MISCELLANEOUS PUBLICATION 92-3 MAY 1992

Field Guide to Geologic Excursions in Utah and Adjacent Areas of Nevada, Idaho, and Wyoming

Prepared for the Geological Society of America,
Rocky Mountain Section Meeting in Ogden, Utah, May 13-15, 1992

Edited by James R. Wilson
Dept. of Geology, Weber State University
Ogden, UT 84408-2507

THE GEOLOGICAL SOCIETY OF AMERICA
Rocky Mountain Section

UTAH GEOLOGICAL SURVEY
a division of
UTAH DEPARTMENT OF NATURAL RESOURCES

UTAH GEOLOGICAL SURVEY
2363 South Foothill Drive
Salt Lake City, Utah 84109-1491

THE UTAH GEOLOGICAL SURVEY is organized into three geologic programs with Administration, Editorial, and Computer Resources providing necessary support to the programs. The ECONOMIC GEOLOGY PROGRAM undertakes studies to identify coal, geothermal, uranium, hydrocarbon, and industrial and metallic mineral resources; to initiate detailed studies of the above resources including mining district and field studies; to develop computerized resource data bases; to answer state, federal, and industry requests for information; and to encourage the prudent development of Utah's geologic resources. The APPLIED GEOLOGY PROGRAM responds to requests from local and state governmental entities for engineering geologic investigations; and identifies, documents, and interprets Utah's geologic hazards. The GEOLOGIC MAPPING PROGRAM maps the bedrock and surficial geology of the state at a regional scale by county and at a more detailed scale by quadrangle. Information Geologists answer inquiries from the public and provide information about Utah's geology in a non-technical format.

THE UGS manages a library which is open to the public and contains many reference works on Utah geology and many unpublished documents on aspects of Utah geology by UGS staff and others. The UGS has begun several computer data bases with information on mineral and energy resources, geologic hazards, stratigraphic sections, and bibliographic references. Most files may be viewed by using the UGS Library. The UGS also manages a sample library which contains core, cuttings, and soil samples from mineral and petroleum drill holes and engineering geology investigations. Samples may be viewed at the Sample Library or requested as a loan for outside study.

The UGS publishes the results of its investigations in the form of maps, reports, and compilations of data that are accessible to the public. For information on UGS publications, contact the UGS Sales Office, 2363 South Foothill Drive, Salt Lake City, Utah 84109-1491, (801) 467-7970.

The papers in this guidebook were solicited by the organizers of these field trips for the Geological Society of America, Rocky Mountain Section Meeting for 1992. They have been edited and given a common format. They have not been formally reviewed for style or content by the Utah Geological Survey.

Frontispiece

Hayden Survey camp of 1872 near the present Ogden High School. Taylor Canyon (left), Mount Ogden (center), and Malans Peak (right) are visible to the east in the Wasatch Range.
The 1871 and 1872 Hayden Surveys were important in the scientific exploration of the west and in the creation of Yellowstone National Park. Photograph by W.H. Jackson, U.S. Geological Survey Photo Archive 1250.

UTAH GEOLOGICAL SURVEY

Miscellaneous Publication 92-3

1992

Field Guide to Geologic Excursions in Utah and Adjacent Areas of Nevada, Idaho, and Wyoming

Prepared for the Geological Society of America,
Rocky Mountain Section Meeting in Ogden, Utah, May 13-15, 1992

Edited by James R. Wilson
Dept. of Geology, Weber State University
Ogden, UT 84408-2507

Field Guide to Geologic Excursions in Utah and Adjacent Areas of Nevada, Idaho, and Wyoming

Edited by James R. Wilson

Preface

This guidebook contains articles and road logs for field trips planned in conjunction with the 1992 meeting of the Rocky Mountain Section of the Geological Society of America held at Ogden, Utah. The field trip articles and road logs are arranged in the order in which they were numbered for the meeting. Most of the field trips have several technical articles addressing various aspects of the geology seen on the field trip and an effort was made to have each of these papers reviewed by one or more geologists with expertise in that area. Because of time constraints, not every paper was reviewed or edited as thoroughly as might have been desired, but this is somewhat unavoidable in a guidebook. Actually, authors were encouraged to discuss ideas that would generate discussion on the field trips and at subsequent symposia, therefore, some views expressed in the articles and road logs are backed by less evidence than might normally be found in a journal article.

With those caveats in mind, it should be noted that much of the information presented in these papers is new and not currently available in any other publication. In particular, the papers on structure and metamorphism in the eastern Great Basin, papers on structure and mineral deposits of the Oquirrh Mountains, papers on stratigraphy and structure in the Lakeside Mountains, and the papers on vertebrate paleontology will be of interest to many readers.

Two of the field trips were designed specifically for public school teachers (General Geology of the Ogden Area and Geologic Processes and Principles along the Wasatch Front) and therefore, their road logs are not as detailed as others and there are no accompanying technical papers. The geology of Antelope Island, in the Great Salt Lake, has and will be described in a series of publications by the Utah Geological Survey, thus, this important area has only a descriptive road log.

As editor, I would like to express my appreciation to all the authors who helped to make this guidebook a valuable, lasting contribution to the geologic literature of Utah. I would especially like to thank the small number of authors who valiantly adhered to the announced deadlines in the face of their other responsibilities. All papers were reviewed by the editor, but I would like to thank the following geologists for their assistance in technical reviews of some papers: Sidney Ash, James P. Evans, David D. Gillette, Susanne Janecke, Robert Q. Oakes, W. T. Parry, Mike Shubat, Danny Vaughn, Paula N. Wilson, and W. Adolf Yonkee.

TABLE OF CONTENTS PAGE

QUATERNARY VOLCANISM, TECTONICS, AND SEDIMENTATION IN THE IDAHO NATIONAL ENGINEERING LABORATORY AREA

William R. Hackett and Richard P. Smith
Idaho National Engineering Laboratory, EG&G Idaho, Inc., Geosciences, MS 2107
P.O. Box 1625, Idaho Falls, ID 83415

INTRODUCTION

In this article, we discuss the regional context and describe localities for a two-day field excursion in the vicinity of the Idaho National Engineering Laboratory (INEL) (Fig. 1). We address several geologic themes: (1) Late Cenozoic, bimodal volcanism of the Eastern Snake River Plain (ESRP), (2) the regional tectonics and structural geology of the Basin and Range province to the northwest of the ESRP, (3) fluvial, lacustrine, and aeolian sedimentation in the INEL area, and (4) the influence of Quaternary volcanism and tectonics on sedimentation near the INEL. Recent overviews of the Quaternary history, geomorphology, volcanic geology and tectonics of the Eastern Snake River Plain include Baker and others (1987), Kuntz and others (in press), Kuntz (in press), Pierce and Morgan (1990 and in press), and Malde (1991).

HISTORICAL AND TECHNOLOGICAL SIGNIFICANCE OF THE INEL

Established in 1949 as the National Reactor Testing Station, the INEL today includes a number of facilities within an 890-square-mile area of sagebrush desert, on the Eastern Snake River Plain of Idaho. The climate is semi-arid, with an average annual precipitation of about 8.5 inches (216 mm). The site was originally chosen for nuclear-safety research because of its isolation and unsuitability of the land for agriculture. In 1951 the INEL hosted one of the most significant accomplishments of the century — the first use of nuclear fission to produce electricity, in Experimental Breeder Reactor 1, now a National Historic Landmark. Fifty-two reactors, most of them first-of-a-kind facilities, have been built here. Several are still operable, and others were phased out upon completion of their research missions.

The INEL is also a National Environmental Research Park, preserving habitat and fostering biologic, archaeologic, and geologic research within its relatively undisturbed environment. Today, the INEL is administered by the U.S. Department of Energy, together with about seven major contractors. It is an important center for nuclear-safety research, defense programs, nuclear-waste technology, and advanced energy concepts.

Geotechnical data, including regional geology and geophysics, are widely used by INEL scientists and engineers in the design, construction, and safety analysis of INEL facilities. Thus, much of the information we present in this article has been obtained within the context of our attempts to assess the potential impacts of future volcanic, seismic, and climatic events on INEL facilities.

REGIONAL GEOLOGIC SETTING OF THE IDAHO NATIONAL ENGINEERING LABORATORY

The INEL is located near the northwestern margin of the ESRP, and lies in an area influenced by two distinct geologic provinces (Fig. 1). The ESRP is a northeast-trending zone of late Tertiary and Quaternary volcanism that transects the northwest-trending, normal-faulted mountain ranges of the surrounding Basin and Range province. The topographically subdued ESRP, the dominant geomorphic feature of southern Idaho, is a relatively aseismic region in the midst of the high-relief, seismically active Basin and Range province.

Volcanic and sedimentary rocks of the Snake River Plain form a 60- to 100-kilometer-wide belt, extending about 600 km from the Idaho-Oregon border to the Yellowstone Plateau. The inception of voluminous silicic volcanism on the Snake River Plain becomes younger toward the northeast (Fig. 2), supporting the interpretation of the Eastern Snake River Plain as the track of a mantle plume, formed during the past 16 Ma due to southwestward relative movement of the North America plate at a rate of about 3.5 cm/yr (Armstrong and others, 1975; Rodgers and others, 1990; Pierce and Morgan, 1990 and in press). The plume now underlies the Yellowstone Plateau (Iyer and others, 1981), and is the source of heat for the spectacular geothermal features and more than 6,000 km^3 of Quaternary silicic-volcanic rocks comprising the Yellowstone Plateau volcanic field (Hildreth and others, 1991). No basalt has yet erupted within the Yellowstone caldera, but in the wake of the plume, extensive late Tertiary and Quaternary mafic volcanism and sedimentation have occurred on the ESRP.

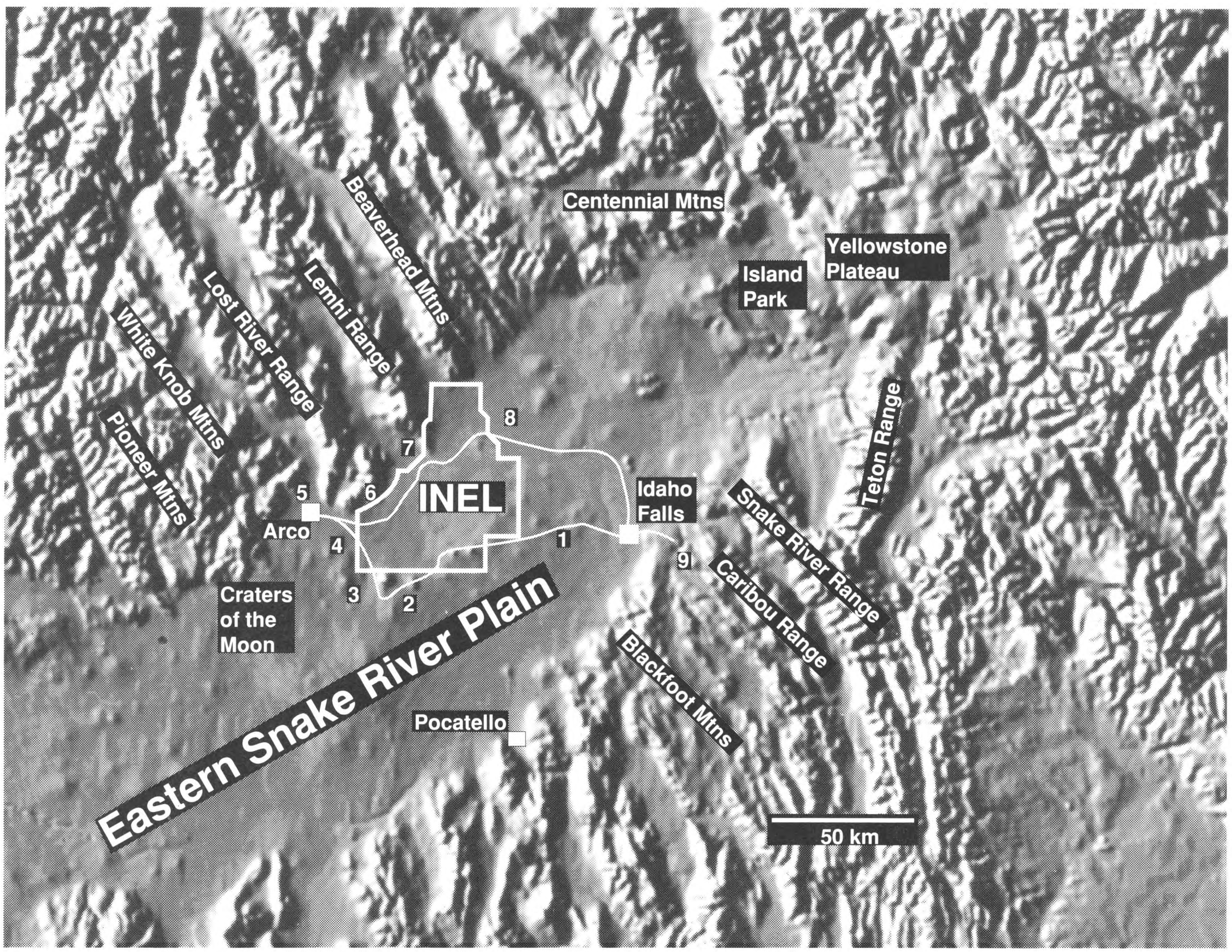

Figure 1. Index map, showing the location of the Idaho National Engineering Laboratory on the Eastern Snake River Plain volcanic province, the surrounding Basin and Range tectonic province, the field-trip route, locations of stops 1-9, and selected points of geographic and geologic reference; BSB = Big Southern Butte, CB = Cedar Butte, MB = Middle Butte, EB = East Butte, JB = Juniper Buttes. The digital-topographic base is from Richard Pike, U.S. Geological Survey.

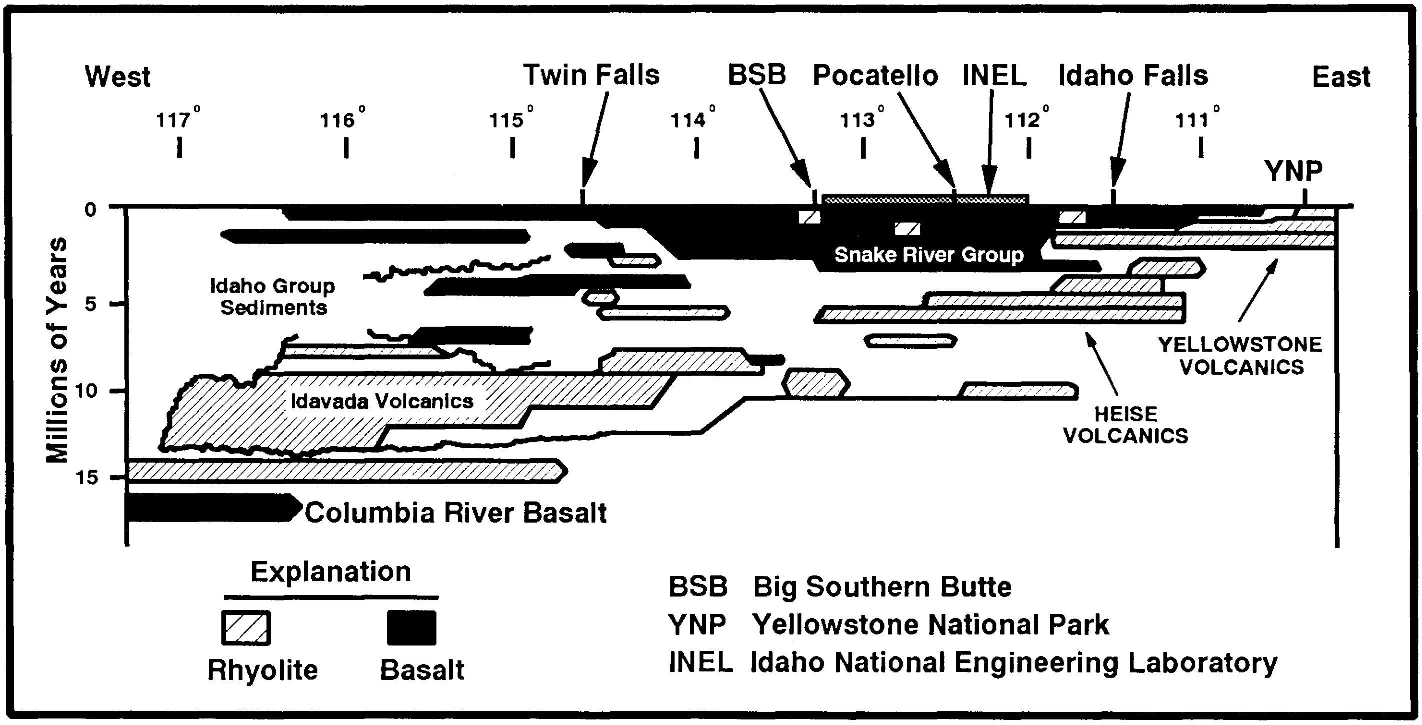

Figure 2. Age-distance plot of late Cenozoic, bimodal volcanism in the Snake River Plain-Yellowstone province (adapted from Armstrong and others, 1975; Hackett and Morgan, 1988; Rodgers and others, 1990). Two features are emphasized: the onset of voluminous rhyolitic volcanism becomes progressively younger toward the northeast, and the Tertiary eruptive complexes have been subsequently covered by Quaternary basalts and sediments of the Snake River Group.

Neogene Silicic Volcanism

Neogene silicic tuffs and lava flows of the Heise volcanic field are considered to be the oldest plume-related volcanic rocks of the ESRP, and are the ancestral equivalents of the Quaternary Yellowstone volcanics (Morgan and others, 1984; Morgan, 1988; Pierce and Morgan, 1990 and in press). Three widespread and voluminous rhyolitic ignimbrites are key lithostratigraphic units of the Heise volcanics, occurring in outcrops around the margins of the ESRP and in deep drillcores of the ESRP (Fig. 3). The major ignimbrites are the 6.5-Ma tuff of Blacktail, the 6.0-Ma Walcott Tuff (formerly the tuff of Blue Creek), and the 4.3-Ma tuff of Kilgore (Morgan, 1988). Vent regions of the Heise tuffs and lavas are largely covered by Quaternary/late Tertiary basalts and sediments of the Snake River Group (Fig. 2), but lithologic, paleomagnetic and structural evidence strongly suggests that they were erupted from calderas buried beneath basalts and sediments of the ESRP (Fig. 4) (Morgan, 1988). Such evidence includes the petrology and volcanic facies of the tuffs themselves; the possible occurrence of ring fractures and related faults in isolated places on both ESRP margins; contemporaneous silicic lava flows which may have issued from ring-fracture zones, and the great thicknesses of rhyolite found in the two deep INEL drillholes beneath the Quaternary basalt-sediment pile [ca. 2500 m of rhyolite in INEL-1 (Doherty, 1979), and 380 m in WO-2 (Hackett and others, unpublished data)]. These thicknesses are substantially greater than those of equivalent outflow-facies ignimbrites exposed outside the ESRP. To the northeast, the Island Park region (Fig. 1) is a transitional area between the basaltic-lava plains of the ESRP and the Yellowstone Plateau, where no basalt has yet erupted within the Yellowstone caldera. Partial filling of the Quaternary Henrys Fork caldera at Island Park by basaltic lava flows (Christiansen, 1982) is an example of the beginning of the burial process. Concurrent with basaltic volcanism, subsidence of the ESRP is predicted by thermal modelling of the response of the continental lithosphere to passage of the mantle plume (Blackwell, 1989).

Quaternary Basalt, Sediment and Rhyolite

Basalts and sediments of the ESRP are part of the Snake River Group, composed largely of tholeiitic-basalt lava flows emplaced during the past 4 million years (Fig. 2). Most eruptions were effusive, and typical landforms of Quaternary mafic volcanism on the ESRP are small shield volcanoes with summit pit craters, fissure-fed lava flows associated with zones of tensional fracturing, and relatively uncommon tephra cones of magmatic or phreatomagmatic origin (Greeley, 1982).

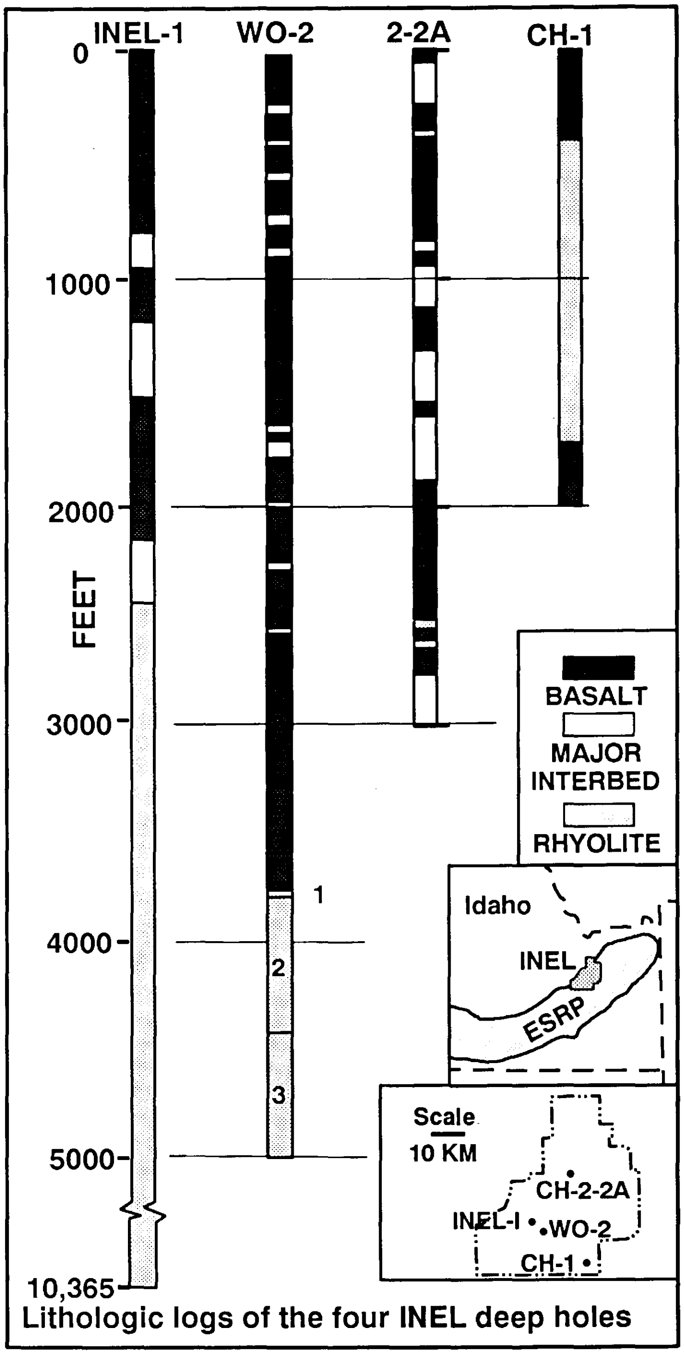

Figure 3. Simplified lithologic logs from deep drillholes in the INEL area. Only INEL-1 and WO-2 intersect Tertiary rhyolite, beneath basalts and sediments of the Snake River Group. Lithologic data are from Doherty and others (1979) for INEL-1 ; Doherty (1979a) for hole CH-1; and Doherty (1979b) for corehole 2-2A.

Based on field mapping, and limited geochronometry and paleomagnetic data, Kuntz and others (1990) (Fig. 5) identify five Quaternary basalt lava-flow groups in the INEL area, ranging in age from 5,200 years to greater than 730,000 years. The estimated ages of most lava flows in the INEL area are based on qualitative geomorphic and stratigraphic criteria: the youngest lava fields show little or no eolian sand and loess cover, and are largely unweathered. Older flows are covered by progressively thicker sediment and are more deeply weathered. These factors, together with stratigraphic-age relationships among adjacent lava fields, form the subjective basis for assigning lava fields to their respective age units.

Basaltic vents on the ESRP typically form linear arrays of fissure flows, small shields and pyroclastic cones, pit craters and open fissures, which collectively define northwest-trending volcanic rift zones (Fig. 6). Volcanic rift zones have similar trends as normal faults in the adjacent Basin and Range province to the north, but are not strictly colinear with those faults. The most well-known and recently active of ESRP volcanic rift zones is the Great Rift (Kuntz and others, 1988), where eight eruptive episodes occurred at Craters of the Moon, and several smaller, monogenetic lava fields were formed during the past 15,000 years. In the INEL area, most basaltic rift-zone volcanism seems to have occurred during Pleistocene time, generally between about 0.1 and 0.7 Ma. Most subaerially exposed lavas have normal magnetic polarity, and are therefore younger than about 730,000 years. Several well-dated Holocene lava fields (Kuntz and others, 1986) erupted from northwest-trending fissures to the south of the INEL, on the northeast-trending axial volcanic zone.

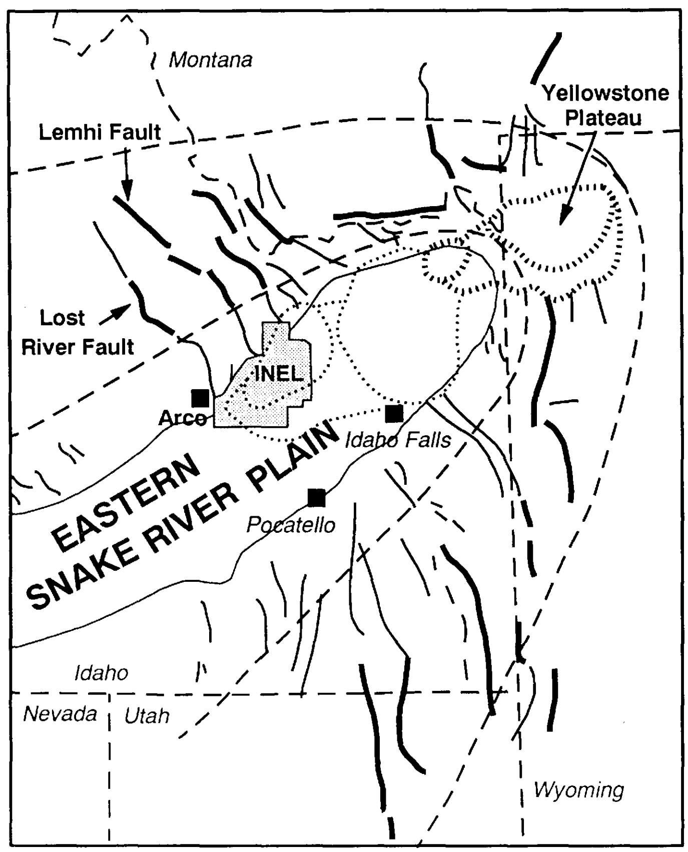

Figure 4. Map showing the generalized locations of Neogene silicic calderas (dotted ellipses) that are inferred to be buried beneath the ESRP (Morgan and others, 1984; Morgan, 1988), the exposed Quaternary calderas of the Yellowstone Plateau volcanic field (Christiansen, 1984), the parabolic region of historical seismicity centered on the Yellowstone plateau (enclosed by dashed curves; Anders and others, 1989), and major normal faults around the ESRP (bold lines indicate fault segments with Holocene displacement).

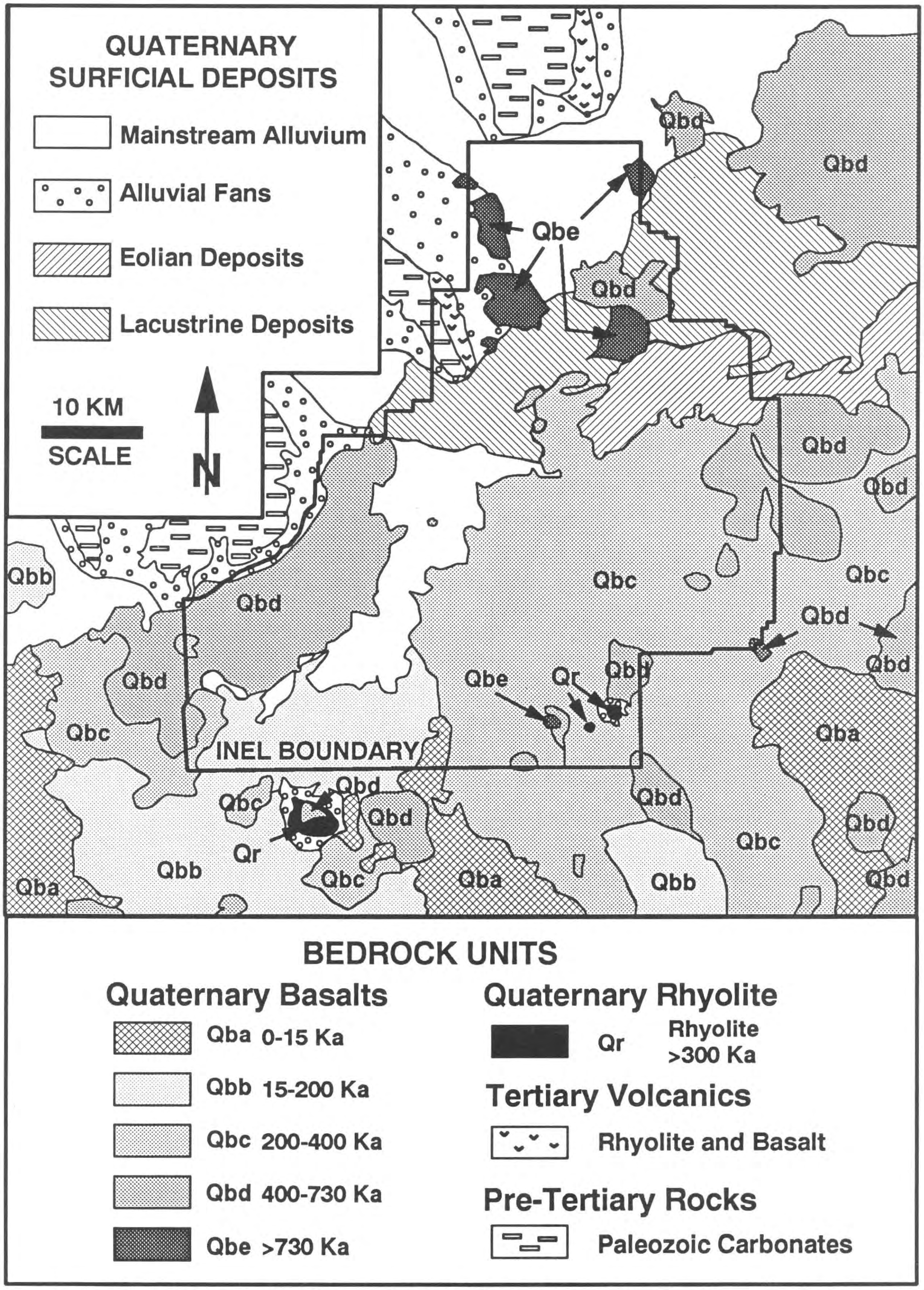

Figure 5. Generalized geologic map of the INEL area, showing the distribution of major basalt lava-flow groups and sedimentary deposits (adapted from Kuntz and others, 1990; Scott, 1982).

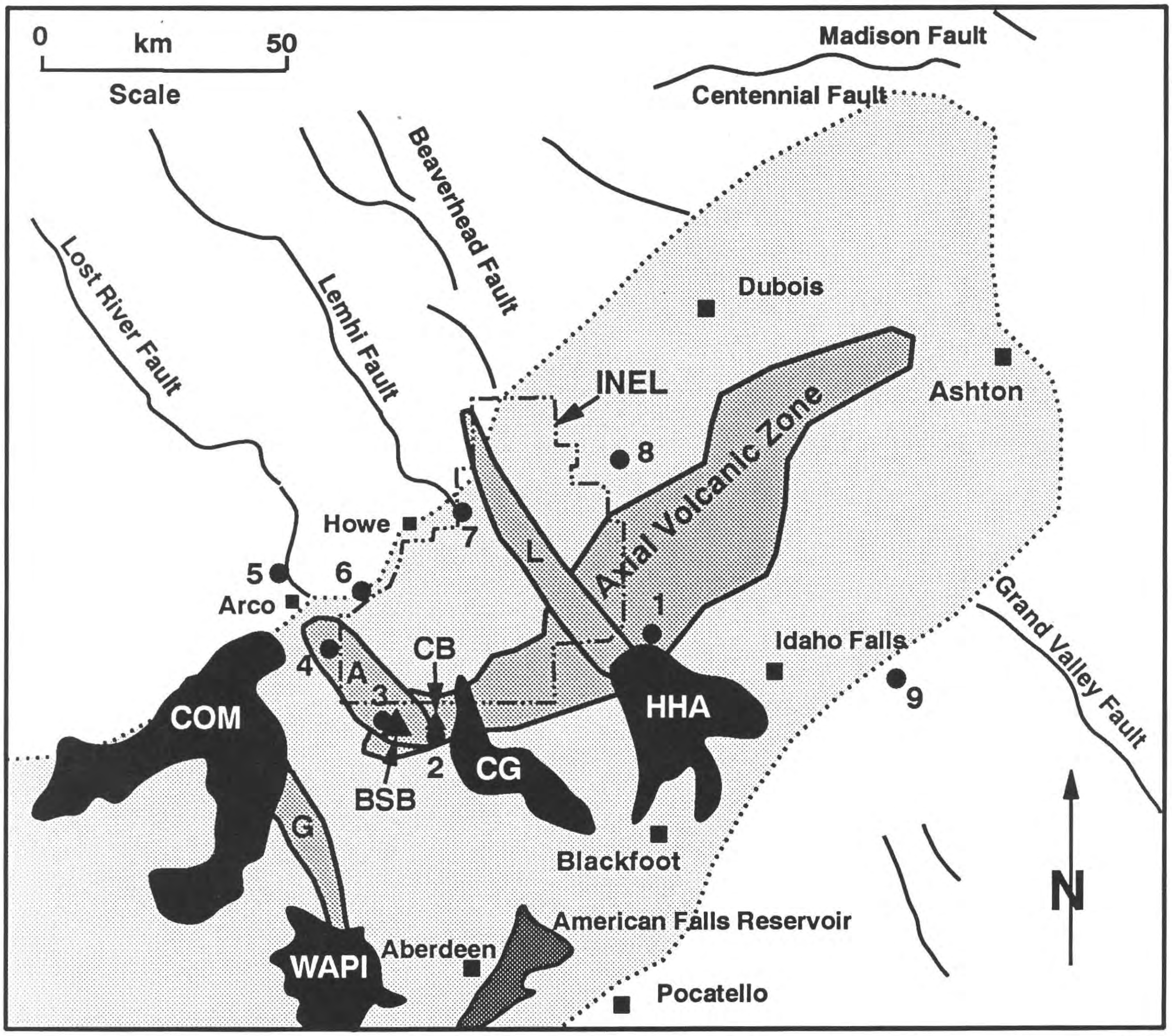

Figure 6. Map showing the major volcanic and tectonic elements of the INEL area, including northwest-trending normal faults of the Basin and Range tectonic province, northwest-trending volcanic rift zones on the ESRP, and the northeast-trending axial volcanic zone (a central, constructional region of volcanic vents). Holocene lava fields near the INEL are Hell's Half-Acre (HHA), Cerro Grande (CG), Wapi, and Craters of the Moon (COM). Locations of stops 1-9 are indicated.

Pleistocene rhyolite domes also occur along the axial volcanic zone on the ESRP (Fig. 7). Big Southern Butte is formed of two, coalesced exogenous rhyolite domes (Spear and King, 1982), with an uplifted, north-dipping block of basalts, ferrolatites and sedimentary interbeds on its north flank (Fishel, 1992). The Cedar Butte eruptive center (Spear, 1979; Hayden, 1992) is a complex assemblage of landforms and lava types, mostly mafic in composition but including a small, undated rhyolitic dome. A topographic escarpment southeast of the Cedar Butte summit may be the result of uplift associated with late-stage silicic-magma intrusion beneath the complex, or the draping of mafic lava flows over a steep-sided silicic flow. Middle Butte is a stack of about twenty basalt lava flows, apparently uplifted in pistonlike fashion by a buried silicic intrusion (cryptodome) of unknown age. East Butte is an exogenous rhyolitic dome, in places containing centimeter-sized clots and blocks of mafic material.

Northern Basin and Range Province

The INEL is located near the northwestern margin of the ESRP (Figs, 1 and 2), where the low-lying lava plains terminate abruptly against the northern Basin and Range province, represented by the Lost River Range, Lemhi Range, and Beaverhead Mountains. Hypocenters of historical earthquakes occur in a parabolic region surrounding the ESRP and centered on the Yellowstone Plateau (Anders and others, 1989; Pierce and Morgan, 1990 and in press) (Fig. 4). The southern limb of the parabola is part of the Intermountain Seismic Belt, which continues south to the Wasatch front of Utah and marks the eastern edge of the seismically active Basin and Range tectonic province. The northern limb of the parabola is the Centennial Tectonic Belt, which extends westward from the Yellowstone Plateau and includes the epicentral area of the 1983 Borah Peak earthquake. The central, relatively aseismic area enclosed by the

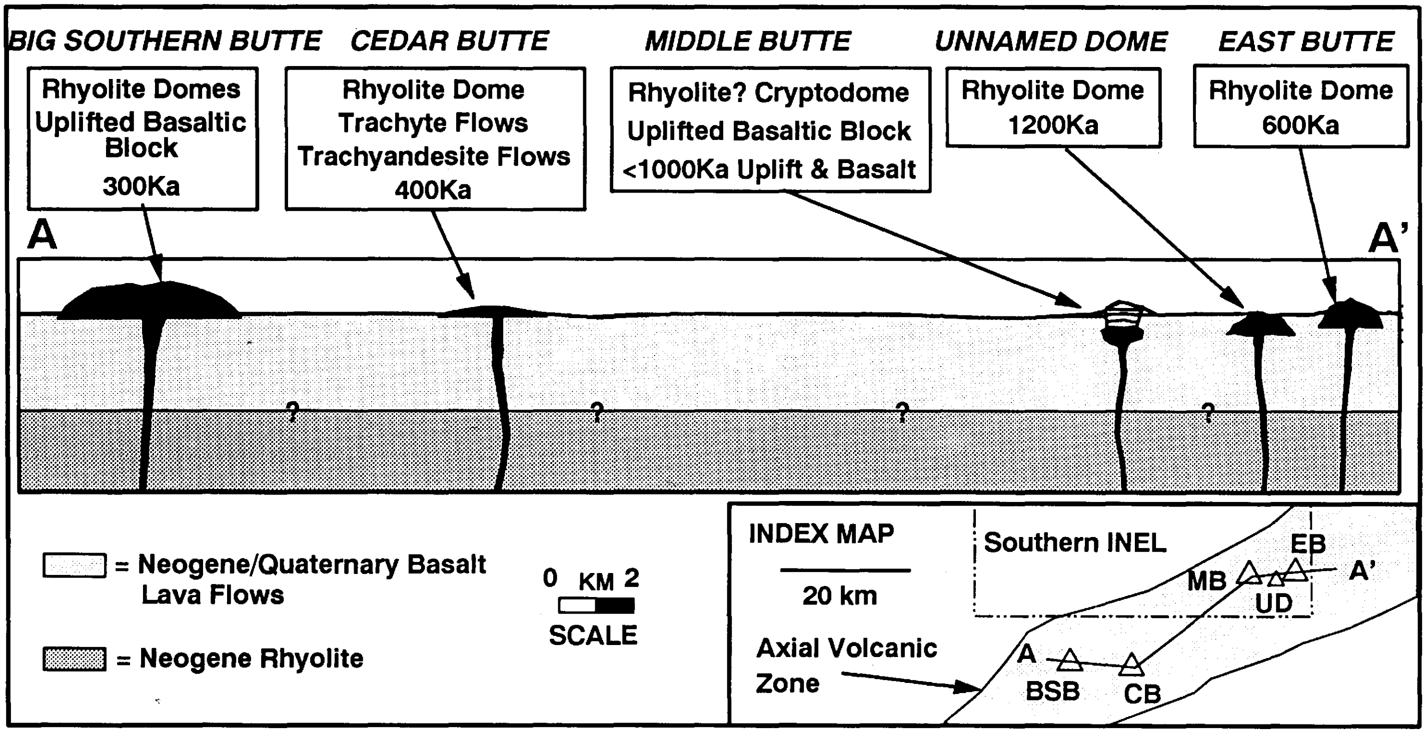

Figure 7. Schematic cross section along the axial volcanic zone of the ESRP, showing the ages, rock types and known or inferred lithostratigraphic relationships of Pleistocene silicic volcanic domes (adapted from Kuntz and Dalrymple, 1979; Spear and King, 1982; and authors' unpublished data).

seismic parabola includes not only the ESRP, but also adjacent portions of basin-and-range normal faults.

Northwest of the INEL, basin-and-range mountains are episodically uplifted along high-angle normal faults, as shown by paleoseismic investigations of fault scarps along the Lost River and Lemhi faults (Malde and others, 1971; Malde, 1987; Pierce, 1988; Hemphill-Haley and others, 1991), and coseismic deformation associated with the 1983 Borah Peak earthquake on the Lost River fault (Crone and others, 1987). Geologic mapping and fault-scarp excavations suggest that Quaternary normal faults to the north of the INEL are broken into discrete, 20- to 30-km-long segments that probably rupture independently (Crone and Haller, 1991), and that Holocene movements have not occurred on their southernmost segments adjacent to the ESRP (Pierce and Morgan, 1990 and in press) (Fig. 9). The northern Basin and Range mountains end abruptly against the low-lying ESRP (Figs. 1 and 6), suggesting that the normal faults also terminate.

Quaternary Surficial Deposits

Most lava flows in the INEL region are Pleistocene in age, have been subaerially exposed for several hundred thousand years, and are therefore blanketed with unconsolidated sedimentary deposits of eolian, alluvial and lacustrine origin (Scott, 1982) (Fig. 5). Although little is known of the detailed Quaternary lithostratigraphy of the ESRP subsurface, data from INEL drillcores generally indicate that relatively long (10^5-year) periods of sedimentation and volcanic quiescence, represented by major sedimentary interbeds, were punctuated by relatively brief ($<10^2$- to 10^3-year) episodes of basaltic volcanism, the latter represented by rapidly emplaced lava-flow groups (Kuntz and Dalrymple, 1979; Kuntz and others, 1979, 1980; Champion and others, 1988; Anderson and Lewis, 1989; Anderson, 1991). The present distribution of surficial deposits is probably qualitatively analogous to that of subsurface deposits, involving intermittent blanketing of lava flows by loess, and the deposition of fluvial/lacustrine sediments in low-lying areas between constructional volcanic zones.

Alluvial deposits of two types are found in the INEL area: alluvial-fan deposits and mainstream alluvium. Alluvial fans are developed on the steep lower flanks of basin-and-range mountains and contain clastic material of local origin, commonly subangular/subrounded, moderately sorted gravel, dominated by Paleozoic carbonate clasts. Pierce (1988) uses carbonate-coat thicknesses and $^{230}Th/^{234}U$ disequilibrium dating to identify five age groups of alluvial-fan gravels on the southern Lost River Range, deposited about 15 ka to 160 ka. Where they have been displaced by faulting, alluvial-fan deposits are important targets in fault-scarp excavations, because they provide a sedimentological context for deciphering the absolute and relative chronology of paleoseismic events. Typically, wedges of scarp-derived colluvium are intercalated with loess or other fine-grained sediment, and the latter deposits can commonly be dated using such methods as thermoluminescence and radiocarbon.

Mainstream-alluvial deposits are associated with the channels of the Big Lost River, Little Lost River, and Birch

Creek, which longitudinally drain the northern Basin and Range province and flow southward onto the ESRP (Pierce and Scott, 1982). None of these streams reach the Snake River to the south. Instead, their ephemeral waters percolate into permeable lava flows and sediments at the Lost River Sinks of the northern INEL, a local recharge area for the Snake River Plain aquifer. Mainstream deposits are generally better sorted, rounded and bedded than those of alluvial fans, and clasts are predominantly quartzite, chert, silicified Eocene volcanic rocks, and other resistant lithologies.

Evidence for catastrophic flooding is well-known in the upper Snake River drainage where the effects of at least two Pleistocene, probably ice-dammed flood events are recognized, with likely sources on the Yellowstone Plateau (Scott, 1982). Effects of the Bonneville flood in southeast Idaho are even better known (Malde, 1968; Scott and others, 1982). Less well-known are glacial-outburst flood features of the Big Lost River (Rathburn, 1988; 1991). Near the western INEL boundary, channeled scablands, boulder bars and hyperconcentrated stream-flow deposits are products of a glacial-outburst flood. The floodwaters probably originated in the Copper Basin area, about 50 miles from the INEL, where Pinedale moraines and kame deposits are abundant. Preliminary results indicate the Big Lost River flood occurred about 19.8 ± 1.4 ka, based on cosmogenic ^{3}He and ^{21}Ne dating of geomorphic surfaces that were exposed during the event (Cerling and others, 1991).

Lacustrine deposits: volcanic eruptions and tectonism have periodically impounded the Snake River and its tributaries, forming lacustrine basins or areas of impeded drainage (Malde, 1982; Howard and Shervais, 1982; Scott and others, 1982; Hackett and Morgan, 1988). In the INEL region, the axial volcanic zone obstructed drainage from areas north of the ESRP. During glacial/pluvial periods, the resulting basins received more runoff than now, and contained large shallow lakes, in contrast to the present small playas of the Lost River Sinks. One such basin in the area that is now the northern INEL (Fig. 5) was occupied by Lake Terreton, whose Pleistocene deposits have been cored in the upper part of drillhole 2-2A (Fig. 3). Lake Terreton formerly covered a wide area near the present Mud Lake. Its shoreline generally follows the 4,800-foot topographic contour on the ESRP and is marked by beaches, bars and deltas. Lake Terreton sediments are the major source of material for Holocene dunes to the northeast.

Eolian deposits: Pleistocene loess deposits are widespread on the ESRP, and reach their greatest thickness along its southeastern margin. Several episodes of loess deposition are inferred from studies of loess stratigraphy and paleopedology (Pierce and others, 1982; Lewis and Fosberg, 1982; Scott, 1982). Holocene basalt flows on the ESRP have accumulated little or no loess (Kuntz and others, 1986), indicating that major loess deposition ceased about 10 to 15 ka. Late Pleistocene basalt flows and geomorphic surfaces are overlain by a single loess blanket, whereas older surfaces are generally mantled by several loess units, separated by paleosols or erosional surfaces. Pierce and others (1982) identify two widespread loess units in southeast Idaho; the upper loess (unit A) was deposited about 10-70 ka, while the lower (unit B) is less well dated but probably accumulated about 140-200 ka.

Dunes and sheets of Holocene eolian sand near Mud Lake (Fig. 5) have sources in the deflated alluvial surfaces of the Lost River Sinks, and in the abandoned shoreline and floor of former Lake Terreton to the southwest.

INTERACTION OF QUATERNARY VOLCANIC AND TECTONIC PROCESSES ON THE EASTERN SNAKE RIVER PLAIN

The ESRP is surrounded by the northern Basin and Range province, a region of actively extending lithosphere. The question of whether the ESRP is extending along with the surrounding terrain has recently been addressed by several writers. Anders and others (1989) consider that basin-and-range structures die out toward the ESRP because the integrated strength of the continental lithosphere beneath the ESRP is too great to permit extension, owing to the introduction of mantle-derived, mafic material at depth. Although the geophysical evidence of seismic refraction and regional heat flow data support the introduction of voluminous mafic-magmatic material into the middle crust and probably also the lithospheric mantle (Sparlin and others, 1982; Blackwell, 1989), the absence of strike-slip faults along the margins of the ESRP argues against decoupling of a static volcanic province from its extended surroundings. We and our colleagues have recently developed an explanation: the ESRP is extending at much the same rate as the surrounding Basin and Range province, but it does so by mafic-dike intrusion rather than by normal faulting (Smith and others, 1989; Rodgers and others, 1990; Parsons and Thompson, 1991) (Fig. 8).

Evidence in support of these two contrasting extensional mechanisms includes geologic and geophysical data, as outlined by Hackett and others (1991): Basaltic rift zones on the ESRP are aligned northwest, parallel to the trends of normal faults in the northern Basin and Range province. Rift-zone characteristics on the ESRP are similar to those of active rifts in Iceland and Hawaii, and include both ground deformation (open fissures, small-displacement normal faults, graben) and linear volcanic features. The surface-deformation features associated with ESRP basaltic volcanism are dissimilar in style and displacement to range-bounding normal faults in the surrounding tectonic province, but are identical to those of active rift zones in other regions such as Iceland, where dike-induced extension is unequivocal. Northwest-trending, positive aeromagnetic anomalies (Zietz and others, 1978) may indicate subsurface dike swarms beneath volcanic-rift zones. Several anomalies extend beyond the margins of the ESRP, suggesting the continuation of mafic-dike swarms into the adjacent Basin and Range tectonic province. Such outboard dike intrusion may explain the general observation of decreased paleoseismicity along southern normal-fault segments adjacent to the ESRP. In

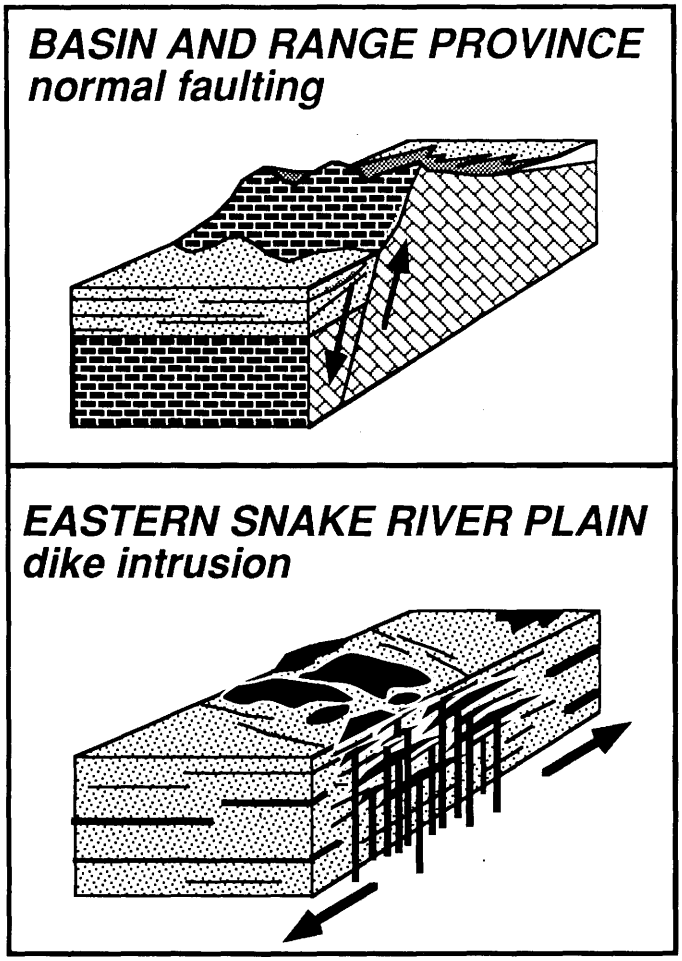

Figure 8. Schematic block diagrams showing the different modes of extension in the INEL region. On the Eastern Snake River Plain, the lithosphere apparently extends by mafic-dike intrusion. In the surrounding Basin and Range province, the lithosphere extends by normal faulting.

addition, northwest-trending, late-Quaternary volcanic rift zones are best developed on the northern half of the ESRP, adjacent to the most actively extending, northern part of the Basin and Range province.

The absence of borehole breakouts in the 3.2-km INEL-1 drillhole indicates that deviatoric stresses in the ESRP are low (Thompson and others, 1990), despite the presumed northeast-southwest extension of the ESRP. The dilation of dike walls due to the magma overpressure required for intrusion keeps ESRP deviatoric stresses low. Magma intrusion therefore effectively prevents normal faults from extending into the Snake River Plain.

By summing the inferred dike widths across Holocene eruptive centers and rift zones, we estimate total Holocene extension due to dike intrusion in the ESRP to be on the order of 10 to 20 meters. This is comparable to the estimated Holocene extension in the northern Basin and Range province, as derived from paleoseismic investigations of fault segments showing Holocene movement.

These contrasting extensional processes explain not only the strong topographic contrast between the Basin and Range tectonic province and the ESRP volcanic province, but also the relative aseismicity of the ESRP in contrast to its surroundings. Normal faults in the Basin and Range tectonic province generate large earthquakes, due to the accumulation and periodic release of elastic-strain energy. In contrast, ascending dikes would produce low-magnitude earthquake swarms, since shallow country rocks are weak under tension and little strain accumulation takes place prior to failure. Thus, although volcanic rift zones on the ESRP are potentially seismogenic sensu stricto, they are probably incapable of generating large-magnitude earthquakes, and magma overpressure in the ESRP prevents accumulation of the elastic strain that is necessary to produce large earthquakes.

INTRODUCTION TO THE FIELD GUIDE

Features to be visited on the two-day excursion include Holocene basaltic lava fields; eruptive and structural features of Quaternary basaltic-rift zones near the INEL; the southern segments of two major, basin-and-range faults near the INEL; Pleistocene rhyolitic domes along the central axis of the ESRP; Quaternary tectonic, sedimentary and volcanic features along the northern margin of the ESRP; late-Pleistocene, glacial-outburst features on the ESRP; and caldera-related, Neogene rhyolites around the margins of the ESRP.

Related guidebooks, maps and other literature of general interest include Scott, 1982; Link and Hackett, 1988; Alt and Hyndman, 1989; Bonnichsen and others, 1989; Ruebelmann, 1989; Kuntz and others, 1990; and Malde, 1991. Topographic maps of the field-trip area include the Idaho Falls 1 x 2-degree sheet, and the Arco, Craters of the Moon, Circular Butte, and Blackfoot 1:100,000 (metric) sheets.

SECURITY AND SAFETY ON THE IDAHO NATIONAL ENGINEERING LABORATORY

Our work at the INEL involves research and information affecting the defense and security of the United States. As a result, visitors to the INEL must be accompanied by an authorized escort at all times. Upon presentation of a picture identification/proof of U.S. citizenship (a valid driver's license is sufficient), security personnel may issue a visitor pass, which must be worn in plain view between the neck and waist. Personal equipment is permitted on site, but must be tagged by security. Boxes, briefcases, purses, etc. will be searched when entering and exiting controlled areas. Prohibited items include firearms and incendiary devices, alcohol and illegal drugs, portable transmitting or recording devices, and cameras. Your escort will direct you in case of an emergency situation, but two telephone numbers are important to know when visiting DOE facilities: for fire or medical emergencies dial 777; for other emergencies dial 526-1515.

LOCALITY DESCRIPTIONS

Stop 1. Hell's Half-Acre lava field

Holocene basaltic lava fields ranging in age from about 15 to 2 ka cover about 13% of the ESRP. Most are associated with either the Great Rift or the axial volcanic zone. The Hell's Half-Acre lava field was emplaced about 5.2 ± 0.15 ka, according to radiocarbon studies (Kuntz and others, 1986). The lava field is composed of about eight lobes of rapidly emplaced, basaltic pahoehoe flows, and marks the southern end of the Lava Ridge - Hell's Half-Acre volcanic rift zone (Kuntz and others, 1979). The hummocky lava-flow surfaces are typical of sheetlike basaltic lava flows worldwide, and are deflation features resulting from drainage of magma and gas from beneath the solidified lava crust. Generalized features of the Hell's Half-Acre lava field, which also apply to other lava fields on the ESRP, are shown in Fig. 9. The vent region is marked by a basaltic-shield volcano on the northwestern part of the lava field, with numerous aligned pit craters and small spatter mounds along a northwest-trending eruptive fissure. These features, together with two sets of parallel, noneruptive fissures extending northwestward beyond the lava field, indicate that the lava effusions were fed by one or more basaltic dikes.

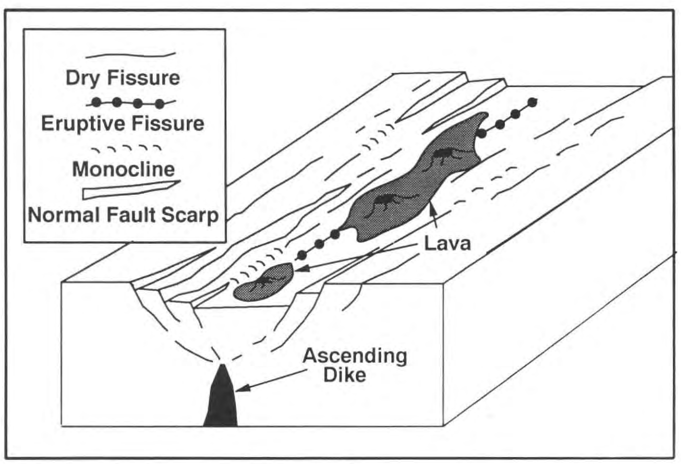

Figure 9. Schematic block diagram, showing typical eruptive and ground-deformation features of a monogenetic, dike-fed basaltic lava field such as Hell's Half-Acre.

Field studies, elastic-strain models, and the empirical results of "sand-box" experiments (Rubin and Pollard, 1988; Mastin and Pollard, 1988) have shown that ascending dikes produce overlying extensional features. Extensional structures such as graben, monoclines and open fissures commonly develop in tandem zones, symmetrically disposed around the intruded dike or its eruptive fissure. These features develop due to tensional stresses above the propagating dike tip, as country rocks are shouldered aside.

Dikes, and hence their associated ground-deformation features, are sensitive indicators of the regional-stress field. Because the ESRP is a young volcanic province, few dikes are exposed, but ground-deformation features associated with dike intrusion beneath volcanic-rift zones are nearly always northwest-trending, and thus have similar orientations as normal faults in the surrounding Basin and Range province.

Stop 2. Cedar Butte eruptive center

Cedar Butte is a composite eruptive center located near the intersection of the Arco rift zone and the axial volcanic zone on the Eastern Snake River Plain (Fig. 10) (Spear, 1979; Hayden, 1992). Geologic mapping of the Cedar Butte eruptive center has identified three vent areas: a large arcuate spatter rampart, a cinder cone, and a small fissure vent to the south of the cinder cone (figure 10). Lavas and tephra exhibit a wide range of bulk compositions from about 54 to 74 weight % SiO_2 (figure 12), and include basaltic trachyandesite, trachyandesite, trachyte, and rhyolite. The arcuate spatter vent is the source of the evolved basaltic flows covering the northern portion of the eruptive center. The cinder cone is held up by erosionally resistant spatter deposits, consisting of strongly to weakly welded lapilli tuff containing red, black and white pumice lapilli in a matrix of hybrid spatter. Basaltic spatter containing mixed-magma pumice lapilli occurs on the southwestern cone rim. About one-half kilometer south of the cone, a fissure vent erupted a widespread, thin flow of basaltic trachyandesite. An older, steep-sided rhyolite lava flow at the southern margin of the volcanic complex is mostly covered by trachyte and basaltic trachyandesite flows. The volcanic stratigraphy and mixed-magma lithologies at Cedar Butte show that diverse magma types were erupted in close spatial and temporal proximity. Evidence for co-eruption and commingling of mafic-to-silicic magmas occurs at all scales of observation, from disequilibrium phenocryst assemblages, to individual clasts of hybrid pumice, mixed-tephra pyroclastic beds, and a hybrid dike.

At **Stop 2,** a hybrid dike cuts the eastern part of the cinder cone (Fig. 10), outcropping in three segments along a small gully. The dike contains an inner, silicic core (62 to 73% SiO_2), with a mantle of basaltic trachyandesite (56% SiO_2). The dike is thus an intrusive counterpart of the hybrid and mixed-tephra deposits of the cinder cone.

Stop 3. Big Southern Butte

The most conspicuous landmark on the ESRP, Big Southern Butte rises 760 m from the surrounding lava plains, at the intersection of the axial volcanic zone and the Arco-Big Southern Butte volcanic rift zone. Armstrong and others (1975) give potassium-argon dates of 0.30 ± 0.002 and 0.60 ± 0.01 Ma from rhyolite of Big Southern and East buttes, respectively. The geology of Big Southern Butte is described by Spear and King (1982) as a dome of sugary, flow-banded to massive, nearly aphyric rhyolite. The northern flank of the butte is composed of a north-dipping slab of mafic lavas,

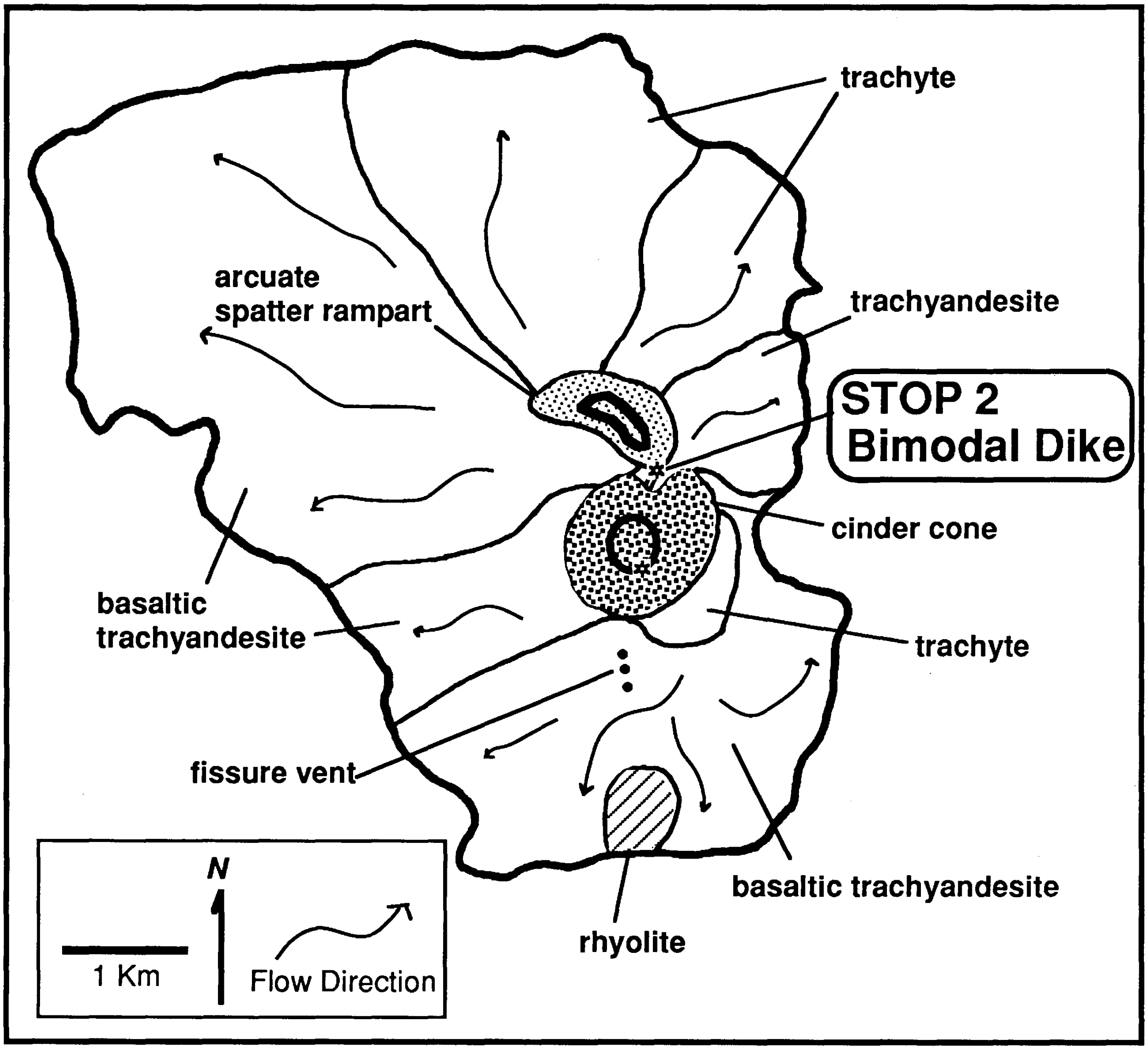

Figure 10. Generalized geologic map of the Cedar Butte eruptive center (data from Hayden, 1992), showing major map units, vent areas and position of Stop 2. All rock units are Quaternary in age, and the nomenclature of rock units is based on the geochemical data of Figure 12.

uplifted during growth of the rhyolite dome. Fishel (1992) (Fig. 11) shows that the uplifted slab of mafic lavas has a total stratigraphic thickness of about 900 m, and consists of at least thirty, 2- to 18-meter-thick lava flows, together with a few poorly exposed sedimentary interbeds. Bulk compositions of the uplifted Snake River Plain lavas range from about 45% to 67% SiO_2 (Fishel, 1992). Most rocks are tholeiitic basalts, but evolved lavas occur at the base and top of the exposed section (Fig. 11): ninety meters of welded-pyroclastic trachybasalts occur at the base of the section, and the uppermost lava flows are trachydacitic in composition. The latter are compositionally and petrographically similar to Cedar Butte eruptives (Fig. 12), suggesting that the source of the uppermost, mafic-to-intermediate lava flows on Big Southern Butte is the Cedar Butte eruptive center, about 7 km to the east.

Stop 4. Arco volcanic rift zone (multiple localities)

Volcanism and dike-induced surface deformation: A zone of northwest-elongate volcanic vents, extensional fissures, monoclines and small normal faults extends for a distance of more than 20 km between the town of Arco, Idaho and Big Southern Butte (Kuntz, 1978a,b; Smith and others, 1989; Kuntz and others, 1990). The 6-km-wide rift zone is colinear with the surface trace of the west-dipping Lost River fault, and is thus developed in the footwall of that structure. A generalized geologic map is given in Fig. 13, and Fig. 14 is an oblique-aerial photograph of a graben in the northern part of the Arco rift zone.

Surface deformation in the Arco rift zone is similar to that of active volcanic-rift zones in Iceland and Hawaii, and

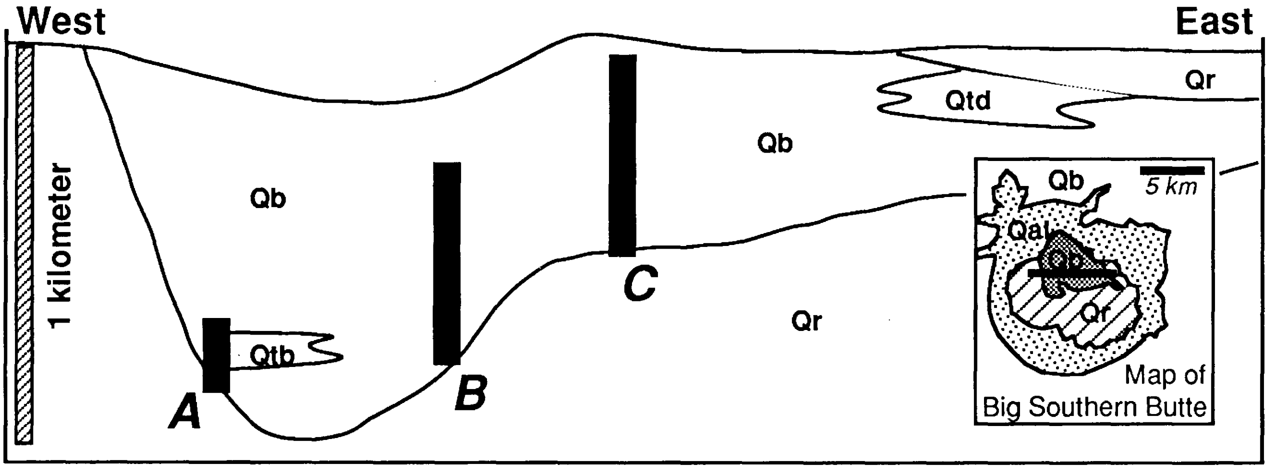

Figure 11. Schematic cross section of the uplifted slab of mafic-to-intermediate volcanic rocks exposed on the north flank of Big Southern Butte (data from Fishel, 1992). Locations of measured stratigraphic sections used in the compilation are shown as A, B, C; units dip about 45 degrees north. All deposits are of Quaternary age: Qal = alluvial-fan deposits; Qr = rhyolite of Big Southern Butte; Qb = Snake River Plain basalt lava flows; Qtb = lower trachybasalts; Qtd = upper trachydacites. See Fig. 12 for composition and nomenclature of selected rock units.

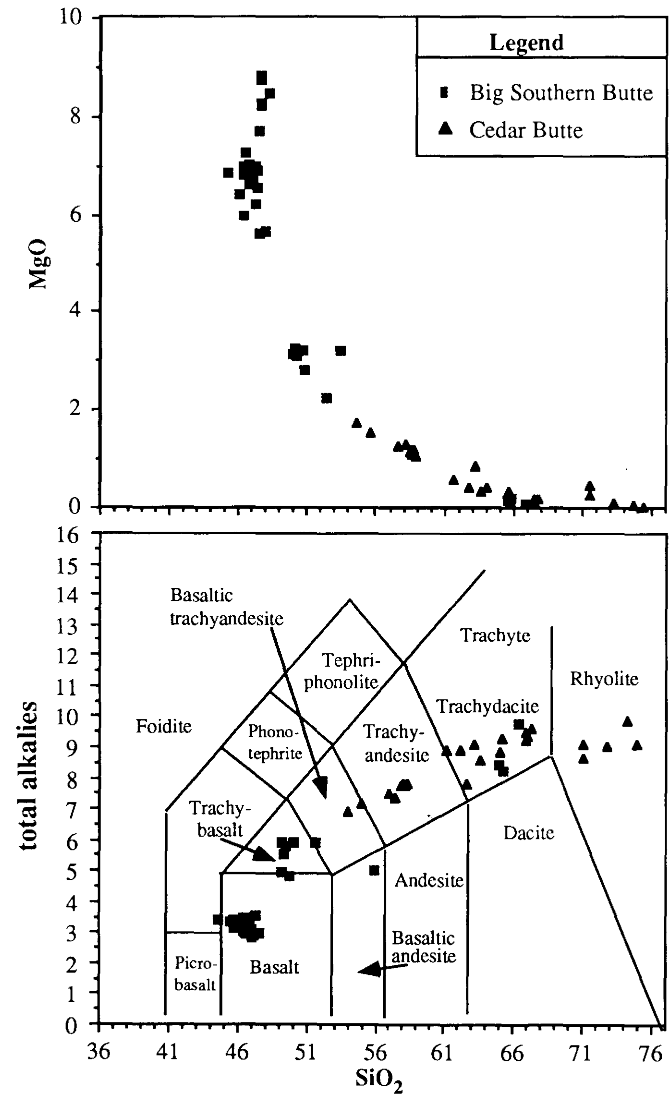

Figure 12. Bulk compositions of volcanic rocks from the Cedar Butte eruptive center and from uplifted, mafic-to-intermediate volcanic rocks on the north flank of Big Southern Butte (data from Fishel, 1992; and Hayden, 1992). Compositional fields and nomenclature are from LeBas and others, 1986.

consists of fissures, faults and monoclinal flexures that cut Quaternary basalt lava flows. Some fissures occupy the hinges of monoclines and are therefore of flexural origin, but most fissures are open vertical cracks with purely dilational displacement. Individual fissures are up to 3 km long, with dilations up to 1 meter. Although the fissures likely penetrate to basaltic-dike tips at depths of hundreds of meters to several kilometers (see Hell's Half-Acre discussion), observable depths seldom exceed 6 meters as a result of infilling by basalt rubble and loess. Fissures make up 80% of the total length of ground-deformation features in the Arco rift zone.

Fault scarps and monoclines commonly alternate with each other along linear zones. The maximum vertical displacement on faults in the Arco rift zone is about 10 meters (Fig. 13) and the maximum fault length is about 6 km. Most offsets are down-to-the-southwest, but down-to-the-northeast offsets are common. Constructional volcanic features consist of northwest-trending eruptive fissures, marked by aligned pyroclastic mounds and elongate shield volcanoes. We interpret the extensional features of the Arco rift zone as having been largely — if not entirely — caused by the intrusion of basaltic dikes, because of their close association with fissure-erupted basalts, and because the magnitude and style of displacement along faults, monoclines and open fissures are similar to those of active basaltic rift zones in Hawaii, Iceland and elsewhere. The presence of subsurface dikes beneath the Arco rift zone is also suggested by a 300-gamma, positive aeromagnetic anomaly over the area (Zietz and others, 1978). The relatively steep gradient of the water table beneath the area suggests that the subsurface basaltic dikes are aquitards.

Age and polygenetic origin of the Arco rift zone: The probable age of Arco-rift-zone volcanism and associated surface deformation ranges from about 600 ka to 100 ka. Fissures are apparently younger than about 600 ka: in the northwest part of the Arco rift zone near Box Canyon they cut basalt lavas that have been radiometrically dated at about 500 ka to 600 ka (Kuntz and others, 1990). Fissuring

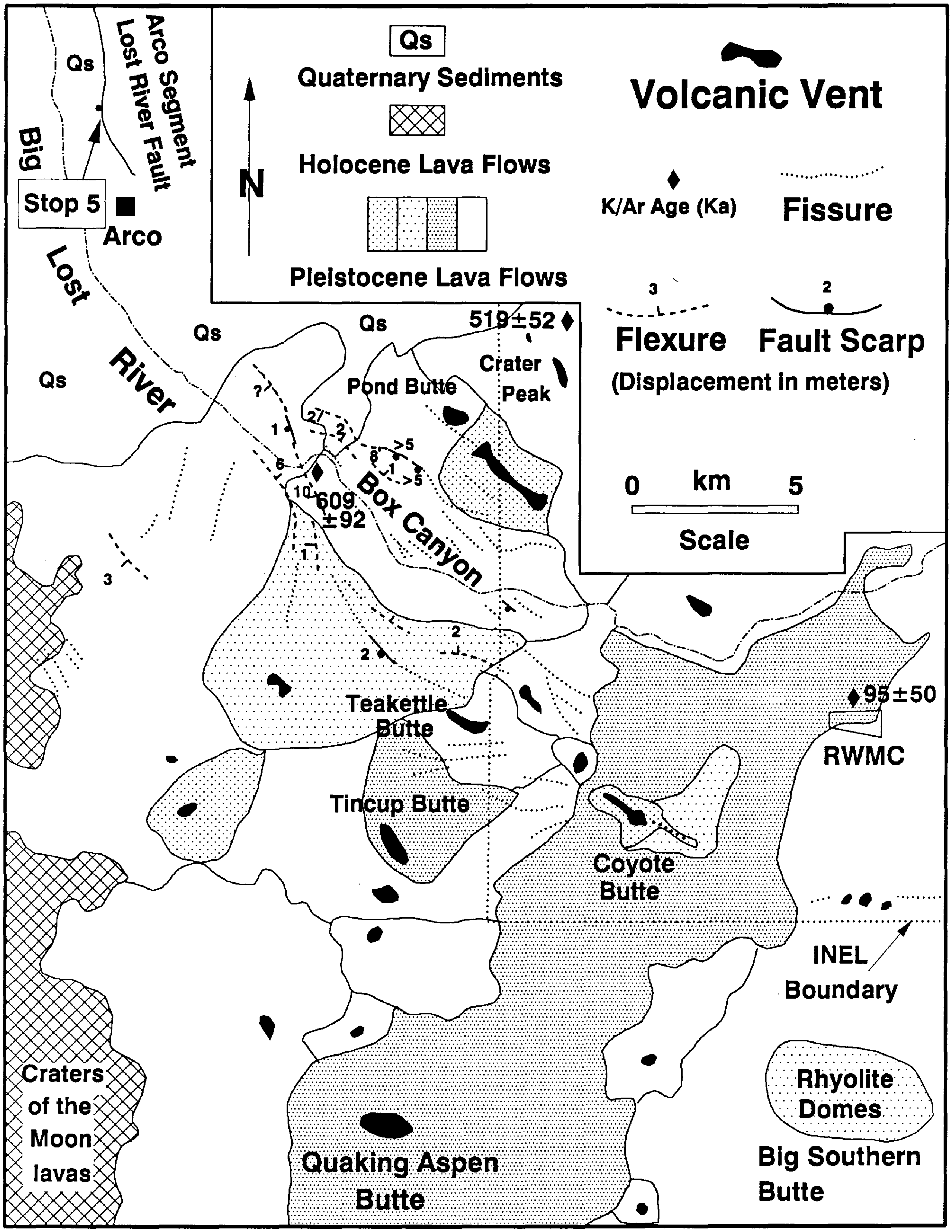

Figure 13. Generalized geologic map of the Arco rift zone (Smith and others, 1989; Kuntz and others, 1990).

and volcanism of the Arco rift zone is older than about 100 ka because a lava flow from Quaking Aspen Butte has been dated at 95 ± 50 ka, and that flow covers older lavas and fissures of the southern Arco rift zone.

In contrast to the monogenetic Hell's Half-Acre lava field, the more-complex Arco rift zone is almost certainly a polygenetic feature, as shown by the presence of multiple eruptive fissures, and several discrete groups of ground-deformation features. The fissures, monoclines and faults that we infer to have accompanied basaltic volcanism and dike intrusion are probably also polygenetic, and the large (up to 10 m) cumulative vertical displacement along one fault (Figs. 13 and 14) suggests multiple-uplift events. Geomorphic evidence supports our assertion that multiple uplifts account for the 10-meter displacement along the eastern border of the graben: the Big Lost River has incised the 15-meter-deep Box Canyon into basalt-lava flows to the east of the graben. Incision of the river apparently kept pace with multiple, meter-scale vertical displacements. Conversely, it is difficult to envision that the river could incise Box Canyon after a single, 10-meter-displacement event, and would likely have been displaced southward rather than occupying its present eastward course through Box Canyon.

Late Pinedale glacial-outburst flooding: Climatic fluctuations associated with Pleistocene glacial and interglacial episodes induced catastrophic flooding of the Big Lost River through Box Canyon (Rathburn, 1988). This large, rare event and subsequent streamflow left distinctive, mappable fluvial deposits along the length of the river. Erosional features associated with the catastrophic flooding include arcuate basalt cataracts, smoothed and scoured basalt outcrops, and a loess scarp (Rathburn, 1991). Boulder bars, and erratics of intrusive and metamorphic rocks derived from the Pioneer Mountains are the primary depositional features of the flooding. A peak discharge of 2 to 4 million cfs is estimated for the event (Rathburn, 1991), which occurred 19.8 ± 1.4 ka, based on cosmogenic ^{3}He and ^{21}Ne measured from exposed surfaces of large flood-transported boulders (Cerling and others, 1991).

Stop 5. Trench site, Arco segment of the Lost River fault

Three, segmented normal faults occur to the north and west of the INEL, in the northern Basin and Range province (Fig. 1). All are of concern in seismic-safety issues at the INEL, because of their proximity to the site, and evidence for Quaternary paleoseismicity. Quaternary faulting and scarp-degradation studies in the southern Lost River Valley are discussed by Pierce (1988), from which the following summary is adapted. Along the estern side of the southern Lost River Range near the town of Arco, the scarp of the Lost River fault is about 16 to 23 meters high, and is formed in older Quaternary alluvial-fan gravels. Pierce (1985; 1988) uses geologic relations such as carbonate-coat thicknesses on alluvial-fan clasts, and U-Th disequilibrium dating to infer the history of faulting near a deep trench that was first excavated and described by Malde (1971). The total vertical displacement of units exposed in the trench is estimated at about 20 meters, and two wedges of fault-derived colluvium are exposed in the bottom of the trench. The colluvial units are overlain by loess containing volcanic ash dated at 76 ± 34 ka (N.D. Naeser, pers. comm., in Pierce, 1988), and the oldest exposed alluvial-fan deposit (160 ± 30 ka; Pierce, 1988) had been offset 4 to 7 meters by the time the ash was deposited. The youngest surface faulting along the Arco

Figure 14. North-looking, oblique-aerial photograph of the 0.3-km-wide graben in the northern part of the Arco rift zone. The Big Lost River flows from left to right, and Box Canyon is incised to the right (east) of the graben. Cumulative vertical displacement along the east side of the graben where it is intersected by the river is about 10 meters. We consider the graben, together with associated tensional fissures and monoclines, to have been produced by dike intrusion. The southern end of the Lost River Range is in the upper left, and the Arco Hills are in the upper right.

segment is estimated to have occurred about 30 ka. This contrasts with more northern segments of the Lost River fault, which show evidence of Holocene, and in places historical, offset: the 1983 Borah Peak earthquake and its associated scarp occurred on the Lost River fault, about 30 miles north of Arco (Crone, 1988).

Stop 6. Nontectonic scarp along the northern margin of the Eastern Snake River Plain

The abrupt geographic transition from the northern Basin and Range tectonic province to the ESRP volcanic province, together with the comparatively low-lying terrain of the ESRP suggests that major northeast-trending, southeast-downthrown faults may be present along the northern margin of the ESRP, although no evidence for such features has yet been found (Rodgers and others, 1990). The identification of any such northeast-trending faults — especially those showing evidence for Quaternary displacement — would be important in seismic-hazard evaluation at the INEL. A subdued, northeast-trending scarp on the northern margin of the ESRP near the Arco Hills was previously mapped as a fault scarp (Scott, 1982) and was excavated in order to determine whether the feature is tectonic in origin (Breckenridge and Othberg, 1991). The now-backfilled, 3-by-40-meter trench excavation is located north of highway 33, within the INEL boundary and near the center of the north edge of section 25, T4N, R23E. Loess and alluvial-fan gravel deposits exposed in the trench walls are not offset, and the feature is therefore of nontectonic origin. The late Pleistocene loess deposit overlying alluvial-fan deposits thins across the topographic scarp, and the scarp is therefore of erosional origin, involving partial removal of the loess cover on the downhill (southeast) side. The explanation we favor is that the scarp is the result of differential erosion across a fire scar, and is similar in origin to other subdued, northeast-trending features on the ESRP. Fire scars have abrupt linear edges, and destruction of vegetation on the burnt area commonly leads to eolian stripping of loess. In places, fire scars are apparently further modified by redeposition of stripped loess within the unburned sagebrush along the edge of the fire scar, forming a subdued linear mound or scarp.

Stop 7. Howe Point, southern tip of the Lemhi Range

Features to be observed and discussed at Howe Point include Neogene rhyolitic volcanics, lake-margin sediments of pluvial Lake Terreton, and the structural geology of the southern Lemhi Range. On the west side of the southern Lemhi Range, the Lemhi fault terminates in a number of splays, displacing Paleozoic carbonate rocks and Neogene volcanic tuffs, but apparently not unconsolidated eolian deposits of late Pleistocene or Holocene age (Ron Bruhn, written commun., 1991).

Figure 15 shows the stratigraphy of Neogene rhyolitic tuffs exposed at Howe Point, an important locality for

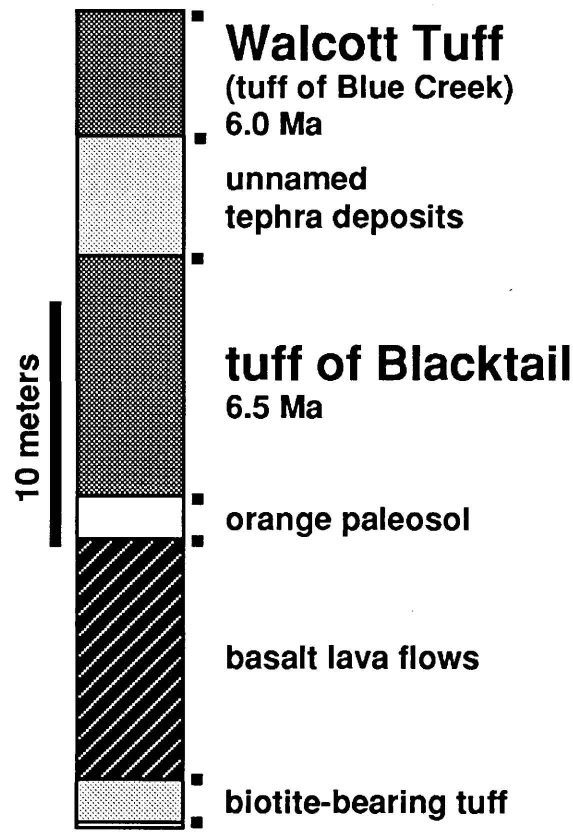

Figure 15. Simplified, composite-stratigraphic section of volcanic rocks exposed at Howe Point, Stop 7 (adapted from Hackett and Morgan, 1988).

reconstructing the nature of silicic volcanism and caldera collapse of the Heise volcanic field (Morgan, 1988). On the north side of highway 33, the 6.0-Ma tuff of Blue Creek (Walcott Tuff), one of three voluminous and regionally distributed Heise ignimbrite sheets, forms the top of the section. The tuff of Blue Creek (Walcott Tuff) at this locality is a near-vent ignimbrite, judging from its large and abundant phenocrysts and lithic-rock fragments, together with an underlying meter-thick, welded, pumice-rich, plinian-fall deposit. In addition, zones of brecciation, marked by angular tuff clasts within a white, vapor-phase-altered matrix of the same tuff, occur along faults that are interpreted as caldera ring fractures (Morgan, 1988). Below the tuff of Blue Creek (Walcott Tuff) and associated ash deposits is the 6.5-Ma tuff of Blacktail, which also has lithologic features suggesting near-source deposition.

The Lost River Sinks occur south of highway 33 within a subdued topographic basin. The basin is developed between alluvial valleys and bedrock ranges to the north, and the axial volcanic zone of the ESRP. The Sinks currently receive ephemeral water and alluvial sediment from the Big and Little Lost Rivers, but in late Pleistocene time an area approximately within the 4800-foot topographic contour was occupied by pluvial Lake Terreton, whose modern remnant is Mud Lake. As mapped by Scott (1982), the deposits of Lake Terreton cover about 600 square miles, but are concealed in places by stabilized linear dunes (see Stop 8). Near Howe Point, weakly bedded, fine lacustrine sands containing gastropod-shell fragments are exposed along curved erosional scarps, marking a former Lake Terreton shoreline.

Stop 8. Holocene/late Pleistocene longitudinal dunes, southwest of Mud Lake

Eolian sand occurs on the ESRP as stabilized dunes, and in places as active dunes (Scott, 1982; Baker and others, 1987; Malde, 1991). One area of stabilized linear dunes forms a broad band 15 km wide, stretching about 80 km northeastward from the Lost River Sinks along the margin of the ESRP. The area is marked by long, straight parallel ridges about 1 to 7 m high, 20 to 60 m wide, and tens of km long. The longitudinal dunes overlie deposits of Lake Terreton and their distribution suggests that the dunes were derived from those lacustrine deposits. Hence, the dunes are of late Pleistocene to Holocene age.

Stop 9. Rhyolitic tuffs at the Blacktail Recreation Area

About 12 miles east of Idaho Falls, several localities at the Blacktail Recreation area on Ririe Reservoir contain excellent exposures of Neogene rhyolitic tuffs. The locality is important in reconstructing the nature and regional distribution of tuffs from the Heise volcanic field. In addition, the Blacktail area contains outstanding exposures of all three genetic categories of pyroclastic deposit: fall, flow and surge. The following discussion is adapted from Hackett and Morgan (1988). Fig. 16 shows the volcanic stratigraphy.

The localities are near the inferred structural margin of the Blacktail caldera, source of the 6.5-Ma tuff of Blacktail. The basal unit is the tuff of Blacktail. North of the boat ramp, it exceeds 150 m in thickness, is crystal-rich, and contains tight flowage folds; this thick tuff represents the ponded intracaldera facies. At the boat ramp near reservoir level, the tuff thins into an undeformed outflow sheet with a basal, spherulitic vitrophyre; a massive, devitrified, densely welded interior; an upper vapor-phase zone; and a several-meter-thick cap of black vitrophyre. The tuff of Wolverine Creek is a local, obsidian-rich, nonwelded ignimbrite containing fluid-escape pipes, capped by ash-cloud (?) surge deposits. Overlying the tuff of Wolverine Creek are unnamed, planar-bedded lapilli tuffs of probable plinian-fall origin. The uppermost rhyolitic deposits are the 2.0-Ma Huckleberry Ridge Tuff, from the Yellowstone Plateau volcanic field. In places, Quaternary basalt lava flows unconformably overlie the rhyolitic tuffs.

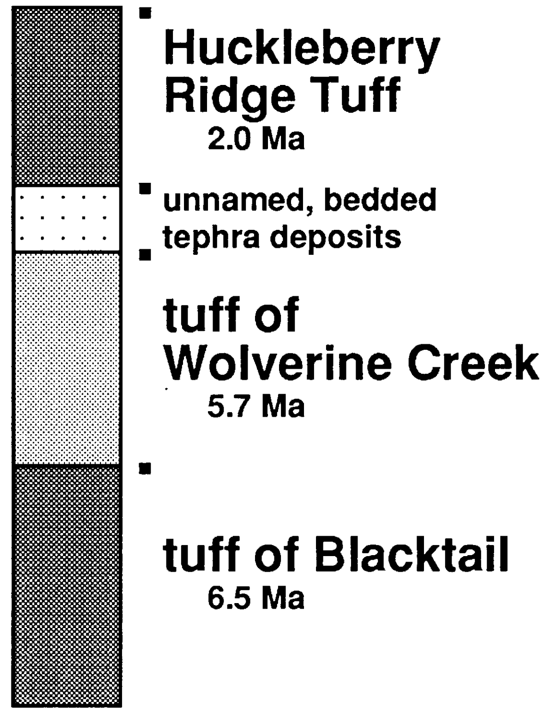

Figure 16. Generalized stratigraphy of Quaternary and Neogene rhyolitic tuffs exposed at the Blacktail Recreation area along the southern margin of the ESRP, Stop 9 (data from Morgan, 1988; Hackett and Morgan, 1988). The total section is about 300 m thick; relative thickness of the tuffs is not drawn to scale.

ACKNOWLEDGMENTS

In compiling this overview, we have drawn heavily from the data and constructive criticism of colleagues who have worked with us on the Eastern Snake River Plain. We thank Steve Anderson, Mel Kuntz, Lisa Morgan and Ken Pierce of the U.S.G.S.; Mark Hemphill-Haley, Tom Sawyer and Ivan Wong of Woodward-Clyde Consultants; Kevin Coppersmith of Geomatrix Consultants; Randy Kath, Ken Moser, Don West, and Ric Zepeda of Golder Associates; Steve Forman of Ohio State University; Dave Rodgers of Idaho State University; Peter Knuepfer of SUNY Buffalo; George Thompson of Stanford University; Ron Bruhn of the University of Utah; and Jim Wilson, the patient editor of this volume. Stan Mertzman of Franklin & Marshall College supplied the geochemical data presented here. We thank Mark Fishel, Karl Hayden and Mike McCurry of Idaho State University for information on Big Southern and Cedar buttes, and for logistical assistance. Carroll Knutson reviewed the manuscript. In spite of all this help, any errors or blunders are our own responsibility.

Work performed under the auspices of the U.S. Department of Energy, DOE Idaho Field Office Contract DE-AC07-761D01570.

REFERENCES CITED

Alt, David, and Hyndman, D.W., 1989, Roadside geology of Idaho: Mountain Press Publishing Company, Missoula, Montana, 393 p.

Anders, M.H., Geissman, J.W., Piety, L.A., and Sullivan, J.T., 1989, Parabolic distribution of circum-eastern Snake River Plain seismicity and latest Quaternary faulting: Migratory pattern and association with the Yellowstone hotspot: Journal of Geophysical Research, v. 94, p. 1589-1621.

Anderson, S.R., 1991, Stratigraphy of the unsaturated zone and uppermost part of the Snake River Plain aquifer at the Idaho Chemical Processing Plant and Test Reactors Area, Idaho National Engineering Laboratory, Idaho: U.S. Geological Survey Water-Resources Investigations Report 91-4010, 71 p.

Anderson, S.R., and Lewis, B.D., 1989, Stratigraphy of the unsaturated zone at the Radioactive Waste Management Complex, Idaho National Engineering Laboratory, Idaho: U.S. Geological Survey Water-Resources Investigations Report 89-4065, 54 p.

Armstrong, R. L., Leeman, W. P., and Malde, H. E., 1975, K-Ar dating, Quaternary and Neogene rocks of the Snake River Plain, Idaho: American Journal of Science, v. 275, p. 225-251.

Baker, V.R., Greeley, Ronald, Komar, P.D., Swanson, D.W., and Waitt, R.B., 1987, Columbia and Snake River Plains, *in* Graf, W.L., editor, Geomorphic systems of North America: Boulder, Colorado, Geological Society of America, Centennial Special Volume 2, p. 403-468.

Blackwell, D.D., 1989, Regional implications of heat flow of the Snake River Plain, northwestern United States: Tectonophysics, v. 164, p. 323-343.

Bonnichsen, Bill, Christiansen, R.L., Morgan, L.A., Moye, F.J., Hackett, W.R., Leeman, W.P., Honjo, Norio, Jenks, M.D., and Godchaux, M.M., 1989, Excurion 4A: Silicic volcanic rocks in the Snake River Plain-Yellowstone Plateau province: New Mexico Bureau of Mines and Mineral Resources Memoir 47, p. 135-182.

Breckenridge, R.M., and Othberg, K.L., 1991, Geologic interpretation of a trench near the Arco Hills on the northwest margin of the Eastern Snake River Plain, Idaho (abst.): Geological Society of America Abstracts with Programs, v. 23, no. 4, p. 7.

Cerling, T.E., Craig, H., Poreda, R., and Rathburn, S.L., 1991, Dating catastrophic-flood events using cosmogenic ^{3}He and ^{21}Ne: Geological Society of America Abstracts with Programs, v. 23, no. 5, p. A98.

Champion, D.E., Lanphere, M.A., and Kuntz, M.A., 1988, Evidence for a new geomagnetic reversal from lava flows in Idaho: Discussion of short polarity reversals in the Brunhes and late Matuyama polarity chrons: Journal of Geophysical Research, v. 93, p. 11,667-11,680.

Christiansen, R. L., 1982, Late Cenozoic volcanism of the Island Park area, eastern Idaho, *in* Bill Bonnichsen and R. M. Breckenridge, editors, Cenozoic geology of Idaho: Idaho Bureau of Mines and Geology Bulletin 26, p. 345-368.

Christiansen, R. L., 1984, Yellowstone magmatic evolution: its bearing on understanding large-volume explosive volcanism, in Explosive volcanism: inception, evolution, and hazards: National Academy Press, Washington, D.C., p. 84-95.

Crone, A.J., 1988, Field guides to the Quaternary geology of central Idaho: Part D., Surface faulting and groundwater eruptions associated with the 1983 Borah Peak earthquake, *in* Link, P. K., and Hackett, W. R., editors, Guidebook to the geology of central and southern Idaho: Idaho Geological Survey Bulletin 27, p. 227-232.

Crone, A.J., Machette, M.N., Bonilla, M.G., Lienkaemper, J.J., Pierce, K.L., Scott, W.E., and Bucknam, R.C., 1987, Surface faulting accompanying the Borah Peak earthquake and segmentation of the Lost River fault, central Idaho: Bulletin of the Seismological Society of America, v. 77, p. 739-770.

Crone, A.J., and Haller, K.M., 1991, Segmentation and the coseismic bahavior of basin-and-range normal faults; examples from east-central Idaho and southwestern Montana, U.S.A., Journal of Structural Geology, v. 13, p. 151-164.

Doherty, D.J., 1979a, Drilling data from exploration well 1, NE ¼, sec. 22, T.2N., R. 32E., Bingham County, Idaho: U.S. Geological Survey Open-file Report 79-1225, 1 p.

Doherty, D.J., 1979b, Drilling data from exploration well 2-2A, NW ¼, sec. 15, T. 5 N., R. 31 E., Idaho National Engineering Laboratory, Butte County, Idaho: U.S. Geological Survey Open-file Report 79-851, 1 p.

Doherty, D. J., McBroome, L. A., and Kuntz, M. A., 1979, Preliminary geologic interpretation and lithologic log of the exploratory test well (INEL-1), Idaho National Engineering Laboratory, eastern Snake River Plain, Idaho: U. S. Geological Survey Open-File Report 79-1248, 10 p.

Fishel, M.L., 1992, Geology and petrology of uplifted mafic lavas on the north flank of Big Southern Butte, Eastern Snake River Plain, Idaho: Masters thesis, Idaho State University, Pocatello, Idaho.

Greeley, Ronald, 1982, The style of basaltic volcanism in the eastern Snake River Plain, Idaho, *in* Bonnichsen, Bill, and Breckenridge, R.M., editors, Cenozoic geology of Idaho: Idaho Bureau of Mines and Geology Bulletin 26, p. 407-422.

Hackett, W.R., Smith, R.P., and Josten, N.E., 1991, Interaction of Quaternary volcanic and tectonic processes, eastern Snake River Plain, Idaho: Geological Society of America Abstracts with Programs, v. 23, no. 2, p. 32.

Hackett, W.R., and Morgan, L.A., 1988, Explosive basaltic and rhyolitic volcanism of the eastern Snake River Plain, Idaho, *in* Link, P. K., and Hackett, W. R., editors, Guidebook to the geology of central and southern Idaho: Idaho Geological Survey Bulletin 27, p. 283-301.

Hayden, K.P., 1992, Geology and petrology of the Cedar Butte eruptive center, Eastern Snake River Plain, Idaho: Masters thesis, Idaho State University, Pocatello, Idaho.

Hemphill-Haley, M.A., Sawyer, T.L., Wong, I.G., Knuepfer, P.L.K., Forman, S.L., and Smith, R.P., 1991, Quaternary faulting along the southern Lemhi fault near the Idaho National Engineering Laboratory, southeastern Idaho: Proceedings, Third DOE Natural Hazards Phenomena Mitigation Conference.

Hildreth, Wes, Halliday, A.N., and Christiansen, R.L., 1991, Isotopic and chemical evidence concerning the genesis and contamination of basaltic and rhyolitic magma beneath the Yellowstone Plateau volcanic field: Journal of Petrology, v. 32, p. 63-138.

Howard, K. A., Shervais, J. W., and McKee, E. H., 1982, Canyon-filling lavas and lava dams on the Boise River, Idaho, and their significance for evaluating downcutting during the last two million years, *in* Bonnichsen, Bill, and Breckenridge, R. M., editors, Cenozoic geology of Idaho: Idaho Bureau of Mines and Geology Bulletin 26, p. 629-641.

Iyer, H.M., Evans, J.R., Zandt, G., Stewart, R.M., Coakley, J.M., and Roloff, J.N., 1981, A deep low-velocity body under the Yellowstone caldera, Wyoming: Delineation using teleseismic p-wave residuals and tectonic interpretation: Geological Society of America Bulletin, v. 92, Part II, p. 1471-1476.

Kuntz, M.A., 1978a, Geology of the Arco-Big Southern Butte area, eastern Snake River Plain, and potential volcanic hazards to the Radioactive Waste Management Complex and other waste storage and reactor facilities at the Idaho National Engineering Laboratory, Idaho: U. S. Geological Survey Open-File Report 78-691, 70 p.

Kuntz, M.A., 1978b, Geologic map of the Arco-Big Southern Butte area, Butte, Blaine and Bingham counties, Idaho: U. S. Geological Survey Open-File Report 78-302, 1:48,000 scale.

Kuntz, M.A., in press, A model-based perspective of basaltic volcanism, eastern Snake River Plain, Idaho, *in* Link, P.K., Kuntz, M.A., and Platt, L.W., Regional geology of eastern Idaho and western Wyoming: Geological Society of America Memoir.

Kuntz, M.A., Champion, D.E., Lefebvre, R.H., and Covington, H.R., 1988, Geologic map of the Craters of the Moon, Kings Bowl, and Wapi lava fields, and the Great Rift volcanic rift zone, south-central Idaho: U. S. Geological Survey Miscellaneous Investigations Series Map I-1632, 1:100,000 scale.

Kuntz, M.A., Covington, H.R., and Schorr, L.J., in press, An overview of basaltic volcanism of the eastern Snake River Plain, Idaho, with emphasis on latest Pleistocene and Holocene lava fields, volcanic rift zones, and interrelated Neogene and Quaternary volcano-tectonic structures, *in* Link, P.K., Kuntz, M.A., and Platt, L.W., Regional geology of eastern Idaho and western Wyoming: Geological Society of America Memoir 179.

Kuntz, M.A., and Dalrymple, G.B., 1979, Geology, geochronology and potential volcanic hazards in the Lava Ridge-Hell's Half Acre area, eastern Snake River Plain, Idaho: U. S. Geological Survey Open-File Report 79-1657, 65 p.

Kuntz, M. A., Dalrymple, G.B., Champion, D.E., and Doherty, D.J., 1980, Petrography, age and paleomagnetism of volcanic rocks at the Radioactive Waste Management Complex, Idaho National Engineering Laboratory, Idaho, with an evaluation of volcanic hazards: U.S. Geological Survey Open-File Report 80-388, 63 p.

Kuntz, M.A., Scott, W.E., Skipp, Betty, Hait, M.H., Embree, G.F., Hoggan, R.D., and Williams, E. J., 1979, Geologic map of the Lava Ridge-Hell's Half Acre area, eastern Snake River Plain, Idaho: U. S. Geological Survey Open-File Report 79-1657, 1:48,000 scale.

Kuntz, M.A., Skipp, B., Lanphere, M.A., Scott, W.E., Pierce, K.L., Dalrymple, G.B., Morgan, L.A., Champion, D.E., Embree, G.F., Smith, R.P., Hackett, W.R., and Rodgers, D.W., 1990, Revised geologic map of the Idaho National Engineering Laboratory and adjoining areas, eastern Idaho: U.S. Geological Survey Open-File Report 90-333, 37 p. with 1:100,000-scale map.

Kuntz, M. A., Spiker, E.C., Rubin, Meyer, Champion, D.E., and Lefebvre, R.H., 1986, Radiocarbon studies of latest Pleistocene and Holocene lava flows of the Snake River Plain, Idaho: data, lessons, interpretations: Quaternary Research, v. 25, p. 163-176.

LeBas, M.J., LeMaitre, R.W., Streckeisen, A., and Zanettin, B., 1986, A chemical classification of volcanic rocks based on the total alkali-silica diagram: Journal of Petrology, v. 27, p. 745-750.

Lewis, G.C., and Fosberg, M.A., 1982, Distribution and character of loess and loess soils in southeastern Idaho, *in* Bonnichsen, Bill, and Breckenridge, R. M., editors, Cenozoic geology of Idaho: Idaho Bureau of Mines and Geology Bulletin 26, p. 705-716.

Link, P.K., and Hackett, W.R. (editors), 1988, Guidebook to the geology of central and southern Idaho: Idaho Geological Survey Bulletin 27, 319 p.

Mastin, L.G., and Pollard, D.D., 1988, Surface deformation and shallow dike intrusion processes at Inyo Craters, California: Journal of Geophysical Research, v. 93, p. 13221-13235.

Malde, H.E., 1968, The catastrophic late Pleistocene Bonneville flood in the Snake River Plain, Idaho: U.S. Geological Survey Professional Paper 596, 52 p.

Malde, H.E., 1971, Geologic investigations of faulting near the National Reactor Testing Station, Idaho, with a section on microearthquake studies by A.M. Pitt and J.P. Eaton: U.S. Geological Survey Open-File Report 71-338, 167 p.

Malde, H. E., 1982, The Yahoo Clay, a lacustrine unit impounded by the McKinney Basalt in the Snake River canyon near Bliss, Idaho, *in* Bonnichsen, Bill, and Breckenridge, R. M., editors, Cenozoic geology of Idaho: Idaho Bureau of Mines and Geology Bulletin 26, p. 617-628.

Malde, H.E., 1987, Quaternary faulting near Arco and Howe, Idaho: Bulletin of the Seismological Society of America, v. 77, p. 847-867.

Malde, H.E., 1991, Quaternary geology and structural history of the Snake River Plain, Idaho and Oregon, *in* Morrison, R.B., editor, Quaternary nonglacial geology; Conterminous United States: Boulder, Colorado, Geological Society of America, The Geology of North America, v. K-2, p. 251-281.

Morgan, L. A., 1988, Explosive rhyolitic volcanism on the eastern Snake River Plain, Idaho: Ph.D. dissertation, University of Hawaii, Manoa.

Morgan, L. A., Doherty, D. J., and Leeman, W. P., 1984, Ignimbrites of the eastern Snake River Plain: evidence for major caldera-forming eruptions: Journal of Geophysical Research, v. 89, p. 8665-8678.

Parsons, Tom, and Thompson, G.A., 1991, The role of magma overpressure in suppressing earthquakes and topography: worldwide examples: Science, v. 253, p. 1399-1402.

Pierce, K.L., 1985, Quaternary history of faulting on the Arco segment of the Lost River fault, central Idaho, *in* Stein, R.S. and Bucknam, R.C., editors, Proceedings of Conference XXVIII — the Borah Peak, Idaho earthquake: U.S. Geological Survey Open-File Report 85-290.

Pierce, K.L., 1988, Field guides to the Quaternary geology of central Idaho, Part E. History of Quaternary faulting and scarp-degradation studies, southern Lost River Valley, *in* Link, P. K., and Hackett, W. R., editors, Guidebook to the geology of central and southern Idaho: Idaho Geological Survey Bulletin 27, p. 233-240.

Pierce, K. L., and Scott, W. E., 1982, Pleistocene episodes of alluvial-gravel deposition, southeastern Idaho, *in* Bonnichsen, Bill, and Breckenridge, R. M., editors, Cenozoic geology of Idaho: Idaho Bureau of Mines and Geology Bulletin 26, p. 685-702.

Pierce, K.L., Fosberg, M.A., Scott, W.E., Lewis, G.C., and Colman, S.M., 1982, Loess deposits of southeastern Idaho: age and correlation of the upper two loess units, *in* Bonnichsen, Bill, and Breckenridge, R. M., editors, Cenozoic geology of Idaho: Idaho Bureau of Mines and Geology Bulletin 26, p. 717-725.

Pierce, K.L., and Morgan, L.A., 1990, The track of the Yellowstone hotspot: volcanism, faulting and uplift: U.S. Geological Survey Open-File Report 90-415, 68 p.

Pierce, K.L., and Morgan, L.A., in press, The track of the Yellowstone hotspot: volcanism, faulting and uplift, *in* Link, P.K., Kuntz, M.A., and Platt, L.W., Regional geology of eastern Idaho and western Wyoming: Geological Society of America Memoir 179.

Rathburn, S.L., 1988, Glacial-lake outburst flooding along the Big Lost River, central Idaho: Geological Society of America Abstracts with Programs, v. 20, no. 4, p. 283.

Rathburn, S.L., 1991, Quaternary channel changes and paleoflooding along the Big Lost River, Idaho National Engineering Laboratory: EG&G Informal Report WM-9909, 33 p.

Rodgers, D.W., Hackett, W.R., and Ore, H.T., 1990, Extension of the Yellowstone plateau, eastern Snake River Plain, and Owyhee plateau: Geology, v. 18, p. 1138-1141.

Rubin, A.M., and Pollard, D.D., 1988, Dike-induced faulting in rift zones in Iceland and Afar: Geology, v. 16, p. 413-417.

Ruebelmann, K.L., 1989, editor, Field-Trip Guidebook T-305: Snake River Plain-Yellowstone volcanic province: Washington, D.C., American Geophysical Union, 103 p.

Scott, W.E., 1982, Surficial geologic map of the eastern Snake River Plain and adjacent areas, 111 to 115 degrees W., Idaho and Wyoming: U.S. Geological Survey Miscellaneous Investigations Series Map I-1372, 2 sheets, 1:250,000.

Scott, W.E., Pierce, K.L., Bradbury, J.P., and Forester, R.M., 1982, Revised Quaternary stratigraphy and chronology in the American Falls area, southeastern Idaho, *in* Bonnichsen, Bill, and Breckenridge, R. M., editors, Cenozoic geology of Idaho: Idaho Bureau of Mines and Geology Bulletin 26, p. 581-596.

Smith, R.P., Hackett, W.R., and Rodgers, D.W., 1989, Geologic aspects of seismic-hazards assessment at the Idaho National Engineering Laboratory, southeastern Idaho: Proceedings, Second DOE Natural Phenomena Hazards Mitigation Conference, p. 282-289.

Sparlin, M.A., Braile, L.W., and Smith, R.B., 1982, Crustal structure of the eastern Snake River Plain determined from ray-trace modelling: Journal of Geophysical Research, v. 87, p. 2619-2633.

Spear, D.B., 1979, The geology and volcanic history of the Big Southern Butte-East Butte area, eastern Snake River Plain, Idaho: Ph.D. dissertation, State University of New York at Buffalo , 136 p.

Spear, D. B. and King, J. S., 1982, The geology of Big Southern Butte, Idaho, *in* Bonnichsen, Bill, and Breckenridge, R. M., editors, Cenozoic geology of Idaho: Idaho Bureau of Mines and Geology Bulletin 26, p. 395-403.

Thompson, G.A, Parsons, Tom, and Smith, R.P., 1990, Examples of magma overpressure suppressing normal faulting and inhibiting seismicity: Snake River Plain, Idaho; Yucca Mountain, Nevada; and Mono Craters, California (abstract): EOS, Transactions American Geophysical Union, v. 71, no. 43, p. 1622.

Zietz, I., Gilbert, F.P., and Kirby, J.R., 1978, Aeromagnetic map of Idaho: U.S. Geological Survey Geophysical Investigations Map GP-920, 1:1 million scale.

STRUCTURE AND FABRIC OF METAMORPHIC TERRAINS IN THE NORTHEASTERN GREAT BASIN: IMPLICATIONS FOR MESOZOIC CRUSTAL SHORTENING AND EXTENSION

Phyllis A. Camilleri, Department of Geology and Geophysics, University of Wyoming, Laramie, WY 82071-3006
David M. Miller, U.S. Geological Survey, 345 Middlefield Road, Menlo Park, CA 94025
Arthur W. Snoke, Department of Geology and Geophysics, University of Wyoming, Laramie, WY 82071-3006
Michael L. Wells, U.S. Geological Survey, 345 Middlefield Road, Menlo Park, CA 94025

INTRODUCTION

Complex deformational and metamorphic histories were suggested for the metamorphic terrains exposed in the northeastern Great Basin in several early studies (e.g., Misch, 1960; Misch and Hazzard, 1962; Armstrong and Hansen, 1966; Thorman, 1970). These workers ascribed all deformation and metamorphism to shortening in the hinterland of the late Mesozoic to early Tertiary Sevier fold and thrust belt. Subsequent studies have indicated that some of the deformation and metamorphism postdated the development of the Sevier belt and was most likely related to crustal extension (Armstrong, 1972; Compton et al.,1977; Snoke, 1980; Snoke and Miller, 1988). More recently, some investigators have argued that much of the contractile deformation and metamorphism is Late Jurassic in age (Allmendinger et al., 1984; Glick, 1987; Miller et al., 1987; Snoke and Miller, 1988; Hudec, 1990) predating the development of imbricate foreland thrusts of the Sevier belt. Other workers have favored chiefly a Cretaceous history for much of the deep-seated deformation of the hinterland (Miller and Gans, 1989). Local Jurassic and Cretaceous structures and fabrics that are extensional in origin have also been recognized and, although poorly understood in places, are inferred to be a by-product of crustal contraction or magmatism (Allmendinger and Jordan, 1984; Snoke and Miller, 1988; Wells and Allmendinger, 1990; Wells, et al., 1990; Miller and Allmendinger, 1991; Camilleri, this volume; Miller and Hoisch, this volume). In this paper we bring together new structural, metamorphic, and geothermobarometric data from the Raft River Mountains, Pilot Range, Toano Range, Pequop Mountains, Wood Hills, and northern East Humboldt Range to present a more detailed picture of the structural and tectonic complexities in the "hinterland" of the northeastern Great Basin. Unless otherwise cited, this paper draws heavily from data and ideas presented in accompanying papers in this volume by Wells (eastern Raft River Mountains), Snoke (Clover Hill and northeastern East Humboldt Range), Miller and Hoisch (Pilot Range and Toano Range), and Camilleri (Wood Hills and Pequop Mountains.

The field trip transects much of northwestern Utah and northeastern Nevada (Figs 1 and 2), passing through several Mesozoic metamorphic terrains, which roughly parallel a fundamental bend in the North American Precambrian and Paleozoic continental shelf margin (Fig. 3). Along the bend, Paleozoic lithofacies belts trend east-west (Miller et al., 1991; P. A. Camilleri [unpublished data]). Miller et al. (1991) suggested that Paleozoic depositional patterns in this region were influenced by Proterozoic structural discontinuities, such as the approximately east-striking structural zone that separates the Archean Wyoming Province rocks from accreted Proterozoic rocks. Mesozoic contractile structures also change orientation from dominantly E-directed where the margin trends north to dominantly SE-directed along the bend (Figs. 1 and 3). We suggest that along the bend in the continental shelf margin, Proterozoic to Paleozoic inhomogeneities (structural or perhaps lithologic) influenced the localization and kinematics of Mesozoic contractile structures and that these structures influenced the kinematics of subsequent major middle Tertiary (middle Eocene to Miocene) extensional structures. We also document Mesozoic extensional features that are probably synchronous with shortening, and we suggest that some of these extensional features may facilitate moderation of topography during crustal shortening.

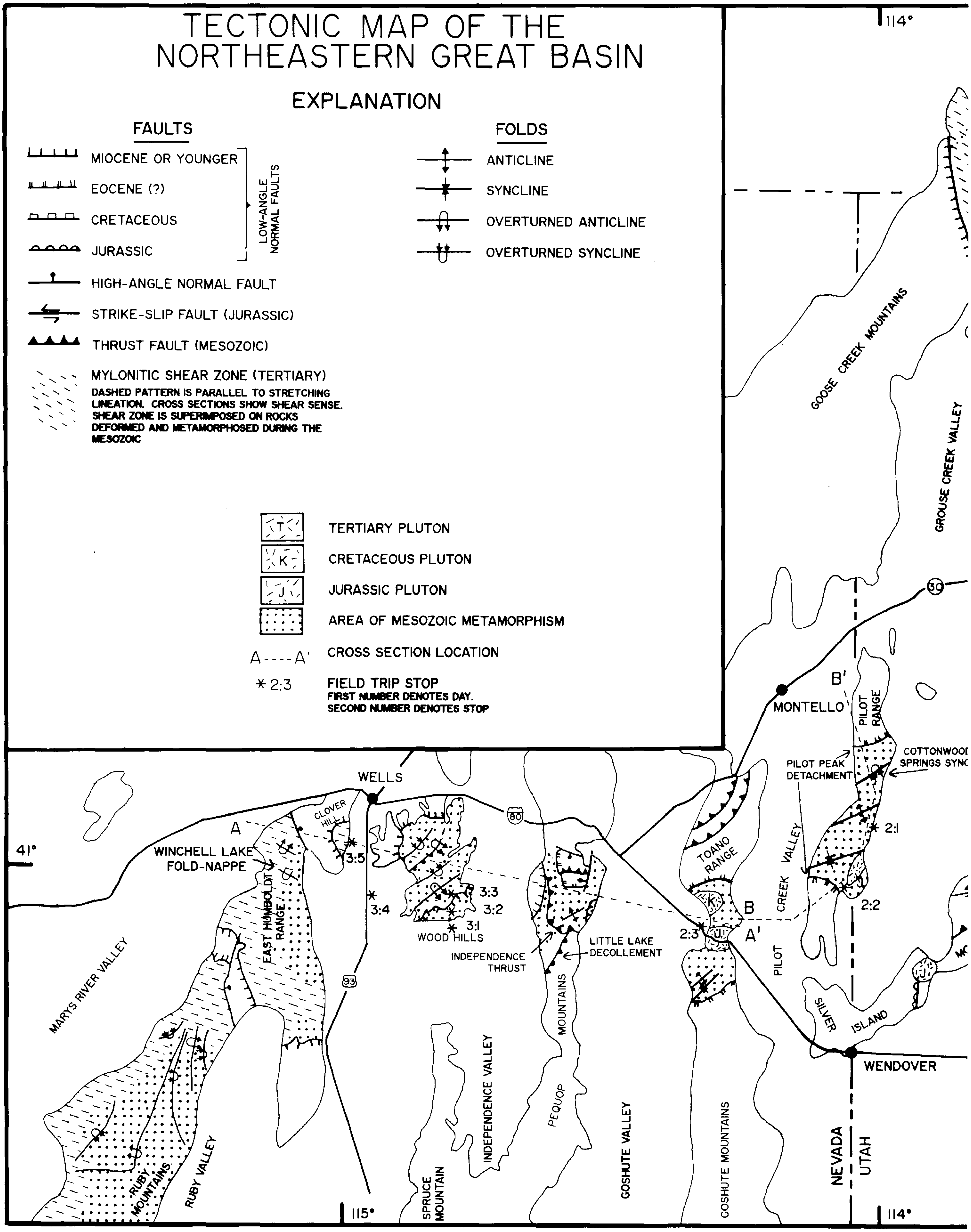

Figure 1. Tectonic map of the northeastern Great Basin. Data used in compilation of this map are from Doelling (1980), Smith (1982), Wells and Allmendinger (1990), M. L. Wells (unpublished mapping), V. R. Todd (unpublished mapping), Jordan (1983), Saltzer and Hodges (1988), Malavielle (1987), Camilleri (this volume), P. A. Camilleri (unpublished mapping), Glick (1987), Allmendinger and Jordan (1984) Miller et al., (1987), D. M. Miller (unpublished mapping), and Snoke and Lush (1984).

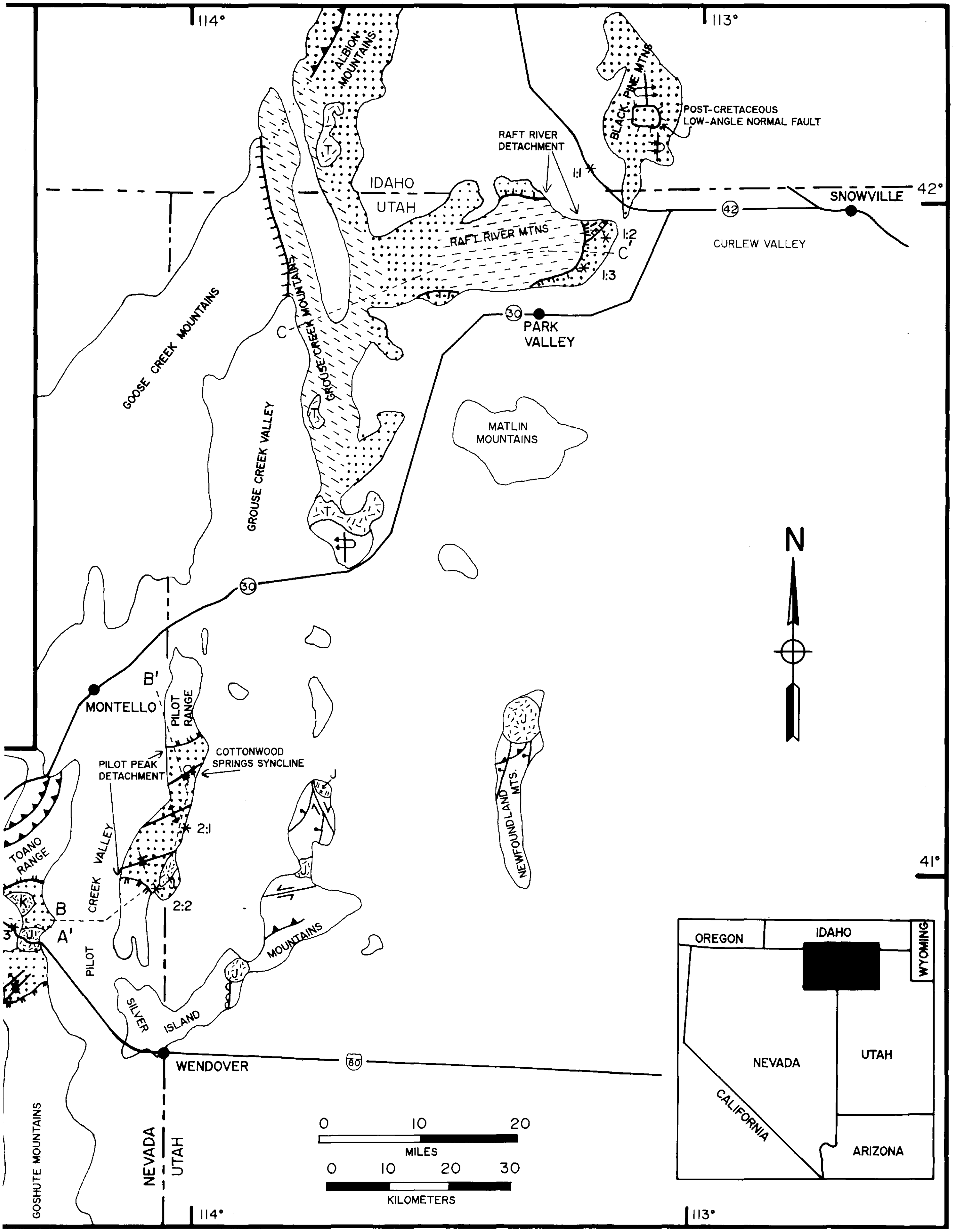
114°
113°
ALBION MOUNTAINS
BLACK PINE MTNS
POST-CRETACEOUS
LOW-ANGLE NORMAL FAULT
RAFT RIVER
DETACHMENT
IDAHO
UTAH
42°
SNOWVILLE
42
CURLEW VALLEY
RAFT RIVER MTNS
1:1
1:2
1:3
C
C'
30
PARK
VALLEY
GOOSE CREEK MOUNTAINS
GROUSE CREEK MOUNTAINS
GROUSE CREEK VALLEY
MATLIN
MOUNTAINS
T
N
30
B'
MONTELLO
PILOT RANGE
PILOT PEAK
DETACHMENT
COTTONWOOD
SPRINGS SYNCLINE
J
2:1
2:2
TOANO RANGE
CREEK VALLEY
B
A'
PILOT
NEWFOUNDLAND MTS.
41°
MOUNTAINS
SILVER
ISLAND
WENDOVER
80
OREGON
IDAHO
WYOMING
NEVADA
UTAH
CALIFORNIA
ARIZONA
0 10 20
MILES
0 10 20 30
KILOMETERS
GOSHUTE MOUNTAINS
NEVADA
UTAH
114°
113°

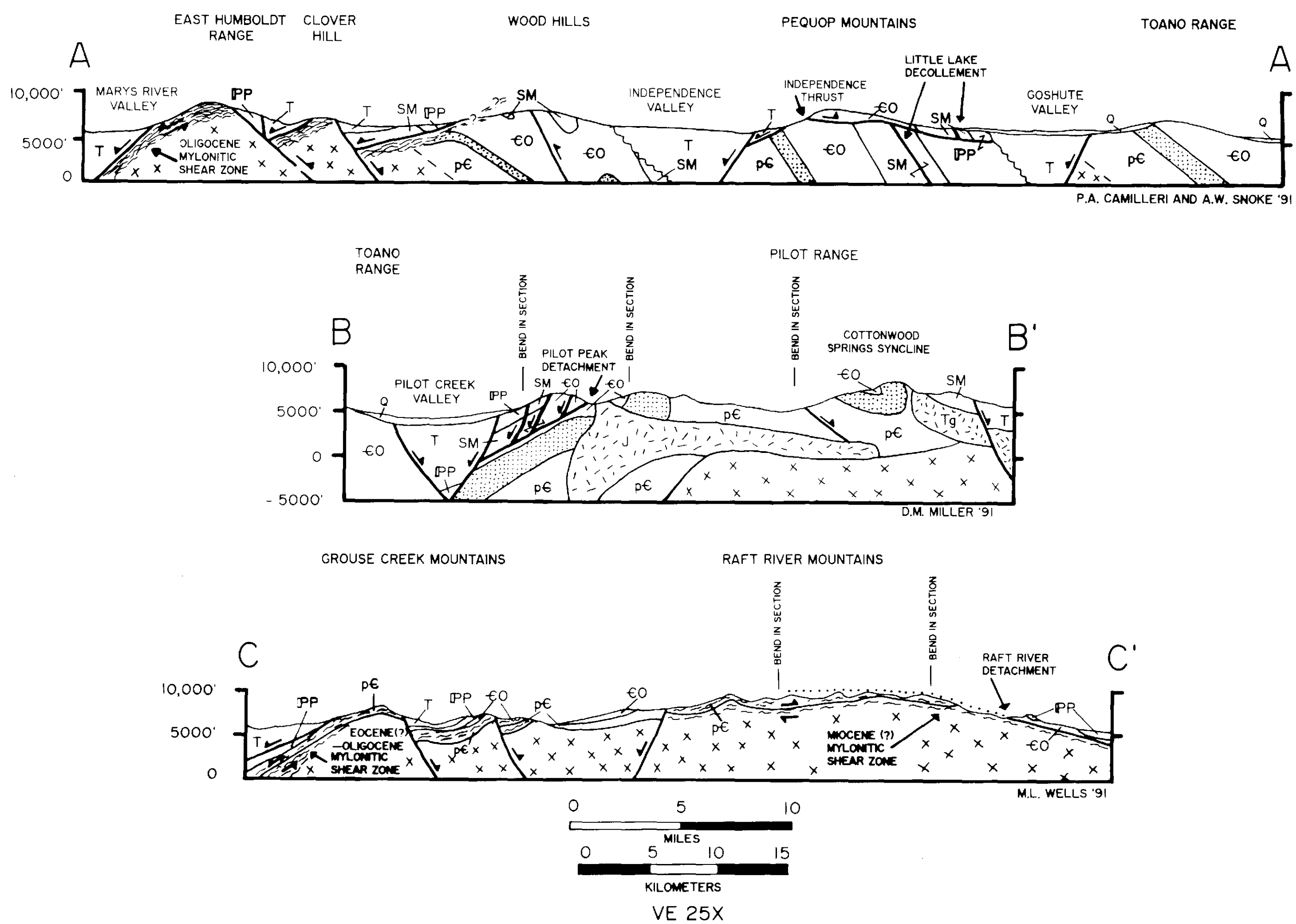

Figure 2. Geologic cross sections. See Figure 1 for locations. p €= Precambrian strata; €O = Cambrian and Ordovician strata; SM = Silurian, Devonian, and Mississippian strata; **PP** = Pennsylvanian and Permian strata; T = Tertiary strata; Q = Quaternary strata. Random dash patterns in section B-B′ represent plutons; J = Jurassic; Tg = Tertiary granitoid rocks. Stippled pattern in cross sections A-A' and B-B' represents the Late Proterozoic and Cambrian Prospect Mountain Quartzite. Cross pattern represents Archean basement. Wavy pattern represents mylonitic shear zone.

Eastern Raft River Mountains

The Raft River, Grouse Creek, and Albion mountains comprise a regionally extensive Mesozoic metamorphic terrain (Fig. 1). Mesozoic metamorphic fabrics and structures were exhumed by Cretaceous low-angle normal faults and by two Tertiary, oppositely-rooted, extensional mylonitic shear zones, which are developed in Archean to Paleozoic rocks (Figs. 1 and 2). The west side of the Albion Mountains exposes a belt of mylonitic rocks which record Oligocene and possibly Eocene top-to-the-WNW shear (Saltzer and Hodges, 1988). Fabrics in these mylonitic rocks are probably continuous with similar fabrics within the Grouse Creek Mountains and in the western Raft River Mountains (and are shown as such in Fig. 1). The central and eastern parts of the Raft River Mountains expose a belt of mylonitic rocks which records Miocene top-to-the-east sense-of-shear (Compton et al., 1977; Sabisky, 1985; Malavielle, 1987). This shear zone directly underlies, and is inferred to be genetically and kinematically related to, the Raft River detachment fault (Figs. 1 and 2).

Rocks in the hanging wall of the Raft River detachment in the eastern Raft River Mountains (Fig. 1) show no effects of Tertiary mylonitization and metamorphism and preserve a complex Mesozoic structural history. These rocks comprise two allochthons. The lower allochthon, directly above the Raft River detachment, consists of metamorphosed Cambrian(?), Ordovician, and Pennsylvanian(?) rocks and the overlying allochthon is composed of less metamorphosed Pennsylvanian and Permian rocks. The earliest Mesozoic deformational event involved the development of a pre-Late Cretaceous (Fig. 4) prograde metamorphic fabric interpreted to be a product of NE-directed shortening. This event was followed by marked attenuation of stratigraphic section

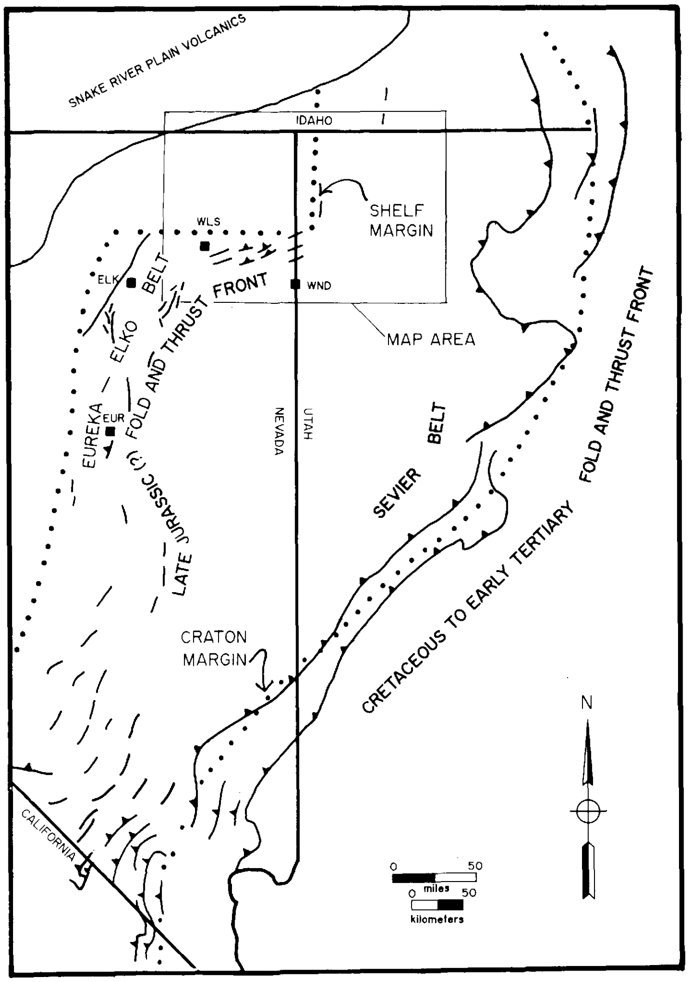

Figure 3. Tectonic map of the eastern Great Basin showing trends of contractile structures. WND = Wendover; WLS = Wells; ELK = Elko; EUR = Eureka. This Figure is modified after Speed et al. (1988) and incorporates data from Figure 1 as well as from Stewart (1980), Fryxell (1988), Bartley and Gleason (1990) and Camilleri (1988). The position of the continental carbonate platform margin is modified after Miller et al. (1991).

along top-to-the-west, low-angle normal faults that truncate bedding at a shallow angle. The most impressive of these structures is a fault that places metamorphosed limestone of the Pennsylvanian Oquirrh Formation over Ordovician rocks, omitting the entire Silurian, Devonian, and Mississippian section. These two events predate Late Cretaceous cooling of muscovite through ~350° C (Fig. 4). The faults and the earlier metamorphic fabric were subsequently deformed into Mesozoic(?) map-scale recumbent folds, which in turn were cut by a regionally extensive post-metamorphic (post-Late Cretaceous to pre-Miocene) low-angle normal fault along which the overlying allochthon was emplaced. All of the aforementioned structures are cut by the Miocene Raft River detachment fault.

Pilot Range and Toano Range

The structural histories of the Pilot and Toano Ranges are remarkably similar. Both ranges expose a west-rooted, Eocene low-angle normal fault (Fig. 1). Hanging-wall rocks in the Pilot and Toano Ranges consist of unmetamorphosed Cambrian to Permian strata. Hanging-wall rocks in the Toano Range are cut by two east-directed imbricate thrusts of small separation that are probably Mesozoic in age (Glick, 1987; Fig. 1). Plastically deformed upper amphibolite to greenschist facies Proterozoic and Cambrian strata comprise footwall rocks in both ranges. In the Toano Range, footwall rocks contain a Jurassic regional metamorphic fabric that predates emplacement of a Late Jurassic pluton (Glick, 1987). In the Pilot Range, footwall rocks were deformed into map-scale SE-vergent folds (Fig. 1) and metamorphosed synchronously with emplacement of a Late Jurassic pluton. The metamorphic rocks in the Pilot Range also contain Jurassic synmetamorphic bedding-parallel low-angle normal faults that may be products of stratal thinning along limbs of the map-scale folds as well as minor thrust faults that may have accommodated thickening in the hinge regions of the folds. Following metamorphism in the Pilot Range, east-directed plastic normal faults with moderate dips formed prior to Late Cretaceous cooling of muscovite to ~350° C.

Mesozoic deformation was followed by the development of late Eocene top-to-the-WNW low-angle normal faults (Fig. 1). Slip along these faults is estimated at 10 to 50 km, and directed nearly opposite to Jurassic shortening. One or more episodes of extension following Eocene detachment faulting resulted in low- and high-angle normal faults as young as late Miocene to Holocene.

Pequop Mountains, Wood Hills, and Northern East Humboldt Range

Along a west-to-east transect, the northern East Humboldt Range, Wood Hills, and northern Pequop Mountains expose a faulted cross section of miogeoclinal rocks that preserve the transition from Mesozoic middle crust to upper crust. These rocks were exhumed largely during Tertiary extension. From south to north, the Ruby Mountains-East Humboldt Range (Fig. 1) present a continuously exposed crustal cross section. Rocks of the Late Proterozoic McCoy Creek Group of Misch and Hazzard (1962) in the southern Ruby Mountains were not buried much in excess of stratigraphic depths and can be traced continuously into the northern East Humboldt Range (Hudec, 1990) where they were buried to depths perhaps as much as 26 km in excess of stratigraphic depths (Hodges et al., in press; Snoke, this volume) and metamorphosed to upper amphibolite facies during the Mesozoic. These data suggest that the Ruby Mountains-East Humboldt Range experienced significant tectonic burial on its northern end during the Mesozoic. A similar transition from structurally deep to shallow rocks occurs from west to east, although exposure is not continuous. In the Wood Hills, strata were metamorphosed to upper amphibolite facies and buried to a minimum of 10 km in excess of stratigraphic depths (Hodges et al., in press; Camilleri, this volume). Strata in the Pequop Mountains range from lower amphibolite and greenschist facies to unmeta-

SELECTED STRUCTURAL, AGE, METAMORPHIC, GEOBAROMETRIC, AND THERMAL DATA FOR METAMORPHIC TERRAINS IN THE NORTHEASTERN GREAT BASIN

	KINEMATICS AND AGE OF EARLIEST TERTIARY EXTENSIONAL FAULTS OR SHEAR ZONES	MAJOR MESOZOIC CONTRACTILE FOLD VERGENCE/SHEAR SENSE AND AGE (EXCLUDES BACK FOLDS AND THRUSTS)	MESOZOIC METAMORPHIC GRADE AND AGE OF REGIONAL METAMORPHISM	GEOBAROMETRY (RECORDS MESOZOIC PRESSURES)	TEMPERATURE (°C) JURASSIC	TEMPERATURE (°C) EARLY CRETACEOUS	TEMPERATURE (°C) LATE CRETACEOUS
RAFT RIVER MOUNTAINS	WNW-DIRECTED EOCENE(?)-OLIGOCENE	UPPER PLATE OF THE RRD* NE-DIRECTED ≥ 90 Ma LOWER PLATE OF THE RRD* NW-DIRECTED MESOZOIC (?)	GREENSCHIST–AMPHIBOLITE FACIES ≥ 90 Ma	UPPER PLATE OF THE RRD* > 4 kb LOWER PLATE OF THE RRD* DATA NOT AVAILABLE	?	~500	325–350
PILOT RANGE	WNW-DIRECTED EOCENE	SE-DIRECTED JURASSIC	GREENSCHIST–AMPHIBOLITE FACIES ~165–150 Ma	~3.5 kb (JURASSIC)	575–625 max.	>350	325–350
TOANO RANGE	WNW(?)-DIRECTED EOCENE(?)	SE(?)-DIRECTED JURASSIC(?)	GREENSCHIST–AMPHIBOLITE FACIES ≥ 162 Ma	~3.4 kb (JURASSIC)	~500 max.	>350	325–350
PEQUOP MOUNTAINS	~W-TO NW-DIRECTED ≥ EOCENE	SE-DIRECTED JURASSIC(?)	GREENSCHIST–AMPHIBOLITE FACIES ≥ 115–105 Ma	DATA NOT AVAILABLE	?	~300	?
WOOD HILLS	~W-TO NW-DIRECTED ~OLIGOCENE (?)	~SE-DIRECTED JURASSIC(?)	AMPHIBOLITE FACIES ≥ 115–105 Ma	5-6 kb (JURASSIC?)	? ←	~550 630	?
NORTHERN EAST HUMBOLDT RANGE	WNW-DIRECTED OLIGOCENE	SW(?)-DIRECTED LATE CRETACEOUS(?)	AMPHIBOLITE FACIES ≥ 128 Ma	> 10 kb (JURASSIC?) 5-6.4 kb (pre-mid-CRETACEOUS)	~500 540	~550 630	~550 650

*RRD = RAFT RIVER DETACHMENT FAULT

Figure 4. Table listing kinematics of Mesozoic and Cenozoic structures, timing of regional metamorphism, and geobarometric and thermal data for metamorphic terrains in the northeastern Great Basin. Data from Hodges et al. (in press), Thorman and Snee (1988), Snoke and Lush (1984), Miller et al. (1987), Wells et al. (1990), Dallmeyer et al. (1986), Glick (1987), Saltzer and Hodges (1988), Miller and Hoisch (this volume), Wells (this volume), and Camilleri (this volume).

morphosed, and therefore, represent a yet higher structural level. Like the Ruby Mountains-East Humboldt Range, the Pequop Mountains also appear to have been tectonically buried on its northern end in that miogeoclinal rocks only in the northern part of the Pequop Mountains were duplicated by thrust faulting (Fig. 1; also see Fig. 1 in Camilleri [this volume]). These regional relations suggest that during the Mesozoic, the East Humboldt Range, Wood Hills, and northern Pequop Mountains represent an area of localized large magnitude crustal thickening during the Mesozoic.

Structural data from the Wood Hills and Pequop Mountains suggest that at least two major Mesozoic contractile events are responsible for the large magnitude crustal thickening in this region. The first contractile event involved Jurassic(?) SE-directed thrusting. Metamorphic rocks in the Wood Hills, Pequop Mountains, and northern East Humboldt Range are inferred to have once comprised the footwall to a SE-tapering and -directed thrust wedge (see Camilleri, this volume) beneath the Little Lake decollement, which is exposed in the Pequop Mountains (Fig. 1). Metamorphic grade and burial depth of this footwall decreases in the direction of hanging-wall transport. Footwall metamorphic rocks were deformed into a prograde metamorphic L-S tectonite and in places an S tectonite with foliation nearly parallel to stratigraphic boundaries. Marked attenuation of stratigraphic section accompanied development of the tectonite and, based on metamorphic microstructures, is interpreted to reflect dominantly pure shear of the footwall at peak metamorphic grade. Stretching of the footwall may be a direct response to tectonic loading by thrust faulting and attendant thermal weakening due to burial.

The second contractile event overprints the tectonite and also involved SE-directed thrusting. Structures formed during this event include the Independence thrust in the Pequop Mountains (Fig. 1) and associated NW-vergent back-folds and thrusts (these structures occur in the upper plate of the Independence thrust in the Pequop Mountains and in the Wood Hills [Fig.1]). In comparison to the first event the second event probably only resulted in a minor amount of crustal thickening.

Unroofing of the Mesozoic fabrics and structures was largely accomplished by one or more west-rooted normal fault systems. Age constraints on the extensional faults or shear zones range from Cretaceous(?) to pre-middle Eocene (Pequop Mountains; Fig. 1), Oligocene (mylonitic shear zone in the East Humboldt Range; Figs. 1 and 2), and Miocene or younger (faults of this age occur in all three ranges; Fig. 1). It is not clear if extensional episodes were continuous or temporally distinct. In the Pequop Mountains-East Humboldt Range region, earliest Tertiary extension was directed opposite to that of Mesozoic shortening.

DISCUSSION

The age of regional metamorphism and major contractile structures along the continental shelf margin in the northeastern Great Basin, where dated by relationships with plutons, is constrained to be Late Jurassic. In areas where no such plutons exist (in the northern East Humboldt Range, Wood Hills, Pequop Mountains, and Raft River Mountains), metamorphism is constrained by mica and hornblende $^{40}Ar/^{39}Ar$ cooling ages which suggest that the age of metamorphism is Early to Late Cretaceous or older (Fig. 4). It is possible that much of the localized contractile deformation and regional metamorphism along the continental shelf margin is Late Jurassic in age. Bartley and Taylor (1991) proposed that east-directed structures in the so-called Eureka fold and thrust belt (Fig. 3), although poorly dated, may be synchronous with Jurassic deformation in northeast Nevada. If true it would appear that the Jurassic fold and thrust front is regionally localized along the continental shelf margin (Fig. 3). This contrasts with the Cretaceous to early Tertiary Sevier belt in which folds and thrusts are localized along the craton margin (Fig. 3). The structurally deepest rocks presently exposed in the northeastern Great Basin, occur in the northern East Humboldt Range, along the western salient in the sigmoidal bend in the continental shelf margin (Figs. 1 and 3). Deep structural burial in this region may reflect a localized concentration of strain at this crustal anomaly during crustal shortening and hence deep burial (Miller and Hoisch, this volume).

Although Mesozoic strain in the northeastern Great Basin reflects convergence at the plate boundary and bulk crustal shortening/thickening, it records localized extensional deformation. Mesozoic extensional features in the northeastern Great Basin are diverse in structural style, age, and interpretation. These extensional features can be grouped into four general categories, which are listed below.

Penetrative layer-parallel plastic attenuation of stratigraphic section: Metamorphic rocks in the Wood Hills and Pequop Mountains inferred to have comprised the footwall to a Jurassic(?) SE-tapering and -directed thrust wedge, were deformed into a prograde metamorphic L-S tectonite and in places an S tectonite, with foliation nearly parallel to stratigraphic boundaries. Fifteen to fifty percent attenuation of stratigraphic section that varies directly with metamorphic grade and burial depth was synchronous with the development of the tectonite and is interpreted to reflect dominantly pure shear of the footwall at peak metamorphic grade during and/or following tectonic loading. Thermally driven extension of footwall stratigraphic units may have allowed stretching as well as a decrease in flexural rigidity of the footwall and hence allow sinking or isostatic accommodation of the overlying load as well as reduction in topography.

Extensional faulting along the limbs of major folds. The limbs of synmetamorphic map-scale overturned folds in the Pilot Range contain bedding-parallel low-angle faults that omit stratigraphic section. These faults developed synchronous with metamorphism and with the development of the folds (Miller and Hoisch, this volume). Thus, these extensional features probably are a by-product of major shortening structure.

Low- and high-angle normal faults associated with magmatism: The Silver Island Mountains and Newfoundland Mountains (Fig. 1) contain small-scale, low- and high-angle normal faults that are cut by Jurassic plutons, (Allmendinger and Jordan, 1984; Miller and Allmendinger, 1991). Allmendinger and Jordan (1984) suggest that some of the normal faults may have developed as a result of pluton emplacement.

Low-angle normal faulting: Low-angle normal faults of presumed Late Cretaceous age are present in the Pilot Range and in the Raft River Mountains. The faults omit stratigraphic section and have only minor to moderate stratigraphic separation, and variable displacements as large as 10 km (Wells [this volume] and Miller and Hoisch [this volume]). The Late Cretaceous age of these normal faults suggests that they were active during documented shortening in the foreland (e.g. Armstrong and Oriel, 1965; Heller et al., 1986). Furthermore, it is known from various geologic and geophysical constraints that foreland thrusts root into Precambrian basement towards the west (Royse et al., 1975; Allmendinger, in press). Therefore, upper- to mid-crustal extension can be inferred to have occurred synchronously with shortening at deeper structural levels. This contemporaneity of shortening and extension has been documented recently for a number of convergent margin settings (e.g., Dalmayrac and Molnar, 1981; Burchfiel and Royden, 1985; Selverstone, 1988). The most probable explanation is that these structures moderate crustal thickness during contractional orogenesis. Compressional boundary forces which develop topography by means of crustal shortening are working against gravitational body forces (resulting from increases in topography and topographic slope) which tend to thin the lithosphere via extension. If gravitational body forces locally overcome compressional boundary stresses, the rocks will undergo subhorizontal extension. A corollary of this treatment of mountain belts as orogenic wedges is that alternating periods of extension and shortening can occur episodically, as in the eastern Raft River Mountains (Wells, this volume).

The direction of earliest Tertiary extension along the bend in the continental shelf margin is kinematically approximately opposite to the direction of Mesozoic shortening (Fig. 4). We hypothesize that along the region of the bend in the continental shelf margin, Mesozoic contraction produced a southeastward tapering wedge of thickened crust that was subsequently extended. In the northeastern Great Basin, tectonic heredity may have played a role in localizing Mesozoic shortening and subsequent first phases of Tertiary extension.

ACKNOWLEDGMENTS

Field work for preparation of the road log was partially supported by Geological Society of America, American Association of Petroleum Geologists, Sigma XI, and Wyoming Geological Association research grants to P.A. Camilleri, and National Science Foundation research grant EAR 87-07435 to A.W. Snoke. M.L. Wells acknowledges support from Geological Society of America, and Cornell Graduate School research grants and National Science Foundation research grant EAR 87-20952 (awarded to R. W. Allmendinger). We appreciate reviews of earlier manuscripts by V. R. Todd, D. M. Morton, and A. Yonkee.

DAY 1: ROAD LOG FROM SNOWVILLE, UTAH TO RAFT RIVER MOUNTAINS AND WENDOVER, UTAH

by

Michael L. Wells and David M. Miller

Day one of this field trip will focus on the geometry, timing, and kinematics of pre-Miocene structures within Paleozoic rocks comprising the hanging wall of the Tertiary Raft River detachment fault. We will view and discuss the evidence for large-magnitude extension of Late Cretaceous age, and probable contractional deformations which both post- and pre-date this extension. Additionally, we will view and explore the evidence for two later episodes of detachment faulting. For the background geologic information on this region, see the accompanying article (Wells, this volume).

MILEAGE		DESCRIPTION
Incremental	Cumulative	
		The road log begins in Snowville, Utah, an hour and twenty minute drive from Ogden. To reach Snowville, drive north on I-15, take 84W near Tremonton for 34 miles to Snowville. Get off at the Utah State Highway # 30 exit to Park Valley and Malta.
0.00	0.00	Junction of Interstate 84 and Highway 30, just west of Snowville, Utah.
		As we drive across Curlew Valley, the Raft River Mountains are on the west. We are looking down the axis of the range, which has an overall geometry of an east-west trending, doubly plunging anticline. Off to our right are the Black Pine Mountains. The roads on the east flank of the Black Pine Mountains are within the newly redeveloped Black Pine mining district. Exploration by Noranda has defined five separate ore bodies totaling 5.2 million tons of 0.06 ounce per ton gold (Hefner et al., 1990) within Pennsylvanian and Permian rocks of the Oquirrh Formation.
11.9	11.9	At ~200 yds past mile marker 79, a Bonneville terrace exposing basalt is on the right.
3.0	14.9	At~200 yds past mile marker 76 is a Bonneville terrace with exposures of the Pennsylvanian and Permian Oquirrh Formation.
0.3	15.2	Curlew Junction (junction of Highways 30 and 42). About 8 kilometers east and southeast from here three wells encountered Devonian, Mississippian, and Pennsylvanian rocks (Pease, 1956). Within the Black Pine Mountains, Devonian strata and up to 2000 meters of Mississippian strata (thickened by folding) are present (Smith, 1982). This is in marked contrast to the absence of Devonian and Mississippian rocks in the eastern Raft River Mountains ten kilometers to the west-southwest.
4.6	19.8	A prong of the Oquirrh Formation extends from the Black Pine Mountains to the highway. These exposures, and exposures of the Oquirrh Formation on the flanks of the eastern Raft River Mountains, nearly provide a bedrock link across the valley with a gap in exposure of only 3 kilometers.
0.2	20.0	On the south side of the road is a beautiful exposure of a Bonneville barrier bar, with gravel overlain by marl.
0.15	20.10	Cedar Creek Road intersects highway from the south.
0.3	20.40	Exposures of the Oquirrh Formation on either side of road.

3.0 23.40 **STOP 1 (Fig. 1).**

Strevell, and intersection of Naf road and Highway 42. View of Raft River Mountains from northeast side of range. The Raft River Mountains exhibit many features characteristic of other metamorphic core complexes. A domal-shaped subhorizontal Tertiary detachment fault (the Raft River detachment) is superimposed on an older mylonite zone. The Raft River detachment separates Archean and Proterozoic rocks in the footwall (autochthon) from Paleozoic rocks in the hanging wall, or upper plate. Here we see isolated klippen of upper plate rocks scattered across the crest of the range, and the large exposure of these upper plate rocks at the eastern end of the range. The detachment is subparallel to lithologic contacts and the mylonitic foliation in the underlying autochthon. The morphology of the detachment is well expressed because of a laterally continuous resistant quartzite unit (the Elba Quartzite) in the footwall. The autochthon in the footwall of the detachment consists of Archean intrusive rocks and schists, and unconformably overlying Proterozoic(?) rocks. The mylonite zone is >200 meters thick and represents an extensional, top-to-the-east ductile shear zone.

The upper plate of the Raft River detachment is composed of a lower allochthon of Cambrian(?), Ordovician, and Pennsylvanian(?) rocks, and a middle allochthon of Pennsylvanian and Permian rocks. The pre-Miocene structural history of the Cambrian(?) to Permian rocks of the upper plate includes: (1) early NE-directed interbed plastic flow, (2) top-to-the-west attenuation faulting, (3) recumbent folding of the attenuated strata and low-angle faults of the lower allochthon, (4) emplacement of the middle allochthon of Pennsylvanian and Permian (Oquirrh Formation) rocks over the folded lower allochthon along a low-angle fault localized in the Mississippian Manning Canyon Shale, and (5) folding of both the lower and middle allochthons into upright, open folds.

To the north-northeast lie the Black Pine Mountains. The southern Black Pine Mountains are composed of three major bedrock units: the Pennsylvanian and Permian Oquirrh Formation (Smith, 1982; 1983), Upper Mississippian and Lower Pennsylvanian Manning Canyon Shale, and the Devonian Guilmette Formation. In general, low-angle faults separate these stratigraphic units and place younger rocks over older rocks. The Guilmette Formation forms the structurally lowest allochthon and its basal contact is not exposed. Generally, no significant thickness of section is missing across these faults, with the exception of the fault which places Chesterian rocks of the Manning Canyon Shale on Devonian limestone; there, slivers of Kinderhookian limestone occur along the fault contact locally.

Five metamorphic and/or deformational events are recorded in the Black Pine Mountains (Wells and Allmendinger, 1990). From oldest to youngest these include: 1) static metamorphism (M_1) to 350-400°C recorded by pretectonic chloritoid porphyroblasts in the Manning Canyon Shale and conodont color alteration indices of 5 to 5.5, possibly synchronous with emplacement of Late Jurassic sills; 2) east-west layer-parallel elongation of 160% associated with synkinematic metamorphism (M_2) and growth of white mica along cleavage; 3) generally top-to-the-west low-angle faulting and overturned to recumbent folding; and, although their relative sequence is not known, 4) doming, and 5) high-angle normal faulting.

Within the Raft River Basin, approximately 1700 meters of upper Cenozoic deposits are present (Williams et al., 1982). Many of these volcanic and volcaniclastic deposits are well exposed in the Jim Sage Mountains, the first range we see to the west across the valley. Within the central part of the basin, subsurface studies based on drilling show that these faulted and tilted Cenozoic deposits lie structurally above a relatively flat fault that in turn lies above metamorphosed Precambrian rocks lithologically equivalent to those exposed within the Raft River Mountains. These and other Tertiary deposits within the Raft River Basin are westdipping, and probably were caused by down-to-the-east faulting in the upper plate of the detachment fault which floors this structural basin (Covington, 1983). Here at Strevell, Tertiary basin-fill deposits reach depths of only 340 meters, and overlie the Oquirrh Formation.

The principal stop for today (Stop 3 at Ten Mile Canyon; Fig. 5) will feature: (1) a traverse through footwall rocks of the Raft River detachment and the Cenozoic top-to-the-east extensional shear zone, (2) overviews of the geometry of F_5 upright folding within the upper plate, (3) examination of the middle detachment fault, (4) outcrop study of D_1 fabrics, and (5) overview of the geometry of D_2 attenuation faults and F_3 recumbent folds. We will end up on Crystal Peak (Fig. 5), the high point in the low hills directly to the south that expose upper plate. An optional stop at Emigrant Spring Canyon (Stop 2) will focus on the rock fabric within marble mylonite associated with a major D_2 attenuation fault of Late Cretaceous age. See Wells (this volume) for a description of the structural events on the eastern Raft River Mountains. Note: stops 2 and 3 are on private land and you must have permission from the land owners for access. Additionally, many of the gates in this region are locked.

Turn vehicles around. Head back southeast on Highway 42.

3.3 26.7 Turn right (south) on Cedar Creek Road. As we drive along this road we are very near the maximum highstand for Lake Bonneville. Here, a thin veneer of Quaternary deposits overlie Tertiary deposits. Lake Bonneville platforms are cut into this stratigraphy, locally exposing Tertiary deposits on the cut surfaces behind the platforms.

2.8 29.5 If you are bypassing Stop 2 go to mileage 32.3 of the road log (not your odometer) to continue.

Turn right through southernmost of two gates and onto property of Juddabeth Land and Livestock.

0.5 30.0 Drive straight through gate in fence.

0.1 30.1 Bear left.

0.1 30.2 Bear left where road comes in from right.

0.1 30.3 Bear right.

0.1 30.4 Bear right and proceed up canyon.

0.2 30.6 Drive straight through gate.

0.1 30.7 Just past trailer on right side of road, the road crosses a drainage and proceeds up south side of canyon. If road is not in good condition, one can park here and proceed on foot up the valley. If proceeding on foot, continue up canyon past piles of granulated and pulverized rocks of the Eureka Quartzite. Continue up wash through the Swan Peak Quartzite, which is composed of interbedded sandy limestone, brown and white quartzite, brown-weathering calcareous sandstone, but also contains a lower phyllite and an upper dolomite. Note the ENE-trending lineations defined by pressure shadows around pyrite and by calcite streaking. Road to south ends at quartzite quarry.

30.9 **STOP 2** (Figs. 5 and 6).

If driving, continue up road until it ends at quartzite quarry. At road's end there is a turnaround spot. Proceed up wash past quartzite mine. Continue in main drainage center, left of quarry wall through large blocks. Continue up wash until ridge is visible on left.

Scramble up the creek bank to west and climb to the ridge and note contact between Ordovician dolomite (buff grey) and Pennsylvanian limestone (blue-grey). Note chips of brown-weathering quartzite and phyllite along the contact. These chips are the remnants of the entire Mississippian section. A fine-grained marble tectonite with isoclinal folds is developed within the underlying Pennsylvanian marble. Proceed directly up this ridge to peak 6160. Here, mylonitic fabrics within this tectonite are well developed. Stretching lineations trending 95 to 105 are prominent. Walk fifty feet to the northwest down the ridge to a fault contact with Ordovician dolomite. Again note chips of Mississippian rocks (Chainman? Shale) and the fine-grained marble tectonite. Isoclinal folds within this zone (all removed by sampling) have axes trending parallel to the stretching lineation in the coarser grained marble above. Calcite C-axis texture from this horizon is strongly asymmetric indicating top-to-the-west shearing. Additionally, oblique subgrain fabric within the coarse-grained crinoidal marble above also indicates westward shearing. Muscovite from the marble tectonite collected 500 m to the south yields a $^{40}Ar/^{39}Ar$ plateau age of 88.5 ± 0.3 Ma.

Retrace steps back to the quartzite quarry and vehicles.

1.4 32.3 Return to Cedar Creek Road and turn right (south).

5.1 37.4 Turn right before fence, and drive west along fence line.

0.2 37.6 Bear right at "Y" road intersection.

0.9 38.5 Drive straight through fence line.

0.2 38.7 Drive through fence with a gate.

0.2 38.9 Turn left at the corral.

0.1 39.0 Proceed through the fence, then bear right.

1.3 40.3 Cross the wash.

0.1 40.4 Turn left at "T".

0.8 41.2 Bear right as road comes in from left.

0.3 41.5 Drive straight through the gate. Enter mouth of Ten Mile Canyon. Exposures of Cambrian (?) quartzite of Clarks Basin on slope to the right (south). As we proceed up Ten Mile Canyon, note the exposures of brown-weathering, muscovite-biotite-quartz schist of the older schist unit of Compton (1972).

1.6 43.1 **STOP 3** (Figs. 5 and 7).

Turn vehicles around, one at a time, where canyon to northeast joins main canyon at ~ elevation of 6310, and park vehicles facing downhill. This hike will take about 5 hours, so pack and carry with you the appropriate materials. The elevation gain will be about 1400 feet, and boots are highly recommended. See Figure 7 for a geologic map of this area.

Proceed up road in the canyon for ~2000 feet, until a prominent canyon joins from the right (northeast). Climb up the northwest-trending ridge separating the two canyons. This climb will take us through rock units comprising the lower plate (autochthon) of the Raft River detachment fault. We will walk from rocks exhibiting little Tertiary fabric into rocks that were highly deformed during Tertiary top-to-the east shearing. The dark rock exposed on the lowest (200′) slopes of this ridge as well as along the road is amphibolitic schist and granular amphibolite exhibiting varying degrees of fabric development. Near the top of this unit, foliation is flat-lying and exhibits a stretching lineation trending ~ 086. Above the amphibolitic schist is the oldest rock unit in the Raft River Mountains (older schist unit of Compton, 1972;

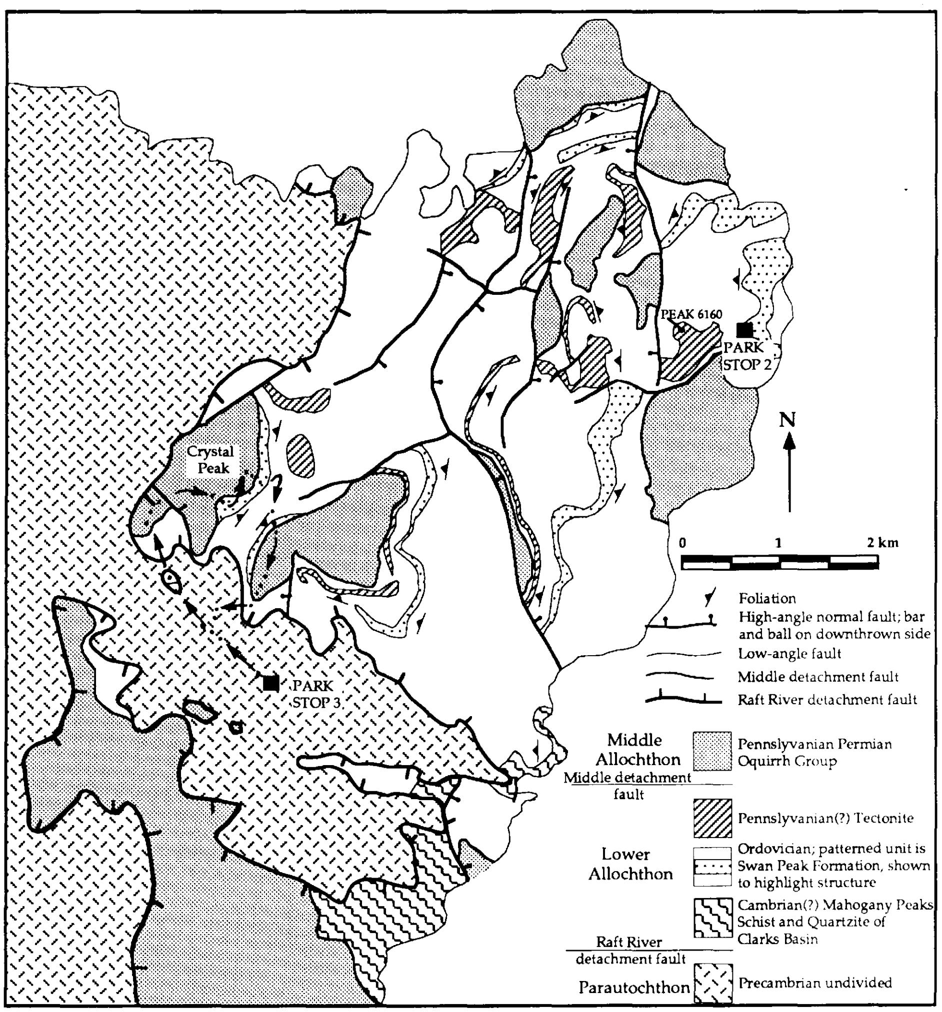

Figure 5. Geologic map of the eastern Raft River Mountains illustrating distribution of structural plates and location of field trip stops 2 and 3. Data from M.L. Wells (unpublished mapping).

EXPLANATION FOR FIGURES 6 AND 7

MAP UNITS

Qal	Alluvium
Qls	Landslide Deposits
Qc	Colluvium
Qaf	Alluvial Fan Deposits
Ts	Sedimentary Rocks (Tertiary)
Po	Oquirrh Formation (Permian and Pennsylvanian)
Pot	Oquirrh Formation Tectonite (Pennsylvanian ?)
OSd	Ordovician - Silurian Dolomite
Oe	Eureka Quartzite (Ordovician)
Osp	Swan Peak Quartzite (Ordovician)
Ogc	Garden City Formation (Ordovician)
P€es	Schist Member of Elba Quartzite (Proterozoic?)
P€e	Elba Quartzite (Proterozoic?)
P€ad	Adamellite (Archean)
P€mi	Mafic Igneous Rocks (Archean)
P€os	Older Schist (Archean)

CONTACT

HIGH-ANGLE FAULT

Bar and ball on downthrown side

LOW-ANGLE FAULT

Teeth on hanging wall

BEDDING ATTITUDES

43

inclined vertical

FOLD AXIAL TRACE

Anticline Syncline

Overturned anticline Overturned syncline

RAFT RIVER DETACHMENT

Hachures on hanging wall

MIDDLE DETACHMENT

Double hachures on hanging wall

FAULT OF UNCERTAIN GEOMETRY

FOLIATION ATTITUDES

inclined vertical

MINERALOGIC LINEATIONS

22

Inclined Horizontal

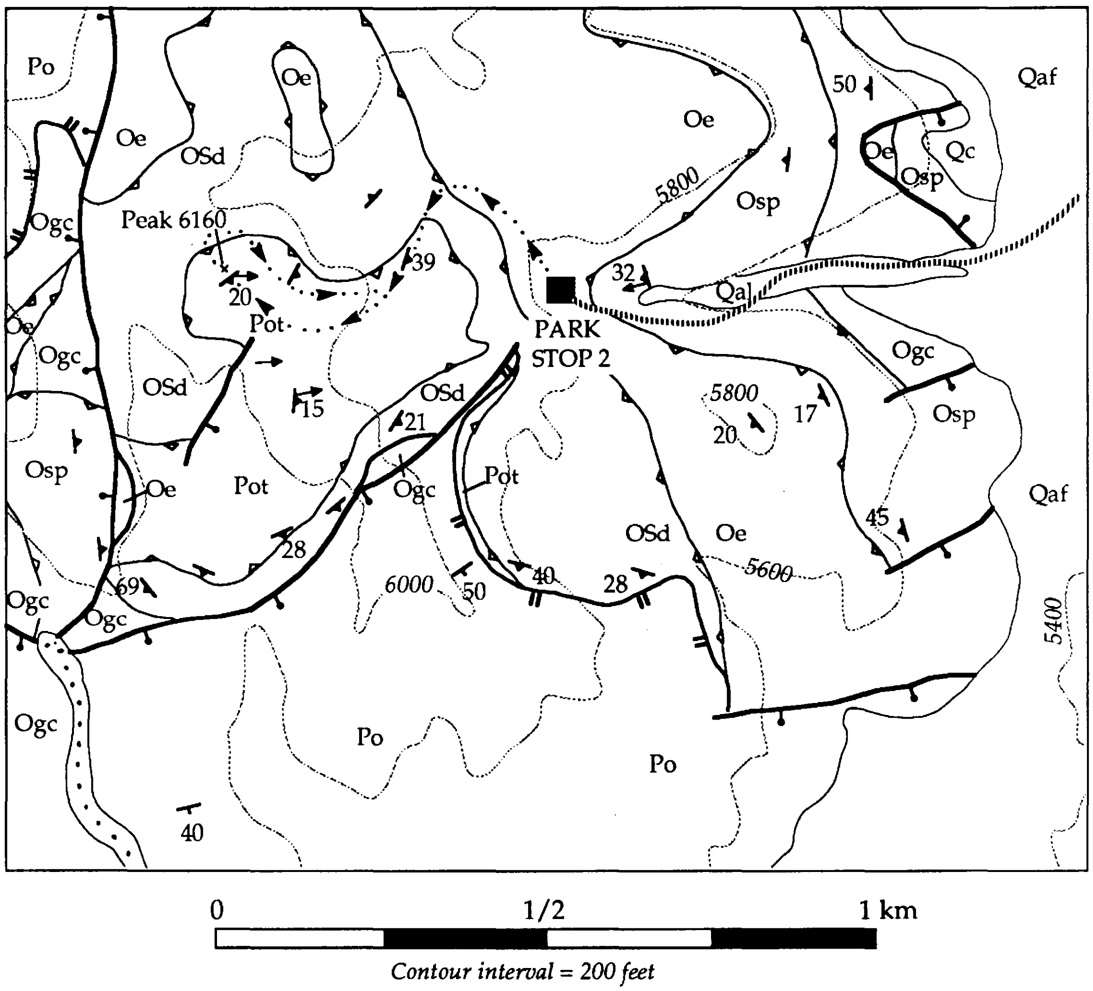

Figure 6. Geologic map of area traversed on Stop 2, Emigrant Spring. Data from M.L. Wells (unpublished mapping).

1975), a fine-grained mica-feldspar-quartz schist and semischist. Above this schist lies the Elba Quartzite. Note the prominent flat-lying foliation and N85E-trending stretching lineations. Proceed up the ridge through a dark grey to black weathering quartzose schist. Immediately overlying this schist is the brittle detachment fault demarcated by scraps of brecciated and altered carbonate rocks.

Proceed up ridge across a klippe of Ordovician rocks to the summit of small knob 7240. This knob offers a vantage point from which to view several important elements in the structural history that predated detachment faulting.

Off to the NW, we see a prominent stripe of quartzite running across the slope on the south flank of Crystal Peak. Directly above this stripe composed of the attenuated Eureka Quartzite lies the middle detachment, which here places Pennsylvanian

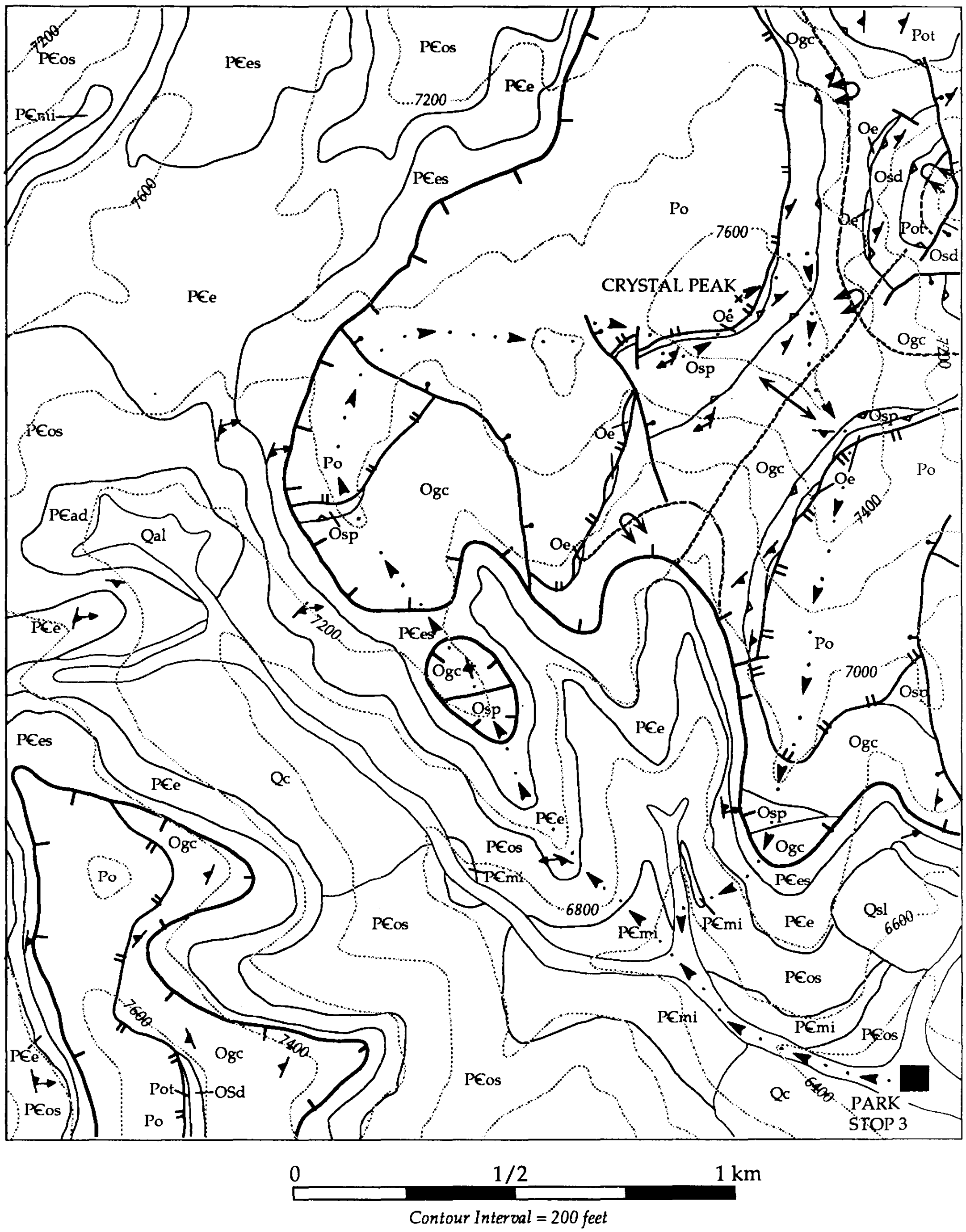

Figure 7. Geologic map of area traversed on of Stop 3, upper Ten Mile Canyon. Data from M.L. Wells (unpublished mapping).

rocks of the Oquirrh Formation over Ordovician rocks. Beneath the Eureka Quartzite lies an upright sequence of the Swan Peak Quartzite and the overlying Garden City Formation. The Garden City Formation forms the grey-colored craggy slopes, and phyllite of the basal part of the Swan Peak Quartzite forms the grass covered slopes above. Both the middle detachment fault and the underlying strata were folded about an upright, open fold whose axis is slightly oblique to our vantage point. The fold is truncated by high-angle faults which sole into, but do not cut, the Raft River detachment fault.

Proceed to the NW, down across small saddle in the schist member of the Elba Quartzite and continue up the ridge. At elevation 7410 we cross the middle detachment and then walk through the poorly exposed Oquirrh Formation. Follow the ridge up as it bends to the right and walk up to peak 7620, noting fusulinids in the sandstone along the way. From this vantage point we have a clear view to the east of the middle detachment fault, which is offset down-to-the east along a high-angle normal fault. Looking to the west, the domal morphology of the range is highlighted by the resistant Elba Quartzite. Scattered klippen of Ordovician and Pennsylvanian rocks are visible along the crest of the range.

Our next stop will be at the cedar-topped outcrops ~100 feet below the band of the Eureka Quartzite. Proceed east across the saddle, over the quartzite ledge and down to limestone outcrops of the Swan Peak Quartzite. Walk along the base of the limestone outcrop, uphill to the northwest, to best view the array of structures. At this locality, D_1 fabrics are well-developed. Here, discernible bedding and D_1 foliation lie at a much larger angle to each other than is usual. D_1 foliation dips westward relative to a transposed bedding. Stretching lineations are defined by white-calcite streak ing and calcite and quartz pressure shadows around pyrite. Two episodes of "folding" are apparent. Foliation is axial planar to the principal small-scale recumbent folds whose axes are subparallel to the stretching lineation. Foliation intersects a highly transposed bedding at higher angles in sandy zones, and lower angles in the dominantly calcite-rich zones. This relationship of apparent cleavage refraction could be a result of finite-strain refraction, differential volume loss between beds, differential shear strain between layers of differing competency, or combinations of these processes. An apparent second "folding" is evident in exposures oriented NW (viewed to the NE). Foliation is not only refracted between layers but is apparently back-rotated. The paradox here is that bedding is recumbently folded and foliation is axial planar to these folds, yet foliation is locally folded or back-rotated about apparently younger folds and bedding is not. Perhaps this back rotation is due to continued shortening and tightening of the now recumbent folds after the initial cleavage formation and refraction processes.

Proceed uphill to the band of the Eureka Quartzite. Here, the Eureke Quartzite is internally brecciated, and within a fault zone above the Eureka Quartzite is minor dolomite and a minor exposure of the Chainman Shale (apparent only as sooty soil), all beneath the Oquirrh Formation. The Oquirrh Formation from the top of Crystal Peak has yielded conodonts with CAI values of 5, indicating metamorphic temperatures of 350 to 400° C. In contrast, metamorphic temperatures in the Ordovician rocks are 490 to 520° C, as indicated by oxygen isotopic geothermometry and CAI values >7 from the Swan Peak Quartzite (Wells et al., 1990; J.E. Repetski, personal communication, 1988).

Proceed up-hill to the top of Crystal Peak (elev. 7770) for a panoramic view including the Raft River Valley to the north and the Black Pine Mountains to the northeast.

Walk down the NW-trending ridge to the contact between the Swan Peak Quartzite and Garden City Formation, then contour to the northeast to outcrops of the Garden City Formation at the top of a steep slope. From this vantage point we can look into Crystal Hollow, which provides an overview of upright and overturned stratigraphic units and a major Cretaceous normal fault. The smooth weathering slopes on the northwest-trending ridge to the southeast are underlain by the Pennsylvanian and Permian Oquirrh Formation of the middle allochthon. The middle allochthon is in fault contact with metamorphosed Pennsylvanian rocks of the Oquirrh Formation of the lower allochthon, the prominent cliff-forming blue-grey band projecting westward into Crystal Hollow. The Pennsylvanian marble structurally overlies a greatly attenuated Ordovician and Silurian(?) dolomite section, not visible from this vantage point. The fault separating the Ordovician and Silurian(?) dolomite from the Pennsylvanian marble is interpreted to represent a Late Cretaceous normal fault of large displacement, which omits Silurian, Devonian, and Mississippian strata. This stratigraphic omission is present over an east-west distance as great as 11 km. Synkinematic muscovite within the marble mylonite adjacent to this fault yields a $^{40}Ar/^{39}Ar$ plateau age of 88.5 ± 0.3 Ma (Wells et al., 1990). The Ordovician and Silurian(?) dolomite is underlain by the Eureka Quartzite which forms the prominent flat-lying bench along the ridge. Beneath the Eureka Quartzite lie the Swan Peak and Garden City Formations, which together comprise an upright stratigraphic section.

We are standing on the uppermost part of the Garden City Formation, which is overlain by the Swan Peak Quartzite and an attenuated section of the Eureka Quartzite. Down slope, structurally beneath the Garden City Formation, are white to tan outcrops and float of the Ordovician and Silurian(?) dolomite, and discontinuous slivers of Eureka Quartzite occur between these units. Below the Ordovician and Silurian(?) dolomite is Pennsylvanian marble. This overturned section beneath us, together with upright strata to the northwest, comprise a recumbent fold whose axial surface lies within the Garden City Formation. The Cretaceous normal faults are folded about this recumbent fold, which in turn is cut by the middle detachment.

Proceed down the ridge, bearing to the right when you reach sandstone of the Oquirrh Formation of the middle allochthon. At ~elevation 6900 feet, in faulted Ordovician rocks, walk downslope to the west across the Raft River detachment, and work your way down slope through parautochonous rock units. From the valley bottom, turn left and follow the valley to the junction with Ten Mile Canyon: proceed down the road in the canyon back to the vehicles.

5.7 48.8 Return to Cedar Creek Road. Turn right (south).

0.9 49.7 Turn right at paved road, heading southwest toward Park Valley on Utah State Highway 30.

1.0 50.7 Basalt flows cut by Bonneville lake terraces are exposed north and south of the highway. Lithologically similar basalt flows nearby were dated at about 3 Ma by K-Ar (Todd, 1983) but D.W. Fiesinger (written communication, 1991) has dated the same at about 7 Ma. White deposits in the valleys are composed of calcareous silt (white marl) from the floor of Lake Bonneville, derived from tuffaceous Miocene strata underlying the basalt. As we top the rise, a pit in shoreline gravel deposits is visible on the left.

White, south-facing dip slopes in the Raft River Mountains composed of the Elba Quartzite overlie darker slopes formed on Archean rocks. At the base of the range, many klippen of younger rock units overlie the Elba Quartzite along the Raft River detachment fault. Low-angle fault-bounded klippe on top and on the flanks of the mountains presumably once covered the older rocks. Strata in the klippen are mainly Ordovician units and the Oquirrh Formation.

3.3 54.0 Ahead and to the right Bonneville shorelines have cut bluffs at the highest stand of the lake.

5.7 59.7 The north-trending ridge ahead and to the left of the microwave tower is composed of Miocene tuffaceous mudstone, sandstone, and conglomerate of the Salt Lake Formation.

1.9 61.6 Park Valley, one of the quarrying locations for the beautiful flagstone (micaceous quartzite) occurring in the Raft River Mountains.

4.6 66.2 Rosette.

1.3 67.5 Intersection of Palmer Ranch/Montgomery Road; continue south on Utah State Highway #30. We are moving away from the east-trending Raft River Mountains toward the Grouse Creek Mountains in the distance to the right. The Grouse Creek Mountains are part of the same metamorphic core complex.

8.2 75.7 Hills on the left are just above the high stand of Lake Bonneville. They contain Miocene tuffaceous siltstone and vitric tuff of the Salt Lake Formation. On the right, the Grouse Creek Mountains form the skyline.

Approximately 12 miles to the southeast are the Matlin Mountains, which consist of a complex allochthon that was emplaced in the same approximate time span (middle to late Miocene) as the upper allochthon of the Grouse Creek Mountains to the west of the Highway (Todd, 1983). The Matlin

Mountains, named for a water stop of the first transcontinental railroad, were islands in the northwestern part of Lake Bonneville and are surrounded by, and partly covered by, lacustrine sedimentary deposits. They expose a sequence of five thin displaced sheets that consist of upper Paleozoic and lower Mesozoic rocks and Tertiary strata. This displaced sequence rests in low-angle fault contact on a rooted upper Paleozoic section to the east. The thickness of the displaced sheets is typically less than 200 m and the exposed extent of individual sheets is roughly 10 to 20 km from north to south and 5 to 10 km from east to west. The entire displaced sequence appears to dip gently westward toward the Grouse Creek Mountains. Two of the five low-angle faults that form the boundaries of the displaced sheets divide the displaced terrane into two composite plates, which appear to have had different histories and to have moved separately. One of these faults, the East fault, is the basal fault which separates the displaced terrane from the rooted section. The other, the West fault, probably dips westward and joins the basal fault at depth. These two faults juxtapose plates that differ significantly in lithology, metamorphism and structural character and they probably have the largest displacements of the faults in the Matlin displaced terrane.

3.4 79.1 Muddy Ranch Road. Light-colored outcrops to the left are Miocene strata of the Salt Lake Formation.

5.3 84.4 Emigrant trail road (not marked) to the left (east) is the road to the Matlin Mountains.

3.3 87.7 Historic Marker:

Rich in history of exploration and travel, Park Valley has witnessed the passage of great men and events.

Jedediah Smith, mountain man and explorer, traversed this region in 1826, seeking beaver and a river flowing west from Great Salt Lake. Two years later, Peter Skene Ogden, in command of a Hudson Bay Co. fur trapping party, explored Park Valley. Other explorers and traders subsequently passed near the site. Joseph R. Walker, fur trapper turned explorer and guide, led a party through to California in 1833. Portions of his route were followed by the Bartleson-Bidwell party in 1841, the first wheeled vehicle immigrant train in Utah. The Salt Lake Cutoff branch of the California Trail offered passage to the thousands of "49'ers" who made their way to the goldfields in the 1850's.

The first transcontinental railroad completed at Promontory, Utah, May 10, 1869, bisected this county 2 miles south of this site. Settlement in the Valley followed soon on the heels of the railroad.

4.6 92.3 The craggy outcrops between 2:00 and 3:00 are granodiorite which makes up the Immigrant Pass intrusion. This approximately 38-Ma pluton intruded the Oquirrh Formation. The pluton extends for 3 miles to the north and 8.5 miles to the west, and was dated by R. Zartman as approximately 38 Ma by the Rb-Sr method (Compton et al., 1977). Also visible are the high wave-cut benches of Lake Bonneville and a level-topped gravel beach that extends from the mountain front northeast to a low, craggy spur exposing granodiorite.

At 10:00 in the distance are the Newfoundland Mountains. The Late Jurassic Newfoundland stock at the north end cuts a thrust fault that duplicates part of the Ordovician section, and also cuts normal faults (Allmendinger and Jordan, 1984).

At 11:00 in the distance are the Silver Island Mountains and at 12:00 in the distance is the Pilot Range.

3.3 95.6 Just before the right hand bend in the highway is a prominent outcrop of unmetamorphosed rocks of the Silurian Laketown Dolomite, with bedding dipping 60° or so to the northeast.

1.1 96.7 Slow down but do not stop. For the next mile or so we will view the south end of the Grouse Creek Mountains. The high mountain mass is called Bovine Mountain and its geology has been studied in detail by Jordan (1983). It exposes an unusually thick sequence of the Oquirrh Formation that has been deformed broadly by folding on east-verging recumbent folds that predate or are coeval with the 38-Ma pluton. Most of the exposures on the mountain are in an overturned limb, and rocks dip at moderate angles to the west. The pale gray rocks around the base of the mountain are another structural element-a plate consisting of an unnamed limestone member of the overturned Oquirrh Formation, lying on a low-angle fault that dips toward the highway. The fault parallels bedding in the limestone member but clearly cuts across bedding in sandstone of the Oquirrh Formation (brownish outcrops) that forms the main ridge immediately to the north. A third structural element is exposed in the low, dark (desert-varnished) outcrops that extend from a point near the highway for about 0.6 miles to the north. These are overturned Ordovician and Silurian strata that are unique within the entire area of the core complex and its cover in that they are only slightly metamorphosed and texturally unstrained. These rocks are separated from limestone of the Oquirrh Formation by a fault that parallels bedding in both fault blocks and that is folded by northeast-trending folds that predate the Immigrant Pass intrusion.

2.2 98.9 Pigeon Mountain at 10:00 is composed of Permian and Triassic strata juxtaposed by several thrust faults.

1.5 100.4 White Miocene vitric water-laid tuff is well exposed in outcrops and in a quarry on the right (north) side of the road. The beds are broadly folded on roughly west-trending axes and dip at low angles (12 to 20°) to the north and south.

1.6 102.0 Small dirt road marked by a B.L.M. sign to Immigrant Pass and Rosebud Station. Four buttes to the northwest of the road are separate rhyolite plugs or thick flows that are cut by high shorelines of Lake Bonneville; the plugs were dated as 11.7 Ma (Compton, 1983; K-Ar on sanidine). The plugs intrude a thick sequence of middle Miocene tuff and interstratified sedimentary rocks that underlie the smooth-surfaced hills rising to the northeast of the road. The Miocene sequence ranges in age from approximately 15 Ma to 11.5 Ma. The Miocene rocks are in fault contact with the older rocks of the range at the break in slope where the smooth hills meet the more jagged slopes of Bovine Mountain. The fault here dips approximately 25° WSW. The same fault has been mapped continuously for 24 miles to the north and from that point it has been mapped discontinuously to the Idaho state line, a total distance of 39 miles. The Miocene rocks 4.8 miles to the north are tectonically intercalated with Permian(?) and Triassic rocks, and these rocks together comprise a detachment sheet along the western side of the Raft River-Grouse Creek core complex (includes the uppermost allochthonous sheet of Compton et al., 1977).

2.7 104.7 Permian and Triassic strata form the sharp hills rising from the valley floor to the southwest.

1.0 105.7 Rabbit Springs road. The springs to the south are used for watering trail herds of both cattle and sheep. The springs were originally developed for the transcontinental railroad.

3.0 108.7 Crossroads; Grouse Creek to the right and Lucin to the left. Permian and Triassic strata is exposed in the nearby hills to the south and Miocene rhyolite plugs and minor related outflow volcanic rocks are exposed to the north. Variscite has been mined from cherty Permian rocks in the area.

2.8 111.5 Bridge over wash. Gravel and sand in the road cuts on either side of Grouse Creek were deposited as a narrow delta as Lake Bonneville receded. Underlying light-colored deposits are fine-grained deltaic deposits and marl.

1.6 113.1 Ahead for the next few miles we pass close by Permian rocks underlying the hills on our right and Ordovician rocks underlying Gartney Mountain on the left.

4.4 117.5 State Line.

1.6 119.1 Crossing of Thousand Spring Creek. The road was washed out here during the winter and spring of 1984; heavy rainfall and snowfall in the huge drainage basin of this creek turned it from a trickle to a torrent for several months.

The Pilot Range to the south exposes a nearly complete section of sedimentary rocks of Late Proterozoic to Permian age, granitic rocks of Mesozoic and Cenozoic age, and volcanic rocks and intercalated sedimentary rocks of Eocene, Oligocene, and Miocene age. Horizontal rhyolite lava flows at the north end are about 9 Ma (K-Ar on sanidine).

1.0 120.1 Dake Reservoir on right.

4.9 125.0 Refining mill set up to process gold in the region but never used. To the left behind us on the skyline, the tallest peak is Bald Eagle Mountain. To its right the reddish-orange cuts are on Copper Mountain, part of the Lucin mining district. The cut is an open-pit mine in the Devonian Guilmette Formation. Devonian and older sedimentary rocks in the district occur in several low-angle fault slices that were cut by higher angle faults and subsequently intruded by the latest Eocene McGinty Monzogranite. Mineralization is related to plutonism. The district produced abundant rich oxide ore from 1870 to 1920, and at a lower production rate until 1966. Total values shipped were about $4 million.

3.4 128.4 Montello is an old railroad town, first settled in the 1800's when the original east-to-west railroad line was built. Its population has fluctuated from several thousands to less than a hundred.

We drive west through Tecoma Valley, which was a broad and relatively shallow (300 ft deep at highstand) arm of Lake Bonneville. The fine-grained lake deposits around us locally form sand dunes due to reworking by wind following the recession of the lake. To the west rise the Leach Mountains, composed of Permian through Triassic strata. The Permian strata are structurally detached from underlying fragments of Mississippian clastic rocks. No older rocks crop out in the Leach Mountains. Permian rocks exposed in the Leach Mountains apparently exceed 3,000 m in thickness. To the north are complexly faulted hills composed of upper Paleozoic strata and Tertiary sedimentary and volcanic rocks.

1.6 130.0 Highway turns south and crosses railroad track.

3.0 133.0 Intersection with gravel road to the southeast. Turn left and head southeast past the gravel pit.

0.9 133.9 To the left, in the distance at the north end of the Pilot Range, note the white tuff beds below the buttes discussed earlier. Straight ahead is another view of Copper Mountain.

0.6 134.5 At this point Paleozoic strata in the northern Pilot Range are well displayed (Fig. 8). Pale cliffs near the crest of the range are composed of the Guilmette Formation, which is underlain by the slope-forming Simonson Dolomite and underlying Silurian and Devonian thick-bedded dolomite. Above the cliffs are tree-covered brown cliffs of brecciated jasperoid and above these cliffs are grassy slopes underlain by Mississippian strata. Just south of this prominently exposed stratigraphic section is a broad pass underlain by latest Eocene granite. South of the pass are higher peaks underlain by metamorphosed Proterozoic and Cambrian strata.

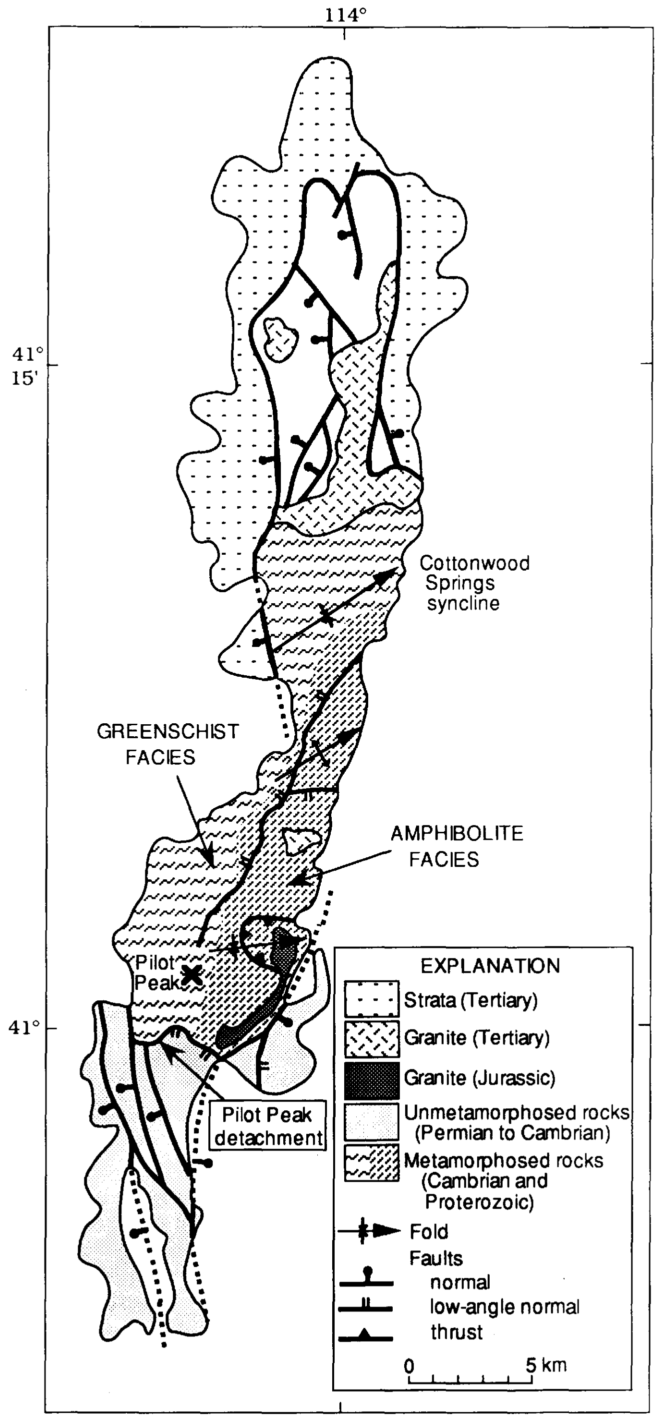

Figure 8. Generalized geologic map of the Pilot Range. Metamorphic rocks lie south of Tertiary pluton and north of Pilot Peak detachment fault and are patterned to distinguish metamorphic facies.

11.9 146.4 Pilot Range overview (Fig. 8). We have driven nearly the length of the Pilot Range. Beginning in the north we passed a Paleozoic sedimentary succession, followed by an Eocene pluton, and finally drove along an expanse of the Late Proterozoic McCoy Creek Group of Misch and Hazzard (1962). At this point Pilot Peak is nearly due east from us and shows as a triple-humped knife edge, all of which is above 10,600 ft. elevation. It is underlain by the talus slope- and cliff-forming Prospect Mountain Quartzite, with older rocks below. The Prospect Mountain Quartzite dips about 30° southward at the slope extending south from the peak and are cut by a nearly bedding-parallel fault, the Pilot Peak detachment. Above the detachment and forming the tree-covered peaks at about 7,000 to 8,000 feet high, are the Cambrian and Ordovician Notch Peak and Ordovician Garden City Formations. South ward in the trailing tip of the range are younger units of the Paleozoic succession.

The Pilot Peak detachment juxtaposes older rocks which are metamorphosed to greenschist and amphibolite facies with younger rocks that are texturally unmetamorphosed. The youngest rocks beneath the detachment are Middle Cambrian in age, and the oldest rocks above the detachment are Late Cambrian, but at all exposures of the detachment, strata are cut out. The detachment is cut by latest Eocene granodiorite, indicating that detachment in the Pilot Range began by 40 Ma or earlier.

2.0	148.4	To the southwest, the northern Toano Range is composedof Upper Cambrian to Mississippian strata that were intruded by Jurassic, Cretaceous, and Eocene plutons. Thrust faults predate the Cretaceous pluton, and normal faults postdate all plutons.
		Dry wildcat oil wells spudded near our present location encountered several thousand feet of Tertiary sedimentary rocks without hitting Paleozoic bedrock.
0.6	149.0	To the left is an excellent view of the south-dipping beds in the hanging wall of the Pilot Peak detachment.
11.3	160.3	The large plant ahead is Continental Lime's quicklime plant. High-calcium limestone for the plant is mined nearby from the Guilmette Formation. The primary market for the lime is the booming gold industry of northern Nevada.
1.7	162.0	Leppy Hills ahead on left. The Leppy Hills consist of tilted fault-bounded blocks. The blocks consist of Cenozoic volcanic rocks of felsic to intermediate composition that lie on Devonian through Permian sedimentary rocks. Most of the rocks dip 10° to 60° westward. Although the faulting pattern is complex, the range can be described generally as a north- to northwest-trending horst.
1.3	163.3	Historic marker.
		The high, symmetrically shaped mountain seen rising to the north is Pilot Peak. In the period 1845-1850, it was a famous landmark and symbol of hope and relief to the Reed-Donner Party and all other wagon train pioneers who traveled the 70-odd deadly, thirst and heat-ridden miles of the Great Salt Lake Desert. Across this desert, between the Cedar Range on the east and Pilot Peak on the west, stretched perhaps the worst section of the infamous Hastings Cutoff of the California Emigrant Trail.
		The peak was named by John C. Fremont on his expedition of 1845. Kit Carson, the expedition's guide, was sent ahead to locate water and found a line of springs at the peak's eastern base, now known as McKellar Springs. Carson is reputed to have guided the rest of Fremont's expedition across the salt desert by sending up smoke signals from the peak; hence, Fremont's name for it.
		During the years 1847-1850, relief parties sallied forth periodically with water from the Pilot Peak springs to rescue and succor the thirst-crazed emigrants and their livestock struggling across the terrible salt desert to the east.
		Proceed under interstate overpass.
0.1	163.4	I-80, turn left onto eastbound entrance ramp.
8.7	172.1	View of Salt Lake Desert ahead. Tertiary rhyolitic lava flows (12 Ma) on both sides of the road.
2.2	174.3	Leave the freeway at Exit #410 to Wendover and Alt. U.S. Highway 93.
0.3	174.6	Turn right at the stop sign at the end of the exit ramp and enter West Wendover, Nevada.
		Wendover is divided by the state line between Nevada and Utah. The Nevada side is one of the fastest growing towns in the state. Its population has risen from 307 to more than 2,200 since 1980 primarily due to its growing gaming industry. Wendover (Utah side) was an Army Air Corps Base in World War II. Paul Tibbets trained here; he flew the Enola Gay, which dropped the first atomic bomb at Hiroshima in 1945. Wendover (Utah side) is also known for the Bonneville Salt Flats, located 7 miles to the east, where numerous land-speed records have been set.
0.1	174.7	Turn left at stop sign onto Wendover Boulevard.
0.2	174.9	Intersection of U.S. Alt 93. Continue east (straight ahead) to our lodgings at the Stateline Inn on the left side of Wendover Blvd. in Wendover, Utah. This is beyond the waving cowboy (Wendover Will) on the right.
0.9	175.8	Stateline Inn on left—enter parking lot.

DAY 2:
ROAD LOG FROM THE PILOT RANGE TO WELLS, NEVADA

by
David M. Miller and Phyllis A. Camilleri

This part of the trip continues from Wendover, passing through the Silver Island Mountains, Pilot Range, and then west to the Toano Range, Pequop Mountains, and Wood Hills. Exposed in these ranges are several low-angle normal faults of Cenozoic age, beneath which are rocks ranging from high-level unmetamorphosed strata to somewhat deeper amphibolite facies rocks. In general, metamorphic rocks brought to the surface by extensional complexes contain the best evidence for Mesozoic tectonism, but many structures in unmetamorphosed rocks are no doubt also Mesozoic in age. In the Pilot Range, we will examine amphibolite facies strata that were metamorphosed in the Jurassic, as well as the anatomy of a detachment fault zone that places tilted, slightly metamorphosed lower Paleozoic strata upon greenschist to amphibolite facies rocks. This tectonic assemblage resulted from extension along a gently dipping detachment at a deeper level than that of the Leppy Hills, but footwall rocks represent a shallower level than those recognized as "metamorphic core complexes." Driving westward to the Toano Range, we will pass through a similar middle-level detachment system developed on metamorphic and plutonic rocks of Jurassic age. From there westward to the East Humboldt Range the depth of detachment currently exposed appears to increase.

MILEAGE		DESCRIPTION
Incremental	Cumulative	
0.0	0.0	Underpass beneath I-80, West Wendover. Turn right onto I-80 East.
1.6	1.6	We are passing through road cuts in the Guilmette Formation, here highly faulted. The Leppy Range here is a northwest-trending horst, with bounding systems of normal faults that dip east and west (Schneyer, 1990). Within the range, normal faults have both steep and gentle dips, and curving fault geometries are preserved. Extension was accommodated by contrasting modes of deformation in contrasting materials. Massive limestone deformed brittlely, typically with 'space problems' accommodated by massive white calcite solution fillings and solution breccia. These features are vivid in the road cuts. Shale deformed ductilely, as seen by folded and sometimes wildly contorted beds. Schneyer (1984) argued that most, if not all, of the normal faulting occurred after deposition of Miocene (11.9 Ma) rhyolite on Permian strata, chiefly because the rhyolite and the Paleozoic strata are similarly rotated within some fault blocks.
3.2	4.8	Exit 4, Bonneville Speedway. Exit here and turn north.
1.2	6.0	Bear left at the fork in road onto gravel road. Straight ahead, gently folded Pennsylvanian limestone dips west in the lower slopes, and Miocene rhyolite lava forms the rugged hill crests.
3.1	9.1	Leppy Pass. Bear left at fork in road. We now have a sweeping view of Pilot Valley playa, with the Pilot Range on the left and the Silver Island Mountains on the right. We will proceed north along the west side of the playa.
9.5	18.6	Pilot Valley playa lies on our right.
14.3	32.9	Turn left on small road that heads due west to Pilot Range. At this point we see mostly rocks of the Late Proterozoic McCoy Creek Group of Misch and Hazzard (1962) in the center of the tectonic window be-

neath the Pilot Peak detachment fault (Fig. 8).

2.0 34.9 Cross Lake Bonneville highstand.

0.9 35.8 **STOP 1** (Fig. 9).

Park at the gated fence. We are in the bottom of a strike valley in the uppermost unit (unit G) of the McCoy Creek Group (Fig. 9). To the south is a high ridge underlain by the steeply north-dipping Prospect Mountain Quartzite that is overturned. The browner slopes facing us are the basal part of unit G. The gentler north side of the canyon is underlain by several units of the upper part of the McCoy Creek Group, all overturned and folded about NE to NNE axes. These folds and associated low-angle faults are cut by the Late Eocene Bettridge Canyon Granodiorite, dated by U-Pb on zircons at 38.9 ± 0.9 Ma (Miller and others, 1987).

We will examine schists and quartzites of the McCoy Creek Group and the igneous rocks that intrude them. Throughout this area, strata bear a prominent foliation at low angles to bedding (S_1). Rare folds that are nearly isoclinal probably represent F_1 stage deformation. Common upright folds and mineral lineations with a northeast trend deform S_1 and are assigned to F_2 and L_2, respectively. Synkinematic mineral assemblages here include musc-qtz-gar-tour and musc-qtz-gar-tour-and: nearby to the north, sillimanite is present, indicating upper amphibolite facies conditions.

Southward, metamorphic hornblende in amphibolite-facies rocks yielded a $^{40}Ar/^{39}Ar$ plateau age of 149 ± 0.9 Ma, indicating cooling following peak metamorphism in the Late Jurassic. Since metamorphism was in part coeval with emplacement of Jurassic granite (155 to 165 Ma, U-Pb zircon), the mineral growth and development of structures and fabrics here in Bettridge Canyon was also Late Jurassic in age (Miller et al., 1987).

Cross the ridge to the north and drop down to the next, broad, valley. The valley is floored by poorly exposed biotite-hornblende granodiorite of the Late Eocene Bettridge Canyon Granodiorite. Xenoliths of dark igneous rock are common, in many cases elongate parallel to weak magmatic foliation. Foliation is inconsistently oriented and weak, in contrast to tectonite fabric in the wall rocks.

Return to road fronting the Pilot Range.

2.9 38.7 Turn right (south) along main gravel road.

4.7 43.4 Bear right at fork.

4.0 47.4 Turn right (west) on dirt road leading to Pilot Range.

The view straight ahead is of Pilot Peak, underlain by Late Proterozoic quartzite. The forested lower hills to the south are underlain by Paleozoic carbonate strata structurally overlying the quartzite.

2.2 49.6 Road turns right on Bönneville shoreline gravels.

1.8 51.4 Pass mine dump and buildings. The ridge above the mine is underlain by Upper Cambrian carbonate strata dipping moderately eastward. The mine enters a shattered zone of carbonate rocks and farther in intersects altered granodiorite. This same granodiorite is common within the detachment fault. The hornblende-biotite granodiorite was dated at 37.5 ± 2.6 Ma by K-Ar on slightly altered biotite. Proceed up road.

0.3 51.7 **STOP 2** (Fig. 10). Turn out to right in clearing beyond aspen grove.

We will examine the anatomy of the detachment fault (Pilot Peak detachment) that separates tilted packets of Cambrian and Ordovician strata from underlying schist, marble, phyllite, and quartzite. If time permits, we will examine some typical rock types and structures in the metamorphosed sequence.

As shown in Figure 10, much of the Cambrian system is missing at the detachment fault. Under the fault are metamorphosed Late Proterozoic to Middle Cambrian strata, and above the fault are Upper Cambrian to Lower Ordovician strata. These units are described in more detail by Miller (1984). Regionally, a similar detachment fault in mountain ranges to the east and west omits strata that range from Middle Cambrian to Middle Ordovician in age, but strata are consistently omitted.

Walk up the road to the point where brown cliffs of marble are on the left and climb these rocks. We will proceed south, upslope, and climb through the detachment system.

The brown cliffs are the upper part of the Killian Springs Formation, and the strike of bedding projects to the north to bold outcrops of the unit (Fig. 10). The sandy to silty limestone was metamorphosed to amphibolite facies here, producing the mineral assemblages: Musc-biot-epid-plag-sph, musc-biot-epid-trem-calc-sph, phlog-

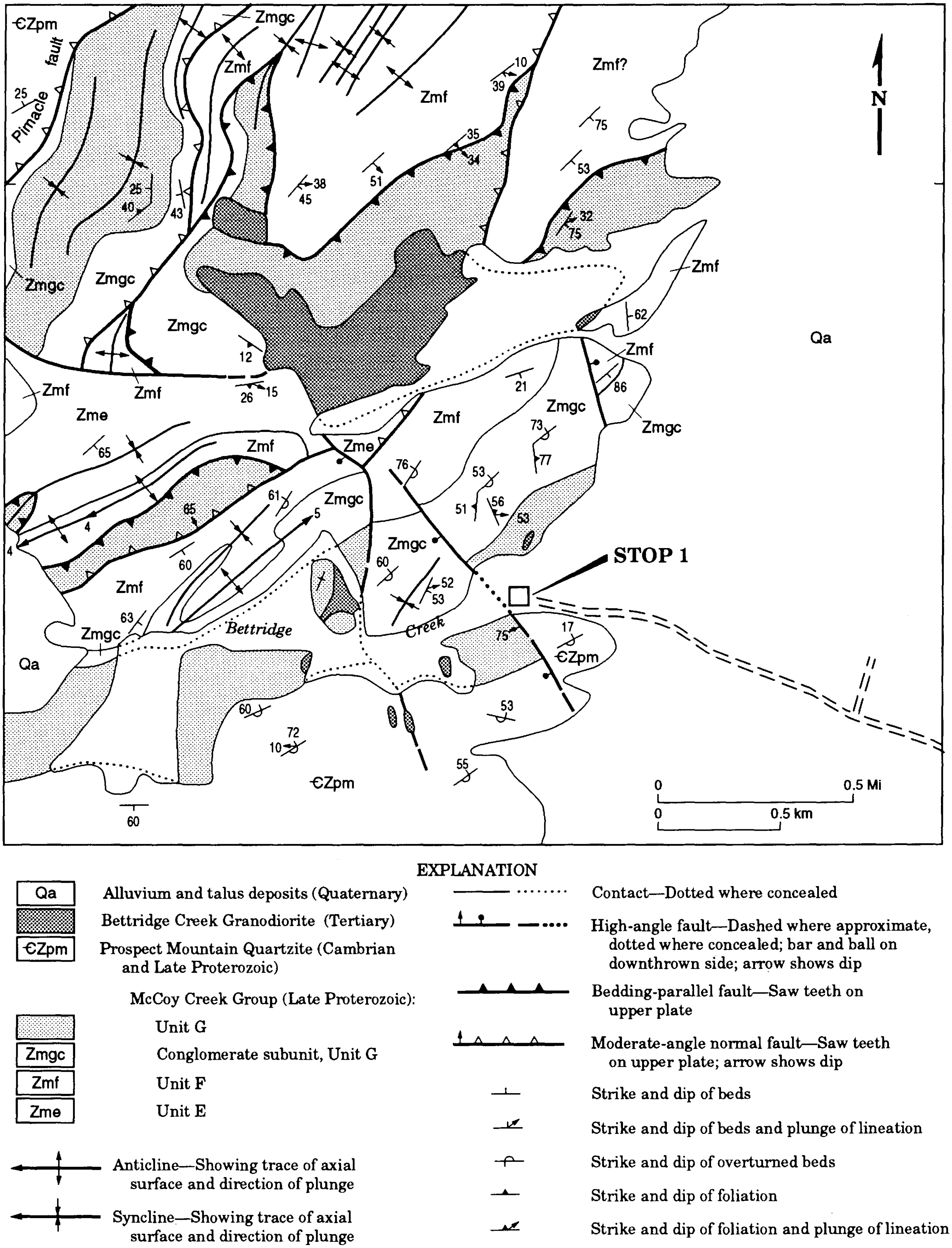

Figure 9. Geologic map of Bettridge Creek area. After Miller and Lush (in press).

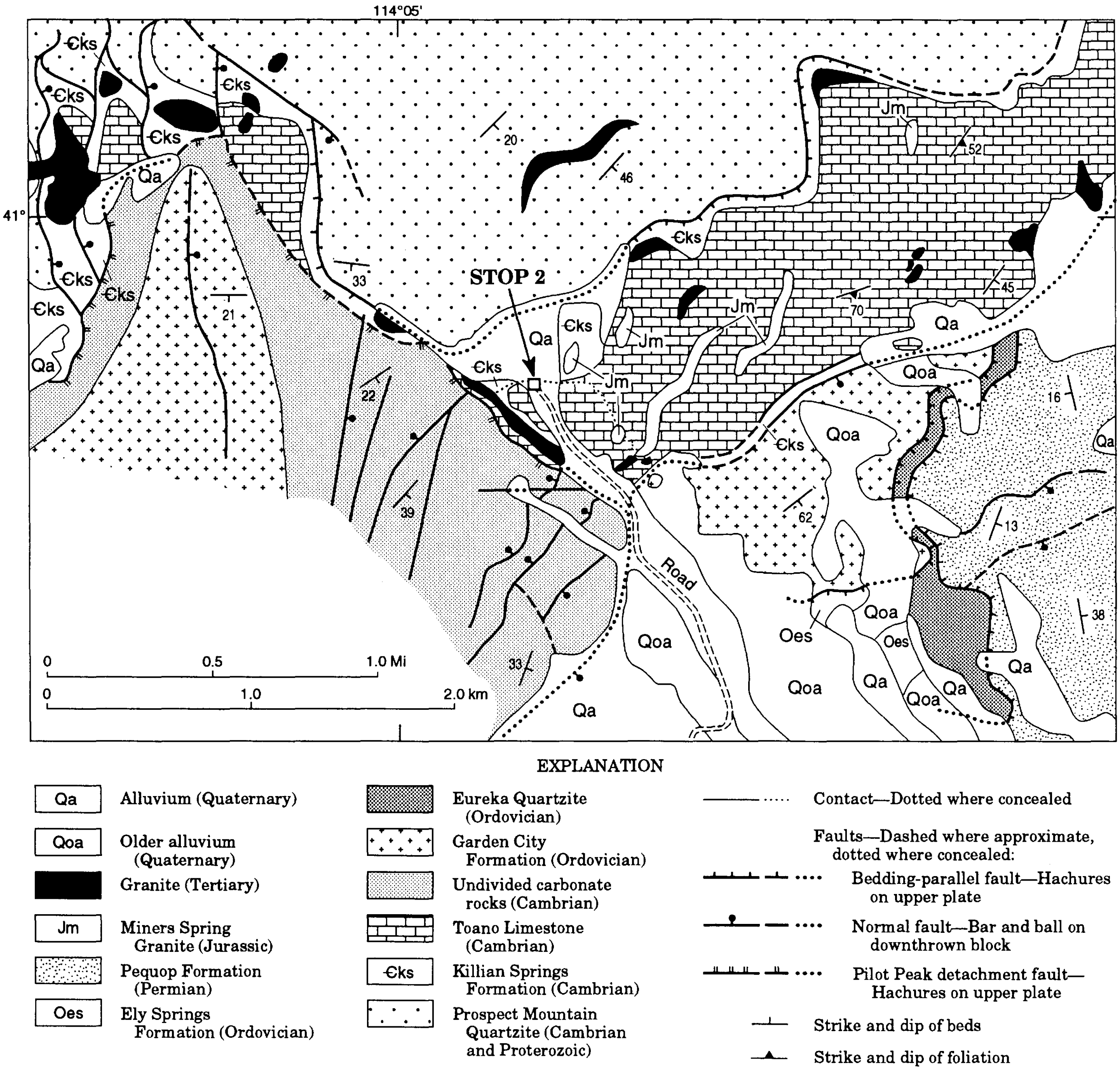

Figure 10. Geologic map of Miners Canyon area . After Miller and Lush (in press) and Miller (unpublished mapping). Trip route shown by dotted line.

chlor-calc-dol, and musc-qtz-trem-calc-sph. The marble is strongly foliated and in places folded. To the north, the brown marble is overlain by white marble of the Toano Limestone. Rocks in both units are more highly metamorphosed here than 5 km west in the Pilot Range, where they are only slightly metamorphosed (Miller and Lush, 1981). Granitoid dikes of probable Jurassic age cut this marble. Also present is a small mafic igneous body, of probable Jurassic age. Upslope, beyond a short covered zone, the marble is strongly folded, and further upslope the marble acquires an easterly strike, an orientation which we will see is subparallel to the detachment above. Next upslope is a broad area of modestly fractured and altered granodiorite. This body crops out as an extensive sill along the canyon wall (Fig. 11). Exposures are poor, but outcrops of dark gray silty limestone interspersed among granodiorite outcrops suggest inclusions or septa of these wall rocks, which belong to a less metamorphosed lower Toano Limestone similar-to that cropping out 5 km to the west. Also

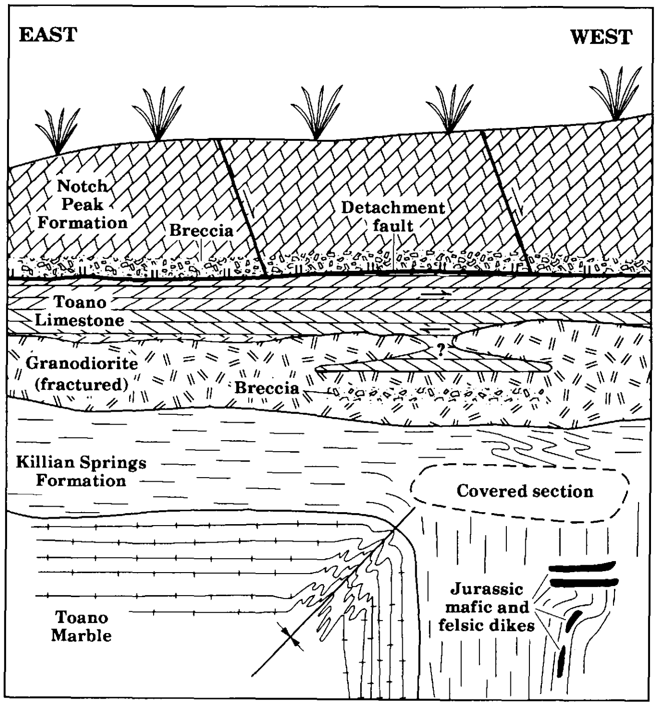

Figure 11. Diagrammatic relations on south wall of Miners Canyon. White marble of the Toano Limestone lies in core of large fold; brown micaceous marble of the Killian Springs Formation wraps around the fold. Less metamorphosed slices of the Toano Limestone lie above granodiorite sill and are involved in multiphase shear along a detachment fault.

exposed at one place is brecciated granodiorite. The granodiorite sill has yielded K-Ar dates of 30.1 ± 0.5 Ma (biotite) and 54.6 ± 1.6 Ma (hbld) at nearby areas, and is probably closely related to lithologically similar granodiorite in a pluton dated at 38.9 ± 0.9 Ma by U-Pb on zircon about 6 km to the north.

Upslope from the granodiorite are large outcrops of black silty limestone, somewhat metamorphosed, of the lower part of the Toano Limestone. Its metamorphic grade is distinctly lower than that of the Killian Springs Formation (marble) below. Upward, the Toano is highly faulted along closely spaced low-angle faults. This deformation contrasts with that in immediately overlying dolomite breccia from above the detachment fault.

Fabrics within these Cambrian rocks suggest a three-stage history. First, ductile deformation coeval with amphibolite-facies mineral growth took place in the Late Jurassic (Miller et al., 1987). Jurassic granite cuts mafic dikes, which are boudinaged in the metamorphic rocks. This north-striking Jurassic fabric is folded to an east strike by a second event, the drag suggesting top-to-east shear. Lower grade exposures of the Toano Limestone above the east-striking fold limb contains syntaxial calcite and quartz veins within which fibers indicate top-to-east shear. A third event is suggested by yet another fabric superimposed on the Toano Limestone immediately beneath the detachment fault, where several sets of brittle fractures combine to resemble pencil cleavage; the features are much like S-C fabrics. Lineations in the pencil cleavage trend N70W to west and are parallel to local slickenlines. Pseudo-S-C fabrics and offset veins yield top-to-west sense of shear; fracture of the veins indicates that this shear postdates that of event 2. Dolomite breccia and oolitic limestone lie above the detachment; presumably the breccia formed during event 3.

Timing information for these three events suggests a Mesozoic to early Cenozoic evolution of the rocks. Event 1 is Late Jurassic in age. Event 2 postdates peak metamorphism (Late Jurassic) but is partly ductile in character, so probably predates K-Ar ages (Late Cretaceous) for metamorphic micas. Thus, top-to-the-east shear here is probably late Mesozoic in age. Because the shear system duplicates strata, it may represent shortening. The shear also placed low-grade rocks on high-grade rocks, but these relations do not require extension because rapid metamorphic facies changes are common within single stratigraphic units in the Pilot Range. Event 3 cannot be dated at this outcrop, but elsewhere along the Pilot Peak detachment fault breccia is cut by granodiorite sills that are only modestly fractured. These relations led Miller and others (1987) to infer that most detachment faulting predated late Eocene dike emplacement.

A scenario for tectonism here is (1) Late Jurassic metamorphism and fabric development caused by local heating adjacent to a pluton during deformation, (2) east-directed low-angle faulting in the Late Cretaceous, and (3) west-directed detachment faulting in the late Eocene.

Proceed downslope to the northeast, aiming slightly down the canyon from the parking spot. The white marble is the Toano Limestone; it overlies the Killian Springs Formation in the ridge to the north, and is exposed near the slope base. Bedding in the white marble strikes northerly at the slope base (as does bedding in the underlying Killian Springs Formation) and turns to an easterly strike farther upslope. Folds in the core of this fold are well exposed.

A number of constraints can be placed on the offset along the detachment fault. The major offset took place at the base of brecciated dolomite, where structural, metamorphic, and stratigraphic contrasts suggest tens of kilometers of offset. Top-to-the-WNW movement is indicated by tilted panels above the fault and by regional sedimentary facies patterns in Cambrian strata: offshore deposits from the west and northwest were structurally emplaced beneath shallow platform deposits.

For an optional continuation of this field trip stop, cross the stream north of the parking area and contour to the first major ridge northeast of Miners Canyon. Follow along the south side of the ridge crest, observing white, leucocratic Jurassic dikes (155-165 Ma by U-Pb) that are moderately deformed but cut foliation in the marble. Folds in the marble are complex, but appear to group into three sets, two of which fold the Jurassic dikes. This relation roughly constrains the onset of ductile deformation to the Late Jurassic. Metamorphism is dated by high-grade minerals in syntectonic fabrics that deform the Jurassic granite and by an approximately 150-Ma cooling $^{40}Ar/^{39}Ar$ date on metamorphic hornblende. Micas in the high-grade rocks cooled to "blocking temperatures" by Cretaceous time.

The last bedrock exposures on this ridge lie in the saddle, where undeformed Tertiary hornblende-biotite granodiorite dikes cut the marble. Float in the eastern part of the saddle suggests that rocks typical of the detachment fault are present: blocks of phyllitic rocks of the Toano Limestone and a few patches of brown sandstone and siltstone of the Killian Springs Formation. Nearby to the east, the Ordovician Garden City Formation of the upper plate is exposed in a prospect pit. To the northeast, these structural relations can be clearly seen in a ridge about 1 km in the distance: marble is structurally beneath the brown Garden City Formation along a gently east-dipping fault. Reactivation of the detachment as a range-bounding fault during Miocene time is probable because this fault is oriented at right angles to the detachment fault. Walk south to the cottonwood grove in Miners Canyon and up the canyon to the vehicles.

4.2 55.9 Turn right on graded road.

12.1 68.0 Bear right at road junction in Leppy Pass.

3.1 71.1 Turn right on to paved road.

1.2 72.3 Enter I-80 west-bound. We drive again through road cuts north of Wendover that display the typical brittle response of massive limestone to extensional faulting: solution breccia and complex closely spaced faults.

7.1 79.4 Just west of Wendover, we drive through road cuts of tilted 12-Ma rhyolite that unconformably overlies tilted Permian strata. Cut into, and deposited near the western exposures of, the rhyolite are exceptionally well developed wave abrasion platforms and gravel bars from Pleistocene Lake Bonneville.

West of Wendover, we approach and cross the Toano Range. Silver Zone Pass, utilized by the highway and a railroad, is underlain by a large Jurassic (about 162 Ma, J.E. Wright, personal commun.) hornblende-biotite granodiorite pluton. It intruded and contact metamorphosed previously regionally metamorphosed Cambrian strata correlative with those we examined beneath the Pilot Peak detachment at Miners Canyon. Weak fabric in the Cambrian rocks distant from the pluton is discordant to, and overprinted by, a strong foliation adjacent to the pluton. These relations led Glick (1987) to propose a regional Jurassic metamorphism and deformation in the Cambrian strata.

North of Silver Zone Pass, in this part of the Toano Range, Glick (1987) showed that Upper Cambrian and younger strata that are essentially unmetamorphosed rest structurally on metamorphosed Middle and Lower Cambrian strata in a relation much like that of the Pilot Peak detachment. South of the pass, the metamorphosed sequence includes rocks as young as Middle Ordovician and is structurally juxtaposed with overlying Devonian(?) rocks. Gross similarities in structure and stratigraphy suggest that the Toano Range occupied a position close to the Pilot Range prior to late Cenozoic extension.

13.6 93.0 Roadcuts expose highly foliated Cambrian marble adjacent to the Silver Zone Pass pluton. Foliation is steep and parallel to the pluton margin. Spectacular examples of chocolate-tablet boudinage exist.

2.7 95.7 Roadcuts expose the hornblende-biotite granodiorite that makes up the pluton. It is undeformed, contains common xenoliths, and in this exposure is cut by several steep mafic dikes.

4.2 99.9 **STOP 3** (Fig. 1; OPTIONAL). Shafter exit. Poorly exposed road cuts are in lacustrine and fluvial strata of Miocene age. North of the highway are dark-colored hills underlain by 13-Ma topaz-bearing rhyolite flows.

OPTIONAL STOP. Cross the overpass to the south side of Interstate 80. Proceed east on frontage gravel road for 3.5 miles, crossing the railroad, to a poorly marked intersection on the right. Take that road *(WARNING: high-clearance vehicles only!)* to the south, climbing up an alluvial fan about 1.3 mi to a narrow canyon mouth. Park here and examine strong fabrics in the Middle Cambrian Cliffside Limestone next to the intrusive contact with the Silver Zone Pass pluton. This zone of highly deformed marble, which continues eastward adjacent to the pluton for 4 km, contrasts sharply with the undeformed granodiorite and with only slightly foliated limestone present at distances greater than about 1 km from the pluton. The highly foliated marble is axial planar to an overturned anticline that faces the pluton margin. Proximity to the pluton suggests that deformation was caused by pluton emplacement, in much the same manner as deformation described in the Silver Island Mountains (Miller and Allmendinger, 1991).

Return to Shafter exit. At Shafter exit we have an excellent view of the Pequop Mountains and Goshute Valley. If you look to the south, at about 9:00, the trace of the Independence thrust is visible. The trace of the thrust lies approximately at the base of the tree-covered slopes. In this locality, hanging wall rocks consist of metamorphosed Ordovician rocks of the Pogonip Group and footwall rocks (barren slopes) consist of unmetamorphosed Mississippian Chainman Shale and Diamond Peak Formation (See Fig. 1 in Camilleri [this volume] for a geologic map of the Pequop Mountains).

Proceed west on Interstate 80 to Wells. As we cross the Pequop Mountains we will drive down-section through Devonian to Pennsylvanian carbonate and siliciclastic rocks. These rocks comprise part of the hanging wall of the Independence thrust (see Fig. 1 in Camilleri [this volume]).

11.1 111.0 Barren reddish brown slopes on both sides of the freeway are composed of the undivided Chainman Shale and Diamond Peak Formation.

1.9 112.9 Tree covered slopes at 9:00 comprise the Mississippian Tripon Pass Limestone.

2.3 115.2 On both sides of the freeway gray, cliff-forming limestone of the Devonian Guilmette Formation is exposed.

1.7 116.9 Independence Valley and the Wood Hills are straight ahead.

7.6 124.5 High peaks immediately to the south are composed of metamorphosed rocks of the Devonian Guilmette Formation.

2.0 126.5 Low-lying hills immediately to the south of the freeway are composed of Miocene (Thorman et al., 1990) clastic and volcaniclastic strata (see Fig. 1 in Camilleri [this volume]). Bedding within these rocks, although not visible from this vantage point, dips around 25-35° east. These rocks consist of volcaniclastic strata, sandstone, siltstone, and conglomerate. Clasts consist of unmetamorphosed upper Paleozoic rocks. This sequence also contains "room-" to "house"-sized clasts of unmetamorphosed Pennsylvanian(?) and Permian(?) limestone. The contact between the Miocene rocks and regionally metamorphosed rocks within the Wood Hills is not exposed. Thorman et al. (1990) suggested that the Miocene rocks, like other Miocene rocks within the region, are in low-angle normal fault contact with the metamorphosed rocks.

0.8 127.3 East-dipping Tertiary strata are exposed in the roadcut on the south side of the freeway.

4.8 132.1 Unmetamorphosed Permian strata are exposed immediately to the south. These rocks lie in low-angle normal fault contact above the metamorphosed sequence in the Wood Hills (see Fig. 1 in Camilleri [this volume]).

1.6 133.7 Take second Wells exit. Arrive in Wells.

DAY 3: ROAD LOG TO THE WOOD HILLS PEQUOP MOUNTAINS, CLOVER HILL AND NORTHERN EAST HUMBOLDT RANGE, NEVADA

by
Phyllis A. Camilleri and Arthur W. Snoke

Today we will discuss and observe elements of the Mesozoic tectonic history of the East Humboldt Range, Wood Hills, and Pequop Mountains. This region experienced two main phases of Mesozoic contractile deformation (for details see Camilleri [this volume] and Snoke [this volume]).

Metamorphosed miogeoclinal strata in East Humboldt Range, Wood Hills, and Pequop Mountains are inferred to have comprised a NW-dipping footwall to a Late Jurassic(?) top-to-the-SSE ductile decollement in Mississippian limestone, the Little Lake decollement (Fig. 1). Footwall rocks were buried to perhaps as much as 26 km in excess of stratigraphic depths in the northern East Humboldt Range and to at least 10 km in excess of stratigraphic depths in the Wood Hills, and footwall rocks in the Pequop Mountains represent an even higher structural level. Metamorphic grade increases with structural depth of the footwall and dies out up section in the Pequop Mountains. Regional metamorphism is interpreted to be a product of tectonic burial coupled with igneous intrusion in the deeper structural levels. Metamorphosed footwall rocks were deformed into a prograde metamorphic L-S to S (S_1 and L_1) tectonite and attenuated synchronously with fabric development. The amount of attenuation of stratigraphic units increases with structural depth in concert with metamorphic grade.

The second phase of deformation involved Late Jurassic or Cretaceous SE-directed thrusting and associated back-folding and back-thrusting, which overprints metamorphic fabrics formed during the first event. Probable structures of this event occur in all three ranges: (1) the Independence thrust in the Pequop Mountains and NW-directed back-folds and back-thrusts in the Wood Hills and Pequop Mountains, and (2) the southward-closing Winchell Lake fold-nappe in the East Humboldt Range. The character of phase 2 structures somewhat reflects increasing temperature and pressure from east to west. Structures in the Pequop Mountains have associated brittle fault rock and folds are generally upright and tend to be kink-like in geometry. In contrast, folds in the southern Wood Hills are asymmetric and overturned and in the central, structurally deeper part of the Wood Hills, folds are recumbent. In the East Humboldt Range, the Winchell Lake fold-nappe is also recumbent but much more tightly appressed.

In the Wood Hills and East Humboldt Range we will observe attenuated stratigraphic section, the L-S tectonite, and kyanite-bearing schists developed during the first event. We will also view the Little Lake decollement, and observe overprinting relationships of phase 1 and 2 structures and fabrics. We will view the Independence thrust in the Pequop Mountains, an overturned back-fold in the Wood Hills, and the Winchell Lake fold-nappe.

MILEAGE Incremental	Cumulative	DESCRIPTION
0.0	0.0	The road log begins at the intersection of U.S. Highway 93 and Interstate 80 in Wells, Nevada. Proceed south on Highway 93.
		The hills immediately to the east consist of unmetamorphosed Devonian to Permian strata that are in low-angle normal fault contact above the upper amphibolite facies metamorphic terrain in the Wood Hills (see Camilleri, this volume, Fig. 1).
		To the right at about 2:00 is "Clover Hill", which is the site of Stop 5 (Fig. 12).

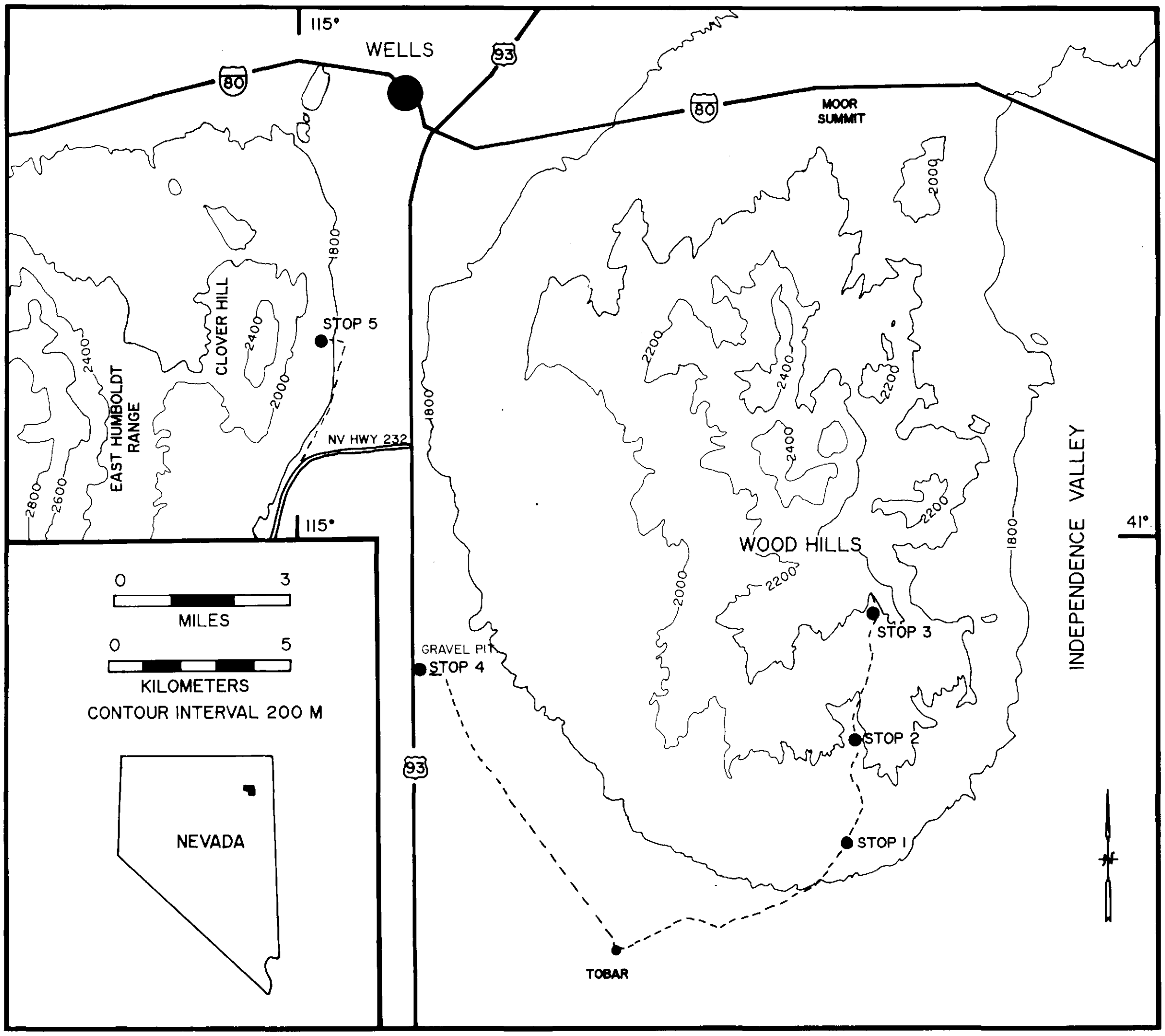

Figure 12. Map showing location of day 3 field trip stops.

4.2 4.2 To the east the metamorphic sequence of the Wood Hills is exposed.

3.9 8.1 Turn left onto dirt road at the gravel pit. Cross over the cattle guard and take the road that veers to the right.

The hills straight ahead consist of metamorphosed Ordovician rocks of the Pogonip Group.

0.7 8.7 Dirt road bifurcates at the railroad tracks. Turn right and proceed south.

1.6 10.3 At 1:00 is Spruce Mountain. The highest peak on Spruce Mountain is 10,076 ft high and is composed of low-grade metamorphosed Ordovician strata of the Pogonip Group (Hope, 1972). The low-lying ridge or prong of Spruce Mountain extending to the north is composed of unmetamorphosed Pennsylvanian and Permian strata intruded by a Mesozoic or Tertiary hornblende diorite pluton (Hope, 1972).

3.8 14.1 Dirt road bifurcates. Take road to the left towards Warm Springs.

0.9 14.3 Cross railroad tracks. Immediately after crossing the tracks there are four dirt roads. Take the third road from the railroad tracks on your right (or second road from the tracks on your left).

1.4 15.7 The Pequop Mountains are straight ahead.

2.0 17.7 Turn left on dirt road that heads towards the southern Wood Hills.

1.0 18.7 **STOP 1** (Figs. 12 and 13).

Overview of the structures and fabrics in the Wood Hills and Pequop Mountains.

Pequop Mountains. From this point we can observe two major Mesozoic contractile structures in the northern Pequop Mountains: the Independence thrust and the Little Lake decollement (Fig. 1 and 2; see also Fig. 1 in Camilleri [this volume]). The approximate trace of the Independence thrust can be delineated by observing the truncation of footwall strata, in particular the Ordovician Eureka Quartzite, which appears as a prominent white band. At the point of truncation, the Cambrian Dunderberg Shale [phyllite] structurally overlies the Eureka Quartzite. Nearly the entire Paleozoic section is exposed in the footwall of the Independence thrust. The stratigraphically lowest unit is the upper part of the basal Cambrian Prospect Mountain Quartzite and the stratigraphically highest (from this vantage point) is the Mississippian Chainman Shale, which underlies the barren slopes at the crest of the range.

The Independence thrust cuts an earlier metamorphic strain gradient within the Paleozoic section (see Fig. 1 in Camilleri [this volume]) in both its hanging wall and footwall. The stratigraphically lowest rocks were deformed and metamorphosed to form a lower amphibolite to greenschist facies prograde L-S to S (S_1 and L_1) tectonite in which foliation is nearly parallel to, or at a low-angle to, stratigraphic boundaries. Metamorphism and strain die out stratigraphically upward: Upper Ordovician or Silurian and younger rocks are unmetamorphosed and generally lack strain features. This transition occurs just above the level of the Eureka Quartzite. However, silty limestone of the Devonian Guilmette Formation (the cliff-forming limestone beneath the barren slopes of the Chainman Shale) in a few places contains a related moderate to weak cleavage. Because metamorphic facies boundaries are more or less parallel to stratigraphic boundaries, the Independence thrust juxtaposes more metamorphosed rocks over less metamorphosed rocks near the base of the range. In contrast, near the range crest the thrust juxtaposed metamorphosed rocks on top of unmetamorphosed rocks. At the range crest, metamorphosed Lower Ordovician strata of the Pogonip Group lie structurally above unmetamorphosed rocks of the Mississippian Chainman Shale.

Between the Chainman Shale and the Guilmette Formation in the footwall of the Independence thrust is the Little Lake decollement (Figs. 1 and 2). The Independence thrust cuts the decollement (Figs. 1 and 2). The decollement occurs within the Mississippian Joana Limestone and is marked by a prominent white band of mylonitized limestone that contrasts with the original dark to medium gray color of the Joana Limestone. Although most of the Joana Limestone is deformed, in a few places undeformed rocks of the Joana Limestone crop out as gray blocky material above the white mylonite zone and below the Chainman Shale. The mylonite zone varies in thickness from a few meters to a few tens of meters. Stretching lineations within the mylonite dominantly trend SSE.

Wood Hills. Looking to the north in the Wood Hills, we can see southeast-dipping gray Ordovician to Devonian dolomite. These rocks constitute part of the upright limb of a NW-vergent overturned anticline (Fig. 13; see also Figs. 1 and 5 in Camilleri [this volume]). The pre-folding structure and fabric of the southernmost Wood Hills resemble that of the Pequop Mountains in that (1) metamorphic grade decreases upsection, and (2) the penetrative metamorphic fabric (S_1 and L_1) dies out upsection. In the southern Wood Hills Silurian and Devonian dolomite contain no calc-silicate minerals and are generally unstrained. However, towards the center of the range these rocks contain a strong penetrative metamorphic fabric and contain abundant calc-silicate minerals.

Return to vans. Proceed north on dirt road.

0.8 19.5 On the left or east side of the canyon is the basal sandy (quartzose) dolostone of the Simonson Dolomite. Although the rocks are metamorphosed they lack a penetrative metamorphic fabric and upon close inspection cross-bedding is visible. As we proceed up the canyon from south to north we will traverse down-section through Ordovician to Devonian dolostone. Degree of recrystallization of dolomite and of fabric development increases down-section such that Ordovician and Silurian dolomite is a fine-grained marble and contains a well devel-

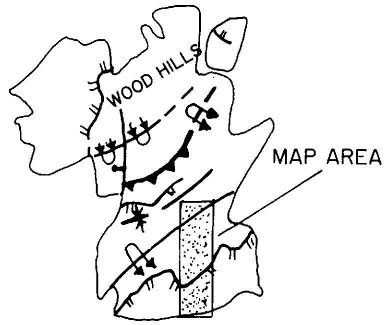

EXPLANATION

Qs	Surficial deposits (Quaternary) alluvium and colluvium	
DSOd	Fish Haven, Laketown, Sevy, and Simonson Dolomite (Ord., Sil., and Dev.) dolomitic marble and dolostone; sandy dolostone near the base of the Simonson Dolomite	
Oe	Eureka Quartzite (Ordovician)	
Opl	Lehman Formation (Ordovician) micaceous calcite marble	POGONIP GROUP
Opc	Unit C (Ordovician) phyllite or schist near the top (= Kanosh Shale), micaceous calcite marble in the middle, and ~ 50' thick quartzite at the base	POGONIP GROUP
Opb	Unit B (Ordovician) micaceous calcite marble and calcite marble with minor phyllite or schist	POGONIP GROUP
Opa	Unit A (Ordovician) cherty, micaceous calcite marble	POGONIP GROUP
Ꞓnp	Notch Peak Formation (Cambrian) cherty calcite marble and calcite marble with dolomite marble and cherty dolomite marble near the top	POGONIP GROUP
Ꞓu	Dunderberg Shale, Oasis and Shafter Formations undifferentiated (Cambrian) schist with minor micaceous calcite marble near the top (= Dunderberg Shale]; calcite marble, micaceous calcite marble, and minor dolomitic marble (= Oasis and Shafter Formations undifferentiated)	
	High-angle normal fault	
	Low-angle fault	
	Axis of overturned anticline	
24	Strike and dip of S_1	
17	Trend and plunge of stretching lineation (L_1)	

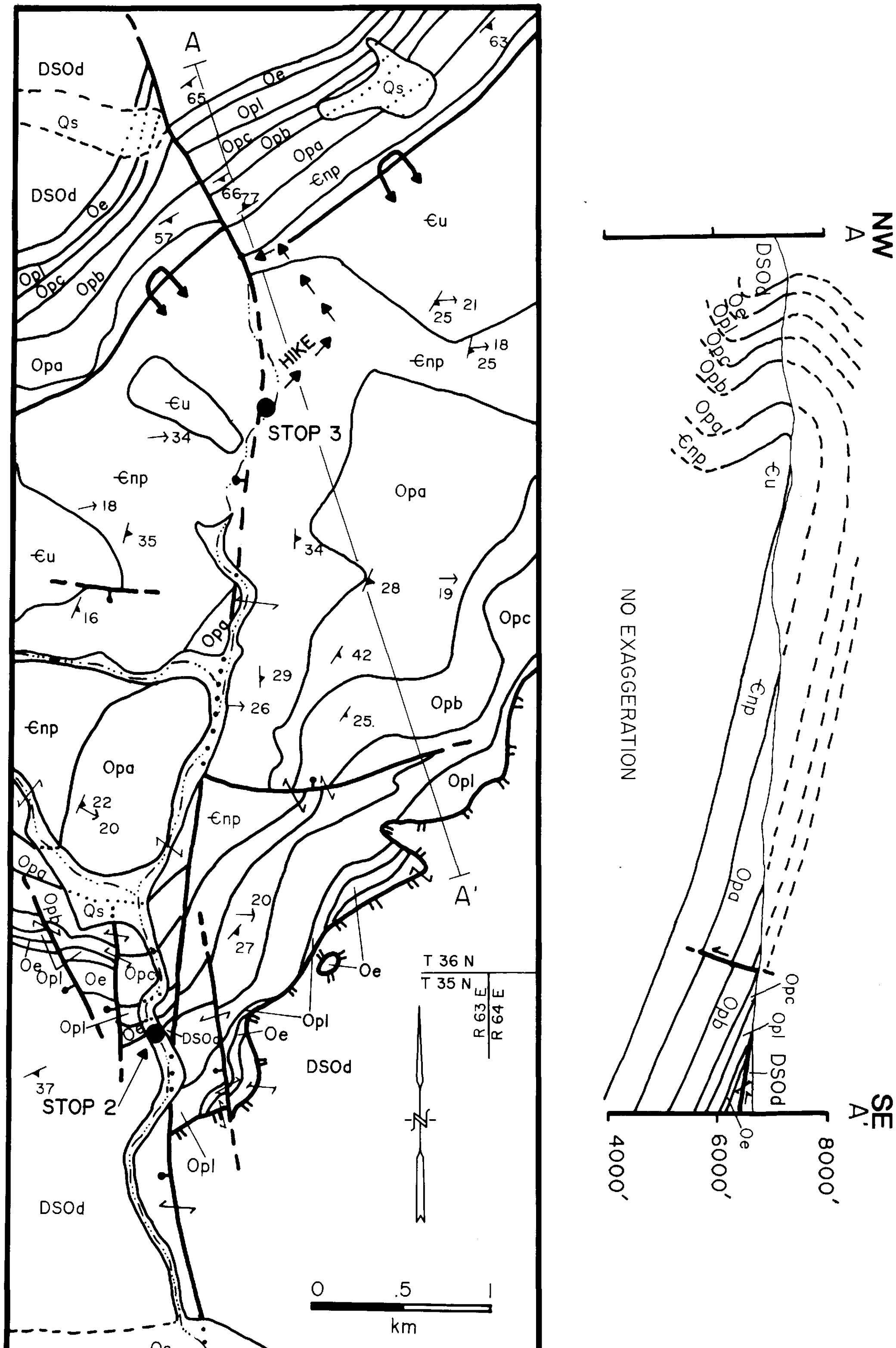

Figure 13. Geologic map and cross section of a part of the southern Wood Hills. Data from P. A. Camilleri (unpublished mapping).

oped bedding-parallel cleavage or foliation.

1.1 20.6 **STOP 2** (Figs. 12 and 13). Park on dirt road. On this stop we will observe the prograde metamorphic L-S tectonite in Ordovician rocks. On the east side of the canyon, foliated and lineated rocks of the Ordovician Lehman Formation, Eureka Quartzite, and Fish Haven Dolomite are exposed. From here we can see that foliation is approximately parallel to stratigraphic boundaries and we can observe a complete but plastically attenuated section of the Eureka Quartzite. Here, the Eureka Quartzite is approximately 75′ thick, whereas regionally the Eureka Quartzite is generally 200′ thick or greater.

Hike up the hillside to observe S_1 fabric elements. At the base of the hill, fine-grained micaceous marble of the Lehman Formation is exposed. Foliation dips about 30 degrees to the southeast and pronounced stretching lineations and approximately 23 degrees to the east-southeast. The overlying Eureka Quartzite has a well developed foliation, but lineation is less well pronounced. The Fish Haven Dolomite consists of dark gray dolostone with chert lenses and abundant tiny pelmatozoan fragments and has a strong bedding-parallel foliation. Stretching lineations are poorly developed and are generally only visible on chert lenses.

Return to vans. Proceed north on dirt road.

2.3 22.9 **STOP 3** (Figs. 12 and 13).
Park on the side of the dirt road. At this stop we will hike up into the Dunderberg Shale [schist] in the core of the northwest-vergent overturned anticline (Fig. 13). We will observe the overprinting effects of the fold on S_1. Bring lunch and water.

Hike up the hillside to the north-trending ridge on the east side of the canyon (Fig. 13). Near the base of the hill, micaceous cherty marble of the basal part of the Cambrian Notch Peak Formation is exposed. Further up the hill we will see evidence of transposition of bedding, as indicated by small-scale isoclines, within S_1 in outcrop and float. Once on top of the ridge proceed north through the Notch Peak Formation and stop at the outcrop immediately before descending into the saddle on the ridge. In this area, calcite marble contains a moderate to strong axial-planar grain-shape foliation ("S_2") that overprints S_1 (compositional layering). Cleavage or foliation (S_2) related to the northwest-vergent folds is generally restricted to the vicinity of the fold axis. Descend into the saddle where the Upper Cambrian Dunderberg Shale [schist] is exposed. On the northern slope of the saddle the Notch Peak Formation is exposed again in the overturned limb of the anticline.

The Dunderberg Shale contains porphyroblastic garnet, staurolite, kyanite, and biotite. The general metamorphic mineral assemblage is biotite-staurolite-kyanite-garnet-muscovite-quartz-plagioclase-allanite-rutile-ilmenite. Geothermobarometric analysis of this assemblage yields burial depths of around 18 to 24 km (Hodges et al., in press). This is a minimum of about 10 km in excess of probable Mesozoic stratigraphic depths (Camilleri, this volume).

An L-S tectonite in the Dunderberg Shale [schist] is largely overprinted by a L-tectonite fabric resulting from constrictional strain in the core of the anticline. Stretched biotite porphyroblasts define the stretching lineation. In thin sections cut parallel to lineation, biotite contains symmetrical recrystallized tails, whereas in thin sections cut perpendicular to lineation, deformation and rotation of porphyroblasts and crenulation of S_1 is evident.

Eat lunch. Proceed due west down the hill from the saddle. Intersect dirt road and proceed south on the road back to the vans. Return, exactly the way we came, to the intersection of Highway 93 and the dirt road adjacent to the gravel pit.

14.6 37.5 Arrive at Highway 93. **STOP 4** (Fig. 12). From this locality we have an excellent overall view of the east face of the East Humboldt Range, Clover Valley, Signal Hill (about N65W from present locality), and "Clover Hill" (about N25W from present locality and the site of STOP 5). The large cirque directly ahead is Lizzie's Basin (about S80W from present locality) where the deepest structural level in the East Humboldt Range is exposed (Fig. 14). Farther northward along the East Humboldt Range we can see the Winchell Lake fold-nappe (about N80W from present locality; Fig. 15). This fold-nappe is cored by a Precambrian gneissic complex consisting of Late Archean biotite monzogranitic orthogneiss (Lush et al., 1988) and Early Proterozoic (?) pelitic to quartzitic paragneisses. Recent geochronometric studies (J.E. Wright, 1991, unpublished data)

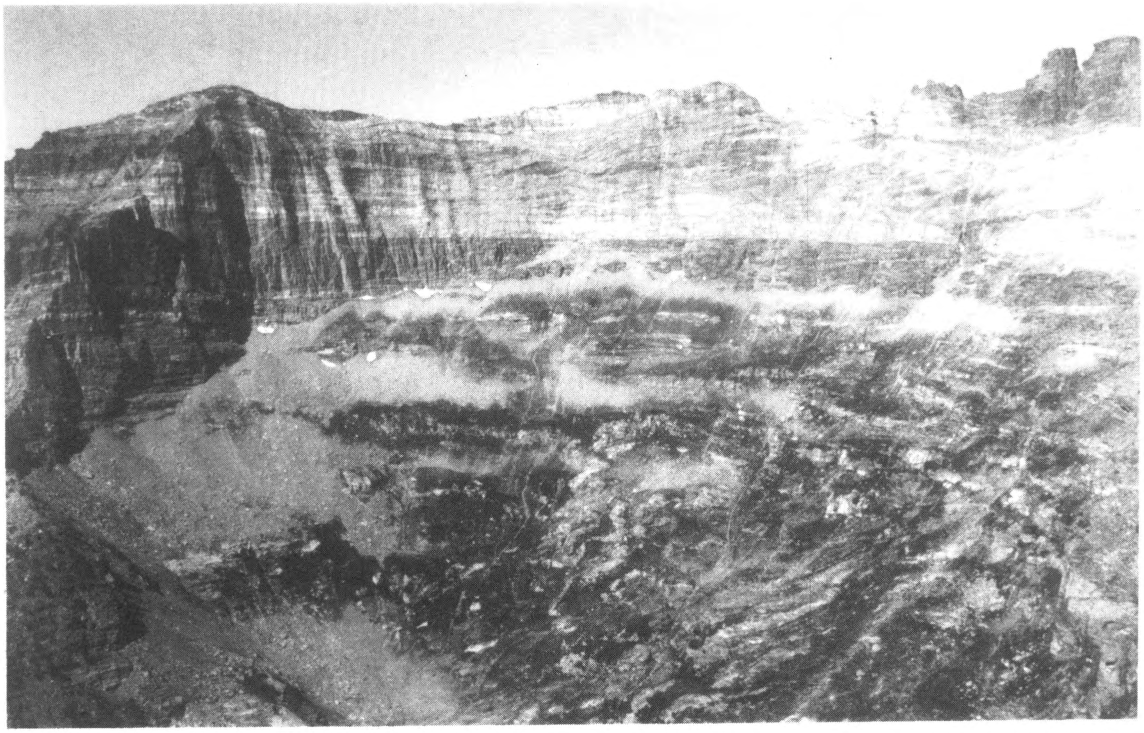

Figure 14. Variably mylonitic, WNW-lineated metasedimentary rocks-gneiss domain, west wall of Lizzie's Basin cirque, central East Humboldt Range; hqd = hornblende-biotite quartz diorite orthogneiss, lg = pegmatitic leucogranite, DЄmu = Cambrian to Devonian metacarbonate rocks, Tmg = Tertiary biotite monzogranitic orthogneiss. Photograph by A. W. Snoke, sketch by Phyllis A. Ranz.

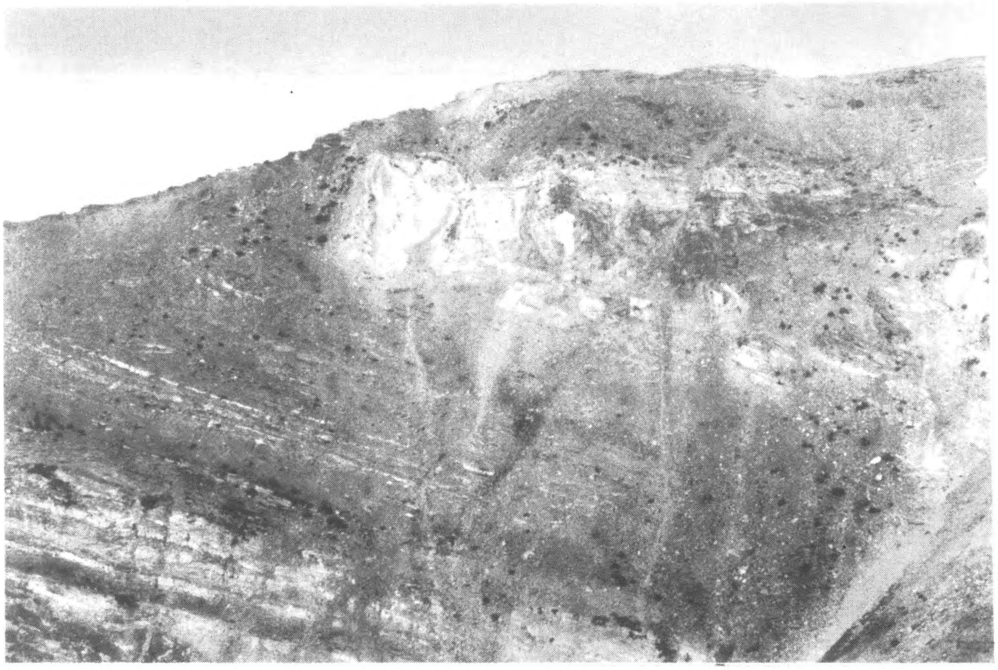

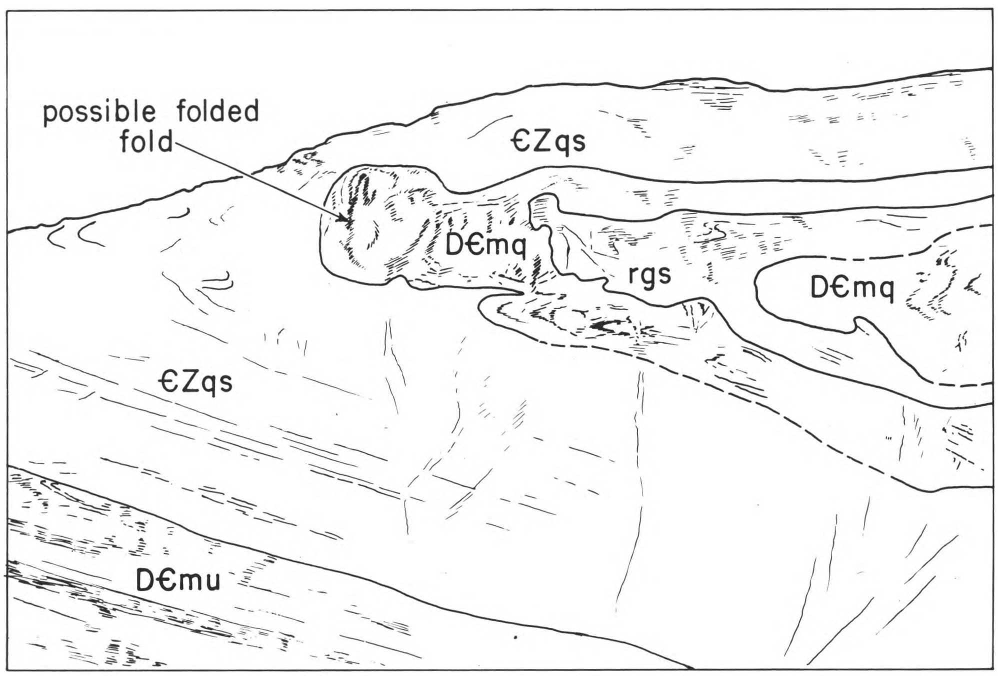

Figure 15. Hinge zone of the Winchell Lake fold-nappe as exposed along the back wall of Winchell Lake cirque on the eastern face of the northern East Humboldt Range. The core of the fold at this locality consists of dark outcrops of rusty-weathering graphitic paragneiss surrounded by white-weathering Cambrian and Ordovician marble and Ordovician metaquartzite. Enveloping the fold is a thick sequence of Late Proterozoic and Lower Cambrian flaggy quartzite and schist. These metasedimentary rocks, particularly the metaclastic units, all contain abundant sheet-like bodies of leucogranitic orthogneiss. The hingeline of this major structure trends WNW, approximately parallel to mineral elongation lineations in the deformed rocks. Closure is to the south. To the north, the fold is cored by Archean and Early Proterozoic gneisses, and a pre-folding low-angle fault is inferred to separate the metasedimentary rocks shown in this photograph from the basement complex enclosed in the core of the fold. €Zqs = Cambrian and Late Precambrian quartzite and schist, rgs = rusty-weathering graphitic schist, D€mq = Cambrian to Devonian metacarbonate rocks and quartzite. D€mu = Cambrian to Devonian metacarbonate rocks. Photograph by A. W. Snoke, sketch by Phyllis A. Ranz.

coupled with detailed geologic mapping (A. J. McGrew, work in progress) suggest that the Winchell Lake fold-nappe evolved in the Late Cretaceous. The fold-nappe was subsequently flattened and attenuated during the development of an Oligocene mylonitic shear zone.

From this vantage point, we can also see a portion of the road that switchbacks up to Angel Lake in the northern East Humboldt Range. At Angel Lake, both the core of the Winchell Lake fold-nappe and the upper and lower limbs of the foldnappe, consisting of metamorphosed Paleozoic sedimentary rocks intruded by abundant granitic rocks, are well exposed. The upper limb of the fold-nappe is strongly overprinted and thinned by the Oligocene mylonitic shear zone.

The low range east of the East Humboldt Range includes Signal Hill and "Clover Hill", part of a composite hanging wall that has been downdropped with respect to the main East Humboldt Range (see Figs. 2, 3, and 4 in Snoke [this volume]). "Clover Hill" has a complex criss-crossing road system on its east face related to mining activity (see Lipten, 1984, for details). Signal Hill and the tree-covered part of Clover Hill are underlain chiefly by unmetamorphosed middle Paleozoic carbonate rocks (Guilmette Formation and Silurian and Devonian dolomite), although Lush (1982) mapped some exposures of the Pilot Shale on the east side of Signal Hill. These middle Paleozoic sedimentary rocks are in low-angle normal (?) fault contact with a lower plate of chiefly lower amphibolite-facies, impure calcite marble of Cambrian and Ordovician protoliths. The low reddish exposures between the East Humboldt Range and Signal Hill are Miocene quartz porphyry rhyolite.

1.6 39.1 Railroad crossing.

2.2 41.3 Intersection on the left with Nevada 232 (Clover Valley Road). Turn left onto this road.

0.65 41.95 Cross railroad tracks.

1.25 43.2 Intersection with Clover Hill access road. Turn right onto this road.

0.15 43.35 Gate. At times, this gate has been padlocked, thus you may have to seek permission (and a key) from the local ranch leasing Southern Pacific Railroad lands (presently the Mike Bush Ranch in Clover Valley). Note: Access to Clover Hill can also be made from the north via Wells. Start at Sixth St. and Shoshone Avenue and go due south on Shoshone Avenue; you will cross several fence lines, and the gates are typically closed but not locked. In the past, the land has not been posted, but it is checkerboard land with ownership alternating between the Southern Pacific Land Company and Bureau of Land Management.

0.8 44.15 Road to mine area on left, continue straight.

0.85 45.0 A dirt road angles off to the left, continue straight.

0.45 45.45 Road intersection on left, turn left onto this road and drive toward the range front.

0.2 45.65 Pass small corral on left, follow road toward range front.

0.25 45.9 **STOP 5** (Fig. 12). Fence line. The road leads into a small pasture associated with a range front spring. Either drive forward a short distance and park or park off the road outside the fence (probably the best option if there are cows in the pasture).

This stop is a traverse up the east face of Clover Hill; it consists of four specific localities (A-D) and involves about 1400 feet of vertical climb (see Fig 3 in Snoke [this volume]). Some of you may not want to take in the complete climb, but we urge you to visit sites A, B, and C. Float blocks derived from site D are visible along the lower part of the traverse, thereby eliminating the need for a direct examination of the exposures. We will begin our traverse by walking west upslope to a series of low outcrops (locality A) that expose various phases of the gneissic complex of Clover Hill which includes Archean rocks. The rock types in these exposures are Tertiary(?) medium-grained biotite monzogranitic orthogneiss, pin-striped augen orthogneiss (Late Archean?), and pegmatitic leucogranite (age uncertain). Compositional layering in the pin-striped augen orthogneiss is locally folded and in turn was intruded by discordant but internally deformed Tertiary orthogneiss. Similar orthogneiss collected near Angel Lake has been dated by U-Th-Pb techniques as 29 ± 1 Ma (J.E. Wright, unpublished data).

After you have examined the various relationships exposed at locality A, head toward the prominent rocky knob (locality B) about a third of the way up the east face of Clover Hill. You must cross a gully and walk on the next ridge to the north from locality A to reach locality B (see Fig. 3 in Snoke [this volume] for approximate relative location). At the base of locality B and throughout much of this exposure are rocks of the gneissic complex, but at the top of the exposure are flaggy, micaceous quartzites which include pale green fuchsitic quartzite. Thus, we cross a deformed, metamorphosed, locally intruded unconformity between Early(?) Proterozoic quartzite and schist and the gneissic complex. Note that fabrics in these flaggy quartzites probably result from strong Tertiary plastic deformation associated with the shear zone deformation, locally present in the metamorphic complex of Clover Hill.

We continue to traverse uphill toward locality C, crossing the poorly exposed Early(?) Proterozoic sequence, consisting chiefly of migmatitic quartzite and schist, but including probable infolds of the gneissic complex. We climb to the upper part of Clover Hill (stay on the same ridge that exposes the fuchsitic quartzite) and head toward a group of angular-appearing outcrops (locality C). Before we get to these outcrops, we will cross a pre-folding, low-angle fault that separates the underlying Early(?) Proterozoic sequence from lower and middle Paleozoic metacarbonate rocks (unit D€mu on Fig. 3 in Snoke, this volume). These metacarbonate rocks form a highly attenuated, recumbent syncline sandwiched between quartzite and schist sequences above and below. In the midst of these metacarbonate rocks is a lenticular mass (tectonic inclusion) of very deformed (mylonitic) quartzite and quartzose metaconglomerate. Could these rocks be the metamorphosed equivalents of the Pennsylvanian and Mississippian clastic rocks that are common in northeastern Nevada?

If you wish to visit locality D, you must climb an additional 300 feet vertically. Please see Fig. 3 in Snoke (this volume) for the suggested route. As we climb toward locality D, we will cross a low-angle fault that separates mylonitic and migmatitic Late Proterozoic and Cambrian quartzite and schist from the underlying metacarbonate rocks. This low-angle fault is probably a Tertiary feature superimposed on the upper limb of the Winchell Lake fold-nappe. Included in the Proterozoic and Cambrian sequence is pelitic schist correlated with unit G of the McCoy Creek Group of Misch and Hazzard (1962). This pelitic schist, well exposed at locality D, contains the mineral assemblage: kyanite-sillimanite-garnet-plagioclase-biotite-muscovite-ilmenite-rutile. Geothermobarometric data (GARB-GASP) from this locality indicate approximately T = 625° and P = 5 kb for final equilibration, although the presence of relic GRAIL mineral phases suggests significant decompression prior to this equilibration (sample locality 1-15-17; Hodges et al., in press). The schist bears a strong WNW-ESE Tertiary (?) lineation. Many kyanite crystals are oriented subparallel to this lineation, but importantly some are not aligned. Hornblende from a quartz dioritic orthogneiss closely associated with kyanite-rich pelitic schist at a locality approximately 1.25 km northeast was analyzed by $^{40}Ar/^{39}Ar$ techniques. Results suggest that the kyanite-grade metamorphism predated 128 Ma (sample H16, Dallmeyer et al., 1986). Textural data suggest two distinct phases of aluminosilicate growth; kyanite is prekinematic to the main phase foliation whereas sparse sillimanite is synkinematic (Hodges et al., in press). Subsequently, this Mesozoic metamorphic history was overprinted by a strong middle Tertiary mylonitic deformation. The fabric of most of the metamorphic rocks exposed on Clover Hill is a composite of these two superposed deformations.

Return to your vehicle and backtrack to the main dirt road (about 0.45 miles). At this point, turn right and drive to the gate (about 2.1 miles) and eventually to Nevada 232 (0.15 miles more). At this intersection, turn left and drive to U.S. Highway 93 (1.9 miles). To reach Wells, Nevada (about 5.5 miles to the north), turn left.

REFERENCES CITED

Allmendinger, R.W., in press, Thrust and fold tectonics of the western United States, exclusive of the accreted terranes, *in* Burchfiel, B. C., Lipman, P., and Zoback, M. L., eds., The Cordilleran orogen: Boulder Colorado, Geological Society of America, v. G 3.

Allmendinger, R.W., and Jordan, T.E., 1984, Mesozoic structure of the Newfoundland Mountains, Utah: Horizontal shortening and subsequent extension in the hinterland of the Sevier belt: Geological Society of America Bulletin, v. 95, p. 1280-1292.

Allmendinger, R. W., Miller, D. M., and Jordan, T. E., 1984, Known and inferred Mesozoic deformation in the hinterland of the Sevier belt, northwest Utah, *in* Kerns, J.G., and Kerns, R. L., Jr., eds., Geology of northwest Utah, southern Idaho, and northeast Nevada: Utah Geological Association Publication 13, p. 21-34.

Armstrong, F. C., and Oriel, S. S., 1965, Tectonic development of the Idaho-Wyoming thrust belt: American Association of Petroleum Geologist Bulletin, v. 49, p. 1847-1866.

Armstrong, R. L., and Hansen, E., 1966, Cordilleran infrastructure in the eastern Great Basin: American Journal of Science, v. 264, p. 112-127.

Armstong, R. L. 1972, Low-angle (denudation) faults, hinterland of the Sevier orogenic belt, eastern Nevada and wester Utah: Geological Society of America Bulletin: v. 83, p. 1729-1754.

Bartley, J. M., and Gleason, G., 1990, Tertiary normal faults superimposed on Mesozoic thrusts, Quinn Canyon and Grant Ranges, Nye County, Nevada: Geological Society of America Memoir 176, p. 195-212.

Bartley, J. M., and Taylor, W. J., 1991, Central Nevada thrust belt formed in the Jurassic Elko orogeny?: Geological Society of America Abstracts with Programs, v. 23, p. A192.

Burchfiel, B. C., and Royden L. H., 1985, North-south extension within the convergent Himalyan region: Geology, v. 13, p. 679-682.

Camilleri, P. A., 1988, Superposed compressional and extensional strain in metamorphosed lower Paleozoic rocks of the northwestern Grant Range, Nevada [M.S. thesis]: Corvallis, Oregon, Oregon State University, 84 p.

Compton, R. R., 1972, Geologic map of Yost quadrangle, Box Elder County, Utah, and Cassia County, Idaho: U. S. Geological Survey, Miscellaneous Geologic Investigations Map I-672.

Compton, R. R., 1975, Geologic map of Park Valley quadrangle, Box Elder County, Utah, and Cassia County, Idaho: U. S. Geological Survey, Miscellaneous Geologic Investigations Map I-873.

Compton, R.R., 1983, Displaced Miocene rocks on the west flank of the Raft River-Grouse Creek core complex, Utah, *in* Miller, D.M., Todd, V.R., and Howard, K.A., eds., Structural and stratigraphic studies in the eastern Great Basin: Geological Society of America Memoir 157, p. 271-279.

Compton, R.R., Todd, V.R., Zartman, R.E., and Naeser, C.W., 1977, Oligocene and Miocene metamorphism, folding, and low-angle faulting in northwestern Utah: Geological Society of America Bulletin, v. 88, p. 1237-1250.

Covington, H. R., 1983, Structural evolution of the Raft River Basin, Idaho, *in* Miller, D. M., Todd, V. R., and Howard, K. A., eds., Tectonic and stratigraphic studies in the Eastern Great Basin: Geologic Society of America Memoir 157, p. 229-237.

Dallmeyer, R.D., Snoke, A.W., and McKee, E.H., 1986, The Mesozoic-Cenozoic tectonothermal evolution of the Ruby Mountains, East Humboldt Range, Nevada: A Cordilleran metamorphic core complex: Tectonics, v. 5, p. 931-954.

Dalmayrac, B., and Molnar, P., 1981, Parallel thrust and normal faulting in Peru and the constraints on the state of stress: Earth and Planetary Science Letters, v. 55, p. 473-481.

Doelling, H., 1980, Geology and Mineral resources of Box Elder County, Utah: Utah Geologic and Mineral Survey Bulletin 115, 251 p.

Fryxell, J. E., 1988,Geologic map and descriptions of stratigraphy and structure of the west-central Grant Range, Nye County, Nevada: Geological Society of America Map and Chart Series MCH064, 16 p.

Glick, L.L., 1987, Structural geology of the northern Toano Range, Elko County, Nevada [M.S. thesis]: San Jose, California, San Jose State University, 141 p.

Hefner, M. L., Loptien, G. D., and Ohlin, H. N., 1990, Geology and mineralization of the Black Pine Gold Deposit, Cassia County, Idaho, *in* Shaddrick, D. R., Kizis, J. A., and Hunsaker, E. L., eds., Geology and ore deposits of the northeastern Great Basin, Geological Society of Nevada, p. 167-173.

Heller, P. L., Bowdler, S. S., Chambers, H. P., Coogan, J. C., Shuster, M. W., Winslow, N. S., and Lawton, T. F., 1986, Time of initial thrusting in the Sevier orogenic belt, Idaho-Wyoming and Utah: Geology, v. 14, p. 388-391.

Hodges, K.V., Snoke, A.W., and Hurlow, H.A., 1992, Thermal evolution of a portion of the Sevier hinterland: the northern Ruby Mountains-East Humboldt Range and Wood Hills, northeastern Nevada: Tectonics, in press.

Hope, R. A., 1972, Geologic map of the Spruce Mountain quadrangle Elko County, Nevada: U.S. Geological Survey Map GQ-942.

Hudec, M. R., 1990, The structural and thermal evolution of the central Ruby Mountains, Elko County, Nevada [Ph.D. thesis]: Laramie, Wyoming, University of Wyoming, 272 p.

Jordan, T. E., 1983, Structural geometry and sequence, Bovine Mountain, northwestern Utah, *in* Miller, D. M., Todd, V. R., and Howard, K. A., eds., Tectonic and stratigraphic studies in the Eastern Great Basin: Geological Society of America Memoir 157, p. 215-288.

Lipten, E.J.H., 1984, The geology of Clover Hill and classification of the Wells tungsten prospect, Elko County, Nevada [M.S. thesis]: West Lafayette, Indiana, Purdue University, 239 p.

Lush, A.P., 1982, Geology of part of the northern East Humboldt Range, Elko County, Nevada [M.S. thesis]: Columbia, South Carolina, University of South Carolina, 138 p.

Lush, A.P., McGrew, A.J., Snoke, A.W., and Wright, J.E., 1988, Allochthonous Archean basement in the northern East Humboldt Range, Nevada: Geology, v. 16, p. 349-353.

Malavielle, J., 1987, Kinematics of compressional and extensional ductile shearing deformation in a metamorphic core complex of the northeastern Basin and Range: Journal of Structural Geology, v. 9, p. 541-554.

Miller, D.M., 1984, Sedimentary and igneous rocks in the Pilot Range and vicinity, Utah and Nevada, *in* Kerns, G.J. and Kerns, R.L., Jr., eds., Geology of northwest Utah, southern Idaho and northeast Nevada: Utah Geological Association Publication 13, p. 45-63.

Miller, D.M., and Allmendinger, R.W., 1991, Jurassic normal and strike-slip faults at Crater Island, northwestern Utah: Geological Society of America Bulletin, v., 103, p. 1239-1251.

Miller, D.M., and Lush, A.P., 1981, Preliminary geologic map of the Pilot Peak and adjacent quadrangles, Elko County, Nevada, and Box Elder County, Utah: U.S. Geological Survey Open-File Report 81-658, 21 p., 2 sheets, scale 1:24,000.

Miller, D. M., and Lush, A. P., in press, Geologic map of the Pilot Peak quadrangle, Box Elder County, Utah, and Elko County, Nevada: Utah Geological Survey.

Miller, D.M., Hillhouse, W.C., Zartman, R.E., and Lanphere, M.A., 1987, Geochronology of intrusive and metamorphic rocks in the Pilot Range, Utah and Nevada, and comparison with regional patterns: Geological Society of America Bulletin, v. 99, p. 866-879.

Miller, D. M., Repetski, J. E., and Harris, A. G., 1991, East-trending Paleozoic continental margin near Wendover, Utah, *in* Cooper, J. D., and Stevens, C. H., eds., Paleozoic paleogeography of the western United States—II: Society of Economic Paleontologists and Mineralogists, Pacific Section, v. 67, p. 439-461.

Miller, E. L., and Gans, P. B., 1989, Cretaceous crustal structure and metamorphism in the hinterland of the Sevier thrust belt, western U. S. cordillera: Geology, v. 17, p. 59-62.

Misch, P., 1960, Regional structural reconnaissance in central-northeast Nevada and some adjacent areas: observation and interpretation, in Guidebook to the geology of east-central Nevada: Intermountain Association of Petroleum Geologists and Eastern Nevada Geological Society, p. 17-42.

Misch, P., and Hazzard, J. C., 1962, Stratigraphy and metamorphism of the late Precambrian rocks in central northeastern Nevada and adjacent Utah: American Association of Petroleum Geologists Bulletin, v. 46, p. 289-343.

Pease, F. S., 1956, History of exploration for oil and gas in Box Elder County, Utah, and vicinity: Utah Geological Society Guidebook to the Geology of Utah, no. 11, Geology of parts of northwestern Utah, p. 17-31.

Royse, F., Warner, M. A., and Reese, D. L., 1975, Thrust belt structural geometry and related stratigraphic problems, Wyoming-Idaho-northern Utah, *in* Bolyard, D. W., ed, Deep drilling frontiers of the central Rocky Mountains: Denver, Colorado, Rocky Mountain Association of Geologists, p. 41-54.

Sabisky, M. A., 1985, Finite strain, ductile flow, and folding in the central Raft River Mountains, northwestern Utah [M. S. thesis]: Salt Lake City, Utah, University of Utah, 69 p.

Saltzer, S. D., and Hodges, K. V., 1988, The Middle Mountain shear zone, southern Idaho: Kinematic analysis of an early Tertiary high-temperature detachment: Geological Society of America Bulletin, v. 100, p. 96-103.

Schneyer, J.D., 1984, Structural and stratigraphic complexities within an extensional terrain: Examples from the Leppy Hills area, southern Silver Island Mountains, near Wendover, Utah, *in* Kerns, G.J., and Kerns, R.L., Jr., eds., Geology of northwest Utah, southern Idaho and northeast Nevada: Utah Geological Association Publication 13, p. 93-116.

Schneyer, J.D., 1990, Geologic map of the Leppy Peak quadrangle and adjacent area, Elko County, Nevada and Tooele County, Utah: U.S. Geological Survey Miscellaneous Investigations Map 1938, scale 1:24,000.

Selverstone, J., 1988, Evidence for east-west crustal extension in the Eastern Alps: Implications for the unroofing history of the Tauern window: Tectonics, v. 7, p. 87-105.

Smith, J. F., 1982, Geologic Map of the Strevell 15 minute quadrangle, Cassia County, Idaho: U.S. Geological Survey, Map 1-1403.

Smith, J. F., 1983, Paleozoic rocks in the Black Pine Mountains, Cassia County, Idaho: U.S. Geological Survey Bulletin 1536, 36 p.

Snoke, A. W., 1980, The transition from infrastructure to suprastructure in the northern Ruby Mountains, Nevada, *in* Crittenden, M. D., Jr., Coney, P.J., and Davis G. H., eds., Cordilleran metamorphic core complexes: Geological Society of America Memoir 153, p. 287-333.

Snoke, A. W., and Lush, A. P., 1984, Polyphase Mesozoic-Cenozoic deformational history of the Ruby Mountains-East Humboldt Range, Nevada, *in* Lintz, J., Jr., ed., Western geological excursions: Geological Society of America annual meeting field trip guidebook, Mackay School of Mines, Reno, Nevada, v. 4, p. 232-260.

Snoke, A. W., and Miller, D. M., 1988, Metamorphic and tectonic history of the northeastern Great Basin, *in* Ernst, W. G., ed., Metamorphism and crustal evolution of the western United States (Rubey Volume VII): Englewood Cliffs, New Jersey, Prentice Hall, p. 606-648.

Speed, P., Elison, M. W., and Heck, F. R., 1988, Phanerozoic tectonic evolution of the Great Basin, *in* Ernst, W. G., ed., Metamorphism and crustal evolution of the western United States (Rubey Volume VII): Englewood Cliffs, New Jersey, Prentice Hall, p. 572-605.

Stewart, J. H., 1980, Geology of Nevada, a discussion to accompany the geologic map of Nevada: Nevada Bureau of Mines and Geology Special Publication 4, 136 p.

Thorman, C. H., 1970, Metamorphosed and nonmetaporphosed Paleozoic rocks in the Wood Hills and Pequop Mountains, northeast Nevada: Geological Society of America Bulletin, v. 81, p. 2417-2448.

Thorman, C. H., and Snee, L. W., 1988, Thermochronology of metamorphic rocks in the Wood Hills and Pequop Mountains, northeastern Nevada: Geological Society of America Abstracts with Programs, v. 20, p. A18.

Thorman, C. H., Ketner, K. B., Brooks, W. E., Snee, L. W., and Zimmerman, R. A., 1990, Late Mesozoic-Cenozoic tectonics in northeastern Nevada, *in* Shaddrick, D. R., Kizis, J. A., Jr., and Hunsaker, E. L., eds., Geology and ore deposits of the northeastern Great Basin: Geological Society of Nevada 1990 meeting, p. 25-45.

Todd, V.R., 1983, Late Miocene displacement of pre-Tertiary and Tertiary rocks in the Matlin Mountains, northwestern Utah, *in* Miller, D.M., Todd, V.R., and Howard, K.A., eds., Tectonic and stratigraphic studies in the eastern Great Basin: Geological Society of America Memoir 157, p. 239-270.

Wells, M. L., and Allmendinger, R. W., 1990, An early history of pure shear in the upper plate of the Raft River metamorphic core complex; Black Pine Mountains, southern Idaho: Journal of Structural Geology, v. 12, p. 851-868.

Wells, M. L., Dallmeyer, R. D., and Allmendinger, R. W., 1990, Late Cretaceous extension in the hinterland of the Sevier thrust belt, northwestern Utah and southern Idaho: Geology, v. 18., p. 929-933.

Williams, P. L., Covington, H. R., and Pierce, K. L., 1982, Cenozoic stratigraphy and tectonic evolution of the Raft River basin, Idaho, *in* Bonnichsen, B., and Breckinridge, R. M., eds., Cenozoic geology of Idaho: Idaho Bureau of Mines and Geology Bulletin 26, p. 491-504.

KINEMATICS AND TIMING OF SEQUENTIAL DEFORMATIONS IN THE EASTERN RAFT RIVER MOUNTAINS

Michael L. Wells
Department of Geological Sciences
Cornell University
Ithaca, NY 14853
currently at U.S. Geological Survey
345 Middlefield Road, MS975
Menlo Park, CA 94025

ABSTRACT

The Raft River Mountains of northwestern Utah contain an unusually complete record of sequential Mesozoic and Cenozoic deformations. Through geologic mapping, macro- and microscopic kinematic and strain analyses, and isotopic studies, constraints on the geometry, kinematics and timing of these deformations have been determined.

In the eastern Raft River Mountains, two allochthons comprise the upper plate of the Raft River detachment fault. Cambrian(?) through Pennsylvanian(?) strata within the lower allochthon were dramatically attenuated as a result of ductile, west-vergent low-angle faulting and earlier intrabed plastic flow. Oxygen isotopic geothermometry and conodont color alteration indices indicate peak metamorphic temperatures of 500° C. Attenuated strata, together with complete structural omission of Devonian and Mississippian units, suggest large magnitude horizontal extension. $^{40}Ar/^{39}Ar$ analyses of metamorphic muscovite from rocks within the lower allochthon consistently yield plateau ages between 82 and 90 Ma. Subsequent to stratigraphic attenuation, the lower allochthon was recumbently folded, followed by post-metamorphic westward transport of the middle allochthon. Open folding about generally north-trending axes followed westward translation. All of these structures formed prior to the development of the Miocene Raft River detachment.

These data suggest that upper crustal extension was occurring in the Mesozoic hinterland synchronous with shortening in the foreland. Additionally, the deformation sequence suggests that sequential (episodic) reversals in contraction and extension occurred during the Mesozoic to early Cenozoic evolution of the Sevier belt hinterland.

INTRODUCTION

The eastern Raft River Mountains are part of a large, contiguous metamorphic core complex that includes the Raft River, Albion, and Grouse Creek mountains in northwestern Utah and southern Idaho. Superimposed Mesozoic and Cenozoic deformations produced a greatly attenuated stratigraphic section. Although deformational fabrics at all scales have been identified and documented by various workers for both Mesozoic and Cenozoic deformations, the regional effects of these events, in particular the Mesozoic deformations, remain elusive. What are the kinematics and timing of the Mesozoic deformations and do they record contraction or extension? What are the relative contributions of Mesozoic and Cenozoic deformations to the stratigraphic attenuation visible today? Detailed geologic mapping, and structural and isotopic analyses from the eastern Raft River Mountains demonstrate key relationships that bear directly on these questions.

The focus of this paper is the deformation history within Paleozoic rocks in the upper plate of the Cenozoic Raft River detachment fault in the eastern Raft River Mountains. In contrast to rocks in the southern Albion and Grouse Creek mountains, these rocks were far removed from Oligocene plutons, and were not thermally overprinted in the Tertiary. Additionally, unlike lower plate rocks, upper plate rocks were not subjected to Cenozoic mylonitization and metamorphism, and thus preserve a more coherent Mesozoic history. Of particular importance to our understanding of the tectonics of this region are: an episode of large magnitude extension of Late Cretaceous age coeval with shortening in the foreland (suggesting that the Cordilleran thrust belt hinterland experienced significant topographic development): and, the suggestion in the deformation sequence that sequential (episodic) alternations from contraction to extension occurred during the Mesozoic to early Cenozoic.

GEOLOGIC SETTING

The Raft River Mountains lie within the hinterland of the Mesozoic Sevier orogenic belt (Armstrong, 1968a), to the west of the classic foreland fold and thrust belt (Armstrong and Oriel, 1965) (Fig. 1). Within the hinterland of northwestern Utah, southern Idaho, and northeastern Nevada, faults that place older rocks on younger, or place higher grade metamorphic rocks on lower grade, are rare, in marked contrast to the foreland. More commonly, low-angle faults within the Sevier belt hinterland place younger rocks on older, and unmetamorphosed rocks on metamorphosed (Armstrong, 1972). Many of these younger-over-older faults have documented Cenozoic ages. For example, low-angle faults of known Cenozoic age are present in the Pilot Range (Miller and others, 1987), the Goshute Range (Day and others, 1987), the Ruby Mountains (Snoke and Lush, 1984), the Snake Range (E. Miller and others, 1983), the Grouse Creek Mountains (Compton, 1983), and the Albion Mountains (Saltzer and Hodges, 1988).

Despite the common association of low-angle younger-over-older faults with Eocene and younger extensional deformation, many younger-over-older faults are apparently Mesozoic to early Tertiary in age. Notable examples

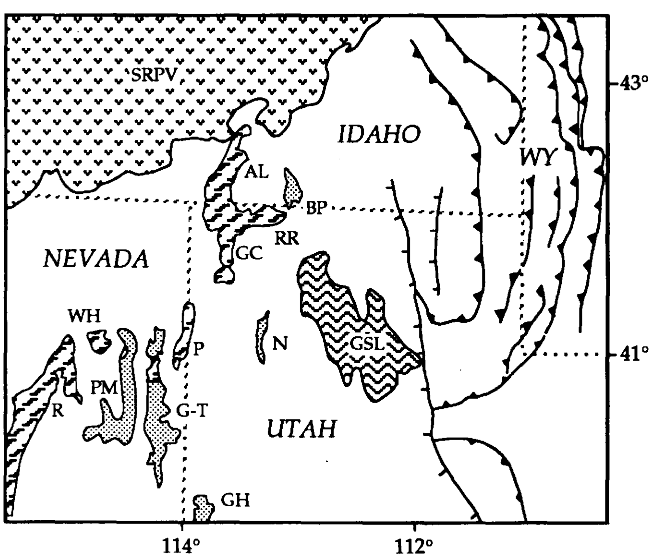

Figure 1. Generalized location and tectonic map of the northeastern Great Basin illustrating location of hinterland metamorphic rocks and other ranges mentioned in text. Barbed lines are thrusts of the Sevier belt, hachured lines are normal faults of the Wasatch system. Labeled geographic and structural elements: AL, Albion Mountains; BP, Black Pine Mountains: GC, Grouse Creek Mountains; GH, Gold Hill; GSL, Great Salt Lake; G-T, Toano-Goshute Mountains; N, Newfoundland Mountains; P, Pilot Range; PM, Pequop Mountins; R, Ruby Mountains; RR, Raft River Mountains; SRPV, Snake River Plain volcanic rocks; WH, Wood Hills; WY, Wyoming. Exposures of metamorphic rocks shown with diagonal wavy pattern.

occur within the Newfoundland Mountains (Allmendinger and Jordan, 1984), the Pilot Mountains (Miller and Hoisch, this volume), Gold Hill (Robinson, 1990), and possibly Bovine Mountain (Jordan, 1983).

Both Cenozoic and Mesozoic younger-over-older faults are present in the eastern Raft River Mountains. In the larger Raft River-Albion-Grouse Creek metamorphic core complex, a generally consistent structural stratigraphy is present throughout an area greater than 4000 km^2. Within this stratigraphic succession, several low-angle faults divide the rocks into 4 major allochthons and an autochthon, as defined by Compton and others (1977) and Miller (1980) (Figs. 2 and 3). Within these allochthons, numerous smaller low-angle faults occur. All of these faults, with few exceptions, place younger rocks on older rocks, and apparently are subparallel to bedding over large areas.

STRATIGRAPHY OF THE RAFT RIVER, ALBION, AND GROUSE CREEK MOUNTAINS

In the Raft River, Albion, and Grouse Creek mountains, a sequence of Proterozoic(?) to Triassic rocks unconformably overlies an Archean basement complex (Armstrong, 1968b; Compton and others, 1977). Within the eastern Raft River Mountains, these rocks can be subdivided into three tectonostratigraphic units (Fig. 3), which are generally correlative with the autochthon and allochthons present elsewhere in the Raft River, Grouse Creek and Albion mountains (Fig. 2). From structurally lowest to highest (Fig. 4), these are: (1) the autochthon, (2) the lower allochthon, and (3) the middle allochthon.

Autochthon

In the autochthon, an Archean basement complex (Green Creek complex of Armstrong, 1968b) comprised of 2.5 Ga gneissic adamellite, schist, trondhjemite and amphibolite (Compton, 1975; Compton and others, 1977), is unconformably overlain by the Elba Quartzite and an overlying schist unit. These latter units correlate with the lowermost part of the Raft River Mountains sequence of Miller (1983), and have been assigned various ages including Paleozoic, Middle Proterozoic, and Late Proterozoic (Armstrong, 1968b; Compton and others, 1977; Compton and Todd, 1979; Crittenden, 1979). The youngest unit in the autochthon in the eastern Raft River Mountains (Kelton Pass Quadrangle) is 25 m of quartz-muscovite schist and foliated cataclasite which overlies the Elba Quartzite and is probably correlative with the schist member of the Elba Quartzite of Compton (1975). The overlying rocks, present within the autochthon to the west, have apparently been structurally removed.

Lower Allochthon

The lower allochthon consists of Cambrian(?) quartzite and schist; Ordovician calcitic marble, phyllite, quartzite and dolomite; Silurian(?) dolomite; and Pennsylvanian(?)

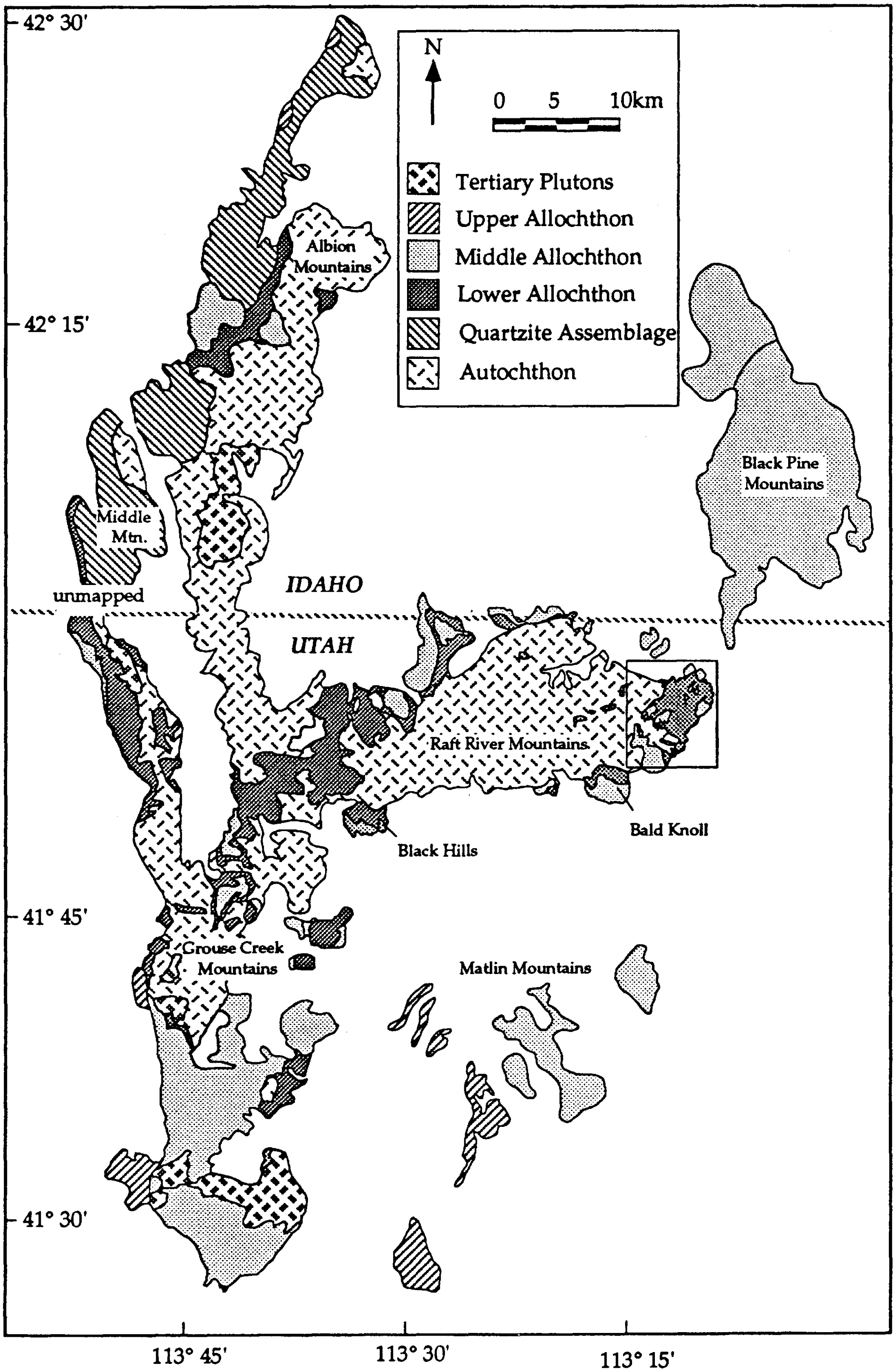

Figure 2. Tectonostratigraphic map of the Raft River, Black Pine, Albion, Grouse Creek, and Matlin mountains. Box outlined in eastern Raft River Mountains indicates location of more detailed geologic map shown in Figure 4. Modified from Compton (1975), Compton and others (1977), Todd (1980, 1983), Miller (1983), Malavielle (1987b), and author's mapping. Note that Bovine Mountain is shown as interpreted by Compton and others (1977), and differs from the interpretation of Jordan (1983).

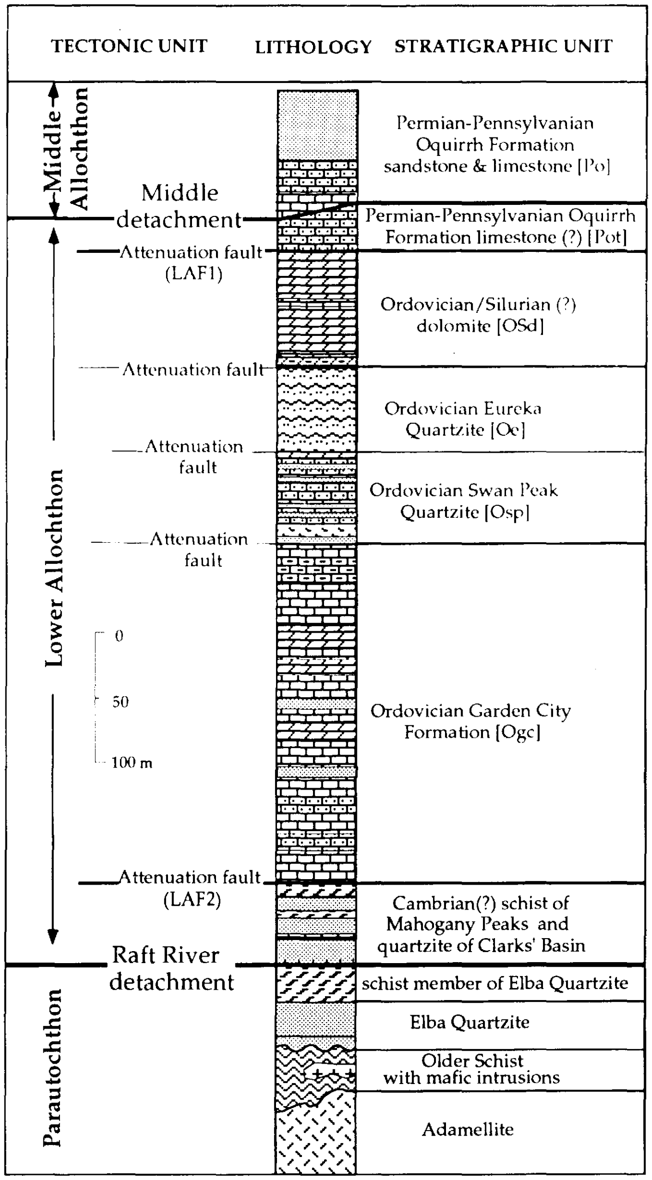

Figure 3. Stratigraphy of the eastern Raft River Mountains. Thicknesses are approximately maximums, and are highly variable. Positions of major faults are indicated. Note that all stratigraphic contacts within the lower allochthon are low-angle faults.

marble. These units are consistent with those mapped earlier within the lower allochthon to the west (Compton, 1975; Compton and others, 1977; Compton and Todd, 1979), although I will describe two modifications to this stratigraphy.

The oldest units present within the lower allochthon are the quartzite of Clarks Basin and the schist of Mahogany Peaks. These units were thought to be Cambrian in age by Compton (1972, 1975), but Crittenden (1979) considered their age to be Middle Proterozoic. The quartzite of Clarks Basin consists of characteristically flaggy muscovite quartzite, with lesser interbedded schist and marble. The schist of Mahogany Peaks consists of porphyroblastic garnet-staurolite and biotite schist 0-10 meter thick. The stratigraphically lowest Ordovician unit mapped by Compton (1972, 1975) is the Pogonip Group. Here, the Pogonip Group is subdivided into the Garden City Formation and the overlying Swan Peak Quartzite. The Garden City Formation consists of up to 300 m of calcitic marble, dolomite, and subordinate sandstone and quartzite. Typically, this unit has a three-part stratigraphy, although these parts were not mapped separately. The lower part is primarily thin-bedded and laminated brown-weathering silty to sandy limestone, with a few beds of brown quartzite and muscovite phyllite. The middle of the unit is mainly massive light grey dolomite, with subordinate laminated limestone and quartzite. The upper part consists of medium- to thick-bedded, light grey to buff limestone, with abundant silty laminations. The top of this part is a characteristically clean, finely laminated marble, and is underlain by 2 to 10 meters of chert-rich limestone. Conodonts extracted from the upper part of the Garden City Formation yield lower Ordovician ages, confirming its stratigraphic assignment (J. E. Repetski, written communication, 1990).

The Garden City Formation is overlain by a unit as thick as 70 m that consists of (from base to top) brownish quartzite, muscovite phyllite, interbedded quartzite and sandy limestone, and dolomite. The limestone is dark grey, and commonly contains quartz and feldspar sand, muscovite, and much pyrite. The quartzite is commonly reddish brown, well-bedded, with interbeds of clean white quartzite. The lower part of this unit is correlated to the Kanosh Shale to the southwest, and the lower member of the Swan Peak Quartzite in northeastern Utah (Oaks and others, 1977). In the absence of biostratigraphic control, I tentatively correlate the upper part of the unit to the middle member of the Swan Peak Quartzite in northeastern Utah, and the Lehman Formation and Swan Peak Quartzite in western Utah.

As much as 60 m of clean, vitreous white quartzite characterize the overlying Eureka Quartzite. The Eureka is overlain by up to 130 m of dolomite which typically is rich in black chert at its base, and grades upward into buff, white, laminated to massive dolomite. The lower cherty part of this unit probably correlates with the Ordovician Fish Haven or Ely Springs Dolomite; however, it is not biostratigraphically constrained and upper sections of this unit could either be Ordovician or Silurian dolomite. Attempts to extract conodonts from the dolomite for biostratigraphic control were unsuccessful.

The Ordovician/Silurian(?) dolomite unit is overlain by less than 40 m of banded, fossiliferous, light grey to buff and dark blue-grey limestone. Abundant crinoids, minor brachiopods, lenses of siltstone and chert, the dark blue-grey color, and the banded nature of this unit make it easily recognizable. The basal contact of this unit is a major low-angle fault, and chips of oxidized muscovite phyllite and black quartzite lie within the fault zone. Two stratigraphic correlations are possible. First, this marble may represent limestone of the lower Oquirrh Formation, with chips of phyllite and quartzite representing the remains of the Mississippian Chainman-Diamond Peak Formations. Alternatively, this marble could represent metamorphosed Kinderhookian limestone (Joana Limestone), and the phyllite and

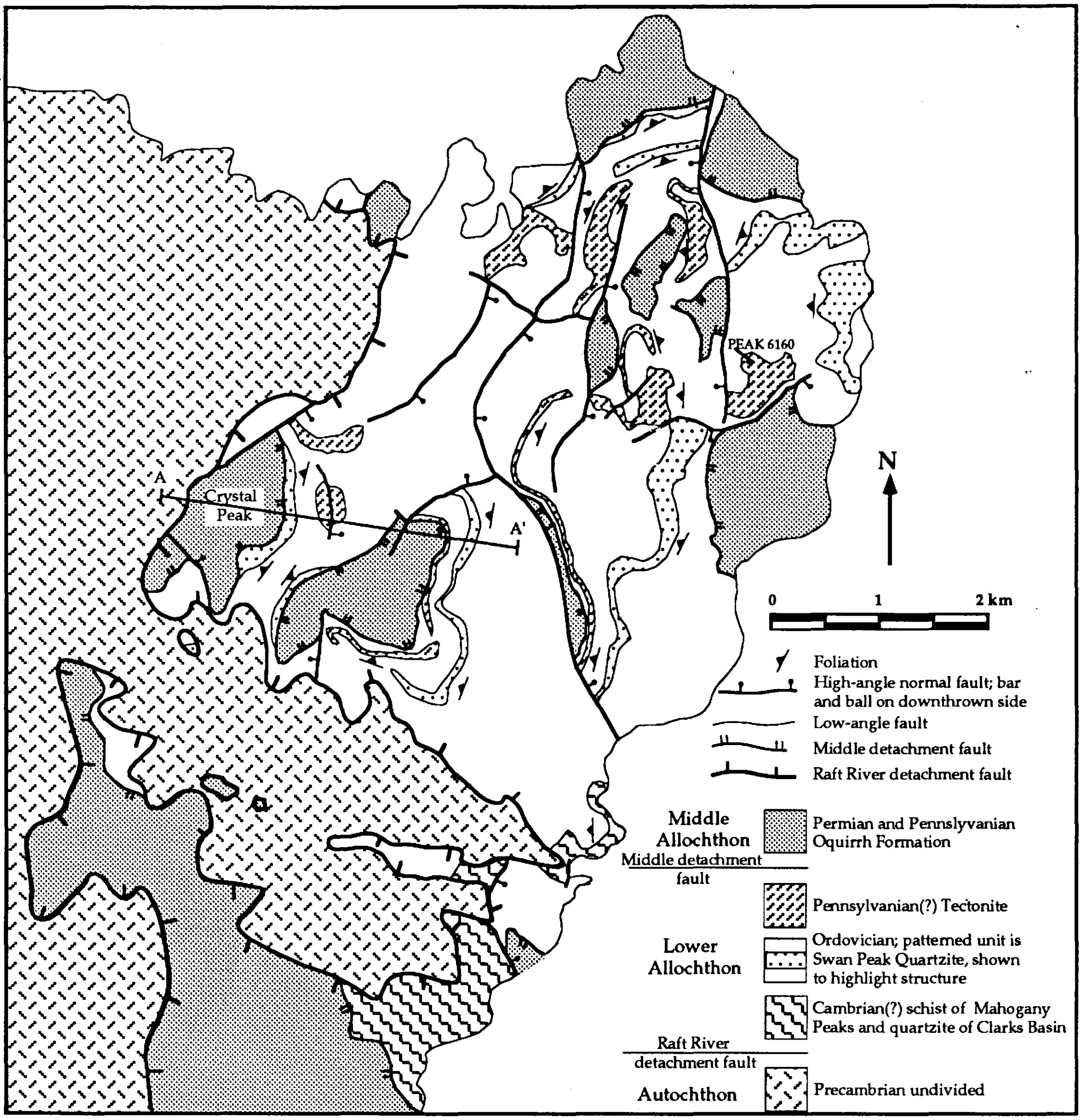

Figure 4. Generalized geologic map of the eastern Raft River Mountains from mapping by author. This base map is utilized in Figures 11 and 12 where various structural features are plotted.

quartzite would correlate to the Pilot Shale. The former correlation is favored, based on a remarkable similarity in appearance between this marble tectonite and marble assigned to the lower Oquirrh Formation exposed in the Grouse Creek Mountains—where it overlies a thick section of metamorphosed Chainman-Diamond Peak (Todd, 1980; Miller and others, 1983)—and the lack of quartzite in the Pilot Shale to the SW. Attempts to extract conodonts for biostratigraphic control were unsuccessful, and brachiopods are too highly strained and recrystallized for identification.

Middle Allochthon

The middle allochthon is separated from the lower allochthon by the middle detachment fault. Rocks of the middle allochthon are composed mainly of the Permian and Pennsylvanian Oquirrh Formation, with a thin (0- to 5-m-thick) sliver of Mississippian Manning Canyon Shale locally present along its base. The Oquirrh Formation has a general internal stratigraphy consisting of three units which were not mapped separately. The lower unit consists of a lower dark blue-grey limestone with sandy interbeds and common bryozoans and brachiopods. The Lower Pennsylvanian age for the lower limestone has been confirmed by conodont identification (J. E. Repetski, written communication, 1989, 1990). The lower limestone is overlain by platy, tan, maroon, and grey weathering sandy to silty limestone. The upper unit is dominantly sandstone and calcareous sandstone, locally with fusilinids, and is the most common lithology in the middle allochthon.

STRUCTURAL GEOLOGY

Review of Previous Studies

Detailed studies of the stratigraphy, structural geology, and metamorphism have been carried out by many workers at various localities within the Raft River, Albion, and Grouse Creek mountains. Of particular importance are studies by Armstrong (1968b, 1976); Compton (1972, 1975); Compton and others (1977); Miller (1980, 1983), and Todd (1980, 1983). Additionally, several recent investigations have focused on determining the kinematics of deformation utilizing more recently described shear-sense criteria (Sabisky, 1985; Malavielle, 1987a, 1987b; Saltzer and Hodges, 1988). These studies illustrate well the complexity of the deformation history of these rocks. As many as four distinct deformations, identified by associated flat-lying foliations, lineations, and lineation-parallel fold axes, are present locally within the metamorphic terrane. These deformations will be discussed with reference to their associated stretching lineations.

Two presumed Mesozoic deformations have been documented in the northern Albion Mountains (Miller, 1980); the earliest exhibits NE-trending lineations (L_1 of Miller (1980), with top-to-the-NE shear; Malavielle, 1987b) and the second has northwest-trending lineations (L_2 of Miller (1980), with top-to-the-NW shear). Rocks containing these fabrics have yielded eight conventional K-Ar cooling ages (biotite, muscovite, and hornblende) ranging from 66 to 81 Ma (Armstrong, 1976). A third lineation trending WNW is present in the western Albion Mountains, and is best developed at Middle Mountain. Here, a west-dipping extensional shear zone (the Middle Mountain shear zone, Saltzer and Hodges, 1988) exhibits a WNW-trending lineation with top-to-the-west shear sense. The Middle Mountain shear zone is younger than the development of L_2 of Miller (1980) and metamorphic minerals synkinematic with this lineation yield Oligocene cooling ages (Armstrong, 1976; Miller and others, 1983; Saltzer and Hodges, 1988).

In the Grouse Creek and western Raft River mountains, two lineations are present; a NNE-trending lineation (with top-to-the NNE shear; Malavielle, 1987b) that is probably correlative to the Mesozoic NE-trending lineation in the rest of the metamorphic terrane, and a younger NW-trending lineation that yields top-to-the NW shear (Compton and others, 1977; Todd, 1980; Compton, 1983; Malavielle, 1987b). The age and correlation of this second lineation is problematic due to the similarity in trend and associated kinematics with the Mesozoic L_2 of Miller (1980) in the northern Albion Mountains and the Cenozoic WNW-trending lineation of the Middle Mountain shear zone. However, as noted by Miller and others (1983), the NW-trending lineations within the Grouse Creek Mountains might represent two sets, one older than the 38 Ma Immigrant Pass pluton, and the other synchronous with intrusion of 25 Ma Red Butte Canyon Stock. In the central and eastern Raft River Mountains, an additional fabric set is developed. Prominent flat-lying foliations and an east-trending lineation demarcate a Cenozoic top-to-the-east shear zone which is cut by the brittle Raft River detachment fault (Sabisky, 1985; Malavielle, 1987a).

Eastern Raft River Mountains

In the eastern Raft River Mountains, the Cenozoic Raft River detachment fault separates the Precambrian autochthon from the overlying upper and middle allochthons (Figs. 4 and 5). As in other core complexes in the western United States (Crittenden and others, 1980), a mylonite zone directly underlies the brittle detachment fault, and both the mylonites and cataclasites related to the detachment fault exhibit the same kinematics, here top-to-the-east shearing. The upper plate rocks at the extreme east end of the range have proven to be an ideal area to reconstruct the sequence of pre-detachment faulting deformations, as well as to provide constraints on their ages. This earlier history is well recorded because no Tertiary metamorphism affected these upper plate rocks, and their moderate metamorphic grade promoted development of penetrative fabrics and growth of metamorphic minerals useful for dating.

The following progression of deformations has been determined by detailed geologic mapping in the eastern Raft River Mountains. (1 & 2) Attenuation of units within the lower allochthon via early NE-directed intrabed plastic flow and later top-to-the-west younger-over-older faulting. (3) Recumbent folding (F_3) of attenuated strata and faults. (4) Emplacement of the middle allochthon over the lower allochthon along the middle detachment. (5) Upright, open folding (F_5) of the middle and lower allochthons. (6) Progressive eastward normal-sense shearing along the autochthon shear zone and superposed Raft River detachment fault, with concomitant high-angle normal faulting of the upper plate. (7) Doming of the Raft River detachment fault and earlier structures. The relationship among some of these structures can be seen by inspection of the cross section in Figure 5.

(1) D_1 Deformation. *Generalities.* The Cambrian (?) through Pennsylvanian (?) units within the lower allochthon have been markedly attenuated, during both plastic and brittle deformations. This stratigraphic section, which in neighboring ranges is from 4 to 7 km thick, varies in thickness from 50 to 500 meters (Fig. 6). The attenuation has been achieved by NE-directed penetrative deformation (D_1) and later (D_1) low-angle younger-over-older ductile and brittle faulting (referred to as attenuation faulting). For the following reasons the attenuation faults are thought to be distinct from and postdate penetrative foliation development: (1) attenuation faults locally truncate D_1 foliation; (2) mylonitic fabrics within ductile attenuation fault zones are preserved and non-annealed; and (3) the penetrative D_1 fabrics have distinct kinematics from the attenuation faults - D_1 is NE-directed and D_2 is west-directed.

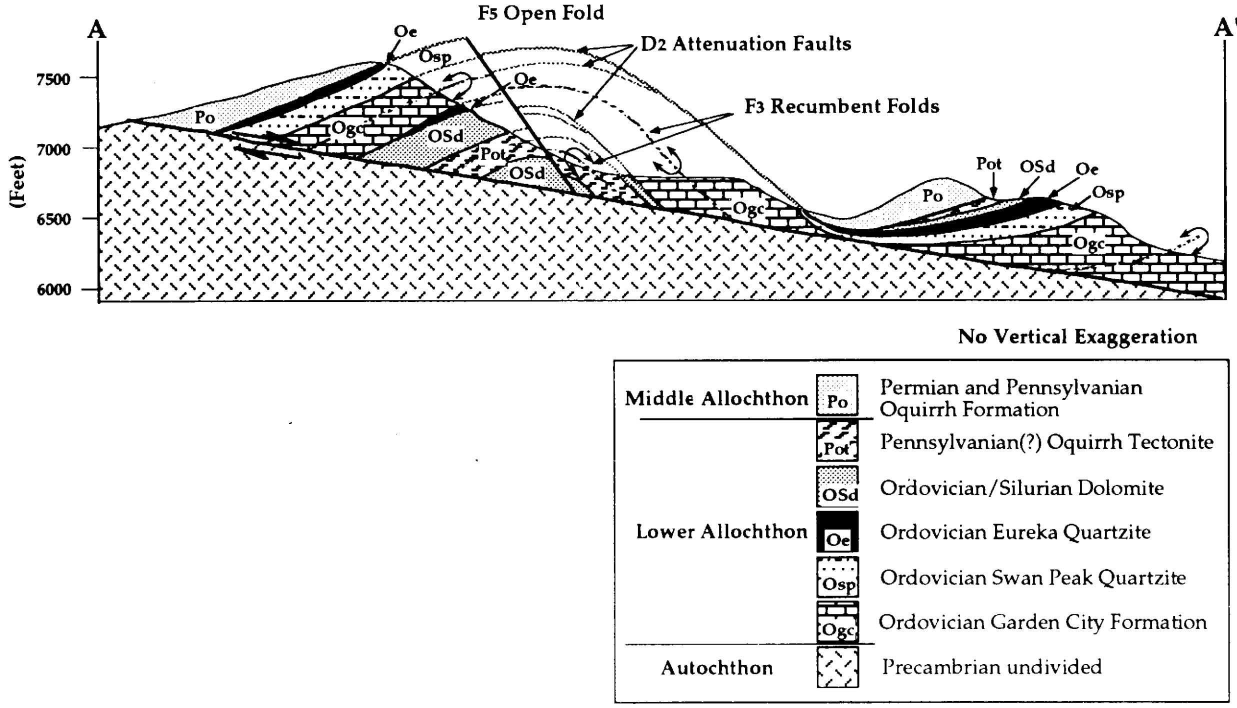

Figure 5. Simplified geologic cross section A-A' from the eastern Raft River Mountains. Note the D_2 attenuation faults which omit much of the stratigraphic section. These faults are folded about F_3 recumbent folds. D_2 attenuation faults, F_3 recumbent fold axial surfaces, and the middle detachment are folded about F_5 open folds. See Figure 4 for location of cross section.

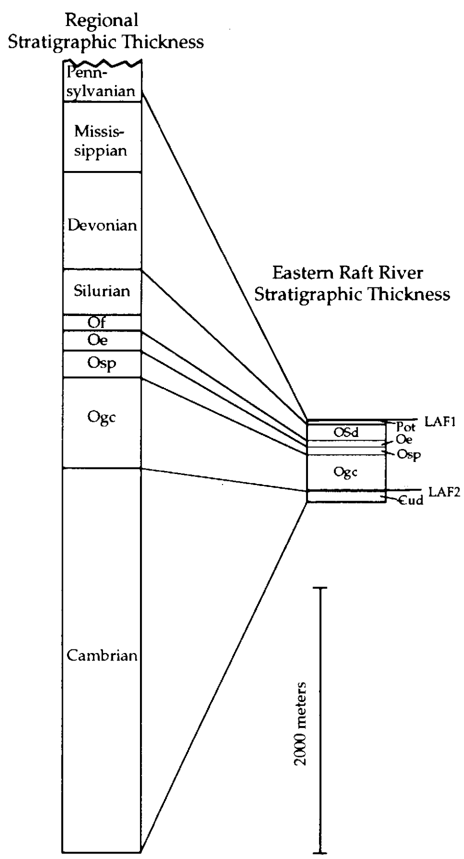

Figure 6. Comparison between attenuated stratigraphic thicknesses within the eastern Raft River Mountains and representative stratigraphic thicknesses from nearby localities taken from Hintze (1988). Of = Fish Haven Dolomite.

The most pervasive fabric in the lower allochthon is the D_1 penetrative foliation which occurs at low angles to both bedding and attenuation fault zones. Bedding is highly transposed by foliation, and at all locations where both bedding and foliation are identifiable, foliation consistently is slightly inclined to the southwest relative to bedding, suggesting the possibility of NE-directed deformation. Lineations are variably developed, generally trending NE. A few asymmetric structures indicate E and NE shearing, however the majority of strained features are symmetric, suggesting a major component of flattening strain. The details of D_1 fabric development are described below, according to lithology.

Carbonate. All carbonate units within the lower allochthon display a well-developed foliation. Where discernible, relict bedding is commonly highly transposed, and foliation generally dips WSW relative to bedding in both upright and overturned rocks (Fig. 7a). The only recognized F_1 folds are sparse mesoscopic eastward-overturned folds with axes generally trending NNE. Lineations are generally scarce; however, locally they are well developed. These lineations are most commonly defined by elongate quartz and calcite pressure shadows about pyrite grains, elongate calcite grains (evident in thin sections), and stretched and recrystallized crinoid fragments. Finite strains within these rocks are highly variable, and principal extensions are locally as great as 600%.

Kinematic indicators within Pennsylvanian(?) and Ordovician marble are not pervasive and only locally present. Many outcrops exhibited symmetric structures, including pressure shadows around rigid objects and boudinage of quartzite and chert interbeds. Additionally, many outcrops exhibited asymmetric structures, but few showed consistent sense of asymmetry. At localities where a consistent shear sense was present, all indicated a uniformly top-to-the-NE shear sense (i.e., Fig. 7b). These observations, coupled with the SW dip of foliation relative to bedding, suggest that D_1 fabrics record NE-directed deformation resulting from a combination of flattening strain and simple shear.

Quartzite. The Ordovician quartzites, except those within D_2 ductile attenuation fault zones, do not exhibit a macroscopic stretching lineation. Thin sectioning parallel to foliation revealed a moderate grain-shape elongation lineation; however, the degree of development of this lineation is highly variable. Thin sections examined parallel to lineation and perpendicular to foliation exhibit large (1.5 to 2 mm) elongate detrital quartz grains, with much recrystallization at grain boundaries. The elongate detrital grains exhibit variably developed undulatory extinction and discrete extinction domains with both sharp and diffuse domain boundaries.

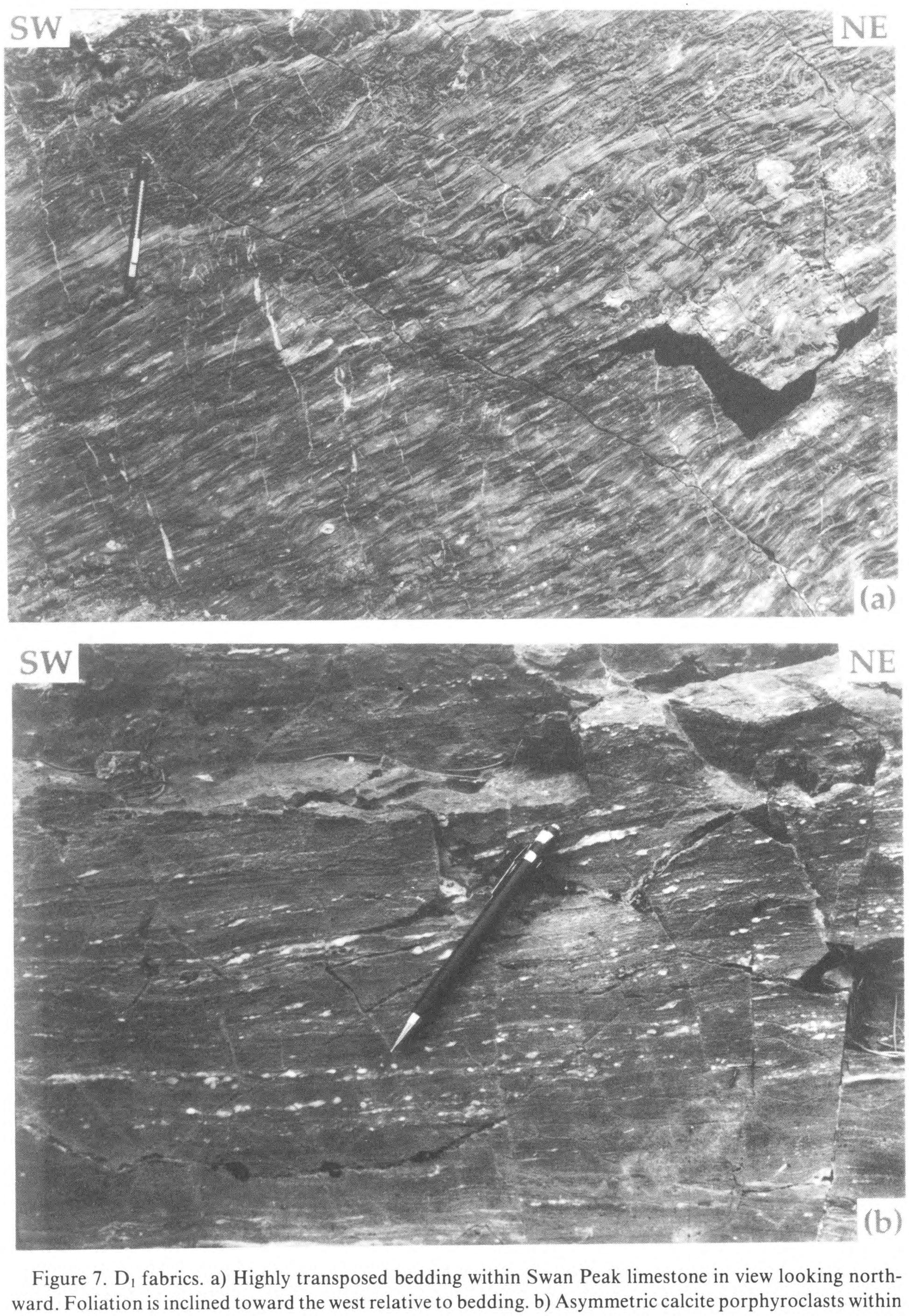

Figure 7. D_1 fabrics. a) Highly transposed bedding within Swan Peak limestone in view looking northward. Foliation is inclined toward the west relative to bedding. b) Asymmetric calcite porphyroclasts within Pennsylvanian(?) marble.

Where boundaries between extinction domains are diffuse, this microstructure is termed banded undulatory extinction; where extinction domain boundaries are sharp they are deformation bands or subgrains, depending on whether they do or do not exhibit internal undulatory extinction, respectively (White, 1973). Differences in crystallographic alignment are generally about 5° across subgrain boundaries.

C-axes within Ordovician quartzites are subparallel to deformation band boundaries, suggesting that they are prismatic subgrain boundaries. Extinction bands and subgrain boundaries are oriented between 42° and 68° from the foliation, with the large majority inclined towards the west relative to the principal foliation. Internal foliations defined by subgrains which are oblique to the principal foliation have been proposed as a reliable shear criteria (Law and others, 1984; Law, 1986; Lister and Snoke, 1984). The crystallographic preferred orientation suggested by the preferential alignment of prismatic subgrains is also indicated by petrographic examination with the gypsum plate. Although these quartzites have not been analyzed by x-ray pole figure goniometry or universal stage measurement, the inferred crystallographic orientation and the subgrain fabric of these quartzites consistently suggests a component of northeastward shearing.

The quartzite of Clarks Basin, at the lowest structural level, exhibits well-developed mylonitic fabrics, with an E-W trending stretching lineation defined by elongate muscovite and quartz grains, and a foliation defined by parallel-aligned muscovite and a mild quartz grain-shape fabric. These quartzites exhibit a microstructure similar to the Ordovician quartzites. Again, inclined boundaries separate domains of differing crystallographic orientation, and are interpreted to represent subgrain boundaries. In the Clarks Basin quartzite, these microstructures, coupled with preliminary examination of the preferred orientation using the gypsum plate, indicate a component of eastward shearing. Currently, these fabrics are thought to be related to D_1. However, in light of the intensity of fabric development, the east rather than NE lineation trends, and the structural position of these rocks, it cannot be ruled out that these Cambrian (?) rocks were once within the Tertiary shear zone in the now lower plate, and have since been accreted to the upper plate by structural incision.

(2) D_2 Attenuation Faults and Fabrics. *Faults.* Two major stratigraphic discontinuities are present within the lower allochthon; the lower allochthon fault 1 (LAF1) and the lower allochthon fault 2 (LAF2) (Fig. 3). The LAF1 places Pennsylvanian (?) tectonite marble on top of Ordovician/Silurian (?) dolomite. This fault removes the majority or all of the Silurian, all of the Devonian, and all but centimeter-scale slivers of Mississippian rocks, throughout the entire mapped area.

There is, however, another possible explanation for the absence of the Silurian through Mississippian strata in this region; an extensive unconformity could lie at the top of the Ordovician/Silurian (?) dolomite (Armstrong, 1968b). There is no general agreement on this issue among geologists mapping in this region as well as amoung stratigraphers who have extensively studied the northern Great Basin (Armstrong, 1968b; Compton and others, 1977, Hintze, 1988). For the following reasons, I attribute the lack of section to low-angle faulting.

First, the Pennsylvanian (?) calcitic marble lying above this discontinuity contains a distinct mylonite zone adjacent to the contact; thus, the mylonitic fabrics are spatially associated with the stratigraphic discontinuity. Second, chips of phyllite (Mississippian) are generally present along this contact throughout the map area. Erosional processes resulting in the preservation of a ~ centimeter-thick layer of shale over tens of square kilometers seems highly unlikely. A low-angle fault localized within a shale horizon, however, could produce this distribution, and similar stratigraphic relationships are seen along many low-angle normal faults. Third, and most importantly, there are many examples of structural discordance across this contact. Finally, the removal of rock units by low-angle faulting is characteristic of deformation within the lower allochthon, as shown by various mapped relationships within the Cambrian (?), Ordovician, and Pennsylvanian (?) rocks.

The second major stratigraphic discontinuity (LAF2) is more enigmatic. It occurs within the lower allochthon and separates the Cambrian (?) schist of Mahogany Peaks and quartzite of Clarks Basin from the Ordovician carbonates. The Mahogany Peaks schist and Clarks Basin quartzite were tentatively assigned a Cambrian age due to the apparent depositional contact with overlying Pogonip Group strata (here divided into Swan Peak Quartzite and Garden City Formation) by Compton (1975), and Compton and Todd (1979). However, because of this anomalous stratigraphy, Crittenden (1979) suggested that these are instead Middle Proterozoic strata, which would require omission of 4500 to 7600 m of upper Precambrian and Lower Cambrian clastic strata and 1400 m of Middle and Upper Cambrian carbonate. Even if the Mahogany Peaks schist is Early Cambrian in age as suggested by Compton, 1400 m of Middle and Upper Cambrian carbonates are still missing. Therefore, irrespective of the debate on the age of the Mahogany Peaks schist and underlying formations, a large thickness of strata apparently is absent along the contact between Mahogany Peaks schist and Ordovician carbontate. As suggested by Crittenden (1979), this stongly implies the presence of a concealed low-angle fault. This suggestion was discounted by Compton and Todd (1979) for several reasons including the conformity of attitudes between units above and below this contact, the regional persistence of a 35 m thick Mahogany Peaks schist below this contact, and the absence of fragments of other units along this contact. This contact is only exposed for a few hundred meters in the eastern Raft River Mountains, and my structural observations from this discontinuity alone are not compelling. Nevertheless, the similarity in style to other bedding-parallel faults within the Raft River Mountains (i.e., faults which consistently omit the same thickness of section along their trace), coupled with the regional stratigraphic arguments presented by Crittenden (1979) strongly suggests that this contact represents a synmetamorphic attenuation fault.

The regional-scale geometry of these two large-displacement faults suggests that, in general, the exposed segments of these structures are bedding-parallel flats in a low-angle fault with ramp and flat geometry; in general, hanging wall and footwall stratigraphic levels do not change over large distances. However, there are exceptions within the footwall of the LAF1 fault. In several localities Ordovician strata are truncated across this fault, suggesting that these are exposures of a footwall ramp against a hanging wall flat.

In addition to the two major low-angle faults described above, all other stratigraphic contacts within the lower allochthon are low-angle faults. These low-angle attenuation faults are identified both by textural and stratigraphic criteria. These faults generally are subparallel to foliation (and bedding) in the adjacent units and are recognized by high-strain zones localized along bedding-parallel contacts between stratigraphic units, along which section is commonly missing; however, locally there is miderate discordance between the fault zone and the adjacent unit, and between units bounding faults. Slivers of units are commonly strung out along low-angle faults and, locally, units have been completely omitted. Commonly, 1 to 2 meter-thick ledges of mylonitic to cataclastic quartzite or dolomite, representing in-sequence stratigraphic units, mark low-angle faults bounding calcitic marbles (e.g., Fig. 8a). Where the faulted nature of stratigraphic contacts is not evident by field inspection, significant lateral changes in map-scale unit thicknesses attest to their presence.

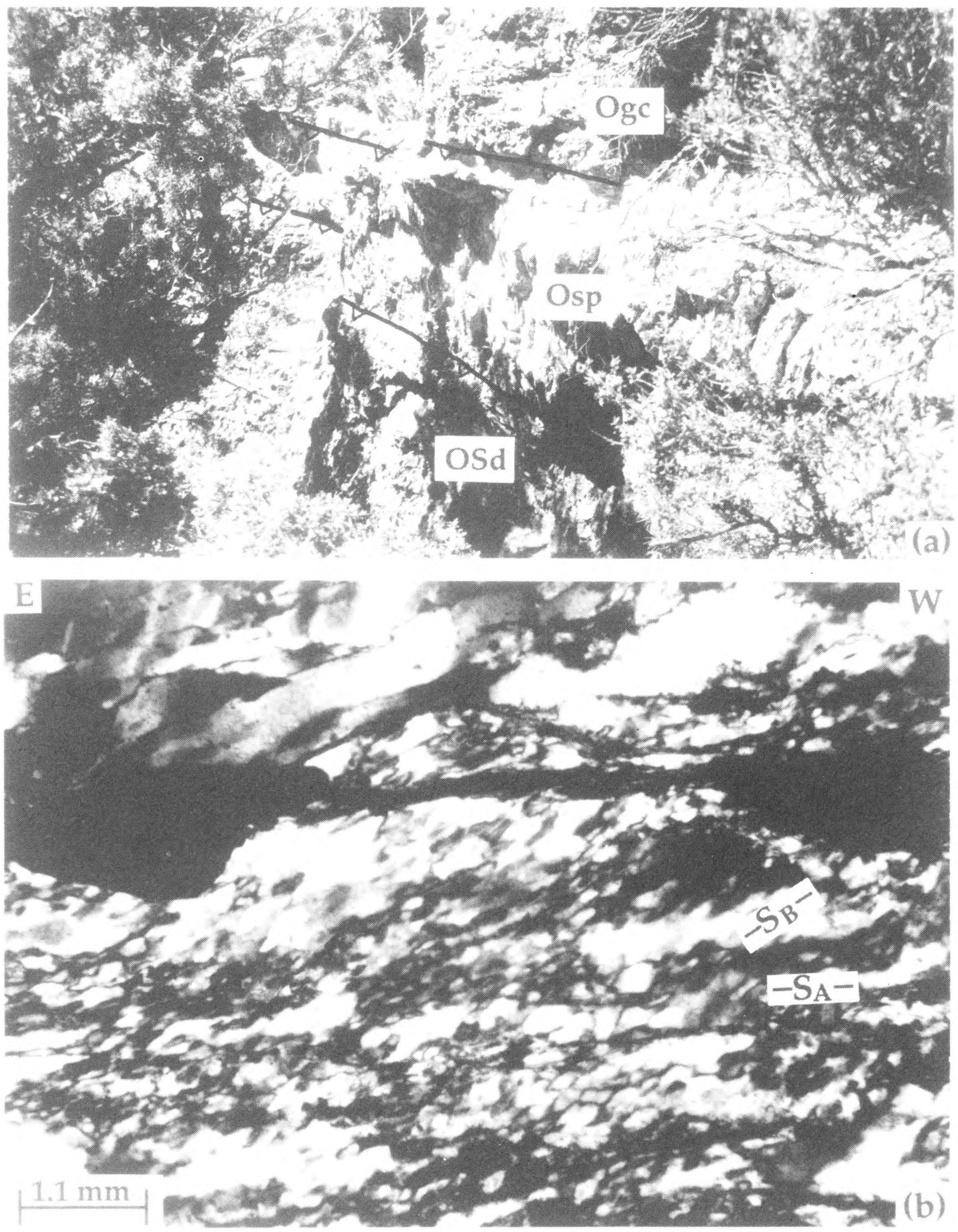

Figure 8. D_2 attenuation faults and fabrics. a) Overturned sequence consisting of 1 meter thick sliver of Swan Peak Quartzite tectonically overlain by Garden City Formation and underlain by Ordovician/Silurian (?) dolomite. b) Detail of oblique grain-shape fabric within quartzite, indicating dextral shear.

Fabrics. Within attenuation fault zones, fabrics range from ductile to brittle, and in many localities a progression from early ductile to later brittle shearing is evident. Macroscopic foliation within these shear zones is subparallel to D_1 foliation, except in rare localities where D_1 foliation is clearly truncated by the D_2 shear zones. The majority of observations from within these fault zones suggest top-to-the-west shearing.

Mylonitic shear zones are locally present within greatly attenuated Swan Peak and Eureka Quartzite which lie in fault zones separating Ordovician/Silurian (?) dolomite from Garden City Formation. These shear zones are highly localized, and range in thickness from one to 150 cm. For example, east of Crystal Peak, discrete Type 2 S-C mylonite zones (Lister and Snoke, 1984) occur within quartzite. C-surfaces are oriented subparallel to bedding, and S-surfaces are inclined relatively towards the east, indicating top-to-the-west shearing. Oblique grain-shape fabrics within these quartzites confirm this shear sense (Fig. 8b). Elsewhere, in finely laminated quartzite and phyllite, shear bands or extensional crenulation cleavage (Platt and Vissers, 1980) dips westward relative to foliation. Foliation is deformed into sigmoidal trajectories between these inclined shear bands, and the axes of the sigmoids are consistently oriented N-S. Again, westward shearing is indicated.

The basal part of the Pennsylvanian (?) marble, adjacent to the fault which removes Silurian through Mississippian units (LAF1), is commonly transformed into an extremely fine-grained marble tectonite (Fig. 9a). This marble is highly foliated, and locally contains a well-developed stretching lineation which is parallel to fold axes of locally developed isoclinal folds. In thin section, a porphyroclastic texture is defined by a few porphyroclasts of calcite which are slightly elongate parallel to a foliation defined by parallel alignment of fine-grained muscovite. The matrix is composed of fine-grained (8 to 20 um) calcite which lacks a grain-shape fabric. Because of the extremely small grain size in this carbonate rock, the deformation kinematics of one sample were investigated using crystallographic texture analysis, determined using x-ray pole figure goniometry. This sample exhibits a strong preferred orientation of a-axes. The a-axis girdle and inferred c-axis maxima are asymmetric with respect to foliation, and indicate westward shearing (Fig. 9b). Other west-vergent shear indicators from this marble tectonite include: a secondary grain-shape fabric of recrystallized grains which is oblique and inclined eastward relative to the mylonitic foliation, and deformed fold limbs which are boudinaged where inclined eastward and folded where inclined westward relative to foliation. Common late brittle fault networks consistently indicate the same sense of shearing.

Although these structures within fault zones are not ubiquitous, the kinematic consistency of these observations suggests that westward shearing is characteristic for these faults. It is noteworthy that the microstructures and crystallographic textures which record westward shearing are preserved and have not been annealed.

In the field, orientation alone is insufficient to distinguish

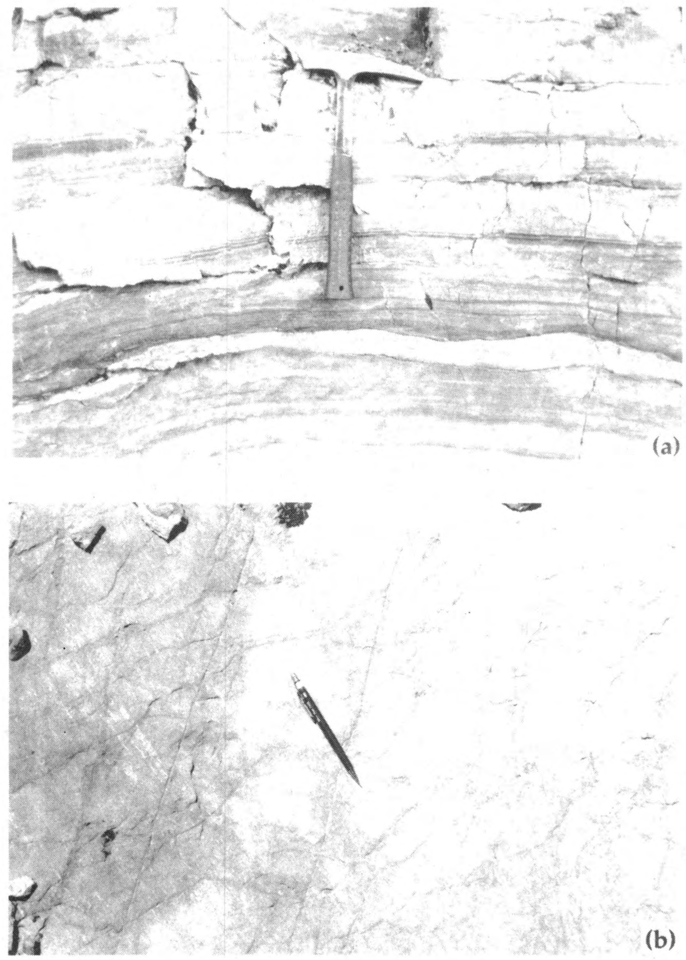

Figure 9. Pennsylvanian(?) marble tectonite adjacent to LAF1. a) Mylonitic foliation. b) Stretching lineations viewed on foliation surface.

lineations related to westward D_2 shearing from those related to NE-vergent D_1 fabrics. This difficulty stems from the gradational nature of many of the contacts between W-vergent attenuation shear zones and the surrounding domains of D_1 fabrics, the difficulty in determining kinematics from macroscopic structures in these rocks, and the overlapping ranges in orientation of each set. Because of these uncertainties, all lineations from the lower allochthon are plotted together as shown in Figure 10. Their diversity in azimuth, generally between 200° and 280°, is in part due to folding about F_3 and F_5 map-scale folds, and subsequent rotation during high-angle normal faulting. Additionally, part of the variability is original, representing two generations of lineations; the majority of lineation measurements from fabrics yielding westward shearing have E trends, while most of the NE-verging structures contain NE-trending lineations. The NE-trending lineations probably predate attenuation faulting, whereas many of the E-trending lineations are clearly related to attenuation faulting.

(3) F_3 Recumbent folding. Large inverted sequences of Ordovician and Pennsylvanian (?) rocks coupled with upright packages of the same rocks are common in the lower allochthon. These relationships indicate the presence of upright

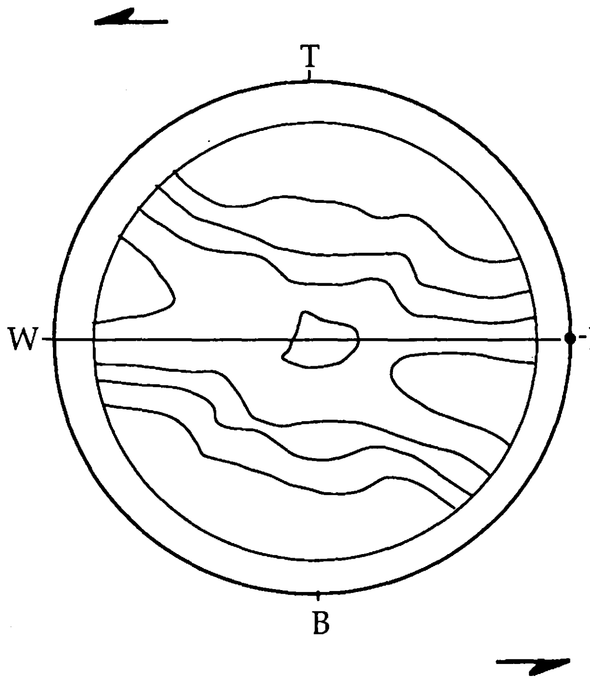

Figure 10. X-ray derived a-axis pole figure for Pennsylvanian (?) tectonite, determined using Huber 4-circle x-ray pole figure goniometer. The E-W line represents the macroscopic cleavage plane and the lineation is indicated by the filled circle. Contours of 1, 1.5, 2.0, and 2.5 of random distribution.

and overturned limbs of large recumbent folds. The hinges of these inferred folds, however, are not unequivocally exposed and, because later high-angle normal faults have since altered their limb dips, their geometries are not known. The youngest unit involved in the recumbent folding is the Pennsylvanian (?) tectonite, and it generally occupies the cores of recumbent synclines (Fig. 11). Because no rocks younger than Pennsylvanian (?) are involved in these folds, the originally overlying rocks are inferred to have been decoupled during folding. Presently, the D_1 foliation consistently dips more steeply westward than transposed bedding on both upright and overturned limbs, suggesting that the foliation either predates or postdates, but is not synchronous with, folding.

The development of F_3 recumbent folds is bracketed as younger than D_2 attenuation faulting and older than D_4 movement along the middle detachment. Because attenuation faults occur in both upright and overturned limbs and several consistently remove the same amount of stratigraphic section (for example, the fault separating Pennsylvanian(?) from Ordovician/Silurian(?) strata), recumbent folding postdated attenuation faulting within the lower allochthon. Because the middle allochthon presently rests on various structural levels of both upright and overturned sequences, F_3 recumbent folding preceded emplacement of the middle allochthon.

The overturned limbs commonly are more highly attenuated than upright limbs. There are two possible explanations for this observation, 1) further attenuation accompanied recumbent folding or, 2) overturned limbs preferentially underwent later shearing during movement on the overlying middle detachment. The available data do not allow differentiation between these two alternatives.

(4) Emplacement of the Middle Allochthon Along the Middle Detachment. Subsequent to recumbent folding, Permian and Pennsylvanian Oquirrh Formation rocks of the middle allochthon were emplaced along the middle detachment fault. The middle detachment in many localities cuts across structure within the lower allochthon; however, there is no consistency in whether it cuts up or down structure relative to the footwall in any given direction. In part, this is due to uncertainties in the number of recumbent anticline-syncline pairs contained within the lower allochthon, which make correlation of structural level within the lower allochthon difficult. In some localities, such as at Crystal Peak, the middle detachment is approximately parallel to lithologic layering in the footwall (Fig. 4).

Along the base of the middle allochthon, a thin sliver of Manning Canyon Shale is present locally. In most places, this is indicated only by shale chips in float and the development of sooty-colored soil. However, at Bald Knoll (Figure 2), a 5-meter thickness of black shale is exposed. Pressure shadows around pyrite are ubiquitous and impart a strong WSW-trending stretching lineation in this shale. In thin sections cut parallel to the lineation and perpendicular to foliation, the pressure shadows are strongly asymmetric relative to foliation (Fig. 12). The morphology of these fibers is similar to that described by Etchecopar and Malavielle (1988) for rigid, face-controlled fibers growing around euhedral pyrite during non-coaxial flow. These pressure shadows are interpreted as recording top-to-the-WSW shearing. Because this shale occurs as a thin sliver at the base of the middle allochthon, probably within a fault zone, the kinematics of deformation within this shale is extrapolated to movement along the middle detachment. This translation direction is substantiated by highly lineated Manning Canyon Shale and lower Oquirrh Formation limestone adjacent to the middle detachment in the Black Hills, 19 km to the east (Fig. 2). This is also consistent with data from the Black Pine Mountains which also indicate westward transport of the middle allochthon (Wells, 1988).

Movement along the middle detachment fault probably occurred during low ambient temperatures. This is evident by the metamorphic discontinuity across this fault in the study area and further to the west (Compton and others, 1977). Conodonts from the lower Oquirrh Formation within the middle allochthon at Crystal Peak yield CAI values of 5 indicating metamorphic temperatures of 350-400° C, whereas metamorphic temperatures in the footwall were 490 to 520° C, as indicated by oxygen isotopic geothermometry and CAI values >7 (Wells and others, 1990; J. Repetski, personal communication, 1988). Therefore the displacement along the middle detachment was probably late- to post-metamorphic.

(5) F_5 Open Folding. Both the lower and middle allochthon are folded into broad, upright, open folds whose axes generally trend N-S. Axial traces of these folds are illustrated in Figure 11, with Pi diagrams of poles to bedding

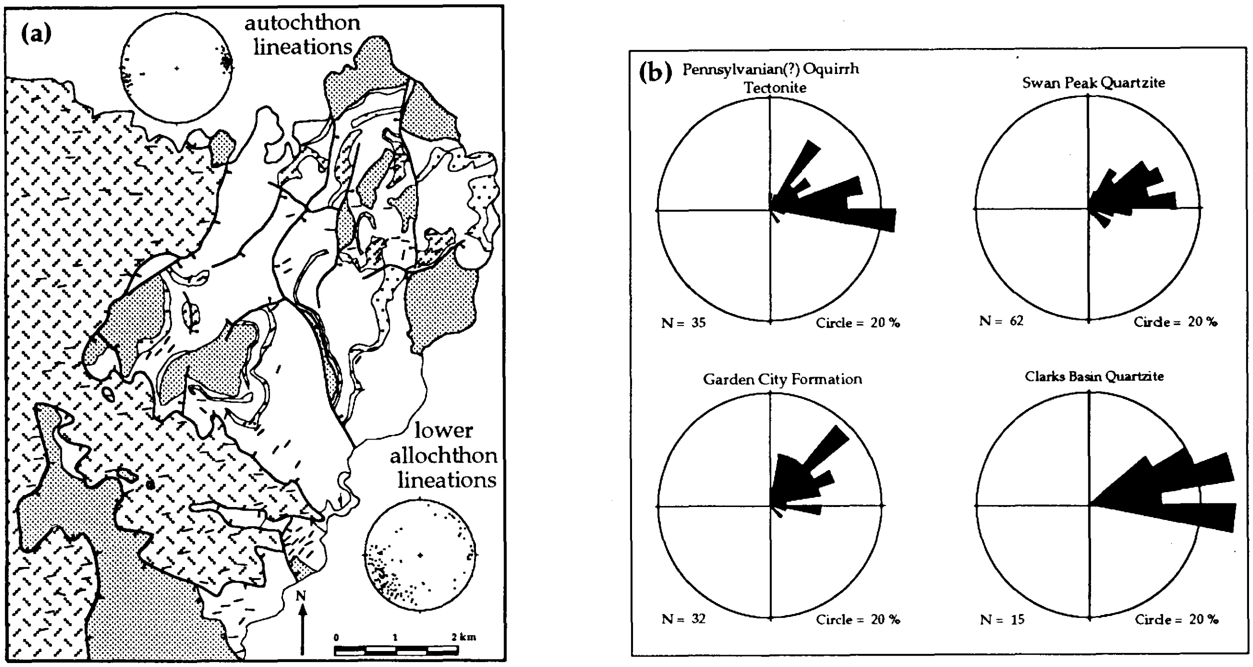

Figure 11. Lineations from the eastern end of the Raft River Mountains. a) Lineation map with stereographic projections of lineations from the autochthon and from the lower allochthon. b) Rose diagrams of azimuths of lower allochthon lineations divided by lithology. The predominance of E-W lineations within the Pennsylvanian(?) tectonite reflects the greater development of lineations related to westward D_2 attenuation faulting.

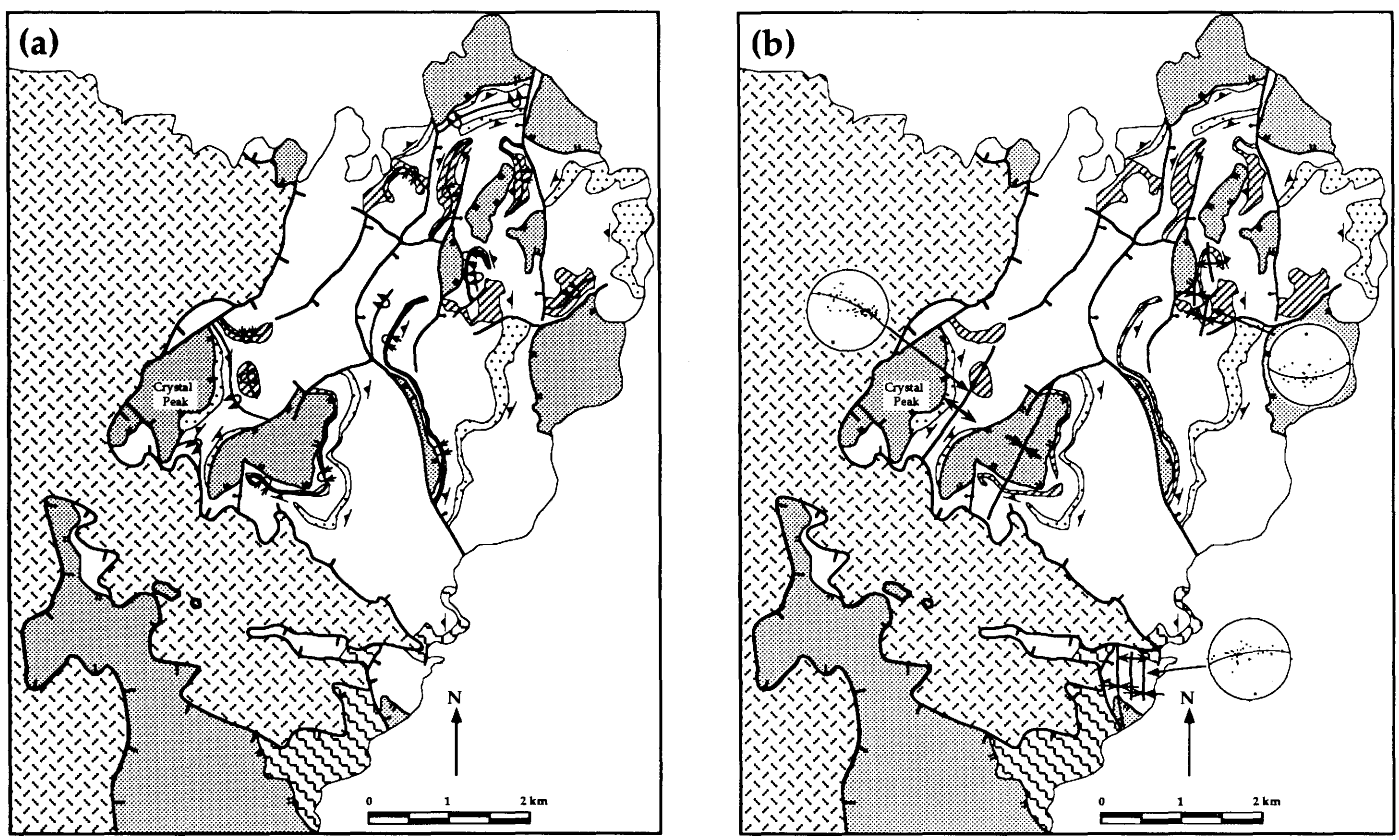

Figure 12. Generalized geologic map of the eastern Raft River Mountains indicating axial traces of F_3 recumbent folds (a) and axial traces of F_5 open folds (b). Note that the Pennsylvanian (?) marble commonly occurs within the cores of recumbent synclines. Stereonets are Pi-diagrams of poles to foliation from the indicated localities of F_5 folds, pole to best-fit great circle indicated with a box is the fold axis. See Figure 4 for explanation of symbols.

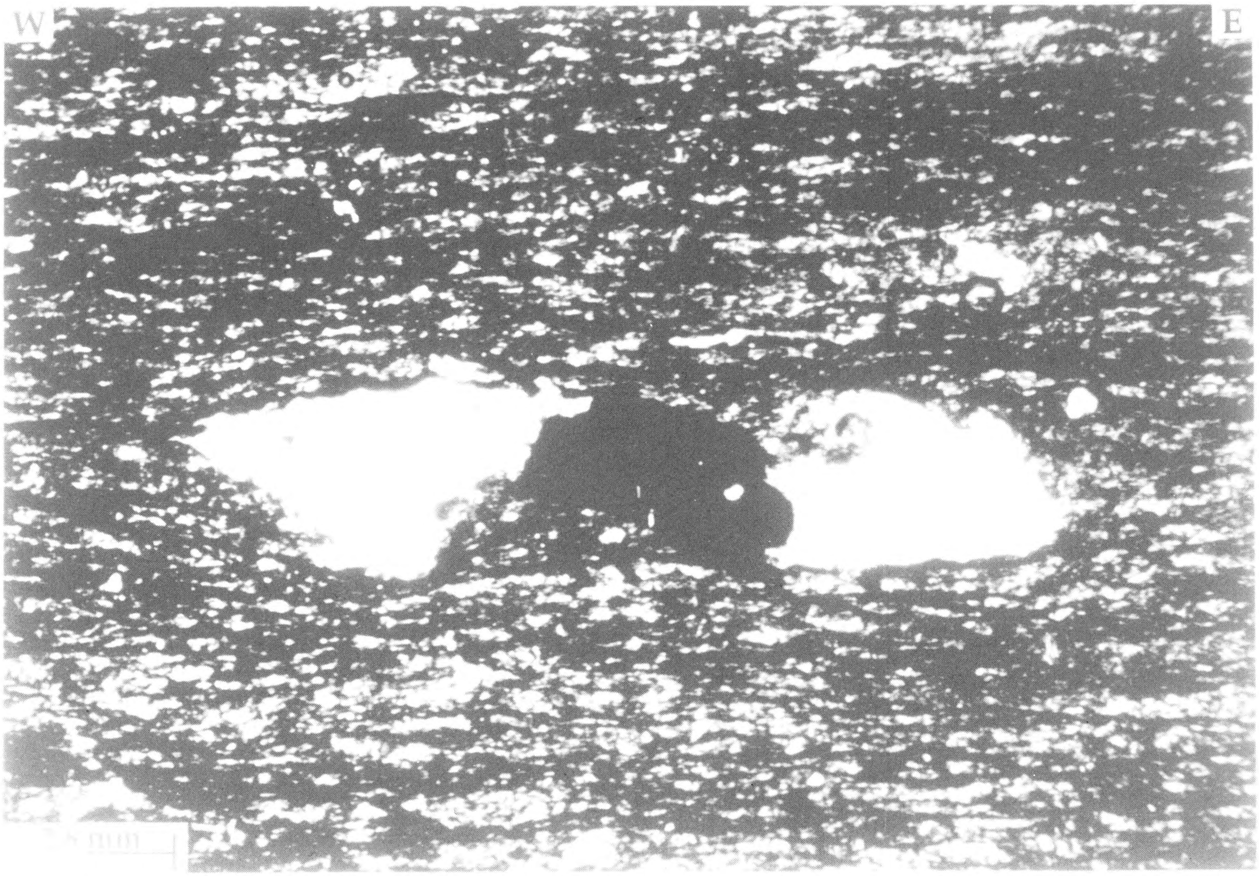

Figure 13. Photomicrograph of pressure shadow from Manning Canyon Shale at base of middle allochthon at Bald Knoll. Asymmetric quartz-calcite pressure shadow around pyrite, which are ubiquitous within this shale, indicates westward shearing.

from various localities. The wavelengths of these folds are highly variable. Due south of Crystal Peak, an F_5 open fold with a wavelength greater than 1500 meters is well exposed (Figs. 11 & 13). This fold clearly deforms both the middle detachment and underlying low-angle faults within the lower allochthon, and is truncated by the Raft River detachment. At other localities, the folds have wavelengths of 30 to 150 meters.

(6) Footwall Shear Zone and Raft River Detachment Fault. Beneath the Raft River detachment and within the autochthon lies a shear zone that is generally parallel to bedding in the Proterozoic (?) units, and the underlying unconformity with Archean rocks. Previous studies of the shear zone farther west have documented large-scale top-to-the-east displacement along this ~300 m-thick zone (Compton, 1980; Sabisky, 1985; Malavielle, 1987a). The shear zone is continuous to the extreme eastern exposures of the autochthon, apparently maintaining its bedding-parallel nature over a distance greater than 21 km parallel to the transport direction. Mylonitic fabrics are the most highly developed within the Elba Quartzite and its schist member, and fabric intensity related to eastward shearing dies out downward within the Green Creek Complex.

Stretching lineations within the Elba Quartzite and overlying schist consistently trend 083 ± 10° (Fig. 10), and are defined by elongation of quartz grains, quartz ribbons, and mica, and the long axes of clasts in conglomeratic horizons. The preferred orientation of quartz c-axes, asymmetric feldspar porphyroclasts, oblique grain-shape foliations, and mica fish consistently indicate eastward shearing. Within the schists of the Green Creek Complex, shear bands or extensional crenulation cleavage (Platt and Vissers, 1980) yielding eastward shear-sense are ubiquitous.

Superimposed on the shear zone in the autochthon is the brittle Raft River detachment fault. This fault lies above the schist member of the Elba Quartzite, and in the eastern Raft River Mountains, marks a major structural discontinuity. Although this fault is concordant with foliation and bedding within the lower plate, structures within the upper plate are commonly truncated. The fault surface is not exposed, but float blocks of brecciated and oxidized carbonate are commonly present. However, in the SE end of the Raft River Mountains, the fine-grained schist which is present in the footwall adjacent to the detachment has been subject to cataclasis. Here, resistent ledges of black cataclasite demarcate the detachment fault. Both brittle and ductile cataclastic rocks are present as are many shear fabrics common to ductile shear zones.

As in other Cenozoic metamorphic core complexes, there is a close spatial and kinematic association between the Raft

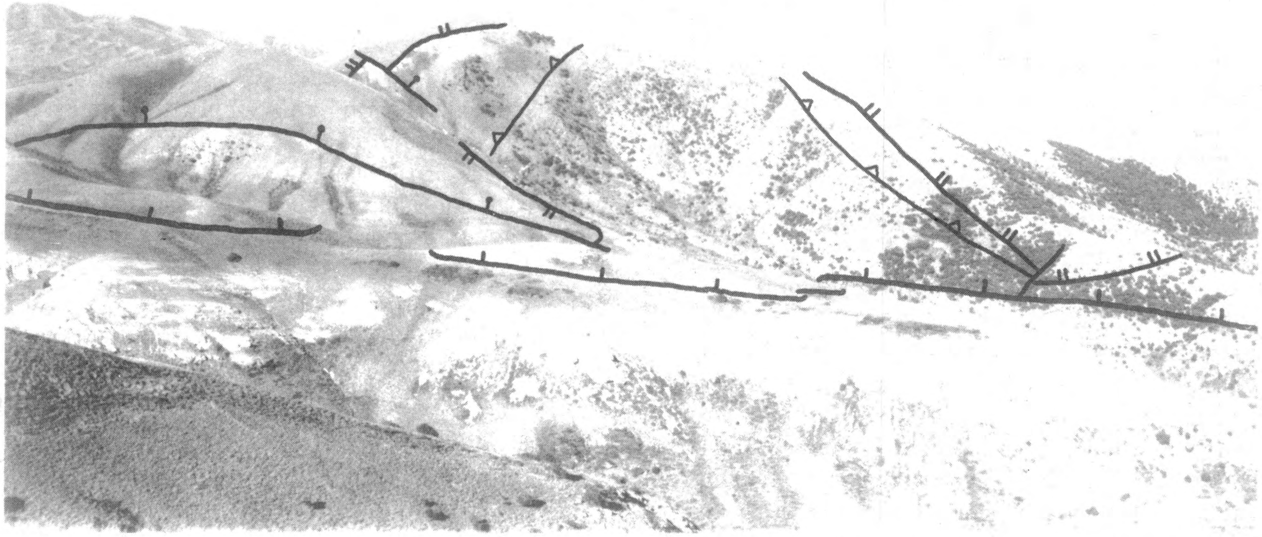

Figure 14. Photograph of F_5 open fold on south side of Crystal Peak. The Raft River detachment truncates the broad fold, which folds both D_2 attenuation faults and the middle detachment.

River detachment fault and the underlying shear zone. Fabrics within the uppermost shear zone are commonly retrograded, and where a brittle cataclasite is present beneath the detachment fault, a progression between lower mylonite and upper cataclasite is commonly evident. Both plastic and brittle deformations exhibit the same kinematics of top-to-the-east shearing.

Existing geochronology from the autochthon is scarce and incomplete given the complexity of the data; however, all ages are in marked contrast to the Late Cretaceous muscovite ages from the lower allochthon (Wells and others, 1990). In Clear Creek canyon, autochthon metamorphic ages are: 19 ± 0.5 Ma ($^{40}Ar/^{39}Ar$ muscovite, Malavielle, 1987b) from the Elba Quartzite; 20 ± 10 and 20 ± 4 Ma (apatite and sphene fission track, respectively, Compton and others, 1977) from adamellite; 57 + 8/ -3 Ma (biotite conventional K-Ar, with 22% chlorite and 3% feldspar and quartz, Armstrong and Hansen, 1966) from adamellite 2.5 km southwest; and 10.2 ± 1.9 and 12.4 ± 2.4 Ma (apatite and sphene fission track, Compton and others, 1977) from older schist 2.6 km to the SE. These ages, taken as a whole, are difficult to interpret. However, in exclusion of the biotite age (possibly justified both by its impurity and use of conventional K-Ar dating), these ages suggest somewhat rapid cooling during the Miocene, probably during footwall uplift related to both displacement and unroofing. Additionally, although these cooling ages need not imply that these rocks were plastically deforming in the Miocene, the presence of preserved intracrystalline strain as well as low-temperature strain features (i.e., quartz deformation lamellae) suggest that the rocks were deforming as they were uplifting.

(7) Broad Folding. The present morphology of the Raft River Mountains is that of an east-west-trending, doubly plunging anticline of 26 km and 1.2 km of exposed structural relief. The axis of the elongate anticline is parallel to the transport direction for both the footwall shear zone and the brittle deformation associated with the detachment fault. The shear zone, the strata in the autochthon, and the detachment fault outline this large structure. This anticline may be viewed as an interference structure formed by the interaction of two anticlines; one with an axis parallel to, and the other with an axis perpendicular to, the stretching lineation.

Nonplanar detachment faults of comparable geometry are present within many other core complexes, in particular core complexes of the Colorado River trough region (Spencer, 1982). The broad folding along axes perpendicular to the transport direction has been linked to flexural uplift of the denuded footwall, following detachment faulting (Spencer, 1984; Buck, 1988). The origin of lineation-parallel folds, on the other hand, is a subject that is less well understood. It has been proposed that they are primary features such as large-scale fluting structures developed during shearing within the fault zone (John, 1984), or alternatively that they form secondarily from decompression caused by unloading of the footwall (Spencer, 1982). The near parallelism of the shear zone detachment fault to the footwall strata over a wide area of the Raft River Mountains, particularly in the orientation perpendicular to the anticlinal axis, strongly suggests that the fold developed after faulting. Additionally, deformed upper Miocene beds along the flanks of the Raft River Mountains suggest that folding about an E-W axis took place in Pliocene time (Compton and others, 1977).

DISCUSSION

Age of Upper Plate Ductile Extension

Previously it was postulated (Wells and others, 1990) that the D_2 attenuation faults were related to the D_1 fabrics, and that both were Late Cretaceous, in part based on the similarity in $^{40}Ar/^{39}Ar$ ages of muscovites collected from domains characterized by each fabric. Although this interpretation requires refinement in light of the new kinematic data and observations, which indicate that the attenuation faults are younger than the D_1 fabrics, the interpretation of the absolute age of the fault zones remains unaltered.

As described in Wells and others (1990), $^{40}Ar/^{39}Ar$ ages were determined for muscovite from 4 sampes of marble and schist from the lower allochthon. Muscovite separates from samples of the Garden City Formation containing D_1 fabrics yielded ages of 81.7 ± 0.2, 87.8 ± 0.3, and 90.4 ± 0.3 Ma; a muscovite separate from Pennsylvanian (?) marble tectonite within a D_2 fault zone (LAF1) yielded a similar age, 88.5 ± 0.3 Ma. I now interpret, based on new fabric and texture analysis, that there are two generations of rock fabrics which yield similar muscovite ages. The similarity in ages from both D_1 and D_2 fabrics indicates that both fabrics developed prior to or synchronous with the cooling ages indicated by the $^{40}Ar/^{39}Ar$ age spectra.

Possible Eocene Deformation

Preliminary geochronology presented in Wells and others (1990) from the eastern Raft River Mountains indicates a 50 Ma thermal event that is mildly expressed in the low-temperature increments of all muscovite $^{40}Ar/^{39}Ar$ age spectra, and is much more evident in the whole-rock phyllite analysis. This thermal event postdates D_2 attenuation faulting, and probably corresponds with either F_3 recumbent folding, or emplacement of the middle allochthon. The Raft River-Albion-Grouse Creek core complex is the northernmost core complex south of the Snake River Plain. North of the Snake River Plain, extensional shearing in both the Pioneer and Bitterroot core complexes is Eocene in age (Garmezy and Sutter, 1983; Silverberg, 1988); possibly, the Eocene thermal event in the Raft River Mountains is also related to extension.

Existence of Mesozoic Plateau and Hinterland Extension

A much debated question is whether or not the interior of the hinterland to the foreland thrust belt was an uplifted plateau in Mesozoic time, that locally failed in upper crustal extension. By analogy with active mountain belts of similar tectonic setting such as the South American Andes, where a continental plateau separates the foreland thrust belt from the magmatic axis, it is likely that the hinterland of the Sevier belt was also an uplifted plateau in Mesozoic time (Jordan and others, 1983). Although much speculation over this possibility has taken place, the question remains unresolved. For example, it has been suggested that the metamorphic core complexes are remnants of a thickened Mesozoic hinterland crust (that supported a high-standing topography) that collapsed in extension due to the lateral variation in crustal thickness (Coney and Harms, 1984). This tendency for topographically uplifted and crustally thickened orogenic interiors to later collapse and spread laterally has been used to explain the commonly observed transition from early contractional to later extensional deformation in many mountain belts (e.g., Molnar and Tapponnier, 1978; Selverstone, 1988). However, other factors could have led to the Tertiary extension in the Basin and Range Province, and Tertiary extension does not necessarily require Mesozoic crustal thickening.

Central to any discussion of the Mesozoic paleogeography of the northeastern Great Basin is the regionally extensive unconformity separating Tertiary rocks from upper Paleozoic and Mesozoic rocks, with only minor angular discordance. This sub-Tertiary unconformity has been used to argue for the lack of significant erosion and structural relief in the Mesozoic (Armstrong, 1968, 1972; Gans and Miller, 1983). However, if the hinterland was a high-standing plateau, it could have been internally drained as is the case for other continental plateaus (e.g., Jordan and Alonso, 1987), effectively buffering the plateau against erosion. In fact, internal drainage for Late Cretaceous to early Tertiary basins in eastern Nevada figured prominently in recent regional paleogeographic reconstructions (Vandervoort and Schmidt, 1990). Additionally, if uplift was related to crustal thickening at depth, the upper crustal rocks could have remained relatively flat-lying. Thus, rather than preclude topographic development within the Mesozoic hinterland, the sub-Tertiary unconformity could constrain the geometry of uplift.

Several recent studies of active contractional mountain belts have indicated that the upper crust of high-standing plateaus can undergo extension contemporaneously with shortening at depth and in the adjacent foreland (e.g., Dalmayrac and Molnar, 1981; Burchfiel and Royden, 1985; Molnar and Lyon-Caen, 1988). This scenario might apply to the Sevier belt hinterland; if there was significant topography within the hinterland during Mesozoic time, then the delicate balance between topography, topographic slope, and compressional boundary stresses could locally have been upset, and the upper crust could have failed in extension. Additionally, application of thrust belt wedge models (Dahlen and Suppe, 1988) to orogenic belts suggests that extension can be produced within the rear of contractional orogenic wedges to accommodate changes in topographic slope, basal rheology, or compressional boundary stresses (Platt, 1986). Furthermore, this treatment of mountain belts as orogenic wedges suggests that alternating periods of shortening and extension can be episodically produced by these changing parameters (Platt, 1986). If late Mesozoic extensional structures, coeval with overall contraction, are present within the hinterland, this would strongly suggest that the hinterland was a region of high-standing topography.

The D_2 attenuation faults from the eastern Raft River Mountains are interpreted to record crustal extension (Wells and others, 1990). Combined with structural and isotopic work from the Black Pine Mountains, this extension is constrained as occurring in the early Late Cretaceous. The development of extensional deformation at upper crustal levels in the Mesozoic hinterland synchronously with shortening in the foreland (and probable shortening at depth in the hinterland) strongly suggests that the hinterland had a high-standing topography. This topography is inferred to have developed due to substantial shortening of the lower and middle crust.

Recumbent Folding and Possible Kinematic Reversals

The F_3 recumbent folds which developed within the lower allochthon remain an enigma. Because of their poorly understood geometry, the vergence of these structures remains undetermined. Presently, foliation and bedding generally dip westward, suggesting east-vergent folds. However, much of this westward tilt is probably caused by rotation concurrent with down-to-the-east normal faulting within the upper plate of the Raft River detachment. The similarity between structural sequences in the Raft River and Black Pine mountains suggests that the Raft River folds may have the same westward vergence as the recumbent folds within the Black Pine Mountains. The absence of rocks younger than lower Pennsylvanian involved in recumbent folding suggests that the folds were detached during their development.

It is possible that these folds developed during extension. For example, kilometer-scale recumbent folds are developed within the autochthon extensional shear zone in the Raft River Mountains (Compton, 1980; Sabisky, 1985; Malavielle, 1987a). These folds are developed within zones of very high shear strain and may represent a-type and sheath folds (e.g., Cobbold and Quinquis, 1980; Carreras and others, 1977). However, it is doubtful that the recumbent folds within the eastern Raft River lower allochthon represent sheath folds for several reasons including the lack of coeval fabrics recording high shear strains related to recumbent folding. A more feasible extensional analog is the recumbent folds related to the Himalayan detachment system, which occur in moderately strained rocks and are apparently nucleated at ramps in normal faults (K. V. Hodges, personal communication, 1989). If these F_3 folds did develop during extension, then deformations D_2 through D_4 record a protracted period of extension prior to the development of the Cenozoic Raft River detachment.

The alternative and favored interpretation, is that the F_3 recumbent folds developed within a regime of regional shortening. Recumbent folds with axes perpendicular to the transport direction are well-recognized from the internal parts of most fold and thrust belts. In this case, the D_1 fabrics and the D_3 recumbent folds record shortening, whereas the D_2 attenuation faults and the D_4 middle detachment record extension, requiring alternating extensional and contractional episodes. This interpretation is supported by the structural sequence observed in the Black Pine Mountains (Wells and Allmendinger, 1990); there, coaxial bedding-parallel extensional fabrics of Late Cretaceous age (Wells and others, 1990) are folded about west-verging overturned to recumbent folds, which in turn are cut by west-verging low-angle, younger-over-older faults correlative with the middle detachment in the eastern Raft River Mountains. The implication is that during the Mesozoic to early Cenozoic evolution of the Cordilleran hinterland, extension transpired episodically, interspersed with contractional deformation. This is an attractive interpretation for two reasons: (1) Mesozoic age in the northeastern Great Basin (e.g., Miller this region, as well as elsewhere within the Cordilleran hinterland (Hodges and Walker, 1990; Hodges and others, in press), strongly suggests that locally there was high-standing topography. This being the case, we would expect alternations from extension to contraction, to accommodate changes in the boundary conditions of the orogenic wedge, such as the width of the mountain belt, degree of underplating and consequent topographic development, and convergence rate. (2) Presently, there are many conflicting reports of probable extensional and contractional structures of Mesozoic age in the northeastern Great Basin (e.g.,Miller and Gans, 1989; Snoke and Miller, 1988; Wells and others, 1990). A model invoking reversals in contraction and extension would explain these apparent kinematic inconsistencies.

Correlations to the Raft River-Albion-Grouse Creek Metamorphic Core Complex

Although lineations from rocks exhibiting D_1 fabrics in the eastern Raft River Mountains are highly variable, the general NE trend is similar to L_1 of Miller (1980) in the Albion Mountains and L_1 lineations from the Grouse Creek Mountains (Compton and others, 1977; Todd, 1980). Fabrics associated with these lineations in the Albion and Grouse Creek mountains have been shown to record top-to-the-NE shearing (Malavielle, 1987b).

Seven Mesozoic K-Ar ages have been reported from rocks containing NE-trending L_1 lineations from the Albion Mountains (Armstrong, 1976; Miller, 1980). Because of the similarity in cooling ages between the eastern Raft River Mountains and the northern Albion Mountains, and because of the similarity in kinematics, correlation of these events is tentatively proposed. These early NE-directed fabrics have been suggested to be related to regional shortening (Miller, 1980; Malavielle, 1987b). The D_1 fabrics within the eastern Raft River Mountains possibly also developed during an early contractional deformation.

One possible contractional structure with which D_1 fabrics could be linked is the Basin-Elba fault in the northern Albion Mountains, which places Proterozoic to early Paleozoic(?) rocks over Archean through Ordovician rocks (Miller, 1980; Hodges and McKenna, 1986). Thermobarometric work by Hodges and McKenna (1986) suggests that this fault places rocks with mineral assemblages yielding estimates of 480-540 MPa and 532-562 °C, over rocks with P-T conditions of 350-410 MPa and 477-527 °C. Mesozoic K-Ar cooling ages (Armstrong, 1976) from rocks within this fault zone combined with these thermobarometric estimates suggest that this structure is a Mesozoic thrust fault (Hodges and McKenna, 1986; Malavielle, 1987b). However, there is no consensus on whether the Basin-Elba fault is a D_1 or younger structure (Hodges and McKenna, 1986; Malavielle, 1987b).

Compton and others (1977) described a regional detachment which emplaced variably metamorphosed Mississippian, Pennsylvanian, and Permian rocks over metamorphosed Ordovician and older rocks of the lower allochthon, omitting Silurian, Devonian, and much of the Mississippian strata. In the eastern Raft River Mountains, this structure corresponds to what I have mapped as the middle detachment, which separates the middle allochthon from the lower allochthon (Fig. 3 and 4). Compton and others (1977), however, did not recognize the LAF1 described here, and therefore did not recognize the stratigraphic omission which is present within the lower allochthon. One significant aspect of the recognition of LAF1 is that the stratigraphic omission of Silurian through Mississippian units previously assigned to motion along the middle detachment (Compton and others, 1977) actually occurred much earlier in the structural history; omission of these rocks in the eastern Raft River Mountains occurred prior to emplacement of the middle allochthon and prior to recumbent folding within the lower allochthon. The middle allochthon, then, cut across a previously folded lower allochthon which was *already missing* Silurian through Mississippian strata, and was juxtaposed against various structural levels of the lower allochthon. It is important to note that, although these relationships and distinctions hold for the eastern Raft River Mountains, they may not apply to the much larger area described by Compton and others (1977).

CONCLUSIONS

Geologic mapping, macro- and microscopic kinematic and strain analyses, and $^{40}Ar/^{39}Ar$ studies of rocks within the eastern Raft River Mountains provide constraints on the geometry, kinematics, and timing of Mesozoic and Cenozoic deformations. These results have important implications for several questions regarding the tectonics of the Sevier belt hinterland, including the timing of the onset of extension and the possible existence of a high-standing topography in the Mesozoic. Two ductile deformation episodes precede recumbent folding of Cambrian(?) through Pennsylvanian(?) strata of the lower allochthon; the first is penetrative throughout these rocks, and probably records NE-directed contractional deformation. The second set of ductile fabrics is localized along discrete shear zones that are generally parallel to lithologic contacts and accomplish significant stratigraphic attenuation. These attenuation fault zones record top-to-the-west shearing. Synkinematic muscovite from both generations of fabrics record very similar $^{40}Ar/^{39}Ar$ cooling ages, indicating that both events occurred prior to 82-90 Ma.

The D_2 attenuation faults are interpreted to record extensional deformation. Combined with structural and isotopic work from the Black Pine Mountains, this extension is constrained as occurring in the early Late Cretaceous. The development of extensional deformation at upper crustal levels in the Mesozoic hinterland strongly suggests that the hinterland had a high-standing topography. This topography is inferred to have developed due to substantial contractional deformation of the lower and middle crust in the hinterland. The production of earlier NE-vergent ductile structures by shortening is strongly suggested by fabric correlations within the Grouse Creek and Albion mountains. Perhaps these features are related to the crustal thickening that could have produced this elevated topography.

Both sets of ductile fabrics were subsequently folded about enigmatic D_3 recumbent folds, which could have developed during extension or shortening. An areally extensive allochthon of dominantly Pennsylvanian and Permian rocks was emplaced along the low-angle middle detachment fault, cutting across various structural levels of the recumbently folded lower allochthon. If D_3 recumbent folds developed during shortening, the D_1 through D_4 structural sequence records episodic reversals in contraction and extension.

Early to middle Tertiary extension is recorded in the development of a ~300 m-thick ductile shear zone in Precambrian(?) rocks, and the late, superimposed Raft River detachment fault. Progressive crystal-plastic to brittle shearing and the kinematic consistency between brittle and ductile shearing is compatible with the evolving low-angle shear zone model.

ACKNOWLEDGMENTS

This research was supported by National Science Foundation Grant EAR-8720952 (awarded to R. W. Allmendinger), the Geological Society of America, Sigma XI, and the Graduate School at Cornell University. Kenneth Tillman and Trenton Cladouhos provided very able assistance in the field. Rick Allmendinger, David Miller, Phyllis Camilleri and an anonymous reviewer provided many useful comments and suggestions on this manuscript.

REFERENCES

Allmendinger, R. W., and Jordan, T. E., 1984, Mesozoic structure of the Newfoundland Mountains, Utah: Horizontal shortening and subsequent extension in the hinterland of the Sevier belt: Geological Society of America Bulletin, v. 95, p. 1280-1292.

Allmendinger, R. W., Miller, D. M., and Jordan, T. E., 1984, Known and inferred Mesozoic deformation in the hinterland of the Sevier belt, northwestern Utah, *in* Kerns, G. J., and Kerns, R. L., eds., Geology of northwestern Utah, southern Idaho and northeast Nevada: Utah Geological Association, Publication 13, p. 21-34.

Armin, R.A. and Mayer, L., 1983, Subsidence analysis of the Cordilleran miogeocline: implications for timing of late Proterozoic rifting and amount of extension: Geology, v. 11, n. 2, p. 702-705.

Armstrong, F. C., and Oriel, S. S., 1965, Tectonic development of the Idaho-Wyoming thrust belt: American Association of Petroleum Geologists Bulletin, v. 49, p. 1847-1866.

Armstrong, R. L., 1968a, Sevier orogenic belt in Nevada and Utah: Geological Society of America bulletin, V. 79, p. 429-458.

————, 1968b, Mantled gneiss domes in the Albion Range, southern Idaho: Geological Society of America Bulletin, v. 79, p. 1295-1314.

————, 1972, Low-angle (denudation) faults, hinterland of the Sevier orogenic belt, eastern Nevada and western Utah: Geological Society of America Bulletin, v. 83, p. 1729-1754.

————, 1976, The geochronology of Idaho (Part 2): Isochron/West, no. 15, p. 1-33

Buck, W. R., 1988, Flexural rotation of normal faults: Tectonics, v. 7, p. 959-973.

Burchfiel, B. C., and Royden, L. H., 1985, North-south extension within the convergent Himalayan region: Geology, v. 13, p. 679-682.

Carreras, J., Estrada, A., and White, S., 1977, The effects of folding on the c-axis fabrics of a quartz mylonite: Tectonophysics, v. 39, p. 3-24.

Cobbold, P., and Quinquis, H., 1980, Development of sheath folds in shear regimes: Journal of Structural Geology, v. 2, p. 119-126.

Compton, R. R., 1972, Geologic map of Yost quadrangle, Box Elder County, Utah, and Cassia County, Idaho: U. S. Geological Survey, Miscellaneous Geologic Investigations Map I-672.

————, 1975, Geologic map of Park Valley quadrangle, Box Elder County, Utah, and Cassia County, Idaho: U.S. Geological Survey, Miscellaneous Geologic Investigations Map I-873.

————, 1980, Fabrics and strains in quartzites of a metamorphic core complex, Raft River Mountains, Utah, *in* Crittenden, M. D., Jr., Coney, P. J., and Davis, G. H., eds., Cordilleran metamorphic core complexes: Geological Society of America Memoir 153, p. 385-398.

————, 1983, Displaced Miocene rocks on the west flank of the Raft River-Grouse Creek core complex, Utah, *in* Miller, D. M., Todd, V. R., and Howard, K. A., eds., Tectonic and stratigraphic studies in the eastern Great Basin: Geological Society of America Memoir 157, p. 271-279.

Compton, R. R., Todd, V. R., Zartman, R. E., and Naeser, C. W., 1977, Oligocene and Miocene metamorphism, folding, and low-angle faulting in northwestern Utah: Geological Society of America Bulletin, v. 88, p. 1237-1250.

Compton, R. R., and Todd, V. R., 1979, Oligocene and Miocene metamorphism, folding, and low-angle faulting in northwestern Utah: Reply: Geological Society of America Bulletin, v. 90, p. 307-309.

Crittenden, M. D., Jr., 1979, Oligocene and Miocene metamorphism, folding, and low-angle faulting in northwestern Utah: Discussion: Geological Society of America Bulletin, v. 90, p. 305-306.

Crittenden, M.D., Jr., Coney, P.J., and Davis, G.H., eds, 1980, Cordilleran metamorphic core complexes: Geological Society of America Memoir 153, 490 p.

Dalmayrac, B., and Molnar, P., 1981, Parallel thrust and normal faulting in Peru and the constraints on the state of stress: Earth and Planetary Science Letters, v. 55, p. 473-481.

Dahlen, F. A., and Suppe, J., 1988, Mechanics, growth, and erosion of mountain belts, *in* Clark, S. P., Jr., Burchfiel, B. C., and Suppe, J., eds., Processes in continental lithospheric deformation: Boulder, Colorado, Geological Society of America, Special Paper 218, p. 161-178.

Day, W. C., Elrick, M., Ketner, K. B., Vaag, M. K., 1988, Geologic Map of the Bluebell and Goshute Peak Wilderness study areas, Elko Country, Nevada: U. S. Geological Survey, Miscellaneous Field Studies Map MF-1932.

Dietrich, D., and Song, H., 1984, Calcite fabrics in a natural shear environment, the Helvetic nappes of western Switzerland: Journal of Structural Geology, v. 6, p. 19-32.

Etchecopar, A., and Malavielle, J., 1988, Computer models of pressure shadows: a method for strain measurement and shear-sense determination: Journal of Structural Geology, v. 9, p. 667-677.

Felix, 1952, Geology of the eastern part of the Raft River Range, Box Elder County, Utah, *in* Eardley, A. J., and Hardy, G. T., eds., Geology of parts of northwestern Utah: Utah Geological Society Guidebook to the Geology of Utah, no. 11, p. 76-97.

Gans, P. B., and Miller, E. L., 1983, Style of mid-Tertiary extension in east-central Nevada: Utah Geological and Mineral Survey Special Studies, 59, p. 107-139

Garmezy, L., and Sutter, J. F., 1983, Mylonitization coincident with uplift in an extensional setting, Bitterroot Range, Montana-Idaho: Geological Society of America Abstracts with Programs, V. 15, p. 578.

Handin, J. W., and Griggs, D. T., 1961, Deformation of the Yule marble, part II: Geological Society of America Bulletin, v. 62, p. 863-886.

Hintze, L.F., 1978, Sevier orogenic attenuation faulting in the Fish Springs and House Ranges, western Utah: Brigham Young University Geology Studies, v. 25, part 1, p. 11-24.

Hintze, L. F., 1988, Geologic history of Utah: [Provo, Utah], Brigham Young University, Geology Studies Special Publication 7, 202 p.

Hodges, K. V., and McKenna, L., 1986, Structural and metamorphic characteristics of the Raft River-Quartzite Allochthon juxtaposition, Albion Mountains, southern Idaho: Geological Society of America Abstracts with Programs, v. 18, p. 117.

Hodges, K. V., and Walker, J. D., 1990, Petrological constraints on the unroofing history of a metamorphic core complex, Funeral Mountains, California, J. Geophys. Res., v. 95, p. 8437-8445.

Hodges, K. V., Snoke, A. W., and Hurlow, H. A., in press, Thermal evolution of a portion of the Sevier hinterland: the northern Ruby Mountains-East Humboldt Range and Wood Hills, northeastern Nevada: Tectonics.

John, B. E., 1984, Primary corrugations in Tertiary low-angle normal faults, SE Californian: Porpoising mullion structures: Geological Society of America Abstracts with Programs, v. 16, p. 291.

Jordan, T. E., 1983, Structural geometry and sequence, Bovine Mountain, northwestern Utah, *in* Miller, D. M., Todd, V. R., and Howard, K. A., eds., Tectonic and stratigraphic studies in the eastern Great Basin: Geological Society of America Memoir 157, p. 215-228.

Jordan, T. E., and Douglass, R. C., 1980, Paleogeography and structural development of the Late Pennsylvanian to Early Permian Oquirrh basin, northwestern Utah, *in* Fouch, T. D., and Magathan, E. R., eds., Paleozoic paleogeography of west-central United States: Society of Economic Paleontologists and Mineralogists, Rocky Mountain Section, West-central United States Paleogeography Symposium 1 , p. 217-238.

Law, R. D., 1986, Relationships between strain and quartz crystallographic fabrics in the Roche Maurice quartzites of Plougastel, western Brittany: Journal of Structural Geology, v. 8, p. 493-515.

Law, R. D., Knipe, R. J., and Dayan, H., 1984, Strain path partitioning within thrust sheets: microstructural and petrofabric evidence from the Moine thrust zone at Loch Eriboll, northwest Scotland: Journal of Structural Geology, v. 6, p. 477-498.

Lister, G. S., and Snoke, A. W, 1984, S-C mylonites: Journal of Structural Geology, v. 6, p. 617-639.

Malavielle, J., 1987a, Extensional shearing and kilometer-scale a type folds in a Cordilleran metamorphic core complex (Raft River Mountains, northwestern Utah): Tectonics, v. 6., p. 423-448.

Malavielle, J., 1987b, Kinematics of compressional and extensional ductile shearing deformation in a metamorphic core complex of the northeastern Basin and Range: Journal of Structural Geology, v. 9, p. 541-554.

Miller, D. M., 1980, Structural geology of the northern Albion Mountains, south-central Idaho, *in* Crittenden, M. D., Jr., Coney, P. J., and Davis, G. H., eds., Cordilleran Metamorphic core complexes: Geological Society of America Memoir 153, p. 399-423.

Miller, D. M., 1983, Allochthonous quartzite sequence in the Albion Mountains, Idaho, and proposed Proterozoic Z and Cambrian correlatives in the Pilot Range, Utah and Nevada, *in* Miller, D. M., Todd, V. R., and Howard, K. A., eds., Tectonic and stratigraphic studies in the eastern Great Basin: Geological Society of America Memoir 157, p. 191-213.

Miller, D. M., Armstrong, R. L., Compton, R. R., and Todd, V. R., 1983, Geology of the Albion-Raft River-Grouse Creek Mountains area, northwestern Utah and southern Idaho: Utah Geological and Mineral Survey Special Studies, 59, p. 1-59.

Miller, D. M., Hillhouse, W. C., Zartman, R. E., and Lanphere, M. A., 1987, Geochronology of intrusive and metamorphic rocks in the Pilot Range, Utah and Nevada, and comparison with regional patterns: Geological Society of America Bulletin, v. 99, p. 880-885.

Miller, E. L., Gans, P. B., and Garing, J., 1983, The Snake Range decollement: An exhumed mid-Tertiary ductile-brittle transition: Tectonics, v. 2, p. 239-263.

Miller, E. L., and Gans, P. B., 1989, Cretaceous crustal structure and metamorphism in the hinterland of the Sevier thrust belt, western U.S. Cordillera: Geology, v. 17, p. 59-62.

Molnar, P. and Lyon-Caen, H., 1988, Some simple physical aspects of the support, structure, and evolution of mountain belts, *in* Clark, S. P., Jr., Burchfiel, B. C., and Suppe, J., eds., Processes in continental lithospheric deformation: Boulder, Colorado, Geological Society of America, Special Paper 218, p. 197-207.

Nolan, T. B., 1935, The Gold Hill mining district, Utah: U. S. Geological Survey Professional Paper 177, 172 p.

Oaks, R. Q., James, W. C., Francis, G. G., and Schulingkamp, W. J., 1977, Summary of Middle Ordovician stratigraphy and tectonics, northern Utah, southern and central Idaho: Wyoming Geological Association Guidebook, 27th Annual Field Conference, p. 101-118.

Platt, J. P., 1986, Dynamics of orogenic wedges and uplift of high-pressure metamorphic rocks: Geological Society of America Bulletin, v. 97, p. 1037-1053.

Platt, J. P., and Vissers, P. L., 1980, Extension structures in anisotropic rocks: Journal of Structural Geology, v. 2, p. 397-410.

Poole, F. G., 1974, Flysch deposits of the Antler foreland basin, western United States, *in* Dickinson, W. R., ed., Tectonics and Sedimentation: Society of Economic Paleontologists and Mineralogists Special Publication 22, p. 59-82.

Ramsay, J. G., and Huber, M. I., 1983, The techniques of modern structural geology Volume 1: Strain Analysis: New York, Academic Press, 307 p.

Robinson, J., 1990, A comprehensive study of the structural geology and regional tectonics of the Gold Hill area, northern Deep Creek Mountains, western Utah [Ph.D. Dissertation]: Ithaca, Cornell University, 287 p.

Sabisky, M. A., 1985, Finite strain, ductile flow, and folding in the central Raft River Mountains, northwestern Utah [M.S. thesis]: Salt Lake City, University of Utah, 69 p.

Saltzer, S. D., and Hodges, K. V., 1988, The Middle Mountain shear zone, southern Idaho: Kinematic analysis of an early Tertiary high-temperature detachment: Geological Society of America Bulletin, v. 100, p. 96-103.

Silverberg, D., 1988, Petrologic, $^{40}Ar/^{39}Ar$ isotopic and structural constraints on the Tertiary tectonic evolution of the Pioneer core complex, south-central Idaho: Geological Society of America Abstracts with Programs, v. 20, p. A18.

Snoke, A. W., and Lush, A. P., 1984, Polyphase Mesozoic-Cenozoic deformational history of the northern Ruby Mountains-East Humboldt Range, Nevada, *in* Lintz, J., Jr., ed., Western Geological Excursions: Reno, Nevada, Geological Society of America 1984 Annual Meeting, p. 232-260.

Snoke, A. W., and Miller, D. M., 1988, Metamorphic and tectonic history of the northeastern Great Basin, *in* Ernst, W. G., ed., Metamorphism and crustal evolution of the western United States: Englewood Cliffs, New Jersey, Prentice Hall, Rubey Volume VII, p. 606-648.

Spencer, J. E., 1982, Origin of folds of Tertiary low-angle fault surfaces, southeastern Californian and western Arizona: *in* Frost, E G., and Martin, D. L., eds., Mesozoic-Cenozoic Tectonic Evolution of the Colorado River Region, California, Arizona, and Nevada, Cordilleran Publishers, San Diego, CA, p. 123-134.

Spencer, J. E., 1984, Role of tectonic denudation in warping and uplift of low-angle normal faults: Geology, v. 12, p. 95-98.

Stewart, J. H., 1972, Initial deposits in the Cordilleran geosyncline: Evidence of a late Precambrian (850 m.y.) continental separation: Geological Society of America Bulletin, v. 8, p. 1345-1360.

Stewart, J. H., 1980, Geology of Nevada: Nevada Bureau of Mines and Geology, Special Publication 4, 136 p.

Stewart, J. H., and Poole, F. G., 1974, Lower Paleozoic and uppermost Precambrian Cordilleran miogeocline, Great Basin, western United States, *in* Dickinson, W.R., ed., Tectonics and sedimentation, Society of Economic Paleontologists and Mineralogists Special Publication #22, p. 28-57.

Stewart, J. H., and Suczek, C. A., 1977, Cambrian and latest Precambrian paleogeography and tectonics in the western United States, *in* Stewart, J.H., Stevens, C.H., and Fritsche, A.E., eds., Paleogeography of western United States, Society of Economic Paleontologists and Mineralogists, Pacific Section, Pacific Coast Paleogeography Symposium, 1st, p. 1-18.

Todd, V. R., 1980, Structure and petrology of a Tertiary gneiss complex in northwestern Utah, *in* Crittenden, M. D., Jr., Coney, P. J., and Davis, G. H., eds., Cordilleran metamorphic core complexes: Geological Society of America Memoir 153, p. 349-383.

Todd, V. R., 1983, Late Miocene displacement of pre-Tertiary and Tertiary rocks in the Matlin Mountains, northwestern Utah, *in* Miller, D. M., Todd, V. R., and Howard, K. A., eds., Tectonic and stratigraphic studies in the eastern Great Basin: Geological Society of America Memoir 157, p. 239-270.

Treagus, S. H., 1983, A theory of finite strain variation through contrasting layers, and its bearing on cleavage refraction: Journal of Structural Geology, v. 5, p. 351-368

Turner, F. J., 1953, Nature and dynamic interpretation of deformation in calcite of three marbles: American Journal of Science, v. 251, p. 276-298.

Turner, F. J., Griggs, D. T., and Heard, H. C., 1954, Experimental deformation of calcite crystals: Geological Society of America Bulletin, v. 65, p. 883-934.

Turner, F. J., Griggs, D. T., Clark, R. H., and Dixon, R. H., 1956, Deformation of the Yule marble, part VII: Geological Society of America Bulletin, v. 67, p. 1259-1294.

Vandervoort, D. , and Schmidt, J. G., 1990, Cretaceous to early Tertiary paleogeography in the hinterland of the Sevier thrust belt, east-central Nevada: Geology, v. 18, p. 567-570.

Wells, M. L., 1988, Structural geometry, sequence, and kinematics of the Black Pine Mountains, southern Idaho: Implications from the cover rocks to metamorphic core complexes [M.S. Thesis]: Ithaca, New York, Cornell University, 95 p.

Wells, M. L., and Allmendinger, R. W., 1990, An early history of pure shear in the upper plate of the Raft River metamorphic core complex; Black Pine Mountains, southern Idaho: Journal of Structural Geology, v. 12, p. 851-868.

Wells, M. L., Dallmeyer, R. D., and Allmendinger, R. W., 1990, Late Cretaceous extension in the hinterland of the Sevier thrust belt, northwestern Utah and southern Idaho: Geology, v. 18., p. 929-933.

Wernicke, B., 1981, Low-angle normal faults in the Basin and Range province: nappe tectonics in an extending orogen: Nature, v. 291, p. 645-648.

White, S., 1973, Deformation lamellae in naturally deformed quartz: Nature, v. 245, p. 26-28.

MESOZOIC STRUCTURE, METAMORPHISM, AND MAGMATISM IN THE PILOT AND TOANO RANGES

David M. Miller

U.S. Geological Survey
345 Middlefield Road, MS-975
Menlo Park, CA 94025

and

Thomas D. Hoisch

Department of Geology
Northern Arizona University
Flagstaff, AZ 86011

ABSTRACT

Mesozoic tectonic events in the Pilot and Toano Ranges of the northeastern Great Basin are dated by Late Jurassic and Late Cretaceous plutons and by ages of metamorphic minerals. A Jurassic pluton in the Pilot Range was emplaced at ~13 km depth into ductilely deforming crust between 155 and 165 Ma. Metamorphism at this time in the Pilot Range produced mineral assemblages in Late Proterozoic and Cambrian strata that indicate ~150°C temperature changes over just 3 km in like strata. Highest grade assemblages, present near the Jurassic pluton, indicate relatively high T (575-625°C), low P (3-4 kb) amphibolite facies metamorphism, probably induced by heat from nearby magma. Reinforcing this interpretation are $^{40}Ar/^{39}Ar$ age data that indicate peak metamorphism closely followed plutonism. Greenschist facies metamorphism farther from the pluton occurred under lower temperature conditions (~ 400°C) that require a slightly elevated geothermal gradient of ~ 30° C/km. Shortening manifested by southeast-vergent 10-km-scale folds, minor thrust faults, and local thinning of stratigraphic section accompanied metamorphism in the Pilot Range. A 162-Ma pluton in the Toano Range that intruded greenschist to lower amphibolite facies rocks also was at about 13 km depth. The pluton truncated bedding-parallel foliation and north- to northeast-trending folds that formed during metamorphism.

During the Late Cretaceous, mica Ar systems were set in all metamorphic rocks in the Pilot and Toano Ranges. Tectonic models for Cretaceous cooling are not well constrained in these ranges; ductile normal faults that produced horizontal extension in the Pilot Range, and hence footwall cooling, may be Cretaceous in age, whereas a single strongly peraluminous 80-Ma pluton in the Toano Range indicates at least locally elevated temperatures at that time.

Middle and Late Jurassic tectonism, dated by relations with widespread ~160- to 165-Ma plutons and dikes, varies considerably across the northeastern Great Basin. East of the Pilot Range, plutons were emplaced into shallow crust (depths less than 9 km) that was undergoing or had recently undergone approximately WNW-directed extension. Thrust faults predate the normal faults and plutons; the thrusts ramp up to the east and southeast through Ordovician strata, and probably have a few km of offset. Throughout this region and in the Pilot and Toano Ranges, Jurassic pressures determined from plutonic hornblende compositions are compatible with stratigraphic burial depths from reconstructed Paleozoic and Mesozoic strata. In contrast, Paleozoic rocks apparently metamorphosed during the Jurassic in the central Ruby Mountains to the west were deeper in the crust and require tectonic thickening, indicating larger-scale crustal shortening. If the Ruby Mountains metamorphism was Jurassic, a tectonic scenario for the Jurassic is magmatism-induced rifting in the east, modest

shortening in and near the Pilot Range, and larger-scale shortening farther west closer to the margin of the continental crust. However, considerable uncertainty exists about the timing of high-pressure metamorphism in the western belt.

Widespread cooling of metamorphic rocks is the hallmark of Late Cretaceous tectonics in the northeastern Great Basin. Whereas this event locally represents heating by Cretaceous magmas followed by cooling, most rocks in the Pilot Range region likely remained at 12-15 km depth and were able to maintain temperatures in excess of 300°C from 160 to 80 Ma. Modest upper-crustal extension, perhaps coupled with refrigeration by a cool shallow subduction slab that removed the hot mantle, best accounts for the Late Cretaceous cooling event.

INTRODUCTION

Over the last decade, substantial progress has been made in understanding Great Basin tectonics by separating data that unambiguously record Mesozoic tectonics from data that may record Cenozoic tectonics or a combination of the two. Much of the new data for Mesozoic tectonism has stemmed from combined geochronology and structural studies and, more recently, petrologic studies. Although the data still do not uniquely confirm specific tectonic models, they nonetheless provide firm constraints for models and point to fruitful directions for future studies.

Three regional aspects of Mesozoic tectonics of the northeastern Great Basin must be considered in addition to local data. (1) Early Cretaceous to middle Eocene east-directed shortening in the frontal fold and thrust belt (Sevier orogenic belt of Armstrong, 1968a) (Armstrong and Oriel, 1965; Crittenden, 1972; Heller and others, 1986) took place along faults that project westward beneath western Utah. These include the earliest identified frontal breakouts of thrusts. (2) Across much of the region west of the frontal thrust belt and east of the continental margin (Fig. 1), lower Tertiary deposits were laid concordantly on upper Paleozoic rocks, precluding major structures at the surface before the Eocene (Armstrong, 1968a). (3) Triassic and Lower Jurassic strata near Currie, Nevada (Fig. 1), correlate with Colorado Plateau strata (Stewart, 1980), indicating regionally uniform depositional environments until at least the Early Jurassic. Mesozoic tectonic events probably began in the Middle Jurassic, when orogenic deposits first became common in basins in central Utah (Jordan, 1985).

Our studies focus on a region of the Great Basin near the Utah-Nevada border at approximately 41°latitude (Fig. 1). Archean and Early Proterozoic metamorphic and igneous rocks underlie the region and form the basement upon which Late Proterozoic to Triassic sedimentary sequences were deposited. A poorly constrained east-trending boundary between Archean crust to the north and Early Proterozoic crust to the south lies between latitudes 40° and 41°N (Stacey and Zartman, 1978; Lush and others, 1988; Wright and Wooden, 1991). This boundary may have controlled the

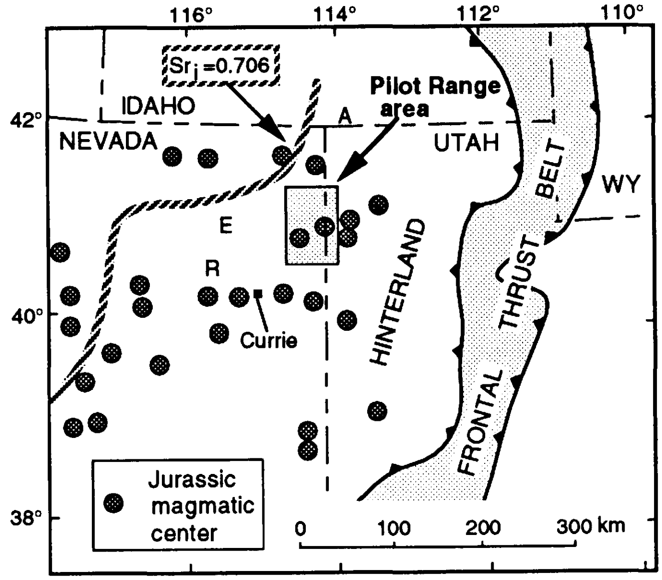

Figure 1. Location map of the eastern Great Basin, showing Mesozoic tectonic features. Initial strontium line (Sr_i = 0.706) is taken as the edge of Precambrian continental crust. Pilot Range area is shown in Figure 2. Letters indicate mountain ranges: A = Albion, E = East Humboldt, R = Ruby. Raft River and Grouse Creek Mountains lie in Utah south of the Albion Mountains. Shaded area shows zone of frontal thrust of Cretaceous to Eocene age. Hinterland is region west from frontal thrusts to magmatic arc (west of area shown in figure).

position of orthogonal bends in the Paleozoic carbonate shelf margin (Miller and others, 1991). The miogeocline received a total of 11 to 15 km of Late Proterozoic siliciclastic rocks, Cambrian to Devonian carbonate rocks, and Mississippian to Lower Triassic mixed siliciclastic and carbonate rocks (Hintze, 1988).

Jurassic tectonism included normal, strike-slip, and thrust faulting (Allmendinger and Jordan, 1984; Miller and Allmendinger, 1991) in various parts of northern Utah, as well as large-scale folding and fabric development associated with metamorphism in the Pilot Range (Miller and others, 1987; Miller and Lush, in press). Late Jurassic magmatism, an event currently limited to about 155 to 165 Ma (Miller and others, 1990), accompanied tectonism.

Whereas Late Cretaceous metamorphism and deformation is well documented in east-central Nevada (Miller and others, 1988), Cretaceous events are documented in only a few places in northeastern Nevada and northern Utah. Widespread setting of K-Ar systems in metamorphic micas at ~85 to 65 Ma (Miller and others, 1987) indicates a regional cooling event possibly caused by a combination of magmatism, tectonism, and gradual uplift from erosion, but the origin of this event is not well understood. Possible evidence for Early Cretaceous (~110 Ma) metamorphism and deformation near Wells, Nevada, (Camilleri, this volume; Snoke, this volume) add to the puzzles for Cretaceous regional tectonism.

We have studied the Pilot Range and Toano Range (Fig. 2) to quantify the Mesozoic history of that area as fully as possible, and herein report new pressure and temperature constraints for metamorphic and plutonic rocks. Although metamorphic rocks locally are middle amphibolite facies,

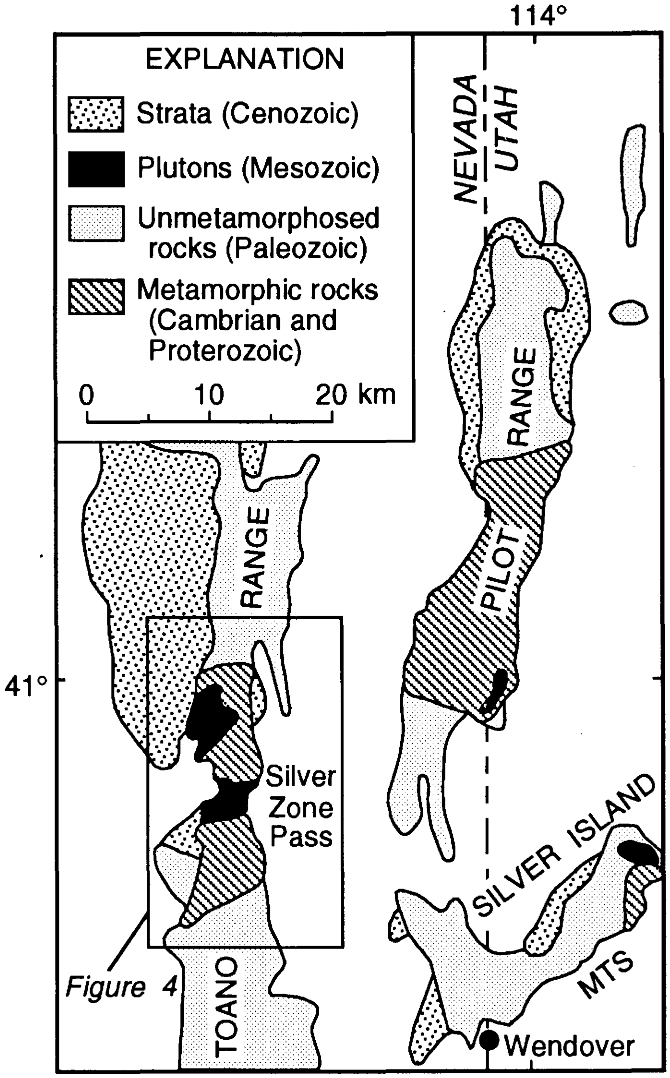

Figure 2. Generalized geologic map of the Pilot and Toano Ranges, Utah and Nevada, showing locations of metamorphic rocks. Unmetamorphosed rocks tectonically lie above metamorphosed rocks along Cenozoic low-angle normal faults.

they and nearby plutonic rocks were at most about 13 km deep. Mesozoic tectonism apparently did not bury rocks currently exposed at the surface in this region.

MAGMATISM

Numerous Jurassic plutons and dikes were intruded across the region between 155 and 165 Ma (Fig. 1). A Cretaceous pluton in the Toano Range is about 80 Ma, and is the only known Cretaceous pluton in the region. Ages and descriptions of plutons in the Pilot and Toano Ranges were given by Miller and others (1987, 1990). Geochemical and isotopic compositions of plutonic rocks provide restrictions on the involvement of continental crust in the processes of magmatism and provide insight on crustal tectonics during intrusion. Mineral chemistry of some plutonic rocks can provide barometric data for crystallization assemblages, yielding depths for emplacement.

Pilot Range

The Miners Spring Granite crops out in a 6 x 2 km area of the southeastern Pilot Range (Fig. 3). It is represented by dikes, commonly less than 1 m wide, and net-vein complexes. No pluton is observed, but a pluton is inferred to underlie the diked area and to have been the source for the dikes.

The Miners Spring Granite is composed of medium-grained, equigranular, muscovite-biotite granite. Muscovite-enriched and garnet-bearing phases are common, as are leucocratic pegmatite and aplite dikes (Miller and others, 1990). The Miners Spring consists of potassic, silicic granite that is moderately peraluminous. Despite being peraluminous and therefore of possible crustal-melt origin, its initial Sr ratio is 0.7104 and ε_{Nd} is -6.4 (Wright and Wooden, 1991), both much less evolved than typical crustal melts. These data suggest that the magma only modestly interacted with middle and upper crustal rocks.

Zircons dated by U-Pb methods gave discordant results that were interpreted by Miller and others (1987) as indicating a crystallization age between 155 and 165 Ma. The lower and upper limiting ages were derived from models of inherited zircons and Pb loss, respectively. We favor, but cannot prove, an age close to 165 Ma on the basis of Pb loss from the extremely U-rich zircons.

Toano Range

Two Mesozoic plutons crop out in the northern Toano Range (Fig. 4). At Silver Zone Pass, a homogeneous pluton of Jurassic age is composed of undeformed hornblende-biotite granodiorite. Granodiorite is coarse-grained, subequigranular, and carries sparse poikilitic potassium feldspar phenocrysts. The pluton is cut by fine-grained mafic dikes of uncertain age; a few granodiorite dikes extend into the Middle Cambrian country rock. Zones of mafic (cumulate?) rock lie along part of the north margin of the pluton. The Silver Zone Pass pluton is slightly potassic and its isotopic signature ($Sr_i = 0.7053$, $\varepsilon_{Nd} = -2.5$) is that of lower crust or upper mantle (Farmer and DePaolo, 1983; Wright and Wooden, 1991). A concordant U-Pb age on one zircon fraction is 162 Ma, although the most reliable K-Ar biotite age is 152 Ma (Coats and others, 1965; Miller and others, 1990). Barometric analysis for emplacement of the pluton, derived from the aluminum-in-hornblende barometer of Johnson and Rutherford (1989), yields 3.4 kb. It is in accord with stratigraphic data, verifying emplacement of the pluton at about 13 km.

The Toano Springs pluton is a muscovite-phenocrystic silicic granite body containing abundant potassium feldspar phenocrysts; it is cut by numerous garnet-bearing pegmatite and aplite dikes (Lee and others, 1981; Glick, 1987). The granite is strongly peraluminous and was inferred on this basis and by isotopic data ($Sr_i = 0.7250$, $\varepsilon_{Nd} = 23.2$) to be a melt from the crust (Lee and others, 1981; Wright and Wooden, 1991). However, Barton (1990) considered that

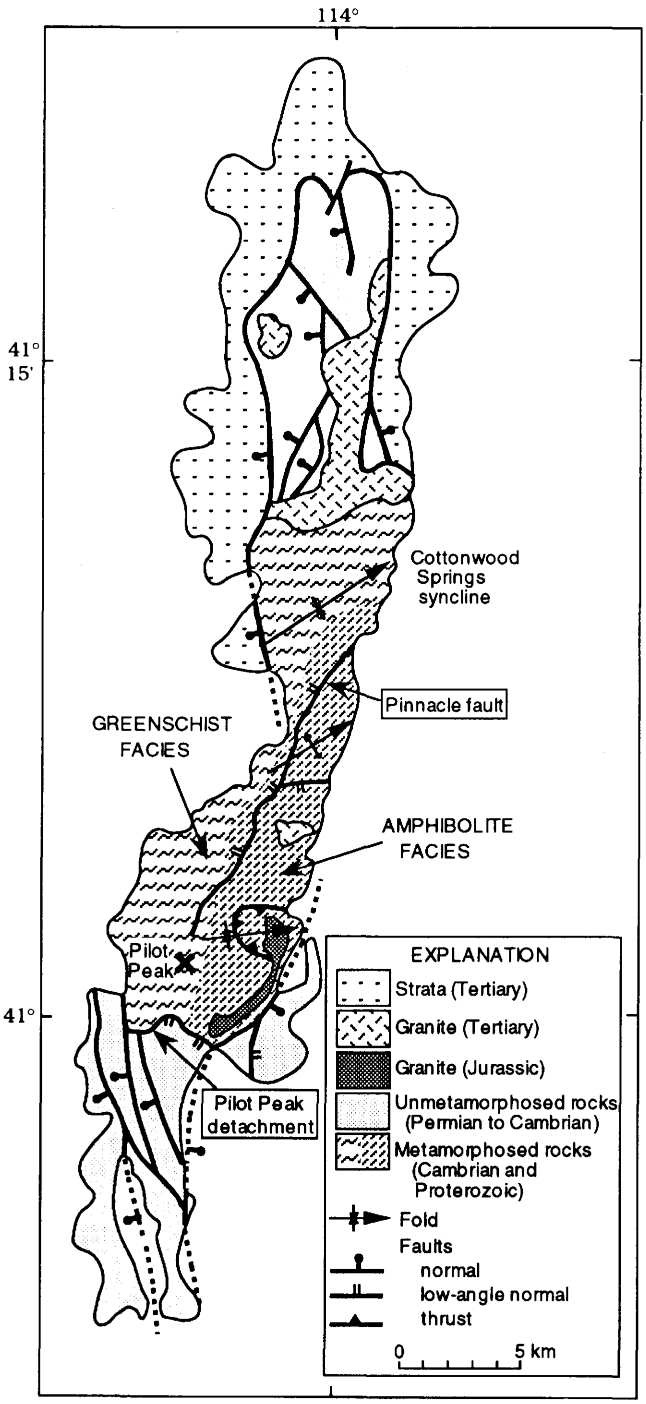

Figure 3. Map of major structures and rock units in the Pilot Range. Metamorphic facies belts indicated by different patterns. Map area of Jurassic Miners Spring Granite represents zone of abundant dikes. Northeast-trending folds such as Cottonwood Springs syncline are overturned to the southeast.

Cordilleran peraluminous granites could have a subcrustal source in part. Its age is about 80 Ma (Miller and others, 1990).

Synthesis

Jurassic plutons in the Pilot Range region and those scattered farther to the east, west, and south (Fig. 1) share many characteristics. Most are hornblende-biotite granodiorite (contrast Barton, 1990) with slightly alkalic chemical tendencies and unevolved Sr and Nd isotopic signatures. These characteristics, along with minor mafic bodies, indicate an origin in the lower crust or mantle (Miller and others, 1989; Wright and Wooden, 1991). The plutons were emplaced into Cambrian to Permian strata, suggesting emplacement depths from 13 to 6 km, unless major structural thickening or thinning took place before plutonism. Barometric data verify shallow emplacement for several plutons.

Unevolved isotopic data for Jurassic plutons are difficult to reconcile with data indicating shallow emplacement in miogeoclinal rocks overlying Archean or Early Proterozoic basement. We consider the hypothesis of Wright and Wooden (1991), that these plutons intruded through greatly thinned continental crust near the boundary between continental and oceanic crust and then were thrust eastward over little-changed crust, extremely unlikely because mio-

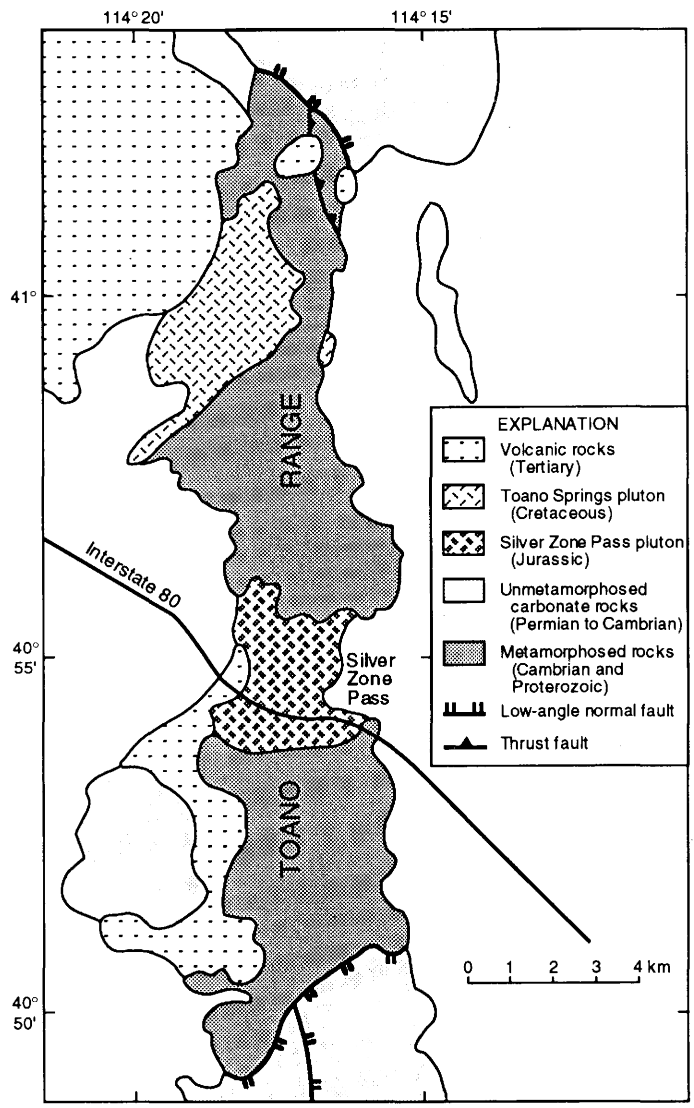

Figure 4. Map of major structures and rock units in the Toano Range. All metamorphic rocks are greenschist facies except one small area in hanging wall of thrust northeast of the Toano Springs pluton. Map based on Glick (1987) and unpublished mapping by D.M. Miller and K.B. Ketner.

geoclinal strata into which the plutons intruded were deposited on stable, and only slightly thinned, continental crust. We prefer an explanation invoking rapid ascent of magmas through the crust, most likely in an extending (rifting) crust. Rapid ascent could inhibit crustal contamination, allowing the magmas to retain unevolved isotopic signatures in robust systems such as Sr and Nd but not for systems easily modified by minor assimilation such as Pb (Miller and others, 1989). Alkalic chemical tendencies are in accord with the hypothesis of magmatism in a rift environment. Muscovite and garnet in the Miners Spring Granite may indicate considerable differentiation of more mafic magma, rather than assimilation of, or melting from, upper crust.

Cretaceous magmatism is represented by a single pluton, but that pluton is similar to other strongly peraluminous granites scattered through eastern Nevada (Lee and others, 1981; Snoke and Miller, 1988) that have been proposed as the cause of widespread upper crustal metamorphism (Miller and Gans, 1989). No metamorphism can be directly linked to the Toano Springs pluton, which appears to cut Jurassic fabrics associated with peak metamorphism (Miller and others, 1990). Although the proposed upper-crustal melting origin of the Toano Springs pluton might indicate large-magnitude crustal thickening and (or) a major heat influx into the upper crust, we consider that lack of evidence for widespread melting favors a model for localized melting, such as intrusion of mafic magma into the middle crust. Barton (1990) arrived at a similar conclusion on the basis of continental magmatic-arc affinities exhibited by trace elements, which probably reflect subcrustal components in the peraluminous granites.

METAMORPHISM

Most Paleozoic rocks in the northeastern Great Basin were heated to about 300°C, judging from conodont alteration data (Harris and others, 1980), but with few exceptions post-Ordovician rocks in the Pilot and Toano Ranges bear no textural evidence for metamorphism. Dynamothermal metamorphism is evident in rocks within tectonic windows of Cenozoic age in the Pilot and Toano Ranges and westward to the Ruby Mountains (Fig. 1), as well as within metamorphic core complexes to the north in the Albion, Raft River, and Grouse Creek Mountains. Metamorphism in these rocks has been summarized by Misch (1960), Armstrong and Hansen (1966), Armstrong (1968b, 1982), Snoke and Miller (1988), and Miller (1990).

Pilot Range

Miller and Lush (1981) first documented amphibolite-facies metamorphism in the Pilot Range and Miller and others (1987) demonstrated that the metamorphism was Jurassic in age. Greenschist facies assemblages exist in Late Proterozoic to Cambrian strata along the west side of the range and mainly amphibolite facies assemblages exist in like strata on the east side (Fig. 3). Quartzites with no diagnostic mineral assemblages lie between the east and west facies belts. High-grade rocks were multiply deformed, and the Miners Spring Granite both intruded foliated rock and was folded and foliated with its wallrocks; it is interpreted as syntectonic. Foliated granite has a 155- to 165-Ma U-Pb zircon age, thus dating deformation as Jurassic. A $^{40}Ar/^{39}Ar$ age of metamorphic hornblende is about 150 Ma. This age is interpreted to result from cooling following peak metamorphism, corroborating field relations indicating synchronous metamorphism and plutonism (Miller and others, 1987).

Along the west side of the Pilot Range, semi-pelitic rocks, now slate and phyllite, contain assemblages indicating biotite-zone metamorphism. Typical greenschist facies assemblages in these rocks are: quartz + muscovite + chlorite + epidote ± biotite ± albite. Primary chlorite is present in most pelitic rocks; coexistence of chlorite and quartz indicates that metamorphism was not in the amphibolite facies. Temperatures required for the mineral assemblages are about 400°C, but pressures are not constrained. We consider that the wide extent of these assemblages indicates that the metamorphism was regional in scope and was not an aureole of a pluton.

Mineral assemblages along the east side of the range indicate low pressure middle amphibolite facies metamorphism. Semipelitic rocks contain muscovite + quartz + biotite + andalusite ± staurolite ± garnet ± sillimanite ± fibrolite ± tourmaline. Graphite schist contains the assemblage andalusite + graphite + muscovite + quartz. Impure calcareous rocks contain calcite + quartz + muscovite + tremolite + sphene ± biotite ± diopside ± microcline. Syntectonic and post-tectonic hydrothermal alteration is suggested by coarse replacement muscovite in porphyroblasts and by ubiquitous unoriented chlorite, respectively. Hydrothermal alteration outlasting peak temperatures is suggested by the partial replacement of staurolite, andalusite, and fibrolite by sericite, and of biotite by chlorite.

Coexisting sillimanite and andalusite, in conjunction with stable muscovite, quartz, biotite, and staurolite, indicate temperatures of about 575 to 625 °C and pressures of about 3.5 kb (Fig. 5), or tectonic depths of about 13.5 km. Tectonic thickening or tilting of the range to expose deeper rocks on the east side do not explain amphibolite facies metamorphism because the change to greenschist facies conditions takes place laterally over 3 km, across comparatively minor structures, and in rocks of the same age. The known stratigraphic thickness of rocks overlying the metamorphosed Cambrian rocks is 11.3 km, but the best thickness estimate is 12.8 ± 0.5 and thickness possibly could be as much as 14 km, if probable post-Early Triassic strata are included. This best estimate corresponds well with the pressure determination for amphibolite facies metamorphism. These data, when combined with the temperature estimate for greenschist facies rocks of similar stratigraphic position from the west side of the range, require a reasonable thermal gradient of 30° C/km. No tectonic thickening is required to explain the pressures estimated for regional metamorphism. A plausible

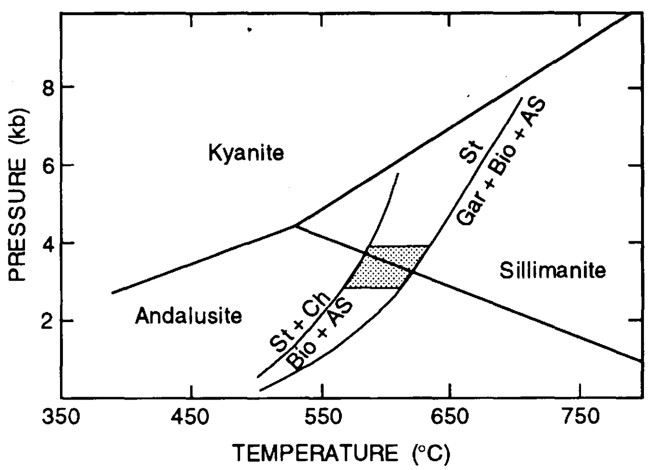

Figure 5. Pressure and temperature constraints for amphibolite-facies mineral assemblages from the Pilot Range, based on the petrogenetic grid of Spear and Cheney (1989) and the aluminosilicate triple point calibration of Bohlen and others (1991). Mineral abbreviations: St = staurolite, Ch = chlorite, Bio = biotite, AS = aluminosilicate, Gar = garnet.

explanation for the ~600 °C metamorphism along the east side of the Pilot Range is a pronounced thermal gradient that locally increased temperatures by 150 to 200 °C near the Jurassic pluton. On the basis of distribution of amphibolite facies rocks, the pluton probably underlies, at minimum, a 20 x 5 km area in the eastern Pilot Range.

Timing of metamorphism is Middle to Late Jurassic as determined by relations with the syntectonic Miners Spring Granite and by the 150-Ma cooling of metamorphic hornblende. However, K-Ar ages for metamorphic micas along the east side of the Pilot Range record cooling to 250 to 350 °C by 83 to 56 Ma (Miller and others, 1987). These data suggest that, following Jurassic amphibolite facies metamorphism, rocks returned to ambient conditions of about 400 °C. During the Late Cretaceous, a regional cooling event allowed micas to close with respect to Ar diffusion.

Toano Range

Metamorphic rocks in the Toano Range were described by Glick (1987) and Miller and others (1990). Like the Pilot Range, metamorphosed Late Proterozoic and Cambrian rocks are exposed in a Cenozoic tectonic window. Greenschist facies metamorphism is widespread and characterized by muscovite, biotite, and chlorite in pelitic rocks, and muscovite, chlorite, and tremolite in calcareous rocks. At one location, pelitic schist contains muscovite + biotite + staurolite + garnet, indicating amphibolite facies metamorphism. Foliation that developed during growth of these metamorphic minerals is cut by the undeformed Late Jurassic Silver Zone Pass pluton and its dikes, indicating a pre-Late Jurassic age for metamorphism. In many rocks, chlorite is both oriented as part of foliation-defining fabric and is randomly oriented. Muscovite and tremolite also occur in random orientations. Unoriented mineral growth is spatially associated with the Silver Zone Pass pluton, but not with the Cretaceous Toano Springs pluton. Jurassic fabrics evidently were overgrown by randomly oriented minerals during heating by the Silver Zone pass pluton.

Peak temperatures for metamorphism varied, but probably were between 400 and 500°C. Pressure can be estimated by depth for crystallization of the Jurassic Silver Zone Pass pluton, about 3.4 kb. Cooling ages for metamorphic micas near the Late Cretaceous pluton are close to the age of the pluton. In contrast, micas greater than one km distant yielded ages of 94.5 Ma (biotite) and 69.7 Ma (muscovite), suggesting prolonged cooling from earlier mica growth and cooling at the same time as rocks in the Pilot Range (Miller and others, 1990).

Synthesis

Although metamorphic facies vary within the Pilot and Toano Ranges, all metamorphism appears to be of fairly low pressure, and consistent with no tectonic burial. Elevated temperatures in the Pilot Range are therefore most likely due to heating by nearby large Jurassic peraluminous magma bodies. Ages of metamorphic minerals and evidence for pervasive hydrothermal alteration during and after metamorphism support this conclusion. Metamorphism was therefore primarily Jurassic in age and grades higher than greenschist may be localized around plutons, thereby affecting only a small volume of the upper crust. If any large-magnitude shortening took place in the Jurassic, it did not cause tectonic burial of rocks exposed in these ranges.

A second metamorphic pulse may be indicated by regional cooling of metamorphic micas through ~250-350 °C during the Late Cretaceous. However, metamorphic rocks more likely underwent protracted cooling from the Jurassic event and synchronously cooled during a Cretaceous regional tectonic event such as extension.

STRUCTURE

Pre-Cenozoic rocks in the Pilot and Toano Ranges can be divided into largely unmetamorphosed rocks in hanging walls of major low-angle normal faults and pervasively metamorphosed rocks beneath those faults. The low-angle fault in the Pilot Range, the Pilot Peak detachment fault (Fig. 3), is latest Cretaceous or early Cenozoic in age (Miller and others, 1987); its counterpart on the northern side of the window of metamorphic rocks in the Toano Range is remarkably similar (Glick, 1987). Many structures in the hanging walls of the detachment faults are plausibly Mesozoic in age, but they are undated and will not be described in this paper. It is the metamorphic rocks in the footwalls that demonstrably record Mesozoic tectonism.

Pilot Range

Metamorphic rocks beneath the Pilot Peak detachment fault record two phases of widespread ductile deformation and a later, more localized, ductile-brittle event, all of which predate ~40-Ma granitoids. Ductile fault zones formed during, and possibly before, the two phases of ductile deformation. Evidence for Mesozoic deformation stems from field relations with a Jurassic pluton and K-Ar studies of metamorphic minerals.

Metamorphosed Late Proterozoic and Cambrian strata underwent ductile deformation on all scales from overturned folds with 10 km wavelengths to microscopic folds and preferred crystallographic and grain-shape orientations of minerals. Schist and quartzite display orderly minor structures, whereas structures in marble are less systematic. The oldest penetrative foliation (S_1) is oriented nearly parallel with bedding and contains rare, generally east-trending, mineral-elongation lineations. Rare isoclinal folds (F_1) with axes oriented parallel to the lineation probably are associated with S_1. This oldest foliation is deformed by steeply northwest-dipping penetrative foliation (S_2) that is axial planar to small folds (F_2) with shallowly northeast-plunging axes. East-trending penetrative lineations locally are folded about northeast-trending F_2 folds. Metamorphic minerals aligned with S_1 and S_2 foliations indicate similar metamorphic conditions during the formation of both fabrics. The F_2 folds are generally open to moderately tight and are similar in geometry and orientation to major southeast-vergent folds, best exemplified by the Cottonwood Springs syncline (Fig. 3). Another fold east of Pilot Peak is probably also a major northeast-trending syncline that is deformed by subsequent broad folds. Strain associated with both ductile deformation events is represented throughout the Pilot Range, and therefore is interpreted as regional, rather than caused by granite emplacement. S_1 does not appear to be produced as axial-plane foliation in large-scale recumbent folds, so it may indicate more or less homogeneous flattening of the rocks. Second phase structures are associated with regional shortening; fabrics are locally accentuated in the aureole of the Miners Spring Granite, but show no evidence of being directly caused by granite emplacement. Similarity of metamorphic assemblages in first and second phase fabrics suggests a continuum of deformation and metamorphism, rather than discrete events.

Faults of Pilot Peak are nearly parallel to bedding, primarily ductile, and formed early in the metamorphic cycle, as indicated by: (1) absence of breccia, (2) similar metamorphic assemblages across the faults, (3) abundant ductile minor structures near the faults, and (4) folding about F_2 synclines. A thrust fault (Fig. 3) duplicates the upper part of the Prospect Mountain Quartzite (Miller and Lush, in press) and overlying schist, and other structurally higher and smaller thrusts further duplicate schist. In contrast, a bedding-plane fault south of the thrusts truncates the uppermost part of the Prospect Mountain Quartzite and much of the overlying schist, omitting several hundred meters of section. Both thrust and normal faults east of Pilot Peak are pre- to syn-metamorphic and they are folded by the F_2 syncline. Their relation to S_1 fabrics has not been established.

Bedding-plane faults in the central part of metamorphic exposures omit Late Proterozoic rock units. The faults are ductile, exhibit normal-sense stratigraphic separation, and appear to be younger than the bedding-plane faults east of Pilot Peak because they postdate F_2 folds. Quartzite near the bedding-plane faults is mylonitic with prominent southeast-trending stretching lineations. The grain-size reduction of mylonitic rocks suggests declining temperatures and(or) water content following peak metamorphism.

Moderate-angle faults that cut bedding at moderate to steep angles are common north of the main outcrop of the Prospect Mountain Quartzite in the Pilot Peak area. These faults are normal, strike north-northeast, and appear to have behaved in a brittle-ductile manner. The largest, the Pinnacle fault (Fig. 3), displays brecciated quartzite and grain-size-reduced marble and schist in a zone as much as 50 m wide. We interpret the brittle-ductile aspect of the fault zone as indicating deformation at temperatures below those of peak metamorphism. However, muscovite is stable in the deformed rocks, suggesting some fault movement at low metamorphic temperatures. The Pinnacle fault, and parallel faults to the east, dip west, whereas faults with northerly strikes lying west of the Pinnacle fault dip east, possibly as conjugate faults.

The Pinnacle fault dies out southward and upward in the section of the thick, competent Prospect Mountain Quartzite, which is arched in a large, complex, north-trending fold that refolds earlier folds. The maximum stratigraphic separation on the Pinnacle fault, near the northernmost exposures, is about 1.5 km. No metamorphic contrasts are noted in assemblages across the fault, but textural grade changes approximately at the fault, with schist in the footwall and phyllite and minor schist in the hanging wall. The termination of the Pinnacle fault southward is partly caused by merging with antithetic faults to the west and partly by complex kink folding within the Prospect Mountain Quartzite. This faulting and folding apparently resulted in net thinning of the stratigraphic section and complex rotation of strata in individual fault blocks.

Open, kink-style folds, and small faults that break nearly parallel to axial planes of the kink folds, appear to be related to the Pinnacle fault. The folds trend north to north-northeast, have nearly planar limbs and tight hinges, and are hundreds of meters in wavelength. They verge eastward on the east side of the Pinnacle fault and westward west of the fault. Sparse small-scale folds, related to the kink folds, have no axial-plane foliation and minerals such as biotite and quartz in the hinge zones are deformed but not recrystallized. Low- and moderate-angle faults that break near the hinges of the kink folds parallel the Pinnacle fault and have normal separations. These faults apparently developed as the asymmetric folds broke along surfaces nearly parallel to axial planes in the tight hinge zones.

The two ductile fabrics and pre- to syn-metamorphic bedding-plane faulting took place during the Jurassic. The 155- to 165-Ma Miners Spring Granite intruded foliated rocks, thrusts, and other low-angle faults, and is itself variably deformed by F_2 folds. Metamorphic hornblende east of Pilot Peak cooled to ~450 °C by 149 Ma, following peak metamorphism, indicating that much ductile deformation and peak amphibolite facies metamorphism was Jurassic in age. Metamorphic temperatures, recorded by Ar systems in micas, had declined to 250 to 350°C by 83 Ma (Miller and others, 1987). This Late Cretaceous cooling might be due to extension recorded by the Pinnacle and related faults and folds, and corresponding exhumation of metamorphic rocks.

The Pilot Peak detachment fault, which places essentially unmetamorphosed Upper Cambrian strata on metamorphosed Lower and Middle Cambrian strata in the southern Pilot Range (Fig. 2), postdates metamorphism and predates latest Eocene to Oligocene granodiorite dikes (Miller and others, 1987). The Pilot Peak detachment is marked by highly sheared and locally shattered slivers of metamorphosed Cambrian strata and brecciated limestone. Kinematic markers within and below the detachment provide evidence for two episodes of movement after Jurassic metamorphic fabrics formed. During episode one, lower grade phyllite was placed on amphibolite-facies schist about 10 m beneath the detachment. The phyllite contains syntaxial calcite and quartz veins within which fibers indicate top-to-the-east shear, and antitaxial pressure shadows. Structurally higher, another fabric representing episode two is superimposed on the phyllite immediately beneath the detachment fault; brittle fractures and cleavage form a composite fabric much like S-C fabrics. Lineations within the composite fabric trend N70°W to N90°W and are parallel to local slickenlines. S-C pseudofabrics and offset veins yield top-to-west sense of shear; fracture of the veins indicates that this shear postdates that of the first episode.

The first episode of movement on the detachment fault postdates peak metamorphism, but is partly ductile in character, so probably predates or is synchronous with regional K-Ar ages (Late Cretaceous) for metamorphic micas. Thus, top-to-the-east shear here is probably late Mesozoic. The second episode is probably Eocene in age because breccia at the Pilot Peak detachment fault is cut by Eocene granodiorite sills that are only modestly fractured. Lineations associated with the brittle second episode indicate top-to-the-west-northwest shear. A similar conclusion is reached by contrasting sedimentary environments for Cambrian strata above and below the detachment (McCollum and Miller, 1991), which indicates several tens of kilometers of offset (Miller and others, 1991).

Toano Range

Metamorphic rocks in the Toano Range are similar to those in the Pilot Range in that they contain metamorphic minerals and associated fabrics that are established as Mesozoic in age (Glick, 1987), but structures in unmetamorphosed rocks are of unknown age. A broad fold around the Toano Springs pluton, minor folds in schistose rocks, and variably developed foliations and lineations are described by Glick (1987).

Early foliation is nearly parallel to bedding and is defined by oriented metamorphic minerals such as mica, amphibole, and chlorite. Near the Silver Zone Pass pluton, this foliation is discordant to the margin of the unfoliated pluton. The foliation is overprinted by unoriented growths of chlorite, tremolite, and muscovite that increase in grade toward the pluton, indicating a pre-plutonic origin for the early foliation. Small folds plunge north to northeast, and in places are accompanied by parallel mineral lineations. The folds deform the early foliation but predate unoriented mineral growth. Folds formed in carbonate rocks north of the Silver Zone Pass pluton verge to the west.

Normal and thrust faults nearly parallel to bedding were mapped by Glick (1987) in a few places. Normal faults eliminate tens of meters of strata. A thrust fault northeast of the Toano Springs pluton carries amphibolite facies schist in its hanging wall, and duplicates several hundred meters of strata. The north-trending folds deform the normal faults, and all are warped around the east margin of the Cretaceous Toano Springs pluton.

After foliation, faults, and folds developed, static mineral growth in all rocks took place. This growth is spatially related to the Silver Zone Pass pluton, but not to the Toano Springs pluton, suggesting a Late Jurassic age. Despite this evidence for a post-metamorphic thermal event, quartz in many rocks displays subgrains, deformation lamellae, and deformation bands, indicating yet later minor deformation.

Synthesis

Thrust faults and overturned folds in the Pilot and Toano Ranges document shortening during the Jurassic. Shortening was southeast-directed in the Pilot Range and at least in part west-directed in the Toano Range, and was broadly synchronous with plutonism at ~160-165 Ma. Ductile faults about parallel to bedding both truncated and duplicated strata; these faults formed during or before metamorphism and indicate varying strain conditions during overall shortening.

East-directed low-angle extensional faults in the Pilot Range are plausibly Late Cretaceous in age. Resulting upper-crustal denudation may have set K-Ar ages for metamorphic micas. Locally, heating by intrusions like the Toano Springs pluton in the Late Cretaceous, followed by passive cooling (Miller and others, 1990), may account for the mica ages.

REGIONAL RELATIONS

Jurassic

Late Jurassic plutons and dikes, present in many mountain ranges in the northeastern Great Basin (Fig. 1), indicate a widespread magmatic event at about 155 to 165 Ma that was first identified by Armstrong and Suppe (1973) and recently reviewed by Miller and others (1990). Most plutons apparently were emplaced at depths of about 6 to 13 km on the basis of reconstructed stratigraphy of the wallrocks;

these depths are supported by our preliminary barometric studies. Even though the intrusions in some cases are associated with high-grade metamorphism, the depth of emplacement of those in the Toano Range and to the east is shallow and requires no additional sedimentary or tectonic load.

Most Jurassic plutons are composed of alkali-enriched hornblende-biotite granodiorite, but compositions vary, with felsic granite in the Pilot Range and mafic diorite, monzodiorite, and quartz monzonite in the Silver Island, Deep Creek, and Dolly Varden Mountains (Fig. 6). Initial Sr ratios for plutons, whether felsic or mafic, are only slightly more evolved than bulk earth, which is more typical of granitoids melted from lower crust or mantle than of granite and granodiorite that was derived from middle and upper Precambrian crust. Miller and others (1989) suggested that these isotopic signatures, coupled with the alkalic compositions and common association with normal faults, indicate a rift-related environment for emplacement that was much like a back-arc, but without basinal sediments.

East of the Pilot Range, Jurassic tectonism is well-preserved in the Newfoundland Mountains (Allmendinger and Jordan, 1984) and the northern and central Silver Island Mountains (Miller and Allmendinger, 1991; D.M. Miller, 1991, unpubl. mapping). Common to all of these areas are three main elements: (1) Jurassic plutons and dikes, (2) contemporaneous or older normal faults that indicate generally east-directed subhorizontal extension, and (3) yet older thrust faults that document generally east-directed shortening. Orientation of Jurassic dikes indicates a minimum compressive stress orientation that is parallel to the extension direction indicated by normal faults, indicating that the dikes were intruded during a similar stress regime as that for normal faulting. Normal faults are inferred on this basis, and by field relations indicating age close to magmatism, to be late Middle or early Late Jurassic in age. The normal faults probably are restricted to sites of magma intrusion, but collectively outline a province with roughly east-oriented extension.

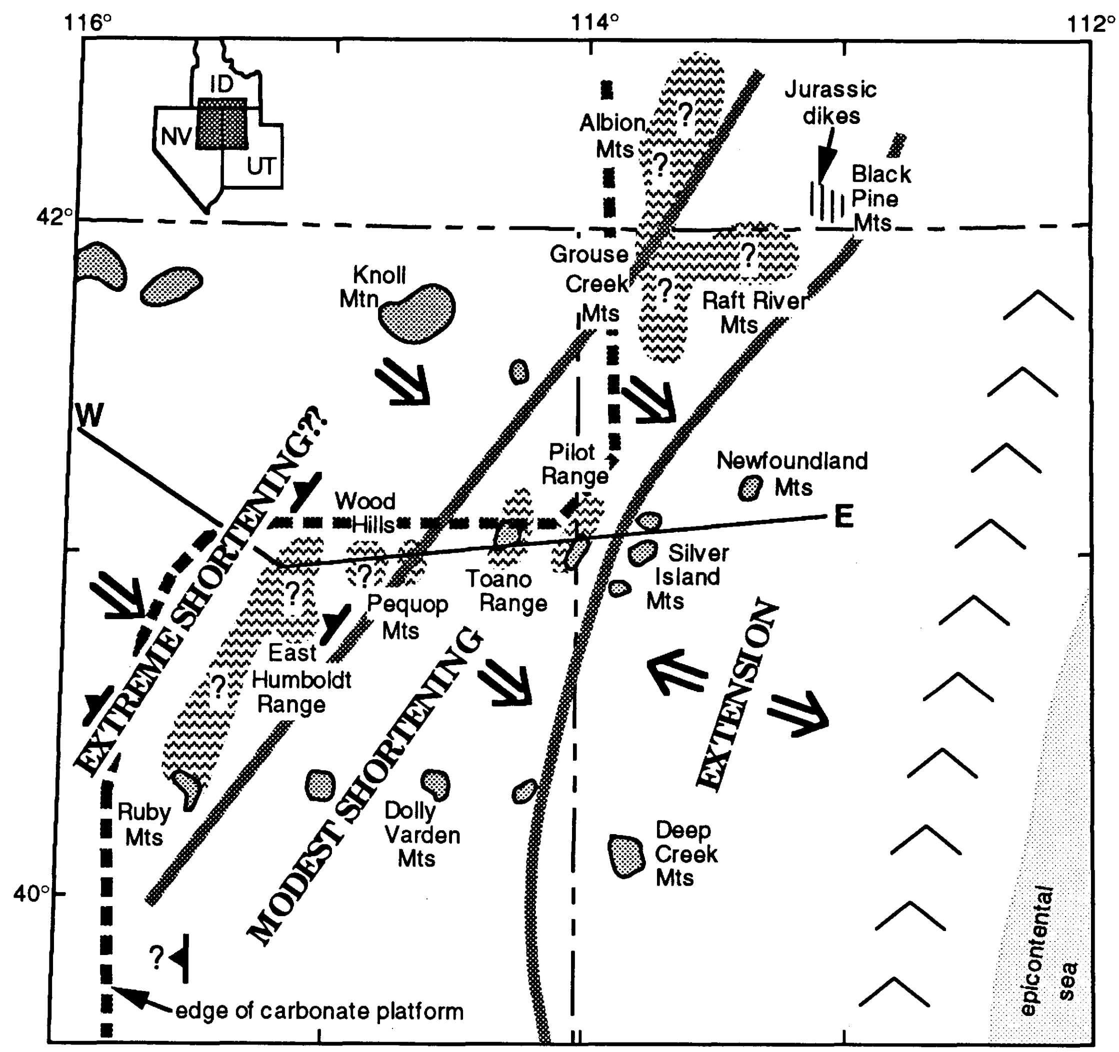

Figure 6. Map showing late Jurassic tectonic provinces in the northeastern Great Basin. Dark-shaded areas are plutons. Wavy pattern represents metamorphic rocks, queried where possibly Cretaceous in age. Line of cross section shown in Figure 7 is labeled W-E.

Paleogeography of the eastern part of the orogen is partly constrained by the sedimentary record of the shallow epicontinental sea of eastern Utah (Jordan, 1985). Strata in this basin thicken modestly to the west, and include tuff and lithic sandstone, recording a western orogenic source. However, sediment in the basin is not as thick as is typical for thrust-belt foreland basins, and little sediment is coarse-grained. We suggest that Jurassic mountains were not very high in western Utah, and that sediment from probably higher volcanic edifices in Nevada, which probably were prolific sediment sources, was either trapped or diverted to other basins. The extensional province in western Utah (Fig. 6) may have been up-bowed or depressed; in either case, it probably had uplifts along both flanks like most rifts. A likely scenario is that the rift province was a sediment trap of low relief, and the epicontinental sea only received detritus from the adjacent flank uplift on the east side of the rift province (Fig. 6).

Westward, such as in the Pilot Range, low-angle normal faults subparallel to bedding, large-scale folds overturned to the southeast, and thrust faults indicate modest Jurassic shortening, which was accompanied by greenschist to amphibolite facies metamorphism. Although precise times for southeast-directed shortening in the Pilot Range are not known, available data point to about 160 to 165 Ma, which is probably synchronous with east-directed extension in ranges to the east. The incompatibility of these strain patterns emphasizes the distinction between the eastern extensional province and the province of shortening in and near the Pilot Range. At Knoll Mountain (Fig. 6) (also referred to as the H-D Range), thrust stacks near the Jurassic contact pluton are cut by pluton-related radiating dikes (Coats and Riva, 1983). Rocks associated with these thrusts are deformed into tight southeast-verging folds, taken as the transport direction. In the Dolly Varden Mountains, tight folds are cut by Jurassic plutons (Atkinson and others, 1982); although some folds may have formed during intrusion, one north-trending fold predates the pluton. In addition, normal and thrust faults predate Jurassic granite in the Deep Creek Mountains (Nolan, 1935; Miller, 1990).

In addition to Jurassic metamorphism in the Pilot and Toano Ranges, early metamorphism in metamorphic core complexes of this region may be Jurassic in age. In the Albion Mountains, Mesozoic first-phase fabrics formed at middle amphibolite facies may be Jurassic in age (Armstrong, 1968b, 1976, 1982), but are only constrained as older than Late Cretaceous. Hodges and McKenna (1986) showed that first phase structures in one thrust plate in the Albion Mountains equilibrated at 6 kb. West of the Pilot Range, in the central Ruby Mountains, Hudec (1990) showed that metamorphism near a Jurassic pluton occurred at 6 kb. Metamorphic fabrics farther north in the East Humboldt Range equilibrated first at 9 kb; although known as Early Cretaceous or older, they may also be Jurassic in age (Dallmeyer and others, 1986; Hodges and others, in press). Because these examples of known and possible Jurassic metamorphism affect lower Paleozoic rocks that were stratigraphically buried by 12 to 14 km, 10 km of tectonic thickening is required in the Ruby Mountains, and as much as 20 km of tectonic thickening may have occurred in the East Humboldt Range during the Jurassic. Uncertainty about the timing of high-pressure metamorphism in the metamorphic core complexes creates vital ambiguities for interpreting Jurassic tectonics of those areas.

Jurassic Models

The overall Jurassic tectonic pattern of western North America is one of shortening (Elison, 1991). Oceanic plates were subducting roughly eastward under the North American plate, probably inducing shortening within the continental plate. However, extensional tectonics in north-central Utah and a lack of major frontal breakouts of thrusts challenge simple thrust-belt models.

Jurassic tectonism in the northeastern Great Basin close in time to plutonism varies from brittle extension at shallow levels in the east to ductile shortening at similar to somewhat deeper levels westward. The data support a model for regional shortening for which local conditions were chiefly controlled by plutonism. We distinguish three tectonic provinces (Fig. 6) in the northeastern Great Basin during the early Late Jurassic: (1) An extensional province of voluminous plutons, in northwestern Utah; pluton emplacement was accompanied by normal faulting. Thrust faults older than plutonism probably only slightly modified the crust, since the faults seem to be of small offset (Allmendinger and Jordan, 1984) and because emplacement depths for plutons are appropriate for stratigraphic thicknesses. (2) A province of modest shortening west of the zone of plutons, in northeastern Nevada and extreme northwestern Utah. As exemplified by the Pilot Range, strata in this province were metamorphosed near plutons and did not undergo net extension; these rocks continued to shorten during plutonism. Rocks in this province also were not tectonically buried. (3) A province of modest to extreme shortening farther west near the edge of the Precambrian continental crust (Ruby Mountains area) in which crustal shortening possibly was of larger magnitude, as suggested by pre-110 Ma high-P metamorphism. If this model is correct, Jurassic tectonism in the eastern Great Basin primarily resulted from regional stresses imprinted by back-arc magmatism. The formerly undisturbed brittle crust of north-central Utah underwent extension in response to magmatism, whereas the weaker crust to the west underwent shortening, with ductile response probably restricted to parts of the middle and upper crust that were thermally softened by magmatism.

If province 3 rocks underwent high-pressure metamorphism during the Jurassic, the crust may have deformed into a large-scale duplex that produced complexly folded and faulted metamorphic rocks, structurally overlain by broadly warped strata (Snoke and Miller, 1988). Because no frontal breakout of a major thrust is known, such a duplex would have to be overlain by a west-directed roof thrust, in the overall geometry of a tectonic wedge (Fig. 7A). Such a wedge is possible farther east at depths not currently exposed, although it is unlikely in our view because that crust deformed primarily by extension and, by our paleogeographic interpretation, no large mountains existed to the east. We submit that, if present, large-magnitude crustal shortening in the Ruby Mountains area was caused by focusing of thrust faults (Fig. 7A) at a boundary in the ancient Precambrian crust that has controlled lithofacies patterns and tectonic features since the Late Proterozoic (Miller and others, 1990). Overthrusting of much greater magnitude than elsewhere could have been localized by this crustal feature, perhaps creating a tectonic belt (province 3) extending from the Albion Mountains through central Nevada to the Ruby Mountains (Camilleri and others, this volume). This crustal feature undergoes a sharp bend near the East Humboldt Range, perhaps causing localized extreme shortening at this rheological salient in the crust.

Alternatively, province 3 rocks underwent moderate- or low-pressure metamorphism during the Jurassic and high-pressure metamorphic assemblages of the Ruby Mountains, East Humboldt Range, and Albion Mountains are Early Cretaceous in age. By this interpretation, Jurassic tectonism and metamorphism probably were controlled by locally softened crust caused by magmatically produced elevated temperatures (Fig. 7B), similar to the model proposed by Collins and Vernon (1991). Magmatism provided local heat sources for metamorphism as fairly broad zones at 10-15 km depth and as narrow aureoles at shallower depths. Ductile deformation recorded regional stress fields at broad zones of thermally softened crust near masses of plutons.

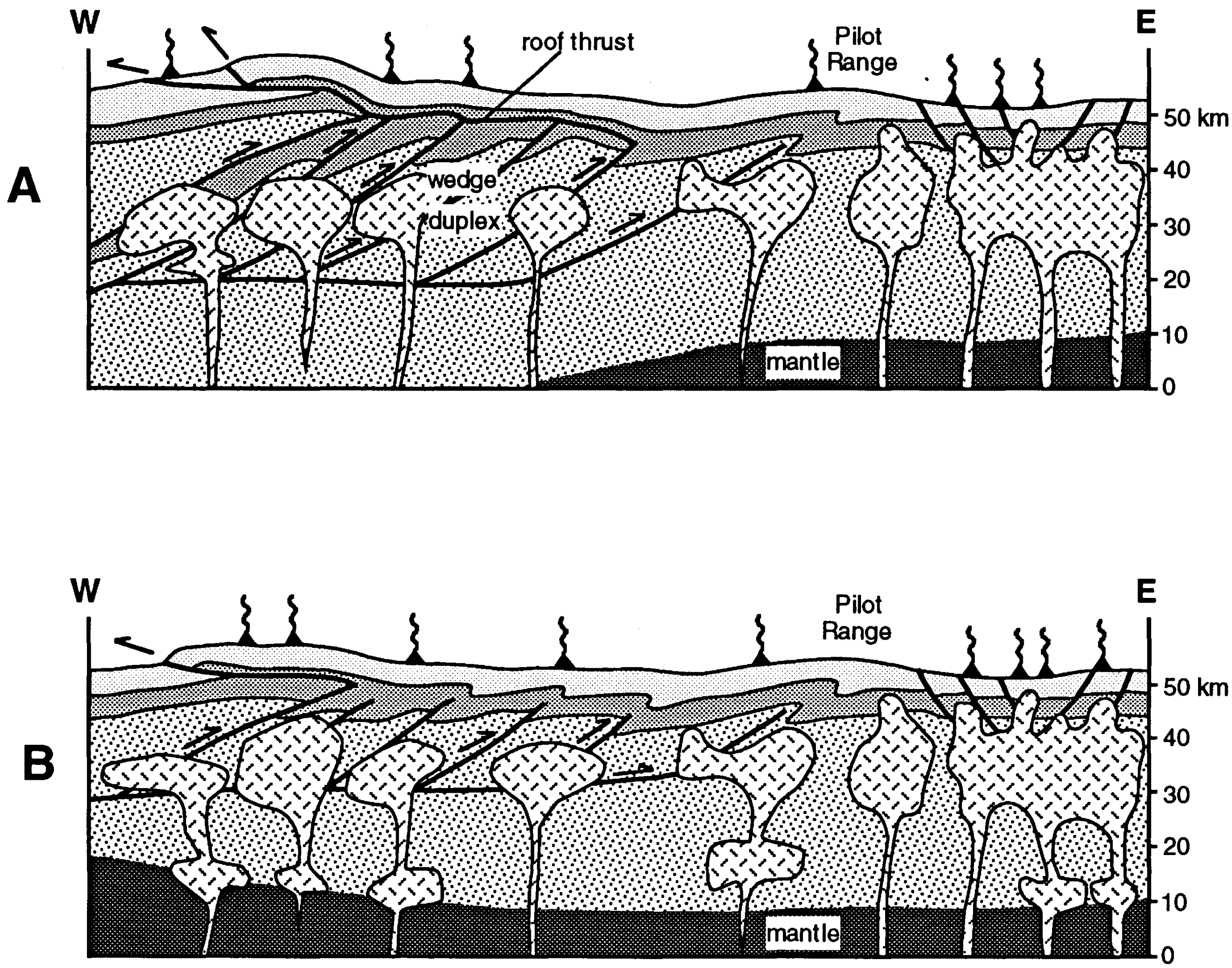

Figure 7. Cross sections depicting tectonic models at about 165 Ma. A. High-pressure metamorphism in East Humboldt Range is assumed to be Jurassic, which requires extreme shortening. Crust is assumed to deform primarily by footwall deformation. B. High-pressure metamorphism in East Humboldt Range is assumed to be Cretaceous.Only modest shortening and extension occur in the northeastern Great Basin. Ductile structures are limited to areas near Jurassic plutons.

Cretaceous

Some 40 m.y. after the Jurassic magmatism, the frontal fold and thrust belt (Sevier orogenic belt of Armstrong, 1968a) began forming in the eastern part of the northeastern Great Basin (Fig. 1). These thrust faults extended west to deeper levels (Royse and others, 1975), but direct evidence for them in the hinterland remains undocumented. Metamorphism in north-central Nevada, possibly Early Cretaceous in age, yielded high-pressure metamorphic assemblages (Hodges and McKenna,1986; Dallmeyer and others, 1986; Hodges and others, in press) that suggest crustal thickening. Scattered strongly peraluminous Late Cretaceous plutons intruded approximately synchronously with widespread cooling recorded by Late Cretaceous K-Ar ages on micas. At about the same time, upper-crustal extension took place above the shortening lower crust in the eastern Raft River and Black Pine Mountains (Wells and others, 1990; Wells, this volume), possibly in the Pilot Range, and perhaps elsewhere in the region (Armstrong, 1972).

Much of the Late Cretaceous thrusting in southwestern Wyoming took place between 85 and 65 Ma, synchronous with widespread cooling in the northeastern Great Basin hinterland (Miller and others, 1987). One interpretation of the coincident cooling in the hinterland is that a major thrust fault, rooted beneath hinterland rocks, placed metamorphic rocks eastward over cold rocks (Armstrong, 1982) and resulted in erosional or tectonic denudation of the metamorphic rocks. This interpretation is supported by seismic reflection data in central Utah, which were interpreted by Allmendinger and others (1983) as possibly illustrating Mesozoic thrust ramps deep in the crust just east of the metamorphic belt at that latitude.

As an indirect or direct result of shortening, upper-crustal tectonic and erosional denudation may have rapidly unroofed and cooled this thickened crust of the metamorphic belt. Recently documented Cretaceous extension in this region increases the viability of this interpretation. In addition, nonmarine, fault-bounded basins of Late Cretaceous to Eocene age are scattered to the south and west of the northeastern Great Basin, suggesting that extensional sedimentary basins may have formed above the metamorphic belt roughly at the time that K-Ar systems were closed to diffusion at depth. However, regional lower Tertiary strata lie concordantly on upper Paleozoic strata, precluding large-scale erosion or exhumation, and attendant cooling.

Another interpretation calls for a mild Late Cretaceous heating event accompanied by little or no deformation. Such an event most likely would be caused by magmas, and would be most evident by its subsequent cooling. Peraluminous magmas were emplaced into the upper crust at least locally, and Miller and Gans (1990) proposed that widespread plutons of this age caused regional metamorphism farther south. However, Cretaceous plutons are rare in the northeastern Great Basin and therefore would likely cause only local heating effects. In addition, some K-Ar ages, such as in the Toano Range, are older than nearby Late Cretaceous granites and therefore cannot reflect cooling from a magmatism-related metamorphic event. These data and the regionwide nature of cooling preclude the magmatic-heating interpretation as the sole cause.

We consider that the most viable interpretation for Cretaceous cooling is a combination of regional upper-crustal extension and subcrustal refrigeration; local magmatic heating doubtless contributed to the pattern of K-Ar ages in some places. Metamorphism in the Toano and Pilot Ranges requires no crustal thickening in the Jurassic and contains no record of a Cretaceous thickening event, suggesting that these rocks were not part of a thrust plate brought from greater depth in the Cretaceous. Following Jurassic metamorphism, temperatures at 13 km depth plausibly remained as high as 350°C, and therefore K-Ar ages were not set, until tectonic or erosional removal of 2 to 4 km of overburden. Modest exhumation of the upper crust could produce the necessary small temperature decrease that would result in regional setting of K-Ar ages and yet preserve in most places the upper Paleozoic strata on which Tertiary volcanic rocks were deposited. Within the resolution of K-Ar dating, extension took place roughly at the same time as proposed crustal refrigeration. Gradual cooling of the upper crust may have been produced by subduction of cold lithosphere during low-angle Laramide subduction (Dumitru and others, 1991) beginning at about 80 Ma. The cooling effects are observed in the upper crust some 5 to 25 m.y. after refrigeration began, depending on depth of the cold slab and the position in the upper crust. Perhaps cooling caused by exhumation at the surface and lessening of the geothermal gradient by refrigeration beneath the crust coincided to produce a regionally recognized cooling event.

CONCLUSIONS

Rocks in the Toano and Pilot Ranges underwent widespread greenschist facies metamorphism during the Jurassic and localized amphibolite facies metamorphism near plutons about 160 Ma. Pressures during metamorphism were about 3.5 kb, which corresponds closely to the calculated sedimentary load, and therefore precludes tectonic thickening to produce metamorphism; magmatic heating is the most likely thermal source. Accompanying Jurassic metamorphism was southeast-directed folding and minor thrust faulting. Cretaceous events in these ranges are limited to intrusion of one strongly peraluminous pluton at about 80 Ma, and cooling to Ar retention temperatures in micas from 85 to 65 Ma, although minor east-directed extension in the Pilot Range is possibly Late Cretaceous.

A scenario for Jurassic tectonism is magmatism-induced rifting east of the Pilot Range, modest shortening in and near thermally softened upper crust of the Pilot Range, and possible large-scale shortening farther west closer to the margin of the continental crust. If this model is correct, Jurassic tectonism in the eastern Great Basin resulted from back-arc magmatism imprinting a normal-fault fabric on the brittle crust inboard of the ductilely shortening weaker crust. Tectonism probably records regional stresses at middle and upper crustal zones of thermal softening, induced by voluminous magmatism. Tectonic inheritance of Proterozoic structures influenced patterns of Mesozoic tectonism, best exemplified by the 20-km burial of Paleozoic rocks on the crustal salient at the East Humboldt Range.

ACKNOWLEDGMENTS

We thank R.W. Allmendinger, L.L. Glick, L.W. Snee, M.L. Wells, and J.L. Wooden for informative discussions on various aspects of the geology of the Pilot Range area. K.B. Ketner generously provided unpublished geologic maps of part of the Toano Range. We thank D.S. Harwood and M.L. Wells for helpful reviews of this paper.

REFERENCES CITED

Allmendinger, R.W., and Jordan, T.E., 1984, Mesozoic structure of the Newfoundland Mountains, Utah: Horizontal shortening and subsequent extension in the hinterland of the Sevier belt: Geological Society of America Bulletin, v. 95, p. 1280-1292.

Allmendinger, R.W., Sharp, J.W., Von Tish, D., Serpa, L., Brown, L., Kaufman, S., Oliver, J., and Smith, R.B., 1983, Cenozoic and Mesozoic structure of the eastern Basin and Range province, Utah, from COCORP seismic-reflection data: Geology, v. 11, p. 532-536.

Armstrong, F.C., and Oriel, S.S., 1965, Tectonic development of Idaho-Wyoming thrust belt: American Association of Petroleum Geologists Bulletin, v. 49, p. 1847-1866.

Armstrong, R.L., 1968a, Sevier orogenic belt in Nevada and Utah: Geological Society America Bulletin, v. 79, p. 429-458.

—1968b, Mantled gneiss domes in the Albion Range, southern Idaho: Geological Society America Bulletin, v. 79, p. 1295-1314.

—1972, Low-angle (denudation) faults, hinterland of the Sevier orogenic belt, eastern Nevada and western Utah: Geological Society of America Bulletin, v. 83, p. 1729-1754.

—1976, The geochronometry of Idaho, Pt. 2: Isochron/West, v. 15, p. 1-33.

—1982, Cordilleran metamorphic core complexes—From Arizona to southern Canada: Annual Reviews of Earth and Planetary Sciences, v. 10, p. 129-154.

Armstrong, R.L., and Hansen, E., 1966, Cordilleran infrastructure in the eastern Great Basin: American Journal of Science, v. 264, p. 112-127.

Armstrong, R.L., and Suppe, J., 1973, Potassium-argon geochronometry of Mesozoic igneous rocks in Nevada, Utah, and southern California: Geological Society America Bulletin, v. 84, p. 1375-1392.

Atkinson, W.W., Jr., Kaczmarowski, J.H., and Erickson, A.J., Jr., 1982, Geology of a skarn-breccia orebody at the Victoria Mine, Elko County, Nevada: Economic Geology, v. 77, p. 899-918.

Barton, M.D., 1990, Cretaceous magmatism, metamorphism, and metallogeny in the east-central Great Basin, *in* Anderson, J.L., ed., The nature and origin of Cordilleran magmatism: Geological Society of America Memoir 174, p. 283-302.

Bohlen, S.R., Montana, A., and Kerrick, D.M., 1991, Precise determinations of the equilibria kyanite—sillimanite and kyanite-andalusite and a revised triple point for Al2SiO5 polymorphs: American Mineralogist, v. 76, p. 677-680.

Coats, R.R., Marvin, R.F., and Stern, T.W., 1965, Reconnaissance of mineral ages of plutons in Elko County, Nevada, and vicinity: U.S. Geological Survey Professional Paper 525-D, p. 11-15.

Coats, R.R., and Riva, J.F., 1983, Overlapping overthrust belts of late Paleozoic and Mesozoic ages, northern Elko County, Nevada, *in* Miller, D.M., Todd, V.R., and Howard, K.A., eds., Structural and stratigraphic studies in the eastern Great Basin: Geological Society of America Memoir 157, p. 305-327.

Collins, W.J., and Vernon, R.H., 1991, Orogeny associated with anticlockwise P-T-t paths: Evidence from low-P, high-T metamorphic terranes in the Arunta inlier, central Australia: Geology, v. 19, p. 835-838.

Crittenden, M.D., Jr., 1972, Willard thrust and the Cache allochthon, Utah: Geological Society of America Bulletin, v. 83, p. 2871-2880.

Dallmeyer, R.D., Snoke, A.W., and McKee, E.H., 1986, The Mesozoic-Cenozoic tectonothermal evolution of the Ruby Mountains, East Humboldt Range, Nevada: A Cordilleran metamorphic core complex: Tectonics, v. 5, p. 931-954.

Dumitru, T.A., Gans, P.B., Foster, D.A., and Miller, E.L., 1991, Refrigeration of the western Cordilleran lithosphere during Laramide shallow-angle subduction: Geology, v. 19, p. 1145-1148.

Elison, M.E., 1991, Intracontinental contraction in western North America: Continuity and episodicity: Geological Society of America Bulletin, v. 103, p. 1226-1238.

Farmer, G.L., and DePaolo, D.J., 1983, Origin of Mesozoic and Tertiary granite in the western United States and implications for pre-Mesozoic crustal structure — 1. Nd and Sr isotopic studies in the geocline of the northern Great Basin: Journal of Geophysical Research, v. 88, p. 3379-3401.

Glick, L.L., 1987, Structural geology of the northern Toano Range, Elko County, Nevada: Unpubl. M.S. Thesis, San Jose State Univ., San Jose, CA, 141 p.

Harris, A.G., Wardlaw, B.R., Rust, C.C., and Merrill, G.K., 1980, Maps for assessing thermal maturity (conodont color alteration index maps) in Ordovician through Triassic rocks in Nevada, Utah, and adjacent parts of Idaho and California: U.S. Geological Survey Miscellaneous Investigations Series Map I-1249.

Heller, P.L., Bowdler, S.S., Chambers, H.P., Coogan, J.C., Hagen, E.S., Shuster, M.W., Winslow, N.S., and Lawton, T.F., 1986, Time of initial thrusting in Sevier orogenic belt, Idaho-Wyoming and Utah: Geology, v. 14, p. 388-391.

Hintze, L.F., 1988, Geologic history of Utah: Brigham Young University Geology Studies Special Publication 7, 202 p.

Hodges, K.V., and McKenna, L., 1986, Structural and metamorphic characteristics of the Raft River-Quartzite Assemblage juxtaposition, Albion Mountains, southern Idaho: Geological Society of America Abstracts with Programs, v. 18, p. 117.

Hodges, K.V., Snoke, A.W., and Hurlow, H.A., in press, Thermal evolution of a portion of the Sevier hinterland: the northern Ruby Mountains-East Humboldt Range and Wood Hills, northeastern Nevada: Tectonics.

Hudec, M.R., 1990, Mesozoic history of the central part of the Ruby Mountains-East Humboldt Range metamorphic core complex, Nevada: Geological Society of America Abstracts with Programs, v. 22, p. 30.

Johnson, M.C., and Rutherford, M.J., 1989, Experimental calibration of the aluminum-in-hornblende geobarometer with applications to Long Valley caldera (California) volcanic rocks: Geology, v. 17, p. 837-841.

Jordan, T.E. 1985, Tectonic setting and petrography of Jurassic foreland basin sandstones, Idaho-Wyoming-Utah, *in* Kerns, G.J. and Kerns, R.L., Jr., eds., Orogenic patterns and stratigraphy of north-central Utah and southeastern Idaho: Utah Geological Association Publication 14, p. 201-213.

Lee, D.E., Kistler, R.W., Friedman, Irving, and Van Loenen, R.E., 1981, Two-mica granites of northeastern Nevada: Journal of Geophysical Research, v. 86, p. 10607-10616.

Lush, A.P., McGrew, A.J., Snoke, A.W., and Wright, J.E., 1988, Allochthonous Archean basement in the northern East Humboldt Range, Nevada: Geology, v. 16, p. 349-353.

McCollum, L.B., and Miller, D.M., 1991, Cambrian stratigraphy of the Wendover area, Utah and Nevada: U.S. Geological Survey Bulletin 1948, 43 p.

Miller, D.M., 1990, Mesozoic and Cenozoic tectonic evolution of the northeastern Great Basin, *in* Shaddrick, D.R., Kizis, J.A., Jr., and Hunsaker, E.L., III, eds., Geology and ore deposits of the northeastern Great Basin: Geological Society of Nevada Field Trip No. 5, p. 43-73.

Miller, D.M., and Allmendinger, R.W., 1991, Jurassic normal and strike-slip faults at Crater Island, northwestern Utah: Geological Society of America Bulletin, v. 103, p. 1239-1251.

Miller, D.M., and Lush, A.P., 1981, Preliminary geologic map of the Pilot Peak and adjacent quadrangles, Elko County, Nevada, and Box Elder County, Utah: U.S. Geological Survey Open-File Report 81-658, 21 p., 2 sheets, scale 1:24,000.

—in press, Geologic map of the Pilot Peak quadrangle, Box Elder County, Utah, and Elko County, Nevada: Utah Geological Survey Map, scale 1:24,000.

Miller, D.M., Hillhouse, W.C., Zartman, R.E., and Lanphere, M.A., 1987, Geochronology of intrusive and metamorphic rocks in the Pilot Range, Utah and Nevada, and comparison with regional patterns: Geological Society of America Bulletin, v. 99, p. 866-879.

Miller, D.M., Nakata, J.K., and Glick, L.L., 1990, K-Ar ages of Jurassic to Tertiary plutonic and metamorphic rocks, northwestern Utah and northeastern Nevada: U.S. Geological Survey Bulletin 1906, 18 p.

Miller, D.M., Repetski, J.E., and Harris, A.G., 1991, East-trending Paleozoic continental margin near Wendover, Utah, *in* Cooper, J.D., and Stevens, C.H., eds., Paleozoic paleogeography of the western United States-II: Pacific Section, Society of Economic Paleontologists and Mineralogists, v. 67, p. 439-461.

Miller, D.M., Wooden, J.L., and Wright, J.E., 1989, Mantle-derived Late Jurassic plutons emplaced during possible regional extension of the crust, northwest Utah and northeast Nevada: Geological Society of America Abstracts with Programs, v. 21, p. 117.

Miller, E.L., and Gans, P.B., 1989, Cretaceous crustal structure and metamorphism in the hinterland of the Sevier thrust belt, western U.S. Cordillera: Geology, v. 17, p. 59-62.

Miller, E.L., Gans, P.B., Wright, J.E., and Sutter, J.F., 1988, Metamorphic history of the east-central Basin and Range Province: Tectonic setting and relationship to magmatism, *in* Ernst, W.G., ed., Metamorphic and crustal evolution of the western United States: Prentice-Hall, Englewood Cliffs, New Jersey, p. 650-682.

Misch, Peter, 1960, Regional structural reconnaissance in central-northeast Nevada and some adjacent areas-observations and interpretations, *in* Geology of east-central Nevada: Intermountain Association of Petroleum Geologists Guidebook 11, p. 17-42.

Nolan, T.B., 1935, The Gold Hill mining district, Utah: U.S. Geological Survey Professional Paper 177, 172 p.

Royse, Frank, Jr., Warner, M.A., and Reese, D.L., 1975, Thrust belt structural geometry and related stratigraphic problems, Wyoming-Idaho-northern Utah, *in* Bolyard, D.W., ed., Deep drilling frontiers of the central Rocky Mountains: Denver, Rocky Mountain Association of Geologists, p. 41-54.

Snoke, A.W., and Miller, D.M., 1988, Metamorphic and tectonic history of the northeastern Great Basin, *in* Ernst, W.G., ed., Metamorphic and crustal evolution of the western United States: Prentice-Hall, Englewood Cliffs, New Jersey, p. 606-648.

Spear, F.S., and Cheney, J.T., 1989, A petrogenetic grid for pelitic schists in the system SiO_2-Al_2O_3-FeO-MgO-K_2O-H_2O: Contributions to Mineralogy and Petrology, vo. 101, p. 149-164.

Stacey, J.S., and Zartman, R.E., 1978, A lead and strontium isotopic study of igneous rocks and ores from the Gold Hill mining district, Utah: Utah Geology, v. 5, p. 1-15.

Stewart, J.H., 1980, Geology of Nevada, a discussion to accompany the geologic map of Nevada: Nevada Bureau of Mines and Geology Special Publication 4, 136 p.

Wells, M.L., Dallmeyer, R.D., and Allmendinger, R.W., 1990, Late Cretaceous extension in the hinterland of the Sevier thrust belt, northwestern Utah and southern Idaho: Geology, v. 18, p. 929-933.

Wright, J.E., and Wooden, J.L., 1991, New Sr, Nd, and Pb isotopic data from plutons in the northern Great Basin: Implications for crustal structure and granite petrogenesis in the hinterland of the Sevier thrust belt: Geology, v. 19, p. 457-460.

MESOZOIC STRUCTURAL AND METAMORPHIC FEATURES IN THE WOOD HILLS AND PEQUOP MOUNTAINS, NORTHEASTERN NEVADA

Phyllis A. Camilleri
Department of Geology and Geophysics
University of Wyoming, Laramie, WY 82071-3006

ABSTRACT

The Wood Hills and Pequop Mountains, respectively, lie successively to the east of the Ruby Mountains-East Humboldt Range metamorphic core complex. These three ranges, from west to east, provide a nearly continuous cross section of metamorphosed miogeoclinal rocks representing Mesozoic middle to upper crust. Miogeoclinal strata were structurally buried to at least 26 km in excess of stratigraphic depths on the west, and structural depth and metamorphic grade decreases to the east. Much of the Mesozoic tectonic history is strongly obscured or overprinted by a penetrative top-to-the-NW mylonitic extensional shear zone in the East Humboldt Range. In contrast, the Pequop Mountains and Wood Hills mainly record Mesozoic deformation and therefore are critical to understanding the mode and geometry of crustal thickening responsible for deep structural burial of the miogeoclinal section in this region.

New structural data from the Wood Hills and the Pequop Mountains indicate that two major contractile deformational events were responsible for tectonic burial of the miogeoclinal section. The first event involved Jurassic (?) SE-directed thrusting. Metamorphosed miogeoclinal rocks in the Wood Hills and Pequop Mountains are inferred to have once comprised the footwall to a top-to-the-SE, NW-dipping ductile decollement exposed in Mississipian strata (Little Lake decollement). Geobarometric and structural data suggest that footwall rocks were structurally buried to at least 10 km in excess of stratigraphic depths towards the northwest (Wood Hills), and burial depth decreases to the SE (Pequop Mountains). Within the footwall metamorphic grade decreases from upper amphibolite facies to lower greenschist facies commensurate with decreasing structural depth. These rocks may have lain below an eastward tapering contractionally thickened wedge above the Little Lake decollement or may have comprised a horst in a duplex system. Footwall rocks were deformed into a prograde metamorphic L-S to S tectonite (S_1 and L_1) with foliation subparallel to stratigraphic boundaries. Attenuation of stratigraphic section accompanied development of the tectonite. Amount of attenuation ranges from around fifteen to fifty percent and varies directly with metamorphic grade and burial depth. Based on metamorphic microstructures, attenuation of section is largely a product of bulk pure shear with the flattening plane nearly parallel to stratigraphic units at peak metamorphic grade. Attenuation may be a byproduct of thermal weakening and spreading during or following structural burial, due perhaps to reequilibration of thermal gradients. Such attenuation of section may be a natural response to significant loading of a footwall. In effect, stretching of the footwall may facilitate isostatic accommodation of the load (i.e., sinking) and a consequent reduction of topography.

The second major Mesozoic contractile event affecting rocks in the Wood Hills and Pequop Mountains was the development of Jurassic or Cretaceous, post-S_1 map-scale thrust faults and folds. A regionally extensive top-to-the-SE thrust fault (the "Independence thrust") in the Pequop Mountains cuts through nearly the entire Paleozoic section. The Independence thrust is inferred to have rooted beneath

the Wood Hills. Smaller scale NW-vergent back folds and back thrusts occur in the hanging wall of the Independence thrust in the Pequop Mountains and the Wood Hills.

Structures that postdate contractile structures comprise low-angle normal faults that appear to be rooted to the west. These structures are remnants of normal fault systems responsible for unroofing of the once-structurally-deep Mesozoic fabrics or structures. Age constraints on these faults range from pre-middle Eocene to Miocene or younger. Extension of the load created during Mesozoic contractile deformation appears to be roughly kinematically opposite the direction of shortening.

INTRODUCTION

The Wood Hills and Pequop Mountains are Mesozoic metamorphic complexes that are situated within a belt of metamorphic core complexes in northeast Nevada (see Fig. 1 in Camillleri et al., this volume). This region lies in what has been traditionally referred to as the "hinterland" of the Cretaceous to early Tertiary Sevier fold and thrust belt, but this region may also comprise the "hinterland" to a Late Jurassic fold and thrust belt (see Camilleri et al., this volume). Within the metamorphic core complexes structurally deep metamorphosed miogeoclinal rocks that contain Mesozoic metamorphic fabrics and structures have been exhumed, overprinted, and dismembered by Tertiary plastic to brittle extensional structures. The Wood Hills and Pequop Mountains are unique in that they comprise extensive, intact terrains of polydeformed, structurally deep to shallow metamorphosed miogeoclinal rocks that lack a strong Tertiary extensional overprint and hence preserve the Mesozoic tectonic and metamorphic history.

The Wood Hills and Pequop Mountains lie east of the northern East Humboldt Range, which is the northernmost part of the Ruby Mountains-East Humboldt Range metamorphic core complex (Fig. 1). In these three ranges Tertiary extensional fault systems have unroofed contractile Mesozoic metamorphic fabrics and structures developed at mid-crustal to supracrustal levels.

The northern East Humboldt Range exposes upper amphibolite facies, migmatitic rocks which are overprinted by a mid-Tertiary top-to-the-northwest extensional, mylonitic shear zone (Snoke and Lush, 1984). Footwall rocks consist of Carboniferous to Proterozoic miogeoclinal strata and Archean basement record Mesozoic upper amphibolite facies metamorphism and complex plastic strain (Snoke and Lush, 1984). Geothermobarometric and geochronologic data from Proterozoic Z rocks (McCoy Creek Group Unit G) in the Clover Hill area of the northern East Humboldt Range (Fig.1) suggest that these rocks were structurally buried to depths of at least 35 km during the Mesozoic (Hodges et al., in press). This is roughly 26 km in excess of probable Mesozoic stratigraphic depths based on estimates of the thicknesses of Paleozoic-Mesozoic rocks (Fig. 4) and stratigraphic thickness of Precambrian strata (Miller, 1984). This metamorphic sequence is inferred to have been partially exhumed by extensional processes during the Mesozoic (Hodges et al., in press).

The Wood Hills comprise an extensive tract of upper amphibolite facies Cambrian to Devonian strata that mainly record Mesozoic metamorphism and contractile strain at a structural level above that in the adjacent East Humboldt Range. Geothermobarometric data on an upper Cambrian schist in the southern Wood Hills suggest burial depths of 18 to 24 km (Hodges et al., in press), which is at least 10 km in excess of Mesozoic stratigraphic depths (Fig. 4). Cambrian to Triassic strata in the Pequop Mountains mainly record Mesozoic contractile strain and metamorphism at yet higher structural levels above that recorded in the Wood Hills.

Although much of the Mesozoic history in the northern East Humboldt Range has been obscured by subsequent Tertiary deformation, rocks in the Wood Hills and Pequop Mountains preserve much of this history. Because the Wood Hills and Pequop Mountains expose a relatively continuous transition of rocks that represent Mesozoic mid-crustal to supracrustal levels, they are critical to understanding Mesozoic metamorphic and tectonic processes that resulted in deep structural burial of the miogeoclinal section in the Wood Hills and northern East Humboldt Range.

Thorman (1970) originally mapped the Wood Hills and Pequop Mountains. He suggested that polydeformed, regionally metamorphosed rocks in both ranges lie structurally below low-angle faults that contain unmetamorphosed Paleozoic rocks in the upper plates (Fig. 2). He interpreted all the low-angle faults as being remnants of a regionally extensive, post-metamorphic top-to-the-east thrust fault termed the "Wood Hills thrust" (Fig. 2). Snoke and Miller (1988) noted that the fault omits metamorphic grade and that an extensional origin is more probable. In the footwall of the Wood Hills thrust in the Wood Hills, Thorman (1970) mapped a series of map-scale northwest-vergent folds, which he suggested postdated the development of regional metamorphic fabric but predated the "Wood Hills thrust." In the Pequop Mountains, Thorman (1970) mapped a major east-directed thrust fault (the valley view thrust; Fig. 2) in the hanging wall of the "Wood Hills" thrust that he interpreted to have evolved synchronously with the Wood Hills thrust. Thorman (1970) inferred that all deformation and metamorphism in the footwall of the "Wood Hills thrust" was Mesozoic, and recently Thorman and Snee (1988) confirmed a Mesozoic age.

I present a brief synthesis of work in progress in the Wood Hills and Pequop Mountains, concentrating mainly on Mesozoic metamorphism and deformation. In this paper I present new geologic mapping, and structural and metamorphic data that suggest: (1) regionally metamorphosed rocks in the Wood Hills and Pequop Mountains do not lie beneath a single regionally extensive thrust fault that places unmetamorphosed rocks on top of metamorphosed rocks, (2) regional metamorphism in the Pequop Mountains dies out up section through continuous stratigraphic sections, and (3) regionally metamorphosed rocks in the Wood Hills and Pequop Mountains record two major Mesozoic con-

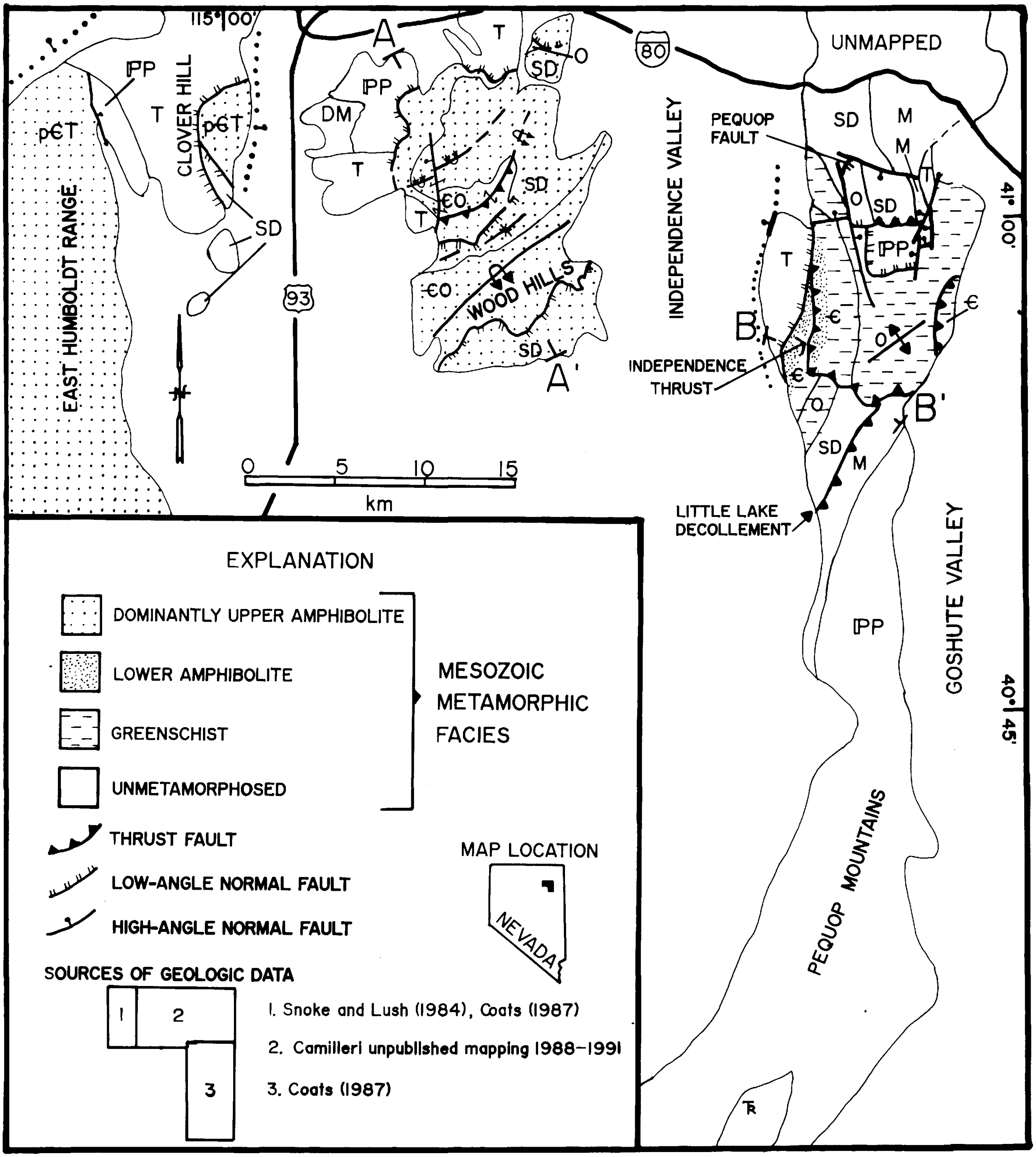

Figure 1. Simplified geologic map of the Wood Hills and Pequop Mountains region. p€T is Precambrian to Tertiary metasedimentary rocks (in part migmatitic) and granitoids; € is Cambrian strata; O is Ordovician strata; €O is Cambrian and Ordovician strata; SD is Silurian and Devonian strata; M is Mississippian strata; IPP is Pennsylvanian and Permian strata; ҇R is Triassic strata, and T is Tertiary strata and volcanic rocks. Unit "T" is Miocene in age in the East Humboldt Range, Wood Hills, and on the western flank of the Peqoup Mountains and is Eocene in age on the east flank of the Pequop Mountains.

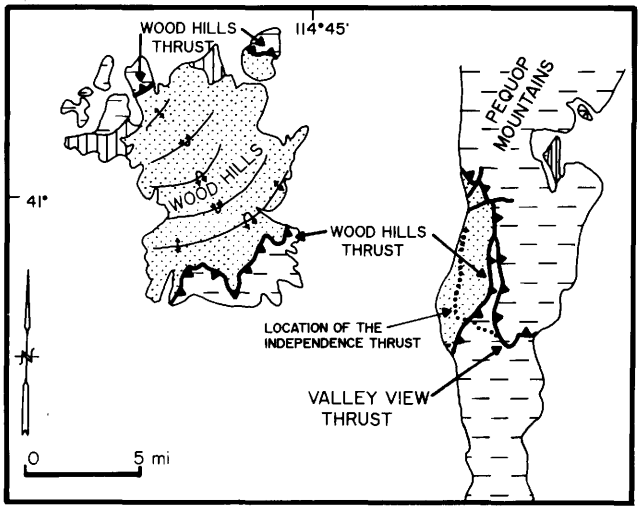

Figure 2. Simplified geologic map of the Wood Hills and Pequop Mountains illustrating major structural features (Thorman, 1970). Stippled pattern represents regionally metamorphosed Cambrian to Devonian strata. Horizontally ruled pattern represents unmetamorphosed Ordovician to Permian strata. Vertically ruled pattern represents Tertiary strata. The bold stippled line represents the location of the Independence thrust, which is shown on Figure 1 (see text for explanation). This figure is modified after Thorman (1970).

tractile events: the first involved Jurassic (?) SE-directed thrusting that resulted in large-magnitude crustal thickening and the development of a prograde metamorphic L-S tectonite fabric (S_1 and L_1) within structurally deep rocks, and the second event involved the development of a Jurassic or Cretaceous, regionally extensive post-S_1 top-to-the-SE thrust fault and associated back folds and back thrusts.

STRUCTURE AND FABRIC IN THE WOOD HILLS

The Wood Hills expose a continuous, regionally extensive tract of upper amphibolite facies Upper Cambrian to Upper Devonian strata. In the northwestern part of the Wood Hills the metamorphic sequence lies in low-angle normal fault contact beneath unmetamorphosed Upper Devonian to Permian strata (Fig. 1). Metamorphosed rocks in the Wood Hills record four main phases of deformation: (1) the development of a prograde metamorphic L-S (S_1 and L_1) tectonite, (2) the development of a normal fault that either predates or postdates phase #1 but predated phase #3, (3) the development of map-scale, post-S_1 NW-vergent folds and an associated thrust fault, and (4) the development of brittle and plastic low-angle normal faults that postdate all previous phases of deformation.

Regional Metamorphism and Fabric Development

The oldest synmetamorphic deformational event recorded in the Wood Hills is the development of a prograde metamorphic L-S tectonite fabric with foliation nearly parallel to stratigraphic units. Based on $^{40}Ar/^{39}Ar$ data on micas, metamorphism is constrained to be Early Cretaceous (115-105 Ma) or older (Thorman and Snee, 1988). The L-S tectonite is characterized by a strong foliation (S_1) with scarce small-scale isoclinal folds (vergence, if any, is indeterminate) and an ENE- to ESE-trending elongation lineation (L_1; Fig. 3). L_1 is defined by minerals, graphite streaks and grain aggregates. In the southernmost Wood Hills, on the upright limb of the NW-vergent overturned anticline (Fig. 1 and 5), S_1 and L_1 die out up section such that Silurian to Devonian strata lack penetrative fabric. Attenuation of stratigraphic section was a component of the development of S_1 because stratigraphic sections have been thinned to an average of 40-50 % of their original thickness (Fig. 4).

Metamorphic assemblages within particular stratigraphic units are generally uniformly consistent throughout the Wood Hills (with one exception discussed below). Diagnostic metamorphic assemblage in Cambrian pelitic schist (Dunderberg Shale) is biotite-staurolite-kyanite-garnet-muscovite-quartz-plagioclase-allanite-rutile-ilmenite. Diopside and tremolite are prominent in Cambrian to Devonian impure carbonates. Ordovician to Devonian impure dolomite in the southernmost Wood Hills contains no calc-silicates and this is also the section of rock where penetrative metamorphic fabric dies out. This may reflect a southward decrease in metamorphic grade. Moreover, grain size increases from south to north. For example, in the southernmost Wood Hills marbles are generally fine-grained and pelitic rocks are phyllite, whereas in the central and northern Wood Hills marbles are coarse- to medium-grained and pelitic rocks are schist. Thermobarometric analysis of the metamorphic mineral assemblage in the Dunderberg Shale [schist] suggests a burial depth of 18 to 24 km (Hodges et al., in press). This depth requires a minimum of approximately 10 km of structural overburden in excess of probable Mesozoic stratigraphic depths of around 8 km (Fig. 4).

In general, metamorphic minerals display equilibrium textures and porphyroblasts exhibit evidence of having grown syntectonically. In thin sections of schist cut parallel

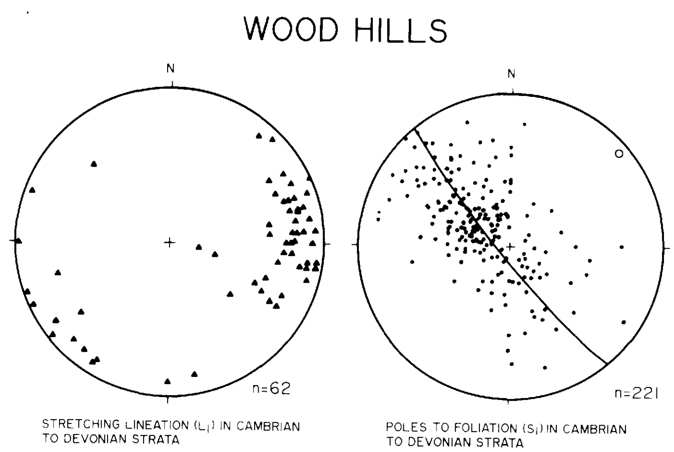

Figure 3. Lower hemisphere projection of L_1 and poles to S_1 from both limbs of the overturned anticline in the southernmost Wood Hills (Fig. 1). Lineations on the overturned limb dominantly trend SW. Best fit great circle to poles to S_1 suggests a NE—trending fold axis (large open circle), which is consistent with the mapped orientation of the fold axis (Fig. 1).

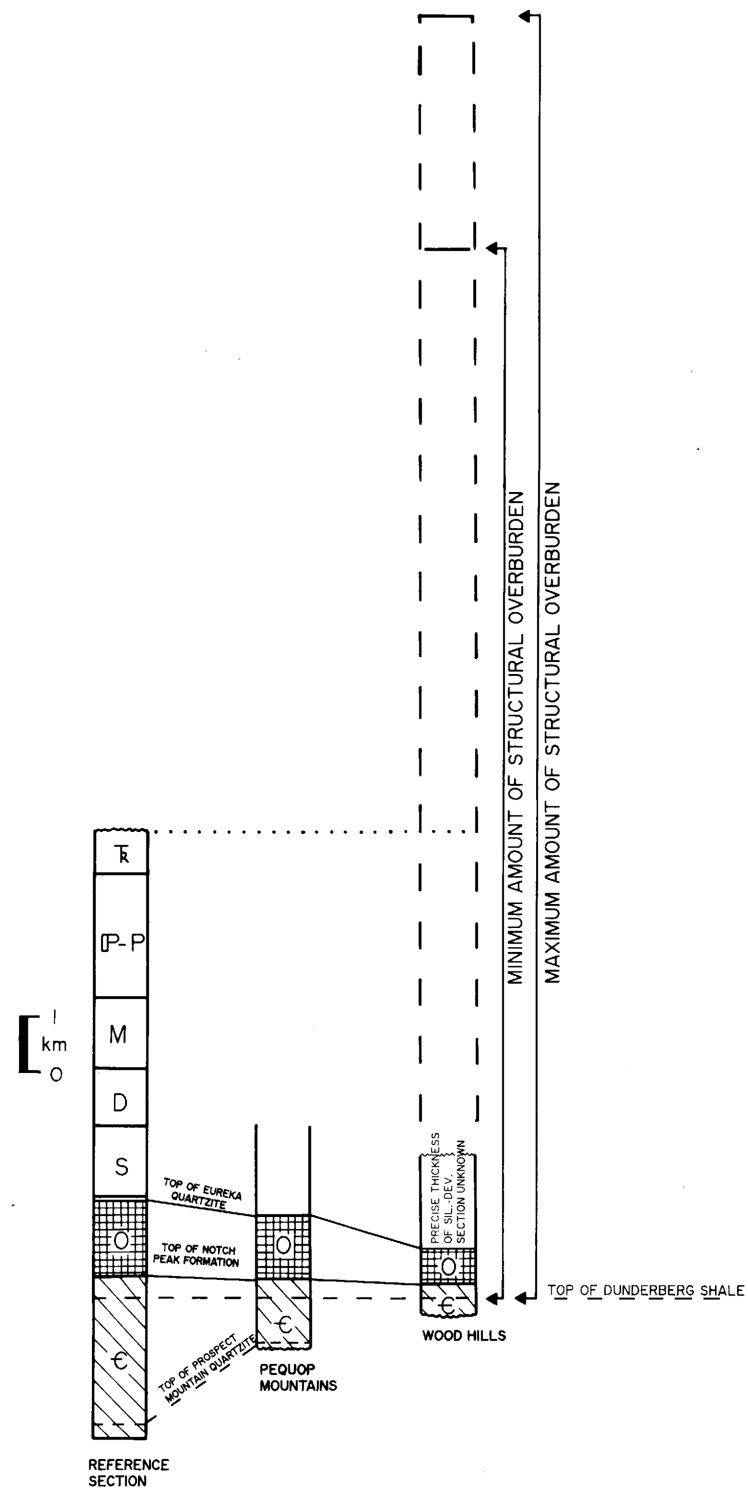

Figure 4. Comparison of minimum stratigraphic thicknesses of regionally metamorphosed and deformed Cambrian and Ordovician sections in Pequop Mountains and Wood Hills with a standard, undeformed Paleozoic reference section. All stratigraphic columns are hung on the top of the Upper Cambrian Dunderberg Shale for comparative purposes. The reference section was constructed using data from McCollum and Miller, 1991; D. M. Miller, 1984; Glick, 1987; Thorman, 1970; Robinson, 1961; and Fraser 1986. Amount of attenuation of the Cambrian-Ordovician sections in the Wood Hills and Pequop Mountains (see text for explanation) was determined by comparison of Cambrian and Ordovician sections in the Wood Hills with undeformed Cambrian and Ordovician sections/type sections exposed in the Toano Range, which is described by Glick (1987) and McCollum and Miller (1991). The estimates of percent attenuation (see text) does not account for any possible regional stratigraphic thickness variation. In ascending order, Cambrian stratigraphic units consist of the Prospect Mountain Quartzite, Killian Springs Formation, Toano Limestone, Cliffside Limestone, Morgan Pass Formation, Decoy Limestone, Shafter Formation, Oasis Formation, Dunderberg Shale, and Notch Peak Formation. Ordovician units consist of the Pogonip Group, Eureka Quartzite, and Fish Haven Dolomite, Silurian units consist of the Laketown Dolomite, Roberts Mountain Formation, and Lone Mountain Dolomite. Devonian units consist of the Simonson Dolomite and Guillmette Formation. Mississippian units consist of Joana Limestone (in the footwall of the Independence thrust) or Tripon Pass Limestone (in the hanging wall of the Independence thrust) and Chainman Shale-Diamond Peak Formation. This figure illustrates maximum and minimum amount of structural overburden in the southern Wood Hills as required by data of Hodges et al. (in press).

to elongation lineation and perpendicular to foliation, kyanite and staurolite porphyroblasts generally contain inclusion trails that are parallel to external foliation and that are commonly elongate in the plane of schistosity. Biotite and microline porphyroblasts tend to have characteristic "eye shapes" with the long axis of the porphyroblast parallel to foliation and elongation lineation. Where present porphyroblast pressure shadows are symmetrical, and biotite porphyroblasts commonly display evidence of having grown into their own pressure shadow. These microfabric relationships and the lack of any asymmetric microstructures suggest growth of metamorphic minerals during peak metamorphism in a dominantly coaxial strain regime. In-progress quartz petrofabric studies will test such a strain history.

The high pressure metamorphic assemblage in the Dunderberg Shale suggests that S_1 is a result of a major contractile or crustal thickening event, yet S_1 also records plastic extension or attenuation of stratigraphic units. Microstructural relationships, as well as the fact that S_1 is approximately parallel to stratigraphic units, suggest dominantly pure shear with the flattening plane parallel to stratigraphic units during peak metamorphism, hence attenuation of section would be a direct consequence of this type of strain. An apparent contradiction to an entirely layer-parallel bulk pure shear history for the development of S_1 is the presence of small-scale isoclinal folds with axial planes parallel to foliation. Because foliation is parallel to stratigraphic units this does not seem compatible with fold development in a coaxial strain regime. These seemingly incompatible micro- and macrostructural relationships can be resolved if the rocks experienced a more complex strain history. One possibility is an early history of dominantly bulk simple shear nearly parallel to bedding followed by bulk pure shear with the flattening plane parallel to stratigraphic units during peak metamorphic conditions. Alternatively, the same relationships could be produced by an early bulk pure shear at an angle to bedding (thereby producing folds) with subsequent rotation of principal strain axes during peak metamorphism such that the flattening plane is parallel to stratigraphic units. An important point to note is the metamorphic rocks lack pre-S_1 foliations so that if folding predates peak metamorphism either no strong foliations were produced, or any foliations that were produced were rotated into parallelism with stratigraphic units (as in bulk progressive simple shear) or were obscured or obliterated during bulk pure shear at peak metamorphism.

Northwest-vergent Folds and Thrust Fault

S_1 is deformed by map-scale NW-vergent folds and a thrust fault (Fig. 1 and Fig. 5). In the southern Wood Hills the NW-vergent folds comprise an overturned anticline-syncline pair in the hanging wall of a top-to-the-NW thrust fault. In the northern Wood Hills a recumbent syncline occurs in the footwall of the thrust (Fig. 5). The map-scale folds contain scarce parasitic mesoscopic folds and in a few places, generally near the hinges of the map scale folds, a weakly developed axial-planar grain-shape foliation, solution cleavage, or crenulation is developed. There is little evidence of metamorphic retrogression (production of new mineral assemblages) in rocks deformed during the development of the thrust and folds, although recrystallization of deformed minerals or growth of new white mica is common.

Low-angle Normal Faults

The Wood Hills expose four major low-angle normal faults, three of which are probably Tertiary and one that is likely Paleozoic or Mesozoic.

A low-angle normal fault that juxtaposes unmetamorphosed Tertiary strata and middle to upper Paleozoic rocks on top of upper amphibolite facies lower to middle Paleozoic rocks is exposed in the northwestern corner of the Wood Hills. Footwall rocks are partially stratigraphic and age equivalent to hanging wall rocks. Although this fault duplicates stratigraphic section, it is interpreted as a normal fault because it omits metamorphic grade. Such relationships are likely the result of extensional excision of a thrust fault. This low-angle normal fault is inferred to be top-to-the-west because it cuts down section to the west in the hanging wall and footwall (Fig. 5).

A plastic low-angle normal fault that juxtaposes hanging-wall metamorphosed Devonian strata on metamorphosed Ordovician strata (Fig. 1) is exposed in the northeastern corner of the Wood Hills. S-C fabrics in mylonite in Ordovician quartzite beneath the fault overprint S_1 and yield a top-to-the-west sense-of-shear, which is consistent with offsets of stratigraphic units. Based on map relations the amount of slip on this fault probably ranges from tens of meters to a few kilometers. Although the age of this fault is not well constrained, the fault is geometrically and kinematically similar to fabrics and structures associated with the development of the thick Tertiary mylonitic extensional shear zone in the Ruby-East Humboldt core complex (Snoke and Lush, 1984), and may be a product of this system. Moreover, Tertiary(?) top-to-the-W to-NW outcrop-scale mylonitic shear zones are common in metamorphic rocks in the northernmost part of the Wood Hills.

A brittle low-angle fault (Fig. 1) that cuts Middle Ordovician to Silurian strata and omits a minor amount of stratigraphic section is exposed in the southern Wood Hills. The fault is at a low angle to bedding and foliation in the hanging wall and footwall (Fig. 5). Sense of slip on this fault is difficult to constrain. However, offset units require a sense of slip in the general domain of N to WSW (see Fig. 5), and amount of slip probably ranges from tens of meters to a few kilometers. The age of this fault is unconstrained, however it is kinematically similar to other Tertiary low-angle normal faults in the Wood Hills and East Humboldt Range (Snoke and Lush, 1984). Thus this fault may be a rotated Tertiary normal fault.

The low-angle normal faults in the southern, northwestern, and northeastern corners of the Wood Hills were previously inferred to be remnants of a once continuous top-to-the-east thrust fault called the "Wood Hills thrust" (Fig. 2;

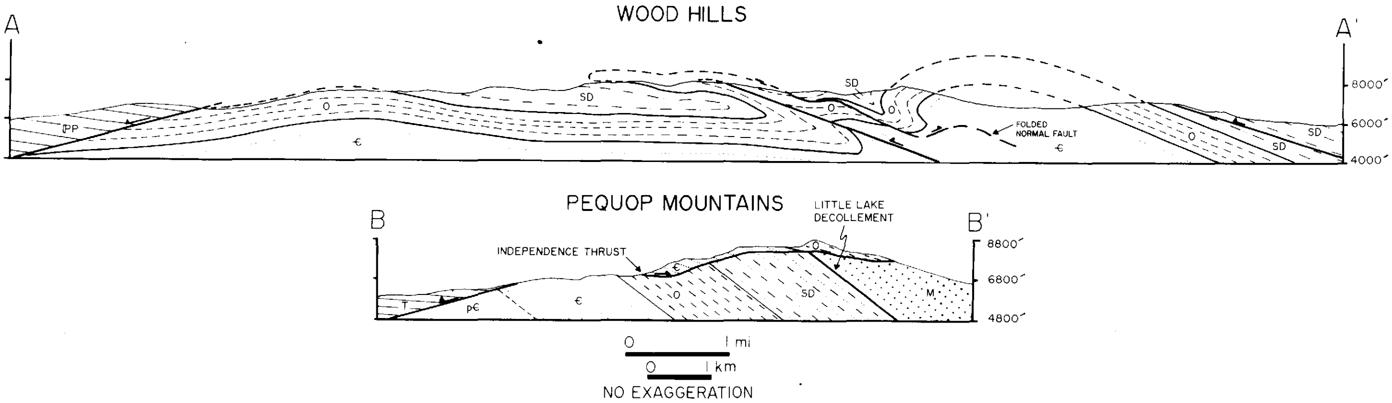

Figure 5. Simplified NW-SE cross section through the Wood Hills (A-A'; see Fig. 1 for location of section) and the Pequop Mountains (B-B', see Fig. 1 for location of section). No vertical exaggeration. Note that the Pequop Mountains cross section is drawn oblique to the inferred slip direction of the Independence thrust.

Thorman, 1970). However, the new data presented here suggest that the faults are likely Tertiary, probably rooted towards the west, and extensional in origin. Moreover, the contrasting large amount vs. small amount of displacement and brittle vs. plastic deformation along the three segments of the "Wood Hills thrust" precludes them from being a single fault surface.

In the central part of the Wood Hills an additional low-angle normal fault is exposed (Fig. 1). This fault is folded by the NW-vergent folds (Fig. 5). Although the normal fault surface is not exposed, map relations indicate that the fault is at a low angle to foliation. It is not clear whether the fault predates or postdates the development of S_1; however, S_1 does not appear to be overprinted adjacent to the fault contact suggesting that S_1 is coeval with or younger than faulting. The age of this fault, if pre-metamorphic, would then be constrained as Devonian (the youngest rocks cut by the fault) to pre-Early Cretaceous.

STRUCTURE AND FABRIC IN THE PEQUOP MOUNTAINS

According to Thorman (1970; Fig. 2) the Pequop Mountains contain two major thrust faults, one of which he correlated with the "Wood Hills thrust" and the other he named the "valley view thrust." Thorman (1970) suggested regionally metamorphosed Cambrian to Devonian strata were confined to the footwall of the "Wood Hills thrust" (Fig. 2), although he noted uncertainty in stratigraphic correlations. Detailed mapping of rocks in the footwall of the "Wood Hills thrust" indicates that they consist of two stratigraphically continuous Cambrian sections transected by a thrust fault (herein named the "Independence thrust", cf. Fig. 1 and Fig. 2). In addition, no break in metamorphic grade or omission or duplication of section exists at the mapped location of the "Wood Hills thrust." The Independence thrust, however, is continuous with the east-trending segment of the "valley view thrust" (cf. Fig. 1 and Fig. 2). Based on new mapping, the north-trending segment of the "valley view thrust" in general parallels a stratigraphic boundary and lacks evidence for a fault contact along its entire length and hence is interpreted as a stratigraphic contact.

I recognize four main phases of deformation in the Pequop Mountains (Fig. 1). These are the development of: (1) a prograde metamorphic L-S tectonite, (2) the Little Lake decollement in Mississippian limestone that formed prior to, during, or after phase #1 but clearly predates phase #3, (3) the post-metamorphic Independence thrust and associated back fold and back thrust, and (4) low-angle normal faults. One of the low-angle normal faults (the Pequop fault, Fig. 1) contains a thrust fault in its hanging wall. The age of this thrust fault relative to the first 3 phases of deformation is unknown.

Regional Metamorphism and Fabric Development

Rocks in the hanging wall and footwall of the Independence thrust record the same synmetamorphic strain history. In both structural blocks metamorphic grade and regional metamorphic fabric die out stratigraphically upwards whereby Silurian to upper Ordovician and younger rocks are essentially unmetamorphosed (Fig. 1) and generally lack penetrative fabric. Lower to Middle Cambrian rocks are lower amphibolite to upper greenschist facies and constitute a prograde metamorphic L-S tectonite (S_1 and L_1) with foliation nearly parallel to stratigraphic units. S_1 is characterized by scarce small-scale isoclinal folds and an elongation lineation (L_1) defined by minerals or elongated grain aggregates with a dominant E to ESE trend (Fig. 6). At stratigraphically higher levels (Upper Cambrian to Ordovician) and lower metamorphic grade (greenschist facies) cleavage or foliation is parallel or at a low angle to bedding, and elongation lineations are scarce. Cleavage that is at a low angle to bedding would dip shallowly towards the west if bedding is rotated to horizontal. Upper Silurian to Lower Devonian dolostone contains no cleavage, but, in places Upper Devonian silty limestone contains a weak to moderate cleavage that is at a low angle to bedding and is geometrically identical to that in stratigraphically lower greenschist facies rocks.

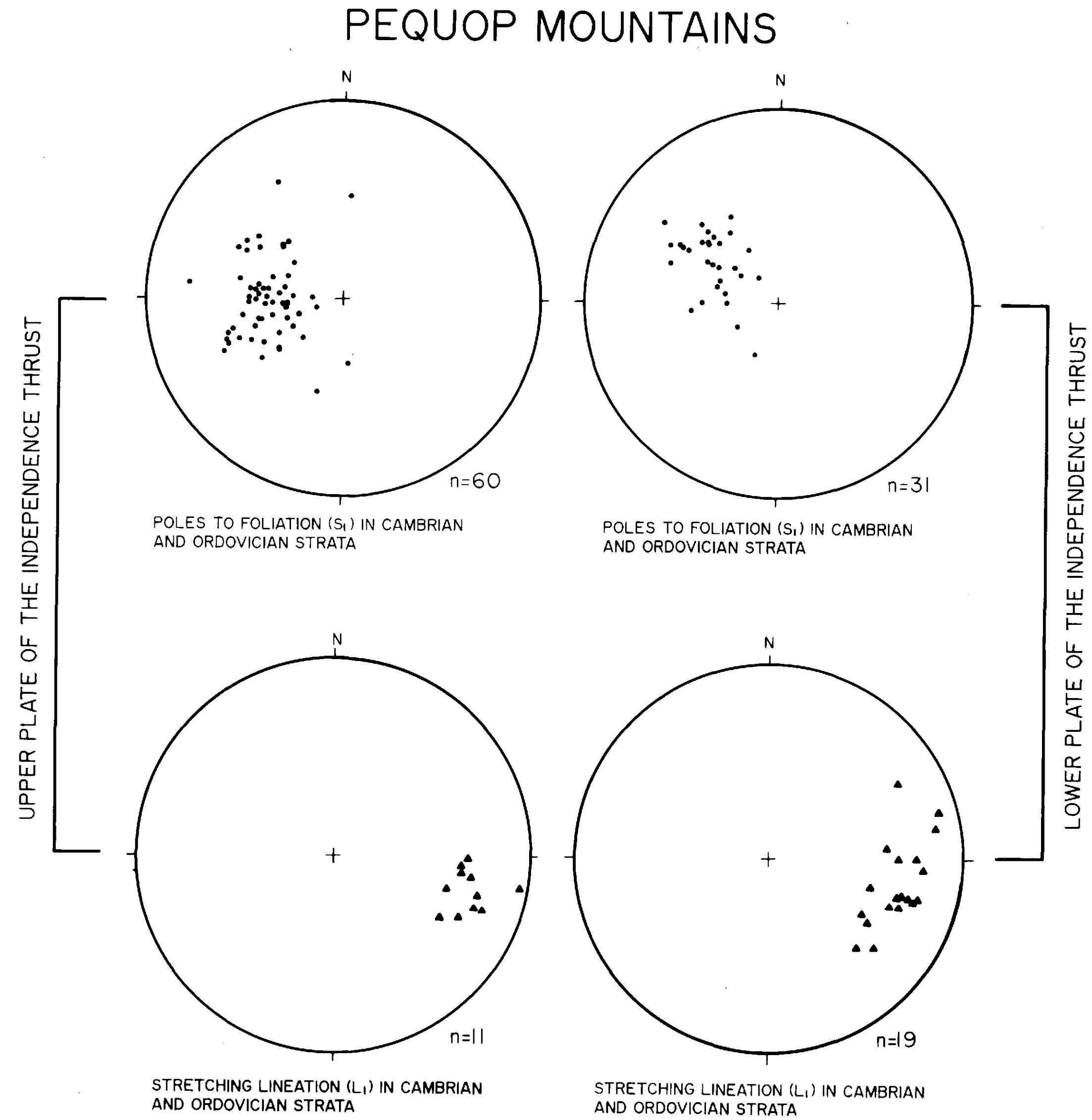

Figure 6. Lower hemisphere projections of poles to S_1 and elongation lineations (L_1) in the hanging wall and footwall of the Independence thrust. For the purpose of comparison of L_1, the data are from the extreme west flank on the Pequop Mountains where foliation in the hanging wall and footwall have similar orientation. Hanging wall strata in the central and eastern part of the range are deformed by post-S_1-L_1 back folds and a back thrust and are therefore not shown.

Bulk attenuation of stratigraphic section appears to have been part of the process responsible for the development of S_1. The amount of stratigraphic attenuation varies directly with metamorphic grade of the rocks (Fig. 4). The amount of attenuation of the Cambrian-Ordovician section collectively varies within the range from approximately 15 to 30%.

In the hanging wall and footwall of the Independence thrust metamorphic grade decreases stratigraphically up section generally commensurate with decrease in penetrative fabric. Diagnostic metamorphic assemblages in stratigraphically lowest, lower amphibolite facies rocks are biotite-garnet-muscovite in impure quartzite, biotite-muscovite-chlorite-epidote in pelite, and hornblende-sphene-biotite-white mica or tremolite in impure carbonate. In stratigraphically higher greenschist facies rocks, pelites were metamorphosed to sericite phyllite and impure carbonates contain no calc-silicates. As a comparison, the Dunderberg Shale in the Pequop Mountains contains the general assemblage biotite-muscovite-allanite-epidote-quartz ± chlorite whereas Dunderberg Shale [schist] in the Wood Hills contains kyanite, staurolite and garnet and no prograde metamorphic chlorite. The latter assemblage attests to greater metamorphic grade for the section in the Wood Hills.

The microstructural character of the metamorphic rocks in the Pequop Mountains is generally identical to that previously described for the Wood Hills. As in the Wood Hills, I interpret the development of S_1 in the Pequop Mountains to be largely a product of bulk pure shear with the flattening plane approximately parallel to or at a low-angle to stratigraphic units at peak metamorphic conditions.

Metamorphism is constrained to have occurred at 115 to 105 Ma or earlier (Thorman and Snee, 1988). Hence the development of S_1 shares the same age constraints.

Independence Thrust and Related Structures

Perhaps the most impressive structure in the Pequop Mountains is the Independence thrust, which cuts through nearly the entire Paleozoic section (Fig. 1; see also cross section in Figure 5 but note that cross section is oblique to inferred slip direction of the thrust). The thrust postdates metamorphism and associated strain, and hence cuts metamorphic gradients (Fig. 1). Thus the Independence thrust emplaced higher grade strata over lower grade strata and metamorphosed strata over unmetamorphosed strata (Fig. 1). Stratigraphic units and metamorphic foliation (S_1) in the footwall of the thrust uniformly dip approximately 35° to 45° to the east. However, stratigraphic units and S_1 in the hanging wall have been deformed by a map-scale NW-vergent back fold and a back thrust (Fig. 1).

Three lines of evidence can be used to infer sense of slip on the Independence thrust. First, the thrust ramps on footwall upper Ordovician to Devonian strata. The ramp appears to trend NE-SW: assuming that sense of slip on the thrust is nearly orthogonal to trend of the ramp suggests that sense of slip is top-to-the SE. Second, if sense of slip on the thrust is inferred to be perpendicular to the map-scale NW-vergent back-fold (Fig. 1), then sense of slip is top-to-the-SE. Third, slickenlines in rocks adjacent to the thrust trend NNW-SSE and indicate the latest slip direction. Therefore, I infer a top-to-the-SE sense of slip on the Independence thrust.

Little Lake Decollement

A bedding-parallel mylonitic shear zone (herein named the Little Lake decollement) occurs at the base of the Mississippian section in the footwall of the Independence thrust (Fig. 1). The Independence thrust cuts, and is therefore younger than, the decollement. The decollement is marked by a prominent white band of mylonitized Joana Limestone (undeformed Joana Limestone is dark gray), which is visible on aerial photographs and when viewed from surrounding ranges west of the Pequop Mountains. The mylonite zone varies in thickness from a few meters to a few tens of meters, and in some places all of the Joana Limestone is deformed. I found no evidence for macroscopic unidirectional sense of shear criteria within mylonitized rocks, however elongation lineations dominantly trend SSE-NNW and would require sense of slip to be either top-to-the-NNW or -SSE.

I have found no evidence for a mylonite zone within Mississippian limestone (Tripon Pass Limestone) in the hanging wall of the Independence thrust (Fig 1). Thorman (1970), however, mapped a decollement at the top of the Tripon Pass Limestone (or base of the Mississipian Chainman Shale) in this region. In this area, the contact between the Tripon Pass Limestone and the Chainman Shale is folded ("room-size" folds) and these folds are cut by high-angle normal faults with displacements of a few meters. Although the contact is not exposed, there is no noticeable repetition or omission of section within the Tripon Pass Limestone. Ascertaining omission or duplication of section within the Chainman Shale at the contact would be difficult because of the lack of exposure and the lithologic monotony of stratigraphic section. However, limestone immediately below, and shale immediately above, the contact is highly fractured and in some places sheared. Deformation at the contact could be a product of folding, high-angle faulting or a decollement or a combination of all three. Thus, it is equally likely that the contact between the Tripon Pass Limestone and Chainman Shale is either depositional or tectonic; the data are inconclusive. It is also possible that the Little Lake decollement is present within the Chainman Shale. However, detecting this would be extremely difficult because this unit is only rarely exposed and is lithologically monotonous. In summary, the Little Lake decollement may or may not be present within the hanging wall of the Independence thrust.

Low-angle Normal Faults

The Pequop Mountains expose two major low-angle normal faults (Fig. 1), both of which appear to be top-to-the west. The Pequop fault is a gently east-dipping, low-angle normal fault that juxtaposes unmetamorphosed Permian to Ordovician strata on top of metamorphosed Ordovician to unmetamorphosed Mississippian strata in the hanging wall of the Independence thrust (Fig. 1). In the hanging wall of the Pequop fault, Permian strata lie in thrust fault contact below a sequence of unmetamorphosed Ordovician to Mississippian strata; this thrust fault is cut by the Pequop fault (Fig.1). Unmetamorphosed Ordovician strata in the hanging wall of the Pequop fault are stratigraphically equivalent to Ordovician regionally metamorphosed and plastically strained strata in the footwall. These relationships are most likely the result of extensional excision, along the Pequop fault, of a thrust fault with an unmetamorphosed upper plate that once lay structurally above the Independence thrust. The Pequop fault is inferred to have been west-rooted because it cuts down section to the west.

The Pequop fault is middle Eocene or older in age because volcanic rocks as old as middle Eocene (41 Ma; Thorman et al., 1990) on the northeastern flank of the Pequop Mountains (shown as Tertiary rocks on Fig. 1) appear to depositionally overlie the fault (Camilleri unpublished mapping, 1990). Moreover, a high-angle, down-to-the-south normal fault cuts the Pequop fault at its northernmost extent, and this fault is also depositionally overlain by the Eocene volcanic rocks (Fig. 1). From these data, the thrust fault in the hanging wall of the Pequop fault is constrained to be premiddle Eocene as well. The Pequop fault truncates broad flexures in hanging wall strata of the Independence thrust. These flexures are likely related to the Independence thrust and hence the Pequop fault probably postdates the Independence thrust. However, age relationships between the thrust in the hanging wall of the Pequop fault and the Independence thrust are unconstrained.

A west-dipping, top-to-the-west low-angle normal fault bounds the west flank of the Pequop Mountains (Fig. 1).

This fault contains Tertiary strata in its hanging wall. The Tertiary section contains clasts and slide blocks of metamorphic rocks derived from the Pequop Mountains as well as Middle to Late Miocene vitric air fall tuff. This indicates that the metamorphic rocks in the Pequop Mountains were exhumed by at least Middle to Late Miocene and that the normal fault is at least this age as well.

DISCUSSION

Metamorphism and many of the deformational events recorded in the Wood Hills and Pequop Mountains are similar enough to permit compelling correlation of structural styles as well as sequence of events. The earliest correlative event in both ranges was the development of the prograde metamorphic L-S to S tectonite. Based on Thorman and Snee's (1988) data, I infer the development of the tectonite to be 115 to 105 Ma or older. Directly to the east of the Pequop Mountains, in the Toano Range, regional metamorphism has been constrained to be Late Jurassic or older (Glick, 1987), and in the central Ruby Mountains regional metamorphism and crustal thickening is constrained as Late Jurassic (Hudec, 1990). These data suggest that regional metamorphism, and the development of S_1 in the Wood Hills-Pequop Mountains region could be Jurassic in age as well. S_1 in the Wood Hills and Pequop Mountains is nearly parallel to stratigraphic units, and in both ranges L_1 (except where folded) dominantly trends E to SE (cf. Figs. 3 and 6). The tectonite is developed within upper amphibolite facies rocks in the Wood Hills and within lower amphibolite to greenschist facies rocks in the Pequop Mountains. In the Pequop Mountains, metamorphic grade and fabric die out up section. As in the Pequop Mountains, S_1 in the southernmost Wood Hills dies out up section coincident with a decrease in metamorphic grade. In both ranges, plastic attenuation of section accompanied development of S_1. Amount of attenuation of stratigraphic section varies directly with metamorphic grade and is reflected in the fact that: (1) the section in the Wood Hills is more attenuated than that in the Pequop Mountains, and (2) within the Pequop Mountains attenuation and metamorphic grade decrease up section. The metamorphic mineral assemblage in metapelite that indicates 5 to 6 kb pressure from the Wood Hills (Hodges et al., in press) suggests that S_1 is the result of a major crustal thickening event. Although no geobarometric data are available for the Pequop Mountains, metamorphic assemblages do not require excessive structural overburden. In both ranges, I interpret S_1 to be largely a product of a bulk pure shear at peak metamorphic grade with the flattening plane nearly parallel to stratigraphic units and a general stretch direction of NW-SE. The similarity of S_1 and L_1 in both ranges as well as the occurrence of a metamorphic-strain gradient in the Pequop Mountains and in the southern Wood Hills suggests that the metamorphosed Paleozoic sections in both ranges, prior to post-S_1 deformation, could have comprised a continuous Paleozoic section. Because the Wood Hills section requires significant structural burial, the metamorphosed Paleozoic section must have comprised the footwall to a thrust fault. A likely interpretation for the Little Lake decollement (Fig. 1) is that it represents the upper bounding decollement for the metamorphosed footwall. This assumption would require the presence of the Little Lake decollement in the hanging wall of the Independence thrust (see description of the Little Lake decollement). Reconstruction of this footwall, taking into account for tectonic thicknesses of stratigraphic sections, distribution of metamorphic facies, and probable structural depths, suggests a westward-dipping footwall in which metamorphic grade and attenuation of stratigraphy increases with structural depth (Fig. 7 A and 8 A). Based on the trend of stretching lineations in the Little Lake decollement, the sense of shear on the thrust system is top-to-the-SSE.

The extent of the proposed thrust system can be inferred from regional relationships. The earliest prograde metamorphic fabric (S_1) in regionally metamorphosed rocks in the East Humboldt Range (A.W. Snoke personal communication; Snoke and Lush, 1984; Taylor, 1981) is described as an L-S tectonite, the development of which involved marked attenuation of stratigraphic section. These characteristics are very similar to S_1 in the Wood Hills and Pequop Mountains suggesting that metamorphosed miogeoclinal strata in the northern East Humboldt Range which record 10 kb pressure (Hodges et al., in press) may represent the structurally deepest part of the proposed footwall in Figure 8 A. These structurally deep rocks can be traced continuously southward through decreasing structural depth and metamorphic grade into the Ruby Mountains where the miogeoclinal section was not buried much in excess of stratigraphic depth during the Mesozoic (Hudec, 1990). A similar relationship occurs in the Pequop Mountains. The structurally lowest rocks in the Pequop Mountains occur in the lower plate of the Independence thrust and these rocks can be traced from the stratigraphically lowest rocks in the range (the upper part of the basal Cambrian Prospect Mountain Quartzite) southward through a relatively continuous stratigraphic sequence into unmetamorphosed Triassic strata in the southernmost Pequop Mountains (Fig. 1). Strata in the southern Pequop Mountains do not appear to have been structurally buried much in excess of stratigraphic depths (R. F. Swenson, personal communication 1991). The northern Pequop Mountains therefore appear to have been tectonically loaded by crustal shortening, whereas the southern end was not (Fig. 1). These data suggest that metamorphosed rocks in the northern East Humboldt Range, Wood Hills and northern Pequop Mountains comprised an area of *localized*, large-magnitude Jurassic (?) crustal thickening.

Assuming that metamorphosed Paleozoic sequences in the Wood Hills and Pequop Mountains and possibly the East Humboldt Range were part of the same west-dipping footwall requires an overlying wedge-shaped thrust plate or contractionally thickened wedge above the Little Lake decollement (such as depicted in Fig. 8 A), most or all of which was extensionally excised in the Cenozoic or Late Mesozoic. An alternate interpretation for the metamorphosed footwall is that it represents a horst in a duplex system. Footwall

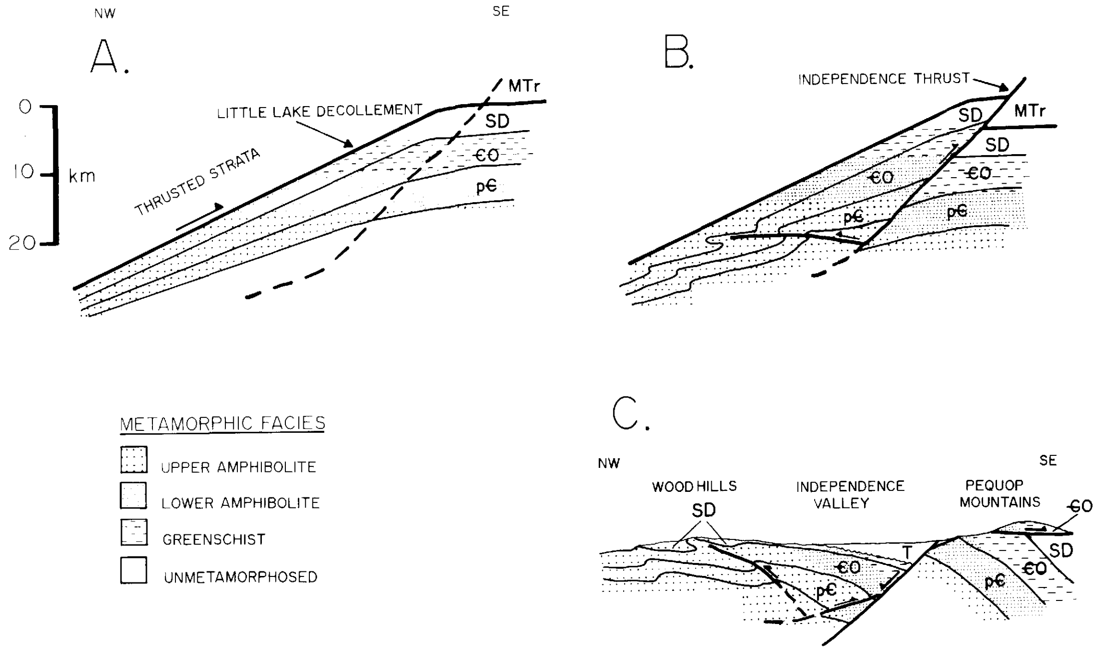

Figure 7. Schematic reconstruction of the metamorphic sequences in the Wood Hills and Pequop Mountains. T is Tertiary strata; MTr is Mississippian to Triassic strata; SD is Silurian to Mississippian strata; €O is Cambrian and Ordovician strata; p€ is PreCambrian strata. Thickness of the Precambrian section is inferred. Cross section is drawn approximately parallel to line A-B′ (Fig. 1). A = inferred Jurassic (?) geometry and distribution of metamorphic facies within the footwall of the Little Lake decollement. B = development of Jurassic or Cretaceous post-metamorphic thrust faults and folds (for simplicity back-folds and thrusts in the Pequop Mountains section are not shown) C = after Mesozoic (?) to Cenozoic extension.

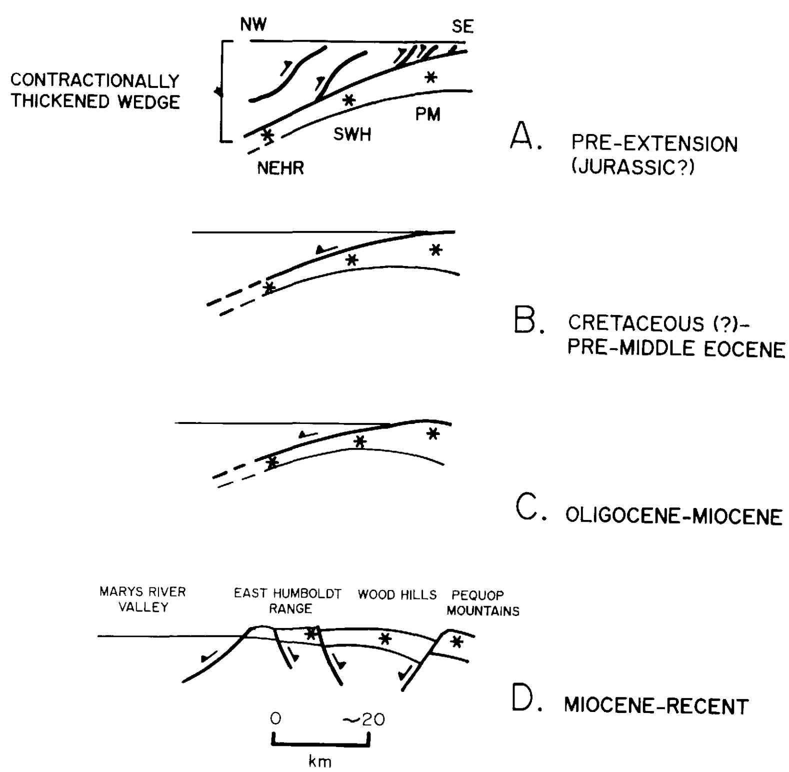

Figure 8. Cartoon illustrating extensional exhumation of the contractionally thickened wedge. For simplicity post-S_1 contractile structures are not shown. NEHR is the metamorphic sequence in northern East Humboldt Range; SWH is the southern Wood Hills; PM is the northern Pequop Mountains. Reconstruction is roughly parallel to line A-B′ shown in Figure 1.

attenuation during peak metamorphic conditions may be a consequence of thermal weakening and spreading under the weight of the overlying "contractionally thickened wedge." This would account for the westward increase in thinning of stratigraphic section that accompanies the westward increase of structural overburden and metamorphic grade (Fig. 7 A). Thermal weakening of the footwall and consequent stratal attenuation may be related to a late stage rise in temperature that could reflect: (1) an increase in temperature due to a regional magmatic event at depth, (2) nearly isobaric heating due to reequilibration of thermal gradients once significant structural overburden is developed (e.g., as shown in PTt paths for thickening of continental crust by Thompson and England, 1984), and (3) a combination of #1 and #2. In the scenarios depicted in Figures 7 A or 8 A, attenuation of stratigraphy could be envisioned as one way of isostatically accommodating the localized thickened area. In effect, stretching of the footwall would allow, to some degree, isostatic sinking of the wedge and attendant reduction in topography.

The second correlative deformational event that affected rocks in the Wood Hills and Pequop Mountains was the development of map-scale NW-vergent folds and thrust faults that fold or cut S_1. The NW-vergent structures occur throughout the Wood Hills and in the Pequop Mountains only in the hanging wall of the Independence thrust where they comprise a back fold and a back thrust (Fig. 1). If the metamorphic sequences in both ranges were once part of a continuous Paleozoic section prior to post-S_1 folding and thrust faulting then the Independence thrust would root beneath the section exposed in the Wood Hills (Fig. 7 B). Therefore folds and thrusts in the Wood Hills could be back folds and thrusts developed in the hanging wall of the Independence thrust (Fig. 7 B). Post-S_1 folds in the northern East Humboldt Range, such as the Winchell Lake fold-nappe (Snoke, this volume), may have formed during this deformational event as well. The age of this deformational event is poorly constrained, it could be Jurassic or perhaps Cretaceous and related to the development of the Sevier fold and thrust belt.

Unroofing of the metamorphic rocks in the northern East Humboldt Range, Wood Hills, and Pequop Mountains is inferred to have been largely accomplished by extensional processes in Mesozoic and Tertiary time (Hodges et al., in press). Any regional inferences on style, timing and kinematic evolution of extensional structures must consider the following published thermochronologic and structural data as well as data presented in this paper.

East Humboldt Range

(1) Based on geochronologic and geothermobarometric data, metamorphic rocks in Clover Hill are inferred to have been extensionally exhumed from around 35 km or greater to around 15 km depth in Cretaceous time (Hodges et al., in press). These rocks subsequently cooled to ~300°C by extensional exhumation along the top-to-the-NW mylonitic shear zone during Late Oligocene (Dallmeyer et al., 1986).

Wood Hills

(1) Rocks in the southern Wood Hills record cooling to ~300°C during Early to Middle Eocene (56-47 MA; Thorman and Snee, 1988; Thorman and Snee, personal communication, 1990). These cooling ages may reflect early Eocene or older extensional exhumation. No thermochronologic data for the northern Wood Hills exist at this time.

(2) All of the faults in the Wood Hills that are inferred to be Tertiary low-angle normal faults were rooted in a westerly direction.

(3) The presence of Wood Hills type metamorphic clasts in Middle to Late Miocene sedimentary rocks in the Clover Hill area indicate that the Wood Hills metamorphic sequence was exhumed by at least this time (Snoke and Lush, 1984).

Pequop Mountains

(1) The Pequop fault represents a pre-Middle Eocene (41 Ma) phase of west-rooted normal faulting.

(2) The metamorphic rocks were exhumed by at least Middle to Late Miocene.

Utilizing these timing and kinematic constraints, Figure 8 shows a simplified model of extensional excision of the inferred contractionally thickened wedge along a west-rooted detachment. For simplicity post-S_1 thrust faults and folds are not shown and I only show the unroofing of the metamorphic rocks along a single detachment. It is, however, very probable that a series of west-rooted detachment systems are responsible for unroofing the metamorphic footwall. If this model is correct it would predict that $^{40}Ar/^{39}Ar$ mica cooling ages in the Wood Hills would young from 56-47 Ma (Thorman and Snee, 1988) in the southern Wood Hills to about 24 Ma in the northwesternmost Wood Hills, assuming that they would be similar to ~24 Ma mica cooling ages in the Clover Hill area (Dallmeyer et al., 1986). The evolution of such a detachment(s) depicted in Figure 8 involves isostatic rebound of the footwall with progressive extension (e.g., Spencer, 1984; Wernicke and Axen, 1988). In essence, Figure 8 A depicts asymmetric contractional loading of a thrust plate and subsequent extension (Fig. 8 B, C, and D) of the load kinematically opposite the direction of shortening. I make this inference because the trend of Mesozoic elongation lineations in the Wood Hills and Pequop Mountains are roughly similar in orientation to NW-SE-trending Tertiary elongation lineations within the top-to-the-NW mylonitic extensional shear zone in the Ruby Mountains-East Humboldt Range metamorphic core complex (see Snoke and Lush, 1984). Thus Tertiary extensional flow or slip lines in this region are similar to the earliest Mesozoic contractile flow or slip lines suggesting that the Mesozoic structural grain or geometry has in part influenced the development and kinematics of Tertiary extensional fabric and structures. The scenarios depicted in Figures 7 and 8 should be treated as preliminary hypotheses and no doubt will be modified as new data are generated.

ACKNOWLEDGMENTS

Dedicated to Nancy O. Camilleri and Paul A. Camilleri. My research was supported by GSA, AAPG, Sigma Xi, and Wyoming Geological Association research grants and in part by NSF grant EAR 87-07435 (awarded to A. W. Snoke). Material support for this project was provided by the U. S. Geological Survey and Chevron USA. David M. Miller, Linda McCollum, and Mike McCollum assisted me in confirmation of correlation of Cambrian stratigraphy in the Pequop Mountains with Cambrian sections and/or type sections exposed in the Pilot and Toano Ranges. Matthew J. Camilleri, Jack E. Deibert, and J. Amory provided some field assistance. I thank Chuck Thorman for continued, open discussion about the geology of this region and also thank Chuck and Larry Snee for discussing their thermochronologic data in the Wood Hills and Pequop Mountains. The development of my research/this paper has benefited from reviews or discussions with B. Fred Swenson, A.W. Snoke, D. M. Miller, M. L. Wells, B.R. Frost, C. Thorman, K. Mueller, and T. MacCready. I thank Jim Evans for a constructive review of the final version of this paper.

REFERENCES CITED

Coats, R. R., 1987, Geology of Elko County, Nevada: Nevada Bureau of Mines and Geology Bulletin 101, 112 p.

Dallmeyer, R. D., Snoke, A. W., and McKee, E. H., 1986, The Mesozoic and Cenozoic tectonothermal evolution of the Ruby Mountains-East Humboldt Range, Nevada: Tectonics, v. 5, p. 931-945.

Fraser, G. S., Ketner, K. B., and Smith, M. C., 1986, Geologic map of the Spruce Mountain 4 Quadrangle, Elko County, Nevada: U. S. Geological Survey Map MF-1846.

Glick, L. L.,1987, Structural geology of the northern Toano Range, Elko County, Nevada [M.S. thesis]: San Jose, California, San Jose State University, 141 p.

Hodges, K. V., Snoke, A. W., and Hurlow, H. A., in press, Thermal evolution of a portion of the Sevier hinterland: the northern Ruby Mountains-East Humboldt Range and Wood Hills, northeastern Nevada: Tectonics.

Hudec, M.R., 1990, The structural and thermal evolution of the central Ruby Mountains, Elko County, Nevada [Ph.D. thesis]: Laramie, Wyoming, University of Wyoming, 272 p.

McCollum, L. B., and Miller, D. M., 1991, Cambrian stratigraphy of the Wendover area, Utah and Nevada: U. S. Geological Survey Bulletin 1948, 43 p.

Miller, D. M., 1984, Sedimentary and igneous rocks of the Pilot Range and vicinity, Utah and Nevada, *in* Kerns, G.J., and Kerns, R.L., eds., Geology of northwest Utah, southern Idaho and northeast Nevada: Utah Geological Association, Field Conference No. 13, p. 45-63.

Robinson, G. B., Jr., 1961, Stratigraphy and Leonardian fusilinid paleontology in central Pequop Mountains, Elko County, Nevada: Brigham Young University Geological Studies, v. 8, p. 93-146.

Snoke, A. W., and Lush, A. P., 1984, Polyphase Mesozoic-Cenozoic deformational history of the Ruby Mountains-East Humboldt Range, Nevada, *in* Lintz, J., Jr., ed., Western geological excursions: Geological Society of America annual meeting field trip Guidebook, Mackay School of Mines, Reno, Nevada, v. 4, p. 232-260.

Spencer, J. E., 1984, The role of tectonic denudation in the warping and uplift of low-angle normal faults: Geology, v. 12, p. 95-98.

Taylor, G. K., 1984, Stratigraphy, metamorphism, and structure of the southeastern East Humboldt Range, Elko County, Nevada [M.S. thesis]: Columbia, South Carolina, University of South Carolina, 148 p.

Thompson, A.B., and England, P. C., 1984, Pressure-temperature-time path of regional metamorphism II. Their inference and interpretation using mineral assemblages in metamorphic rocks: Journal of Petrology, v. 25, p. 929-955.

Thorman, C. H., 1970, Metamorphosed and nonmetamorphosed Paleozoic rocks in the Wood Hills and Pequop Mountains, northeast Nevada: Geological Society of America Bulletin, v. 81, p. 2417-2448.

Thorman, C.H., Ketner, K.B.,Brooks, W.E., Snee, L. W., and Zimmerman, R.A., 1990, Late Mesozoic-Cenozoic tectonics in northeastern Nevada: *in* Shaddrick, D.R., Kizis, J.A., Jr., and Hunsaker, E.L., III, eds., Geology and ore deposits of the northeastern Great Basin, Geological Society of Nevada 1990 meeting, p. 25-45.

Thorman, C.H., and Snee, L.W., 1988, Thermochronology of metamorphic rocks in the Wood Hills and Pequop Mountains, northeastern Nevada: Geological Society of America Abstracts with Programs, v. 20, p. A18.

Wernicke, B., and Axen, G. J., 1988, On the role of isostasy in the evolution of normal fault systems: Geology, v. 16, p. 848-851.

CLOVER HILL, NEVADA: STRUCTURAL LINK BETWEEN THE WOOD HILLS AND EAST HUMBOLDT RANGE

Arthur W. Snoke
Department of Geology and Geophysics
University of Wyoming
Laramie, WY 82071-3006

ABSTRACT

Clover Hill, Elko County, Nevada, provides an excellent cross-section through a Tertiary plastic-to-brittle extensional shear zone superposed on rocks that record a complex Mesozoic magmatic-metamorphic-deformational history. Archean gneissic rocks intruded by Oligocene monzogranitic orthogneiss are the structurally deepest rocks exposed at Clover Hill. A Lower Proterozoic(?) sequence of quartzite and schist is structurally and apparently stratigraphically above the Archean gneissic rocks. These Precambrian rocks form the core of an inferred recumbent fold and are separated from an overlying Devonian to Cambrian marble and quartzite unit by a pre-folding, low-angle fault. The Devonian to Cambrian unit is complexly folded and greatly attenuated. A tectonic inclusion of quartzite-metaconglomerate within the Devonian to Cambrian unit suggests that even younger rocks (Pennsylvanian-Mississippian?) were involved in the large-scale transposition that this unit has experienced. In turn, the marble and quartzite unit is structurally overlain by an extensive quartzite and schist unit (Cambrian and Upper Proterozoic) that locally includes kyanite-rich metapelites. A fault-bounded sheet of impure marble occurs above the quartzite-schist unit, and in turn is overlain by low-grade tectonic slices of metadolomite and Devonian Guilmette Formation as well as a younger allochthon consisting of northeast-dipping mid-Eocene(?) to Upper Miocene volcanic and sedimentary rocks. The presence of Archean gneissic rocks at Clover Hill provides a definite structural link with the northern East Humboldt Range which exposes a major southward-closing, basement-cored fold-nappe. The uppermost plate of impure marble occupies a structural position equivalent to the Mesozoic metamorphic terrane exposed in the Wood Hills directly to the east, but at Clover Hill these rocks have been attenuated in a Tertiary shear zone. An early history (Late Jurassic?) of crustal thickening is indicated by the high-pressure metamorphism preserved at Clover Hill, however, this history has been overprinted by Late Cretaceous and especially mid-Tertiary magmatism, metamorphism, and deformation.

INTRODUCTION

The term "Clover Hill" was apparently first used by Snelson (1957) for the elongate, domical hill that exposes pre-Tertiary rocks north of Clover Valley and east of the northern East Humboldt Range. This term is informal, for it does not appear on any U.S. Geological Survey topographic map. Clover Hill (CH), located about 7.5 km south-southwest of Wells, Nevada, is situated east of the northern East Humboldt Tertiary metamorphic core complex and west of the Wood Hills Mesozoic metamorphic terrane and is, therefore, a key link in the structural evolution of the region. In this light, CH provides an excellent cross-section through a Tertiary brittle-to-plastic shear zone superposed on a complex Mesozoic metamorphic-deformational history.

An important aspect of CH is that the highest pressure metamorphic rocks in the Ruby-East Humboldt metamorphic core complex (Fig. 1) are preserved at this locality. Other parts of the core complex no doubt also are comprised of rocks that have experienced similar high pressures but

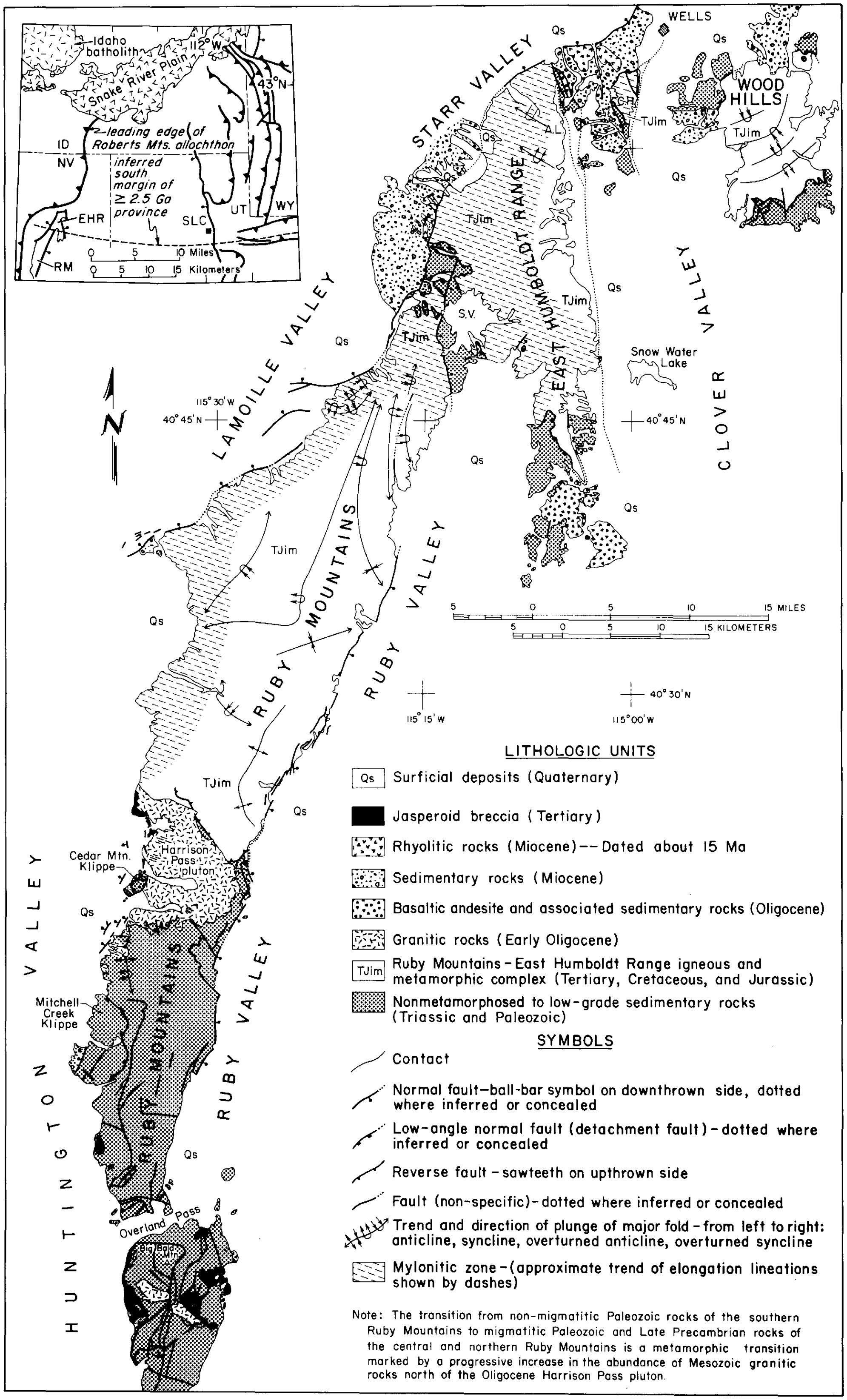

Figure 1. Generalized geologic map of the East Humboldt Range, Wood Hills, Ruby Mountains, and Big Bald Mountain, Nevada. C.H. = Clover Hill. A.L.=Angel Lake. The inset map shows the location of the Ruby Mountains (RM) and East Humboldt Range (EHR) with respect to large-scale tectonic features in the region.

have apparently been strongly overprinted by younger, high-temperature recrystallization (Hodges and others, in press). These rocks occur within an allochthonous sheet of Cambrian-Upper Proterozoic quartzite and schist (Fig. 2, note starred localities) which is interpreted as a displaced part of the upper limb of the Winchell Lake fold-nappe (Lush and others, 1988). In turn, this allochthon lies structurally above a complexly folded suite of younger rocks whose apparent protoliths range from Cambrian to Pennsylvanian-Mississippian(?). The structurally deepest rocks exposed on CH include a migmatitic suite of Lower Proterozoic(?) and Late Archean rocks which are here interpreted as part of the core of the Winchell Lake fold-nappe. A traverse through these various rock units, is the focus of STOP 5 (Day 3) in the accompanying field guide (Camilleri and others, this volume). The purpose of this article is to provide a detailed overview of CH so as to place the field trip stop into a larger context. This report also serves as the first formal publication on the geology of CH.

PREVIOUS STUDIES

Although King (1878) recognized CH as part of extensive exposures of probably Precambrian metamorphic and granitic rocks in the "Humboldt Range" (included both East Humboldt Range and Ruby Mountains of present usage), Snelson (1957) prepared the first geologic map of CH. On this map, Snelson (1957) showed two units: Precambrian metamorphic rocks undifferentiated and Ordovician-Devonian strata; he argued that the younger sedimentary/metasedimentary rocks were thrust over the older crystalline rocks. Furthermore, he separated the Tertiary rocks to the west from the older rocks by a steep, east-dipping reverse fault with the east side upthrown. As part of an evaluation of landholdings of the Southern Pacific Land Company, Oesterling (1961) and Anctil (1961) prepared geologic reports on CH and the surrounding area. Within these reports is included a detailed geologic map of CH (1:24,000) plotted on a topographic base. These authors concluded that the rocks mapped by Snelson (1957) as "Precambrian" were actually highly metamorphosed and deformed Paleozoic rocks. Furthermore, they recognized and mapped several low-angle faults between the various units. All these faults were interpreted as contractile related to Mesozoic deformation. These data plus additional geologic reconnaissance of the CH area by Roger A. Hope were included on the "Geologic map of Elko County, Nevada" (Coats, 1987).

The most recent studies of the CH area have concentrated on various topical aspects and have included: $^{40}Ar/^{39}Ar$ radiometric dating (Dallmeyer and others, 1986), fission-track dating (Dokka and others, 1986), Tertiary stratigraphy (Snoke and others, 1983), economic geology (Lipten, 1984), and geothermobarometry (Hodges and others, in press).

ROCK UNITS

Structural Stacking

The rock units exposed on CH are commonly separated by low-angle faults of various origin and character (Figs. 3 and 4). The oldest low-angle fault is the boundary that separates Archean (Wgn) and Lower Proterozoic(?) (Xqs) rocks from a structurally overlying Devonian-Cambrian marble and quartzite unit (D€mu). This fault is pre-fold-nappe, but its relationship to Mesozoic metamorphism is uncertain. This contact was also mapped by Oesterling (1961) as a fault and referred to in his report as the "Wells thrust". Another low-angle fault separates D€mu from a structurally higher Cambrian-Upper Proterozoic quartzite and schist unit (€Zqs). This low-angle fault is interpreted as post-fold-nappe, because it crosscuts the inferred folded, low-angle fault contact as well as various metamorphic structures in both its upper and lower plates. €Zqs is tectonically overlain by a stack of younger-on-older, low-angle faults. Immediately overlying €Zqs is a sheet of Ordovician(?)-Cambrian impure marble (O€m). This fault contact was incorrectly correlated by Oesterling (1961) with the structurally lower "Wells thrust". In turn, remnants of Devonian-Silurian dolomite/metadolomite (DSd), Devonian Guilmette Formation (Dg), and Miocene Humboldt Formation (Th) occur as fault-bounded slices above the older rocks. This unusual structural stacking is the product of a complex superposed deformational history that ranged from Mesozoic contraction and perhaps extension to Tertiary plastic-to-brittle extension. Multiple metamorphic events accompanied this complex structural developmental history. Previous workers [e.g., Snelson (1957); Oesterling (1961)] considered all these low-angle faults to be contractional with the exception of the faulted contact that separates the Humboldt Formation from the older rocks which was mapped as a west-dipping normal fault by Oesterling (1961) and Anctil (1961).

Gneissic Complex

Archean(?) gneissic rocks intruded by Oligocene(?) monzogranitic orthogneiss form the core of a recumbent fold in the structurally deepest level exposed at Clover Hill (Figs. 4 and 5A). Coarse-grained, muscovite leucogranite of uncertain age also forms segregations and layers within the Archean(?) gneissic rocks.

The Archean rocks are chiefly augen orthogneisses of biotite monzogranite protolith; they are strongly foliated, characterized by a "pin-striped" gneissosity (Fig. 5B). This compositional layering is locally folded by flexural flow folds (so-called "F_2 folds"). Although no geochronometric studies have yet been attempted on this orthogneiss unit, its lithic character is identical to the radiometrically dated Late Archean biotite monzogranitic orthogneiss of Angel Lake (Lush and others, 1988; see Fig. 2 for location of dated sample). Various paragneissic rocks have also been included within the gneissic complex for mapping convenience,

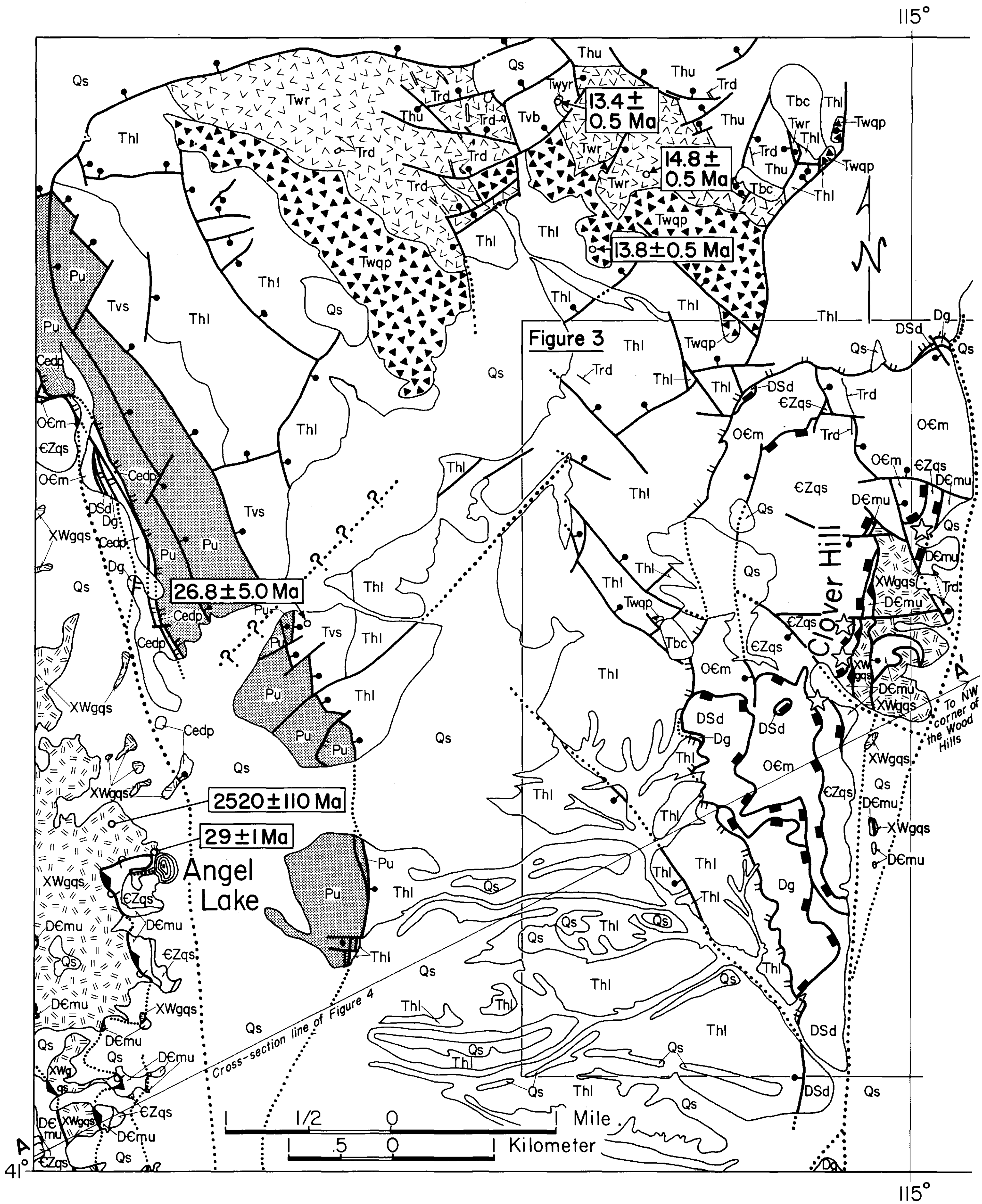

Figure 2. Geologic map of the northeastern East Humboldt Range, Nevada. The area of Figure 3 is outlined and cross-section line AA' (Fig. 4) is delineated.

GEOLOGIC MAP OF THE NORTHEASTERN EAST HUMBOLDT RANGE, NEVADA

Lithologic units

- Qs Surficial deposits (Quaternary)
- Tbc Boulder conglomerate (Pliocene or late Miocene)
- Thu Upper Humboldt Formation (Miocene)
- Twyr Rhyolite (~13.4 Ma)
- Tvb Volcaniclastic breccia (Miocene)
- Twqp Rhyolite quartz porphyry (~13.8 Ma), Trd =dikes
- Twr Rhyolite (~14.8 Ma)
- Thl Lower Humboldt Formation (Miocene)
- Tvs Volcaniclastic conglomerate, sandstone, andesite-rhyolite (Eocene?)
- Pu Permian undivided (Murdock Mtn. & Pequop formations)
- Cedp Ely Limestone & Diamond Peak Formation (Carboniferous)
- Dg Guilmette Formation (Devonian)
- DSd Metadolomite (Devonian & Silurian)
- OЄm Impure calcite marble & calc-silicate rock (Ordovician & Cambrian)
- PЄmu Metasedimentary rocks undivided (Devonian to Cambrian)
- ЄZqs Impure quartzite & schist (Cambrian & Proterozoic Z)
- XWgqs Orthogneiss & paragneiss (Archean) & quartzite, schist, & amphibolite (Proterozoic?)

Symbols

- Contact
- Pre-folding low-angle fault; overturned on right
- Low-angle fault, plastic-to-brittle
- Low-angle fault, brittle
- Normal fault, high-angle; dotted where covered
- ☆ Kyanite-rich metapelite (Clover Hill)

although their exact relationship with the orthogneiss is uncertain. These paragneisses are quartzitic to pelitic and commonly contain migmatitic leucogranite segregations.

Much younger, Oligocene(?) orthogneiss occurs as discordant, sheet-like intrusions which locally truncate the compositional layering and tight folds in the Archean(?) orthogneiss (Fig. 5A). These younger orthogneisses are, however, internally foliated and locally well-lineated, indicating that plastic strain accompanied their emplacement. These orthogneisses are petrographically similar to the Oligocene, medium-grained biotite monzogranitic orthogneiss of Angel Lake dated as about 29 Ma (Wright and Snoke, 1986; see Fig. 2 for location of dated sample). Streaky biotitic lineations, commonly localized along mm-scale shear zones, occur in the younger orthogneisses.

Lower Proterozoic(?) Quartzite and Schist

The gneissic complex is overlain by a quartzite and schist unit which I here suggest may correlate with Lower Proterozoic metaclastic rocks extensively exposed in the Raft River Mountains, northwest Utah, (Compton, 1972; 1975) as well as in the basal part of the Willard thrust sheet of the central Wasatch Mountains, northern Utah (i.e., Facer Formation of Crittenden and Sorensen, 1980). In this light, I therefore interpret the boundary between the gneissic complex and the structurally overlying quartzite and schist unit as a deformed and metamorphosed unconformity. This boundary is also extensively exposed in the northern East Humboldt Range which Lush and others (1988) as well as A.J. McGrew (unpublished data) also interpret as a deformed and metamorphosed unconformity between Archean rocks and a younger, Lower Proterozoic sequence. Pale green fuchsitic quartzite is a distinctive lithic type in these suspected Lower Proterozoic rocks; and this rock type is also distinctive of the possible correlative strata in Utah (Crittenden and Sorensen, 1980). Other lithotypes include pelitic schist and very mafic amphibolite. However, conglomeratic quartzite, characteristic of the Elba Quartzite in northwest Utah, has not been recognized (Compton, 1972; 1975). The rocks of this possible Lower Proterozoic(?) suc-

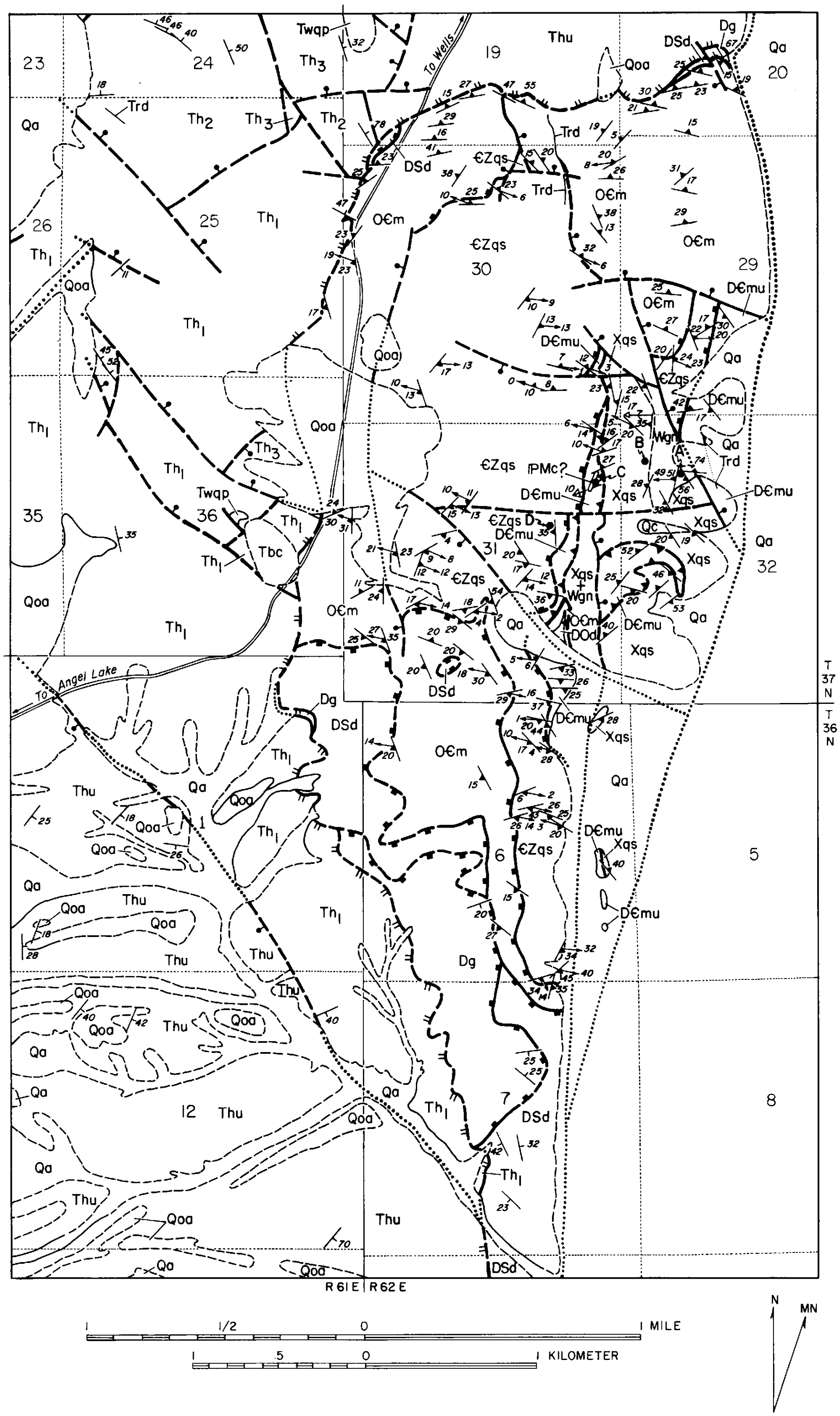

Figure 3. Geologic map of the Clover Hill area. Geologic mapping by A.W. Snoke (intermittently 1980-83, 88-89) with additions compiled from Lush (1982) along the southwestern flank of CH.

EXPLANATION

Lithologic units

Qa	Younger alluvium (Quaternary)
Qc	Colluvium (Quaternary)
Qoa	Older alluvium (Quaternary)
Tbc	Boulder conglomerate (Pliocene or Late Miocene)
Trd	Rhyolite dike (Miocene)
Twqp	Quartz + feldspar porphyry rhyolite, Willow Creek complex (Miocene)
Th_3, Th_2, Th_1, Thu	Humboldt Formation, units 3, 2, 1 or undifferentiated (Miocene)
ℙMc?	Metaclastic rocks, Diamond Peak Formation ? (Pennsylvanian & Mississippian)
Dg	Guilmette Formation (Devonian)
DЄmu	Marble and quartzite unit (Devonian to Cambrian)
DSd	Dolomite (Devonian & Silurian)
OЄm	Impure marble unit (Ordovician & Cambrian)
ЄZqs	Quartzite and schist (Cambrian & Upper Proterozoic)
Xqs	Quartzite and schist (Lower Proterozoic?)
Wgn	Gneissic complex (Archean & younger intrusive rocks)

Symbols

Contact; dashed where approximate

High-angle normal fault; dashed where approximate, dotted where concealed

Low-angle normal fault (brittle); dashed where approximate, dotted where concealed

Low-angle normal fault (plastic-to-brittle), dashed where approximate

Low-angle fault (pre-folding), dashed where approximate

28 Strike and dip of bedding

15 9 10 Strike and dip of foliation (left); trend and plunge of lineation on a foliation surface (right)

A Locality associated with STOP 5, DAY 3 (see Camilleri and others, this volume)

cession are migmatitic, locally containing abundant coarse-grained, muscovite leucogranite. Critical metamorphic mineral assemblages for geothermobarometric studies have not been recognized, although no detailed sampling program has been attempted. Fibrolitic sillimanite occurs in pelitic rocks and green hornblende in the amphibolites. The rocks of this unit are inferred to have probably experienced multiple phases of Mesozoic (Jurassic and Cretaceous) upper amphibolite facies metamorphism as well as Oligocene dynamothermal shear zone metamorphism.

Devonian-Cambrian Marble and Quartzite Unit

A heterogeneous, structurally complex sequence of impure calcite marble, calc-silicate marble, graphitic paragneiss, white quartzite, and metadolomite forms a mappable unit at CH. Clearly, this unit is an aggregate of various lower to mid-Paleozoic (Devonian to Cambrian) miogeoclinal units, now highly metamorphosed and deformed. A similar, but considerably less dismembered, sequence is well-exposed in the northern Ruby Mountains (Howard, 1971; Snoke, 1980) and southeastern East Humboldt Range (Taylor, 1984).

The metasedimentary rocks that comprise this composite unit are rotated and deformed into numerous mesoscopic, nearly isoclinal recumbent folds and intruded by coarse-grained, muscovite leucogranite of uncertain age. Distinctive, compositional layers can be locally traced for tens of meters but eventually are dismembered by plastic flowage within the folds. This composite unit has experienced transposition and attenuation during the multiple deformational history experienced by the metamorphic rocks of CH.

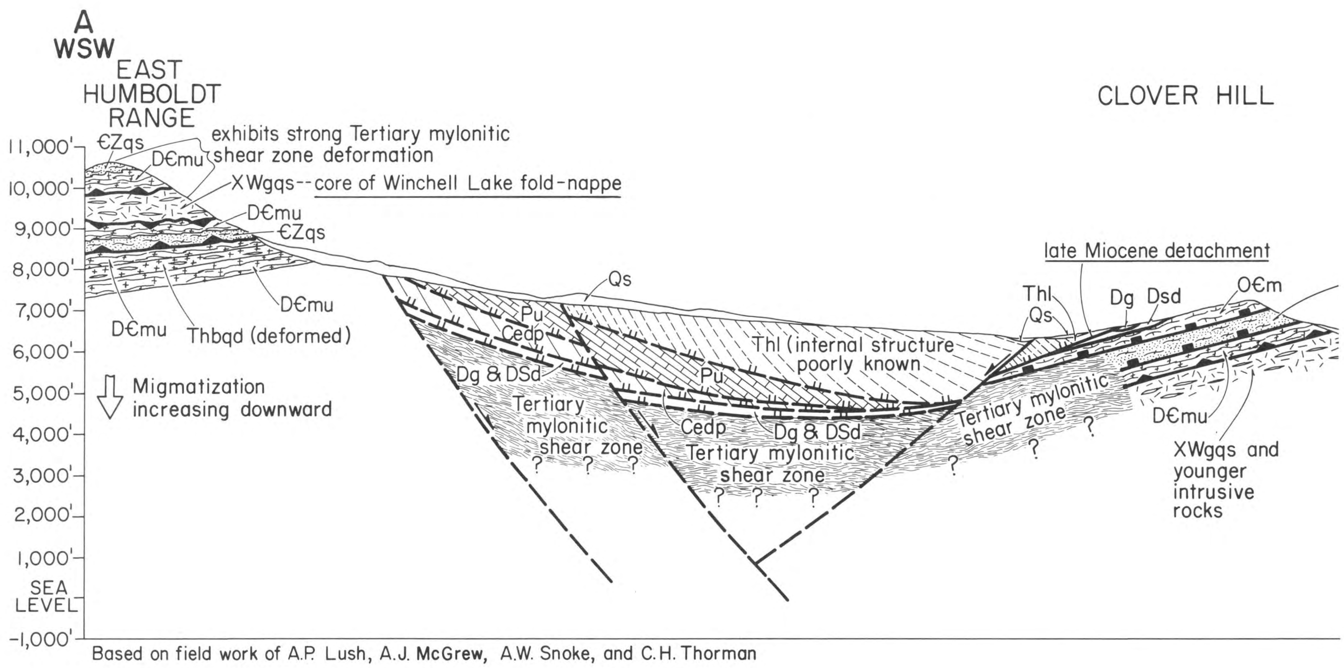

Figure 4. Generalized cross-section AA' across the northern East Humboldt Range, Clover Hill, and northwestern Wood Hills. Geologic data in the northern East Humboldt Range derived from unpublished geologic mapping and structural analysis of A.J. McGrew (work in progress) and Lush (1982), and in the Wood Hills from Thorman (1970). Symbols are the same as used in Figure 2 except Thbqd = Tertiary hornblende-biotite quartz diorite and Mc = Chainman Formation.

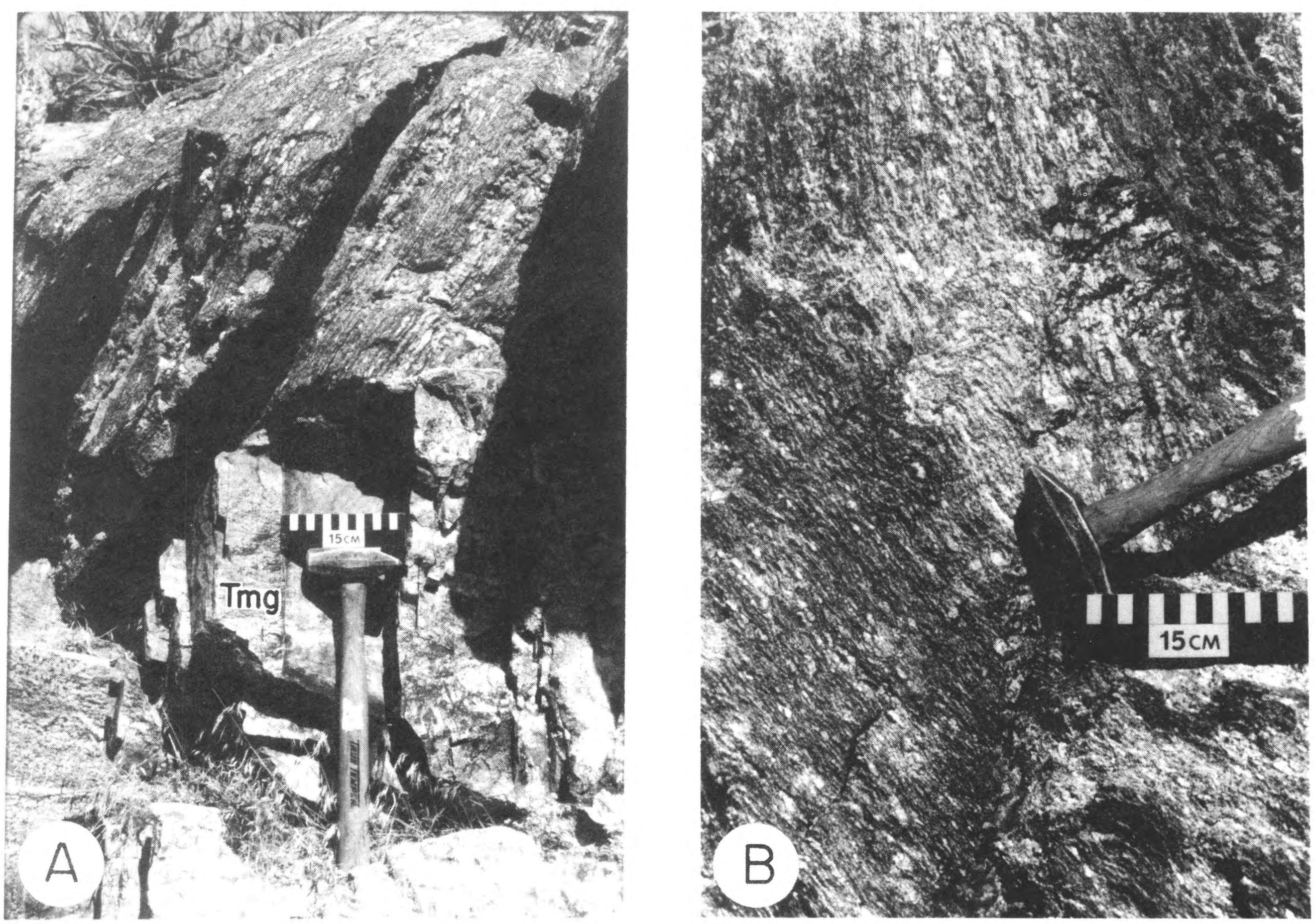

Figure 5. Photographs of deformational features in the metamorphic rocks of Clover Hill. A. Compositional layering in Late Archean(?) orthogneiss truncated by intrusive sheet of Oligocene(?) biotite monzogranitic orthogneiss (Tmg) which is internally foliated. B. Steeply dipping compositional layering in "pin-striped" augen orthogneiss (Late Archean?) near the hinge zone of "F_2-type" fold.

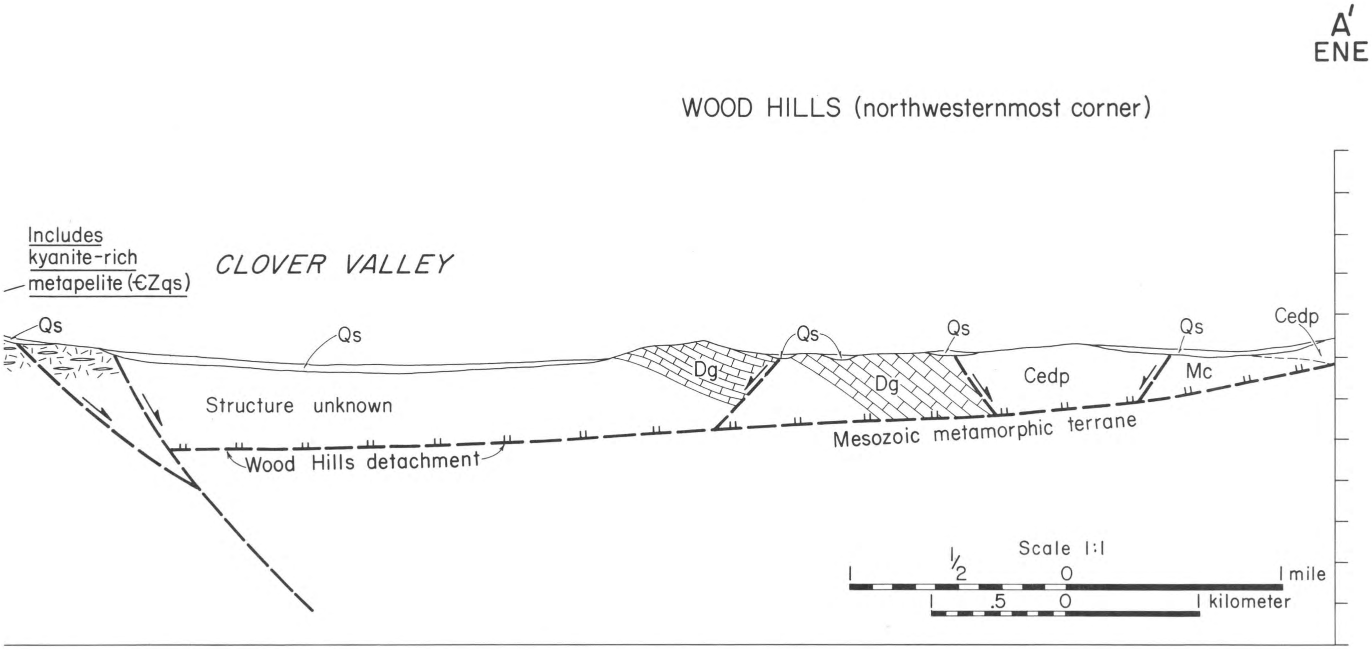

Pennsylvanian-Mississippian(?) Quartzite and Metaconglomerate "Tectonic Inclusion"

A distinct lenticular mass of mylonitic, *non-migmatitic* quartzite-metaconglomerate occurs within the Devonian-Cambrian marble-quartzite unit (Fig. 3). This "tectonic inclusion" may occupy the core of a recumbent isocline, although folds within the quartzite-metaconglomerate unit have relatively steep-dipping axial surfaces. These folds are late in the deformational history, for they fold the mylonitic foliation. In this light, they are perhaps Tertiary in age and may indicate local shortening during non-coaxial shear zone deformation. A unique correlation between the rocks of the tectonic inclusion and the Paleozoic stratigraphy of the region is uncertain. However, the silicic character of the rocks coupled with the conglomeratic aspect suggest a possible correlation with Pennsylvanian-Mississippian clastic rocks which are widespread in northeastern Nevada (e.g., Diamond Peak Formation).

Cambrian-Upper Proterozoic Quartzite and Schist

A sequence of flaggy, micaceous-feldspathic quartzite and subordinate pelitic schist forms another mappable unit (Fig. 6A). The gross lithic character of this unit resembles the Lower Proterozoic(?) unit, although some important distinctions exist. The inferred younger quartzite-schist unit does not contain fuchsitic quartzite; the pelitic schist commonly contains conspicuous kyanite and garnet porphyroblasts; a distinct biotite-hornblende quartz dioritic orthogneiss occurs as deformed intrusive layers near the structural base of the unit; and amphibolite is very uncommon in this unit. I correlate the quartzite-schist unit with Proterozoic Z

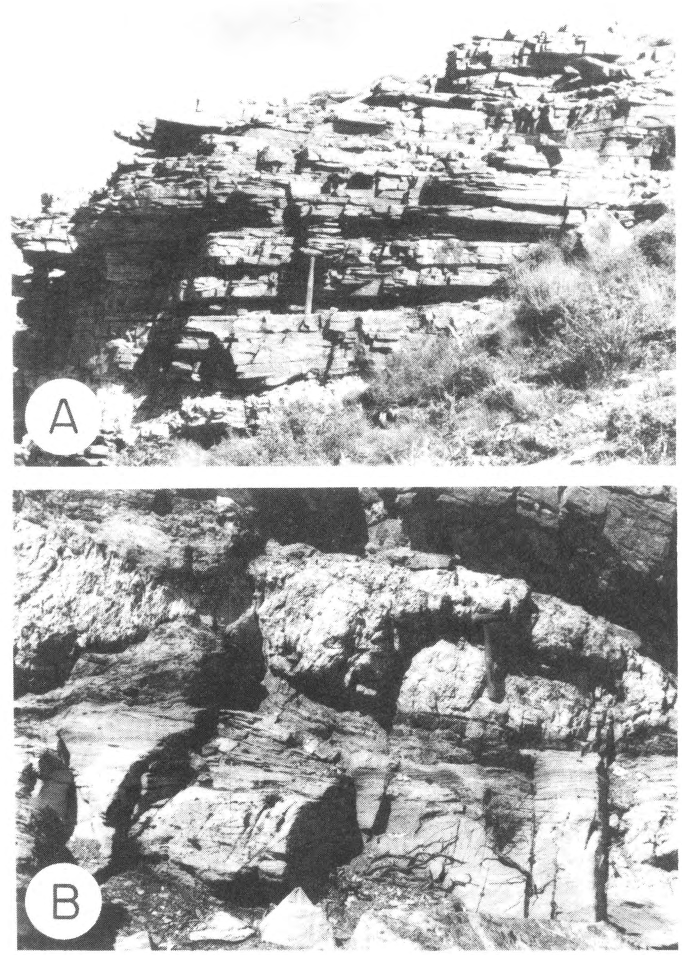

Figure 6. A. Typical exposure of flaggy, mylonitic quartzite of the Cambrian-Upper Proterozoic quartzite and schist unit. B. Boudinaged mass of coarse-grained, leucocratic muscovite granite in banded mylonitic calcite marble of the Ordovician(?)-Cambrian impure marble unit.

and Lower Cambrian rocks extensively exposed in parts of eastern Nevada [e.g., Proterozoic Z McCoy Creek Group of Misch and Hazzard (1962), and the Cambrian-Proterozoic Z Prospect Mountain Quartzite (Hague, 1883; Nolan and others, 1956)].

Ordovician(?)-Cambrian Impure Marble Unit

This unit occurs as a fault-bounded allochthon which appears to represent the metamorphic and structural transition between the high-grade rocks of the Cambrian-Upper Proterozoic quartzite and schist unit and the low-grade metasedimentary rocks of the overlying, younger-on-older fault slices. Pale gray muscovitic, graphitic calcite ± dolomite marble with a distinctive platy cleavage is a common lithic type; whereas in the structurally lower parts of the allochthon, calc-silicate marble is widespread, commonly containing abundant diopside and biotite. Yellow-brown-weathering metadolomite is another lithic type common in the lower parts of this allochthon. These various lithic units no doubt reflect a complex Cambrian and Ordovician(?) stratigraphy. Distinctive mappable formations, as recognized by McCollum and Miller (1990) in other parts of the northeastern Great Basin, have not yet been individually delineated. It is important to note that this unit does *not* include infolded layers of Ordovician Eureka metaquartzite or mid-Paleozoic metadolomite as typical of the structurally lower Devonian-Cambrian marble and quartzite unit. Scattered masses of coarse-grained, leucocratic muscovite (±biotite) granite are a component of this unit (Fig. 6B). The age of these intrusive granitoids is uncertain, although similar leucogranites in the southeastern East Humboldt Range have yielded a Late Cretaceous age (U-Th-Pb monazite, J.E. Wright, personal comm.).

Devonian-Silurian Dolomite/Metadolomite

Unmetamorphosed dolomite to low-grade metadolomite forms a fault-bounded slice on the southwestern flank of CH and forms much of Signal Hill to the south (Lush, 1982). According to Lush (1982), the lithotypes present include thick-bedded medium to dark gray dolomite, laminated black fine- to medium-grained dolomite, scarce platy dark gray argillaceous limestone, and a distinctive quartz sandstone. These lithic characteristics suggest that some of the Silurian Laketown Dolomite may be present, but the bulk of the unit probably consists of Devonian Sevy and Simonson dolomites [see Nolan (1935) for type section descriptions]. These dolomites are commonly brecciated with a carbonate or siliceous vein-filling cement between the fragments. A small, but mappable, slice of white, tremolite-bearing metadolomite also occurs near the northwestern corner of CH (Fig. 3).

Guilmette Formation

The Guilmette Formation (Nolan, 1935) forms a southwest-dipping fault slice on the southwestern flank of CH but also occurs as a small, fault-bounded slice along the northern margin of CH (Fig. 3). The rocks of this unit are massive to platy, medium to dark gray, locally dolomitic limestone. This unit is fossiliferous, containing stromatoporoids, bryozoa, corals, crinoid debris, gastropods, and brachiopods (Lush, 1982). Merriam (1940) and Snelson (1957) reported that fossil assemblages collected from the southern end of CH and the hills to the south indicate an Upper Devonian age.

Carboniferous and Permian Rocks

Although Carboniferous and Permian strata are not exposed at CH, extensive exposures of these rocks form a north-northwest-striking band along the northeastern flank of the northern East Humboldt Range (Fig. 2). These units are fault-bounded and include: Diamond Peak Formation (Hague, 1882, 1883; also see Nolan and others, 1956; Brew, 1971), Ely Limestone (Lawson, 1906; Spencer, 1917), Pequop Formation (Steele, 1960), and Murdock Mountain Formation (Wardlaw and others, 1979) . These rocks are unmetamorphosed and have experienced only brittle, upper crustal strain. If the stratigraphic correlation of the quartzite-metaconglomerate "tectonic inclusion" with the Diamond Peak Formation is correct, the unmetamorphosed Diamond Peak Formation of the northeastern East Humboldt Range clearly was derived from a different (i.e., much shallower) structural level than the possible metamorphic equivalent exposed at CH.

The unmetamorphosed Paleozoic rocks of the northeastern East Humboldt Range probably originally formed part of the subjacent older rocks upon which mid-Eocene(?) to Miocene volcanic and sedimentary rocks were deposited. This unconformable boundary is not preserved in the northern East Humboldt Range, but possible equivalent Eocene(?) volcanic rocks rest depositionally on Lower Triassic Thaynes Formation in the southeastern East Humboldt Range (Taylor, 1984; Snoke and Howard, 1984, STOP 18).

Humboldt Formation

Steeply dipping, Miocene Humboldt Formation occurs in the hanging wall of a low-angle normal fault that frames the metamorphic rocks of Clover Hill (Figs. 2, 3, and 7). The Humboldt Formation is a lithologically diverse unit reflecting its deposition in an alluvial fan-lacustrine complex that evolved during regional extension and volcanism. The lower part of the formation consists chiefly of conglomerate and sandstone with prominent intercalations of megabreccia and fine-grained lacustrine limestone. This part of the formation is overlain by a rhyolitic complex including lava flows, shallow-level intrusive rocks, and volcaniclastic breccia (Fig. 2). These rhyolitic rocks range in age from about 15 to 13.4 Ma (Fig. 2) and are informally referred to as the Willow Creek rhyolitic complex (Snoke and others, 1983; Snoke and Lush, 1984). The part of the Humboldt Formation that overlies the rhyolitic complex consists of polymictic conglo-

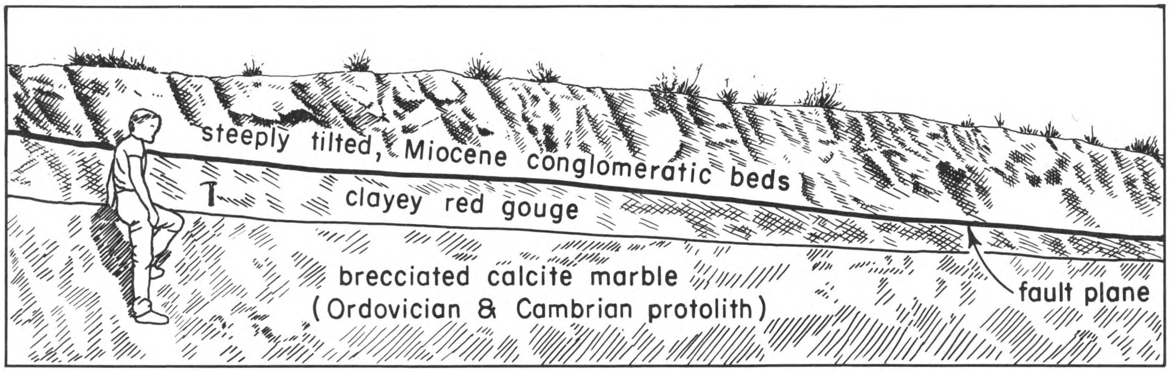

Figure 7. Roadcut exposure of a low-angle normal fault exposed on the west flank of Clover Hill separating steeply dipping fanglomerate of the Humboldt Formation from a footwall of brecciated, strongly foliated calcite marble. A red gouge zone forms a distinct layer along the fault surface.

merate, accretionary lapilli tuff, vitric tuff, and scattered limestone beds.

Rhyolitic and Basaltic Dikes

Massive, yellow-orange-weathering rhyolite porphyry locally occurs as dikes in the metamorphic complex (Fig. 3). The rhyolite is quartz+feldspar-phyric with oxidized (hematitic) Fe-Ti oxides as the only mafic minerals in this hypabyssal rock. The dikes are probably related to the mid-Miocene Willow Creek rhyolitic suite. Scattered basaltic dikes also occur in the metamorphic complex; they probably are related to a widespread suite of basaltic dikes that apparently ranges in age from about 17 to 15 Ma (Snoke, 1980; Hudec, (1990).

STRUCTURAL HISTORY

Pre-mylonitic (Mesozoic?) Deformational History

A thorough understanding of the pre-mylonitic Mesozoic deformational history of the metamorphic rocks exposed at CH is essential in deciphering the history of this specific area as well as the region. The largest pre-mylonitic structural feature in the northern East Humboldt Range is the Winchell Lake fold-nappe (Lush, 1982; Lush and others, 1988). This basement-cored, recumbent fold is exceptionally well-exposed along the east face of the northern East Humboldt Range (see STOP 4, Day 3 in Camilleri and others, this volume), and I infer that a part of the upper limb of this great fold is also exposed at CH.

As in the northern East Humboldt Range, Precambrian rocks including Late Archean(?) monzogranitic orthogneiss and Lower Proterozoic(?) quartzite and schist are an important component of this inferred eastward extension of the Winchell Lake fold-nappe. These rocks are separated from a heterogeneous suite of Devonian to Cambrian marble and quartzite by a mappable contact interpreted as a pre-folding, low-angle fault (Figs. 3 and 8A). The rocks above this boundary are complexly folded, attenuated, and locally are stratigraphically inverted. The tectonic character of the low-angle fault that separates the Precambrian rocks (Wgn and Xqs) from D€mu is uncertain; for example, this boundary may be a contractional or extensional fault depending on how the fold-nappe is unfolded. Lush (1982) as well as Lush and others (1988) interpreted the Winchell Lake fold-nappe of the northern East Humboldt Range as a south-directed, recumbent anticline that was cored by Precambrian rocks but surrounded by an allochthonous and downward-facing succession of miogeoclinal rocks ranging from Upper Precambrian to Devonian. If this interpretation is correct, an early history of stratigraphic inversion, most likely related to large-scale recumbent folding, is required prior to the development of the Winchell Lake fold-nappe. The south-directed, recumbent anticline interpretation is also adopted here for a fundamental, early phase in the structural development of CH. At CH, the allochthonous, downward-facing succession(?), subsequently folded during nappe development, perhaps includes rocks as young as Carboniferous.

Mesoscopic isoclinal folds occur at scattered localities in the metamorphic rocks exposed at CH (Fig. 8B). These folds

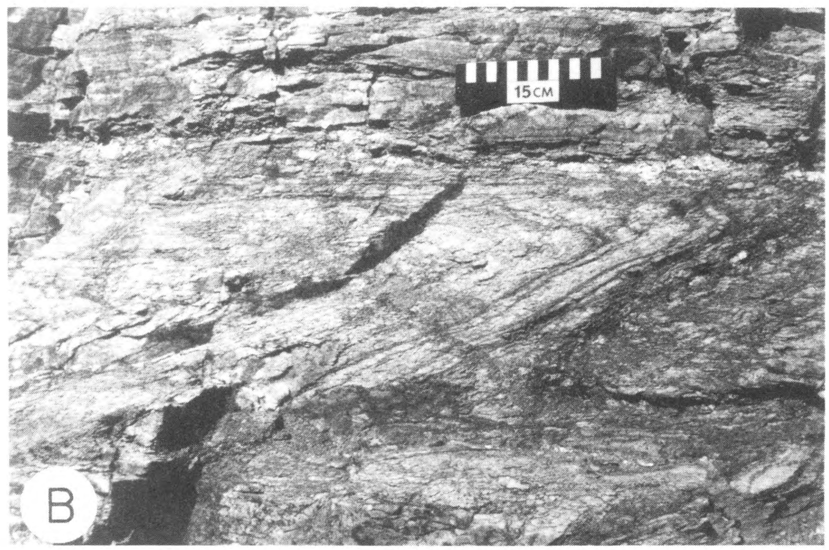

Figure 8. Photographs of deformational features in the metamorphic rocks of Clover Hill. A. Adit along contact between overlying Devonian-Cambrian marble and quartzite unit and underlying Lower Proterozoic(?) quartzite and schist unit (Xqs). This contact is interpreted as a pre-folding, low-angle fault, presently in the upper limb of the Winchell Lake fold-nappe. B. Tight fold of compositional layering ("F_2-type" fold) in Cambrian-Upper Proterozoic quartzite and schist unit. This fold has been overprinted (flattened and attenuated) during Tertiary mylonitic-shear zone deformation.

rotate compositional layering which appears to be an earlier metamorphic foliation. Consequently, such isoclines are called "F_2-type" folds, although the exact numerical chronologic sequence is uncertain. These folds were overprinted by the mylonitic shear zone deformation, and consequently, are flattened and attenuated (Fig. 8B). These isoclines are probably parasitic to the inferred recumbent fold-nappe. Lush (1982) reported analogous folds from the northern East Humboldt Range; and he argued that they exhibit a consistent geometric form (S-, M-, and Z-shaped folds) and vergence related to the upper limb, hinge zone, and lower limb, respectively, of the Winchell Lake fold-nappe.

Oligocene Mylonitic Shear Zone Deformation

A mylonitic foliation and associated stretching lineation is characteristic of many rocks which comprise the amphibolite-facies metamorphic terrane exposed on CH. This mylonitic deformation is locally well-developed in parts of the Ordovician(?)-Cambrian impure marble unit, but is especially pervasive in the Cambrian-Upper Proterozoic quartzite and schist unit (Figs. 6A, 8B, 9, 10). At deeper structural levels the mylonitic deformational fabric is also well-developed in the Lower Proterozoic(?) quartzite and schist unit (Figs. 3, 9, 10). In the gneissic complex, the mylonitic fabric is chiefly developed in intrusive sheets of Oligocene(?) monzogranitic orthogneiss, whereas an older, truncated fabric is characteristic of the late Archean(?) orthogneiss (Fig. 5A).

Stretching lineations in these various units are consistent, trending WNW-ESE with a generally low plunge (Fig. 10). Interestingly, the hingelines of the few measured mesoscopic folds diverge somewhat from the tight cluster defined by the stretching lineations (Fig. 10). As previously indicated, I interpret these folds as pre-mylonitic; their present orientation reflects partial reorientation associated with attenuation and flattening related to the mylonitic deformation. No systematic study of sense-of-shear has been attempted for the mylonitic rocks exposed on CH, although scattered observations suggest top-to-the-WNW as characteristic of areas further south and west (Snoke and Lush, 1984; McGrew and Snoke, 1990).

Plastic-to-brittle Low-Angle Normal Faults

A system of plastic-to-brittle, low-angle faults has partitioned the pre-Tertiary rocks of CH into a stack of thin allochthons. These faults in turn are locally truncated and structurally overlain by an extensive allochthon consisting of Tertiary rocks (Figs. 2 and 4). Bedding in the Tertiary rocks of this uppermost allochthon is commonly moderately to steeply dipping and is truncated at a high angle by a brittle, low-angle normal fault (Fig. 7). In contrast, bedding and foliation in the pre-Tertiary rocks is only moderately to shallowly dipping and is subparallel to the fault surfaces, although local discordances across the low-angle faults are obvious. Aside from the pre-folding, low-angle fault between D€mu and Xqs, I interpret all the other low-angle faults exposed on CH as Tertiary in age, related to crustal

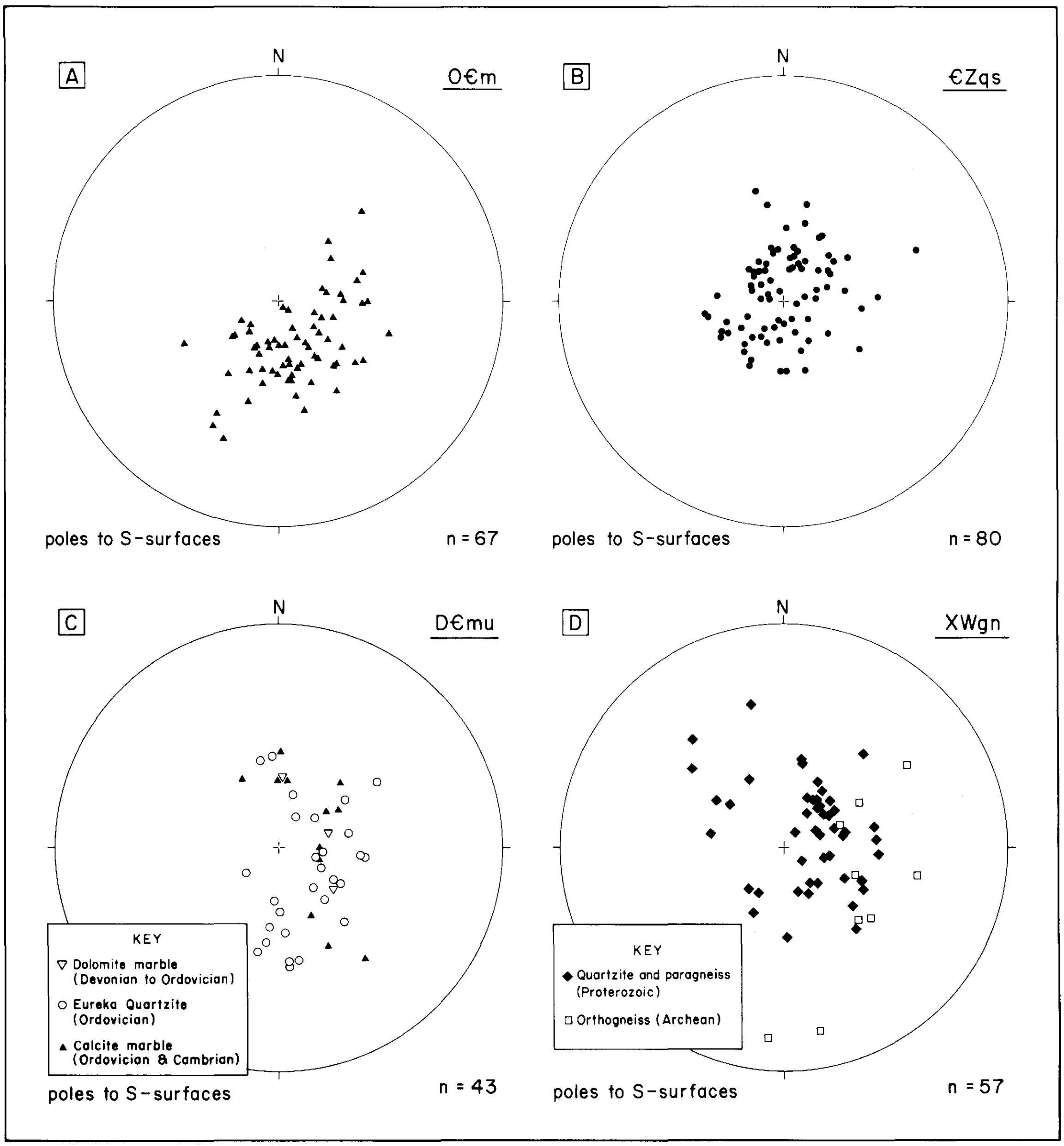

Figure 9. Equal-area, lower-hemisphere projections showing distribution of S-surfaces in contrasting lithologies as exposed in the Clover Hill area.

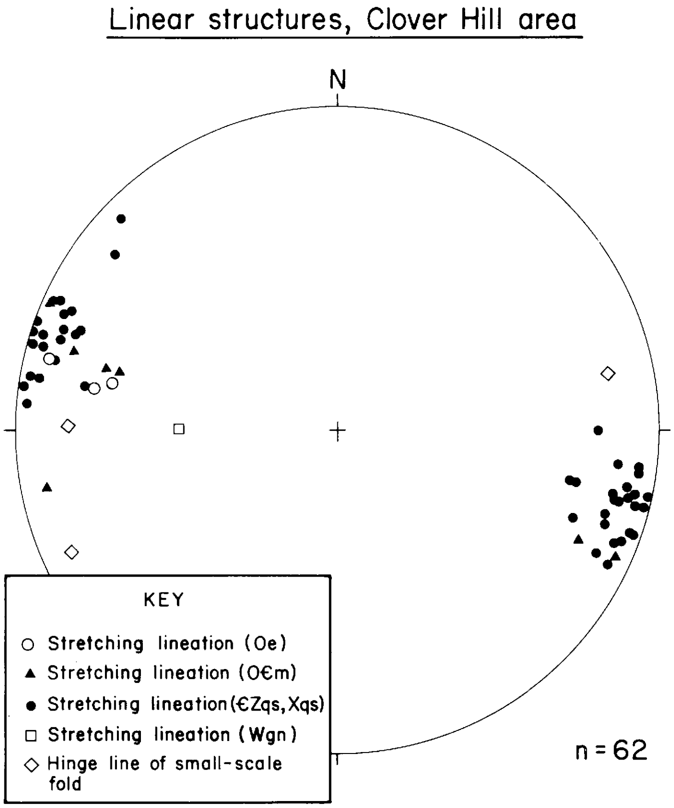

Figure 10. Equal-area, lower-hemisphere projection showing linear structural features from the metamorphic rocks of the Clover Hill area.

extension. Parts of these faults locally truncate the Tertiary mylonitic foliation at low angles, although very fine-grained, calc-mylonites are also associated with parts of the fault zones. At other localities, breccias are present indicating a brittle regime during part of the displacement history. These low-angle faults therefore appear to be the manifestation of strain localization in the footwall of a Tertiary shear zone during progressive unroofing through the plastic-to-brittle transition. Detailed geologic mapping and cross-section preparation of Tertiary extensional faults between the northern East Humboldt Range and the Windermere Hills (Mueller and Snoke, in review) indicate a long-lived (mid-Eocene to Present), west-rooted extensional fault system. The mylonitic rocks and low-angle faults exposed on Clover Hill are part of this west-rooted, extensional fault system, and therefore, reflect part of the rheological evolution of this fault system.

High-angle Normal Faults

A major east-dipping, high-angle normal fault forms the eastern boundary of CH (Fig. 4). This fault is an east-stepping, en echelon segment of the eastern rangefront system (Sharp, 1939). This fault zone truncates older high-angle as well as low-angle faults in its footwall. It is important to note that this normal fault clearly truncates the west-rooted, brittle low-angle fault that frames CH and has Miocene Humboldt Formation in its hanging wall (Figs. 3 and 4).

The high-angle faults within CH form a complex, intersecting pattern including both NW- to NNW-striking and EW-striking faults. These high-angle faults generally appear younger than the low-angle plastic-to-brittle faults that cut the metamorphic rocks exposed at CH, but are themselves truncated by the brittle, low-angle normal fault that frames the pre-Tertiary rocks (Figs. 2 and 3). An obvious exception is a small, NW-striking fault in section 20, T 37 N, R 62 E, which cuts the brittle, low-angle fault in the northeastern-most corner of the map area (Fig. 3). Furthermore, many normal faults in the hanging-wall, Tertiary sequence are truncated by the brittle, low-angle fault. In summary, the overprinting history derived from map relationships indicates the following general fault sequence: 1) low-angle plastic-to-brittle faults that cut the pre-Tertiary rocks; 2) high-angle faults within the range; 3) west-rooted, brittle low-angle fault with Miocene Humboldt Formation in hanging wall (Fig. 7); and 4) the east-dipping high-angle range-front fault.

METAMORPHIC HISTORY

The most interesting and important metamorphic rocks exposed at CH are kyanite-rich metapelitic schists which occur at several localities (see starred localities on Fig. 2) in probable McCoy Creek G of the Cambrian-Proterozoic quartzite and schist unit. These rocks are conspicuously porphyroblastic containing large (typically about 1 cm long), bluish, blade-like crystals of kyanite as well as red garnet (3-4 mm in diameter). The complete metamorphic mineral assemblage in these metapelitic rocks is: quartz-muscovite-biotite-plagioclase-kyanite-garnet-sillimanite-rutile-ilmenite. Textural studies suggest that this assemblage may be polymetamorphic and disequilibrium textures are locally apparent (e.g., kyanite porphyroblasts are pre-kinematic to the main schistosity whereas sparse fibrolitic sillimanite growth is synkinematic; Hodges and others, in press). Geothermobarometric data employing the Gibbs' Method approach suggest that the pelitic schists have experienced a high-pressure metamorphism (at depths in excess of 35 km) and then subsequent decompression prior to sillimanite growth (Hodges and others, in press). These rocks equilibrated at about 550-630°C and 500-640 MPa in pre-mid-Cretaceous time (Hodges and others, in press). An $^{40}Ar/^{39}Ar$ hornblende spectrum (H16, Dallmeyer and others, 1986) indicating probable Early Cretaceous or Late Jurassic cooling through the Ar closure temperature for hornblende (~ 500°C, McDougall and Harrison, 1988) suggests that the high-temperature, Late Cretaceous magmatic-metamorphic overprint was less pervasive at CH than in the northern Ruby Mountains-East Humboldt Range (Snoke and others, 1979; J.E. Wright, 1991, personal comm.). In regard to the Oligocene shear zone deformation, late Oligocene $^{40}Ar/^{39}Ar$ biotite plateau ages (Dallmeyer and others, 1986) and the lack of extensive retrogression in the pelitic schists suggest probable upper greenschist (biotite stable rather than chlorite) to lower amphibolite facies conditions during mylonitization.

CONCLUSIONS

Structural, metamorphic, and magmatic relationships exposed at CH indicate a complex history of overprinting and polyphase evolution. Sparse geochronometric data suggest high pressure metamorphism prior to the mid-Cretaceous (Dallmeyer and others, 1986; Hodges and others, in press); however, regional relationships indicate that this deep-seated history was commonly overprinted by a strong Late Cretaceous magmatic-metamorphic event (Miller and Gans, 1989; Barton, 1990) as well as by mid-Tertiary magmatism and shear zone deformation (Wright and Snoke, 1986). The oldest structural feature preserved at Clover Hill is the pre-folding, low-angle fault that separates D€mu from Xqs and Wgn. This fault apparently occurs both in the upper and lower limbs of the Winchell Lake fold-nappe (Lush, 1982; Lush and others, 1988). If the fold-nappe is unfolded as originally suggested by Lush (1982), D€mu and €Zqs would have formed an allochthonous, inverted upper plate of miogeoclinal rocks above the Precambrian rocks (Xqs and Wgn). Recent geochronometric data (U-Th-Pb, monazite, J.E. Wright, personal comm., 1991) coupled with geologic mapping (A.J. McGrew, work in progress) suggest that the Winchell Lake fold-nappe is probably a Late Cretaceous structural feature. An early history (Late Jurassic?) of crustal thickening is indicated by the high-pressure metamorphism preserved at CH, however, this history has been overprinted by probable but weak Late Cretaceous and especially mid-Tertiary magmatism, metamorphism, and deformation. In the northern Ruby Mountains and East Humboldt Range, the Late Cretaceous event is manifested by the intrusion of peraluminous leucogranite and high-temperature metamorphism as well as apparently large-scale fold-nappes. The mid-Tertiary to Holocene tectonic history is extensional in character ranging from a 1.5- to 2.0-km-thick mylonitic shear zone to plastic-to-brittle, low-angle normal faults to brittle, high-angle normal faults. Widespread, episodic magmatism was coincident with the Tertiary extensional history, manifested chiefly in the metamorphic terrane as intrusive sheets of granitic orthogneiss (Wright and Snoke, 1986) and in the Neogene succession as a rhyolitic suite (Snoke and others, 1983).

ACKNOWLEDGMENTS

This study is part of an ongoing geologic mapping project in the East Humboldt Range that began in 1979. This project has been supported by National Science Foundation Grants EAR 7904204, EAR 82-14236, EAR 84-18390, EAR 87-07435. E.A. Winter of Phelps Dodge Corporation generously supplied some large-scale ($\sim$1″=1200′), black and white aerial photographs which greatly facilitated the geologic mapping of Clover Hill. R.L. Parratt of Southern Pacific Land Company provided copies of the unpublished reports of Anctil and Oesterling which included much useful information for geologic mapping and interpretation. Thought-provoking discussions with A.P. Lush, A.J. McGrew, K.J. Mueller, P.A. Camilleri, and W.B. Hamilton have caused me to rethink and re-evaluate various concepts concerning the geology of CH. I also thank Phyllis A. Ranz for her help in preparing the final figures for this article. Finally, review comments by Adolph Yonkee improved the clarity and organization of the manuscript.

REFERENCES CITED

Anctil, R.J., 1961, Geology and mineral resources of Township 36, North Ranges 61 and 62 East, Mount Diablo Meridian, Elko County, Nevada: Southern Pacific Land Company, unpublished report.

Barton, M.D., 1990, Cretaceous magmatism, metamorphism, and metallogeny in the east-central Great Basin, *in* Anderson, J.L., ed., The nature and origin of Cordilleran magmatism: Boulder, Colorado, Geological Society of America Memoir 174, p. 283-302.

Brew, D.A., 1971, Mississippian stratigraphy of the Diamond Peak area, Eureka County, Nevada: U.S. Geological Survey Professional Paper 661, 84 p.

Coats, R.R., 1987, Geology of Elko County, Nevada: Nevada Bureau of Mines and Geology Bulletin 101, 112 p.

Compton, R.R., 1972, Geologic map of the Yost quadrangle, Box Elder County, Utah, and Cassia County, Idaho: U.S. Geological Miscellaneous Investigations Series Map I-672.

Compton, R.R., 1975, Geologic map of the Park Valley quadrangle, Box Elder County, Utah, and Cassia County, Idaho: U.S. Geological Miscellaneous Investigations Series Map I-873.

Compton, R.R., Todd, V.R., Zartman, R.E., and Naeser, C.W., 1977, Oligocene and Miocene metamorphism, folding, and low-angle faulting in northwestern Utah: Geological Society of America Bulletin, v. 88, p. 1237-1250.

Crittenden, M.D., Jr., Sorensen, M.L., 1980, The Facer Formation, a new Early Proterozoic unit in northern Utah: U.S. Geological Survey Bulletin 1482-F, p. F1-F28.

Dallmeyer, R.D., Snoke, A.W., and McKee, E.H., 1986, The Mesozoic-Cenozoic tectonothermal evolution of the Ruby Mountains, East Humboldt Range, Nevada: A Cordilleran metamorphic core complex: Tectonics, v. 5, p. 931-954.

Dokka, R.K., Mahaffie, M.J., and Snoke, A.W., 1986, Thermochronologic evidence of major tectonic denudation associated with detachment faulting, northern Ruby Mountains-East Humboldt Range, Nevada: Tectonics, v. 5, p. 995-1006.

Hague, A., 1882, Administrative report of Mr. Arnold Hague: U.S.Geological Survey 2nd Annual Report, p. 21-35.

Hague, A., 1883, Abstract of report on the geology of the Eureka district, Nevada: U.S. Geological Survey 3rd Annual Report, p. 237-290.

Hodges, K.V., Snoke, A.W., and Hurlow, H.A., 1992, Thermal evolution of a portion of the Sevier hinterland: the northern Ruby Mountains-East Humboldt Range and Wood Hills, northeastern Nevada: Tectonics, in press.

Howard, K.A., 1971, Paleozoic metasediments in the northern Ruby Mountains, Nevada Geological Society of America Bulletin, v. 82, p. 259-264.

Hudec, M.R., 1990, The structural and thermal evolution of thecentral Ruby Mountains, Elko County, Nevada [Ph.D.dissertation]: Laramie, Wyoming, University of Wyoming, 272 p.

King, C., 1878, Systematic Geology - geological exploration of the Fortieth Parallel, v. 1: Washington, D.C., U.S. Government Printing Office, 803 p.

Lawson, A.C., 1906, The copper deposits of the Robinson mining district, Nevada: University of California Publications, Department of Geology Bulletin, v. 4, p. 287-357.

Lipten, E.J.H., 1984, The geology of Clover Hill and classification of the Wells tungsten prospect, Elko County, Nevada [M.S. thesis]: West Lafayette, Indiana, Purdue University, 239 p.

Lush, A.P., 1982, Geology of part of the northern East Humboldt Range, Elko County, Nevada [M.S. thesis]: Columbia, South Carolina, University of South Carolina, 138 p.

Lush, A.P., McGrew, A.J., Snoke, A.W., and Wright, J.E., 1988, Allochthonous Archean basement in the northern East Humboldt Range, Nevada: Geology, v. 16, p. 349-353.

McCollum, L.B., and Miller, D.M., 1991, Cambrian stratigraphy of the Wendover area, Utah and Nevada: U.S. Geological Survey Bulletin 1948, 43 p.

McDougall, I., and Harrison, T.M., 1988, Geochronology and thermochronology by the $^{40}Ar/^{39}Ar$ method: New York, Oxford University Press, 212 p.

McGrew, A.J., and Snoke, A.W., 1990, Styles of deep-seated flow in an extending orogen: the record from the East Humboldt Range, Nevada: Geological Society of America Abstracts with Programs, v. 22, no. 3, p. 66.

Merriam, C.W., 1940, Devonian stratigraphy and paleontology of the Roberts Mountains region, Nevada: Geological Society of America Special Paper 25, 114 p.

Miller, D.M., 1983, Allochthonous quartzite sequence in the Albion Mountains, Idaho, and proposed Proterozoic Z and Cambrian correlatives in the Pilot Range, Utah and Nevada, *in* Miller, D.M., Todd, V.R., and Howard, K.A., eds.,Tectonic and stratigraphic studies in the eastern Great Basin: Geological Society of America Memoir 157, p. 191-213.

Miller, E.L., and Gans, P.B., 1989, Cretaceous crustal structure and metamorphism in the hinterland of the Sevier thrust belt, western U.S. Cordillera: Geology, v. 17, p. 59-62.

Misch, P., and Hazzard, J.C., 1962, Stratigraphy and metamorphism of late Precambrian rocks in central northeastern Nevada and adjacent Utah: American Association of Petroleum Geologists Bulletin, v. 46, p. 289-343.

Mueller, K.J., and Snoke, A.W., in review, Progressive overprinting of normal fault systems and their role in Tertiary exhumation of the East Humboldt-Wood Hills metamorphic complex, northeast Nevada: Tectonics.

Nolan, T.B., 1935, The Gold Hill mining district, Utah: U.S. Geological Survey Professional Paper 177, 172 p.

Nolan, T.B., Merriam, C.W., and Williams, J.S., 1956, The stratigraphic section in the vicinity of Eureka, Nevada: U.S. Geological Survey Professional Paper 276, 77 p.

Oesterling, W.A., 1961, Geology and mineral resources of Township 37 North, Ranges 61 and 62 East, Mount Diablo base and meridian, Elko County, Nevada: Southern Pacific Land Company, unpublished report.

Sharp, R.P., 1939, Basin-range structure of the Ruby-East Humboldt Range, northeastern Nevada: Geological Society of America Bulletin, v. 50, p. 881-920.

Snelson, S., 1957, The geology of the northern Ruby Mountains and the East Humboldt Range, Elko County, Nevada [Ph.D. thesis]: Seattle, Washington, University of Washington, 268 p.

Snoke, A.W., 1980, Transition from infrastructure to suprastructure in the northern Ruby Mountains, Nevada, *in* Crittenden, M.D., Jr., Coney, P.J., and Davis, G.H., eds., Cordilleran metamorphic core complexes: Geological Society of America Memoir 153, p. 287-333.

Snoke, A.W., and Lush, A.P., 1984, Polyphase Mesozoic-Cenozoic deformational history of the northern Ruby Mountains-East Humboldt Range, Nevada, *in* Lintz, J., Jr., ed., Western geological excursions (Geological Society of America annual meeting guidebook, Volume 4): Reno, Nevada, Mackay School of Mines, p. 232-260.

Snoke, A.W., and Howard, K.A., 1984, Geology of the Ruby Mountains-East Humboldt Range, Nevada: A Cordilleran metamorphic core complex, *in* Lintz, J., Jr., ed., Western geological excursions (Geological Society of America annual meeting guidebook, Volume 4): Reno, Nevada, Mackay School of Mines, p. 260-303.

Snoke, A.W., McKee, E.H., and Stern, T.W., 1979, Plutonic, metamorphic, and structural chronology in the northern Ruby Mountains, Nevada — A preliminary report: Geological Society of America Abstracts with Programs, v. 11, p. 520-521.

Snoke, A.W., McCall, R.G., McKee, E.H., 1983, Tertiary stratigraphy and structure in the northern East Humboldt Range, Nevada — A clue to Cenozoic regional tectonic patterns: Geological Society of America Abstracts with Programs, v. 15, p. 403.

Spencer, A.C., 1917, The geology and ore deposits of Ely, Nevada: U.S. Geological Survey Professional Paper 96, 189 p.

Steele, G., 1960, Pennsylvanian-Permian stratigraphy of east-central Nevada and adjacent Utah, *in* Guidebook to the geology of east-central Nevada: Intermountain Association of Petroleum Geologists, 11th Annual Field Conference, p. 91-113.

Taylor, G.K., 1984, Stratigraphy, metamorphism, and structure of the southeastern East Humboldt Range, Elko County, Nevada [M.S. thesis]: Columbia, South Carolina, University of South Carolina, 148 p.

Wardlaw, B.R., Collinson, J.W., and Maughan, E.K., 1979, The Murdock Mountain Formation: a new unit of the Permian Park City Group, *in* Wardlaw, B.R., ed., Studies of the Permian Phosphoria Formation and Related Rocks, Great Basin-Rocky Mountain Region: U.S. Geological Survey Professional Paper 1163-B, p. 5-8.

Wright, J.E., and Snoke, A.W., 1986, Mid-Tertiary mylonitization in the Ruby Mountains-East Humboldt Range metamorphic core complex, Nevada: Geological Society of America Abstracts with Programs, v. 18, p. 795.

EXTRAORDINARY SYNOROGENIC AND ANOXIC DEPOSITS AMIDST SEQUENCE CYCLES OF THE LATE DEVONIAN-EARLY MISSISSIPPIAN CARBONATE SHELF, LAKESIDE AND STANSBURY MOUNTAINS, UTAH

K.M. Nichols and N.J. Silberling
U.S. Geological Survey, MS-919
Denver, CO 80225
and
Patricia H. Cashman and James H. Trexler, Jr.
Department of Geological Sciences
Mackay School of Mines
University of Nevada, Reno, NV 98557

INTRODUCTION

The Late Devonian marked a time of major change in the depositional regime of the Cordilleran miogeocline. The thick Ordovician to Devonian section of dolomitic sabkha deposits in northwest Utah is succeeded abruptly by open-marine limestones and clastic rocks of Late Devonian to Mississippian age. Giving emphasis to this change, some of the Upper Devonian and Lower Mississippian strata bear evidence of unusual depositional histories. Different levels in this interesting part of the section record episodes of local tectonic disturbance, depositional cycles involving a variety of carbonate rocks, and widespread restriction and anoxia on the shelf. A number of different depositional and tectonic scenarios have been proposed for these Upper Devonian and Lower Mississippian rocks, but an overriding concern is how these rocks might reflect Antler tectonism and the inferred emplacement of the Roberts Mountains allochthon farther outboard along the North American continental margin. This field guide is focused on strata in the Lakeside and Stansbury Mountains and at Stansbury Island that illustrate some of the depositional features that bear on the interpretation of the history of this enigmatic part of the Cordilleran Paleozoic record. The route of this field trip and the localities to be visited are shown on Figure 1.

Formational nomenclature for Devonian and Mississippian strata in northwestern Utah is not entirely standardized nor does it reflect a modern understanding of the depositional record. The stratigraphic nomenclature used in this field guide is listed on Figure 2. As such, this nomenclature expresses the continuity of the major lithosomes, but it overlooks a number of unresolved problems in defining and extending the boundaries between named units.

FIELD TRIP ROAD LOG

DAY ONE:

Travel via U.S. Interstate 15 (I-15) from Ogden, Utah, south to U.S. Interstate 80 (I-80). Travel west on I-80 to Exit 77.

MILEAGE (in miles)		DISCUSSION
Cumulative	Incremental	
0.0	(0.0)	Exit I-80 via Exit 77, turn right (north) onto paved frontage road. Proceed on frontage road which heads west and then turns northward, crossing railroad tracks at

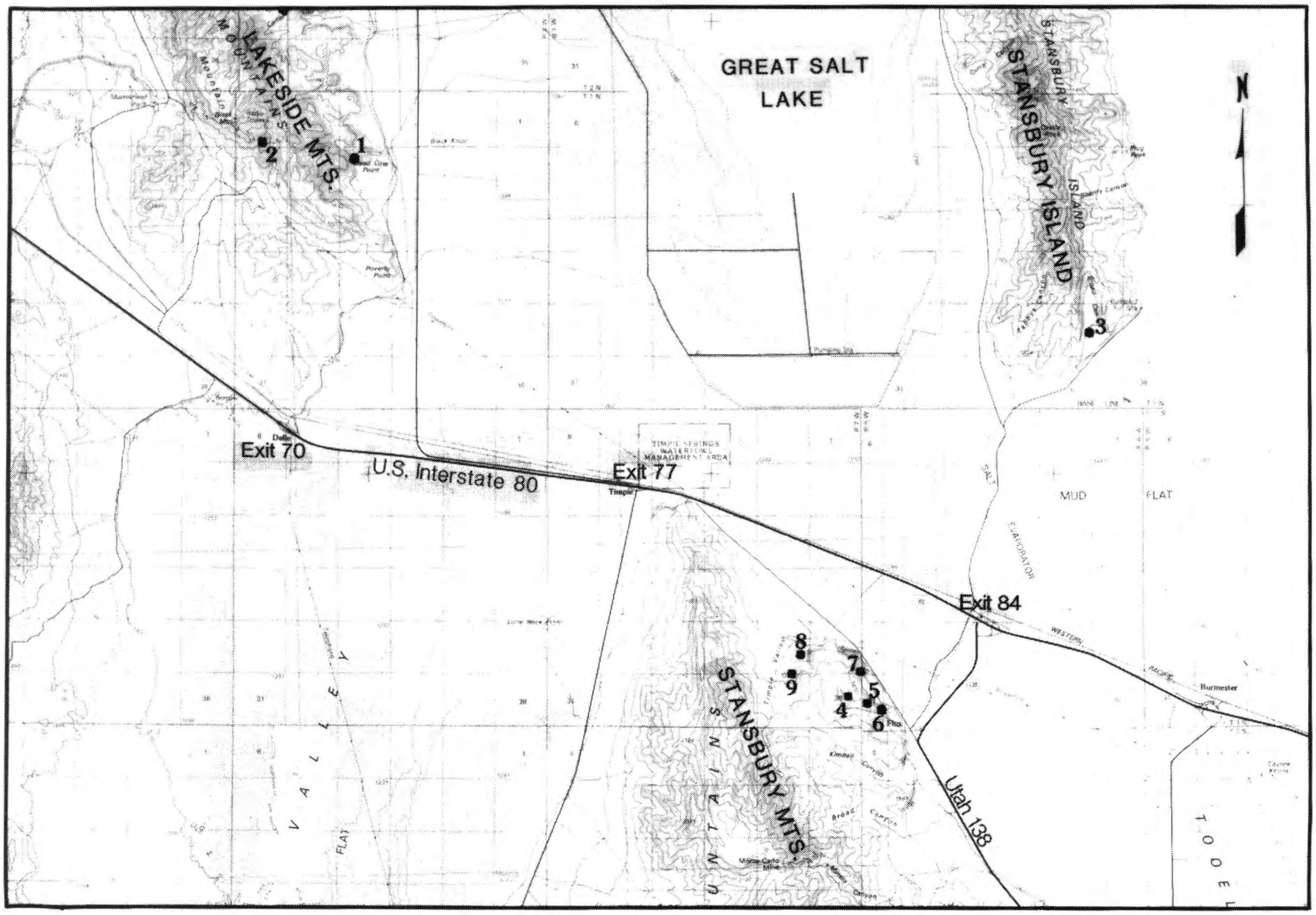

Figure 1. Map of region including field-trip stops.

LAKESIDE MTS.	STANSBURY MTS. and STANSBURY ISLAND	MAJOR DEPOSITIONAL CYCLES
Great Blue Ls. (Upper Miss.)	Great Blue Ls. (Upper Miss.)	IV
Humbug Fm. (Upper Miss.)	Humbug Fm. (Upper Miss.)	———
Woodman Fm. (Up. & Low. Miss.) Delle Phosphatic Mbr.	Deseret Ls. (Up. & Low. Miss.)	III
Gardison Ls. (Lower Miss.)	Gardison Ls. (Lower Miss.)	
Fitchville Fm. (Low. Miss. & Up. Dev.) ?	Fitchville Fm. (Lower Miss.)	II
? Pinyon Peak Ls. (Upper Devonian) ?	Stansbury Fm. (Upper Devonian) ?	I
Devonian dolostone		
	Silurian to Cambrian rocks	

Figure 2. Formational nomenclature used in this field guide.

4.5 (4.5). This paved road leads to the magnesium extraction plant of the Magnesium Corporation of America whose smoke stacks can be seen ahead along the shore of Great Salt Lake. At this plant magnesium metal is recovered from solar-concentrated Great Salt Lake brines. Continue north to

7.0 (2.5) and turn left (west) onto gravel road that leads to a quarry in the Lakeside Mountains where limestone was produced from the Upper Mississippian Great Blue Limestone. Travel west on this road to near the range front at

7.6 (0.6) and turn right (north) onto dirt road. Travel north, passing by large-scale cross-stratification in sandy Great Blue Limestone occurring just above the contact with the underlying Humbug Formation at

8.2 (0.6). Some of the Humbug outcrops along here are heavily coated by Pleistocene Bonneville calcareous tufa. At

9.7 (1.5) turn left (just south of "Dead Cow Point"). Cuestas of upper part of the Delle Phosphatic Member on far left. Bear right at

10.3 (0.6) and then continue to

10.75 (0.45) which is STOP 1. Parking area is on the Devonian dolostone unit which has been referred to here as the Jefferson Dolomite, Guilmette Formation, or Beirdneau Formation by previous workers. The Upper Devonian and Lower Mississippian carbonate rocks of interest overlie these sabkha deposits of primary or penecontemporaneous dolostone, eogenetic secondary dolostone, and quartzite, and they are well exposed in the cliffs to the west from here, except where they are covered by cemented Bonneville gravels. The stratigraphy, petrology, and sedimentation of these rocks are discussed in the accompanying Guidebook article (Silberling and Nichols, this volume).

Backtrack to intersection with quarry road at

14.5 (3.75) and continue, generally southward, on the unpaved range-front road. A large normal fault strikes down the valley to the west, downdropping Pennsylvanian and Lower Permian rocks of the Oquirrh Group on its southwest side against lower parts of the section examined at Stop 1. Continue south to another intersection at

15.4 (0.9) and bear right, following the unpaved road around the southeasternmost point of the Lakeside Mountains. Cross railroad tracks at what used to be the Delle section stop and then turn right (west) onto the paved frontage road at

16.3 (0.9). Travel west on frontage road to 19.3 (3.0) where the road turns north. Cross back over railroad tracks at

19.7 (0.4) and take right fork on gravel road. The Oquirrh Group forms low hills on either side of valley; the east-dipping Devonian and Mississippian section forms the range front at the head of the valley below the array of electronic antennae on Black Mountain. Travel north on gravel road to mouth of canyon, passing a gravel pit on the east side of the road at

23.45 (3.75). Continue on gravel road up the canyon to STOP 2 at

24.9 (1.45). This stop is at the type section of the Delle Phosphatic Member, which was originally defined as a member of the Woodman Formation, the type section of which is at Gold Hill about 115 km to the southwest. The Delle Phosphatic Member typifies the initiation of the widespread Delle phosphatic or anoxic event. For a description of these rocks, and an interpretation of their depositional environment, see Silberling and Nichols (1991), which is reproduced in this field guide and is an expanded and more fully illustrated version of Nichols and Silberling (1990). For a much different description and interpretation of the rocks at this stop see Sandberg and Gutschick (1984).

Salient features of the Delle Phosphatic Member that can be observed at this stop include:

—Evidence for episodic dissolution of limestone, especially at the contact between the Delle and underlying Gardison Limestone and higher in the section where pinch-and-swell structures resulted from dissolution of limestone beds.

—Thin, stratigraphically isolated beds of black chert, evidently replacing sparsely radiolarian limestones.

—Peloidal and oolitic phosphorite layers, mainly as reworked, detrital aggregates, but possibly also as replacements of limestone.

—Ubiquitous secondary dolostone as cement in clastic rocks; second to quartz, dolostone is volumetrically the most important mineral in these rocks.

—Subordinate amount of black shale in section.

—Suggestion that the several red layers may have resulted from episodes of syndepositional oxidation of original iron sulfides.

—Prevalence of planar (upper? plane-bed flow regime) lamination in siltstones and fine-grained sandstones.

—Appearance of dense, featureless, yet distinctive "ostracode lime mudstone" units, particularly that at the top of the type Delle, which contains wood-grained chert nodules.

Backtrack 5.4 miles to frontage road on north side of freeway and proceed 3.75 miles eastward to I-80 interchange (Exit 70) and enter I-80 eastbound. The prominent, well-bedded roadcut on the south side of I-80 just past exit 77, at the north end of the Stansbury Mountains, is part of the Ordovician section. Macroscopic folds at the north end of the range (visible from I-80) have moderately dipping west-facing limbs and gently dipping east-facing limbs. The apparent westward vergence implied by this geometry is an artifact of the westerly dip of Silurian and older units below the sub-Stansbury unconformity (see Cashman, this volume). Turn off of I-80 at Exit 84. Follow the off ramp around and turn right (north) onto Solar Road at the sign. Pass under the freeway, turn left (west) at the Stansbury Island sign, cross railroad tracks, and then turn right (north) onto the Stansbury Island levee road that crosses the main E-W railroad tracks at

00.00.		Pavement ends at
0.8	(0.8).	Continue to
3.6	(2.8)	and take the right fork. Proceed to
4.05	(0.45)	and take the left fork; cross the ditch, bear right, and drive through the gravel pit. Continue northeast on the lakeshore drive to
5.2	(1.15)	and bear left on the unimproved road. View to the north of Stansbury Formation quartzite resting unconformably on the Silurian Laketown(?) Dolomite. Continue on this road, bear left at
5.70	(0.5)	and continue on to STOP 3 at
6.45	(0.75)	(For the following stops, refer to the papers by Trexler and Cashman in this guidebook for maps, related data, and detailed description).

STOP 3: This stop is at the top of the measured section of the Stansbury Formation (Tabby's Canyon section, Fig. 3 in Trexler, this volume). Based on correlation with the stratotype at Flux (Stop 4, tomorrow) the Stansbury is Late Devonian to possibly earliest Mississippian in age here (Stokes and Arnold, 1958; Chapusa, 1969). At the head of Broad Canyon, the stratigraphically highest quartzites of the Stansbury are separated from the overlying Kinderhookian cherty limestones of the Fitchville Formation by about 15 m of partly calcareous fine-grained terrigenous clastic rocks and minor limestone containing marine fossils at some levels. These strata can be regarded as partly the top of the Stansbury Formation, by analogy with its type section, and partly mudstone and impure limestone at the base of the Fitchville Formation; Sandberg and Gutschick (1978) assign different levels of this relatively thin interval to several successive formations and members recognized elsewhere.

The Stansbury Formation seen here is unique among known exposures of this unit. This section of quartz arenite is 240 meters thick, and unlike the type section, contains no conglomerate at all. The dominant sedimentary structures are low-angle tabular cross-stratification. Data gathered from these cross-strata indicate an opposed bimodal pattern, with trends both east and west. Other structures include oscillation ripples, and faint tabular structures that may be infaunal burrows. Sand at the base and at the top is calcareous. This section is interpreted as a shallow-shelf, sand-wave deposit, with opposed currents causing the thick accumulation. These currents may be tidal or storm set-up and return flow. The oscillation ripples suggest that the setting was open marine rather than estuarine. This section of the Stansbury Formation is so different from the type Stansbury that it can be considered a separate but possibly coeval unit. There are quartz-arenite beds at Flux, but they do not share the same depositional environment with the quartz-arenites at Stansbury Island. Further, the thick, coarse conglomerate beds that are characteristic of the type Stansbury are entirely missing here.

(End of day one; overnight in Tooele, Utah.)

DAY TWO

00.00		Depart from Tooele at the intersection of Main Street (Utah Route 36) and Utah Route 112. Travel west on Utah 112 to intersection with Utah Route 138 just east of Grantsville at
8.65	(8.65).	Turn left (west) and proceed on Utah 138 through Grantsville and on to the north-

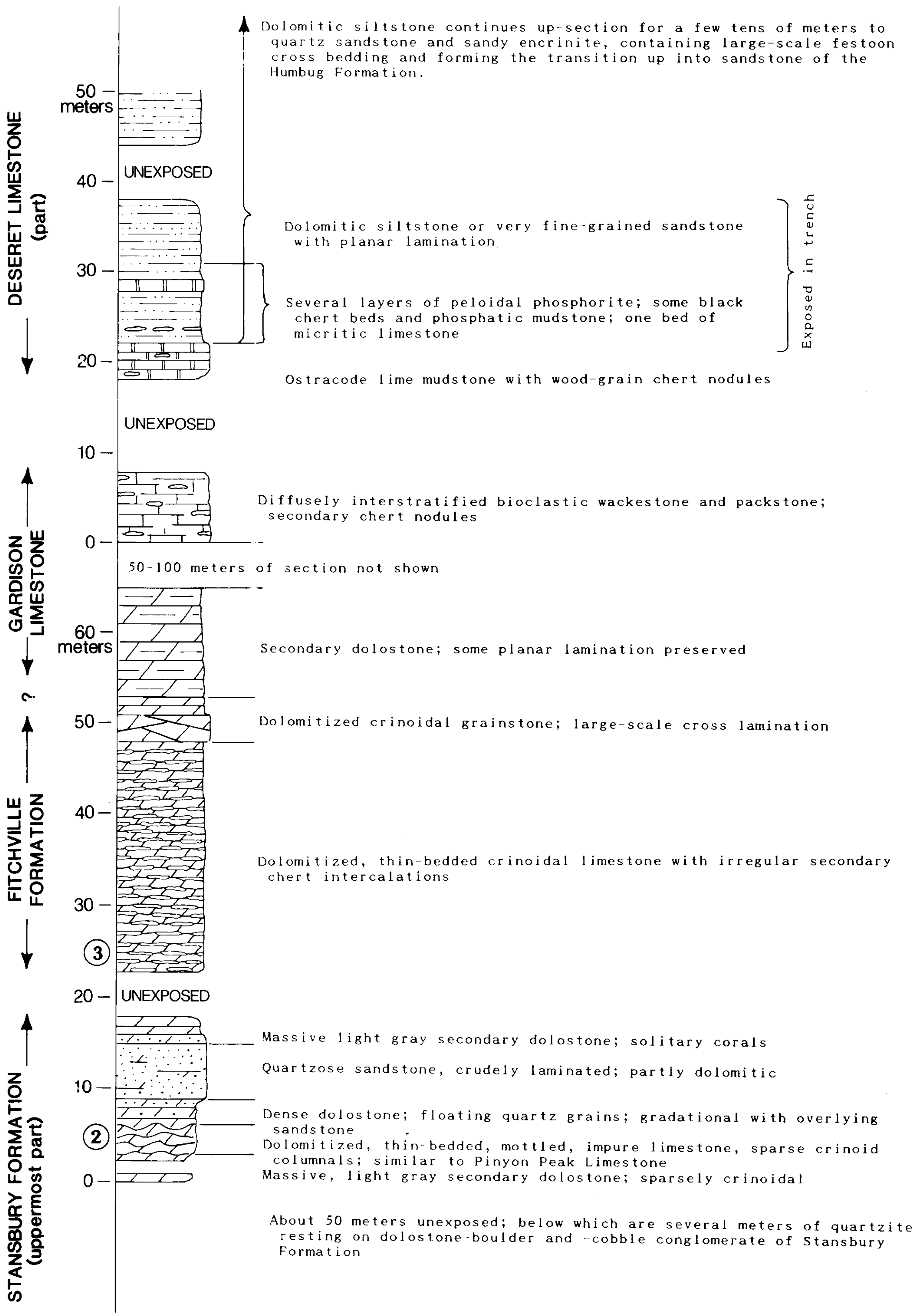

Figure 3. Columnar section showing strata from the uppermost part of the Stansbury Formation to the lower part of the Deseret Limestone. Stops 5 and 6, spur north of Flux Canyon, northern Stansbury Range. Encircled numbers to left of column indicate the level of conodont samples 2 and 3, Appendix A, in Silberling and Nichols, this volume.

west along the northeast side of the Stansbury Mountains. The commodity that was quarried along the east flank of the Stansbury Mountains is limestone of high purity in the Upper Mississippian Great Blue Limestone. Turn left on the road to Flux at

18.1 (9.45). Stay on paved road to

18.4 (0.3) and then bear left onto the road leading to the entrance to the limestone processing plant. Cross railroad tracks and then, before entering the limestone plant, turn right onto the gravel road that continues around the power sub-station and the north side of the plant and on up Flux Canyon. Continue on this road to the saddle at

19.0 (0.6) and turn left onto unimproved dirt track. At

19.5 (0.5) bear right and continue to STOP 4 at

19.7 (0.2). STOP 4: The resistant quartzite rib here is the "lower quartzite member" (Stokes and Arnold, 1958) of the Stansbury Formation. Their type section was measured on the ridge to the south of this stop, and was remeasured recently (see Trexler, this volume). We will look briefly at the quartzite here, and then walk south up the hill to the basal unconformity of the Stansbury.

Lower quartz-arenite beds: The well-bedded quartz-arenite near the road here is typical of quartz-arenite throughout the type section. The dominant feature is tabular cross-stratification with low-angle reactivation surfaces, and there are fine-grained calcareous beds throughout. Paleocurrent data in these quartz-arenites invariably indicate a west-trending current direction (contrast with Stansbury Island). These lenses of quartz sand are laterally limited individually, but this stratigraphic level invariably contains one or more lenses.

Stansbury basal unconformity: Climb the ridge to the south of this stop to the pronounced lake-terrace bench. The basal beds of the Stansbury Formation here are laminated, gray dolostone. They lie with angular unconformity on undivided Ordovician and Silurian strata, as mapped by Stokes and Arnold (1958). The basal gray dolostone of the Stansbury is overlain by a distinctive, black dolostone that contains open-marine macrofossil fragments. Above this is the "lower quartzite member" of the Stansbury. A short walk east along the lake terrace will bring you to excellent exposures of the quartzite lenses, and the overlying conglomerate.

Structural note: Stokes and Arnold (1958) invoked a high-angle fault to explain the apparent offset of individual horizons in the Stansbury Formation across Flux Canyon. An alternative explanation for both the apparent offset and the slight change in bedding orientation across the canyon is tilting of strata (north side down) around an east-west axis. This explanation is supported by the fact that the axis of the Deseret anticline also changes orientation (to plunge more steeply northward) 1.5 km west of here (Stop 8).

Backtrack 0.20 mi. to STOP 5, which is at a spectacular exposure of conglomerate in the upper part of the Stansbury Formation.

STOP 5: The conglomerate exposed here is characteristic of the dolostone-clast conglomerate found throughout the type section, and elsewhere in the northeastern Stansbury Mountains. It is typically matrix-supported and very coarse, with a variety of dolostone lithologies representing subjacent Paleozoic strata. Other clast types include quartzite rip-ups from the intercalated quartz-arenite beds. Viewing this outcrop down-dip, one can see the nested-channel geometry characteristic of most of the section. Although imbrication has not been found at this locality, it is fairly common along the type section, and clast-orientation data indicate transport of these conglomerates to the northeast. These conglomerates are interpreted as submarine debris-flow deposits, shed into a shallow basin margin facing northeast. The source of the conglomerates is presumed to be nearby to the southwest, where the sub-Stansbury unconformity cuts deepest into the Paleozoic section.

From here walk north about 0.10 mi. to east end of low saddle and continue upsection to examine uppermost Stansbury Formation (which includes a few meters of sparsely crinoidal, impure, mottled carbonate rock that resembles the Pinyon Peak Limestone), the Fitchville equivalent, and basal Gardison Limestone (see Fig. 3). The original limestones in all of these units have been secondarily dolomitized. The items of interest here are: (1) the Stansbury taking the place in the section of most of the Pinyon Peak, (2) the apparently disconformable (albeit covered) contact between the Stansbury and overlying Fitchville equivalent, and (3) the general similarity lithically and in depositional history of the

Fitchville equivalent and Gardison here with these units in the Lakeside Mountains.

Backtrack down canyon another 0.50 miles to STOP 6. Here, the contact between the Gardison Limestone and Deseret Limestone, which corresponds to the initiation of the Delle phosphatic event, is covered (see Fig. 3). Exposed in the bulldozer trench are beds in the lower part of the Deseret that are equivalent to part of the Delle Phosphatic Member in the Lakeside Mountains. The ammonites reported by Petersen (1969) were obtained from this section about 15 m above the ostracode lime mudstone unit at the base of the exposed Deseret (Sandberg and Gutschick, 1978, fig. 8). The same genus of ammonite, *Beyrichoceras,* occurs from level 15 of the type Delle Phosphatic Member in the Lakeside Mountains (Silberling and Nichols, 1991), indicating that the thick ostracode lime mudstone unit that defines the top of the type Delle is not represented in the section here at Flux. Instead, irregularly laminated dolomitic siltstone and cross-bedded sandstone and encrinite form a transition upward into the Humbug Formation.

Continue backtracking down canyon for short distance to intersection on saddle at 20.25 (0.55). Turn left (north) and follow gravel road to STOP 7 at

21.25 (1.0). STOP 7: View here to the north is of the ridge behind the Chemstar plant at Dolomite; note the pronounced angular discordance in the section, and the anomalous, thick section of bedded dolostone high in the Stansbury section. This dolostone "block" was interpreted by Stokes and Arnold (1958) as a slide block of Silurian strata included in the clastic Stansbury section and emplaced in Stansbury time. Although early work did not reveal it, this is not an unusual relationship. A very similar situation occurs at the same place in the section at Miner's Canyon, about 7 km to the south. The angular truncation of Stansbury strata seems to preclude a slide-block interpretation, either ancient or modern. The "block" is clearly part of the section; it is depositionally overlain by more conglomerate and quartz arenite. An alternative explanation is that this internal discordance represents uplift, tilt and erosion, and renewed subsidence during the filling of the Stansbury basin. If time permits, the unconformity is readily accessible on the south-facing hillside.

Backtrack to the Flux turnoff on Utah 138 at

22.85 (1.6). Turn left onto paved road paralleling railroad and follow it to the plant at

24.75 (1.9) operated by Chemstar Inc. This plant produces type-S dolomitic hydrate used in building materials. Continue past the plant on unpaved road and turn left at

25.25 (0.5). Turn right at

25.55 (0.3) then turn left at

25.8 (0.25). Continue to STOP 8 at

26.05 (0.25). STOP 8: The steeply plunging anticline at this stop is the northernmost exposure of the Deseret anticline (Lambert, 1941; Rigby, 1958), which cores the range. The shortening accommodated by this fold is dramatically smaller here than in the center of the range; much of the shortening is taken up at this latitude by the Timpie Ridge anticline (Rigby, 1958), an en echelon fold to the west and northwest (see Cashman, this volume). Here, the anticline is in the Upper Mississippian Humbug Formation and Great Blue Limestone. An axial plane, pressure solution cleavage is well developed in the limestone layers. The steep northward plunge of the hingeline is a local phenomenon, probably related to the lateral termination of the fold and/or to larger lateral changes in the thrust belt. Continue to STOP 9 at

26.6 (0.55). STOP 9: View southward along the Broad Canyon fault. This subvertical fault is an enigmatic feature, and is characterized by highly variable stratigraphic separations along its length. Here, the fault juxtaposes Upper Cambrian Ajax Dolomite on the east against Upper Mississippian Great Blue Limestone on the west, a stratigraphic separation of 2,000 m. At West Canyon, 11 km to the south, Great Blue Limestone is on both sides of the fault. At Pope Canyon, 1.5 km farther south, Pennsylvanian and Lower Permian Oquirrh Group is on the east and Great Blue Limestone on the west. The Broad Canyon fault is shown on the cross-sections of Rigby (1958) as a west-dipping reverse fault along the length of the range, and it was reinterpreted by Tooker and Roberts (1971) to be a west-dipping thrust fault. New evidence (see Cashman, this volume) suggests that it is an east-dipping reverse fault and that it postdates the east-verging folding found throughout the range.

END OF TRIP!

REFERENCES CITED

Cashman, P.H., 1992, Structural geology of the northeastern Stansbury Mountains: (this volume).

Chapusa, F.W.P., 1969, Geology and structure of Stansbury Island: Unpubl. M.S. Thesis, University of Utah, Salt Lake City.

Lambert, H.C., 1941, Structure and stratigraphy in the southern Stansbury Mountains, Tooele County, Utah: Unpubl. M.S. Thesis, University of Utah, Salt Lake City.

Nichols, K.M., and Silberling, N.J., 1990, Delle Phosphatic Member: An anomalous phosphatic interval in the Mississippian (Osagean-Meramecian) shelf sequence of central Utah: Geology, v. 18, p. 46-49.

Petersen, M.S., 1969, The occurrence of ammonoids from the lower Deseret Limestone, northern Stansbury Mountains, Tooele County, Utah: Geological Society of America Abstracts with Programs, v. 1, p. 63.

Rigby, J.K., 1958, Geology of the Stansbury Mountains: Utah Geological Society Guidebook 13, p. 1-134.

Sandberg, C.A., and Gutschick, R.C., 1978, Biostratigraphic guide to Upper Devonian and Mississippian rocks along the Wasatch Front and Cordilleran hingeline, Utah: U.S. Geological Survey Open-File Report 78-351, 52 p.

—1984, Distribution, microfauna, and source-rock potential of Mississippian Delle Phosphatic Member of Woodman Formation and equivalents, Utah and adjacent states, *in* Woodward, Jane, Meissner, F.F, and Clayton, J.L., eds., Hydrocarbon source rocks of the greater Rocky Mountain region: Denver, Colorado, Rocky Mountain Association of Geologists, p. 135-178.

Silberling, N.J., and Nichols, K.M., 1991, Petrology and regional significance of the Mississippian Delle Phosphatic Member, Lakeside Mountains, northwestern Utah, *in* Cooper, J.D., and Stevens, C.H., eds., Paleozoic paleogeography of the western United States II: Pacific Section Society of Economic Paleontologists and Mineralogists, v. 67, p. 425-438.

—, 1992, Depositional cycles of the Upper Devonian-Lower Mississippian limestone succession in the southern Lakeside Mountains, Utah: (this volume).

Stokes, W.L., and Arnold, D.E., 1958, Northern Stansbury Range and the Stansbury Formation: Utah Geological Society Guidebook 13, p. 135-139.

Tooker, E.W., and Roberts, R.J., 1971, Structures related to thrust faults in the Stansbury Mountains, Utah: U.S. Geological Survey Professional Paper 750-B, p.1-12.

Trexler, J.H., Jr., 1992, The Stansbury Formation at Stansbury Island and the northeast Stansbury Mountains: (this volume).

DEPOSITIONAL CYCLES OF THE UPPER DEVONIAN-LOWER MISSISSIPPIAN LIMESTONE SUCCESSION IN THE SOUTHERN LAKESIDE MOUNTAINS, UTAH

By N.J. Silberling and K.M. Nichols
U.S. Geological Survey
Box 25046, Federal Center
Denver, CO 80225

With an appendix on the

IDENTIFICATION AND AGE INTERPRETATIONS OF CONODONT FAUNAS

By Robert G. Stamm
U.S. Geological Survey
National Center
Reston, VA 22092

ABSTRACT

The succession of Upper Devonian-Lower Mississippian marine limestones in the southern Lakeside Mountains is about 200 m thick and accumulated on the continental shelf of the Antler foreland. This limestone succession abruptly and disconformably overlies inner-shelf, peritidal-cyclic dolostones of Devonian age and is overlain by phosphatic, dolomitic and cherty, fine-grained siliciclastic rocks that mark the initiation of the Delle phosphatic event. Despite some minor problems in the definitions of formational units, limestones of this succession represent, in ascending order, the Pinyon Peak Limestone, Fitchville Formation, and Gardison Limestone, all of which are typified in the East Tintic district about 100 km to the south-southeast of the Lakeside Mountains. In the Lakeside Mountains this succession includes seven distinct lithic units whose interpretation in terms of sedimentary environments supports the recognition of three distinct depositional cycles. In the context of sequence stratigraphy, cycles I and III in Utah reflect local tectonic control of deposition in what can be interpreted as the back-bulge region of the Antler foreland during, respectively, latest Devonian time and from late Early to Late Mississippian time.

INTRODUCTION

Upper Devonian-Lower Mississippian limestones in the southern Lakeside Mountains, exemplify the succession characteristic of a large area in northwest Utah. Their map relations in the southern Lakeside Mountains are shown on Figure 1, which is reproduced from Young (1955) who used the names "Madison Limestone" and "Deseret Limestone" for these rocks. Although these names are misapplied, the map pattern is still generally correct and useful.

In addition to their inherently interesting depositional history and their significance for interpreting subsequent structural rearrangement, these Upper Devonian-Lower Mississippian limestones provide the context for understanding unusual parts of the stratigraphic record in the region such as the partly correlative, coarse-clastic Stansbury Formation in ranges immediately to the east and southeast of the Lakeside Mountains and the anoxic deposits of the Delle phosphatic event (Silberling and Nichols, 1991, reproduced in this volume) that cap the Upper Devonian-Lower Mississippian limestone succession over a broad area. Both the upper and lower limits of this succession, which in the Lakeside Mountains is about 200 m thick, are sharply delimited. Its base marks a distinct change to more

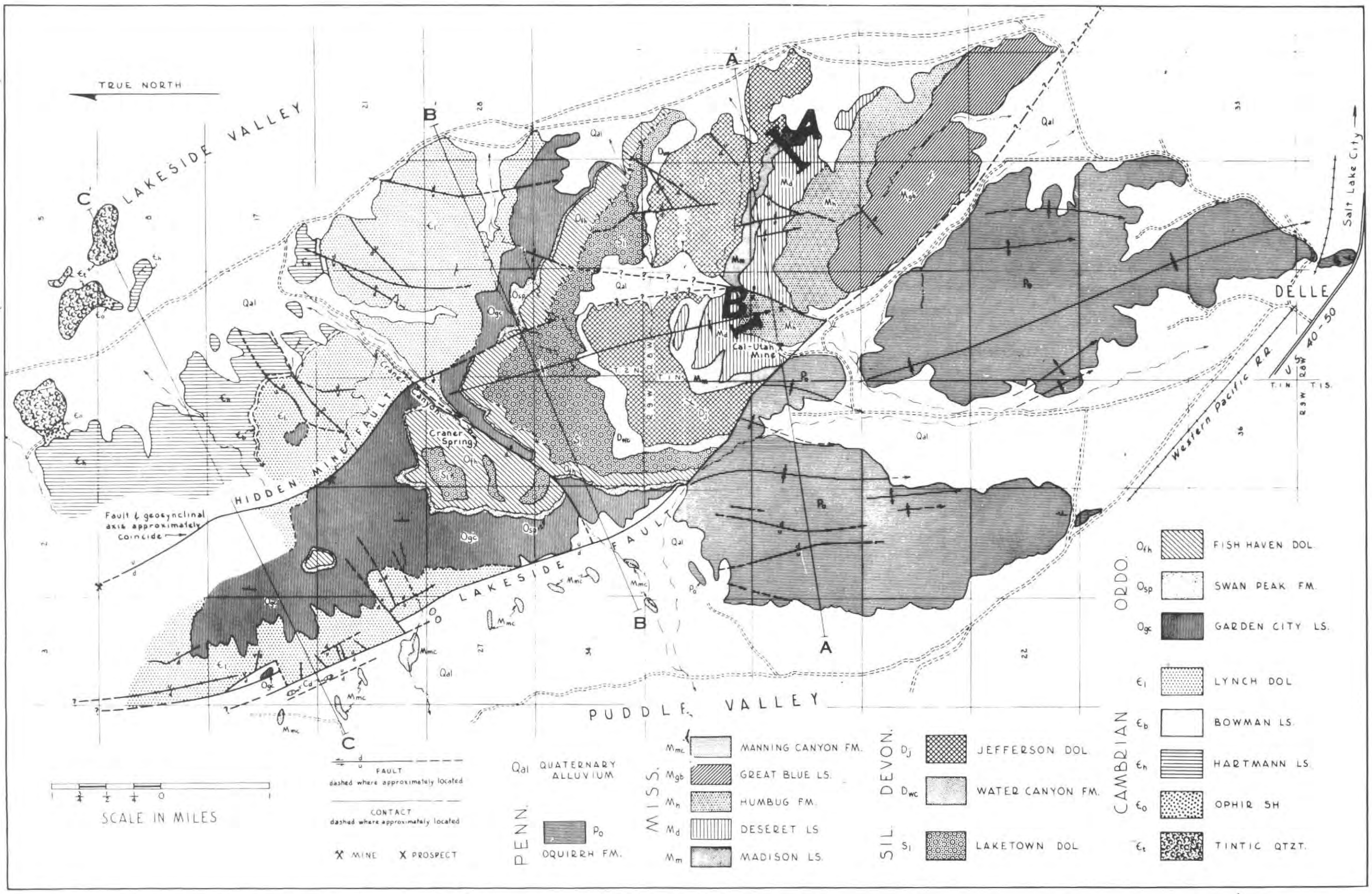

Figure 1. Geologic map of the southern Lakeside Mountains reproduced from Young (1955). A and B, (annotations added to map) locations of sections discussed in text (respectively, stops 1 and 2 in Road Log, this volume). Upper Devonian-Lower Mississippian limestone succession included in "Madison Ls," and "Deseret Ls." of map explanation.

open marine conditions in late Famennian time, following a long period during which a thick sequence of Devonian and older dolostones was deposited on the inner shelf. Its top marks the advent of the Delle phosphatic event, which abruptly interrupted shelf carbonate deposition in Osagean time (Nichols and Silberling, 1989).

The formation names most applicable to the uppermost Devonian-Lower Mississippian limestone succession in the southern Lakeside Mountains are, from oldest to youngest, the Pinyon Peak Limestone, Fitchville Formation, and Gardison Limestone, all named from exposures in the East Tintic district (ETD on Fig. 2) (Morris and Lovering, 1961) about 100 km south-southeast of the southern Lakeside Mountains. On the geologic map of the southern Lakeside Mountains (Fig. 1), reproduced from Young (1955), the basal contact of the Pinyon Peak corresponds to that of the "Madison Limestone," and the top of the Gardison corresponds to the base of the "Deseret Limestone". The "Humbug Formation" as mapped on Figure 1 includes in its lower part the rocks equivalent to the typical Deseret Limestone (type section at OP on Fig. 2). Although problems with the definition of the type Pinyon Peak and the recognition of its contact with the overlying Fitchville are unresolved, as explained below in discussing the application of these names in the southern Lakeside Mountains, these two formations plus the Gardison correspond at least in a general way to two of the principal cycles of latest Devonian to Mississippian deposition in northwest Utah and the initial part of a third cycle. In the East Tintic district (ETD on Fig. 2), cycle I is represented by the Pinyon Peak, as used herein, and the lowermost part of the Fitchville Formation. Cycle II is represented by the remainder of the Fitchville Formation, and the lower part of cycle III by the Gardison Limestone. For the sake of objectivity in describing the Upper Devonian-Lower Mississippian limestone succession in the Lakeside Mountains, it is divided into seven units as shown on Figure 3. Nomenclature and sequence stratigraphy are discussed in terms of their relationship to these units.

A thick section of Devonian and older dolostone and some quartzite underlies the Pinyon Peak Limestone that forms the base of the uppermost Devonian and younger limestones that are the subject of interest here. Much of this dolostone section is the characteristic inner-shelf association of alternating one to several meter thick units of light-colored p-dolostone (i.e., "primary" or "penecontemporaneous," dense, locally microbially laminated dolostone) and gray, sugary, crystalline eogenetic secondary dolostone of the kind described by Nichols and Silberling (1980). The

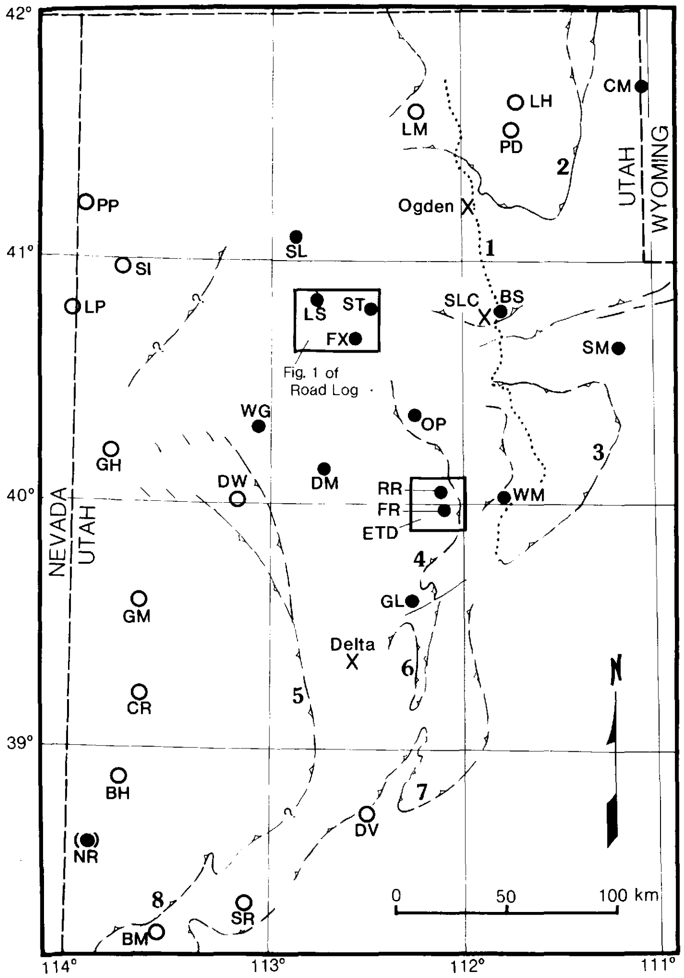

Figure 2. Map of most of western Utah showing location of significant Upper Devonian-Lower Mississippian sections: BH, Burbank Hills; BM, Blawn Mountain; BS, Becks Spur, Wasatch Range; CM, Crawford Mountains; CR, Confusion Range; DM, Davis Mountain; DV, Dog Valley, Pavant Range; DW, Dugway Range; FR, Fitchville Ridge, East Tintic district; FX, Flux, northern Stansbury Mountains; GH, Gold Hill; GL, Gilson Mountains; GM, Granite Mountain; LH, Leatham Hollow, Bear River Range; LM, Little Mountain; LP, Leppy Hills; LS, southern Lakeside Mountains; OP, Ophir Canyon, Oquirrh Mountains; NR, Needle Range; PD, Porcupine Dam, Bear River Range; PP, Pilot Peak; RR, Rattlesnake Ridge, East Tintic district; ST, Stansbury Island; SI, Silver Island; SL, Sally Mountain, northern Lakeside Mountains; SR, Star Range; SM, Samak, west end of Uinta Mountains; WG, Wig Mountain; WM, West Mountain.

Abbreviated place names: ETD, East Tintic district; SLC, Salt Lake City.

Faults: 1, Wasatch fault zone; 2, Paris-Willard thrust; 3, Charleston-Nebo thrust; 4, East Tintic thrust (in part); 5, House Range detachment, interpreted as reactivated thrust following Villien (1984); 6, Canyon Range thrust; 7, Pavant thrust; 8, Wah Wah thrust. Structural features modified from Allmendinger and others (1983), Levy and Christie-Blick (1989), Miller (1990), Morris (1983), and others. Region west of Wasatch fault zone has been tectonically extended in Tertiary time; the highly extended belt of Gans and Miller (1983) lies west of a line connecting GM and SL. Solid circles, secitons where unit 6 (as described in text) is recognized; in parentheses (at NR) where poorly developed. Open circles, sections that include the stratigraphic level of unit 6, but unit 6 is not represented.

unit of this type of peritidal-cyclic dolostone that immediately underlies the Pinyon Peak Limestone in the Lakeside Mountains has been referred to at different times in the literature as the Jefferson Dolomite (e.g., Fig. 1), Guilmette Formation, and Beirdneau Formation; the name Victoria Formation, derived from the East Tintic district (Morris and Lovering, 1961), is also applicable.

The description of the Upper Devonian-Lower Mississippian limestone section herein is based mainly on observations made in the NW¼ sec. 9, T.1 N., R.8 W. on the northwest-facing slope of the spur on the east side of the southern Lakeside Mountains west of Dead Cow Point (section A on Fig. 1; Stop 1 in Road Log, this volume). Exposures of unit 1 through the lower part of unit 6 (Fig. 3) are particularly good here despite the partial cover of cemented gravels related to Pleistocene Lake Bonneville. Views of section A at Stop 1 in the Road Log are shown on Figures 4 and 5. The highest beds of the limestone succession in unit 7 (Fig. 3) are best examined in the section that includes the typical Delle Phosphatic Member of the Woodman Formation in south central sec. 6, T.1 N., R.8 W. on the road to the electronic facility atop Black Mountain (B on Fig. 1; Stop 2 in Road Log).

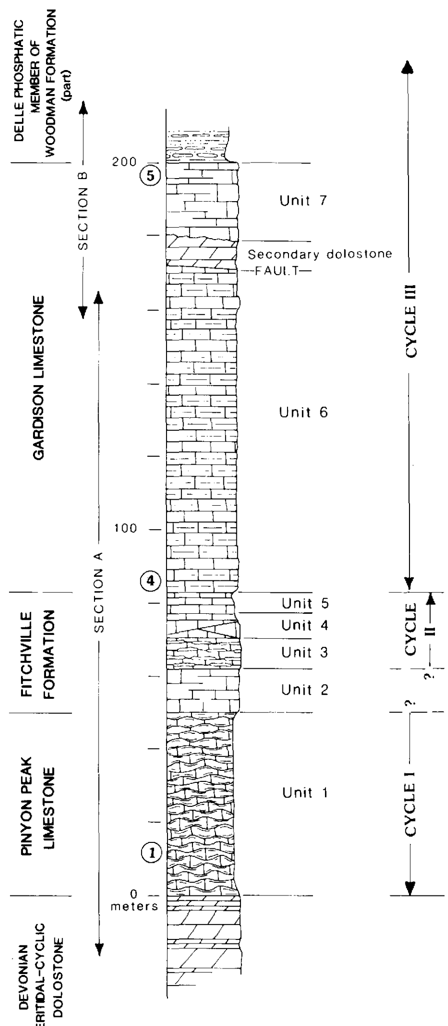

Figure 3. Composite columnar section of the Upper Devonian-Lower Mississippian limestone succession and enclosing strata, southern Lakeside Mountains. Encircled numbers to left of column are conodont samples 1, 4, and 5 in Appendix A.

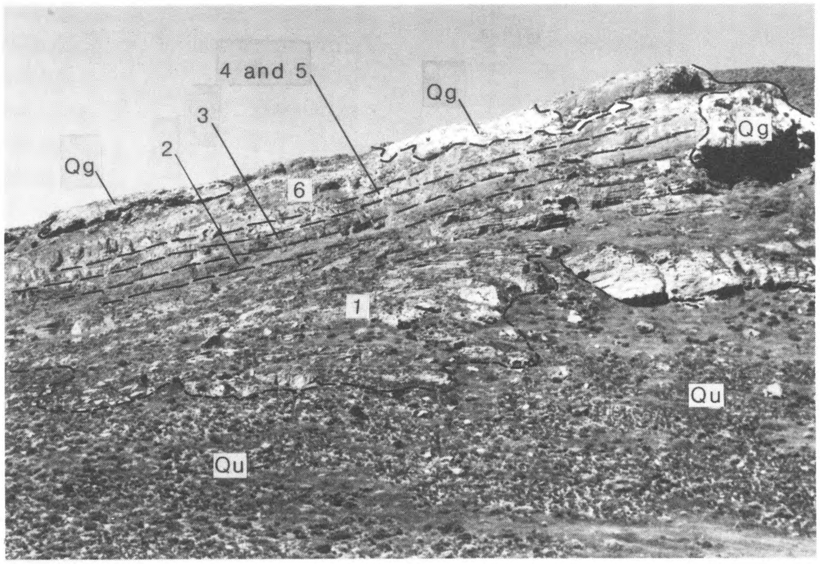

Figure 4. View of section A (Fig. 1) showing units 1 to 6. Qu, undifferentiated Quaternary cover; Qg, cemented Bonneville gravels.

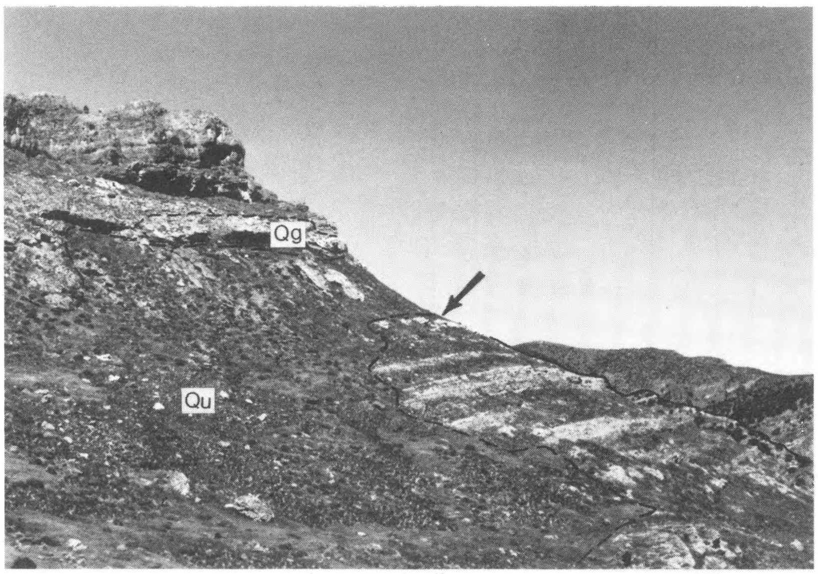

Figure 5. View of section WNW of section A, showing location of exposure of base of unit 1 (Fig. 8); Qu, undifferentiated Quaternary cover; Qg, cemented Bonneville gravels.

DESCRIPTION OF UNITS

Unit 1

Unit 1 is composed of mottled, thin-bedded, irregularly slabby to platy, impure limestone (Fig. 6) which contains nodules and thin lenses of gray bioclastic packstone and wackestone enclosed in generally subordinate, anastomosing, argillaceous to silty, yellow brown weathering streaks and layers. It is fairly homogeneous throughout its 50 m thickness in the southern Lakeside Mountains; the main variations are in the degree of solution compaction (Fig. 7) and in the appearance in the uppermost 15 m of conspicuous megafossils, including both solitary and colonial corals and brachiopods. In section A (Fig. 1) southwest of the low saddle between the drainages on either side of the outlying hills that form Dead Cow Point, the base of unit 1 is not exposed. However, in an isolated outcrop (Fig. 5) about 300 m west this section, the sharp contact (Fig. 8) with the underlying p-dolostone is well displayed. Although not present here, sandstone averaging "1 foot but ... up to 3 feet thick" is reported at the base of unit 1 by Young (1955).

Among the mid and upper Paleozoic strata of western Utah, unit 1 is lithically unique. On the outcrop it is characterized by its nodular thin bedding and by the ubiquitous, albeit locally scarce, presence of megascopically visible crinoid columnals. Unit 1 is distinguished petrographically from other thin-bedded, impure, nodular or mottled limestones, such as those forming part of the somewhat older, pelletal West Range Limestone in westernmost Utah, by its wackestone and fine-grained packstone fabric of open-marine bioclasts (derived from crinoids, brachiopods, bryozoans, etc.) coupled with the only minor occurrence of pellets among its allochems (Fig. 9). Limestones such as

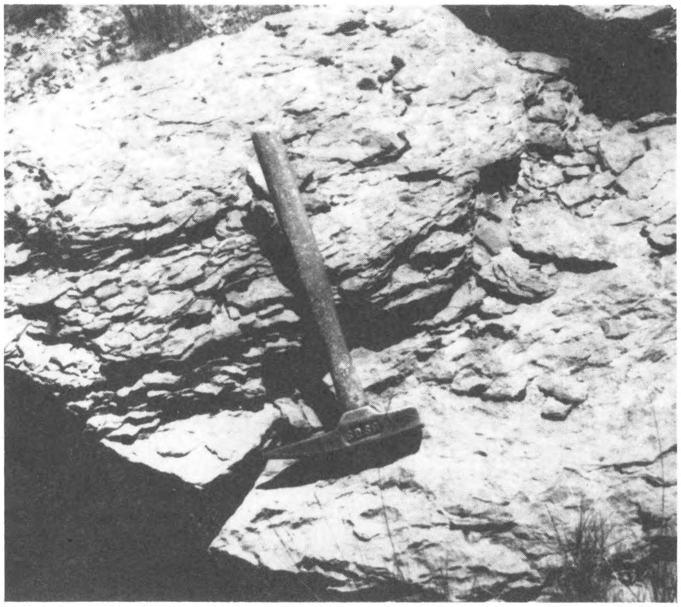

Figure 6. Thin-bedded, irregularly slabby to plate, impure limestone in lower part of unit 1.

Figure 8. Sharp contact (just below hammer head) between impure, thinly nodular, crinoidal limestone and underlying p-dolostone (see text).

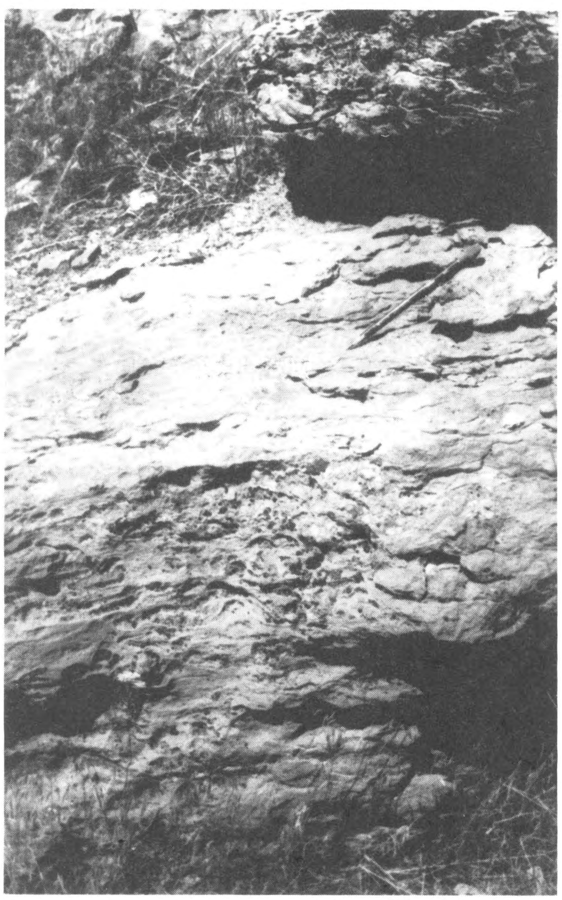

Figure 7. Solution compacted, impure limestone near top of unit 1; pencil points to in-place colonial coral.

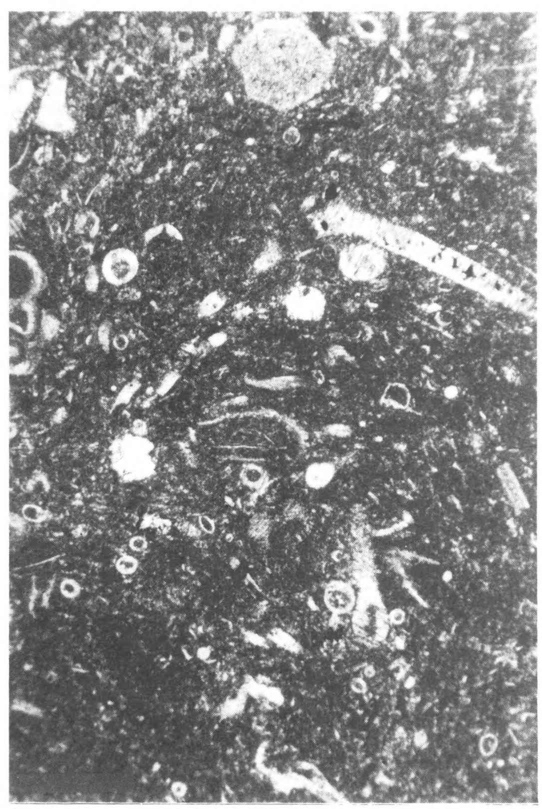

Figure 9. Photomicrograph of wackestone/fine-grained packstone in lower part of unit 1 showing crinoid columnals and other bioclasts and the scarcity of pellets. Bar scale = 0.5 mm.

these are generally interpreted as well-oxygenated periplatform deposits formed below normal wave base (Wilson, 1969; Cook and Taylor, 1977; Dorobek and Read, 1986). Such deposits may record an episode of rapid transgression and flooding of the shelf (Barnaby and Read, 1990).

Unit 1 is lithically equivalent to what is generally regarded as the Pinyon Peak Limestone in Utah. However, the original definition of this unit in the East Tintic mining district (Lindgren and Loughlin, 1919) allows this name to be used in some genetically unnatural ways. For example, Sandberg and Poole (1977, and in subsequent papers by them and other coauthors) restrict strata having the character of unit 1 to an upper member of the Pinyon Peak and recognize as a lower member a disconformably underlying, discontinuous, inner-platform unit up to a few tens of meters thick composed of light-colored, fine-grained, peloid or grapestone grainstone and fenestrate calcisphere, ostracode wackestone. This lower member is not present in the Lakeside Mountains. In the East Tintic district the Pinyon Peak Limestone is overlain by the Fitchville Formation, the base of which was originally defined by Morris and Lovering (1961) on the presence of a thin stringer of fine-grained quartz sandstone (the "sand grain marker bed"). In its type section on Fitchville Ridge (FR on Fig. 2) the lower 3 m of the Fitchville Formation above the "sand grain marker bed" is lithically identical to the underlying Pinyon Peak Limestone (Morris and Lovering, 1961, p.76). Overlying these basal strata of the Fitchville are massive, solution-compacted crinoid grainstones that are quite distinct. This confusing situation, whereby the basal rocks of the type Fitchville are lithically the same as those at the top of the Pinyon Peak, was used by Sandberg and Dreesen (1984) in support of assigning the coral-bearing upper 14 m of unit 1 in the Lakeside Mountains to the Fitchville Formation rather than to the Pinyon Peak. Also, according to Sandberg and Dreesen (1984, Fig. 7) the upper part of unit 1 belongs to the Middle *Palmatolepis expansa* (originally called the Lower *Bispathodus costatus*) conodont Zone and is correlative with the massive crinoidal limestones in the lower part of the Fitchville Formation. If Sandberg's largely undocumented conodont-age determinations are accepted, and if the massive crinoidal limestones of the lower part of the type Fitchville are regarded as representing the platform margin with respect to the strata of the Pinyon Peak (such as those of unit 1 that are subtidal shelf flat or ramp deposits), then northward or northwestward progradation of the Fitchville over the Pinyon Peak is suggested. The lower and major share of unit 1 in the Lakeside Mountains and rocks lithologically like unit 1 regionally belong to the Lower *expansa* (formerly the Upper *Polygnathus styriacus*) Zone (as reported by C.A. Sandberg and coauthors in numerous papers, for example, Johnson and others, 1991, and confirmed here for exposures in the Lakeside Mountains, sample 1, Appendix A).

Where unit 1 rests directly on older Devonian sabkha dolostones and quartzites in ranges south of the Lakeside Mountains, its thickness ranges from 40 to 60 m. A few meters of strata like those of unit 1, and of the same age (sample 2, Appendix A), conformably occur within the uppermost part of the Stansbury Formation above its substantial thicknesses of subaqueous sandstone and conglomerate in the Stansbury Mountains and at Stansbury Island (FX and ST on Fig. 2) (Trexler, this volume). Thus, unit 1 and the enigmatic Stansbury Formation bear some direct relationship to one another.

Unit 2

Unit 2 is composed of dark gray, diffusely and irregularly interlayered, fine-grained crinoidal packstone and wackestone having a total thickness of about 12 m. In contrast with the limestones of unit 1, those of unit 2 are massively bedded and have irregularly stylolitic, medium to thick parting. In addition to the ubiquitous crinoid columnals, other bioclasts conspicuous in thin section include finely comminuted bryozoan and brachiopod skeletal debris (Fig. 10). For the most part, the bioclasts do not exhibit micritized margins, and in size and kind they resemble those of the underlying unit 1 limestones. The lime-mudstone matrix in unit 2 is faintly pelleted.

Limestones of unit 2 represent an open-marine, fairly energetic environment; they may be prograding bank deposits at the top of the sedimentary cycle that begins with unit 1 and be equivalent to the massive crinoidal limestones in the lower part of type Fitchville in the East Tintic district mentioned above. This correlation is not compelling, and unit 2 might be part of the latest Devonian cycle rather than the base of the overlying Early Mississippian cycle. Thus, the position of the boundary between cycles I and II with respect to unit 2 is uncertain; it may be either at the base or top of unit 2.

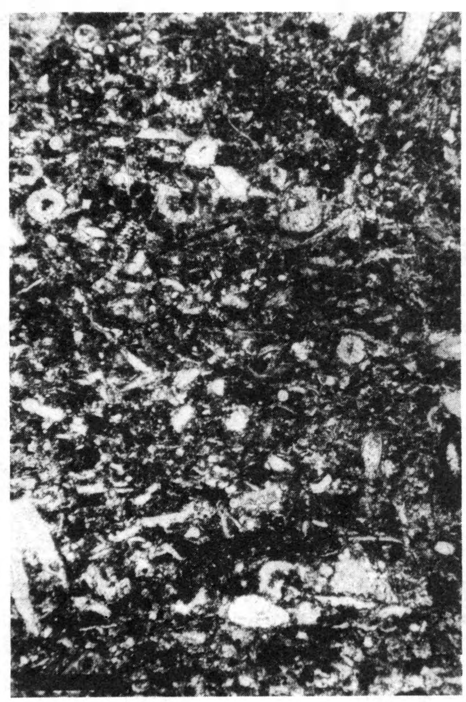

Figure 10. Bioclastic packstone of unit 2 showing similarity in kind and size of bioclasts with those of unit 1 (Fig. 9). Bar scale = 0.5 mm.

At Sally Mountain in the northern Lakeside Mountains (SL on Fig. 2) the limestone unit that occupies the same relative stratigraphic position and that is about the same thickness as unit 2 is quite different. It is mainly composed of massive crinoidal grainstone having about a meter of coarse-grained, oncolitic, *Renalcis*-like algal grainstone in its lower part (Fig. 11). Again, whether this limestone represents the prograded upper part of sequence cycle I or drowning at the base of cycle II is uncertain; it is a shoal-water deposit but appears to grade up into the rhythmically bedded, cherty shelf-flat limestones of unit 3 in cycle II (Fig. 3).

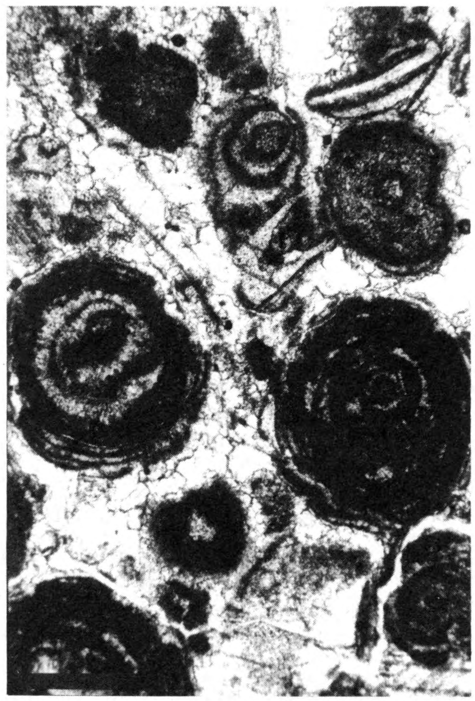

Figure 11. Oncolitic grainstone containing *Renalcis*-like algae and other bioclasts in a limestone unit at Sally Mountain (SL on Fig. 2) corresponding in stratigraphic position to that of unit 2 in the southern Lakeside Mountains. Bar scale = 0.5 mm.

Unit 3

Unit 3 consists of continuous, but highly irregular, alternating layers of gray limestone and yellow-brown weathering chert. The total thickness of this unit is 7 m, about one-quarter to one-third of which is composed of chert. Layers of chert vary widely in thickness along strike and are associated with compensating dissolution compaction of the intervening, nodular to lenticular, thin- to medium-thick layers of limestone. The chert retains remnants of limestone fabric and is thus mainly replacive, but the layers of secondary chert most likely were seeded by fine-grained siliciclastic partings within a limestone originally having regular, rhythmic bedding. The limestone beds are mainly lime mudstone and bioclastic wackestone (Fig. 13). Some interbedded packstone either forms discrete layers between beds of wackestone (Fig. 14) or make up the lower part of wackestone beds, suggesting normal grain-size grading. Bioclasts are primarily crinoid columnals along with some other open-marine skeletal debris.

Unit 3 is the counterpart of the approximately 10 m of thin-bedded limestone that disconformably overlies the 28 m-thick massive crinoidal grainstone in the basal part of the type Fitchville Formation in the East Tintic district (ETD on Fig. 2). Late Kinderhookian conodonts (sample 3, Appendix A) have been recovered from the lower part of the lithic

Figure 12. Thin- to medium-bedded limestone intercalated with chert comprising unit 3.

Figure 13. Photomicrograph of crinoidal-bryozoan bioclastic wackestone of unit 3. Bar scale = 0.5 mm.

Figure 14. Evenly thin- to medium-bedded limestone having either impure-limestone or chert-replacement partings and showing a shelly packstone bed (behind hammer handle) intercalated with wackestone beds. Unit 3 at Sally Mountain (SL on Fig. 2), northern Lakeside Mountains.

equivalent to unit 3 near Flux in the northern Stansbury Mountains (FL on Fig. 2). Regionally, unit 3 and its lateral equivalents represent the subtidal, shelf-flat and ramp deposits that mark the transgressive part of cycle II.

Unit 4

Unit 4 is composed of 6.5 m of massive, roughly cross laminated grainstone that grades up from the crinoid-rich upper part of unit 3 and in turn is gradationally overlain by massive wackestone and lime mudstone of unit 5. Allochems of unit 4 grainstone are distinctive in being mainly conspicuously micritized crinoid columnals and equivalent-sized peloids (Fig. 15). Some peloids may be completely micritized skeletal grains. Others may be intraclasts, as shown by the presence of rare rounded intraclastic grains composed of finely pelletal limestone. In addition to endothyrids, some large shelly bioclasts are also represented in these grainstones that represent the progradational margin of an intrashelf, carbonate-buildup. Where not obscured by eogenetic secondary dolomitization, as in the type Fitchville (FR on Fig. 2) in the East Tintic district, massive grainstones characterized by micrititized columnals, peloids, and intraclasts are distinctive of equivalent deposits in this cycle at least as far south as the Needle Range in westernmost Utah (NR on Fig. 2).

Unit 5

Massive fine-grained crinoidal packstone and wackestone in the lower part of unit 5 form a transition from the grainstones of unit 4 up into the 3.5 m of massive wackestone and lime mudstone that makes up most of unit 5. These limestones are capped by about 1 m of buff-weathering lime mudstone that locally exhibits microbial-mat lamination and suggests restricted, inner-platform deposition. The thickness of unit 5 is about 5 m.

Despite its inconspicuous appearance and thickness, the progradational shallowing represented by unit 5 at the top of cycle II can be recognized regionally. It provides a means of correlating from the Crawford Mountains in northernmost Utah (CM on Fig. 2), south through the East Tintic district (ETD on Fig. 2), where the equivalent of unit 5 includes the "curley limestone" stomatolitic marker bed (Proctor and Clark, 1956), to the Star Range in southern Utah (SR on Fig. 2). At some places, as in the East Tintic district, Gilson Mountains and West Mountain (respectively, ETD, GL, and WM on Fig. 2), the equivalents of unit 5 include p-dolostones and other indications of desiccation such as fenestrate lime mudstones. This sea-level minimum at the top of cycle II also provides a means of correlating with the rocks generally referred to as the Joana Limestone in the upper plate of the House Range detachment in westernmost Utah, as at localities CR, BH, NS, and NR (Fig. 2).

Unit 6

Unit 6 makes up the major share of the Gardison Limestone and is an unmistakable part of the pre-Tertiary section throughout north-central Utah. It is distinguished by dark-gray, very finely grainy, conspicuously laminated limestone punctuated at intervals by discrete tempestite beds. The laminated limestone generally lacks megascopic fossils, is

Figure 15. Photomicrograph of grainstone from unit 4 containing micritized crinoid columnals, peloids, and possible intraclasts. Bar scale = 0.5 mm.

regularly medium- to thick-parted, and the sets of planar lamination exhibit low-angle, commonly nearly imperceptible, truncation of one set by another (Fig. 16). Hummocky cross stratification is suggested at a number of places in unit 6 in the southern Lakeside Mountains and elsewhere. It is especially well developed at Sally Mountain in the northern Lakeside Mountains (Fig. 17; SL on Fig. 2). In thin section the laminated limestones of unit 6 are markedly pelletal, fine-grained packstones and grainstones composed mainly of well-sorted, well-rounded pellets 50-100 microns in diameter and subordinate abraded echinoderm fragments (Fig. 18). Pellets tend to be concentrated in stringers and clots elongated parallel to bedding and separated by flat-shaped, ragged pores filled by spar that is mostly rim cement on the echinoderm fragments. These pore fillings account for as much as 20% of the total rock volume. Besides pellets, well sorted bioclasts, including crinoid-columnal fragments, form a subordinate share of the allochems, and very fine-grained detrital quartz occurs in trace amounts. Tempestite beds, mostly of medium thickness, are intercalated in the section of laminated limestones at meter to several-meter intervals, and they are either normally or reverse graded (Fig. 19). Clasts in the tempestites are body fossils, such as small horn corals, crinoid columnals, and large shells, especially of snails, and in some beds, rip-up intraclasts of the enclosing pelletal limestone.

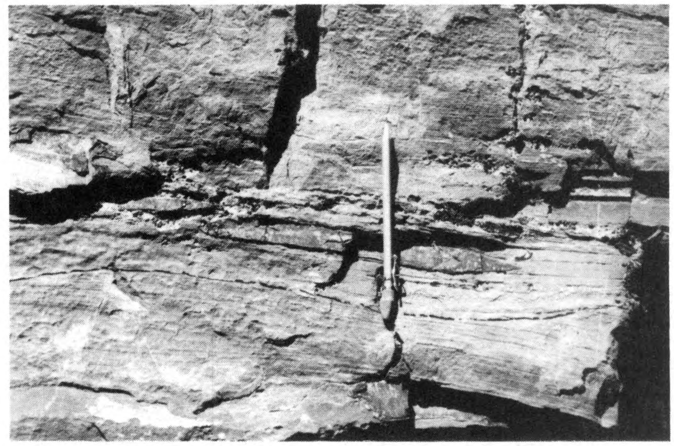

Figure 17. Hummocky cross stratification low in unit 6 at Sally Mountain (SL on Fig. 2), northern Lakeside Mountains. Hummocky surface traced on outcrop by felt-pen line behind pencil eraser.

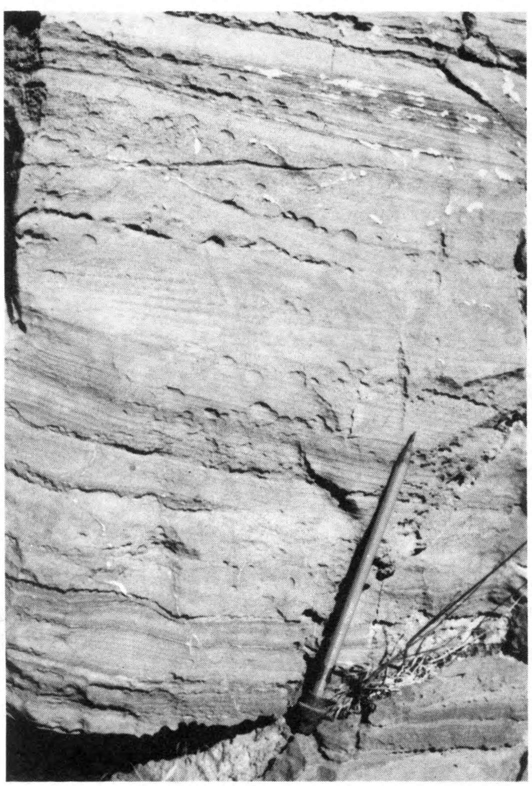

Figure 16. Low truncation angle, planar cross lamination characteristic of unit 6. Large talus block at foot of cliffs at section A.

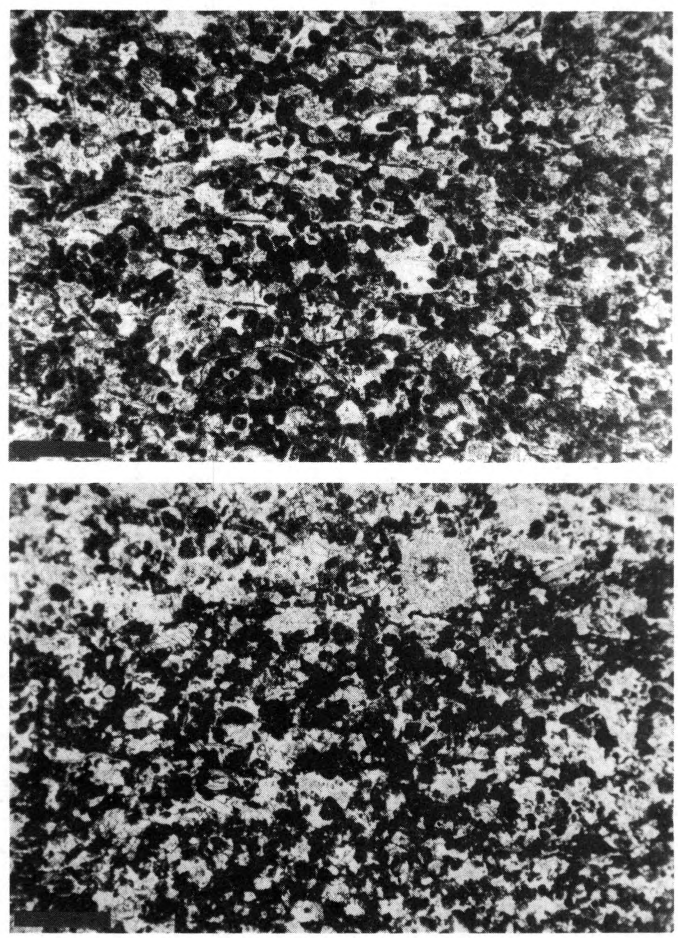

Figure 18 A and B. Photomicrographs of laminated pelletal fine-grained packstone/grainstone of unit 6. Horizontally flattened, rim cemented pores separate elongated stringers and clots of pellets. A, Talus block illustrated in Figure 16. B, upper part of unit 6, section A; note conspicuous crinoid columnal. Bar scale = 0.5 mm.

Figure 19. Inversely graded tempestite bed within unit 6, Sally Mountain (SL on Fig. 2), northern Lakeside Mountains. Note cross-section of large low-spired snail at left end of outcrop.

In the southern Lakeside Mountains unit 6 is partly covered in the vicinity of section A and is cut by obvious bedding-parallel faults at section B (Fig. 1); its estimated thickness is at least 90 m. The sections where unit 6 is recognized regionally are shown on Figure 2. Its thickness varies from about 70 m at SM (on Fig. 2) in the west end of the Uinta Mountains (Dockal, 1980; Nichols and Silberling, 1991), to about 105 m at RR and GR in the vicinity of the East Tintic district, to as much as 125 m at SL in the northern Lakeside Mountains (Nichols and Silberling, unpubl. data). These sections of unit 6 are entirely composed of the distinctive laminated limestones and tempestites except for relatively thin transitions into the underlying and overlying units. In the southern Lakeside Mountains a little more than a meter of massive finely crinoidal wackestone separates the lowest laminated limestone of unit 6 from the top of unit 5. This wackestone is considerably neomorphosed, partly cherty, and contains a few percent of authigenic quartz crystals. Conodonts from this level are late Kinderhookian in age (sample 4, Appendix A). Assuming that these conodonts are not reworked, which in this transgressive setting is a distinct possibility, the age of these conodonts indicates that any hiatus at the sequence boundary between units 5 and 6 is insignificant. This follows because conodont-based ages of units 3 and 4 are mid- to late Kinderhookian regionally.

At SL, SM, RR, and GL (Fig. 2), oolitic grainstones occur within a few meters of the base of unit 6. Those at SL (Fig. 20), though conspicuous in outcrop, are only about 15 cm thick and are present about 1 m above the level exhibiting hummocky cross stratification. In addition to their occurrence in unit 6, oolites also characterize the equivalent stratigraphic level in western Utah at SR, BM, NR, BH, and CR (Fig. 2); occurrences at other stratigraphic levels in the Mississippian of Utah are unknown. The oolitic part of the section is present both below and above the Wah Wah thrust (labelled 8 on Fig. 2). It thus provides a means of lithically correlating across this structure which appears to be the southern continuation of the House Range detachment (5 on Fig. 2). The apparent juxtaposition of largely different Devonian-Mississippian sections across the Wah Wah-House Range detachment suggests to us that this surface was originally a large-scale, pre-Tertiary contractile structure, as proposed by Villien (1984), although it may have been reactivated during Tertiary extension. At NR, the southernmost Mississippian section in the House Range detachment sheet (and upper plate of the Wah Wah thrust), units of massive ooid grainstones characterize the 47 m of section immediately overlying inner-shelf limestone correlated with unit 5, the regional sea-level minimum unit, of the southern Lakeside Mountains section. The upper 10 m of these oolitic rocks intertongue with and are then overlain by another 12 m of laminated pelletal packstone/grainstone the same as that forming unit 6. An expression of unit 6 may thus be represented in the southern part of the Wah Wah-House Range structural plate, and if substantial southeastward thrusting of such a plate occurred (Miller, 1966), then the western limit of unit 6 originally may have been considerably to the west of the well-developed sections of unit 6 in north-central Utah.

The transition at the top of unit 6 into unit 7 is obscured by both faulting and lack of exposure in the southern Lakeside Mountains. Sections farther south and east in Utah exhibit one or more units of crinoidal grainstone in the upper part of unit 6, the highest such unit intervening between units 6 and 7. These grainstone units are on the order of meters thick, exhibit large-scale planar cross-stratification, and are interpreted as submarine-dune deposits.

The depositional environment of the main body of laminated limestone and tempestites forming unit 6 is especially interesting considering its thickness and great, apparently continuous original extent (Fig. 2). The pelletal, evenly fine-grained allochem content, open-marine bioclasts, and cleanly washed nature of the laminated limestones, coupled with their pervasive low-angle cross lamination, lack of bioturbation, and the occurrence in them of interbedded coarse-

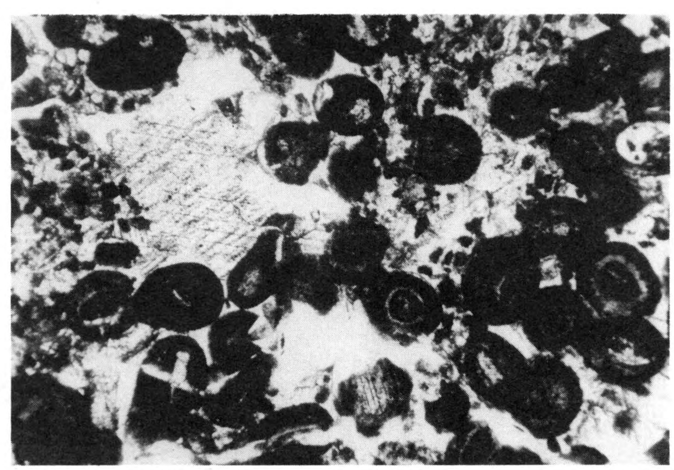

Figure 20. Photomicrograph of oolitic grainstone, lower part of unit 6. Sally Mountain (SL on Fig. 2). Bar scale = 0.5 mm.

grained tempestites, indicates deposition under a regime of energetic currents at shallow, fairly uniform, subtidal, or even partly intertidal, water depths. The most persistent depositional factor appears to have been the system of water currents that may have been produced by some combination of tides, prevailing wind set-up, and wave action. The unusually good preservation of lamination may have been enhanced by development of microbial mats, an idea suggested to us by Jorg Trappe (oral commun., 1991) that would explain the prevalence of the bedding-parallel pores described above and the ubiquitous occurrence in tempestite beds of large shells of snails that were presumably microbial-mat grazers. Other common shelly components of tempestite beds have been transported and redistributed from minor crinoid and solitary-coral build-ups on the shallow subtidal flat.

Unit 7

Unit 7 is characterized by the diffuse, intergradational interstratification of irregularly thick layers of abundantly crinoidal wackestone and packstone that form generally massive or at least poorly bedded outcrops. In addition to crinoid columnals, pellets are abundant in the more matrix-rich layers, and a wide variety of open-marine bioclasts including those of bryozoans, brachiopods, mollusks, etc., are represented. Conspicuous megafossils include isolated specimens of solitary corals, spiriferid brachiopods, and fenestrate bryozoa. Lenticular lag deposits of crinoid-bryozoan grainstone are interstratified in the higher parts of unit 7. In contrast to the underlying rocks of unit 6, large irregularly shaped nodules and bedding-parallel stringers of secondary chert are well developed in unit 7. A complete exposure of unit 7 has not been observed in the southern Lakeside Mountains; its thickness here is estimated at 20-30 m. Conodonts from the top of unit 7 at section B (Fig. 1) are indicative of the Lower *Gnathodus typicus* to middle Upper *typicus* Zones of early Osagean age (sample 5, Appendix A), in agreement with the age assigned by Sandberg and Gutschick (1984) who, however, placed the beds at this level in the basal part of their Delle Phosphatic Member.

Unit 7 is widespread in western Utah. It is equivalent to the upper member of the type Gardison Limestone (Morris and Lovering, 1961) at RR (Fig. 2). Everywhere the distinctive laminated packstones and tempestites of unit 6 occur, they are overlain by limestones having the character of unit 7, although up to 15 m of cross-stratified crinoidal grainstone intervenes between them at some localities. Where in sequence with unit 6, unit 7 mostly ranges from 20-40 m in thickness, the greatest thickness being 60 m at SM (Fig. 2). Beyond the limits of unit 6, at localities such as SR and BM (Fig. 2) in southwest Utah, unit 7 is as much as 15 m thick and overlies shoal-water deposits of crinoidal or oolitic grainstone that laterally replace unit 6.

Unit 7 is an open shelf deposit. It exhibits the activity of a wide variety of organisms and the pervasive effects of scour and current action. This unit is interpreted to be a retrograde blanket over the shallow subtidal or intertidal underlying deposits and to represent gradual transgression over a very low gradient shelf.

In the southern Lakeside Mountains, as well as at other localities where the top of the Gardison has been observed, the upper meter or so of unit 7 has undergone limestone dissolution, compaction, partial replacement by phosphate, and hardground development related to the initiation of the Delle phosphatic event as described in Silberling and Nichols (1991; reproduced in this volume). Rocks deposited during the Delle event, which in the southern Lakeside Mountains belong to the Delle Phosphatic Member of the Woodman Formation, contrast greatly with the underlying limestones of unit 7 and represent an abrupt change in depositional regime on the shelf. Initiation of the Delle event is interpreted to correspond with a relative sea-level maximum. In the jargon of sequence stratigraphy, the Delle event commences with the beginning of deposition of the transgressive systems tract of the stratigraphic sequence for which the Gardison Limestone and its lateral correlatives represent the shelf-margin systems tract.

REGIONAL IMPLICATIONS

The limestones of latest Devonian to Early Mississippian age in the southern Lakeside Mountains are the record on the shelf of three successive cycles of deposition. The regional significance of these depositional cycles and their relationship to regional tectonism, eustatic sea level change, or both, is largely unresolved. Not only is interpretation of the ages and depositional settings of strata that regionally record these cycles still incomplete, but also their post-depositional rearrangement in the eastern Great Basin by contractional and extensional tectonism, though obviously significant, is poorly constrained.

The initiation of cycle I, deposits of which correspond in northwest central Utah to unit 1 as exemplified in the Lakeside Mountains (Fig. 3), represents a flooding event that established open-marine conditions over what had been the Devonian inner shelf. Unit 1—corresponding generally to the Pinyon Peak Limestone — is correlated with younger parts of the Pilot Shale (e.g., Johnson and others, 1991) that extends from eastern Nevada into westernmost Utah (as at LP, GM, CR, BH, and NR on Fig. 1) and with equivalents of the Pilot such as the Leatham Formation on the Paris-Willard thrust plate (as at LH on Fig. 1). The Pilot Shale has been reasonably interpreted by Goebel (1991) as having been deposited in the back-bulge part of the Antler foreland that was characterized by local tectonic instability and variable rates of subsidence. Thus, at least partial control of cycle I deposition by Antler foreland tectonism is a strong possibility. Closer to the part of Utah where unit 1 actually occurs, strata having the age and the character, though secondarily dolomitized, of unit 1 are included in the uppermost part of the orogenic deposits of the Stansbury Formation in the northern Stansbury Mountains (as at FX, Fig. 1) (Trexler, this volume). Again, tectonic control of cycle I deposition is district and to units 3, 4, and 5, and possibly also 2, in the southern Lakeside Mountains (Fig. 3). These carbonate rocks in west-central Utah form a clear-cut record of abrupt transgression over a surface of disconformity followed by progradation, all of which took place during late Kinderhookian time according to available conodont dating. Progradation of open marine shelf-flat limestones by more continentward inner-shelf carbonate rocks at the top of this highstand systems tract was on the order of 100 s of kilometers in a northwesterly direction. Age equivalents of cycle II deposits occur in northwesternmost and northernmost Utah and adjacent states, but their facies and palinspastic relationships to the strata of interest here in west-central Utah have yet to be established. Eustatic sea-level change by itself could have been the primary depositional control on these rocks in Utah.

The deposits of cycle III, the initiation of which is recorded by units 6 and 7 in the Lakeside Mountains (Fig. 3), are particularly instructive with respect to the problem of choosing between eustatic and regional tectonic depositional controls. Units 6 and 7 belong to the shelf-margin systems tract forming the lower part of cycle III. They document the aggradation of the shelf under widespread conditions of more or less constant, shallow subtidal water depth, giving way upward to somewhat deeper, agitated, open shelf deposition. The relative sea-level maximum over this broad shelf on which units 6 and 7 accumulated coincides with initiation of the Delle phosphatic event and anoxic, condensed deposition (Nichols and Silberling, 1990; Silberling and Nichols, 1991). Deposits of the Delle event represent the transgressive systems tract of this sequence cycle. This system tract is then followed by the progradational highstand tract represented in Utah by strata such as those in higher parts of the Deseret Limestone, the similar rocks in the Lakeside Mountains assigned to the Woodman Formation, the lower part of the Humbug Formation, and correlative rocks of the Brazer Dolomite. Maximum progradation and the beginning of the next sequence cycle is recorded within the Humbug Formation in rocks of Late Mississippian age. A much different interpretation of the sedimentary environments and paleogeographic setting of the strata representing cycle III is presented by Sandberg and Gutschick (1984) and Poole and Sandberg (1991).

Strata of cycle III, from the Lakeside Mountains southward and eastward, beginning with the Gardison Limestone (formed of units 6 and 7) and including the younger retrograde deposits of the Delle event and subsequent prograde deposits, form a textbook example of a type-2 stratigraphic sequence (for example, see Van Wagoner and others, 1988, Fig. 4). However, to the west of the Lakeside Mountains in the Leppy Hills (LP on Fig. 2), deposits of the Delle event depositionally overlie a limestone unit that resembles unit 2 and is only about 7 m thick. Conodonts from this unit have been dated as Kinderhookian in age (sample 6, Appendix A). Equivalents of the Gardison Limestone at this locality were evidently either eroded or never deposited owing to tectonic uplift prior to the Delle event. Thus, while the Gardison Limestone (units 6 and 7) was accumulating on the continental shelf, as represented by the section in the southern Lakeside Mountains, more oceanward parts of the shelf were experiencing tectonic activity, possibly related to the development of a foreland bulge (Goebel, 1991). As hypothesized by Silberling and Nichols (1991), such tectonism may have resulted in silling of the shelf, trapping fine-grained siliciclastic sediment that otherwise would have bypassed the shelf and causing the water on the shelf to become stratified and anoxic. The stratigraphic sequence related to cycle III thus may record subsidence in a back-bulge region laterally linked with uplift of a foreland bulge in the pattern predicted by flexural loading models.

REFERENCES CITED

Allmendinger, R.W., et al., 1983, Cenozoic and Mesozoic structure of the eastern Basin and Range province, Utah, from COCORP seismic-reflection data: Geology, v. 11, p. 532-536.

Barnaby, R.J., and Read, J.F., 1990, Carbonate ramp to rimmed shelf evolution: Lower to Middle Cambrian continental margin, Virginia Appalachians: Geological Society of America Bulletin, v. 102, p. 391-404.

Cook, H.E., and Taylor, M.E., 1977, Comparison of continental slope and shelf environments in the Upper Cambrian and lowest Ordovician of Nevada, *in* Cook, H.E., and Enos, Paul, eds., Deep-water carbonate environments: Society of Economic Paleontologists and Mineralogists Special Publication 25, p. 51-81.

Dockal, J.A., 1980, Petrology and sedimentary facies of Redwall Limestone (Mississippian) of Uinta Mountains, Utah and Colorado: Iowa City, University of Iowa, Ph.D. thesis, 440 p.

Dorobek, S.L., and Read, J.F., 1986, Sedimentology and basin evolution of the Siluro-Devonian Helderberg Group, central Appalachians: Journal of Sedimentary Petrology, v. 56, p. 601-613.

Gans, P.B., and Miller, E.L., 1983, Style of mid-Tertiary extension in east-central Nevada: Utah Geological and Mineral Survey Special Studies 59, p. 107-160.

Goebel, K.A., 1991, Paleogeographic setting of Late Devonian to Early Mississippian transition from passive to collisional margin, Antler foreland, eastern Nevada and western Utah, in Cooper, J.D., and Stevens, C.H., eds., Paleozoic paleogeography of the western United States-II: Pacific Section SEPM, v. 67, p. 401-418.

Johnson, J.G., Sandberg, C.A., and Poole, F.G., 1991, Devonian lithofacies of western United States, *in* Cooper, J.D., and Stevens, C.H., eds., Paleozoic paleogeography of the western United States-II: Pacific Section SEPM, v. 67, p. 83-105.

Levy, Marjorie, and Christie-Blick, Nicholas, 1989, Pre-Mesozoic palinspastic reconstruction of the eastern Great Basin (western United States): Science, v. 245, p. 1454-1462.

Lindgren, Waldemar, and Loughlin, G.F., 1919, Geology and ore deposits of the Tintic mining district, Utah: U.S. Geological Survey Professional Paper 107, 282 p.

Miller, D.M., 1990, Mesozoic and Cenozoic tectonic evolution of the northeastern Great Basin, *in* Shaddrick, D.R., Kizis, J.A., Jr., Hunsaker, E.L., III, eds., Geology and ore deposits of the northeastern Great Basin: Reno, Geological Society of Nevada, p. 43-73.

Miller, G.M., 1966, Structure and stratigraphy of southern part of Wah Wah Mountains, southwest Utah: American Association of Petroleum Geologists Bulletin, v. 50, p. 858-900.

Morris, H.T., 1983, Interrelations of thrusts and transcurrent faults in the central Sevier orogenic belt near Leamington, Utah: Geological Society of America Memoir 157, p. 75-81.

Morris, H.T., and Lovering, T.S., 1961, Stratigraphy of the East Tintic Mountains, Utah: U.S. Geological Survey Professional Paper 361, 145 p.

Nichols, K.M., and Silberling, N.J., 1980, Eogenetic dolomitization in the pre-Tertiary of the Great Basin, *in* Zenger, D.J., Dunham, J. B., and Effington, R.L., eds., Concepts and models of dolomitization: Society of Economic Paleontologists and Mineralogists Special Publication 28, p. 237-246.

—, 1989, Shelfal nature of Lower and Middle Mississippian rocks, northwest Utah: Geological Society of America Abstracts with Programs, v. 21, p. 143.

—, 1990, Delle Phosphatic Member: An anomalous phosphatic interval in the Mississippian (Osagean-Meramecian) shelf sequence of central Utah: Geology, v. 18, p. 46-49.

—, 1991, Petrology and depositonal setting of Mississippian rocks associated with an anoxic event at Samak, western Uinta Mountains, Utah: U.S. Geological Survey Bulletin 1787-S, p. S1-S13.

Poole, F.G., and Sandberg, C.A., 1991, Mississippian paleogeography and conodont biostratigraphy of the western United States *in* Cooper, J.D., and Stevens, C.H., eds., Paleozoic paleogeography of the western United States-II: Pacific Section SEPM, v. 67, p. 107-136.

Proctor, P.D., and Clark, D.L., 1956, The Curley limestone—an unusual biostrome in central Utah: Journal of Sedimentary Petrology, v. 26, p. 313-321.

Sandberg, C.A., and Dreesen, Roland, 1984, Late Devonian icriodontid biofacies models and alternate shallow-water conodont zonation: Geological Society of America Special Paper 196, p. 143-178.

Sandberg, C.A., and Gutschick, R.C., 1984, Distribution, microfaunal, and source-rock potential of Mississippian Delle Phosphatic Member of Woodman Formation and equivalents, Utah and adjacent states, *in* Woodward, Jane, Meissner, F.F., and Clayton, J.L., eds., Hydrocarbon source rocks of the Greater Rocky Mountain region: Denver, Colorado, Rocky Mountain Association of Geologists, p. 135-178.

Sandberg, C.A., and Poole, F.G., 1977, Conodont biostratigraphy and depositional complexes of Upper Devonian cratonic-platform and continental-shelf rocks in the western United States, *in* Murphy, M.A., Berry, W.B.N., and Sandberg, C.A., eds., Western North America: Devonian: University of California, Riverside Campus Museum Contribution 4, p. 144-182.

Schneyer, J.D., 1990, Geologic map of the Leppy Peak Quadrangle and adjacent area, Elko County, Nevada, and Tooele County, Utah: U.S. Geological Survey Miscellaneous Investigations Map I-1938, scale 1:24,000.

Silberling, N,J., and Nichols, K.M., 1991, Petrology and regional significance of the Mississippian Delle Phosphatic Member, Lakeside Mountains, northwestern Utah, *in* Cooper, J.D., and Stevens, C.H., eds., Paleozoic paleogeography of the western United States-II: Pacific Section SEPM, v. 67, p. 425-438.

Trexler, J.H., Jr., 1992, The Stansbury Formation at Stansbury Island and the northeastern Stansbury Mountains: this volume.

Van Wagoner, J.C., Posamentier, R.M., Mitchum, R.M., Vail, P.R., Sarg, J.F., Loutit, T.S., and Hardenbol, J, 1988, An overview of the fundamentals of sequence stratigraphy and key definitions, *in* Wilgus, C.K., et al., eds., Sea-level changes: an Integrated approach: society of Economic Paleontologists and Mineralogists Special Publication 42, p. 39-45.

Villien, Alain, 1984, Central Utah deformation belt: Boulder, University of Colorado, Ph.D. thesis, 283 p.

Wilson, J.L., 1969, Microfacies and sedimentary structures in "deeper water" lime mudstones, *in* Friedman, G.M., ed., Depositional environments in carbonate rocks: Society of Economic Paleontologists and Mineralogists Special Publication 14, p. 4-19.

Young, J.C., 1955, Geology of the southern Lakeside Mountains, Utah: Utah Geological and Mineralogical Survey, Bulletin 56, 110 p.

APPENDIX A: Identification and Age Interpretations of Conodont Faunas

by R.G. Stamm, U.S. Geological Survey

[Conodonts from the samples listed below are deposited in the conodont reference collections of the Paleontology and Stratigraphy Branch, U.S. Geological Survey, National Center, Reston, Virginia, 22092]

Sample 1. Field no. 90-S-241 (USGS colln. 12198-SD). Impure, sparsely crinoidal, nodular limestone in lower part of Pinyon Peak Limestone, section A, Figs 1 and 3, southern Lakeside Mountains. Initial Wt. 4.74 kg.
Polygnathus experplexus Sandberg & Ziegler, 2 Pa elements
P. semicostatus Branson & Mehl, 27 Pa
Palmatolepis rugosa rugosa Branson & Mehl, 2 Pa
Bispathodus stabilis Branson & Mehl, 7 Pa
Mehlina? stigosa (Branson & Mehl), 4 Pa
Apatognathus varians varians Branson & Mehl, 24 unassigned elements
A. v. klapperi Druce, 88 unassigned elements
Icriodid simple cones, 10
Age: late Famennian (Lower *Palmatolepis expansa* Zone).

Sample 2. Field no. 90-S-832 (USGS colln. 12199-SD). Dolomitized, Pinyon Peak Limestone-like beds in uppermost part of Stansbury Formation, spur north of Flux Canyon, northern Stansbury Mountains. See Figure 3 of Road Log, this volume. Initial Wt. 8.12 kg.
Polygnathus experplexus Sandberg & Ziegler, 56 Pa
P. semicostatus Branson & Mehl, 104 Pa
P. semicostatus Branson & Mehl, morphotype 2, 29 Pa
P. extralobatus Schafer, 6 Pa
P. perplexus Thomas, 1 Pa
P. granulosa Branson & Mehl, 1 Pa
P. sp. Four Pa elements with morphologic characteristics of the *"P. nodocostatus Group"* of Famennian age.
Palmatolepis rugosa rugosa Branson & Mehl, 3 Pa
Bispathodus stabilis Branson & Mehl, 87 Pa
Icriodus costatus (Thomas), 6 Pa, 15 cones
Mehlina? sp.6 Pa
Branmetila sp.?, 4 Pa
Apatognathus varians varians Branson & Mehl, 11 Pb, 79 S elements
A. v. klapperi Druce, 39 S elements
Age: late Famennian (middle Lower *expansa* to middle Middle *expansa* Zones).

Sample 3. Field no. 90-S-834 (USGS colln. 31274-PC). Dolomitized, thin-bedded crinoidal limestone interlayered with chert in lower part of Fitchville Formation (as exposed), spur north of Flux Canyon, northern Stansbury Mountains. See Figure 3 of Road Log, this volume. Initial Wt. 5.16 kg.
Siphonodella quadruplicata (Branson & Mehl)
S. crenulata (Cooper), 1 Pa
S. cooperi Hass, morphotype 2
S. obsoleta Hass
Polygnathus longipostica Branson & Mehl, 24 Pa
P. triangulata Voges, 3 Pa
P. communis Branson & Mehl, 47 Pa
P. inornata Branson & Mehl, 12 Pa
Bispathodus stabilis (Branson & Mehl), 27 Pa
Pseudopolygnathus cf. *P. fusiformis* Branson & Mehl, 2 Pa
Hindeodus sp. (Branson & Mehl), 5 Pa
Branmetila inornata (Branson & Mehl), 1 Pa
Age: late Kinderhookian (Lower *Siphonodella crenulata* to Middle *Siphonodella isosticha*-Upper *crenulata* Zones).

Sample 4. Field no. 90-S-251 (USGS colln. 31275-PC). 2.5 m above base of Gardison Limestone, section A, Figs 1 and 3, southern Lakeside Mountains. Initial Wt. 5.44 kg.
Patrognathus andersoni Klapper, 16 Pa
Siphonodella cf. *S. isosticha* (Cooper), 4 juvenile Pa, 9 ramiform elements
Bispathodus stabilis (Branson & Mehl), 4 Pa
Hindeodus sp., 13 Pa, 1 Pb, 1 Sa, 1 Sb, 3 Sc
Kladognathus sp., 18 M, 5 Sa, 23 Sc Age: late Kinderhookian (Lower *crenulata* and *isosticha*-Upper *crenulata* Zones).

Sample 5. Field no. 88-N-62 (USGS colln. 31276-PC). 25 cm below top of highest coherent limestone of Gardison Limestone, (level 1 on Fig. 1 of Silberling and Nichols, 1991), section B, Figures 1 and 3, southern Lakeside Mountains.
Bispathodus utahensis Sandberg & Gutschick, 3 Pa
Gnathodus cf. *G. typicus* Cooper, 1 juvenile Pa element of morphotype 1 (Lane, Sandberg, & Ziegler).
Bactrognathus sp., various elements
Age: early to middle Osagean (Lower *Gnathodus typicus* to *Scaliognathus anchoralis-Dolignathus latus* Zones)

Sample 6. Field no. 90-S-152 (USGS colln. 31277-PC). Current-layered crinoidal grainstone/packstone 0.5-1.0 m below replacement chert at top of "Joana Limestone" of Schneyer (1990) A-1 Canyon, Leppy Hills, Nevada (LP on Fig. 2). Initial Wt 7.10 kg.
?Patrognathus andersoni Klapper, 3 Pa
Polygnathus inornatus Branson, 2 Pa
P. cf. *P. lacinatus* Huddle, 1 juvenile Pa
Hindeodus cf. *H. crassidentatus* (Branson & Mehl), 8 Pa, 2 Sb, 1 Sb, 1 Sc.
Age: late Kinderhookian (Lower *crenulata* and Upper *crenulata-isosticha* Zones).

PETROLOGY AND REGIONAL SIGNIFICANCE OF THE MISSISSIPPIAN DELLE PHOSPHATIC MEMBER, LAKESIDE MOUNTAINS, NORTHWESTERN UTAH

N.J. Silberling and K.M. Nichols
U.S. Geological Survey, Denver, Colorado 80225

ABSTRACT

Phosphatic rocks are a distinctive part of the mid-Mississippian rock record in northwestern Utah and are particularly significant because of their influence on interpretations about the paleogeography and depositional framework of this part of the Paleozoic section. These rocks have been incorporated in the Delle Phosphatic Member, which at its type section in the Lakeside Mountains, northwestern Utah, is about 60 m thick and is tentatively regarded as the basal member of the Woodman Formation. Deposition of the Delle Phosphatic Member was initiated by an abrupt anoxic event, herein referred to as the "Delle phosphatic event (DPE)" of Silberling and Nichols (1990). Regionally, the boundary marking the onset of the DPE is characterized by corrosion and dissolution of pre-existing limestone and represents an interruption in deposition. The typical Delle Phosphatic Member and the rocks deposited during the DPE throughout western Utah are characterized by the absence of benthic shelly fossils, by the dissolution and chert replacement of limestone, by the occurrence of pelletal, pisolitic and oolitic phosphorite, and by megascopically unfossiliferous, distinctive massive lime mudstone. Deposits of the DPE, which in their more eastern occurrences are only a few meters thick, are sandwiched within thick sequences of normal-marine subtidal and peritidal Mississippian shelf-carbonate and craton-derived siliciclastic rocks. Endolithic algal boring of phosphorite layers in the Delle Phosphatic Member, the absence of sedimentary features characteristic of slope environments, and the stratigraphic context of the DPE indicate a shelf setting for rocks deposited during the DPE. Initiation of the DPE resulted from flooding of the Early Mississippian carbonate shelf by nutrient-rich, organically productive water and coincided with the appearance on the shelf of fine-grained, craton-derived, siliciclastic sediment dispersed by a shelf-wide current system. As an hypothesis, the unusual shelf waters may have been derived from upwelling in the Antler foredeep in central Nevada, and restriction and stratification of shelf waters may have resulted from silling of the shelf by the foreland bulge that would have been a consequence of foreland basin development. Deposition of the typical Delle Phosphatic Member and the onset of the DPE is thus viewed as a modification of the Mississippian shelf and not the result of a deep marine basin existing in central Utah as required by the "Deseret deep starved basin" model of the previous authors.

INTRODUCTION

Occurrence of phosphatic rocks has long been known within the Mississippian section at various localities in northwestern Utah (Cheney, 1957; Morris and Lovering, 1961; Schell and Moore, 1970; Gutschick, 1976). These and associated rocks that reflect anoxic deposition are anomalous with respect to the thick, laterally variable sequence of normal subtidal to peritidal shelf carbonate rocks that stratigraphically underlie them, as well as to the thick sequence of peritidal carbonate and/or craton-derived siliciclastic rocks that overlie them. The Delle Phosphatic Member was established by Sandberg and Gutschick (1984) to include these phosphatic rocks which were regarded as being characteristic of their "Deseret deep starved basin." The typical Delle Phosphatic Member in the Lakeside Mountains, Utah, was interpreted as the basal member of the Woodman Formation, and the unit was extended by Sandberg and Gutschick (1984), over a wide area of western Utah, northeastern Nevada, and southeastern and central Idaho as the basal member of several different Mississippian formations. However, away from the vicinity of its type section in the Lakeside Mountains, we cannot recognize the top of the Delle Phosphatic Member using a consistent set of lithic criteria. Consequently, for the purpose of regional discussion we find it more useful to treat the rocks in question as those affected by an abrupt, widespread anoxic depositional event, which initiated deposition of the Delle Phosphatic Member in the Lakeside Mountains. This anoxic event caused diagenetic alteration of pre-existing carbonate rocks. Its effect on deposition diminishes up section in varying ways at different places. The term "Delle phosphatic event (DPE)" was applied by Silberling and Nichols (1990) to this particular phenomenon and is used herein in the same sense.

Rocks deposited during the DPE, even where relatively thin, are of particular interest not only because of their peculiar depositional and diagenetic history, but also because they form the basis for inferences about economically important paleogeographic features such as the nature and location of the Mississippian shelf margin. Furthermore, assumptions by previous workers about depositional environments during the DPE and conjecture about the sedimentology of the postulated "Deseret deep starved basin" have significantly influenced interpretations of regional Mississippian facies and ostracode biofacies, and the paleotectonic history of Utah, Nevada, and Idaho (Rose, 1976; Sando and others, 1976; Poole and Sandberg, 1977; Sandberg and Gutschick, 1977, 1979, 1980, 1984, 1989; Gutschick and others, 1980; Lane and others, 1980; Sandberg and others, 1980; Sando and others, 1981; Sandberg and others, 1982; DeCelles and Gutschick, 1983; Gutschick and Sandberg, 1983; Poole and Claypool, 1984; Gutschick, 1987; Sohn and Sando, 1987.

Throughout northwestern Utah, rocks deposited during the DPE are characterized by the absence of normal marine shelf benthic fossils, the occurrence of pelletal, pisolitic, or oolitic phosphorite, stratigraphically isolated massive beds or units of a distinctive, megascopically unfossiliferous, ostracode-bearing lime mudstone, the rare occurrence of pelagic goniatites and radiolarians, and the pervasive dissolution and replacement by silica of limestones other than those of the ostracode lime mudstone. According to Sandberg and Gutschick (1984), the rocks immediately older than the DPE lie within the *Gnathodus typicus* conodont zone (Osagean), and this is permissibly confirmed by our conodont collections as interpreted by B.R. Wardlaw (written commun., 1990). These rocks are thus evidently about the same age everywhere the DPE is recognized.

Exposures in the Lakeside Mountains that include the type section of the Delle Phosphatic Member were chosen for detailed sedimentologic and petrographic study, the results of which serve to constrain depositional and paleotectonic interpretations of the anomalous Delle interval. In the type section, which is easily accessible, pelletal, pisolitic, and oolitic phosphorite and associated rock types occur at more stratigraphic levels and through a greater thickness and variety of rocks than in other expressions of the DPE in the region.

The stratigraphic nomenclature we use in the Lakeside Mountains (Fig. 1) is shown on Figure 2. Rocks beneath the type section of the Delle Phosphatic Member in the Lakeside Mountains were assigned by Sandberg and Gutschick (1984) to the Lodgepole Limestone, but are here reassigned to the Gardison Limestone, as explained below in the discussion of this unit. The type Delle was interpreted as the the lower member of the Woodman Formation, and strata immediately overlying the type Delle were interpreted as the Needle Siltstone Member of the Woodman Formation by Sandberg and Gutschick (1984). We do not endorse applying the concept of the Needle Siltstone Member in the Lakeside Mountains for reasons explained below.

In our map of the type area of Delle (Fig. 1B), we choose to follow Hintze (1988) and to include in the Humbug Formation the sandstones that occur above both the Delle and its superjacent unit of fine-grained clastic rocks. Thus, the Delle and the superadjacent fine-grained clastic unit (the "Needle" of Sandberg and Gutschick, 1984, fig. 6) overlie the Gardison Limestone and underlie the Humbug Formation. These rocks occupy the stratigraphic position of the Deseret Limestone in sections farther south and east in Utah, and in the Lakeside Mountains they have been assigned to the Deseret by previous workers (e.g., Hintze, 1988). However, the Deseret is predominantly limestone (Gilluly, 1932; Morris and Lovering, 1961), whereas this interval in the Lakeside Mountains is mainly siliciclastic. Despite the lack of a complete type section of the Woodman Formation in the structurally disrupted Gold Hill area (G on Fig. 1A) of western Utah (Nolan, 1935; Robinson, in press), the lower part of the type Woodman is predominantly plane-bed laminated, carbonate-cemented siltstone and fine-grained sandstone, and it has a weak expression of the DPE at its base. Therefore, we provisionally follow Sandberg and Gutschick (1984) in retaining both the type Delle and the overlying fine-grained clastic unit in the Woodman Formation. However, recognition of the Needle Siltstone Member, a name introduced in an unpublished Ph.D. thesis by Sadlick (1965) for the basal member of the Chainman Shale in the Confusion Range of west-central Utah (C on Fig. 1A), as a member of the Woodman Formation in the Lakeside Mountains and the Gold Hill area, as advocated by Sandberg and Gutschick (1984, fig. 6), would require a more complete knowledge of the lateral continuity of these rocks than presently exists.

Much useful stratigraphic and geochemical data have been provided for the Delle Phosphatic Member in the Lakeside Mountains by Sandberg and Gutschick (1984). However, our interpretation of the petrology and depositional environment of the Delle Phosphatic Member in this expanded and more fully documented version of Nichols

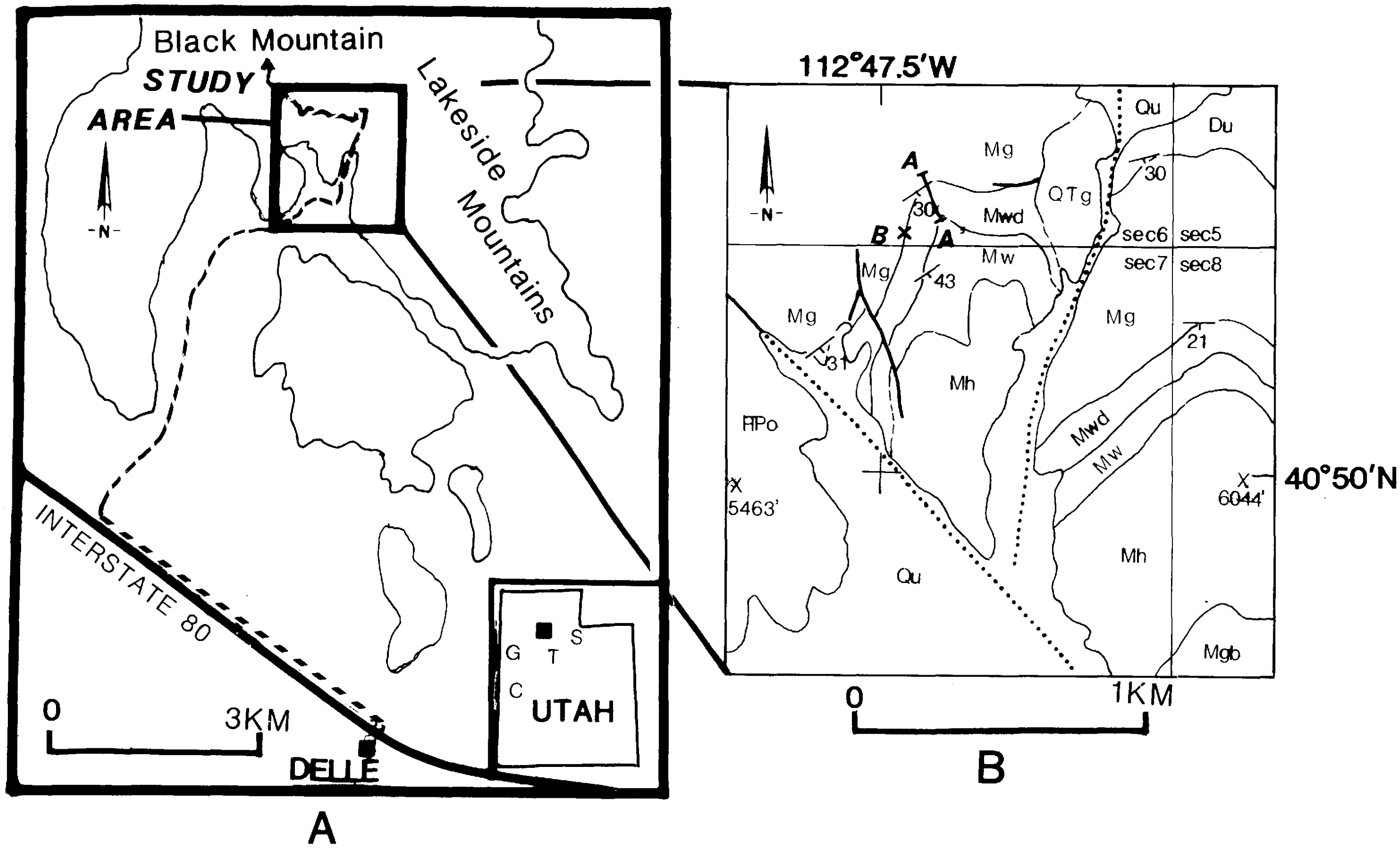

Figure 1A and B. A: Location of study area in southern Lakeside Mountains, Utah. C, Confusion Range; G, Gold Hill area; S, Samak area; T, East Tintic Mountains. B: Geologic map of type area of Delle Phosphatic Member of the Woodman Formation, T.1 N., R.8 W. Qu, Quaternary deposits, undifferentiated; QTg, Quaternary or Tertiary gravel; PPo, Permian and Pennsylvanian Oquirrh Formation; Mgb, Mississippian Great Blue Limestone; Mh, Mississippian Humbug Formation; MW, Mississippian Woodman Formation; Mwd, Mississippian Delle Phosphatic Member of Woodman Formation; Mg, Mississippian Gardison Limestone; Du, Devonian, undifferentiated. A-A', Type section of Delle Phosphatic Member; B, location of trenched section. Base from Delle, Utah 7.5' quadrangle.

and Silberling (1990; in press a) differs from that proposed by them and indicates a much different mid-Mississippian (Osagean-Meramecian) paleogeography.

PETROLOGIC OBSERVATIONS

Gardison Limestone

In the Lakeside Mountains the Delle Phosphatic Member of the Woodman Formation overlies about 115 m of carbonate rocks assigned to the Gardison Limestone. In the section that includes the type Delle (line A-A', Fig. 1B), the Gardison is cut by low-angle, bedding-plane faults along which some strata may have been omitted about 30 m below the base of the Delle (Fig. 2). Massive, secondary dolomite obliterates 10-12 m of the limestone above this fault zone. Below the fault zone is a thick sequence of regularly thin- to medium-parted, fecal-pelleted lime packstone, much of which exhibits pronounced planar lamination (Fig. 3A). Partly graded, discontinuous interbeds as thick as 10 cm and composed of crinoidal, coralline, and shelly debris occur at 0.2- to several-meter-thick intervals in the laminated lime packstone sequence and are interpreted as storm deposits or tempestites (Fig. 3B). Only the uppermost 10 m of this sequence is shown on the columnar section (Fig. 2). The total thickness of the Gardison Limestone in the Lakeside Mountains is about 85 m, and it is the same widespread unit that forms most of the 115 m-thick lower member of the Gardison Limestone (Morris and Lovering, 1961) at its type section in the East Tintic Mountains, Utah (T on Fig. 1A). The pelleted fabric, pervasive lime-packstone, current lamination, and above wave base, tempestite layers in this unit are features characteristic of mid-shelf environments (e.g., Enos, 1983).

In the section that includes the type Delle, the uppermost unit of the Gardison, beginning above the secondary dolomite of the fault zone and about 18 m below the top of the Gardison, is massive, pelleted, crinoidal lime wackestone grading upward into bioturbated, diffusely interstratified, fecal-pelleted lime wackestone and packstone (Fig. 4). These rocks contain an abundance of crinoid columnals and other bioclasts, including a few solitary corals and brachiopod shells, and conspicuous bedding-parallel stringers and nodules of secondary chert. This normal marine, cherty, diffusely interbedded wackestone and packstone unit, which

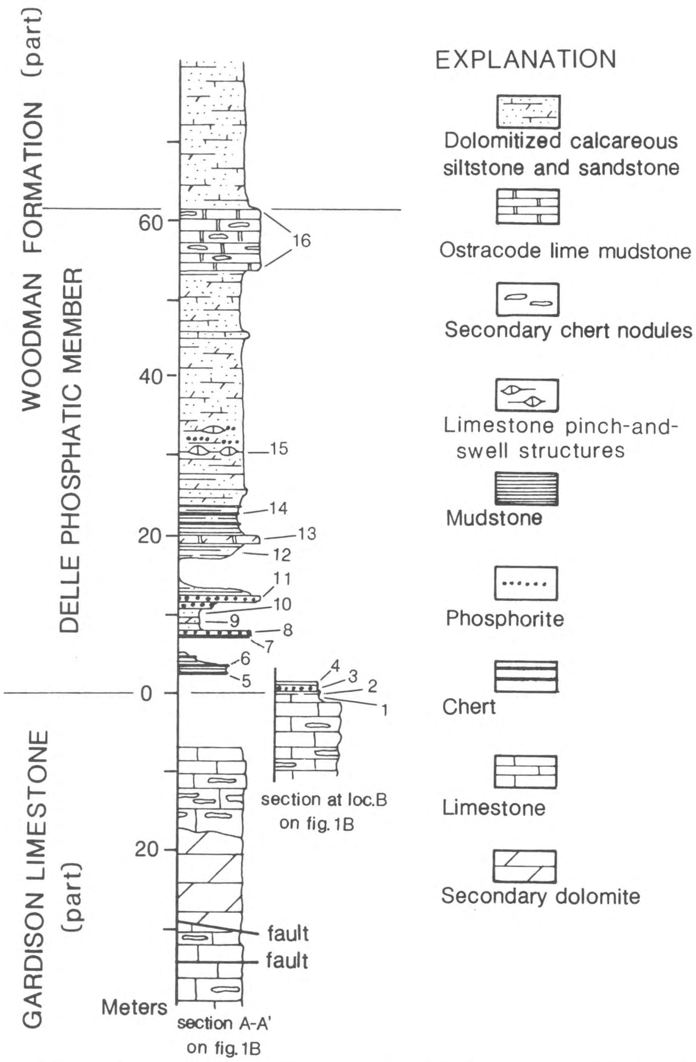

Figure 2. Generalized stratigraphy of type Delle Phosphatic Member of the Woodman Formation and adjoining strata, Lakeside Mountains. Numbers label stratigraphic levels discussed in text.

is no thicker than about 30 m in the Lakeside Mountains, corresponds lithically with the upper member of the typical Gardison Limestone (Morris and Lovering, 1961) which is about 35 m thick in the East Tintic Mountains.

In section A-A' (Fig. lB), which is along a ridge crest, the upper 7-8 m of this wackestone-packstone unit is not exposed, but it can be observed in the gully leading south downhill from the base of the Delle type section. Trenching, as at locality B (Fig. lB), is required to expose the actual contact between the Gardison and the Delle. Here, the uppermost 10-20 cm of the Gardison Limestone (level 1, Fig. 2) is blotched, red-stained, solution-compacted fecal-pelleted, bioclastic wackestone (Fig. 5). Phosphate is present in this rock both as replacement bodies within the remaining limestone matrix and as void fillings within the pores of crinoid columnals, bryozoans, and other bioclasts. This partly dissolved, compacted limestone is the "deep-water winnowed encrinite" of Sandberg and Gutschick (1984, p. 140, 142). Immediately above the highest coherent limestone of the Gardison (level 1), and exposed by trenching at locality B, is 0.5 m of punky, red, dissolution-compacted, microcrystalline quartz and illitic clay (level 2) containing scattered, partially dissolved, calcitic bioclasts similar in kind to those of the immediately underlying limestone. Above this residuum is a 40-cm-thick resistant level (level 3) composed of silicified limestone nodules that appear to be dissolution remnants in a matrix of laminated, siliceous mudstone and pelleted phosphorite. Features interpreted as burrow cavities as wide as several millimeters in the secondarily silicified nodules are infilled by phosphate pellets (Fig. 6). The stratigraphically lowest occurrence of detrital phosphate pellets (level 3, Fig. 2) and the base of the Delle Phosphatic Member are thus associated with carbonate dissolution and apparent burrowing. The pelletal phosphorite that marks the beginning of the "DPE" elsewhere in central and western Utah commonly either fills complexly pinnacled solution cavities in the underlying limestone (Fig. 7)

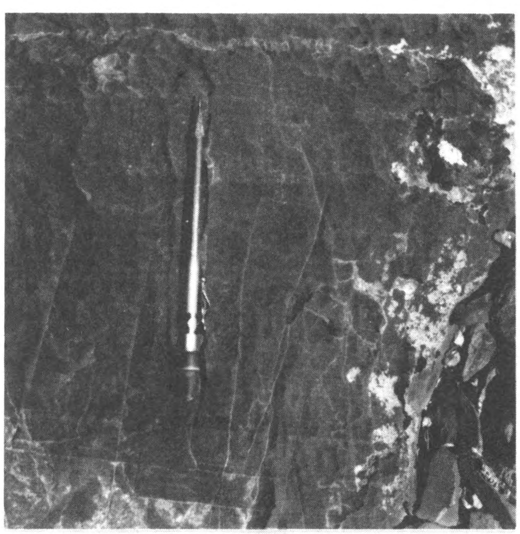
A

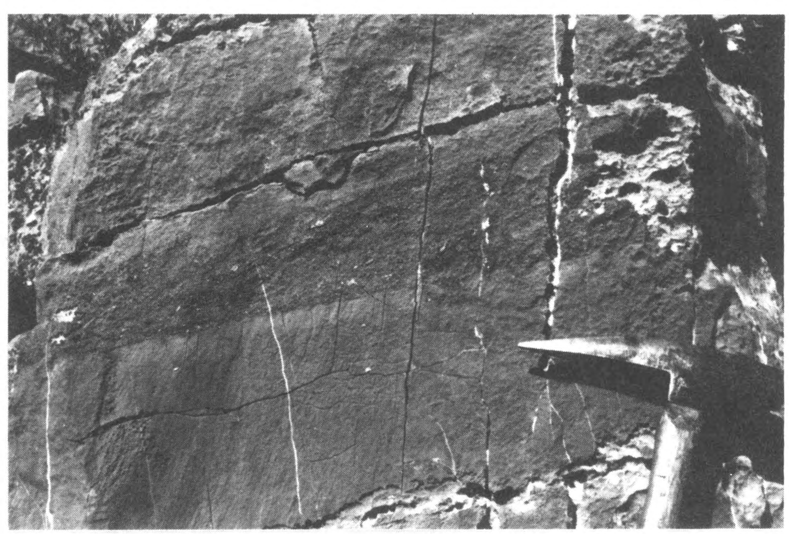
B

Figure 3A and B. A: Laminated fecal(?)-pellet packstone from same part of section as Figure 3B, but from east side of Lakeside Mountains. B: Example of a tidal-flat storm deposit or tempestite within lime mudstone in the upper part of the Gardison Limestone underlying type section of the Delle Phosphatic Member, Lakeside Mountains.

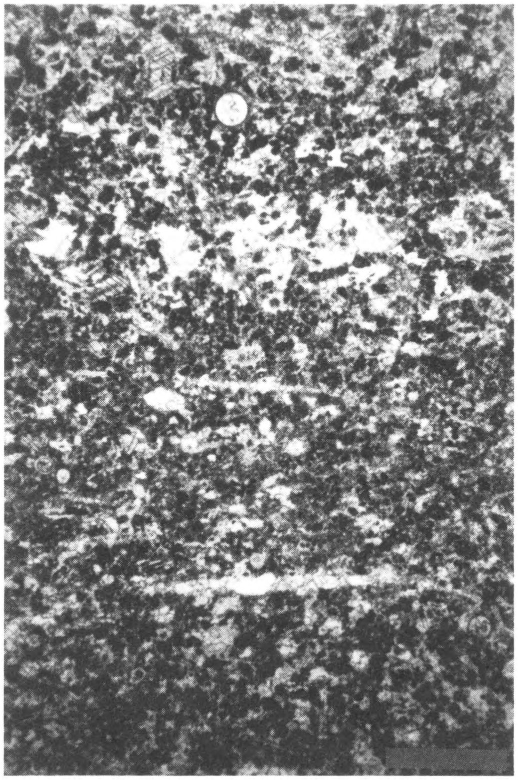

Figure 4. Photomicrograph of fecal(?)-pellet, crinoidal packstone 8 m below the top of the Gardison Limestone underlying type section of the Delle Phosphatic Member, Lakeside Mountains. Scale bar = 0.2 mm.

Figure 5. Photomicrograph of strongly solution-compacted, partly phosphatic, fecal(?)-pellet, crinoidal wackestone from the top of the Gardison Limestone immediately underlying type section of the Delle Phosphatic Member at locality B (Fig. lB), Lakeside Mountains. Scale bar = 0.2 mm.

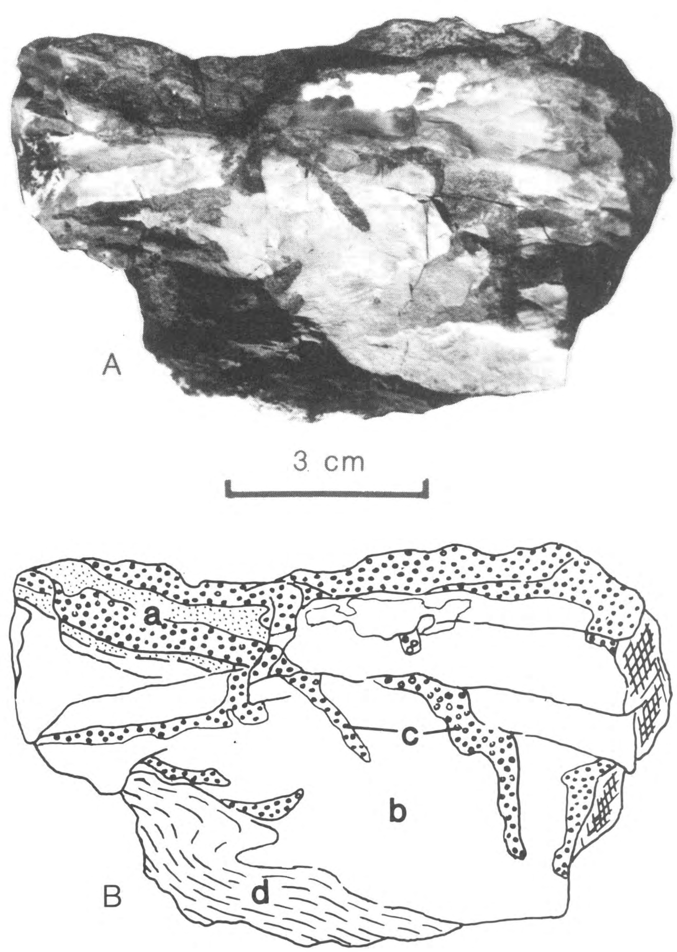

Figure 6A and B. A: Cross-sectional surface of remnant silicified limestone nodule from level 3 (Fig. 2) at contact between Gardison Limestone and Delle Phosphatic Member at locality B (Fig. lB), Lakeside Mountains. B: Sketch of Figure 6A showing scale; laminated pelletal phosphorite and siliceous mudstone (a); dense, silicified limestone (b); burrows in silicified limestone filled with pelletal phosphorite (c); red, quartz-illite, limestone-solution residuum (d).

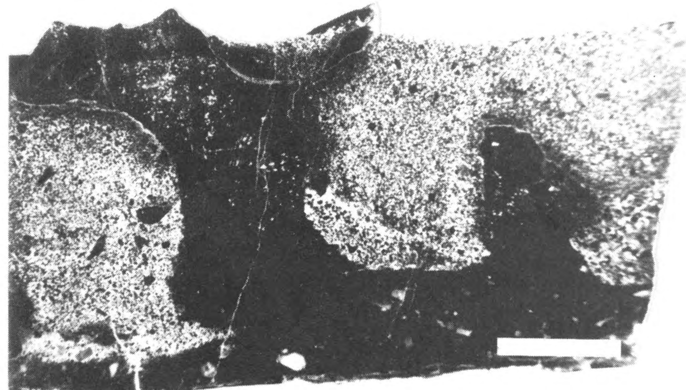

Figure 7. Slabbed cross-sectional surface showing contact between rocks formed during the DPE and underlying limestone assigned to Gardison Limestone by Bromfield and others (1970), central Wasatch Mountains, Utah, about 120 km east-southeast of the study area in Lakeside Mountains. Complex, pinnacled relief on the surface of underlying crinoidal packstone filled by detrital phosphatic ooids, peloids, and bioclast (mainly ossicle) replacements. Scale bar = 2 cm.

(Sandberg and Gutschick, 1984, plate 1B) or is associated with a layer of insolubles as much as a meter in thickness produced by dissolution of the underlying limestone. Dissolution of limestone at the onset of the DPE was thus regionally widespread. Conodonts, along with other insolubles such as inorganic phosphate grains, have been concentrated by carbonate dissolution in the limestones immediately underlying rocks of the DPE. This high yield of conodonts has been interpreted as evidence for basinal or slope depositional environments (Lane and others, 1980, p. 125; Sandberg and Gutschick, 1979, p. 130), whereas it is more likely the result of concentration by limestone dissolution and compaction.

Delle Phosphatic Member

Natural exposures of the lower 20 m of the type Delle Phosphatic Member, below level 13 (Fig. 2) are poor, but this part of the section is a heterogeneous succession of diagenetically reconstituted rocks characterized by phosphorite and by replacement silica and dolomite associated with mudstone and siltstone.

In the trenched section at locality B (Fig. 1B), four thin, indurated layers of pale-yellowish-brown, phosphatic, siliceous mudstone or impure chert occur in the otherwise punky, deeply weathered material that characterizes the basal 1.0 m of the Delle above level 3 that is regarded as the basal bed of the Delle. In a particularly cherty layer (level 4) bands of scattered, round or ellipical voids as much as 200 microns in diameter may represent the former presence of calcified radiolarians. Phosphate grains occur in these layers as flattened pellets.

In the type section of the Delle (A-A′ on Fig. 1B), fresh exposures beginning about 0. 5 m stratigraphically higher than level 4 were created in late 1989 or early 1990 by bulldozing for road gravel along the road leading to the radio towers on top of Black Mountain. In the stratigraphic position of levels 5 and 6, which were originally exposed in a low road cut, about 3.0 m of completely exposed section could be observed in the summer of 1990. These beds consist of pale and moderate yellowish-brown, siliceous, more or less silty mudstone with subordinate interbeds, 2-10 cm thick, of black, phosphatic, chert bearing scattered radiolarians. Thirteen of these thin chert layers occur in a stratigraphic thickness of 2.8 m. The black phosphatic cherts at this level, and higher in the section, as at levels 7 and 14, have a distinctive solution-compacted fabric of laterally discontinuous, lenticular and sinuously flattened grains of internally featureless phosphate, along with sparse silica-filled and recrystallized radiolarians, enveloped in microcrystalline silica. These rocks are interpreted to have been relatively pure, sparsely radiolarian and spiculitic, limestone beds, probably lime mudstones, that first were partially replaced by phosphate in pelletal form and then underwent solution compaction prior to or during silicification. Laminae of uncompacted, phosphate pellets in grain-to-grain contact occur within some of these cherts (Fig. 8) and support the interpretation that the flattened fabric was produced by dissolution of a limestone matrix in parts of the rock where scattered pellets were originally matrix supported. Thus, rather than being primary biogenic siliceous rocks, or "lydites" as they were called by Sandberg and Gutschick (1984, p. 143), we interpret these black, phosphatic, chert beds to be secondary replacements of limestones that originally contained some siliceous bioclasts such as radiolarians.

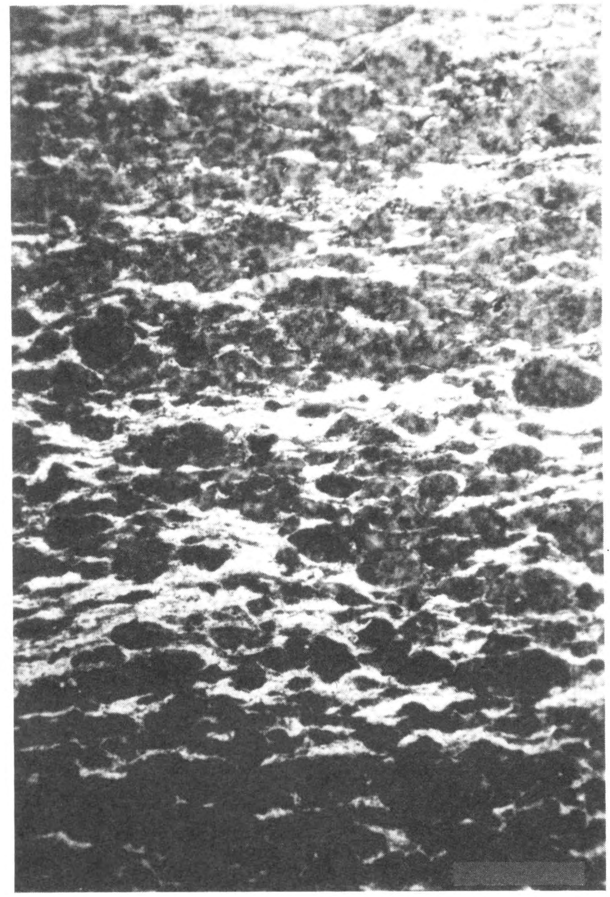

Figure 8. Photomicrograph showing flattened phosphate pellets in solution-compacted secondary chert (light areas), Delle Phosphatic Member, level 14 (Fig. 2). Note less-compacted fabric of phosphate pellets in more grain-supported layer in lower part of view. Scale bar = 0.2 mm.

Above the exposures near the road, in the lower part of the type Delle, the next 17 m of the Delle is poorly exposed up to level 13 (Fig. 2). Relatively resistant rock types that crop out within this poorly exposed lower Delle interval represent less than 20 percent of the section and are: (1) black, phosphatic-chert replacement of limestone (for example, level 7), (2) black, pelletal, pisolitic, and oolitic phosphorite in conspicuous beds as thick as 10 cm (levels 8 and 11), (3) yellowish-brown, illitic, siliceous mudstone and impure secondary chert (for example, at level 10), and (4) dolomitized, calcareous, siliciclastic mudstone and silty limestone (levels 9 and 12). More than a decimeter of vivid red-weathering mudstone or shale overlies the phosphorite bed of level 11, and another red-weathering zone overlies a phosphatic chert bed exposed by recent bulldozing between levels 11 and 12. A few fragments of thin-shelled brachiopods were found in siltstones of level 12 and are the stratigraphically lowest megafossils observed in the Delle section. Authigenic ammonium feldspar, or buddingtonite (Fig. 9; x-ray diffraction identification by R.M. Pollastro, oral commun., 1988), occurs in phosphatic, cherty, and dolomitized beds at several levels (levels 3, 4, 5, 9) (Fig. 9) and is associated with pseudomorphs after framboidal iron sulfide in level 9. Both buddingtonite and framboidal iron sulfide indicate strongly reducing in-sediment conditions. In contrast to these diagenetically anomalous rocks, a conspicuous and laterally persistent 0.6-m-thick unit of evenly bedded, partly dolomitic, megascopically unfossiliferous lime mudstone occurs at level 13. Lithologically this limestone at level 13 is like the ostracode lime mudstone that forms the limestone unit (level 16) at the top of the type Delle.

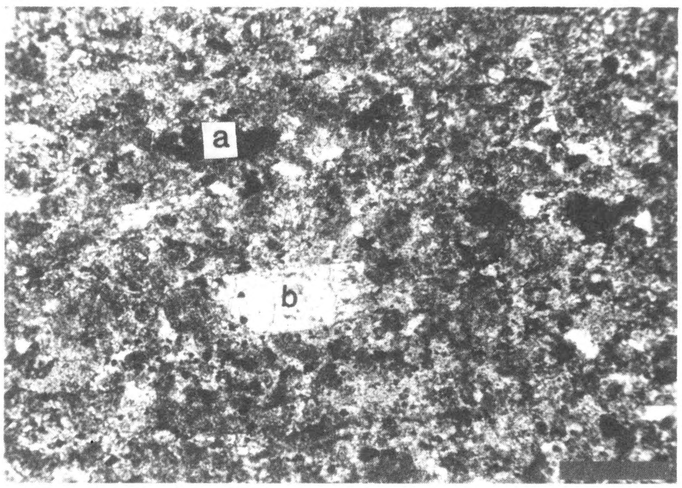

Figure 9. Photomicrograph of dolomitized calcareous mudstone, Delle Phosphatic Member, level 9 (Fig. 2). Framboidal ferric oxides after pyrite (a); authigenic ammonium feldspar or buddingtonite (b). Scale bar = 0.2 mm.

Conspicuous, well-indurated, laterally discontinuous beds of pelletal and oolitic phosphorite occur at levels 8 and 11 (Fig. 2) in the lower part of the Delle. Phosphate grains are closely packed in these rocks, which have little or no matrix; the pore space between the phosphate grains is filled with large, commonly cloudy, poikilitic calcite crystals that are in optical continuity from void to void. Laterally within single beds, and from bed to bed, the character of the phosphate grains and the manner in which they are aggregated changes among three different types. These are: (1) pelletal, phosphatic crust composed of closely packed aggregates of internally featureless phosphate pellets cemented by an isopachous, delicately lamellar, phosphate cement (Fig. 10); (2) pisolitic phosphorite composed of poorly size-sorted aggregates of concentrically coated phosphate grains (Fig. 11); and (3) detrital aggregates of ooidal and other kinds of phosphate grains most likely formed by erosion and reworking of the pisolitic phosphorite (Fig. 12). Any one of these three types can constitute an entire bed as thick as 10 cm.

Within the pisolitic phosphorite of level 11 the grain size of pisoids tends to decrease both stratigraphically upward and downward, bordering irregular layers of dense, black phosphorite a few millimeters thick. These massive layers, or crusts, are reworked into oolitic detrital beds as solid lumps as large as 2 cm. The pisolitic and pelletal-crust phosphorite occurring in the lower Delle resembles that described by Southgate (1986) from the Cambrian of Australia and interpreted by him as phoscrete formed in the surficial sediment on semi-emergent flats associated with an epeiric marine basin. In further support of a phoscrete origin for some of the phosphorites in the Delle, particularly that at level 11, are well developed endolithic algal borings (Figs. 13 and 14) in both the pisolitic and detrital oolitic phosphorite. These borings range from 10-20 microns in diameter and are as long as a few hundred microns. In size and configuration they are virtually identical to borings in carbonate substrates by modern blue-green algae such as *Hyella* (Golubic, 1969; Budd and Perkins, 1980). They are both too large and of the wrong shape to be fungal borings, and they lack the verrucose surface texture indicative of sponge borings. In modern marine environments, living blue-green algae, such as *Hyella*, are restricted to the upper photic zone (intertidal to about 20 m water depth) (Budd and Perkins, 1980). In the Delle these borings are at least indicative of water depths within the zone of light penetration. Microbial boring in the phosphorite of the Delle took place after authigenic quartz euhedra had grown in some grain interiors (Figs. 13 and 14), strongly indicating that diagenesis of the phosphorite and possibly the dissolution of its probable original lime-mud matrix preceeded exposure at the sediment surface and algal infestation. The complexly interwoven pattern of algal borings in the phosphorite of level 11 are filled with the same single-crystal poikilitic calcite cement that fills the intergranular areas.

The upper two-thirds of the Delle type section, between levels 13 and 16, is mainly yellowish-brown-weathering, plane-bed laminated, and secondarily dolomitized, calcareous siltstone and fine-grained sandstone along with subordinate mudstone and silty secondary dolomite. Marine benthic fossils, such as bryozoans, occur sparsely at a few levels. In addition to quartz, these clastic rocks contain detrital mica, K-feldspar and plagioclase, indicating their derivation from the craton, not from the Roberts Mountains allochthon, as argued by previous authors (Sandberg and Gutschick, 1984, p. 143). Other rock types in the lower 25 m of this interval are black, phosphatic, replacement chert (at and near level 14), and laminae of phosphate pellets associated with limestone pinch-and-swell structures (as at level 15).

The limestone pinch-and-swell structures were regarded as concretions by Sandberg and Gutschick (1984) but appear instead to have resulted from partial dissolution of once continuous limestone beds (Fig. 15). Phosphate pellets occur scattered within these pinch-and-swell structures as well as in thin, discontinuous selvages or crusts on their top surfaces and as partings within the surrounding siltstone and mudstone. Even though radiolarians tend to be well-preserved in these limestone bodies, mostly as ferric-oxide replacements,

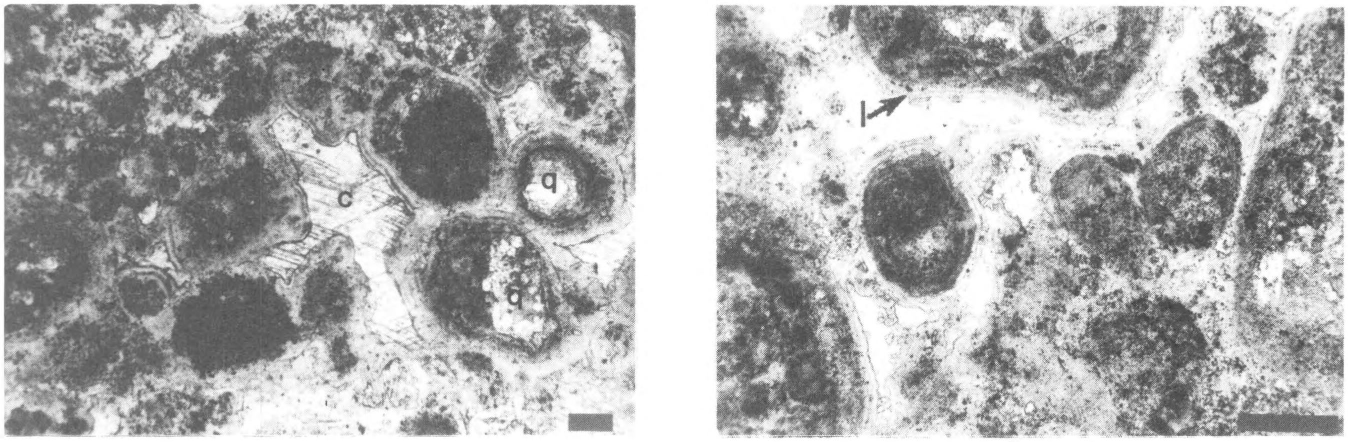

A B

Figure 10A and B. Photomicrographs of pelletal phosphate crust, Delle Phosphatic Member, level 11 (Fig. 2). A: Poikilitic, single-crystal late calcite cement (c); authigenic quartz euhedra (q). Scale bar = 0.2 mm. B: Closer view of different field of view; same slide; laminated, isopachous, phosphate cement (1). Scale bar = 0.2 mm.

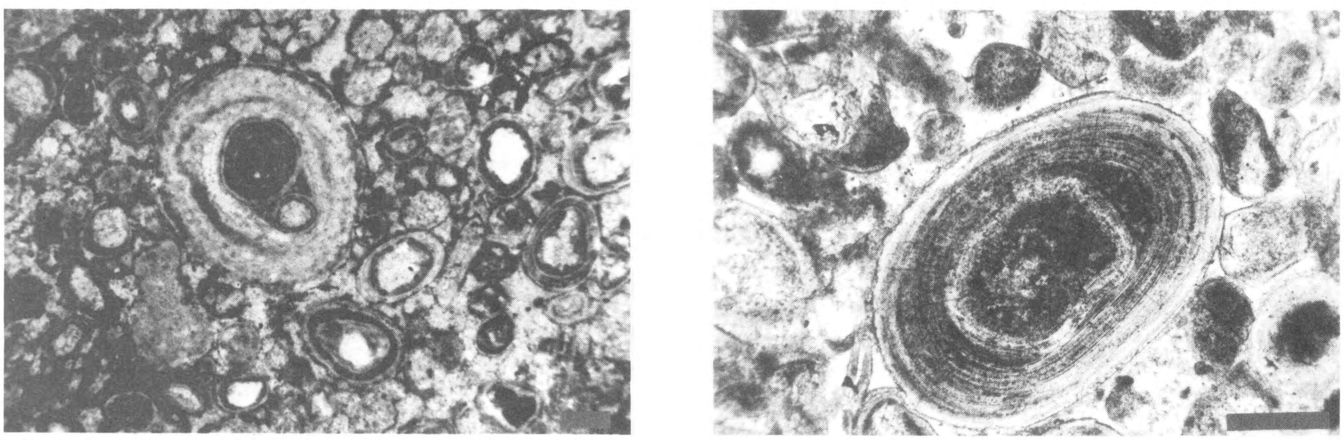

A B

Figure 11A and B. Photomicrographs of pisolitic and oolitic phosphorite, Delle Phosphatic Member, level 11 (Fig. 2). A: pisolitic phosphorite. B: Oolitic phosphorite. Scale bars = 0.2 mm.

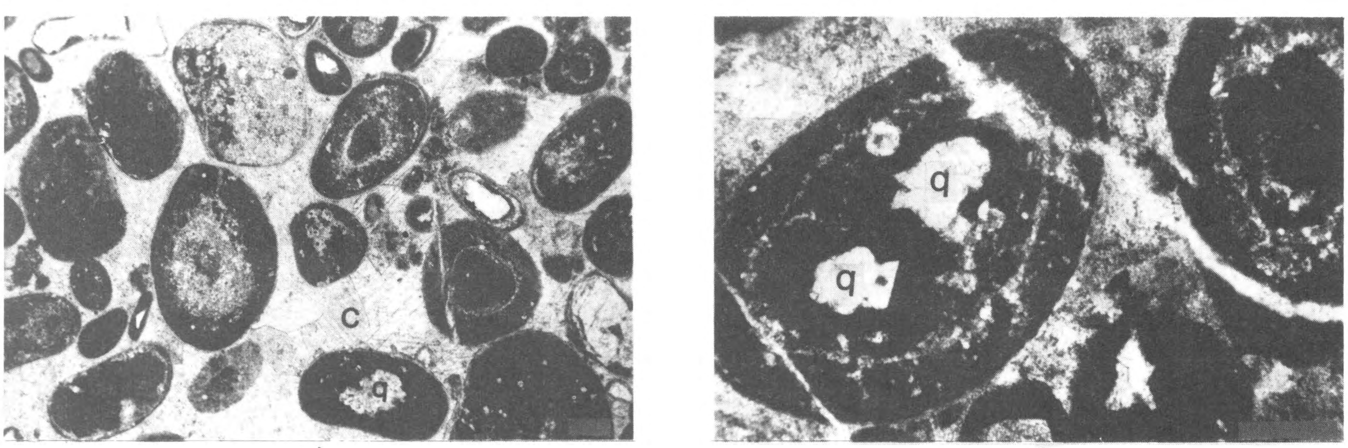

A B

Figure 12A and B. Photomicrographs of detrital oolitic and pelletal phosphorite, Delle Phosphatic Member, level 8 (Fig. 2). Poikilitic late calcite cement (c); grain-interior aggregates of authigenic euhedral quartz (q). Scale bars = 0.2 mm.

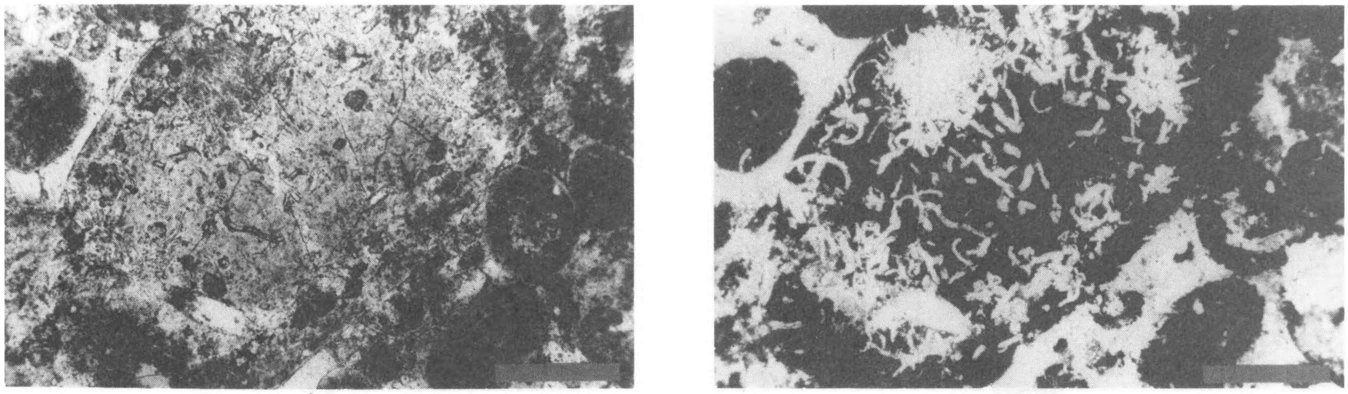

A B

Figure 13A and B. Photomicrographs of a bored phosphate grain, Delle Phosphatic Member, level 8 (Fig. 2). Calcite fillings of borings are in optical continuity with intergranular cement. A: Plane light. B: Crossed nicols. Scale bars m 0.2 mm.

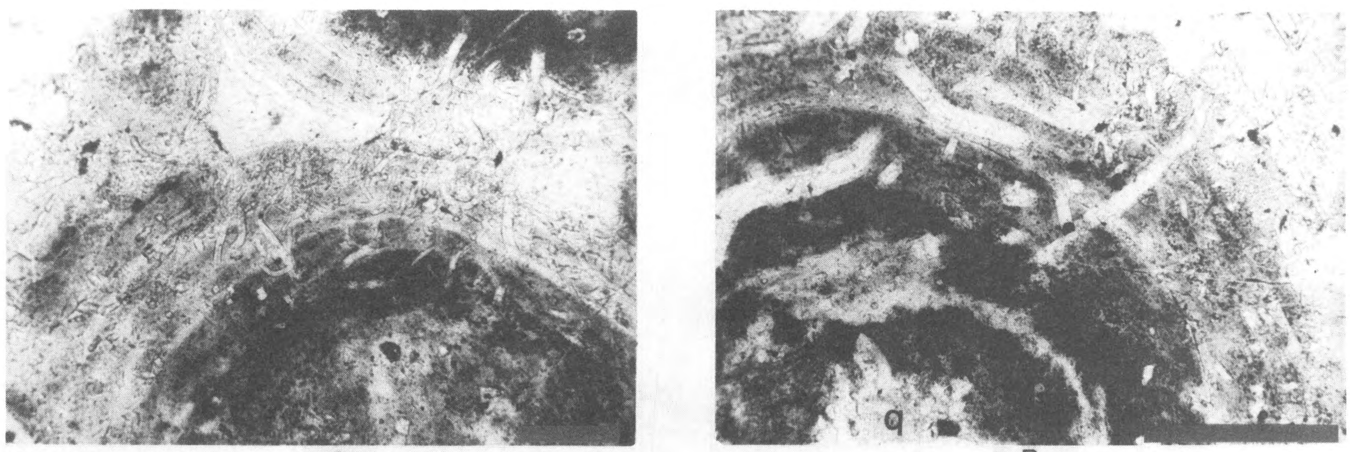

A B

Figure 14A and B. Photomicrographs of endolitic algal borings in oolitic phosphate grains, Delle Phosphatic Member, level 11 (Fig. 2). Aggregate of authigenic euhedral quartz in B (q). Scale bars = 0.2 mm.

Figure 15. Limestone pinch-and-swell structure enveloped by stratification in enclosing dolomitic mudstone, Delle Phosphatic Member, level 15 (Fig. 2). Maximum thickness of structure about 25 cm.

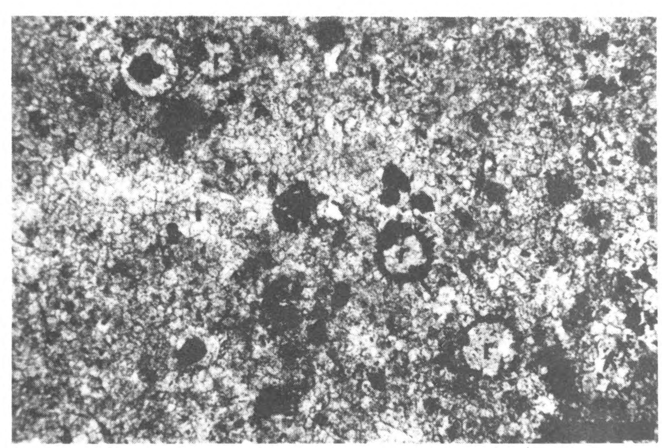

Figure 16. Photomicrograph of neomorphosed limestone composing a pinch-and-swell dissolution structure, Delle Phosphatic Member, level 15 (Fig. 2). Radiolaria (r). Scale bar = 0.2 mm.

the original limestone fabric is coarsely neomorphosed (Fig. 16). Well-preserved radiolarians and large numbers of conodonts have been reported by Sandberg and Gutschick (1984) from these pinch-and-swell structures, which are their "concretions."

The prominently outcropping unit (level 16) of dense, medium-bedded limestone (Fig. 17), the ostracode lime mudstone, which defines the top of the type Delle is megascopically featureless except for many nodules of "wood-grained" secondary chert (DeCelles and Gutschick, 1983). Fossils of marine-shelf benthic organisms, such as small solitary corals, occur but are exceedingly rare. In most thin sections (e.g., Fig. 18) cross sections of ostracodes are conspicuous and are the only recognizable bioclasts in a matrix that is commonly composed of minutely fragmented bioclastic material. Because of its unusual ostracode content, this limestone and the similar, but dolomitized limestone lower in the section at level 13, are believed to represent deposition in a restricted, either brackish or hypersaline, low-energy environment, and limestones of this kind are a distinctive, although minor, component of the rock record influenced by the DPE throughout central and western Utah. Both these rocks and those of the same character that formed during the DPE elsewhere in Utah were interpreted as regionally significant gravity and slope deposits by Sandberg and Gutschick (1984, p. 138), but nowhere do they bear evidence of gravity-flow deposition, slump folding, or any other features characteristic of such deposits, and their peculiar bioclast content makes such an interpretation highly unlikely.

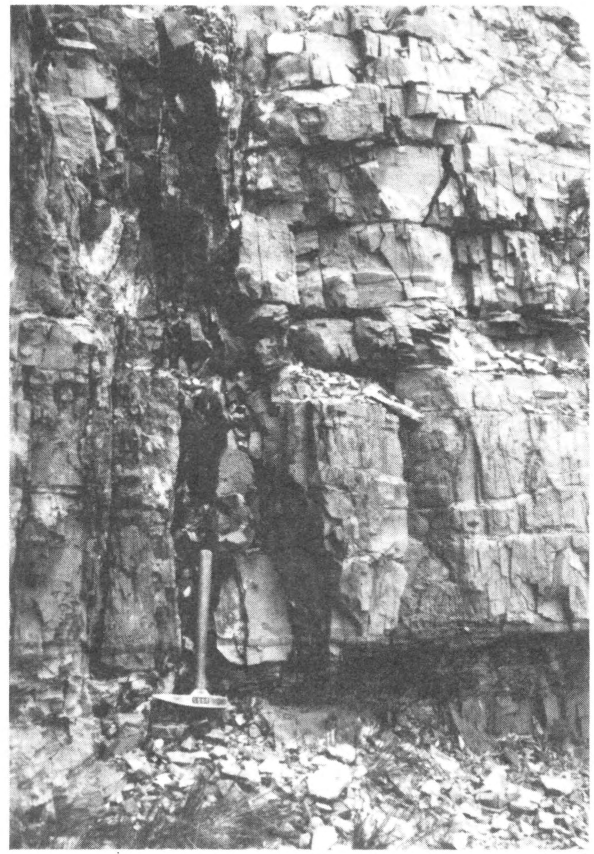

Figure 17. Megascopically featureless, regularly thin- to medium-parted ostracode lime mudstone containing secondary chert nodules. This rock type defines the top of the type Delle Phosphatic Member, Lakeside Mountains, level 16 (Fig. 2). Hammer for scale.

Younger Rocks

Immediately overlying the Delle Phosphatic Member in its type section are generally unfossiliferous, dolomitized calcareous siltstone and fine-grained sandstone similar in composition and bedding characteristics to those that form much of the upper part of the type Delle. Plane-bed lamination is prevalent where not obscured by an abundance of bedding-plane burrows. These fine-grained, siliclastic rocks are about 75 m thick and are referred to simply as part of the Woodman Formation on Figures 1B and 2. The next higher map unit (Mh, Fig. 1B) is coarser and more conspicuously cross-bedded, quartzose sandstone to which the name Humbug Formation is applied. This unit is lithologically unlike either the Needle Siltstone Member of the Chainman Formation or the Woodman Formation, and in assigning it to the Humbug Formation we are following Hintze (1988), who applied the name Deseret Limestone to much or all of the underlying interval here included in the Woodman Formation. The siltstones and sandstones here assigned to the upper part of the Delle and to the Woodman and Humbug show only the effects of current-entrainment transport, mainly plane-bed lamination and cross stratification. These rocks exhibit none of the characteristics of slope-controlled, gravity-flow deposits.

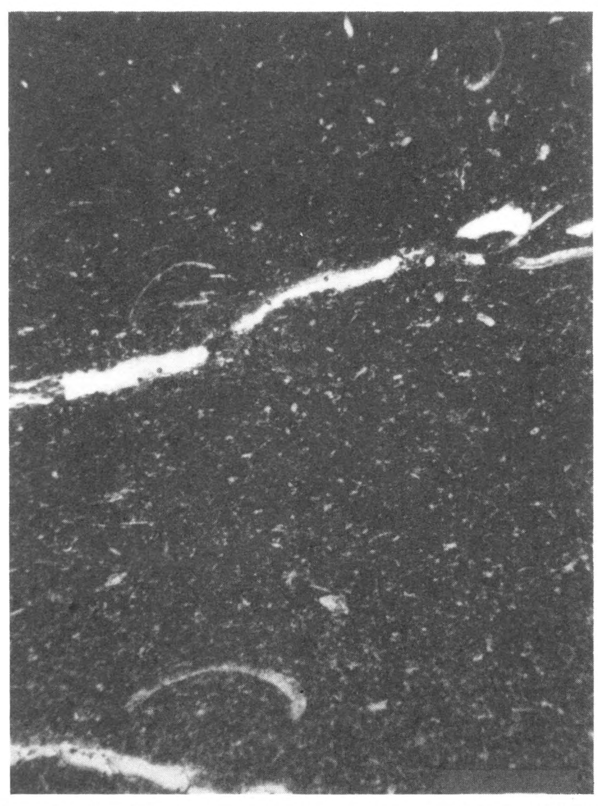

Figure 18. Photomicrograph of ostracode lime mudstone, Delle Phosphatic Member, Lakeside Mountains, level 16 (Fig 2). Scale bar = 0.2 mm.

DISCUSSION

The heterogeneous, anomalous rocks that occur relatively low in the type Delle Phosphatic Member record fluctuating depositional and diagenetic environments, the effects of which have been complexly superimposed on one another. Anoxia in bottom water, related to the overproduction and accumulation of organic matter during deposition of this part of the section, can explain the absence of normal-marine shelf benthic fossils and bioclasts. Reducing, organic-rich conditions within the sediment are indicated by the occurrence of phosphorite, ammonium feldspar, the development of iron sulfides, and possibly some of the secondary dolomite, the formation of which might have been enhanced by sulfate reduction. Episodes of oxidation, on the other hand, are indicated by the low (mostly < 0.5 percent) organic carbon content in the Delle (Sandberg and Gutschick, 1984, p. 177), the general lack of black organic pigments in much of the section, and burrowed siliciclastic intervals. Episodic penecontemporaneous oxidation of iron sulfide may have produced the layers of vivid red mudstone that overlie some phosphorite beds such as that at level 11. A little higher, beginning in the recently exposed few meters of section between levels 11 and 12, the upward sequence of phosphatic chert, red mudstone, sparsely fossiliferous siltstone (level 12), and ostracode lime mudstone (level 13) suggests a progression toward increasing oxygenation. Perhaps significantly, the ostracode lime mudstone of level 13, which would be the most oxygenated part of this cycle, was not affected by dissolution, whereas the limestone pinch-and-swell structures that occur still higher in the section were.

Although similar in some respects to basinal deposits, a deep-water origin for the anomalous rocks produced by the anoxic event is not required by their sedimentary features and biotic content, and it is especially implausible because of their stratigraphic context. The Delle Phosphatic Member in the Lakeside Mountains abruptly overlies normal-marine shelf limestone. Regionally, the relationships are the same, and over much of western Utah deposits of the DPE abruptly overlie the same uppermost unit of the Gardison Limestone. In their most eastern occurrences, such at that at Samak at the west end of the Uinta Mountains (S on Fig. 1A) (Lane and others, 1980; Nichols and Silberling, in press b), the depositionally and diagenetically peculiar rocks of the DPE are relatively thin (less than 10 m in thickness) and grade upward into normal-marine shelf carbonate rocks. Farther west in Utah, as in the Confusion Range (C on Fig. 1A), effects of the DPE persist upwards through hundreds of meters of the partly fine-grained siliciclastic Chainman Shale. Nowhere in Utah, however, in rocks associated with the DPE is there evidence for regionally significant slope environments in the form of thick sequences of turbidites or significant products of gravity-flow deposition.

As an hypothesis, the petrology and stratigraphic setting of rocks of the DPE can be explained by the incursion onto the Mississippian shelf of nutrient-rich, organically productive, openmarine water. Such water would have favored the presence of pelagic organisms, such as radiolarians and goniatites, while the anoxia resulting from high organic productivity caused extermination of the normal-marine shallow, shelly benthos. Water depth on the shelf had to have been sufficiently deep to maintain stratification and restriction. The biofacies argument of Sandberg and Gutschick (1984) for their interpretation of a truly deep, basinal depositional environment can also be applied to shelf environments of modest depth influenced by unusual, anoxic water chemistry.

The apparent condensation of rocks affected by the anoxic event, in comparison with shelf carbonate rocks of supposed equivalent age (Sandberg and Gutschick, 1980), can be explained by the absence as rock-forming constituents of the usual calcareous bioclasts, such as crinoid columnals, by the penecontemporaneous dissolution of calcareous material, for which there is abundant evidence as described above, and perhaps by one or more interruptions in deposition. A disconformity associated with the initiation of the DPE is suggested by the corrosion, dissolution, and phosphatic replacement of pre-existing limestones such as those that directly underlie the Delle Phosphatic Member. Moreover, initiation of the DPE, in addition to corresponding to an abrupt change in water chemistry, coincided with the abrupt influx of fine-grained siliclastic sediment over the more western parts of the pre-existing carbonate shelf. Only in the easternmost of the sections in Utah where the DPE is recorded, is its age apparently tightly constrained (Lane and others, 1980) within the Osagean. Elsewhere, existing biostratigraphic age control for inception of the DPE, that is both accurately placed in the stratigraphic sequence and adequately documented, allows for the possibility of the onset of the DPE being associated with regional disconformity, the hiatus of which might increase westward to span part of Osagean and early Meramecian time. In the Lakeside Mountains, however, any hiatus at the base of the Delle would be brief, as indicated by age-diagnostic goniatites that were collected by T.W. Henry and the authors from the lowest pinch-and-swell structures (level 15) that are 30 m above the base of the type Delle Phosphatic Member. These fossils, like those reported by Petersen (1969) from a similar stratigraphic level about 25 km to the southeast in the Stansbury Mountains, are identified as species of *Beyrichoceras* and *Dzhaorakoceras* and dated as late Osagean by Mackenzie Gordon (oral commun., 1990). This assignment agrees with that of Sandberg and Gutschick (1984) who place this level in the lower *Gnathodus texanus* conodont zone and recognize the Osagean-Meremecian boundary as being between the lower and upper parts of this zone. In the absence of others kinds of fossils, dating of radiolarians from siliceous rocks near the base of the Delle, or dating of palynomorphs from fine-grained siliclastic rocks where these occur low in the more western deposits of the DPE, could resolve the uncertainty regarding the possibility of a disconformity between the Delle and underlying Lower Mississippian carbonate rocks.

PALEOGEOGRAPHIC IMPLICATIONS

The Delle Phosphatic Member in the Lakeside Mountains exemplifies the Delle phosphatic event which was similar to the subsequent anoxic/phosphatic event that resulted in deposition of the Phosphoria Formation in Permian time (e.g., Morris and Lovering, 1961). These two unusual and widespread phenomena, the DPE and the similar event that produced the Phosphoria, affected overlapping regions of the broad late-Paleozoic shelf of western North America. We are impressed that they roughly correlate with deformation, respectively, of the the Antler and Sonoma orogenies and the inferred emplacement of accretionary tectonic complexes onto the continental margin. This coincidence implies paleotectonic control of these anoxic depositional events (Silberling and Nichols, 1989).

In the case of deposits of the DPE, their sedimentology and stratigraphic context precludes the existence of part of the Antler foredeep in the eastern Great Basin of Nevada and Utah, and yet the high-nutrient, marine water that influenced their deposition could not have been generated on a normal shelf. Therefore, we hypothesize, following Roberts (1979), that the Early Mississippian carbonate shelf in Utah was flooded, and normal deposition modified, by waters produced through upwelling in the Mississippian Antler foredeep. This speculation would be particularly attractive if deep-marine circulation could have been maintained by a paleogeographic configuration that permitted connection along the trend of the Antler foredeep with the oceanic marginal sea, or "Schoonover-Havallah basin," which coexisted with the foredeep (Miller and others, 1984). Restriction and stratification of shelf waters of the inner Antler foreland could thus be the consequence of silling of the shelf by tectonic development of a foreland bulge as would be predicted to accompany the formation of a foredeep by flexural loading (e.g., Speed and Sleep, 1982). Restriction of the shelf, deposition thereupon influenced by the DPE, and retention on the shelf of fine-grained siliclastic sediment originally of cratonic provenance, would then have taken place during the time when the actual foredeep and its deposits, the Diamond Range sequence of Trexler and Nitchman (1990), were being developed much farther (probably more than 200 km farther) west. According to Trexler and Cashman (1990) the full expression of these mid-Mississippian foredeep deposits is no longer preserved owing to a subsequent contractional phase of Antler orogenesis in Late Mississippian time. Thus the DPE regionally, and its expression in the Lakeside Mountains in the form of the Delle Phosphatic Member, are viewed as phenomena of the inner Antler foreland. They resulted from profound modification of the sedimentary regime, but not the bathymetry, of the pre-existing Early Mississippian shelf and were the direct consequence of tectonic emplacement of the Roberts Mountains allochthon during a protracted Antler orogeny.

ACKNOWLEDGMENTS

Among our many colleagues, we are especially grateful to Katie Goebel, Dave Miller, Hal Morris, and Jim Trexler for sharing their ideas and data with us in both the office and in the field. We thank Mitch Henry and Pete Isaacson for reviewing the present manuscript.

REFERENCES CITED

Bromfield, C.S., Baker, A.A., and Crittenden, M.D., Jr., 1970, Geologic map of the Heber quadrangle, Wasatch and Summit Counties, Utah: U.S. Geological Survey Map GQ-864, scale 1:24,000.

Budd, D.A., and Perkins, R.D., 1980, Bathymetric zonation and paleoecological significance of microborings in Puerto Rican shelf and slope sediments: Journal of Sedimentary Petrology, v. 50, p. 881-904.

Cheney, T.M., 1957, Phosphate in Utah: Utah Geological and Mineralogical Survey Bulletin 59, 54 p.

DeCelles, P.G., and Gutschick, R.C., 1983, Mississippian wood-grained chert and its significance in the western interior United States: Journal of Sedimentary Petrology, v. 53, p. 1175-1191.

Enos, P., 1983, Shelf environment, *in* Scholle, P.A., Bebout, D.G., and Moore, C.H., eds., Carbonate depositional environments: American Association of Petroleum Geologists Memoir 33, p. 267-295.

Gilluly, J., 1932, Geology and ore deposits of the Stockton and Fairfield quadrangles, Utah: U.S. Geological Survey Professional Paper 173, 171 p.

Golubic, S., 1969, Distribution, taxonomy and boring patterns of marine endolithic algae: American Zoologist, v. 9, p. 747-751.

Gutschick, R.C., 1976, Preliminary reconnaissance study of Lower and lower-Upper Mississippian strata across northwestern Utah: U.S. Geological Survey Open-File Report 76-200, 40 p.

——1987, Letter: Geology, v. 15, p. 684.

Gutschick, R.C., and Sandberg, C.A., 1983, Mississippian continental margins of the conterminous United States, *in* Stanley, D.J., and Moore, G.T., eds., The shelf-break; critical interface on continental margins: Society of Economic Paleontologists and Mineralogists Special Publication 33, p. 79-96.

Gutschick, R.C., Sandberg, C.A., and Sando, W.J., 1980, Mississippian shelf margin and carbonate platform from Montana to Nevada, *in* Fouch, T.D., and Magathan, E.R., eds., Paleozoic paleogeography of the west-central United States: Denver, Rocky Mountain Section, Society of Economic Paleontologists and Mineralogists, Rocky Mountain Paleogeography Symposium 1, p. 111-128.

Hintze, L.F., 1988, Geologic history of Utah: Brigham Young University Geology Studies Special Publication 7, 202 p.

Jansma, P.E., and Speed, R.C., 1985, Antler foreland basin tectonics: new data: Geological Society of America Abstracts with Programs, v. 17, p. 363.

Lane, H.R., Sandberg, C.A., and Ziegler, W., 1980, Taxonomy and phylogeny of some Lower Carboniferous conodonts and preliminary standard post-*Siphonodella* zonation: Geologica et Palaeontologica, v. 14, p. 117-164.

Miller, E.L., Holdsworth, B.K., Whiteford, W.B., and Rodgers, D., 1984, Stratigraphy and structure of the Schoonover sequence, northeastern Nevada: implications for Paleozoic plate-margin tectonics: Geological Society of America Bulletin, v. 95, p. 1063-1076.

Morris, H.T., and Lovering, T.S., 1961, Stratigraphy of the East Tintic Mountains, Utah: U.S. Geological Survey Professional Paper 361, 145 p.

Nichols, K.M., and Silberling, N.J., 1990, The Delle Phosphatic Member: An anomalous part of the Mississippian (Osagean-Meramecian) shelfal sequence of central Utah: Geology, v. 18, p. 46-49.

——in press a, Petrology and significance of a Mississippian (Osagean-Meramecian) anoxic event, Lakeside Mountains, northwestern Utah: U.S. Geological Survey Bulletin 1787.

——in press b, Petrology and depositional setting of Mississippian rocks associated with an anoxic event at Samak, western Uinta Mountains, Utah: U.S. Geological Survey Bulletin 1787.

Nolan, T.B., 1935, The Gold Hill mining district, Utah: U.S. Geological Survey Professional Paper 117, 172 p.

Petersen, M.S., 1969, The occurrence of ammonoids from the lower Deseret Limestone, northern Stansbury Mountains, Tooele County, Utah: Geological Society of America Abstracts with Programs, v. 1, p. 63.

Poole, F.G., and Claypool, G.E., 1984, Petroleum source-rock potential and crude-oil correlation in the Great Basin, *in* Woodward, Jane, Meissner, F.F., and Clayton, J.L., eds., Hydrocarbon source rocks of the greater Rocky Mountain Region: Denver, Rocky Mountain Association of Geologists, p. 179-229.

Poole, F.G., and Sandberg, C.A., 1977, Mississippian paleogeography and tectonics of the western United States, *in* Stewart, J.H., Stevens, C.H., and Fritsche, A.E., eds., Paleozoic paleogeography of the western United States: Los Angeles, Pacific Section, Society of Economic Paleontologists and Mineralogists, Pacific Coast Paleogeography Symposium 1, p. 67-85.

Roberts, A.E., 1979, Northern Rocky Mountains and adjacent plains region, *in* Craig, L.C., and Conner, C.W., coords., Paleotectonic investigations of the Mississippian System in the United States: U.S. Geological Survey Professional Paper 1010, p. 221-247.

Robinson, J.P., in press, Geologic map of the Gold Hill 7.5′ quadrangle, Tooele County, Utah: Utah Geological Survey Map, scale 1:24,000.

Rose, P.R., 1976, Mississippian carbonate shelf margins, western United States: U.S. Geological Survey Journal of Research, v. 4, p. 449-466.

Sadlick, W., 1965, Biostratigraphy of the Chainman Formation (Carboniferous), eastern Nevada and western Utah [Ph.D. thesis]: Salt Lake City, University of Utah, 227 p.

Sandberg, C.A., and Gutschick, R.C., 1977, Paleotectonic, biostratigraphic, and economic significance of Osagean to early Meramecian starved basin in Utah: U.S. Geological Survey Open-File Report 77-121, 16 p.

——1979, Guide to conodont biostratigraphy of Upper Devonian and Mississippian rocks along the Wasatch front and Cordilleran hingeline, Utah, *in* Sandberg, C.A., and Clark, D.L., eds., Conodont biostratigraphy of the Great Basin and Rocky Mountains: Brigham Young University Geology Studies, v. 26, p. 107-134.

——1980, Sedimentation and biostratigraphy of Osagean and Meremecian starved basin and foreslope, western United States, *in* Fouch, T.D., and Magathan, E.R., eds., Paleozoic paleogeography of the west-central United States: Denver, Rocky Mountain Section, Society of Economic Paleontologists and Mineralogists, Rocky Mountain Paleogeography Symposium 1, p. 128-147.

——1984, Distribution, microfauna, and source-rock potential of Mississippian Delle Phosphatic Member of Woodman Formation and equivalents, Utah and adjacent states, *in* Woodward, Jane, Meissner, F.F., and Clayton, J.L., eds., Hydrocarbon source rocks of the greater Rocky Mountain Region: Denver, Rocky Mountain Association of Geologists, p. 135-178.

——1989, Deep-water phosphorite in the early Carboniferous Deseret starved basin, Utah, *in* Notholt, A.J.G., Sheldon, R.P., and Davidson, D.F., eds., Phosphate deposits of the world, v. 2, Phosphate rock resources: Cambridge Earth Science Series, p. 18-23.

Sandberg, C.A., Gutschick, R.C., Johnson, J.G., Poole, F.G., and Sando, W.J., 1982, Middle Devonian to Late Mississippian geologic history overthrust belt region, western United States, *in* Powers, R.B., ed., Geologic studies of the Cordilleran thrust belt, v. 2: Denver, Rocky Mountain Association of Geologists, p. 691-719.

Sandberg, C.A., Poole, F.G., and Gutschick, R.C., 1980, Devonian and Mississippian stratigraphy and conodont zonation of Pilot and Chainman Shales, Confusion Range Utah, *in* Fouch, T.D., and Magathan, E. R., eds., Paleozoic paleogeography of the west-central United States: Denver, Rocky Mountain Section, Society of Economic Paleontologists and Mineralogists, Rocky Mountain Paleogeography Symposium 1, p. 71-79.

Sando, W.J., Dutro, J.T., Jr., Sandberg, C.A., and Mamet, B.A., 1976, Revision of Mississippian stratigraphy, eastern Idaho and northeastern Utah: U.S. Geological Survey Journal of Research, v. 4, p. 467-479.

Sando, W.J., Sandberg, C.A., and Gutschick, R.C., 1981, Stratigraphic and economic significance of Mississippian sequence at North Georgetown Canyon, Idaho: American Association of Petroleum Geologists Bulletin, v. 65, p. 1433-1443.

Schell, E.M., and Moore, K.P., 1970, Stratigraphic sections and chemical analyses of phosphatic rocks of Permian and Mississippian age in Weber County, Utah: U.S. Geological Survey Circular 635, 11 p.

Silberling, N.J., and Nichols, K.M., 1989, Arcs, allochthons, and forelands--parallels and predictions in Antleran and Sonoman histories: Geological Society of America Abstracts with Programs, v. 21, p. 143.

——1990, Tectonic implications of wide-spread anoxia on the Mississippian shelf, western and northern Utah: Geological Society of America Abstracts with Programs, v. 22, p. 83-84.

Sohn, I.G., and Sando, W.J., 1987, Paleobathymetric significance of ostracodes from the Paine Member of the Lodgepole Limestone (Early Mississippian), north-east Utah: U.S. Geological Survey Bulletin 1690-E, 7 p.

Southgate, P.N., 1986, Cambrian phoscrete profiles, coated grains, and microbial processes in phosphogenesis; Georgina Basin, Australia: Journal of Sedimentary Petrology, v. 56, p. 429-441.

Speed, R.C., and Sleep, N.H., 1982, Antler orogeny and foreland basin—A model: Geological Society of America Bulletin, v. 93, p. 815-828.

Trexler, J.H., Jr., and Cashman, P.H., 1990, The Diamond Mountain phase of the Antler orogeny: Late Mississippian compressional deformation in east-central Nevada: Geological Society of America Abstracts with Programs, v. 22, p. A274.

Trexler, J.H., Jr., and Nitchman, S.P., 1990, Sequence stratigraphy and evolution of the Antler foreland basin, east-central Nevada: Geology, v. 18, p. 422-425.

THE DEVONIAN-MISSISSIPPIAN STANSBURY FORMATION AT STANSBURY ISLAND AND IN THE NORTHEASTERN STANSBURY MOUNTAINS, UTAH

James H. Trexler, Jr.
Department of Geological Sciences
University of Nevada, Reno

ABSTRACT

The Devonian-Mississippian Stansbury Formation is a locally thick sequence of dolomite-clast conglomerate, quartz-arenite, and dolomite that is exposed only in the Stansbury Mountains and adjacent ranges in western Utah. At Flux in the northeast Stansbury Mountains, the type section comprises 540 meters of coarse conglomerate deposited as submarine debris flows, intercalated with quartz-arenite that represents near-shore accumulation by shore-parallel currents. Paleocurrent data from the conglomerate indicates a northeast-dipping slope, while cross-stratification in the quartz-arenite suggests a west-trending shoreline. The conglomerate had a source nearby to the southwest, and the quartz-arenite came from far to the east on the craton. Conglomeratic Stansbury Formation is restricted to the Stansbury Mountains; elsewhere, at Stansbury Island and in the Oquirrh Mountains and Wasatch Range, correlative strata comprise only quartzite, limestone, and dolomite. The quartz-arenite-dominated section at Stansbury Island is interpreted as a marine sand-wave accumulation attributed to cyclic, opposed currents on a shallow shelf.

In the northern Stansbury Mountains, Stansbury strata sit with angular unconformity on Paleozoic rocks from Cambrian through Devonian in age. The Stansbury Formation is thickest where it rests on relatively young strata, and missing where pre-Stansbury erosion was deepest. Internal angular unconformities within the Stansbury sequence may indicate local uplift and tilting during basin fill.

The Stansbury Formation represents deposition due to local but significant subsidence in the Late Devonian. The Uinta arch has been invoked to account for this activity, but its location is well to the south, and arch-uplift may not account for such rapid subsidence. An alternative may be early craton-margin deformation related to the onset of obduction of the Antler allochthon.

This paper discusses strata visited during the 1992 Geological Society of America, Rocky Mountain Section field trip to the area. The text describes the rocks in the same order that they are described in the roadlog (this volume), and is restricted to those localities. For a more complete treatment of the Stansbury Formation, see Trexler (in review).

INTRODUCTION

Devonian through Mississippian strata in the ranges south of the Great Salt Lake (Fig. 1) mostly comprise a regionally similar section of dolomite, limestone, and minor quartzite (Fig. 2). In the Stansbury Mountains, this section is interrupted by a pronounced angular unconformity, and strata of Cambrian through Silurian age are overlain by a locally thick, dolomite-clast conglomerate unit, the Stansbury Formation of Stokes and Arnold (1958). The Stansbury Formation type section at Flux in the northeastern Stansbury Mountains consists of 540 meters of dolomite-clast conglomerate, quartz-arenite, dolomite, and limestone. On the west side of Timpie Valley, just a few kilometers west

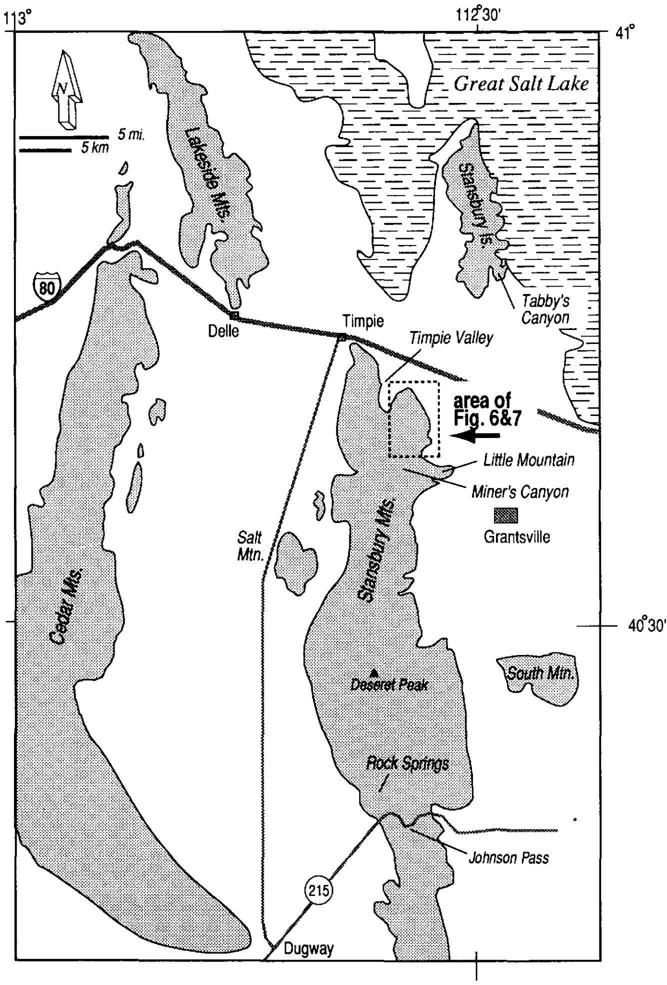

Figure 1. Regional geography in west-central Utah, and localities mentioned in text.

of Flux, the Stansbury Formation is missing due to either erosional removal or pinchout. In the southern and western Stansbury Mountains at Salt Mountain and Rock Springs, the formation is only 75 meters thick and the conglomerate is not as coarse as at Flux, but otherwise these strata resemble the Flux section. At Stansbury Island the formation is 240 meters thick, but is mostly quartz-arenite with minor carbonate and no conglomerate. Limestone beds in the upper Stansbury Formation at Flux are dated as Late Devonian to Early Mississippian (N. Silberling, written commun., 1991), and are correlative with the widespread Pinyon Peak Formation.

The Stansbury Formation is bounded by a basal unconformity and an upper disconformity throughout the region. At Flux, the basal contact is an angular unconformity with sub-unconformity dips that range from 15° to 30°, and the Stansbury Formation lies on undifferentiated Ordovician and Silurian dolomite. In the northwestern Stansbury Mountains, a thin limestone unit mapped as Pinyon Peak (Rigby, 1959) is the only representative of Stansbury strata, and it lies with angular discordance on Cambrian rocks. It is not presently known whether the Stansbury Formation is erosionally truncated there, but no angular discordance between the Stansbury or Pinyon Peak and overlying, lower Mississippian Fitchville equivalent (mapped as Gardner by Rigby, 1959) has been observed anywhere in the Stansbury Mountains. In the western and southern Stansbury Mountains, the basal contact is a disconformity, and strata below are mapped as Silurian (Rigby, 1959), usually based on lithostratigraphy. At Stansbury Island, subjacent strata are disconformable, and are assigned to the Silurian Laketown Dolomite (Chapusa, 1969).

The Stansbury Formation including Pinyon Peak equivalent strata are overlain throughout their regional extent by the Mississippian Fitchville Formation or its equivalents. The most detailed maps of the Stansbury Mountains (e.g., Rigby, 1959) assign these cherty limestones to the Gardner Formation, but this terminology has since been abandoned. As discussed below, the Fitchville limestones are somewhat younger than the youngest known Stansbury Formation, and a diastem or disconformity is implied here.

Stansbury Formation strata that are lithologically similar to the type locality at Flux (Fig. 1) are limited to the Stansbury Mountains. Conglomeratic strata in the Newfound-

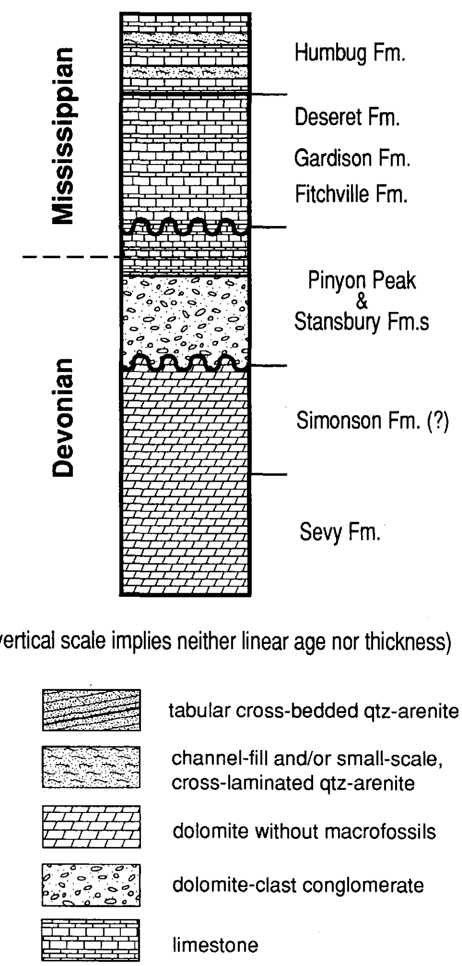

Figure 2. Regional Devonian-Mississippian stratigraphy in the Stansbury and adjacent mountain ranges (after Hintze, 1988; Moore and Sorenson, 1979; Rigby, 1959). Lithologic symbols used here are also used in Figures 3 and 5.

land and Silver Island Mountains north and west of the Great Salt Lake were at one time correlated with the Stansbury Formation (Roberts and Tooker, 1969). However, this compositionally distinct conglomerate in the Silver Island Mountains has more recently been mapped as Chainman/Diamond Peak Formation equivalent (Miller and others, 1990) with a chert-lithic sediment source probably in the Antler foreland or Roberts Mountains allochthon to the west. Recent mapping in the Newfoundland Mountains (Allmendinger and Jordan, 1989) does not recognize a Stansbury Formation lithologic equivalent. The Lakeside Mountains, lying halfway between the Stansbury and Newfoundland ranges, contain no Stansbury Formation strata.

A different version of the Stansbury Formation, with its own depositional history, consists of a quartzite and limestone section cropping out at Stansbury Island, with possible equivalents also occurring in the Oquirrh and Wasatch mountains. These quartz-arenite-dominated sections lack conglomerate and probably represent a separate depositional system, but have been included in the Stansbury Formation by many workers.

STANSBURY ISLAND

From several kilometers away, the dominant visual feature of Stansbury Island is a light-colored "stripe" that delineates a large anticline in the southern part of the island, and tilted blocks of strata to the north. This stripe is the quartzite interval that was mapped by Chapusa (1969) as the Stansbury Formation. Excellent exposures of these strata are easily accessible on the ridge between Tabby's Canyon and Broad Canyon at the south end of the island (Fig. 1). A section measured here (Fig. 3) documents 282 meters of quartz-arenite and minor limestone.

The Stansbury Formation at the southern end of Stansbury Island lies disconformably on Ordovician-Silurian dolomite. Chapusa (1969) identified this underlying unit as the Silurian Laketown Formation, but Palmer (1970) questions this call. These strata comprise interbeds of dolomite and quartzite that are deformed into low-angle, small-scale folds within the larger anticline. The Stansbury Formation does not have these folds; it is not presently known whether these folds are due to pre-Stansbury folding truncated by an unconformity (as seen at Flux, discussed below), or to differential competence and response to Mesozoic deformation that affected all of these strata.

The base of the Stansbury Formation here is taken as the lowest limestone above the Laketown and below the thick quartz-arenite section. This approximates Chapusa's (1969) mapped contact. Limestone at the base of the section contains calcareous algae identified as latest Devonian-earliest Mississippian (B. Mamet, written commun., 1991).

The lowest Stansbury strata in this section are limestone, dolomitized limestone, and calcareous quartz-arenite. The limestone is laminated to massive micrite, with visible fossil fragments. The calcareous quartz-arenite is finely laminated. Overlying these strata is 200 meters of clean, medium-

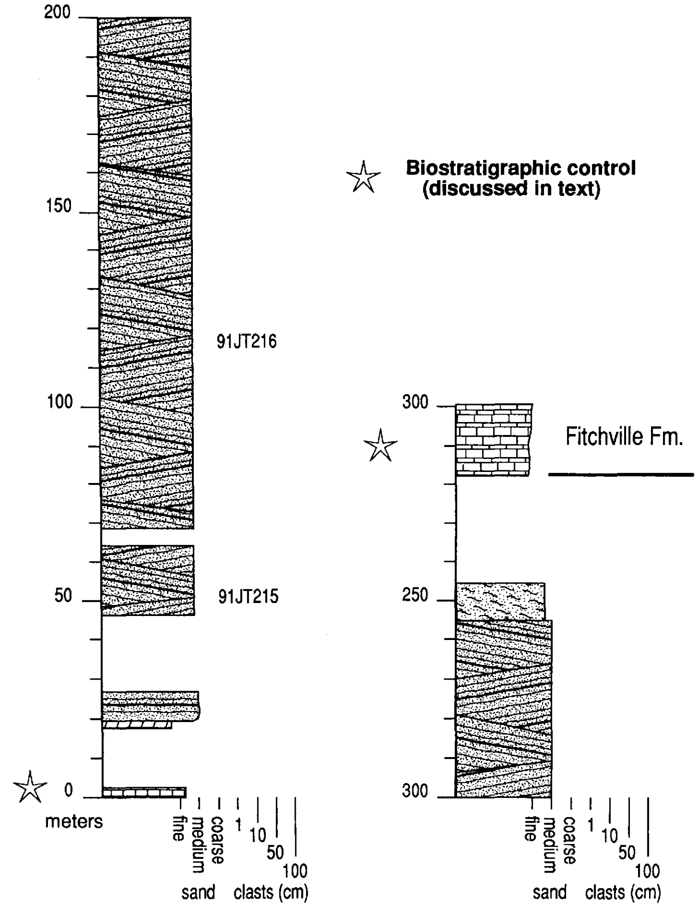

Figure 3. Measured section at Tabby's Canyon, southern Stansbury Island. Numbers adjacent to column refer to paleocurrent localities (Fig. 4).

grained quartz-arenite. The dominant sedimentary structures throughout the quartz-arenite section are low-angle, tabular sets of cross-stratification that are 2 to 5 meters thick. Sets truncate one another along low-angle reactivation surfaces. Ripple cross-lamination was also reported from these strata by Chapusa (1969). The uppermost 10 meters of the exposed section comprises thin-bedded, ripple-laminated calcareous quartz-arenite and thin calcarenite beds. Ripples here are straight-crested and symmetric, with wavelengths from 5 to 10 cm. Twenty meters of cover separate the Stansbury from the overlying Fitchville cherty limestone here.

Cross-stratification orientation data from the quartz-arenite beds at this measured section (Fig. 4) indicate a distinctive bimodal pattern, with opposed trends east and west. Individual sets of cross-strata cluster tightly; larger cosets have opposed directions.

The depositional environment for the Stansbury Formation at Stansbury Island is interpreted to be a submarine, sand wave build-up in relatively shallow water. The intercalated marine limestone beds at the bottom and top of the section, and a complete lack of associated eolian features, indicate that the entire section is marine. The low-angle cross-stratification in sets 2 to 5 meters thick suggest that

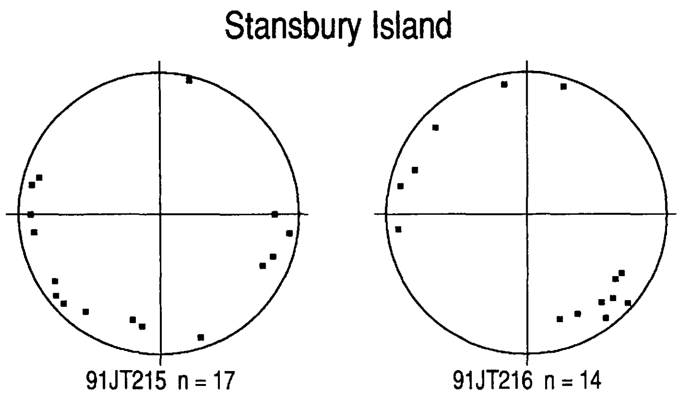

Figure 4. Paleocurrent data from the Tabby's Canyon section of the Stansbury Formation.

small dunes were the dominant bed form. The combination of dune form and grain size indicate that current strength was between 0.5 and 1 m/sec., and the general lack of ripples indicates flow velocities mostly greater than 0.5 m/sec. during deposition (Costello, 1974). Symmetric oscillation ripples suggest that the water depth was above wave-base, at least at the top of the section. The rarity of preserved ripples indicates that any ripples that formed during times of lower flow were usually eradicated by stronger currents.

The opposed paleocurrent directions suggest that these quartz-arenite beds were deposited in a setting where intermittent, opposite currents resulted in a local build-up of sand, in contrast to a throughgoing sand-transport system such as a beach, river delta, or submarine canyon. Such opposed currents may be attributed to tidal reversals or storm set-up and return flow. The reversals probably were not seasonal but more frequent, since opposed paleocurrent directions are found in intercalated cosets. The occurrence of oscillation ripples indicates that the setting may have been offshore rather than estuarine.

As will be seen in the following discussion, the Stansbury Formation at Stansbury Island is very different from the type section at Flux. There is no conglomerate at Stansbury Island, and there is roughly four times as much quartz-arenite as at Flux. The depositional setting of the two localities is quite different. The main feature they share is stratigraphic position.

THE TYPE SECTION AT FLUX

The original stratotype for the Stansbury Formation (Stokes and Arnold, 1958) was measured on the ridge west of the lime plant at Flux, Utah (Fig. 1). For this study, the type section was remeasured in greater detail (Fig. 5), and the local area was remapped (Fig. 6) taking into account a change in the position of the basal contact of the Stansbury. The newly measured section comprises 540 meters of conglomerate, quartz-arenite, and carbonate. The regional attitudes here are prevailing north-south strikes with gentle easterly dips; thus this east-west-trending ridge crest is an ideal traverse through the section. The strata are partly obscured by rock rubble and sparse vegetation, but exposure approaches 100 percent through most of the section and offset of the traverse is required only to follow the ridge crest.

Stokes and Arnold (1958) mapped several members in the Stansbury Formation: a lower quartzite member, and lower conglomerate, an upper quartzite member, and an upper conglomerate. Remapping (Fig. 7) for this project modifies this somewhat, and recognizes three main lithofacies that, while mappable, are not members because they do not occupy specific stratigraphic positions. These lithofacies are dolomite, dolomite-clast conglomerate, and quartz-arenite.

The base of the section is defined here as an angular unconformity between undivided Ordovician-Silurian dolomite (Stokes and Arnold, 1958) and lower Stansbury dolomite. Stokes and Arnold (1958) originally picked the base of the Stansbury at the base of the lowest quartz-arenite bed, so recognition of this angular unconformity and inclusion of a lower dolomite interval adds about 50 meters to the base of the section. New fossil evidence of a latest Devonian age confirms that this dolomite is part of the Stansbury section (see below). Rigby (1958) recognized that the Stansbury

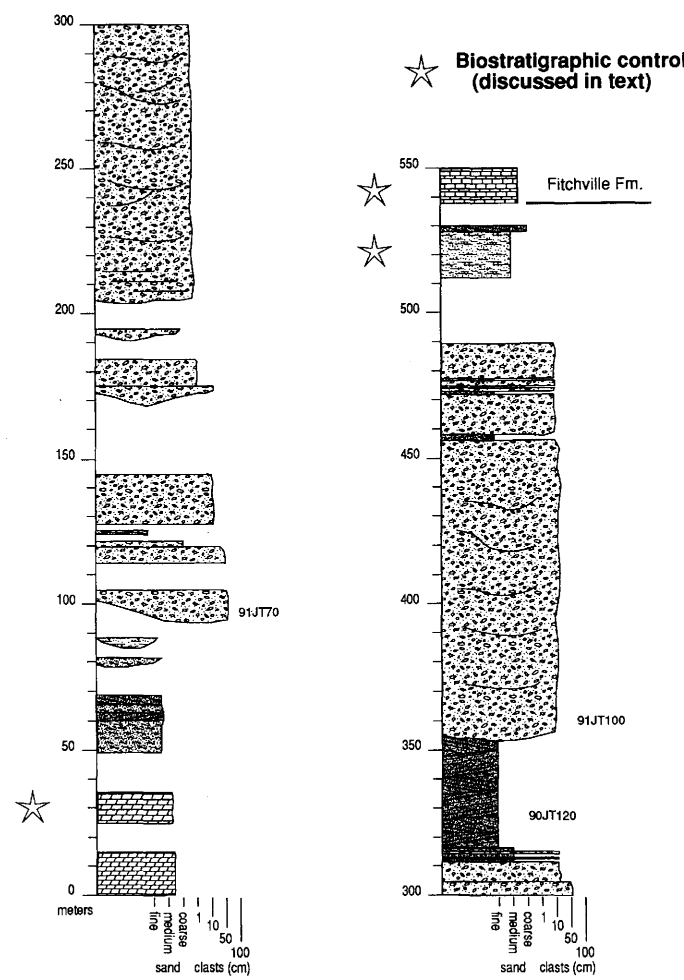

Figure 5. Measured section of the Stansbury Formation stratotype at Flux, Utah.

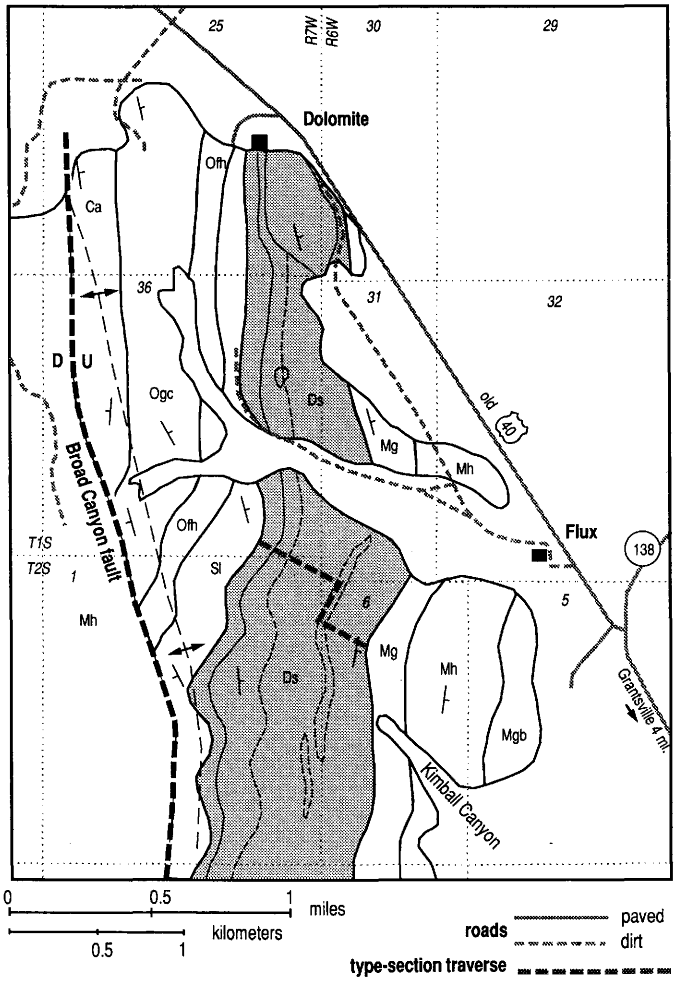

Figure 6. Geologic map of the northeastern Stansbury Mountains. See Figure 1 for location.

Formation contained an unknown thickness of basal dolomite on the west side of the Stansbury Mountains, and the redefined section at Flux corroborates this. Rigby (1958) also stated that strata mapped as Silurian dolomite in the Stansbury Mountains can probably all be assigned to the Sevy Dolomite; rocks assigned to the Simonson Dolomite, although mapped here, probably should be reassigned either to the Sevy or to the Stansbury formations.

The lowest Stansbury beds are laminated, light grey dolomite. Overlying this is 10 meters of a distinctive black dolomite that forms a marker horizon throughout the local area. This black dolomite is a recrystallized open-marine limestone, with abundant macrofossil fragments, including crinoidal debris. Samples collected from this black dolomite have been dated as latest Famennian to earliest Kinderhookian, based on microfossils (B. Mamet, written commun., 1991).

A laterally persistent quartz-arenite overlies the black dolomite throughout the study area. This is the "lower quartzite member" mapped by Stokes and Arnold (1958). At the type section, the lower part of the quartz-arenite comprises pods or lenses that are laterally discontinuous at outcrop scale, but at map scale form a continuous unit. The quartz-arenite pods have convex-down channel geometry, and cut out dolomite below. Quartz-arenite becomes more laterally continuous up section. In the channel bodies, sedimentary structures include flat lamination and small-scale cross-stratification. In the more continuous upper beds of quartz-arenite the most common feature is low-angle, tabular cross-stratification in sets 1 to 3 meters thick. Dolomite pebbles are mixed into the quartz-arenite in places as local lags deposits. Less common features include imbrication of these pebbles, and small-scale trough cross-lamination.

Cross-stratified quartz-arenite in the type section yields abundant paleocurrent data (Fig. 8). Trends are mostly west, with a range of local directions from northwest to southwest. Local variation between sets suggests oblique transport to a prevailing current.

A very coarse, 220-meter-thick, dolomite-clast conglomerate overlies the "lower quartzite member." The base of the conglomerate is irregular, and truncates the quartz-arenite on a surface that has up to 60 meters of relief. Clasts are primarily dolomite, of a variety of colors and textures. Stokes and

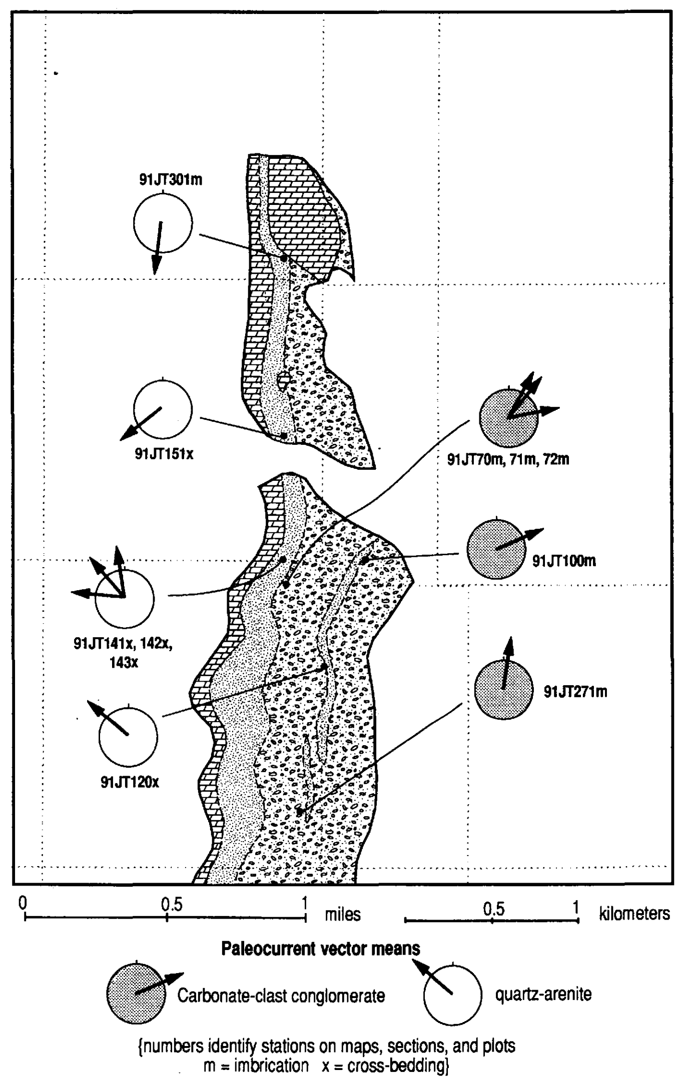

Figure 7. Lithofacies map of the Stansbury Formation, with paleocurrent measurement localities (see Figs. 8 and 9).

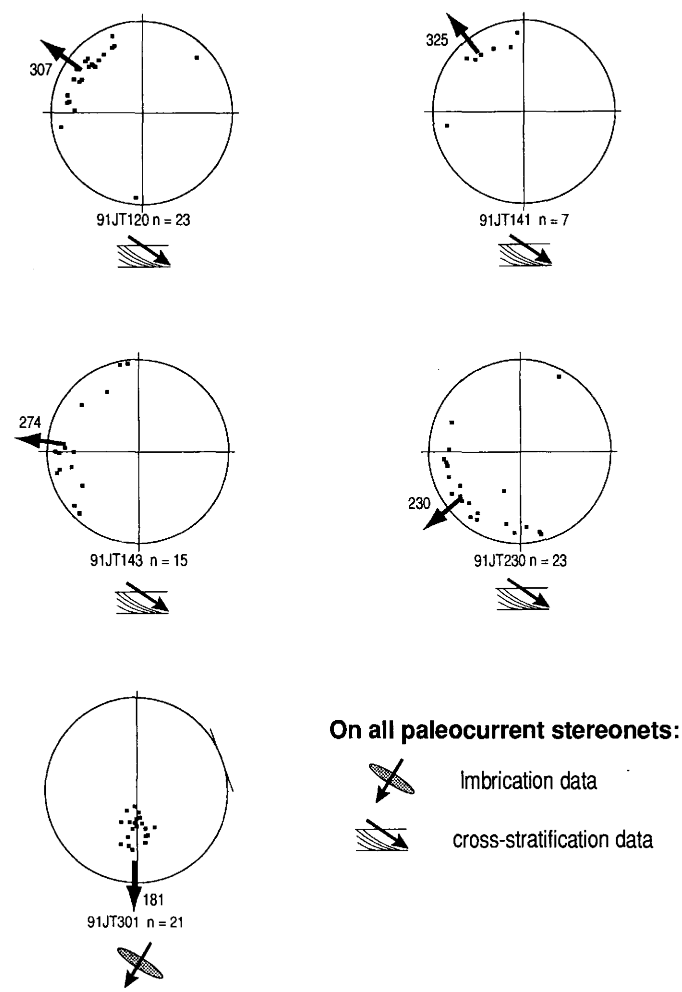

Figure 8. Paleocurrent data from quartz-arenite at Flux (locality numbers from map, Fig. 7).

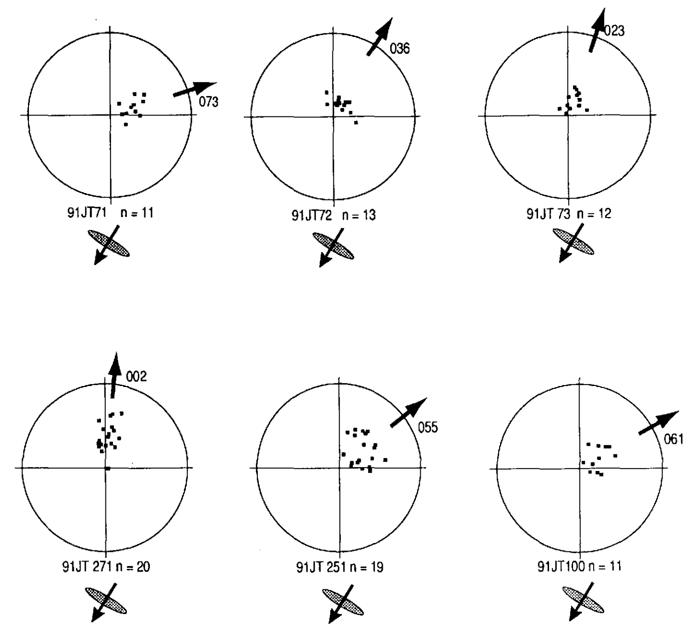

Figure 9. Paleocurrent data from conglomerate at Flux (locality numbers from map, Fig. 7).

Arnold (1958) identified clast compositions that represented all the subjacent Paleozoic strata, including rare quartzite clasts that they interpreted as having a Precambrian source. In some places, quartz-arenite clasts that appear to be rip-ups from the "lower quartzite member" are common.

The conglomerate contains subangular to subrounded and inequant clasts up to 1.5 meters in diameter. The conglomerate is generally matrix supported, and everywhere is matrix rich; the matrix is now dolomite, but originally may have been a dolomitic or calcareous, sandy mud. Although the conglomerate appears massive, there are bed-bounding surfaces within the unit that suggest nested channels. At the bases of these channels in a few places imbrication of the inequant clasts occurs.

Imbrication in the Stansbury Formation conglomerate beds indicates the direction of transport of these boulder gravels (Fig. 9). The principle transport direction was northeast, ranging from nearly north to east-northeast. Orientation of pebbles is generally tightly clustered in any one locality. This northeasterly trend is valid for imbrication measurements throughout the type section.

At the 310 meter level in the type section, conglomerate deposition is interrupted by a second interval of quartz-arenite. This unit is about 50 meters thick, and identical in all respects to the "lower quartzite member". It is, however, much less continuous laterally (Fig. 6, 7), occurring as lenses that pinch out within tens of meters along strike. Paleocurrent measurements from this unit have a similar trend to those in the lower quartz-arenite.

A dolomite-clast conglomerate 140 meters thick overlies the upper quartz-arenite interval. This conglomerate is similar in all respects to the conglomerate below, except that it is somewhat coarser in mean clast size. Above this is 40 meters of calcareous quartz-arenite and limestone that is poorly exposed in the type section. The quartz-arenite contains small-scale cross-lamination, and the limestone has visible fossil fragments and floating quartz grains. Samples from this limestone have a microflora indistinguishable from those collected from the base of the section, and date the unit as latest Famennian to earliest Kinderhookian. Limestones of the upper Stansbury Formation elsewhere in the study area have been dated as upper Famennian (N. Silberling, written commun., 1991).

The top of the Stansbury type section is taken as the base of the ledge-forming, dark, cherty limestone of the Fitchville Formation. The Fitchville represents the entire Kinderhookian series at its stratotype in the Tintic district (Hintze, 1988). This unit is dated here as upper Kinderhookian (N. Silberling, written commun., 1991); the lacuna is attributed to lack of deposition of the lower Fitchville in this area.

The depositional setting of the Stansbury strata at Flux is complex, and represents two overlapping processes. The conglomerates were deposited as submarine debris flows.

Quartz-arenite was brought into the area by shore-parallel currents. Intercalated limestone beds and sedimentary structures throughout indicate that the section is entirely marine.

The unsorted texture, matrix-supported fabric, and very coarse clast size support the interpretation that the conglomerate beds were deposited as subaqueous, gravity driven, density-modified flows. These features have been described as common in submarine debris-flow deposits by many workers (Walker, in Harms and others, 1975; Middleton and Hampton, 1976). Such deposits are reported to contain imbricate fabric such as described here. The convex-down bases to the beds suggest that the flows may have been initially turbulent and erosive.

Several lines of evidence indicate that these debris-flows were subaqueous. Indications of turbulence (imbrication, erosive channel bases, poorly developed stratification, inverse-to-normal grading) are all found in these rocks, and all indicate that fluids were abundant and possibly being entrained as the flows moved downhill. Also, open-marine biosparites are commonly intercalated throughout the section.

Alternative interpretations include subareal fan deposits, and a proximal submarine-fan setting. However, there is a complete lack of features expected on a subareal fan: associated fluvial and lacustrine sediments, levee deposits, sieve deposits, and paleosols. These rocks also lack many features expected on a submarine fan: channelized conglomerates, slumps, channel-wall rip-ups, and interchannel fines are all lacking. In addition, no associated submarine-fan features were found, such as turbidite bedding in more distal facies.

The most striking aspect of these conglomerate beds is their thickness and lateral (albeit local) persistence. It is apparent that these debris flows were not part of a complicated sediment distribution system with many energy levels and transport mechanisms. Rather, very coarse debris was shed into this area by gravity-driven flows, without many interruptions.

These conglomerate beds were probably deposited in a marginal-marine basin in a "Yallahs-type" fan delta (Wescott and Etheridge, 1980), where an alluvial debris fan built outward directly onto a submarine slope. The thickness and coarseness of the deposit, combined with paleocurrent data, suggest that the source of the sediment was nearby to the southwest. This marginal-marine slope need not have been steep; such flows are mobile on subareal slopes of 5 degrees or less (Rodine and Johnson, 1976). Further, the flows were *deposited* rather than flowing here, indicating that the local slope was flattening to the northeast, or there was local impoundment of the flows. Such flows would not "freeze up" unless physically stopped, but rather would dissipate downslope.

Quartz sands were concurrently carried along the basin margin in a westerly direction, presumably by long-shore currents or shore parallel flow driven by wind or tides. Shore-parallel currents of this type are common in many modern basins (McCubbin, 1982). Sedimentary structures reported here are typical of lower flow-regime (<1 m/sec. water flow velocity) migration of small, subaqueous dunes (Leeder, 1980).

The basin margin on which these strata were deposited was roughly east-west-trending and sloped northeast. This paleogeography satisfies the interbedded west-travelling quartz-arenites and northeast-flowing coarse debris-flows. The debris-flows were gravity-driven and necessarily flowed down hill, indicating that the paleoslope had a gentle, generally northeast dip. The conglomerate had a nearby, high-relief source in uplifted, subjacent strata. The quartz-arenite had a source far to the east on the craton.

ANOMALOUS DOLOMITE BEDS WITHIN THE STANSBURY FORMATION

At three localities in the northeastern Stansbury Mountains, dolomite beds occur as anomalous "blocks" within Stansbury Formation strata. They are anomalous in that they do not occur in the type section, nor do they extend very far along strike, and their contacts with the Stansbury strata are angular in places. Two of these blocks, at Miner's Canyon and at Dolomite (Fig. 1, 7) are hundreds of meters across, and the third, located on a ridge north of Flux, is only a few tens of meters across. This latter, small "block" is a fine-grained dolomite that occupies a pod-like cutout in Stansbury strata, and appears to be a dolomitic, mud-filled channel. Unlike the larger blocks, its bedding is concordant with surrounding Stansbury strata.

The two, large anomalous dolomite blocks at Dolomite and Miner's Canyon comprise fine-grained, laminated to massive dolomite beds that are brecciated into what appears to be a pre-lithification, solution-collapse fabric. At both localities, a thick section of this anomalous dolomite lies with angular discordance on Stansbury conglomerate and quartz-arenite. At Dolomite, this basal surface clearly cuts out several tens of meters of lower Stansbury section. At both localities, the dolomite blocks are conformably overlain by Stansbury conglomerate and quartz-arenite in a relatively thin section, that is, in turn, overlain by Fitchville Formation. Lateral contacts of the blocks are not exposed.

The anomalous dolomite block at Dolomite was interpreted by Stokes and Arnold (1958) as a slide block of Silurian rocks, implaced during deposition of the Stansbury by gravity sliding. The similar relationships at Miner's Canyon were not previously recognized. The angular truncation of Stansbury strata under the dolomite beds makes this interpretation unlikely. Further, these laminated, solution-brecciated dolomite beds do not closely resemble the subjacent, massive dolomites of the Ordovician-Silurian.

Alternatively, these dolomite beds may document active uplift, tilt, and erosion and subsidence of strata in the Stansbury basin during its evolution. In this scenario, a block of Stansbury sediments was uplifted and tilted during basin sedimentation. After erosion, subsidence resumed, and the first sediments accumulated were sabkha-type, primary, algal dolomite. As subsidence continued, these dolomite beds were subject to solution-recrystallization and collapse, and were finally buried by clastic sediments of the upper Stansbury Formation. The multiple occurrences and very limited lateral extent of these anomalous blocks suggests that block-faulting may also have played a role in their formation.

STANSBURY FORMATION: IMPLICATIONS

The first evidence of Late Paleozoic, tectonic disruption of the continental margin in western Utah is the pronounced angular unconformity under the Stansbury Formation. Pre-Stansbury (Late Devonian?), local uplift resulted in removal of most of the Paleozoic section in the northern Stanbury Mountains. Folding resulted in strata tilt of at least 30° in places. This uplift has been attributed to activity along the Uinta arch (Rigby, 1959; Roberts and Tooker. 1969), a structure which is thought to intersect the Stansbury Mountains at about the latitude of South Mountain (Fig. 1). If this is true, the area affected by the arch is much more widespread than previously thought, and strata apparently are not much affected in the southern Stansbury Mountains where the arch is thought to have been located.

The Stansbury Formation itself represents the effects of further active uplift and subsidence on the craton margin in Late Devonian-Early Mississippian time. Basin subsidence was apparently most rapid in the area presently just west of Flux, Utah. Uplift was a short distance to the south-southwest. The result was a thick accumulation of coarse conglomerate and quartz sand along a locally northeast-facing basin margin. Quartz sand made its way west from the craton throughout the Late Paleozoic and is represented throughout the Paleozoic section as thin quartzite interbeds. Movement of this sand was not deterred by the local tectonic activity that formed the Stansbury basin, and it continued to be transported west along the east-west-trending shoreline.

The most pronounced effect of the Late Devonian structural disruption is not uplift, but rather subsidence. Although the Stansbury Formation is laterally limited, its thickness is impressive. The slopes that mobilized the coarse debris-flows that filled this basin need not have been steep, but the persistence of these slopes (and vertical accumulation of sediments) suggests that this is a tectonic feature of some consequence.

The Stansbury Formation at Stansbury Island cannot readily be related to the stratotype at Flux. The sedimentology and internal stratigraphy are quite different. The depositional settings could be adjacent systems; the sand-wave setting at Stansbury Island may be the offshore equivalent to the shoreline or near-shore sands at Flux. Conversely, there is no independent reason to believe that these settings were linked in any way; in fact, the paleocurrent data suggest that these two settings cannot be in their original positions relative to each other. Stansbury Island is only about 12 kilometers to the north-northeast of Flux, and is directly in line with the direction of flow of the debris flows that formed the thick conglomerate units. It seems unlikely that none of the debris flows made it as far as the present position of Stansbury Island, and yet there is no conglomerate in the Stansbury Island section.

The tectonic activity that formed the basin into which the Stansbury Formation was deposited is an anomaly in regional tectonic history in several respects. First, the style of the basin seems to be narrow and steep-sided, unlike the subtle tilting, transgression, and regression usually reported as tectonic activity in upper Paleozoic rocks in this area (see, for instance, Johnson and others, 1991; Poole and Sandburg, 1991). Also, as noted above, the Stansbury episode does not particularly fit ideas about the Uinta arch. The east-west-trending basin margin runs at right angles to the general trend of the craton margin, but rapid, lateral facies shifts between Flux and Timpie Valley suggest that there may also have been north-south-trending structural control. It is tempting, but probably premature, to try to tie the Stansbury basin into the onset of obduction of the Antler allochthon, which was occurring at about this time (Johnson and Pendergast, 1981). That event was well to the west in central Nevada, and this would be the first indication of Antler orogeny effects this far east.

ACKNOWLEDGMENTS

This project was funded by a research grant from the Utah Geological Survey. That grant also funded concurrent work on the structural history of the northern Stansbury Mountains by Patricia Cashman; these studies together clarified and helped to resolve many of the stratigraphic problems in the area. Conversations with N. Silberling, K. Nichols and K. Giles aided greatly in understanding regional stratigraphy. Early versions of this paper were read by L.F. Hintze, who helped with stratigraphic nomenclature, J.K. Rigby, Silberling, and Nichols. The final version was edited by J. Wilson and an anonymous reviewer.

REFERENCES CITED

Allmendinger, R.W., and Jordan, T.E., 1989, Geologic map of the Newfoundland Mountains, northwestern Utah: U.S. Geological Survey Miscellaneous Field Studies Map, MF 2087, 1:31,680

Chapusa, F.W.P., 1969, Geology and structure of Stansbury Island: M.S. Thesis, University of Utah, Salt Lake City, 83 p.

Costello, W.R. 1974, Development of bed configurations in coarse sands: Cambridge Mass., Earth and Planetary Science Department, M.I.T. Reprint 74.1.

Harms, J.C., Southard, J., Spearing, D.R., and Walker, R.G., 1975, Depositional enivironments interpreted from primary sedimentary structures and stratification sequences: SEPM Short Course Notes No. 2.

Hintze, L.F., 1988, Geologic history of Utah: Brigham Young University Geology Studies, Special Publication 7, 202 p.

Johnson, J.G. and Pendergast, A., 1981, Timing and mode of emplacement of the Roberts Mountain allochthon, Antler orogeny: Geological Society of America Bulletin, v. 92, p. 648-658.

Johnson, J.G., Sandberg, C.A., and Poole, F.G., 1991, Devonian lithofacies of the western United States, *in* Cooper, J.D. and Stevens, C.H., eds., Paleozoic paleogeography of the Western United States-II, Pacific Section SEPM, v. 67, p. 83-106.

McCubbin, D.G., 1982, Barrier-island and strand-plain facies, *in* Scholle, P.A. and Spearing, D., eds., Sandstone depositional environments: American Association of Petroleum Geologists Memoir 31, p. 247-280.

Middleton, G.V. and Hampton, A., 1976, Subaqueous sediment transport and deposition by sediment gravity flows, *in* Stanley, D.J. and Swift D.J.P., eds., Marine sediment transport and environment management: New York, Wiley, p. 197-218.

Miller, D.M., Jordan, T.E., and Allmendinger, R.W., 1990, Geologic map of the Crater Island quadrangle, Box Elder County, Utah: Utah Geological and Mineral Survey Map 28, 1:24,000.

Moore, W.J., and Sorenson, M.L., 1979, Geologic map of the Tooele 1° x 2° Quadrangle, Utah: United States Geological Survey Miscellaneous Investigation Series, Map I-1132, 1:250,000.

Palmer, D.E., 1970, Geology of Stansbury Island, Tooele County, Utah: Brigham Young University Geology Studies, v. 17, pt. 2, p. 1-30.

Poole, F.G. and Sandberg, C.A., 1991, Mississippian paleogeography and conodont biostratigraphy of the western United States, *in* Cooper, J.D. and Stevens, C.H., eds., Paleozoic paleogeography of the Western United States II, Pacific Section SEPM, v. 67, p. 107-136.

Rigby, J.K., 1958, Geology of the Stansbury Mountains, eastern Tooele County, Utah, *in* Rigby, J.K., ed., Geology of the Stansbury Mountains, Tooele County, Utah: Utah Geological Society, v. 13, p. 1-133.

Rigby, J.K., 1959, Upper Devonian unconformity in central Utah: Geological Society of America Bulletin, v. 70, p. 207-218.

Rodine, J.D. and Johnson, A.M., 1976, The ability of debris, heavily freighted with coarse clastic materials, to flow on gentle slopes: Sedimentology, v. 23, p. 213-234.

Roberts, R. J. and Tooker, E., 1969, Age and regional significance of conglomerate in the Newfoundland and Silver Island Mountains, Utah (abs.): Geological Society of America Abstracts with Program, v. 1, no. 5, p. 69.

Stokes, W.L. and Arnold, D.E., 1958, Northern Stansbury Range and the Stansbury Formation, *in* Rigby, J.K., ed., Geology of the Stansbury Mountains, Tooele County, Utah: Utah Geological Society, v. 13, p. 134-149.

Trexler, J.H., Jr., (in review), Devonian-Mississippian active tectonism and basin formation in the interior craton margin: the Stansbury Formation of western Utah: submitted to Geological Society of America Bulletin.

Walker, R.G., 1982, Deep water sandstone facies and submarine fans, *in* Tillman R.W. and Syed, A.A., eds., Deep water canyons, fans and facies: models for stratigraphic trap exploration: American Association of Petroleum Geologists Reprint Series no. 26, p. 1-35.

Wescott, W.A. and Etheridge, F.G., 1980, Fan-delta sedimentology and tectonic setting — Yallahs fan delta, southeast Jamaica: American Association of Petroleum Geologists Bulletin, v. 64, p. 374-399.

STRUCTURAL GEOLOGY OF THE NORTHEASTERN STANSBURY MOUNTAINS

Patricia H. Cashman
Department of Geological Sciences
University of Nevada, Reno

ABSTRACT

The structure of the Stansbury Mountains is dominated by Mesozoic east-vergent folding and thrusting. This is overprinted on a cryptic Devonian deformation event (Rigby, 1959). The anticline-syncline pair that underlies most of the range is a fault-propagation fold, cored by a blind thrust. The anticline is doubly plunging, and en echelon folds at the north and south ends of the range take up much of the shortening as the main anticline dies out. The macroscopic folds are curvilinear (convex toward the west) at the scale of the range. The Broad Canyon fault, previously interpreted to be a west-dipping thrust fault, is an east-dipping reverse fault that postdates thrust-related deformation. Two additional thrust faults within the range, postulated by Tooker and Roberts (1971), were disproven by this study. A brief deformation history of the Stansbury Mountains is: (1) localized Late Devonian folding, uplift and erosion; (2) Mesozoic east-vergent folding and thrusting which impinged on the structural salient of the Uinta axis, followed by continued eastward propagation of thrust-related deformation to the north and south of the Uinta axis, resulting in curvilinear fold traces; (3) final shortening by back-thrusting along the Broad Canyon fault; (4) Tertiary tilting and normal faulting. The structure of the Stansbury Mountains — in particular, the absence of regional-scale thrusting within the range — places important constraints on the internal stratigraphy of the synorogenic Devonian-Mississippian Stansbury Formation.

INTRODUCTION

The Stansbury Mountains of north-central Utah lie between the well-documented structures of the fold and thrust belt to the east and the metamorphic hinterland to the west (Fig. 1). The range is cored by the doubly-plunging Deseret anticline (Lambert, 1941), which dies out at the northern and southern ends of the range (Rigby, 1958) (Fig. 2). Smaller en echelon folds occur at both ends of the range, where the Deseret anticline dies out. The Deseret anticline and the Little Baldy syncline along its east flank (Rigby, 1958) form an east-verging anticline-syncline pair. These two folds expose rocks ranging from Cambrian to Triassic (Jordan and Allmendinger, 1979) in age, and have a structural relief of at least 10 km. They are separated by the subvertical Broad Canyon fault, which has been interpreted to be a west-dipping reverse fault (Rigby, 1958) or thrust fault (Tooker and Roberts, 1971; Sorensen, 1982; Tooker, 1983). The Stansbury Mountains are bounded on the west by a system of Tertiary normal faults; alluvium-filled basins separate them from the Oquirrh Mountains to the east and Cedar and Lakeside Mountains to the west. The Stansbury Mountains stand across the west end of the "Uinta trend" (Roberts and others, 1965; Crittenden, 1976; and many others), a significant east-west structural feature that extends across the eastern half of Utah and into Colorado.

The dramatic structural relief of the folding in the Stansbury Mountains provides information of stratigraphic, as well as structural, interest. The oldest rocks exposed in the

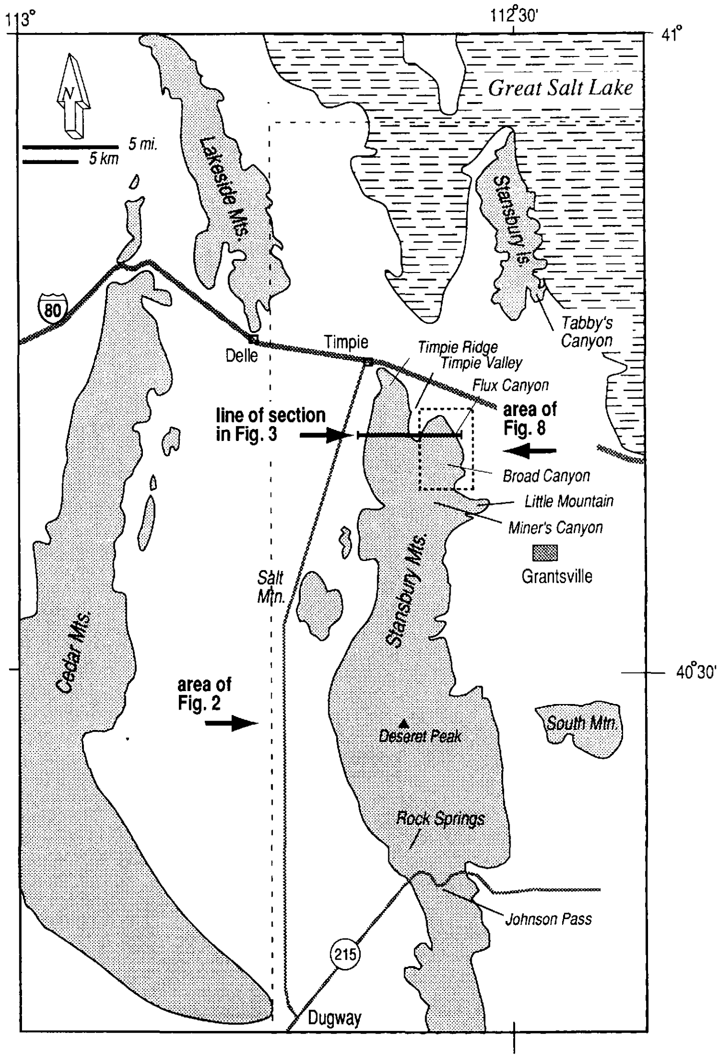

Figure 1. Location map showing major geographic features in the Stansbury Mountains and vicinity.

adjacent ranges are Mississippian, while the complete Paleozoic section is exposed in the Stansburys. Thus the Stansbury Mountains provide one of the few glimpses of the lower Paleozoic stratigraphy in northwestern Utah. One of the most striking aspects of this stratigraphy is a profound Late Devonian unconformity (Rigby, 1959) overlain by the enigmatic coarse conglomerate deposits of the Stansbury Formation (Stokes and Arnold, 1958; Trexler, this volume).

The overall structure and stratigraphy of the range were first described by Rigby (1958). Tooker and Roberts (1971) recognized the pattern of east-verging deformation and related it to thrusting. They interpreted the range to comprise four thrust sheets, in contrast to the two fault blocks described by Rigby. Tooker (1983) elaborated on the thrust interpretation, fitting it into a model for regional correlation of thrust plates in northwestern Utah. Other workers have mapped local areas within the Stansbury Mountains (e.g., Sorensen, 1982; Foose and others, 1989; Foose, 1989) and have debated the existence of some of the thrusts of Tooker and Roberts (1971), but no detailed structural studies have been undertaken. Similarly, the Stansbury Formation has been recognized as anomalous for its age and geographic position, but it has not been re-examined since the original description (Stokes and Arnold, 1958).

The structural study described here was undertaken in conjunction with a detailed sedimentological study of the Stansbury Formation (see Trexler, this volume, and Trexler, in review). The primary intent of the project was to resolve the number of thrusts in the range and to constrain the amount of shortening due to thrust-related deformation, in order to reconstruct the Stansbury depositional basin. Additional objectives were to gather any data pertaining to regional structural issues such as thrust correlation and the termination of the Uinta trend. The results presented here are based on reconnaissance throughout the range and local detailed mapping at the northern end.

In this paper, I will describe the structural geometry and deformational style of the Mesozoic east-verging deformation in the northeastern Stansbury Mountains and of the deformation related to the Broad Canyon fault. These data suggest that the Broad Canyon fault is a west-verging reverse fault with relatively small offset, here interpreted to be a back-thrust. My mapping also eliminates two thrusts proposed by Tooker and Roberts (1971). Therefore, the bulk of the structural shortening expressed within the Stansbury Mountains was accomplished by folding rather than by thrusting. The paper will conclude with the implications of the structural reconstructions for the geometry of the Devonian-Mississippian Stansbury depositional basin and for regional thrust correlations and structure.

EAST-VERGENT THRUSTING

The principal anticline-syncline pair in the Stansbury Mountains (the Deseret anticline and Little Baldy syncline) (Figs. 2, 3) is herein interpreted to be a fault-propogation fold (as defined by Suppe and Medwedeff, 1984; Suppe, 1985). The Stansbury folds have planar limbs and relatively narrow hinges, and the fold shapes change along strike. The folds are asymmetric; west-facing limbs dip gently, whereas the shared east-facing limb is steep to overturned. Overturning is restricted to the central part of the range, but is locally strong (as much as 50°). This fold geometry, particularly in an isolated anticline/syncline pair such as that in the Stansbury Mountains, is typical of fault-propagation folding (Suppe and Medwedeff, 1984; Suppe, 1985). Fault propagation folds form as a thrust fault steps up, most commonly from a bedding-parallel detachment, and represent the deformation immediately ahead of the propagating fault surface (Fig. 4). Although many fault propagation folds are later broken along one of the axial surfaces or the intervening limb by the propagating thrust, this has happened only very locally in the Stansbury Mountains. Thus, although the macroscopic folds are related to thrust faulting, the thrust itself is blind. It can be reasonably inferred to terminate at relatively shallow depths in the core of the Deseret Anticline, based on map relationships and geometric constructions (Fig. 3).

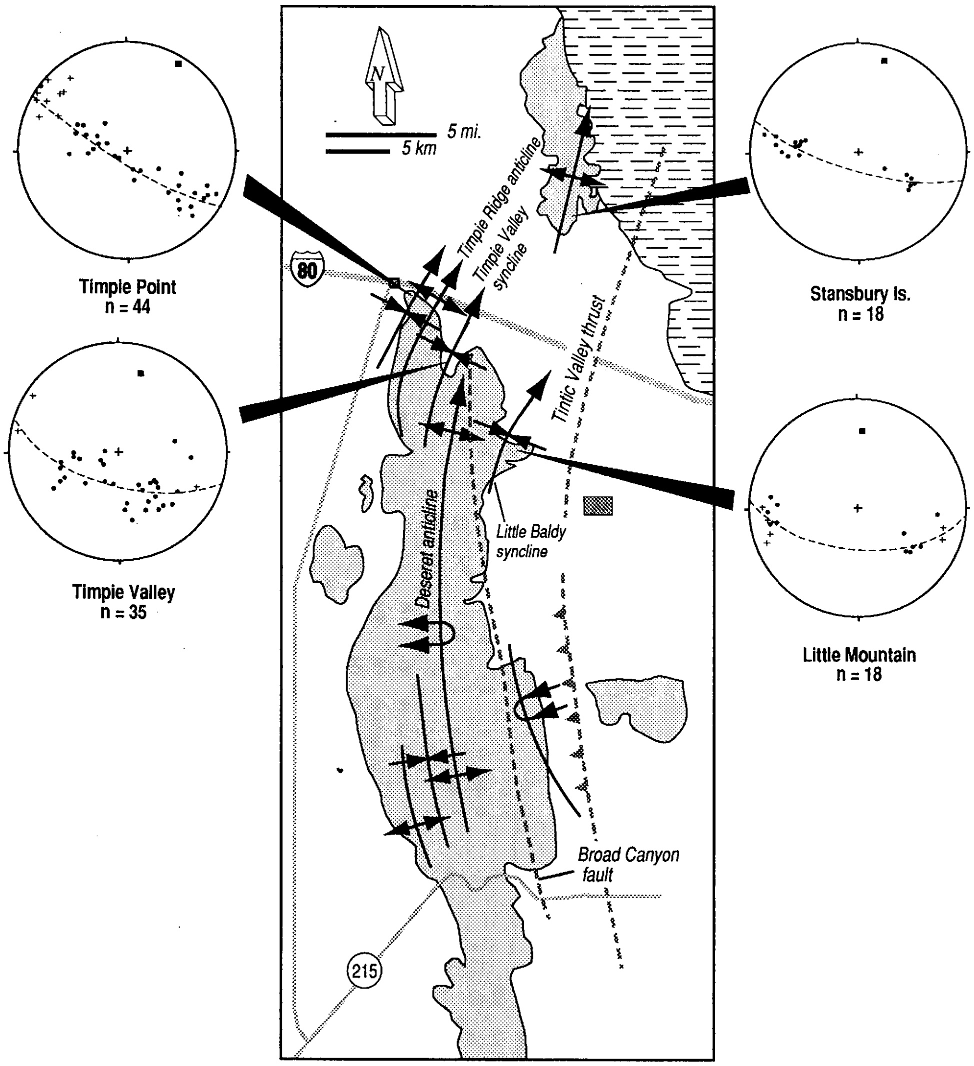

Figure 2. Location map showing major geologic features in the Stansbury Mountains; modified from Rigby (1958). Stereograms show poles to bedding (dots) and poles to cleavage (crosses) for several of the en echelon folds at the north end of the range. Best-fit great circles and fold axes were computed by "Stereonet 4.1" public domain software written by R. Allmendinger. Data from Foose (1989) are included in the stereogram for the Timpie Valley anticline, and data from Chapusa (1969) are used for the stereogram of Stansbury Island. Note that the Timpie Point station is restricted to strata below the mid-Paleozoic unconformities, and the Little Mountain station is restricted to strata above these unconformities. The other stations are a mix of the two, which may explain the greater scatter in these plots.

Although the thrust fault related to the fault propagation fold is a blind thrust, a second fault, generally interpreted to be a thrust fault, is required in the (covered) interval between the Stansbury Mountains and South Mountain (Fig. 2). This fault was recognized by Billingsley and Locke (1939, p. 43), and was named the Tintic Valley thrust by Roberts and others (1965). While stratigraphic juxtapositions actually require three faults (Jordan and Allmendinger, 1979; Tooker, 1983), structural relationships suggest that the eastern of these faults is the major feature, while the western ones are probably imbricates or splays with relatively minor offset. The Tintic Valley thrust is thought to crop out in the Gilson Mountains to the south (H.T. Morris, oral communication, 1967, as cited in Tooker and Roberts (1971)), and its presence has been inferred northward, passing east of Stansbury Island (Crittenden, 1976; Tooker, 1983) (Fig.2).

Two additional thrusts proposed by Tooker and Roberts (1971), were not found in this study. The first of these, termed the Timpie thrust, coincides with the sub-Mississippian unconformity and is in fact an erosional surface. Careful examination of this contact along the west side of Timpie Valley showed none of the mesoscopic structures associated with faulting elsewhere in the range (e.g., local cleavage development or brecciation and veining). The second of these, termed the Delle thrust, was not observed by Tooker and Roberts (1971) on the surface, but was postulated based on the absence of southward continuations of the Timpie Ridge anticline and the Timpie Valley syncline. If these folds are en echelon with the Deseret anticline (growing in amplitude northward as the Deseret anticline decreases in amplitude), the rationale for the Delle thrust disappears.

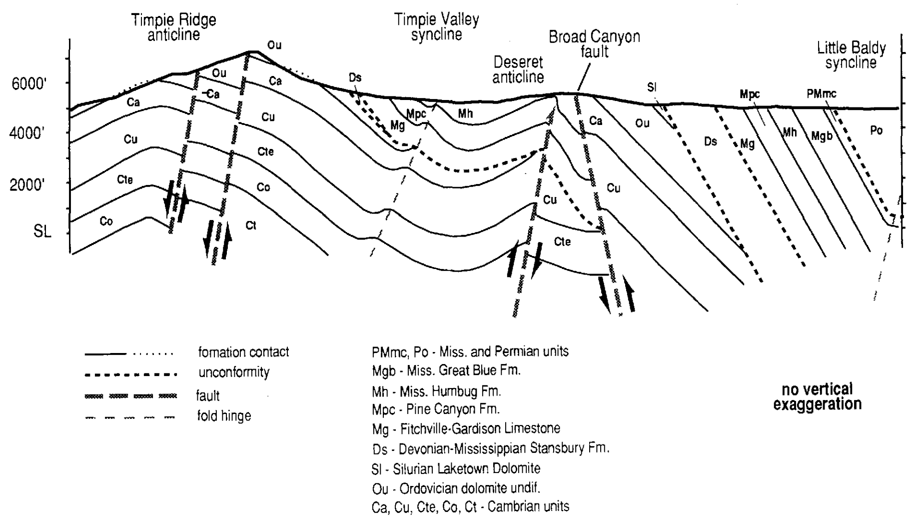

Figure 3. Schematic cross-section across the northern Stansbury Mountains. Map contacts are from Rigby (1958); therefore, his Mississippian stratigraphic units are used, although these are not in agreement with current nomenclature. Note the variable stratigraphic separation across the Broad Canyon fault, and the dramatic lateral thickness changes in the DevonianMississippian Stansbury Formation.

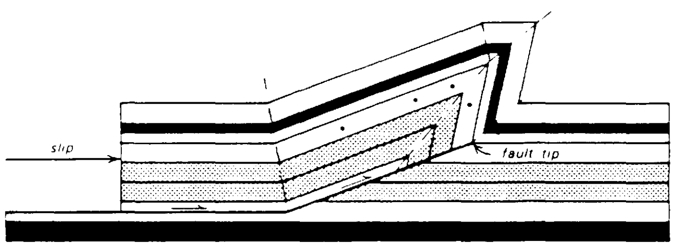

Figure 4. Diagram of an ideal fault propogration fold, from Suppe (1985).

The Deseret anticline dies out near the northern and southern ends of the Stansbury Mountains. Its northern termination is well exposed in eastern Timpie Valley; it is a small, tight fold (wavelength less than 1 km), characterized by a steeply plunging hingeline and well-developed axial planar cleavage. Approximately 1 km south of this final exposure, and extending southward for 2 km, Rigby (1958) maps a fault cutting the steep eastern limb of the fold. This may represent the tip of the thrust that cores the range; if so, it appears to be the only exposure of this otherwise-blind thrust. The strongest penetrative deformation observed in this study was adjacent to and structurally above this fault (see below); the fabric supports the interpretation that this fault is a structurally significant feature.

En echelon anticlines at the northern and southern ends of the range take up much of the shortening from the Deseret anticline (Fig. 2). South of Deseret Peak, the main anticline dies out and a second picks up approximately 3 km to the west. This fold has also been called the Deseret anticline (Teichert, 1959), and was clearly thought by him and by Rigby (1958) to be part of the same fold system as the main fold. North of Miners Canyon, three en echelon folds increase in amplitude as the Deseret anticline dies out —the Timpie Valley syncline, Timpie Ridge anticline (both named by Rigby, 1958), and an unnamed syncline at the northernmost end of the range (Fig. 2).

At first glance, the Timpie Ridge anticline and the unnamed syncline at the northern end of the range appear to contradict the regional east-verging fold pattern. Their style (planar limbs and relatively narrow hinges) and orientation (northeast-plunging hingelines) are consistent with those of other folds in the northern Stansbury Mountains (Fig. 2). However, the west-facing fold limbs dip more steeply than the east-facing limbs, suggesting westward vergence. Mesoscopic kinematic indicators, including well-developed mesoscopic folding in interbedded limestone and siltstone of the Garden City Formation, indicate a west-over-east sense of shear, in spite of the steep west-facing fold limbs (Fig. 5). One possible explanation is that these folds record flexural slip on the limbs of the larger fold. However, the stratigraphic position of the units in these folds suggests another possible solution to the paradox: the rocks exposed in Timpie Ridge underlie the sub-Stansbury unconformity. This unconformity is angular; the underlying units dip moderately west in both Flux Canyon and Timpie Valley, to the east of Timpie Ridge (Fig. 6), and at Salt Mountain, to the west of Timpie Ridge (Fig. 1). East-vergent folds superimposed on a west-dipping homocline can produce folds that have steeper west-facing limbs than east-facing limbs (Fig. 7). The occurrence of the apparent west-verging folds exclusively in pre-Stansbury stratigraphic units suggests that this may be the case in the northern Stansbury Mountains.

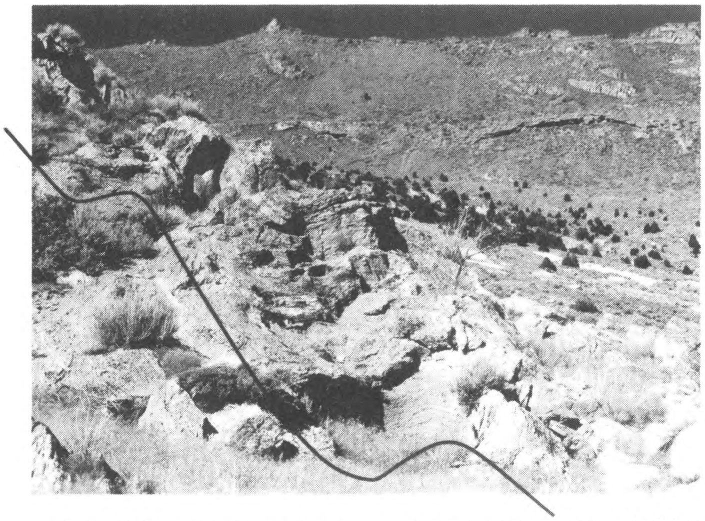

Figure 5. Outcrop photo of east-vergent asymmetric mesoscopic folds from the northern end of the Stansbury Mountains.

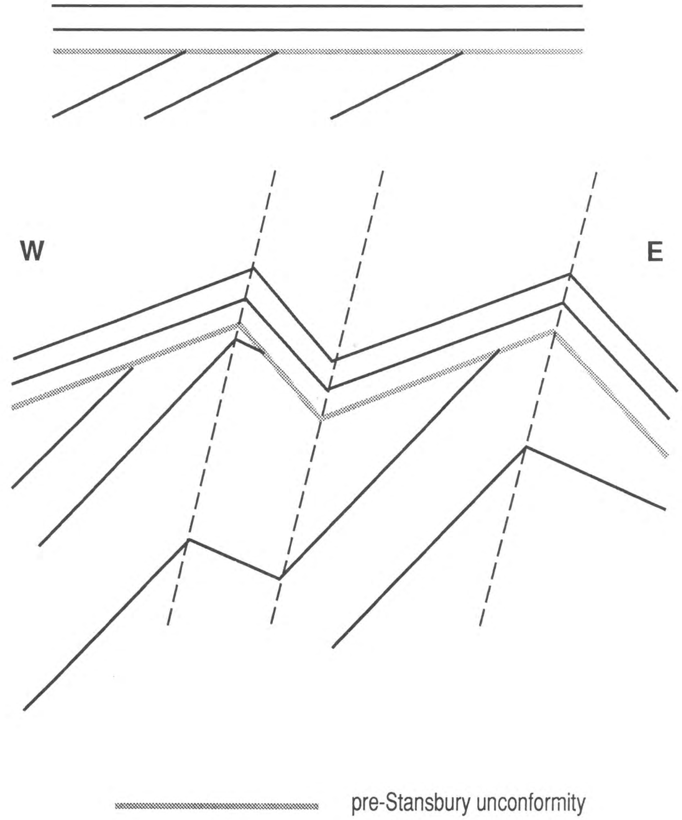

Figure 7. Diagram of the formation of apparent west-vergent folds (by what is actually east-vergent folding) due to the presence of an angular unconformity within the section.

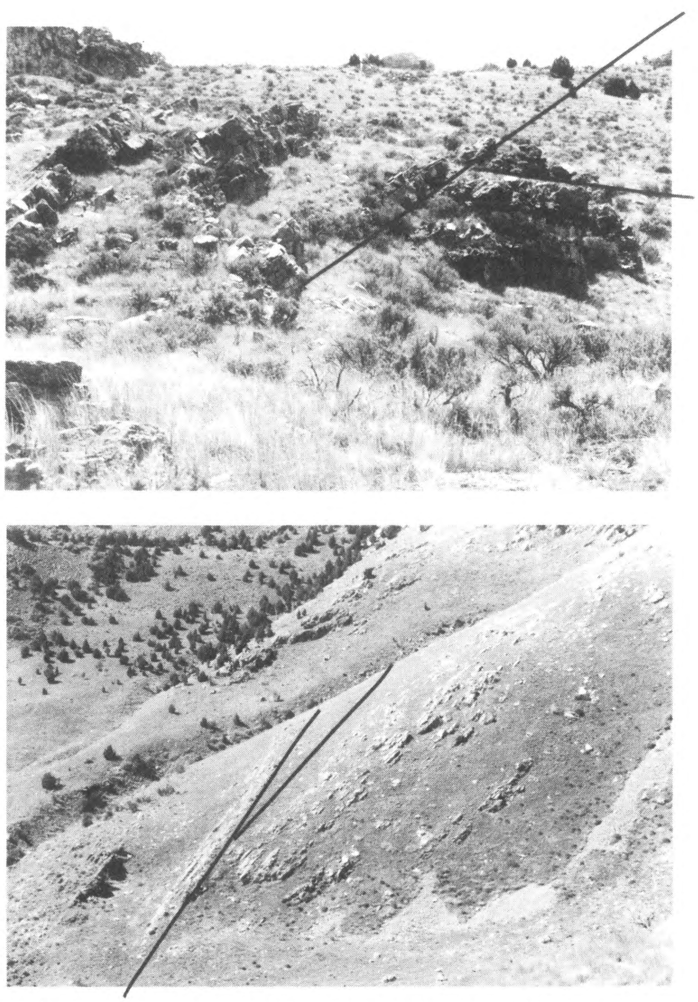

Figure 6. Outcrop photos of the angular relationship under the Devonian unconformity. (a) Flux Canyon (b) west side of Timpie Valley.

Cleavage is associated with the macroscopic, east-vergent folding; it is symmetrical with respect to the fold axial surfaces, fanning slightly around the folds. It is generally restricted to the cores of folds, and even in fold cores its presence is lithologically controlled. Cleavage is represented by closely spaced parallel partings marked by concentrations of clay-rich material. It formed at a high angle to bedding, starting early in the development of the folds. The folding continued during or after formation of the cleavage, as shown by the fanning of cleavage around the fold cores.

The strongest penetrative fabric is developed in the Cambrian carbonates at the southeast end of Timpie Valley. Here the limestones contain boudins and rootless hinges of dolomite in a strongly foliated limestone matrix. The structural position of this locality is near the core of the Deseret anticline; the stratigraphic position is below the sub-Stansbury unconformity. Although this is the locus of the most extreme pre-Mississippian deformation (as shown by the high-angle truncation of the Cambrian units beneath the unconformity — see map in Rigby, 1958), there is no evidence elsewhere of penetrative deformation associated with the pre-Mississippian event. It seems more likely that the penetrative deformation at the southeast end of Timpie Valley is related to the Deseret anticline, and, specifically, to the fault at its core. Near its northern termination, this anticline is locally faulted at the surface, probably by the thrust which cores the fold throughout the range (see above). The fault crops out less than 1 km from the strong foliation in the Cambrian carbonates; further mapping is needed to determine whether the Mississippian rocks adjacent to the fault are also strongly foliated.

Mesoscopic folding is rare in the Stansbury Mountains and, where present, appears to be lithologically controlled. It is absent in most of the massive Paleozoic quartzites and carbonates, but is locally well developed in thinly interbedded units of contrasting competence. Mesoscopic folds range in amplitude from cm to m, but are consistently asymmetric to overturned and east-verging.

THE BROAD CANYON FAULT — AN EAST-DIPPING REVERSE FAULT

The Broad Canyon fault runs the length of the range, separating the Deseret anticline and the Little Baldy syncline. First recognized by Rigby (1958) and interpreted to be a west-dipping reverse fault, it was reinterpreted by Tooker and Roberts (1971) as a west-dipping thrust fault. The thrust interpretation was preferred by most subsequent workers (e.g., Armin, 1979; Moore and Sorensen, 1979; Sorensen, 1982). The field evidence contradicts these interpretations. The fault itself is poorly exposed, but mapping demonstrates that it is offset very little as it crosses topography and is therefore sub-vertical. Arnold (1956) estimated its dip as 75° east in Flux Canyon, and Rigby (1958) estimated its dip as 85° east in Broad Canyon, both at the northeast end of the range (Fig. 7). Scattered erosional remnants of Tertiary volcanic units along the east flank of the Stansbury Mountains dip gently to moderately east, recording Tertiary (post-volcanic) eastward tilting of as much as 35°. When this is removed, the pre-Tertiary dip of the Broad Canyon fault was almost certainly toward the east at a moderate angle.

The stratigraphic separation across the fault is highly variable along its length, and does not help resolve the question of sense of motion along the fault. The Mississippian Great Blue Limestone (or, locally, one of the two adjacent units) forms the footwall of the fault throughout the range (see Fig. 3 for stratigraphic column). Cambrian through Pennsylvanian rocks are adjacent to the fault in the hanging wall, as the fault cuts the Little Baldy syncline in the northeastern Stansbury Mountains. Thus the Broad Canyon fault clearly postdates the folding, and stratigraphic juxtapositions cannot be used to determine sense or amount of motion. The folding may be obscuring yet another reason for the contradictory stratigraphic separations across the Broad Canyon fault: The strata underlying the Devonian unconformity differ on the two sides of the fault, suggesting that the Devonian Stansbury Formation may have been deposited on a surface with significant topographic relief (see below).

This study found evidence for west-directed reverse motion along the Broad Canyon fault. The regional eastward dip on the east flank of the range is reversed adjacent to (east of) the fault (Figs. 3, 8). The zone of westward dip is

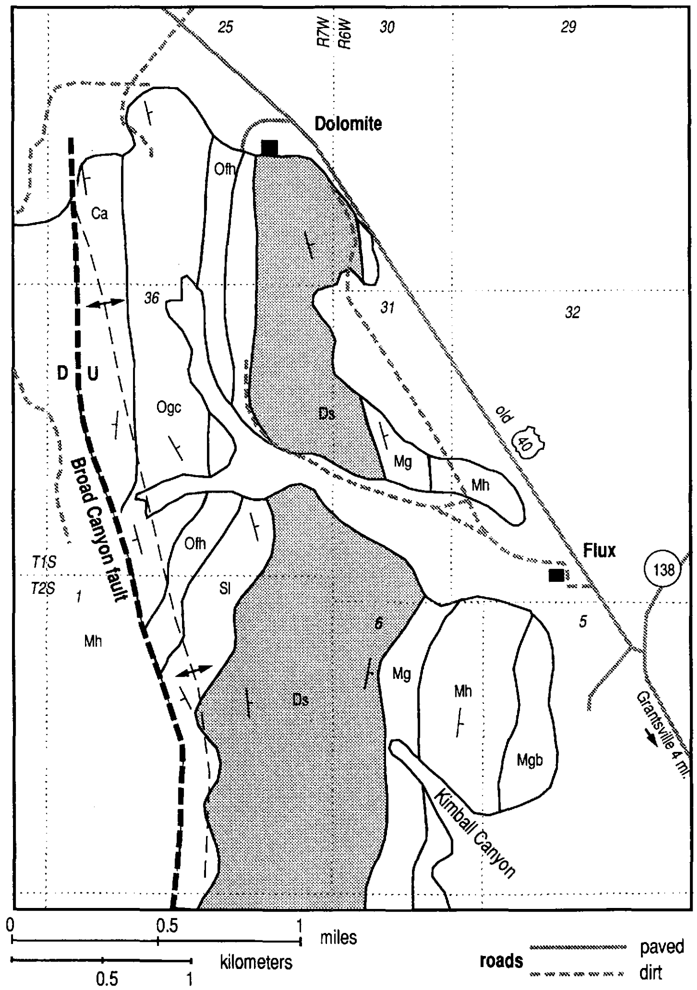

Figure 8. Geologic map of Flux Canyon and vicinity, showing the dip reversal adjacent to the Broad Canyon fault. Mapping from Rigdy (1958), Stokes and Arnold (1958) and this study. See Figure 3 for stratigraphic symbols.

relatively narrow (400 m), and is characterized by a brittle mesoscopic deformation style (see below). These characteristics are compatible with local drag folding caused by east-side-up motion. A comparable drag effect has not been observed west of the fault, probably because the fault is sub-parallel to bedding in the footwall.

The mesoscopic deformational style associated with the Broad Canyon fault also distinguishes it from the eastward-vergent, thrust-related, deformation. Penetrative fabric occurs only very locally along the fault — it was observed in three places during the course of this study, always in a zone < 10 m thick. More typically, the rocks within several tens of meters of the fault are locally strongly brecciated and veined. Brecciation and veining are found in limestones as well as dolomites, demonstrating that the deformation style is not lithologically controlled. Instead, this style indicates that the Broad Canyon fault occurred under more brittle conditions than those associated with the macroscopic folding in the range, and supports the field relations which indicate that it postdates the folding.

Petrographic evidence from the foliated rocks along the Broad Canyon fault supports the field evidence for reverse (east-side-up) motion. The rocks show flattening perpendicular to foliation and sub-vertical extension in the plane of the foliation. Most grains are not internally deformed, and show no evidence of cataclasis or intracrystalline plasticity. Deformation occurred by limited cataclasis of selected grains, and by diffusional mass transfer — as shown by local solution and fiber growth. East-side-up simple shear is well documented petrographically in samples from two localities, and may include a slight left-lateral component. Kinematic indicators include sigma-type porphyroclasts (Passchier and Simpson, 1986) and asymmetric folds.

IMPLICATIONS FOR REGIONAL-SCALE STRUCTURE AND FOR THE STANSBURY DEPOSITIONAL BASIN

In summary, the Stansbury Mountains record a cryptic Late Devonian deformation event followed by well developed Mesozoic thrust faulting. Evidence for the Devonian deformation includes an angular unconformity (Rigby, 1959) and the synorogenic Stansbury Formation (Stokes and Arnold, 1958; Trexler, this volume; Trexler, in review). There is evidence for two Mesozoic thrust faults in the Stansbury Mountains — a blind thrust which cores the range, and the Tintic Valley thrust (recognized by many previous workers) which surfaces immediately to the east of the Stansbury Mountains and is thought to underlie the range. The Broad Canyon fault, previously interpreted to be a west-dipping thrust fault (e.g., Tooker and Roberts, 1971), is in fact an east-dipping reverse fault that postdates the thrust-related deformation. Of two additional thrust faults postulated by Tooker and Roberts (1971), one was found to be an angular unconformity and the second (which was hypothetical even in the original description) is not necessary to explain the observed structures.

The folding in the Stansbury Mountains records a single deformational event; the major anticline-syncline pair that forms the range is interpreted to be a fault-propagation fold. Folds at the north and south ends of the range are interpreted to be en echelon folds that take up the shortening as the main anticline decreases in amplitude. The geometry of one of these folds, the Timpie Ridge anticline, suggests that it, too, is a fault propagation fold cored by a blind thrust. The unusual geometry of this anticline (i.e., apparent westward vergent) is probably due to the presence of an angular unconformity within the Paleozoic section (see above).

This structural interpretation has important implications for the geometry of the Devonian-Mississippian Stansbury depositional basin. Most important, no major thrust faults exist between the type section of the Stansbury Formation (in Flux Canyon), where the unit is over 500 m thick, and Timpie Valley, where it is completely absent. This requires that there be abrupt thickness changes in the Stansbury Formation, most probably because of significant relief on the sub-Stansbury depositional surface. Second, there is no evidence for a fundamental structural boundary between the northern Stansbury Mountains and Stansbury Island, although there may be some minor lateral offset between the two. The anticlinal structure of Stansbury Island (Chapusa, 1969) is consistent with the structural style of the northeastern Stansbury Mountains, and could represent another en echelon fold (Fig. 2). However, the position of this anticline almost exactly along-trend from the Little Baldy syncline suggests either an abrupt transition from one fold to the other or lateral offset between the two folds. If there are no major structures between Stansbury Island and the Stansbury Mountains, dramatic lateral compositional variation within the Stansbury Formation is required (see Trexler, this volume, and Trexler, in review).

The thrust-related structures in the northern Stansbury Mountains also place some intriguing constraints on regional structural interpretations, and suggest several topics for future investigation. The axial traces of the macroscopic, east-vergent folds are curvilinear (convex to the west) at the scale of the range, with the center of the curvature at the center of the range, adjacent to South Mountain (Fig. 2). The maximum overturning of the Deseret anticline also occurs adjacent to South Mountain, along with the maximum structural, stratigraphic and topographic relief in the Stansbury Mountains. The sense of fold curvature — relative to thrust transport direction — is the opposite of the "bow and arrow" pattern typical of thrust belts (Elliott, 1976). The geometry and scale of the curvature cannot be plausibly explained by invoking lateral ramps in the underlying (Tintic Valley) thrust. Rather, the curvature may be related to the interference of the east-west Uinta trend, expressed in South Mountain, (Tooker and Roberts, 1971; Crittenden, 1976) with the north-south thrust belt structures; this interpretation was first suggested by Tooker and Roberts (1971). The Broad Canyon fault does not change orientation adjacent to South Mountain, it cuts across the curved fold trends. The Mesozoic deformational history suggested by these relationships is: (1) the developing east-verging fold-thrust system impinged on the mechanical inhomogeneity of the Uinta axis; (2) the deformation continued to propagate eastward to the north and south of this structural salient, but shortening at the latitude of the salient was accommodated by increasing amplitude and overturning in the anticline/syncline pair; (3) the final shortening may have been accomplished by back-thrusting along the Broad Canyon fault, starting at the Uinta axis and propagating to the north and south across the already-formed east-vergent folds. An alternate interpretation for curvature of the fold axial traces is that it is due to renewed uplift along the Uinta axis at some time after the compressional deformation; however, this would not explain either: (1) the truncation of the east-vergent folds by the Broad Canyon fault, or (2) the change in fold shape (i.e., overturning of the Deseret anticline) in the vicinity of the Uinta axis.

ACKNOWLEDGMENTS

This research was supported by a grant to P. H. Cashman and J. H. Trexler, Jr. from the Mineral Lease Special Projects Program of the Utah Geological Survey. J. K. Rigby generously provided original field maps and encouragement in the early stages of the project; his excellent geologic map (Rigby, 1958) was invaluable throughout the study. My present understanding of the structure and stratigraphy of the Stansbury Mountains was substantially enhanced by conversations with many workers, including R. L. Bruhn, K. M. Nichols, N. J. Silberling, J. H. Trexler, Jr. and W. A. Yonkee. The manuscript was improved by reviews from J. H. Trexler, Jr. and W. A. Yonkee.

REFERENCES

Armin, R.A., 1979, Geology of the southeastern Stansbury Mountains and southern Onaqui Mountains, Tooele County, Utah, with a paleoenvironmental study of part of the Oquirrh Group: unpub. M.S. thesis, San Jose State University, San Jose, California, 105 p.

Arnold, D.E., 1956, Geology of the northern Stansbury Range, Tooele County, Utah: unpub. M.S. thesis, University of Utah, Salt Lake City, 57 p.

Billingsley, P.R. and Locke, A., 1939, Structure of ore districts in the continental framework: New York, Am. Inst. Mining Metall. Engineers, 51 p.

Chapusa, F.W.P., 1969, Geology and structure of Stansbury Island: unpub. M.S. thesis, University of Utah, Salt Lake City, 81 p.

Crittenden, M.D., Jr., 1976, Stratigraphic and structural setting of the Cottonwood area, Utah, *in* Hill, J.G. (ed.), Geology of the Cordilleran Hingeline: Rocky Mountain Association of Geologists Symposium, Denver, p. 363-379.

Elliott, D., 1976, The energy balance and deformation mechanisms of thrust sheets: Phil. Trans. Roy. Soc. Lon. A, v. 283, p. 289-312.

Foose, M.P., 1989, Geologic Map of the North Stansbury Mountains Wilderness Study Area, Tooele County, Utah: U.S. Geological Survey Map MF-2061, 1:24,000.

Foose, M.P., Duttweiler, K.A. and Almquist, C.L., 1989, Mineral resources of the North Stansbury Mountains Wilderness Study Area, Tooele County, Utah: U.S. Geological Survey Bulletin 1745, 18 p.

Jordan, T.E., and Allmendinger, R.W., 1979, Upper Permian and Lower Triassic stratigraphy of the Stansbury Mountains: Utah Geology, v. 6, no. 2, p. 69-74.

Lambert, H.C., 1941, Structure and stratigraphy in the southern Stansbury Mountains, Tooele County, Utah: unpub. M.S. thesis, University of Utah, Salt Lake City, 51 p.

Moore, W.J.,and Sorensen, M.L., 1979, Geologic map of the Tooele 1° by 2° quadrangle, Utah: U.S. Geological Survey Map I-1132, 1:250,000.

Passchier, C.W.,and Simpson, C., 1986, Porphyroclast systems as kinematic indicators: J. Struc. Geol., v. 8, p. 831-843.

Rigby, J.K., 1958, Geology of the Stansbury Mountains, eastern Tooele County, Utah: Utah Geol. Soc. Guidebook, no. 13, p. 1-134.

Rigby, J.K., 1959, Upper Devonian unconformity in central Utah: Geol. Soc. America Bull., v. 70, p. 207-218.

Roberts, R. J., Jr., Crittenden, M.D., Jr., Tooker, E.W., Morris, H.T., Hose, R.K., and Cheney, T.M., 1965, Pennsylvanian and Permian basins in northwestern Utah, northeastern Nevada, and south-central Idaho: American Association of Petroleum Geologists Bulletin, v. 49, p. 1926-1956.

Sorensen, M. L., 1982, Geologic map of the Stansbury roadless areas, Tooele County, Utah: U.S. Geological Survey Map MF-1353-A, 1:62,500.

Stokes, W.L. and Arnold, D.E., 1958, Northern Stansbury Range and the Stansbury Formation: Utah Geol. Soc. Guidebook no. 13, p. 135-149.

Suppe, J., 1985, Principles of Structural Geology: Prentice-Hall, Inc., Englewood Cliffs, NJ, 537 p.

Suppe, J., and Medwedeff, D.A., 1984 (abs), Fault-propagation folding: Geol. Soc. America Abst. with Prog., v. 16, p. 670.

Teichert, J.A., 1959, Geology of the southern Stansbury Range, Tooele County, Utah: Utah Geo. and Min. Surv. Bulletin 65, 75 p.

Tooker, E.W., 1983, Variations in structural style and correlation of thrust plates in the Sevier foreland thrust belt, Great Salt Lake area, Utah: *in* Miller, D.M., Todd, V.R. and Howard, K.A. (eds.), Tectonic and Stratigraphic Studies in the eastern Great Basin: Geol. Soc. America Memoir 157, p. 61-73.

Tooker, E.W. and Roberts, R.J., 1971, Structures related to thrust faults in the Stansbury Mountains, Utah, in U.S. Geological Survey Research 1971: U.S. Geological Survey Prof. Paper 750-B, p. B1-B12.

Trexler, J.H., Jr., 1992, The Stansbury Formation at Stansbury Island and the northeastern Stansbury Mountains: (this volume).

Trexler, J.H., Jr., in review, Devonian-Mississippian active tectonism and basin formation in the interior craton margin: the Stansbury Formation of western Utah.

QUATERNARY GEOLOGY AND GEOLOGIC HAZARDS OF TOOELE AND NORTHERN RUSH VALLEYS, UTAH

Barry J. Solomon
Utah Geological Survey, Salt Lake City, Utah 84109
Benjamin L. Everitt
Utah Division of Water Resources, Salt Lake City, Utah 84116
Donald R. Currey
Department of Geography, University of Utah, Salt Lake City, Utah 84112
Joseph S. Paulick
Industrial Risk Management, Tooele Army Depot, Tooele, Utah 84074
Daning Wu
Department of Geology and Geophysics, University of Utah, Salt Lake City, Utah 84112
Susan Olig
Utah Geological Survey, Salt Lake City, Utah 84109
Ted N. Burr
Salt Lake City, Utah 84102

ABSTRACT

Tooele and Rush Valleys, in east-central Tooele County, contain most of the county's population and are on the western margin of expanding metropolitan Wasatch Front communities. Northern Rush Valley is the site of Tooele Army Depot South (TADS), the staging ground for a massive chemical weapons storage and demilitarization program.

Lake Bonneville sediments predominate on the valley floors, and were deposited between about 28,000 and 13,000 yr B.P. Marginal, shore-zone, and deep-water lacustrine deposits overlie older Quaternary deposits which are commonly etched by lake shorelines. The older deposits also occur on mountain slopes above the Bonneville shorelines. Transgressive and regressive shorelines are both climatically induced and caused by basin-hypsometric factors. Four basin-wide Lake Bonneville shorelines are recognized within Tooele Valley. They are, from oldest to youngest, the Stansbury, sub-Provo, Bonneville, and Provo shorelines. The Lake Bonneville highstand (the Bonneville shoreline) is the oldest recognized shoreline in northern Rush Valley, and one local shoreline (the Provo equivalent) is recognized which was created after regression of the lake from its maximum extent isolated Rush Valley as a separate basin. The Gilbert shoreline formed between 12,000 and 9,400 yr B.P., very early in the history of Great Salt Lake, and is also recognized within Tooele Valley. The Gilbert-equivalent shoreline, as well as a later shoreline which records the highest lake level during the Holocene, are recognized in northern Rush Valley.

Late Pleistocene lacustrine sediments are overlain by late Pleistocene to Holocene alluvial, eolian, mass wasting, playa, and spring deposits. Sediments were deposited within several subenvironments of these categories.

Above-normal precipitation in 1983 and 1984 resulted in basement flooding from shallow ground water in Erda, Tooele Valley. Landslides and debris flows ensued in canyons in the Oquirrh Mountains east of Tooele and Rush Valleys. Potential hazards include the possible contamination of ground water in basin-fill aquifers, debris flows and flash floods in the piedmont zone, and earthquake-related hazards. Unsafe foundation conditions may result from silty and sandy sediments subjected to liquefaction or hydrocompaction, clayey sediments and mud flats subjected to shrinking or swelling, or salt flats subjected to subsidence due to dissolution.

LOCATION AND GENERAL FEATURES

Tooele and northern Rush Valleys are in east-central Tooele County (figure 1). The county is rural with a 1990 population density of about 3.8 persons per sq mi, and a 1990 population of 26,601 (U.S. Census Bureau, 1990). The Oquirrh Mountains form the eastern border of Tooele and northern Rush Valleys, and the Stansbury Mountains form the western border. Great Salt Lake is north of Tooele Valley, which is separated from Rush Valley to the south by South Mountain. Drainage in Tooele Valley is north into Great Salt Lake, whereas Rush Valley is internally drained.

The city of Tooele, in southeastern Tooele Valley, is about 30 mi (50 km) southwest of Salt Lake City. Tooele is the county seat and the largest community in the county with a population of 13,887 in 1990, or more than 52.2 percent of the county total. Grantsville, in northwestern Tooele Valley, is the second largest community with an estimated population of 4,500 in 1990.

Tooele and Rush Valleys have a semi-arid climate with wide seasonal and diurnal temperature variability typical of middle latitude continental regions (National Oceanic and Atmospheric Administration, 1990). Tooele Valley has an approximate mean annual temperature of 50.7°F (10.4°C); mean monthly temperatures are lowest in January (28.8° F; -1.8° C) and highest in July (75.4° F; 24.1° C). Annual precipitation is 16.5 inches (42.0 cm).

PREVIOUS WORK

In an 1854 expedition across the Great Basin, Beckwith (1855) was inspired with the ancient shorelines of "Tuilla Valley" which "will perhaps afford....the means of determining the character of the sea by which they were formed...." In 1859, Simpson (1876) observed similar features in Rush Valley. Henry Engelmann, the geologist for the Simpson Expedition, attributed the varying lake levels to climatic influences. Gilbert crossed Tooele Valley in 1872 for the Wheeler Survey, but the structure of the Oquirrh Mountains interested him more than the characteristics of the adjacent basin (Gilbert, 1875). He travelled the perimeters of Tooele and Rush Valleys in 1877, and returned to the valleys in 1880 (Hunt, 1982). On these later visits, Gilbert devoted considerable attention to geomorphic features related to the history of Lake Bonneville in Tooele and Rush Valleys (Gilbert, 1890). In particular, he used shoreline elevations in Tooele Valley and adjacent basins to illustrate the principle of crustal rebound from isostatic compensation as a result of the lowering of the level of Lake Bonneville and subsequent release of overlying pressure. He also described the morphology of faults along the western edges of the Oquirrh and Stansbury (referred to as the northern part of the Aqui Mountains by Gilbert, 1890) Mountains, and accounted for the unique assemblage of bars and spits which are present near the town of Stockton and continue westward to the northern edge of South Mountain.

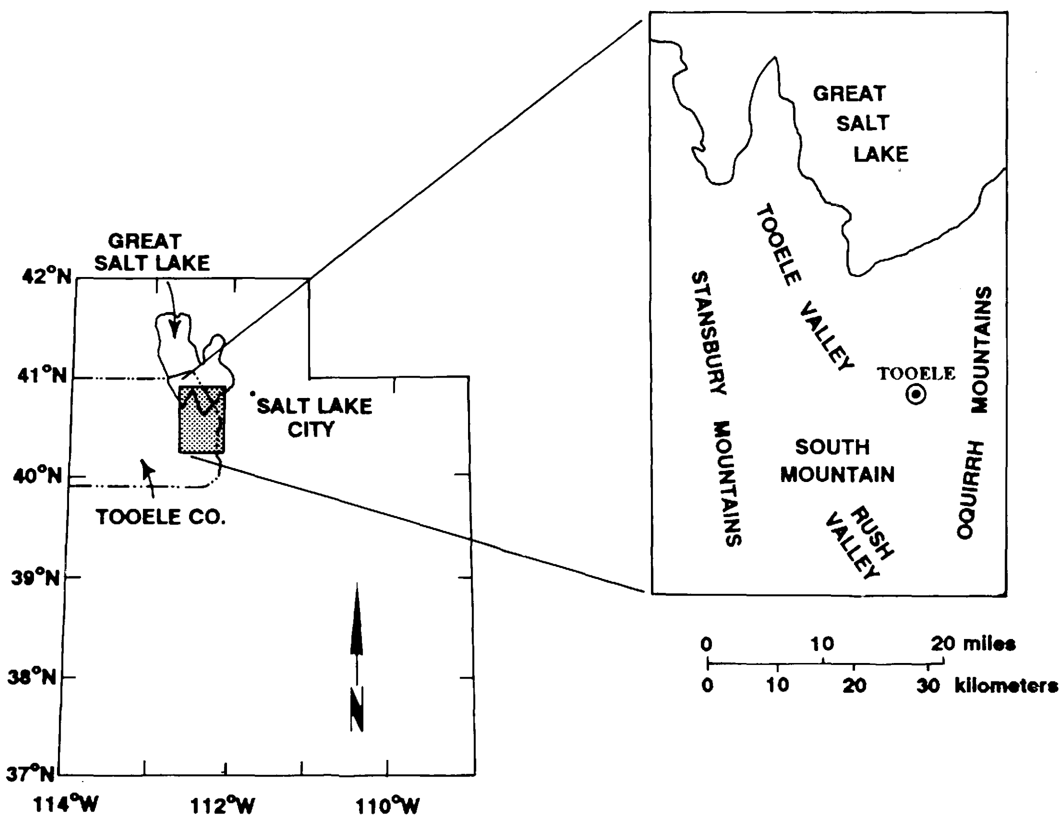

Figure 1. Location map.

A few geologic maps broadly portray Tooele and northern Rush Valley Quaternary deposits. Rigby (1958) categorized the Stansbury Mountains piedmont as either lacustrine, alluvial, or eolian deposits, and described pre-Lake Bonneville geomorphic features. Everitt and Kaliser (1980) supplemented existing geologic maps with air-photo interpretations, and mapped the valleys at a scale of 1:50,000. Several geologic quadrangle maps cover the Oquirrh Mountains piedmont (Tooker, 1980; Tooker and Roberts, 1971a, 1971b; 1988a, 1988b), differentiate Quaternary units, and map faults in such units.

Previous research has emphasized various geological characteristics of the area. Smith and others (1968) relate Lake Bonneville stratigraphy to Pleistocene fish fossils from several locations within the Bonneville Basin, one of which is at Black Rock Canyon at the northern end of the Oquirrh Mountains. McCoy (1987) sampled gastropod fossils from the same canyon in an investigation of Quaternary aminostratigraphy. The Quaternary stratigraphic record was studied in core samples collected near Burmester, in northern Tooele Valley, by Eardley and others (1973).

Regional gravity surveys which cover Tooele and northern Rush Valleys were conducted by Johnson and Cook (1957), Johnson (1958), Cook and Berg (1961), Tanis (1963), Zimbeck (1965), and Cook and others (1975, 1989). Gravity anomalies (Johnson, 1958) indicate that the basin floors are complex collections of structural troughs and ridges rather than single downfaulted grabens. The deepest portion of Tooele Valley is on its north-central margin. The Walker-Wilson No. 1 oil test well penetrated 7,100 ft (2,100 m) of basin fill in this area (Heylmun, 1965), and Everitt and Kaliser (1980) estimate in excess of 8,000 ft (2,400 m) of fill as the basin thickens northward under Great Salt Lake. Other investigators (Bucknam, 1977; Everitt and Kaliser, 1980; Barnhard, 1988; Barnhard and Dodge, 1988) mapped fault scarps on unconsolidated sediments within the valleys, and scarps of erosional or undetermined origin were also mapped by Everitt and Kaliser (1980). Krinitzsky (1989) evaluated earthquake hazards for Tooele Army Depot, Tooele and Rush Valleys, by determining empirical earthquake ground motions. Wu and Bruhn (1990) studied the geometry and kinematics of normal faults along the western flank of the southern Oquirrh Mountains, adjacent to Rush Valley. Gilluly (1928) also studied these faults in the vicinity of Stockton, and postulated a process for the integration of the drainage of Rush Valley with Tooele Valley prior to the highstand of Lake Bonneville (Gilluly, 1929). Shore features that formed during the last deep-lake cycle at the pass between Rush and Tooele Valleys near Stockton were investigated by Burr and Currey (1988) and Burr (1989). The Utah Geological Survey has conducted investigations of proposed construction sites within Tooele Valley (Kaliser, 1971; Lund, 1985b, 1986; Case, 1987a), flood damage in adjacent canyons (Lund, 1985a), and rock-fall hazards in adjacent mountains (Case, 1987b). The U.S. Department of Agriculture Soil Conservation Service has mapped soils in the area (unpublished data, 1989) and has made engineering interpretations regarding erosion hazard, permeability, and land use. Data on Quaternary geology and engineering properties of soils were also generated for highway construction (Utah State Department of Highways, 1963).

Several ground-water studies provide information on Tooele and Rush Valleys. Carpenter (1913) included the valleys in his comprehensive northwestern Utah ground-water investigation. He located streams, springs, and wells, and attributed recharge of the valley floors to precipitation on mountain slopes and infiltration in the piedmont zone. Thomas (1946) differentiated eolian from lacustrine deposits on the floor of Tooele Valley, and recognized the presence of fault blocks within the basin based upon geologic and hydrologic data. More recent hydrologic investigations of Tooele and Rush Valleys demonstrate that ground water in Tooele Valley flows northward into Great Salt Lake (Gates, 1963, 1965; Gates and Keller, 1970; Razem and Steiger, 1981; Ryan and others, 1981), whereas northern Rush Valley is essentially a closed hydrologic basin in which recharge flows from surrounding mountains into Rush Lake (Hood and others, 1969). The possibility of faults within Tooele Valley which might serve as ground-water barriers and complicate ground-water flow was discussed in four investigations (Thomas, 1946; Gates, 1962, 1965; Razem and Steiger, 1981).

A comprehensive study of the Quaternary geology and potential geologic hazards of Tooele and northern Rush Valleys has been conducted by the Utah Geological Survey (Solomon, in preparation[a,b]). The surficial geology of the valleys has been mapped at a scale of 1:24,000, and overlays have been prepared which show the potential for various geologic hazards within the valleys and adjoining mountain slopes.

PRE-LAKE BONNEVILLE PLEISTOCENE GEOLOGY

Tooele and Rush Valleys occupy structural basins in the Basin and Range physiographic province (Hunt, 1967). Late Cenozoic crustal extension formed the dominant north-south-trending fault-block topography that dominates most of the province (Hintze, 1973).

The surficial geology of the valley floors is dominated by Quaternary materials deposited from 13,000 to 28,000 years ago by Lake Bonneville. The lake's basin, however, has been an area of closed drainage for much of the past 15 million years, and several lakes existed in the basin during this time. Surficial evidence of geologic processes prior to 28,000 years ago (yr B.P.) is scant, but remnants of older Quaternary deposits are extant on mountain foothills at elevations greater than the Lake Bonneville highstand. Pre-Lake Bonneville coalescing alluvial fans and alluvial-terrace deposits are present in both Tooele and Rush Valleys on the margins of the Oquirrh and Stansbury Mountains and near South Mountain. These older fans are now abandoned and incised. Relative ages of pre-Lake Bonneville alluvial deposits are based upon the degree of fan or terrace incision, and relative elevation of adjacent geomorphic surfaces. No outcrops of contemporaneous lacustrine material are present, but pre-

Lake Bonneville lacustrine sediments are buried in the valleys.

LAKE BONNEVILLE AND LATER LACUSTRINE CHRONOLOGY

The valleys are geomorphic subbasins of the Bonneville Basin as a consequence of their integration with Lake Bonneville for part of the late Pleistocene Bonneville lacustral cycle (Gilbert, 1890; Eardley and others, 1957; Currey and others, 1984; Currey and Oviatt, 1985). The Bonneville cycle was essentially coincident with the last global ice age of marine isotope stage 2, and lasted from about 28,000 to 13,000 years ago (Currey, 1990). Four regional shorelines were created by Lake Bonneville: the Stansbury, sub-Provo, Bonneville, and Provo. A fifth regional shoreline, the Gilbert, was created by early Great Salt Lake. Each shoreline is actually a complex association of shorelines which record lake fluctuations.

Transgression of the lake was well underway by about 25,000 yr B.P. (Spencer and others, 1984). The lake experienced a major oscillation between 22,000 and 20,000 yr B.P. which resulted in the formation of the Stansbury shoreline (Oviatt and others, 1990). Shoreline deposits at the south end of Tooele Valley (the unnamed shoreline complex of Burr and Currey, 1988) mark what seems to be one or more important stillstands or moderate oscillations during the transgressive phase of the Bonneville lake cycle as the lake rose above the Stansbury level. Sack (1990), who notes casual references to similar deposits elsewhere in Utah by previous researchers, applied the term "sub-Provo" to the deposits where they occur in Tule Valley of west-central Utah. This sub-Provo lake level formed between 20,000 and 16,400 yr B.P., and was so named because it lies just below the later Provo shoreline.

Lake Bonneville occupied its highest shoreline, which Gilbert (1875) named the Bonneville beach, after 16,400 yr B.P., and perhaps as late as 15,000 yr B.P. (Currey and Oviatt, 1985). Prior to the lake transgression, the drainage of Rush Valley had been integrated with that of Tooele Valley (Gilluly, 1929). During the highest stage of Lake Bonneville, Rush Valley was an embayment connected with Tooele Valley by a strait at the pass between the two valleys near Stockton. After the catastrophic incision of the Zenda threshold in southern Idaho and the rapid drawdown of Lake Bonneville, Rush Valley was isolated when Lake Bonneville receded below the Stockton Bar barrier between Rush and Tooele Valleys. Rush Valley then became the site of a succession of independent pluvial lakes which include Lake Shambip, Lake Smelter, and Rush Lake (Burr and Currey, 1988).

In Tooele Valley, and in the remainder of the Bonneville Basin, Lake Bonneville stabilized at a lower threshold and formed the very prominent Provo shoreline (Gilbert, 1875, 1890). About 14,000 yr B.P. climatic factors induced regression from the Provo level (Currey and Oviatt, 1985). In less than 2,000 years the lake level was below the elevation of the present Great Salt Lake. Transgression was subsequently renewed and the earliest post-Bonneville oscillation, known as the Gilbert, began about 12,000 yr B.P. (Murchison, 1989). The lake finally regressed sometime between 9,400 and 9,700 yr B.P. A late Holocene lake rise, between 3,440 and 1,400 yr B.P., resulted in the highest static lake level reached during the Holocene, and is commonly referred to as the Holocene high (Murchison, 1989). Three shorelines of local extent formed in the adjacent northern Rush Valley pluvial lakes and reflect lake levels within the remainder of the Bonneville Basin. The three shorelines comprise the Provo shoreline equivalent which enclosed Lake Shambip, the Gilbert shoreline equivalent which enclosed Lake Smelter, and the Rush Lake shoreline during the historic high of the 1980s, which is essentially coincident with the level of the Holocene high (Burr and Currey, 1988).

Lake Bonneville sediments vary in grain size with the environment in which they were deposited. Coarser material was derived from Paleozoic bedrock and reworked from older alluvial fans, and is common near shorelines along the basin margin. Thick gravel and sand deposits occur near the Bonneville level along the Oquirrh and Stansbury range fronts, as well as in spits and bars on the northern edge of South Mountain and in the pass near the town of Stockton. Finer material was deposited further offshore, and is common in central Tooele and Rush Valleys. Marl is rare, and occurs as interbeds within other lacustrine sequences. Tufa was deposited along the lake shore, and is particularly common at shorelines near the north end of the Stansbury and Oquirrh Mountains, as well as near the crest of the Stockton bar.

NON-LACUSTRINE HOLOCENE GEOLOGY

As Lake Bonneville and subsequent Great Salt Lake receded, sediments were deposited in several non-lacustrine, continental environments. These deposits form complex patterns on valley floors and piedmont slopes. Alluvial and eolian deposits predominate.

Alluvial sediments include fan deposits on the piedmont slopes along valley margins, and channel deposits from perennial streams originating in mountain slopes near the pass between Tooele and Rush Valleys. Eolian sediments include barchan silt dunes in northern Tooele Valley, and longitudinal siliceous dunes on Tooele Army Depot North (TADN). Mud and salt flats occur immediately south of the shore of Great Salt Lake, and playa deposits are present within the basin of Rush Lake. Spring deposits occur at the northern end of Tooele Valley near the junction of piedmont slopes with flat-lying lacustrine beds. Landslide blocks of bedrock occur at the northern end of the Oquirrh Mountains, near the head of Soldier Canyon southeast of Stockton, and at the confluence of Morgan and East Hickman Canyons on the eastern slope of the Stansbury Mountains adjacent to northern Rush Valley. Mud and debris-flows are present on the northern edge of the Stockton Bar as well as in mountain canyons east of Tooele.

GEOLOGIC HAZARDS

The study of Quaternary geology provides information to evaluate geologic hazards that must be considered for safe and efficient development in Tooele Valley and adjacent northern Rush Valley. The type of geologic material and Quaternary depositional environment, and the relation between Quaternary units and geologic structures in the valleys, can be used to evaluate the potential for many geologic hazards.

Earthquakes, and the hazards which may accompany them, are of particular significance to development in Tooele and Rush Valleys. These valleys lie in the Intermountain seismic belt (ISB), an active seismic area in the western United States (Smith and Sbar, 1974). Whereas earthquakes in the ISB generally do not coincide with known geologic structures, there is evidence that at least one structure in the field trip area, the Northern Oquirrh fault zone (NOFZ) on the eastern edge of Tooele Valley (STOP 1), has offset unconsolidated Quaternary sediments younger than the Lake Bonneville highstand (about 15,000 yr B.P.; Barnhard and Dodge, 1988) and is thus capable of generating large, surface-faulting earthquakes. The Mercur fault zone, on the eastern edge of Rush Valley, has also offset Quaternary unconsolidated sediments but the age of most recent movement, postulated by Everitt and Kaliser (1980) to be younger than the Bonneville highstand and by Barnhard and Dodge (1988) to be older, is unclear (STOP 6). The valleys may also be subject to earthquake hazards from more distant sources, notably the Wasatch fault zone, which is as close as 20 mi (30 km) to the east.

Potential earthquake hazards in the field trip area include: 1) surface fault rupture, most likely along the NOFZ; 2) liquefaction in northern Tooele and Rush Valleys, where granular soils deposited in Lake Bonneville are saturated with shallow ground water; 3) earthquake-induced landslides, particularly on mountain slopes underlain by the clay-rich Manning Canyon Shale of Mississippian age; 4) earthquake-induced rock falls, particularly on mountain slopes above wave-cut benches of the Bonneville shoreline; 5) tectonic subsidence related to movement on the NOFZ; 6) ground shaking, from both local and distant earthquakes; 7) ground failure due to loss of strength in sensitive clays, possible in fine-grained Lake Bonneville deposits on the valley floors; 8) subsidence caused by vibratory settlement in granular materials; 9) flooding in northern Tooele Valley caused by seiches in Great Salt Lake; and 10) flooding from increased ground-water discharge or surface-water diversions, including dam failures.

Potential earthquake hazards, while important, are not the only geologic hazards in the field trip area. Significant damage occurred in the area following above-normal precipitation in 1983 and 1984 (Kaliser and Slosson, 1988; Arnow and Stephens, 1990). The precipitation, and abrupt spring warming which resulted in rapid snowmelt and runoff, caused geologic hazards which may be repeated should conditions recur. Landslides; rock falls; debris slides, flows, and floods; stream and lake flooding; and shallow ground-water problems all occurred during the "wet years." Downslope movement of rock and soil occurred in Oquirrh and Stansbury Mountain canyons, disrupting roadways and water supplies; floodwaters flowed down the streets of Tooele; and basements flooded in Erda in northern Tooele Valley (Lund, 1985a, 1986). The rising water of Great Salt Lake, which peaked at 4,211.85 ft (1,283.77 m) on June 3, 1986 (Arnow and Stephens, 1990), caused flood damage to recreation facilities along the lake's south shore, and required raising of a railroad bed on a solid-fill causeway at the south end of the lake. Mountain canyons, and piedmont slopes underlain by Holocene alluvial-fan deposits, are particularly subject to mass-movement hazards; the north end of both Tooele and Rush Valleys are subject to shallow ground-water hazards; and northern Tooele Valley may be inundated by Great Salt Lake.

Still other potential geologic hazards may occur in the valleys. Expansive soils may crack foundations and road surfaces, and plug wastewater disposal systems, in areas underlain by fine-grained lake deposits on valley floors. Piping may occur in Lake Bonneville deposits containing marl or silt. Elevated levels of indoor radon may occur in buildings constructed on well-drained rock or soil with relatively high amounts of uranium. Although the distribution of these hazards is not precisely defined, their potential may be estimated by a knowledge of Quaternary deposits and geologic structures in the field trip area. Detailed site investigations are required for an accurate determination of geologic-hazard potential.

FIELD TRIP OVERVIEW

Features related to Lake Bonneville chronology provide important data to evaluate the type, magnitude, and recurrence of potential geologic hazards in the field trip area. The physical properties of lake sediments determine the geologic stability of foundation materials, as well as the role of such sediments in ground-water protection. Lake shorelines are important time horizons from which the characteristics of surface-faulting earthquakes may be estimated. The characteristics of pre-and post-Lake Bonneville deposits, although of small aerial extent, also contribute to the evaluation of geologic hazards.

Geologic features along the field trip route, their relevance to land use within the valley and to geologic-hazard evaluation, and appropriate reference citations, are noted in the field trip road log. Although the field trip concentrates on Tooele and northern Rush Valleys, relevant geologic features are also indicated along the route from its start in Ogden to the first encounter with Tooele Valley at the northern end of the Oquirrh Mountains (Figure 2). Once in Tooele Valley, five items of significance will be inspected in detail at seven field trip stops: 1) the paleoseismicity and kinematics of the zone of normal faults in bedrock and unconsolidated Quaternary deposits on the eastern edge of Tooele and Rush Valleys (stops 1 and 6); 2) the relationship between activities

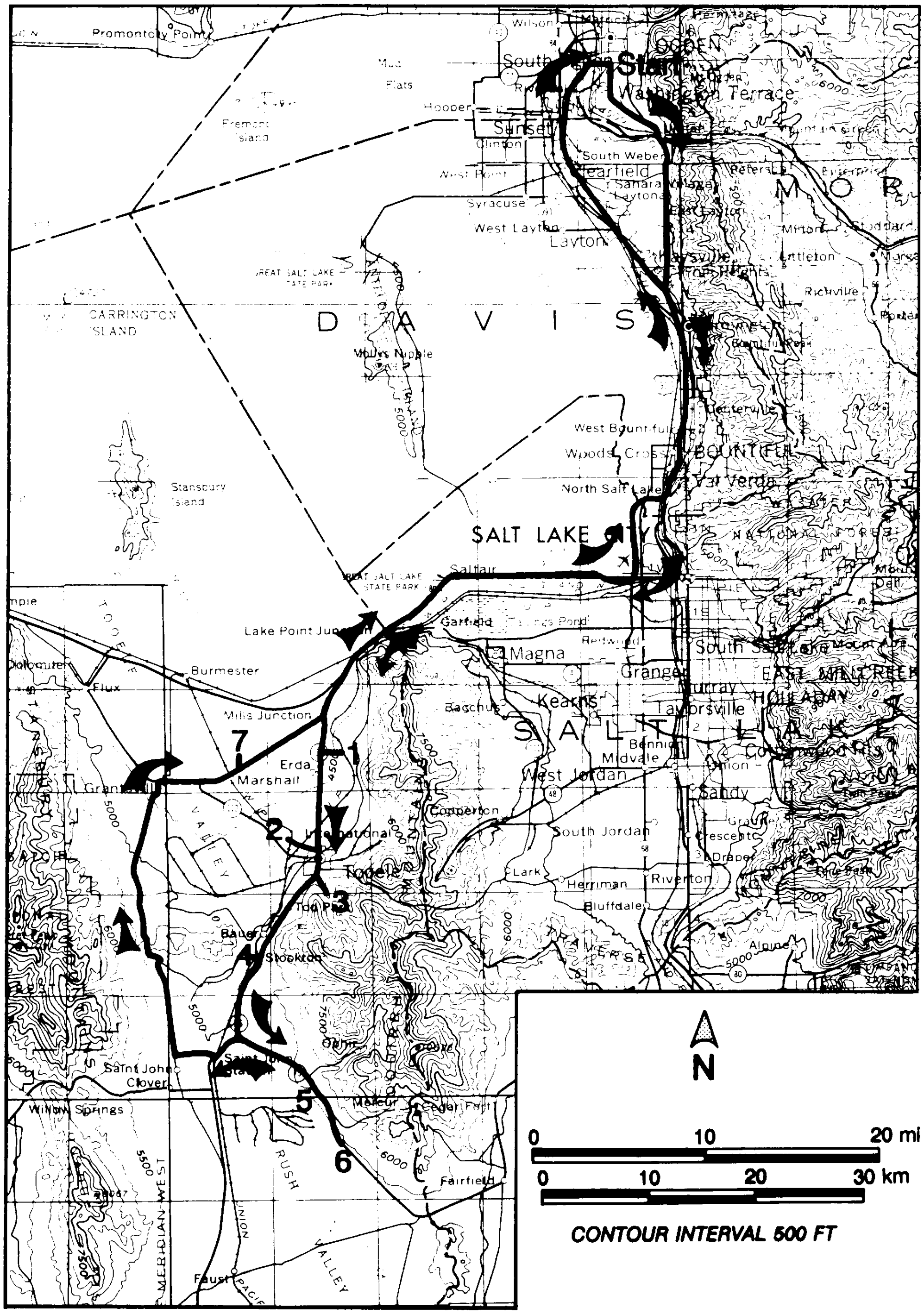

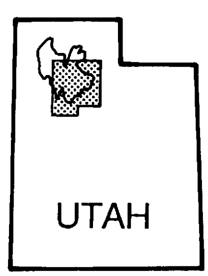

Figure 2. Field trip route with stops.

at Tooele Army Depot and the ground water of Tooele and northern Rush Valleys (stops 2 and 5); 3) evidence of flooding and debris flows near the expanding urban area of Tooele (stop 3); 4) exceptional Lake Bonneville shoreline features at the pass between Tooele and Rush Valleys (stop 4); and 5) enigmatic elliptical depressions at the northern end of Rush Valley, and their possible relationship to shallow ground water and seismicity (stop 7). An index to maps of field trip stops and other significant features, presented within the road log, appears in figure 3. Interesting features are also noted along the return route to Ogden where it differs from the initial route.

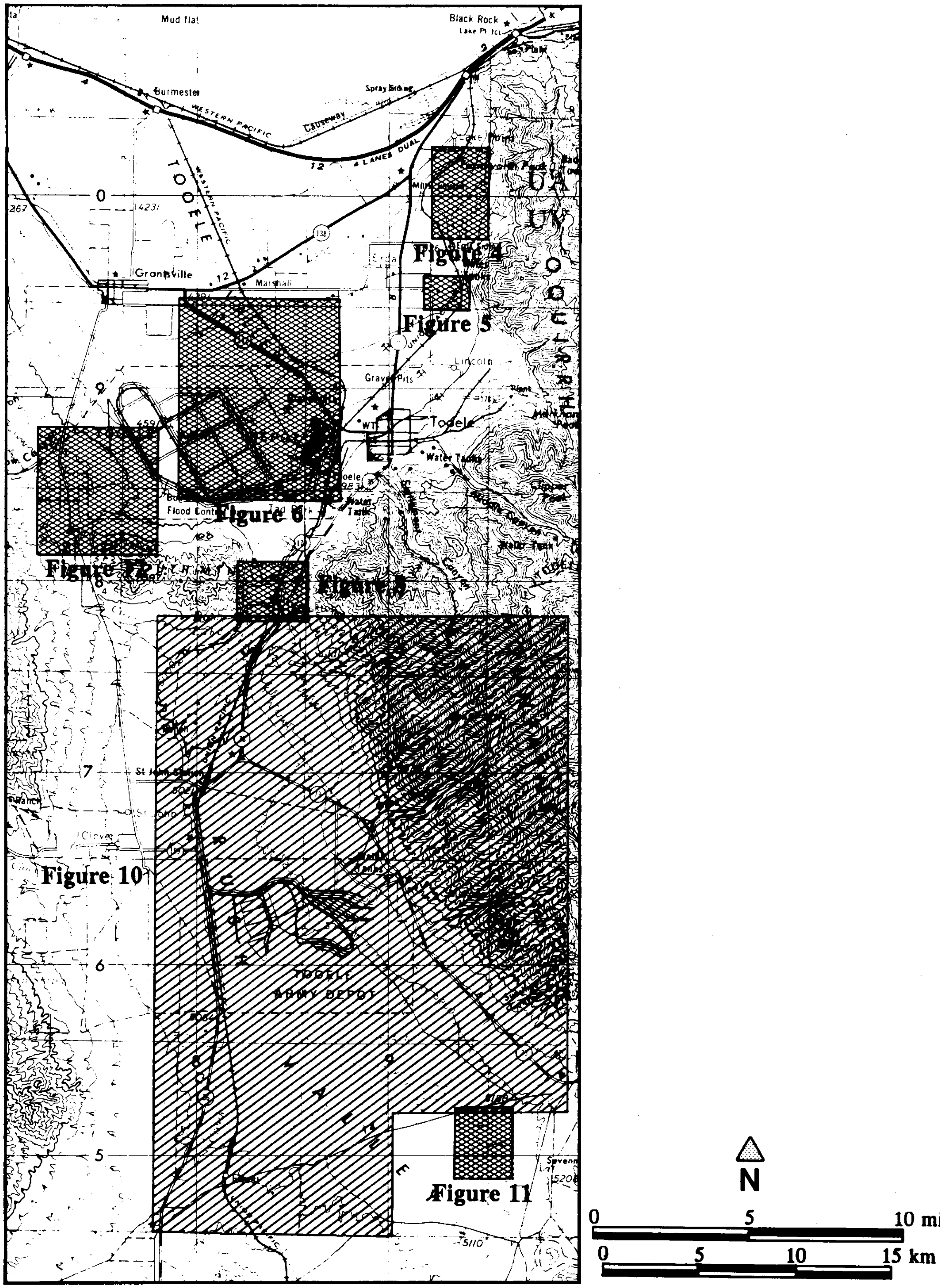

Figure 3. Map index for the field trip road log.

FIELD TRIP ROAD LOG

Mileage Incremental	Cumulative	Description
		Ogden to Tooele Valley
0.0	0.0	Depart from front entrance to Weber State University at intersection of 3850 South and Harrison Boulevard, Ogden, Utah. Proceed south on Harrison Boulevard. Note the Bonneville shoreline, at an elevation of about 5,200 ft (1,585 m), cut into the side of the Wasatch Range to the left.
2.2	2.2	The upland surface is the top of the Provo-stage delta, with remnants of Bonneville-stage deposits and Holocene alluvial fans to the left (Nelson and Personius, 1990).
0.6	2.8	Turn left from Harrison Boulevard onto U.S. Highway 89. The terrace below the "U" on the mountainside is the abrasion platform of the Bonneville shoreline.
0.7	3.5	The highway begins its descent into the Weber River valley, underlain by Holocene alluvium. The river has cut into upper Pleistocene Lake Bonneville deltaic deposits. To the right is the town of Uintah, location of the highest residential indoor radon level yet reported in the state (Sprinkel and Solomon, 1990). A likely source for the radon may be uranium in permeable alluvium derived from both the metamorphic Precambrian Farmington Canyon Complex and the rhyolitic Eocene Norwood Tuff. These rocks are extensive in the Weber River drainage basin of the Wasatch Range.
0.9	4.4	Cross the Union Pacific Railroad tracks. In 1981, sand and silt of the Lake Bonneville deltaic deposits failed, damaging both the railroad and power line (Kaliser, 1983).
0.6	5.0	Cross the Weber River.
0.2	5.2	Sand and gravel pits both east and west of the highway are excavated into Quaternary fluvial deposits of the Weber River. The dry pit floors indicate a considerable depth to the water table; a well located in one of the pits encountered water at a depth of 157 ft (48 m) (Plantz and others, 1986). The mouth of the canyon here is believed to be one of the primary recharge areas for the Delta aquifer, a part of the East Shore aquifer system (Clark and others, 1990). The Delta aquifer farther to the west supplies a large part of the ground water used in Weber County. The Bonneville shoreline forms the abrasion platform midway up the hillside, with associated triangular facets above. Immediately to the left are scarps of the Wasatch fault zone.
1.8	7.0	The toe of an alluvial fan from the adjacent small canyon forms a hump in the road. Mudflows came from many of the small canyons nearby during the 1983-84 "wet years" of above normal precipitation along the Wasatch Front, and many of the alluvial fans are composed mostly of mudflow deposits.
0.5	7.5	On the left is a small graben along a strand of the Wasatch fault zone. This fault zone forms the structural boundary between the Basin and Range province to the west and the Colorado Plateaus and Middle Rocky Mountains provinces to the east. It extends about 200 mi (320 km) from Malad City, Idaho, south to Fayette, Utah, and passes through the heavily urbanized part of the Wasatch Front between Ogden and Provo, including Salt Lake City. The Wasatch fault zone exhibits evidence for recurrent surface faulting during late Quaternary time (Machette and others, 1991).
0.8	8.3	Farmington Bay lies ahead; this is the proposed site of a water-storage reservoir to be enclosed by dikes (Everitt, 1991). Antelope Island, part of the state parks system, is to the right. Causeways to the island were flooded and destroyed by the 1983-87 rise in Great Salt Lake. Great Salt Lake is the fourth largest terminal lake in the world (Greer, 1977). At the average historic lake level of about 4,200 ft (1,280 m) above mean sea level, it covers about 1,700 sq mi (4,400 sq km) with a maximum depth of 34 ft (10 m) (Arnow and Stephens, 1990). Historic lake salinity has varied from as much as 28 percent salt (eight times that of ocean water), to about 6 percent in 1984 (in the south arm of the lake).
1.3	9.6	The flat-topped hills to the left are remnants of the Bonneville shoreline platform.
1.0	10.6	The community of Fruit Heights lies near the mouth of Holmes Creek canyon, from which mudflows came in 1983-84. To the right, south of Antelope Island, are the Oquirrh Mountains. The distant range east of the Oquirrh Mountains is the Stansbury Mountains. Tooele Valley lies between these ranges.
3.0	13.6	The headscarp of the Farmington Siding landslide, a liquefaction-induced lateral spread of Holocene age, lies to the left (Van Horn, 1973). The slide may be associated

with the penultimate surface-faulting earthquake on the Weber segment of the Wasatch fault zone (Everitt, 1991; Foreman and others, 1991). Nearby, at the foot of the mountain, is the site of the Kaysville trench, the first trench excavated across the Wasatch fault zone to specifically study and date fault displacement (Schwartz and others, 1983).

1.8 15.4 Return to Interstate 15. On the left is Lagoon amusement park. When the area was first inhabited it was a wetland, and there is still marshy ground on both sides of the highway. The poor drainage is probably due to a combination of tectonic backtilting toward the Wasatch fault zone and disruption of drainage by the Farmington Siding landslide.

2.0 17.4 Between here and Centerville, 1.6 mi (2.6 km) to the south, it is common for foundation excavations to encounter layers of peat a foot (0.3 m) or more thick. To the right is the site of the Guffey and Galey #1 oil test well, drilled to 2,000 ft (610 m) in 1904, and abandoned in "lake deposits" (Hansen and Bell, 1949).

1.6 19.0 Centerville. To the right is the former location of the Farmington gas field, which produced methane from organic-rich lake beds at depths of from 400 to 700 ft (120 to 210 m) for a short time around the turn of the century (Hansen and Bell, 1949). Destructive debris flows and debris floods, generated by late spring snowfall and rapid warming in the spring of 1983, traveled down steep canyons along the mountain front to the left (Keaton and others, 1988).

2.1 21.1 Near exit 321 to Bountiful the highway is on fine-grained lake deposits near the present level of Great Salt Lake. The prominent benches on the mountain front to the east are at the Bonneville (upper) and Provo (lower) shoreline levels of Lake Bonneville. This part of the Wasatch Range is underlain by rocks of the Farmington Canyon Complex.

2.3 23.4 The ridge ahead which extends from the mountain front is the Salt Lake salient, a slice of rock between two strands of the Wasatch fault zone, the Rudy's Flat fault to the east and the Warm Springs fault to the west. The salient is mostly composed of Tertiary conglomerate and volcanic rocks. The quarries on the west end are in Paleozoic dolomite and limestone beneath a veneer of Lake Bonneville sand and gravel.

3.1 26.5 Take exit 316 to Interstate 215. Conglomerate of the Eocene Wasatch Formation is exposed on the hillside to the left, on the upthrown side of the Warm Springs fault (Bryant, 1990). Proceed west on Interstate 215 onto the flood plain of the Jordan River. The course of the river along the range front is likely a result of tectonic subsidence accompanying faulting.

1.6 28.1 Cross the Jordan River. Nearby, Western Petroleum drilled an oil test well in 1931. It was abandoned at about 2,000 ft (610 m) in "lake beds."

2.2 30.3 To the left, the steep front of the Salt Lake salient is adjacent to the Warm Springs fault. The surface trace of the fault extends southeastward and disappears beneath downtown Salt Lake City. The domed state capitol building, visible in the distance, is underlain by deltaic deposits from City Creek, associated with the Stansbury level of Lake Bonneville.

2.1 32.4 Take exit 22A to Interstate 80, west. The interchange crosses small scarps of the West Valley fault zone (Bryant, 1990).

0.9 33.3 Salt Lake City International Airport is on the right. The highway crosses the Jordan surplus canal.

0.8 34.1 To the left, the Bingham Canyon open-pit mine is visible on the east flank of the Oquirrh Mountains, within the Bingham mining district. A conveyor system brings ore north along the east side of the range to the concentrator, mill, and smelter on the north end. Just north of the Bingham Canyon mine, excavation is underway at the newly developed Barneys Canyon gold deposit.

Copper became an important commodity from the district in 1896, although copper, molybdenum, and gold are now produced from the Bingham Canyon open-pit mine (Tripp and others, 1989). The Kennecott Copper Corporation operated the mine for several decades beginning in 1936, and was influential in the economic development of Wasatch Front communities. Ownership of the mine has since been transferred between several companies, and today the mine is owned by the RTZ Corporation. In recognition of the significant role that Kennecott historically played, the division of RTZ which operates the mine does so under the Kennecott name.

1.9 36.0 The International Center office complex on the right is constructed on the saturated, unconsolidated, fine-grained deposits of the Jordan River delta of Holocene age, at about the level of the Holocene high (elevation 4,221 ft; 1,287 m) of Great Salt Lake.

1.4 37.4 In the foreground to the left is the north end of the Oquirrh Mountains; the north end of the Stansbury Mountains is visible in the distance. To the right of the highway is Antelope Island, and opposite the Stansbury Mountains to the right is Stansbury Island. The south end of Antelope Island is composed of Precambrian rock of the Farmington Canyon Complex, and the north end of the Oquirrh Mountains is Pennsylvanian and Permian rock of the Oquirrh Group. The large gap in the stratigraphic record, and attitude of the strata, implies a substantial buried structure between the two locations.

2.6 40.0 The flat-topped mesa to the left contains the Kennecott mill tailings pond. North of the mesa is the Morton Company salt plant. The pond is one of the largest in the world. It covers an area of 8 sq mi (21 sq km) to a depth of about 200 ft (60 m) and weighs about 90 million tons (80 million metric tons). This significant load is in the vicinity of a local concentration of earthquake epicenters, including the 1962 Magna earthquake of magnitude 5.2 (Arabasz and others, 1979). No relationship has been established, however, between the tailings pond and possible induced seismicity.

1.4 41.4 The roadway on the right was raised in 1984 to keep storm surges from flooding the interstate at a time when Great Salt Lake was rising to record historic levels. The roadway has been lined with concrete barricades, but they also prevent travellers from viewing the lake. To the left are the Morton Salt Company evaporation ponds.

1.3 42.7 On the right is the sewage lagoon which serves the state parks along the Great Salt Lake shore. Three miles to the north is the site of the Whitlock No. 1 Morton Salt oil test well drilled in 1956 (Davis, 1984). The well encountered Tertiary strata at 962 ft (293 m), Precambrian strata at 3,656 ft (1,114 m), and bottomed at 4,231 ft (1,290 m) (Heylmun and others, 1965).

A USGS study of ground-shaking induced by distant nuclear explosions at the Nevada Test Site (NTS) indicated that the south shore area, underlain by thick alluvial and lacustrine deposits, experienced spectral velocities about 10 times larger than sites underlain by bedrock (Carver and King, 1987). Amplifications for earthquake sources closer and larger than the NTS explosions are still being debated.

1.0 43.7 The Morton Salt Company pumping station is on the right. The intake canal was excavated through a 2-ft (0.6-m) thick bed of Glauber's salt (hydrous sodium sulfate; Wilson and Wideman, 1957; Eardley, 1966).

0.3 44.0 The causeway extending into the lake is the roadbed of the railway which went to the Saltair pavilion, the last and largest of the lake resorts. Saltair was completed in 1893, and after abandonment in the 1960s due to the low lake level, the remaining buildings were destroyed by fire in 1971 (Travous, 1980). The pavilion was built on pilings inserted in holes melted with steam through the hard Glauber's salt bed which underlies the southeast shore area (Miller, 1980).

0.3 44.3 Mudflats on the south shore of Great Salt Lake, part of the state park system (Great Salt Lake State Park South Shore), are to the right. From 1984 to 1986, when the lake level was high, the area was popular with windsurfers.

0.7 45.0 The bump in the road marks the beginning of a section of the Interstate highway raised in 1984 in response to the rising level of Great Salt Lake.

0.8 45.8 New Saltair to the right, a privately developed replica of the original pavilion, was opened for business in March, 1983, one month before the lake level rose and inundated the facility.

1.3 47.1 Beyond the concrete barricades to the right is the Great Salt Lake Boat Harbor and Sunset Beach, which was one of the last remaining swimming beaches on the south shore. Sunset Beach was covered with rock fill in 1984 to prevent erosion from the rising lake. The Kennecott smelter slag pile is on the left.

Tooele and Northern Rush Valleys

1.5 48.6 On the right, near the intersection of Interstate 80 and State Route 201 (the road to Magna), Black Rock is a megablock of detached bedrock near the edge of Great Salt Lake (Tooker and Roberts, 1971a). Emplaced by a Quaternary rock fall from high on the north end of the Oquirrh Mountains, Black Rock is an offshore stack at high stages of Great Salt Lake and a land-tied tombolo at low stages. The elevation of the tombolo is about 4,205 ft (1,282 m). Black Rock is the site of one of the first resorts on the south shore of the lake, built in 1880, and also is the site of the earliest gauge to measure the level of the lake, a staff gauge operated from 1875 to 1876 (Arnow and Stephens, 1990).

On the left near the same intersection, Black Rock Canyon is the site of a gravel pit that, during the construction of Interstate 80, yielded the most prolific freshwater fish fauna ever recovered from Lake Bonneville sediments (Smith and others, 1968). Black Rock Caves in the canyon, and Deadman Cave at the north end of the Stansbury Mountains, yielded archaeological remains which have basal dates from 5,000 to 7,000 yr B.P. (Simms, 1977; Madsen, 1980).

1.0 49.6 The remains of the Garfield Landing resort are on the left, and of the Garfield Beach resort are on the right. Both resorts were constructed in the 1880s (Miller, 1980). A staff gauge to measure the lake level operated at Garfield from 1881 to 1901 (Arnow and Stephens, 1990). All of the deepwater beaches close to Salt Lake City have now been filled or made inaccessible by highway and railroad construction.

0.8 50.4 On the left as Interstate 80 rounds the northwest corner of the Oquirrh Mountains, overhanging ledges (surmounted by powerline poles) of tufa-cemented gravels mark the Stansbury shoreline. About 240 ft (73 m) above modern lake stages, the Stansbury shoreline formed between 22,000 and 20,000 yr B.P. (^{14}C years before present; Oviatt and others, 1990), about midway in the 12,000-year transgression of Lake Bonneville. Similar tufa encrustations occur at the Provo level nearby, and at both the Provo and Stansbury levels on the north end of the Stansbury Mountains to the west.

0.8 51.2 At Lake Point, take exit 99 to State Route 36 (Mills Junction-Tooele Road). The Southern Pacific Railroad causeway, to the right, was raised 10 ft (3 m) in the 1980s to avoid damage from the rising lake.

Also on the right, a service road leads to the evaporation ponds and salt piles of the Lake Point salt works. The road follows the crest of one of three parallel beach ridges that form the Holocene highstand shoreline in this area. Reaching an elevation of 4,221 ft (1,287 m) above sea level, the highest stage of Great Salt Lake during the last 10,000 years occurred between 3,440 and 1,400 yr B.P. (Murchison, 1989). As at many other Holocene highstand sites, oolitic sand is an important constituent of these beaches.

2.6 53.8 Turn left on Big Canyon Road from State Route 36.

1.4 55.2 Cross the railroad tracks and follow the dirt road to the intersection.

0.2 55.4 Turn left at the intersection and continue on the dirt road until the next intersection.

0.2 55.6 Turn right at the intersection and continue on the dirt road.

0.5 56.1 Follow the dirt road to **STOP 1.** Tooele Valley is at the western edge of the ISB, a zone of diffuse seismicity extending from Arizona north into Montana (Smith and Sbar, 1974). Earthquakes in the ISB are shallow and are rarely coincident with known Quaternary structures, which complicates the evaluation of earthquake hazards. One significant geologic structure in Tooele Valley with evidence for recurrent surface faulting during late Quaternary time is the NOFZ.

The NOFZ bounds the west side of the northern Oquirrh Mountains, generally strikes north-south, and dips to the west. It is a zone of normal faults that extends roughly 14 mi (23 km) from Lake Point, on the north, to Middle Canyon south of Tooele. The NOFZ can be divided into two sections: 1) a northern section, roughly 7 mi (11 km) long, marked by discontinuous fault scarps that offset Lake Bonneville deposits; and 2) a southern section, which places older Quaternary alluvium in fault contact with Paleozoic rocks along the range front (Barnhard and Dodge, 1988).

Four potential trench sites have been selected by the UGS to investigate the size and timing of surface-faulting events on the northern section of the NOFZ. Information from the trenches may constrain the characteristics of the most recent and penultimate events, and latest Quaternary recurrence intervals and slip rates.

STOP 1 is the most promising trench site. Geology of the site vicinity is shown on figure 4 (trench location A). At this site a multiple-event main fault scarp and a short antithetic fault scarp form a wide, shallow graben in Lake Bonneville deposits (Solomon, in preparation[b]). The graben has served as a sediment trap for Holocene debris-flow and flash-flood deposits, and is a favorable setting for finding charcoal-bearing sediments or possibly pond organics in stratigraphic relation to faulting. In

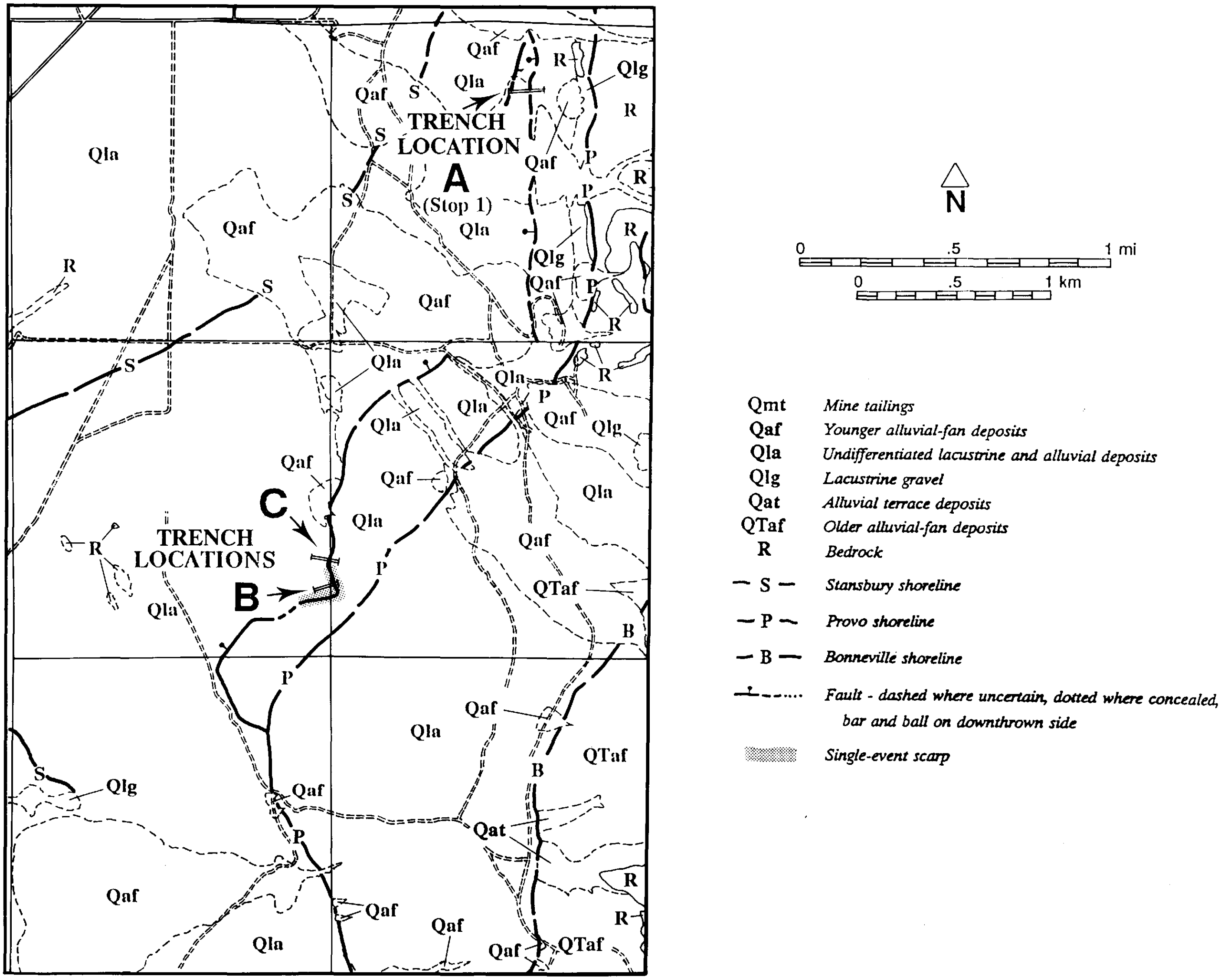

Figure 4. Surficial geologic map of a portion of the northern Oquirrh fault zone (Solomon, in preparation [b]) showing proposed trench locations A (STOP 1), B, and C. See figure 3 for location. Geology by Barry Solomon, 1989-1990.

addition to providing information on the timing of the most recent surface-faulting event, an evaluation may be possible of the timing of the penultimate event with respect to the chronology of Lake Bonneville.

To the south, two potential trench sites, located 2.0 mi (3.2 km) east and 1.3 mi (2.1 km) north of the intersection of State Route 36 and Bates Canyon Road, are in an area where a single-event scarp diverges from the trend of a multiple-event scarp. This is one of the few places along the fault zone where a single-event scarp is preserved (T.P. Barnhard, written communication, 1990). A trench across this scarp (trench location B, figure 4) should expose evidence of the most recent surface-faulting event uncomplicated by a pre-existing scarp or the formation of a graben. A trench across the adjacent multiple-event scarp (trench location C, figure 4) should provide information on the relationship of penultimate faulting to the Bonneville lake cycle.

The fourth potential trench site is located north of Flood Canyon, 2.1 mi (3.4 km) east of State Route 36 (trench location D, figure 5). Here, a single scarp offsets the Provo shoreline and post-Provo (younger than 13,500 yr B.P.) alluvial-fan deposits (Solomon, in preparation[b]). However, the potential for useful information at this site is complicated by shallow bedrock. There are exposures of highly fractured quartzite from the Oquirrh Group of Pennsylvanian and Permian age (Tooker, 1980) on both the upthrown and downthrown sides of the fault scarp.

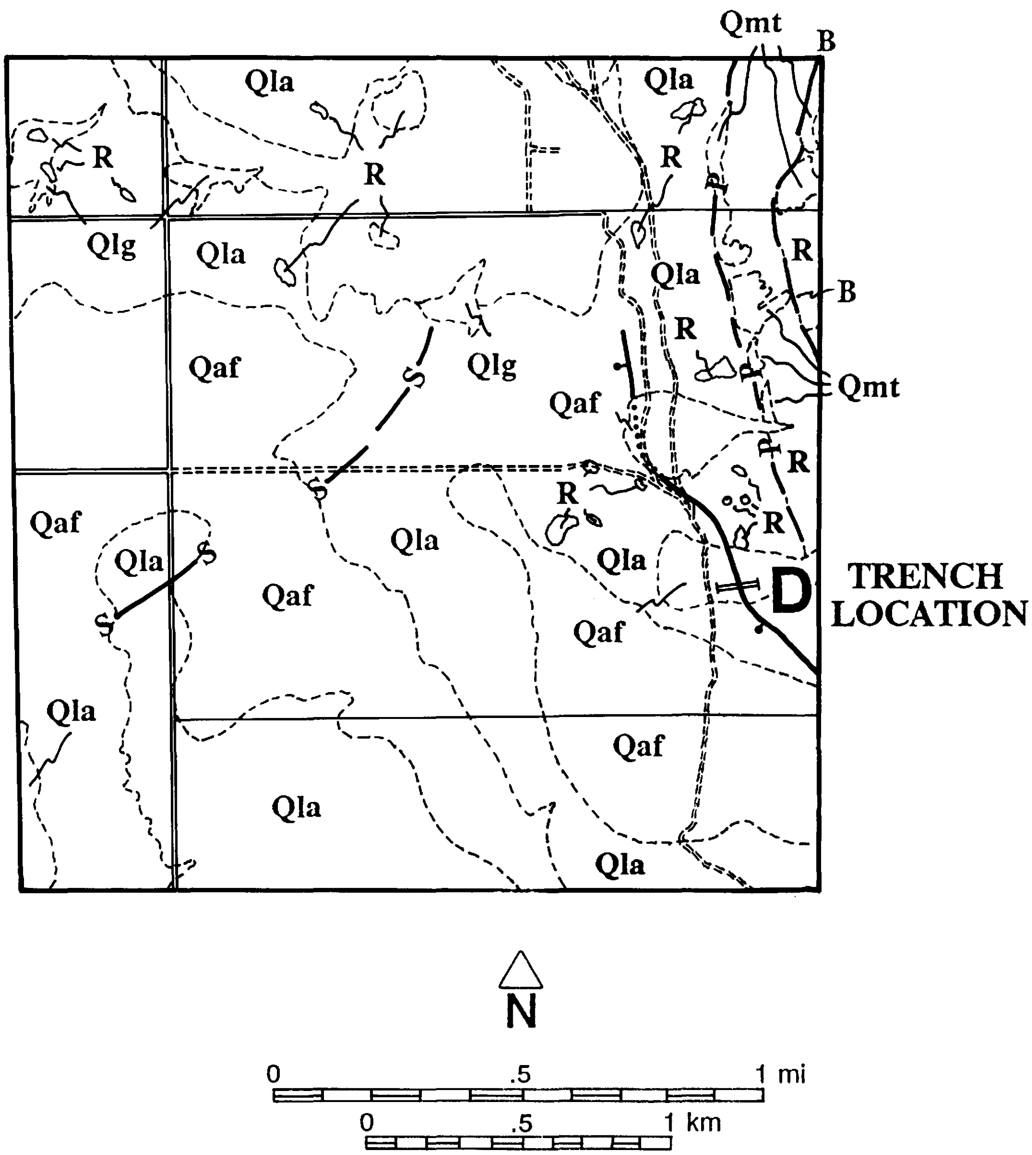

Qmt	*Talus*
Qaf	*Younger alluvial-fan deposits*
Qla	*Undifferentiated lacustrine and alluvial deposits*
Qlg	*Lacustrine gravel*
QTaf	*Older alluvial-fan deposits*
R	*Bedrock*
— S —	*Stansbury shoreline*
— P —	*Provo shoreline*
— B —	*Bonneville shoreline*
⊥ – – –	*Fault - dashed where uncertain, dotted where concealed, bar and ball on downthrown side*

Figure 5. Surficial geologic map of a portion of the northern Oquirrh fault zone (Solomon, in preparation [b]) showing proposed trench location D. See figure 3 for location. Geology by Barry Solomon, 1989-90.

2.3 58.4 Return to State Route 36 and turn left.

0.5 58.9 On the left is Adobe Rock, a stack eroded from an outcrop of the Pennsylvanian and Permian Oquirrh Group (Tooker and Roberts, 1971b) by the surf of Lake Bonneville. On the right is Dunne's Pond Spring, one of the large springs of the valley which provides water to the Kennecott mill and smelter. Flow from the spring is reported to be 4,200 gpm (265 L/s) (Razem and Steiger, 1981).

0.4 59.3 Near the intersection of State Route 36 and State Route 138 (Salt Lake City-Grantsville Road), the Mills Junction spit of Gilbert shoreline age projects toward the southwest, away from its sediment sources in the Oquirrh Mountains (Eardley and others, 1957). The Gilbert shoreline-forming interval occurred between 12,000 and 10,000 yr B.P. (Murchison, 1989), very early in the history of Great Salt Lake and under end-of-Pleistocene paleoclimatic conditions that remain something of a mystery. Here at an elevation of 4,262 ft (1,299 m), the crest of the highest Gilbert shoreline beach ridge has historically served three functions: 1) its lagoon side provided natural topographic closure for a mill pond that was a source of water power in the nineteenth century; 2) more recently, that topographic closure was exploited in the landscape architecture of the artificial lake on the north side of Stansbury Park; and 3) for over a century, the crest of the Mills Junction spit has provided a well-drained site for several miles of the Salt Lake City-Grantsville Road, which will be the return route of this field trip.

1.0 60.3 To the right is Mill Pond Spring, which also supplies water to Kennecott. Its flow is reported as 3,400 gpm (215 L/s) (Razem and Steiger, 1981).

To the left is a salient that extends westward from the Oquirrh Mountains. The surficial deposits consist of Lake Bonneville transgressive gravel accumulations. Several bedrock knobs are present on the margin of the salient and these, as well as gravity contours (Johnson, 1958; Cook and Berg, 1961) and the continuity of Lake Bonneville shorelines, indicate that the salient is largely underlain by shallow bedrock that was a preexisting topographic high during deposition of Lake Bonneville sediments. No evidence of post-Bonneville faulting on the margins of the salient has been found, although the NOFZ does trend northward across the salient.

1.8 62.1 The highway bears left in Erda. To the right is the site of USGS ground-water test well No. 3, drilled in 1978 and abandoned at a depth of 365 ft (111 m) because of uncontrollable artesian flow (Ryan and others, 1981).

The inferred trace of the Occidental Fault trends northwest through Erda, and extends southeast along the margin of the Oquirrh Mountains. The presence of this fault was inferred by Gates (1962) because of a gravity anomaly and a discontinuous ridge of gravel on the ground surface, and because his data showed differences in the potentiometric surface and chemical quality of the water from one side of the suspected fault to the other. Gates (1965) stated that this fault was the only known barrier to ground-water movement in the valley fill. Data from newer wells, however, indicate that the fault is not a barrier to ground-water movement, and that differences in chemical quality are a function of depth rather than related to a fault (Razem and Steiger, 1981). The fault likely exists, but there is no evidence to indicate that the fault has ruptured surficial unconsolidated sediments (Solomon, in preparation[b]).

0.2 62.3 To the left is the site of USGS ground-water test well No. 4, completed to a depth of 1,500 ft (460 m) in alluvial basin fill. The hole encountered interbedded sand, gravel and clay with fresh water to a depth of 900 ft (270 m), and mostly clay with brackish or saline water below that depth.

0.3 62.6 A mile to the east on the toe of the alluvial apron is the site of USGS ground-water test well No. 8, drilled to 1,511 ft (461 m) in alluvial basin fill, with results similar to those of well No. 4.

0.1 62.7 The Erda Center store. To the left is a good view of the steep front of the Oquirrh Mountains. The northern Oquirrh fault zone forms low scarps in Pleistocene lakebeds on the piedmont slope. The row of talus-covered triangular facets just above the base of the mountain marks the beach cliff above the Bonneville shoreline. The association of talus with this shoreline is typical along the western flank of the Oquirrh Mountains (Case, 1987b).

1.9 64.6 To the left is the site of the International smelter. The copper, lead, and zinc smelter was constructed in 1910, and operated into the 1970s (Hansen, 1963). The deposit of black slag at the mouth of Pine Canyon, nearby, is the only remaining visible evidence of the smelter. Further up Pine Canyon stands a concrete headframe, approximately 300 ft (90 m) high, the most prominent remaining feature of Anaconda's Carr Fork Mine.

Northeast of the smelter are Pass and Swensons Canyons. During the wet years of 1983-84, debris floods in these canyons deposited sand and gravel on alluvial fans east of the town of Lincoln (Harty and Lowe, in preparation). The farthest of these deposits reached nearly 1.2 mi (1.9 km) beyond the base of the mountains. Along the range front are more faceted spurs above the Bonneville shoreline, one of the most prominent marked with the letter "T."

1.3 65.9 To the right after crossing the railroad overpass, the wave-cut platform and bluff of the Provo shoreline trend toward the southwest, around the northwest side of Tooele and into Tooele Army Depot North (TADN) at an elevation of about 4,860 ft (1,480 m). The Provo shoreline formed between 14,500 and 14,000 yr B.P., following Lake Bonneville's rapid descent during the Bonneville Flood in southern Idaho (Currey and Oviatt, 1985). Gravels removed from north of Tooele entered an energetic longshore transport system, which carried them 6 mi (10 km) to the southwest and deposited them near the south edge of TADN. The Provo shoreline depositional sequence there contains dozens of parallel beach ridges.

1.5 67.4 Turn right on State Route 112 from State Route 36.

2.4 69.8 **STOP 2.** State Route 112 (Gransville-Tooele Road), TADN, ammunition gate. TADN operated an unlined industrial waste lagoon (IWL) from about 1965 until November, 1988. Organic solvents and metals from this operation have contaminated ground water in the vicinity. Trichlorethylene (TCE) was the most significant contaminant (figure 6). Information from 79 monitoring wells contributed to the determination that the contaminant plume contains 36 billion gallons (136 billion liters) of TCE-contaminated ground water. The ground water is in a generally unconfined aquifer consisting of both unconsolidated sediments and bedrock. The unconsolidated sediments consist of poorly sorted, subangular, silty sand, gravel, and cobbles with layers of clay, sand, or gravel up to 5 ft (2 m) thick. The sand, gravel, and cobbles are composed of limestone and quartzite from the Oquirrh Mountains. The aquifer is recharged by subsurface seepage from the Oquirrh Mountains, upward flow from deeper confined aquifers, percolation of precipitation, and minor subsurface flow from adjacent areas. Depth to ground water at TADN ranges from about 200 to 400 ft (60 to 120 m) below the ground surface. Ground water flows from south to north, toward the center of Tooele Valley.

The Army and the State of Utah entered into a consent decree on January 13, 1986, to have the IWL closed by November, 1989, and corrective action implemented. A wastewater treatment system was constructed, and discharge to the IWL ceased on November 8, 1988. The IWL was closed on November 1, 1989. A contract for ground-water cleanup was awarded on March 28, 1991. The contaminated ground water will be extracted, put through an air stripping treatment system, and the clean water will be re-injected into the ground. It is anticipated that treatment will last approximately 15 years, at a cost of $7.5 million.

2.4 72.2 Return to the intersection of State Route 112 and State Route 36. Turn right on State Route 36.

1.0 73.2 On the south outskirts of Tooele, State Route 36 curves to the right (southwest) and ascends to the Bonneville shoreline, which here is at elevations from 5,170 to 5,230 ft (1,575 to 1,595 m). Lake Bonneville occupied this zone discontinuously between 16,400 and 15,000 yr B.P., prior to the Bonneville Flood (Currey and Oviatt, 1985). As at the Gilbert and Provo shorelines, longshore transport carried gravelly sediments several miles to the southwest, in the same direction as southbound State Route 36. From high-energy sediment sources south of Tooele, large volumes of material moved to low-energy sediment sinks in the complex depositional features that comprise the Stockton Bar depocenter.

0.3 73.5 Turn left on Settlement Canyon Road.

0.6 74.1 **STOP 3.** Settlement Canyon Reservoir has been the site of numerous floods during periods of rapid snowmelt (Lund, 1985a; Harty and Lowe, in preparation). In 1973, snowmelt runoff rapidly filled the reservoir causing an uncontrolled spill for almost

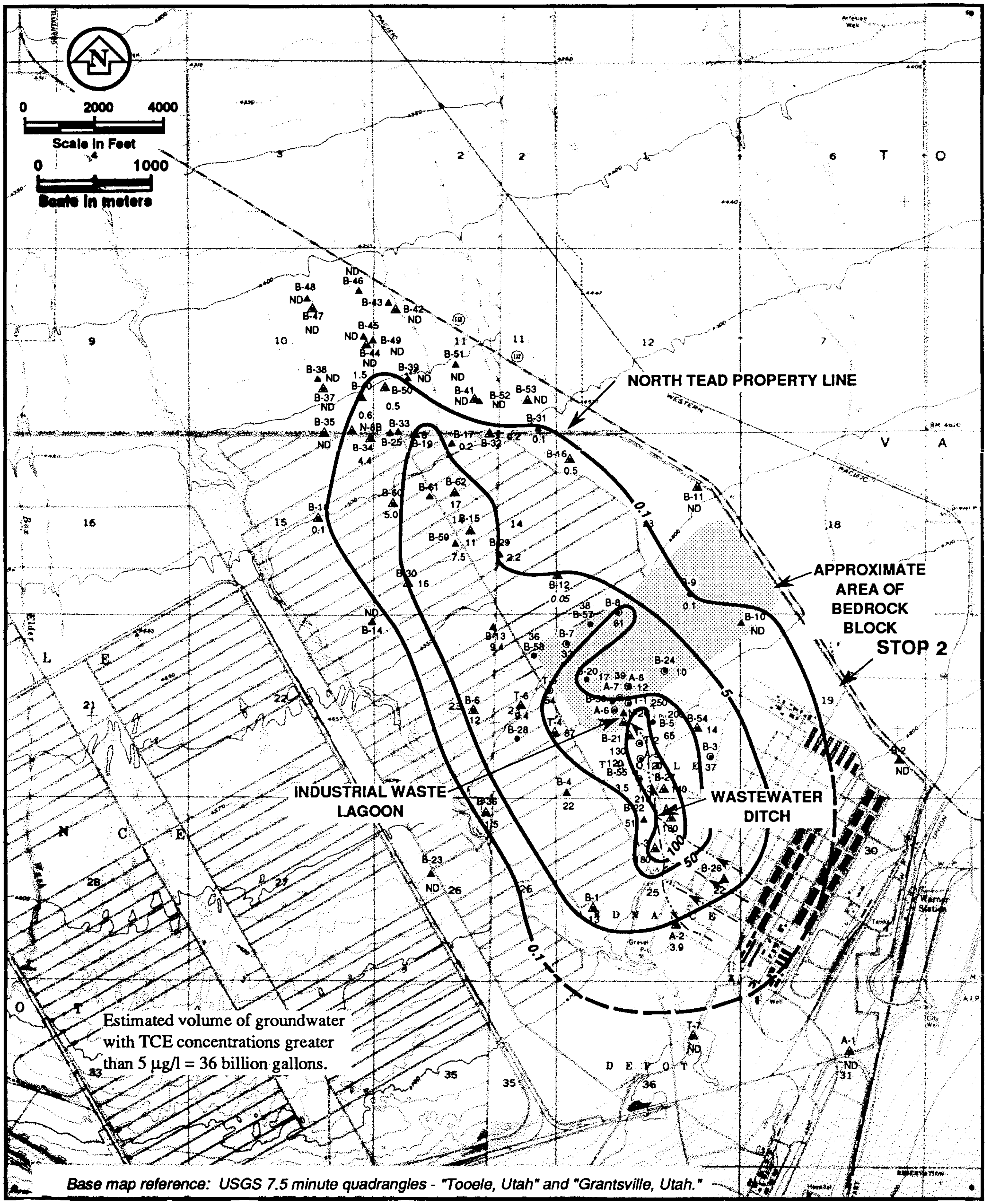

EXPLANATION

- ▲ Alluvial monitoring well location
- ● Bedrock monitoring well location
- ▲ Deep Alluvial monitoring well location (>110 ft. BSWL)
- ● Deep Bedrock monitoring well location (>110 ft. BSWL)
- 0.14 Concentration of TCE in groundwater measured during 1986, 1987, & 1988 sampling (µg/l)
- 0.05 Isoconcentration line, dashed where inferred (contour interval varies)
- ND Not detected

Figure 6. Isoconcentration map for TCE at Tooele Army Depot north area, STOP 2 (modified from James M. Montgomery, Inc., 1989, figure 2). See figure 3 for location.

three months. In 1983, stream inflow exceeded safe levels of outflow for release from the reservoir, and flood waters were released from the overflow outlet into Tooele Valley. A similar incident occurred in 1984. Streets in Tooele were inundated during the three events, and in 1983 and 1984 house and property damage occurred when floodwaters breached a dike.

Settlement Canyon has also been the site of large earth movements (Harty and Lowe, in preparation; Harty, Nelson, and Lowe, in preparation; figure 7). Two large rock slides are present in the upper portion of the canyon, although the date of movement is unknown. A summer rainstorm in 1983 generated a debris flow about 7 mi (11 km) up the canyon that buried a large part of the canyon road. In the spring of 1984, a series of debris flows and floods trapped three men in the canyon for seven hours, and a pick-up truck parked in the canyon was destroyed and washed away. The material continued to flow downstream into the reservoir, burying the outlet with about 6 or 7 ft (2 m) of sediment.

0.6 74.7 Return to State Route 36 and turn left.

0.3 75.0 On the left between Tooele and the main gate of TADN, a bedrock platform at the base of the truncated mountain front indicates that up to 300 ft (90 m) of highly fractured Pennsylvanian quartzite were removed in a few hundred years, mostly by waves from across Lake Bonneville's long northwest-southeast fetch.

1.3 76.3 On the left near the main gate of TADN, the toe of a pre-Bonneville alluvial fan was notched by wave erosion at the Bonneville shoreline. Most of the gravel that was removed from this fan (at least 4,000,000 cubic yards; 3,000,000 cubic meters) now resides in the Stockton Bar depocenter, 2 to 3 mi (3 to 5 km) farther southwest.

2.1 78.4 An extensive tailings pond at Bauer, to the right, is related to a selective flotation plant. The plant, now inactive, processed metallic ore which was transported from the Honerine Mine in the adjacent Oquirrh Mountains through a long adit excavated in Quaternary lacustrine and alluvial deposits (Gilluly, 1932). The adit was over 13,000 ft (4,000 m) long and discharged water at the rate of about 1,500 to 1,900 gpm (95 to 120 L/s).

0.2 78.6 **STOP 4.** On the left near the crest of State Route 36, the longshore process mode at the Bonneville shoreline changes from erosion (to the northeast) to deposition (to the southwest). Front-right, a communications relay station is situated on the highest spit in the Stockton Bar depocenter (Burr and Currey, 1988; Burr, 1989; figure 8).

Figure 7. Debris flow in upper Settlement Canyon, STOP 3, deposited during wet years of 1983 or 1984. Alignment of logs on debris-flow surface, from upper left to lower right, indicates flow direction. Photograph by Kimm Harty, 1990.

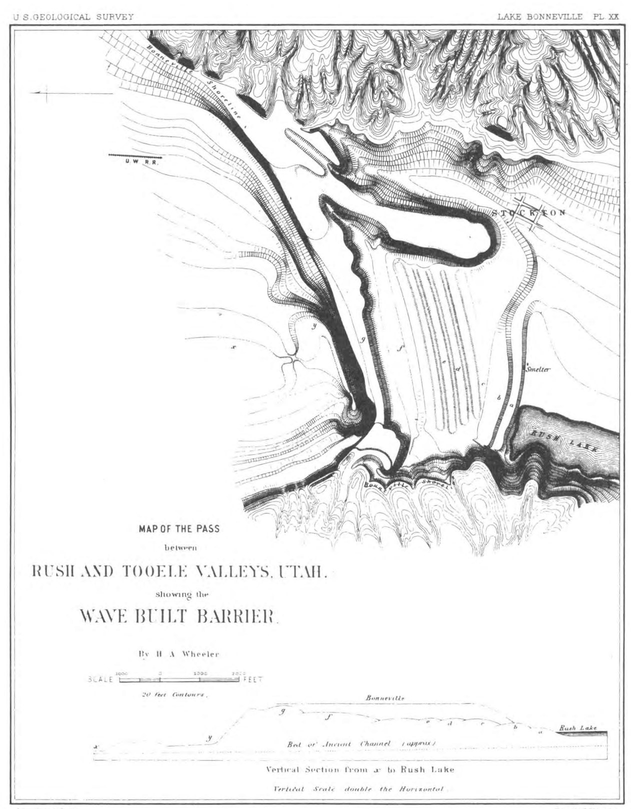

Figure 8. Contour map and vertical section of the Stockton Bar, STOP 4 (Gilbert, 1890, plate XX). See figure 3 for location.

The many morphostratigraphic units that comprise the Stockton Bar depocenter are reviewed in more detail in the article by Burr and Currey in this guidebook.

1.7 80.3 To the right, Rush Lake was reportedly the size of a "small pond" in 1862 (Gilbert, 1980). The lake is thought to have reached its greatest height in 1876 or 1877, but by 1959 the lake was dry (Harty and Christenson, 1988). The lake began rising again in 1978, and between 1983 and 1985 the lake level rose 10 ft (3 m). The recent level, though, is several feet lower than the historic high of the 1870s.

0.7 81.0 On the left 1 mi (2 km) south of downtown Stockton, the Soldier Creek alluvial fan was constructed and then deeply entrenched in pre-Bonneville time. This suggests that the pre-Bonneville drainage of Soldier Creek must have been free to exit Rush Valley, which of course is now closed by deposits of the Stockton Bar depocenter (Gilluly, 1929). Apparently all of Rush Valley drained freely into ancestral Great Salt Lake in pre-Bonneville time, and Rush Lake has existed only in post-Bonneville time.

The large Soldier Canyon landslide of early to middle Holocene age lies on the south flank of Soldier Canyon, about 3.5 mi (5.6 km) to the left (Tooker and Roberts, 1988a). The Manning Canyon Shale of Mississippian age underlies the flanks of the canyon and is likely involved in this slope failure. This is the only deep-seated landslide in the Oquirrh Mountains within the field trip area.

Soldier Canyon was also the site of flooding and earth movement during the 1983-84 wet years. Extensive road damage in the canyon occurred from flooding during the spring of both years (Harty and Lowe, in preparation). A debris flow or debris flood during the summer of 1983 destroyed four secitons of a main culinary water line (Kaliser, 1989).

4.1 85.1 Turn left onto State Route 73.

6.8 91.9 **STOP 5.** State Route 73, Tooele Army Depot South (TADS), near east gate. Chemical weapons have been in existence since World War I. Since then, the United States has maintained its own chemical stockpile as a deterrent force. In 1985, the U.S. Congress passed Public Law 99-145 which directed the Department of Defense to destroy our country's stockpile of unitary chemical weapons, some of which are more than 40 years old. These unitary weapons contain pre-mixed, live chemical agents and are becoming obsolete for modern U.S. defense systems. More importantly, the weapons are beginning to deteriorate in storage, and they could become a risk to public safety and the environment.

TAD has in storage 42 percent of this country's chemical weapons. A plant currently under construction at TADS is a major project in the chemical weapons disposal program (figure 9). The plant utilizes the technology developed and tested at a similar plant located at TADS for the past 12 years. Operations at the new plant are scheduled to begin in 1994. Seismic and hydrologic considerations are critical elements in the design, construction, and safe operation of the plant.

2.0 93.9 Continue south on State Route 73. Turn left on Mercur Canyon Road.

0.4 94.3 **STOP 6.** A zone of normal faults is present along the western flank of the southern Oquirrh Mountains, on the margin of Rush Valley. The fault zone is composed mainly of three subsidiary fault zones, which trend N25°W and dip 55 to 65°W, in a right-stepping pattern separated by northeast- and northwest-trending cross faults. The subsidiary zones have differing amounts of displacement.

The three right-stepping fault zones were designated by Gilluly (1932) as the Soldier Canyon, Lakes of Killarney, and West Mercur fault zones (F1, F2, and F3, from north to south; figure 10). Most of the faults occur in or adjacent to bedrock, but the southern West Mercur fault zone forms scarps on unconsolidated sediments, and is designated by Barnhard and Dodge (1988) as the Mercur fault zone. These scarps are on two sub-parallel faults about 3-mi (5-km) long. Maximum slope angles on the scarps reach 19°, with a maximum tectonic displacement of 20.0 ft (6.1 m). These are the most prominent late Quaternary fault scarps on the west flank of the southern Oquirrh Mountains.

The Bonneville shoreline is well preserved near the fault zone. The shoreline scarp height varies from about 50 ft (15 m) west of Soldier Canyon to about 7 ft (2 m) west of Mercur Canyon. Four periods of alluvial deposition have been identified nearby. The oldest deposits are alluvial fans designated on figure 10 as Qaf_1 to Qaf_3, from youngest to oldest; the youngest deposit,

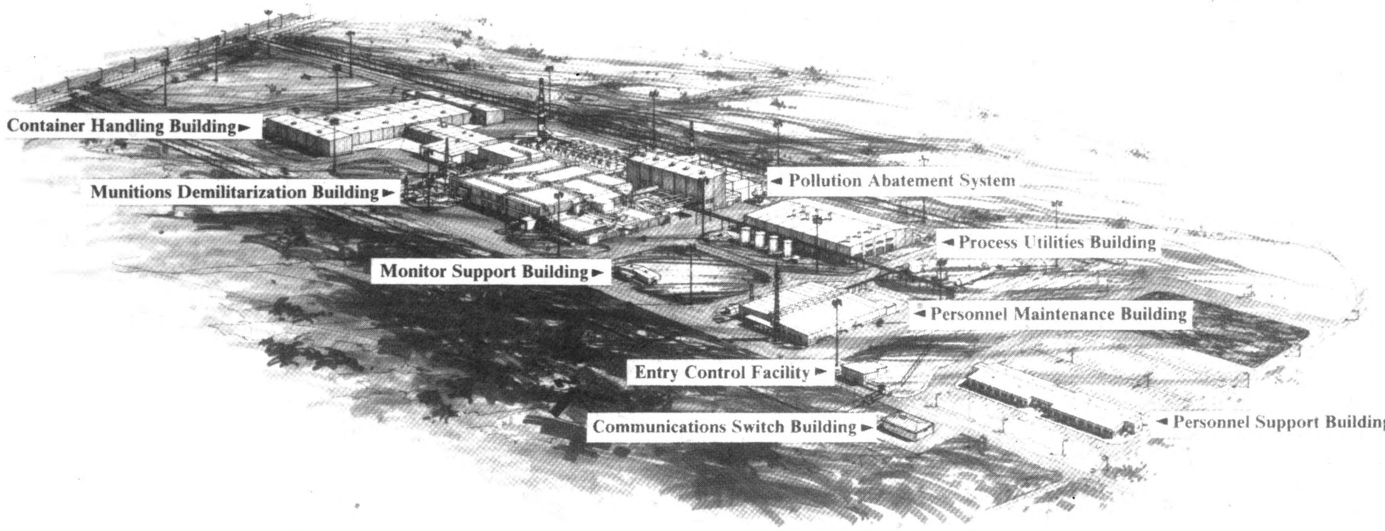

Figure 9. Artist's concept of the Chemical Stockpile Disposal Plant under construction at Tooele Army Depot south area, STOP 5.

not mappable at the scale shown, includes alluvium deposited on the valley floor. The age of fan deposition (Qaf_1 to Qaf_3) has been estimated by comparison with the characteristics and chronology of other Wasatch Front alluvial fans. The oldest fans (Qaf_3) were deposited about 100,000 to 200,000 yr B.P. (Machette, 1984). These fans are offset by the southern West Mercur fault zone, and by part of the south end of the western branch of the Lakes of Killarney fault zone. The younger two fan deposits (Qaf_1 and Qaf_2) are as old as 16,000 to 32,000 yr B.P. (Scott and others, 1983), and are older than the Bonneville shoreline which is eroded into the fans. The youngest alluvium (not mapped) is post-Bonneville age, and extends into the Holocene.

There has been debate regarding the age of offset along the West Mercur fault zone. Everitt and Kaliser (1980, plate VIIa) mapped a scarp of this zone which crossed the Bonneville shoreline onto a post-Bonneville alluvial fan, and concluded that at least 2 ft (0.6 m) of offset was post-Bonneville (figure 11). They also reported the presence of deformed Lake Bonneville or younger sediments in a trench excavated to investigate the fault (Everitt and Kaliser, 1980, plate VIIb). Barnhard and Dodge (1988), however, interpret the trench sediments as unfaulted and uncomformably draped over a pre-existing fault scarp by the transgressive rise of Lake Bonneville. They measured 11 fault-scarp profiles and found that the regression-equation line for the West Mercur fault zone scarps (the Mercur fault zone of Barnhard and Dodge, 1988) plots below and parallel to the Bonneville shoreline regression-equation line, indicating that the last surface-faulting event predates the shoreline. Geologic mapping along the fault zone north of the trench site (figure 10) shows that younger fan deposits (Qaf_1 and Qaf_2) are not cut by faults, and the faults themselves terminate against the Bonneville shoreline south of Mercur Canyon, where the shoreline apparently runs along the old fault scarp. Faults in this area, therefore, are older than the Bonneville shoreline and Qaf_2.

Vertical displacement in the West Mercur fault zone appears largest near Mercur Canyon and decreases toward both the south and north. However, the lengths of the three right-stepping subsidiary fault zones decrease from south to north: 9 mi (15 km) for the West Mercur fault zone, 6 mi (10 km) for the Lakes of Killarney fault zone, and 4 mi (7 km) for the Soldier Canyon fault zone. This decrease in length is coincident with a decrease in apparent tectonic displacement: about 20 ft (6 m) for the West Mercur fault zone in alluvial-fan deposits north of Mercur Canyon, 7 ft (2 m) for the Lakes of Killarney fault zone for fault scarps developed in limestone bedrock, and 3 ft (1 m) for bedrock scarps in the Soldier Canyon fault zone. Gravity data (Cook and others, 1989) show that the basement under Rush Valley is deepest to

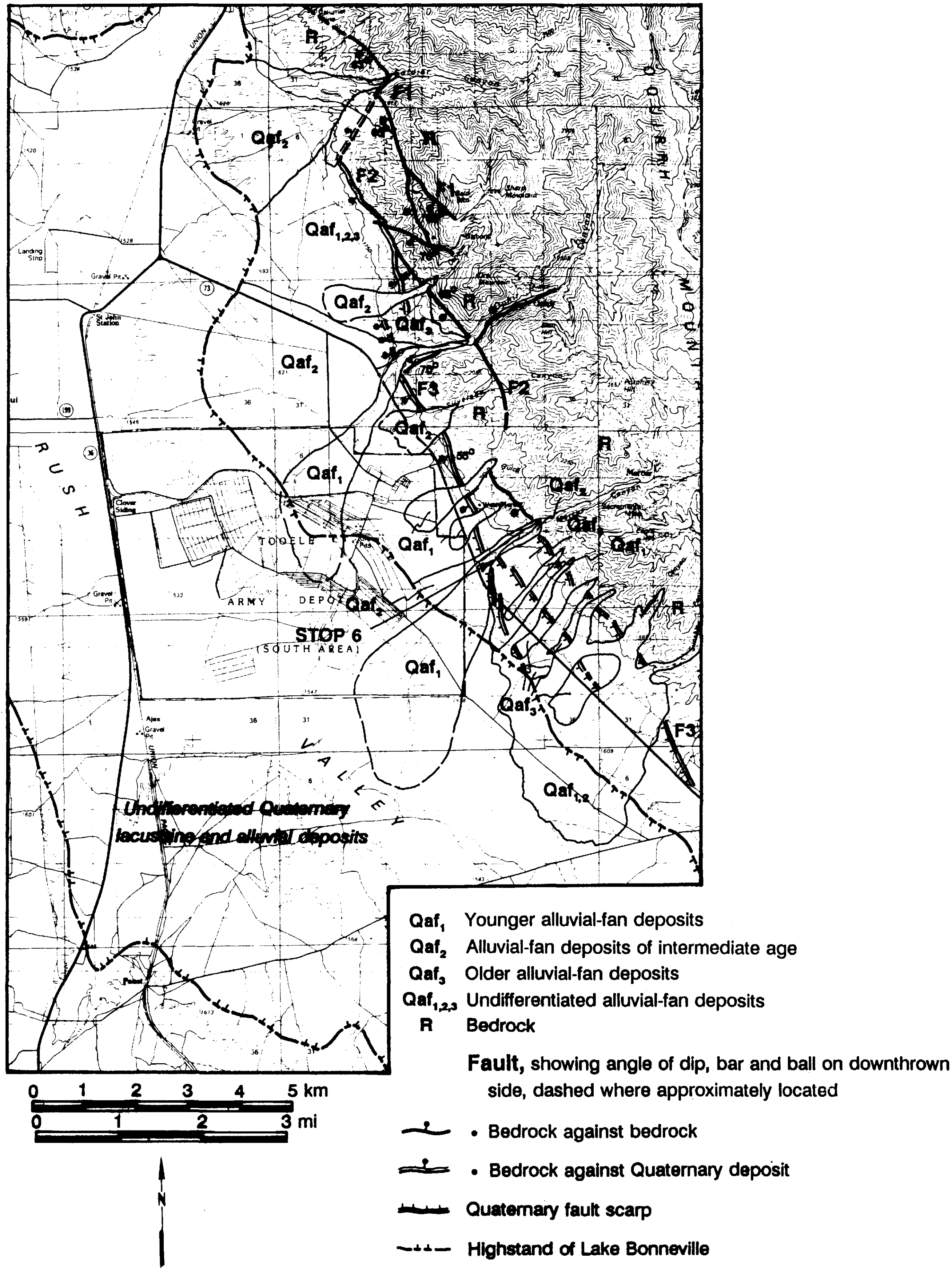

Figure 10. Geologic map of northeastern Rush Valley showing a zone of normal faults on the western margin of the southern Oquirrh Mountains. Qaf_1, Qaf_2, and Qaf_3, from youngest to oldest, are late Pleistocene alluvial fans. F1, F2, and F3 are, respectively, the Soldier Canyon, Lakes of Killarney, and West Mercur fault zones of Gilluly (1932). Fault scarps of the West Mercur fault zone formed on unconsolidated sediments near the mouth of Mercur Canyon will be inspected at STOP 6. See figure 3 for location. Geology by Daning Wu, 1990.

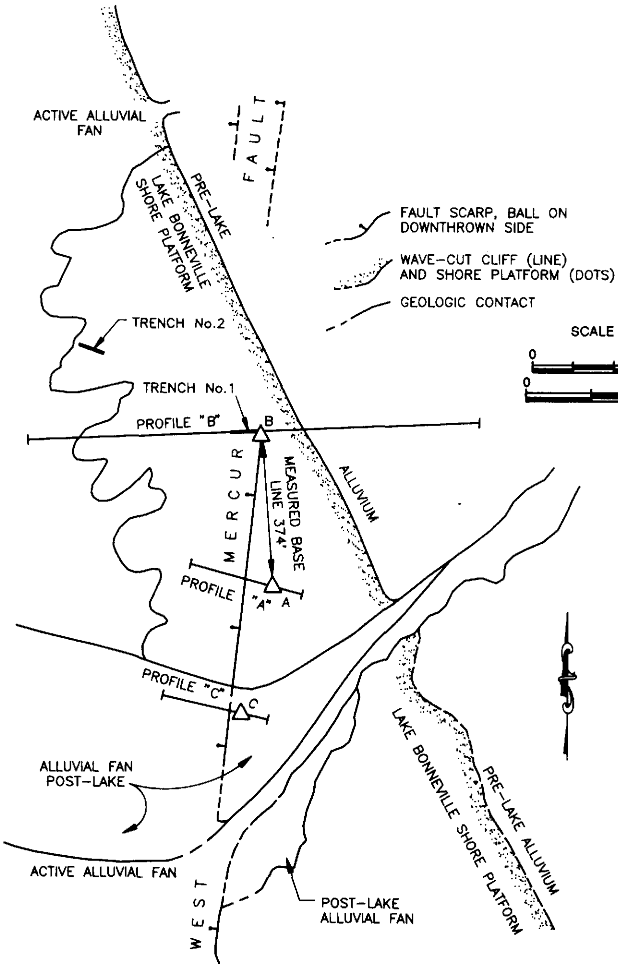

Figure 11. Surficial geology at the intersection of the West Mercur fault and the Bonneville shoreline, SE¼ Sec. 1, T. 7 S., R. 4 W., Tooele County, Utah. This map is from Everitt and Kaliser, 1980, figure VIIa, and corrects the image reversal of the original illustration. See figure 3 for location. Geology by Ben Everitt and Bruce Kaliser, 1979.

the south, and becomes shallower to the north. Thus, increased displacement along valley-margin faults to the south coincided with increased basin subsidence in the southern portion of Rush Valley, and with increased subsidiary fault zone length. Late Pleistocene basin subsidence to the south initiated a southerly shift in the Rush Valley depocenter which may be reflected in the morphology of the youngest alluvial fans (Qaf_1), whose distal portions extend southward as opposed to a more westerly orientation of older alluvial-fan deposits (Qaf_2 and Qaf_3).

Scarp morphology and fault geometry suggest that the three subsidiary fault zones could rupture synchronously during an earthquake event similar to the surface-rupture pattern of the 1915 Pleasant Valley earthquake, Nevada (Wallace, 1984). Most of the Lakes of Killarney and Soldier Canyon fault zones offset bedrock, however, and do not have well-preserved late Quaternary fault scarps. Because of this, even careful paleoseismic studies may not yield conclusive evidence with regard to synchronous displacement.

0.4 94.7 Return to State Route 73. Turn right.

8.8 103.5 Return to the intersection of State Routes 36 and 73 and turn left on State Route 36.

1.7 105.2 Turn right at St. John Station. Near St. John Station a series of northwest-trending, discontinuous scarps occur in Quaternary alluvium of pre-Bonneville age. These scarps, both northeast and southwest facing, are referred to as the Saint John Station fault zone by Barnhard and Dodge (1988). The lack of offset spits, noted by Everitt and Kaliser (1980), indicates that the surface faulting is older than the spit deposits of Lake Bonneville (about 15,000 yr B.P.).

2.4 107.6 Turn right onto the St. John-Grantsville Road.

5.7 113.3 In 1983, a large landslide in Manning Canyon Shale occurred at the confluence of Morgan and East Hickman Canyons to the left (Harty, Robison, and Lowe, in preparation). The slide damaged the East Hickman Canyon Road, and access to vehicular traffic has only recently been restored.

2.4 115.7 In the right foreground near the south edge of TADN, the St. John-Grantsville Road descends to and parallels the Bonneville shoreline. Less than a mile (1 km) farther east, near the west edge of TADN, enormous south-trending spits indicate that longshore transport along the east flank of the Stansbury Mountains was similar to that elsewhere in Tooele Valley, with a net movement from north to south (figure 12). The gravels in these spits were derived from pre-Bonneville alluvial fans as far north as Grantsville.

3.4 119.1 Abandoned alluvial-fan deposits which predate the highstand of Lake Bonneville are present between East Hickman and North Willow Canyons, in the foothills of the Stansbury Mountains. These deposits are formed by coalescing alluvial fans which have developed bajadas, characterized by gentle down-fan slopes and undulating cross-fan topography. These deposits have been divided into three units based upon the relative elevation of adjacent fan surfaces and the degree of dissection (Solomon, in preparation[b]). The youngest aban-

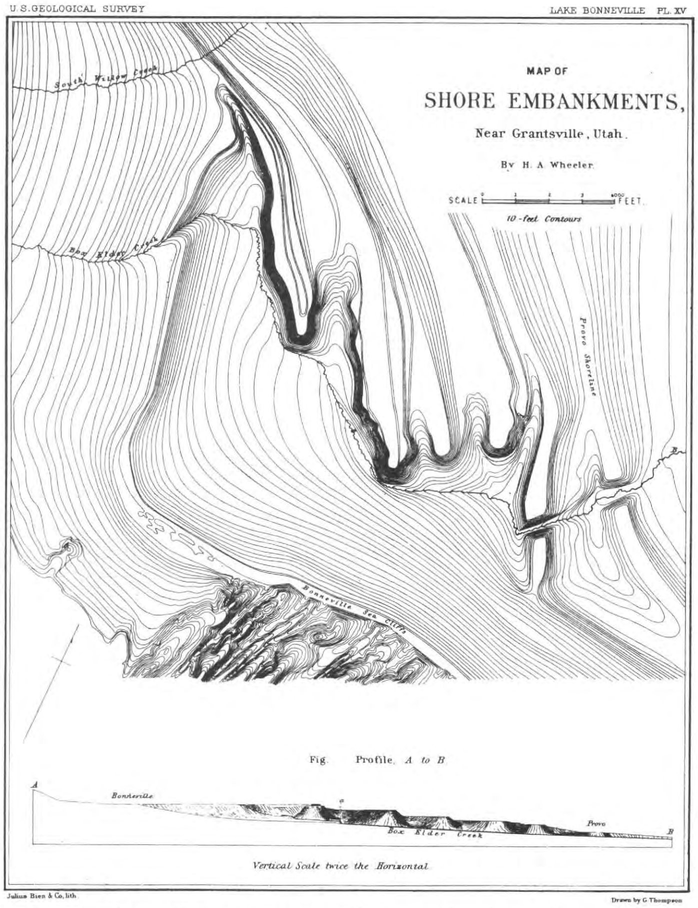

Figure 12. Contour map and vertical section of south-trending spits near the west edge of Tooele Army Depot north area (Gilbert, 1890, plate XV). See figure 3 for location.

doned alluvial fans have relatively smooth, convex surfaces truncated by the Bonneville shoreline. The surface of older deposits are more incised, and are truncated by younger deposits. More extreme dissection occurs in the oldest deposits, which may be as old as late Tertiary. These deposits were abandoned prior to Lake Bonneville transgression. The deposits do not occur below the Bonneville level, and are probably eroded and buried by younger material.

Alluvial-terrace deposits formed prior to the Bonneville shoreline also occur in the same canyons, and are particularly well developed in the vicinity of East Hickman Canyon, where five terrace levels occur. Between South Willow and Box Elder Canyons, three levels are present.

The embankment on the bajada between North and South Willow Canyons is part of the Grantsville Irrigation Company reservoir. The 70-ft (20-m) high, zoned earth-fill dam was constructed in 1984. Excavation for fill within the reservoir basin showed the pre-Bonneville alluvium to consist of gravelly, silty clay cut by channels filled with sandy gravel.

1.0 120.1 Crossing the St. John-Grantsville Road obliquely from northwest to southeast, the Provo shoreline in this area is a shore platform, with a wave-cut bluff/inner platform that is fringed by a wave-built outer platform.

1.4 121.5 In the extensive piedmont zones of the Oquirrh and Stansbury Mountains, surficial material consists mainly of alluvial-fan deposits of pre-Bonneville age that were only moderately reworked by lacustrine processes. As a result, the alluvial-fan deposits are overlain by a thin cover of lacustrine sediment. The lacustrine sediment is coarser grained in the middle and upper piedmont, and finer grained in the lower piedmont, because the pre-lake fan material was finer near the distal ends of the fans. In these places the unit is commonly expressed geomorphically as pre-Bonneville alluvial fans etched by Lake Bonneville shorelines.

1.8 123.3 Thomas (1946) reported that the area south and east of Grantsville was covered by dunes "as recent as any geologic features in the valley, having been developed chiefly during the drought years of 1934 and 1935, when the vegetative cover was destroyed by desiccation over large areas." There are no signs of these dunes in the immediate vicinity of Grantsville now, but such material does exist at TADN, eroded from very fine-grained lacustrine beds.

0.2 123.5 After the road bears right, it makes a sharp left into Grantsville.

0.7 124.2 In the town of Grantsville, turn right onto State Route 138 from the St. John-Grantsville Road. To the left, in Grantsville, is the site of USGS ground-water test well No. 6. The well, completed in 1978, recovered tuffaceous sandstone from a depth of 728 ft (222 m). Pollen analysis showed that the sample was of Pliocene age (Everitt and Kaliser, 1980).

At the base of the Stansbury Mountains, 3 to 6 mi (5 to 10 km) northwest, mine dumps are present near Flux, where high-calcium limestone was once mined, and near Dolomite, where dolomite extraction is ongoing (Chemstar, Inc., 1990).

Barchan dunes with predominantly silt-sized grains, and with lesser amounts of clay, fine sand, and sodic material, are present in the northwestern portion of

Tooele Valley, 3 mi (5 km) north of Grantsville. The sand is locally oolitic with a core of silt. The silt dunes occur on the margin of, and overlie, erosional remnants of Lake Bonneville lacustrine sediments; the remnants are commonly surrounded by younger deposits of playa mud. The silt dunes appear to have accumulated from eroded, fine-grained Lake Bonneville beds, and serve as a protective barrier for the lakebed remnants. Fine-grained lakebeds are common in northern Tooele Valley, between piedmont slopes to the south, and mudflats to the north.

4.6 128.8 To the right of the road, near the town of Marshall, is the site of USGS ground-water test well No. 1, drilled to a depth of 1,513 ft (461 m) in unconsolidated basin fill. There is fresh water in thin gravel beds to a depth of about 800 ft (245 m).

0.6 129.4 Turn left onto the dirt road. There is a locked gate at the entrance; permission from the owner must be granted for access.

0.7 130.1 **STOP 7.** Elliptical depressions, from 5 to 50 ft (2 to 15 m) in diameter, occur in a restricted area northeast of Grantsville (figure 13). The area is underlain by fine-grained Lake Bonneville beds with local interbedded sand. Many of the depressions are surrounded by a raised rim of sand, and springs emanate from within some of them. Depressions without springs are commonly plugged by dark, peaty clay. These features superficially resemble liquefaction-induced sand boils, but their origin is enigmatic. The features may also be due to artesian pressure and flowage beneath a confining layer (Obermeier and others, 1990).

About 1 mi (2 km) to the north are two oil test wells. One well, Hickey No. 1 Cassity, encountered Paleozoic strata at 4,830 ft (1,470 m) while the other, Walker-Wilson No. 1, less than a mile (2 km) west of the Hickey well, bottomed in Tertiary strata at 7,100 ft (2,200 m) (Heylmun, 1965). This bedrock relief confirms a locally steep gravity gradient, and has been used to infer the presence of a subsurface fault (Johnson, 1958).

0.7 130.8 Return to State Route 138 and turn left.

1.8 132.6 On the right, houses near Erda were subject to basement flooding in the spring of 1985. Ground water occurs under both artesian

Figure 13. Elliptical depressions northeast of Grantsville, STOP 7. Photograph by Ben Everitt, 1990.

and water-table conditions in the Erda area (Gates and Keller, 1970). Subsurface flow from bedrock aquifers in the Oquirrh Mountains probably accounts for the largest percentage of total recharge to the artesian aquifers. A principal source of recharge to the shallow water table is upward leakage from the underlying artesian aquifers. Greater than normal precipitation was recorded in the valley during the five years preceding basement flooding, and between March, 1984 and March 1985, increases in hydrostatic head in the artesian aquifer of between 15 and 45 ft (5 and 14 m) were recorded (Arnow, 1985). The sustained pattern of increased precipitation and upward leakage from the artesian aquifer into unconfined beds resulted in basement flooding (Lund, 1986).

1.1 133.7 On State Route 138 between 6 and 9 mi (10 and 14 km) northeast of Grantsville, beach ridges that comprise the Mills Junction spit of Gilbert shoreline age are evident to either side of, and beneath, the right of way. This leg of the field trip is exactly counter to the direction of longshore transport that prevailed about 10,500 yr B.P.

2.6 136.3 Turn left at Mills Junction, the intersection of State Route 138 and State Route 36.

3.6 139.9 Take the entrance to Interstate 80 east toward Salt Lake City.

Tooele Valley to Ogden

16.2 156.1 Retrace the ingoing route on Interstate 80. At the intersection with Interstate 215, go north to Ogden.

5.9 162.0 Continue on Interstate 215. At the intersection with Interstate 15, go north to Ogden.

11.1 173.1 Continue on Interstate 15; do not take the exit for U.S. Highway 89.

1.0 174.1 The freeway rises onto the right lateral margin of the Farmington Siding landslide.

2.0 176.1 Antelope Island is visible to the left, across Farmington Bay.

5.0 181.1 From the top of the overpass at exit 335, the skyline to the north is the surface of the Provo stage of the Weber River delta. The freeway here is on the Provo-stage lake bottom. The hill to the right is also part of the Provo-stage delta, with Hill Air Force Base constructed on the hill's flat upper surface.

3.0 184.1 The freeway rises over the nose of the Pleistocene Weber River delta at an elevation of about 4,600 ft (1,400 m).

2.0 186.1 The Lake Bonneville plain in front of the delta stretches to the edge of present Great Salt Lake.

1.0 187.1 Promontory Point is visible to the northwest. In 1869, the first transcontinental rail line was completed near Promontory Summit, a pass in the mountains about 30 mi (50 km) north of Promontory Point. This route, however, had steep grades and sharp curves and was abandoned in 1904 in favor of a more direct route. The new route consisted of a wooden-trestle causeway from Promontory Point to Lakeside (Newby, 1980). Replacement of the trestle with rock fill in 1959 is one of the local geotechnical legends, and involved the national engineering community (Casagrande, 1965). The fill was raised in response to the rising lake level from 1984 to 1986; storms closed the rail line for substantial lengths of time during these years.

2.0 189.1 The highway descends into the valley of the Weber River, running northward, which has cut into the Lake Bonneville delta. Hills on the left are remnants of deltaic deposits. To the right is Weber Canyon, where the Weber River cuts the Wasatch Range from Morgan Valley. North of Weber Canyon is Ogden Canyon from the Pineview Reservoir in Ogden Valley. Further north is the North Ogden Divide.

1.0 190.1 Leave Interstate 15 at exit 344 and travel east to return to Weber State University.

2.4 192.5 Turn right on Washington Boulevard.

0.8 193.3 Turn left on 36th Street.

1.6 194.9 Turn right on Harrison Boulevard.

1.0 195.9 Return to the front gate of Weber State University at the intersection of Harrison Boulevard and 3850 South.

ACKNOWLEDGMENTS

This manuscript was reviewed by Gary E. Christenson of the UGS and Jim Wilson of Weber State University, and we thank them for their critical comments and helpful suggestions. Paleolake research was supported, in part, by USGS Grant 14-08-0001-G1536 to Donald R. Currey.

REFERENCES CITED

Arabasz, W.J., Smith, R.B., and Richins, W.D., editors, 1979, Earthquake studies in Utah, 1850-1978: University of Utah Seismograph Stations, Department of Geology and Geophysics, Salt Lake City, 548 p.

Arnow, Ted, 1985, Ground-water levels rise throughout most of Utah for third consecutive year: U.S. Geological Survey in cooperation with the Utah Department of Natural Resources Division of Water Rights, Water-level-change report and maps, 20 p.

Arnow, Ted, and Stephens, Doyle, 1990, Hydrologic characteristics of the Great Salt Lake, Utah: 1847-1986: U.S. Geological Survey Water-Supply Paper 2332, 32 p.

Barnhard, T.P., 1988, Fault-scarp studies of the Oquirrh Mountains, Utah, *in* Machette, M.N., ed., In the Footsteps of G.K. Gilbert — Lake Bonneville and Neotectonics of the Eastern Basin and Range Province: Utah Geological and Mineral Survey Miscellaneous Publication 88-1, p. 52-54.

Barnhard, T.P., and Dodge, R.L., 1988, Map of fault scarps formed on unconsolidated sediments, Tooele 1° x 2° quadrangle, northwestern Utah: U.S. Geological Survey Miscellaneous Field Studies Map MF-1990, scale 1:250,000.

Beckwith, E.G., 1855, Explorations from the mouth of the Kansas River, Missouri, to the Sevier Lake, in the Great Basin: Pacific Railroad Reports, vol. 2, Washington, D.C.

Bryant, Bruce, 1990, Geologic map of the Salt Lake City 30'x60' quadrangle, north-central Utah, and Uinta County, Wyoming: U.S. Geological Survey Miscellaneous Investigations Map I1944, scale 1:100,000.

Bucknam, R.C., 1977, Map of suspected fault scarps in unconsolidated deposits, Tooele 20 sheet, Utah: U.S. Geological Survey Open-File Report 77-495, scale 1:250,000.

Burr, T.N., 1989, Hydrographic isostatic modelling of thresholdcontrolled shorelines of Lake Bonneville: University of Utah, Salt Lake City, M.S. thesis, 62 p.

Burr, T.N., 1989, Hydrographic isostatic modelling of threshold-controlled ed., In the Footsteps of G.K. Gilbert — Lake Bonneville and Neotectonics of the Eastern Basin and Range Province: Utah Geological and Mineral Survey Miscellaneous Publication 88-1, p. 66-73.

Carpenter, Everett, 1913, Ground water in Box Elder and Tooele Counties, Utah: U.S. Geological Survey Water-Supply Paper 333, 90 p.

Carver, D.L., and King, K.W., 1987, Ground response study — interisland dike location, Great Salt Lake, Utah: Preliminary U.S. Geological Survey Report to Utah Division of Water Resources, 4 p.

Casagrande, Arthur, 1965, Role of the "calculated risk" in earthquake and foundation engineering: American Society of Civil Engineers Proceedings, Journal of the Soil Mechanics and Foundations Division, v. 91, no. SM4, p. 1-40.

Case, W.F., 1987a, Proposed spring drainage trench site, Erda, Tooele County, Utah, *in* Mulvey, W.E., comp., Technical Reports for 1986-Site Investigation Section: Utah Geological and Mineral Survey Report of Investigation 215, p. 118-124.

—-1987b, Rock-fall hazard susceptibility due to earthquakes, central Wasatch Front, Utah: U.S. Geological Survey Open-File Report 87-585, p. V1-V36.

Chemstar, Inc., 1990, Chemstar lime: Chemstar, Inc., Grantsville, Utah, 10 p.

Clark, D.W., Appel, C.L., Lambert, P.M., and Puryear, R.L., 1990, Ground-water resources and simulated effects of withdrawals in the east shore area of Great Salt Lake, Utah: Utah Department of Natural Resources Technical Publication No. 93, 150 p.

Cook, K.L., and Berg, J.W., 1961, Regional gravity survey along the central and southern Wasatch Front, Utah: U.S. Geological Survey Professional Paper 316-E, p. 75-89.

Cook, K.L., Bankey, Viki, Mabey, D.R., and DePangher, Michael, 1989, Complete Bouguer gravity anomaly map of Utah: Utah Geological and Mineral Survey Map 122, scale 1:500,000.

Cook, K.L., Montgomery, J.R., Smith, J.T., and Gray, E.F., 1975, Simple Bouguer gravity anomaly map of Utah: Utah Geological and Mineral Survey Map 37, scale 1:1,000,000.

Currey, D.R., 1990, Quaternary palaeolakes in the evolution of semidesert basins, with special emphasis on Lake Bonneville and the Great Basin, U.S.A.: Palaeogeography, Palaeoclimatology, Palaeoecology, v. 76, p. 189-214.

Currey, D.R., and Oviatt, C.G., 1985, Duration, average rates, and probable causes of Lake Bonneville expansions, stillstands, and contractions during the last deep-lake cycle, 32,000 to 10,000 years ago, *in* Kay, P.A., and Diaz, H.F., eds., Problems of and Prospects for Predicting Great Salt Lake Levels: Center for Public Affairs and Administration, University of Utah, Salt Lake City, p. 9-24.

Currey, D.R., Oviatt, C.G., and Czarnomski, J.E., 1984, Late Quaternary geology of Lake Bonneville and Lake Waring, *in* Kerns, G.J., and Kerns, R.L., Jr., eds., Geology of Northwest Utah, Southern Idaho, and Northeast Nevada: Utah Geological Association Publication 13, p. 227-237.

Davis, F.D., 1984, Mineral resources of the central Wasatch Front: Utah Geological and Mineral Survey Map 54-D, scale 1:100,000.

Eardley, A.J., 1966, Sediments of Great Salt Lake, in Stokes, W.L., ed., The Great Salt Lake: Utah Geological Society Guidebook to the Geology of Utah No. 20, p. 105-120.

Eardley, A.J., Gvosdetsky, Vasyl, and Marsell, R.E., 1957, Hydrology of Lake Bonneville and sediments and soils of its basin: Geological Society of America Bulletin, v. 68, p. 1141-1201.

Eardley, A.J., Shuey, R.T., Gvosdetsky, Vasyl, Nash, W.P., Picard, M.D., Grey, D.C., and Kukla, G.J., 1973, Lake cycles in the Bonneville basin, Utah: Geological Society of America Bulletin, v. 84, no. 1, p. 211-216.

Everitt, B.L., 1991, Stratigraphy of eastern Farmington Bay: Utah Geological and Mineral Survey, Survey Notes, v. 24, no. 3, p. 27-29.

Everitt, B.L., and Kaliser, B.N., 1980, Geology for assessment of seismic risk in the Tooele and Rush Valleys, Tooele County, Utah: Utah Geological and Mineral Survey Special Studies 51, 33 p.

Foreman, S.L., Nelson, A.R., and McCalpin, J.P., 1991, Thermoluminescence dating of fault-scarp derived colluvium: Deciphering the timing of paleoearthquakes on the Weber segment of the Wasatch fault zone, north-central Utah: Journal of Geophysical Research, v. 96, no. B1, p. 595-605.

Gates, J.S., 1962, Geohydrologic evidence of a buried fault in the Erda area, Tooele Valley, Utah, in Geological Survey Research 1962 - Short Papers in Geology, Hydrology, and Topography, Articles 120-179: U.S. Geological Survey Professional Paper 450-D, p. D78-D80.

—-1963, Selected hydrologic data, Tooele Valley, Tooele County, Utah: Utah State Engineer Basic Data Report 7, 23 p.

—-1965, Re-evaluation of the ground-water resources in Tooele Valley, Utah: Utah State Engineer Technical Publication 12, p. 68.

Gates, J.S., and Keller, O.A., 1970, Ground water in Tooele Valley, Utah: Utah Department of Natural Resources Water Circular 2, 15 p.

Gilbert, G.K., 1875, Report upon the geology of portions of Nevada, Utah, California, and Arizona, examined in the years 1871 and 1872, *in* Wheeler, G.M., ed., Report upon Geographical and Geological Explorations and Surveys West of the One Hundredth Meridian, v. III—Geology: Washington, D.C., Government Printing Office, p. 17-187.

—-1890, Lake Bonneville: U.S. Geological Survey Monograph 1, 438 p.

Gilluly, James, 1928, Basin Range faulting along the Oquirrh Range, Utah: Geological Society of America Bulletin, v. 39, p. 1103-1130.

—-1929, Possible desert-basin integration in Utah: Journal of Geology, v. 37, p. 672-682.

—-1932, Geology and ore deposits of the Stockton and Fairfield Quadrangles, Utah: U.S. Geological Survey Professional Paper 173, 171 p.

Greer, D.C., 1977, Desertic terminal lakes, in Desertic Terminal Lakes: Proceedings from the International Conference on Desertic Terminal Lakes, Utah Water Research Laboratory, Utah State University, Logan, p. 1-24.

Hansen, G.B., 1963, Industry of destiny — copper in Utah: Utah Historical Quarterly, v. 31, no. 3, p. 262-279.

Hansen, G.H., and Bell, M.M., 1949, Oil and gas possibilities in Utah: Utah Geological and Mineral Survey Special Bulletin, 341 p., 9 plates.

Harty, K.M., and Christenson, G.E., 1988, Flood hazards from lakes and failures of dams in Utah: Utah Geological and Mineral Survey Map 111, scale 1:750,000, 8 p.

Harty, K.M., and Lowe, Mike, in preparation, Debris flows, debris floods, and stream flooding, *in* Solomon, B.J., ed., Geologic Hazards and Land-Use Planning in Tooele Valley and the West Desert Hazardous Industry Area, Tooele County, Utah: Utah Geological Survey Open-File Report.

Harty, K.M., Nelson, C.V., and Lowe, Mike, in preparation, Rock fall, *in* Solomon, B.J., ed., Geologic Hazards and Land-Use Planning in Tooele Valley and the West Desert Hazardous Industry Area, Tooele County, Utah: Utah Geological Survey Open-File Report.

Harty, K.M., Robison, R.M., and Lowe, Mike, in preparation, Landslides, *in* Solomon, B.J., ed., Geologic Hazards and Land-Use Planning in Tooele Valley and the West Desert Hazardous Industry Area, Tooele County, Utah: Utah Geological Survey Open-File Report.

Heylmun, E.B., 1965, Reconnaissance of the Tertiary sedimentary rocks in western Utah: Utah Geological and Mineral Survey Bulletin 75, 38 p.

Heylmun, E.B., Cohenour, R.E., and Kayser, R.B., 1965, Drilling records for oil and gas in Utah, 1954-1963: Utah Geological and Mineral Survey Bulletin 74, 518 p.

Hintze, L.F., 1973, Geologic history of Utah: Brigham Young University Geology Studies, v. 20, Pt. 3, 181 p.

Hood, J.W., Price, Don, and Waddell, K.M., 1969, Hydrologic reconnaissance of Rush Valley, Tooele County, Utah: Utah Division of Water Rights Technical Publication 23, 63 p.

Hunt, C.B., 1967, Physiography of the United States: W.H. Freeman and Co., New York, 480 p.

—-editor, 1982, Pleistocene Lake Bonneville, ancestral Great Salt Lake, as described in the notebooks of G.K. Gilbert, 1875-1880: Brigham Young University Geology Studies, vol. 29, part 1, 225 p.

James M. Montgomery Consulting Engineers, Inc., 1989, Corrective action plan for groundwater remediation: Prepared for the U.S. Army Corps of Engineers.

Johnson, J.B., 1958, Regional gravity survey of part of Tooele County, Utah: University of Utah, Salt Lake City, M.S. thesis, 38 p.

Johnson, J.B., and Cook, K.L., 1957, Regional gravity survey of parts of Tooele, Juab, and Millard Counties, Utah: Geophysics, v. 22, no. 1, p. 49-61.

Kaliser, B.N., 1971, Preliminary reconnaissance of the Finch Tailer Court, Lake Point, Tooele County, Utah: Utah Geological and Mineral Survey Report of Investigation 52, 2 p.

—-1983, Engineering geologic problems along Utah's urban corridor, *in* Gurgel, K.D., ed., Geologic Excursions in Neotectonics and Engineering Geology in Utah, Geological Society of America Guidebook - Part IV: Utah Geological and Mineral Survey Special Studies 62, p. 91-109.

—-1989, Water-related geologic problems of 1983 — Utah occurrences by county: Utah Geological and Mineral Survey Miscellaneous Publication 89-4, 24 p.

Kaliser, B.N., and Slosson, J.E., 1988, Geologic consequences of the 1983 wet year in Utah: Utah Geological and Mineral Survey Miscellaneous Publication 88-3, 109 p.

Keaton, J.R., Anderson, L.R., and Mathewson, C.C., 1988, Assessing debris flow hazards on alluvial fans in Davis County, Utah, *in* Fragaszy, R.J., ed., Proceedings of the 24th Symposium on Engineering Geology and Soils Engineering: Washington State University, Pullman, p. 89-108.

Krinitzsky, E.L., 1989, Empirical earthquake ground motions for an engineering site with fault sources, Tooele Army Depot, Utah: Bulletin of the Association of Engineering Geologists, v. XXVI, no. 3, p. 283-308.

Lund, W.R., 1985a, Helicopter reconnaissance of Settlement, Middle, and Butterfield Canyons, Oquirrh Mountains, Utah, *in* Harty, K.M., comp., Technical Reports for 1984 - Site Investigation Section: Utah Geological and Mineral Survey Report of Investigation 198, p. 240-243.

——1985b, Investigation of fatal trench cave-in, AMAX Magnesium Corporation facility near Rowley, Utah, *in* Harty, K.M., comp., Technical Reports for 1984 — Site investigation Section: Utah Geological and Mineral Survey Report of Investigation 198, p. 244-248.

——1986, Preliminary evaluation of high ground-water conditions in Erda, Tooele County, Utah, *in* Mulvey, W.E., comp., Technical Reports for 1985 - Site Investigation Section: Utah Geological and Mineral Survey Report of Investigation 208, p. 228-236.

Machette, M.N., 1984, Preliminary investigations of Late Quaternary slip rates along the southern part of the Wasatch fault zone, central Utah, *in* Hays, W.W., and Gori, P.L., eds., Proceedings of Conference XXVI, a Workshop on "Evaluation of Regional and Urban Earthquake Hazards and Risk in Utah," August 14-16, 1984, Salt Lake City: U.S. Geological Survey Open-File Report 84-763, p. 391-406.

Machette, M.N., Personius, S.F., Nelson, A.R., Schwartz, D.P., and Lund, W.R., 1991, The Wasatch fault zone, Utah—segmentation and history of Holocene earthquakes: Journal of Structural Geology, v. 13, no. 2, p. 137-149.

Madsen, D.B., 1980, The human prehistory of the Great Salt Lake region, *in* Gwynn, J.W., ed., Great Salt Lake - a Scientific, Historical and Economic Overview: Utah Geological and Mineral Survey Bulletin 116, p. 19-31.

McCoy, W.D., 1987, Quaternary aminostratigraphy of the Bonneville Basin, western United States: Geological Society of America Bulletin, v. 98, p. 99-112.

Miller, D.E., 1980, Great Salt Lake: a historical sketch, *in* Gwynn, J.W., ed., Great Salt Lake - a Scientific, Historical and Economic Overview: Utah Geological and Mineral Survey Bulletin 116, p. 1-14.

Murchison, S.B., 1989, Fluctuation history of Great Salt Lake, Utah, during the last 13,000 years: University of Utah Limneotectonics Laboratory Technical Report 89-2, 137 p.

National Oceanic and Atmospheric Administration, 1990, Climatological data annual summary, Utah: v. 92, no. 13, 40 p.

Nelson, A.R., and Personius, S.F., 1990, Preliminary surficial geologic map of the Weber segment, Wasatch Fault Zone, Weber and Davis Counties, Utah: U.S. Geological Survey Miscellaneous Field Studies Map MF-2132, scale 1:50,000.

Newby, J.E., 1980, Great Salt Lake railroad crossing, *in* Gwynn, J.W., ed., Great Salt Lake a Scientific, Historical and Economic Overview: Utah Geological and Mineral Survey Bulletin 116, p. 393-400.

Obermeier, S.F., Jacobson, R.B., Smoot, J.P., Weems, R.E., Gohn, G.S., Monroe, J.E., and Powars, D.S., 1990, Earthquake-induced liquefaction features in the coastal setting of South Carolina and in the fluvial setting of the New Madrid seismic zone: U.S. Geological Survey Professional Paper 1504, 44 p.

Oviatt, C.G., Currey, D.R., and Miller, D.M., 1990, Age and paleoclimatic significance of the Stansbury shoreline of Lake Bonneville, northeastern Great Basin: Quaternary Research, v. 33, p. 291-305.

Plantz, G.G., Appel, C.L., Clark, D.W., Lambert, P.M., and Puryear, R.L., 1986, Selected hydrologic data from wells in the east shore area of the Great Salt Lake, Utah, 1985: U.S. Geological Survey Open-File Report 86-139, 75 p.

Razem, A.C., and Steiger, J.I., 1981, Ground-water conditions in Tooele Valley, Utah, 1976-1978: Utah Department of Natural Resources Technical Publication 69, 95 p.

Rigby, J.K, 1958, Geology of the Stansbury Mountains, eastern Tooele County, Utah, *in* Rigby, J.K., ed., Geology of the Stansbury Mountains, Tooele County, Utah: Utah Geological Society Guidebook to the Geology of Utah No. 13, p. 1-134.

Ryan, K.H., Nance, B.W., and Razem, A.C., 1981, Test drilling for fresh water in Tooele Valley, Utah: Utah Division of Water Rights Information Bulletin 26, 46 p.

Sack, Dorothy, 1990, Quaternary geology of Tule Valley, west-central Utah: Utah Geological and Mineral Survey Map 124, 26 p., scale 1:100,000.

Schwartz, D.P., Hanson, K.L., and Swann, F.H., III, 1983, Paleoseismic investigations along the Wasatch fault zone: an update, *in* Gurgel, K.D., ed., Geologic Excursions in Neotectonics and Engineering Geology in Utah, Geological Society of America Guidebook - Part IV: Utah Geological and Mineral Survey Special Studies 62, p. 45-49.

Scott, W.E., McCoy, W.D.,, Shroba, R.R., and Rubin, Meyer, 1983, Reinterpretation of the exposed record of the last two cycles of Lake Bonneville, western United States: Quaternary Research, v. 20, p. 261-285.

Simms, S.R., 1977, A Mid-Archaic subsistence and settlement shift in the northeastern Great Basin, *in* Fowler, D.D., ed., Models and Great Basin Prehistory - a Symposium: Desert Research Institute Publications in the Social Science, no. 12, p. 195-210.

Simpson, J.H., 1876, Explorations across the Great Basin territory of Utah for a direct wagon-route from Camp Floyd to Genoa, in Carson Valley, in 1859: U.S. Army Engineer Department, 518 p.

Smith, G.R., Stokes, W.L., and Horn, K.F., 1968, Some Late Pleisotocene fishes of Lake Bonneville: Copeia, v. 4, p. 807-816.

Smith, R.B., and Sbar, M.L., 1974, Contemporary tectonics and seismicity of the western United States with emphasis on the Intermountain seismic belt: Geological Society of America Bulletin, v. 85, p. 1205-1218.

Solomon, B.J., editor, in preparation(a), Geologic hazards and land use planning in Tooele Valley and the West Desert Hazardous Industry Area, Tooele County, Utah: Utah Geological Survey Open-File Report.

—-in preparation(b), Quaternary geology of Tooele Valley, northern Rush Valley, and the West Desert Hazardous Industry Area, Tooele County, Utah: Utah Geological Survey Open-File Report, scale 1:24,000.

Spencer, R.J., Baedecker, M.J., Eugster, H.P., Forester, R.M., Goldhaber, M.B., Jones, B.F., Kelts, K., McKenzie, J., Madsen, D.B., Rettig, S.L., Rubin, M., and Bowser, C.J., 1984, Great Salt Lake, and precursors, Utah — The last 30,000 years: Contributions to Mineralogy and Petrology, v. 86, p. 321-334.

Sprinkel, D.A., and Solomon, B.J., 1990, Radon hazards in Utah: Utah Geological and Mineral Survey Circular 81, 24 p.

Tanis, J.T., 1963, Isostasy and crustal thickness in Utah and adjacent areas as revealed by gravity profiles: University of Utah, Salt Lake City, Ph.D. thesis.

Thomas, H.E., 1946, Ground water in Tooele Valley, Tooele County, Utah: Utah State Engineer Technical Publication 4, 238 p.

Tooker, E.W., 1980, Preliminary geologic map of the Tooele quadrangle, Tooele County, Utah: U.S. Geological Survey Open-File Report 80-623, scale 1:24,000.

Tooker, E.W., and Roberts, R.J., 1971a, Geologic map of the Garfield (later renamed Farnsworth Peak) quadrangle, Salt Lake and Tooele Counties, Utah: U.S. Geological Survey Map GQ-922, scale 1:24,000.

—-1971b, Geologic map of the Mills Junction quadrangle, Tooele County, Utah: U.S. Geological Survey Map GQ-924, scale 1:24,000.

—-1988a, Interim geologic maps and explanation pamphlet for parts of the Stockton and Lowe Peak 7.5-minute quadrangles, Utah: U.S. Geological Survey Open-File Report 88-280, scale 1:24,000.

—-1988b, Preliminary geologic map, cross sections, and explanation pamphlet for the Bingham Canyon 7.5-minute quadrangle, Salt Lake and Tooele Counties, Utah: U.S. Geological Survey Open-File Report 88-699, scale 1:24,000.

Travous, K.E., 1980, Recreation on the Great Salt Lake, *in* Gwynn, J.W., ed., Great Salt Lake — a Scientific, Historical and Economic Overview: Utah Geological and Mineral Survey Bulletin 116, p. 33-45.

Tripp, B.T., Shubat, M.A., Bishop, C.E., and Blackett, R.E., 1989, Mineral occurrences of the Tooele 1° x 2° quadrangle, west-central Utah: Utah Geological and Mineral Survey Open-File Report 153.

U.S. Census Bureau, 1990, Census of the United States, 1990: U.S. Department of Commerce, Census Bureau.

Utah State Department of Highways, 1963, Materials inventory, Tooele County: 25 p.

Van Horn, Richard, 1973, Largest known landslide of its type in the United States - a failure by lateral spreading in Davis County, Utah: Utah Geological and Mineral Survey, Utah Geology, v. 2, no. 1, p. 83-88.

Wallace, R.E., 1984, Fault scarps formed during the earthquakes of October 2, 1915, in Pleasant Valley, Nevada, and some tectonic implications: U.S. Geological Survey Professional Paper 1274-A, 33 p.

Wilson, S.R., and Wideman, F.L., 1957, Sodium sulfate deposits along the southeast shore of Great Salt Lake, Salt Lake and Tooele Counties, Utah: U.S. Bureau of Mines Information Circular 7773, 10 p.

Wu, Daning, and Bruhn, R.L., 1990, Geometry and kinematics of normal faults, western flank of Oquirrh Mountains, Utah: American Geophysical Union Fall, 1990 Meeting Program, p. 18.

Zimbeck, D.A., 1965, Gravity survey along northward-trending profiles across the boundary between the Basin and Range province and Colorado Plateau: University of Utah, Salt Lake City, M.S. thesis, 111 p.

HYDROGRAPHIC MODELLING AT THE STOCKTON BAR

by
Ted Burr
Salt Lake City, Utah
and
D.R. Currey
Geography Department
University of Utah
Salt Lake City, Utah

INTRODUCTION

Lake Bonneville was the largest body of water in the Great Basin during late Pleistocene time. At its highest level it inundated a large portion of northwestern Utah, southeastern Idaho, and northeastern Nevada (figure 1). Shorelines in pluvial lake basins generally form under hydrographically closed conditions. However, a special case prevailed during the culminating phase of the last deep-lake cycle in the Bonneville basin when shorelines formed under open-basin, threshold-controlled conditions. Shore features that formed during the last deep-lake cycle are well developed and well preserved at many localities in the Bonneville basin. However, the pass between Rush and Tooele Valleys—formerly a Lake Bonneville strait—near Stockton, Utah, is exceptional, if not world class, in the details of paleolake history that are recorded in its suite of littoral deposits.

G.K. Gilbert first crossed the pass on July 14, 1877, on which occasion he made a preliminary sketch of the "Bonneville Bar" (Hunt, 1982a, p. 38). Gilbert returned to the area three years later, at which time he made a detailed drawing (figure 2) of "The Great Bar at Stockton, Utah" (retouched version in Gilbert, 1890, plate IX; original field version in Hunt, 1982a, p. 170). Gilbert's topographers also prepared a detailed map of the area (figure 3; Gilbert, 1890, plate XX). Gilbert's field notes (Hunt, 1982a, p. 169-174) recorded 252 leveling stations, include several sketches, and clearly indicate that by the end of a week's field work he had a firm understanding of the coastal geomorphology of the Stockton area. Work in recent years has added greatly to the detail, but has invalidated very little of the substance of Gilbert's original interpretations.

HYDROGRAPHIC HISTORY

In order to place the open-basin threshold-controlled shorelines of Lake Bonneville into context, it is helpful to outline briefly the hydrographic history of the last deep-lake cycle in the Bonneville basin, which is called the Bonneville lake cycle. The general history of Lake Bonneville has been known since the work of Gilbert (1890). Currey and Oviatt's (1985) summary of Lake Bonneville fluctuations portrays the most current model of the lake's oscillations. The following summary is based mainly from their work.

The Bonneville lake cycle spanned the interval from about 32,000 to 13,000 years ago, which is approximately coincident with the last global ice age, that is, marine oxygen-isotope stage 2. In general, the cycle comprised three major phases: a protracted phase of closed-basin, predominantly transgressive stages lasting from about 32,000 to 15,500 yr B.P.; a phase of intermittently open-basin, threshold-controlled stages, which occurred between about 15,500 and 14,200 yr. B.P.; and a brief phase of closed-basin, rapidly regressive stages after about 14,200 yr. B.P. (figure 4). The catastrophic Bonneville Flood occurred about 14,500 yr B.P. when alluvial material at the threshold failed (Gilbert, 1890; Malde, 1968; Jarrett and Malde, 1987).

The most prominent shorelines marked on the piedmont of the Bonneville basin are the Stansbury shoreline complex (SSC), the Bonneville shoreline complex (BSC), and the Provo shoreline complex (PSC), which postdates the Bonneville Flood (Gilbert, 1890; Currey and Oviatt, 1985) (figure 4). At its deepest, Lake Bonneville contained about 10,000 km^3 of water. At its highest level, the paleolake was controlled by an external threshold near Zenda, Idaho (fig-

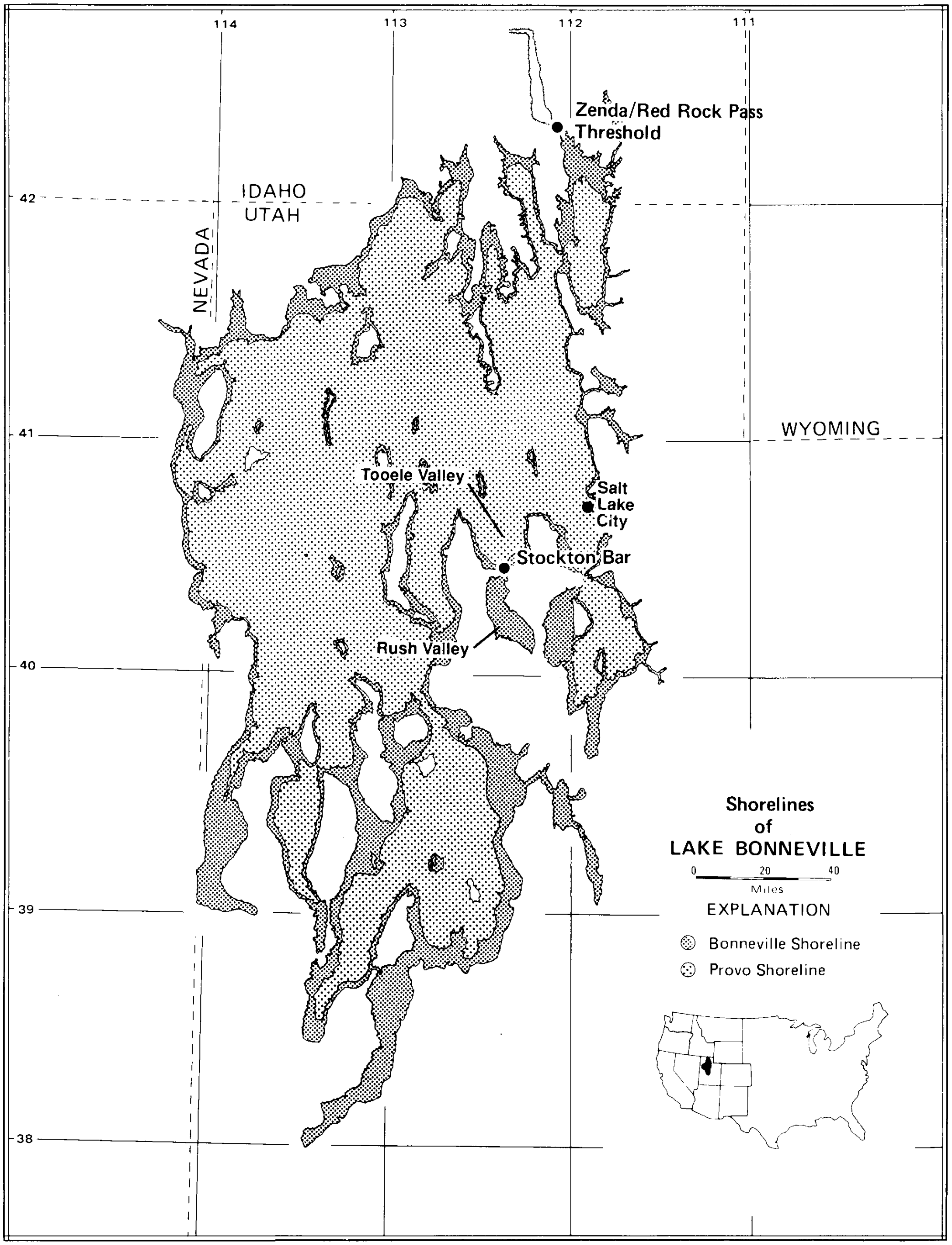

Figure 1. Map showing the Bonneville shoreline and the Provo shoreline (after Burr, 1989).

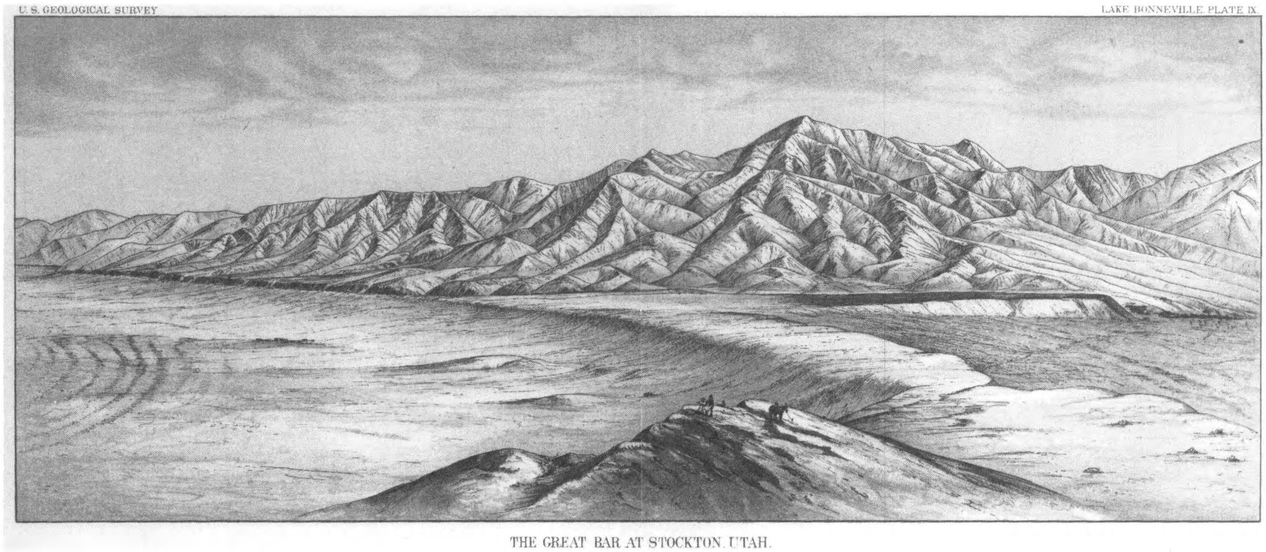

Figure 2. View southeastward from South Mountain, showing The Great Bar at Stockton, Utah (Gilbert, 1890, plate IX).

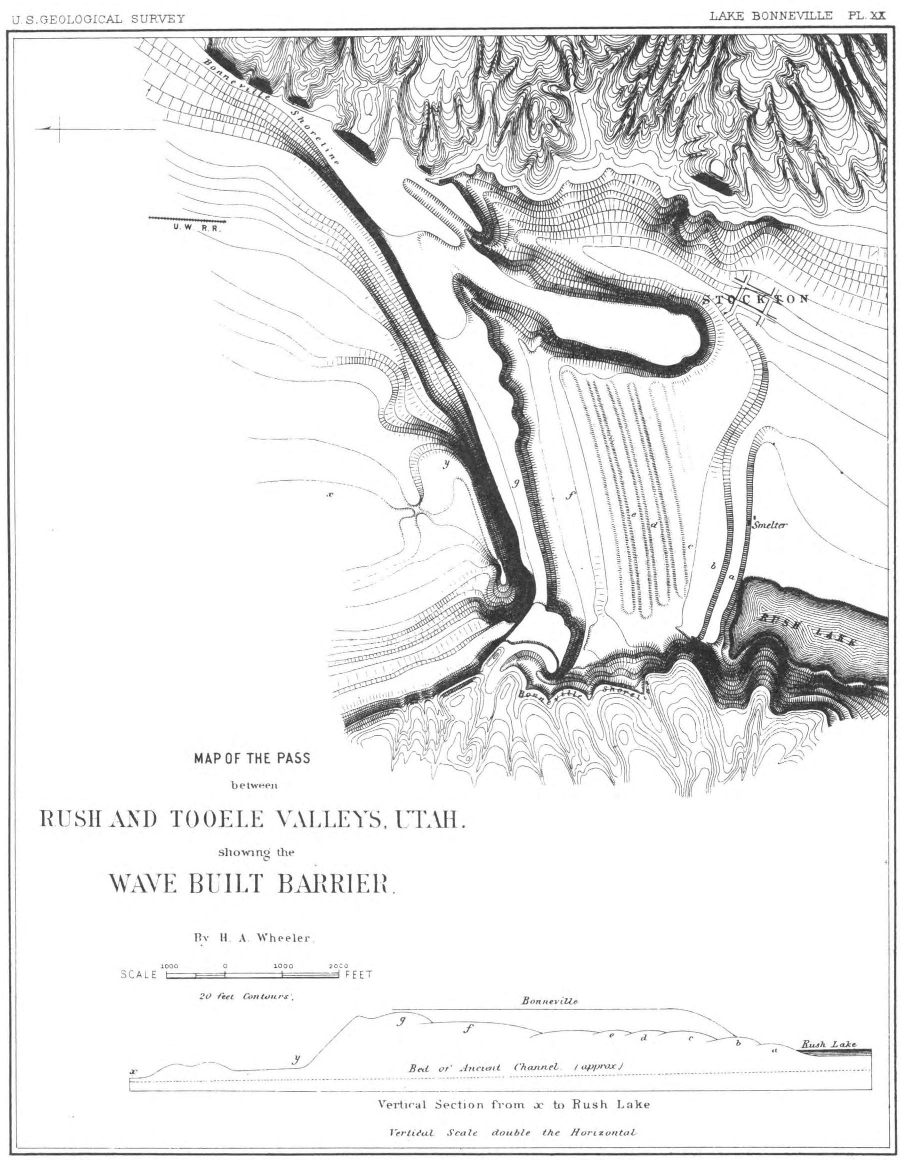

Figure 3. Contour map and vertical section of the Stockton Bar (Gilbert, 1890, plate XX).

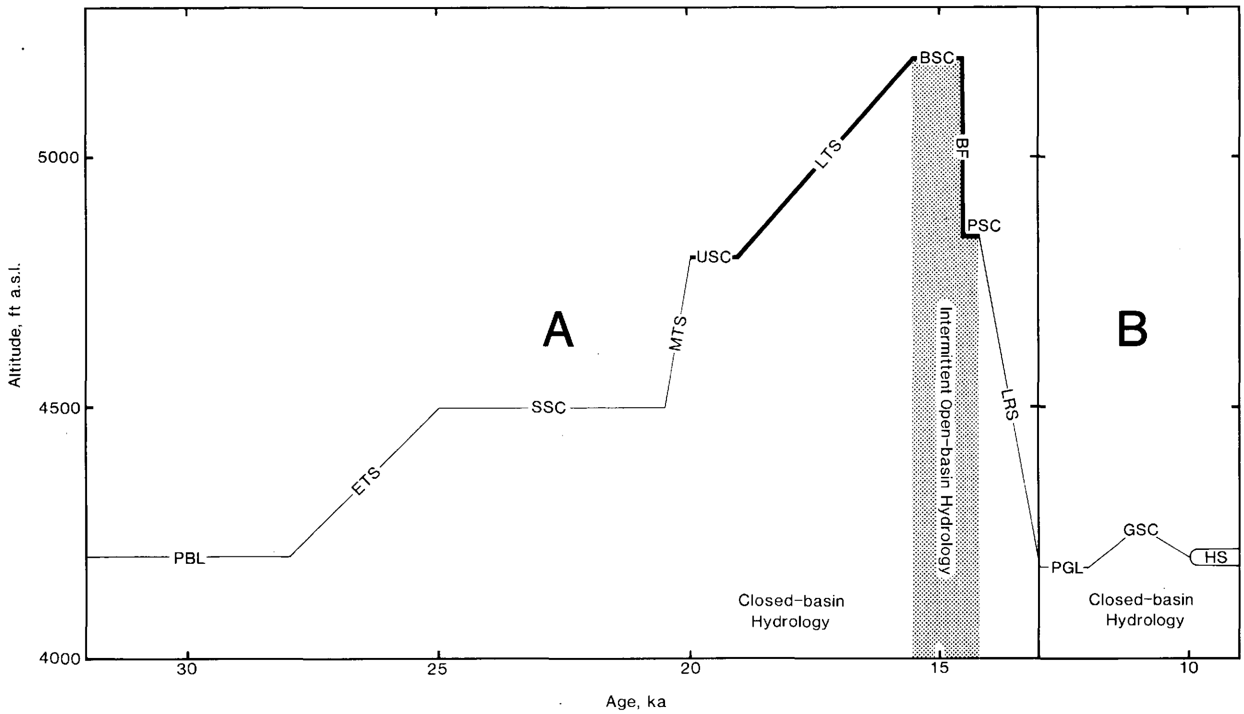

Figure 4. Schematic hydrograph of the Bonneville basin, showing generalized paleolake stages during the Bonneville lake cycle, A, and in early post-Bonneville time, B. Segments of the hydrograph are: PBL, pre-Bonneville low stages; ETS, early transgressive stages; SSC, Stansbury shoreline complex; MTS, middle transgressive stages; USC, unnamed shoreline complex; LTS, late transgressive stages; BSC, Bonneville shoreline complex; BF, Bonneville Flood; PSC, Provo shoreline complex; LRS, late regressive stages; PGS, pre-Gilbert low stages; GSC, Gilbert shoreline complex; and HS, Holocene stages. Stages USC through PSC (heavy line) are exceptionally well represented by littoral morphostratigraphic units at or near the Stockton Bar (after Burr and Currey, 1983).

ure 1), at an elevation of about 5090 feet (1551 m) (Currey, 1980). Lake Bonneville discharged intermittently over the Zenda threshold for about 1000 yr (Currey and Burr, 1988), during which time the Bonneville shoreline complex was formed. The shorelines that formed during this stage were complicated by isostatic subsidence of the basin interior due to the hydro-isostatic load of Lake Bonneville. Formation of the Bonneville shoreline complex ceased when catastrophic failure of the Zenda threshold released the Bonneville Flood and caused the water level to fall to a new threshold at Red Rock Pass, Idaho (Currey, 1980). Besides the vertical lowering of the threshold, the floodwaters headwardly eroded the Snake River-Bonneville basin drainage divide southeastward about 2 miles (3.2 km) (Gilbert, 1890; Currey, 1982). Post-Flood threshold discharge at Red Rock Pass continued for about 300 yr (Currey and Burr, 1988), during which time the Provo shoreline complex was formed.

MORPHOSTRATIGRAPHY

Morphostratigraphic complexes at the Stockton locality are defined as assemblages of relict littoral landforms whose external form and internal deposits accumulated over space and time (figure 5). They are the spatiotemporal assemblages that collectively comprise the topography. A morphostratigraphic unit in a coastal depositional environment is a spatiotemporal assemblage of littoral sediments, and several morphostratigraphic units can constitute a morphostratigraphic complex. At the Stockton Bar depocenter morphostratigraphic units are barriers, spits and beach ridges. Coastal morphostratigraphic subunits are the bottomsets, topsets, backsets, and foresets that comprise morphostratigraphic units.

CHRONOSTRATIGRAPHY

The chronology of late Quaternary events in the Bonneville basin is constrained to varying degrees by radiocarbon age determinations on more than two hundred samples of lacustrine and related materials from dozens of localities in Utah, Nevada, and Idaho (e.g., Currey and Oviatt, 1985). Five ^{14}C age determinations have been obtained on lacustrine carbonate materials from selected morphostratigraphic subunits at the Stockton Bar (Table 1). The age of the B_0 shoreline, which was the lake level at the start of the Bonneville Flood, is constrained by SI-4227C and Beta-10244 thusly: the $\delta^{13}C$ value of Beta-10244 suggests that the unadjusted ^{14}C age of SI-4227C is probably a few hundred years too young, i.e., 14,260 ^{14}C yr B.P. is a minimum limiting age. The age of the L_5 shoreline subunit that is designated $L_{5.1}$ (Table 1), which formed midway through the late transgressive stages of Lake Bonneville, is constrained by Beta-10245 thusly: since about 7% of the original aragonite in the gastropod shells has weathered into calcite, probably by exposure to isotopically younger carbonic acid, 16,450 ^{14}C yr B.P. is a minimum limiting age.

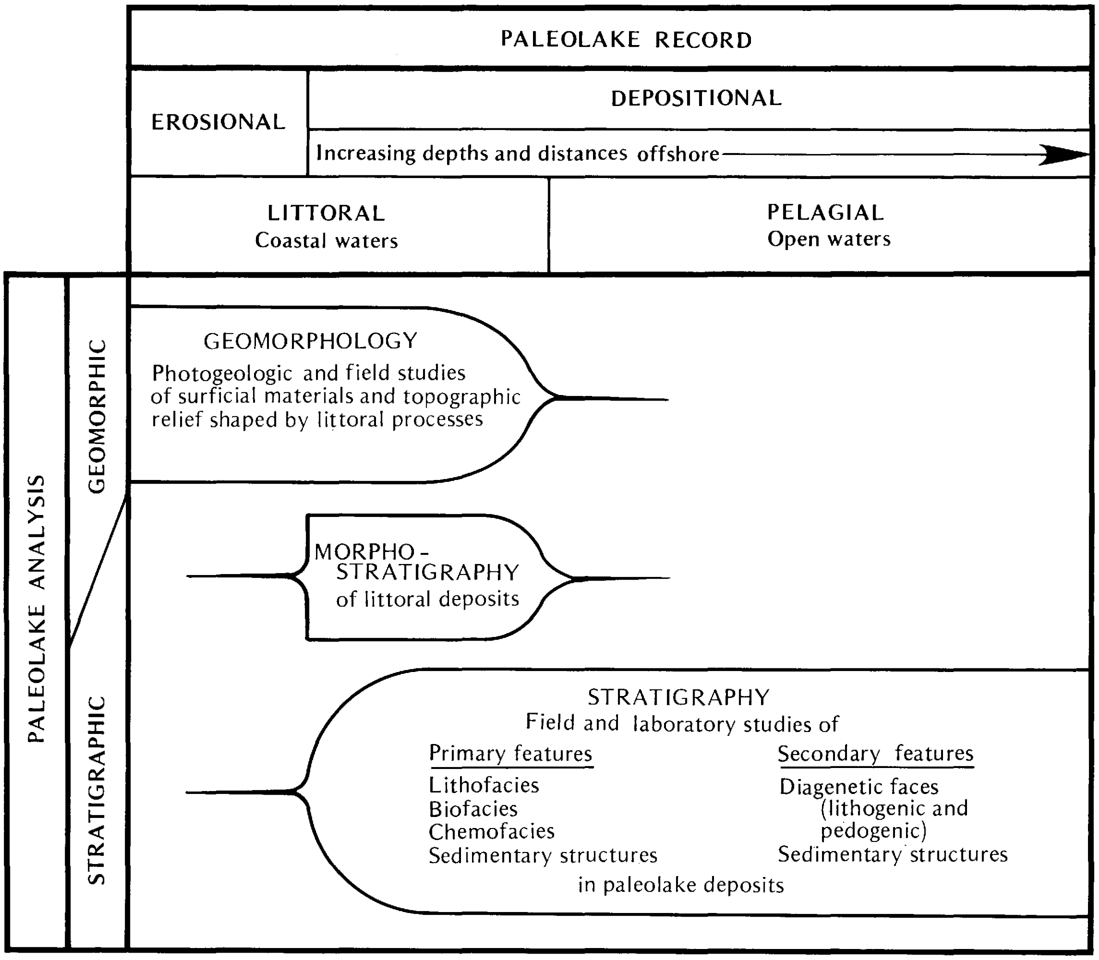

Figure 5. The morphostratigraphy of littoral deposits, which combines the methods of geomorphology and stratigraphy, is a powerful tool in the analysis of paleolake records (after Currey and Burr, 1988).

TABLE 1.
RADIOCARBON AGES OF LACUSTRINE CARBONATE MATERIALS FROM SELECTED MORPHOSTRATIGRAPHIC SUBUNITS AT THE STOCKTON BAR, UTAH.

Lab No.	Material	Elev.(m)	Subunit	^{14}C Years B.P.	δ ^{13}C	Adj. ^{14}C Age	Notes
SI-4227A	tufa polyp	1573	B_8	13,480 $\pm$ 90			1, 2
SI-4227B	same	same	same	13,970 $\pm$ 95			1, 3
SI-4227C	same	same	same	14,260 $\pm$ 100			1, 4
Beta-10244	tufa polyp	1573	B_8	12,540 $\pm$ 150	+3.36	13,010 $\pm$ 150	1, 5
Beta-10245	gastropods	1521	$L_{5.1}$	16,050 $\pm$ 160	-0.66	16,450 $\pm$ 160	1, 6

1. morphostratigraphic subunit designations as in figure 6;
2. 16.3-40.7% in from surface of polyp (outermost 16.3% removed before evolving sample CO_2);
3. 40.7-81.7% in from surface of polyp;
4. innermost 18.3% of polyp;
5. 95 +/- 3% calcite, remainder aragonite;
6. 7 +/- 1% calcite, remainder aragonite. See figure 6 for locaiton of lacustrine carbonate samples.

INTERPRETATION

The portion of the Bonneville Lake cycle that is represented by the littoral deposits at and near the Stockton Bar is indicated by the heavy line in figure 4. The purpose of the Stockton Bar segment of this trip is to examine and discuss morphostratigraphic evidence pertaining to the unnamed shoreline complex (USC), late transgressive stages (LTS), Bonneville shoreline complex (BSC), Bonneville Flood (BF), and Provo shoreline complex (PSC), as well as post-flood shorelines that are unique to Rush Valley. The physical nature and significance of this evidence is summarized below.

UNNAMED SHORELINE COMPLEX (USC)

Approximately 20,000 yr B.P. the transgressing body of water began to attack pre-Lake Bonneville alluvial fans at 4800 feet (1463 m) a.s.l. Longshore currents primarily from the northeast started to build a series of retrograding coastal landforms at the southern end of Tooele Valley. The USC is a large cross-valley barrier (figure 6,[U]) and, as at many other localities in the Bonneville basin, is partly concealed by overlying PSC deposits (Sack, 1988). Sack (1988) applied the term subProvo to transgressive Lake Bonneville shoreline deposits that lie just below the elevation of the regressive Provo shoreline complex. SubProvo deposits probably constitute at least a portion of the unnamed shoreline complex as employed in this paper. The unnamed shoreline complex/ subProvo morphostratigraphic evidence marks what seems to be an important stillstand or oscillation during the transgressive phase of the Bonneville lake cycle (Sack, 1988).

LATE TRANSGRESSIVE STAGES (LTS)

The transgressing lake continued to develop spits and barriers in Tooele Valley, including a bayhead barrier, constructed at an altitude about 4900 feet (1493 m) (figure 6, [L_2]). Chemical and mine tailings reclamation activities at Bauer have used the lagoon behind the barrier at this altitude as a settling pond.

As Lake Bonneville transgressed into Rush Valley (figure 6,[L_5]) the retrograding and aggrading pattern of spit-barrier development shifted to a prograding and aggrading pattern. This may have been due to an increasing rate of local hydro-isostatic subsidence. Surface drainage from Rush Valley was blocked as the spit-barrier development continued to prograde and aggrade (Gilbert, 1890, Plate XX; Gilluly, 1929). The spit-barrier construction continued to about 5160 feet (1572 m) (figure 7, B_0), at which altitude in the Stockton Bar area the lake became a threshold-controlled water body, under the influence of the Zenda threshold far to the north; this marks the beginning of the BSC, the first threshold controlled morphostratigraphic unit.

BONNEVILLE SHORELINE COMPLEX (BSC)

At many localities morphostratigraphic evidence of the culminating, open-basin phase of the Bonneville lake cycle suggests that four stages of non-catastrophic discharge at the Zenda threshold 5090 feet (1552 m) were interrupted by three sub-threshold lake stages, all of which were complicated by an isostatically subsiding basin (Currey and Burr, 1988). In the Stockton Bar area, as well, morphostratigraphic features B_1, B_3, B_5, and B_8 show evidence of four periods of threshold-controlled deposition that occurred during non-catastrophic discharge at Zenda. [B_1] in figure 6 and B_1 in figure 7, a cross-valley baymouth barrier at about 5180 feet (1579 m), was built approximately 15,350 yr. B.P. by vertical accretion that occurred at essentially the same rate that local hydro-isostatic subsidence was occurring relative to the threshold-controlled water plane. A long, lakeward-dipping abrasion platform extends from Tooele southwestward to the proximal end of BSC depositional features near Stockton (figure 8). It marks the avenue along which material travelled during longshore transport. As in the late transgressive phase, unconsolidated material from pre-Lake Bonneville alluvial fans, mainly readily rounded clasts of Pennsylvanian quartzite, provided the sediments that comprise the BSC barrier and spits. Baymouth barrier B_1 formed by prolongation and aggradation of a spit that eventually extended across the Tooele-Rush strait to South Mountain.

The area continued to subside during a sub-threshold interval. After threshold control resumed, a massive spit ([B_3] in figure 6 and B_3 in figure 7) aggraded and extended southward into Rush Valley about 1.5 miles (2.4 km), attaining a maximum altitude of 5212 feet (1588 m) approximately 15,150 yr B.P. After a second sub-threshold interval, the massive B_3 spit was followed by the construction of a smaller spit [B_5] in figure 6 and B_5 in figure 7) that aggraded at the rate of local subsidence and attained an altitude of 5231 feet (1594 m) approximately 15,000 yr B.P. The B_5 spit marks the maximum elevation of the BSC near the Stockton Bar, and correlative features mark the Bonneville maximum elsewhere throughout the basin. Direct evidence of the two sub-threshold lake stages that occurred between B_1, B_3, and B_5 has not yet been found in the Stockton Bar area, although those stages can be identified elsewhere in the Bonneville basin (e.g., lower beach ridges of Gilbert, 1890, plate XI).

After the development of the highest, B_5 component of the BSC, the Zenda threshold underwent about 40 feet (12 m) of non-catastrophic incision approximately 15,000 yr B.P. (Currey and Burr, 1988). The conclusion of this early Zenda incision is marked by the Stockton Bar area by a boulder beach ([B_6] in figure 6, and B_6 in figures 7 and 9) at an elevation of about 5191 feet (1582 m), where the regressing water plane lingered only long enough to winnow the pebbly sand matrix from between cobbles and boulders that had been deposited approximately 200 years earlier in the construction of the massive B_3 spit.

The short-lived development of the B_6 shoreline was fol-

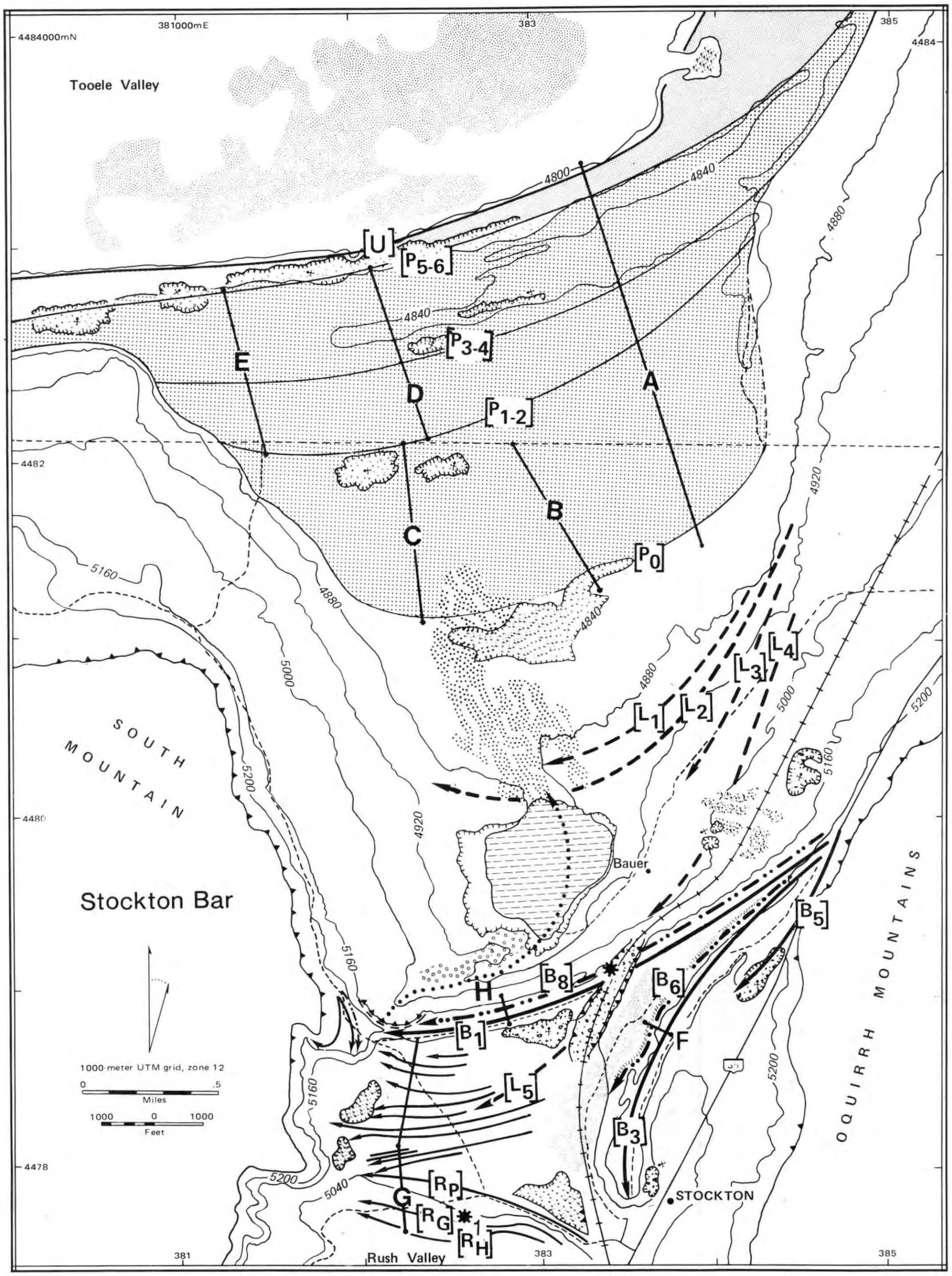

Figure 6. Map of the Stockton Bar area, showing the morphostratigraphic units of the unnamed shoreline complex [U], late transgressive stages [L_1-L_5], Bonneville shoreline complex [B_0-B_8], and Provo shoreline complex [P_0-P_6], and Rush Valley post-flood shorelines (R_P, R_G, R_H] (after Burr and Currey, 1988).

* = Radiocarbon sample location for subunit B_8 listed in table 1.

* = Radiocarbon sample location for subunit $L_{5.1}$ listed in table 1.

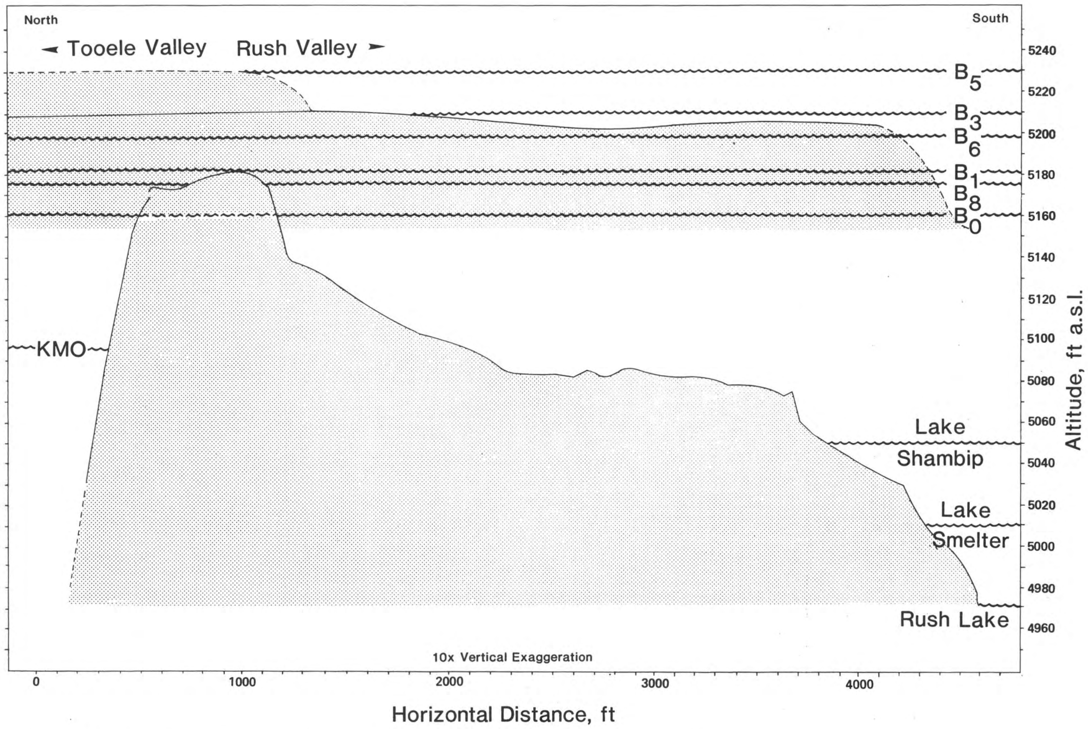

Figure 7. North-south composite profile of the Stockton Bar, showing hypsometric relations among several of the morphostratigraphic units that are mapped in figure 6 (after Burr and Currey, 1988). See figure 6 for location of profiles.

Figure 8. View southwestward from the south edge of Tooele, showing the Stockton Bar in middle distance and the B_5 shoreline angle and shore platform at the toe of the Oquirrh Mountains (to the left of what is now Utah Highway 36). The Stockton Bar was the sediment sink for longshore transport from sediment sources that included the now scree-mantled quartzite cliffs in the left foreground and the arcuate bluff in highly erodible pre-Bonneville fan gravels in the left middle ground. Photo by Barnum Brown, 1934.

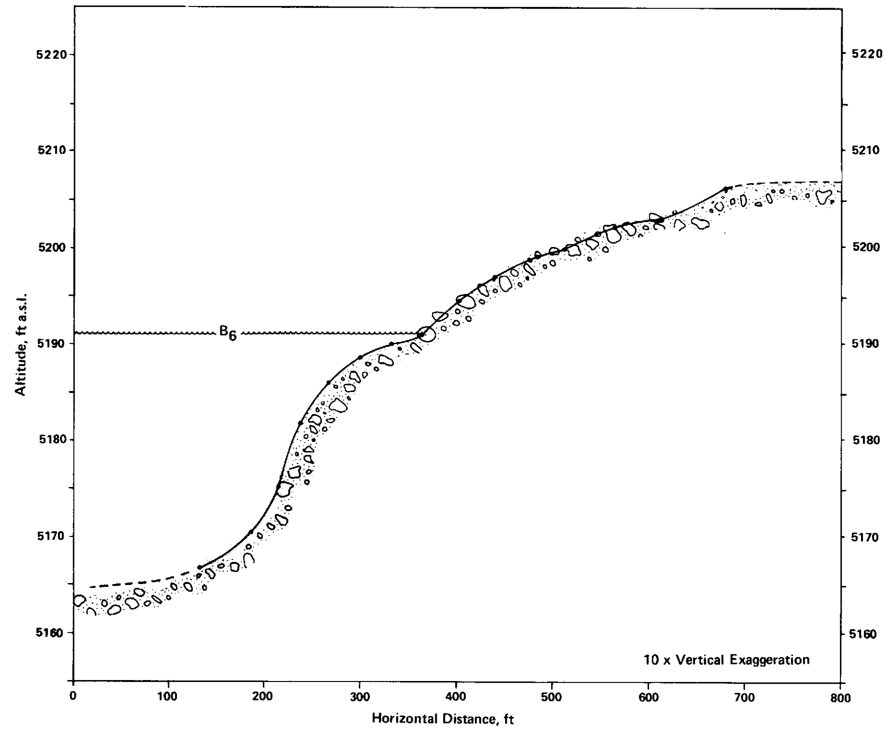

Figure 9. Profile of the B_6 boulder beach, which formed after the Zenda threshold was lowered 40 feet during the non-catastrophic early Zenda incision. The water plane lingered only long enough to winnow the pebbly sand matrix from between cobbles and boulders that had been deposited approximately 200 years earlier in the construction of the massive B_3 spit (after Burr and Currey, 1988).

lowed by a major sub-threshold cycle between approximately 15,000 and 14,550 yr B.P. This Keg Mountain oscillation (KMO) of Currey and others (1983; Currey and Burr, 1988; clearly reflects significant hydroclimatic forcing. During the regressive phase of the KMO, the lake receded about 100 feet (30 m)(figure 7, KMO) below the previous B_6 stage. The basin underwent partial hydro-isostatic unloading and reloading during the KMO with the net result bing measurable isostatic rebound. At the conclusion of the KMO, after having deposited a tufa drapery on the north-facing slope of the Stockton Bar, the lake returned to threshold control at an elevation of about 5170 feet (1575 m). Between approximately 14,550 and 14,500 yr B.P. the lake transgressed at the local rate of hydro-isostatic subsidence to an elevation of 5177 feet (1578 m), where the final tufa-encrusted BSC beach ridge ([B_8 figure 6; B_8 in table 1 and figure 7) was deposited.

Further development of the Bonneville shoreline complex was prevented by catastrophic incision of the Zenda threshold and the rapid drawdown of the lake that occurred as a consequence. The early Zenda incision and the short duration of Zenda threshold control after the KMO prevented the basin from subsiding to its previous maximum, and thereby reduced somewhat the volume of water that otherwise would have been released.

BONNEVILLE FLOOD (BF)

The Bonneville Flood (Malde, 1968), which occurred about 14,500 ^{14}C yr B.P., rapidly released the upper 340 feet (104 m) of Lake Bonneville into the Snake River system. The floodwaters headwardly eroded the Snake River-Bonneville basin (Pacific Ocean-Great Basin) drainage divide southeastward about 2 miles (3.2 km)(Currey and others 1983, Smith and others, 1989); and lowered it 340 feet (104 m). The current consensus is that the duration of the flood exceeded 8 weeks (e.g., Jarrett and Malde, 1987), but probably did not exceed one year. As measured at and near the Stockton Bar, the stage change that occurred during the flood is the vertical difference between the B_8 shoreline, which was the highest that formed during post-KMO time, and the base of the small bluff ([P_0] in figure 6 and P_0 in figure 10) that began to form on day one of control by the newly excavated threshold at Red Rock Pass. Total threshold lowering, including the early Zenda incision, was about 380 feet (116 m).

PROVO SHORELINE COMPLEX (PSC)

The Provo shoreline north of the Stockton Bar is, in essence, an enormous ramp of prograding and aggrading

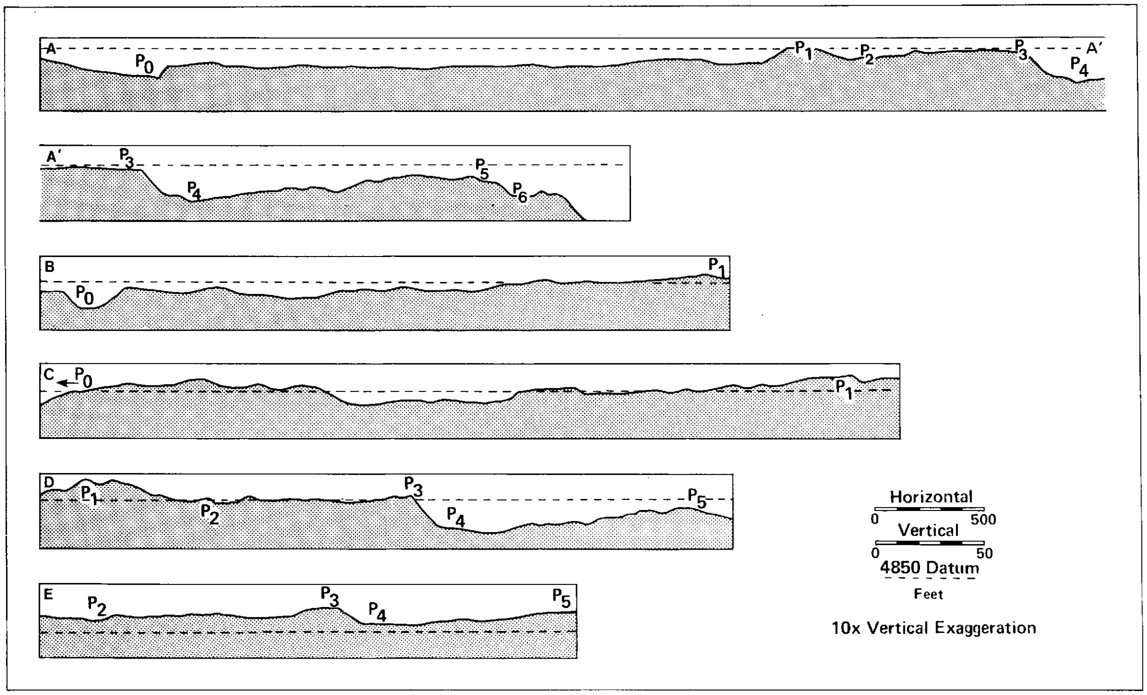

Figure 10. Profiles of the Provo shoreline complex north of the Stockton Bar, depicting the shore-face accretion that prograded and aggraded ramp-like to the north (right), and which was interrupted a few times by small downward steps in the locus of littoral deposition. See figure 4 for locations of profiles (after Burr and Currey, 1988).

beach ridges; continuity of the ramp is interrupted by small downward steps (P_2, P_4, and P_6 in figure 10). This morphostratigraphic signature, which is seen basin wide, resulted from persistent landsliding in the flood-scoured threshold area, and from intermittent incision of the post-flood outlet channel across the 5-mile-long (8 km) toe of the landslide (Currey and Burr, 1980; Smith and others, 1989). After the Provo water plane stabilized initially at P_0, landsliding gradually raised the Red Rock Pass threshold and caused the first beach ramp to prograde and aggrade from P_0 to P_1. A threshold incision of about 5 feet (1.5 m) shows up in the figure 10 profiles at P_2. Subsequent landsliding resulted in continuing beach ramp construction to P_3, after which 15 feet (4.5 m) of threshold downcutting is indicated in the figure 10 profiles at P_4. Threshold incision was again followed by landsliding and beach ramping to P_5. A final threshold incision of 10 feet (3m) appears in the figure 10 profiles at P_6. Threshold-controlled littoral deposition continued briefly, until approximately 14,200 yr B.P., when the lake finally regressed below Red Rock Pass. Shore-face accretion on the well-developed beaches of the PSC was then replaced by incipient development of littoral features during the transient regressive stages that characterized LRS time.

RUSH VALLEY SHORELINES

The post-flood shorelines on the Rush Valley side of the Stockton Bar (figures 6 and 7) comprise the Provo shoreline equivalent, R_P, at about 5050 feet (1539 m), and what is likely the Gilbert Shoreline equivalent, R_G, at about 5010 feet (1527 m). The 4970-foot (1515-m) level of Rush Lake during the highstoric high of the 1980s. R_H, seems to have been approximately coincident with the level of the Holocene high in Rush Valley. The independent lake that existed within Rush Valley during Provo shoreline time is called Lake Shambip (Currey and others, 1983); in this paper the independent lake that existed in Rush Valley during Gilbert shoreline time is named Lake Smelter.

Shorelines that formed on the Rush Valley side of the Stockton Bar during and subsequent to Provo shoreline complex time were not addressed in detail by Gilbert (1890), but he did note historic fluctuations of Rush Lake (Gilbert, 1890, p. 228-229). He also recognized that Rush Valley retained a separate body of water when Lake Bonneville receded below the Stockton Bar barrier between Rush and Tooele Valleys (Gilbert, 1890, p. 149). The morphostratigraphic record in Rush Valley at the elevations mentioned above clearly indicates that post-flood coastal processes did rework littoral sediments that earlier had been deposited as Lake Bonneville transgressed into Rush Valley.

HYDROGRAPHIC MODEL

From empirical constraints and modelling constraints, a probable scenario of hydrographic, isostatic, and geomorphic events at the Zenda threshold can be postulated for the open-basin phase of Lake Bonneville (Currey and Burr, 1988). As modelled in Figure 11, Lake Bonneville first became a threshold-controlled water body at B_0 and trans-

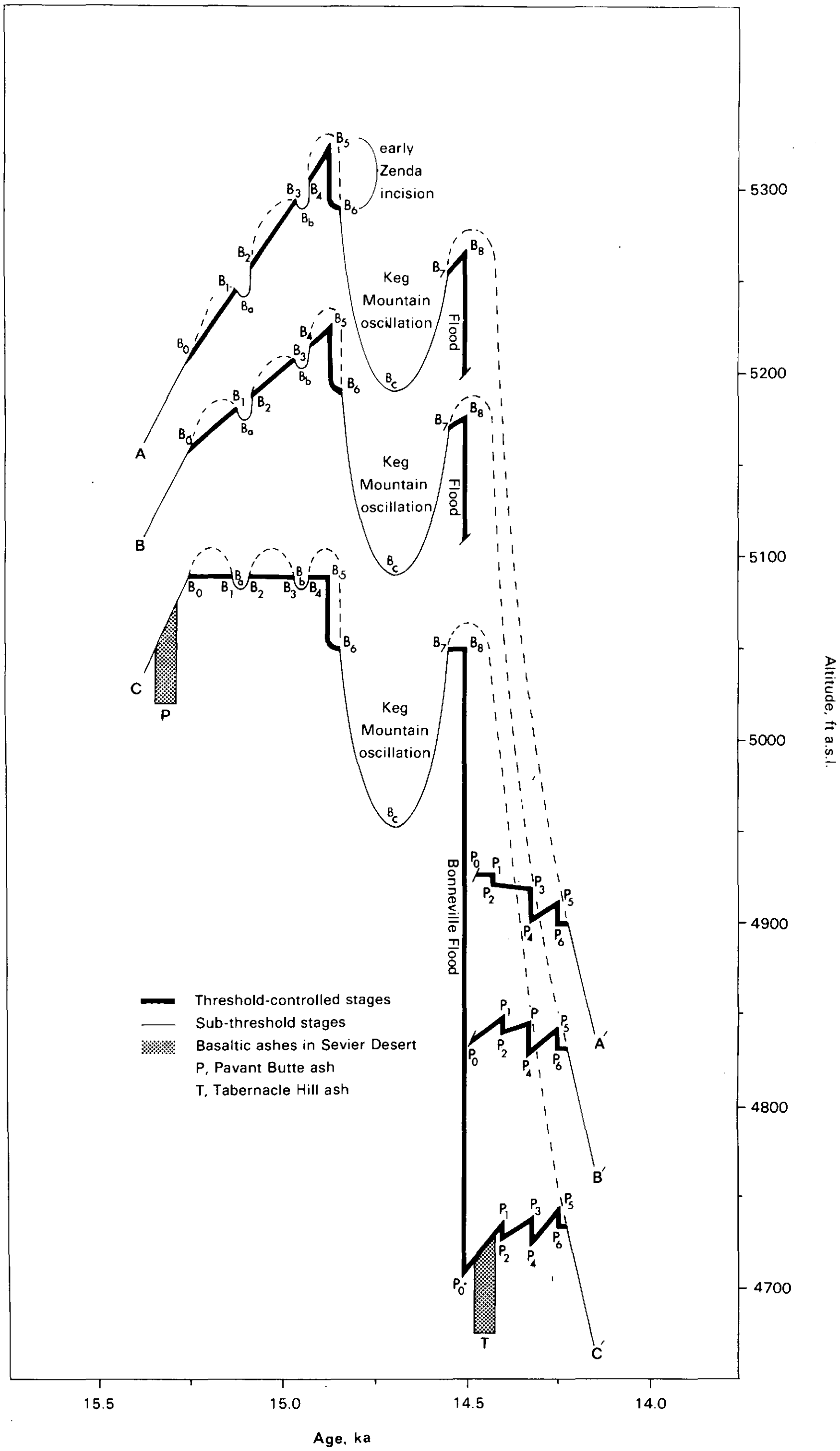

Figure 11. Threshold-controlled stages of Lake Bonneville in the region of maximum hydro-isostatic deflection, A-A'; at a typical basin-interior locality (Stockton Bar), B-B', and in the threshold region and other basin perimeter regions of minimum deflection, C-C'. Stages B_0-B_8 comprise the Bonneville shoreline complex (BSC) and stages P_0-P_6 comprise the Provo shoreline complex (PSC) (after Currey and Burr, 1989).

gressed to B_1 at the local rate of hydro-isostatic subsidence. The Zenda threshold apparently remained basically undissected during that transgression. Hydroclimatic factors probably caused the lake to fall slightly below threshold control between B_1 and B_2, while rates of isostatic subsidence remained relatively constant. According to this hypothesis, threshold control resumed at B_2, and the lake transgressed to B_3, keeping pace with the local rate of isostatic subsidence and remaining under the control of the undissected threshold. Hydroclimatic factors seem to have caused the lake to fall slightly below the minimum divide elevation between B_3 and B_4, while isostatic subsidence continued. Threshold control resumed at B_4 and the lake transgressed to B_5, again approximately at the local rate of isostatic subsidence and under the control of a basically undissected threshold. Evidence suggests that incision of the Zenda threshold then became significant, initially causing the lake to regress about 40 feet (12 m) to B_6 from its all-time high at B_5. The B_6 shoreline was abandoned when hydroclimatic factors caused the lake to fall many tens of feet below threshold control between B_6 and B_7; this subthreshold cycle is what Currey and others (1983) termed the Keg Mountain oscillation. The field evidence at Stockton supports the contention of Currey and others (1983) that during the oscillation, hydro-isostatic deflection in the basin interior changed from subsidence to rebound and back to subsidence, with net deflection in the basin being rebound during KMO.

According to the present model, threshold control resumed at B_7 and the lake briefly transgressed to B_8 at the local rate of isostatic subsidence and with negligible threshold incision. Because no post-B_8 Bonneville shoreline evidence has been found anywhere in the Bonneville basin and because the B_8 component is a small feature in the Bonneville shoreline complex, B_8 is interpreted as marking a brief period of post-Keg Mountain oscillation threshold control. Subsequent failure of the alluvial threshold at Zenda resulted in the Bonneville Flood and rapid additional lowering of the lacustrine base level by about 340 feet (104 m), to the Red Rock Pass threshold. As measured at Stockton, total threshold lowering between B_5 and the end of the Bonneville Flood was about 380 feet (116 m); net isostatic rebound during that interval locally ranged from negligible near the perimeter of the basin to about 24 feet (7 m) in the region of greatest water depth (between 1200 and 1300 feet; 365-400 m) (Currey and Burr, 1988).

Not only did the Bonneville Flood cause deep incision of the Zenda threshold, it also over-steepened the east flank of the adjacent Malad Range, and thereby probably triggered recurrent major landsliding (Currey and Oviatt, 1985). The earliest landslide occurred during the Bonneville Flood (Currey and Oviatt, 1985), and briefly deflected the axis of incision to the east. In the Red Rock Pass-Zenda threshold area, landslide activity probably continued along a 5-mile (8 km) segment of the range front long after the earliest post-Flood level of the lake stabilized at P_0 (D.R. Currey, 1988). Landsliding steadily elevated the Red Rock Pass threshold about 25 feet (7.6 m), but the observed net difference in elevation between P_0 and P_1 is less than that over most of the basin. This may have resulted if local isostatic rebound partly counteracted the threshold rise. The regression from P_1 to P_2 could have been caused by a 5-foot (1.5 m) incision of the landslide at the Red Rock Pass threshold. Continued landsliding steadily elevated the Red Rock Pass threshold about 8 feet (2.4 m), however, the net transgression from P_2 to P_3 in the basin interior was slight because local isostatic rebound could have largely counteracted the threshold rise. The regression of the lake from P_3 to P_4 was probably caused by a 15-foot (4.5 m) incision of the landslide at Red Rock Pass. Landsliding continued and steadily elevated the Red Rock Pass threshold about 18 feet (5.5 m). The net transgression from P_4 to P_5, however, was less than 18 feet (5.5 m) over most of the basin. Local isostatic rebound may have partly counteracted the threshold rise. It appears that a final 10 feet (3 m) of incision of the landslide at Red Rock Pass may have caused the lake to regress from P_5 to P_6, shortly before it reverted to closed-basin conditions by finally regressing below its threshold elevation.

CONCLUSIONS

The hypsometric constraints of the linear model presented here have important hydro-isostatic and geomorphic implications.

1. Approximately half of the lake load that was depressing crust at any basin-interior locality occurred during threshold-controlled stages B_0 to B_5.

2. About 10 percent of the net isostatic rebound at any basin-interior locality occurred during the Keg Mountain oscillation, before the Bonneville Flood; about 90 percent occurred after the Flood.

3. The Zenda threshold was incised twice with approximately 10 percent of the total downcutting occurring non-catastrophically during a pre-Keg Mountain oscillation event; about 90 percent of the downcutting occurred catastrophically during the Bonneville Flood.

The hypsometric constraints of the linear model together with the chronometric constraints provided by other workers (e.g., Currey and Oviatt, 1985) imply several interesting kinematic relations.

1. The average rate of change of lake stage during the Keg Mountain oscillation, from the beginning of the regression to the end of the transgression, was about 0.4 feet/yr (.12 m/yr).

2. The rate of isostatic subsidence during the stage from B_0 to B_5 varied basinwide, from a negligible minimum at the perimeter to a basin-interior maximum of about 0.24 feet/yr (.07 m/yr).

3. The rate of isostatic rebound during stages P_0 to P_5 varied basinwide, from an approximately negligible minimum at the basin perimeter to a basin-interior maximum of about 0.17 feet/yr (.05 m/yr).

REFERENCES

Burr, T.N., 1989, Hydrographic isostatic modelling of threshold-controlled shorelines of Lake Bonneville: University of Utah, Salt Lake City, M.S. thesis.

Burr, T.N., and Currey, D.R., 1988, The Stockton Bar: Utah Geological and Mineral Survey Miscellaneous Publication 88-1, p. 66-73.

Currey, D.R., 1980, Threshold-controlled shorelines of Lake Bonneville: Great Plains-Rocky Mountain Geographical Journal, v. 9, p. 103-104.

Currey, D.R., 1982, Lake Bonneville: selected features of relevance to neotectonic analysis: U.S. Geological Survey Open-File Report 82-1070, 31 p.

Currey, D.R., and Burr, T.N., 1988, Linear model of threshold-controlled shorelines of Lake Bonneville: Utah Geological and Mineral Survey Miscellaneous Publication 88-1, p. 104-110.

Currey, D.R., and Oviatt, C.G., 1985, Durations, average rates, and probable causes of Lake Bonneville expansions, stillstands, and contractions during the last deep-lake cycle, 32,000 to 10,000 years ago, *in* Kay, P.A., and Diaz, H.F., eds., Problems of and prospects for predicting Great Salt Lake levels: Salt Lake City, University of Utah Center for Public Affairs and Administration, p. 9-24.

Currey, D.R., Oviatt, C.G., and Plyler, G.B., 1983, Lake Bonneville stratigraphy, geomorphology, and isostatic deformation in west-central Utah: Utah Geological and Mineral Survey Special Studies 62, p. 63-82.

Gilbert, G.K., 1890, Lake Bonneville: U.S. Geological Survey Monograph 1, 438 p.

Gilluly, J., 1929, Possible desert-basin integration in Utah: Journal of Geology, v. 36, p. 672-682.

Hunt, C.B., ed., 1982, Pleistocene Lake Bonneville, ancestral Great Salt Lake, as described in the notebooks of G.K. Gilbert, 1875-1880: Brigham Young University Geology Studies, v. 29, Pt 1, 225 p.

Jarrett, R.D., and Malde, H.E., 1987, Paleodischarge of the late Pleistocene Bonneville Flood, Snake River, Idaho, computed from new evidence: Geological Society of America Bulletin, v. 99, p. 127-134.

Malde, H.E., 1968, The catastrophic late Pleistocene Bonneville Flood in the Snake River Plain, Idaho: U.S. Geological Survey Professional Paper 596, 52 p.

Sack, D., 1988, Studies of G.K. Gilbert, Lake Bonneville chronology reconstructions, and the Quaternary geology of Tule Valley, west-central Utah: University of Utah, Salt Lake City, Ph.D. thesis, 138 p.

Smith, G.I., L.B., Benson, and Currey, D.R., 1989, Quaternary Geology of the Great Basin: IGC Field Trip Guide Book T117.

GEOLOGIC EVOLUTION OF ANTELOPE ISLAND: MULTIPLE EPISODES OF DEFORMATION AND METAMORPHISM

by
Grant C. Willis, Hellmut H. Doelling
Utah Geological Survey
2363 S. Foothill Drive, Salt Lake City, UT 84109
W. Adolph Yonkee
Department of Geology, Weber State University, Ogden, UT 84408
Mark E. Jensen
Utah Department of Health and Environmental Quality
Salt Lake City, UT 84114

INTRODUCTION

Antelope Island, the largest island in the Great Salt Lake, is a showcase for geologic features including Archean to Early Proterozoic igneous and high-grade metamorphic rocks, Late Proterozoic low-grade metasedimentary rocks, thrust faults and folds produced during the Cretaceous to early Tertiary Sevier orogeny, normal faults and Tertiary sedimentary rocks that formed during basin-and-range extension, and shorelines of Pleistocene Lake Bonneville. In addition to its geologic features, Antelope Island is a haven for wildlife and a place of unique and pristine scenic beauty. The island is currently owned by the State of Utah and is administered as a state park by the Department of Natural Resources through the Division of Parks and Recreation. Access to the island was by a northern causeway until the causeway was flooded during a high stand of the Great Salt Lake in the early 1980s. The Division of Parks and Recreation plans to reopen the north causeway to the public in 1992. The route for this field trip enters the island from a southern causeway, but part of this route crosses private property and is not open to the public. Future users of this guide should check with the Division of Parks and Recreation for any restrictions on access to and across the island.

Field trip participants will examine the long and complex geologic history of Antelope Island. Specific topics will include: (1) the Archean(?) to early Proterozoic metamorphic and igneous history of basement rocks in the Farmington Canyon Complex, (2) the stratigraphy and tectonic significance of Late Proterozoic to Cambrian low-grade metasedimentary rocks, (3) features produced by internal shortening and their relation to regional thrusting during the Sevier orogeny, and (4) the stratigraphy and tectonic setting of late Tertiary strata. Much of the information presented on this field trip was gathered by workers of the Utah Geological Survey who mapped the island in the late 1980s (Doelling and others, 1990; and other publications by the Utah Geological Survey), and by Yonkee (1990). Previous work on the island was done by King (1878), Larsen (1957), Bryant and Graff (1980), and Bryant (1988).

ROAD LOG
FIRST DAY

mileage	cumulative	
0.0	0.0	Leave Quality Inn located at 5575 West Amelia Earhart Dr., near junction of Interstate 80 (I-80) and 5600 West, Salt Lake City, Utah.
0.5	0.5	Junction with I-80. Turn right and head west on I-80. Highway crosses flood-plain and delta deposits of the Jordan River. This area was covered by about 800 feet (250 m) of water 15,000 years ago during the high stand of Lake Bonneville.
2.7	3.2	Junction with frontage road. Leave I-80 at exit 111, turn right and then left, and proceed west on frontage road. The Oquirrh Mountains are visible to the southwest, Stansbury Island is to the west, and Antelope Island is to the northwest. Quaternary alluvial fans, and benches cut along the Provo and Bonneville shorelines of ancient Lake Bonneville are visible on the eastern side of the Oquirrh Mountains.
2.4	5.6	Junction with gravel road. Turn right and head north on gravel road past radio towers. The Morton-Thiokol salt plant is on the south side of I-80. Mud flats flank the gravel road.
0.9	6.5	Gate. Continue heading north toward the Great Salt Lake. The road crosses private land for the next 2.4 miles (3.8 km). Wetlands along the road provide important nesting and feeding habitat for waterbirds.
2.4	8.9	Gate. Cross canal and continue northwest toward Antelope Island.
2.0	10.9	STOP 1. Antelope Island overview (Fig. 1). After discussion proceed northwest on causeway toward Antelope Island.

Antelope Island consists primarily of Archean(?) to Early Proterozoic high-grade metamorphic and igneous rocks of the Farmington Canyon Complex. These basement rocks underwent a complicated history of metamorphic and igneous activity including initial deposition of sedimentary and volcanic(?) rocks, an early period of metamorphism and deformation, intrusion of large granitic plutons, a second period of intense deformation and metamorphism, and late intrusion of granite and pegmatite. A thin cover sequence was unconformably deposited over the basement and includes 100 to 300 feet (30 to 100 m) of upper Proterozoic diamictite, dolomite, and slate, of the Mineral Fork and Kelley Canyon Formations, and about 1,000 feet (300 m) of Cambrian Tintic Quartzite.

Basement and cover rocks on Antelope Island were internally deformed and locally metamorphosed to greenschist facies during the Cretaceous to early Tertiary Sevier orogeny. These rocks lie on the western limb of a regional basement-cored anticline and are probably imbricated by the Ogden thrust system at depth (Yonkee, 1990; in press). Basement and cover rocks were translated eastward by about 40 miles (60 km) during regional thrusting.

Tertiary strata, including conglomerate, sandstone, ash beds, and marl, unconformably overlie basement and cover rocks and thrust-related structures. Tertiary rocks dip an average of 35° east, reflecting rotation during post-Miocene extension. Lacustrine deposits of Pleistocene Lake Bonneville and Holocene alluvial and colluvial deposits mantle much of the bedrock.

Basement rocks are also exposed to the east in the Wasatch Range along the eastern limb of the basement-cored anticline. The Wasatch Range is bounded on its west side by the Wasatch fault zone. This normal fault zone has accommodated up to 35,000 feet (11 km) of slip during the last 17 m.y. (Parry and Bruhn, 1986), and has had repeated Holocene surface-rupturing earthquakes (Machette and others, 1991). The Wasatch fault zone is capable of generating magnitude 7.0 to 7.5 earthquakes and the average recurrence interval between major earthquakes for the entire fault zone is about 400 years.

The Oquirrh Mountains to the south are underlain by more than 25,000 feet (7,500 m) of mixed sandstone and carbonate of the Permo-Pennsylvanian Oquirrh Group, and by a thick section of Mississippian to Cambrian miogeoclinal rocks. A thick miogeoclinal section of Mississippian to Upper Proterozoic rocks is also exposed on Stansbury Island (southwest of Antelope Island). The prominent light band is the Devonian Stansbury Formation, a coarse clastic unit deposited during a localized orogenic event. Stansbury Island and the Oquirrh Mountains probably lie within the southern continuation of the Willard thrust sheet, although these two areas may be separated by smaller imbricate thrusts. Antelope Island is separated from the Oquirrh Mountains and Stansbury Island

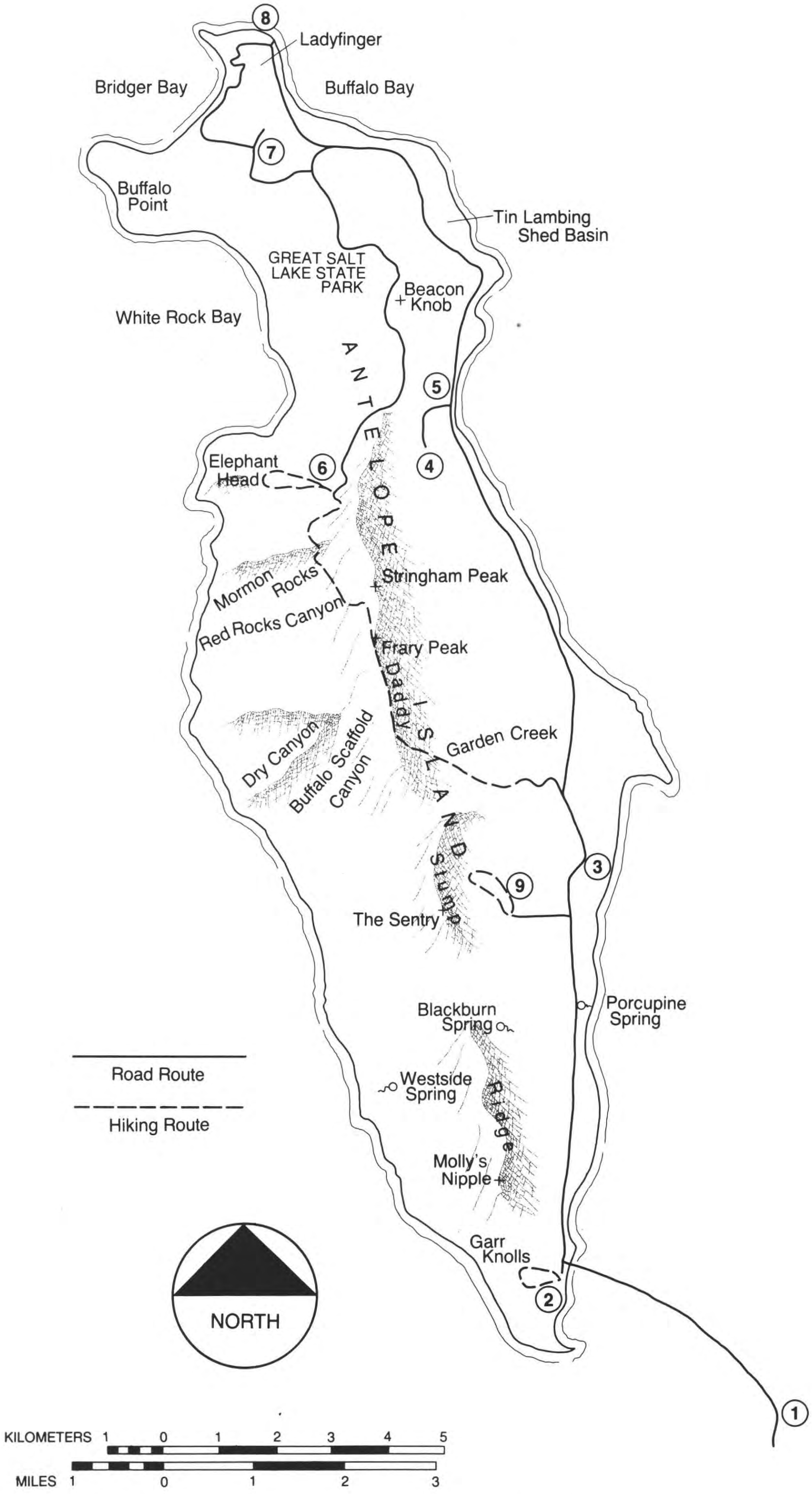

Figure 1. Index map of Antelope Island. Route of field trip is indicated and stops are numbered.

by the Willard thrust system and by younger normal faults.

0.6 11.5 Gate. Continue across causeway.

John C. Fremont explored the Great Salt Lake in 1843 and visited Antelope Island in 1845. At that time, the level of the lake was low and he reached the island by horseback across a peninsula. The lake has fluctuated in elevation since that time from a historic high of 4,211.5 feet (1,283.7 m) in 1873 and 1987 to a low of 4,191 feet (1,277.4 m) in 1963.

Antelope Island is currently a state park administered by the Utah Department of Natural Resources, Division of Parks and Recreation. The state purchased the northern end of the island in 1967, and built a causeway, public swimming facilities, and camp grounds. The park was a favorite among the public, with visits approaching 1 million per year. In 1981 the state acquired the rest of the island, but the dramatic rise in lake level beginning in 1983 flooded the north and south causeways, causing closure of the park. Other than a short period when ferry service was provided, the park has remained closed to the public since that time. Construction to restore the northern causeway and public facilities is currently underway (1992).

2.4 13.9 Reach Antelope Island. Turn left off main gravel road and head south on dirt road.

0.3 14.2 STOP 2. Early geologic history of the Farmington Canyon Complex. Take hike to examine characteristics of basement rock types exposed on the southern part of the island. The hiking route entails a rise of about 750 feet (230 m) in elevation up to Garr Knolls, extends about 1.2 miles (2.0 km), and will take about 2 hours. After hike return to main gravel road and drive north along the eastern side of island.

Precambrian high-grade metamorphic and igneous rocks of the Farmington Canyon Complex exposed on Antelope Island provide a partial record of the early geologic history of northern Utah. Basement rocks on Antelope Island have been divided into 10 types based on petrographic and geochemical properties, and these rock types are closely related to the map units of Doelling and others (1990). Rock types include: (1) layered gneiss, which corresponds to parts of the layered and mixed gneiss map units of Doelling and others (1990); (2) biotite schist, which forms lenses in the layered gneiss; (3) quartz-rich gneiss, which corresponds to the quartz-plagioclase gneiss map unit; (4) metamorphosed ultramafic rock, which forms isolated lenses in layered gneiss; (5) hornblende-plagioclase gneiss, which corresponds to the amphibolite map unit and forms lenses in other units; (6) banded gneiss, which corresponds to part of the mixed gneiss map unit; (7) granitic gneiss, which corresponds to the red granitic and migmatitic granitic gneiss map units (8) granite and pegmatite, which correspond to the coarse-grained and pegmatitic granite map units and form dikes and pods within other units; (9) chloritic gneiss, which partly corresponds to the chloritized and hematitized gneiss, phyllonite, and mylonite map unit; and (10) phyllonite and mylonite within shear zones. On this hike we will examine rock types 1 to 5, which are interpreted to be the oldest rocks exposed on the island. The other rock types will be examined at later stops.

Layered gneiss, with concordant lenses of biotite schist and quartz-rich gneiss, crop out in elongate regions within the central and southern parts of the island (Fig. 2). Some layered gneiss grades into biotite- and quartz-rich gneiss, consistent with a sedimentary protolith, but other layered gneiss grades into granitic gneiss and may have had an igneous protolith. Layered gneiss is migmatitic and contains quartz, plagioclase, K-feldspar, biotite, garnet, rare sillimanite, and rare cordierite, recording metamorphism at high temperatures ($<$600°C) and relatively low pressures (3 to 6 kbar). The presence of muscovite in some gneiss layers may reflect local retrograde metamorphism.

Hornblende-plagioclase gneiss is generally dark in color and consists of varying amounts of hornblende and plagioclase (Fig. 3), with lesser amounts of biotite, quartz, and clinopyroxene. This type of gneiss forms pods and layers that vary from being concordant to locally discordant to layered gneiss. Pods and layers of the gneiss probably represent metamorphosed mafic igneous rocks emplaced over a protracted history.

Ultramafic rock, consisting of variably altered pyroxene, amphibole, and rare olivine, forms isolated pods that are generally surrounded by mafic gneiss. These pods may represent dismembered parts of oceanic crust or layered mafic intrusions.

Layered gneiss, and lenses of biotite schist

Figure 2. Layered gneiss on southern part of island consists of alternating gray quartzo-feldspathic layers, white quartz-rich layers, darker biotite-rich layers, and dark amphibolite.

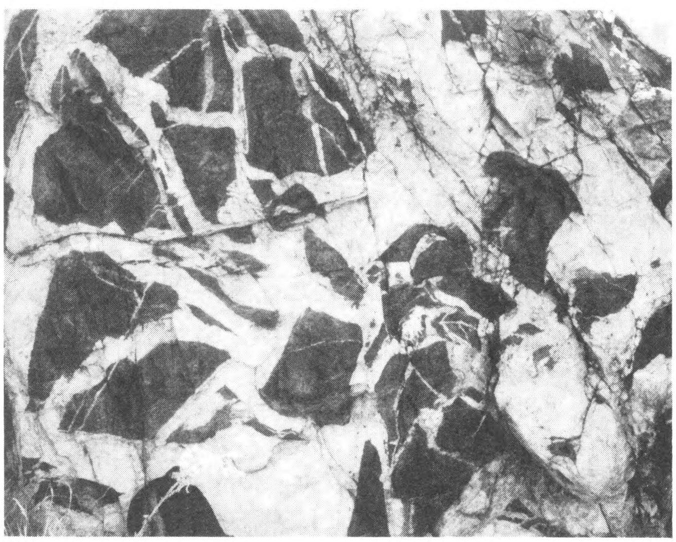

Figure 3. Dark hornblende-plagioclase gneiss is cut by light-colored pegmatite dikes and pods.

and quartz-rich gneiss, represent part of a sedimentary sequence that may have been deposited on oceanic crust, now preserved as isolated ultramafic pods. Mafic lava flows or intrusive dikes, now hornblende-plagioclase gneiss, were also incorporated into this sequence. Locally preserved interference fold patterns and multiple foliations record an early phase of deformation. A dominant foliation formed in the gneisses during a second phase of deformation, and this foliation can be traced into the younger banded and granitic gneiss units.

1.0 15.2 Abandoned road-fill pit on the left (west) extends 3.5 miles (5.3 km) to the north. Material removed from the pit was transported to the mainland on a 13-mile-long (20-km-long) conveyor belt for the construction of I-80 west of the Salt Lake City International Airport. After the project was completed, the pit was contoured and reseeded. Trees along the lower slope to the west denote the presence of springs.

0.4 15.6 Tertiary red conglomerate visible along the west end of the pit unconformably overlies the Farmington Canyon Complex and consists of weathered basement clasts sitting in a sandy arkosic matrix. The red conglomerate dips 35° east and is overlain by gray conglomerate consisting of quartzite, carbonate, and Eocene volcanic clasts in a calcareous matrix. Poorly exposed white to light-gray sandstone, marl, and ash beds of the Miocene(?) Salt Lake Formation overlie the gray conglomerate and are locally exposed near the road.

0.5 16.1 "Bird Bone" hill, composed of buried large boulders discarded from the road fill quarrying operation, is visible to the east. The hill is littered with the bones of waterbirds that nested there.

0.5 16.6 The bedrock hills on the west side of the pit consist of banded gneiss. Banded gneiss is the dominant rock type on the eastern side of the island and probably represents part of a deformed granitic pluton.

Buffalo are often observed in this area grazing on grasses and shrubs. Buffalo were introduced to the island in 1893 and have prospered since. The island currently supports a herd of about 600 animals. Recent testing by the Division of Parks and Recreation found that the herd has a distinct genetic makeup, making these animals particularly valuable in breeding programs.

0.8 17.4 Hay shed to east.

0.7 18.1 Approximate northern boundary of the road-fill pit. Trees to the west mark the site of Mushroom Springs. The Sentry, a lone prominent point bounded by flat benches cut by Lake Bonneville, is visible on the crest of Daddy Stump Ridge to the west.

1.0 19.1 STOP 3. Old ranch house. Turn right off main gravel road, proceed east to ranch house for a short discussion on the recent history of the island, then return to main gravel road and head north. The ranch house was constructed between the fall of 1848 and spring of 1849 by Fielding Garr and was used continuously as a residence until the 1970s. Captain Howard Stansbury made his camp on the island while surveying the Great Salt Lake in 1849-1850 and befriended Fielding Garr. Garr provided logistical assistance to the survey party. Freshwater springs underlie the marshy area east of the ranch house.

0.5 19.6 View east to Farmington Canyon and Francis Peak (site of a radar facility) in the Wasatch Range. Sea Gull Point juts out from Antelope Island just to the east.

1.6 21.2 Frary Peak, the highest point on Antelope Island, can be seen on Daddy Stump Ridge to the west. Frary Peak will be climbed on the second day of the field trip. The peak has an elevation of 6,597 feet (2,011 m) and stands about 2,400 feet (730 m) above the Great Salt Lake.

0.6 21.8 Slope failure in Bonneville lacustrine gravel created the large slump and landslide west of the road.

1.1 22.9 The East Stringham Peak fault crosses the gap north of Frary Peak. Proterozoic cover rocks, visible as folded light and dark bands, are exposed north of the fault.

0.6 23.5 Quaternary deposits along the shoreline to the east have slumped toward the lake. Precambrian rocks exposed to the west are mostly non-foliated pegmatitic granite.

0.9 24.4 Banded gneiss with small pods of amphibolite and pegmatite is exposed on both sides of road.

0.3 24.7 Junction with small side road. Turn left and head west-southwest along side road toward abandoned drill pad.

0.3 25.0 STOP 4 (optional). Granitic intrusions of the Farmington Canyon Complex. Stop at abandoned drill pad for discussion of granitic intrusions and later retrograde metamorphism. Return to the main road after stop.

Relatively unaltered banded gneiss grades westward into chloritic gneiss across the drill pad. Banded gneiss, the dominant rock type within the central and eastern parts of the island, surrounds a large elliptical region of granitic gneiss on the west side of the island. Multiple sets of less deformed pegmatite dikes cross-cut banded and granitic gneiss in most outcrops (Fig. 4). Banded gneiss and granitic gneiss consist of 30 to 35 vol% quartz, 20 to 40% plagioclase, 15 to 40% K-feldspar, and 5 to 15% mafic minerals (mostly hornblende and magnetite). Granitic gneiss has a greater average content of K-feldspar and a lower content of mafic minerals compared to banded gneiss. Banded gneiss displays well-developed compositional layering and strong foliation defined by preferred orientations of hornblende and quartz aggregates, and grades into more homogeneous and less strongly foliated granite gneiss. Both types of gneiss are mineralogically, chemically, and texturally gradational, and are interpreted to represent part of a zoned pluton that was intruded into the layered gneiss unit. Hedge and others (1983) reported an age of about 2000 Ma for granitic gneiss on Antelope Island, and this date has been interpreted to record approximately synchronous intrusion and metamorphism (Bryant, 1988).

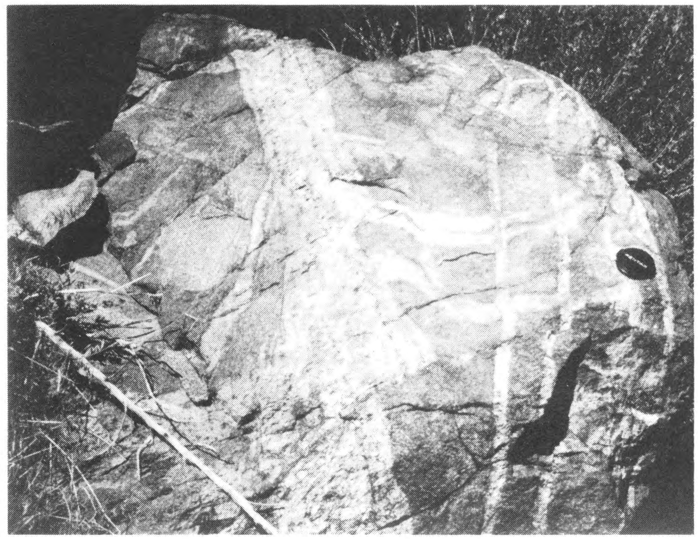

Figure 4. Granitic gneiss displays weak foliation and is cross cut by multiple sets of pegmatite dikes.

Granitic gneiss is locally cross cut by widely spaced fractures with limited greenschist-facies alteration, and grades into chloritic gneiss with increasing alteration. Chloritic gneiss is found along shear zone boundaries and near the contact with the overlying sedimentary cover. Chloritic gneiss displays complex fracture networks, minor shear zones, veins, and local protomylonitic foliation, reflecting variable cataclasis, plastic deformation, and alteration. Alteration minerals include chlorite, sericite, quartz, epidote, albite, and stilpnomelane. These alteration minerals both seal and are granulated along fractures, recording overlapping alteration and deformation. Chloritic gneiss is generally enriched in chlorite and sericite and depleted in feldspar compared to the protolith. With increasing alteration and deformation phyllonite and mylonite are produced. Syntectonic sericite from phyllonite on Antelope Island and in the Wasatch Range has ages mostly between 140 and 110 m.y., recording internal deformation that largely preceded large-scale folding and thrusting of the regional basement-cored anticline (Yonkee, 1990).

0.4 25.4 Junction with main gravel road. Turn left and head north on gravel road.

0.6 26.0 STOP 5 (optional). Retrograde metamorphism and deformation of basement rocks. Examine additional effects of Cretaceous deformation and retrograde metamorphism.

Basement rocks underwent localized internal deformation and retrograde alteration during the Sevier orogeny, resulting in development of chloritic gneiss and shear zones that contain phyllonite and mylonite (Fig. 5). Phyllonite and mylonite display pervasive chlorite and sericite alteration, and strong cleavage defined by preferred orientation of mica and plastically recrystallized quartz aggregates. Shear zones locally cross cut earlier Precambrian fabrics in the basement, and define several sets that vary between structural domains. Structural domains corresponding to the north and central parts of the island meet in this general area (Yonkee, 1990; in press). The central domain has steeply east-dipping and west-dipping sets of shear zones with reverse slip, reflecting subhorizontal east-west shortening. Gently dipping zones with top-to-the-east shear are also locally developed. Cleavage dips steeply west and stretching lineations trend west down the dip of cleavage. Shear zones in the northern domain include steeply northwest-dipping sets with normal slip and gently northwest-dipping sets with reverse slip; these two sets are mutually offset and define a conjugate pair. Other sets include steeply dipping, northeast- to east-striking shear zones with dextral and sinistral oblique slip. Some zones are curviplanar and sets locally grade into one another. Cleavage is moderately west to northwest-dipping, subparallel to the acute bisector of the conjugate pair. Stretching lineations vary from west- to northwest-trending. The kinematics of shear zones in the northern domain is complex and may reflect combined east-west shortening, as well as dextral wrench shear and top-to-the-east shear partly associated with footwall deformation beneath the Willard thrust.

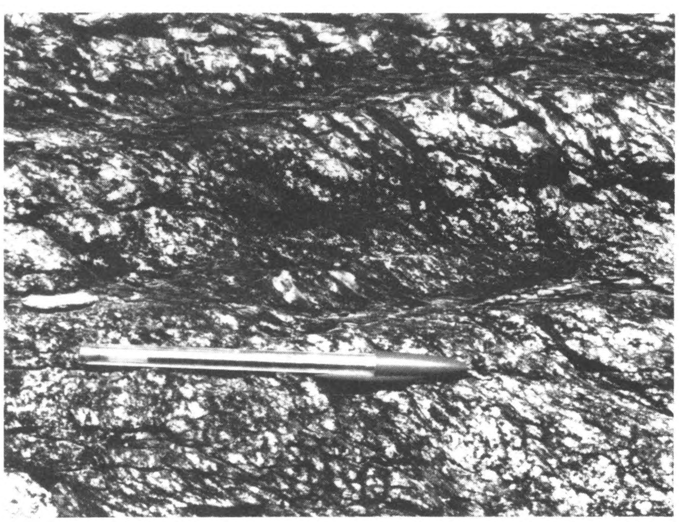

Figure 5. Minor shear zones cut granitic gneiss. Shear zones display phyllonitic cleavage and pervasive alteration.

2.3 28.3 The Gilbert-level shoreline is well developed in Tin Lambing Shed Basin immediately east of the road. The Gilbert level represents the last significant rise in lake level and is about 50 feet (15 m) above the historic average level of the Great Salt Lake. The Weber River delta is visible farther east toward the Wasatch Range.

1.2 29.5 Large boulders of Tintic Quartzite on the slope to the west were moved about in the wave zone of Lake Bonneville.

0.7 30.2 Junction. Turn left on dirt side road.

0.3 30.5 Keep left of buffalo pens and head south. Brecciated Tintic Quartzite crops out on both sides of road.

0.9 31.4 Road rises across several intermediate shorelines of Lake Bonneville. The most prominent is the Provo level.

2.1 33.5 Cross ridge. White Rock, a small island composed of dolomite of the Proterozoic Kelley Canyon Formation, is visible in the bay to the west.

0.9 34.4 Road turns southwest and descends from ridge. Erosion along old road is evident to the right.

1.3 35.7 STOP 6. Stratigraphy and deformation of Late Proterozoic cover rocks. Take hike around Elephant Head to examine characteristics of Late Proterozoic rocks (Fig. 6). The hiking route is about 2 miles (3.2 km) long over gentle topography and will take about 2 hours. Return to vehicles and retrace route to buffalo pens.

A thin sequence of Late Proterozoic sedi-

Figure 6. View of Elephant Head. The reason for this name is apparent when the area is viewed from an airplane. Rocks on Elephant Head display some of the most intense deformation on the island.

mentary and low-grade metasedimentary rocks on Antelope Island consists of diamictite and rare quartzite of the Mineral Fork Formation, overlain by dolomite, argillite and slate of the Kelley Canyon Formation. The diamictite is composed of sand-size to boulder-size clasts of quartzofeldspathic gneiss, schist, and quartzite that sit in a dark micaceous matrix (Fig. 7). Diamictite is very poorly sorted and massive, and unconformably overlies basement rock, varying in thickness from about 0 to 200 feet (0 to 60 m). Dolomite of the Kelley Canyon Formation is finely crystalline and forms light-gray resistant benches (Fig. 8), which contrast with the underlying diamictite. Dolomite is massive to finely laminated and has a thickness of 20 to 30 feet (6 to 9 m). Argillite or slate overlies the dolomite and is composed mostly of fine-grained quartz, sericite, and chlorite. It is locally calcareous and varies in color from gray to purple to reddish brown. This unit is thin bedded and varies in thickness from 50 to 250 feet (15 to 75 m).

These cover rocks were internally deformed during regional thrusting associated with the Sevier orogeny. Diamictite displays cleavage defined by flattened clasts and preferred orientation of mica (Fig. 7). Cleavage dips shallowly to moderately northwest, and can be traced directly upward from the basement. Cleavage, however, locally decreases in dip and intensifies within the diamictite, reflecting top-to-the-east simple shear parallel to the basement-cover contact, and local limited detachment of the cover (Yonkee, in press). Some clasts are bounded by asymmetric tails and pressure shadows, also recording top-to-the-east simple shear. Dolomite displays open folds, fractures, and thin veins in most outcrops, but is locally intensely folded with development of crenulation cleavage (Fig. 8). Slate on Elephant Head displays intense cleavage defined by preferred orientation of mica. Cleavage is locally rotated by shear bands that accommodated heterogeneous simple shear and by kink bands.

Figure 7. Diamictite of the Mineral Fork Formation exposed on Elephant Head is cut by well-developed cleavage. Cleavage is defined by flattened clasts and preferred orientation of mica.

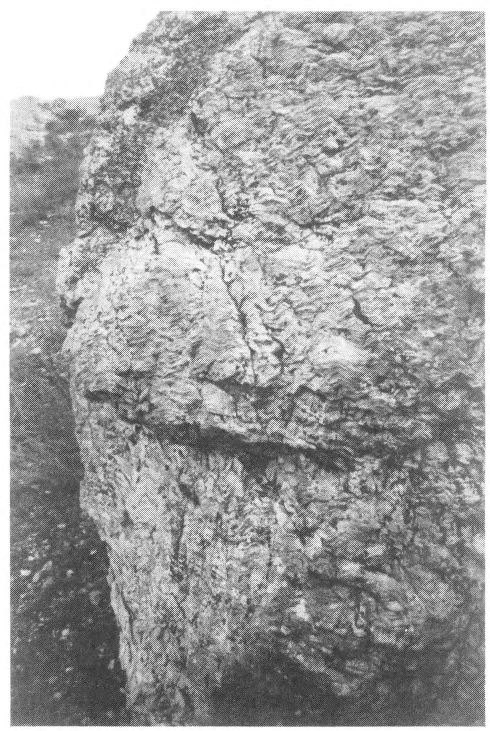

Figure 8. Dolomite of the Kelley Canyon Formation exposed on Elephant Head is locally folded and cut by crenulation cleavage.

5.5 41.2 Junction. Turn left at north end of buffalo pens and head southwest on gravel road.

0.2 41.4 Turn right on gravel road and pass northeast of park maintenance facilities.

0.6 42.0 Junction. Turn right and head north on paved road.

0.5 42.5 STOP 7. Deformation of Cambrian Tintic Quartzite. Hike about 0.25 mile (0.4 km) southeast toward low outcrops of quartzite. Examine deformed pebbles, shear bands, and minor folds. Return to vehicles, and head back south on paved road.

Most outcrops of Tintic Quartzite on the island display weakly to strongly developed cleavage defined by flattened pebbles and quartz aggregates (Fig. 9). Vein arrays at high angles to cleavage are also widespread, and minor folds are locally developed. Shapes of deformed pebbles have been used to estimate finite strain, and record 10 to 80% principal shortening perpendicular to cleavage, 0 to 30% intermediate extension, and 10 to 180% principal extension (Yonkee, 1990; in press). Cleavage dips moderately to steeply west to northwest in most areas and stretching lineation generally trend west to northwest at high to oblique angles to minor fold axes. This pattern is consistent with overall east-west shortening and top-to-the-east-southeast simple shear parallel to bedding. Outcrops of quartzite in this area, however, display relatively intense deformation compared to most other locations on the island, and stretching lineations are at low angles to minor fold axes. Clasts in conglomeratic layers are rotated into and intensely deformed along shear bands that are both subparallel and at high angles to bedding. These shear bands may record wrench shear parallel to an oblique or lateral ramp in the Willard thrust which covered this area prior to Tertiary erosion.

0.2 42.7 Junction. Turn right and head west on paved road toward Bridger Bay. Oolite and quartz sand dunes are on both sides of road. Some dunes are unstable and have periodically covered the roadway.

0.9 43.6 Beach facilities at Bridger Bay were damaged by undercutting storm waves during high-water period of 1985-1988.

1.1 44.7 Ladyfinger Point and Egg Island, visible to the north, consist of scattered bedrock outcrops of Tintic Quartzite that have been brecciated and relithified. The brecciation is the result of brittle deformation, and probably represents a later (Tertiary?) structural event.

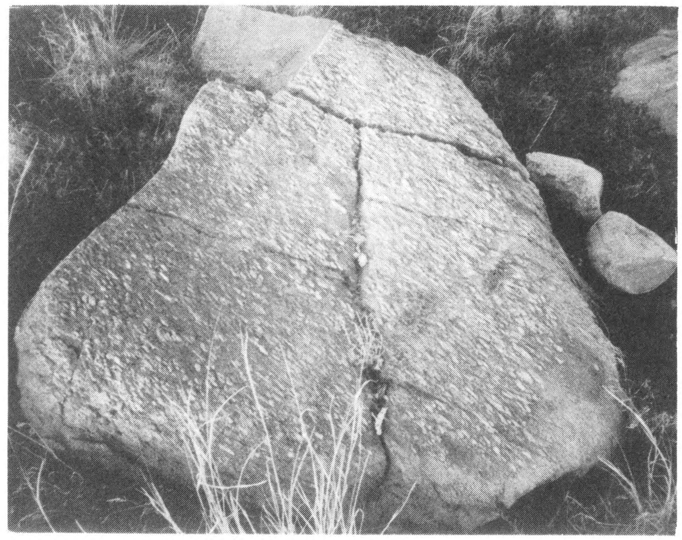

Figure 9. Stretched pebbles in outcrop of Tintic Quartzite on north end of the island.

0.2 44.9 Parking area to north. Continue east on paved road.

0.6 45.5 Turn left and head toward northern causeway, then immediately turn left (northwest), and continue in large arc until facing southwest. Proceed to outcrops exposed in pit and wave-cut slope. Promontory Point and Fremont Island, visible to the north, consist of a thick sequence of Late Proterozoic low-grade metasedimentary rocks within the Willard thrust sheet. The trace of the Willard thrust lies between Fremont and Antelope Islands.

0.2 45.7 STOP 8. Tertiary rocks at Ladyfinger Point. Examine faulted and tilted late Tertiary rocks. Return to vehicles and retrace route to pavement.

Tertiary strata in a pit were exposed when gravel was excavated for causeway construction after 1967 (Fig. 10). Strata are overturned to steeply southeast-dipping, cut by numerous small-displacement faults, and are in unconformable or fault contact with the Tintic Quartzite. Faults dip steeply north and have both dip-slip and strike-slip movement. The Tertiary rocks consist of interbedded sedimentary breccia, poorly sorted conglomerate, and thick beds of volcanic glass shards. Clast types include quartzite derived from the Cambrian Tintic Quartzite, olive-green shale, silty limestone, and dolomite derived from the Cambrian Ophir and Maxfield Formations, and argillite and feldspathic quartzite derived from Late Proterozoic strata in the Willard thrust sheet. Individual carbonate and shale clasts display intense foliation and complex vein arrays, reflecting concentrated shear strain that accumulated prior to erosion and deposition of the clasts. These clasts were probably eroded from nearby exposures of footwall rocks just below the Willard thrust. A glide horizon within Cambrian strata along the Willard thrust in part of the Wasatch Range may have extended to the north end of Antelope Island just above the rocks now exposed.

0.2 45.9 Junction. Travel south on paved road.

0.4 46.3 Junction. Turn left on gravel road.

0.9 47.2 Cross fence and continue south on main gravel road along the east side of island, following earlier route.

10.1 57.3 Old ranch house. Continue south on main road.

0.6 57.9 Junction. Turn right and head west on obscure dirt road.

0.5 58.4 STOP 9. Tertiary megaconglomerate. Take short hike of about 1 mile (1.6 km) to examine Tertiary conglomerate. Return to vehicles and retrace route to main road.

Eocene to Oligocene clastic rocks are exposed in the lower slopes at this stop. The basal beds consist of coarse conglomerate (Fig. 11). Boulders up to 11 feet (3.5 m) in diameter from this conglomerate were incorporated into nearby beach deposits of Lake Bonneville. Boulder types in the conglomerate include Mississippian carbonate, silty limestone probably derived from Cambrian strata, and quartzite probably derived from the Tintic Quartzite. Mississippian rocks are not preserved on the island, but the extremely large clast size indicates a local source. The most likely source was from erosion of rocks in the footwall of the Willard thrust, requiring a footwall ramp up to Mississippian rocks toward the south end of the island. A similar ramp in the Willard thrust is exposed to the northeast in part of the Wasatch Range. Beds in the conglomerate dip 30 to 40° east, reflecting tilting during late Tertiary extension.

0.5 58.9 Junction with main gravel road. Turn south and retrace route across southern causeway, to frontage road, to I-80, and back to motel.

17.1 76.0 Return to Quality Inn. End of first day.

SECOND DAY.

0.0 0.0 Leave Quality Inn, and proceed to Antelope Island via southern causeway as on first day. Follow former route to first day's

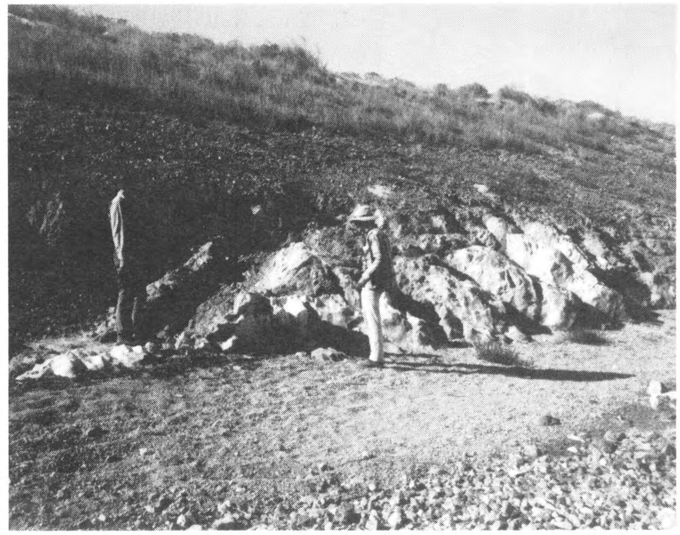

Figure 10. Tertiary Salt Lake Formation is exposed in a pit near Ladyfinger Point. Lighter-colored beds are volcanic ash, and darker-colored beds are interbedded conglomerate and breccia. Underlying Tintic Quartzite is highly brecciated.

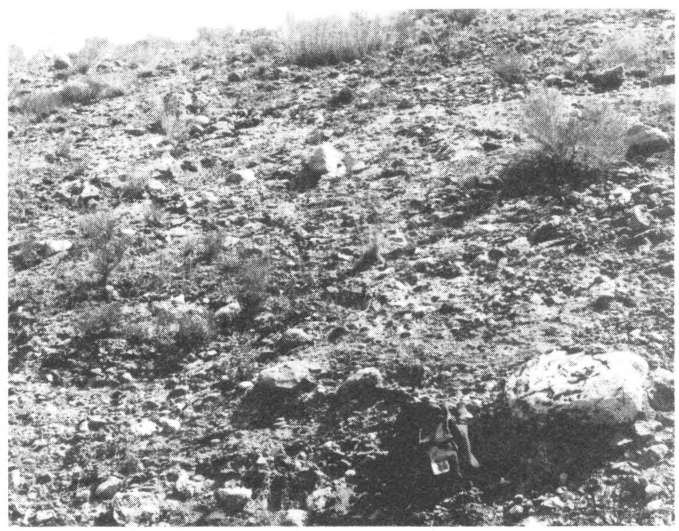

Figure 11. Boulder conglomerate of probable Eocene age on the southeast part of the island contains clasts derived from Mississippian to Cambrian carbonate and sandstone.

STOP 6 on Elephant Head.

34.3 34.3 HIKE ALONG DADDY STUMP RIDGE. A strenuous hike of about 6 miles (10 km) will entail climbing from an altitude of 4,800 feet (1,460 m) to about 6,600 feet (2,010 m), and then descending to 4,650 feet (1,420 m). On the hike we will examine the Archean(?) to Early Proterozoic metamorphic, igneous, and deformation history of the Farmington Canyon Complex, stratigraphy and deformation features in Late Proterozoic and Cambrian low-grade metasedimentary rocks, the geometry and kinematics of structures that developed during the Sevier orogeny, and the stratigraphy and tectonic significance of Tertiary strata. Features along the hike will include a reverse fault that juxtaposed basement rocks of the Farmington Canyon Complex over Cambrian and Late Proterozoic strata (Fig. 12), slate and quartzite with complex folds and cleavage, and Tertiary megaconglomerate. Views from Daddy Stump Ridge provide a spectacular view of the regional geology and physiography. Lunch will be on Frary Peak, the highest point on the island. Meet vehicles on east side of island.

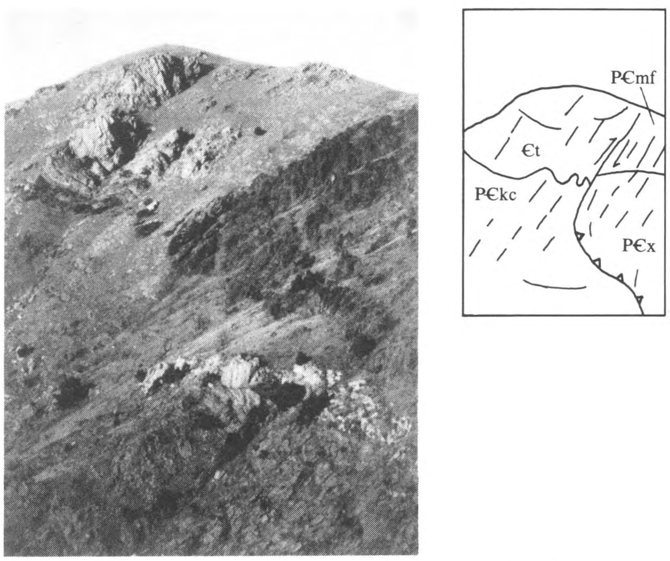

Figure 12. View to north of southeast-dipping reverse fault along Daddy Stump Ridge. The fault juxtaposes basement and diamictite on the east against dolomite, slate, and quartzite on the west. Cleavage is steeply dipping and continues up from the basement into the cover. Line drawing illustrates structural geometry of fault and cleavage (short dashed lines). Units are P€x-basement rocks of the Farmington Canyon Complex, P€mf-Mineral Fork Formation, P€kc-Kelley Canyon Formation, and €t-Tintic Quartzite.

17.3	51.6	Vehicles driven around to pickup point. Proceed back to motel via south causeway.
19.9	71.5	Return to Quality Inn. End of Second day.

REFERENCES

Bryant, B., 1988, Geology of the Farmington Canyon Complex, Wasatch Mountains, Utah: U.S. Geological Survey Professional Paper 1476, 54 p.

Bryant, B., and Graff, P.J., 1980, Metaigneous rocks on Antelope Island: Geological Society of America Abstracts with Programs, v. 12, p. 269.

Doelling, H. H., Willis, G. C., Jensen, M. E., Hecker, S., Case, W. F., and Hand, J. S., 1990, Geologic map of Antelope Island, Davis County, Utah: Utah Geological and Mineral Survey Map 127, scale 1:24,000.

Hedge, C. E., Stacey, J. S., and Bryant, B., 1983, Geochronology of the Farmington Canyon Complex, Wasatch Mountains, Utah, *in* Miller, D. M., Todd, V. R., and Howard, K. A., eds., Tectonic and stratigraphic studies in the eastern Great Basin: Geological Society of America Memoir 157, p. 37-44.

King, C., 1878, Systematic geology: U.S. Geological Exploration 40th parallel, v. 1 and 2.

Larsen, W. N., 1957, Petrology and structure of Antelope Island, Davis County, Utah: [Ph.D. dissertation], Salt Lake City, University of Utah, 142 p.

Machette, M. N., Personius, S. F., Nelson, A. R., Schwartz, D. P., and Lund, W. R., 1991, The Wasatch fault zone, Utah — Segmentation and history of Holocene earthquakes: Journal of Structural Geology, v. 13, p. 137-149.

Parry, W. T., and Bruhn, R. L., 1986, Pore-fluid chemistry and chemical reactions on the Wasatch normal fault, Utah: Geochimica et Cosmochimica Acta, v. 52, p. 2053-2063.

Yonkee, W. A., 1990, Geometry and mechanics of basement and cover deformation, Farmington Canyon Complex, Sevier orogenic belt, Utah [Ph.D. dissertation]: Salt Lake City, Utah, The University of Utah, 255 p.

——, in press, Basement-cover relations, Sevier orogenic belt, northern Utah: Geological Society of America Bulletin.

GEOLOGIC HAZARDS OF THE OGDEN AREA, UTAH

by
Mike Lowe
Utah Geological Survey
Bill D. Black
Utah Geological Survey
Kimm M. Harty
Utah Geological Survey
Jeffrey R. Keaton
Sergent, Hauskins & Beckwith
William E. Mulvey
Utah Geological Survey
E. Fred Pashley, Jr.
Weber State University
Department of Geology
Scott R. Williams
Davis County Flood Control

ABSTRACT

The Ogden area is in the Intermountain seismic belt, an active earthquake zone extending from northwestern Montana to southwestern Utah. Earthquake hazards in the Ogden area include ground shaking, surface fault rupture, tectonic subsidence, liquefaction, and seismically-induced slope failure and/or flooding. The largest historical earthquake in the Ogden area occurred in 1914 and was an estimated magnitude 5.5. Trenching studies along the Wasatch fault zone indicate that earthquakes of magnitude 7.0-7.5 could occur near Ogden. Tectonic subsidence due to surface-faulting events could cause ponding of shallow ground water in the Ogden area, and, in central Davis County to the south of Ogden, could also cause flooding along the shore of Great Salt Lake. Shoreline flooding could also be caused by earthquake-induced seiches. Liquefaction of saturated fine sandy deposits could accompany large earthquakes in the Ogden area where several prehistoric liquefaction-induced landslides have been identified.

Geologic hazards in the Ogden area not necessarily caused by earthquakes include landslides, debris flows, rock falls, problem soils, flooding, and shallow ground water. Landslides are especially common in fine-grained lacustrine deposits, primarily along steep bluffs created by stream incision into deltas deposited into Pleistocene Lake Bonneville by the Ogden and Weber Rivers, and in mountainous areas underlain by the Precambrian Farmington Canyon Complex. Debris flows, triggered by both snowmelt-induced landsliding and cloudburst-rainstorm-induced erosion, have caused significant historical damage in the vicinity of Ogden. Rock falls have been common during historical time only in Ogden Canyon, but could be widespread along the mountain front during large earthquakes. Compressible soils associated with peat deposits have been identified near Ogden. Flood damage has occurred along streams and the shoreline of Great Salt Lake. Shallow ground water is common at lower elevations.

INTRODUCTION

Potential geologic hazards in the vicinity of Ogden, Utah include earthquakes (ground shaking, surface fault rupture, tectonic subsidence, liquefaction, and seismically-induced slope failure and/or flooding), slope failures, problem soils, flooding, and shallow ground water. During this one-day field trip, which will consist of nine stops between the cities of North Ogden and Centerville (figures 1 and 2), we will present examples of many geologic hazards and case histories of geologic-hazard investigations. Considerable background material is presented on the nature of geologic hazards in an attempt to make this paper more valuable to engineering geologists unfamiliar with the Ogden area, to geologists outside of the engineering geology subdiscipline, to earth-science teachers, and to the educated layperson. Much of this background material is taken largely from Lowe (1990d, 1990e) and papers by the Wasatch Front County Geologists in Gori (1990). A selected bibliography of geologic maps and reports covering the Ogden area, which have not been cited in this text, is presented at the end of this paper for those seeking additional information.

BACKGROUND AND HISTORY

The field trip area is located between approximately 41° 15′ and 40° 52′ N. latitude and 111° 56′ and 111° 51′ W. longitude in Weber and Davis Counties, Utah (figures 1 and 2). Most cities in Weber and Davis Counties were founded shortly after the Mormon pioneers settled the Salt Lake Valley in 1847. These cities were generally founded near major streams such as the Ogden and Weber Rivers, or on alluvial fans at the mouths of the smaller canyons where water was readily available. Ogden is the county seat of Weber County; Farmington is the county seat of Davis County. Weber and Davis Counties have a combined population of slightly less than 350,000.

SETTING

The Ogden area is located in the Ogden Valley Segment of the Wasatch Front Valleys Section of the Basin and Range Physiographic Province (Stokes, 1977). The Ogden Valley Segment is a north-south-trending structural trough which has been the site of accumulation of great thicknesses of sediment since the advent of Basin and Range normal faulting approximately 15 million years ago (Hintze, 1988). The Wasatch Range and the west-dipping Wasatch fault zone bound the trough to the east, and geophysical data indicate that Little Mountain may be part of a horst which bounds the trough to the west (Feth and others, 1966). Sediments filling the trough are predominantly of fluvial, lacustrine, and deltaic origin. Geophysical data indicate that, in some areas, these sediments may be as much as 1,800 to 2,700 m (6,000-9,000 ft) thick (Feth and others, 1966).

Great Salt Lake is located in the western portion of Weber and Davis Counties. Major tributaries flowing into Great Salt Lake include the Bear River to the north, the Weber River to the east, and the Jordan River to the south. Great Salt Lake is located in a closed hydrologic basin, called the Lake Bonneville basin, and water flowing into this basin leaves predominantly by direct evaporation. The Lake Bonneville basin has been an area of internal drainage for much of the last 15 million years, and lakes of varying sizes likely existed in the area during all or most of that time (Currey and others, 1984).

CLIMATE

The Ogden area has a temperate and semiarid climate and four distinct seasons. Average annual precipitation increases from less than 30 cm (12 in) in the valley bottom near the shore of Great Salt Lake to more than 50 cm (20 in) along the mountain front (Clark and others, 1990). Estimated average annual precipitation in higher peaks of the Wasatch Range, where some peaks exceed 2,700 m (9,000 ft) in elevation, is 60 to 75 cm (25 to 30 in). The average annual temperature in the Ogden area is generally in the low 50s; the range between average summer and winter temperatures is about 40 degrees Fahrenheit (Erickson and others, 1968). In general, winds are light to moderate (11-16 km/h, 7-10 mi/h), although strong, damaging winds occur occasionally (Feth and others, 1966).

GROUND WATER

Ground water occurs in unconsolidated and semi-consolidated basin-fill deposits of Tertiary and Quaternary age, and the following description is taken from Feth and others (1966) and Clark and others (1990). Figure 3 shows the relationships of unconfined, confined, and perched ground water in the Ogden area. The basin fill consists of coarse gravel to clay size sediments eroded from the mountain ranges to the east and deposited in the valley as interbedded alluvial and lacustrine deposits. Near the mountains, the basin fill consists mostly of coarse-grained fluvial, alluvial-fan, and deltaic sediments; near Great Salt Lake in the center of the valley, the basin fill consists mostly of fine-grained lacustrine sediments. The basin fill in the Ogden area is estimated to be approximately 1,800 to 2,700 m (6,000-9,000 ft) thick.

Aquifers in the Ogden area are part of the East Shore aquifer system; ground water in this system is predominantly confined, but unconfined conditions exist in the recharge areas along the mountain front. Two major aquifers, the Sunset and Delta, have been delineated in the central part of the East Shore aquifer system. The Delta aquifer is the primary source of ground water in the Ogden area and is composed primarily of Weber River fluvial and deltaic sediments. The top of the Delta aquifer is between 150 and 200 m (500 and 700 ft) below the ground surface at most locations in the Ogden area. The Delta aquifer is estimated to be 15 to 46 m (50-150 ft) thick. The shallower Sunset aquifer is used to a lesser extent than the Delta aquifer as a source of ground water, primarily because of its lower permeability. The top of the Sunset aquifer is typically 76 to 122 m (250-

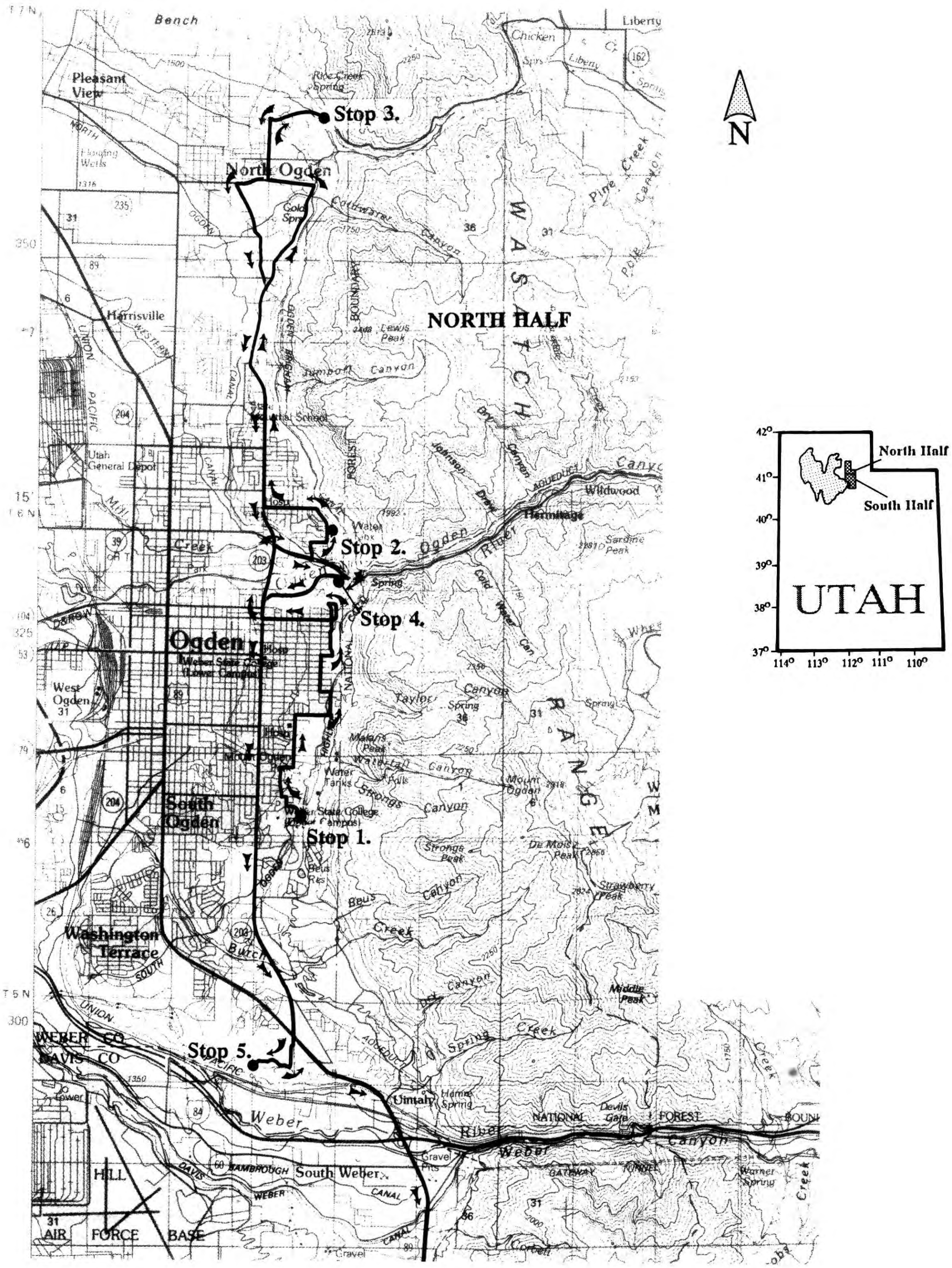

SCALE

0 1 2 3 4 5 mi

0 1 2 3 4 5 6 7 8 9 10 km

CONTOUR INTERVAL 50 METERS

Figure 1. Field trip route and stops, north half.

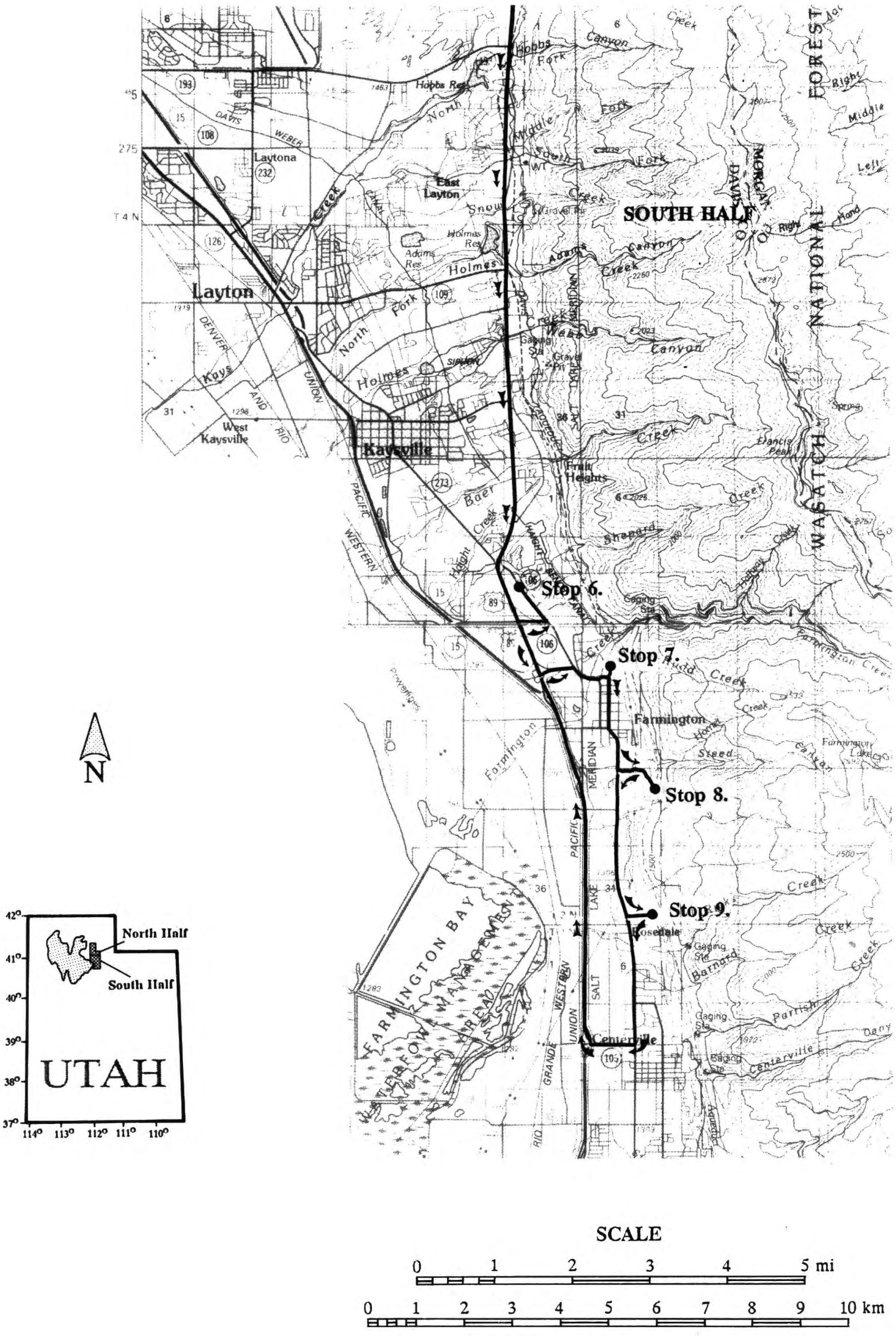

Figure 2. Field trip route and stops, south half.

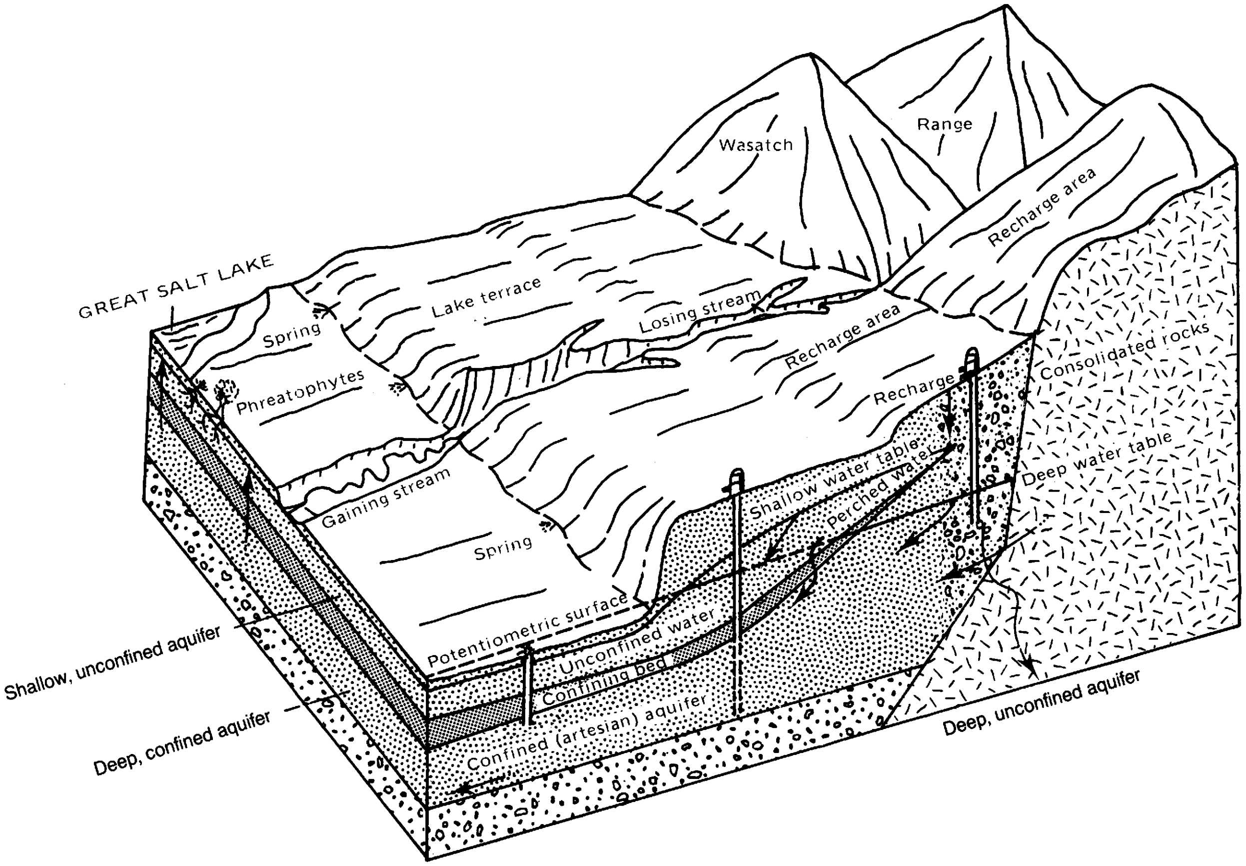

Figure 3. Generalized block diagram showing ground-water conditions in the Ogden area, Utah (modified from Hely and others, 1971).

400 ft) below the ground surface, but at some locations is as shallow as 61 m (200 ft). The Sunset aquifer ranges from 15 to 61 m (50-200 ft) in thickness. Fine-grained confining beds overlie both aquifers.

GEOLOGIC HAZARDS

Earthquake Hazards

Earthquakes — The Ogden area is in the Intermountain seismic belt (figure 4), an active earthquake zone which extends from northwestern Montana to southwestern Utah (Smith and Sbar, 1974). The largest magnitude historical earthquake in the Ogden area occurred in 1914 near Ogden and had an estimated Richter magnitude 5.5 (figure 5; Arabasz and others, 1979). Numerous smaller earthquakes have occurred in the area during historical time. Many of these earthquakes cannot be attributed to known active faults, although faults thought to be capable of generating earthquakes are present in the area. The Wasatch fault, which trends north-south along the mountain front in the eastern Ogden area, is of most concern because of its recency of movement, potential for generating large earthquakes, and proximity to urban areas. It consists of a zone of faults and crustal deformation, in places as much as several thousand feet wide, and is considered capable of generating earthquakes up to magnitude 7.0-7.5 (Schwartz and Coppersmith, 1984; Machette and others, 1991). Other fault zones, such as the Hansel Valley or East Cache fault zones, are capable of generating earthquakes which could cause ground shaking in the Ogden area.

Ground Shaking — Ground shaking is the most widespread and frequently occurring of the earthquake hazards and has been responsible for the majority of earthquake-caused damage throughout the world. The extent of property damage and loss of life in an earthquake due to ground shaking is determined by several factors including: 1) strength of seismic waves reaching the surface (horizontal accelerations are the most damaging), 2) frequency, amplitude, and duration of ground shaking, 3) proximity to fault zones or epicenters, 4) foundation materials, and 5) building design (Costa and Baker, 1981). Foundation materials are important because ground shaking can be amplified by local site conditions, and the site response is influenced by the nature and thickness of underlying unconsolidated deposits (Hays and King, 1982).

The severity of ground shaking is chiefly dependent on the magnitude of the earthquake. Based on expected shaking levels at bedrock sites, the Uniform Building Code (UBC) places the Ogden area in seismic zone 3 and gives minimum specifications for earthquake-resistant design and construction. The Utah Seismic Safety Advisory Council (USSAC), which existed from 1977 to 1981, placed the Ogden area in seismic zone U-4 and recommended application of UBC

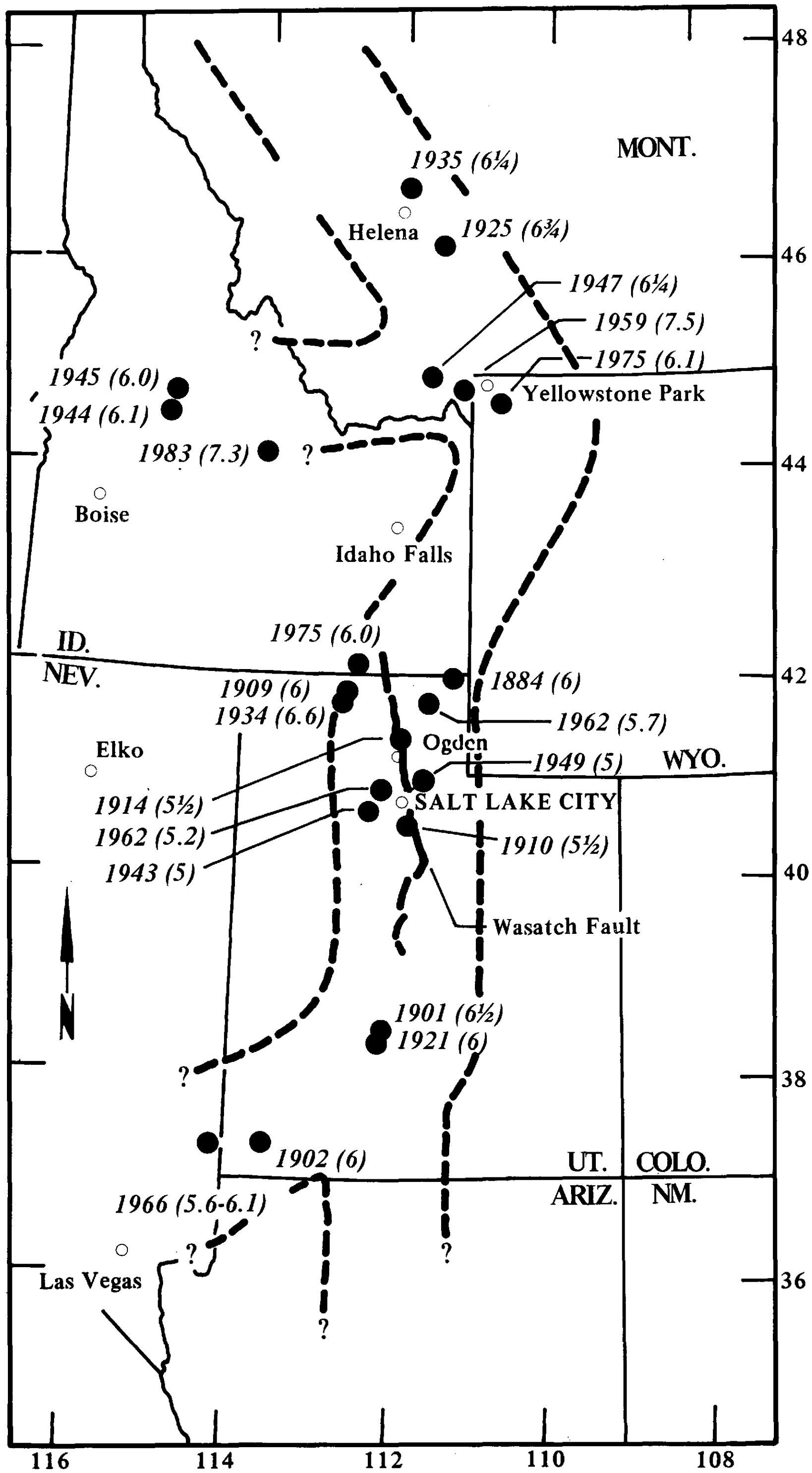

Figure 4. Epicenter map of the Intermountain Seismic Belt (modified from Lund and others, 1990).

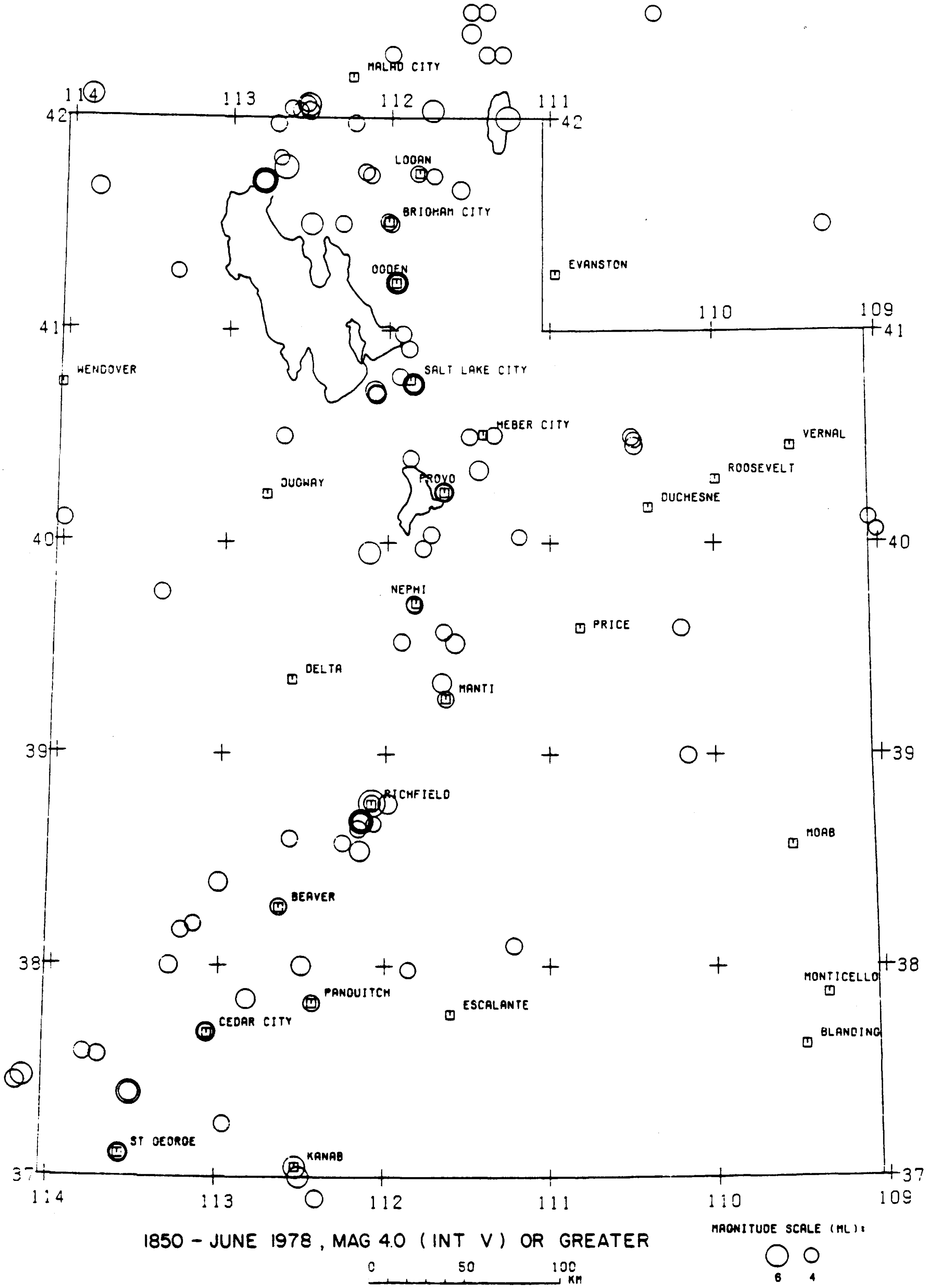

Figure 5. Earthquakes, magnitude 4.0 (intensity V) or greater, 1850 to June, 1978 (from Arabasz and others, 1979).

zone 3 specifications with more stringent review and inspection to ensure compliance.

Both the UBC and USSAC seismic zonations are based on expected ground shaking in bedrock. It is important to understand that when the fundamental frequency of a building is the same as the dominant frequency of the ground motion, the potential for damage increases. Short-period waves (0.1 to 0.2 seconds) are most destructive to 1 to 2 story buildings, whereas waves with 0.2 to 0.7.second periods are most destructive to 3 to 7 story buildings. Longer period waves may cause damage to taller buildings with relatively little effect on other structures. In the Ogden area, peak horizontal ground accelerations with a 10 percent probability of exceedance in a 50-year period could be more than 30 percent of the force of gravity; peak horizontal ground accelerations with a 10 percent probability of exceedance in a 250-year period could be as high as 60 percent of the force of gravity (figure 6; Youngs and others, 1987). Maximum Modified Mercalli intensities associated with these ground accelerations could be as high as XIII and X, respectively (Bolt, 1978).

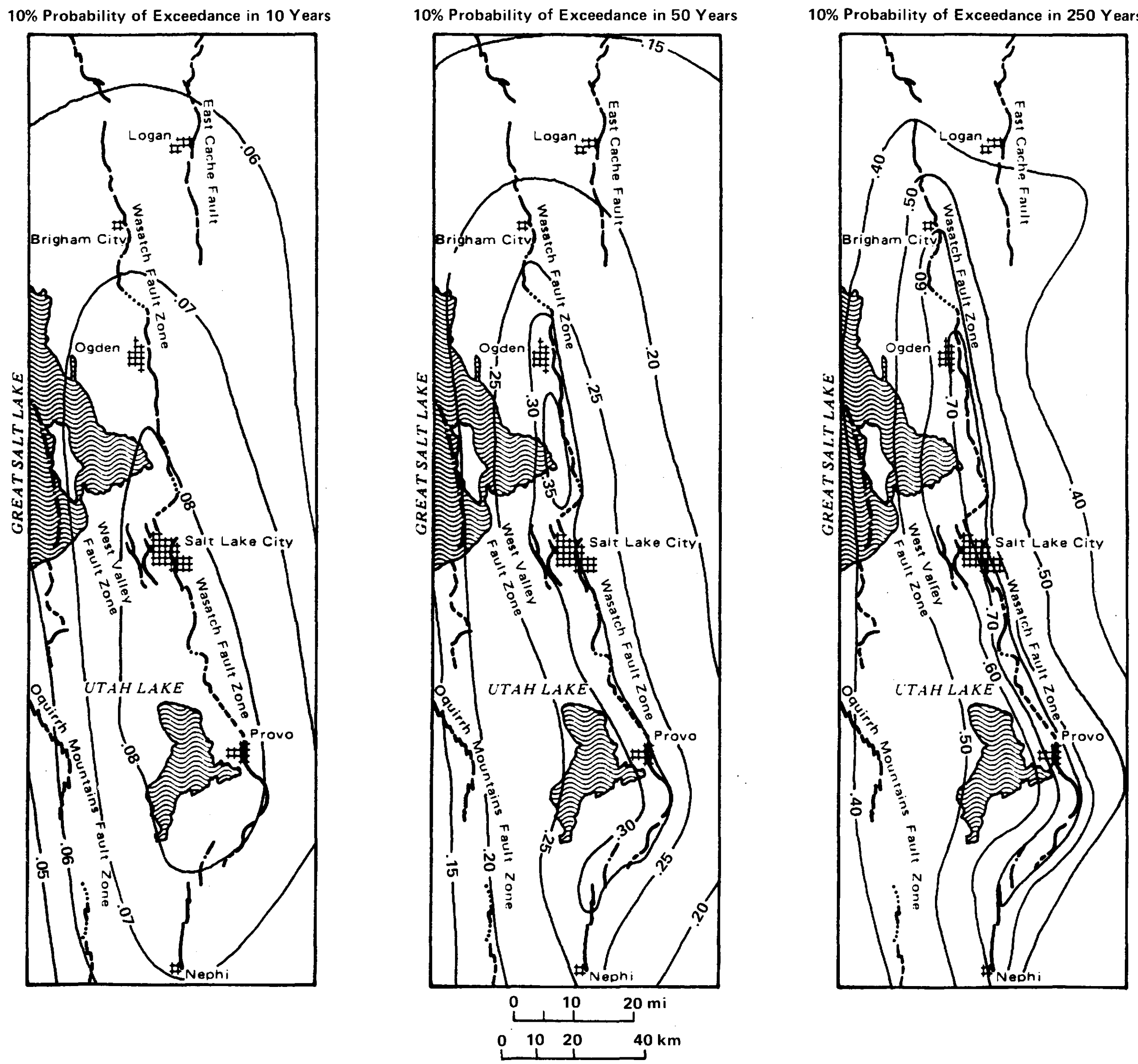

Figure 6. Contours of peak ground acceleration on soil sites with 10 percent probability of being exceeded in 10 years, 50 years, and 250 years (Youngs and others, 1987).

Surface Fault Rupture — Studies along the Wasatch fault zone (Schwartz and Coppersmith, 1984) and elsewhere indicate that the most likely areas for surface fault rupture are along areas of previous (prehistoric) rupture. During large-magnitude earthquakes (magnitude 6.0-6.5+), ruptures generally propagate to the surface as one side of the fault is uplifted and the other side downdropped, resulting in a scarp with a near-vertical slope. Wasatch fault scarps, which are generally near the range front in the Ogden area, will be viewed at many locations during the field trip.

The Wasatch fault zone extends from near Malad City in southern Idaho to Fayette in central Utah, a distance of about 343 km (213 mi) (Machette and others, 1989). The fault zone trends roughly north-south and, at the surface, dips steeply to the west. The Wasatch fault zone is commonly not a single fault plane, but a zone of deformation containing many individual subparallel faults, cracks, and tilted or displaced blocks (figure 7). This zone of deformation may be a few inches to several hundred feet wide. The Wasatch fault zone is not expected to rupture along its entire length during a single earthquake, but rather discrete segments of varying lengths will probably rupture independently. Originally, 6 segments were proposed, but more recent studies indicate there may be as many as 10 (figure 8; Schwartz and Coppersmith, 1984; Machette and others, 1987, 1989, 1991). These segments generally control the length of the expected surface rupture, the starting or stopping points of ruptures, and place physical constraints on the maximum magnitudes of potential earthquakes. Surface-faulting events along the central Wasatch fault zone have an average recurrence interval of 395 ± 60 years (Machette and others, 1991). The most recent rupture along the Wasatch fault zone may have occurred on the Nephi fault segment in Juab County, 300-500 years ago (Schwartz and Coppersmith, 1984); Jackson and Ruzicka (1988), however, suggest that this event may have occurred 500 or slightly more years ago.

The Wasatch fault-zone segment in the Ogden area, the Weber segment, is the longest segment of the zone (57 km; 35 mi). The Weber segment extends from the southern edge of the Pleasant View salient near North Ogden to the northern edge of the Salt Lake salient near North Salt Lake (Machette and others, 1987). A trenching study near Fruit Heights (Kaysville site) indicated that the most recent surface faulting on the southern portion of the Weber segment occurred slightly before 700 and 900 years ago (McCalpin and others, in prep.). Studies of an exposure near the mouth of Garner Canyon in North Ogden (Nelson and others, 1987) and trenches just north of Ogden Canyon (East Ogden trench site; Stop 2 on the field trip) indicate that the last major surface faulting event on the segment occurred prior to about 1,000 years ago (Nelson, 1988; Forman and others, 1991). More limited evidence at the East Ogden site suggests a small event occurred prior to 600 years ago (Nelson, 1988). The penultimate surface-faulting event on the Weber segment occurred between 2,000 and 3,000 years ago in the northern portion at the Garner Canyon and East Ogden sites (Nelson and others, 1987; Nelson, 1988; Forman and others, 1991). As many as 5-6 surface-faulting events may have occurred during the last 12,000 years at the Kaysville trench site (McCalpin and others, in prep.). Average ground-surface displacement along the main trace of the fault at the Garner Canyon exposure was 1.4 m (4.6 ft) (Nelson and others, 1987). Displacements during surface-faulting events at the East Ogden site ranged from 0.6 to 3.5 m (2-11 ft) (see field trip road log, Stop 2). At the Kaysville site, average

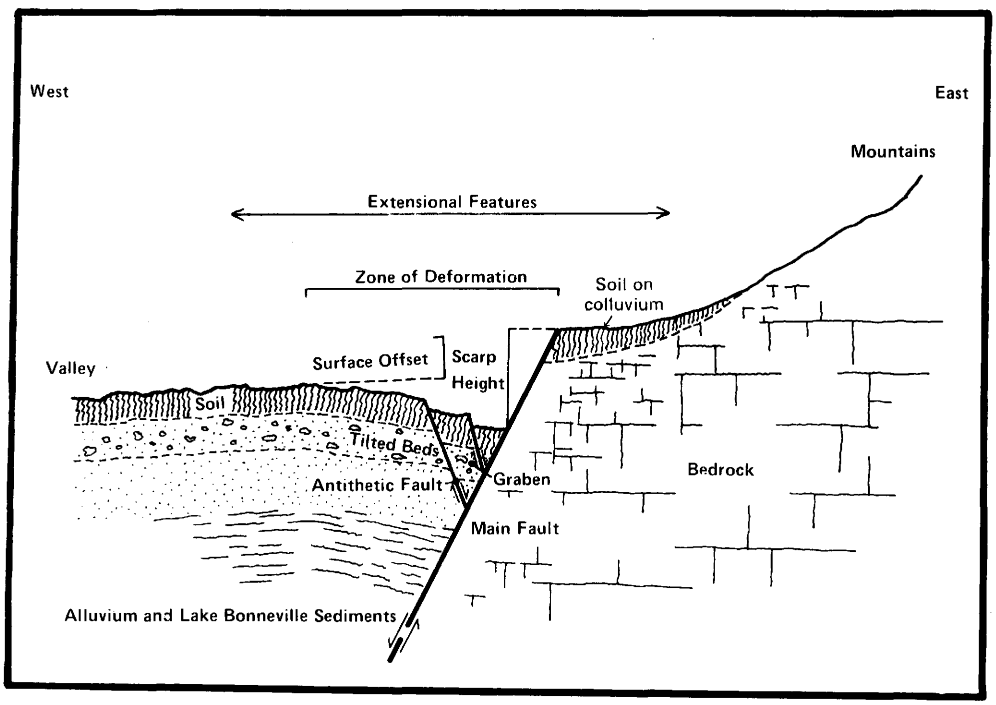

Figure 7. Schematic diagram of near-ground-surface features commonly associated with the Wasatch fault zone. The sketch is not to scale (from Robison, 1990a).

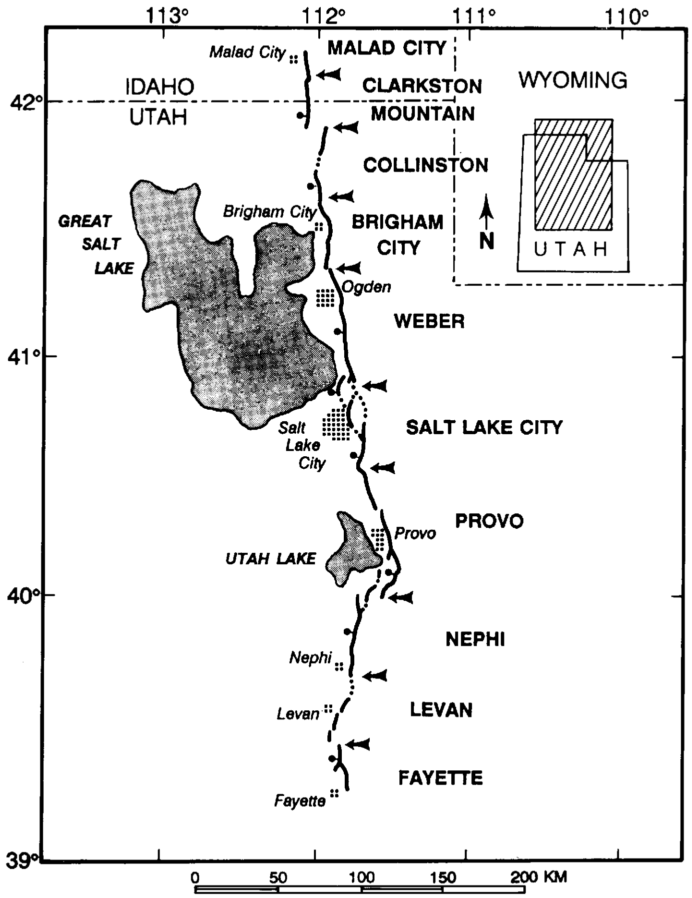

Figure 8. Map of the Wasatch fault zone segments (adapted from Machette and others, 1991).

ground-surface displacement was 1.4 to 3.4 m (4.6-11.2 ft) (McCalpin and others, in prep.).

Tectonic Subsidence — Tectonic subsidence of large areas may accompany surface faulting during large earthquakes as the downthrown block undergoes regional downdropping and tilting toward the fault (Keaton, 1987). Tectonic subsidence could cause flooding along the shoreline of Great Salt Lake in the Ogden area as depicted diagrammatically in figure 9; the amount of inundation depends on lake levels at the time of the event. The expected area of subsidence along the Wasatch fault zone extends as far as 16 km (10 mi) west of the fault zone, with the majority of deformation occurring within about 5 km (3 mi) (Keaton, 1986a). Tectonic deformation maps for the Wasatch fault indicate subsidence due to the "characteristic" Wasatch fault earthquake (magnitude 7.0-7.5) to be about 1.5 m (5 ft) along the mountain front in the Ogden area (Keaton, 1987). Eastward tilting of the ground surface may be as much as 9.5 cm/km (0.5 ft/mi), and could adversely affect gravity-flow structures such as storm sewers, and sanitary sewers which feed wastewater-treatment plants (figure 9) (Keaton, 1987). These tectonic deformation maps also indicate that flooding caused by tectonic subsidence could occur due to ponded shallow ground water (figure 9) in the eastern portion of the Ogden area.

Liquefaction — Earthquake ground shaking causes a variety of phenomena which can damage structures and threaten lives. One of these is soil liquefaction. Ground shaking can cause an increase in the pressure in the pore water between soil grains, which decreases the stresses between the grains. The loss of intergranular stress can cause the shear strength of some soils to decrease nearly to zero. When this happens, the soil behaves like a liquid, and therefore is said to have liquefied. When liquefaction occurs, foundations may crack; buildings may tip; buoyant buried structures, such as septic tanks and storage tanks, may rise; and even gentle slopes may fail as liquefied soils and overlying materials move downslope (Lowe, 1990c).

The potential for liquefaction depends both on soil and groundwater conditions, and on the severity and duration of ground shaking. Soil liquefaction most commonly occurs in areas of shallow ground water (less than 9 m; 30 ft) and loose sandy soils which are common in western Weber and Davis Counties. In general, an earthquake of magnitude 5 or greater is needed to induce liquefaction (Kuribayashi and Tatsuoka, 1975, 1977; Youd, 1977). For larger earthquakes, liquefaction has a greater likelihood of occurrence and will occur at greater distances from the epicenter (the point on the earth's surface directly above the focus of the earthquake). Earthquakes of magnitude 7.0-7.5 are the largest expected along the Wasatch Front (Schwartz and Coppersmith, 1984; Machette and others, 1991); during such earthquakes liquefaction has occurred up to 270 km (170 mi) (1977 Romanian earthquake, magnitude 7.2) from the epicenter (Youd and Perkins, 1987).

Liquefaction itself does not necessarily cause damage, but it may induce ground failure of various types which can be very damaging. Four types of ground failure commonly result from liquefaction: 1) loss of bearing strength, 2) ground oscillation, 3) lateral-spread landslides, and 4) flow landslides (Youd, 1978a, 1978b; Tinsley and others, 1985). Youd and others (1975) relate these types of ground failure to the slope of the ground surface.

Loss of bearing strength beneath a structure can occur during earthquake ground shaking when the underlying soil liquefies and loses strength (figure 10) (Tinsley and others, 1985); these types of failures are most common in areas where slopes are generally less than about 0.5 percent (Anderson and others, 1982). The soil mass is then susceptible to deformation that allows buildings to settle and/or tilt (Tinsley and others, 1985). Among the more spectacular examples of a bearing-capacity failure was the tilting of four four-story buildings, some as much as 60 degrees, in the Kwangishicho apartment complex during the 1964 Niigata, Japan, earthquake (National Research Council, 1985). Buoyant buried structures such as gasoline storage or partially empty septic tanks may float upward in thick layers of liquefied soils as a result of a loss of bearing strength (Tinsley and others, 1985). Buried septic tanks rose as much as one meter (three feet) during the 1964 Niigata earthquake (Tinsley and others, 1985).

Ground oscillation takes place when liquefaction occurs beneath the ground surface below soil layers that do not

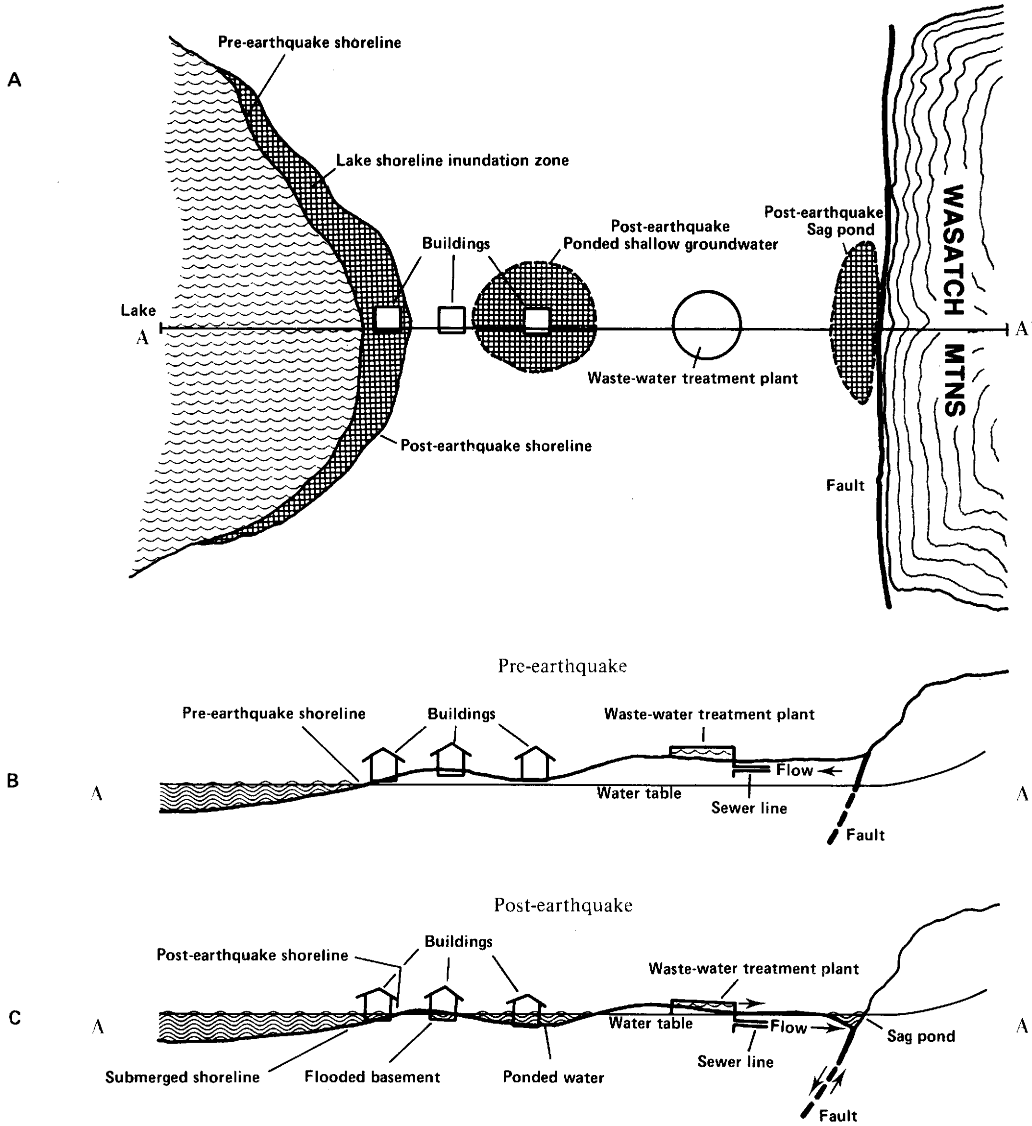

Figure 9. Schematic diagram of phenomenon that may occur due to tectonic subsidence. The sketch is not to scale. Cross sections are between points A-A' on the map (modified from Robison, 1990b).

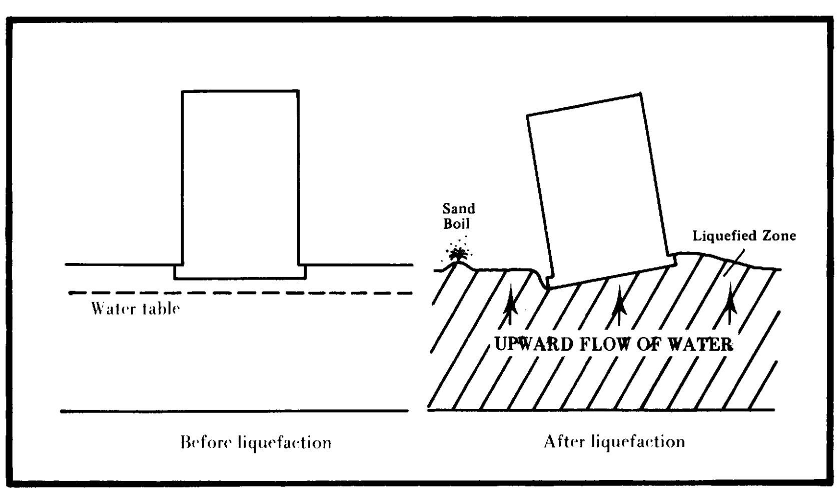

Figure 10. Tilting of a building due to liquefaction and loss of bearing strength in the underlying soil (modified from Youd 1984, in National Research Council, 1985).

liquefy, and where slopes are too gentle for lateral displacement to occur (figure 11) (Tinsley and others, 1985). Under these conditions, "liquefaction at depth commonly decouples overlying soil blocks, allowing them to jostle back and forth on the liquefied layer during an earthquake" (National Research Council, 1985). The decoupled layer vibrates in a different mode than the underlying and surrounding firm ground, causing fissures to form and impacts to occur between oscillating blocks and adjacent firm ground (National Research Council, 1985; Tinsley and others, 1985). Overlying structures and buried facilities can be damaged due to this type of ground failure as a result of ground settlement, the opening and closing of fissures, and sand boils which commonly accompany the oscillations (Tinsley and others, 1985).

Where the ground surface slope ranges between 0.5 and 5.0 percent, failure by lateral spreading may occur (figure 12) (Anderson and others, 1982). Lateral spreads occur as surficial blocks of sediment are displaced laterally downslope as a result of liquefaction in a subsurface layer (National Research Council, 1985). The surface layer commonly breaks up into blocks bounded by fissures which may tilt and settle differentially with respect to one another (National Research Council, 1985). The ground surface can be displaced laterally several yards, perhaps tens of yards, depending on soil and ground-water conditions and the duration of earthquake shaking (Tinsley and others, 1985). Lateral spread landsliding can be especially destructive to pipelines, utilities, bridge piers, and other structures with shallow foundations (Tinsley and others, 1985). Lateral spread landslides with ground displacements of only a few feet caused every major pipeline break in San Francisco during the 1906 earthquake (Youd, 1978a); hence, liquefaction was largely responsible for the inability to control the fires that caused 85 percent of the damage to the city (Tinsley and others, 1985).

Where ground surface slopes are steeper than about 5.0 percent, slope failure may occur in the form of flow landslides (figure 13) (Anderson and others, 1982). Flow failure is the most catastrophic mode of liquefaction-induced ground failure (Tinsley and others, 1985). Flow landslides are comprised chiefly of liquefied soil or blocks of intact material riding on liquefied layers (National Research Council, 1985). Flow failures can cause soil masses to be displaced tens of yards; under favorable conditions, flow failures have displaced materials miles at relatively high velocities (Tinsley and others, 1985). Extensive damage due to flow landslides occurred in the cities of Seward and Valdez, Alaska, during the 1964 Alaska earthquake (Tinsley and others, 1985). A flow landslide during the 1906 San Francisco earthquake knocked a powerhouse from its foundation near the Mount Olivet Cemetery (Youd, 1973).

Anderson and others (1982, 1990) have produced liquefaction-potential maps for the Ogden area. Large areas of Weber and Davis Counties have moderate to high potential for liquefaction during earthquake ground shaking, including most of the area west of I-15. For high liquefaction-potential areas, the approximate probability that the critical acceleration needed to induce liquefaction in susceptible soils will be exceeded in 100 years is greater than 50 percent. Seven slope failures covering a combined total of more than 62 km^2 (24 mi^2) have been mapped in Weber and Davis Counties and interpreted as prehistoric lateral-spread failures probably induced by past earthquake ground shaking (Van Horn, 1975a, 1982; Miller, 1980; Anderson and others, 1982; Nelson and Personius, 1990; Harty, 1991). The Utah Geological Survey is presently mapping and studying the history of movement on these landslides (Lowe and others, 1991).

Seiches in Great Salt Lake — A seiche is the oscillation of the surface of a lake or other landlocked body of water; seiches vary in period from a few minutes to several hours. Seiches can be likened to the oscillations produced by the sloshing of water in a bowl or a bucket when it is shaken or jarred (Nichols and Buchanan-Banks, 1974). The magnitude of oscillation of the water surface is determined by the degree of resonance between the water body and the periodic driving force such as earthquake ground shaking and wind. When the periodic driving force is oscillating at the same frequency at which the water body tends to oscillate naturally, the magnitude of the oscillation is greatest. The oscillation may take the form of unusually large waves that break at considerable height and with great suddenness along the coastline (Costa and Baker, 1981).

The effects of seiches are in part determined by water depth, the configuration of the local shoreline, and the lake bottom. These parameters determine the lake's natural period of oscillation and inherent system of long waves, much as the natural frequency of a pendulum is determined by its physical characteristics (Lin and Wang, 1978). The system of long waves includes an infinite number of species of waves, usually called the normal modes. The fundamental mode refers to the wave with the longest wavelength. It is the fundamental mode that is generally observed during surging and seiching. The period of the fundamental mode of Great Salt Lake's South Arm is 6 hours (Lin and Wang, 1978). Studies from other areas have shown that seiches may raise and lower a water surface from inches to many yards, causing severe flooding and damage from wave action (Blair and Spangle, 1979).

Seiches may be generated by wind, landslides, and/or earthquakes (ground shaking, surface fault rupture, and earthquake-induced landslides). The principle area at risk from seiches in the Ogden area is along the shore of Great Salt Lake, although seiches could also occur in reservoirs on streams east of Ogden. Wind seiches in Great Salt Lake have been studied and the maximum wave amplitude generated by this type of seiche is expected to be about 0.6 m (2 ft) (Lin and Wang, 1978). No systematic or theoretical studies of landslide or earthquake-induced seiching in Great Salt Lake have been completed. Seiches were reported along the southern shoreline of Great Salt Lake at Saltair and at the trestle at Lucin during the magnitude 6 Hansel Valley earthquake of October 5, 1909 (Williams and Tapper, 1953). The elevation of Great Salt Lake was 1280.8 m (4202.0 ft) on October 1, 1909 (U.S. Geological Survey lake elevation

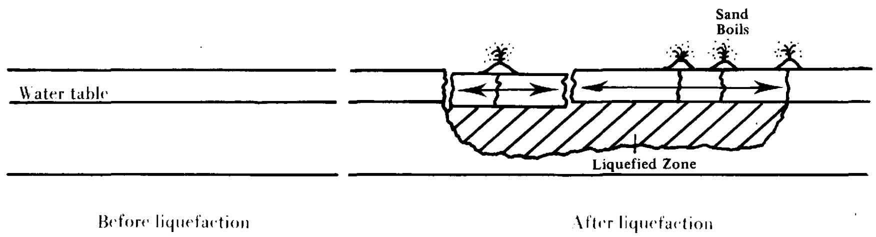

Figure 11. A diagram of liquefaction-induced ground oscillation (modified from Youd, 1984, in National Research Council, 1985). Liquefaction occurs in the cross-hatched zone.

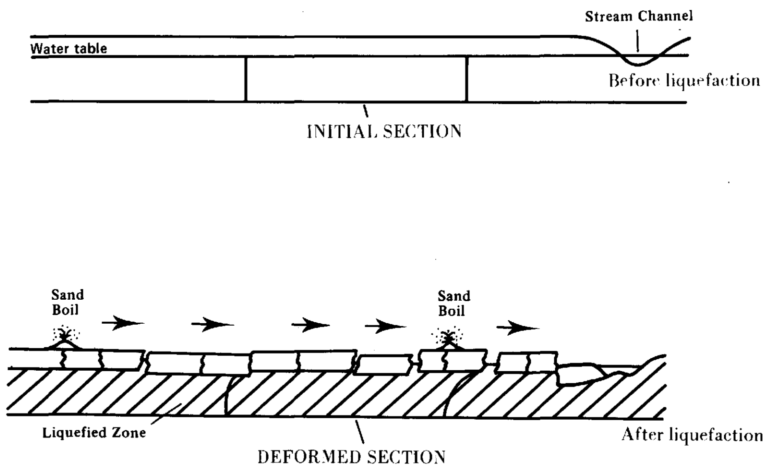

Figure 12. Diagram of a lateral spread (modified from Youd, 1984, in National Research Council, 1985). Liquefaction occurs in the cross-hatched zone. The ground surface slopes slightly to the right.

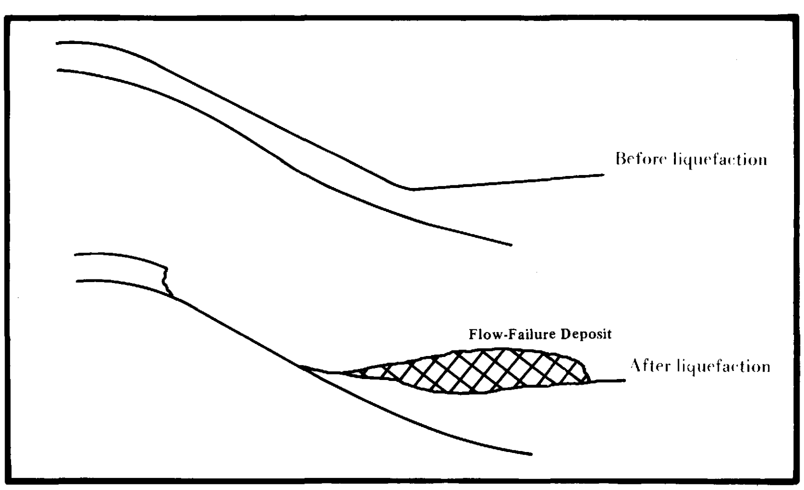

Figure 13. Diagram of a flow failure (modified from Youd, 1984, in National Research Council, 1985). Liquefaction beneath the ground surface causes a loss of shear strength, allowing the soil mass to flow down the steep slope.

records). The seiche generated by the 1909 Hansel Valley earthquake overtopped the Lucin cutoff railroad trestle which had an elevation of 1284.7 m (4214.85 ft) (Southern Pacific Transportation Company records). Assuming that reports of the seiche overtopping the trestle are true and that lake and trestle elevation records were accurately reported, the seiche wave generated by the magnitude 6 Hansel Valley earthquake was more than 3.5 m (12 ft) high (Lowe, 1990a).

Mass Wasting

Landslides — Landsliding historically has been one of the most damaging geologic processes occurring in the Ogden area, where more than a thousand landslides have been mapped (unpublished maps; Weber County Planning Commission, 1988; Davis County Planning Commission, 1988). Costa and Baker (1981, p. 243) define landslides as "mass movements of rock or soil downslope under the direct influence of gravitational forces without an aiding transporting medium such as water, air, or ice." The term landslides, as used in this paper, includes rotational and translational slides and associated earth flows (figure 14; Varnes, 1978). Landslides may be caused by any of several conditions, including: 1) oversteepening of slopes, 2) loss of lateral support, 3) weighting of the head, 4) increased pore pressure, and 5) earthquake ground shaking. Older landslides may be particularly susceptible to reactivation due to conditions which exist in a displaced soil mass such as increased permeability and established failure planes (Robison and Lowe, 1990a).

Landslides are likely to occur in the Odgen area if a moderate to strong earthquake occurs in northern Utah. Ground failures, including landslides, commonly accompany earthquakes with magnitudes greater than 4.5 (Keefer, 1984). Some form of landslide or ground failure (predominantly rock fall or rockslide) has been noted in the descriptions of 12 earthquakes that occurred in or immediately adjacent to Utah from 1850 to 1986 (magnitudes 4.3 to 6.6) (Keaton and others, 1987). Future earthquakes of magnitude 7.0-7.5 could cause slope failures as far as 300 km (185 mi) from the epicenter (Keaton and others, 1987).

Landslides are also likely to occur in years of abnormally high precipitation. Many landslides occurred in the Ogden area during the most recent wet cycle (1982-1985), causing significant damage to homes and property. Most of this damage was caused by the Memorial Day 1983 Rudd Canyon debris flow which damaged 35 houses, 15 severely (Lowe and others, 1989). This debris flow, which resulted in deposition of more than 80,000 m^3 (100,000 yd^3) of earth material at the canyon mouth, was initiated by landsliding of less than 15,300 m^3 (20,000 yd^3) near the head of Rudd Canyon in the Wasatch Range (Wieczorek and others, 1983). Landslides also occur during dryer periods, however; examples include the "railroad landside" in Washington Terrace landslide complex in 1981, and the Rainbow Gardens landslide in Ogden River landslide complex in 1987 (see field trip road log, Stop 4).

Several geologic units in the Ogden area are susceptible to landslides. The Precambrian Farmington Canyon Complex weathers in a manner which provides much unstable hillside

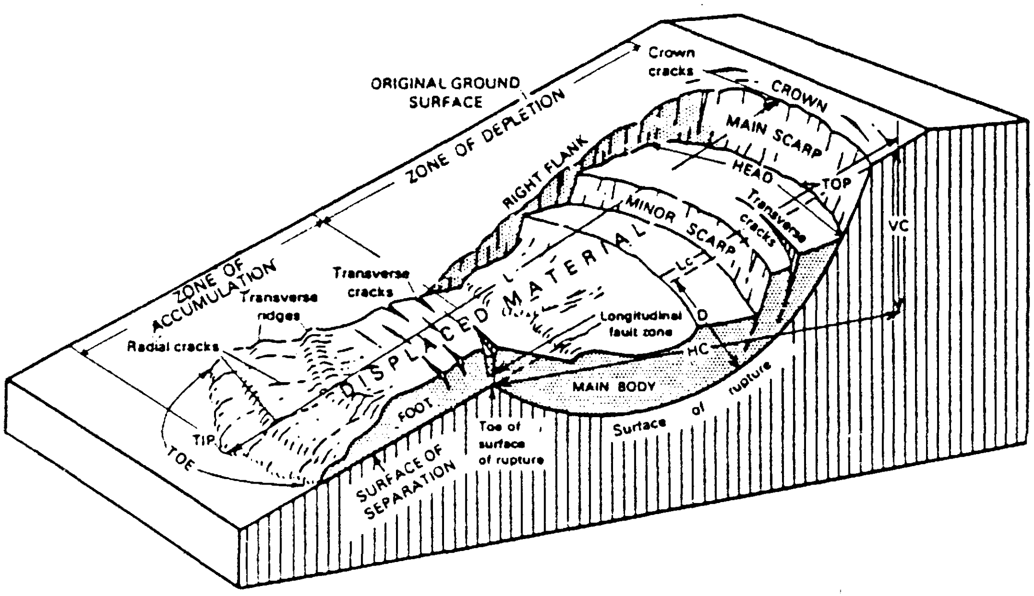

Figure 14. Block diagram of features commonly associated with a rotational slump and earth flow. The surface of rupture (failure plane) is planar, like the surface of separation beneath the foot, for translational landslides (adapted from Varnes, 1978).

debris (colluvium), and debris slides are common. Debris slides in colluvium derived from the Farmington Canyon Complex were responsible for initiating many of the debris flows which occurred in the Ogden area in 1983 and 1984. Other landslide-prone bedrock units include the Precambrian Perry Canyon and Maple Canyon Formations, and the Cambrian-age Maxfield Limestone, Ophir Shale, and Nounan Dolomite.

Landslides are also common in areas underlain by the sediments of Pleistocene Lake Bonneville. Rotational landslides (slumps) are particularly common where stream incision into the Weber River delta has created high bluffs and exposed silts and clays deposited during the high stand of Lake Bonneville. Numerous springs along these bluffs increase the landslide susceptibility of the area. Areas of landsliding in the Weber River delta area include the Washington Terrace, South Weber, and Ogden River landslide complexes (Pashley and Wiggins, 1972). Landslides also occur where smaller streams have eroded into the delta deposits near Layton and Kaysville.

Debris Flows — Debris flows are mixtures of water, rock, soil, and organic material (70-90 percent solids by weight; Costa, 1984) that form a muddy slurry much like wet concrete, and flow downslope, commonly in surges or pulses, due to gravity. They generally remain confined to stream channels in mountainous areas, but may reach and deposit debris over large areas on alluvial fans at and beyond canyon mouths. The eastern portion of Davis County is particularly susceptible to debris-flow hazards because of the steep mountains and the weathering characteristics of the bedrock (the Precambrian Farmington Canyon Complex) which provides much unstable hillside debris (Wieczorek and others, 1983; Pack, 1985). Debris flows have occurred frequently in the Ogden area during historical time and have caused damage to property and loss of life (table 1).

Other forms of alluvial-fan sedimentation events are also considered in this section because debris flow, debris flood (hyperconcentrated streamflow), and normal streamflow form a continuum of sediment/water mixtures that grade into each other as the relative proportion of sediment to water changes and as stream gradient changes (Pierson and Costa, 1987). Deposition of sediment transported by these types of flows ultimately takes place on alluvial fans at and beyond canyon mouths. Deposition on alluvial fans is caused by the decrease in channel gradient and increase in channel area, resulting in a decrease in depth and velocity of flow and an increase in internal friction of the flowing debris as the stream leaves its constricted channel and enters the main valley floor (Jochim, 1986).

Table 1. Historical Ogden area debris flows.

DRAINAGE	YEARS	REPORTED DAMAGE OR LOSS OF LIFE
"Slide Canyon", North Ogden	1991	1 home destroyed, 8 received minor damage
Coldwater Canyon Creek	1983	basements filled with water and debris.
Waterfall Canyon	1923	
Lightning Canyon	1984	house damaged.
Middle Fork, Kays Creek	1947, 1953	
South Fork, Kays Creek	1912, 1923, 1927, 1945, 1947	
North Fork, Holmes Creek	1983	
South Fork, Holmes Creek	1917	
Baer Creek	1983	
Shepard Creek	1923, 1930, 1983	
Farmington Creek	1878, 1923, 1926, 1930, 1947,1983	1923 - 7 deaths, several houses damaged.
Rudd Creek	1983, 1984	1983 - 35 houses damaged, 15 severely.
Steed Creek	1923	
Davis Creek	1878, 1901, 1923	
Ricks Creek	1923, 1929, 1930	1923 - 1 house damaged; 1930 - 1 house damaged.
Parrish Creek	1930 (several events)	several houses destroyed, school damaged.
Stone Creek	1983	houses damaged.
Mill Creek	1983	

Data from (from Marsell, 1972; Croft, 1981; Wieczorek and others, 1983; and Lowe, 1990b).

Debris flows can form in at least two different ways. In the mountainous Wasatch Range east of the Ogden area, where cloudburst rainstorms are common, overland flow and flood waters can scour materials from the ground surface and stream channels, thereby increasing the proportion of soil materials to water until the mixture becomes a debris flow (Wieczorek and others, 1983). The size and frequency of debris-flow events generated by rainfall are dependent upon several factors including the amount of loose material available for transport, the magnitude and frequency of the storms, the density and type of vegetative cover, and the moisture content of the soil (Campbell, 1975; Pack, 1985; Wieczorek, 1987). Debris flows during the 1920s and 1930s in Davis County were generated by overland erosion during summer cloudburst storms which fell on watersheds depleted of vegetative cover by overgrazing and burning (Copeland, 1960).

Debris flows can also mobilize directly from debris slides. A debris slide is a type of landslide in which the material involved is predominantly coarse-grained debris, chiefly colluvium, and the form of movement is mainly translational (Varnes, 1978). A debris flow may be generated when the debris slide reaches a stream, or when the water content is increased in the debris slide by some other means until sufficient to permit flow. Debris flows during the springs of 1983 and 1984 in the Ogden area were mobilized from debris slides caused by rapid melting of an unusually thick snowpack (Wieczorek and others, 1983, 1989).

As the relative proportion of water to sediment increases with either the addition of more water or removal of sediment by deposition, debris flows become hyperconcentrated streamflows. Hyperconcentrated streamflows are often referred to as debris floods or mud floods. In hyperconcentrated streamflow, soil materials are transported by fast-moving flood waters (Wieczorek and others, 1983). Solids account for 40% to 70% of the material by weight (Costa, 1984). These flows can originate either through progressive incorporation of materials into flood waters or through dilution of debris flows (Waitt and others, 1983; Wieczorek and others, 1983). Because of difficulties in distinguishing hyperconcentrated streamflow from flood stages of normal streamflow, there is no adequate record of historical hyperconcentrated-streamflow events in the Ogden area.

In normal streamflow, solids account for less than 40% of the water/sediment mixture by weight (Costa, 1984). Snowmelt flooding in the Ogden area is a nearly annual event and abnormally high snowmelt floods occurred in 1922, 1952 (Marsell, 1972), 1983, and 1984. Snowmelt-induced flood magnitudes are somewhat predictable and depend on the volume of snow in the mountains and the rate of temperature increase in the spring. Summer cloudburst floods account for more localized but often very destructive flooding and can occur with little warning. Davis and Weber Counties experienced 86 cloudburst floods between 1850 and 1969 (Butler and Marsell, 1972). The clear-water flooding hazard has been significantly reduced in recent years by the construction of flood-detention structures and improvements in storm-sewer systems and stream channels.

The frequency of occurrence (recurrence) of debris-flow events in a drainage basin depends upon climatic factors as well as the availability of debris (see field trip log, Stop 7). Recurrence intervals for different magnitude debris-flow events are not currently available for most drainages in the Ogden area.

Loss of life during debris-flow, hyperconcentrated-streamflow, and normal-streamflow events may result from drowning, high-velocity impact, or burial. The following discussion of damages associated with debris flows is taken chiefly from Campbell (1975). The effects on residential structures range from simple inundation to complete destruction by high-velocity impact. The velocity of a debris flow is an important consideration in determining the level of damage to structures. Many debris flows move with speeds on the order of 12 m/sec (27 mi/h; 40 ft/sec), but others move as slowly as 0.3 m/sec (1 ft/sec) as they flow down relatively gentle slopes. Debris flows of sufficient volume and momentum have destroyed residential structures and moved the remains off their foundations. Debris flows of relatively small volume but high momentum have broken through outside walls and even completely through structures. Low-velocity debris flows may enter dwellings through open doors or push laterally through windows and doorways and flood interiors. All three types of flows may fill basements with mud, water, and debris, or pile debris around structures. Debris may also bury yards, streets, parks, driveways, parking lots, and any ground-level structure. In the distal portions of the alluvial fans, damage is usually comparatively minor, consisting primarily of mud and water damage to outer walls of buildings, basements, and yards.

Rock Fall — Rock fall occurs when erosional processes and gravity forces cause rock clasts to be dislodged from slopes (Nelson, 1988, 1990). Large rock masses, traveling at relatively high velocities, can cause significant damage to structures and threaten lives. Potential clast sources in the Ogden area include outcrops broken by bedding surfaces, joints, or other discontinuities (which are common in the Tintic Quartzite near Ogden), and boulders on Bonneville lake-cycle shoreline benches. Case (1987, 1988) mapped rock-fall sources on mountain-front spurs along the Wasatch Front, including the Ogden area. Rock-fall clasts may travel great distances by rolling, bouncing, and sliding down slopes. Triggering mechanisms for rock falls include water in outcrop discontinuities and earthquake ground shaking (Nelson, 1990). Rock falls may occur in earthquakes as small as magnitude 4.0 (Keefer, 1984). In the Ogden area, rock falls have caused problems along canyon roads by blocking traffic or occasionally striking vehicles. Historical rock-fall damage has also occurred to homes in Ogden Canyon.

Problem Soils

Potential problem soils include collapsible (hydrocompactable) soils, compressible organic soils, and soils with a high shrink-swell potential. Problems with soils can also occur due to differential compaction when construction occurs on sediments with different characteristics. Erickson and others (1968) mapped the soils in the Ogden area. Soils mostly have only low to moderate shrink-swell potential, but soils of the Kirkham series have a high shrink-swell potential (Erickson and others, 1968). In Ogden and Morgan Valleys, east of the Wasatch Range, much more serious shrink-swell problems occur in soils derived from the pyroclastic Tertiary Norwood Tuff. Compressible organic soils may occur in areas of former swamps or shallow lakes; peat deposits have been identified in Centerville and Bountiful, just east of I-15.

Shallow Ground Water

The term ground water refers to water in saturated zones beneath the land surface. Ground water occurs in fractures and pore spaces in rock and fills voids between grains in unconsolidated deposits (clay, silt, sand, and gravel) at various depths throughout Utah. Ground water is considered to be shallow where the water table is within 9 m (30 ft) of the ground surface.

Problems from shallow ground water generally arise only when the saturated zone is within about 3 m (10 ft) or less of the ground surface because this is the depth to which many building foundations are excavated. Shallow ground water is a significant factor which must be considered when siting waste-disposal facilities and septic-tank soil-absorption systems. Liquefaction can occur in saturated sandy soils to depths of 9 m (30 ft) during earthquakes and result in ground failure (Youd and others, 1978a).

Problems associated with shallow ground water are described in Robison and Lowe (1990b, 1990c) and summarized below. The most significant hazard associated with shallow ground water is the flooding of subsurface facilities (such as basements), utility lines, and septic-tank soil-absorption fields. Structures extending below the water table may experience water damage to foundations as well as contents. Landfills and waste dumps may become inundated and contaminate aquifers. Underground utilities may also experience water damage. Septic-tank soil-absorption fields can become flooded which may cause ground-water contamination as well as system failure. Roads and airport runways may buckle or settle as bearing strength in susceptible soils are reduced by saturation. Wetting of collapsible or expansive soils by ground water may cause settlement or expansion and damage to foundations and structures.

Dissolution of subsurface materials and soil piping causing sinkholes and collapse-induced depressions may also be caused by shallow ground water. Water flowing through bedrock fissures in limestone or gypsiferous rocks can dissolve the rock and create holes which may collapse. Sinkholes and piping can occur in unconsolidated sediments as water flowing through conduits beneath the ground surface erodes sediments to create cavities ("pipes") which may collapse.

Because shallow ground water lies close to the ground surface, contaminants are easily introduced. Pollutants will flow with the ground water and may enter deeper aquifers or seep into wells. About 85 percent of the Utah's wells are located within basin-fill aquifers, and some are becoming increasingly contaminated (Waddell and Maxell, 1987).

Depth to shallow ground-water maps have not been produced for the Ogden area. However, regional maps indicate that depth to ground water may be less than 3 m (10 ft) in many areas (Hecker and others, 1988). Perched ground water is present at many locations in the Ogden area, especially along bluffs above streams incised into the Weber River delta.

Flooding

Stream Flooding — Stream flooding may be caused by direct precipitation, melting snow, or a combination of both. For rivers with large drainage basins and many tributaries, like the Weber River, the primary cause of flooding is rapidly melting snow, usually occurring from late April to early July (U.S. Army Corps of Engineers, 1969; Federal Emergency Management Agency [FEMA], 1982). Snowmelt floods are characterized by large-volume runoff, moderately high peak flows, and marked diurnal fluctuation in flow (FEMA, 1982). They are somewhat predictable because flood levels depend primarily on the volume of snow in the mountains and the rate of temperature increase in the spring. Prior to 1983, the largest snowmelt floods of record on the Weber River occurred in 1893, 1896, 1907, 1909, 1920, 1922, and 1952 (FEMA, 1980). More recently, snowmelt floods occurred in 1983, 1984, and 1985.

Localized, high-intensity, convective-type (cloudburst) thunderstorms centered over tributary areas are most effective in generating flooding in small drainage basins (Costa and Baker, 1981) such as are found in the Wasatch Range. Such storms, which last from a few minutes to several hours, generally occur between mid-April and September (FEMA, 1978; 1982) and usually are characterized by high peaks, high velocity, short duration, and small volume of runoff (FEMA, 1982). The flooding potential of cloudburst rainstorms is dependent upon many factors including: 1) the intensity or amount of rainfall per unit time, 2) the duration or length of time of rainfall, 3) the distribution of rainfall and direction of storm movement over a drainage basin, 4) soil characteristics, 5) antecedent soil-moisture conditions, 6) vegetation conditions, 7) topography, and 8) drainage pattern. Because many of these conditions are generally not known until rain is actually falling on critical areas, the magnitude of flooding from a given cloudburst storm is difficult to predict. Ogden area communities have experienced many cloudburst floods in historical times (table 2).

Lake Flooding — Fluctuating water levels are a problem with all types of lakes, but flooding can be especially acute on lakes which, like Great Salt Lake, have no outlet. Water-level fluctuations on lakes can be caused by both nature and man. Natural factors include precipitation, evaporation, runoff, ground water, ice, aquatic growth, and wind (FEMA, 1985). Man-induced factors include dredging, diversions, consumptive use of water, and regulation by engineering works (FEMA, 1985).

Lake-level fluctuations may be grouped into three categories: 1) long term, 2) seasonal, and 3) short term. Long-term fluctuations are the result of persistent low or high water-supply conditions for more than one year. Figure 15 shows the effects of long-term excess precipitation with respect to Great Salt Lake elevation. Long-term climatic trends play a major role in determining lake levels, as do diversions of water sources by man. The intervals between periods of high and low lake levels and the length of such periods during long-term fluctuations vary widely and erratically (FEMA, 1985). The extreme lake levels are likely to persist even after the factors which caused them have changed.

Seasonal fluctuations reflect the annual hydrologic cycle. Lakes are lowest in winter and generally rise in the spring due to melting snow, heavier rains, and cooler temperatures, until the lake peaks in the early summer (FEMA, 1985). During the summer, more persistent winds, drier air, and warmer temperatures intensify evaporation; also the runoff and ground-water flow to the lake generally decrease significantly. As water supplied to the lake becomes less than the evaporation, the water level begins the downward trend to winter minima (FEMA, 1985). Great Salt Lake elevations generally fluctuate approximately 0.6 m (2 ft) between winter low and summer high lake levels (figure 16).

Short-term fluctuations are caused by strong winds and sharp differences in barometric pressure (FEMA, 1985). These fluctuations usually last less than one day and do not represent any changes in the amount of water in the lake.

Lake flooding in the Ogden area is confined to the area around Great Salt Lake. In prehistoric time, water levels in lakes occupying the Great Salt Lake basin, such as Lake Bonneville, are known to have fluctuated with great elevation differences between high and low stands (figure 17). Geologic evidence indicates that Great Salt Lake reached a post-Lake Bonneville high of approximately 1,286.6 m (4,221 ft) about 2,000 years before present (Murchison, 1989). Archaeological evidence suggests that Great Salt Lake was at 1,285.3 m (4,217 ft) sometime during the 1600s (Utah Division of Comprehensive Emergency Management, 1985; Murchison, 1989). Until the spring of 1986, the historic high of Great Salt Lake was about 1,283.7 m (4,211.5 ft) (Arnow, 1984). This level was reached in the early 1870s and is based on a relative elevation estimate of water depth over the Stansbury bar (Gilbert, 1890). Direct measurements of the lake's elevation have been recorded since 1875 (Currey and others, 1984). The lake dropped slowly from its high in the 1870s, reaching an historic low of 1,277.52 m (4,191.35 ft) in 1963. Above-average precipitation in recent years caused Great Salt Lake to attain a new historical high of 1,283.77 m (4,211.85 ft) in June, 1986, and April, 1987 (U.S. Geological Survey records). This rise in lake level caused significant damage to structures and property along the shoreline and within the lake (power lines, causeways, dikes, buildings, and refuse dumps). Figure 18 summarizes historical levels of Great Salt Lake and illustrates that significant lake fluctuations can occur within a relatively short time.

Table 2. Historic cloudburst floods, Ogden area, Utah.

CITY	YEAR
Bountiful	1908, 1922, 1938, 1948, 1951, 1954, 1955, 1957, 1961, 1968, 1969, 1972, 1977 (2), 1980
Centerville	1901, 1904, 1923, 1930 (3), 1932
Farmington	1878, 1901, 1912, 1923, 1926 (2), 1929, 1930 (4), 1931, 1932, 1936, 1957, 1963, 1969
Kaysville	1892, 1917, 1947
Layton	1967
Clearfield	1953, 1967
Sunset	1963
Syracuse	1956
Uintah	1975, 1981
Riverdale	1956
Roy	1960
Ogden	1888, 1901, 1905, 1908, 1912, 1913 (2), 1916 (2), 1917, 1920, 1921, 1926, 1929, 1930 (2), 1931, 1941, 1942, 1943, 1945, 1947, 1949, 1951, 1955, 1956, 1960, 1963, 1964, 1965, 1966, 1967, 1968, 1973, 1975, 1979
Pleasant View	1961
Harrisville	1991
North Ogden	1991

Data from (Utah Division of Comprehensive Emergency Management, 1981).

Dam-Failure Inundation — Flooding may also result from dam failure. Dam failures generally occur with little warning, and the severity of flooding depends on the size of the reservoir impounded behind the dam and the extent of failure.

The term dam failure includes all unintentional releases of water from manmade dams, including complete failure and release of all impounded water. Only 8 of 33 dam failures documented in Utah prior to 1984 were complete failures; most of these failures were due to overtopping and/or erosion around spillways and outlets during flood events (Harty and Christenson, 1988). Dam failures have also occurred, however, due to structural and foundation failures caused by landsliding, seepage, and piping (Dewsnup, 1987). Most historical dam failures in Utah have been small dams in rural areas; larger dams are less prone to failure because of more rigorous design, construction, and inspection practices (Harty and Christenson, 1988). Earthquake-induced ground shaking, surface faulting, liquefaction, tectonic subsidence, landslides, and seiches, may occur in the Ogden area and could cause dam failures. Failures of dams upstream of the area could result in flooding and failure of other dams downstream. This is particularly true along the Weber River and its tributaries, where four dams (Wilkinson, Echo, Wanship, and Smith-Morehouse) are located upstream of the Wasatch Front, and the Ogden River, where two upstream dams (Causey and Pineview) have been constructed.

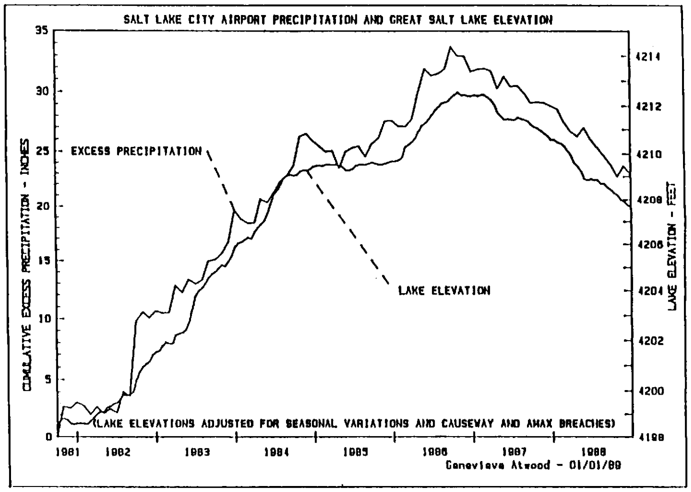

Figure 15. Graph showing the effect of recent cumulative excess precipitation on Great Salt Lake elevation. Lake elevations have been adjusted to remove seasonal water-level variations and the effects of the Great Salt Lake causeway and Amax dike breaches (Atwood and Mabey, written commun., 1989.)

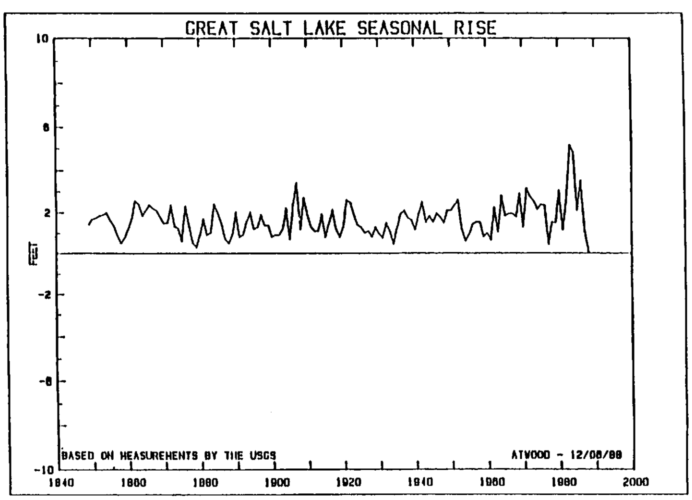

Figure 16. Graph showing the seasonal rise of Great Salt Lake (Atwood and Mabey, written commun., 1989).

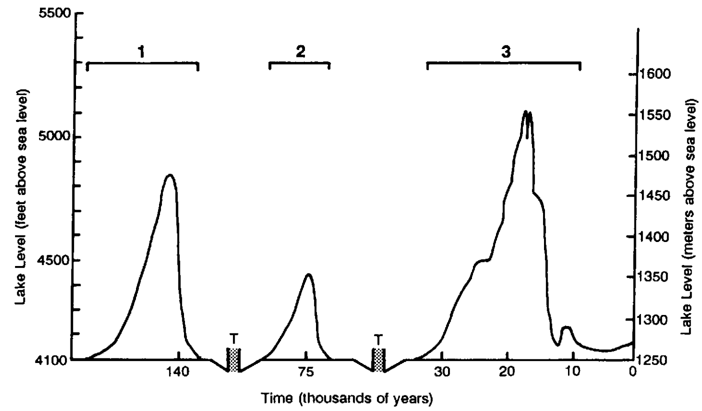

EXPLANATION

1 - Little Valley lake cycle.
2 - Cutler Dam lake cycle.
3 - Bonneville lake cycle.
T - Splice point on graph. Periods of time during interlacustrine phases have been removed to condense graph.

Figure 17. Schematic diagram showing a hydrograph of probable lake levels in the Lake Bonneville (Great Salt Lake) basin for the past 150,000 years. Numbered solid lines above lake-level curves represent time periods when lakes in the basin stood at high levels. Dashed lines represent time periods when lakes in the basin stood at low levels or were nonexistent (modified from Currey and Oviatt, 1985, by Machette and others, 1987, with additional modifications for this report.

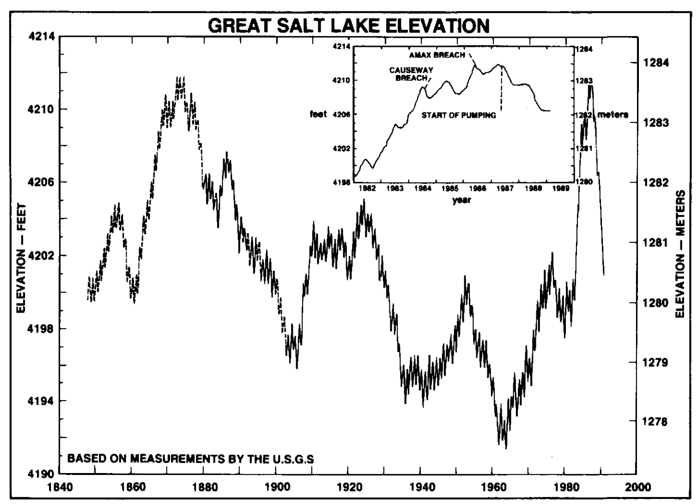

Figure 18. Historical Great Salt Lake hydrograph (modified from Atwood and Mabey, written commun. 1989.)

Effects of Flooding

Loss of lives due to drowning may occur where floodwaters are deep or flowing with high velocity. Water damage accompanies all types of floods and the amount of damage largely depends upon depth of inundation. The damage potential of floodwaters increases dramatically with increases in floodwater velocity (FEMA, 1985). High-velocity floodwaters can cause structures to collapse due to pressures applied by fast-moving water. Moving water can also induce erosion and can undermine structures. The damage potential of floodwaters may be increased hundreds of times when they contain substantial amounts of rock, sediment, ice, or other materials (FEMA, 1985). Areas subject to rapid inundation by floodwaters or flash floods pose special threats to life and property because there is insufficient time for evacuation, emergency floodproofing, or other protective measures (FEMA, 1985).

In areas where flooding may be of long duration, such as along lake shorelines, water damage to structures can be especially serious. This flooding generally is not life-threatening, but may produce permanent property loss or damage. Along the shore of Great Salt Lake the problems associated with flooding are compounded by the presence of salt in the water.

GEOLOGIC HAZARDS AND LAND-USE PLANNING

County Geologist Program Geologic-Hazard Maps

From June 1985 to June 1988, the Weber County Planning Department and the Davis County Planning Department shared a County Geologist as part of the Wasatch Front County Hazards Geologist Program (Christenson, and others, 1987, 1989; Christenson, 1990). This program, which included other County Geologists serving Salt Lake, Utah, and Juab Counties, was conducted by the Utah Geological Survey utilizing funding provided through the U.S. Geological Survey National Earthquake Hazards Reduction Program (NEHRP). As a result of the County Geologist Program, surface-faulting, debris-flow, rock-fall, and landslide hazard maps (1:24,000 scale) and accompanying texts have been prepared for the Weber and Davis County Planning Commissions (Lowe and Christenson, 1990; Lowe, 1990d, 1990e). These products, which are available at the Davis and Weber County Planning Departments, are intended for use by land-use planners and other local government officials, developers, consultants, real estate agents, and prospective home buyers. The maps delineate special-study areas where site-specific studies should be required to address the potential existence of geologic hazards and recommend, if necessary, avoidance or mitigation measures prior to planning commission approval of proposed developments. Technical information regarding the nature of each hazard, its potential consequences, the scope of site investigations needed to evaluate the hazard, and commonly used hazard-reduction techniques have been translated and summarized in reports which accompany the maps. The procedure recommended for use of the products for land-use planning is also included.

The special-study area for surface fault rupture is defined along all active faults by a buffer zone extending 500 feet from the outermost mapped fault scarps. The rock-fall, debris-flow, and landslide hazard special-study areas automatically include all hillsides with slopes greater than 30 percent because slope failures are most common on these slopes and local ordinances restrict building on such grades. Landslide special-study areas extend to slopes less than 30 percent where slope-failure inventory maps, which were compiled as part of the County Geologist Program, identify known landslide deposits. Debris-flow special-study areas extend to slopes less than 30 percent in depositional areas on younger Holocene alluvial fans. Slopes less than 30 percent are included in rock-fall special-study areas based on computer-modeled runout paths.

Other Geologic-Hazard Maps

Other maps depicting geologic hazards in the Ogden area have been produced by a number of investigators. In 1976, a series of 17 thematic maps, which included plates addressing geologic hazards in Davis County, were prepared for the Davis County Planning Commission by the Utah Geological Survey (Kaliser, 1988). Ridd and Kaliser (1978) produced geologic-hazard maps as part of a sensitive-area study for the City of North Ogden. In 1980, the Davis County Planning Commission conducted a foothill development study which included another set of maps depicting geologic-hazard maps for Davis County. Dames & Moore (1980) produced geologic-hazard maps covering a portion of Ogden City for the Ogden City Planning Commission. U.S. Geological Survey NEHRP funding was used to produce maps depicting liquefaction potential (Anderson and others, 1982; 1990), tectonic subsidence (Keaton, 1986; 1987), and seismic slope stability (Keaton and others, 1987).

Geologic-Hazards Ordinances

Whereas most subdivision ordinances have elements which allow planning commissions to require geologic-hazards reports prior to the approval or disapproval of proposed subdivisions, a number of ordinances have been adopted in the Ogden area which are designed to reduce the potential impact of geologic hazards. In 1977, the City of North Ogden adopted an ordinance dealing with sensitive areas, including geologic-hazard areas. In 1985, Ogden City adopted a sensitive area overlay zone ordinance which utilized work by Dames & Moore (1980). In 1983, Ogden City adopted an ordinance that requires existing buildings to be retrofitted for improved seismic safety when they change ownership or type of use. In 1988, the City of Washington Terrace adopted a development overlay zone ordinance addressing geologic hazards. In 1989, the City of Fruit Heights adopted a hillside overlay zone which included geologic-hazard areas.

FIELD TRIP ROAD LOG FOR GEOLOGIC HAZARDS OF THE OGDEN AREA, UTAH

Mileage		Description
Incremental	Cumulative	
0.0	0.0	Meet at Weber State University in Ogden at the parking lot east of Science Lab Building.
0.0	0.0	**STOP 1. Geologic hazards in the vicinity of the Weber State University (WSU) Campus.**

A number of geologic hazards have been identified in the vicinity of WSU. On the mountain front east of the campus, the bowl-shaped scar in the Tintic Quartzite on the mountain front above and east of WSU was the source area for the pre-Lake Bonneville College rock slide (figure 19) discussed by Pashley and Wiggins (1972; p. K3-K5). The landslide is buried by Bonneville lake cycle deposits which obscure the areal extent of the slope failure, but coarse bouldery quartzite debris has been exposed to the west of the source area at some locations in stream cuts (Pashley and Wiggins, 1972).

The WSU campus is located along the Wasatch fault zone (figure 20) and the highest fault scarp in the vicinity of the campus forms the 60-foot-high west-facing hill on which the east bleachers of the football stadium are constructed. Other fault scarps have been mapped along the hillside east of the campus (Nelson and Personius, 1990).

The Allied Health Sciences Building, built in 1984-85, as well as most of the other buildings at Weber State University, are built in the vicinity of the Wasatch fault zone. During 1984 geologists from the Utah Geological Survey (UGS) visited the foundation excavation for the Allied Health Sciences Building and observed several faults cutting Lake Bonneville deposits exposed in the excavation. Because the building was to be located approximately 183 m (600 ft) west of the main trace of the Wasatch fault, the UGS geologists raised questions concerning the activity of the foundation faults and the potential hazard that they would represent to the building. Previous work by Woodward-Clyde (Swan and others, 1980) on the Wasatch fault near Kaysville indicated that the main trace had experienced at least three and probably five surface-faulting events during the past 8,000 ± 2,000 years, and that the elapsed time since the most recent surface-faulting event was about 500 years or slightly less.

Mapping of the foundation excavation by Woodward-Clyde Consultants (1985) revealed that the faults are truncated by Provo-level beach deposits that were deposited between 11,000 and 13,000 years ago. This indicated that the foundation faults had not moved in the last 11,000 to 13,000 years, despite the fact that the nearby Wasatch fault had slipped several times. Woodward-Clyde Consultants (1985) concluded that the foundation faults were not direct splays of the Wasatch fault, and they hadn't acted as sympathetic faults that have slipped in conjunction with surface faulting on the Wasatch fault.

Woodward-Clyde Consultants (1985) suggested that the faults might represent seismically-induced slumping and lateral spreading or gravity-induced sublacustrine sliding at a time when the lake level was high and the deposits were saturated. They concluded, however, that the potential for future tectonic displacement on these faults is extremely low and that the faults do not pose a tectonic surface-faulting hazard to the Allied Health Sciences Building, which was subsequently constructed.

During 1970, a series of deep trenches were dug across the college campus for the purposes of constructing utility tunnels. Dr. Fred Pashley and Ray Wiggins of the Weber State University Department of Geology observed that Bonneville deposits in the trenches were broken by numerous steeply dipping normal faults, were tilted in various directions at fairly steep angles, and at places contained folds that were overturned to the northwest. They mapped 373 faults in 440 m (1443 ft) of trench. Pashley and Wiggins (1972, p. K11 & K16) theorized that the sediments, faults, and folds exposed in the trenches may have been part of a series of translational landslides that moved laterally from the mountain front toward the basin. The features in the Weber State University trenches were similar to features formed by translational

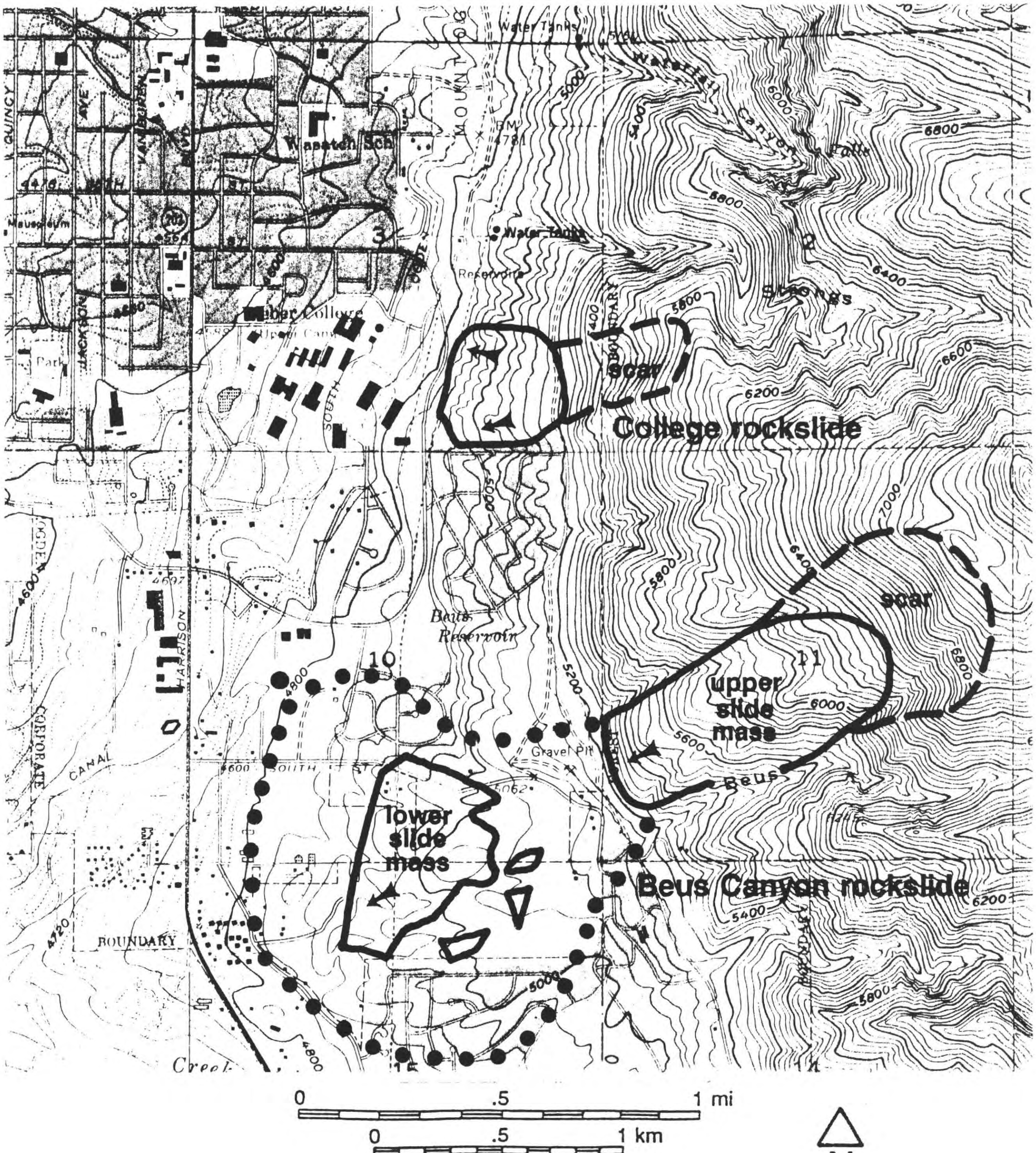

CONTOUR INTERVAL 40 FEET

EXPLANATION

Outline of exposed rockslide units

Outline of probable buried margin of landslide

Outline of rockslide scar

Direction of sliding

Figure 19. Map of the College and Beus Canyon rock slides (from Pashley and Wiggins, 1972).

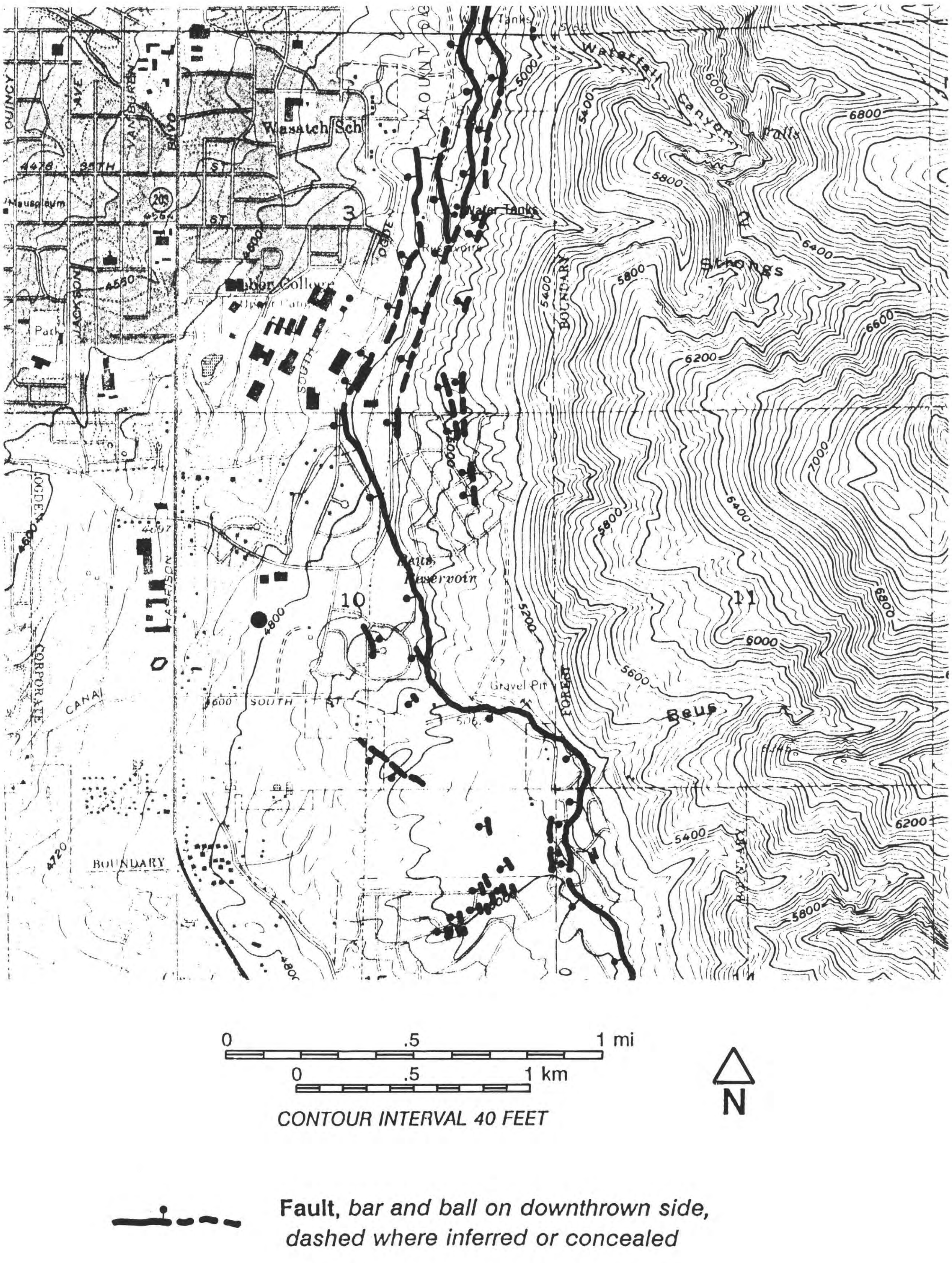

Figure 20. Fault scarps in the vicinity of Weber State University (from Nelson and Personius, 1990).

landsliding in Anchorage, Alaska, during the 1964 Alaskan earthquake.

Damage due to shallow perched ground water has occurred to several buildings on the Weber State University campus. Engineering solutions to the shallow groundwater problem have been required for some of the buildings.

0.0	0.0	Drive north to Campus Drive, turn left and drive west on Campus Drive.
0.2	0.2	Turn right and drive north on Birch Avenue.
0.1	0.3	Turn left and drive west on 36th street.
0.1	0.4	Turn right and drive north on Polk Avenue.
0.3	0.7	At the stop sign, turn right and drive east on Boughton Street.
0.2	0.9	Turn left and drive north on Taylor Avenue.
0.2	1.1	View to the right (east) of mouth of Waterfall Canyon. On Friday, August 13, 1923, a debris flow initiated by a cloudburst rainstorm falling on a watershed denuded by domestic-animal overgrazing caused a debris flow in Waterfall Canyon; debris was deposited westward to what is now Polk Avenue (one block to west) (Croft, 1981).
0.2	1.3	View to the right (east) of two scarps along the mountain front. The lower scarp along the east edge of Mount Ogden Park may be the main scarp of a lateral-spread landslide which underlies much of Ogden City, including Weber State University (described at Stop 1) (Nelson and Personius, 1990). The upper scarp, behind the buildings, is a tectonic scarp of the Weber segment of the Wasatch fault zone.
0.2	1.5	At the stop sign, turn right and drive east on 29th Street.
0.4	1.9	View of the main scarp of the Wasatch fault zone to the east on the south side of Taylor Canyon.
0.0	1.9	Turn left and drive north on Buchanan Avenue.
0.3	2.2	At the stop sign, turn left and drive west on 27th Street.
0.1	2.3	Turn right and drive north on Pierce Avenue.
0.1	2.4	The Cambrian Tintic Quartzite cliffs to the right (east) are extensively fractured and jointed. The boulders at the bottom of the cliffs indicate that rock fall from these cliffs has occurred in the past.
0.3	2.7	At the stop sign, turn right and drive east on 24th Street.
0.2	2.9	Turn left and drive north on Buchanan Avenue.
0.0-0.3	2.9-3.2	View of Tintic Quartzite cliffs to the east (right) behind the Ogden City Reservoir. This area has been mapped by Case (1987) as a potential source of rock-fall clasts. The Tintic Quartzite, at this location, is closely associated with very old compressional (thrust) faulting which has caused intensive fracturing, making it susceptible to rock falls and landsliding. Some of the fracture surfaces in the quartzite cliffs appear to have a valleyward dip. The numerous angular boulders at the base of the cliffs overlying Lake Bonneville deposits provide evidence that many rock falls have occurred at this location in the past 14,000 years. It is likely that rock falls will continue to occur at this location in the future, particularly during earthquake ground shaking. A slab failure, in which a section of these cliffs toppled onto the foothills sometime in the last 14,000 years, was mapped by Olson (1981). Lowe (1990e) constructed rock-fall hazard maps based on computer-modeled run-out paths (Pfeiffer and Higgins, 1988). These maps indicate that the rock-fall hazard area extends as much as 600 m (2,000 ft) west of the base of the cliffs (Lowe, 1990e). This indicates that homes east of Pierce Avenue could potentially suffer damage due to rock fall.
0.0	3.2	The road angles to the east at 22nd Street.
0.0	3.2	Between Buchanan Avenue and the base of the cliffs to the east (right) there are two west-facing normal faults associated with the Weber segment of the Wasatch fault zone (Nelson and Personius, 1990). This is one of the sites visited by G.K. Gilbert during his study of the Lake Bonneville basin. At this location, Gilbert studied the slickensided shear zones and fault gouge in bedrock, observed fault drag in Tintic Quartzite beds adjacent to the fault plane along the main trace of the fault, and mapped the prominent "cross fault" that strikes eastward in the quartzite cliffs (Gilbert, 1928; Nelson, 1988; Nelson and Personius, 1990). Gilbert used this cross fault (70° southwest dip), which joins the Wasatch fault (40° west dip) at this location, as an example of how preexisting structures can control the trace of the fault (Nelson and Personius, 1990). Gilbert concluded from his observations of the orientation and distribution of shear zones and gouge that incremental,

		normal displacement occurred along range-bounding faults (Nelson, 1988).
0.0	3.2	Continue north on Buchanan Avenue.
0.1	3.3	Turn right and drive east on 21st Street.
0.1	3.4	Turn left and drive north on 1850 E. Street.
0.1	3.5	The road turns to the west at 1950 S. Street.
0.0-0.1	3.5-3.6	The houses to the right (north) are located immediately south of the main scarp of an active landslide complex in the 60-meter-high (200 ft) bluff above the south side of the Ogden River (Pashley and Wiggins, 1972). The back yards of the homes have been gradually getting smaller as the main scarp recedes southward, primarily through erosion. This landslide complex will be discussed further at stop 4.
0.05	3.65	Turn left and drive south on Buchanan Avenue.
1.05	3.8	Turn right and drive west on 21st Street.
0.5	4.7	At the stop light, turn right and drive north on Harrison Boulevard.
0.3	5.0	Landslide terrain is visible on the hillside on the south side of the Ogden River to both the left (west) and right (east).
0.2	5.2	The Ogden River.
0.3	5.5	At the stoplight, turn right and drive east on Canyon Road.
0.4	5.9	Turn left and drive north on 1600 E. Street (Fillmore Avenue).
0.2	6.1	Turn right and drive east on 1300 S. Street.
0.2	6.3	View of Ogden River landslides to the right (south).
0.0	6.3	Turn left and drive north on Maxfield Drive.
0.2	6.5	Turn right and drive east on Hislop Drive. Stop at the end of the paved road. Walking, follow the dirt road to the east and then to the north to stop 2.

STOP 2. East Ogden Trench Site.

At this location (figure 21), in September, 1986, five trenches were excavated by the U.S. Geological Survey and the Utah Geological Survey across three scarps of the Wasatch fault zone (Nelson and others, 1987). The purpose of excavating trenches across these fault scarps was to determine: 1) how many surface-fault ruptures have occurred at this location in the recent geologic past, 2) when these ruptures occurred, and 3) how much offset accompanied each rupture.

The sediments exposed in the trenches consisted of thick (greater than 3 m; 10 feet) sequences of bouldery stream- and debris-flow deposits overlying deltaic sands and gravels which were probably deposited near the Provo level of the Bonneville lake cycle about 14,000 years ago (Nelson, 1988). Each prehistoric surface-faulting event formed a near-vertical scarp that gradually eroded back to the natural angle of repose for the alluvial-fan material, while discrete wedges of colluvial material were deposited at the base of the scarp. The number of stacked colluvial wedges exposed in the trench was used to estimate the number of surface-faulting events at the site. The thickness and geometry of the colluvial wedges adjacent to the faults, and displacement of stratigraphic units observed in the trenches, were used to estimate the height of the vertical scarp created by each surface-faulting event. Radiocarbon ages on concentrated organic material from soil A-horizons developed on the colluvial wedges were used to provide estimates of the times of surface-faulting events (Nelson, 1988; Forman and others, 1991).

The two easternmost scarps at the East Ogden site, like most scarps along the Wasatch fault zone, face west because the valley side (west side) has been dropped down relative to the mountain side (east side). The westernmost fault is an antithetic fault that faces east. Along this scarp deposits within the fault zone have been dropped down relative to the valley side. The fault scarps offset both upper Holocene and middle Holocene alluvial-fan surfaces (Nelson and Personius, 1990).

Trenches excavated across the west-facing scarps that offset middle Holocene alluvial-fan deposits (^{14}C dated at about 5,500 years before present) record about 5 m (16 ft) of total displacement on the easternmost scarp (trench 1), and 8 m (26 ft) of total displacement on the westernmost scarp (trench 2). The total displacement on these scarps where they offset upper Holocene alluvial-fan deposits is 1.2 (trench 5) and 1.8 m (trench 3) (4 and 6 ft), respectively (Nelson, 1988). The antithetic fault was trenched where it offset upper Holocene alluvial-fan deposits about 1 m (3.3 ft); this offset occurred during the most recent event on the westernmost west-facing scarp (Nelson and others, 1987).

Data obtained from trenching studies at the East Ogden site are summarized in figure 22. On the easternmost west-facing scarp, two surface-faulting events during the middle Holocene, each with about 2.2

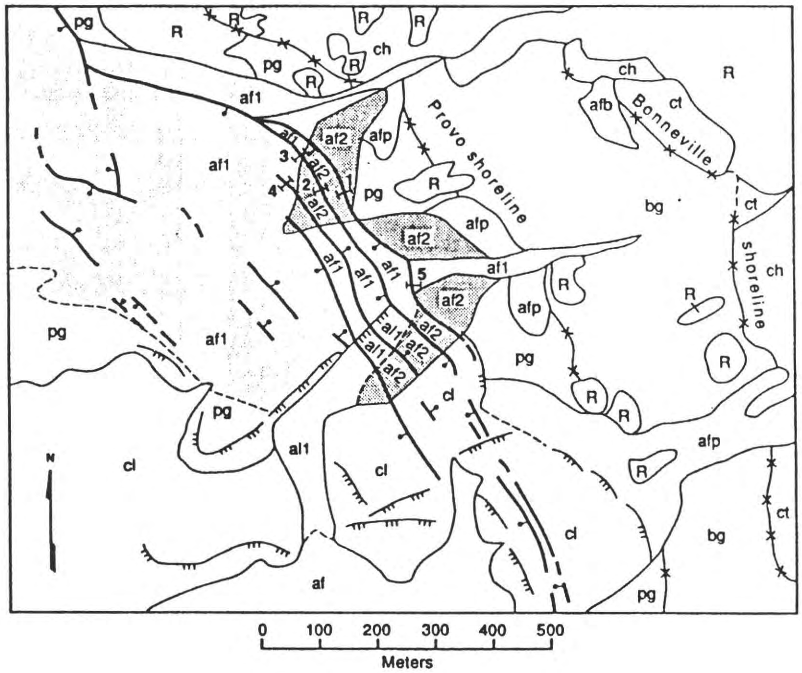

UNITS

al1 - stream alluvium, upper Holocene

Alluvial-fan deposits

af1 - upper Holocene

af2 - lower Holocene

afp - Provo phase

afb - Bonneville phase

pg - lacustrine gravel of Provo phase

bg - lacustrine gravel of Bonneville phase

ct - talus

cl - landslide deposits

ch - hillslope colluvium

R - bedrock

SYMBOLS

landslide scarp

fault scarp

shoreline

backhoe trench

Figure 21. Surficial geologic map of the East Ogden trench site (from Forman and others, 1991).

m (7 ft) of displacement, were followed by a late Holocene surface-faulting event with about 0.9 m (3 ft) of displacement. On the westernmost west-facing scarp, two surface-faulting events during the middle Holocene, with 2.5 and 3.5 m (8 and 11 ft) of displacement respectively, were followed by a late Holocene event with about 1.2 m (4 ft) of displacement. The age estimates for these events are, from oldest to most recent, 4,000 ± 500, 2,750 ± 250, and 1,200 ± 200 (Forman and others, 1991) yr B.P. respectively. Trench 3, on the easternmost west-facing scarp, showed evidence of a recent surface-faulting event with less than 0.6 m (2 ft) of displacement that may have occurred within the past 500-600 years (Nelson, 1988). This event was not identified in any of the other trenches.

In summary, there have been at least three, and possibly four, surface-faulting events at the East Ogden trench site since the approximately 5,500-year-old alluvial-fan sediments were deposited (Nelson, 1988). Displacements during these surface-faulting events range from less than 0.6 to 3.5 m (2-11 ft), the recurrence interval between events during the last 5,500 years has ranged from 400 to 2,000 years for an average recurrence interval of about 1,400 years, and the overall slip rate for the fault zone at this location during this period is about 2 m (7 ft)/ 1,000 years (Nelson, 1988).

View of Landslides and Faults South of the Ogden River

As you walk back to the vehicles, stop 2 also provides a good view to the south of landslides and fault scarps along the south side of the Ogden River. On each side of the Ogden River, clay, silt, and fine sand deposited offshore when Lake Bonneville stood at the Bonneville Shoreline about 15,000 years ago are overlain by a thin cap of deltaic sand and gravel which was deposited by the Ogden River as it flowed into

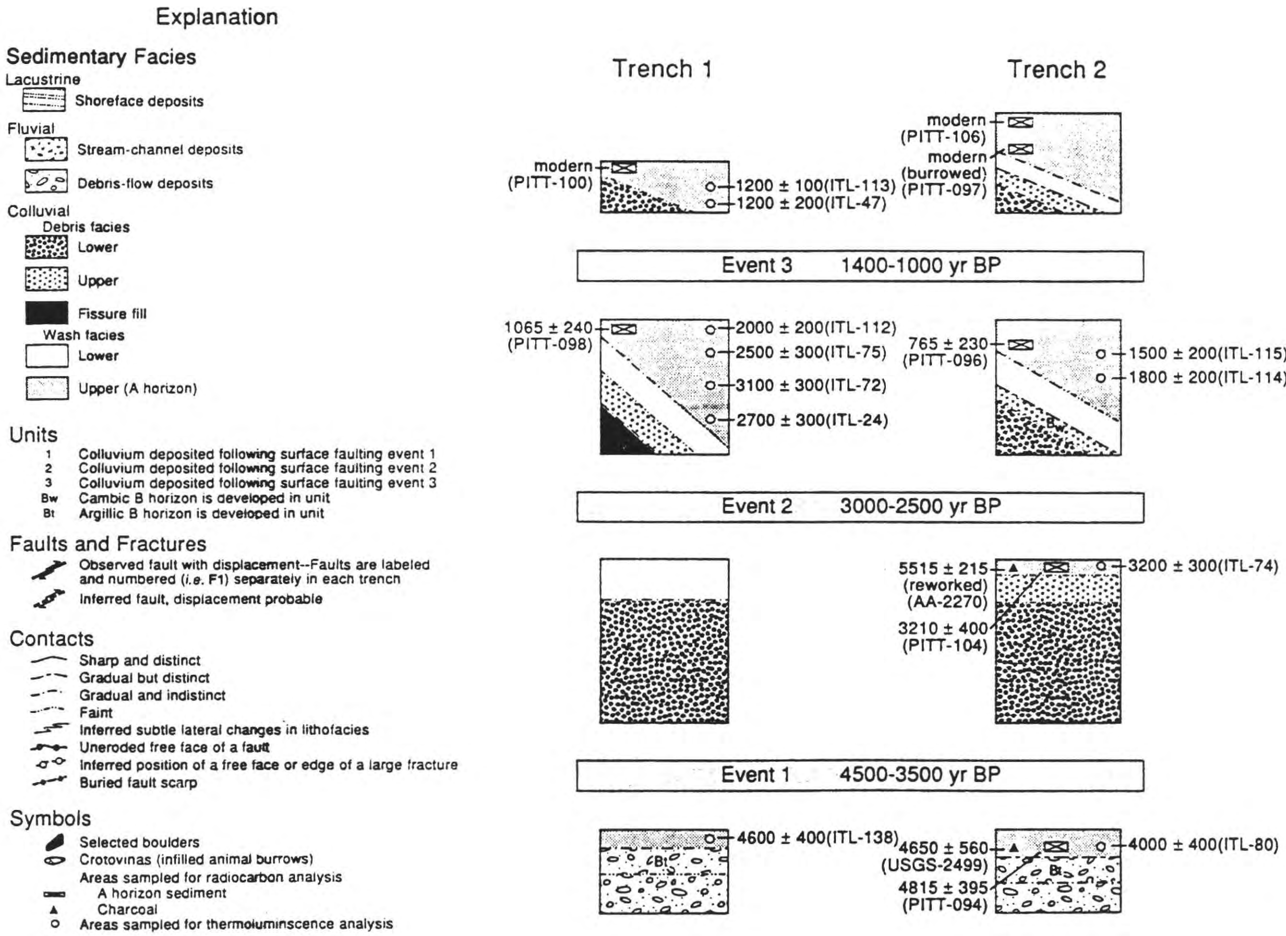

Figure 22. Schematic diagram of the position of samples and age estimates, and the correlation of sedimentary facies within sequences of debris-flow and colluvial deposits exposed in trenches 1 and 2, East Ogden trench site. The intervals of time for the surface-faulting events are based on the synthesis of the age estimates shown in the diagram (modified from Forman and others, 1991).

Lake Bonneville about 14,000 years ago. As Lake Bonneville slowly receded to lower elevations, the Ogden River cut down and eroded laterally into the offshore and deltaic sediments at the mouth of Ogden Canyon leaving bluffs which are steeper than the natural angle of repose of the sediments. These 60-meter-high (200 ft) bluffs have periodically failed by rotational slump/earth flow landsliding, creating two natural amphitheaters on the south side of the Ogden River (Pashley and Wiggins, 1972). The eastern portion of each amphitheater has been active in recent years.

0.0 6.5 Return to the vehicles. Make a U-turn. Drive west on Hislop Drive.

0.0 6.5 Turn right and drive north on Maxfield Drive,

0.3 6.8 Turn left and drive west on 9th Street.

0.6 7.4 Turn right and drive north on Harrison Boulevard (this road later becomes County Boulevard).

2.0 9.4 To the right (east) is a graben along the base of a Wasatch fault scarp.

0.3 9.7 The rocky deposits in the field to the left (west) are part of a pre-Lake Bonneville landslide (Nelson and Personius, 1990) which moved westward from the mountain front to the right (east).

0.3 10.0 The road forks. Take the right fork and drive north on Mountain Road.

0.0 10.0 To the front (north), the main scarp on the North Ogden lateral spread is visible to the left (west) and below the large white house. This lateral spread was first mapped by Miller (1980).

0.1 10.1 The canyon to the right is Garner Canyon. A man-made exposure at the mouth of the canyon provided additional information on past surface-faulting events along the Weber segment of the Wasatch fault zone. Four colluvial wedges produced by displacement along the main trace of the fault were visible in the exposure in 1985 (Nelson and Personius, 1990). Based on wedge stratigraphy, the vertical component of movement for each of the four events was about 1 m (3.3 ft) (Nelson and Personius, 1990). Radiocarbon dating of the two youngest wedges indicates that the two most recent surface-faulting events at this site occurred about 800-1,200 and 1,500-2,000 years ago (Nelson and Personius, 1990).

0.8 10.9 In the spring of 1983, rapid snowmelt caused shallow landsliding to occur near the head of Coldwater Canyon. This landsliding generated a debris flow which just reached the mouth of the canyon (Wieczorek and others, 1983). Landslides provided only part of the material; much was scoured from the channel of the creek as the earth/water mixture moved downstream. The deposits of the 1983 debris flow can be viewed just above the mouth of the canyon. Much of the muddy matrix, which was present in the debris flow during the 1983 event, was subsequently eroded away by Coldwater Canyon Creek, so the deposit now consists mostly of coarse bouldery debris. Several small landslides are present along the north side of the stream channel at the canyon mouth which were caused by channel scouring during the event.

Although the 1983 debris flow was the only known historical event from Coldwater Canyon, deposits at the mouth of the canyon provide evidence for at least one other, presumably prehistoric, debris flow. Debris-flow deposits generally have a ribbon-like morphology, and therefore it is possible that the Coldwater Canyon alluvial fan has been the site of numerous Holocene debris-flow events as the active distributary channel moved back and forth across the fan. The debris basin at the mouth of Coldwater Canyon was built after the 1983 event.

The steep hill behind the debris basin is a Wasatch fault scarp.

0.2 11.1 At the stop sign, turn left and drive west on 2600 N.

0.7 11.8 Turn right and drive north on 1050 E. Street.

0.8 12.6 Turn right and drive east on 3100 N. Street (North Ogden Canyon Road).

0.4 13.0 Pull off onto dirt road to right (south) and park. Walk east on North Ogden Canyon Road about 0.15 miles to stop 3.

STOP 3. Cameron Cove Debris Flow.

A debris flow from an unnamed canyon northeast of Stop 2 (figure 23) caused significant damage in the Cameron Cove Subdivision to the southwest on September 7, 1991. Prior to the debris-flow event, over a 24-hour period, rainfall in the North Ogden area ranged from 6.4 to 21.3 cm (2.5-8.4 in) (Brenda Graham, National Weather Service, oral commun., 1991). This set a new state record for a 24-hour period, and was estimated to be equivalent to a 1000-year storm (Mark Eubank, WeatherBank Inc., oral commun., 1991). Runoff from the storm was concentrated in channels on bedrock (Tintic Quartzite) cliffs at the head of the canyon (Mulvey and Lowe, 1991). During heavy rains, these channels often form waterfalls, cascading several hundred feet to talus slopes at the base of the cliffs (Bruce Dursteler, Mayor, North Ogden, personal commun., 1991). The concentration of heavy runoff apparently mobilized talus and debris in and near tributary channels at the base of the cliffs. As the tributary flows moved downstream and combined with the main channel, additional material was scoured from the channel and incorporated into the debris flow. The flow exited the canyon mouth and traveled down an alluvial fan for a distance of about 400 m (1,300 ft), where the debris damaged several houses in the Cameron Cove Subdivision. Flood waters associated with the storm and debris flow also caused widespread damage in the subdivision.

Examination of the main and tributary channels indicated that stream-channel material, from the base of the cliffs to the mouth of the canyon, had been incorporated into the debris flow. Depth of scour in the main channel averaged 1.5 to 1.8 m (5-6 ft), and in places as much as 4.6 m (15 ft). In general, the drainage-basin slopes did not appear to have contributed much material to the flow. However, on slopes below the cliffs just above 1,770 m (5,800 ft) in elevation there was evidence of contribution from slopewash erosion of drainage-basin soils. Grasses were absent in these areas, cobbles were left standing on pedestals of soil, and small rills were present. This is the only place damaged by the July 30 - August 3, 1990 wild fire that appears to have contributed sediment to the debris flow. Sediment contribution from the 1990 burned area was low because of the rapid revegetation of oakbrush, woody plants, and grasses.

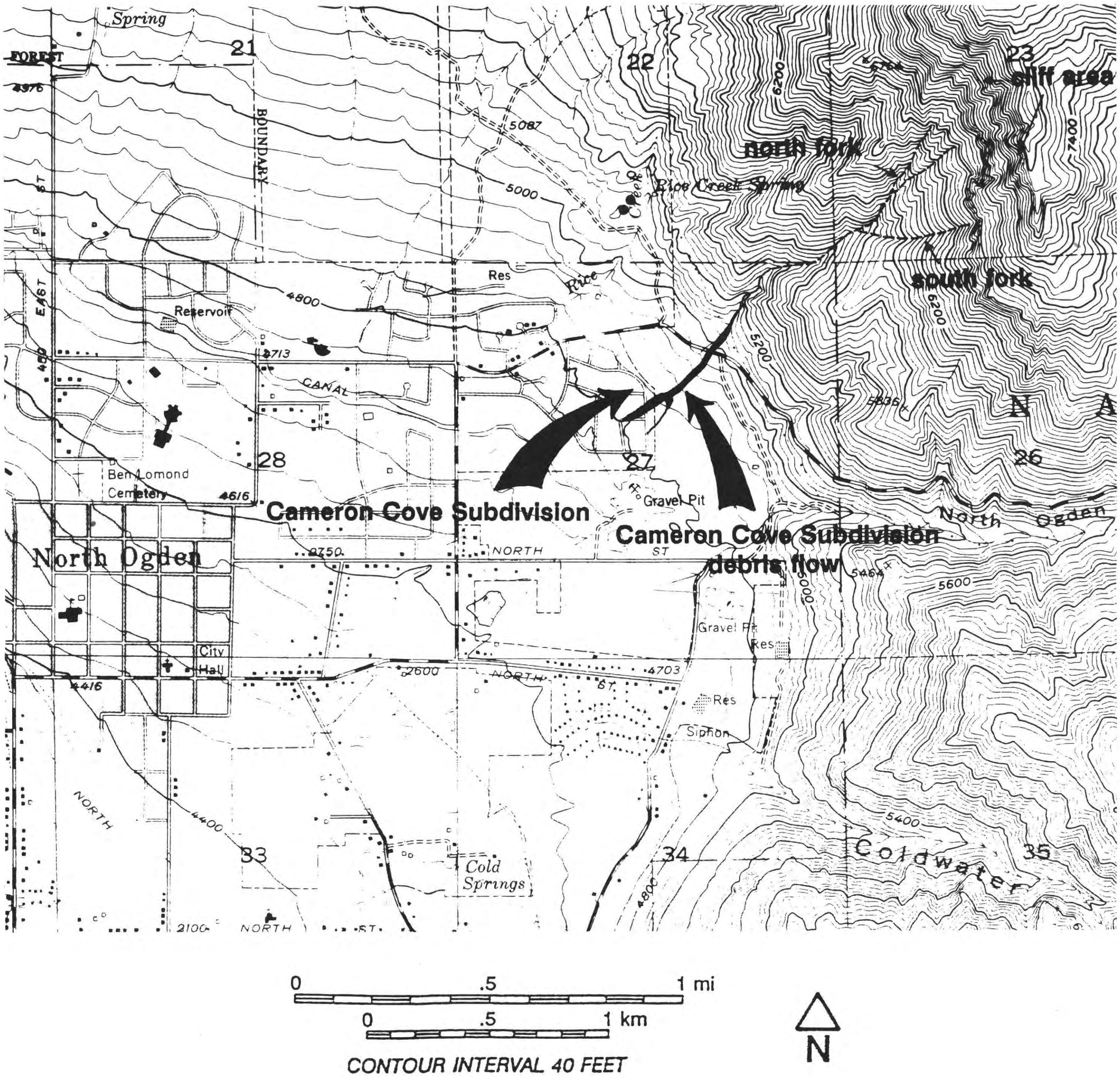

Figure 23. The Cameron Cove Subdivision debris flow, North Ogden, Utah (modified from Mulvey and Lowe, 1991).

Observations in the channel on September 9, 1991, indicated that much debris is still contained in and along the channel itself. Several natural dams composed of large boulders have considerable amounts of debris behind them. In many places along the channel, side-slopes have been destabilized by scour and undercutting of the channel banks. The volume of debris still in the channel is undetermined and accurate estimates of its volume may be difficult to make.

Measurements were made of the width and length of the debris-flow deposit from the mouth of the canyon to within 12 m (40 ft) of the rear of the damaged homes (Mulvey and Lowe, 1991). The volume was estimated at about 10,000 m^3 (13,000 yd^3). This estimate does not include debris around homes and removed from the streets, which was estimated based on the volume of material removed to be about 9,500 m^3 (12,500 yd^3), for a total of 19,500 m^3 (25,500 yd^3).

The potential sediment contribution from slope wash in the drainage was calculated following the fire by Lowe and others (1990) using the Pacific Southwest Inter-Agency Committee (PSIAC) (1968) Sediment Yield Rating Model. They estimated an average-annual post-fire sediment yield of approximately 0.24 acre-feet per year, or 300 m^3 (400 yd^3). Although the sediment yield from a storm of this magnitude may be greater, the large difference between the PSIAC estimate and the actual volume of the debris flow supports field observation that a small percentage of the total volume of debris was derived from the slopes (Mulvey and Lowe, 1991). The majority of debris-flow material was evidently derived from scour of stream channels and talus on slopes immediately below the cliffs.

At present, stream channels in the unnamed canyon still contain debris that could be mobilized and incorporated into another debris flow. Levees from prehistoric debris flows were observed on the alluvial fan at the mouth of the canyon. The active alluvial fan at the canyon mouth indicates that the recent large debris flow was not a geologically unusual event for this canyon, but instead is part of the alluvial-fan-building process. Debris flows will likely occur again on this fan. Houses remain at risk unless a long-term, permanent solution to the problem is pursued.

North Ogden Rock Slide

The hummocky terrain northwest of stop 3 is the North Ogden rock slide described by Pashley and Wiggins (1972). This landslide, first mapped by Eardley (1944), shows little evidence of post-landslide erosion by mountain-front streams. Pashley and Wiggins (1972) subdivided the landslide into four topographically distinct segments (figure 24) or lobes which could represent four distinct landslide events, possibly occurring in rapid succession. Recent exposures behind new houses at the toe of the westernmost segment (lobe number 1; Pashley and Wiggins, 1972, p. K2) indicate that portions of this lobe consist of debris-flow deposits. Mapping by Nelson and Personius (1990) indicate that lobe 4 is covered by Holocene alluvial-fan deposits. The elevation of the North Ogden rockslide ranges from approximately 1,743 m (5,720 ft) at the head to 1,487 m (4,878 ft) at the toe (Nelson and Personius, 1990).

A possible source area for the landslide material indicated by a scar in the south side of the unnamed canyon east of the landslide; the top of the scar has an elevation of about 2,010 m (6,600 ft). The landslide covers an area of approximately 404,700 m^2 (100 acres) and measures about 1,220 m (4,000 ft) long and 335 m (1,100 ft) wide (Pashley and Wiggins, 1972).

Cluff and others (1970) and Pashley and Wiggins (1972) inferred that the landslide postdated the high stand of Lake Bonneville because of the lack of a prominent Bonneville shoreline (elevation approximately 1,585 m; 5,200 ft) cut across the landslide. Nelson and Personius (1990), however, suggest that the rounder, gentler topography of the oldest (westernmost) landslide lobe (lobe number 1; Pashley and Wiggins, 1972) may indicate that Lake Bonneville transgressed across the lower portion of the landslide. A prominent shoreline did not form because the coarse Tintic Quartzite rubble in the landslide mass was resistent to wave erosion and to entrainment of clasts by shore currents. Supporting evidence for a possible pre-Lake Bonneville age for the landslide is: 1) the thick weathering rinds and iron oxide coatings on the surface of clasts in the upper part of the landslide, and 2) the similarity in the height of a fault scarp (20-40 m; 65-130 ft) crossing the middle of the landslide deposits to the height of the same

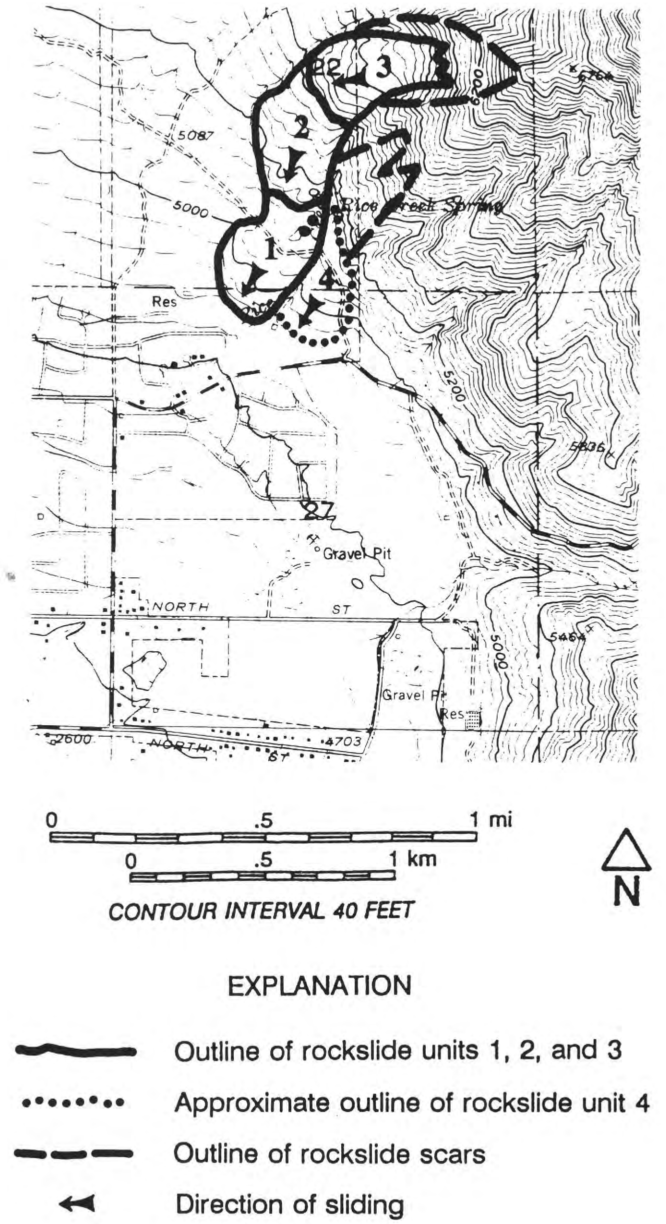

Figure 24. Map of the North Ogden rock slide (from Pashley and Wiggins, 1972).

fault scarp on either side of the landslide (Nelson and Personius, 1990).

0.0	13.0	Leave the dirt road. Turn left and drive west on North Ogden Canyon Road.
0.4	13.4	At the stop sign, turn left and drive south on 1050 E. Street.
0.8	14.2	At the stop sign, turn right and drive west on 2600 N. Street.
0.4	14.6	Turn left and drive south on Fruitland Drive.
0.5	15.1	The steep hill to the left (east) in the distance is the main scarp of the North Ogden lateral-spread landslide.
0.5	15.6	The steep hill immediately on the left (east) side of the road is the main scarp of the North Ogden lateral-spread landslide.
0.3	15.9	Fruitland Drive joins County Boulevard, continue driving south on County Boulevard (which soon becomes Harrison Boulevard).
3.2	19.1	At the stop light, turn left and drive east on 12th Street (Canyon Road).
0.8	19.9	Note the recent detached landslide with a main scarp trending northward up the mountain side on the south side of Ogden Canyon.
0.1	20.0	Make a hard turn to the right and drive west on Valley Drive.
0.1	20.1	Turn left into the Rainbow Imports parking lot.
0.1	20.2	Drive to back (south side) of the parking lot and park.

STOP 4. Rainbow Imports Landslide

This natural amphitheater-like reentrant into the Provo-level delta of the Ogden River is the easternmost area of landsliding (figure 25) discussed by Pashley and Wiggins (1972; p. K9-K10). Slope failures associated with this amphitheater are, in general, rotational slumps in cyclically-bedded, predominantly fine-grained Lake Bonneville deposits. The 60-meter-high (200 ft) bluff along which the landsliding occurs was created by erosion and downcutting by the Ogden River as Lake Bonneville gradually regressed. Landslide deposits associated with this amphitheater cover an area of about 113,300 m^2 (28 acres); the toes of some of the slope failures have been covered or destroyed because the site was previously used as a landfill (Pashley and Wiggins, 1972).

At this location on the afternoon of March 9, 1987, an earth-slump/earth-flow landslide damaged a steel power-transmission tower (figure 26), causing a power failure to much of Ogden's east bench area. Another large mass failed on the night of March 9-10. The landslides occurred on the eastern side of the amphitheater, and most of the material involved in the landsliding was older landslide deposits. Kaliser (1987) estimated that approximately 38,000 m^3 (50,000 yd^3) of material were involved in the 1987 failures and inferred that melting snow and ice, both on the top of the delta and on the toe of the ancient landslide,

Figure 25. Aerial view of the Ogden River landslide complexes. The photograph was taken prior to the 1987 Rainbow Imports landslide.

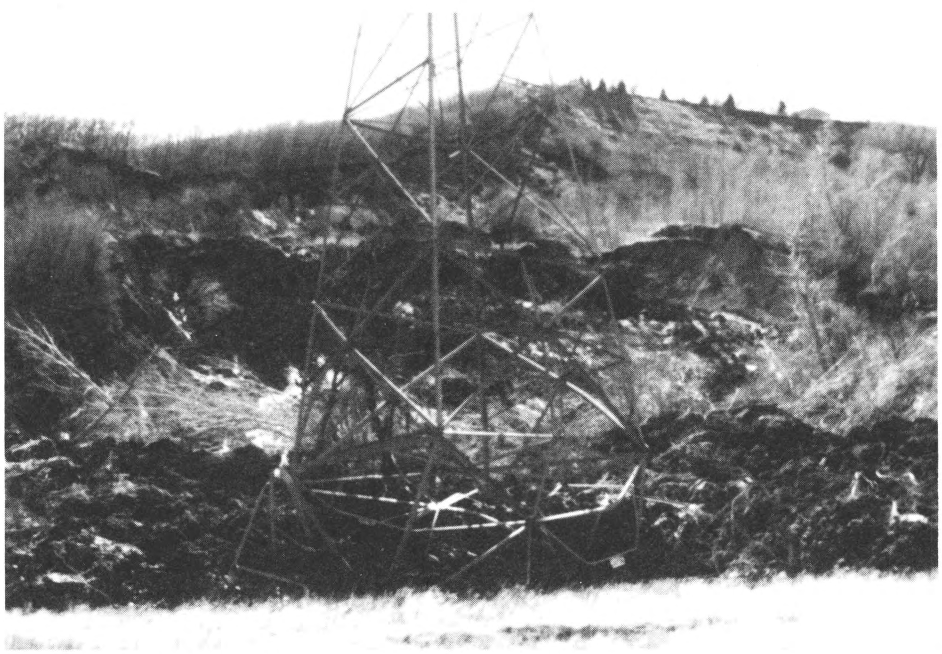

Figure 26. View from the toe of the 1987 Rainbow Imports landslide.

contributed to triggering the 1987 event. More landsliding occurred along the eastern margin of the amphitheater in 1988. Several other areas of recent landslide activity can also be viewed on the west side of this amphitheater.

Along the crown of the landslide amphitheater are a number of houses (figure 25) which may be threatened by landslides and mainscarp retreat in the future. Appraisers working for lending institutions have significantly reduced the amount of money that their companies are willing to loan on some of these houses, making it difficult for the present owners to sell the homes. The Weber County Geologist was contacted a number of times by both homeowners and lending institutions for information concerning how long it will be before the homes are affected by landsliding. Future landsliding in this area will largely be controlled by weather conditions and earthquake activity, and therefore speculations concerning rate of slope retreat are not possible.

0.0 20.2 Return to the vehicles and drive north out of the parking lot.

0.1 20.3 Turn left and drive west on Valley Drive.

0.4 20.7 To the left (south) is an area of active landsliding along the eastern margin of the western amphitheater described by Pashley and Wiggins (1972; p. K9-K10). Landslides associated with this topographic reentrant cover an area of about 255,000 m^2 (63 acres) and display topography that is characteristic of slumping; the landslides form a series of backtilted blocks which gradually become hummocky at the toe where the landslide became an earth flow (Pashley and Wiggins, 1972). The risers (scarps) at the back (south) of each backtilted block represent the individual rupture surfaces along which slumping has taken place (Pashley and Wiggins, 1972). Landsliding along the eastern margin of this landslide complex has caused Valley Drive to be closed a number of times in recent years.

0.2 20.9 The Canyon Cove Apartments to the left (south) are located on landslide deposits associated with the western amphitheater described above. Approval of this development by the Ogden City Planning Commission was based on a consultant's report which concluded that the presence of an Ogden River terrace cut into the landslide deposits to the right (north) of the road, on the Ogden Municipal Golf Course, indicated that the landslide complex in the vicinity of the development was not active. The apartment buildings have suffered extensive structural damage since construction, but it has not been determined if this damage is related to landslide movement, poor foundation conditions, or poor design or construction of the structures.

0.5 21.4 Valley Drive swings to the south and then west again, becoming 20th Street. At the stop light, turn left and drive south on Harrison Boulevard.

1.3 22.7 To the front left (southeast), is the bowl-shaped scar of the College rock slide.

0.9 23.8 To the left (east), another view of the College rock-slide source area.

1.2 25.0 To the left and back (northeast) is another bowl-shaped scar, this time in Precambrian Farmington Canyon Complex bedrock which crops out along the mountain front and the north side of Beus Canyon. This is the source area for the pre-Lake Bonneville Beus Canyon rock slide (figure 19) described by Pashley and Wiggins (1972; p. K5-K7). Below the scar and above the Bonneville shoreline is an extensive deposit of gneiss and metaquartzite rock-slide debris that, due to its position high above the valley and the extremely steep slope on which it rests, could be reactivated in the future, possibly during a large earthquake (Pashley and Wiggins, 1972). The western portion of the landslide mass, below the Bonneville shoreline, has undergone extensive modification due to erosion and deposition, primarily during the Bonneville lake cycle.

1.5 26.5 At the stop light, continue south across the four-lane road (Highway 89) onto 1550 E. Street.

0.1 26.6 Turn right (west) into the gate and continue driving south.

0.1 26.7 Note how thin the gravel cap on the Provo-level Weber River delta is at this location.

0.1 26.8 Park in the parking lot on the left (east) side of the road. Watching carefully for heavy-equipment traffic, cross the street and ask for permission at the Gibbons and Reed Company office (northernmost building) to proceed to stop 5.

0.0 26.8 After obtaining permission, proceed on the Gibbons and Reed Company road to the south. Turn to the right (west) just past (south of) the white gasoline storage tank on the right (west) side of the road.

0.1 26.9 The road forks. Take the right (west) fork. Do not continue down the hill. Drive west

		staying to the left (south) of the gravel piles.
0.1-0.2	27.-27.1	Caution! Loaders may be crossing the dirt road in this area carrying gravel to the conveyor belt to the left (south). The belt conveys gravel down to a hot plant which makes asphalt.
0.0	27.1	The road turns slightly to the northwest at this location. Continue driving west/northwest.
0.3	27.4	The road starts down a hill, turns north, then northeast, and then back to the west.
0.0-0.1	27.4-.5	The pond in the valley below is located in a shallow depression in a flat-bottomed drainage and is probably a sag pond that formed behind a back-tilted landslide block.
0.1	27.6	Park to the right (north) of the road.
0.0	27.6	**STOP 5. Gibbons and Reed Company North Pond Landslide.**

During historical time, the pond to the east was enlarged for irrigation with an embankment along the southest margin. Water from the pond, under natural conditions, flowed out of the pond to the southwest, cutting a steep gully which has been eroding headward (northeast) toward the pond. Landsliding and headward erosion caused the head of the gully to move more than 18 m (60 ft) closer to the pond since 1980 (Varge J. Lowe, Office Manager, Gibbons and Reed Company, oral commun., 1985; Lowe, 1988). To stop this erosion, an overflow drain was placed at the pond outlet and water was piped to the base of the hill where it eventually discharged into the Weber River.

In 1983, a landslide on the southeast side of the gully (southwest of the pond), destroyed the overflow pipe from the pond (figures 27 and 28). The landslide probably initiated as a rotational slump, but mobilized, with the addition of water from the pipe, into a rapid earth flow which eroded the gully and deposited material into the Weber River at the base of the bluff. It is difficult to determine if landsliding first caused the pipe to leak, initiating the rapid earth flow, or if water leaking from the pipe was the primary cause of the landslide. Landslides are common south of the pond, however. Extensive landsliding not associated with the 1983 failure are visible along the east and west slopes of the gully,

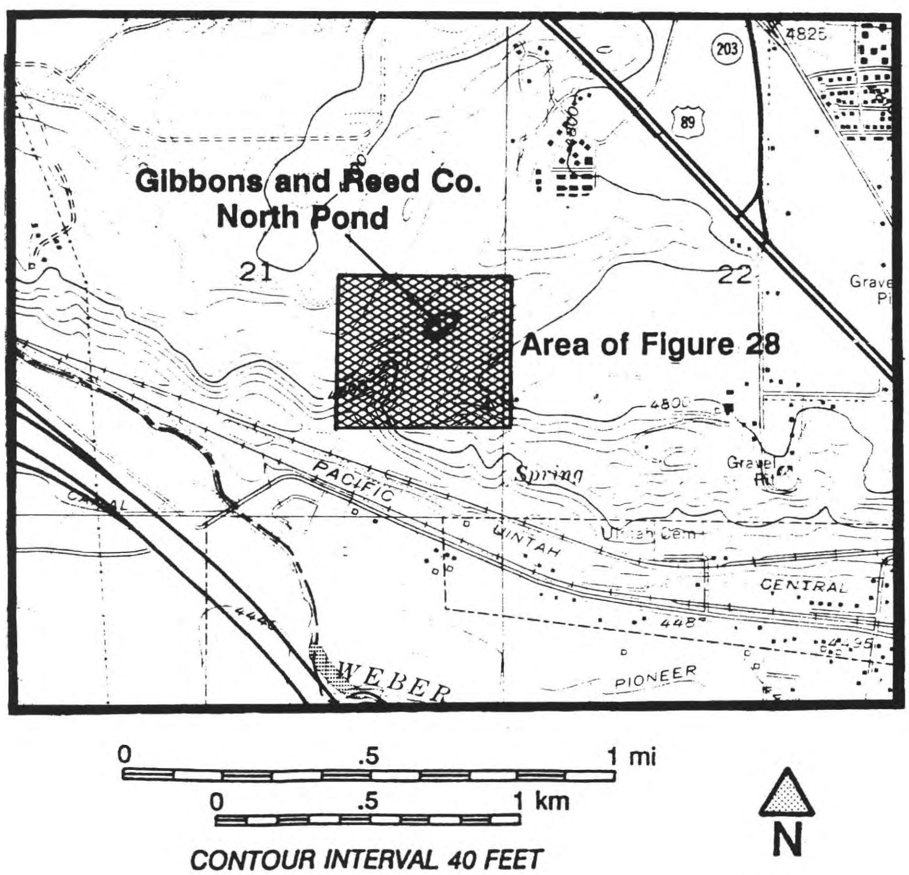

Figure 27. Location map for Gibbons and Reed Company North Pond.

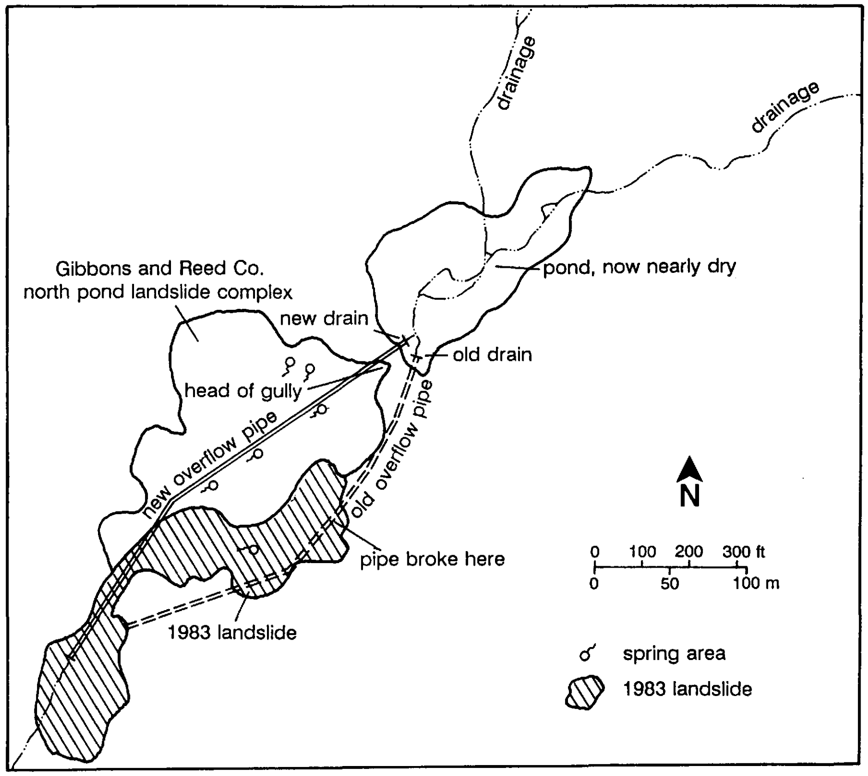

Figure 28. Generalized map view of the Gibbons and Reed Company North Pond landslide complex.

and the main scarp of a slope failure in the gully bottom traverses cross-valley just southwest of the pond. As a result of the 1983 landslide, Weber County installed a new drain in the bottom of the pond, draining most of the water. A new drain pipe was also installed, this time buried in the bottom of the gully where landsliding is less likely to occur.

The Gibbons and Reed landslide and pond are located in the Washington Terrace landslide complex, an area of extensive landsliding that has been studied previously by Feth (1955), Shroder (1971), Pashley and Wiggins (1972), and Van Horn and others (1972). "The Washington Terrace landslide complex is a 7.2-kilometer-long (4.5 mi) crescent-shaped area on the north side of the Weber River that extends from about 3.2 km (2 mi) west of the mouth of Weber Canyon to the northwest side of Washington Terrace" (Pashley and Wiggins, 1972). A number of conditions exist which make this area susceptible to landsliding. The materials in which the landsliding takes place are cyclically-bedded sand, silt, and clay deep-water sediments deposited primarily during the high stand of Lake Bonneville about 15,000 years ago. These deep-water deposits are capped by Provo-level deltaic sediments (cobbles, gravel, and sand) deposited about 14,000 years ago. The Weber River has cut into these sediments as the lake retreated, creating a steep 60-meter-high (200 ft) bluff. Compounding the problems of slope steepness and slide-prone materials is the presence of ground water. Many springs occur along the hillside where impermeable clay beds in the lake sediments prevent downward movement of ground water, resulting in perched ground water. When the deep-water sediments are saturated, they are prone to landsliding. Landslides in this environment usually consist of slumps which mobilize into earth flows at the toe. Features created by landsliding in the Washington Terrace landslide complex include barren slump scarps, closed depressions and lakes, and general hummocky topography (Pashley and Wiggins, 1972).

The 1981 "Railroad Landslide"

Other landslides have occurred within the Washington Terrace landslide complex during historical time, including the "railroad landslide" (figure 29) which derailed eight Union Pacific railroad cars and damaged three Utah Power & Light transmission-line towers on May 17, 1981. This landslide occurred only a few hundred yards west of stop 5. Five flat-cars carrying U. S. Mail, as well as the toe of the landslide, came to rest in the Weber River, subsequently diverting the flow and flooding four homes in the immediate vicinity (Gill, 1981).

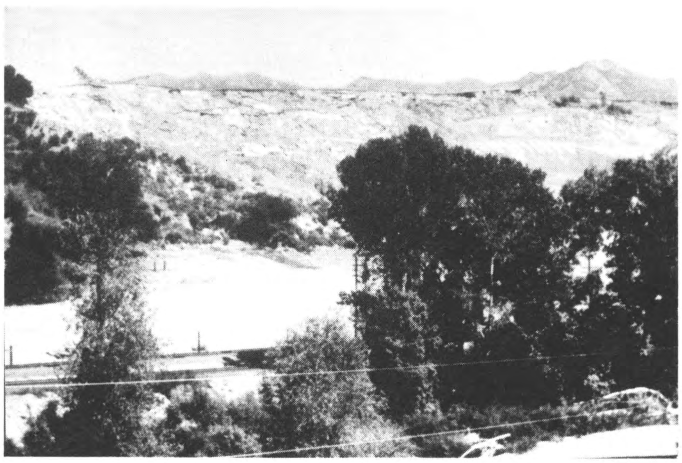

Figure 29. The 1981 "railroad landslide."

The Potential for Future Landsliding

Most of the bluff along the Washington Terrace landslide complex is considered to be either landslide deposits or landslide main scarps. Movement of one slide commonly creates oversteepened conditions around its main scarp which promotes additional landsliding in the scarp area. Earthquake ground shaking can accelerate the landslide process. Dames & Moore (1985) determined that a horizontal acceleration of as little as 0.05 g (5 percent of gravity) can induce significant movements of old landslide deposits along the bluffs above the Weber River. Earthquake-generated horizontal accelerations of 0.05 g have an approximately 95 percent probability of occurring in this region during a 100-year time period (Dames & Moore, 1985). Combined with the fact that topographic, soil-strength, and ground-water conditions permit reactivation of parts of old landslide deposits without earthquake shaking, the likelihood of landsliding in the Washington Terrace landslide complex in the future is high.

During a study for a proposed development immediately south of stop 5 (EarthStore, 1987), stacked colluvial wedges were exposed in trenches across interior scarps in the Washington Terrace landslide complex (figure 30). These colluvial wedges are possibly associated with recurrent landslide movement on interior scarps within the landslide complex, but no radiometric ages were obtained and possible correlations of landslide movements with surface-faulting earthquakes in the region are therefore not possible. As a result of the EarthStore (1987) study, however, it was determined that development should not proceed on the lower, steeper, more active slopes in the landslide complex unless more extensive studies which show development to be safe are completed.

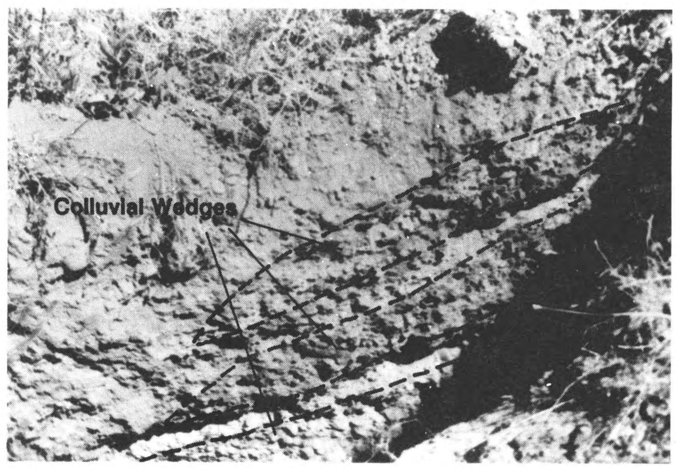

Figure 30. Colluvial wedges exposed in a trench excavated across an interior scarp in the Washington Terrace landslide complex during an EarthStore (1987) landslide-hazard evaluation for a proposed subdivision.

0.0	27.6	Return to the vehicles and drive back up the access road.
0.5	28.1	Gravel piles to the left (north). Beware of loaders feeding the conveyor belt!
0.1	28.2	At the stop sign, turn left and drive north. Stop at the Gibbons and Reed Company office and inform them that you are leaving their property. Continue driving north.
0.4	28.6	At the stop sign, turn left onto 1550 E. Street and drive north.
0.0	28.6	At the stop light, turn right and drive east on Highway 89. Highway 89 soon turns south.
1.6	30.2	Classic triangular facets associated with movement along the Wasatch fault zone can be viewed to the front left (southeast) above the Bonneville shoreline on the south side of Weber Canyon.

0.4 30.6 The Weber River.

0.1 30.7 The floors of the gravel pits to the left (east) and right (west) are well below the level of the Weber River. The lack of water in the pits is indicative of the high permeability associated with fluvial deposits at the mouth of the Weber River. A drillers log of an unused City of South Weber well east of Highway 89 indicates interfingered fluvial sand and gravel deposits containing no clay layers to a depth of at least 60 m (200 ft) below the natural ground surface (Plantz and others, 1986). Little spreading takes place as the river water moves downward to the water table, which is approximately 62 m (207 ft) below the ground surface at the South Weber well site (Plantz and others, 1986).

0.1 30.8 A view to the right front (southwest) of the South Weber landslide complex of Pashley and Wiggins (1972) on the south side of the Weber River. This bluff is affected by landsliding similar to that described in the Washington Terrace landslide complex. Most historical landsliding has taken place well to the west of Highway 89. The Davis-Weber Canal, which flows along the bluff carrying Weber River water to farm land to the west and south, has been affected at many locations by landsliding. In February, 1983, landsliding in the South Weber landslide complex in the City of Riverdale, about 7.2 km (4.5 mi) to the west, damaged seven homes.

0.6 31.4 An exposure immediately west (right) of Highway 89 contains prehistoric debris-flow deposits from Corbett Canyon to the left (east).

0.5 31.9 Note the steep hills in unconsolidated deposits on both sides of Highway 89. Here the highway is in a graben along the Wasatch fault zone.

0.5 32.4 The steep hill behind the Winder Dairy building on the left (west) side of Highway 89 is a Wasatch fault scarp.

0.5 32.9 Note the recent landslides in the road cut to the left (west) above Valley View Drive.

0.2 33.1 The canyon to the west is the Dry Fork of Kays Creek, also known as Lightning Canyon. On May 14, 1984, a debris flow from this canyon damaged a house at the canyon mouth (Mathewson and Santi, 1987). The debris flow (9,000 m^3; 11,800 yd^3) was triggered by landsliding in a tributary drainage on the north side of the canyon. Based on eyewitness accounts by the owner of the damaged house, Mathewson and Santi (1987) described the Lightning Canyon debris flow as a series of flows, each carrying progressively finer-grained materials and containing more water compared to the amount of sediment. The initial flow consisted of "a massive wall of debris containing boulders in a mud matrix." This was followed "shortly thereafter by a second flow containing gravels mixed with clay and silt" that flowed farther down the alluvial-fan surface and contained a relatively greater amount of water per unit volume. A third flow, which consisted primarily of muddy water and which flowed even farther down the fan surface, then occurred. This was followed by clear-water streamflow. This sequence of progressively wetter, finer-grained flows can be identified in alluvial-fan deposits. Fully matrix-supported, unsorted, unstratified debris-flow deposits containing isolated megaclasts, overlain by partially matrix-supported finer-grained transitional flows, overlain by fully clast-supported, even finer-grained hyperconcentrated-sediment-flow (debris-flood) deposits, overlain by still finer-grained normal-streamflow deposits with fining-upward graded bedding, form an ideal alluvial-fan stratigraphic sequence that can be used to interpret exposures in alluvial fans (figure 31, Keaton and others, 1988).

0.0-3.5 33.1-36.6 Many drainages have cut through the Weber River delta in the East Layton area, exposing landslide-prone, fine-grained, cyclically-bedded Lake Bonneville deposits and creating steep slopes along which perched ground water can exit in springs. Many

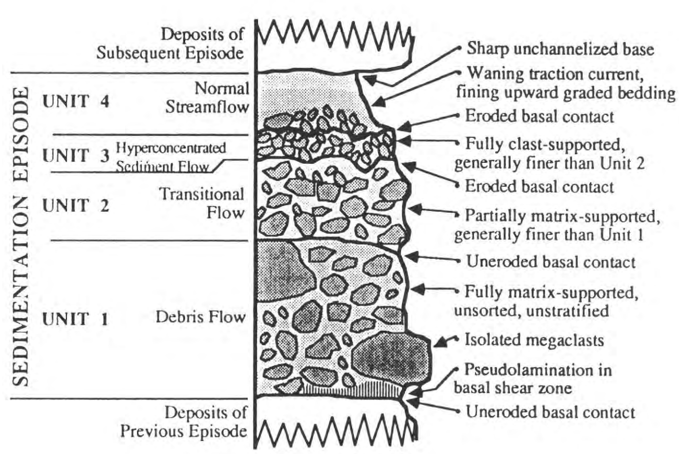

Figure 31. "Ideal alluvial-fan stratigraphic sequence showing features of the characteristic depositional units" (from Keaton and others, 1988).

landslides have occurred along these slopes during historical time.

Examples of these landslides can be viewed along the North Fork Holmes Creek drainage, just west of Holmes Reservoir, in Layton City. Seven areas of recently active landsliding have been identified along this drainage between Holmes Reservoir and approximately 1900 East Gentile Street, including a landslide on the north side of the drainage at approximately 2100 East that damaged a section of Gentile Street on January 26, 1971.

Two landslides on the south side of the drainage can be viewed from approximately 2525 E. Gentile Street. The easternmost of these landslides was reported to Davis County Flood Control on February 24, 1986. At that time, vegetation growing on the slope and the underlying earth material slid into the North Fork Holmes Creek drainage, temporarily blocking the creek and forcing water to flow around the toe of the landslide which extended about 24 m (80 ft) from the base of the hill. The landslide remained active throughout the spring of 1986. Examination of 1985 aerial photographs indicates that landsliding had occurred at this location prior to 1986. Gentile Street residents indicate that the western-most landslide which can be viewed from approximately 2525 E. Gentile Street occurred during the spring of 1983.

0.4 37.0 The canyon to the front left (southeast) is Baer Canyon. Note the many "wet cycle" debris slides on the computer-linked remote weather station established immediately above one of the landslides in the conifers which measures landslide movement with an extensometer, as well as rainfall and soil moisture (Lowe and others, 1988).

1.1 38.1 The Kaysville trench site (figure 32), actually in the City of Fruit Heights, is located to the left (east) immediately below the southernmost houses on the Provo-level terrace. The hill below the houses is a scarp of the Wasatch fault. This site was first trenched in 1978 and was the first such study along the Wasatch fault zone designed to study earthquake recurrence (Swan and others, 1980, 1981; Schwartz and Coppersmith, 1984). Based on radiocarbon dating of charcoal in pond deposits associated with a graben at the base of the main scarp, Swan and others (1980) interpreted that two faulting events occurred sometime after 1580 ± 150 yr B.P., with the most recent event occurring between several hundred and 500 years ago, and that a previous (third) event had occurred some time just prior to 1580 ± 150 years ago.

This trench site was reexcavated in 1988, in part because of the availability of new dating techniques such as radiocarbon analyses of organic concentrates from soil A-horizons (apparent mean residence time or AMRT age dating) and thermoluminescence dating of fine silt in buried A horizons. Based on radiocarbon and thermoluminescence dating of samples collected during the 1988 study, McCalpin and others (1991, in prep.) conclude that: 1) the most recent surface-faulting event at the site occurred slightly more than 700-930 yr B.P., 2) the penultimate surface-faulting event along the Weber segment of the Wasatch fault zone occurred about 2,600-2,800 yr B.P., at the Kaysville site, and 3) the antepenultimate surface-faulting event occurred between 4,700 and 6,300 years ago. The lithofacies from which Swan and others (1980) obtained the 1,580 ± 150 yr B.P. radiocarbon age in 1978 is interpreted by McCalpin and others (1991, in prep.) to have been deposited between 8,500 and 10,000 yr B.P., implying that the charcoal sample from which Swan and others (1980) obtained their radiocarbon age may have been an in situ burned root. The last three faulting events were accompanied by vertical displacements ranging from 1.4 to 3.4 m (4.6-11.2 ft) (McCalpin and others, 1991, in prep.).

0.4 38.5 The canyon to the left (east) is Shepard Creek Canyon. Notice the many debris slides on the canyon side slopes which occurred from 1983 to 1985.

0.3 38.8 The steep hills on both sides of Highway 89 are part of the main scarp of the Farmington Siding lateral-spread landslide which was first mapped by Van Horn (1975).

The wedged-shaped hill in the field to the front right (southwest) is a displaced landslide block which slid from the main scarp of the Farmington Siding lateral spread landslide to the north. The hills in the golf course in the distance are also displaced landslide blocks.

0.1 38.9 At the traffic light, turn left and drive east on Shepard Lane.

1.0 39.9 At the stop sign, turn left and drive north on Highway 106.

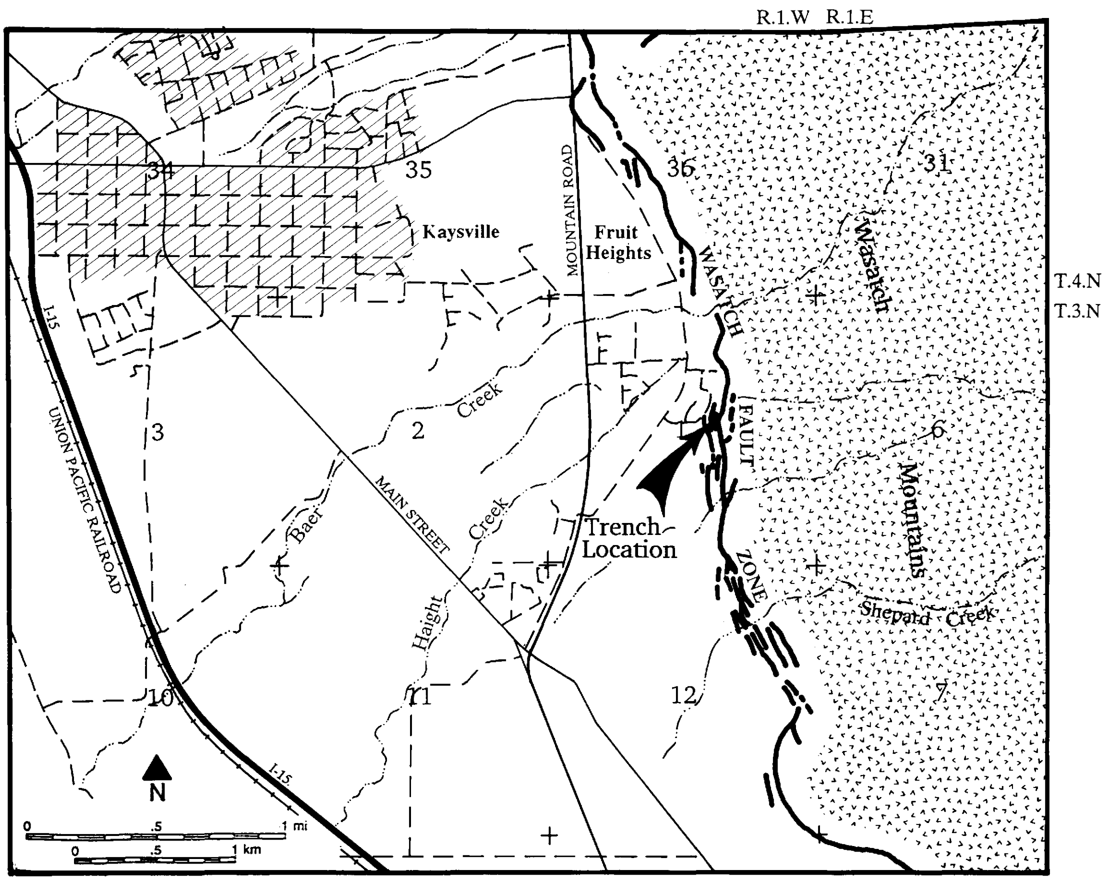

Figure 32. Location map for the Kaysville trench site.

0.6 40.5 Pull off the road to right (east) and park on the north side of 1650 N. Street. Walk back to south to view road cut on east side of Highway 106.

0.0 40.5 **STOP 6. Farmington Siding Lateral-Spread Landslide.**

The Farmington Siding landslide is a large landslide complex believed to be a lateral-spread failure associated with earthquake-induced liquefaction of unconsolidated lacustrine deposits. The Farmington Siding landslide was first identified by Van Horn (1975), and has since been mapped by other researchers (Miller, 1980; Anderson and others, 1982; Nelson and Personius, 1990). The failure was mapped as two separate landslides by Van Horn (1975), Miller (1980), and Anderson and others (1982), but as three separate failures by Nelson and Personius (1990). The southernmost landslide(s) in the complex are thought to be older than the northernmost landslide (Van Horn, 1975; Anderson and others, 1982). The absence of the 10,500-year-old Gilbert shoreline across the failures suggests the lateral spread(s) postdate the formation of this shoreline. Organic clay overlying landslide deposits in Farmington Bay, which may be part of the younger Farmington Siding landlside, provide a radiocarbon age estimate of 2,930 ± 70 yr B.P. (Everitt, 1991). This age estimate (Everitt, 1991) is similar to ages obtained from trenching studies for the penultimate surface-faulting earthquake on the Weber segment of the Wasatch fault (Nelson, 1988; Forman and others, 1991; McCalpin and others, 1991, in prep.).

Geomorphic features on the surface of the Farmington Siding landslide complex are subtle (figure 33). A 15-meter-high (50 ft), steep main scarp separates landslide deposits containing transverse ridges and undrained depressions from undisturbed Lake Bonneville deposits to the north and east. Transverse ridges are subparallel to the main scarp and easily discernible, especially in the northern part of the landslide complex. Farther downslope (to the south and west) the ridges become gradually less distinct. The probable steep pre-failure slope (greater than 5 percent) and the

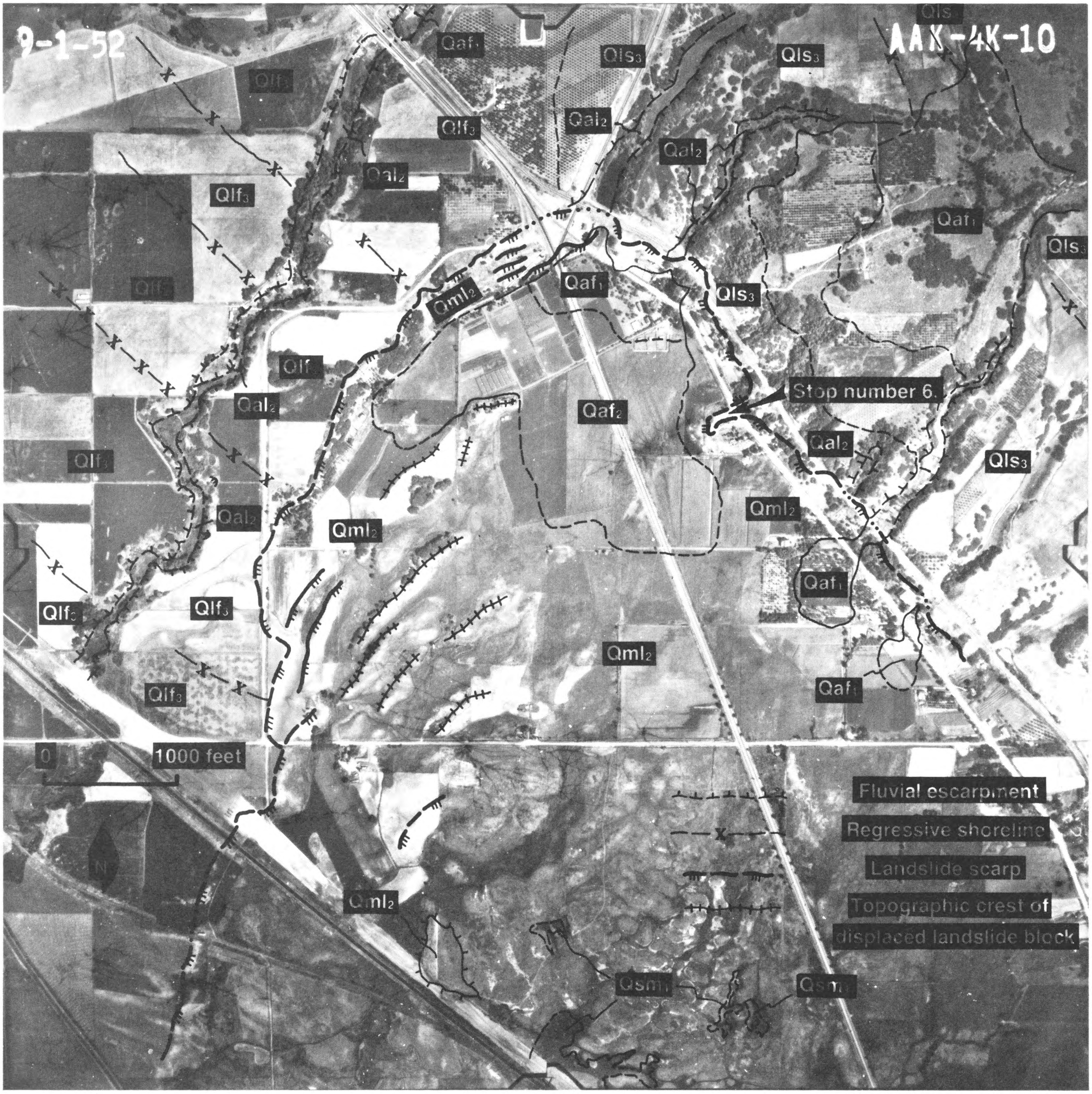

Figure 33. Preliminary photogeologic map of the northern portion of the Farmington Siding landslide complex. Qaf_1 = younger Holocene alluvial-fan deposits, Qaf_2 = older Holocene alluvial-fan deposits, Qal_2 = older Holocene fluvial deposits, Qlf_3 = Lake Bonneville offshore deposits (primarily silt and clay, Qls_3 = Lake Bonneville nearshore deposits (primarily sand and gravel), Qml_2 = Farmington Siding landslide deposits, Qsm_1 = younger Holocene marsh deposits.

hummocky topography (indicating significant disruption and distance of movement) suggest that the Farmington Siding lateral spreads may actually be flow slides.

Both Van Horn (1975) and T. L. Youd (Professor of Civil Engineering, Brigham Young University, oral commun., September, 1991) have identified liquefaction features in exposures of the Farmington Siding landslide. Disrupted and deformed bedding is abundant in exposures, and sand injection features can also be found in some areas. A study of liquefaction-induced landslides along the Wasatch Front was recently initiated by M. Lowe and K.M. Harty of the Utah Geological Survey; determining the age, origin, and hazard potential of the Farmington Siding landslides are major objectives of this study. The road-cut viewed at stop 6 exposes two large recumbent folds, and tilted, faulted, and contorted beds within fine-grained lacustrine sediments (figures 34 and 35). These features are just above the main scarp of one of the "older" Farmington Siding failures and may have been produced by secondary sliding and slumping associated with the landslide. The ongoing study of this landslide may confirm the origin and constrain the age(s) of the failure(s). Results of this study will be of interest to Davis County, because a Criminal Justice Complex has recently been constructed at a cost of more than $20 million on one of the older Farmington Siding landslides.

0.0 40.5 Make a U-turn and drive south on Highway 106.

0.6 41.1 Turn right and drive west on Shepard Lane.

0.4 Turn left at the light and drive south on Highway 89.

0.2 41.7 The canyon to the front left (southeast) is Rudd Canyon, the source of a debris flow which caused extensive damage in Farmington in 1983. The debris slide (figure 36), which is visible in the upper reaches of the canyon, triggered debris flows in both 1983 and 1984.

0.5 42.2 Take the exit to the right to Lagoon Drive (Farmington exit to Highway 225). Do not proceed to I-15. Drive east on Lagoon Drive.

0.4 42.6 The large canyon to the front left (east-northeast) is Farmington Canyon. Seven people died in 1923 during a cloudburst-rainstorm-induced flood along Farming-

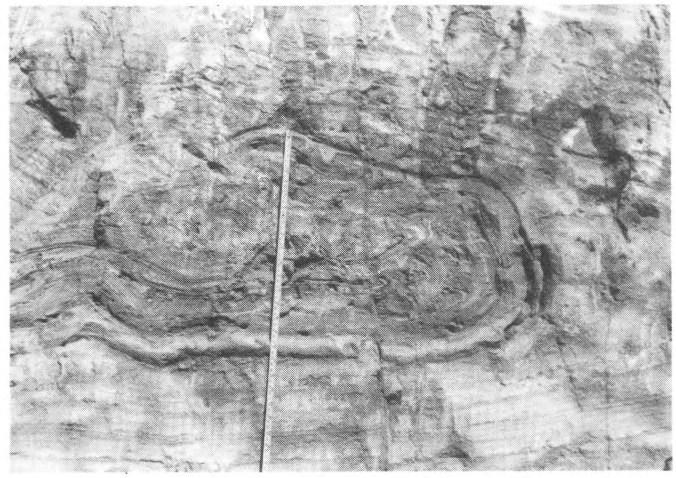

Figure 34. Roadcut exposure of a recumbent fold in fine-grained lacustrine sediments at stop 6. The distance from top to bottom of the folded sand bed is 43 cm (17 in).

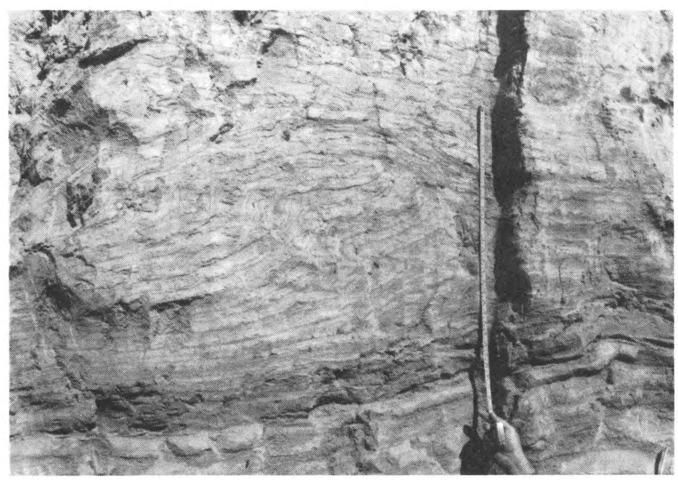

Figure 35. Roadcut exposure of deformed bedding in fine-grained lacustrine sediments at stop 6.

Figure 36. Rudd Canyon debris-slide scar.

ton Creek. Observers reported the flood water coming out of Farmington Canyon to be 23 to 30 meters high (75-100 ft) and 60 meters (200 ft) wide. The flood inundated many campers near the mouth of the canyon.

A Davis County Flood Control unpublished report by Marcia Flocken, compiled primarily from newspaper reports, provides the following account of heroism during that flood. The tent of Mr. and Mrs. Arnold Christensen was one of those in the flood path. Mr. Christensen, 38, was staying in the tent with his wife and two children, who became trapped under the tent when the flood hit. Mr. Christensen was able to pull his wife and one child from the tent, before suffering a heart attack due to overexertion. Mr. Christensen's two-year-old daughter, Margie, was swept away by the flood but rescued downstream by Doc Robinson who pulled her out of the raging waters by her long, black hair. Mr. Christensen died of heart failure before learning that his daughter was alive. Doc Robinson's heroics were not yet ended as he also rescued Mrs. N. O. Pebley, 60, of Farmington. Mrs. Pebley, who had managed to cling to a calf after being swept into the flood torrent, was spotted by Doc Robinson who went in after her. Unfortunately, Doc Robinson cut his legs and feet on a barbed wire fence under the flood waters and contracted tetanus. It took Doc Robinson 18 months to fully recover from the resulting illness. Doc Robinson was awarded the Carnegie Bronze Medal for Bravery as a result of his heroism during the most disastrous flood in Utah history.

The steep escarpment on the left (north) side of Farmington Canyon, which trends up in elevation eastward as it approaches the canyon and then trends down in elevation and westward south of the canyon, is a scarp marking the main trace of the Wasatch fault zone which Gilbert (1890) observed and sketched (figure 37) during his study of the Bonneville Basin. Gilbert spent much time evaluating how fault scarps, shorelines, and fluvial escarpments can be discerned from one another in the field.

Rudd Canyon, the next canyon to the east of Farmington Canyon, can be viewed to the front (east).

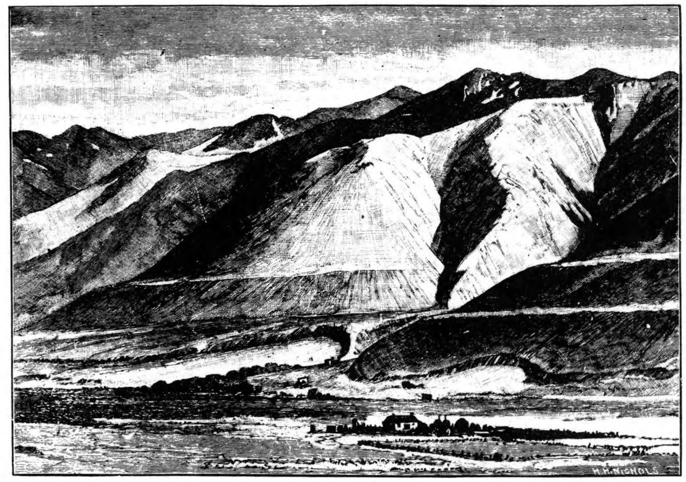

Figure 37. Sketch drawn by G. K. Gilbert (1890) of fault scarps at the mouth of Farmington Canyon.

0.8	43.4	At the stop sign, turn right and drive south on Highway 106 (Main Street). Highway 106 soon turns to the east.
0.2	43.6	As Highway 106 begins to turn back to the south, proceed forward and drive east on 600 N. Street.
0.2	43.8	At the stop sign, turn left and drive north on 100 E. Street.
0.0	43.8	The Rudd Canyon debris basin is to the right (east).
0.1	43.9	Pull off road to right (east) and park.

0.0 43.9 **STOP 7. Rudd Canyon Debris Flow**

On Memorial Day, May 30, 1983, rapid snowmelt caused shallow landsliding to occur near the head of Rudd Canyon. The Rudd Canyon landslide (15,300 m^3; 20,000 yd^3) initiated a debris flow (80,000 m^3; 100,000 yd^3) which damaged 35 houses, 15 severely, in the City of Farmington (Wieczorek and others, 1983; Lowe and others, 1989). Most of the material was scoured from the channel of Rudd Creek itself, as the earth/water mixture moved downstream. A smaller debris flow (1,350 m^3; 1,765 yd^3) occurred in Rudd Canyon in 1984.

The 1983 and 1984 debris flows were the only known historical debris-flow events from Rudd Canyon, but exposures of alluvial-fan deposits on the upthrown side of a Wasatch fault scarp at the mouth of the canyon, and in a small borrow pit about 50 yards north of the canyon, provide evidence for at least five other alluvial-fan sedimentation events (debris flows, transitional flows, and debris floods) from Rudd Canyon (Keaton and others, 1988). The absence of soils developed on the upper surfaces of these prehistoric alluvial-fan deposits suggests that the sedimentation events may have occurred over a relatively short period of time, perhaps around 10,000 years before present (Keaton and others, 1988). The volumes of the prehistoric Rudd Canyon sedimentation events, in order of increasing size, are estimated to have been greater than 250,000; 146,000; 105,000; 94,000; and 64,000 m^3 (325,000; 190,000; 135,000; 120,000; and 80,000 yd^3), respectively (Keaton and others, 1988). The largest of these probably was the earliest post-Lake Bonneville sedimentation event. The 1983 and 1984 sedimentation events at Rudd Canyon did not exceed the capacity of the Rudd Creek channel above the fault scarp and, consequently, did not deposit significant amounts of sediment on the alluvial fan above the fault; prehistoric sedimentation events with magnitudes similar to or smaller than the 1983 and 1984 events may have occurred at Rudd Creek which have not yet been identified (Keaton and others, 1988). Keaton (written commun., 1988) estimates that the recurrence intervals for debris flows of the magnitude of the 1983 event for Rudd Canyon range from 500 years (based on long-term erosion rates from the mountain block), to 1,000 years (over the past 10,000 years), to 3,700 years (based on the historical record).

The Davis County Flood Control Debris-Flow Hazard Evaluation

As a result of the 1983 and 1984 debris-flow and debris-flood events, Davis County formed a Flood Control Department and spent large amounts of taxpayer's money to construct debris basins below those canyons which had produced debris flows or debris floods during historical time. The idea was to "close the barn doors" at the canyon mouths and keep debris from spilling out of the canyons and onto developed alluvial fans.

The debris-flow/flood events of 1983 and 1984 caused damage outside flood plains depicted on Federal Emergency Management Agency (FEMA) Flood Insurance Rate Maps and, consequently, FEMA contracted with the U. S. Army Corps of Engineers to produce new Flood Insurance Rate Maps which take into account debris-flow/flood hazards. These maps are based on the assumption that the 1983 Rudd Creek debris flow was a 100-year event. This assumption was then used to calculate debris-flow potential for all of the canyons in central Davis County, relative to their watershed size on a log-linear scale (table 3). Rudd Creek is one of the smallest watersheds in the study area and, prior to 1983, had not produced a debris flow or debris flood in historical time.

When Davis County received the preliminary debris-flow potential analyses from FEMA, the county discovered that the Corps of Engineers had calculated that most of the debris basins that Davis County had constructed as a result of the 1983/1984 events were inadequate to contain the 100-year debris-flow event (table 3). Mayors and city engineers were concerned over the results of the Corps of Engineers' study and wanted to know why the newly constructed debris basins were inadequate to protect existing and proposed development when their size had been recommended by federally-sponsored studies (Wieczorek and others, 1983) completed after the events of 1983. To further complicate matters, geologic studies of alluvial fans at canyon mouths indicated that these same debris basins had been overdesigned for debris volumes calculated to be produced by the 100-year debris-flow event (Keaton and others, 1988).

To determine which set of conflicting volume estimates were most accurate, Davis County Flood Control began a study of streamchannel conditions in hopes that potential volumes of future debris flows could be predicted (Williams and others, 1988; Williams and Lowe, 1990). Triggering mechanisms for debris-flow/flood events are generally either climatologically-induced erosion or landsliding. Soil characteristics, topography, and vegetative conditions are important in determining the effects of these probabilistic events. The magnitude of the event in terms of amount of debris produced is determined by the volume of debris produced by the triggering event and channel conditions. Debris production and accumulation are slow, intermittent geologic processes. A recently scoured stream channel cannot contribute the same volume of debris during subsequent events as it did during initial events until debris again accumulates in the channel. The potential for large debris-flow

Table 3. Debris-basin capacity and estimated 100-year debris-flow/flood volumes for central Davis County drainages (U.S. Army Cops of Engineers, 1988).

CREEK	DRAINAGE AREA		100-YEAR EVENT VOLUME		DEBRIS-BASIN CAPACITY	
	km^2	(mi^2)	m^3	(yd^3)	m^3	(yd^3)
Shepard	6.0	(2.3)	85,000	(111,000)	24,200	(31,700)
Farmington	27.2	(10.5)	134,000	(175,000)	128,900	(168,600)
Rudd	2.3	(0.9)	64,000	(84,000)	35,200	(46,000)
Lone Pine	2.0	(0.8)	62,000	(81,000)	83,300	(108,900)
Ricks	6.5	(2.5)	86,000	(113,000)	30,600	(40,000)
Barnard	3.6	(1.4)	73,000	(96,000)	4,600	(6,000)
Parrish	5.4	(2.1)	83,000	(108,000)	30,600	(40,000)
Deuel	8.0	(3.1)	92,000	(120,000)	3,400	(4,500)
Stone	16.6	(6.4)	115,000	(150,000)	185,000	(242,000)
Barton	12.9	(5.0)	107,000	(140,000)	252,000	(330,000)
Mill	22.8	(8.8)	122,000	(160,000)	52,800	(69,000)

events is, therefore, deterministically controlled by channel conditions. The ongoing Davis County Flood Control study consists of an assessment of current drainage-specific debris-flow potential for central Davis County based on both channel and drainage-basin conditions. Topographic profiles across stream channels are being constructed and will be used to assess current channel conditions and determine rates of debris accumulation in channels. Drainage-basin conditions (soil conditions, landslides, topography, and vegetation) are also being assessed.

Davis County Flood Control research into the relationship of triggering events, channel conditions, and debris-flow magnitude has already produced some interesting results. Debris volumes produced during alluvial-fan sedimentation events in drainages with perennial streams are largely a function of the length of the stream channel involved. Calculations based on debris volumes from historical events have produced the following relationship:

$$(TDF-TE) / TCCL = CDF$$

where TDF is the total volume of debris measured at the canyon mouth, TE is the estimated volume from the flood source area (sheet erosion or landslide), TCCL is the total contributing channel length and CDF equals the channel debris-production factor (Williams and Lowe, 1990).

For perennial streams, this relationship appears to apply to both the thunderstorm-erosion-generated events of the 1920s and 1930s and the landslide-generated events of 1983 and 1984 (Table 4). Williams and Lowe (1990) suggest that about 30 m^3 of debris per lineal meter (12 yd^3 per lineal foot) of channel may represent a characteristic maximum debris volume for first events from Davis County Canyons. Pristine canyons are those which have not had a historical or recent prehistoric debris-flow event that cleaned out debris in the channel bottom. This volume (30 m^3/m; 12 yd^3/ft) may also indicate a physical limit for potential debris production per unit of channel length for perennial stream canyons underlain by the Farmington Canyon Complex.

The shape of profiles across the stream channels can be used to evaluate potential production from Davis County canyons (figure 38). Rudd Canyon and Parrish Canyon have similar U-shaped channel profiles and sidechannel slopes, in spite of the fact that the Parrish Canyon debris flows occurred more than 50 years prior to the Rudd Canyon debris flows. The Parrish Canyon channel is much deeper than the Rudd Canyon channel, perhaps because Parrish Canyon has a much larger drainage basin and flatter average channel gradient (Williams and Lowe, 1990). The Centerville Canyon cross-channel profile, however, has much gentler side slopes and a flat-bottomed shallow V-shape, indicating that the stream channel contains a large volume of material which could be eroded during future debris-flow events (Williams and Lowe, 1990).

Table 4. Selected debris-flow data (Williams and Lowe, 1990).

Canyon/Creek	Farmington	Rudd	Steed	Davis	Parrish
Year	1923	1983	1923	1923	1930
Avg.stream slope	0.127	0.314	0.341	0.305	0.177
TCCL (m)	18,036	1,652	5,354	3,902	6006
TDF - TE (m^3)	524,208	48,708	155,247	111,980	167,676
CDF (m^3/m length)	29.06	29.48	28.99	28.69	27.92
1983 TE (m^3)	17,000	64,000	10,000	min.	1,000

TCCL = total contributing channel length
TDF = total volume of debris measured at the canyon mouth
TE = estimated volume from flood source area (landslide or erosion)
CDF = amount of debris produced per unit length of channel

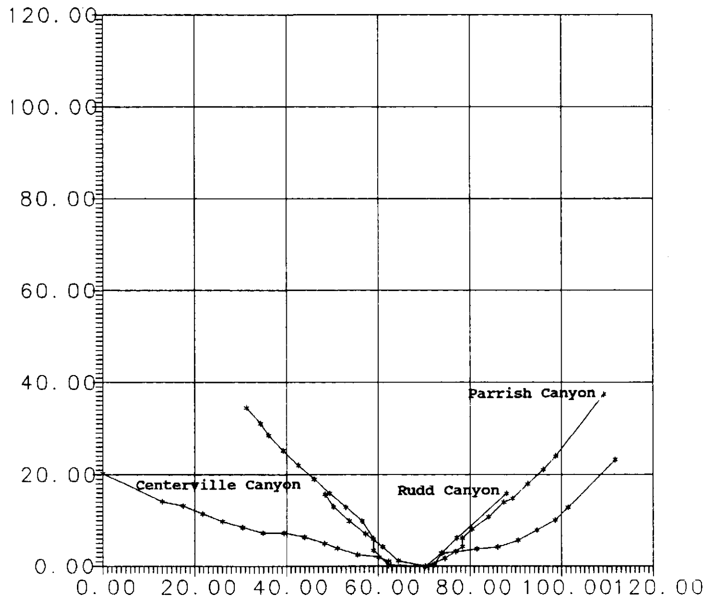

Figure 38. Cross-channel profiles of three central Davis County stream channels.

The amount of bedrock exposed in the channel bottoms of the three stream channels also varies significantly. Williams and Lowe (1990) estimated that the bottom of Rudd Canyon's stream channel is 50 to 70 percent bedrock. Although the Parrish Canyon debris flow occurred more than 50 years before the Rudd Canyon debris flow, Williams and Lowe (1990) estimated that 40-50 percent of the Parish Canyon stream channel is underlain by bedrock at shallow depths (Williams and Lowe, 1990). Willams and Lowe (1990) estimated the amount of bedrock exposed in the Centerville Canyon stream channel at 10 percent or less.

These observations lead to the conclusion that for climatic conditions such as those experienced in central Davis County during the past 50 years, the rate of debris accumulation in stream channels is very low. Until the stream channels are reloaded with debris, drainages that have been cleaned out by recent debris flows will likely produce much smaller debris volumes than pristine, debris-choked canyons. In 1991, based on the preliminary results presented above, and augmented with the results of the Keaton and others (1988) study of central Davis County alluvial fans, Davis County and Centerville City challenged the methodology used to construct the new FEMA flood maps. The maps are currently being revised to reflect a more realistic sediment yield from scoured canyons.

Rudd Canyon Water Tanks

The steep hill behind the debris basin is a fault scarp created by displacement during past surface-faulting events. The main trace of the Wasatch fault was exposed in the excavation for the water tanks which are located just north of the Rudd Canyon debris basin. The potential rupture of these tanks during future surface-faulting events is a significant hazard to homes below the tanks.

0.0 43.9 Make a U-turn and drive south on 100 E. Street.

0.2 44.1 Note the large scarp on the Wasatch fault zone to the left (east).

0.5 44.6 At the stop sign, angle to left and drive south on Highway 106 (which becomes 200 E. Street.

0.6 45.2 Turn left and drive east on 500 S. Street.

0.3 45.5 Note the rock retaining walls for the houses on the left. These rocks may become destabilized during future earthquakes. The steep hill to the front (east) where the road turns to the south is a scarp on the Wasatch fault.

0.1 46.5 The road turns to the south. Park where the paved road ends. Walk south up the road to the small building on the left side of the road.

STOP 8. Davis Canyon Fault Exposure.

Exposures of the Wasatch fault are relatively rare along the Wasatch Front. At stop 8 on the south side of the canyon, cyclically bedded silt and clay beds, deposited during the high stand of Lake Bonneville, have been downdropped on the valley side of the fault so that they are now adjacent to shoreline sand and gravel beds deposited during the slow rise of Lake Bonneville about 22,000 years ago. Frictional drag along the fault plane has caused the beds on each side of the fault plane to be bent during movement. The water tank near the mouth of Davis Canyon, on the west side of the road to the north, is below the exposure of the fault, but could still be in the zone of deformation associated with surface faulting.

0.0 46.5 Make a U-turn and drive north. The road soon turns left. Continue driving west.

0.5 47.0 At the stop sign, turn left and drive south on 200 E. Street (Highway 106).

1.4 48.4 The hummocky terrain to the left (east) is a large pre-Lake Bonneville landslide. The small drainage bisecting the landslide is Lone Pine Canyon.

0.5 48.9 Turn left and drive east on 1825 N. Street.

0.2 49.1 Pull into the church parking lot to right (south) and park.

0.0 49.1 **Stop 9. Rolling Hills Estates Subdivision.**

Three geologic reports were completed for the proposed Rolling Hills Estates in 1979 as part of the subdivision review process (Goode, 1979; Montgomery, 1979a, 1979b). Recommendations concerning avoidance or mitigation of geologic hazards, which were made in the reports, included: 1) stabilization of gravel pit slopes by revegetation, 2) mitigation of hazards created by several large boulders above the site by either breaking the boulders into small fragments using explosives, or dropping the boulders into excavations dug on the upslope side, and 3) accurate location of the Wasatch fault zone with respect to each lot so that no structure would be built across it.

Initial phases of the subdivision were approved based on an understanding that recommendations made in the reports would be followed. In February, 1986, Centerville City requested Mike Lowe (then the Davis County Geologist) to review subsequent phases of the subdivision. At that time it was found that: 1) although an effort had been made to revegetate the gravel-pit slopes, revegetation had not taken place and erosion problems were affecting completed phases of the subdivision, 2) the three large boulders which the geologic reports identified as hazardous to the proposed subdivision were still present at their original locations, and 3) the next phase of the subdivision included lots on the east side of the upper street-light-lined road, which would mean that some of the homes would be placed into the hill (a fault scarp) and potentially across the main trace of the fault.

Rock-fall hazard maps by Case (1987) show the spur above the Rolling Hills Estates Subdivision to be a potential source of rock-fall clasts. The three boulders identified in the geologic reports for the subdivision, including "Sheep Rock," the large boulder which is easily visible on the Bonneville shoreline, are but the largest of many potential rock-fall clasts which could be mobilized downslope by vandals, erosion, or earthquake ground shaking. Because development now exists below the three larger boulders identified in the reports, it is no longer feasible to use explosives to break them up. Because the majority of the potential rock-fall clasts threaten only the completed phases of the subdivision, and because the current developer was not involved in the early phases, it was not possible to require the construction of rock-fall mitigation structures as part of the requirements for approval of subsequent phases. It is therefore likely that the rock-fall hazard at the site will never be mitigated, indicating the need for a process by which recommendations made in geologic reports during the subdivision process will be required to be completed prior to construction of structures.

The 1979 geologic reports for the proposed subdivision contained a plot of the main trace of the fault, as determined from three natural exposures at this location. One of these exposures can be seen just above the upper road with light poles on the west side. At this exposure, bedded silt and clays deposited during the high stand of Lake Bonneville have been dropped down about 6 m (20 ft) and are now adjacent to gravel beds deposited during the slow rise of Lake Bonneville about 22,000 years ago.

Although the main trace of the fault was identified in the 1979 studies, no mention was made in the reports of possible secondary faults or post-rupture erosion and deposition. To identify any secondary faults at the site, it would be necessary to dig a continuous trench across the site. The present developers had purchased the land with the understanding that the 1979 geologic reports had been accepted as adequate. To limit the risk of placing homes across secondary faults, without requiring additional studies, the County Geologist recommended a 15-meter (50 ft) setback from the main trace of the fault. This policy has been in effect in Ogden City for several years. A compromise was reached with the developer in which the setback was reduced to 13.7 m (45 ft). This setback was recorded as a permanent faultline easement on the subdivision plat.

0.0	49.1	Leave the parking lot. Turn left and drive west on 1825 N. Street.
0.2	49.3	At the stop sign, turn left and drive south on 200 E. Street (Highway 106).
0.3	49.6	Note the buildings on the left (east) side of the road constructed behind the field-stone wall. The wall is the downstream section of a debris basin that was constructed along Ricks Creek on privately owned land in the 1930s. When the owner applied for a building permit in the 1970s, Davis County required that the owner sign a waiver releasing the County from any responsibility for future flood or debris-flow damage. In 1983, however, when this and other property along Ricks Creek were threatened by debris floods, the County constructed another debris basin inside the old field-stone walls to protect development. The land on which the new debris basin was constructed was purchased by Davis County.
0.3	49.9	Note the two rows of homes to the left (east) at the base and crest of a scarp on the Wasatch fault.
0.8	50.7	At the stop light, turn right and drive west on Parrish Lane.
0.7	51.4	Turn right and drive north on I-15. Return to Weber State University.

ACKNOWLEDGMENTS

To all those who reviewed this manuscript and provided valuable suggestions: Gary E. Christenson, Utah Geological Survey; James P. McCalpin, Geo-Haz Consultants; Alan R. Nelson, U.S. Geological Survey; Wilf Sommerkorn, Davis County Planning Department; and Jim Wilson, Department of Geology.

REFERENCES CITED

Anderson, L.R., Keaton, J.R., Aubry, Kevin, and Ellis, S.J., 1982, Liquefaction potential map for Davis County, Utah: Logan, Department of Civil and Environmental Engineering, Utah State University, and Dames & Moore Consulting Engineers, Salt Lake City, 50 p.

Anderson, L.R., Keaton, J.R., and Bay, J.A., 1990, Liquefaction potential map of the northern Wasatch Front, Utah: Logan, Department of Civil and Environmental Engineering, Utah State University, 150 p.

Arabasz, W.J., Smith, R.B., and Richins, W.D., eds., 1979, Earthquake studies in Utah, 1850-1978: Salt Lake City, University of Utah Seismograph Stations, 548 p.

Arnow, Ted, 1984, Water-level and water quality changes in Great Salt Lake, Utah, 1847-1983: U. S. Geological Survey Circular 913, 22 p.

Blair, M.L., and Spangle, W.E., 1979, Seismic safety and land-use planning — selected examples from California: U. S. Geological Survey Professional Paper 941-B, 82 p.

Bolt, B.A., 1978, Earthquakes; A Primer: San Francisco, W.H. Freeman and Company, 241 p.

Butler, Elmer, and Marsell, R.E., 1972, Cloudburst floods in Utah, 1939-69: Utah Department of Natural Resources, Division of Water Resources, Cooperative Investigations Report No. 11, 103 p.

Campbell, R.H., 1975, Soil slips, debris flows, and rainstorms in the Santa Monica Mountains and vicinity, southern California: U. S. Geological Survey Professional Paper 851, 51 p.

Case, W.F., 1987, Rock fall hazards in Utah's urban corridor: Geological Society of America Abstracts with Programs, v. 19, no. 7, p. 614.

———1988, Rock-fall hazards in Cache, Salt Lake, and Tooele valleys, Wasatch Front, Utah: Utah Geological and Mineral Survey, unpublished maps, scale 1:24,000.

Christenson, G.E., 1990, Wasatch Front County Hazards Geologist Program, *in* Gori, P.L., ed., Assessment of Regional Earthquake Hazards and Risk Along the Wasatch Front, Utah, v. IV: U.S. Geological Survey Open-File Report 90-225, p. FF-1-21.

Christenson, G.E., Lowe, Mike, Nelson, C.V., and Robison, R.M., 1987, Geologic hazards and land-use planning, Wasatch Front, Utah: Geological Society of America Abstracts with Programs, v. 19, no. 5, p. 265-266.

———1989, Wasatch Front County Hazards Geologist Program: Association of Engineering Geologists 32nd Annual Meeting Abstracts and Program, p. 56-57.

Clark, D.W., Appel, C.L., Lambert, P.M., and Puryear, R.L., 1990, Ground-water resources and simulated effects of withdrawals in the East Shore area of Great Salt Lake, Utah: Utah Department of Natural Resources Technical Publication No. 93, 150 p.

Copeland, O.L., 1960, Watershed restoration: a photo-record of conservation practices applied in the Wasatch Mountains of Utah: Journal of Soil and Water Conservation, v. 15, no. 3, p. 105-120.

Costa, J.E., 1984, Physical geomorphology of debris flows, *in* Costa, J.E., and Fleisher, P.J., eds., Developments and Applications of Geomorphology: New York, Springer-Verlag, p. 268-317.

Costa, J.E., and Baker, V.R., 1981, Surficial geology, building with the earth: New York, John Wiley and Sons, Inc., 498 p.

Croft, A.R., 1981, History of development of the Davis County Experimental Watershed: U.S. Department of Agriculture, Forest Service, Intermountain Region, Ogden, Utah, 42 p.

Currey, D.R., Atwood, Genevieve, and Mabey, D.R., 1984, Major levels of Great Salt Lake and Lake Bonneville: Utah Geological and Mineral Survey Map 73, 1:750,000 scale.

Currey, D.R., and Oviatt, C.G., 1985, Durations, average rates, and probable causes of Lake Bonneville expansions, stillstands, and contractions during the last deep-lake cycle, 32,000 to 10,000 years ago, *in* Kay, P.A., and Diaz, H.F., eds., Problems of and Prospects for Predicting Great Salt Lake levels, Conference Proceedings, Center for Public Affairs and Administration: Salt Lake City, University of Utah, p. 9-24.

Dames and Moore, 1980, Report, geologic hazards evaluation, a portion of Ogden City, for Ogden City Planning Commission: Unpublished consultant's report, 16 p.

———1985, Report, geotechnical and engineering geology investigation, project area for proposed sewer line south of St. Benedicts Hospital, Weber County, Utah, for City of Washington Terrace: Unpublished consultant's report, 11 p.

Davis County Planning Commission, 1988, Geologic hazards and land-use planning: background, explanation, and guidelines for development in Davis County in designated geologic hazards special study areas as required in Davis County Subdivision Ordinance: Unpublished Davis County Planning Commission report and maps, 73 p., 4 pls., scale 1:24,000.

Dewsnup, W.G., 1987, Local government pre-disaster hazard mitigation guidebook: Utah County Comprehensive Emergency Management Project in cooperation with Utah Division of Comprehensive Emergency Management, 86 p.

Eardley, A.J., 1944, Geology of the north-central Wasatch Mountains, Utah: Geological Society of America Bulletin, v. 55, p. 819-894.

EarthStore, 1987, Report, Engineering geology study of potential landslide hazard, southern portion of Stephens property, Washington Terrace, and adjoining property to east, Weber County, Utah, for Mr. Doug Stephens: Unpublished consultant's report, 14 p.

Erickson, A.J., Wilson, LeMoyne, Hughie, V.K., Nielson, Woodrow, and Chadwick, R.S., 1968, Soil survey of the Davis-Weber area, Utah: U.S. Department of Agriculture, Soil Conservation Service, in cooperation with Utah Agricultural Experiment Station, 149 p.

Everitt, Ben, 1991, Stratigraphy of eastern Farmington Bay: Utah Geological and Mineral Survey, Survey Notes, v. 24, no. 3, p. 27-29.

Federal Emergency Management Agency, 1978, Flood insurance study, City of Bountiful, Utah, Davis County: Federal Emergency Management Agency Federal Insurance Administration Community Panel Number 490039, 21 p.

———1980, Flood insurance study, City of South Weber, Utah, Davis County: Federal Emergency Management Agency Federal Insurance Administration Community Panel Number 490049, 11 p.

———1982, Flood insurance study, Weber County, Utah, Unincorporated Areas: Federal Emergency Management Agency Federal Insurance Administration Community Panel Number 490187, 25 p.

———1985, Reducing losses in high risk flood hazard areas: a guidebook for local officials: Federal Emergency Management Agency Publication No. 116, 225 p.

Feth, J.H., 1955, Sedimentary features in the Lake Bonneville Group in the East Shore area near Ogden, Utah, *in* Eardley, A.J., ed., Tertiary and Quaternary Geology of the Eastern Bonneville Basin: Utah Geological Society Guidebook to the Geology of Utah, no. 10, p. 45-69.

Feth, J.H., Barker, D.A., Moore, L.G., Brown, R.J., and Veirs, C.E., 1966, Lake Bonneville: geology and hydrology of the Weber Delta District, including Ogden, Utah: U. S. Geological Survey Professional Paper 518, 76 p.

Forman, S.L., Nelson, A.R., and McCalpin, J.P., 1991, Thermoluminescence dating of fault-scarp-derived colluvium: deciphering the timing of paleoearthquakes on the Weber segment of the Wasatch fault zone, north central Utah: Journal of Geophysical Research, v. 96, no. B1, p. 595-605.

Gilbert, G.K., 1890, Lake Bonneville: U. S. Geological Survey Monograph 1, 438 p.

———1928, Studies of Basin-Range structure: U.S. Geological Survey Professional Paper 153, 89 p.

Gill, H.E., 1981, Geologic investigation of a major slope failure in the Washington Terrace landslide complex near the mouth of Weber Canyon, Weber County, Utah: Utah Geological and Mineral Survey Report of Investigation 163, 18 p.

Goode, H.D., 1979, Geologic study of the Rolling Hills Estates, Centerville, Utah: Unpublished consultant's report to Centerville City, 4 p.

Gori, P.L., ed., 1990, Assessment of Regional Earthquake Hazards and

Risk Along the Wasatch Front, Utah, Volume IV: U.S. Geological Survey Open-File Report 90-225, 449 p.

Harty, K.M., 1991, Landslide map of Utah: Utah Geological and Mineral Survey Map 133, 28 p., scale 1:500,000.

Harty, K.M., and Christenson, G.E., 1988, Flood hazard from lakes and failure of dams in Utah: Utah Geological and Mineral Survey Map 111, 8 p., scale 1:750,000.

Hays, W.W., and King, K.W., 1982, Zoning of the earthquake ground-shaking hazard along the Wasatch fault zone, Utah: Third International Microzonation Conference Proceedings, v. 3, p. 1307-1317.

Hecker, Suzanne, Harty, K.M., and Christenson, G.E., 1988, Shallow ground water and related hazards in Utah: Utah Geological and Mineral Survey Map 110, 17 p.

Hely, A.G., Mower, R.W., and Harr, C.A., 1971, Water resources of Salt Lake County, Utah: Utah Department of Natural Resources Technical Publication 79, 54 p.

Hintze, L.F., 1988, Geologic history of Utah, a field guide to Utah's rocks: Brigham Young University Special Publication 7, 202 p.

Jackson, M.E., and Ruzicka, J., 1988, Holocene paleoseismic history of the Levan and Nephi segments, Wasatch fault zone, Utah: application of the thermoluminescence (TL) method: Geological Society of America Abstracts with Programs, v. 20, no. 5, p. 54.

Jochim, C.L., 1986, Debris-flow hazard in the immediate vicinity of Ouray, Colorado: Colorado Geological Survey Special Publication 30, 63 p.

Kaliser, B.N., 1987, Rainbow Gardens landslide of 3/9/87, Weber County: Utah Geological and Mineral Survey Memorandum, 2 p.

——1988, Thematic mapping applied to hazards reduction, Davis County, Utah: Utah Geological and Mineral Survey Open-File Report 135, 18 p.

Keaton, J.R., 1986, Potential consequences of tectonic deformation along the Wasatch fault: Final report to the U.S. Geological Survey for Earthquake Hazards Reduction Program Grant 14-08-0001-G1174.

——1987, Potential consequences of earthquake-induced regional tectonic deformation along the Wasatch Front, north-central Utah, *in* McCalpin, James, ed., Proceedings of the 23rd Symposium on Engineering Geology and Soils Engineering: Logan, Utah State University, p. 19-34.

Keaton, J.R., Anderson, L.R., and Mathewson, C.C., 1988, Assessing debris flow hazards on alluvial fans in Davis County, Utah, *in* Fragaszy, R.J., ed., Proceedings of the 24th Symposium on Engineering Geology and Soils Engineering: Pullman, Washington State University, p. 89-108.

Keaton, J.R., Anderson, L.R., Topham, D.E., and Rathbun, D.J., 1987, Earthquake-induced landslide potential in and development of a seismic slope stability map of the urban corridor of Davis and Salt Lake Counties, Utah: Salt Lake City, Dames & Moore Consulting Engineers, and Department of Civil and Environmental Engineering, Utah State University, 47 p.

Keefer, D.K., 1984, Landslides caused by earthquakes: Geological Society of America Bulletin, v. 95, p. 406-421.

Kuribayashi, Eiichi, and Tatsuoka, Fumio, 1975, Brief review of liquefaction during earthquakes in Japan: Soils and Foundations, v. 15, no. 4, p. 81-92.

——1977, History of earthquake-induced liquefaction in Japan: Japan Ministry of Construction, Public Works Research Institute Bulletin, v. 31, p. 26.

Lin, Anching, and Wang, Po, 1978, Wind tides of the Great Salt Lake: Utah Geology, v. 5 no. 1, p. 17-25.

Lowe, Mike, 1988, Report of geologic reconnaissance: landslide southwest of Gibbons and Reed Company north pond, west of Uintah, Weber County: Utah Geological and Mineral Survey Report of Investigation 218, p. 76-79.

——1990a, Earthquake-induced ground-failure in sensitive clays, vibratory settlement, and hydrologic hazards; a guide for land-use planning in Davis County, Utah, *in* Gori, P.L., ed., Assessment of Regional Earthquake Hazards and Risk Along the Wasatch Front, Utah, v. IV: U.S. Geological Survey Open-File Report 90-225, p. MM-1-16.

——1990b, Debris-flow hazards; a guide for land-use planning in Davis County, Utah, *in* Gori, P.L., ed., Assessment of Regional Earthquake Hazards and Risk Along the Wasatch Front, Utah, v. IV: U.S. Geological Survey Open-File Report 90-225, p. JJ-1-25.

——1990c, Liquefaction hazards; a guide for land-use planning in Davis County, Utah, *in* Gori, P.L., ed., Assessment of Regional Earthquake Hazards and Risk Along the Wasatch Front, Utah, v. IV: U.S. Geological Survey Open-File Report 90-225, p. KK-1-26.

——, ed., 1990d, Geologic hazards and land-use planning: background, explanation, and guidelines for development in Davis County in designated special study areas: Utah Geological and Mineral Survey Open-File Report 198, 73 p.

——, ed., 1990e, Geologic hazards and land-use planning: background, explanation, and guidelines for development in Weber County in designated special study areas: Utah Geological and Mineral Survey Open-File Report 197, 70 p.

Lowe, Mike, and Christenson, G.E., 1990, Geologic hazards maps for land-use planning, Davis and Weber Counties, Utah: Geological Society of America Abstracts with Programs, v. 22, no. 6, p. 37.

Lowe, Mike, Harty, K.M., and Christenson, G.E., 1991, Hazard potential and paleoseismic implications of liquefaction-induced landslides along the Wasatch Front, Utah, *in* Jacobson, M.L., compiler, National Earthquake Hazards Reduction Program, Summaries of Technical Reports, v. XXXII: U.S. Geological Survey Open-File Report 91-352, p. 549.

Lowe, Mike, Harty, K.M., and Rasely, R.C., 1990, Reconnaissance of area burned by wild fire northeast of North Ogden and evaluation of potential sediment yield: Unpublished Utah Geological and Mineral Survey Memorandum to Dennis R. Shupe, North Ogden City Administrator, 5 p.

Lowe, Mike, Robison, R.M., Nelson, C.V., and Christenson, G.E., 1989, Slope-failure hazards in mountain front urban areas, Wasatch Front, Utah: Association of Engineering Geologists 32nd Annual Meeting Abstracts and Program, p. 90-91.

Lowe, Mike, Williams, S.R., and Smith, S.W., 1988, The Davis County flood warning and information system: Utah Geological and Mineral Survey Open-File Report 151, 15 p.

Lund, W.R., Christenson, G.E., Harty, K.M., Hecker, Suzanne, Atwood, Genevieve, Case, W.F., Gill, H.E., Gwynn, J.W., Klauk, R.H., Mabey, D.R., Mulvey, W.E., Sprinkel, D.A., Tripp, B.T., Black, B.D., and Nelson, C.V., 1990, Geology of Salt Lake City, Utah, United States of America: Bulletin of the Association of Engineering Geologists, v. 27, no. 4, p. 391-478.

Machette, M.N., Personius, S.F., and Nelson, A.R., 1987, Quaternary geology along the Wasatch Front: segmentation, recent investigations, and preliminary conclusions, *in* Gori, P.L., and Hays, W.W., eds. Assessment of Regional Earthquake Hazards and Risk Along the Wasatch Front, Utah, v. I: U. S. Geological Survey Open-File Report 87-585, p. A-1-72.

Machette, M.N., Personius, S.F., Nelson, A.R., Schwartz, D.P., and Lund, W.R., 1989, Segmentation models and Holocene movement history of the Wasatch fault zone, Utah, *in* Schwartz, D.P., and Sibson, R., editors, Proceedings of Conference XLV—Fault Segmentation and Controls on Rupture Initiation and Termination: U.S. Geological Survey Open-File Report 89-315, p. 229-242.

——1991, The Wasatch fault zone — segmentation and history of Holocene earthquakes: Journal of Structural Geology, v. 13, no. 2, p. 137-149.

Marsell, R.E., 1972, Cloudburst and snowmelt floods, *in* Hilpert, L.S., ed., Environmental Geology of the Wasatch Front, 1971: Utah Geological Association Publication 1, p. N1-N18.

Mathewson, C.C., and Santi, P.M., 1987, Bedrock ground water: source of sustained post-debris flow stream discharge, *in* McCalpin, James, ed., Proceedings of the 23rd Annual Symposium on Engineering Geology and Soils Engineering: Logan, Utah State University, p. 253-265.

McCalpin, James, Forman, S.L., and Lowe, Mike, in prep., Reinterpretation of Holocene faulting at the Kaysville trench site, Weber segment of the Wasatch fault zone, Utah: 38 p.

Miller, R.D., 1980, Surficial geologic map along part of the Wasatch Front, Great Salt Lake Valley, Utah: U. S. Geological Survey Miscellaneous Field Studies Map MF-1198, scale 1:100,000.

Montgomery, S.B., 1979a, Potential rock-fall study above Rolling Hills Subdivision: Unpublished consultant's report for Kimball-Lodder Development Company, 5 p.

——1979b, Geologic foundation evaluation progress report for Rolling Hills Subdivision: Unpublished consultant's report for Kimball-Lodder Development Company, 5 p.

Mulvey, W.E., and Lowe, Mike, 1991, Cameron Cove Subdivision debris flow, North Ogden, Utah: Utah Geological Survey Technical Report 91-13, 4 p.

Murchison, S.B., 1989, Fluctuation history of Great Salt Lake, Utah, during the last 13,000 years: Salt Lake City, University of Utah, unpublished Ph.D. dissertation, 137 p.

National Research Council, 1985, Liquefaction of soils during earthquakes: Washington D.C., National Academy Press, 240 p.

Nelson, A.R., 1988, The northern part of the Weber segment of the Wasatch fault zone near Ogden, Utah, *in* Machette, M.N., ed., In the footsteps of G.K. Gilbert—Lake Bonneville and neotectonics of the eastern Basin and Range Province: Geological Society of America Annual Meeting Field Trip Guidebook, Utah Geological and Mineral Survey Miscellaneous Publication 88-1, p. 26-32.

Nelson, A.R., and Personius, S.F., 1990, Preliminary surficial geologic map of the Weber segment of the Wasatch fault, Weber and Davis Counties, Utah: U.S. Geological Miscellaneous Field Studies Map MF-2132, scale 1:50,000.

Nelson, A.R., Klauk, R.H., Lowe, Michael, and Garr, J.D., 1987, Holocene history of displacement on the Weber segment of the Wasatch fault zone at Ogden, northern Utah: Geological Society of America Abstracts with Programs, v. 19, no. 5, p. 322.

Nelson, C.V., 1988 Preparation and use of earthquake ground-shaking and rock-fall hazard maps, Wasatch Front, Utah: Geological Society of America Abstracts with Programs, v. 20, no. 6, p. 459.

——1990, Rock-fall hazards: a guide for land-use planning, Salt Lake County, Utah, *in* Gori, P.L., ed., Assessment of Regional Earthquake Hazards and Risk Along the Wasatch Front, Utah, v. IV: U.S. Geological Survey Open-File Report 90-225, p. I-1-15.

Nichols, D.R., and Buchanan-Banks, J.M., 1974, Seismic hazards and land-use planning: U. S. Geological Survey Circular 690, 33 p.

Olson, E.P., 1981, Geologic hazards of the wasatch Range, Part 1, Ward Canyon to south side Ogden Canyon: U.S. Department of Agriculture, Forest Service, R-4 Intermountain Region, unpublished 1:24,000 scale maps of selected quadrangles within U.S. Forest Service boundaries.

Pacific Southwest Inter-Agency Committee, 1968, Report on factors affecting sediment yield in the Pacific Southwest area and selection and evaluation of measures for reduction of erosion and sediment yield: Report of the Water Management Subcommittee, 10 p.

Pack, R.T., 1984, Debris flow initiation in Davis County, Utah, during the spring snowmelt period of 1983 (abstract): Proceedings of the 21st Annual Symposium on Engineering Geology and Soils Engineering.

——1985, Multivariate analysis of relative landslide susceptibility in Davis County, Utah: Logan, Utah State University, unpublished Ph.D. dissertation, 233 p.

Pashley, E.F., Jr., and Wiggins, R.A., 1972, Landslides of the northern Wasatch Front, *in* Hilpert, L.S., ed., Environmental Geology of the Wasatch Front, 1971: Utah Geological Association Publication 1, p. K1-K16.

Pfeiffer, T.J., and Higgins, J.D., 1988, Colorado rock-fall simulation program users manual: Final report prepared for the Colorado Department of Highways, 107 p.

Pierson, T.C., and Costa, J.E., 1987, A rheologic classification of subaerial sediment-water flows, *in* Costa, J.E., and Wieczorek, G.F., eds., Debris Flows/Avalanches: Process, Recognition, and Mitigation: Geological Society of America Reviews in Engineering Geology, v. 7, p. 1-12.

Plantz, G.G., Appel, C.L., Clark, D.W., Lambert, P.M., and Puryear, R.L., 1986, Selected hydrologic data from wells in the East Shore area of the Great Salt Lake, Utah, 1985: U.S. Geological Survey Open-File Report 86-139, 75 p.

Ridd, M.K., and Kaliser, B.N., 1978, North Ogden sensitive area study: Unpublished report to North Ogden Planning Commission, 124 p.

Robison, R.M., 1990a, Surface fault rupture: a guide for land-use planning, Utah and Juab Counties, Utah, *in* Gori, P.L., ed., Assessment of Regional Earthquake Hazards and Risk Along the Wasatch Front, Utah, v. IV: U.S. Geological Survey Open-File Report 90-225, p. GG-1-25.

——1990b, Tectonic subsidence hazard: a guide to land-use planning, Utah and Juab Counties, Utah, *in* Gori, P.L., ed., Assessment of Regional Earthquake Hazards and Risk Along the Wasatch Front, Utah, v. IV: U.S. Geological Survey Open-File Report 90-225, p. LL-1-12.

Robison, R.M., and Lowe, Mike, 1990a, Landslide hazards; a guide for land-use planning in Davis County, Utah, *in* Gori, P.L., ed., Assessment of Regional Earthquake Hazards and Risk Along the Wasatch Front, Utah, v. IV: U.S. Geological Survey Open-File Report 90-225, p. HH-1-26.

——1990b, Shallow ground water, *in* Lowe, Mike, ed., Geologic Hazards and Land-Use Planning: Background, Explanation, and Guidelines for Development in Weber County in Designated Geologic Hazards Special Study Areas: Utah Geological and Mineral Survey Open-File Report 197, p. J1-J5.

——1990c, Shallow ground water, *in* Lowe, Mike, ed., Geologic Hazards and Land-Use Planning: Background, Explanation, and Guidelines for Development in Davis County in Designated Geologic Hazards Special Study Areas: Utah Geological and Mineral Survey Open-File Report 198, J1-J5.

Schwartz, D.P., and Coppersmith, K.J., 1984, Fault behavior and characteristic earthquakes — examples from the Wasatch and San Andreas fault zones: Journal of Geophysical Research, v. 89, no. B7, p. 5681-5698.

Shroder, J.F., 1971, Landslides of Utah: Utah Geological and Mineral Survey Bulletin 90, 51 p.

Smith, R.B., and Sbar, M.L., 1974, Contemporary tectonics and seismicity of the western United States with emphasis on the Intermountain Seismic Belt: Geological Society of America Bulletin, v. 85, p. 1205-1218.

Stokes, W.L., 1977, Subdivisions of the major physiographic provinces in Utah: Utah Geology, v. 4, no. 1, p. 1-17.

Swan, F.H., III, Schwartz, D.P., and Cluff, L.S., 1980, Recurrence of moderate to large magnitude earthquakes produced by surface faulting on the Wasatch fault, Utah: Bulletin of the Seismological Society of America, v. 70, no. 5, p. 1431-1462.

Swan, F.H., III, Schwartz, D.P., Hansen, K.L., Knuepfer, P.L., and Cluff, L.S., 1981, Study of earthquake recurrence intervals on the Wasatch fault at the Kaysville site, Utah: U.S. Geological Survey Open-File Report 81-228, 30 p.

Tinsley, J.C., Youd, T.L., Perkins, D.M., and Chen, A.T.F., 1985, Evaluating liquefaction potential, *in* Ziony, J.I., ed., Evaluating Earthquake Hazards in the Los Angeles Region — an Earth Science Perspective: U. S. Geological Survey Professional Paper 1360, p. 263-315.

U.S. Army Corps of Engineers, 1969, Flood plain information, Jordan River Complex, Salt Lake City, Utah: U. S. Army Corps of Engineers, Sacramento District, Sacramento, California, 39 p.

——1988, Mudflow modeling, one- and two-dimensional, Davis County, Utah: Omaha District, U. S. Army Corps of Engineers, 53 p.

Utah Division of Comprehensive Emergency Management, 1981, History of Utah floods, 1847 to 1981: Utah Department of Public Safety, 46 p.

——1985, Hazard mitigation plan — executive summary, Great Salt Lake Beneficial Development Area-Utah 1985: Utah Department of Public Safety, 21 p.

Van Horn, Richard, 1975a, Largest known landslide of its type in the United States—a failure by lateral spreading in Davis County, Utah: Utah Geology, v. 2, no. 1, p. 83-87.

——1982, Surficial geologic map of the Salt Lake City North Quadrangle, Davis and Salt Lake Counties, Utah: U. S. Geological Survey Miscellaneous Investigation Series Map I-1404, scale 1:24,000.

Van Horn, Richard, Baer, J.L., and Pashley, E.F., Jr., 1972, Landslides along the Wasatch Front, Utah, *in* Hilpert, L.S., ed., Environmental Geology along the Wasatch Front, 1971: Utah Geological Association Publication 1, p. J1-J16.

Varnes, D.J., 1978, Slope movement types and processes, *in* Schuster, R.L., and Krizek, R.S., eds., Landslides; Analysis and Control: Washington D. C., National Academy of Sciences, Transportation Research Board, Special Report 176, p. 12-33.

Waddell, K.M., and Maxell, M.H., 1987, Utah ground-water quality, *in* Moody, D.W., Carr, Jerry, Chase, E.B., and Paulson, R.W., comps., National Water Summary 1986: U.S. Geological Water Supply Paper 2325, p. 493-500.

Waitt, R.B., Pierson, T.C., Maclead, N.S., Janda, R.J., Voight, B., and Holcomb, R.T., 1983, Eruption-triggered avalanche, flood, and lahar at Mount St. Helens — effects of winter snowpack: Science, v. 221, no. 4618, p. 1394-1397.

Weber County Planning Commission, 1988, Geologic hazards and land-use planning: background, explanation, and guidelines for development in designated geologic hazards special study areas as required in Weber County ordinances: Unpublished Weber County Planning Commission report and maps, 69 p., 4 pls., scale 1:24,000.

Wieczorek, G.F., 1987, Effect of rainfall intensity and duration on debris flows in central Santa Cruz Mountains, California, *in* Costa, J.E., and Wieczorek, G.F., eds., Debris Flows/Avalanches: Process, Recognition, and Mitigation: Geological Society of America Reviews in Engineering Geology, v. 7, p. 93-104.

Wieczorek, G.F., Ellen, Stephen, Lips, E.W., Cannon, S.H., and Short, D.N., 1983, Potential for debris flow and debris flood along the Wasatch Front between Salt Lake City and Willard, Utah, and measures for their mitigation: U. S. Geological Survey Open-File Report 83-635, 45 p.

Wieczorek, G.F., Lips, E.W., and Ellen, S.D., 1989, Debris flows and hyperconcentrated floods along the Wasatch Front, Utah, 1983 and 1984: Bulletin of the Association of Engineering Geologists, v. 26, no. 2, p. 191-208.

Williams, J.S., and Tapper, M.L., 1953, Earthquake history of Utah, 1850-1948: Bulletin of the Seismological Society of America, v. 43, no. 3, p. 191-218.

Williams, S.R., and Lowe, Mike, 1990, Process based debris-flow prediction method, *in* French, R.H., ed., Proceedings of the International Sympsoium on the Hydraulics/Hydrology of Arid Lands (H^2AL): San Diego, American Society of Civil Engineers, p. 66-71.

Williams, S.R., Lowe, Mike, and Smith, S.W., 1989, The discrete debris-mud flow risk analysis method, in Proceedings of the Conference on Arid West Floodplain Management Issues, Las Vegas, Nevada, October 19-21, 1988: Association of State Floodplain Managers, p. 157-167.

Woodward-Clyde Consultants, 1985, Evaluation of fault activity and potential for future tectonic surface faulting — Allied Health Science Building site, Weber State College, Ogden, Utah: Unpublished consultant's report, 10 p.

Youd, T.L., 1973, Liquefaction, flow, and associated ground failure: U. S. Geological Survey Circular 688, 12 p.

———1977, Discussion of "Brief review of liquefaction during earthquakes in Japan" by Kuribayashi, Eiichi, and Tatsuoka, Fumio, 1975: Soils and Foundations, v. 17, no. 1, p. 82-85.

———1978a, Major cause of earthquake damage is ground failure: Civil Engineering, v. 48, no. 4, p. 47-51.

———1978b, Mapping liquefaction-induced ground failure potential: Proceedings of the American Society of Civil Engineers, Journal of Geotechnical Engineering Division, v. 4 no. 674, p. 433-446.

———1984, Geologic effects — liquefaction and associated ground failure: U.S. Geological Survey Open-File Report 84-760, p. 210-232.

Youd, T.L., Nichols, D.R., Helley, E.J., and Lajoie, K.R., 1975, Liquefaction potential, *in* Studies for Seismic Zonation in the San Francisco Bay Region: U. S. Geological Survey Professional Paper 941-A, p. A68-A74.

Youd, T.L., and Perkins, D.M., 1987, Mapping of liquefaction severity index: Journal of Geotechnical Engineering, v. 113, p. 1374-392.

Youngs, R.R., Swan, F.H., Power, M.S., Schwartz, D.P., and Green, R.K., 1987, Probabilistic analysis of earthquake ground shaking hazard along the Wasatch Front, Utah, *in* Hays, W.W., and Gori, P.L., eds., Assessment of Regional Earthquake Hazards and Risk Along the Wasatch Front, Utah, v. II: U.S. Geological Survey Open-File Report 87-585, p. M-1-110.

BIBLIOGRAPHY OF OTHER GEOLOGIC PAPERS WHICH INCLUDE THE OGDEN AREA

Early Reports

Blackwelder, Eliot, 1910, New light on the geology of the Wasatch Mountains, Utah: Geological Society of America Bulletin, v. 21, p. 517-542.

Hague, Arnold, and Emmons, S.F., 1877, Descriptive geology, v. 2 of report of the geological exploration of the fortieth parallel: Professional Papers of the Engineer Department of the U.S. Army, no. 18.

King, Clarence, 1878, Systematic geology, v. 1 of report of the geological exploration of the fortieth parallel: Professional Paper of the Engineer Department of the U.S. Army, no. 18.

Stansbury, Howard, 1853, Exploration and survey of the Great Salt Lake of Utah, including a reconnaissance of a new route through the Rocky Mountains: U.S. 32nd Congress Special Session, Senate Executive Document 3, 487 p.

Zirkel, Ferdinand, 1876, Microscopical petrography, v. 6 of report of the geological exploration of the fortieth parallel: Professional Paper of the Engineer Department of the U.S. Army, no. 18.

General Geology and Geologic Maps

Armstrong, R.L., 1968, Sevier orogenic belt in Nevada and Utah: Geological Society of America Bulletin, v. 67, no. 2, p. 429458.

Bell, G.L., 1951, Farmington Complex of the north-central Wasatch: Salt Lake City, University of Utah, unpublished Ph.D., thesis, 101 p.

———1952, Geology of the northern Farmington Mountains, *in* Marsell, R.E., ed., Geology of the Central Wasatch Mountains: Utah Geological Society Guidebook to the Geology of Utah, no. 9, p. 38-51.

Bruhn, R.L., and Beck, S.L., 1981, Mechanics of thrust faulting in crystalline basement, Sevier orogenic belt, Utah: Geology, v. 9, no. 5, p. 200-204.

Bryant, Bruce, 1978, Farmington Canyon Complex, Wasatch Mountains, Utah: Geological Society of America Abstracts with Programs, v. 10, no. 5, p. 211.

———1980, Metamorphic and structural history of the Farmington Canyon Complex, Wasatch Mountains, Utah: Geological Society of America Abstracts with Programs, v. 12, no. 5, p. 269.

———1984, Reconnaissance geologic map of the Precambrian Farmington Canyon Complex and surrounding rocks in the Wasatch Mountains between Ogden and Bountiful, Utah: U. S. Geological Survey Miscellaneous Investigation Series Map I-1447, 1:50,000 scale.

———1988, Geology of the Farmington Canyon Complex, Wasatch Mountains, Utah: U.S. Geological Survey Professional Paper 1476, 54 p., scale 1:50,000.

Bryant, Bruce, Hedge, C.E., and Stacey, J.S., 1980, Geology of the Farmington Canyon Complex, north-central Utah: Guidebook for Field Trip, no. 6, Precambrian Rocks of the northern Wasatch: Geological Society of America, Rocky Mountain Section Meeting, Ogden, Utah, 18 p.

Crawford, A.L., 1935, Archean metaquartzites east of Bountiful, Utah: Utah Academy of Science, v. 12, p. 167.

Crittenden, M.D., Jr., 1972, Willard thrust and the Cache Allochthon, Utah: Geological Society of America Bulletin, v. 83, p. 2871-2880.

Crittenden, M.D., Jr., and Sorensen, M.L., 1985, Geologic map of the North Ogden quadrangle and part of the Ogden and Plain City quadrangles, Box Elder and Weber Counties, Utah: U.S. Geological Survey Miscellaneous Investigations Series Map I1606, scale 1:24,000.

Davis, F.D., 1983, Geologic map of the central Wasatch Front: Utah Geological and Mineral Survey Map 54-A, scale 1:100,000.

———1985, Geologic map of the northern Wasatch Front: Utah Geological and Mineral Survey Map 53-A, scale 1:100,000.

Eardley, A.J, 1933, Strong relief before block faulting in the vicinity of the Wasatch Mountains, Utah: Journal of Geology, v. 41, p. 243-267.

———1939, Structure of the Wasatch-Great Basin region: Geological Society of America Bulletin, v. 50, p. 1277-1310.

———1969, Willard thrust and Cache uplift: Geological Society of America Bulletin, v. 80, p. 669-680.

Eardley, A.J., and Brasher, G.K., 1953, Tectonic map of northern Utah, southeastern Idaho, and western Wyoming, *in* Guide to the Geology of Northern Utah and Southeastern Idaho: Intermountain Association of Petroleum Geologists Fourth Annual Field Conference, p. 78-79.

Eardley, A.J., and Hatch, R.A., 1940, Precambrian crystalline rocks of north-central Utah: Journal of Geology, v. 48, p. 58-72.

Hedge, C.E., and Stacey, J.S., 1980, Precambrian geochronology of northern Utah: Geological Society of America Abstracts with Programs, v. 12, no. 62, p. 275.

Hedge, C.E., Stacey, J.S., and Bryant, Bruce, 1983, Geochronology of the Farmington Canyon Complex, *in* Miller, D.M., Todd, V.R., and Howard, K.A., eds., Tectonic and Stratigraphic Studies in the Eastern Great Basin: Geological Society of America Memoir 157, p. 37-44.

Naeser, C.W., Bryant, Bruce, Crittenden, M.D., Jr., and Sorensen, M.L., 1983, Fission-track ages of apatite in the Wasatch Mountains, Utah — an uplift study, *in* Miller, D.M., Todd, V.R., and Howard, K.A., eds., Tectonic and Stratigraphic Studies in the Eastern Great Basin: Geological Society of America Memoir 157, p. 29-36.

Royse, F., Jr., Warner, M.A., and Reese, D.L., 1975, Thrust-belt structural geometry and related stratigraphic problems, Wyoming-Idaho-northern Utah, *in* Bolyard, D.W., ed., Deep Drilling Frontiers of the Central Rocky Mountains: Rocky Mountain Association of Geologists Symposium, p. 41-54.

Schirmer, T.W., 1982, Multiple decollements and associated structures in the Wasatch Range near Ogden, Utah: Geological Society of America Abstracts with Programs, v. 14, no. 6, p. 349.

———1984, Correlation of the Ogden thrust, Durst Mountain thrust and allochthonous Precambrian Farmington Canyon Complex in the north-central Wasatch Range, Utah: American Association of Petroleum Geologists Abstracts, v. 68, no. 7, p. 948.

———1985, Sequential thrusting beneath the Willard thrust, Wasatch Range, Ogden, Utah: Logan, Utah State University, unpublished M.S. thesis, 199 p.

———1985, Basement thrusting in north-central Utah: a model for the development of the northern Utah highland, *in* Kerns, G.J., and Kerns, R.L., eds., Orogenic Patterns and Stratigraphy of North-Central Utah and Southeastern Idaho: Utah Geological Association Publication 14, p. 129-143.

———1988, Structural analysis using thrust-fault hanging-wall sequence diagrams: Ogden duplex, Wasatch Range, Utah: American Association of Petroleum Geologists Bulletin, v. 72, no. 5, p. 573-585.

Sorensen, M.L., and Crittenden, M.D., Jr., 1972, Preliminary geologic map of part of the Wasatch Range near North Ogden, Utah: U.S. Geological Survey Miscellaneous Field Studies Map MF-428, scale 1:24,000.

Temple, D.C., 1969, Mount Ogden Granite: Salt Lake City, University of Utah, unpublished M.S. thesis, 30 p.

Van Horn, Richard, 1975, Unevaluated reconnaissance geologic map of Salt Lake and Davis Counties, west of the Wasatch Front, Utah: U.S. Geological Survey Open-File Report 75-616, scale 1:100,000.

———1981, Geologic map of pre-Quaternary rocks of the Salt Lake City North Quadrangle, Davis and Salt Lake Counties, Utah: U.S. Geological Survey Miscellaneous Investigations Series Map I-1330, scale 1:24,000.

Ground Water

Bolke, E.L, and Waddell, K.M., 1972, Ground-water conditions in the East Shore area, Box Elder, Davis, and Weber Counties, Utah: Utah Department of Natural Resources Technical Publication 35, 59 p.

Dennis, P.E., 1952, Ground-water recharge in the East Shore area, Utah: U.S. Geological Survey Open-File Report, 17 p.

Dennis, P.E., and McDonald, H.R., 1944, Ground water in the vicinity of Ogden, Utah: U.S. Geological Survey Open-File Report, 106 p.

Smith, R.E., and Gates, J.S., 1963, Ground-water conditions in the central part of the East Shore area, Utah, 1953-61: Utah Geological and Mineral Survey Water-Resource Bulletin 2, 41 p.

Thomas, H.E., and Nelson, W.B., 1948, Ground water in the East Shore area, Utah; part 1, Bountiful district, Davis County: Utah State Engineer 26th Biennial Report, p. 52-206.

Seismicity

Brown, E.D., Arabasz, W.J., Pechmann, J.C., McPherson, Erwin, Hall, L.L., Oehmich, P.J., and Hathaway, G.M., 1986, Earthquake data for the Utah region, January 1, 1984 to December 31, 1985: Salt Lake City, University of Utah Seismograph Stations, 83 p.

Cook, K.L., 1972, Earthquakes along the Wasatch Front — the record and the outlook, *in* Hilpert, L.S., ed., Environmental Geology of the Wasatch Front, 1971: Utah Geological Association Publication 1, p. H1-H29.

Nava, S.J., Pechmann, J.C., Arabasz, W.J., Brown, E.D., Hall, L.L., Oehmich, P.J., McPherson, Erwin, and Whipp, J.K., 1990, Earthquake catalog for the Utah region, January 1, 1986 to December 31, 1988: Salt Lake City, University of Utah Seismograph Stations, 96 p.

Richins, W.D., Arabasz, W.J., Hathaway, G.M., Oehmich, P.J., Sells, L.L., and Zandt, George, 1981, Earthquake data for the Utah region, July 1, 1978 to December 31, 1980: Salt Lake City, University of Utah Seismograph Stations, 127 p.

Richins, W.D., Arabasz, W.J., Hathaway, G.M., McPherson, Erwin, Oehmich, P.J., and Sells, L.L., 1984, Earthquake Data for the Utah region, January 1, 1981 to December 31, 1983: Salt Lake City, University of Utah Seismograph Stations, 111 p.

Smith, R.B., 1972, Contemporary seismicity, seismic gaps, and earthquake recurrences of the Wasatch Front, *in* Hilpert, L.S., ed., Environmental Geology of the Wasatch Front, 1971: Utah Geological Association Publication 1, p. I-1 I-19.

Smith, R.B., and Richins, W.D., 1984, Seismicity and earthquake hazards of Utah and the Wasatch Front—Paradigm and paradox, *in* Hays, W.W., and Gori, P.L., eds., Workshop on "Evaluation of Regional and Urban Earthquake Hazards and Risk in Utah": U.S. Geological Survey Open-File Report 84-763, p. 73-112.

Earthquake Ground Shaking

Campbell, K.W., 1987, Predicting strong ground motion in Utah, *in* Hays, W.W., and Gori, P.L., eds., Assessment of Regional Earthquake Hazards and Risk Along the Wasatch Front, Utah: U.S. Geological Survey Open-File Report 87-585, v. II, p. L-1-90.

Hays, W.W., 1987, Site amplification in the Salt Lake City-Ogden-Provo, Utah, corridor and the implications for earthquake-resistant design, *in* Hays, W.W., and Gori, P.L., eds., Assessment of Regional Earthquake Hazards and Risk Along the Wasatch Front, Utah, v. II: U.S. Geological Survey Open-File Report 87-585, p. K-1-69.

Hays, W.W., and King, K.W., 1984, The ground-shaking hazard along the Wasatch fault zone, Utah: Eighth World Conference on Earthquake Engineering Proceedings, v. 1, p. 7-14.

——1984, The ground-shaking hazard along the Wasatch fault zone, *in* Hays, W.W., and Gori, P.L., eds., Proceedings of Conference XXVI, A Workshop on "Evaluation of Regional and Urban Earthquake Hazards and Risk in Utah": U.S. Geological Survey Open-File Report 84-763, p. 133-147.

King, K.W., Hays, W.W., and McDermott, P.J., 1983, Wasatch Front urban area seismic response data report: U.S. Geological Survey Open-File Report 83-452, 66 p.

Wasatch Fault Zone

Bruhn, R.L., Gibler, P.R., and Parry, W.T., 1987, Rupture characteristics of normal faults — An example from the Wasatch fault zone, Utah, *in* Coward, M.P., Dewey, J.F., and Hancock, P.L., eds., Continental Extensional Tectonics: Geological Society of London Special Publication No. 28, p. 337-353.

Cluff, L.S., Brogan, G.S., and Glass, C.E., 1970, Wasatch fault, northern portion, earthquake fault investigation and evaluation, prepared for the Utah Geological and Mineral Survey: Oakland, California, Woodward-Clyde and Associates, 27 p., 21 maps, scale 1:24,000.

Crone, A.J., and Harding, S.T., 1984, Near-surface faulting associated with Holocene fault scarps, Wasatch fault zone, Utah — a preliminary report, *in* Hays, W.W., and Gori, P.L., eds., Proceedings of Conference XXVI — A Workshop on "Evaluation of Regional and Urban Earthquake Hazards and Risk in Utah": U.S. Geological Survey Open-File Report 84-763, p. 241-268.

Forman, S.L., Jackson, M.E., McCalpin, James, and Maat, Paula, 1988, The potential of using thermoluminescence to date buried soils developed on colluvial and fluvial sediments from Utah and Colorado, U.S.A.: preliminary results: Quaternary Science Review, v. 7, p. 287-293.

Lund, W.R., 1989, Paleoseismicity of the Wasatch fault zone, current understanding and portent for the future: Association of Engineering Geologists 32nd Annual Meeting Abstracts and Program, p. 91.

Marsell, R.E., 1964, The Wasatch fault zone in north central Utah, *in* Marsell, R.E., ed., The Wasatch Fault Zone in North Central Utah: Utah Geological Society Guidebook to the Geology of Utah no. 18, p. 1-14.

Morisawa, Marie, 1972, The Wasatch fault zone general aspects, *in* Hilpert, L.S., ed., Environmental Geology of the Wasatch Front, 1971: Utah Geological Association Publication 1, p. D1-D17.

Nelson, A.R., and Personius, S.F., 1987, A nonconservative barrier to Holocene rupture propagation in the northern Wasatch fault zone, Utah: Proceedings of XII INQUA Congress, July 31-August9, 1987, Ottawa, Canada.

Schwartz, D.P., Swan, F.H., and Cluff, L.S., 1984, Fault behavior and earthquake recurrence along the Wasatch fault zone: U.S. Geological Survey Open-File Report 84-763, p. 113-125.

Wheeler, R.L., and Krystinik, K.B., 1987, Persistent and nonpersistent segmentation of the Wasatch fault zone, Utah — statistical analysis for evaluation of seismic hazard, *in* Hays, W.W., and Gori, P.L., eds., Assessment of Regional Earthquake Hazards and Risk Along the Wasatch Front, Utah, v. I: U.S. Geological Survey Open-File Report 87-585, p. B-1-124.

Wood, S.H., 1984, Contemporary vertical tectonics along the Wasatch fault zone measured by repeated geodetic leveling, *in* Hays, W.W., and Gori, P.L., eds., Proceedings of Conference XXVI — Workshop on "Evaluation of Regional and Urban Earthquake Hazards and Risk in Utah": U.S. Geological Survey Open-File Report 84-763, p. 269-285.

Zoback, M.L., 1983, Structure and Cenozoic tectonism along the Wasatch fault zone, Utah, *in* Miller, D.M., Todd, V.R., and Howard, K.A., eds., Tectonic and Stratigraphic Studies in the Eastern Great Basin: Geological Society of America Memoir 157, p. 3-27.

Liquefaction

Anderson, L.R., Keaton, J.R., Bay, J.A., and Rice, J.D., 1987, Liquefaction potential mapping, Wasatch Front, Utah, *in* McCalpin, James, ed., Proceedings of the 23rd Annual Symposium on Engineering Geology and Soils Engineering: Logan, Utah State University, p. 1-17.

Mabey, M.A., and Youd, T.L., 1989, Liquefaction severity index maps of the State of Utah, *in* Waters, R.J., ed., Proceedings of the 25th Annual Engineering Geology and Geotechnical Engineering Symposium: Reno, University of Nevada-Reno, p. 305-312.

Sensitive Clays

Parry, W.T., 1974, Earthquake hazards in sensitive clays along the Wasatch Front, Utah: Geology, v. 2, no. 11, p. 559-560.

Landslides

Blackett, R.E., 1979, Landslide hazards in the Weber River Delta near Ogden, Utah: Salt Lake City, University of Utah, unpublished M.S.

thesis, 72 p.

Harp, E.L., Wells, W.G., II, and Sarmiento, J.J., 1990, Pore pressure response during failure in soils: Geological Society of America Bulletin, v. 102, p. 428-438.

Keaton, J.R., 1986, Landslide inventory and preliminary hazard assessment, southeast Davis County, Utah: Association of Engineering Geologists 29th Annual Meeting Program with Abstracts, p. 53.

Monteith, Sara, Anderson, L.R., and Keaton, J.R., 1990, Analysis of Steed Canyòn Landslide, *in* Robinson, Lee, ed., Proceedings of the 26th Annual Symposium on Engineering Geology and Geotechnical Engineering: Pocatello, Idaho State University, p. 31-1-31-17.

Debris Flows, Debris Floods, and Alluvial-Fan Flooding

Ala, Souren, 1989, The influence of bedrock on debris flows along the Wasatch Front, Utah: Association of Engineering Geologists 32nd Annual Meeting Abstracts and Program, p. 48.

———1990, Relationship between bedrock structural fabric and groundwater flow, Wasatch Front, Utah, *in* Robinson, Lee, ed., Proceedings of the 26th Annual Symposium on Engineering Geology and Geotechnical Engineering: Pocatello, Idaho State University, p. 22-1-22-17.

Ala, Souren, and Mathewson, C.C., 1990, Structural control of groundwater induced debris flows, *in* French, R.H., ed., Hydraulics/Hydrology of Arid Lands (H^2AL): American Society of Civil Engineers, p. 590-595.

Anderson, L.R., Keaton, J.R., Saarinen, T.F., and Wells, W.G., II, 1984, The Utah landslides, debris flows, and floods of May and June, 1983: Washington D.C., National Academy Press, 96 p.

Bailey, R.W., 1935, Shackling the mountain flood: American Forests, v. 41, no. 3, p. 101-104.

———1941, Land erosion: normal and accelerated in the semiarid west: Transactions of the American Geophysical Union, v. 22, p. 240-250.

Bailey, R.W., Craddock, G.W., and Croft, A.R., 1947, Watershed management for summer flood control, Utah: U.S. Department of Agriculture Miscellaneous Publication 639, 24 p.

Bailey, R.W., and Croft, A.R., 1937, Contour trenches control floods and erosion on range lands: Washington D.C., Emergency Conservation Work Forestry Publication No. 4, 22 p.

Bailey, R.W., Forsling, C.L., and Becraft, R.J., 1934, Floods and accelerated erosion in northern Utah: U. S. Department of Agriculture Miscellaneous Publication 196, 21 p.

Cannon, S.Q., 1931, Torrential floods in northern Utah, 1930, report of Special Flood Commission: Utah Agricultural Experiment Station Circular 92, 51 p.

Coleman, K.W., 1989, Role of contour trenching in the alteration of hydrogeologic conditions of the Wasatch Front: Association of Engineering Geologists 32nd Annual Meeting Abstracts and Program, p. 57.

———1990, The effect of contour trenching of hydrogeologic conditions of the Wasatch Front: Association of Engineering Geologists 33rd Annual Meeting Abstracts and Program, p. 100.

Craddock, G.W., 1960, Floods controlled on Davis County watersheds: Journal of Forestry, v. 58, no. 4, p. 291-293.

Crawford, A.L., and Thackwell, F.E., 1930, Some aspects of the mudflows north of Salt Lake City, Utah: presented at Utah Society of Engineers Conference, November 19, 1930, 12 p.

Croft, A.R., 1936, Why all these floods?: Utah Farmer, v. 57, no. 6, p. 1-11.

———1962, Some sedimentation phenomena along the Wasatch Mountain Front: Journal of Geophysical Research, v. 67, no. 4, p. 1511-1524.

———1967, Rainstorm debris floods: a problem in public welfare: University of Arizona Agricultural Experiment Station Report 248, 36 p.

Croft, A.R., and Bailey, R.W., 1964, Mountain water: U. S. Forest Service Intermountain Region Publication, 64 p.

Croft, A.R., and Marston, R.B., 1950, Summer rainfall characteristics in northern Utah: Transactions of the American Geophysical Union, v. 31, p. 83-95.

Eblin, J.S., 1990, The influence of colluvial variations on the slope stability of three drainage basins along the Wasatch Front, Davis County, Utah: Association of Engineering Geologists 33rd Annual Meeting Abstracts and Program, p. 94-95.

———1991, A probabilistic investigation of slope stability in the Wasatch Range, Davis County, Utah, *in* McCalpin, J.P., ed., Proceedings of the 27th Symposium on Engineering Geology and Geotechnical Engineering: Logan, Utah State University, p. 18-1, 18-16.

Keaton, J.R., 1988, A probabilistic Model for hazards related to sedimentation processes on alluvial fans in Davis County, Utah: College Station, Texas A&M University, 441 p.

———1988, Stratigraphy of alluvial fan flood deposits, *in* Abt, S.R., and Gessler, Johannes, eds., Hydraulic Engineering: Colorado Springs, Proceedings of the 1988 National Conference of the Hydraulics Division of the American Society of Civil Engineers, p. 149-154.

———1989, Engineering versus geologic approach to evaluating debris flow hazards: Association of Engineering Geologists 32nd Annual Meeting Abstracts and Program, p. 84.

———1990, Predicting alluvial-fan sediment-water slurry characteristics and behavior from sedimentology and stratigraphy of past deposits, in, French, R.H., ed., Hydraulics/Hydrology of Arid Lands (H^2AL): American Society of Civil Engineers, p. 608-613.

Keaton, J.R., and Mathewson, C.C., 1987, Proposed ideal alluvial fan stratigraphy for risk assessment: Geological Society of America Abstracts with Program, v. 19, no. 7, p. 723.

———1988, Stratigraphy of alluvial fan flood deposits, *in* Abt, S.R., and Gessler, Johannes, eds., Hydraulic Engineering: Colorado Springs, Proceedings of the 1988 National Conference of the Hydraulics Division of the American Society of Civil Engineers, p. 149-154.

Keaton, J.R., Mathewson, C.C., and Anderson, L.R., 1987, Hazards and risks associated with alluvial fan processes in Davis County, Utah: Association of Engineering Geologists Abstracts with Program, 30th Annual Meeting, p. 42.

Marston, R.B., 1952, Ground cover requirements for summer storm runoff control on aspen sites in northern Utah: Journal of Forestry, v. 50, no. 4, p. 303-307.

———1958, Parrish Canyon, Utah: a lesson in flood sources: Journal of Soil and Water Conservation, v. 13, no. 4, p. 165-167.

Mathewson, C.C., 1989, Hydrogeology and debris flows in the Farmington Canyon Complex, Davis County, Utah: Association of Engineering Geologists 32nd Annual Meeting Abstracts and Program, p. 93.

Mathewson, C.C., Keaton, J.R., and Santi, P.M., 1990, Role of bedrock ground water in the initiation of debris flows and sustained post-flow stream discharge: Bulletin of the Association of Engineering Geologists, v. 27, no. 1, p. 73-83.

Meeuwig, R.O., 1970, Infiltration and soil erosion as influenced by vegetation and soil in northern Utah: Journal of Range Management, v. 23, p. 185-188.

Olson, E.P., 1985, East Layton debris flow: U. S. Department of Agriculture Forest Service, Intermountain Region, Report G-R-4-85-2, 24 p.

Olson, O.C., 1949, Relations between soil depth and accelerated erosion on the Wasatch Mountains: Soil Science, v. 67, no. 6, p. 447-451.

Paul, J.H., and Baker, F.S., 1923, The floods in northern Utah: University of Utah Bulletin, v. 15, no. 3, 20 p.

Pierson, T.C., 1985, Effects of slurry composition on debris flow dynamics, Rudd Canyon, Utah, *in* Bowles, D. S., ed., Delineation of Landslide, Flash Flood, and Debris Flow Hazards in Utah: Logan, Utah Water Research Laboratory Publication G-85/03, Utah State University, p. 132-152.

Santi, P.M., 1988, The kinematics of debris flow transport down a canyon: College Station, Texas A&M University, unpublished M.S. thesis, 85 p.

———1989, The kinematics of debris flow transport down a canyon: Bulletin of the Association of Engineering Geologists, v. 26, no. 1, p. 5-9.

Santi, P.M., and Mathewson, C.C., 1988, What happens between the scar and the fan? The behavior of a debris flow in motion, *in* Fragaszy, R.J., ed., Proceedings for the 24th Annual Symposium on Engineering Geology and Soils Engineering: Pullman, Washington State University, p. 73-88.

Skelton, R.K., 1990, Investigation to determine the geological control of springs and seeps in the Farmington Canyon Complex, Davis County, Utah: Association of Engineering Geologists 33rd Annual Meeting Abstracts and Program, p. 100.

Stream Flooding

U.S. Army Corps of Engineers, 1984, Wasatch Front and central Utah flood control study, Utah: Sacramento District, U. S. Army Corps of Engineers, 180 p.

Woolley, R.R., 1946, Cloudburst floods in Utah, 1850-1938: U. S. Geological Survey Water-Supply Paper 994, 128 p.

Lake Flooding

Utah Division of Water Resources, 1977, Great Salt Lake hydrologic system management alternatives report: Utah Department of Natural Resources, 32 p.

Dam Failure

Utah Division of Water Rights, 1986-1987, Hydrologic analyses for various dams in Utah: Unpublished computer printouts.

ALTERATION, MINERAL DEPOSITS, AND STRUCTURAL RELATIONSHIPS OF THE OQUIRRH MOUNTAINS, UTAH: ROAD LOG

by
Paula N. Wilson
Dept. of Geology and Geophysics, University of Utah
and
Ricardo D. Presnell
Kennecott Exploration Company

INTRODUCTION

A general road log for this field trip is given below. Because the stops on this trip are predominantly mine tours and because several papers pertaining to the geology and mineral deposits of the Oquirrh Mountains are included in this guidebook, only a generally descriptive road log is presented. The geology of the range, locations of the various mineral deposits, and the route for this trip can be found on Figure 1 (after Presnell, 1992).

This trip will highlight recent geochemical and structural studies of mineral deposits in the Oquirrh Mountains, Utah. This range is unique in its concentration and diversity of mineral deposits, which include porphyry copper, Pb-Zn-Ag-Au fissure controlled replacement, Pb-Zn distal skarn, and disseminated gold deposits. The trip will consist of an overview of the Bingham porphyry copper mine and tours of Kennecott's Barney's Canyon and Barrick's Mercur gold mines. Emphasis will be placed on mineralization, alteration, and structures. Mine tours will include discussions of structural and stratigraphic control of gold deposition, relationships between the Bingham system and gold mineralization, tectonic settings of gold and base metal mineralization, and evidence for a possible Mesozoic age for gold deposits in the Oquirrh Mountains.

Several papers included in this guidebook by Presnell, Kroko, Wilson and Parry, and Wilson and Wilson present new data and genetic theories for the Mercur and Barney's Canyon disseminated gold deposits.

0 Mi.	Exit # 301 on Interstate 15, Salt Lake City, Utah. This is the 72nd South exit at Midvale. Exit interstate and turn west on Hwy. 48 and follow signs to "Copper Mine."
0.2 Mi.	Turn left at traffic light onto 700 West (this is still Hwy. 48).
1.0 Mi	Turn right and stay on Hwy. 48.
5.0 Mi.	Veer left at the Y intersection (stay on Hwy. 48). To the right (1:00) are the dumps and cuts of Kennecott's Barney's Canyon (lower) and Melco (higher and further south) gold deposits. Straight ahead are the large dumps of Kennecott's Bingham Canyon copper mine.
11.4 Mi.	Barney's Canyon Mine entrance road. This mine is not accessible by general public. Continue straight.
13.4	Bingham Mine guard station. The general public is free to visit the mine overlook, but must check in with the guard first. There is a fee for the visit.
15.8 Mi.	Overlook parking lot. The visitors center and bathrooms are located on the south side of the lot. Papers by Presnell relate to the geology of Bingham and the immediate area. An excellent reference for the geology of this deposit is the special issue of Economic Geology devoted to the Bingham Mine area published in 1978, v. 73, no. 7. The Bingham Canyon deposit is a porphyry copper deposit which also contains con-

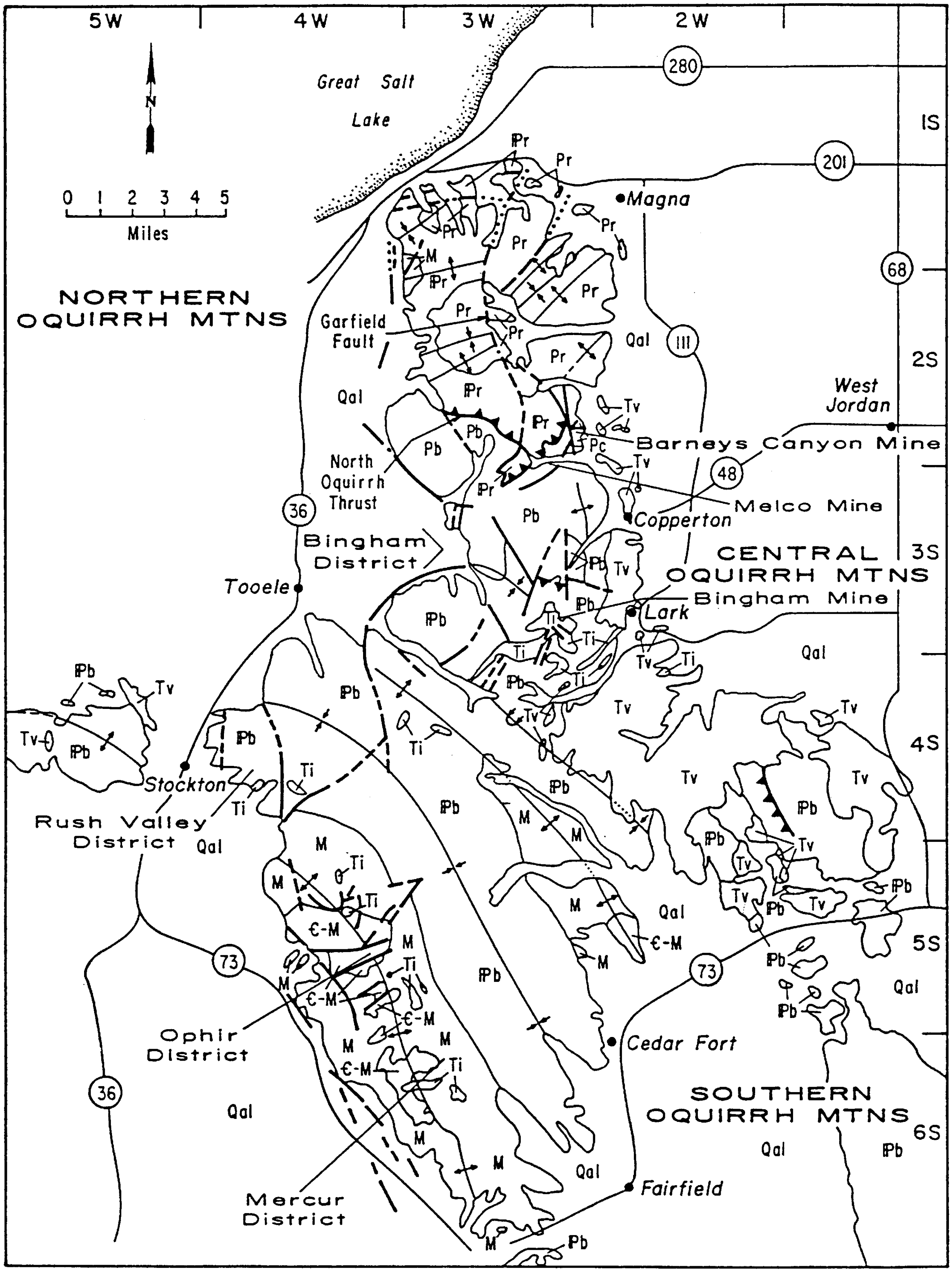

Figure 1. Road map and geologic map for Oquirrh Mountains (from Presnell, 1992).

siderable amounts of gold. Mineralization occurred between 36.6 and 39.8 Ma (Warnaars et al., 1978). Mineralization and alteration are related to and zoned about the quartz monzonite porphyry (Lanier et al., 1978). Mineralization in the immediate district includes Cu-Mo porphyry ore, Cu-(Au) skarn ore, and Cu-Pb-Zn-(Au-Ag) fissure ore.

Fissure-related ore occurs as concordant bedding fissures, crosscutting fissures, and replacement deposits. These ore bodies have been mined for up to 10,000 feet (3,300 m) outward from the center of the Bingham stock. Host rock for these deposits are limestones of varying degrees of alteration. Limestone alteration varies from skarn-like rocks consisting of garnet, wollastonite, diopside, tremolite, and specularite to quartz-chlorite-mica-smectite-calcite alteration to unaltered limestone (Rubright and Hart, 1968).

Considerable debate has centered on the genetic relationship between the Bingham Canyon system and gold mineralization at Barney's Canyon to the north. Because of their close proximity and the gold-rich nature of the Bingham deposit, many people have proposed a genetic link. However, the geothermal cell at Bingham appears to have been too small to have accounted for fluid temperatures at Barney's Canyon (Fig. 2) and Mesozoic ages from illite in gold-bearing fault gouge obtained from bedding plane slip faults resulting from compressive forces have indicated a possible Mesozoic age for the Barney's Canyon system (Presnell, 1992).

15.8 Mi. Retrace route back to Barney's Canyon turnoff.

20.3 Mi. Turn left at the sign onto road to Barney's Canyon. Papers by Gunter, and Presnell relate to the geology of Barney's Canyon and immediate area.

Subsequent mileage does not include distance to Barney's Canyon and back.

22.1 Mi. Turn left (north) onto Hwy. 111. Look left (east) across Salt Lake Valley to the steep, normal fault controlled Wasatch Front. Also note U-shaped glaciated entrance to Little Cottonwood Canyon.

27.9 Mi. Junction of Hwy. 111 and Hwy. 173. Continue straight on Hwy. 111.

34.0 Mi. Kennecott's concentrator and acid plant on left side of road.

41 Mi. (approx.) At the time of planning the trip there was a detour to Interstate 80. The detour brings traffic to the interstate at the Saltair State Park. Under normal circumstances continue straight on Hwy. 111 to the entrance to I-80.

41.9 Mi. (approx.) Enter I-80 westbound. The northern end of the Oquirrh Mountains contains folds and tear faults related to emplacement of the north Oquirrh thrust. The steeply dipping and overturned strata seen behind Kennecott's smelter complex are a result of this event.

42.2 Mi. Great Salt Lake view area.

43.7 Mi. Exit onto Hwy. 36. Proceed south to Tooele. Kessler anticline and the Mill Junction syncline can be seen at 9:00.

46.9 Mi. Note prominent stack from pluvial Lake Bonneville on left side of road.

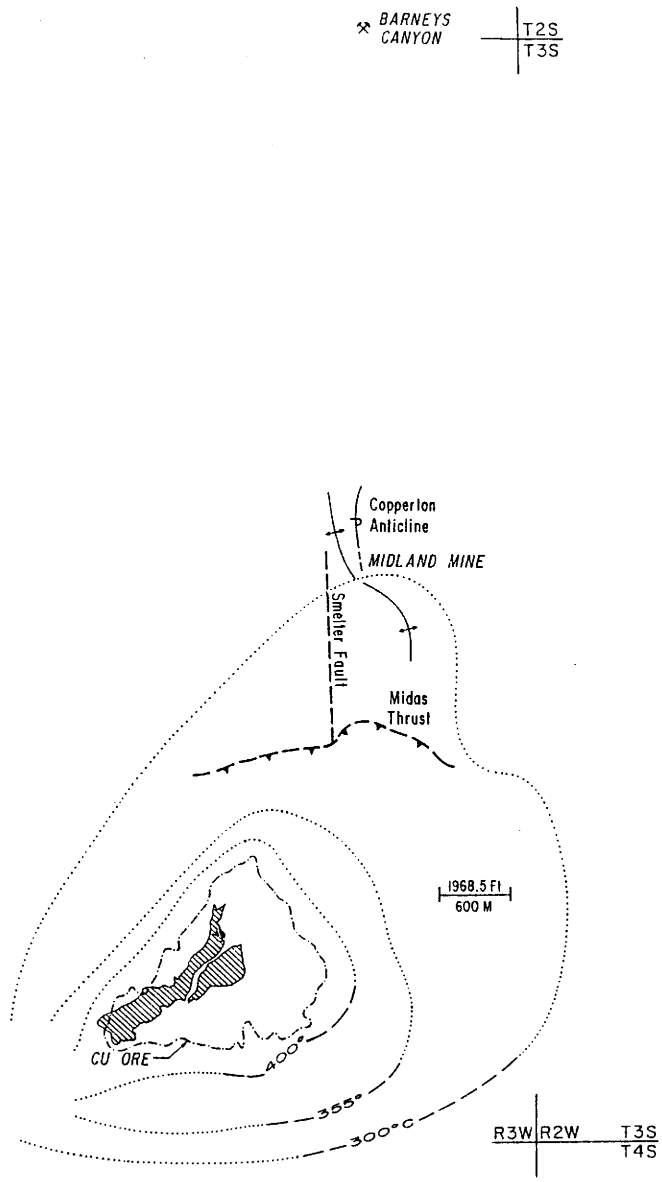

Figure 2. Simplified temperature contour map of the Bingham hydrothermal system from Presnell (1992) based on the fluid inclusion data of Bowman et al. (1987) and Roedder (1971), and alteration of Lanier et al. (1978), and mineral zonation of Atkinson and Einaudi (1978). The 400 °C contour is the limit of potassic alteration and the mean of fluid inclusion homogenization temperatures from within the potassic zone. The 355 °C contour is the limit of propylitic alteration and the mean homogenization temperature from within the propylitic zone. The 300 °C contour represents the limit of the Pb-Zn halo and the average homogenization temperature from within the Pb-Zn halo (Presnell, 1992).

51.7 Mi. Black dump at base of Oquirrh Mountains to left (10:00) is tailings from the Carr Fork skarn deposit, now owned by Kennecott.

55.5 Mi. Tooele.

56.3 Mi. Turn right onto Vine St.

56.8 Mi. Lunch at park located at 200 West and Vine St.

56.8 Mi. Return to Main St. via Vine St.

57.3 Mi. Turn right (south) onto Main St. and continue south.

59.3 Mi. Note green igneous outcrops at base of hill on left side of road. Dated at 32 Ma (F. Brown, pers. comm).

60.2 Mi. Entrance to Tooele Army Depot. View of the Stockton Bar, formed in pluvial Lake Bonneville, ahead and to left. Deseret Peak and Stansbury Mountains visible on west side (right) of valley. Can also see Lake Bonneville shorelines on South Mountain (in center of valley). The top shoreline is the Bonneville level, the lower shoreline is the Provo level.

62.4 Mi. Crossing the Stockton Bar.

62.8 Mi. Here Hwy. 36 parallels a spit extending from the Stockton Bar. This spit continues on into the town of Stockton. Also visible in the hills on the left side of road are mine dumps of the Stockton District. The following description is taken from Gilluly (1932). Deposits here are pod-like Pb-Zn-Ag replacement deposits in limestone which are controlled by N-S-striking fissures which dip steeply west. These deposits are described as having strong stratigraphic control and form only in carbonate beds of the Pennsylvanian Oquirrh formation. Alteration associated with sulfides is slight and usually consists of sericite and silica. Adjacent strata are replaced by lime silicate hornfels which commonly consist of diopside and wollastonite, but the hornfels are rarely associated with sulfides. The ore bodies vary in size with a maximum pitch length of 600 meters (1800 feet). Sulfide mineralogy consists of pyrite, argentiferous galena, sphalerite, and minor chalcopyrite. Gangue minerals are mainly quartz, sericite, calcite, and minor epidote.
These deposits have not been dated, but their many similarities to the fissure ores at Bingham suggest that they are probably related to the Bingham system.

65.7 Mi. Rush Lake visible on the left. Once almost dry, this lake greatly enlarged during the wet years of the early 1980 s. The lake is now beginning to dry up again.

69.1 Mi. Veer left at the Y-intersection, taking Hwy. 73. Head south-east.

73.7 Mi. Turnoff to Ophir Canyon. Dry Canyon is next canyon to north. Mining activity in the Pb-Zn-Ag deposits of this district continued until the late 1970 s. The deposits consist of fissure controlled limestone replacement deposits similar to those of the Stockton district (Gilluly, 1932) and the fissure-controlled distal skarn Pb-Zn-Ag deposit of the Ophir Hill Mine. The Ophir Hill deposit differs from others in the Ophir and Stockton districts in that the sulfides extensively replace skarn and hornfels. A geochemical study of this deposit by Wilson and Parry (1991) has shown that skarn mineralizing fluids varied from initial temperatures near 200 °C and salinities of 5.2 eq. wt. % NaCl during formation of adularia reaction skarn; to temperatures of 425 °C and dropping to 325 °C and salinities of 9 eq. wt. % NaCl during diopside and epidote formation. XCO_2 of skarn fluids was < 0.1 and pressure was about 450 bars. Sulfide precipitation resulted from boiling and mixing of a low salinity, CO_2-rich fluid which appears to have been introduced immediately after boiling. Main stage sulfide mineralization occurred at 300 °C from fluids with salinity of 4 eq. wt. % NaCl and a XCO_2 content of 0.035. Pressure during formation of this deposit varied from hydrostatic at 120 bars (depth of approximately 1.3 km) to partially lithostatic at approximately 440 bars.

75.9 Mi. West Dip. Dumps of black, carbonaceous shale and red oxidized shale containing veins of ammonium illite are visible on left side of road. Gold was mined here in the late 1800 s and from 1913 until 1917. These deposits were in the West Mercur fault, a high-angle normal fault which Gilluly (1932) has interpreted to have moved during both the early Tertiary (pre-Miocene) and during more recent Basin and Range activity. The ore here was similar to that at Mercur, but its relationship, if any, to the West Mercur fault is unknown. This fault system is currently under study by W. T. Parry and R. L. Bruhn (University of Utah) in order to further understand the relationship of faulting and ore.

77.9 Mi. Turnoff to Mercur Canyon. Turn left and proceed up the Canyon to the guard station and visitors center. Mercur Canyon cuts through the Ophir anticline and the change in bedding orientation is visible as you proceed up the road.

81.3 Mi. Barrick Mercur Mine guard station and visitors center. The Mercur Mine is not open to the general public. Papers in this volume by Stanger, Kroko, Wilson and Parry, and Wilson and Wilson relate to the geology of the Mercur Mine. Tour of Mercur Mine. Return to Hwy. 73.

84.7 Mi. Junction with Hwy 73. Turn left (south) onto Hwy. 73.

92.0 Mi. Just past Utah County Line. Turn left onto gravel road. Proceed toward rock piles seen in middle distance. Stay on the main gravel road.

92.8 Mi. Take left fork of road and head for the large limestone rock pile in front of you.

93.2 Mi. Large open pit behind the limestone rock pile. This pit is one of several in the area which is being mined for brick clay. The illite-like, ammonium-rich phyllosilicate, tobelite, has been found in this pit. Dating of a tobelite vein collected here resulted in an age of 189 Ma. Note the oxidation, shale deformation, and occasional gossan development in the shales at the bottom of the pit. Information relating to tobelite and ammonium illite veins here and throughout the southern Oquirrh Mountains and their possible relationships of gold mineralization at Mercur can be found in Wilson and Parry of this volume. Retrace route back to Hwy. 73.

94.9 Mi. Junction of gravel road with Hwy. 73. Turn left (east) onto Hwy. 73.

94.9 Mi. Turn onto dirt road on left and pull off for view up Manning Canyon. Return to Hwy. 73 and proceed east.

112.7 Mi. Lake Mountains to south.

114.7 Mi. Mount Timpanogos straight ahead. Lone Peak is high, gray peak to left at 10:00.

118.8 Mi. Turn left onto 500 West at the Maverick gas station.

119.9 Mi. Turn left onto State St.

120.9 Mi. Junction with I-15. Take northbound entrance to Salt Lake City.

REFERENCES

Atkinson, W. W., Jr., and Einaudi, M. T., 1978, Skarn formation and mineralization in the contact aureole at Carr Fork, Bingham, Utah: Economic Geology, v. 73, p. 1326-1365.

Bowman, J. R., Parry, W. T., Kropp, W. P., Kruer, S. A., 1987, Chemical and isotopic evolution of hydrothermal solutions, Bingham Utah: Economic Geology, v. 82, p. 395-428.

Gilluly, J., 1932, Geology and ore deposits of the Stockton and Fairfield quadrangles, Utah: U.S. Geological Survey Professional Paper 173, 171 p.

Lanier, G., John, E. C., Swenson, A. J., Reid, J., Bard, C. E., Caddey, S. W., and Wilson, J. C., 1978, General geology of the Bingham Mine, Bingham Canyon, Utah: Economic Geology, v. 73, p. 1228-1241.

Presnell, R. D., 1992, In Prep., Geology and geochemistry of the Barneys Canyon gold deposit, Salt Lake County, Utah: Unpub. Ph.D. Dissertation, University of Utah.

Roedder, E., 1971, Fluid inclusion studies on the porphyry-type ore deposits at Bingham, Utah, Butte, Montana, and Climax, Colorado: Economic Geology, v. 66, p. 98-120.

Rubright, R. D., and Hart, O. J., 1968, Non-porphyry ores of the Bingham District, Utah: *in* Ridge, J. D., (ed), Ore Deposits of the United States, 1933-1967, The Graton-Sales Volume, v. 1: The American Institute of Mining, Metallurgical, and Petroleum Engineers, Inc., New York, p. 886-908.

Warnaars, F. W., Smith, W. H., Bray, R. E., Lanier, G., and Shafiqullah, M., 1978, Geochronology of igneous intrusions and porphyry copper mineralization at Bingham, Utah: Economic Geology, v. 73, p. 1228-1241.

Wilson, P. N., and Parry, W. T., 1991, Thermal and chemical evolution of hydrothermal fluids at the Ophir hill mine, Ophir District, Utah, *in* Allison, M. L., (ed.) Energy and mineral resources of Utah: Utah Geological Association Publication 18, 1990 Guidebook, p. 97-112.

LOCAL AND REGIONAL GEOLOGY OF THE OQUIRRH MOUNTAINS

by
Ricardo D. Presnell
Kennecott Exploration Company, Salt Lake City, Utah

ABSTRACT

The Oquirrh Mountains are located in north-central Utah near the boundary between the Basin and Range province and the Colorado Plateau. The Oquirrh Mountains have had a long and complex geologic history. The Oquirrh Mountains occur on a cratonic margin active since the Archean. The late Precambrian Uinta aulacogen coincides with the Archean cratonic margin and extends westward through the Oquirrh Mountains as the Uinta-Cortez axis. The Uinta-Cortez axis became the locus of tectonic and igneous activity throughout the Phanerozoic. During the late Paleozoic, 7.5 kilometers of shallow-water carbonates and siliciclastics were deposited in the Oquirrh basin. Oquirrh basin sediments make up the bulk of the range and host many of the ore deposits in the Oquirrh Mountains. During the Mesozoic the Oquirrh Mountains experienced compressional deformation which formed the folds and thrusts exposed in the range. K-Ar dating of illite veins suggests that this deformation is Jurassic in age. The pattern of folding and thrust faulting has been influenced by the eastward movement of Oquirrh basin sediments against the Uinta arch buttress. During the Cenozoic the Oquirrh Mountains experienced at least two extensional events: 1) Eocene to Oligocene and 2) Miocene to Recent. The present-day location of the Oquirrh Mountains is at the junction of the edge of the Archean craton, the Wasatch line and the Uinta-Cortez axis. The ore deposits in the Oquirrh Mountains are the result of this long and complex geologic history.

INTRODUCTION

The Oquirrh Mountains are located in north-central Utah. North-central Utah straddles the boundary between the Basin and Range and the Colorado Plateau physiographic provinces. The Oquirrh Mountains occur on a cratonic margin active since the Archean and the area of overlap between the Basin and Range extensional terrain and the Cordilleran Fold and Thrust belt. The first part of this paper addresses the geologic history of north-central Utah and its bearing on the geology of the Oquirrh Mountains. The second part discusses the geology of the Oquirrh Mountains with particular emphasis on the Bingham mining district, which occurs in the central part of the range.

REGIONAL GEOLOGY

Archean and Proterozoic History

The margin of the Archean craton (Wyoming Province) trends east-west across northern Utah. The edge of the Archean craton is represented at the southern edge of the Farmington Canyon Complex in the central Wasatch Range (Bryant, 1988). Based on lead isotopes, Stacey et al., (1968) concluded that the crust under the Oquirrh Mountains is either a mix of Archean and 1650 million year old crustal material or reflects a 2000-2300 m.y. B.P. crustal event. These data suggest that the edge of the Archean craton may be at or near the present-day location of the Oquirrh Mountains

(Fig. 1). The edge of the craton extends eastward to the Uinta aulacogen.

Five kilometers of Precambrian sandstone and shale that were deposited in the area of the Uinta Mountains have been interpreted as the fill of an east-trending aulacogen (Bruhn et al., 1986) that appears to coincide with the edge of the Archean craton (Sears et al., 1982). Rifting was initiated 1,550 m.y. B.P. and culminated in a late Proterozoic or early Cambrian rifting event (Sears et al., 1982; Stewart, 1972, 1976; Armin and Mayer, 1983; Bond et al., 1984, 1985). The Uinta aulacogen extends westward as the Uinta-Cortez axis and was reactivated during several epeirogenic uplifts in the Paleozoic (Roberts et al., 1965). The north-south arms of the rift margin are coincident with the Wasatch line of Kay (1951) (Stewart, 1972). The Wasatch line and the Uinta aulacogen became a locus of subsequent tectonic and igneous activity (Stokes, 1976). The present-day location of the Oquirrh Mountains is just west of the intersection of these two crustal breaks (Fig. 1).

Paleozoic History

Until the Late Pennsylvanian, north-central Utah experience subsidence and sedimentation associated with a passive continental margin. During the Upper Pennsylvanian through the Lower Permian 7.5 kilometers (25,000 feet) of shallow water carbonates and siliciclastics were deposited in the Oquirrh basin (Jordan and Douglas, 1980) (see Fig. 1). Sedimentation in the Oquirrh basin was localized by a northwest-trending graben or half-graben (Jordan and Douglas, 1980). Rapid facies changes are common and are a result of the depositional setting rather than being produced by facies being telescoped during subsequent deformation (Jordan and Douglas, 1980).

By the late Permian, north-central Utah returned to a passive margin during deposition of the Phosphoria Formation which is time equivalent to the Grandeur Member of the Park City Formation (Roberts et al., 1965). Strata deposited just before the initiation of the Oquirrh basin host the ore deposits at Mercur, Stockton and Ophir. Sediments deposited at the end of Oquirrh basin sedimentation host the deposits at Melco and Barneys Canyon. Oquirrh basin sedimentary rocks host the replacement deposits adjacent to the Bingham porphyry.

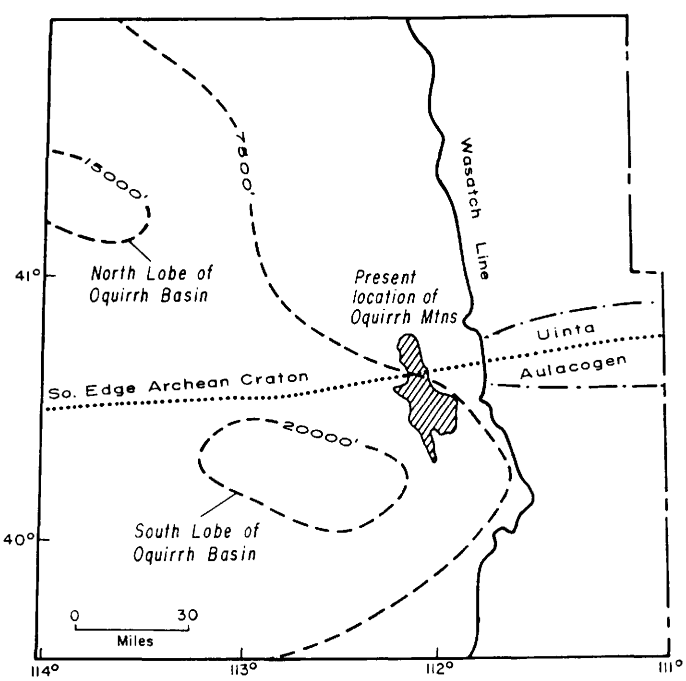

Figure 1. Present-day location of the Oquirrh Mountains and their relationship to regional tectonic features. Modified from Roberts et al. (1965), Bryant (1988), and Jordan and Douglas (1980).

Mesozoic History

During the Mesozoic, north-central Utah had a long and complex deformational history. The actual time-space relationships are difficult to assess due to the overprint by Cenozoic extension. Historically, previous workers assigned all compressional deformation to the Sevier Orogeny of Armstrong (1968), but thrust faults and metamorphism in the hinterland appear to be older than thin-skinned deformation in the fold and thrust belt suggesting that there may be two separate but related orogenic events (Allmendinger et al., 1984).

The hinterland as defined by Armstrong (1968) has been extended eastward by Allmendinger et al. (1984) to the Wasatch Fault based on their definition that the eastern boundary of the hinterland is the line west of which deep stratigraphic levels and crystalline basement were involved in thrusting. Allmendinger and Jordan (1981) recognized a regional detachment cut by a Jurassic pluton in the Newfoundland Mountains and suggested that this detachment was directly related to the fold and thrust belt to the east. Subsequent work (Allmendinger et al., 1984; Snoke and Miller, 1988) has shown more early Mesozoic faulting and metamorphism than previously known. Snoke and Miller (1988) documented the timing of metamorphism and deformation and favored two or more pulses of tectonism rather than a protracted metamorphic and deformational event. The two events are a late Jurassic event and the Cretaceous Sevier orogeny. The Jurassic event is coeval with the Nevadan Orogeny of western Nevada but has recently been named the Elko Orogeny (Thorman et al., 1990 and Thorman et al., 1991).

The age of the Elko Orogeny is based on regional deformation and metamorphism of post-early Jurassic age that are cut by late Jurassic plutons in northeastern Nevada and northwestern Utah (Thorman et al., 1990 and Thorman et al., 1991). Direct dating reported by Snoke and Miller (1988) gave ages of 170-150 Ma in the Pilot range and the Raft-River Albion Range on the Utah Nevada border. K-Ar dating of hydrothermal illites in the southern Oquirrh Mountains yielded Jurassic ages (Wilson and Parry, 1990b).

These dates, along with Jurassic-aged bedding plane gouges at Barneys Canyon, may extend the Elko Orogeny to the Wasatch front (Presnell and Parry, 1991; Presnell, 1992).

The Sevier orogeny was named by Armstrong (1968) for the large-scale east-vergent thrusts and associated folds of the Overthrust Belt of Idaho, Wyoming and Utah. The Orogeny was inferred to have started in the latest Jurassic (Armstrong and Oriel, 1965). However, re-examination of fossil distribution in synorogenic conglomerates shows a late Early Cretaceous (Aptian) initiation (Heller et al., 1986) making it distinct from Jurassic deformation. This supports differentiation of compressional deformation in north-central Utah into two separate, but related orogenic events.

In north-central Utah, Sevier-age folds and thrusts are exposed in the Wasatch Range. The western edge of the Wasatch Range consists of major thrust ramps where the Sevier decollements ramped from a level in the Proterozoic strata to the Mesozoic strata (Bruhn et al., 1986). The northern Wasatch shows thrust relations and age of deformation typical of the Wyoming salient (Royce, Warner and Reese, 1975; Wiltscko and Dorr, 1983; Yonkee, 1990). However further south in the central Wasatch, due to interferences with the Uinta arch, timing and thrust relationships become complex and are not well understood. The Uinta arch segments the overthrust belt into two structural salients (Bruhn et al., 1986). This segmentation was called the Uinta reentrant by Beutner (1977) (Fig. 2).

Based on an unconformity at the top of the Jurassic Preuss, Crittenden (1976) concluded that the Uinta arch had formed by the latest Jurassic to earliest Cretaceous. However, Bryant and Nichols (1989) present sedimentary evidence that the Uinta arch and its related Cottonwood uplift was not active till the Paleocene. Bruhn et al. (1986) suggested that the Uinta arch initially formed during the latest Cretaceous. Bryant and Nichols (1988) concluded that the Uinta arch uplift occurred following emplacement of the Sevier thrust sheets. However, folds mapped in the thrust sheet that carries the Oquirrh Mountains form an arcuate pattern around the projection of the west end of the Uinta arch suggesting that the Uinta arch buttressed the advancing thrust sheets (Beutner, 1977). The evidence to date suggests that the major Uinta arch-Cottonwood uplift began in the late Cretaceous. But, there may have been an earlier uplift that is late Jurassic in age.

In the central Wasatch the thrust belt and foreland uplift interaction has resulted in two major features: the Cottonwood fold and the Charleston allochthon (Fig. 2).

The Cottonwood fold and its associated thrusts occur on the Uinta arch southeast of Salt Lake City (Crittenden, 1976). The Cottonwood fold is a large east-vergent anticline which is directly related to the Uinta arch (Bruhn et al., 1986).

The Charleston allochthon is the major structural feature exposed in the southern Wasatch Range (Fig. 2). The alloch-

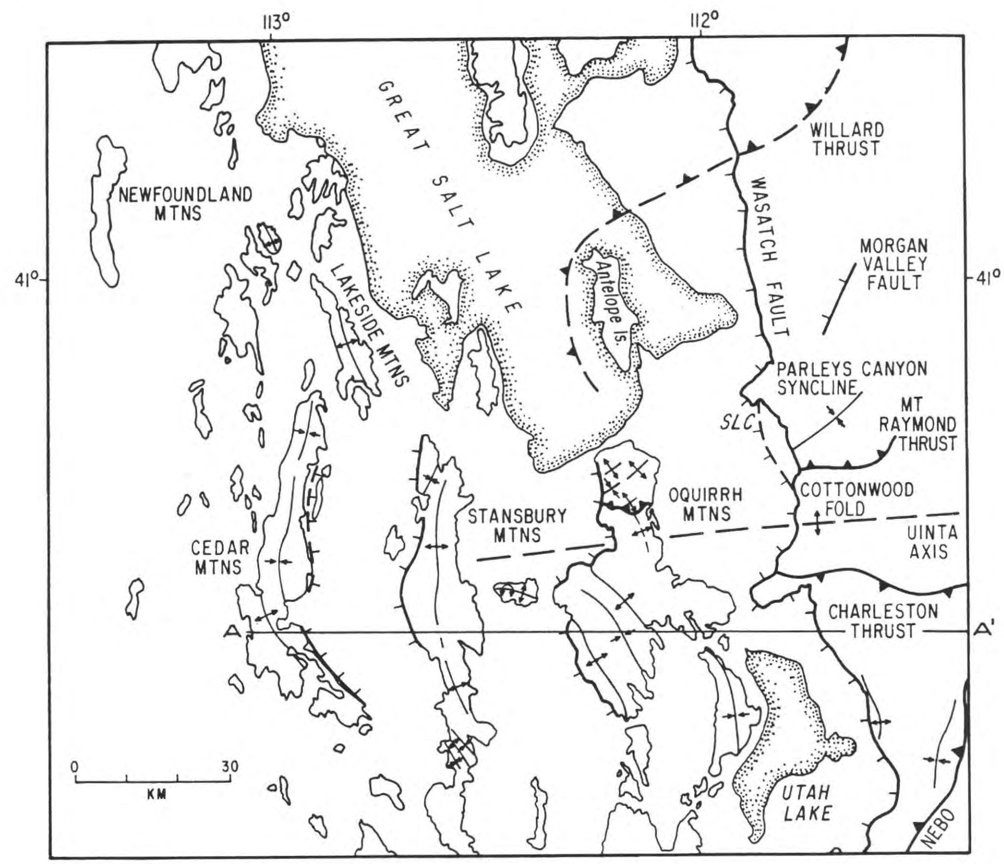

Figure 2. Structure map of north-central Utah after Tooker (1983), Moore and Sorensen (1979), Smith and Bruhn (1984), Yonkee (1990), and Crittenden (1976).

thon is bounded by the Charleston, Nebo and Strawberry thrusts and carried Oquirrh basin sediments over Mesozoic sediments in the latest Cretaceous (Crittenden, 1976; Riess, 1985). The allochthon is not exposed north of the Uinta arch but may be covered by Tertiary sediments in the Salt Lake Valley (Crittenden, 1976). However, a northern extension may not be present and the Oquirrh Mountains may ride on another plate. Total displacement of the allochthon is on the order of 40 kilometers (Riess, 1985). Beutner (1977) suggested that the Uinta arch buttressed the advancing Charleston allochthon separating the thrust belt into two distinct salients.

The Oquirrh Mountains are allochthonous but their relationship to the thrust plates exposed in the Wasatch Range is not well understood and will be addressed in detail later. It has generally been assumed that the Oquirrh Mountains are part of the Charleston allochthon but the northern edge of the Charleston allochthon may be south of the Uinta axis (Beutner, 1977) and therefore would not carry the Oquirrhs.

Cenozoic History

North-central Utah is at the eastern edge of the Basin and Range Province. In northern Utah, the boundary between the Basin and Range and the Colorado Plateau is the Wasatch Fault (Zoback, 1983), which coincides with the Wasatch line (Stokes, 1976). The time and extent of extension in north-central Utah is not well known or constrained. It has been suggested by several workers that the extension may have been controlled by pre-existing structures (Zoback, 1983; Smith and Bruhn, 1984). The following evidence suggests inception of extension as early as the Eocene. The thick package of Eocene Wasatch Conglomerate in the base of the Morgan Valley half-graben, which thickens into the Morgan fault, suggests that there was Eocene extension in the northern Wasatch (Hopkins, 1982). Late Eocene-age NE fissures in the Oquirrh Mountains would corroborate this early extension (Rubright and Hart, 1968). Seismic reflection profiling and well data in the Great Salt Lake show Miocene strata thickening into listric normal faults (Viveiros, 1984; Wilson et al., 1986). The Wasatch fault is at least 18 million years old (Parry et al., 1988). These data suggest that there were at least two periods of extension in north-central Utah: 1) Late Eocene 2) Miocene.

Igneous History

The igneous history of north-central Utah is dominated by the 'Uinta Trend', which is a belt of middle Tertiary plutons that occur along the Uinta-Cortez trend (Moore and McKee, 1983). The Uinta trend extends from east of Park City into Nevada (Stewart et al., 1977; Moore and McKee, 1983). The Uinta trend consists of latest Eocene to latest Oligocene coeval plutons and volcanics (Moore and McKee, 1983). These igneous events were preceded by Jurassic magmatism west of longitude 113° W associated with the Jurassic Cordilleran magmatic arc (Moore and McKee, 1983). In the central Wasatch some small dioritic intrusions are late Cretaceous in age (James, 1979). West of the Oquirrh Mountains the latest igneous activity is represented by scattered basalt and andesite flows of Miocene age (Moore and McKee, 1983).

GEOLOGY OF THE OQUIRRH MOUNTAINS

General Geology

The Oquirrh Mountains are the easternmost range in the Basin and Range Province and straddle the Uinta arch. The arch segments range into southern, central, and northern domains (Fig. 3). The geology of these segments will be addressed individually.

The Oquirrh Mountains are allochthonous and have been assumed (based on the thick Pennsylvanian section in the range) to be part of the Charleston allochthon (Crittenden, 1961; Tooker, 1983) which was emplaced in the late Cretaceous (Lawton, 1985). In order to evaluate this relationship a regional, balanced, east-west cross section was constructed at a scale of 1:500,000 (Fig. 4). This cross section predicts three separate thrusts beneath the Stansbury Mountains, the Oquirrh Mountains and the Wasatch Range. The thrust below the Stansbury Mountains is required by the overturned anticline which makes up the bulk of the range. The thrust below the Oquirrh Mountains interprets the Ophir anticline in the southwestern Oquirrh Mountains to be a ramp anticline formed from the ramping of a thrust from the Cambrian to the Mississippian Manning Canyon Shale. The thrust is here named the Oquirrh thrust and its allochthon the Oquirrh plate. A possible imbricate of this thrust was mapped by Moore (1973) in the West Traverse Mountains in the southeastern part of Figure 3. The thrust below the Wasatch Range is the Charleston-Nebo thrust. The main conclusion derived from the cross section is that the Charleston allochthon ramps from the Precambrian to the Mesozoic east of the Oquirrh Mountains. Riess (1985) reached the same conclusion from a smaller scale and better constrained cross section. Since the Oquirrh Mountains do not ride on the Charleston allochthon, the age of deformation within the Oquirrh Mountains is not necessarily the same as the Sevier-age Charleston-Nebo thrust which was emplaced in the Late Cretaceous. The Oquirrh thrust is analogous to the Midas thrust plate of Tooker (1983), but is renamed so as not to confuse it with the Midas Fault (proper) in Bingham Canyon which has a limited displacement. The Oquirrh thrust ramps from the Precambrian to the Mississippian Manning Canyon Shale beneath Rush Valley and has displaced the Oquirrh Mountains 13 km to the east. The Oquirrh Mountains were subsequently transported further eastward on the Charleston-Nebo thrust during the Sevier Orogeny.

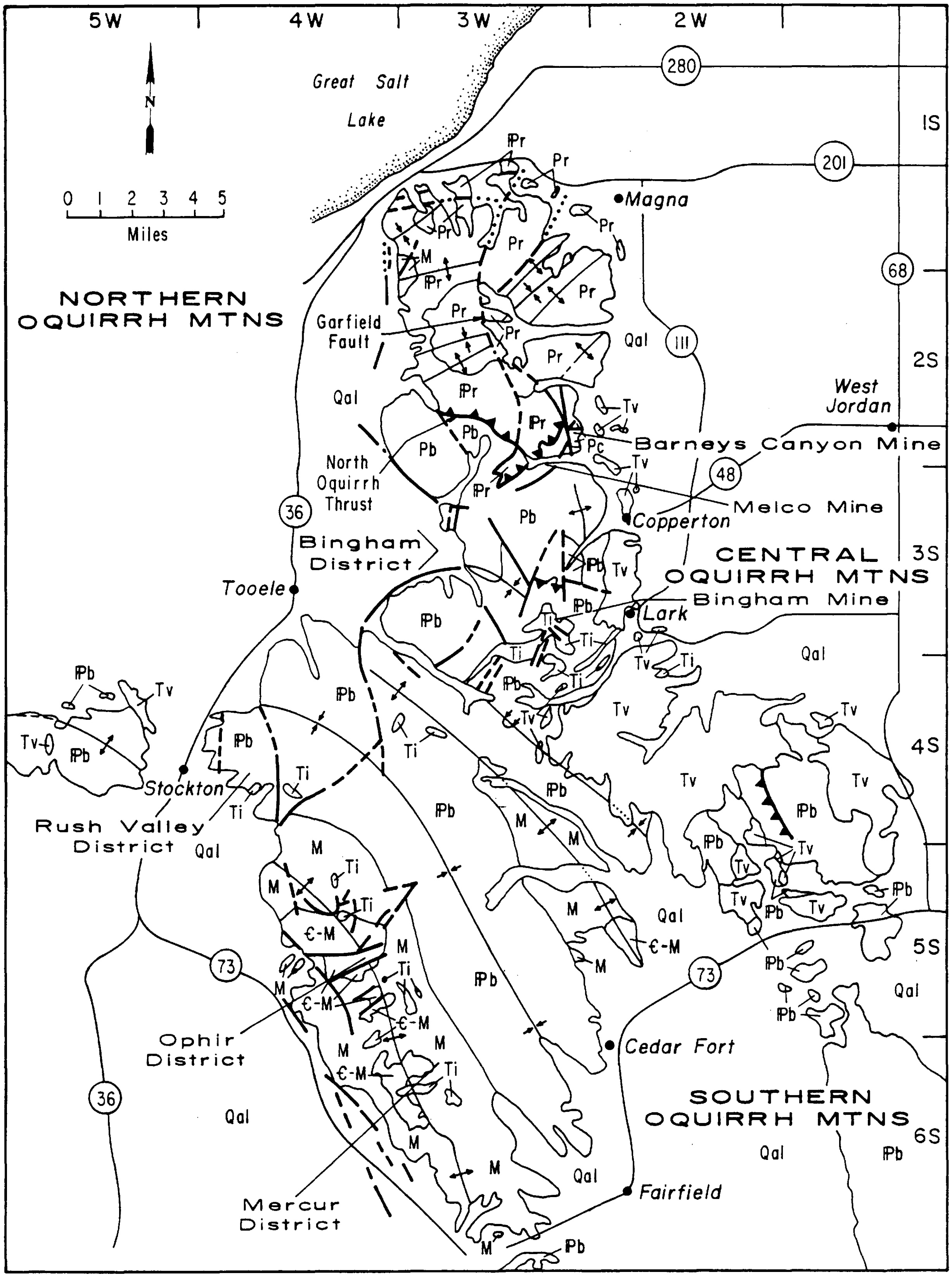

Figure 3. Simplified geologic map of the Oquirrh Mountains after Gilluly (1932), Moore (1973), Moore and Sorensen (1979), Tooker and Roberts (1970) and Swensen (1975).

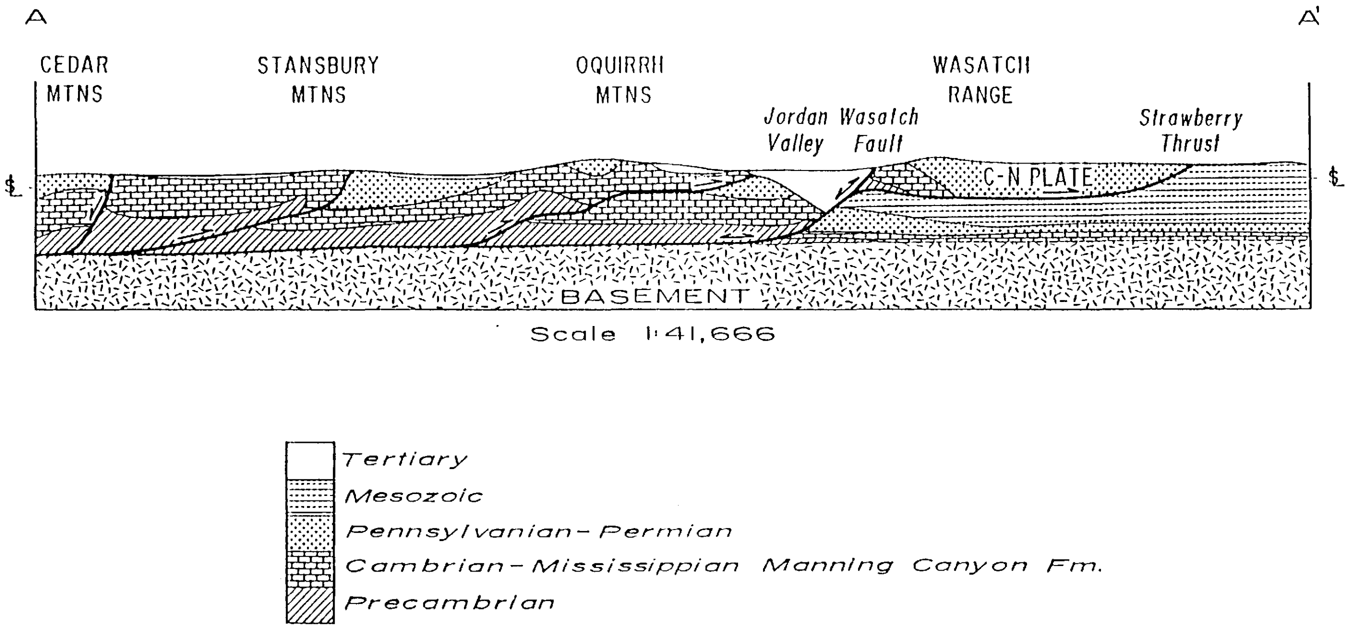

EXPLANATION

Qal — Alluvium and valley fill

Tertiary

- Tv — Volcanics
- Ti — Intrusives

ROGERS CANYON SEQUENCE (upper plate, North Oquirrh Thrust)

Penn. - Permian

- Pr — Park City and Kessler Canyon Fms.
- IPr — Lake Point and Erda Fms.

BINGHAM SEQUENCE (lower plate, North Oquirrh Thrust)

Penn. - Permian

- Pc — Park City Fms.
- Pb — Curry Peak, Freeman Peak, and Kirkman-Diamond Creek Fms.
- IPb — Butterfield Peaks, Bingham Mine, and Oquirrh Fms.

U. Miss.

- M — Manning Canyon Shale and Great Blue Limestone

Cambrian -M. Miss.

- €-M — Cambrian through middle Mississippian sediments

Figure 4. Simplified regional east-west cross section. Line of section is on Figure 2.

The Southern Oquirrh Mountains

General Geology. To date the most comprehensive work on the southern Oquirrh Mountains is by Gilluly (1932). The southern Oquirrh Mountains expose Cambrian through Pennsylvanian strata with some Tertiary and Quaternary cover (Gilluly, 1932). Over 6.4 kilometers (21,000 feet) of sedimentary rocks are exposed, dominated by over 4.6 kilometers (15,000 feet) of Pennsylvanian Oquirrh Formation (Gilluly, 1932).

The southern Oquirrh Mountains are dominated by a series of NW-trending anticline and syncline pairs (Fig. 3). The southern Oquirrh Mountains structural domain extends from Five Mile Pass to the latitude of Tooele where the anticline-syncline pairs make a sharp bend to the west (Fig. 3). These fold trains have been assumed to be Late Cretaceous (Sevier) in age based on the assumption that they are part of the Charleston-Nebo plate. But, as argued above, this may not be the case.

Age Dates. Wilson and Parry (1989, 1990a, and 1990b) dated illite veins and clay separates from altered shales of the Mississippian Great Blue Limestone in the southern Oquirrh Mountains. Vein illites range from 122 to 189 Ma, average 160 Ma, and are similar to the ages of clay-size separates (Wilson and Parry, 1990a and 1990b). The dated illite veins, which generally strike east-west and dip steeply, are in the east limb of the Ophir anticline. A north-south least principal stress direction is consistent with east-west compression. Therefore, the vein ages could record one stage of deformation in the southern Oquirrh Mountains. This interpretation is supported by the presence of Oquirrh Formation clasts in the Sandwash member of the Jurassic Morrison Formation in central Utah (J. Welsh pers. comm. 1990). Therefore, compressional deformation in the southern Oquirrh Mountains could be related to the Elko Orogeny. This would require that the late-Cretaceous Charleston-Nebo thrust reactivated the basal decollement or stepped out of the basement to the east of the Oquirrh Mountains. Alternatively, the illites were formed during a Jurassic metamorphic event, within bedrock joints and were subsequently displaced during the Sevier Orogeny.

Cenozoic History. As is the case for the eastern Basin and Range in general, the Cenozoic history of the southern Oquirrh Mountains is not well understood. Gilluly (1932) recognized an early phase of NE to EW-striking normal faults (i.e., Ophir-Silverado faults). Based on cross-cutting relations, Gilluly suggested that they were older than classic "Basin and Range faults." He concluded that they were either related to formation of the folds, or, because some offset early Oligocene rhyolite dikes, that they were related to an early extensional phase (Gilluly, 1932). Gilluly (1932) recognized a younger set of normal faults which he termed "Basin and Range faults." These are NW-trending, en echelon sets of faults which separate the valley from the range. The faults extend over 45 kilometers and offset unconsolidated Quaternary deposits (Wu and Bruhn, 1990). One of the most prominent is the West Mercur fault which shows clear evidence of rejuvenation (Gilluly, 1932). Based on topographic arguments Gilluly concluded that Basin and Range faulting began in the Miocene or Early Pliocene.

As is the case in the rest of the Basin and Range there appear to have been two extensional events in the southern Oquirrh Mountains: 1) a late Eocene to Oligocene event and 2) a Miocene to recent event. The age and least principal stress directions of the two events are compatible with the regional extensional events in the eastern Basin and Range.

Igneous History. The southern Oquirrh Mountains contain extrusive igneous rocks of latitic and quartz-latitic composition, minor flows of basalt and rhyolite, and numerous plugs, dikes and sills of monzonitic and rhyolitic composition (Gilluly, 1932). The extrusive rocks are generally confined to the Traverse Mountains on the eastern side of the southern Oquirrh Mountains. The intrusive rocks range from 39-31 m.y. B.P. and are coeval with the extrusive rocks (Moore, 1973). In general the higher the silica content the younger the intrusion (Moore, 1973).

Mining Districts. The southern Oquirrh Mountains contain three mining districts: 1) Ophir District, 2) Rush Valley (Stockton) District, and 3) Mercur District. All of the districts occur on the east limb of the Ophir anticline.

The Ophir district contains lead-zinc mineralization with minor silver and copper mineralization as veins and massive replacement of skarn and marble (Wilson and Parry, 1990c). The deposit can be classified as a distal skarn because no major plutonic body has been encountered in the mine (Wilson and Parry, 1990c).

The Rush Valley (Stockton) district contained vein and replacement lead-zinc mineralization with minor silver and copper mineralization as well, but most ore was lead rich (Butler,1920). Gilluly (1932) describes some gold shoots but most ore contained 6-20% Pb, 2-12% zinc, 2 to 8 oz. of silver and virtually negligible gold.

The Mercur mining district contains Carlin-type disseminated gold deposits (Bagby and Berger, 1985). The deposits are hosted by limestones and silty limestones of the Topliff Member of the Mississippian Great Blue Formation (Tafuri, 1987). Hydrothermal alteration is characterized by replacement of the carbonates by silica, phyllosilicates, pyrite, barite, various sulfosalts of As, Hg, Sb and Tl, and micron-sized gold (Jewell and Parry, 1987, 1988). The district consists of two main orebodies: Mercur-Sacramento and Marion Hill, and several satellite deposits: Sunshine, Rover Hill and West Dip (Stanger, 1990). The age of gold mineralization is unknown.

Igneous rocks in the Mercur District are found south and north of the mineralization (Kornze, 1987). The 31.6 Ma Eagle Hill rhyolite occurs to the south and the 36.7 Ma Porphyry Knob quartz monzonite occurs to the north (Moore and McKee, 1983). Classically, the mineralization has been linked to these igneous bodies but the 11 km strike length of alteration, the lack of significant mineralization within the intrusives, and lack of zoning around them argue against a causal relationship (Wilson and Parry, 1990a).

The West Dip deposit occurs within the West Mercur fault located west of the Mercur district (Gilluly, 1932). The West Mercur fault bounds the western side of the Oquirrh Mountains and has suggested to many that the Mercur deposits are Miocene-Pliocene in age. However, the field relationships at West Dip are ambiguous as to whether the fault was the conduit for the ore-bearing fluids or the ore body was dragged and smeared along the fault (Gilluly, 1932).

Wilson and Parry (1990a, 1990b) obtained Jurassic ages for illite from veins and illite-rich clay separates of Mississippian Great Blue shales that are anomalous in Au, As, Hg and other heavy metals. Several illite ages for samples from the Mercur district cluster near 160 Ma, suggesting that Late Jurassic may be a minimum age of gold mineralization (Wilson and Parry, 1990b). However, the highest gold value of a dated sample from the Mercur mine is only .004 oz./ton (Wilson and Parry, 1990b).

To date there is no unequivocal age determination of gold mineralization in the Mercur District.

The Northern Oquirrh Mountains

General Geology. The northern Oquirrh Mountains expose Mississippian through Permian strata with remnants of coarse Tertiary and Quaternary clastics (Tooker and Roberts, 1961) (Fig. 3). The strata are in the hanging wall of the North Oquirrh thrust. Because of stratigraphic and structural differences Tooker and Roberts (1970) separated the age equivalent hanging-wall strata in the northern Oquirrh Mountains from the footwall strata in the central Oquirrh Mountains. Tooker and Roberts (1970) termed the hanging-wall strata the Rogers Canyon sequence and the footwall strata the Bingham sequence (Fig. 5). They state that the main difference between the two sections is that the Rogers Canyon sequence contains Permian Park City Formation and the Bingham sequence does not. Also, the Rogers Canyon sequence contains the Late Pennsylvanian-Early Permian Kessler Canyon Formation which consists of interbedded sandstone, limestone and abundant bedded chert. The top of the Bingham sequence contains age-equivalent Diamond Creek Formation with intertongueing Kirkman Limestone. The Diamond Creek Formation consists of calcareous sandstone with diagnostic intraformational breccias and rare chert (Welsh and James, 1961).

The North Oquirrh thrust plate contains late Mississippian through Early Permian strata which have been thrust over Late Pennsylvanian to Early Permian strata (Tooker and Roberts, 1970). Folds within the North Oquirrh plate trend northeast suggesting emplacement from the northwest (Tooker, 1983). Tooker and Roberts (1970) break the thrust plate into two structural blocks separated by the Garfield fault (Fig. 3). The Garfield fault is a strike-slip fault with dip-slip movement. Rotation of fold axes across the fault suggest right-lateral movement but a case for left-lateral movement can be made (Roberts and Tooker, 1961).

Examination of the trace of the North Oquirrh thrust in the northeast corner of the Bingham mining district (Fig. 3) suggests that the North Oquirrh thrust was emplaced following formation of the northwest-trending folds of the southern and central Oquirrh Mountains. The trace of the thrust on the west side of the range appears to have ridden up and over the northern extensions of the Bingham syncline and the Copperton anticline and ramps from the Lake Point limestone to the Erda Formation. Smith (1975) interpreted this map pattern as being folded by the central Oquirrh structures. But if the North Oquirrh thrust was emplaced prior to formation of the northwest-trending folds, the folds would project into the hanging wall.

The conglomerates in the northern Oquirrh Mountains have been named the Harkers Fanglomerate for exposures in Harkers Canyon and are Pliocene in age (Slentz, 1961). These fanglomerates are underlain by as much as 100 feet of unnamed conglomerate (Tooker and Roberts, 1961). A thin remnant of andesite locally overlies the unnamed conglomerate (Tooker and Roberts, 1961).

Cenozoic Deformation. As is the case in the rest of the region, extensional deformation in the northern Oquirrh Mountains is not well understood. The Pliocene to Recent basin-bounding fault on the west side of the range discussed in the southern Oquirrh section extends north to bound the northern Oquirrhs as well. A basin-bounding fault on the east side of the northern Oquirrh Mountains has not been well established. Some authors (i.e., Zoback, 1983) have suggested that there is not a basin-bounding fault on the east side of the Oquirrhs. They have further suggested that the entire range has been rotated 15 degrees to the east into the Wasatch fault creating a half graben. However, Slentz (1961) recognized a major north-south-striking normal fault along the eastern base of the Oquirrh Mountains, buried in part by the fanglomerate but elsewhere serving as the contact between the Paleozoic and fanglomerate. Aerial photo interpretation and field mapping confirm Slentz's observations and interpretations.

Unequivocal evidence of an earlier (Eocene-Oligocene) extensional event in the northern Oquirrh Mountains has not been found. However, Tooker and Roberts (1961) mapped several NE- to EW-striking normal faults. Their trend would be consistent with the NE-striking Eocene fissures in the Bingham District and the early phase of faulting in the southern Oquirrh Mountains.

Central Oquirrh Mountains

Overview. The central Oquirrh Mountains straddle the Uinta uplift and contain the prolific Bingham mining district. Even though the district has been mined and studied for over 140 years the geology is not completely understood. The district is dominated by the Bingham porphry copper system which was emplaced into a complex structural setting. The central Oquirrh Mountains are the most geologically complex portion of the Oquirrh Mountains because of thrust-belt and foreland interaction and deformation associated with pluton emplacement.

Stratigraphy. The central Oquirrh Mountains expose Pennsylvanian through Permian strata with isolated exposures of Tertiary clastics and volcanic rocks. As previously discussed Tooker and Roberts (1970) divided the north and

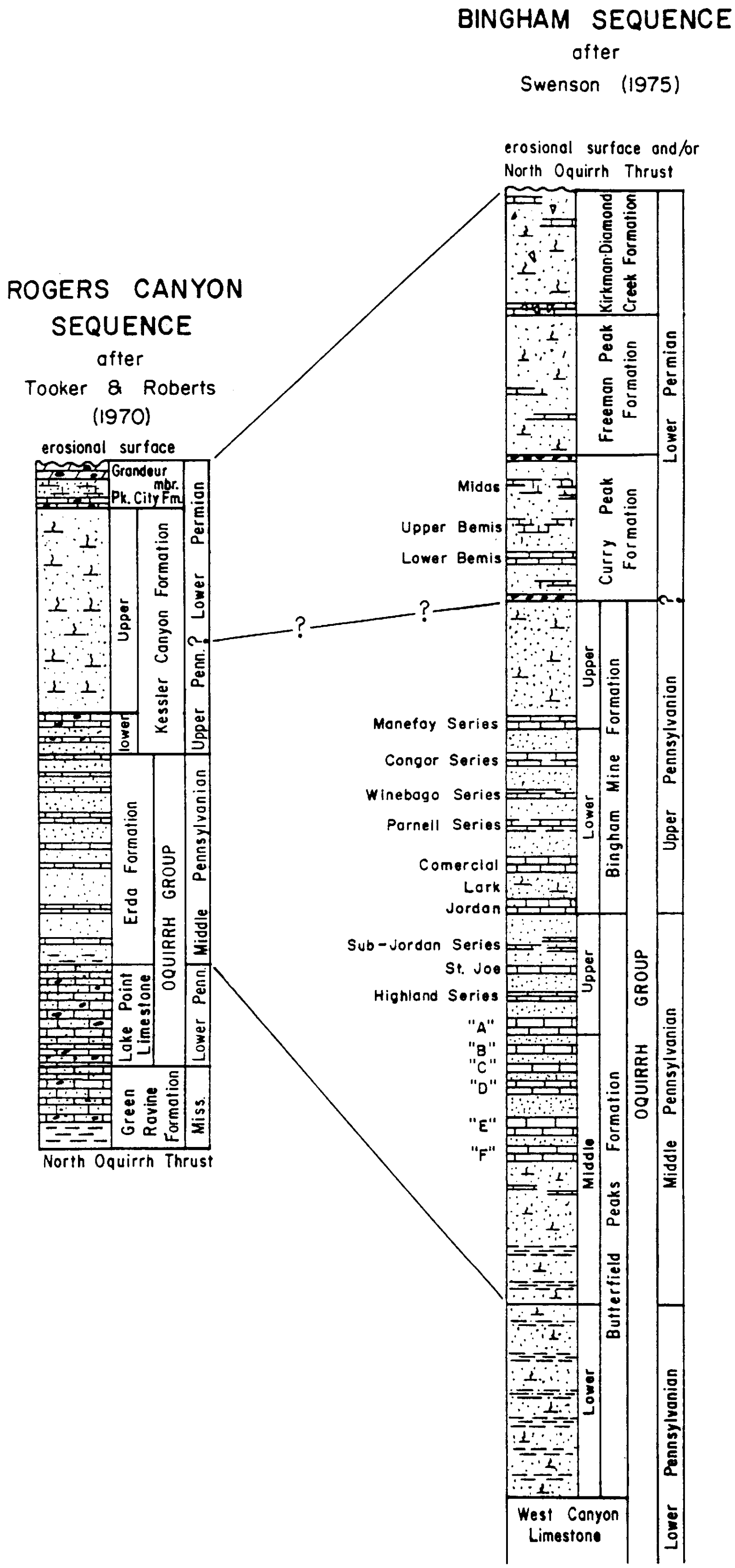

Figure 5. Stratigraphic columns of the Rogers Canyon sequence and the Bingham sequence after Tooker and Roberts (1970) and Swensen (1975).

central Oquirrh Mountains into three tectonostratigraphic units separated by the North Oquirrh thrust and the central Oquirrh Midas thrust (Fig. 3). Swensen (1975) included the strata in the Midas footwall in the Bingham sequence. Therefore, the northern Oquirrhs contain the Rogers Canyon sequence and the central Oquirrhs contain the Bingham sequence separated by the North Oquirrh thrust.

The Bingham sequence consists of the Pennsylvanian Oquirrh Group and lower Permian clastic and carbonate rocks. Welsh and James (1961) called the Pennsylvanian section the Oquirrh Formation after Gilluly (1932). Tooker and Roberts (1970) raised it to group status and raised the members of the section to formation rank. The basal Pennsylvanian formation is the West Canyon Limestone. The West Canyon Formation consists of cyclical, clastic, arenaceous limestones and interbedded thin, cherty , argillaceous limestone and thin calcareous quartzite or siliceous cemented calcareous sandstone (Tooker and Roberts, 1970). The West Canyon Limestone is overlain by the Butterfield Peaks Formation which is predominantly calcareous quartzite with orthoquartzite, calcareous sandstone and arenaceous cherty, argillaceous, and fine-grained dense limestones (Tooker and Roberts, 1970). The Butterfield Peaks Formation is overlain by the Bingham Mine Formation.

The Bingham Mine Formation was named by Welsh and James (1961) for limestone and quartzitic sandstone above the base of the Jordan Limestone. The Jordan and Commercial limestones are the major marker beds in the Bingham District and are also the principal nonplutonic ore hosts. The Jordan and Commercial limestones occur in the lower Bingham Mine Formation which was called the Clipper Ridge member by Tooker and Roberts (1970). Because of invalid type sections, Swensen (1975) did not use the nomenclature of Tooker and Roberts (1970). This paper uses the nomenclature of Swensen (1975). The lower member of the Bingham Mine Formation consists of the Jordan and Commercial markers which are dark gray argillaceous, silty and cherty limestone separated by light gray to tan calcareous quartzite, orthoquartzite and thin calcareous sandstone (Swensen, 1975). The thick section above the Commercial limestone consists predominantly of calcareous quartzites, and orthoquartzites with some interbedded sandstones, limestones, siltstones and shales (Swensen, 1975). The upper member of the Bingham Mine Formation is predominantly light gray to brownish tan, thin-banded orthoquartzite and calcareous quartzite with interbedded thin, light to medium gray, calcareous, sandstones, limestones and siltstones (Swensen, 1975).

The Curry Peak Formation overlies the Bingham Mine Formation and is lower Permian in age (Swensen, 1975). Lithologically, it is principally light gray to light tan, calcareous sandstones and siltstones; and light gray to tan quartzites (Swensen, 1975). The Freeman Peak Formation overlies the Curry Formation and is primarily thick bedded, calcareous quartzites and orthoquartzites with some thin-bedded, calcareous sandstones and argillaceous siltstones and shales (Swensen, 1975).

The Bingham sequence is capped by the Kirkman-Diamond Creek Formation. In north-central Utah the Kirkman-Diamond Creek Formation is two distinct formations: the Kirkman Limestone and Diamond Creek Sandstone, but in the Oquirrh Mountains it is not always possible to completely separate them, so Swensen (1975) mapped them as one formation. In the central Oquirrh Mountains the two units grade into one another laterally and vertically (Schurer, 1979). Schurer (1979) described the formation in the western part of the central Oquirrh Mountains as a chaotic breccia terrane consisting of beds of sandstone and limestone interbedded with stratiform intraformational breccias of both lithologies. But, in some areas there is a distinctive basal package of thin laminated limestones overlain by intraformational brecciated calcareous sandstone (Swensen, 1975).

Igneous Rocks. The central Oquirrh Mountains are dominated by the Bingham intrusive complex. The complex consists of two major stocks: the Last Chance stock and the Bingham stock. The Bingham stock is hydrothermally altered and mineralized but the Last Chance stock is mostly unaltered and unmineralized. The Bingham stock consists of several intrusive phases some of which may have vented to form the volcanic pile on the east side of the range (Lanier et al., 1978). In general, the Bingham stock consists of equigranular monzonites that were intruded by monzonitic to quartz monzonitic porphyry phases (Lanier et al., 1978). The K-Ar ages of the major intrusive phases ranges from 39.8 to 38.8 Ma (Warnaars et al., 1978). The complex also contains numerous dikes and sills. Those of latitic and quartz latitic composition cross-cut all other phases (Lanier et al., 1978). Peripheral to Bingham, the central Oquirrh Mountains contain other small intrusions that are or may be related to the main Bingham system. They are principally latitic to quartz latitic in composition and occur as small sills, dikes and plugs (Swensen, 1975). A latite porphyry dike in Pass Canyon (14-3S-4W) has been dated at 36.5 Ma (Moore, 1973).

Volcanic rocks are preserved on the east side of the central Oquirrh Mountains. They are preserved in part by the eastern tilt of the range by Basin and Range faulting. The most abundant volcanics are biotite hornblende latites (Swensen, 1975). Latitic extrusive rocks in the upper part of the volcanic pile yield ages ranging from 33 to 31 Ma suggesting that plutonism and volcanism in the central Oquirrh Mountains were broadly contemporaneous (Moore, 1973).

General Structure. Recent mapping of the Bingham pit by Kennecott staff requires modification of some of the structural relationships described in previous studies by James et al. (1961), Smith (1975) and Lanier et al. (1978). Incorporation of Anaconda surface data and subsurface data has enhanced the understanding of the district geology as well. This section will focus on the structure in the Bingham district because it is the best documented due to structural control of non-porphyry ores and emplacement of intrusives. Extensive mine excavations have permitted the mapping of most structures in the main part of the Bingham mining district.

The emplacement of igneous rocks in the Bingham mining district was controlled by northwest-trending fold axes and northeast-trending faults (James et al., 1961; Moore, 1973; and Lanier et al., 1978). Figure 6 is a generalized tectonic map of the central Bingham mining district based on Lanier et al. (1978) with modifications from unpublished Kennecott 1989 and 1990 pit maps.

Early Normal Faults. The earliest recognized structure in the district is the east-west-trending Roll fault which has been interpreted to be pre-folding in age (Farmin, 1933; Rubright and Hart, 1968). The Roll fault is offset by all bedding plane faults that are associated with folding, northeast-striking fissures and is locally intruded and mineralized (Rubright and Hart, 1968).

Folds and Thrusts. The Bingham district contains two major folds: the Bingham syncline and the Copperton anticline. The trend of the syncline is similar to the folds in the southern Oquirrh Mountains. The axis of the syncline strikes N60W and plunges 12 NW (James et al., 1961). The location of the syncline has been shifted in Figure 6 from that in Lanier et al. (1978) by more recent mapping (1989, 1990 Bingham pit maps). The fold is broad in the mine area but becomes tighter to the northwest (Lanier et al., 1978). The Bingham stock intruded the axis of the Bingham syncline (Fig. 6) (Rubright and Hart, 1968). The Apex and Rood folds occur on the southwest limb of the Bingham syncline. The Rood fold is a synclinal structure and converges into the Bingham syncline (Lanier et al., 1978). The Apex fold is an anticlinal structure on the west limb of the Bingham syncline and is locally overturned. The Copperton anticline is a north-trending overturned box fold to east of the Bingham syncline separated from the syncline by the Midas thrust. K-Ar dating of illite-bearing bedding-plane gouges on the northern flank of the Copperton anticline in the Barneys Canyon gold mine yielded Jurassic ages suggesting that the Copperton anticline is Jurassic (Presnell and Parry, 1991; Presnell, 1992).

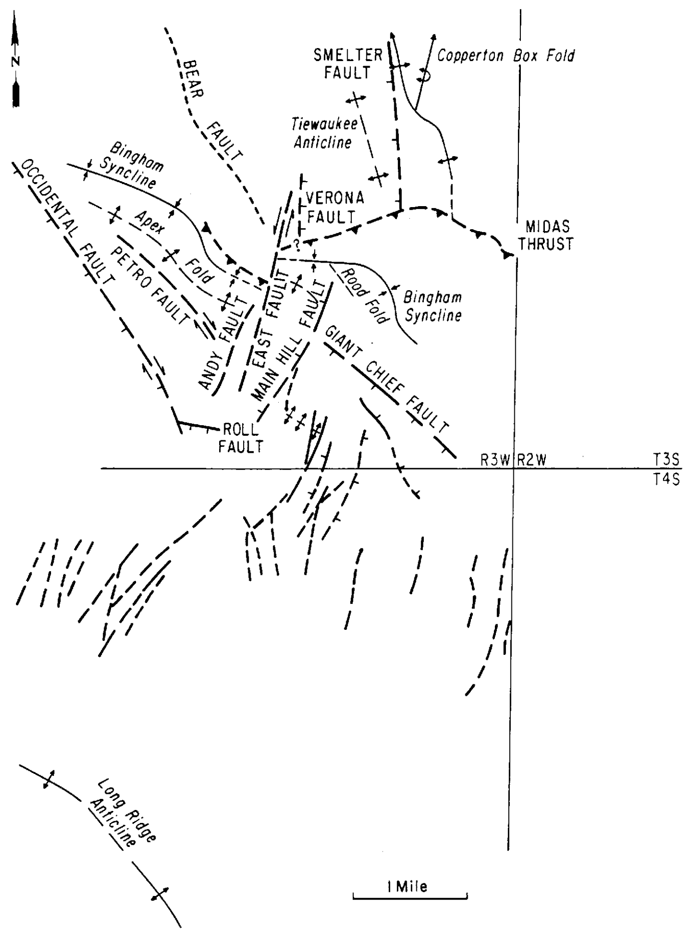

Figure 6 Generalized structure map of the central Bingham mining district after Lanier et al. (1978) and unpublished Kennecott (1989) and (1990) pit maps.

The Bingham mining district contains numerous bedding-plane faults that often occur at the contact between quartzite and limestone but also occur within limestones as well (Rubright and Hart, 1968). The bedding plane faults have been attributed to folding and are the result of flexural slip in the folding process. Rubright and Hart (1968) note several stages of movement along these planes which could be a result of reactivation. The bedding-plane faults are important local ore-controlling structures and have been termed mantos particularly in the lead-zinc zone (Rubright and Hart, 1968).

The Midas thrust fault separates the Bingham syncline from the Copperton anticline. The Midas thrust fault has been termed a regional fault by Tooker (1983) to the east of the Oquirrh Mountains but the actual thrust only occurs in the Bingham Mining District. It was first recognized from its repetition of the Jordan and Commercial limestones. The Midas (proper) occurs in the eastern part of the district. The Bingham syncline is in the hanging wall and the Copperton anticline is in the footwall. Locally, the Midas strikes 70 degrees E and dips 40 degrees southeast. The Midas does not appear to be a major thrust in that offset is on the order of two thousand feet (Swensen, pers. comm., 1990). Its southward dip has suggested to Bruhn (pers. comm., 1990) that it is a sidewall ramp structure, perhaps, related to interference between the Uinta arch and the northwest-trending folds of the southern Oquirrh Mountains.

In the past many authors have correlated the Midas thrust with the Bear Fault having been offset by left-lateral tear faults. However, the Bear fault dips much more steeply (75 degrees).

In the western part of the district, deep drilling by Anaconda revealed the Markham thrust fault which strikes N70W and dips 55 to 65 degrees southwest (Atkinson and Einaudi, 1978). The Markham thrust also repeats the Commercial and Jordan limestones with offset decreasing from 500 meters on the west to 180 meters on the east (Atkinson and Einaudi, 1978). Attempts have been made to correlate the Markham with the Midas but displacement decreases on the Markham towards the Midas.

Northeast Striking Faults. Boutwell (1905) showed that the majority of ore veins and lodes had a northeast strike. The northeast-trending structures are a complex system of nearly parallel, often en echelon, faults and fissures which control mineralization and therefore ore production (Smith, 1975). Most of the faults dip steeply to the west and with few exceptions have minor displacement (Lanier et al., 1978). Boutwell (1905) noted at least two periods of movement along them. Some of them show left lateral offset. The Andy fault was previously thought to be the major sinistral fault in the district (Lanier et al., 1978). But recent mapping and incorporation of subsurface data has shown that the East fault is the major strike-slip fault in the district (Swensen, 1990). As discussed earlier it is not known whether the Midas thrust dies out or is offset by the East fault. Since these faults are mineralized they can be dated by the age of mineralization. In order to be mineralized they had to be open and therefore active during the Late Eocene to Early Oligocene. The Bingham district also contains northwest-striking faults many of which show right-lateral offset (Atkinson and Einaudi, 1978). Although these faults are the most significant in terms of continuity and displacement they are only weakly mineralized where they cut limestone beds (Atkinson and Einaudi, 1978). Boutwell (1905) determined that the northwest-trending faults occurred after an initial northeast-trending event and were followed by a reactivation of northeast-trending faults. Many of the northwest-trending faults experienced strike slip movement followed by dip-slip movement (i.e., the Occidental fault). The productive northeast-striking Leadville fissure is offset by a northwest-striking strike-slip fault (Atkinson and Einaudi, 1978).

In general it is difficult to observe offset of northeast-trending faults by northwest-trending faults, but, this may be due to the discontinuity of the northeast-trending faults. However, where they do intersect, it appears that the northeast-trending faults are offset by the northwest-trending faults. This age relationship is supported by the northeast-trending faults being productive while the northwest-trending faults are barren and probably post-ore in age.

Basin and Range Faulting. The district also contains distinct Basin and Range normal faults as well as Basin and Range reactivation of pre-existing faults. The northwest-trending Occidental fault shows post strike-slip movement down to the south (Atkinson and Einaudi, 1978). The reactivation of the Occidental fault shows that northwest-striking faults had favorable orientation for Basin and Range extension.

Extension in the Bingham Mining District. The two periods of extension in north-central Utah are expressed at Bingham. Late Eocene to early Oligocene extension is clearly recorded by the mineralized northeast-striking faults in the Bingham mining district. A later extensional event in the central Oquirrh Mountains is not as evident. However, the northwest-striking fault sets are parallel to the basin-bounding northwest-trending sets described by Wu and Bruhn, (1990) on the west side of the Oquirrh Mountains.

CONCLUSIONS

The Oquirrh Mountains have had a long and complex geologic history. Compressional deformation formed folds, thrusts and displaced the strata in the range several kilometers to the east. Compressional deformation is at least Cretaceous in age and may be Jurassic. The Oquirrh Mountains experienced at least two extensional events: 1) an Eocene-Oligocene event and 2) a Miocene to Recent event. The present-day location of the Oquirrh Mountains is at the junction of the edge of the Archean craton, the Wasatch line and the Uinta-Cortez axis. The ore deposits of the Oquirrh Mountains are a result of this long and complex geologic history.

ACKNOWLEDGMENTS

This work is based on helpful discussions with R. Bruhn, W.T. Parry, A. Yonkee, G. Ballantyne, J. Swensen, P. Smith, C. Kroko, J. Black and my other colleagues at Kennecott Exploration but does not necessarily reflect their views. I thank Kennecott for use of unpublished data, permission to publish, and funding. The figures were drafted by P. Onstott. I thank M. Shubat for a thorough review of a shorter version of this paper.

REFERENCES

Allmendinger, R.W., and Jordan, T.E., 1981, Mesozoic evolution, hinterland of the Sevier Orogenic belt: Geology v. 9, p. 308-313.

Allmendinger, R.W., Miller, D.M., and Jordan, T.E., 1984, Known and inferred Mesozoic deformation in the hinterland of the Sevier belt, northwest Utah, *in* Kerns, G.J. and Kerns, R.L., eds., Geology of Northwest Utah, Southern Idaho and Northeast Nevada: Utah Geological Association Publication 13, p. 21-34.

Armin, R.A., and Mayer, L., 1983, Subsidence analysis of the Cordilleran miogeocline: Implications for timing of late Proterozoic rifting and amount of extension: Geology, v. 11, p. 702-705.

Armstrong, F.C, and Oreil, S., 1965, Tectonic developement of the Idaho-Wyoming thrust belt: American Association of Petroleum Geologists Bulletin, v. 48, p. 1847-1866.

Armstrong, R.L., 1968, Sevier orogenic belt in Nevada and Utah: Geological Society of America Bulletin, v. 79, p. 429-458.

Atkinson, W.W., Jr., and Einaudi, M.T., 1978, Skarn formation and mineralization in the contact aureole at Carr Fork, Bingham, Utah: Economic Geology, v. 72, p. 1326-1365.

Bagby, W.C., and Berger, B.R., 1985, Geologic characteristics of sediment-hosted, disseminated precious metal deposits in the western United States. *in* Berger, B.R., and Bethke, P.M., eds., Geology and Geochemistry of Epithermal Systems: Society of Economic Geology Reviews in Economic Geology, v.2, p.169-202.

Beutner, E.C., 1977, Causes and consequences of curvature in the Sevier orogenic belt, Utah to Montana, *in* Heisey, E.L. and others, eds. Rocky Mountain Thrust Belt Geology and Resources: Joint WGA-MGS-UGA Guidebook: Wyoming Geological Association, p. 353-366.

Bond, G.C., Christie-Blick, N., Kominz, M.A., and Devlin, W.J., 1985, An early Cambrian rift to post-rift transition in the Cordilleran of western North America: Nature, v. 315, p. 742-746.

Bond, G.C., Nickeson, P.A., and Kominz, M.A., 1984, Breakup of a supercontinent between 625 Ma and 555 Ma: New evidence and implication for continental histories: Earth and Planetary Science Letters, v. 70, p. 325-345.

Boutwell, J.M., 1905, Economic geology of the Bingham mining district, Utah, with a section on areal geology, by Arthur Keith and an introduction on general geology by S.F. Emmons: U.S. Geological Survey Professional Paper 38, 413 p.

Bruhn, R.L., Picard, M.D. and Isby, J.S., 1986, Tectonics and sedimentology of the Uinta Arch, western Uinta Mountains, Uinta Basin, *in* Peterson, J.A., ed., Paleotectonics and Sedimentation in the Rocky Mountain Region: United States: American Association of Petroleum Geologists Memoir 41, p. 333-358.

Bryant, B., 1988, Evolution and early proterozoic history of the margin of the Archean continent in Utah, *in* Ernst, W.C., ed., Metamorphism and Crustal Evolution of the Western United States: Rubey Vol. 7, Prentice Hall p. 432-445.

Bryant, B. and Nichols, D.J., 1988, Late Mesozoic and early Tertiary reactivation of an ancient crustal boundary along the Uinta trend and its interaction with the Sevier Orogenic belt, *in* Schmidt, C.A. and Perry, W.J. eds. Interaction of the Rocky Mountain Foreland and the Frontal Thrust Belt: Geological Society of America Memoir 171, p.411-429.

Butler, B.S., Loughlin, G.F., Heikes, V.C. et al., 1920, The Ore deposits of Utah: U.S. Geological Survey Professional Paper 111, 672 p.

Crittenden, M.D., Jr., 1961, Magnitude of thrust faulting in northern Utah: U.S. Geological Survey Professional Paper 424-D, art. 35, p. D218-D131.

Crittenden, M.D. Jr., 1976, Stratigraphic and structural setting of the Cottonwood area, Utah, *in* Hill, J.G. ed., Symposium on the Geology of the Cordilleran Hingeline: Rocky Mountain Association of Geologists, p. 363-379.

Farmin, R., 1933, Influence of Basin and Range faulting in mines at Bingham Utah: Economic Geology, v. 28, p. 601-606.

Gilluly, J., 1932, Geology and ore deposits of the Stockton and Fairfield quadrangles, Utah: U.S. Geological Survey Professional Paper 173, 171 p.

Heller, P.L., Bowdler, S.S., Chambers, H.P., Coogan, J.C., Hagen, E.S., Schuster, M.W., and Winslow, N.S., 1986, Time of initial thrusting in the Sevier orogenic belt, Idaho-Wyoming and Utah: Geology, v. 14, p. 388-391.

Hopkins, D.L., 1982, A structural study of Durst Mountain and the central Wasatch Mountains, Utah: Master's thesis, University of Utah, Salt Lake City, Utah.

James, A., Smith, W., and Welsh, J., 1961, General geology and structure of the Bingham district, Utah, *in* Cook, D.R., ed., Geology of the Bingham mining district and northern Oquirrh Mountains, Utah: Utah Geological Society Guidebook 16, p. 1-16.

James, L.P., 1979, Geology, ore deposits and history of the Big Cottonwood mining district, Salt Lake Co., Utah: Utah Geological and Mineral Survey Bulletin 114, 98 p.

Jewell, P.W., and Parry, W.T., 1987, Geology and hydrothermal alteration of the Mercur gold deposits, Utah: Economic Geology, v. 82, p. 1958-1977.

Jewell, P.W., and Parry, W.T., 1988, Geochemistry of the Mercur gold deposit, Utah: Chemical Geology, v. 69, p. 245-265.

Jordan, T.E. and Douglas, R.C., 1980, Paleogeography and structural development of the Late Pennsylvanian to Early Permian Oquirrh, northwestern Utah, *in* Fouch, T.D. and Magathan, E.R., eds., Paleozoic Paleogeography of the west-central United States, Rocky Mountain Paleogeography Symposium, Rocky Mountain Section: Society of Economic Paleontologists and Mineralogists, p. 217-230.

Kay, M., 1951, North American Geosynclines: G.S.A. Memoir 48, 143 p.

Kornze, L.D., 1987, Geology of the Mercur gold mine, *in* Johnson, J.L., ed., Bulk Mineable Precious Metals Deposits of the western United States, Guidebook for field trips: Geological Society of Nevada, p. 381-389.

Lanier, G., John, E.C., Swensen, A.J., Reid, J., Bard, S.W., Caddey, S.W., and Wilson, J.C., 1978, General geology of the Bingham mine, Bingham Canyon, Utah: Economic Geology, v. 73, no. 7, p. 1228-1241.

Lawton, T. F., 1985, Style and timing of frontal structures thrust belt, central Utah: American Association of Petroleum Geologists Bulletin, v. 69, no. 7, p. 1145-1159.

Moore, W.J., 1973a, Preliminary geologic map of western Traverse mountains and northern Lake mountains, Salt Lake and Utah counties, Utah: U.S. Geological Survey Miscellaneous Invest. Map I-1132, scale 1:250,000.

Moore, W.J. 1973b, A summary of radiometric ages of igneous rocks in the Oquirrh Mountains, north-central Utah: Economic Geology, v. 68, p. 96-101.

Moore, W.J., and McKee, E.H., 1983, Phanerozoic magmatism and mineralization in the Tooele 1° x 2° quadrangle, Utah, *in* Miller, D.M., Todd, V.R. and Howard, K.A. eds., Tectonic and Stratigraphic Studies in the eastern Great Basin: Geological Society of America Memoir 157, p. 183-190.

Parry, W.T., Wilson, P.N., and Bruhn, R.L., 1988, Pore-fluid chemistry and chemical reactions on the Wasatch normal fault, Utah: Geochimica et Cosmochimica Acta, v. 52, p. 2053-2063.

Presnell, R.D., 1992, Geology and Geochemistry of the Barneys Canyon Gold Deposit, Salt Lake County, Utah: unpublished Ph.D. dissertation, Univ. of Utah, Salt Lake City, Utah, 265 p.

Presnell, R.D. and Parry, W.T., 1991, The Barneys Canyon gold deposit and its relationship to Jurassic tectonism: Geological Society of America Abstracts with Programs, v.23, no. 5, p. A193.

Riess, S.K., 1985, Structural geometry of the Charleston thrust fault, central Wasatch mountains: Utah. Master's Thesis University of Utah, Salt Lake City, Utah, 73 p.

Roberts, R.J., Crittenden, M.D., Jr., Tooker, E.W., Morris, H.T., Hose, R.K., and Cheney, T.M., 1965, Pennsylvanian and Permian basins in northwestern Utah, northeastern Nevada, and south-central Idaho:

American Association of Petroleum Geologists Bulletin, v. 49, p. 1926-1956.

Royce, R.C., Warner, M.A., and Reese, D.L., 1975, Thrust belt of Wyoming, Idaho and northern Utah. Structural geometry and related stratigraphic problems, *in* Boyland, D.W. ed., Deep Drilling Frontiers of the Central Rocky Mountains: Rocky Mountain Association of Geologists Guidebook, p. 41-54.

Rubright, R.D., and Hart, O.J., 1968, Non-porphyry ores of the Bingham district, Utah, *in* Ridge, J.D., ed., Ore Deposits in the United States 1933-1967: American Institute of Mining, Metallurgical and Petroleum Engineers, v. 1, p. 966-991.

Schurer, V.C., 1979, Structural geology of the Kirkman-Diamond Creek Formation, west-central Oquirrh Mountains, Utah: Unpub. Masters's Thesis, University of Utah, Salt Lake City, Utah, 46 p.

Sears, J.W., Graff, P.J., and Holden, G.S., 1982, Tectonic evolution of lower Proterozoic rocks, Uinta mountains, Utah and Colorado: Geological Society of America Bulletin, v. 93, p. 990-997.

Slentz, L.W., 1961, Salt Lake group in the lower Jordan Valley, Utah, *in* Cook, D.R., ed., Geology of the Bingham mining district and northern Oquirrh Mountains, Utah: Utah Geological Society Guidebook 16, p. 23-36.

Smith, R.B. and Bruhn, R.L., 1984, Intraplate extensional tectonics of the eastern Basin-Range: Inferences on structural style from seismic reflection data, regional tectonics and thermal-mechanical models of brittle/ductile deformation: Journal of Geophysical Research, v. 89, p. 5733-5762.

Smith, W.H., 1975, General structural geology of the Bingham district, *in* Bray, R.E., and Wilson, J.C., eds., Guidebook to the Bingham mining district: Society of Economic Geologists, Oct. 23, 1975, Bingham Canyon, Utah, Kennecott Copper Corp., p. 41-48.

Snoke, A.W., and Miller, D.M., 1988, Metamorphic and tectonic history of the northeastern Great Basin, *in* Ernst, W.G., ed., Metamorphism and crustal evolution of the western United States: Rubey vol. 7, Prentice Hall, p. 606-648.

Stacey, J.S., Zartman, R.E., and Nkomo, J.T., 1968, A lead isotope study of galenas and selected feldspars from mining districts in Utah: Economic Geology, v. 63, p. 1345-1360.

Stanger, L.W., 1990, Geology and mineralization of the Lulu graben, Barrick Mercur gold mine, Tooele Co. Utah, *in* Hausen, D.M., ed., Gold '90 Salt Lake City Proceedings, Salt Lake City: American Institute of Mining Engineers, p. 11-20.

Stewart, J.H., 1972, Initial deposits in the Cordilleran geosyncline: evidence of a late Precambrian (<850 m.y.) continental separation: Geological Society of America Bulletin, v. 83, p. 1345-1360.

Stewart, J.H., 1976, Late Precambrian evolution of North America: Plate tectonic implications: Geology v. 4, p. 11-15.

Stewart, J.H., Moore, W.J., and Zietz, I., 1977, East-west patterns of Cenozoic igneous rocks, aeromagnetic anomalies and mineral deposits, Nevada and Utah: Geological Society of America Bulletin, v. 88, p. 67-77.

Stokes, W.L., 1976, What is the Wasatch Line?. *in* Hill, J.M., ed., Symposium on the Geology of the Cordilleran Hingeline: Rocky Mountain Association of Geologists, p. 11-26.

Swensen, A.J., 1975, Sedimentary and igneous rock of the Bingham mining district, *in* Bray, R.E., and Wilson, J.C., eds., Guidebook to the Bingham mining district: Society of Economic Geologists, Oct. 23, 1975: Bingham Canyon Utah, Kennecott Copper Corp., p.21-39.

Tafuri, W.J., 1987, Geology and geochemistry of the Mercur mining district, Tooele Co., Utah: Unpub. Ph. D. dissertation, University of Utah, Salt Lake City, Utah, 180 p.

Thorman, C.H., Ketner, K.B., Brooks, W.E., Snee, L.W., and Zimmerman, R.A., 1991, Late Mesozoic-Cenozoic tectonics in northeastern Nevada, *in* Raines, G.L., Lisle, R.E., Schafer, R.W. and Wilkanson, W.H., eds., Geology and ore deposits of the Great Basin: Geological Society of Nevada, p. 25-45.

Thorman, C.H., Ketner, K.B., and Peterson, F., 1990, The Elko Orogeny-Late Jurassic orogenesis in the Cordilleran miogeocline: Geological Society of America Abstracts with Programs, Cordilleran Section, v. 22, no. 3, p. 88.

Tooker, E.W., 1983, Variation in structural style and correlation of thrust plates in the Sevier foreland thrust belt, Great Salt Lake area, Utah. *in* Miller, D.M.,Todd, V.R. and Howard, K.A., eds., Tectonic and stratigraphic studies in the eastern Great Basin: Geological Society of America Memoir 157, p. 61-74.

Tooker, E.W., and Roberts, R.J., 1961, Stratigraphy of the north end of the Oquirrh Mountains, Utah, *in* Cook, D.R., ed., Geology of the Bingham mining district and northern Oquirrh Mountains, Utah: Utah Geological Society Guidebook 16, p. 17-35.

Tooker, E.W. and Roberts, R.J., 1970, Upper Paleozoic rocks in the Oquirrh Mountains and Bingham mining district, Utah: U. S. Geological Survey Professional Paper 629-A, 76 p.

Viveiros, J. J., 1986, Cenozoic tectonics of the Great Salt Lake from seismic reflection data from the Basin and Range transition: M.S. thesis, University of Utah, Salt Lake City, Utah, 98 p.

Warnaars, F.W., Smith, W.H., Bray, R.D., Lanier, G., and Shafiquallah, M., 1978, Geochronology of igneous intrusions and porphyry copper mineralization at Bingham, Utah: Economic Geology, v. 73, no. 7. p. 1242-1249.

Welsh, J.E., and James, A.H., 1961, Pennsylvanian and Permian stratigraphy of the central Oquirrh Mountains, Utah. *in* Cook, D.R., ed., Geology of the Bingham mining district and northern Oquirrh Mountains, Utah: Utah Geological Society Guidebook 16, p. 1-16.

Wilson, E. A., Saugy, L., and Zimmerman, M. A., 1986, Cenozoic tectonics and sedimentation of the eastern Great Salt Lake area, Utah: Bulletin Societe Geologique France, v. 8, p. 777-782.

Wilson, P.N., and Parry, W.T., 1989, Geochemical characteristics of hydrothermally altered black shales of the southern Oquirrh Mountains and relationships to Mercur-type gold deposits: Utah. Utah Geological and Mineral Survey, Open-file report 161, 64 p.

Wilson, P.N., and Parry, W.T., 1990a, Geochemistry of Mesozoic hydrothermal alteration of black shales associated with Mercur-type gold deposits, *in* Hausen, D.M., ed., Gold '90, Salt Lake City Proceedings, Salt Lake City: American Institute of Mining Engineers, p. 167-179.

Wilson, P.N. and Parry, W.T., 1990b, Mesozoic hydrothermal alteration associated with gold mineralization in the Mercur district, Utah: Geology, v. 18, no. 9, p. 866-869.

Wilson, P.N., and Parry, W.T., 1991, Thermal and chemical evolution of hydrothermal fluids at the Ophir Hill mine, Ophir, district, Utah. *in* Allison, M.L. ed., Energy and Mineral resources of Utah: Utah Geological Association, Publication 18, p. 97-112.

Wiltschko, D.V., and Dorr, J.A., 1983, Timing of deformation in the overthrust belt and foreland of Idaho, Wyoming and Utah: American Association of Petroleum Geologists Bulletin, v. 67, p. 1304-1322.

Wu, D., and Bruhn, R.L. 1990, Geometry and kinematics of normal faults, western flank of Oquirrh Mountains, Utah: Abstract in EOS, Transactions of the American Geophysical Union, v. 71, no. 43.

Yonkee, W.A., 1990, Geometry and mechanics of basement and cover deformation, Farmington canyon complex, Sevier orogenic belt, Utah: Ph.D. dissertation, University of Utah, Salt Lake City, Utah, 255 p.

Zoback, M.L., 1983, Structure and Cenozoic tectonism along the Wasatch fault zone, Utah. *in* Miller, D.M., Todd, V.R. and Howard, K.A. eds, Tectonic and Stratigraphic Studies of the eastern Great Basin: Geological Society of America Memoir 157, p. 3-27.

GEOLOGY OF THE BARNEYS CANYON GOLD DEPOSIT, SALT LAKE COUNTY, UTAH

W.L. Gunter
Kennecott Corporation
Barneys Canyon Gold Mine

ABSTRACT

The Barneys Canyon orebody is a sediment-hosted disseminated gold deposit located 8 km (5 miles) northeast of the Bingham Canyon porphyry copper mine. Micron-sized gold occurs in altered dolomite and siliclastic rocks of Lower Permian-age Park City and Kirkman-Diamond Creek Formation. Geochemically anomalous amounts of As, Sb, Hg, and Tl are associated with gold mineralization. Gold to silver ratios in the deposit greatly exceed 1:1. Gold distributions are controlled by alteration-enhanced permeability contrasts within the lower plate of a thrust fault-repeated stratigraphic sequence. Pre-mineral thrusting and post-mineral normal fault movements are present. Mineralization at Barneys Canyon occurs along a northeast-trending structural corridor dominated by high-angle normal faults, low-angle thrust faults, and alteration.

Gold mineralization at Barneys Canyon is younger than Mesozoic thrusting and older than Tertiary faulting. Barneys Canyon is similar to other epithermal sediment-hosted precious metal deposits of the Basin and Range Province. A conclusive genetic relationship between the Barneys Canyon deposit and the nearby Bingham Canyon porphyry copper deposit has not been established.

INTRODUCTION

The Barneys Canyon project is located in the northern Oquirrh Mountains on the west side of the Salt Lake Valley (Fig. 1). The project consists of two sediment-hosted gold deposits 2.4 km (1.5 miles) apart. The Barneys Canyon orebody contains 8.6 million metric tons (9.65 million short tons) of minable oxide reserves grading 1.64 g/tonne (0.048 oz/ton) gold at a 0.055 g/tonne (0.016 oz/ton) cutoff. The smaller Melco orebody, which lies southwest of the Barneys Canyon Mine, contains 3.5 million metric tons (3.9 million short tons) grading 2.57 g/tonne (0.075 oz/ton) gold at a 0.066 g/tonne (0.019 oz/ton) cutoff. The ore is treated by cyanide heap leach processing. Gold extraction has exceeded eighty-five percent since mining began in 1989. To date the project has produced 10.25 tonnes (329,447 troy ounces) of gold. The current annual production rate is 2.18 metric tons (2.4 million short tons).

HISTORY

Prospecting and mining have taken place in the Oquirrh Mountains since the discovery of lead-silver ore in 1863 (Hammond, 1961). The range has produced approximately 497.65 metric tons (16 million troy ounces) of gold, primarily a byproduct of base metal extraction from the Bingham Canyon porphyry copper system. The Mercur gold mine in the southern Oquirrh Mountains contributed 37.32 metric tons (1.2 million troy ounces) to this total.

REGIONAL GEOLOGY

The Oquirrh Mountains, located 26 km (16 miles) west of the Wasatch Front, form the eastern-most range of the northern Utah Basin and Range Province (Fig. 1). The range consists of Late Paleozoic shallow water carbonate and siliclastic rocks deposited in the northwest-trending Oquirrh structural basin. Jordan and Douglas (1980) report that 7,620 m (25,000 ft) of Upper Pennsylvanian to Lower Permian sedimentary rocks were deposited.

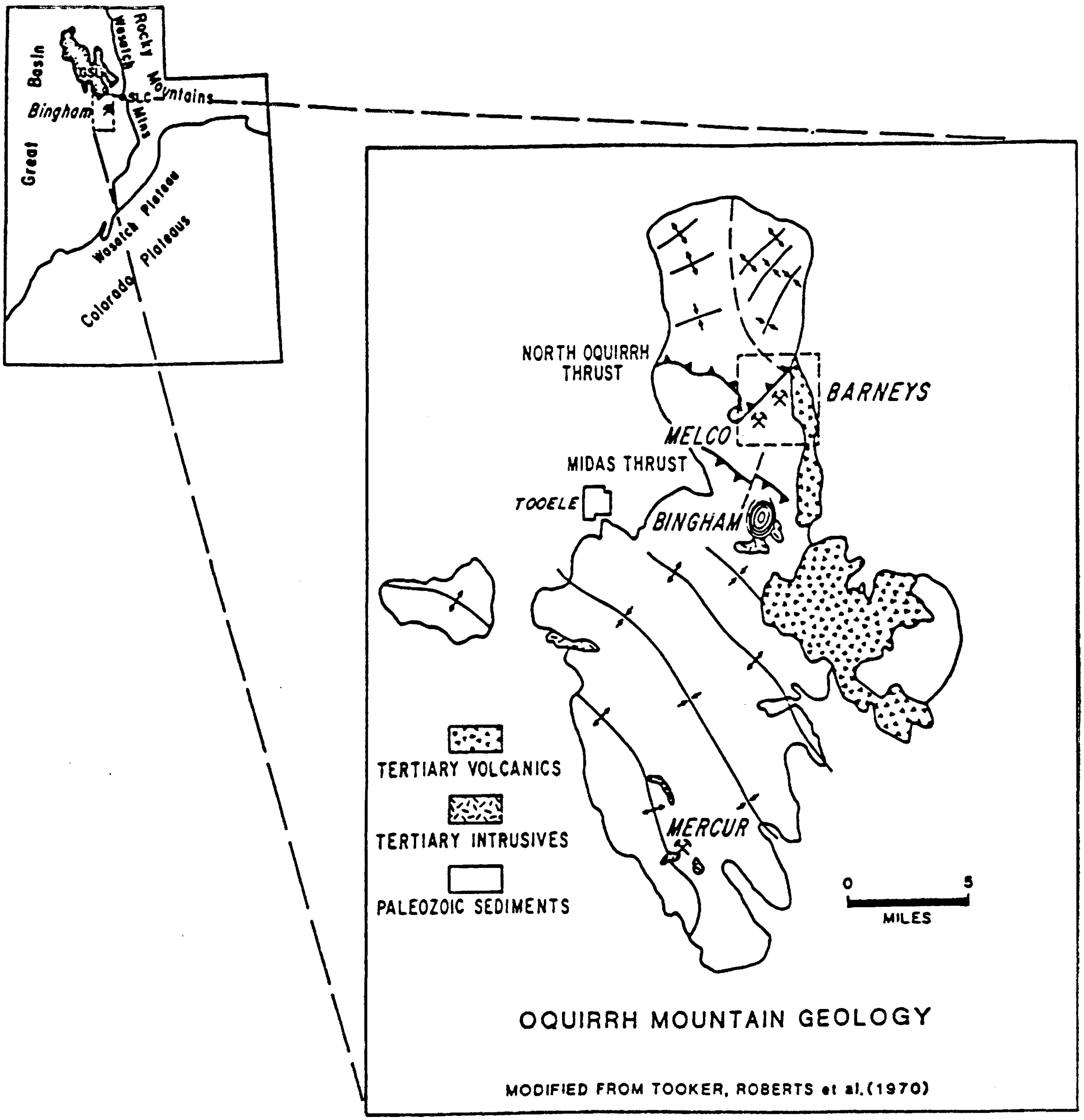

LOCATION MAP OF THE BARNEYS CANYON PROJECT AREA

Figure 1

Mesozoic crustal shortening resulted in extensive thrusting and deformation of Paleozoic strata in the present Basin and Range. Jurassic thrusting circa 150 Ma strongly affected Nevada and western Utah. Recent work by Presnell (1991) suggests that Jurassic thrusting extended much further east than previously thought. The early Cretaceous frontal fold and thrust belt (Sevier Orogeny) began circa 110 Ma, ended in early Eocene, and strongly deformed the strata in central Utah and western Wyoming (Miller, 1990). The frontal thrusts generally propagated eastward in the direction of transport (Miller, 1990). During the Sevier Orogeny sedimentary rocks in the southern Oquirrh Mountains deformed into broad, open, northwest-trending anticlines and synclines. In the northern Oquirrh Mountains, northeast-trending folds formed on the upper and lower plates of the southeast-directed North Oquirrh thrust. The North Oquirrh thrust transposes Pennsylvanian over Lower Permian sedimentary rocks. The north-trending Copperton anticline formed in the lower plate of the Midas thrust north of the Bingham Canyon mine.

Extensional tectonics dominated the Cenozoic Era from Eocene (circa 54 Ma) to present. Igneous intrusive and coeval extrusive rocks were emplaced in the central Oquirrh Mountains (Tooker and Roberts, 1970). Those at Bingham have been dated at 36 to 39 Ma (Moore, 1973). Farther south, dates as young as 31.5 Ma are reported (Moore, 1973). Basin and Range faulting began circa 17 Ma (Miller, 1990).

BARNEYS CANYON DEPOSIT

Stratigraphy

Host strata are Lower Permian cherty and fossiliferous dolomite and dolomitic siltstone of the Park City Formation; and stratigraphically lower siliclastic rocks of the Kirkman-Diamond Creek Formation. Strata strike northwest and dip moderately northeast. The Barneys Canyon thrust structurally thickens the carbonate sequence to 122 m (400 feet) in the mine area (Fig. 2).

The Park City Formation grades conformably into underlying Kirkman-Diamond Creek Formation sandstones. Mineralized sandstone in the mine area displays bedding parallel shear, intense bleaching, calcite flooding, decalcification and argillic alteration. Strongly iron oxide-stained carbonate lenses occur as boudins within altered sandstone.

Structure

The earliest documented structural event is the Barneys Canyon thrust, a probable lower plate imbrication of the North Oquirrh thrust exposed a mile northwest of the mine. The Barneys Canyon thrust causes structural repetition of a distinctive stratigraphic sequence. The fault is a focussed, highly contorted zone of north- to northeast-trending, shallow northeast-plunging upright to overturned folds. Closures are visible on 20-foot benches. Fold orientations indicate an upper plate movement from west northwest to east-southeast. A broad area of bedding parallel slip and gentle ramping surrounds the contorted zone and locally contains ore-grade gold mineralization. Field relationships show that gold emplacement is younger than thrusting.

High-angle normal faults displace older thrust faults, related zones of bedding parallel shear, and gold mineralization in the mine area. The age of these high-angle faults is uncertain. However, the West fault offsets Tertiary-age conglomerates 1.6 km (1 mile) north of the Barneys Canyon mine (G. W. Austin, pers. com., 1991). This establishes that the last movement on the West Fault is no older than Tertiary. Pods of gold mineralization within the West Fault zone and the spatial relationship of the West Fault to other gold prospects indicates that it is a feeder structure for gold mineralization. Displacement is estimated at hundreds of feet. The Park City Formation does not occur west of the West Fault. A strike-slip component of movement is possible.

Geochemistry

Mineralized strata at Barneys Canyon are typically bleached, altered and contain orange-brown to red-brown iron oxides as spots, fracture fillings, and along slip zones. Occasional 1 m (3 ft) clay-bearing iron oxide-rich pods with rare limonite cubes occur within and peripheral to the orebody. The overall orebody is anomalous in Au, As, Sb, Hg, and Tl. The iron oxide pods are anomalous in respect to average orebody values of Au, Fe, As, Sb, Hg, Cu, Pb, Zn, Co, Cd, Tl, Te, Se, Cr, U, Ge, V and W. Silver is often below detection.

Alteration

Subtle alteration patterns and textures resulted from fluid-rock interactions in the mine area. The most pronounced are:

Decalcification. Decalcification is preferentially developed in sparry bioclastic dolomite with thin chert interbeds termed Host Dolomite in the mine, and along high-angle faults and fractures. These rocks are sometimes bleached pale gray to white, are friable, and contain highly fractured and veined chert. Thin sections reveal sparry dolomite rhombs and sand-sized dolomite grains with 5 to 10 percent pore space. This texture is well developed beneath a relatively impermeable dolomitic siltstone unit in both the upper and lower plates of the Barneys Canyon thrust. The lower plate zone of decalcified dolomite contains a significant percentage of the Barneys Canyon orebody, but upper plate decalcified dolomite is weakly anomalous to barren. Decalcification of Host Dolomite apparently preceded gold mineralization.

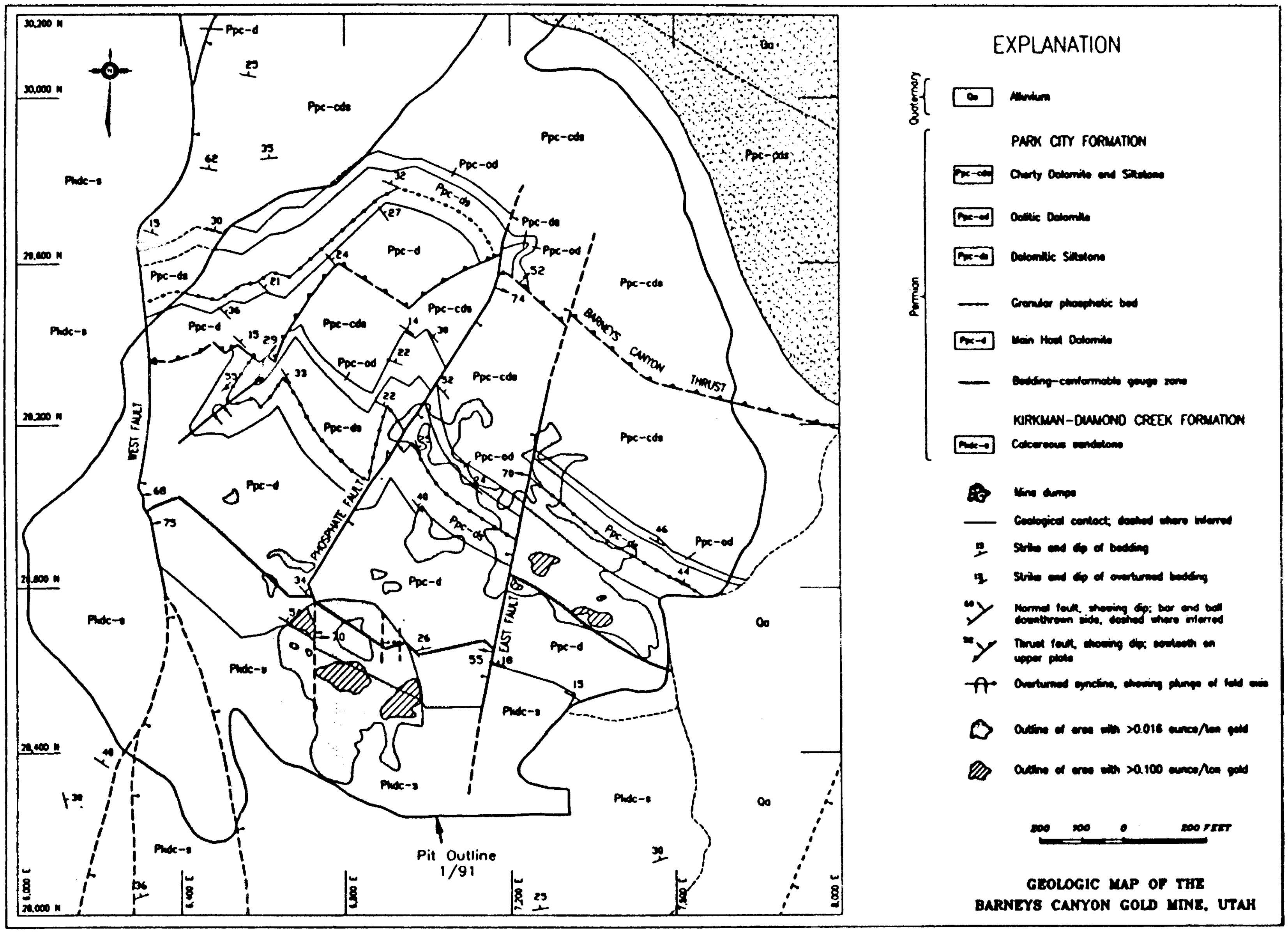
EXPLANATION
Quaternary
Qa Alluvium
PARK CITY FORMATION
Permian
Ppc-cds Cherty Dolomite and Siltstone
Ppc-od Oolitic Dolomite
Ppc-ds Dolomitic Siltstone
Granular phosphatic bed
Ppc-d Main Host Dolomite
Bedding-conformable gouge zone
KIRKMAN-DIAMOND CREEK FORMATION
Pkdc-s Calcareous sandstone
Mine dumps
Geological contact; dashed where inferred
Strike and dip of bedding
Strike and dip of overturned bedding
Normal fault, showing dip; bar and ball downthrown side, dashed where inferred
Thrust fault, showing dip; sawteeth on upper plate
Overturned syncline, showing plunge of fold axis
Outline of area with >0.016 ounce/ton gold
Outline of area with >0.100 ounce/ton gold
200 100 0 200 FEET
WEST FAULT
PHOSPHATE FAULT
EAST FAULT
BARNEYS CANYON THRUST
Pit Outline
1/91
GEOLOGIC MAP OF THE
BARNEYS CANYON GOLD MINE, UTAH

FIGURE 2

Argillic alteration. Argillic alteration occurs dominantly in the sandstone portion of the orebody and to a diminished extent in altered dolomite. Peterson (1989) identified kaolinite and illite as the dominant clay species with subordinate amounts of sericite. Argillic alteration appears to be coeval with decalcification.

Silicification. Massive silicification is not found near the Barneys Canyon deposit. Local, weak to moderate silicification occurs in the mine area. Although macroscopic silicification and gold mineralization have no apparent correlation, Peterson (1989) noted an association between native gold, fine-grained quartz, and iron oxides along microfractures in one ore sample. Other manifestations of silica mobilization within the deposit include silicified fossil fragments in dolomite beds (diagenetic); a zone of bleaching and weak to moderate silicification beneath a bedding parallel gouge zone (hydrothermal ponding); and silicification along exposures of high-angle normal faults. The discovery outcrop of the Barneys Canyon deposit consisted of auriferous jasperoid breccia that displays moderate silicification at the surface. However, the silicification doesn not extend to depth.

Calcite mobilization. Coarse calcite crystal-lined vugs as much as 0.3 m (1 foot) across are present in dolomitic strata within, peripheral to, and overlying gold mineralization. Early stage fluids may have formed these openings which were subsequently filled by remobilized calcite. Calcite cemented fault breccia is found along high angle structures that offset gold mineralization and imply that calcite mobilization followed gold mineralization. Because remobilized calcite haloes gold mineralization, this macroscopic alteration feature could assist recognition of a "blind" orebody.

Mineralization

Bedding, alteration, relative permeability, and structures all control the distribution and intensity of gold mineralization at the Barneys Canyon mine. The orebody, which strikes northwest and dips moderately northeast, subparallel to bedding, is approximately 430 m (1400 ft) long, 370 m (1200 ft) wide, and up to 90 m (300 ft) thick.

Approximately 90 percent of the Barneys Canyon orebody occurs beneath an impermeable siltstone in the lower plate of the Barneys Canyon thrust. Gold grades increase from trace to ore grade at the contact between upper dolomitic siltstone and lower Host Dolomite. Gold values locally continue downward into underlying altered sandstone and display excellent vertical and lateral continuity. In the southwest (up dip) part of the mine, gold mineralization is confined to altered sandstone beneath unaltered dolomite.

Leakage along high-angle structures results in discontinuous gold mineralization above the lower plate dolomitic siltstone. Leakage-related gold mineralization occurs within a broad zone of bedding plane shear and gentle ramping associated with the Barneys Canyon thrust. The original discovery outcrop of "jasperoid breccia" is a leakage phenomenon located 105 m (350 ft) above the main orebody in otherwise barren rock.

Summary of Events at the Barneys Canyon Deposit

The following proposed chronological sequence of events is based upon observations made during definition drilling and mining.

(1) Barneys Canyon thrust repeated distinctive strata in the area.
(2) High angle N- and NNE-striking normal faults and graben structures formed.
(3) Main episode of alteration.
(4) Gold and associated mineralization.
(5) Reactivation of N- and NNE-striking normal faults.
(6) Calcite mobilization.
(7) Erosion and supergene oxidation.

REFERENCES CITED

Gunter, W.L, Hammitt, J.W., Babcock, R.C., Gibson, T.R., and Presnell, R.D., 1990, Geology of the Barneys Canyon and Melco Gold Deposits, Salt Lake County, Utah, *in* Hausen, D.M., ed., Gold '90: AIME, p. 41-50.

Hammond, E.D., 1961, History of Mining in the Bingham District, Utah, *in* Cook, D.R., ed., Geology of the Bingham Mining District and Northern Oquirrh Mountains: Guidebook To the Geology of Utah no. 16, Utah Geologic Society, p. 120-129.

Jordan, T.E., and Douglas, R.C., 1980, Paleozoic Paleogeography of the West-Central United States, *in* Fouch, T.D., and Magatham, E.R., eds., West-Central United States Paleogeography Symposium 1: Rocky Mountain Section S.E.P.M., p. 217-230.

Miller, D. M., 1990, Mesozoic and Cenozoic Tectonic Evolution of the Northeastern Great Basin, *in* Shaddrick, D. R., Kizis, J.A., and Hunsaker, E.L., eds., Geology and Ore Deposits of the Northeastern Great Basin: Geologic Society of Nevada and U. S. Geological Survey, Field Trip #5 Guidebook, p. 43-73.

Moore, W.J., 1973, Igneous rocks in the Bingham mining district, Utah: U.S. Geological Survey Professional Paper 629-B, 42 p.

Peterson, E.U., 1989, Occurrence of Gold in Barneys Canyon Ore: unpublished, University of Utah, 15 p.

Tooker, E.W., Roberts, R.J., 1970, Upper Paleozoic Rocks in the Oquirrh Mountains and Bingham Mining District, Utah: U.S. Geological Survey Professional Paper 629-A, p. 3-10.

ARGILLIC ALTERATION AT THE BARNEYS CANYON GOLD DEPOSIT

by
R.D. Presnell
Kennecott Exploration Company, Salt Lake City, Utah
and
W.T. Parry
University of Utah, Salt Lake City, Utah

ABSTRACT

The Barneys Canyon gold deposit is a sediment-hosted gold deposit of the Carlin-type in Salt Lake Co., Utah. The Barneys Canyon gold deposit exhibits argillic alteration. Phyllosilicates at Barneys Canyon are exclusively illite and kaolinite with some minor to rare interstratified illite-smectite. Evaluation of illite/kaolinite ratios along fences in the strike and dip direction show that the orebody is associated with illite-rich alteration surrounded by kaolinite-rich alteration. Evaluation of illite crystallinity variation along the same drill-hole fences suggest that a lower temperature zone is associated with the orebody. Fluid inclusion data from quartz and barite record two homogenization temperature modes of 225° C and 345° C. But, the lack of pyrophyllite restricts the alteration at Barneys Canyon to the lower temperature event. Two K-Ar ages were obtained from bedding-plane vein illites and yielded Late Jurassic ages (147 Ma and 159 Ma). The alteration at the Barneys Canyon gold deposit was formed at least at 225° C and superimposed on a higher temperature event of Jurassic age.

INTRODUCTION

The Barneys Canyon gold deposit is a sediment-hosted gold deposit of the Carlin-type in Salt Lake County, Utah. Micron-size gold is disseminated in dolomites of the Permian Park City Formation and sandstones of the Permian Kirkman-Diamond Creek Formation. The geology is discussed in a separate paper in this volume by W. Gunter.

Argillization is common in many sediment-hosted disseminated gold deposits (Bagby and Berger, 1985). The phyllosilicates are generally illite and kaolinite with minor smectite (Bagby and Berger, 1985; Percival et al., 1988). Many sediment-hosted disseminated gold deposits exhibit phyllosilicate zonation. In general, the Carlin deposit exhibits a kaolinitic core surrounded by a zone of illite (Arehart et al., 1989; Kuehn, 1989). Within the illitic zones at Carlin the illite polytypes vary and are crudely zoned from 1M converting to 2M towards the orebody (Bagby et al., 1988; Hauff et al., 1989).

Clay zonation and illite crystallinity were evaluated at the Barneys Canyon gold deposit from x-ray diffraction analysis of drill hole composites along two fences of drill holes shown in Figure 1. The strike section is parallel to stratigraphy as well as the strike of the orebody. The dip section is normal to stratigraphy and the trend of the orebody. Illite crystallinity increases systematically with increasing temperature (Kubler, 1967), and has been used as a qualitative estimate of temperature (Weaver, 1961, 1984; Kisch, 1980; Duba and Williams-Jones, 1983). Illite crystallinity was used in this study to obtain a qualitative estimate of temperature distribution within the Barneys Canyon gold deposit.

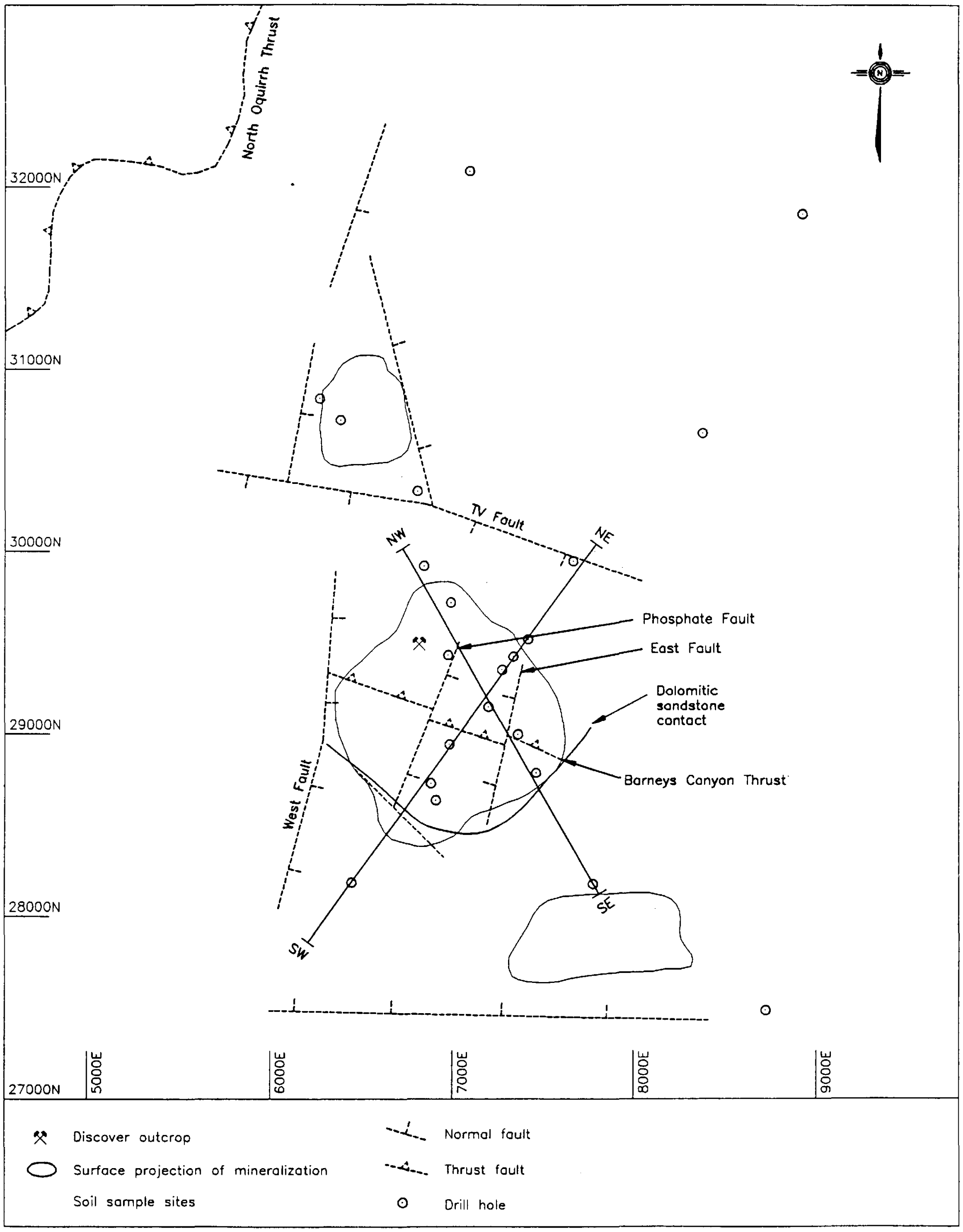

Figure 1. Geologic sketch map of the Barneys Canyon mine showing location of drill hole fences used in this study.

Detailed x-ray diffraction analysis of drill hole pulps and pit samples have shown that phyllosilicates at Barneys Canyon are exclusively illite and kaolinite with some minor to rare interstratified illite-smectite. The phyllosilicates occur in various abundances. The spatial distribution of the relative abundance of illite and kaolinite were evaluated for the two drill hole fences as well as holes peripheral to the deposit.

The peak breadth at half height and the height of the illite (001) and the kaolinite (001) peaks were measured in degrees 2-theta for glycolated <2 micron extract smears from the drill hole composite pulps. The pulps are 20-foot composites made from the original 5-foot sample intervals

In order to determine relative amounts of kaolinite and illite the intensity of the illite peak must be corrected (Pierce, 1969). The illite intensity was corrected by using a multiplication factor of 1.4, determined by ratioing mineral reference intensities given in Moore and Reynolds (1989).

Peak area was calculated by multiplying the height by the breadth at half height. The illite peak area was multiplied by the correction factor. I/K ratios were then calculated and plotted on the strike and dip sections shown as Figures 2a and 2b. Values for peripheral holes are averages of the fifty-foot composites.

Illite crystallinity was determined by measuring the breadth at half height in degrees 2 theta following the method of Kisch (1980). The illite crystallinity values were plotted on the strike and dip sections shown as Figures 3a and 3b.

In strike (Fig. 2a) the variation in I/K ratios does not correspond to the orebody outline and is only roughly parallel to stratigraphy on the eastern side of the deposit. The ratios can be crudely contoured with sub-horizontal zones greater than 2.0 alternating with parallel zones less than 2.0. This suggests that there are alternating zones of kaolinite-rich and illite-rich alteration. In the dip section (Fig. 2b) the variation is roughly sub-parallel to stratigraphy and crudely mimics the orebody. A zone of greater than 2.0 mimics but is within the orebody. The area greater than the 2.0 zone narrows adjacent to the East fault. Below this zone and continuing below the orebody is an area which has ratios less than 2.0 and then the ratios increase towards the sandstone contact. These variations suggest that the core of the orebody is illite-rich and is surrounded by a more kaolinite-rich zone.

In plan view (Fig. 4) the variation is erratic. Values adjacent to the faults are generally lower suggesting higher kaolinite concentrations.

The distribution of illite crystallinity indices in strike and dip are shown in Figure 3a and 3b. In strike (Fig. 3a) the 0.4 contour crudely mimics the orebody. The illite crystallinity index increases towards the core of the orebody particularly within the dolomite adjacent to the East fault. The variation

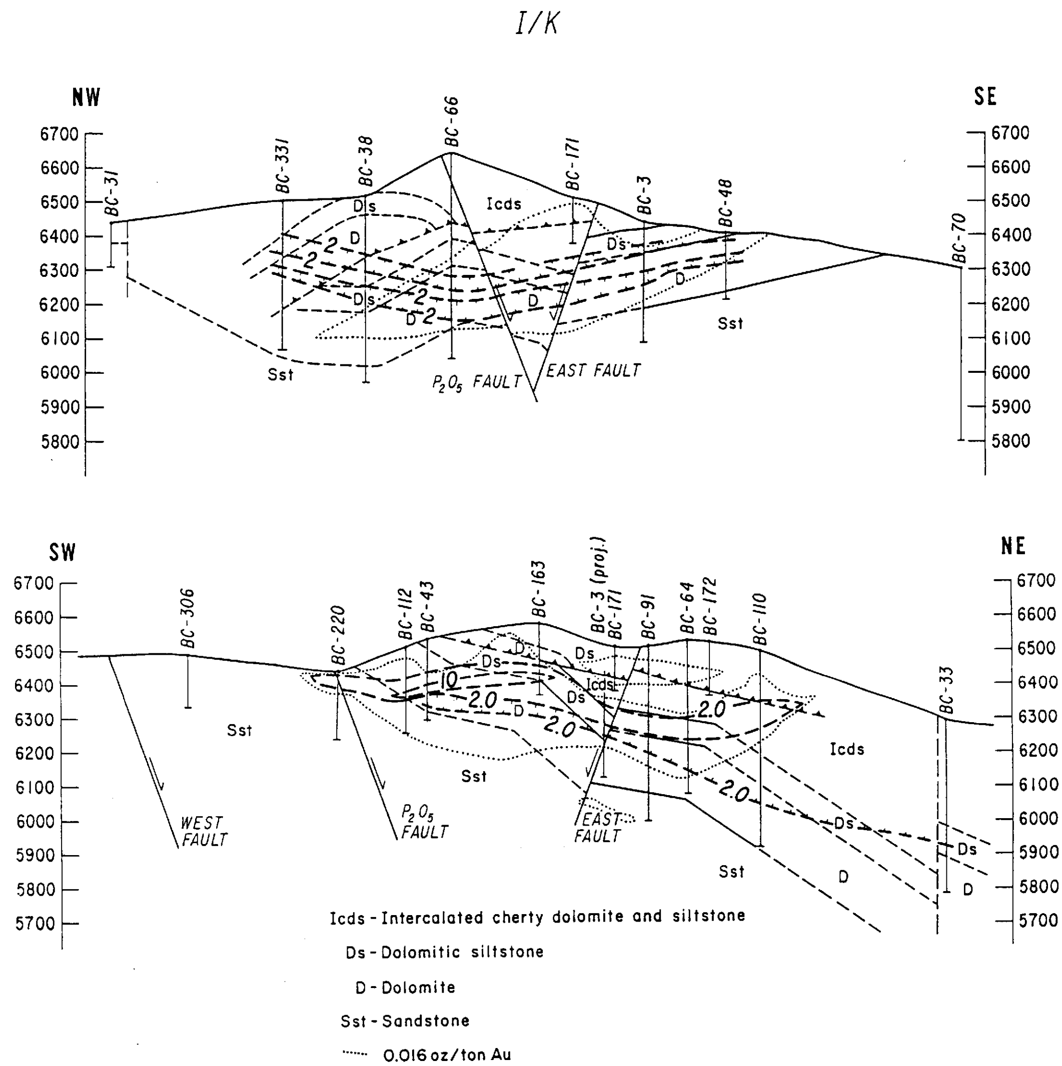

Figure 2. Spatial distribution in strike (2a) and dip (2b) of illite/kaolinite ratios at the Barneys Canyon gold deposit. Data from BC-3 is projected onto section 2b. The 0.016 oz./ton Au contour represents the outline of the orebody.

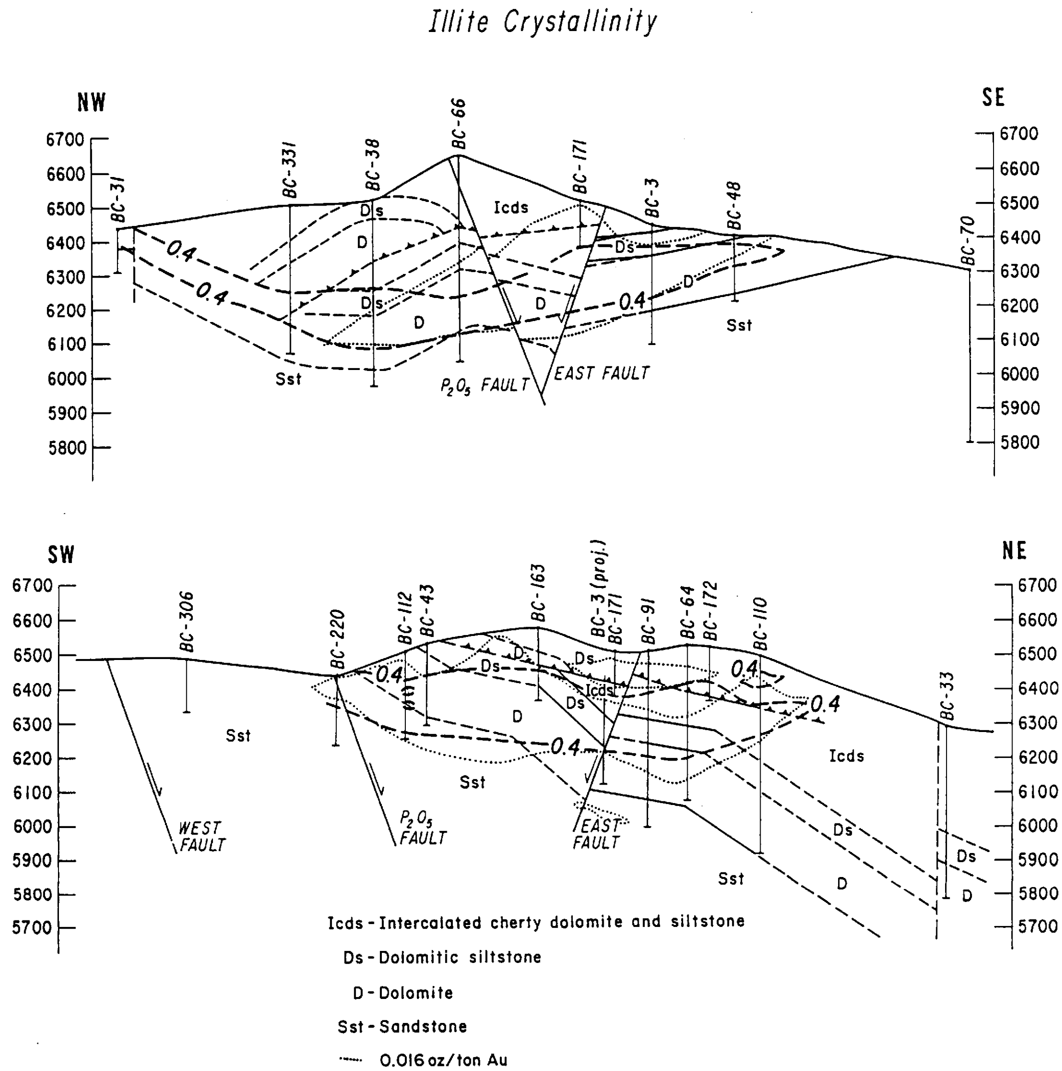

Figure 3. Spatial distribution in strike (3a) and dip (3b) of illite crystallinity (Kubler index) at the Barneys Canyon gold deposit. Data from BC-3 is projected onto section 3b. The 0.016 oz./ton Au contour represents the outline of the orebody.

is relatively continuous. In dip (Fig. 3b) the 0.4 contour mimics the orebody as well.

In plan view (Fig. 5) the core of the orebody tends to be greater than 0.4 but the sparsity and clustering of data do not allow for definitive conclusions. The average values for the peripheral holes do not reflect a pattern in the variation of illite crystallinity.

DISCUSSION

Variation in Illite and Kaolinite

At the Barneys Canyon gold deposit illite and kaolinite coexist but in varying proportions. In strike there are alternating zones of kaolinite-rich and illite-rich alteration, but in dip there is a core of illite-rich alteration surrounded by alteration which is more kaolinite-rich. Phase equilibria between illite and kaolinite is represented by the reaction:

$$3Al_2Si_2O_5(OH)_4 + 2K^+ = 2KAl_3Si_3O_{10}(OH)_2 + 2H^+ + 3H_2O$$

and is therefore controlled by the activities of K+ and H+. It follows that the variation in illite and kaolinite is a result of the fluctuation in either K+, pH or both. Whole rock studies by Presnell (1992) have shown that the K/(K+Al) ratio increases from unmineralized rock to mineralized rock suggesting that potassium was introduced during alteration and may have effected the distribution of illite and kaolinite. However, since the deposit is oxidized, the oxidation of pyrite would lower the pH and possibly convert illite to kaolinite. The various proportions of illite and kaolinite suggest that fluctuations in both K+ and pH effected the distribution of kaolinite and illite.

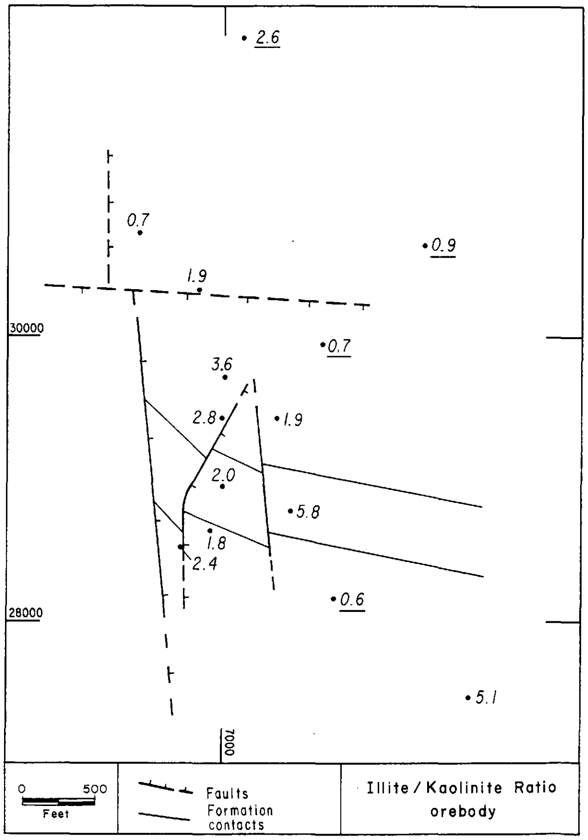

Figure 4. Plan view map through the middle of the Barneys Canyon orebody showing illite/kaolinite ratios relative to geologic features.

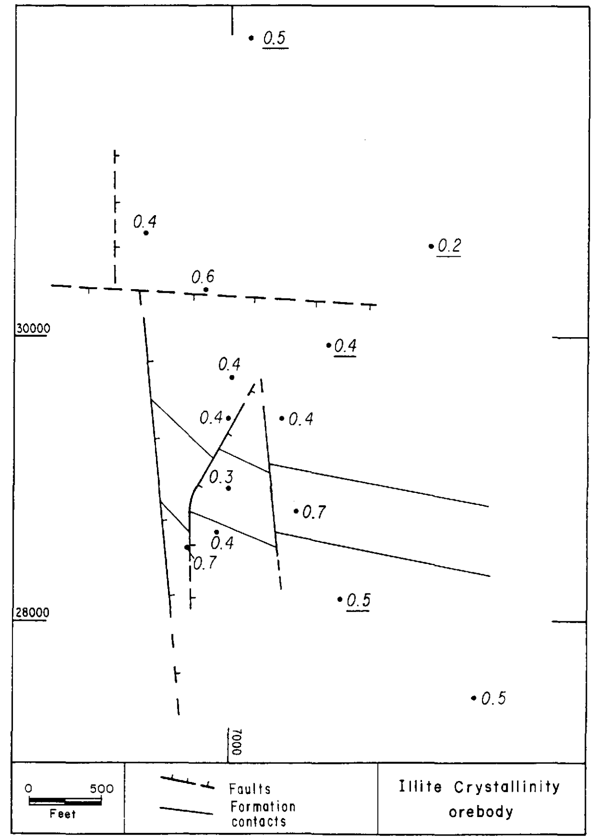

Figure 5 Plan view map through the middle of the Barneys Canyon orebody showing illite crystallinity indices relative to geologic features.

Illite Crystallinity

In general, at the Barneys Canyon gold deposit the illite crystallinity index increases towards and within the orebody. The illite crystallinity index is inversely proportional to temperature (Dunoyer de Segonzac, 1970). Therefore the illite crystallinity at the Barneys Canyon gold deposit records a lower temperature core. Illite crystallinity has been used to characterize very low grade metamorphism from diagenesis to prehnite-pumpellyite metamorphism. Kubler (1967, 1968) recognized and named several degrees of low grade metamorphism. The lowest grade zone is diagenesis followed by the anchizone, and then the epizone which is equivalent to greenschist facies metamorphism (Frey and Kisch, 1987). The 0.4 contour on Figures 3a and 3b corresponds to the onset of the anchizone. The anchizone ranges from illite crystallinity indices of 0.42 to 0.25. Values less than 0.25 are in the epizone. Values greater than 0.42 are related to diagenesis (Kubler, 1967; Weaver, 1984). The anchizone covers a temperature range of 200° to 300° C (Frey and Kisch, 1987; Kisch,1987). The epizone corresponds to vitrinite reflectance of 2.5-5 (Kisch, 1987).

Due to peak interferences from calcite, dolomite and quartz with the diagnostic peaks for distinguishing between 2M and 1M illite polytypes an evaluation of 2M to 1M distribution was not undertaken. However the Kubler index of 0.4 is also the threshold for the conversion of 1M to 2M (Frey and Kisch,1987). This suggests that the orebody is associated with the 1M polytype and maybe surrounded by the higher temperature 2M polytype.

Fluid Inclusion Data

Fluid inclusion data from quartz and barite at the Barneys Canyon gold deposit record two homogenization temperature modes of 225° C and 345° C with temperatures ranging from 129° C to 393° C (Presnell, 1992). However, kaolinite converts to pyrophyllite above 278° C (Hemley et al., 1980). Therefore, the kaolinite must have been formed at the lower temperature event. This also implies that the lower temperature event was superimposed on the higher temperature event.

Age Dates

Two K-Ar ages were obtained from bedding-plane vein illites within the Barneys Canyon orebody and yielded Late Jurassic ages (147 +/-5 and 159 +/-6 Ma). The K-Ar systematics of<4 micron illite will be reset between 250° and 300° C (Hunziker, 1987). Since the lower temperature event was not high enough to reset the K-Ar ages, the dating must record the higher temperature event. Due to the lack of pyrophyllite the alteration at the Barneys Canyon gold deposit was formed at least at 225°C and was superimposed on a higher temperature event of Jurassic age.

Regional Implications

Wilson and Parry (1990a, 1990b) obtained similar ages for 18 illites in the southern Oquirrh Mountains which is described by Wilson and Parry in this volume. Based on dates obtained from vein and whole rock size separates they concluded that the ages date a regional hydrothermal event. Also, illites have been shown to date tectonic events (Hunziker et al., 1986). Since the dated illites from Barneys Canyon are from bedding-plane gouges formed during growth of the Copperton anticline, they may record the age of growth of the anticline. Therefore, structures in the Oquirrh mountains may be Jurassic rather than Cretaceous in age. The Elko orogeny of eastern Nevada and western Utah has been directly dated at 170 to 150 Ma by Snoke and Miller (1988). The Jurassic-age illites in the Oquirrh Mountains extend the Elko orogeny to the Oquirrh Mountains. The higher temperature event recorded at Barneys Canyon is therefore a result of Jurassic metamorphism and tectonism formed during the Elko orogeny.

The age of the Barneys Canyon gold deposit can not be determined from the data and arguments presented above. The outstanding question is how much longer after the higher temperature event was the lower temperature event which is associated with the Barneys Canyon orebody. Incidently, the dated illites at Barneys Canyon have illite crystallinity values consistent with the lower temperature event.

ACKNOWLEDGMENTS

We thank the Kennecott Exploration Company, particularly R. Babcock and P. Smith for funding for this study and release of the data. We also thank the Barneys Canyon mine staff for access and helpful discussions. Discussions with Paula Wilson and her review of the manuscript were indispensable. The figures were drafted by P. Onstott.

REFERENCES

Arehart, G.B., Kesler, S.E., Foland, K.A., and Hubacher, F.A., 1989, Alteration zoning and geochronology of the Post micron gold deposit: Geological Society of America Abstracts with Programs v. 21, no. 6, p. 350.

Bagby, W.C., and Berger, B.R., 1985, Geologic characteristics of sediment-hosted, disseminated gold deposits in the western United States, *in* Berger, B.R., and Bethke, P.M., eds., Geology and geochemistry of epithermal systems: Society of Economic Geology Reviews in Economic Geology v. 2, p. 169-202.

Bagby, W.C., Madrid, R.J., and Bakken, B., 1988, Alteration and vein relationships applied to exploration for sedimentary-rock-hosted, Carlin-type deposits, *in* Extended Oral Abstract volume Bicentennial Gold '88: Melbourne, Australia, May, 1988, p. 161-166.

Duba, D., and Williams-Jones, A.E., 1983, The application of illite crystallinity, organic matter reflectance, and isotopic techniques to mineral exploration: A case study in southwestern Gaspe, Quebec: Economic Geology, v. 78, p. 1350-1363.

Dunoyer de Segonzac, G., 1970, The transformation of clay minerals during diagenesis and low grade metamorphism: a review: Sedimentology, v. 15, p. 281-346.

Frey, M., and Kisch, H.J., 1987, Scope of Subject, *in* Frey, M., ed. Low temperature metamorphism: Blackie, Glasgow and London, p. 1-8.

Hauff, P.L., Kruse, F.A. and Madrid, R.J., 1989, Gold exploration using illite polytypes defined by x-ray diffraction and reflectance spectroscopy, *in* Bhappu, R.B. and Harden, R.J. eds. 1989, Gold Forum on Technology and Practices: World Gold '89 Soc. of Mining, Metallurgy and Exploration, p. 76-82.

Hemley, J.J., Montoya, J.W., Marinenko, J.W., and Luce, R.W., 1980, Equilibria in the system Al2O3-SiO2-H2O and some general implications for alteration/mineralization processes: Economic Geology, v. 75, p. 210-228.

Hunziker, J.C., 1987, Radiogenic isotopes in very low-grade metamorphism, *in* Frey, M., ed., Low temperature metamorphism: Blackie, Glasgow and London, p. 200-226.

Hunziker, J.C., Frey, M., Clauer, N., Dallmeyer, R.D., Friedrichsen, H., Flehmig, W., Hochstrasser, K., Roggwiller, P., and Schwander, H., 1986, The evolution of illite to muscovite: Mineralogical and isotopic data from Glarus, Alps, Switzerland: Contributions to Mineralogy and Petrology, v. 92, p. 413-427.

Kisch, H.J., 1980, Incipient metamorphism of Cambro-Silurian clastic rocks from the Jamatland Supergroup, central Scandinavian Caledonides, western Sweden: Geological Society of London Journal, v. 137, p. 271-288.

Kisch, H.J., 1987, Correlation between indicators of very low-grade metamorphism, *in* Frey, M., ed., Low temperature metamorphism: Blackie, Glasgow and London, p. 227-300.

Kubler, B., 1967, La cristallinite de l'illite et les zones fait superieures du metamorphisme: Etags Tectoniques, Colloq. Neuchabel, p. 105-122.

Kubler, B., 1968, Evaluation quantitative du metamorphisme par la cristallinite de l'illite. Etat des progres realises ces dernieres annees: Bulletine Centre Recherche Pan-SNPA, v. 2, p. 385-397.

Kuehn, C.A., 1989, Studies of disseminated gold deposits near Carlin, Nevada: Evidence for a deep geologic setting of ore formation: Unpub. Ph.D. thesis, Penn. State University, 395 p.

Moore, D.M., and Reynolds, R.C., 1989, X-ray Diffraction and the Identification and Analysis of clay minerals: Oxford University Press, Oxford, New York, 332 p.

Percival, T.J., Bagby, W.C., and Radtke, A.S., 1988, Physical and chemical features of precious metal deposits hosted by sedimentary rocks in the western United States, *in* Schafer, R.W. et al., eds., Bulk mineable precious metal deposits of the western United States: Symposium Proceedings, April, 1987, Geological Society of Nevada, p. 11-34.

Presnell, R.D., 1992, Geology and Geochemistry of the Barneys Canyon Gold Deposit: Unpub. Ph.D. Dissertation, Univ. of Utah, Salt Lake City, Utah, 265 p.

Snoke, A.W., and Miller, D.M., 1988, Metamorphic and tectonic history of the northeastern Great Basin, *in* Ernst, W.G., ed., Metamorphism and Crustal Evolution of the Western United States, Rubey Vol. 7: Prentice Hall p. 606-648.

Weaver, C.E., 1961, Clay minerals of the Ouachita structural belt and the adjacent foreland, *in* Flawn, P.T., Goldstein, A. Jr., King, P.B., and Weaver, C.E., eds., The Ouachita Belt: University of Texas, publication 6120, p. 147-160.

Weaver, C.E., 1984, Shale-Slate Metamorphosis in the Southern Appalachians: Developements in Petrology 10, Elsevier, Amsterdam, 235 p.

Wilson, P.N., and Parry, W.T., 1990a, Geochemistry of mesozoic hydrothermal alteration of black shales associated with Mercur-type gold deposits, *in* Hausen, D.M., ed., Gold '90, Salt Lake City, AIME, p. 167-179.

Wilson, P.N., and Parry, W.T., 1990b, Mesozoic hydrothermal alteration associated with gold mineralization in the Mercur district, Utah: Geology, v. 18, no. 9, p. 866-869.

Wilson, P.N. and Parry, W. T., 1991, Thermal and chemical evolution of hydrothermal fluids at the Ophir Hill mine, Ophir District, Utah, *in* Allison, M. L., ed., Energy and mineral resources of Utah: Utah Geological Association Publication 18, Salt Lake City, Utah, p. 97-112.

BARRICK MERCUR GOLD MINE, MERCUR, UTAH

Larry W. Stanger
Mine Geologist

INTRODUCTION

The Mercur Gold Mine is operated by Barrick Resources (USA) Incorporated. It is located in the southern Oquirrh Mountains in Tooele County, Utah, about 56 km (35 miles) southwest of Salt Lake City and 24 km (15 miles) south of Kennecott's Bingham Copper Mine (Fig. 1).

The Mercur district, as presently permitted, covers 890 hectares (2200 acres). Production began in 1983 and is planned to go through 1999. Planned production is from five separate open pits (Fig. 2). Gold to be produced from 1983 to 1999 will total 48.0 million grams, Mg (1.4 million oz, Moz) along with some silver and mercury.

The Mercur work force consists of about 230 men and women. Work conditions are excellent, contributing to an annual turnover rate of about two per cent, far below an industry average which exceeds 10% (Cummings, A.B., 1991, personal communication). Approximately half of the employees commute from Tooele and the other half commute from Wasatch Front communities.

Reclamation concerns are taken seriously at Mercur. As development has begun on open pits, topsoil has been stripped from within the pit boundaries and stockpiled for future use. Waste dumps will be sloped and topsoil applied and reseeded. Dump leaches will be flushed and drained. A clay cap will then be applied, followed by topsoil and reseeding. The tailings pond will be topsoiled and reseeded. All mill structures will be removed and the areas topsoiled and reseeded. Natural drainages will be reestablished. All reclamation work will be monitored until bond release is given by the state (JBR Consultants Group, 1989). In the end, the public will be able to return to the Mercur area with recreational vehicles and camping equipment to enjoy a safe and visually aesthetic outdoor experience.

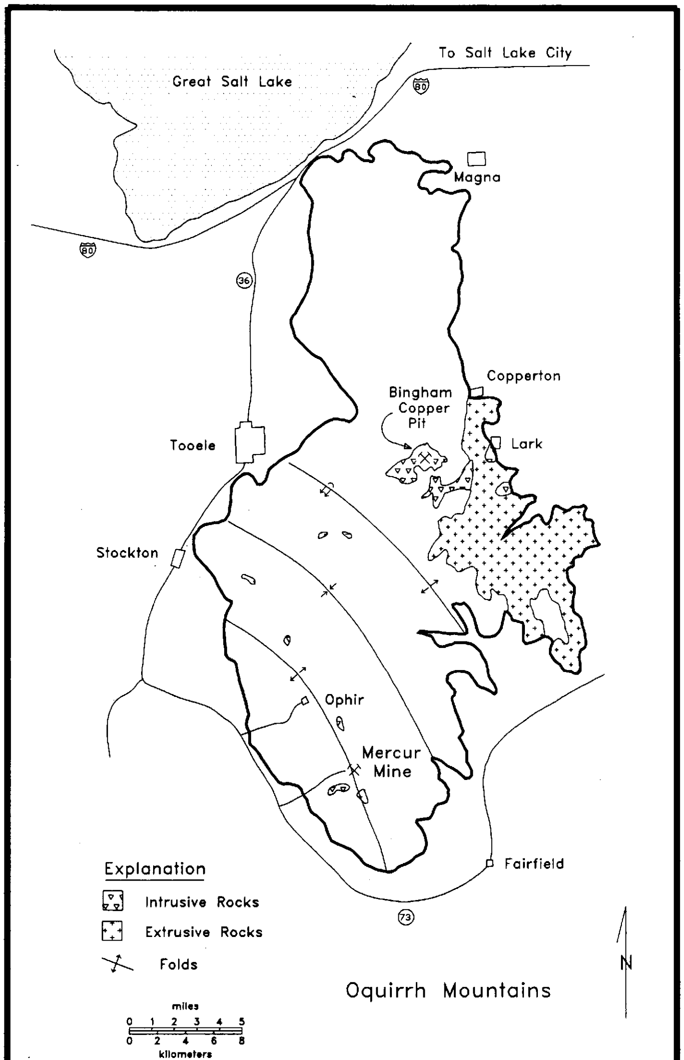

Figure 1

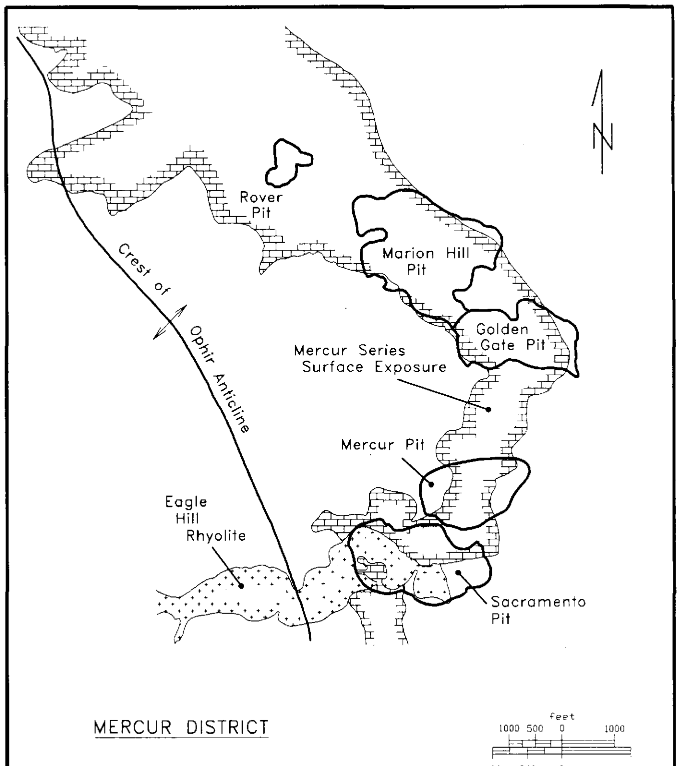

Figure 2

Environmental concerns also receive top priority. Numerous water test wells allow Barrick to monitor water quality both on the mine property and down the hydraulic gradient from the mine. Wildlife are also protected by use of game fences, salt licks and watering troughs. Local wildlife include elk, deer, numerous bird species including bald eagles, mountain lion, coyotes, badgers, red fox, bobcat, and long tailed weasels (JBR Consultants Group, 1989).

HISTORY

The Mercur (Camp Floyd) district has hosted four periods of mining. The first period began in 1870 as a busy, but short-lived silver mining camp called Lewiston. Production was 1.4 Mg (46,000 oz) of silver in three years. Cinnabar was also discovered, though mining of cinnabar was not attempted at the time. In 1879, Arie Pinedo located a claim on what he thought was a cinnabar vein, naming the claim "Mercur," the German word for mercury (Dern, 1904). The red material later proved to be iron oxide staining (Shenon, 1963), but the Mercur claim eventually became the nucleus of the Mercur gold camp (Dern, 1904).

Mercur's second period of mining began when gold was discovered in 1883 (Shenon, 1963). Economic recovery was not possible, however, because of the micron size of the gold particles. In 1891, recovery of gold became feasible with the first successful application in the United States of the McArthur-Forrest cyanide leaching process (Kornze et al., 1984). Gold was mined underground until 1913 when economic problems led to closure of the district's largest mill, the Golden Gate (Requa, 1967). This mill foundation can still be seen as one drives from the lower guard gate to the present mill site.

In 1932, the third mining period began. The price of gold had increased from $0.65 per g ($20.67 per oz) to $1.12 per g ($35 per oz), creating renewed profitability. Ore came from both underground and surface mines. Mining again ceased in 1942 when the Federal Mine Closure Act closed the nation's gold mines (Burger, 1983). Relics from this period can still be seen west of the earlier Golden Gate mill foundation. They include four concrete thickener tanks and numerous wooden or metal structures. The most notable structure is the Ingersoll headframe, which is depicted as a part of the company logo.

The fourth period began in 1973, when Getty Oil Company acquired exploration rights to the district. Exploration was successful, leading to a 1983 start-up of the present mining operation. Texaco Inc. purchased Getty Oil Company in 1984, and Barrick Resources purchased the Mercur Mine from Texaco in 1985.

Total production from the first three periods was 37.3 Mg (1.2 Moz) of gold and minor amounts of silver. The gold had an estimated grade of 7.88 g per metric ton (mt) (0.23 oz per short ton, st) (Klatt and Tafuri, 1976). Mercury production from 1903-1907 was reported as 1,228 kg from cinnabar ore which averaged 7% mercury (Howard, 1913). Current gold production is about 3.6 Mg (115,000 oz) per year with a total planned output of 48.0 Mg (1.4 Moz).

MINING — MILLING

All present mining is by open pit methods. A grid of reverse circulation exploration holes spaced roughly 30 m (100 ft) apart provides information for development of ore bodies and for design of pits. Production drilling is then used to determine actual minable ore zones. Within the pits, four Ingersoll Rand DM-25 drills operate on a grid spacing of 4.3 to 5.5 m (14 to 18 ft). Holes are drilled 7.6 m (25 ft) deep, and sampled for the first and second 3.05 m (10 ft) intervals. The final 1.5 m (5 ft) of hole provides more efficient blasting of rock at the bench toes. Benches are then blasted as 6.1 m (20 ft) levels. Ore is mined as 3.05 m (10 ft) benches in ore zones and as 6.1 m (20 ft) benches where practical in waste rock. Rock is mined by utilizing two Hitachi U-801 track mounted hydraulic shovels, two Caterpillar 992 wheel loaders, two 68 mt (75 st) Wabco haulage trucks, and twelve 77 mt (85 st) Wabco haulage trucks.

Ore is sorted into oxide and refractory, using a 60% laboratory simulated mill recovery as a method of testing. Further sorting is based on grade. The cutoff grade for oxide ore is as low as 0.514 g per mt (0.015 oz per st). Oxide ore below 1.372 g per mt (0.040 oz per st) is sent to leach pads, while oxide ore above 1.372 g per mt is sent to the mill. The cutoff grade for refractory ore is 1.886 g per mt (0.055 oz per st). Refractory ore is processed through an autoclave which articially oxidizes the ore prior to introduciton into the main mill circuit.

The Mercur mine produces 41,800 mt per day (mtpd) (46,000 stpd) ore and waste rock on a five day per week schedule. This supports a mill production of 4500 mtpd (5000 stpd) on a seven day per week schedule.

All millable ore is ground to 80% minus 200 mesh by SAG and ball mills. Ground product is then thickened to approximately 60% solids. Oxide ore reports directly to two parallel CIL circuits with seven tanks in each circuit for leaching. Gold is dissolved with a high pH cyanide solution and adsorbed onto activated carbon granules. Gold is then removed from the carbon and smelted on property to produce a dore' containing gold, silver, and minor impurities. Tails slurry is pumped to the tailings impoundment area for permanent storage of solids. Water is returned to the CIL circuit after solids have settled.

Refractory ore is treated to pressure oxidation in a 725 mtpd (800 stpd) autoclave circuit. High temperature, high pressure, and introduction of oxygen oxidize sulfides in the ore and prepare it for gold leaching in the oxide CIL circuits.

Dump leach ore consists of blasted rock which is hauled directly to the leach pad. There it is dumped and then dozed into 3.7 m (12 ft) lifts and leached with a cyanide solution without further pretreatment. The dump leach forms a closed solution cell because pregnant leachate passes through carbon columns on the bank of the leach pad and returns to service within the pad, which is lined to be an impermeable basin. Leachate application rate averages 0.001 liter per minute per m^2 (0.004 gallons per minute per ft^2) with an ideal concentration of 400 parts per million (ppm) sodium cyanide. Makeup water from the tail pond is used to compensate for evaporation, and dump leach solution can be returned to the tail pond in times of excessive precipitation within the dump leach.

GEOLOGY

Stratigraphy

The Mercur district is located within the southern Oquirrh Mountains, a fault block range near the eastern margin of the Basin-and-Range physiographic province. The southern end of the range consists of folded and faulted Paleozoic sedimentary rocks which were locally intruded during the Oligocene Epoch by igneous rocks of generally acidic composition (Kornze et al., 1985).

Mississippian sedimentary rocks of the Great Blue Formation have been exposed within the mine area. The Great Blue Formation, a 1097 m (3600 ft) thick unit, consists of three members: the Lower Great Blue, the Long Trail Shale, and the Upper Great Blue (Gilluly, 1932). Kornze et al. (1985) further subdivided the Lower Great Blue into a lower half and an upper half. The upper half is known as the Mercur Mine Series, and hosts the bulk of Mercur's gold mineralization.

The Mercur Mine Series has been divided into four mappable units (Fig. 3), which have been described in depth in previous papers (Gilluly, 1932; Tafuri, 1975; Tafuri, 1976; Klatt and Tafuri, 1976; Jewell, 1984; Kornze, et al., 1985; Faddies and Kornze, 1985; Tafuri, 1987). The Upper Beds, usually about 24 m (80 ft) thick are an ore host and consist of thick to thin-bedded fossiliferous limestones and siltstones. The Mercur Beds, generally 12 m (40 ft) thick, are the primary gold host. They consist of highly fossiliferous siltstones and silty thin-bedded limestones. The 18 m (60 ft) thick Barren Beds are typically barren of mineralization and consist of dense, thick-bedded limestones. Finally, the Magazine Sandstone Beds are 12 m (40 ft) thick and consist of fine-grained sand to coarse silt with a medial lime. The Magazine Sandstone is also a gold host.

Igneous Rocks

The Eagle Hill Rhyolite crops out in the southern part of the district. This intrusive is very irregular in form and is in part a sill and in part a dike (Tafuri, 1987). Contact effects with the host rock are slight, usually consisting of a meter or less of bleached and recrystallized limestone (Tafuri, 1987). Moore (1973) dated biotite in the rhyolite at 31.6 m.y.

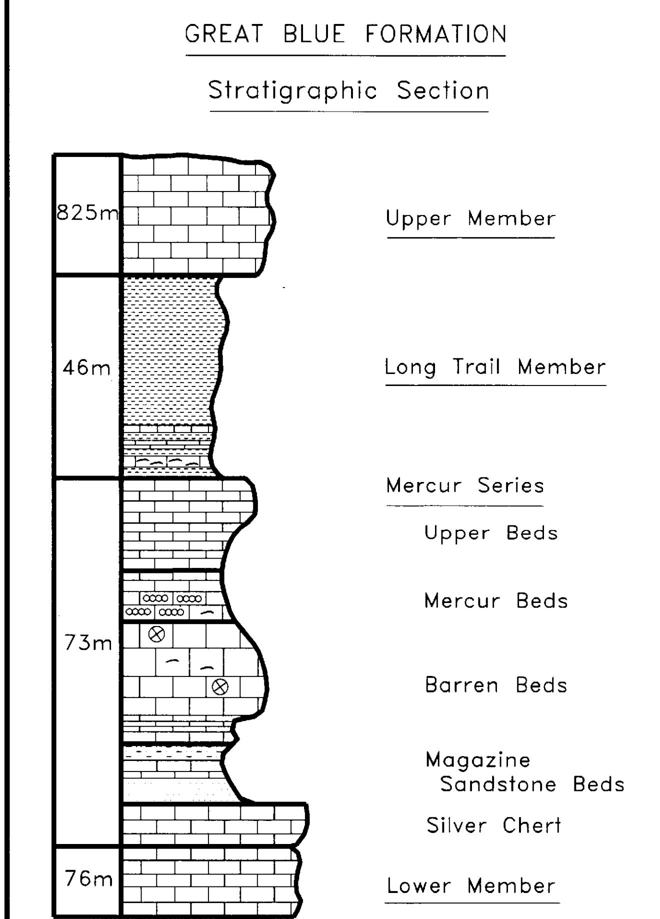

Figure 3

A quartz monzonite crops out about 3 km (2 miles) north of Mercur. The monzonite is predominately a sill with numerous small surficial outcrops. Here again, contact effects with surrounding limestones are slight, with bleaching and recrystallization limited to less than one meter (Tafuri, 1987). Biotite in the quartz monzonite has been dated at 36.7 m.y. (Moore and McKee, 1983).

Structure

The dominant structure at Mercur is the Ophir anticline. It is a broad, locally southeast-plunging fold formed during the first stage of the late Cretaceous Sevier orogeny, (Gilluly, 1932; Eardley, 1951; Roberts and Tooker, 1961; Tafuri, 1987). Mercur centers about 1.6 km (1 mile) east of the crest of the Ophir anticline. Beds at Mercur generally dip 10-30 degrees to the northeast.

Faults. At least three main periods of faulting have been recognized at Mercur (Faddies and Kornze, 1985; Kornze, et al., 1985). The first was contemporaneous with folding and consisted of normal faulting with some strike slip and bedding plane faulting along with overthrusting (Kornze, et al., 1985). Shrier (1989) places the first period faulting contemporaneous with the formation of the Charleston-Nebo thrust. The second period of faulting was the normal, Basin-and-Range block faulting that formed the range front fault along the western margin of the Oquirrh Mountains. Stratigraphic relations indicate this period was not earlier than Oligocene and not later than mid-Pliocene (Kornze et al., 1985). The third period of faulting was a myriad of normal faults which produced minor displacements in the Mercur area. This third period of faulting may, in part, have been contemporaneous with the Basin-and-Range faulting (Kornze, et al., 1985).

Breccia Pipes. Three major breccia pipes have been found in the Mercur district. They are located in the Sacramento Pit, the southern Mercur Pit, and between the Marion Hill and Golden Gate Pits near the old thickener tanks. Tafuri (1987) described the primary features of the three pipes. The Sacramento pipe contains abundant evidence for surging movement of the material in the pipe. This pipe is not mineralized, and may represent a phreatic event associated with the placement of the Eagle Hill rhyolite. The South Mercur Pit pipe appears to be a collapse structure. Brecciation surrounded a central solid core which dropped 60 m (200 ft) relative to surrounding rock. Both clasts and matrix were mineralized. The Marion Hill breccia pipe was also a collapse structure, dropping mineralized Mercur Series rocks into the core of the pipe.

Mineralization

Localization of ore bodies was controlled primarily by steeply dipping faults and fractures. Secondary control of gold mineralization was provided by silty, bioclastic, and thinly bedded lithology. Impermeable or nonreactive reactive limestones, such as the Barren Beds of the Mercur Series and the Lower Great Blue, were mineralized only where fracture intensity sufficiently increased permeability. The intersection of first and second period faults appears to be the primary center for deposition of ore-grade mineralization in the Mercur district.

Alteration

Mercur district alteration has been described by Tafuri (1987). According to Tafuri (1987), the district hosted four major stages of hydrothermal alteration. The earliest stage was silicification. Following silicification was a stage of argillic alteration. Vein and open space filling by carbonates and sulfides characterized the third stage. The final stage of hydrothermal alteration consisted of deposition of barite and halloysite.

Silicification. Silicification of selected horizons of the Lower Great Blue and Mercur Mine Series was the earliest and most widespread form of alteration at Mercur (Jewell, 1984). The most conspicuous horizon was the stratiform and strata-bound Silver Chert jasperoid (Tafuri, 1987) (Figure 3). This jasperoid generally replaced lower beds in the Magazine Sandstone and upper beds in the Lower Great Blue. This is not a perfectly strata-bound unit, because beds were inconsistently replaced by the jasperoid. The unit, however, is bound to the same general sequence of rocks throughout the district (Tafuri, 1987). Some minor silicification is also found in the upper Magazine Sandstone, Mercur Beds, and the lower portion of the Barren Beds (Jewell, 1984).

Ore grade mineralization occurs in the Silver Chert and silicified Magazine Sandstone. Silica encapsulation of the gold has not been noted (R. Klatt and W. Tafuri, written comm. to P. Jewell), suggesting that the main silica stage occurred prior to gold mineralization (Jewell, 1984). The silica stage is also older than the east-northeast and northwest period of faulting because the Silver Chert jasperoid is offset by those faults (Tafuri, 1987).

Argillization. The argillic stage involved decarbonation of limestone and modification of preexisting phyllosilicate minerals (Jewell, 1984). Intensity of alteration does not correlate with the grade of gold mineralization (Tafuri, 1987). Argillic alteration was particularly well developed in the Upper Beds, Mercur Beds, and the lower portion of the Barren Beds. This alteration appears to be preferentially developed in silty and shaly lithologies, but replacement of massive limestones has also been observed (Jewell, 1984).

Carbonate-Sulfide. The third stage involved deposition of calcite, realgar, orpiment, pyrite, marcasite, and organic material within veins and open spaces. The bulk of gold mineralization also appears to have taken place during this stage (Jewell, 1984). This stage is typically developed in the Mercur Beds. Lesser amounts are found in the Upper Beds, and more rarely in the Barren Beds and the median limestone of the Magazine Sandstone (Jewell, 1984). Formation of the veins did not alter the enclosing rock (Jewell, 1984).

Barite-Halloysite. Deposition of barite and halloysite within open spaces and veins in Silver Chert was the final hydrothermal alteration stage (Jewell, 1984).

Oxidation

Hydrothermal oxidation of sulfides affected most of the Magazine Sandstone Bed, as well as silty beds within the rest of the Mercur Mine Series. The Mercur Beds were particularly susceptible to this type of oxidation. Highly visible oxidation plumes are exposed along faults and fissures on mine highwalls. Plumes typically widen with depth, as would be expected of hydrothermal rather than supergene plumes (Tafuri, 1987).

This oxidation, where complete, destroyed the sulfide minerals and the organic matter. Calcite, where still present, was further removed, while clays were not altered nor remobilized (Tafuri, 1987).

SUMMARY

Mercur has had an interesting history dating back to the 1870s. The present operation extracts precious metals previous operations were unable to mine because of unprofitability or presidential order. Environmental concerns receive high priority, which will allow the land to again rest when Barrick has exhausted the present ore body...until the next company comes along with new extractive technology or increased gold prices. At that time, Mercur may come alive again with a fifth life, and the canyons may ring with the sounds of industry.

ACKNOWLEDGMENTS

The management of Barrick Mercur Gold Mine is thanked for allowing preparation of this paper.

REFERENCES CITED

Burger, J.R., 1983, Mercur, Getty's First Gold Mine: Engineering and Mining Journal, p. 48.

Dern, G.H., 1904, The Geology of Mercur: Mines and Minerals, p. 543.

Eardley, A.J., 1951, Structural Geology of North America: New York, Harper and Bros., p. 341.

Faddies, T.B. and Kornze, L.D., 1985, Economic Geology of the Mercur District, Utah: unpublished paper for Getty Mining Company, Mercur, Utah, p. 5-10.

Gilluly, J., 1932, Geology and Ore Deposits of the Stockton and Fairfield Quadrangles, Utah: U.S. Geological Survey Professional Paper 173, p. 29, 73.

Howard, L.O., 1913, History of Milling at the Geyser-Marion and the Sacramento-III: The Salt Lake Mining Review, Vol. 15, No. 9, Aug., p. 13.

JBR Consultants Group, 1989 Revision, "Notice of Intention to Commence Mining Operations and Mining and Reclamation Plan, Barrick Resources (USA), Inc., Mercur Mine, Mercur Hill, Marion Hill, Golden Gate and Sacramento Pits," Aug, Salt Lake City, Utah.

Jewell, P.W., 1984, Chemical and Thermal Evolution of Hydrothermal Fluids, Mercur Gold District, Tooele County, Utah: unpublished M.S. thesis, University of Utah, pp. 9-37.

Klatt, H.R. and Tafuri, W.J., 1976, Gold Mineralization in the Mercur Mining District, Utah: Northwest Mining Association, December 1976, Spokane, p. 6.

Kornze, L.D., et al., 1985, Geology and Geostatistics Applied to Grade Control at the Mercur Gold Mine, Mercur, Utah: Applied Mining Geology: Problems of Sampling and Grade Control, Metz, R.A., ed, AIME, New York, pp. 46-48.

Moore, W.J., 1973, "A Summary of Radiometric Ages of Igneous Rocks in the Oquirrh Mountains, North-Central Utah," Economic Geology, Vol. 65, pp. 99-100.

Moore, W.J. and McKee, E.H., 1983, Phanerozoic Magmatism and Mineralization in the Tooele 1°x2° Quadrangle, Utah: Geol. Soc. Am. Memoir 157, pp. 183-190.

Requa, L.K., 1967, "The Mercur Mining District, Tooele County, Utah," unpublished subject report.

Roberts, R.J. and Tooker, E.W., 1961, Structural Geology of the North End of the Oquirrh Mountains, Utah: in Utah Geological Society Guidebook to the Geology of Utah, No. 16, p. 46.

Shenon, P.J., 1963, "Economic Evaluation of the Consolidated Mercur Gold Mines Co.," unpublished subject report.

Shrier, T., 1989, "Geology of Mercur," unpublished presentation given to mineral investment tour, Mercur Mine.

Tafuri, W.J., 1975, The Lithology and Depositional Environment of the Lower Member of the Great Blue Limestone at Mercur, Utah: Carbonate Petrology, p. 7-10.

Tafuri, W.J., 1976, Geology and Geochemistry of the Gold Deposits at Mercur, Utah: Disseminated Gold Symposium, March 1976, Reno, p. 3-4.

Tafuri, W.J., 1987, Geology and Geochemistry of the Mercur Mining District, Tooele County, Utah: Ph.D. dissertation, University of Utah, p. 24-60.

STRUCTURAL CONTROLS ON GOLD DISTRIBUTION, MERCUR GOLD DEPOSIT, TOOELE COUNTY, UTAH

Caroline T. Kroko
Ronald H. Bruhn
Department of Geology and Geophysics
University of Utah
Salt Lake City, Utah

ABSTRACT

Mercur is a sediment-hosted disseminated gold deposit in the southern Oquirrh Mountains. Gold occurs in clastic and carbonate units of the Mississippian Lower Great Blue Limestone. The Mercur orebodies are part of a linear trend of gold occurrences on the eastern limb of the Ophir anticline, known as the "Mercur Trend" (Kornze, 1984).

The Ophir anticline is modelled as a fault-propagation fold (Suppe, 1985), with a broad gentle crest; a pronounced hingeline on the eastern (leading) limb; and a blind thrust in the core of the fold.

Within the preferred stratigraphy, gold mineralization at Mercur is strongly controlled by high-angle east-northeast and north-northwest-striking faults which occupy a broad linear trend parallel to the anticlinal axis, between the crest of the anticline and the eastern hingeline. The orientation of the ore-controlling faults, and their concentration around the hingeline, suggest that they formed under local extensional strain resulting from flexure of the eastern hingeline.

A structural model for the formation of the Mercur deposit is proposed in which gold-bearing fluids migrated upward along the blind thrust then spread laterally on the high-angle ore-controlling faults to form the deposit.

INTRODUCTION

The Barrick Mercur gold deposit is located on the western slope of the southern Oquirrh Mountains (Fig. 1). Mercur is a Carlin-type disseminated gold deposit hosted by clastic and carbonate sedimentary rocks of the Mississippian Great Blue Limestone. There are two main orebodies at Mercur, the Marion Hill-Golden Gate deposit on the north side of Mercur Canyon, and the Mercur-Sacramento deposit to the south. Both orebodies occur on the gently east-dipping limb of the Ophir anticline (Fig. 2).

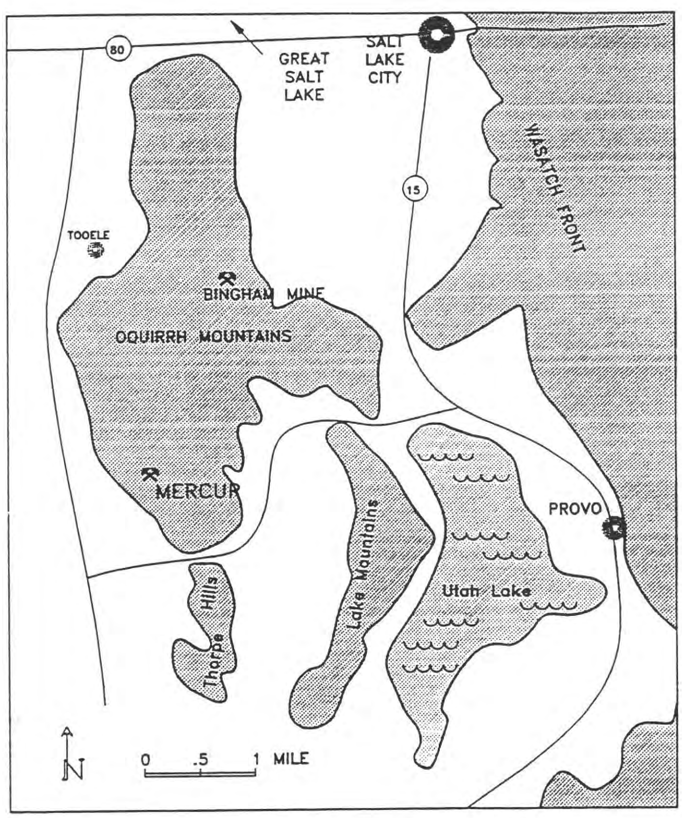

Figure 1. Map showing location of Mercur Mine in the southern Oquirrh Mountains approximately 50 miles southwest of Salt Lake City, Utah.

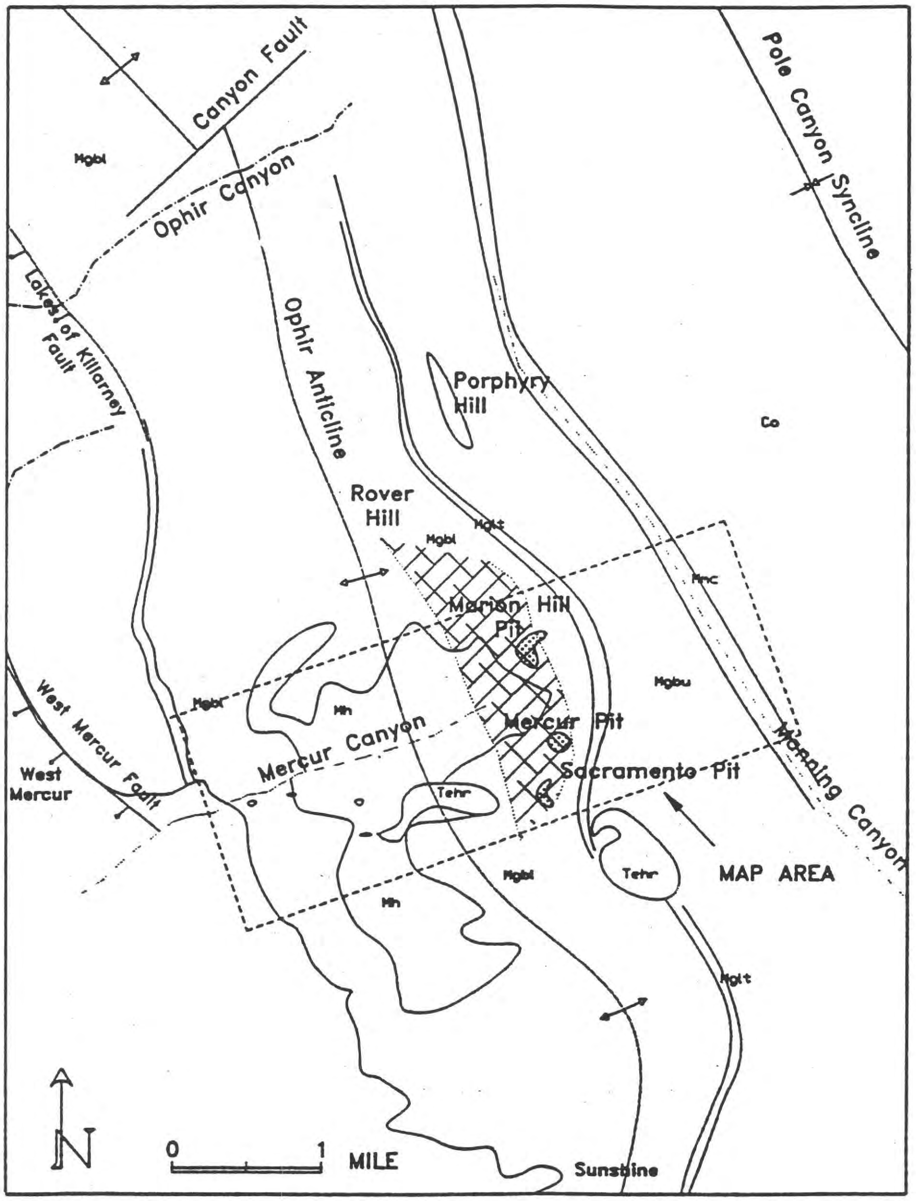

Figure 2. Geologic map of the southwestern Oquirrh Mountains showing the location of the Mercur Mines and the dominant structural features (after Gilluly, 1932). The dashed line encloses the area mapped in detail to produce cross-sections through the Mercur deposits. Map units are: Mississippian Deseret Limestone (Md); Mississippian Humbug Fm (Mh); Mississippian Great Blue Fm — Lower and Upper (Mgbl, Mgbu), separated by Long Trail Shale (Mlt); Mississippian Manning Canyon Shale (Mmc); Pennsylvanian Oquirrh Group (Poq).

The Mercur deposit is part of a north-northwest-striking linear trend of gold occurrences between Rover Hill and the Sunshine Area known as the "Mercur Trend" (Kornze, 1984) (Fig. 3). Coincident with the Mercur gold trend is an area of high-angle, east-northeast and north-northwest-striking faults. High-grade gold mineralization at Mercur is related spatially to these faults (Gilluly, 1932; Kornze et al., 1984; Kornze, 1984; Faddies and Kornze, 1985; Tafuri, 1987; Stanger, 1990).

PURPOSE

The purpose of this report is to establish a link between the structural features of the Mercur trend, and the Mercur gold deposit; and to propose a structural model for the migration of fluids which formed the Mercur deposit.

STRATIGRAPHY

The gold-bearing strata at Mercur were named the Mercur Mine Series by Kornze (1984) (Fig. 4). The Mercur Mine Series consists of approximately 240 feet of clastic and carbonate units capped by the distinctive black carbonaceous Long Trail Shale.

1. Silver Chert Jasperoid — extensively internally brecciated jasperoid which replaces the lowermost carbonate and clastic beds of the Mercur Mine Series
2. The Magazine Sandstone — dominantly clastic unit including medial interval of mudstone, packstone and shale (Jewell, 1985)
3. The Barren Limestone — dense micritic limestone named for the very small amounts of gold it contains
4. The Mercur Beds — mudstones and grainstones which were primary ore hosts in the Mercur orebody
5. The Upper Beds — interbedded wackestones and packstones which hosted some of the highest ore grades in the Mercur orebody

Detailed descriptions of the stratigraphy of the Mercur area and of the southern Oquirrh Mountains are given in Gilluly (1932), Tafuri (1975, 1987), and Tooker (1970, 1983, 1987).

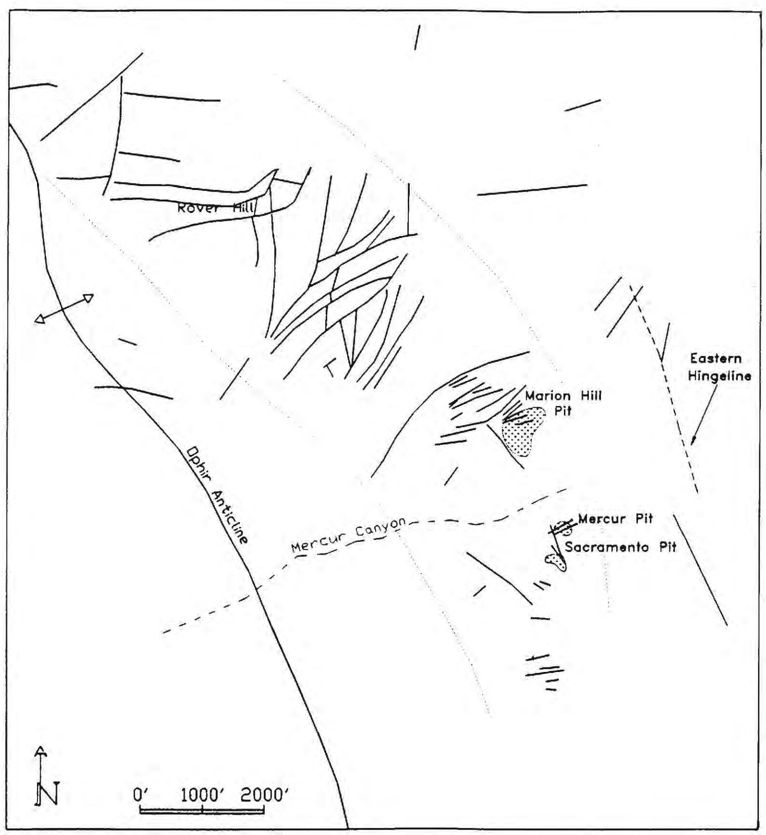

Figure 3. Structure map of the Mercur area showing location of eastern hingeline, crest of the Ophir anticline, and the high-angle normal and normal oblique faults which localize gold mineralization on the Mercur trend (after Tafuri, 1980; mine geologists, 1980 to present). Dotted lines bound area of high-angle ore-controlling faults of the Mercur trend.

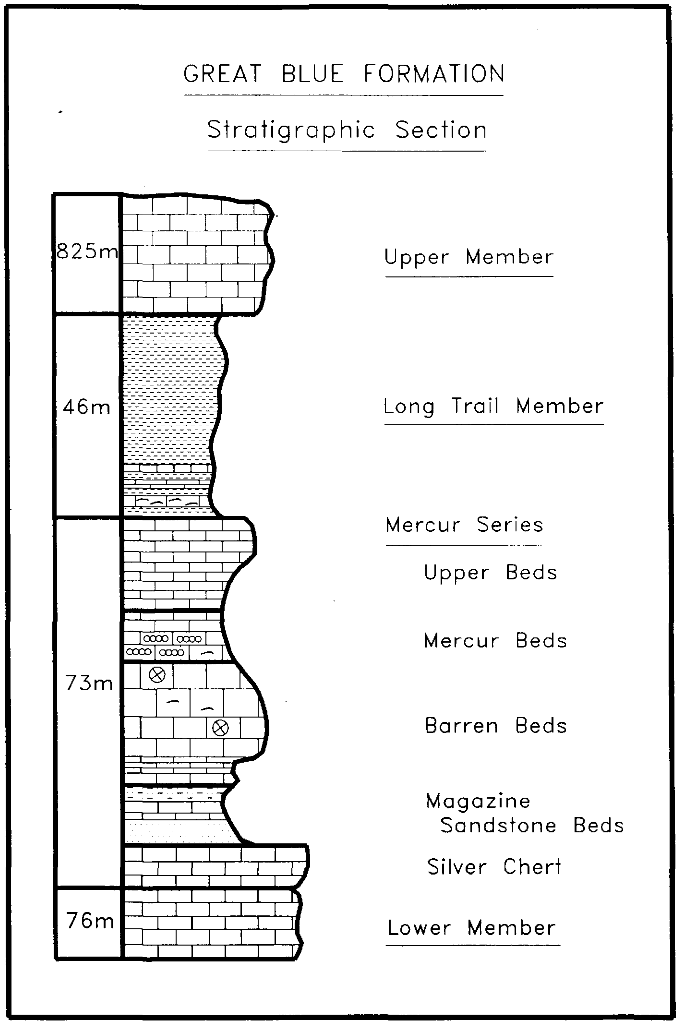

Figure 4. Stratigraphic column of Mercur Mine Series (Kornze, 1984).

THE MERCUR OREBODIES

There are three open-pit mines at Mercur. The Mercur Pit (abandoned), the Marion Hill Pit, and the Sacramento Pit youngest of the three (Fig. 3). Within the Mercur Mine Series, gold distribution is controlled primarily by high-angle faults and secondarily by lithology. The largest ore-controlling faults at Mercur are the east-west-striking Lulu graben and the north-south-striking Twist Fault Zone, which localize high gold grades in the Mercur Pit (Stanger, 1991); and the east-northeast-striking Carrie Steele Fault which hosts high grade gold ore in the Marion Hill Pit.

The analysis of over 200 rock samples collected from the Mercur area, and statistical analysis of over 50,000 blasthole assays (Kroko, 1992) demonstrate the following characteristics of gold grade distribution in the Mercur deposits.

The highest gold grades occur in fault gouge and breccia zones and immediately adjacent to high-angle east-northeast and north-northwest-striking normal and oblique faults which cut the deposit (Fig. 5 and 6).

Gold grade decreases with distance from these faults at a rate which is dependent on lithology. The role of lithology is summarized in Table 1, where the highest overall gold grades occur in clay zones and faults. The second highest range occurs in clastic rocks, sandstones and siltstones, such as those which characterize the Magazine Sandstone. The lowest gold values are in unfractured limestone and dominantly carbonate rocks such as those which dominate the Barren Limestone, the Mercur Beds and the Upper Beds.

STRUCTURE

The Ophir Anticline

The dominant structural feature of the Mercur area is the Ophir anticline. It is one of three major northwest-striking folds in the southern Oquirrh mountains (Fig. 2), from west to east, the Ophir anticline, the Pole Canyon syncline, and the Long Ridge anticline.

The folds ride on the upper plate of at least one regional-scale thrust sheet formed during the Late Cretaceous Sevier orogeny (Gilluly, 1983; Roberts and Tooker, 1961; Tafuri 1987) or during an earlier Jurassic compressional event (Wilson and Parry, 1990; Presnell and Parry, 1991).

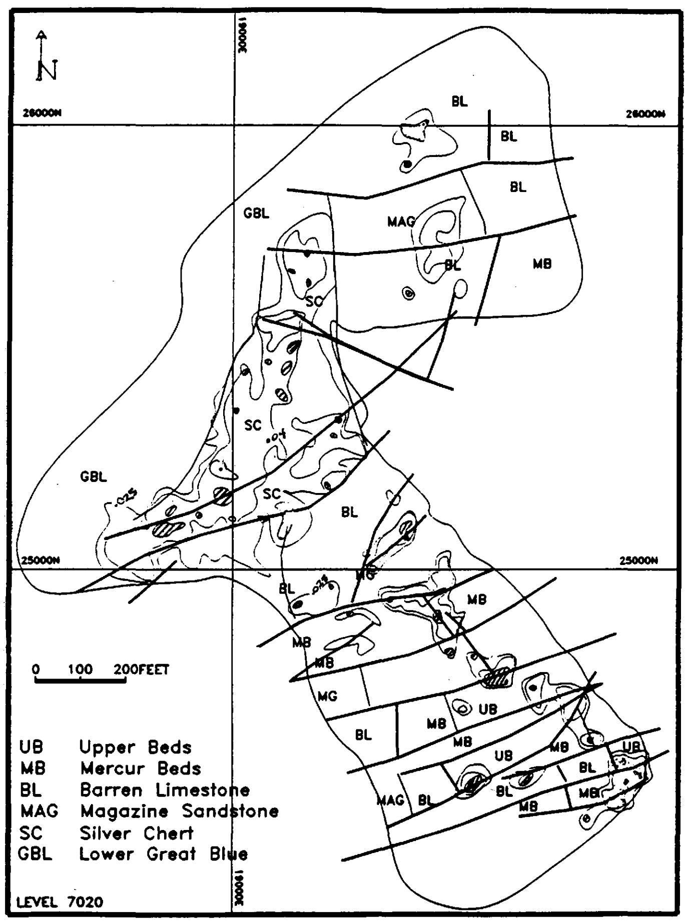

Figure 5. Level plan of gold grade contours, geology, and known faults in the Marion Hill Pit. Contour lines enclose gold grades in ounces per ton: .025 (outermost contour); .04; .1 (inner contour, hachured area). High gold grades in the Silver Chert are disseminated throughout the unit, independent of faults; highest grades in Mercur and Upper Beds occur on faults and dissemination into unfractured rock is slight.

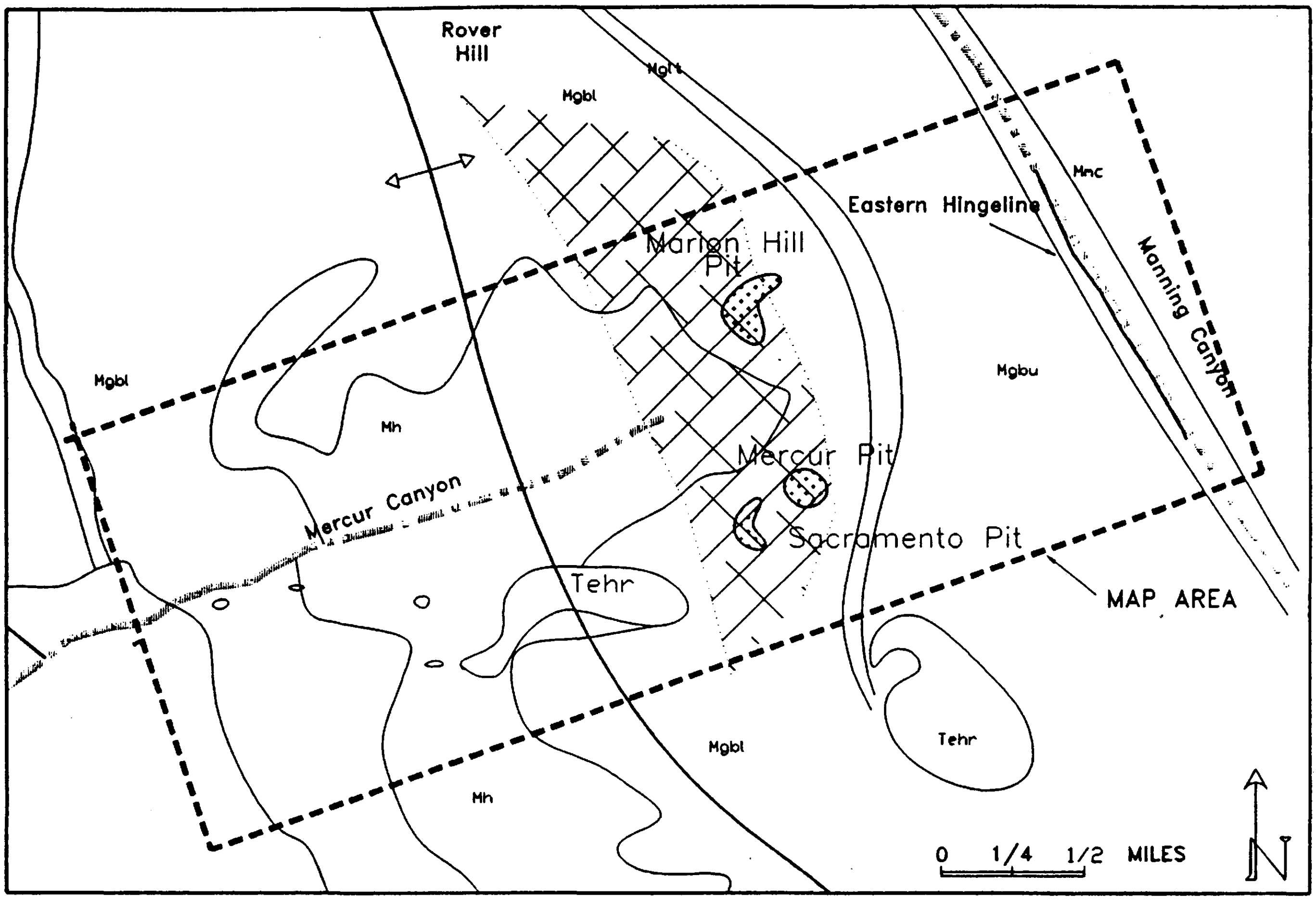

Figure 6. Geologic setting of the present-day Mercur Mines: Marion Hill Pit, Mercur Pit, Sacramento Pit. Map units: Mississippian Deseret Limestone (Md); Mississippian Humbug Fm (Mh); Mississippian Great Blue Fm — Lower and Upper (Mgbl, Mgbu), separated by Long Trail Shale (Mlt); Mississippian Manning Canyon Shale (Mmc); Tertiary volcanic Eagle Hill Rhyolite (Tehr).

Table 1. Gold grade distribution by lithology represented by maximum, minimum and average grades (in ounces per ton) for three sample populations. The highest overall grades occur in gouge and fault zones, and represent the fault-controlled portion of the grade distribution. The highest grades among unfractured rocks are in dominantly clastic units, and the lowest overall gold grades occur in carbonate rocks.

Lithology	Maximum	Minimum	Average
All Samples	0.044	0.00	0.008
Gouge/Faults	0.044	0.00	0.014
Silt/Sandstone	0.026	0.00	0.01
Limestone	0.024	0.00	0.005

Note: all values in ounces/ton.

In cross section, the Ophir anticline is a box-like fold, with a broad gently dipping crest, and a steepened eastern limb, here called the eastern hingeline (Fig. 7a). All of the gold deposits of the Mercur trend lie on the gently dipping portion of the east limb, between the crest of the anticline and the eastern hingeline.

The high-angle faults which localize high-grade gold at Mercur occur in the same region, just west of the eastern hingeline (Fig. 3). A structural analysis of the Ophir anticline shows that the ore-controlling faults may have formed due to local strain perturbations related to the flexure of the hingeline (Kroko, 1992).

In balanced cross section, the geometry of the Ophir anticline is best modelled as a fault-propagation fold (Suppe, 1985; Woodward and Boyer, 1985) (Fig. 7b). The most important feature of this model — as it pertains to structural controls on the Mercur deposit — is the presence of a blind thrust, which cuts up-section from the basal thrust detachment and into the core of the anticline.

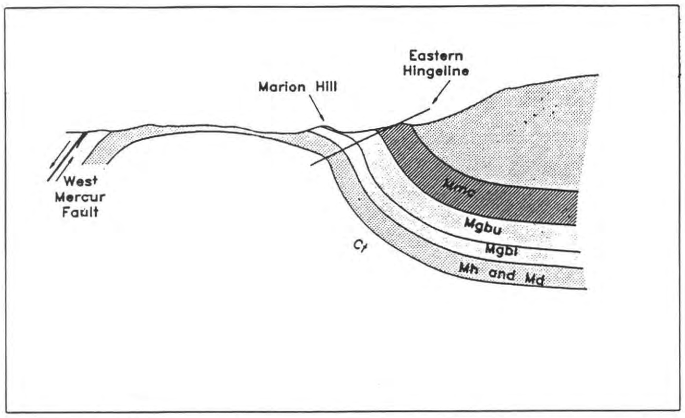

Figure 7a. Diagrammatic cross section, perpendicular to the axis of the Ophir anticline, through the Marion Hill deposit. The eastern hingeline passes beneath the Marion Hill deposit and is exposed in Manning Canyon.

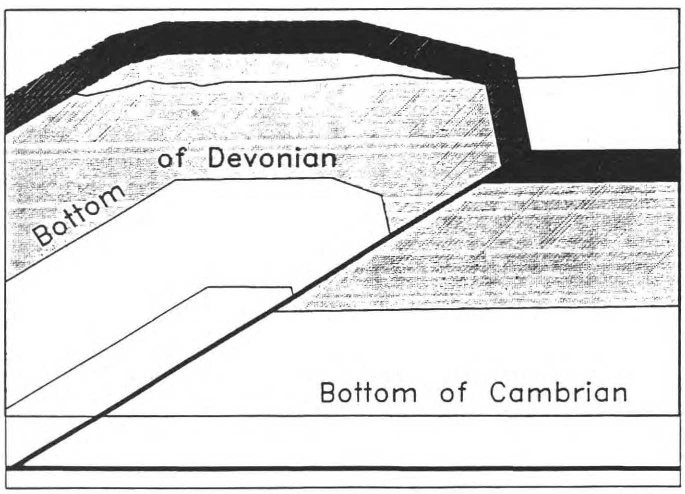

Figure 7b. Analogous portion of a balanced cross section through the Ophir anticline, showing the geometric features of a fault propagation fold: a blind thrust in the core of the anticline and steepened leading limb.

Local Strain Perturbations

Analysis of joints and veins, after the methods of Engelder and Geiser (1980), show two local strain orientations which could account for the formation of the ore-controlling faults (Kroko, 1992). From the crest of the anticline through the eastern hingeline, joint and vein orientations indicate a local axial parallel extension direction overprinting the regional east-west compression. In the area of the eastern hingeline, joint and vein orientations show a second extension direction perpendicular to the axis of the hingeline (Kroko, 1992).

Analogous local strain perturbations have been identified on other anticlines and associated with characteristic fault and fracture orientations which form under these conditions (Stearns and Friedman, 1972; Dunne, 1986; Coleman-Sadd, 1978).

The two sets of fractures proposed by Stearns and Friedman (1972) (Fig. 8) have orientations similar to the major ore-controlling faults at Mercur. Under axial parallel extension (Fig. 8a), fractures form at high angles or perpendicular to the axis of the fold, similar to the Lulu graben, the Carrie Steele Fault, and the numerous high-angle east-northeast-striking faults which localize high-grade gold ore at Marion Hill.

When the local extension direction parallels the fold axis (Fig. 8b), local fractures occur parallel or nearly parallel to the axis of the fold, corresponding to the Twist Fault, and the numerous north-northwest-striking ore-controlling faults at Marion Hill.

It is proposed that these local strain perturbations, which resulted from flexure, are concentrated in areas of the tightest folding. At Mercur, the tightest portion of the anticline occurs at the area of the eastern hingeline, where the high-angle ore-controlling faults are localized.

LOCALIZATION OF GOLD ON THE OPHIR ANTICLINE

The blind thrust in the core of the Ophir anticline and the concentration of high-angle faults around the eastern hingeline are the fundamental structural features which allowed the localization of gold on the Mercur trend.

This model suggests that the intersection of closely spaced faults around the eastern hingeline provided fracture-induced permeability adjacent to the eastern hingeline, along the Mercur gold trend. The blind thrust and its splays in the core of the anticline were the primary conduits for upward migration of gold-bearing fluids from depth.

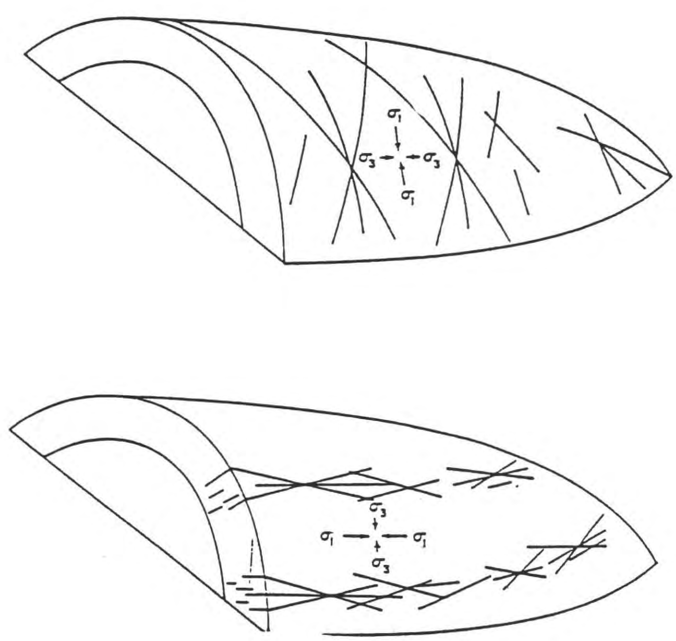

Figure 8. Two strain orientations on a fold, and the resulting fracture orientations (after Stearns and Friedman, 1972). The direction of extension is in the direction of least principle stress, sigma$_3$). A. Extension parallel to fold axis produces fractures at high angles and perpendicular to the axis. B. Extension perpendicular to the fold axis produces fractures at low angles and parallel to the axis.

Figure 9 is a representation of how gold-bearing fluids may have flowed upward from source rocks at depth, along the blind thrust and its branches, then spread out through the network of connecting faults and fractures to form the Mercur deposits.

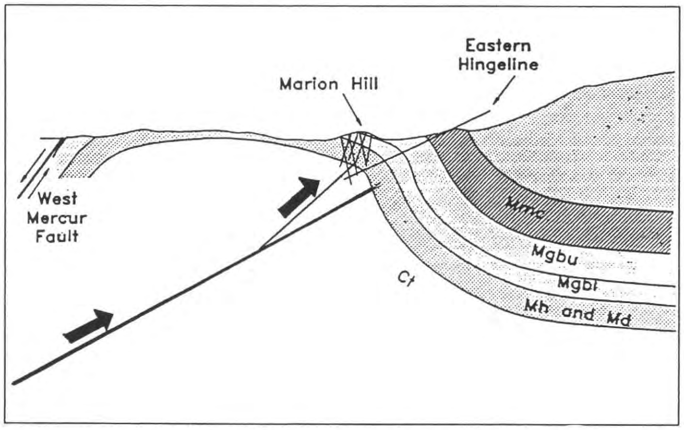

Figure 9. Structural model for migration of gold-bearing fluids up the main blind thrust and its splays to the interconnecting tensional faults at the eastern hingeline. Arrows indicate direction of fluid flow.

SUMMARY

The Mercur deposit is an ideal setting to analyze the structural controls on gold distribution within the deposit as well as the regional structural setting of the deposit.

Detailed sampling in the pits and statistical analysis of blasthole assays (Kroko, 1992) show that high-grade gold is localized on high-angle, north-northwest and east-northeast-striking normal and oblique faults. The degree to which gold is disseminated outward from the ore-controlling faults is a function of lithology, with the overall highest grades occurring in clay zones or clayey layers, the second highest grades in dominantly clastic units, and the lowest overall grades in unfractured limestones (Kroko, 1992).

Cross sections perpendicular to the axis of the Ophir anticline define the box shape of the fold. The orientation of the ore-controlling faults, their proximity to the eastern hingeline, and the analysis of joint and vein orientations across the anticline suggest that the ore-controlling faults formed under local extensional strain, both parallel and perpendicular to the axis (Stearns and Friedman, 1972), which was concentrated in the area of the eastern hingeline.

Finally, a balanced cross section requires the presence of a blind thrust in the core of the anticline (Suppe, 1985; Woodward and Boyer, 1985), which provides a conduit for the upward migration of gold-bearing fluids. It is proposed that gold-bearing fluids flowed upward on the blind thrust and its splays, and then spread outward on the ore-controlling faults and through permeable strata to form the Mercur gold deposit.

ACKNOWLEDGMENTS

This study could not have been accomplished without the assistance and cooperation of staff and management at the Barrick Mercur Gold Mine, especially Tracy Shrier, Rick Simms, Larry Stanger, Bob St. Louis, and Steve Kerr. Reviews and discussions with W.T. Parry and R. Presnell were particularly helpful.

BIBLIOGRAPHY

Coleman-Sadd, S. P., 1978, Fold Development in Zagros Simply Folded Belt, Southwest Iran: American Association of Petroleum Geologists Bulletin, v. 62, no. 6, p. 984-1003.

Dunne, William M., 1986, Mesostructural Development in Detached Folds: An Example from West Virginia: Journal of Geology, v. 94, p. 473-488.

Engelder, Terry and Geiser, Peter, 1980, On the use of Regional Joint Sets as Trajectories of Paleostress Fields During the Development of the Appalachian Plateau: New York, Journal of Geophysical Research, v. 85, no. B11, p. 6319-6341.

Faddies, T. and Kornze, L., 1985, Economic Geology of the Mercur District, Utah: Getty Mining Company, Mercur, Utah, Unpublished, 24 p.

Faill, Rodger R., 1973, Kink-band Folding, Valley and Ridge Province, Pennsylvania: Geological Society of America Bulletin, v. 84, p. 1289-1314.

Gilluly, James, 1932, Geology and Ore Deposits of the Stockton and Fairfield Quadrangles, Utah: U.S. Geological Survey Professional Paper 173, 176 p.

Hintze, Lehi F., 1988, Geologic History of Utah: Brigham Young University Geology Studies, Special Publication 7, Bart J. Kowallis Ed., 202 p.

Jewell, Paul William, 1984, Chemical and Thermal Evolution of Hydrothermal Fluids, Mercur Gold District, Tooele County, Utah: Unpublished Masters Thesis, University of Utah, 77 p.

Klatt, Richard H., Summary Technical Report of Exploration and Metallurgical Investigations in the Mercur Mining District During the Period May, 1973-December, 1979: Getty Oil Company, Unpublished.

Kornze, L. D., Faddies, T. B., Goodwin, J. C., Bryant, M. A., 1984, Geology and Geostatistics Applied to Grade Control at the Mercur Gold Mine, Mercur, Utah: AIME Preprint 84442.

Kornze, L. D., 1984, Geology of the Mercur Gold Mine: *in* Geology of Northwest Utah, Southern Idaho and Northeast Nevada, UGA Publication 13.

Kroko, Caroline T., 1992, Structural Controls on Gold Distribution of the Mercur Gold Deposit, Mercur, Utah: Unpublished Masters Thesis, University of Utah, Salt Lake City, 150 p.

Lenzi, G. W., 1973, Geochemical Reconnaissance at Mercur Utah: Utah Geological and Mineralogical Survey, Special Studies 43, p. 1-16.

Presnell, Ricardo D., and Parry, W. T., 1991, The Barneys Canyon gold deposit and its relationship to Jurassic tectonism: Geol. Soc. of Amer. Abstr. with programs v. 23, no. 5, p. A193.

Roberts R. J. and Tooker E. W., 1961, Structural Geology of the North End of the Oquirrh Mountains, Utah, in Utah Geol. Soc. Guidebook to the Geology of Utah, no. 16, p. 46.

Stanger, Larry H., 1990, Geology and Mineralization of the Lulu Graben, Barrick Mercur gold Mine, Tooele, Utah, *in* Hansen, D. M., ed., Gold '90, Salt Lake City Proceedings: AIME, p. 11-20.

Stearns, David W., and Friedman, Melvin, 1972, Reservoirs in Fractured Rock: American Association of Petroleum Geologists Memoir 16, Stratigraphic Oil and Gas Fields, p. 82-106.

Suppe, J., 1985, Principles of Structural Geology: Prentice Hall Inc., Engelwood Cliffs, New Jersey, p. 309-369.

Tafuri, William J., 1975, The Lithology and Depositional Environment of the Lower Member of the Great Blue Formation at Mercur, Utah: Carbonate Petrology, March 1974, p. 7-10.

Tafuri, William Joseph, 1987, Geology and Geochemistry of the Mercur Mining District, Tooele County, Utah: Unpublished Doctoral Dissertation, University of Utah.

Tooker, Edwin W., and Roberts, R. J., 1970, Upper Paleozoic Rocks in the Oquirrh Mountains and Bingham Mining District, Utah: U.S. Geological Survey Prof. Paper 629A, 76 p.

Tooker, Edwin W., 1983, Variations in structural style and correlation of thrust plates in the Sevier foreland thrust belt, Great Salt Lake area, Utah, *in* Miller and others, eds., Tectonic and Stratigraphic studies in the eastern Great Basin: Geological Society of America, Memoir 157, p. 61-74.

Tooker, Edwin W., 1987, Preliminary Geologic Maps, Cross-Sections, and Explanation Pamphlet for the Ophir and Mercur 7 ½ Minute quadrangles, Utah: U.S. Geological Survey Open-File Report 87-152.

Woodward, Nicholas B., and Boyer, Steven E., 1985, An Outline of Balanced Cross-sections, Notes for a Short Course, Short Course on Balanced Sections, Southeast Section Meeting: Geological Society of America, Knoxville, Tennessee, March 20, 1985, 118 p.

MESOZOIC HYDROTHERMAL ALTERATION IN THE MERCUR DISTRICT AND SURROUNDING AREAS: POSSIBLE RELATIONSHIPS TO ARGILLIC ALTERATION WITHIN THE MERCUR GOLD DEPOSITS

By
Paula N. Wilson and W. T. Parry
Dept. of Geology and Geophysics
University of Utah
Salt Lake City, Utah 84112

ABSTRACT

K/Ar ages and chemical data show that a Mesozoic, gold-bearing, hydrothermal system altered black shales of the Mississippian Great Blue Limestone throughout an area of the southern Oquirrh Mountains, Utah, that includes the Mercur gold district. K/Ar ages of ammonium-illite veins and illite-rich, clay-size separates from the altered shales indicate hydrothermal activity occurred in the time range 193 to 122 Ma. Several ages from within the Mercur district cluster near 160 Ma. Mesozoic igneous rocks do not occur in the area, but these ages are coeval with thrust faulting recognized to the north and west, and with 160 Ma intrusive activity in eastern Nevada.

Preliminary analysis of work in progress on argillic alteration within the gold deposits at Mercur has revealed similarities in alteration mineralogy, replacement textures, and types of interstratified clay species between altered Long Trail Shale and argillically altered carbonate rocks hosting the gold deposits. These common characteristics suggest that the Long Trail Shale alteration may be related to argillic alteration within the Mercur gold deposits.

INTRODUCTION

The Mercur gold district contains several Carlin-type precious-metal deposits which are hosted by the Mississippian Great Blue Limestone and are characterized by replacement of carbonate and silty carbonate rocks by silica, phyllosilicates, pyrite, barite, various As, Hg, Sb, and Tl minerals, and by introduction of micron-size gold (Bagby and Berger, 1985; Tafuri, 1987; Jewell and Parry, 1987; 1988; Wilson and Wilson, 1991). Gold mineralization extends from the Five Mile Pass area north to Ophir Canyon (Fig. 1). The geology of the Mercur district and the southern Oquirrh Mountains is described by Gilluly (1932).

The stratigraphy of interest for the southern part of the range, including the Mercur district, is shown in Figure 2. Most gold mineralization in the Mercur mine occurs in the lower member of the Great Blue Limestone, directly below the Long Trail Shale, although subeconomic gold was found in the Long Trail Shale within the Mercur pit. In the Sunshine Canyon and West Dip areas gold mineralization also occurs within the Long Trail Shale (Wilson and Parry, 1990b) as well as in the overlying limestones (Gilluly, 1932).

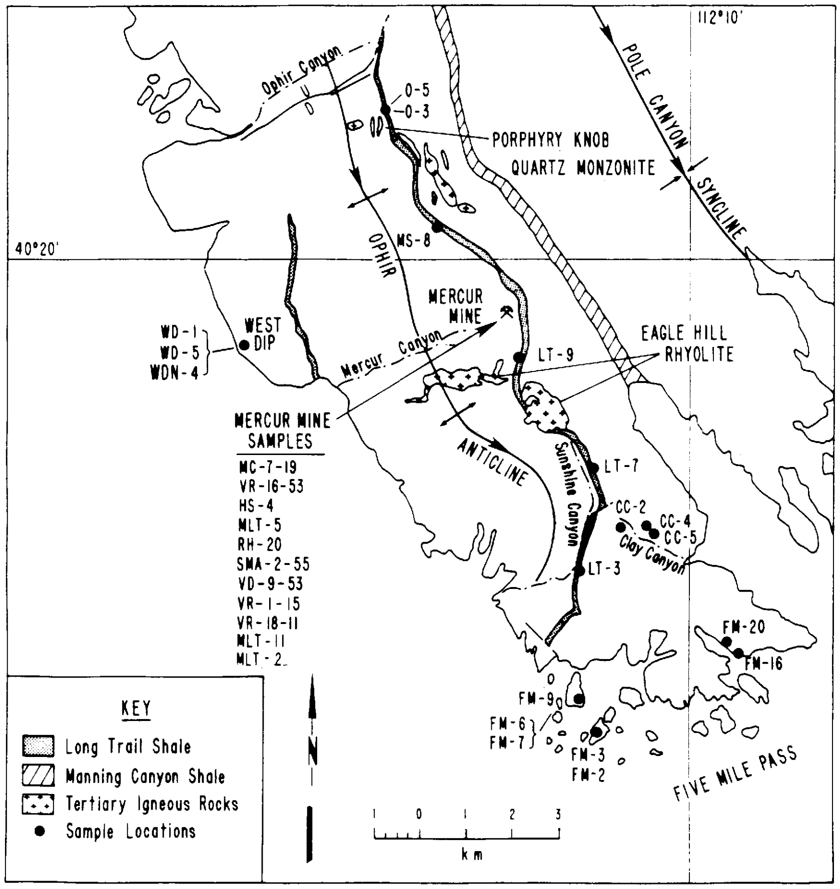

Figure 1. Sample locations and general geology of the southern Oquirrh Mountains. Geology adapted from Gilluly (1932).

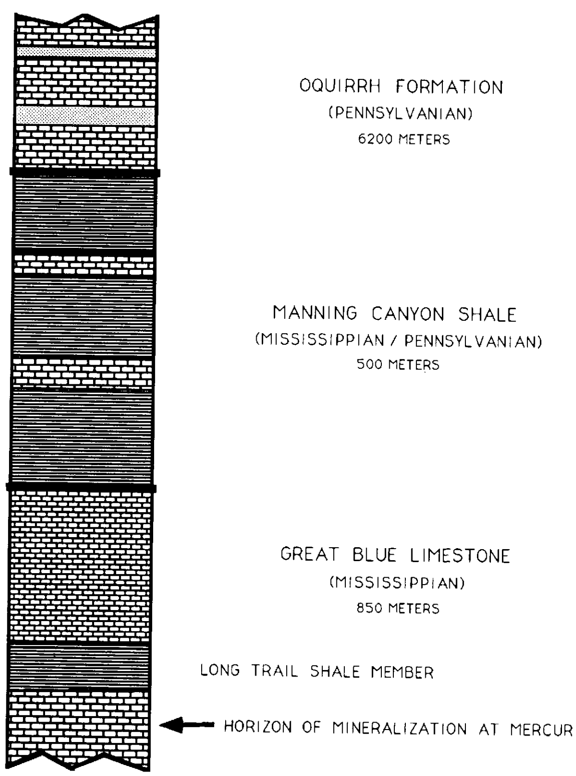

Figure 2. Schematic stratigraphic section of part of the southern Oquirrh Mountain stratigraphy.

In the area south and east of Sunshine Canyon correlation of shales in the Great Blue Limestone is uncertain. Structural complexity and pervasive hydrothermal alteration prevent positive correlation of shale in this area with the Long Trail Shale Member.

Sample locations are shown in Figure 1. Long Trail Shale samples from the Mercur mine were collected from the Mercur pit or were obtained from drill cuttings or core. Other samples were collected from clay pits, road cuts, outcrops, and mine dumps. More detailed accounts of experimental methods and data interpretation applied to the Long Trail Shale can be found in Wilson and Parry (1990a and b).

Most mineralogical analysis was done by X-ray diffraction. Oriented smears of veins, whole rock, and either <4 or <2 μm size fractions of each shale sample were analyzed. Much of the mineralogical discussion in this paper centers on interstratified illite/smectite (I/S). This term refers to a series of phyllosilicate minerals which consist of various combinations of illite-like layers (I) and smectite layers (S) which are stacked parallel to the c-axis. When the smectite layers are numerous ($>50\%$) and the stacking sequence is in random order the material is called R0. When the smectite content is 20-50% and the stacking sequence has statistical ordering, based on repetition of units consisting of IS, the material is called R1 or I/S. When the smectite content is

< 20%, the illitic material is highly ordered, based on repetition of units consisting of ISII, and is referred to as R3 or ISII type. Illite layers may have K^+, NH_4^+, or Na^+ as the interlayer cation. Further explanation of illites and interstratified illite/smectite is available in Srodon and Eberl (1984). Percent smectite and type of interstratification in both the whole rocks and the veins were modeled using the computer program NEWMOD (Reynolds, 1985).

The age of hydrothermal activity in the Mercur district has not been previously determined. A Tertiary age coeval with the 32 Ma age of the Eagle Hill rhyolite or the 37 Ma age of the Porphyry Knob quartz monzonite (Moore and McKee, 1983) has been proposed. However, the small size of these igneous bodies with respect to the 11 km strike length of mineralized sediments (Fig. 1), the lack of significant alteration or mineralization within them, the lack of alteration or mineralization zoning around them, and the failure of any Tertiary hydrothermal system to reset the K/Ar systematics of a Mesozoic-age hydrothermal phyllosilicate vein found within 30 meters of the Eagle Hill rhyolite contact (Wilson and Parry, 1990a) argue against associating Mercur mineralization with this igneous activity.

This paper presents a summary of mineralogical and chemical data from hydrothermally altered shales and hydrothermal veins which provides evidence for a hydrothermal system of regional extent in an area encompassing the Mercur district that appears to have transported gold. In addition, new data pertaining to argillic alteration of carbonates hosting gold mineralization at Mercur are also presented. Although conclusive proof as to the age of the Mercur gold deposits has yet to be obtained, this paper summarizes data which support a Mesozoic, rather than a Tertiary age for these deposits.

HYDROTHERMAL ALTERATION OF THE LONG TRAIL SHALE

The physical and mineralogical aspects of shale hydrothermal alteration are: (1) oxidation and mobilization of organic material, (2) formation of heavy metal-rich ammonium-illite veins, (3) recrystallization of detrital minerals to ordered interstratifications of illite/smectite, ammonium-illite, illite, chlorite, kaolinite, Fe-oxides, and quartz, and (4) "pod" formation, resulting from replacement of fossils by ammonium-illite, chlorite, paragonite, kaolinite, Fe-oxides, and quartz. A description of the dated samples is presented in Table 1.

Veins were only observed in oxidized and recrystallized shale. Veins usually consist of Fe-oxide cores and coarse-grained ammonium-illite or tobelite ± quartz borders. The ammonium illite or tobelite contain 2-3 % interstratified smectite (Wilson and Parry, in prep; Table 1). Maximum vein width is 0.75 cm. Vein length varies from a few centimeters to several meters. The shorter veins usually occur in sets which extend discontinuously over several meters and appear to fill tension gashes. Veins are found throughout the study area, including the gold deposits at Mercur.

The term "pod" describes a hydrothermal texture resulting from replacement of fossils by phyllosilicates, Fe-oxides, and quartz. Pods are elliptical, usually consist of a Fe-oxide core rimmed by coarse-grained ammonium-illite or tobelite and/or chlorite ± quartz and kaolinite, and range up to 2.5 cm long by 5 mm wide (Table 1). In most pods containing both chlorite and illite, illite replaces chlorite. Pods are also found throughout the study area, occasionally with veins.

The presence of ammonium-illite and tobelite in the veins has been documented by microprobe analysis and infrared absorption spectroscopy. Tobelite and ammonium illite are ammonium-rich analogues of illite which contain both NH_4^+ and K^+ in solid solution within the interlayer site. Tobelite is characterized by having $N > K$, $Si \geq 3$, interlayer charge less than one, and a (001) spacing near 10.25 å (Higashi, 1982). A similar phyllosilicate, but with lower NH_4^+ content ($K > N$) and a smaller (001) spacing (about 10.1) has been referred to as ammonium illite (e.g., Stern et al., 1982). The ammonium-bearing phyllosilicates range from 0.19 to 1.88 wt. % N, and 3.16 to 6.19 wt. % K (Wilson et al., in prep). Both vein and pod illites have a similar range in N content. Modeling of the chemical and the XRD data using NEW-MOD (Reynolds, 1985) shows that the ammonium illite and tobelite are interstratified with 2-3 % smectite (Wilson et al., in prep). The presence of ammonium-bearing mica and feldspar in sediment-hosted gold deposits has been documented by Krohn et al. (1988).

Chemical effects of shale alteration include (1) depletion of alkali and alkaline earth metals and associated enrichment in Al, N, and H, (2) a hydrothermal suite in the shales consisting of Al_2O_3, H_2O^+, Sc, Th, Ta, Hf, and Zr, (3) the presence of the gold-pathfinder elements Tl, As, and Hg in all veins and several shale samples, (4) concentration of heavy metals, gold-pathfinder elements, and Sc in ammonium-illite-bearing veins, and (5) presence of trace amounts of gold (Wilson and Parry, 1990b).

Vein samples have high concentrations of the gold-pathfinder elements Hg, As, Tl, Se, and Sc contents as great as 820 ppb, 180 ppm, 29 ppm, 1300 ppm, and 80 ppm, respectively (Table 2). The shales are also enriched in heavy metals and gold-pathfinder elements. Anomalously high Sc concentrations occur throughout the study area.

Gold is present in two shale samples from the Mercur Mine. Samples MC-7-19 and VR-16-53 contain .004 and .001 oz/ton gold, respectively (Barrick assay data). The Long Trail Shale in both of these drill holes is weakly mineralized over several of the intervals assayed. Gold is also present in both the shale and veins of sample LT-3 from Sunshine Canyon and in shales from West Dip (WD-1, WD-5, and WDN-4), but was not detected at other Long Trail Shale localities (Table 2).

ARGILLIC ALTERATION WITHIN GOLD DEPOSITS AT MERCUR

Preliminary results of our study of the argillic alteration in the gold deposits at Mercur are presented here. The data are

Table 1. Description of samples.

Sample	Description
LT-3	Oxidized red shale consisting of illite + kaolinite + chlorite + quartz + Fe-oxides with veins and pods of ammonium-illite (R3, 2% smecitite) + kaolinite + chlorite + quartz + Fe-oxides. Vertical veins strike east-west, maximum 0.25 cm wide. Fe-oxides and ammonium-illite also replace fossils.
FM-2	White, highly oxidized shale with well developed undulating cleavage and greasy feel. Abundant white tobelitic veins; some up to 2–3 mm wide and continuous for one to two meters and oriented parallel to cleavage. Also more abundant tobelitic veinlets 2.5 cm or less in length and discontinuous. Some connected to small pods < 5 mm in diameter of same mineralogy. Veinlets are up to 40% of rock in places. Vein mineralogy is tobelite/smectite (R3, 3% S), and minor I/S (R1, 45% S), kaolinite, and quartz.
FM-3	Oxidized, highly altered, light gray, coarse-grained shale crosscut by discontinuous veins up to 0.25 cm wide of tobelite/smectite (R3, 3%) + kaolinite + Fe-oxides + minor I/S (45% S). Shale is composed of R3 illitic material (up to 100 µm), kaolinite, and angular quartz.
FM-6	Similar to FM-2 with abundant larger tobelitic veins up to 3 mm wide and higher abundance of tobelitic veinlets (40%). More abundant fossil replacement and replaced plant fossils are identifiable. Some Fe-oxide staining. Veins consist of tobelite/smectite (R3, 3% S), very minor kaolinite, and I/S (R1, 45% S).
FM-7	Similar to FM-2. Contains both types of tobelitic veins, but abundance of veinlets is 20%. Vein mineralogy is tobelite/smectite (R3, 3% smectite), and minor kaolinite, quartz, and I/S (R1, 45% S).
FM-9	Light gray, partially oxidized shale consisting of tobelite/smectite (R3, 3% S) + kaolinite + quartz. Replacement of fossils by tobelitic material.
O-2/O-3	Light gray, oxidized, and silicified shale with veins up to 0.5 cm wide of ammonium illite (R3, 2% S) + Fe-oxides + fibrous quartz. Fe-oxide replacement of pyrite in shale is surrounded by illite and fibrous quartz. Shale and pod mineralogy identical to veins.
CC-2	Pinkish-gray, oxidized and partially recrystallized shale. Veins up to 0.75 cm wide of ammonium illite (R2, 2% S) + kaolinite + quartz + chlorite have attitude of N80°E, 80°S. Veins have oxidation and recrystallization selvages. Mineralogy of <4 µm size fraction of shale is R3 illitic material (7% smectite) + quartz + possible feldspar.
MLT-2	Black, organic-rich shale with discontinuous quartz-rich lenses parallel to bedding and up to 1 mm wide. White veins of ammonium illite + chlorite + kaolinite + quartz up to 5 mm wide, 2 to 5 cm long, and discontinous. Shale mineralogy consists of I/S (R1, 32% S) + I/S (R3, 10% S) + kaolinite + chlorite + quartz.
MLT-11	Vein of ammonium illite (R3, 2% S) + pyrite (unoxidized) + kaolinite + chlorite + expandable unknown + gypsum in organic-rich shale. Vein 2 cm wide. Sample obtained within 30 m of contact with Eagle Hill rhyolite.
WD-5	Black, organic-rich, coarse-grained, noncalcareous shale with moderately developed cleavage. Ammonium illite (R3, 2% S), chlorite, kaolinite, and minor quartz replace large brachiopod shells and occasional veins of same mineralogy extend a few mm from replaced fossils. Shale mineralogy is ammonium illite + kaolinite + quartz.

Table 2. Shale heavy metal and minor element geochemistry

SAMPLE	Ag	As	Au (PBB)	Co	Cu	Hf	Hg (PBB)	Mo	Ni	Sb	Sc	Se	Ta	Th	Tl	Zn	Zr
LT-3	<0.5	38	6	2.5	40.0	3.7	22	11	55	3.4	17.0	18	0.9	13.0	<10.0	75	120
LT-3 VEIN	N. S.	180	35	110.0	N. S.	0.9	820	190	N. S.	2.7	80.0	1300	<0.5	2.0	<2.0	N. S.	<10
LT-7	<0.5	40	<5	2.0	6.5	9.0	18	<2	7	0.7	20.4	<2	1.8	17.0	<10.0	11	320
LT-9	<0.5	4	<5	2.0	8.0	5.7	<5	<2	12	5.3	21.5	<2	1.4	15.0	<10.0	22	200
FM-3 VEIN	<0.5	7	<5	2.2	6.5	4.3	60	<2	8	1.5	60.1	<2	1.0	4.6	29.0	42	380
FM-9	<0.5	2	<5	1.2	4.0	2.9	13	<2	6	1.1	15.6	<2	0.7	10.0	<10.0	11	70
FM-16	<0.5	310	<5	29.0	31.0	3.4	23	10	170	2.2	22.7	<2	0.9	10.0	5.0	310	150
FM-20	<0.5	98	<5	11.0	42.0	2.2	44	53	220	6.5	20.2	<2	0.6	7.6	<2.0	330	80
O-3	<0.5	64	<5	1.8	12.0	4.8	80	<2	6	65.0	11.6	<2	0.9	10.0	1.8	10	150
O-5	<0.5	7	<5	11.0	14.0	5.6	<5	<2	62	0.4	23.5	<3	1.5	16.0	10.0	83	170
MS-8	<0.5	3	<5	5.2	26.0	3.4	<5	3	51	0.5	18.4	<2	0.9	11.0	<2.0	74	120
CC-2	<0.5	24	<5	2.3	26.0	4.5	100	4	50	3.2	13.2	<2	1.0	11.0	7.0	93	120
CC-2 VEIN	1.0	120	<5	39.0	490.0	<0.3	480	57	530	1.4	78.4	180	<0.5	1.0	7.0	1900	<10
CC-4	<0.5	19	<5	1.9	9.5	3.4	10	2	35	1.9	11.6	<2	0.8	8.6	<2.0	110	110
CC-5	<0.5	10	<5	4.3	11.0	1.5	81	3	42	0.5	8.0	2	<0.5	4.8	<2.0	61	10
HS-4	<0.5	24	<5	11.0	8.5	5.4	10	2	50	0.6	22.9	5	1.3	14.0	7.0	99	150
MC-7-19	<0.5	53	<5	19.0	13.0	4.3	34	<2	63	0.7	22.4	<2	1.4	14.0	<2.0	120	110
MC-7-20	<0.5	56	<5	22.0	13.0	5.9	170	<2	70	0.8	21.4	<2	1.1	14.0	8.0	97	200
MLT-5	<0.5	12	<5	6.6	10.0	3.5	<5	<2	70	0.3	22.7	<2	0.7	9.5	<2.0	96	130
RH-20	<0.5	12	<5	17.0	21.0	7.1	5	<2	78	0.7	21.8	<2	1.4	15.0	7.0	130	250
SMA-2-55	<0.5	40	<5	13.0	20.0	2.6	70	8	100	2.6	10.9	13	<0.5	6.3	<2.0	370	60
VD-9-53	<0.5	32	<5	18.0	11.0	2.2	62	2	67	2.0	14.8	<2	<0.5	8.5	<2.0	120	30
VR-1-15	<0.5	52	<5	15.0	17.0	4.9	5	2	58	0.7	19.5	<2	0.9	13.0	<2.0	96	170
VR-16-53	<0.5	520	<5	10.0	4.0	2.9	230	<2	43	3.1	17.1	<2	0.7	9.3	8.0	56	120
VR-18-11	<0.5	46	<5	22.0	15.0	4.4	21	<2	60	1.6	20.8	<2	1.0	13.0	6.0	90	120
WD-1	<0.5	1500	130	6.4	14.0	2.3	1000	17	59	7.0	15.3	11	<0.5	6.8	4.0	100	60
WD-5	<0.5	240	130	2.1	12.0	3.9	890	10	47	3.9	15.2	5	0.7	10.0	11.0	37	130
WDN-4	<0.5	150	59	5.5	25.0	1.5	97	24	130	3.7	3.9	11	0.5	4.6	3.0	120	<10

* ALL ANALYSES IN PPM UNLESS OTHERWISE INDICATED. N.D. = NOT DETERMINED. N. S. = INSUFFICIENT SAMPLE

incomplete and the interpretations are tentative pending further data acquisition.

Previous studies of the argillic hydrothermal alteration at Mercur indicate that the mineralogy consists of illite + kaolinite + quartz (Jewell and Parry, 1987; Tafuri, 1987). Our studies of argillic alteration in the upper beds of the lower limestone member of the Great Blue from samples obtained from high-grade ore bodies on the Carrie Steele fault (Marion Hill) and Herschel Fault zone (Sacramento Hill) have also documented this same hydrothermal suite. In a sample suite collected across the Carrie Steele fault, argillic alteration has removed virtually all the limestone and the rock is 95-100% clay minerals and quartz. The degree of argillic mineralization is intense and in most instances the limestone is totally replaced by clay minerals. The resulting rock is fairly dense and only rarely is the more punky and porous texture typical of decalcified limestone present. X-ray diffraction data indicate that the illite is an R3 interstratification with small amounts of smectite ($<10\%$). The typical mineralogy of the $<2\mu m$ size fraction is R3 interstratified illite/smectite ($<10\%$ smectite) and kaolinite. Quartz is a minor component and is often not present.

The argillic alteration also has resulted in phyllosilicate vein formation and fossil replacement identical to that seen in altered Long Trail Shale. In the Carrie Steele fault samples, the veins are generally a few millimeters wide and extend only a few centimeters. Fossil replacement appears to be complete, but the original fossil is often identifiable in contrast to the "pods" that commonly result from fossil replacement in the Long Trail Shale. Illitic material in the veins is also a R3 illite/smectite (2-7% smectite) and generally contains less smectite than the whole rock illites, however the difference is not great. Veins from the Herschel Fault zone (Sacramento Pit) are more extensive, on the order of meters, and are up to 0.5 cm wide. Fossil replacement by clay minerals has not been observed here. The (001) spacings suggest some of the illite from both areas is ammonium-bearing, but confirmation of the presence of nitrogen awaits microprobe analyses. Pyrite or Fe-oxides as replacement of pyrite occur in veins.

Estimates of relative abundances of illite and kaolinite in whole rock were made based on the method described by Moore and Reynolds (1989, p. 297). XRD mineralogical analyses have been completed for the $<2\ \mu$ size fraction of Carrie Steele fault samples and indicate that within about 50 meters of the two strands of the Carrie Steele fault the clay mineralogy averages 90% illite and 10% kaolinite. Beyond about 50 meters, the illite/kaolinite ratio is approximately equal. Veins found throughout the Carrie Steele and Herschel fault suites also consist of illite + kaolinite and generally contain about 50% illite.

Comparison of hydrothermally altered Long Trail Shale from throughout the southern Oquirrhs and hydrothermally altered limestones from the Mercur deposits shows that the Long Trail Shale generally has a more diverse alteration mineralogy that includes chlorite, interstratifications of illite with widely varying amounts of smectite (3-4% smectite), occasional carbonates, and abundant quartz. However, Long Trail Shale from areas enriched in heavy metals and/or near gold mineralization (West Dip, south Sunshine Canyon, Ophir Canyon area, Five Mile Pass, and Clay Canyon) consist of the same mineralogy as the altered carbonates in the gold deposits: R3 illite/smectite (3-10% smectite) and kaolinite plus or minus quartz and Fe-oxides. Veins from these areas are also heavy metal rich and have this same mineralogy, although the illites contain nitrogen in the form of ammonium.

The variation in degree of alteration in rock suites rich in illitic material can be represented on a Watanabe diagram. This type of diagram was explained and applied by Ioune and Utada (1983) and modified by Srodon and Eberl (1984) to show that mineral zoning about a Kuroko deposit was defined, in part, by the amount of smectite involved in the interstratified illite/smectite clay species. Zoning about this deposit progressed from randomly ordered illite/smectite (R0) with large amounts of smectite, to ordered interstratifications of illite/smectite consisting of R1 type, to R3 type as the ore deposit was approached. The change from R0 to R1 and then R3 type reflects continuously decreasing amounts of smectite and correspondingly increasing illite content as the deposit is approached. This zoning of smectite content in illite/smectite is usually interpreted as a result of increasing temperature; however, many important variables involved in changing fluid chemistry could also result in the same trend on this type of diagram and care must be taken when applying an interpretation. In either case, the amount of illite within the illite/smectite is controlled by alteration associated with mineralization and is an indication of alteration intensity.

Figure 3 is a Watanabe plot of diffraction data of illitic material from the Long Trail Shale and altered limestones from the gold deposits. Unmineralized, heavy metal-poor Long Trail Shale has R1 type illite/smectite with about 30% smectite. However, the heavy metal-rich and sometimes gold-bearing Long Trail Shale is characterized by a R3 illite/smectite (3-10% smectite) and by veins containing R3 illite/smectite (2-3 % smectite). We interpret the concentration of heavy metals and the presence of veins as evidence for greater alteration intensity, thus there appears to be a trend of increasing illite content in the interstratified clays as shale alteration increases. Argillically altered limestones of the gold deposits also appear to contain this same trend, progressing from R1 illite/smectite with 23% smectite to R3 illite/smectite with 3-10% smectite as intensity of alteration increases (Fig. 3). However, none of the argillic alteration from within the gold deposits contains the high smectite illite/smectite (25-45% smectite) observed in the less altered Long Trail Shale. Our analyses to date suggest that the most illite-rich interstratified clays sampled within the pits occur nearest to, or within, the gold-bearing rocks; however, more geochemical data are needed to further evaluate this. These altered limestones also contain veins of R3 illite/smectite (2-3% smectite) + kaolinite ± quartz, similar to veins found in the most intensely altered Long Trail Shale.

A suite of samples collected from the Sacramento pit and extending from the Eagle Hill rhyolite contact into adjacent

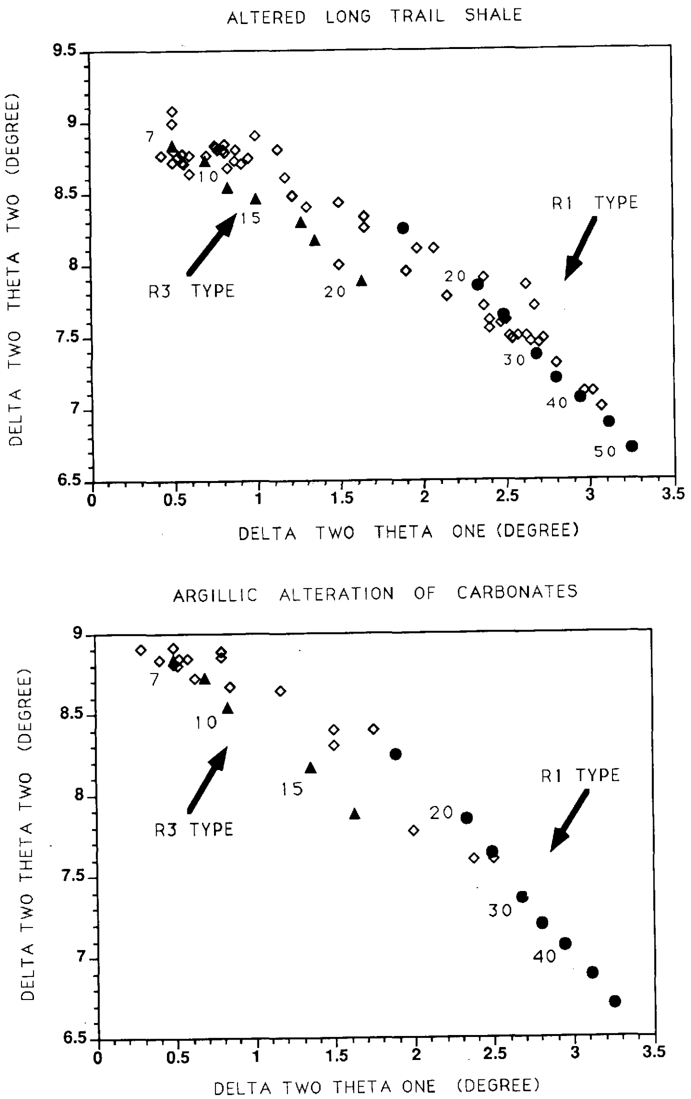

Figure 3. Watanabe diagrams for A) Long Trail Shale from throughout the southern Oquirrh Mountains and B) argillically altered carbonate rocks hosting gold deposits at the MercurMine. Theoretical R1 type interstratified illite/smectite are indicated by solid dots andtheoretical R3 type are indicated by solid triangles. Open diamonds are samples. Numbersby the symbols represent percent smectite within the interstratifications. Delta two theta onerefers to the distance between the 001 and 002 peaks; delta two theta two refers to the distance between 002 and 003 peaks, both measured in degrees two theta. Further explanation of this type of diagram are available in Srodon and Eberl (1984).

argillically altered limestone shows a trend of increasing illite in the interstratified illite/smectite with increasing distance from the rhyolite. The change is from R1 illite/smectite (23% smectite) near the contact to R3 illite/smectite (5-10% smectite) at about 30 meters from the contact. More data is needed before this trend can be interpreted, but the R1 type illite/smectite found closest to the contact is not consistent with the R3 type illite/smectite found in the ore bodies.

As a result of our initial work, we are tentatively proposing that the hydrothermal alteration of the Long Trail Shale is related to the argillic alteration of the host carbonates of the Mercur gold deposits. This is based on (1) the illite + kaolinite ± quartz and Fe-oxides alteration mineralogy common to both highly altered Long Trail Shale and argillically altered carbonate rocks hosting gold, (2) heavy metal signature similarities between these same rock types, and (3) the apparent progressive trend observed in the Long Trail Shale of increasing illite content within the interstratified illite/smectite clays with increasing alteration intensity which culminates in an R3 illite/smectite with <10% smectite similar to the R3 type illite/smectite found in the argillic alteration of the gold deposits (Fig. 3). A new K/Ar dating study is being initiated in order to determine if the age of argillic alteration of the carbonates hosting the gold deposits is similar in age to the alteration of the Long Trail Shale and work is in progress to test if the type of illite/smectite clay is a guide to ore at Mercur.

K/Ar Ages

No unambiguous field geological evidence for the age of gold mineralization in the Mercur district is available. The best alternative is K/Ar dating of hydrothermal phyllosilicates associated with argillic alteration. Determination of concordant K/Ar ages of clay minerals is a well-established method for dating alteration and ore-forming events. However, careful interpretation is required and fine-grained phyllosilicates are susceptible to Ar loss, requiring ages be interpreted as minimum ages (Hunziker et al., 1986; Halliday and Mitchell, 1984; Bethke et al., 1976).

K/Ar ages for vein illites and clay-size, illite-rich separates of Long Trail Shale are presented in Figure 4. Vein illite ages range from 122 to 189 Ma and average 163 Ma. Ages of clay-size separates from whole rock shale range from 124 to 193 Ma and average 161 Ma. All size separates consisted of the <2 μm size fraction except for CC-2 and MC-7-19 which were the <4 and <10 μm size fractions, respectively. The mineralogy of the dated samples is given in Table 1. The <4 μm size fraction of sample CC-2 shale is the only sample in which possible feldspar was detected by XRD analysis.

The range in ages obtained from the vein and the clay-size separates is identical. The average age of both sets of sample ages are also essentially identical at 163 and 161 Ma, respectively. We have interpreted the differences in the K/Ar ages as real and not the result of argon diffusion or other problems (Wilson and Parry, 1990a). The interpretation of the age range as real is based on the overlap of ages obtained from the whole rock shale separates with vein ages, and on the consistency of ages obtained from several samples in and near the Mercur Mine at about 160 Ma. The agreement between the 159 Ma age obtained from the <10 μm size fraction of a mineralized shale (MC-7-19), the average 164 Ma age of the <2 μm size fractions of MS-8, LT-9, and mineralized VR-16-53, and the vein ages of 156 Ma and 147 Ma (O-3 and MLT-11, respectively) is crucial because it indicates (1) that shale temperatures in at least some parts of the Mercur Mine were sufficiently high to reset the <10 μm size fraction, (2) that regional temperatures were high

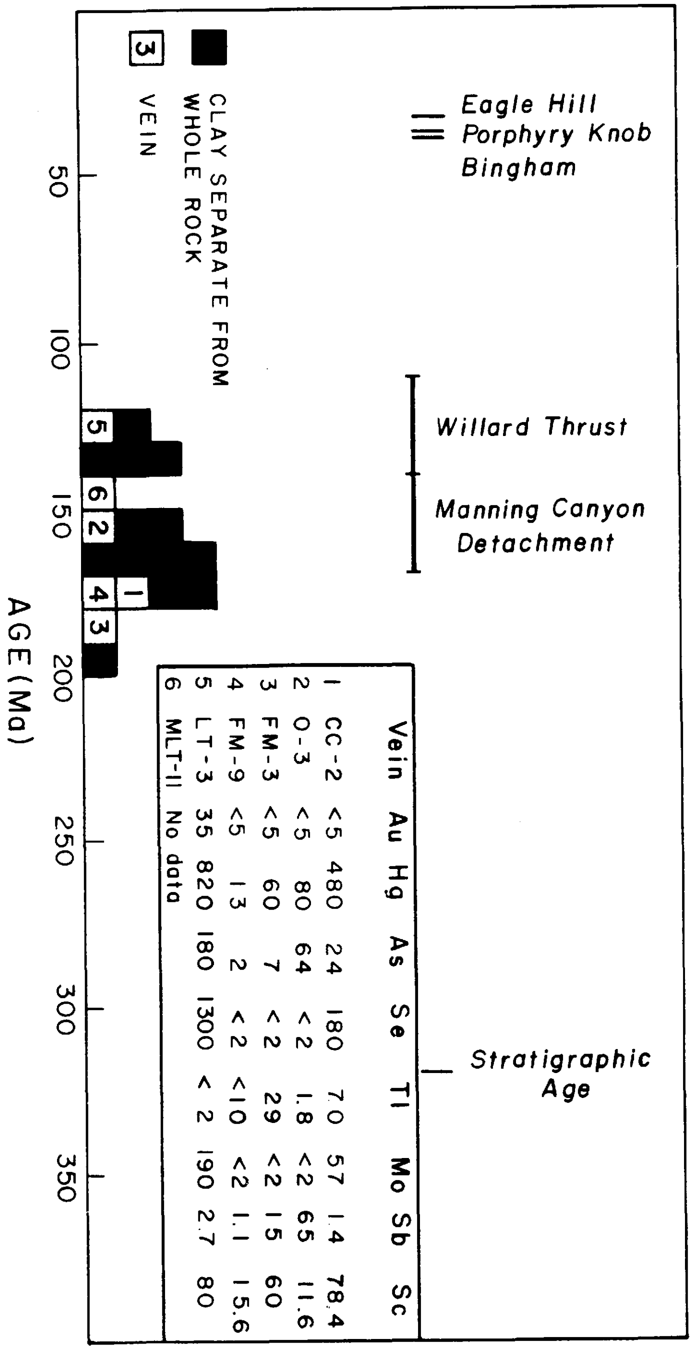

Figure 4. K/Ar ages of clay-size separates of shales (shaded) and veins (numbered) from the southern Oquirrh Mountains. Stratigraphic age of the Long Trail Shale, ages of igneous activity in the Oquirrh Mountains, and Mesozoic thrusting in northern Utah (Allmendinger and Jordan, 1981, 1984; Allmendinger et al., 1984; Heller et al., 1986) are shown for comparison. Trace element content of veins is keyed by number to vein ages. Au and Hg concentrations are in ppb, all others in ppm.

enough to reset at least the $<2\mu$m size fraction, (3) that this age is related to gold mineralization and to gold-pathfinder elements, (4) that this age is related to heavy metal-rich vein formation, and (5) hydrothermal affects related to the Eagle Hill rhyolite were not sufficient to reset the age of MLT-11 vein which was collected within 30 meters of the rhyolite contact.

Gold mineralization has been related to hydrothermal illite (argillic facies) in the Mercur deposits, (Tafuri, 1987; Jewell and Parry, 1987, 1988; Kornze, 1987) and argillic alteration has been related to gold mineralization in other Carlin-type deposits (Bagby and Berger, 1985; Percival et al., 1988). In addition, it is reasonable to assume that the hydrothermal illite in the Mercur mine originated during the time of illite vein formation elsewhere in the southern Oquirrh Mountains. The association of the dated hydrothermal illites with gold and heavy metals in the veins and shales and the concordant ages of different vein assemblages over a wide region, indicate that the K/Ar ages date the minimum age of a gold mineralization event in the Mercur district.

CONCLUSIONS

K/Ar ages and chemical data show that a Mesozoic hydrothermal system altered shales of the Great Blue Limestone and caused mass transport of heavy metals including Au, Sc, As, Hg, and Tl. The hydrothermal system is also characterized by (1) existence over a regional scale, (2) removal of alkali and alkaline earth metals, organic matter, sulfides, carbonates, and concentration of Al, H, and probably N in the shales, and (3) veins of ammonium-illite which are enriched in heavy metals, including Au.

The results of our studies have shown that hydrothermal activity in the southern Oquirrh Mountains is much older than previously supposed, occurring over the approximate time range of 193 to 122 Ma. Several ages of oxidized, recrystallized, and mineralized or gold-pathfinder rich samples from the Mercur Mine and immediate areas have consistent ages near 160 Ma. These ages indicate that a significant gold-bearing hydrothermal system occurred in the district at this time. Whether this hydrothermal system was responsible for the ore-grade gold mineralization at Mercur has not yet been determined. Work is currently underway on the ore deposits themselves in order to answer this question, but initial results indicate that the alteration of the Long Trail Shale and the argillic alteration of the carbonates hosting the gold deposits have many similarities and may be the result of the same hydrothermal system.

The mechanism responsible for this Mesozoic hydrothermal system appears to be unrelated to local igneous activity because there are no igneous rocks older than 40 Ma in the Oquirrh range and the closest Mesozoic igneous rocks are 80 Km to the northeast, in the Wasatch Range (72.4 Ma; James and McKee, 1985). Furthermore, ages of altered shales and vein sampled adjacent to igneous rocks (MLT-11, LT-9, and O-3) are similar to ages of altered shales with no spatial association with igneous rocks. This indicates the thermal effects of Tertiary igneous activity on the shales is minor and that any associated hydrothermal activity was extremely localized.

One possible mechanism for generating and moving hydrothermal fluids might call upon thrust faulting in the manner postulated by Oliver (1986). Ages obtained in this study are shown in comparison to other tectonic, stratigraphic, igneous, and hydrothermal events in the Oquirrh Mountains in Figure 4. All the ages from this study are most closely correlative to Mesozoic thrusting on the Manning Canyon detachment documented in northern Utah and southern Idaho by Allmendinger and Jordan (1981, 1984) and Allmendinger et al. (1984). Dated samples of intensely deformed, thrust faulted, and hydrothermally altered Manning Canyon shale in the adjacent Traverse and Lake Mountains indicate that this deformation and hydrothermal alteration are the same age as the hydrothermal system in the southern Oquirrh Mountains (Wilson and Parry, 1989). The Manning Canyon shale ages may date movement and associated hydrothermal alteration on the Manning Canyon detachment in north-central Utah.

An alternative mechanism for generating the Mercur deposits calls upon hydrothermal activity generated during Mesozoic igneous intrusive activity in eastern Nevada and subsequent rafting of this terrane containing sediment-hosted gold deposits into central Utah during late Cretaceous thrust fault movement. Dating of several intrusives and regional high-grade metamorphism in the Schell Creek and Snake ranges has resulted in a 160 Ma age for both (Miller et al., 1988).

ACKNOWLEDGMENTS

We gratefully acknowledge the Utah Geological Survey, the University of Utah Mineral Leasings Fund, and Barrick-Mercur Gold Mines for funding this study. We also thank Tracy Shrier, Larry Stanger, and Barrick for providing access to Barrick property at Mercur and to drilling samples and logs. Prochnau Mining and Dick Klatt of Gold Standard also provided access to properties. W.P. Nash generously gave of his time to assist in the acquiring microprobe data. Dr. Frank Brown and Dr. Paul Jewell reviewed parts of this manuscript.

REFERENCES CITED

Allmendinger, R.W., and Jordan, T.E., 1981, Mesozoic evolution, hinterland of the Sevier orogenic belt: Geology, v. 9, p. 308-313.

Allmendinger, R.W., and Jordan, T.E., 1984, Mesozoic structure of the Newfoundland Mountains, Utah: horizontal shortening and subsequent extension in the hinterland of the Sevier belt: Geological Society of America Bulletin, v. 95, p. 1280-1292.

Allmendinger, R.W., Miller, D.M., and Jordan, T.E., 1984, Known and inferred Mesozoic deformation in the hinterland of the Sevier Belt, Northwest Utah, *in* Kerns, G.J., and Kerns, R.L. Jr., eds., Geology of northwest Utah, southern Idaho and northeast Nevada: Utah Geological Association Publication 13, p. 21-34.

Bagby, W.C., and Berger, B.R., 1985, Geologic characteristics of sediment-hosted, disseminated precious metal deposits in the western United States, *in* Berger, B.R. and Bethke, P.M., eds., Geology and geochemistry of epithermal systems: Society of Economic Geologists Reviews in Economic Geology, v. 2, p. 169-202.

Bethke, P.M., Barton, P.B., Jr., Lanphere, M.A., and Steven, T.A., 1976, Environment of ore deposition in the Creede Mining District, San Juan Mountains, Colorado: II. Age of mineralization: Economic Geology, v. 71, p. 1006-1011.

Gilluly, J., 1932, Geology and ore deposits of the Stockton and Fairfield Quadrangles, Utah: U. S. Geological Survey Professional Paper 173, 171 p.

Halliday, A.N., Mitchell, J.G., 1984, K-Ar Ages of clay-size concentrates from the mineralization of the Pedroches Batholith, Spain, and evidence for Mesozoic hydrothermal activity associated with the break up of Pangaea: Earth and Planetary Science Letters, v. 68, p. 229-239.

Heller, P.L., Bowdler, S.S., Chambers, H.P., Coogan, J.C., Hagen, E.S., Shuster, M.W., and Winslow, N.S.S., 1986, Time of initial thrusting in the Sevier orogenic belt, Idaho-Wyoming and Utah: Geology, v. 14, p. 388-391.

Higashi, S., 1982, Tobelite, a new ammonium dioctahedral mica: Mineralogical Journal, v. 11, p. 138-146.

Hunziker, J.C., Frey, M., Clauer, N., Kallmeyer, R.D., Friedrichsen, H., Flehmig, W., Hochstrasser, K., Roggwiler, P., and Schwander, H., 1986, The evolution of illite to muscovite: mineralogical and isotopic data from the Glarus Alps, Switzerland: Contributions to Mineralogy and Petrology, v. 92, p. 157-180.

Inoue, A., and Utada, M., 1983, Further investigations of a conversion series of dioctahedral mica/smectites in the Shinzan hydrothermal alteration area, northeast Japan: Clays and Clay Minerals, v. 31, p. 401-412.

James, L.P., and McKee, E.H., 1985, Silver-lead-zinc ores related to possible Laramide plutonism near Alta, Salt Lake County, Utah: Economic Geology, v. 80, p. 497-504.

Jewell, P.W., and Parry, W.T., 1987, Geology and hydrothermal alteration of the Mercur gold deposits, Utah: Economic Geology, v. 82, p. 1958-1977.

Jewell, P.W., and Parry, W.T., 1988, Geochemistry of the Mercur gold deposit, Utah: Chemical Geology, v. 69, p. 245-265.

Kornze, L.D., 1987, Geology of the Mercur gold mine, *in* Johnson, J.L., ed., Bulk Mineable Precious Metal Deposits of the Western United States, Guidebook for Field Trips: Geological Society of Nevada, p. 381-389.

Krohn, M.D., Altaner, S.P., and Hayba, D.O., 1988, Distribution of ammonium minerals at Hg/Au-bearing hot spring deposits: Initial evidence from near-infrared spectral properties, *in* Schafer, R.W., Cooper, J.J., and Vikre, P.G., eds., Bulk Mineable Precious Metal Deposits of the Western United States, Symposium Proceedings: The Geological Society of Nevada, p. 661-679.

Miller, E.L., Gans, P. B., Wright, J. E., and Sutter, J. F., 1988, Metamorphic history of the east-central Basin and Range Province: Tectonic setting and relationship to magmatism, *in* Ernst, W.G., ed., Metamorphism and crustal evolution of the Western United States, Rubey Volume VII: Prentice Hall, Inc., New Jersey, p. 650-682.

Moore, W.J., and McKee, E.H., 1983, Phanerozoic magmatism and mineralization in the Tooele 1° X 2° quadrangle, Utah, in Tectonic and Stratigraphic Studies in the Eastern Great Basin: Geological Society of America Memoir 157, p. 183-190.

Moore, D. M., and Reynolds, R. C., 1989, X-ray Diffraction and the Identification and Analysis of Clay Minerals, Oxford University Press, New York, 332 p.

Oliver, J., 1986, Fluids expelled tectonically from orogenic belts: Their role in hydrocarbon migration and other geologic phenomena: Geology, v. 75, p. 651-671.

Percival, T.J., Bagby, W.C., and Radtke, A.S., 1988, Physical and chemical features of precious metal deposits hosted by sedimentary rocks in the western United States, *in* Schafer, R.W., Cooper, J.J., and Vikre, P.G., eds., Bulk Mineable Precious Metal Deposits of the Western United States, Symposium Proceedings: The Geological Society of Nevada, p. 11-34.

Reynolds, R. C., 1985, Description of program NEWMOD for the calculation of the one-dimensional X-ray diffraction patterns of mixed-layered clays: Dept. of Earth Sciences, Dartmouth College, Hanover, New Hampshire, 23 p.

Srodon, J., and Eberl, D. D., 1984, Illite, in Bailey, S. W., ed., Micas, Reviews in Mineralogy Vol. 3: Mineralogical Society of America, p. 495-544.

Sterne, E. J., Reynolds, R. C., and Zantop, H., 1982, Natural ammonium illites from black shales hosting a stratiform base metal deposit, DeLong Mountains, Northern Alaska: Clays and Clay Minerals v. 30, p. 161-166.

Tafuri, W.J., 1987, Geology and geochemistry of the Mercur mining district, Tooele County, Utah: Unpublished dissertation, University of Utah, 180 p.

Wilson, P.N., and Parry, W.T., 1989, Geochemical characteristics of hydrothermally altered black shales of the southern Oquirrh Mountains and relationships to Mercur-type gold deposits: Utah Geological and Mineral Survey Open-File Report 161, 64 p.

———, 1990a, Mesozoic hydrothermal alteration associated with gold mineralization in the Mercur district, Utah: Geology, v. 18, p. 866-869.

———, 1990b, Geochemistry of Mesozoic hydrothermal alteration of black shales associated with Mercur-type gold deposits, *in* Hausen, D.M., Halbe, D.N., Petersen, E.U., and Tafuri, W.J., eds., Gold '90, Proceedings from the the Gold '90 Symposium, Salt Lake City, Utah, February 26 to March 1, 1990: Society of Mining, Metallurgy and Exploration, Inc., Littleton, Colorado, p. 167-174.

———, in preparation, Tobelitic and ammonium illitic vein phyllosilicates from hydrothermally altered black shale, southern Oquirrh Mountains, Utah: Submitted to Clays and Clay Minerals.

Wilson, J.R., and Wilson, P.N., 1991, Occurrence and paragenesis of thallium sulfosalts and related sulfides at the Barrick Mercur Gold Mine, Utah, *in* Allison, M.L., ed., Energy and Mineral Resources of Utah, 1990 Guidebook, Utah Geological Society, p. 97-112.

SULFIDE AND SULFOSALT MINERALOGY AT THE MERCUR GOLD DEPOSIT, TOOELE COUNTY, UTAH

James R. Wilson
Dept. of Geology
Weber State University
Ogden, UT 84408-2507
and
Paula N. Wilson
Dept. of Geology and Geophysics
University of Utah
Salt Lake City, UT 84112

ABSTRACT

The Mercur gold deposit is a sediment-hosted disseminated gold deposit characterized by the presence of As-, Fe-, Tl-, Sb-, and Hg-minerals which occur in the unoxidized ore as sulfides and sulfosalts. Minerals identified in this study of Mercur include realgar, orpiment, pyrite, marcasite, sphalerite, and the Tl-minerals lorandite, raguinite, gillulyite, and an undescribed Tl-As-S species referred to as "mineral F". Cinnabar has been found at the deposit, but has not been seen in this study. Pyrite occurs as (1) euhedral grains, (2) irregular or rounded zoned grains, and (3) fine-grained "filigree" pyrite. Chemically pyrite can be divided into non-arsenian, moderately arsenian, and strongly arsenian categories. Realgar is common in the deposit and is usually observed being replaced by orpiment. Orpiment is common and can be divided into two geochemical groups based on relative content of minor elements; orpiment with low Tl-high Sb and orpiment with high Tl-low Sb. Gold is found in highest concentrations (avg. 0.1 wt. %) in strongly arsenian pyrite.

INTRODUCTION

The Mercur gold deposit is one of many low-grade, sediment-hosted, disseminated gold deposits found in Nevada and western Utah. These "Carlin-type" deposits are hosted by carbonate and silty carbonate rocks which typically are characterized by some degree of silicification (jasperoid) as well as argillic alteration. The ore in these deposits is anomalously rich in As, Sb, Hg, and Tl, and is characterized by micrometer sized gold (Bagby and Berger, 1985). Bonham (1989) mentions Mo and W as characterizing elements, as well, and notes that Cu, Pb, and Zn are present only in low concentrations, averaging less than 100 g/metric ton in ore.

PREVIOUS WORK

The Mercur gold deposit is located at the former townsite of Mercur, in the southwest part of the Oquirrh Mountains, Tooele County, Utah, approximately 56 km southwest of

Salt Lake City, and is presently being mined by American Barrick Resources, Inc. The general geology of the district is presented in Gilluly (1932) and previous work pertaining to mineralogical relationships and fluid geochemistry include Jewell and Parry (1987,1988) and Tafuri (1987). Ikramuddin et al. (1986) present a number of chemical analyses of rocks from the Mercur gold deposit emphasizing the use of thallium in geochemical exploration.

METHODS

Most of the samples used in this study were collected from the Lulu graben area and elsewhere in the South Mercur Pit where mining has been completed. Other samples are from the Brickyard-Marion Hill Pit. Minerals were examined by reflected light microscopy, and analyzed by x-ray diffraction and electron microprobe. The following elements were sought during microprobe analysis: Tl, As, Fe, Cu, Zn, Ni, Se, Te, Hg, Au, Sb, and S. Standards used were lorandite for Tl (and for As and S on occasion), gallium arsenide for As, marcasite for Fe, cuprite for Cu, sphalerite for Zn, pentlandite for Ni, bismuth selenide for Se, cinnabar for Hg, pure gold for Au, antimony telluride for Sb and Te, and galena for S. Samples were analyzed with an accelerating voltage of 15 kV and a beam current of either 10 or 20 nA. Beam size was generally between 5 and 20μm, however, very small areas were analyzed under high magnification in a scanning electron microscope mode.

MINERALOGY

Occurrence and Composition

The following sulfides and sulfosalts (Table 1) have been identified in unoxidized ore: pyrite, marcasite, realgar, orpiment, sphalerite, and the Tl-bearing minerals lorandite, raguinite, gillulyite, and "mineral F", a new Tl-As-S mineral that has been submitted to the International Mineralogical Association Commission on New Minerals and Mineral Names. Other sulfide and sulfosalt minerals reported at Mercur, but not specifically seen by us, include cinnabar and christite. Stibnite, as residual cores in antimony oxides, is common in the jasperoid. Associated with the sulfide minerals are calcite, barite, and the clay minerals illite and kaolinite. Gold occurs in several of the sulfide minerals as discussed below, but has not been seen as discrete grains. Average analyses of these minerals are presented in Table 2.

Pyrite and Marcasite

Pyrite at Mercur occurs in several habits and with considerable variation in chemical composition. Pyrite habits are as follows:

(1) Euhedral crystals. These are very common in the carbonaceous limestone and are likely diagenetic in most cases. To a lesser extent, these well-formed crystals occur in calcite veins and in the veins of sulfide-sulfosalt minerals. These pyrite crystals are isotropic, have nearly ideal stoichiometry, and seldom have any measurable heavy metals.

(2) Zoned crystals. Zoned pyrite consist of a 3-12 micron overgrowth surrounding a core of relatively pure FeS_2. The overgrowth is almost always enriched in As and usually Tl as well. These rounded or subhedral arsenian pyrite grains are found most often in sulfide-sulfosalt veins, but also occur in barite and in the host rock. In the veins, zoned pyrites are surrounded by orpiment or lorandite. Even grains that seem totally enclosed in barite usually have a thin edge of lorandite between the pyrite and the enclosing barite.

Arsenian pyrite has been reported at a number of gold deposits similar to Mercur such as the Cortez and Carlin deposits, Nevada (Wells and Mullens, 1973), Carlin and Post deposits (Bakken, et al., 1991), and Post/Betze (Arehart et al., 1991). Radtke (1985) reported that Au (up to 0.35 wt. %), As (up to 6.0 wt. %), and Tl (up to 0.25 wt. %) occurred in coatings and films less than 2 microns thick on the surface of pyrite grains.

(3) Filigree pyrite. A darker colored, less reflective, form of pyrite occurs as abundant, very fine-grained stringers of material interstitial to grains in the groundmass. While relatively common, it is not present in every specimen. Analyses of this material usually show significant As and Tl. Gold values are higher in this form of pyrite then in the other two (Table 2). This is similar to observations by Wilson and Rucklidge (1987) that gold concentration is greater in fine-grained, "porous", arsenian pyrite at the Owl Creek deposit, Ontario. Although Cook and Chryssoullis (1990) reported no relationship between the texture of pyrite and gold distribution in limited samples they examined from Canadian mines, they did observe that gold was more enriched in fine-grained arsenopyrite than in coarser material when both textures were present.

Marcasite is relatively abundant, although less common than pyrite, and is recognizable by its lath-like crystal habit and strong anisotropism. It sometimes occurs as large elongate masses of lath-shaped crystals up to 1 mm in length in areas of sulfide-sulfosalt mineralization. These masses (which we refer to as "fishbones") often occur adjacent to grains of raguinite and cross-cut by veins of lorandite. The marcasite itself seldom has appreciable Tl, As, or Au.

Realgar and Orpiment

Realgar is a common mineral in the mine where it most often occurs in calcite veins and fracture fillings. It occasionally can be found as well-formed crystals in vugs with associated calcite crystals. Realgar is earlier than all other sulfide/sulfosalt minerals (except for some pyrite) as it usually is seen being replaced by orpiment. In our analyses, realgar seldom has other metals substituting in its structure, whereas veins of orpiment cutting and replacing realgar have up to 5 wt. % Tl. Orpiment also often has significant amounts of Fe, Hg, and Au with some individual samples having as much Au as some of the pyrite. Orpiment is found as thin scales on fracture surfaces, as blebs in calcite veins, and as thick

Table 1. Sulfide and sulfosalt mineral occurrences at Mercur and other deposits

MINERAL	COMPOSITION	OCCURRENCE AT MERCUR	ALSO KNOWN TO OCCUR AT
pyrite	FeS_2	very common	all other similar deposits
marcasite	FeS_2	common	all other similar deposits
realgar	AsS	common	all other similar deposits
orpiment	As_2S_3	common	all other similar deposits
stibnite	Sb_2S_3	very rare*	Carlin
sphalerite	ZnS	very rare	common at Carlin
lorandite	$TlAsS_2$	scarce	Carlin; Allchar, Yugoslavia
raguinite	$TlFeS_2$	rare	only known at Allchar, Yugoslavia
gillulyite	$Tl_2(As, Sb)_8S_{13}$	rare	known only from Mercur
"mineral F"	Tl_3AsS_4	very rare	only known at Allchar, Yugoslavia
christite	$TlHgAsS_3$	very rare(?)	a rare mineral at Carlin
cinnabar	HgS	scarce(?)	sparsely distributed at Carlin

*antimony is common as a trace or minor consituent of other minerals, but stibnite is rare except in the Silver Chert jasperoid where it is largely oxidized to stibiconite, cervantite, and other antimony oxides.

Table 2. Average composition (wt. %) of sulfide and sulfosalt minerals in the Mercur Gold Deposit

Mineral (# of analyses)	As	Fe	Tl	Au	Sb	Hg	Cu	Zn	S
Pyrite									
Non-arsenian (27)	<.1	45.9	0.1	<.1	<.1	<.1	<.1	<.1	52.9
Moderately arsenian (18)	0.9	44.0	0.7	<.1	<.1	0.1	0.1	0.1	51.3
Strongly arsenian (16)	2.8	41.9	2.2	0.1	<.1	0.3	<.1	<.1	50.2
Marcasite (7)	0.2	46.2	0.1	<.1	<.1	<.1	<.1	<.1	52.4
Orpiment									
Low Tl-High Sb (17)	60.7	<.1	<.1	<.1	0.3	<.1	<.1	<.1	38.6
High Tl-Low Sb (8)	59.3	0.1	1.7	<.1	<.1	0.1	<.1	<.1	37.7
Realgar (10)	70.0	<.1	<.1	<.1	<.1	<.1	<.1	<.1	28.9
Lorandite (29)	21.9	<.1	59.3	<.1	<.1	<.1	<.1	<.1	18.6
Raguinite (8)	1.0	15.9	62.8	<.1	<.1	0.1	<.1	<.1	19.6
Gillulyite (17)	39.3	<.1	28.3	<.1	2.4	<.1	<.1	<.1	28.4
"Mineral F" (5)	9.2	<.1	75.7	<.1	0.1	<.1	0.1	0.1	15.6

subhedral to euhedral crystal masses as much as 3 cm thick and 5 cm long.

Thallium Minerals

Lorandite, a common Tl mineral in most thallium-rich deposits, is the most abundant Tl mineral in the samples that we have examined. It has been found at Mercur as relatively large (1-2 cm), well-formed crystals in an open fracture associated with calcite. More commonly, lorandite occurs as small (2-3 mm) individual crystals in seams of calcite and kaolinite, as small (1-2 mm) botryoidal masses and encrustations in vugs between barite blades, and as large (2 cm) masses associated with orpiment. Microscopically, lorandite occurs as veins crosscutting orpiment and realgar; with raguinite in a vein crosscutting and replacing calcite; as bladed radiating crystal aggregates with a pyritic core; as alteration rims on pyrite; and in veins crosscutting marcasite. It also occurs as tattered framboidal grains up to 100 microns in diameter which may have formed by replacement of fossil material or replacement of framboidal pyrite or marcasite.

Gillulyite is a new Tl mineral discovered at Mercur and named in honor of James Gilluly of the U. S. Geological Survey (Wilson et al., 1991). This mineral was found in the Lulu graben of the South Mercur pit where it was locally abundant. It occurs as cleavable masses and crystal sections up to 2 cm in diameter in hand specimens that also contain minor amounts of lorandite, but has not been found in contact with lorandite or in specimens that contain abundant lorandite. Gillulyite is representative of a relatively Sb-rich zone in that it averages approximately 2 wt. % Sb whereas other sulfide and sulfosalt minerals (other than stibnite) contain little or no Sb. The gillulyite occurs in close association with orpiment. Distinct, sharp grain boundaries between the two minerals are common which may indicate that they are coeval. In some polished sections, blebs of orpiment can be observed within the gillulyite.

Raguinite is a rare Tl mineral that previous to our study was known only from Allchar, Yugoslavia (Picot and Johann, 1982, p. 319). At Mercur it was found in the same area of the Lulu Graben in which the gillulyite occurred. Extremely small (5-8 micron) grains superficially resemble pyrite, but in larger grains the distinctive pink-purple-brown color in plane polarized light and orange color with crossed polars is distinctive. It is found as scattered grains in carbonaceous limestone near lorandite framboids. Larger grains of anhedral raguinite (up to 150 microns) occur in sulfide-sulfosalt veins. It also occurs surrounding and replacing barite; with lorandite in a vein crosscutting and replacing calcite; in close association with, but apparently not replacing, marcasite; and surrounding euhedral pyrite which shows no evidence of replacement or alteration.

Several other Tl minerals have been reported at Mercur but these have not been verified as of this writing. In this category is christite ($TlHgAsS_3$) mentioned by Kornze (1987). Tafuri (1987) reported several thallium-bearing minerals on the basis of qualitative spectrographic analyses, but they were not specifically identified.

We have observed and analyzed other Tl-bearing mineral phases, but have not yet been able to identify and fully characterize them. One of these, currently referred to as "mineral F", Tl_3AsS_4, may be a new mineral species, although it has been described as a synthetic material (Sobott, 1984) and was reported at Allchar, Yugoslavia (Pavicevic and El Goresy, 1988).

Several minerals have been analyzed and found to have relatively complex compositions. It is not clear yet if these phases are separate minerals, intergrowths, and/or partial replacements of earlier sulfides by As- and Tl-bearing fluids. These complex phases usually involve combinations of Fe, As, Zn, Tl, Sb and S. Some of these grains could be interpreted as Tl- and As-bearing pyrite; others may be partially replaced sphalerite. One grain of relatively pure sphalerite has been found, but zinc is generally rare except as a trace constituent.

GOLD IN SULFIDE/SULFOSALT MINERALS

Gold would seem to have been present in the As- and Tl-bearing fluids that formed the orpiment-lorandite suite of minerals. Although realgar is an important gold host at Carlin (Radtke, 1985), our analyses of realgar at Mercur have not detected any gold and, as mentioned above, orpiment veins cutting realgar are significantly enriched in heavy metals. As at other deposits, gold is associated with arsenian pyrite. There also seems to be an enrichment in the filigree pyrite.

SUMMARY

Thus far, our study of sulfides at Mercur has resulted in one new mineral species, gillulyite, and a possible second new species, "mineral F." It has also served to document the sulfide/sulfosalt mineralogy of the deposit, revealing textural relationships that will eventually lead to a meaningful paragenetic model once a larger area has been sampled. The Tl-As-S system is not well defined and by documenting these mineral occurrences we may be able to refine experimental work on the stability of various phases in this system.

ACKNOWLEDGMENTS

We wish to express our appreciation to Larry Stanger, Mine Geologist, and Barrick Mercur Gold Mine, Inc., for their assistance in obtaining samples for this study and for access to various mine properties. W. P. Nash and R. Lambert, University of Utah, gave generously of time and expertise to assist us with the electron microprobe.

REFERENCES

Arehart, G. B., Kesler, S. E., and O'Neil, J. R., (1991) Elemental and sulfur isotopic zoning in iron sulfide grains from sediment-hosted micron gold deposits: implications for deposit genesis: GSA Abstracts with Programs, v. 23, no. 5, p. A228.

Bagby, W. C., and Berger, B. R., 1985, Geologic characteristics of sediment-hosted, disseminated precious metal deposits in the western United States, *in* Berger, B. R. and Bethke, P. M. (eds), Geology and geochemistry of epithermal systems, Society of Economic Geologists Reviews in Economic Geology, v. 71, p. 1006-1011.

Bakken, B. M., Brigham, R. H., and Fleming, R. H., 1991, The distribution of gold in unoxidized ore from Carlin-type deposits revealed by secondary ion mass spectrometry (SIMS):GSA Abstracts with Programs, v. 23, no. 5, p. A228.

Bonham, H. F., Jr., 1989, Bulk minable Au deposits, western United States *in* Keays et al., editor, The Geology of Gold Deposits: The Perspective in 1988, Economic Geology Monograph 6: The Economic Geology Publishing Co., p. 193-207.

Cook, N. J., and Chryssoulis, S. L., 1990, Concentrations of "invisible gold" in common sulfides: The Canadian Mineralogist, v. 28, pt. 1, p. 1-16.

Gilluly, J., 1932, Geology and ore deposits of the Stockton and Fairfield quadrangles, Utah: U. S. Geological Survey Professional Paper No. 173, 171 p.

Ikramuddin, M., Besse, L., and Nordstrom, P. M., 1986, Thallium in Carlin-type gold deposits: Applied Geochemistry, v. 1, p. 493-502.

Jewell, P. W., and Parry, W. T., 1987, Geology and hydrothermal alteration of the Mercur gold deposit, Utah: Economic Geology, v. 82, p. 1958-1966.

Jewell, P. W., and Parry, W. T., 1988, Geochemistry of the Mercur gold deposit (Utah, U.S.A.): Chemical Geology, v. 69, p. 245-265.

Kornze, L. D., 1987, "Geology of the Mercur gold mine", *in* Johnson, J.L., ed., Bulk mineable precious metal deposits of the western United States, Guidebook for field trips: Geological Society of Nevada, p. 381-389.

Pavicevic, M. K., and El Goresy, A., 1988, Crven Dol Tl deposit in Allchar: mineralogical investigation, chemical composition of Tl minerals and genetic implications: Nuclear Instruments and Methods in Physics Research, A271, p. 297-300.

Picot, P. and Johan, Z., 1982, Atlas of ore minerals: Amsterdam, Elsevier Scientific Publishing Co., 482 p.

Radtke, A. S., 1985, Geology of the Carlin gold deposit: U. S. Geological Survey Professional Paper No. 1267, 124 p.

Sobott, R. J. G., 1984, Sulfosalts and Tl_2S-As_2S_3-Sb_2S_3-S phase relations: Neues Jahrbuch fur Mineralogie Abh., v. 150/1, p. 54-59.

Tafuri, W. J., 1987, Geology and geochemistry of the Mercur mining district, Tooele County, Utah: Unpublished dissertation, University of Utah, 180 p.

Wells, J. D., and Mullens, T. E., 1973, Gold-bearing arsenian pyrite determined by microprobe analysis, Cortez and Carlin gold mines, Nevada: Economic Geology, v. 68, p. 187-201.

Wilson, G. C., and Rucklidge, J. C., 1987, Mineralogy and microstructures of carbonaceous gold ores: Mineralogy and Petrology, v. 36, p. 219-239.

Wilson, J. R., Robinson, P., Wilson, P. N., Stanger, L. W., and Salmon, G., 1991, Gillulyite, $Tl_2(As, Sb)8S_{13}$, a new thallium sulfosalt from the Mercur gold mine, Utah: American Mineralogist, v. 76, ¾, p. 653-656.

ROCKY MOUNTAIN SECTION OF THE PALEONTOLOGICAL SOCIETY 1992 FIELD TRIP: UINTA BASIN, UINTA MOUNTAINS, AND THE BRIDGER BASIN

David D. Gillette
Division of State History, 300 Rio Grande
Salt Lake City, Utah 84092

The 1992 field trip sponsored by the Rocky Mountain Section of the Paleontological Society, convening for annual meetings in Ogden, Utah in conjunction with the Rocky Mountain Section of the Geological Society of America, focuses on paleontology and stratigraphy of northeastern Utah and southwestern Wyoming (Fig. 1). From main urban centers along the Wasatch Front (e.g., Ogden, Salt Lake City, Provo), this field trip requires two days of travel. As organized here, the trip originates in Ogden, with travel directly to Vernal, Utah on the first morning. The trip to Dinosaur National Monument is scheduled for the first afternoon. For others who use this roadlog, a full day might be more appropriate, allowing for several hours at the visitor center at the Monument, where dinosaurs are displayed at the most spectacular in situ exhibit in the world. *Stegosaurus, Apatosaurus (=Brontosaurus), Diplodocus, Allosaurus, Barosaurus,* and a wide variety of less famous dinosaurs can be seen in these exhibits. Moreover, this was a center of dinosaur excavations when these giants were first recognized in the American West, dating from the earliest days of discovery. The very roots of dinosaur paleontology are to be found here, a colorful history of exploration and discovery, including legends (and many true stories) of stealth and deception as rival camps sought the prize specimens for their wealthy museum sponsors in the East (the Carnegie Museum of Natural History, the American Museum of Natural History, and the Smithsonian Institution). For readers interested in the history of dinosaur exploration and research, the best account is *Men and Dinosaurs,* by E. H. Colbert (Dutton, New York, 1968), reprinted in 1984 as *The Great Dinosaur Hunters and Their Discoveries* (Dover Press, New York).

Dinosaur research today is a vigorous and popular subdiscipline of paleontology, and the region surrounding Dinosaur National Monument is as important now as it was a hundred years ago. The fruits of much of this research can be seen in the displays at the monument, where paleontologists are actively pursuing the truth about dinosaurs: How did they live? With what other species were they associated? What was their habitat? What were the predator-prey relationships? To what extent did they control their body temperatures? Is there evidence of social organization and care for the young? What accounts for their phenomenal success spanning more than 160 million years? And, inevitably: How and why did they become extinct?

Another important focus of attention in this region has been the spectacular record of evolution of mammals and birds in the early Tertiary. The second day of the field trip focuses attention on this lower Tertiary record, after viewing the Mesozoic rocks north of Vernal en route to the Bridger Basin. The fossils are so abundant and the stratigraphic relations so firmly established that this region has produced the standard reference faunas for four North American Land Mammal Ages (Wasatchian, Bridgerian, Uintan, and Duchesnean Land Mammal Ages), the biochronologic system established by mammal paleontologists and continental stratigraphers for correlation of sites with limited continuity owing to their occurrence in intermontane basins and in circumstances in the Plains states where depositional systems were restricted and not laterally extensive. The Bridger Basin and the Uinta Basin have been mainstays of mammal paleontology fieldwork for more than 100 years, and interest in these faunas continues with increased intensity. Field parties visit the classic sites on annual pilgrimages from museums and universities from near and far, and new approaches are applied regularly as fresh ideas are brought to bear on problems of mammalian evolution.

What is organized for a two-day field trip here would better be expanded for a week or more for dedicated paleontologists. Field trips conducted by local geological societies to these areas have been frequent, and have explored much of this area in much greater intensity than we have organized for this field trip. For those who are interested in more detail and other field trip road logs, the extensive bibliography and historical summary provided by Bilbey (this volume) lists numerous field trip guidebooks and conferences that provide a wealth of information and could be the source of years of field-oriented excursions into this paleontologists' paradise.

Field trip organizers include Sue Ann Bilbey, Alden H. Hamblin, Emmett Evanoff, Logan D. Ivy, Dan Chure, Ann Elder, Scott Madsen, Martin Lockley, Kelly Conrad, Marc Paquette, and John F. Hubert, all of whom have contributed to the road logs and related technical papers. In addition, Martha Hayden has assisted in the organization with her usual good cheer and efficiency. To all these individuals and to others associated with this field excursion, I extend my thanks and congratulations.

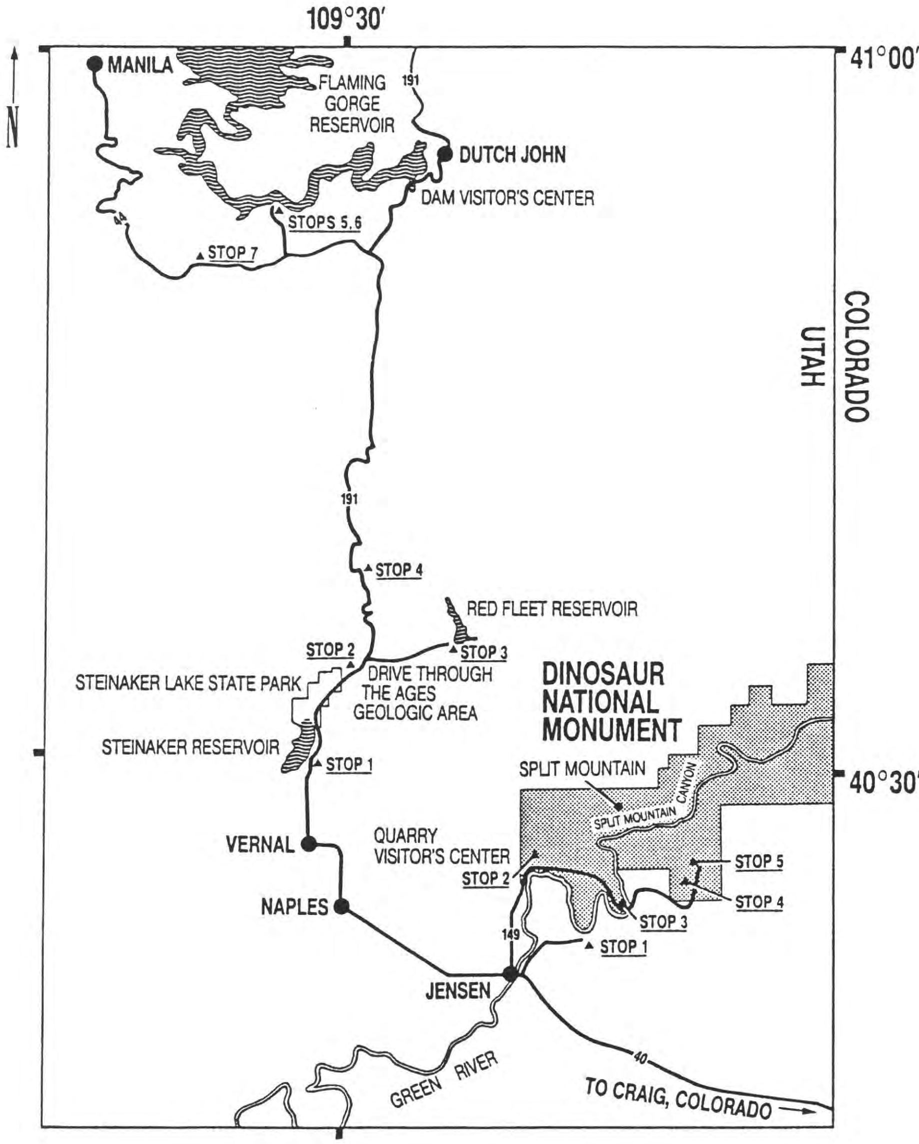

Figure 1: Field trip map for the Utah portions of the road log. The trip is divided into two days. Day 1 originates in Vernal and proceeds eastward to Dinosaur National Monument, with 5 scheduled stops. Day 2 originates in Vernal and proceeds northward to Manila, with 7 scheduled stops; and continues from Manila, Utah, to Fort Bridger, Wyoming. This map corresponds to the road logs by Bilbey (Vernal to Dinosaur National Monument), and Bilbey and Hamblin (Vernal to Manila). A separate field trip map for the Wyoming portion of Day 2 is included with the road log (Manila to Fort Bridger) by Evanoff and Ivy.

UINTA MOUNTAINS AND BASIN — A BRIEF HISTORICAL REVIEW AND SELECTED BIBLIOGRAPHY

Sue Ann Bilbey
Utah Field House of Natural History
235 East Main, Vernal, Utah 84078

INTRODUCTION

Vernal, Utah and Dinosaur National Monument are strategically placed between the Uinta Mountains (the largest, single east-west-trending mountain range in the western hemisphere) and the Uinta Basin (a petroleum-rich intermontane valley). Together these structures encompass almost 3 billion years of earth history, with a fossil record covering more than 600 million years. This record includes most forms of life from primitive algae to highly advanced mammals.

Evidence of human habitation in the Uintas may date back to the Paleo-Indian (12,000 to 7,500 BP) as suggested by the occurrence of several "Clovis" and "Cody Complex" points. Fremont Indians (dating from 1500 BP to 600 BP) were early residents that left abundant pictographs and petroglyphs on desert varnished rock faces, generally in the Navajo or Shinarump sandstones. Modern Utes (Uto-Aztecan people) came into this area about 600 years ago (McNamara, *in* Picard, 1985).

Exploration of this area by white men probably began when early Spanish miners visited in the late 1600 s and early 1700 s. However, the record of their visits is scanty, with most being local legend. It is well documented that in 1776 Spanish Fathers Dominguez and Escalante forded the Green River just south of Split Mountain (very near the Dinosaur National Monument southwest boundary) (Untermann *in* Sears, 1957).

Trappers and explorers visited the Uintas in the early 1800 s, most notably: William H. Ashley, 1825; Antoine Robidoux, 1832 to 1844; John C. Fremont, 1836 and 1844; and John W. Gunnison, 1853. Early Mormon explorers reported in September, 1861 that the area was "one vast contiguity of waste and measurably valueless, excepting for nomadic purposes, hunting grounds for Indians and to hold the earth together" (Deseret News, 1861). One month later President Abraham Lincoln designated most of the "Uintah Valley" as an Indian reservation (about 2 million acres of land).

Three major geologic surveys included portions of the Uintas: 1) the Hayden Survey in northern Utah in 1869 and 1870; 2) the 40th Parallel Survey led by Clarence King in 1869 with Samuel Emmons as the major investigator of the Uinta Mountains; and 3) John Wesley Powell's survey of the Green and Colorado Rivers in 1868 and 1871, and the Uinta Mountains in 1874 and 1875. Most of the well-known geographic names were given during these surveys: King's Peak, Hayden Peak, Flaming Gorge, Red Canyon, Lodore Canyon, Split Mountain to name a few.

Vertebrate fossils were first discovered in the Uinta Basin in 1870 by O. C. Marsh and his students from Yale University. Most of these fossils were of ancient mammals which roamed over North America during late Eocene times, 35 to 45 million years ago. Their discovery was significant enough to the science of paleontology that two North American Mammalian ages are named for them — the Uintan and Duchesnean.

In addition to mammal material Marsh also found turtle bone and *"Megalosaurus"* teeth in steeply dipping beds on the south side of the Uinta Mountains which he interpreted as Cretaceous. These teeth were probably from an *Allosaurus* and he probably collected them from the Jurassic Morrison Formation.

In 1908 Earl Douglass of the Carnegie Museum in Pittsburgh, Pennsylvania, was studying fossil mammals in the Bonanza, Utah area (about 50 miles south east of Vernal). That fall he and Dr. W. J. Holland, Director of the Carnegie Museum, spent several days looking for dinosaur bones in the Jurassic rocks near Split Mountain. A discovery of a large leg bone prompted the decision that Douglass should search the Morrison Formation for more bone the next summer. His search west of Split Mountain led to the discovery, on August 17, 1909, of one of the world's finest concentrations of fossil dinosaur remains. The 140 million year old stratum has revealed during subsequent excavation parts of more than 300 individual animals (12 species of dinosaurs, a crocodile, and 2 turtles.

One of the most significant of Douglass' discoveries was one he did not recognize. During the early days of the excavation it was apparent that they had discovered two nearly complete skeletons of *"Brontosaurus,"* more correctly known as *Apatosaurus.* In November, 1910 a large skull was found associated with these bones. Douglass rejected it as an *Apatosaurus* skull because of its similarity to *Diplodocus* and its difference from the partial skulls identified by Marsh as belonging to the *"Brontosaurus"* (a *Camarasaurus*-like skull). Holland (1915), however, asserted that it was the only verifiable skull ever found associated with an *Apatosaurus.* Professional pressure, however, forced the Carnegie Museum to leave their *Apatosaurus* headless until after Holland's death in 1932. Then the staff placed the *Camarasaurus*-like skull identified by Marsh on the skeleton.

Subsequent study of the skeletons supports Holland's conclusions. It turns out that morphologically the *Apatosaurus* is more closely related to *Diplodocus* than to *Camarasaurus.* McIntosh and Berman (1975) determined, therefore, that the *Camarasaurus* skulls found on all the *Apatosaurus* skeletons in major museums were wrong. Instead the skull found by Douglass at Dinosaur National Monument more appropriately fits. Subsequent changes in displays have corrected the mistake.

Douglass' quarry could not be protected by claiming the mineral rights since fossils do not qualify. Instead President Woodrow Wilson set aside 60 acres surrounding the quarry as a National Monument in 1915. The land was then leased by the Carnegie Museum, the Smithsonian and finally by the University of Utah for further excavation until 1922 when work ceased. In 1938, the Monument was expanded to include the canyons of the Yampa and Green Rivers in Colorado and Utah. In 1958, in fulfillment of Douglass' dreams, the quarry was opened as an in-place exhibit enclosed in a beautiful new building. Subsequent work has exposed more than 1500 bones, most of which remain in situ.

Current research on the fauna of the Morrison Formation has expanded beyond the quarry face. New sites within the Monument boundaries include microvertebrates, several sauropods, and an *Allosaurus.* Outside the Monument scientists have found a partial articulated *Stegosaurus,* a significant Morrison plant site, and numerous isolated dinosaur bones.

Although considerable exploratory research in vertebrate paleontology was done in the Uintas, little detailed work other than dinosaur research has been done until recently. Active projects include dinosaur ichnology in a variety of formations, mammalian paleontology, microvertebrate paleontology, paleobotany, and the study of several new vertebrate species, e.g., a Beryciforme fish, a pliosaur, and a frog. Much remains to be done in the Uintas, a geologist's and paleontologist's paradise.

SELECTED BIBLIOGRAPHY FOR ROAD LOGS

Anonymous, 1981. Drive through the ages: U. S. Forest Service and U. S. Bureau of Land Management (brochure).

Archibald, J. D., Gingerich, P. D., Lindsay, E. H., Clemens, W. A., Krause, D. W., and Rose, K. D., 1987. First North American Land Mammal Ages of the Cenozoic Era, In: Woodburne, M. O. (editor), Cenozoic Mammals of North America. University of California Press, Berkeley, p. 24-73.

Bilbey, S. A., n. d. A study of the Upper Jurassic-Lower Cretaceous rocks at the Cleveland-Lloyd Dinosaur Quarry with a comparison to the Dinosaur National Monument Quarry, Utah. University of Utah Ph. D. Dissertation. In preparation.

——, Kerns, R. L., Jr., and Bowman, J. T., 1974. Petrology of the Morrison Formation, Dinosaur Quarry Quadrangle, Utah. Utah Geological and Mineral Survey Special Studies 48.

Bradley, W. H., 1936. Geomorphology of the north flank of the Uinta Mountains. U. S. Geological Survey Professional Paper 185-I:163199.

Bradley, W. A., 1956. Jurassic and pre-Mancos Cretaceous stratigraphy of the eastern Uinta Mountains, Utah-Colorado. In: Seal, O. G. (editor), Guidebook to the Geology of Northwest Colorado. Intermountain Association of Petroleum Geologists and Rocky Mountain Association of Geologists, p. 21-25.

Brenner, R. L., 1983. Late Jurassic tectonic setting and paleogeography of Western Interior, North America. *In:* Reynolds, M.W. and Dolly, E.D. (editors), Mesozoic Paleogeography of West-central United States. Rocky Mountain Section of the Society of Economic Paleontologists and Mineralogists, p. 119-132.

Bruhn, R. L., Picard, M. D., and Beck, S. L., 1983. Mesozoic and Early Tertiary structure and sedimentology of the central Wasatch Mountains, Uinta Mountains and Uinta Basin. Utah Geological and Mineral Survey Bulletin 59:63-105.

Bruhn, R.L., Picard, M.D., and Isby, J. S., 1986. Tectonics and sedimentology of Uinta Arch, western Uinta Mountains, and Uinta Basin. *In:* Peterson, J. A. (editor), Paleotectonics and Sedimentation. American Association of Petroleum Geologists Memoir 41:333-352.

Cadigan, R. A., 1967. Petrology of the Morrison Formation in the Colorado Plateau Region. U. S. Geological Survey Professional Paper 556, 113 p.

Campbell, J. A. 1975. Structural geology and petroleum potential of the south flank of the Uinta Mountains uplift, northeastern Utah. Utah Geology 2:129-132.

Chure, D. J., 1987. Dinosaur National Monument — A window on the past. *In:* Averett, W.R., (editor), Paleontology and Geology of the Dinosaur Triangle, Guidebook. Museum of Western Colorado, Grand Junction, Colorado, p. 75-78.

Clemens, W. A., Lillegraven, J. A., Lindsay, E. H., and Simpson, G. G., 1979. Where, when, and what — A survey of known Mesozoic mammal distribution, *In:* Lillegraven, J.A., Kielan-Jaworowska, Z., and Clemens, W. A., (editors), Mesozoic Mammals The First Two-thirds of Mammalian History, p. 7-58.

Cockerell, T. D. A., 1915. Some American Cretaceous fish scales, with notes on the classification and distribution of Cretaceous fishes. U. S. Geological Survey Bulletin 603:34-57.

Craig, L. C., Holmes, C. N., Cadigan, R. A., Freeman, V. L., Mullens, T. E., and Weir, G. W., 1955. Stratigraphy of the Morrison and related formations, Colorado Plateau Region — A preliminary report. U. S. Geological Survey Bulletin 1009-E, 168 p.

Crittenden, M. D. and Peterman, Z. E., 1975. Provisional Rb/Sr age of the Precambrian Uinta Mountain Group, northeastern Utah. Utah Geology 2(1):75-77.

Damon, P. E., 1970. Correlation and chronology of ore deposits and volcanic rocks. Tucson, University of Arizona, U. S. Atomic Energy Commission Contract AT(11-1)-689, Annual Progress Report COO-689-130, 77 p.

Dawson, J. C., 1970. The sedimentology and stratigraphy of the Morrison Formation (Upper Jurassic) in northwestern Colorado and northeastern Utah. University of Wisconsin, Ph.D. Dissertation, 125 p.

Dodson, P., Behrensmeyer, A. K., Bakker, R. T., and McIntosh, J. S., 1980. Taphonomy and paleoecology of the dinosaur beds of the Jurassic Morrison Formation. Paleobiology, 6(2):208-232.

Doi, Kentaro, 1990. Geology and paleontology of two primate families of the Raven Ridge, northwestern Colorado and northeastern Utah. M.S. Thesis, Department of Geological Sciences, University of Colorado, 215 pp.

Emmons, S.F., 1877, The Green River Basin. *In:* King, C. (editor), Report of the Geological Exploration of the Fortieth Parallel. Professional Papers of the Engineering Department, U. S. Army, No. 18:191-310.

Emry, R. J., 1981. Additions to the mammalian fauna of the type Duchesnean, with comments of the status of the Duchesnean "Age". Journal of Paleontology 55(3):563-570.

Fouch, T. D., 1975. Lithofacies and related hydrocarbon accumulations in Tertiary strata of the western and central Uinta Basin, Utah. Rocky Mountain Association of Geologists. 1975 Symposium, p. 163-173.

Freeman, W. E., 1976. Regional stratigraphy and depositional environments of the Glen Canyon Group and Carmel Formation (San Rafael Group). Rocky Mountain Association of Geologists 1976 Symposium-Cordilleran Hingeline, p. 247-260.

Gazin, C. L., 1976. Annotated bibliography of Bridger Mammalia. Smithsonian Contributions to Paleobiology 26:13-25.

Gilmore, C. W., 1924. The Dinosaur National Monument and its fossils. Washington Academy of Science Journal 19(15):381.

——, 1936. Osteology of *Apatosaurus,* with special reference to specimens in the Carnegie Museum. Memoirs of Carnegie Museum 11(4):175-300.

Grande, L., 1980. Paleontology of the Green River Formation with a review of the fish fauna. Geological Survey of Wyoming Bulletin 63:xvii + 333 p.

Grande, L., 1984. Paleontology of the Green River Formation with a review of the fish fauna. Geological Survey of Wyoming Bulletin 63:xvii + 333 p. Second Edition.

Hamblin, A. H., 1987. Paleogeography and paleoecology of the Myton Pocket, Uinta Basin, Utah (Uinta Formation-Upper Eocene). Brigham Young University Geology Studies 34(1):33-60.

——, 1987. Road log of the Drive Through the Ages. In: Averett, W. R., (editor), Paleontology and Geology of the Dinosaur Triangle, Guidebook, Museum of Western Colorado, Grand Junction, Colorado, p. 143-148.

Hansen, W. R., 1965. Geology of the Flaming Gorge area, Utah-Colorado-Wyoming. U. S. Geological Survey Professional Paper 490, 196 p.

Hansen, W. R., 1969. The geology of the Uinta Mountains. U. S. Geological Survey Bulletin 1291, 144 p.

——, 1984. Post-Laramide tectonic history of the eastern Uinta Mountains, Utah, Colorado, Wyoming. Mountain Geologist 21:5-29

——, 1977. Geologic map of the Canyon of Lodore South Quadrangle, Moffat County, Colorado. U. S. Geological Survey Geologic Quadrangle Map GQ-1403, scale 1:24,000.

——, 1986. Neogene tectonics and geomorphology of the Eastern Uinta Mountains in Utah, Colorado and Wyoming. U. S. Geological Survey Professional Paper 1356, 78 p.

——, Rowley, P. D., and Carrara, P. E., 1983. Geologic map of Dinosaur National Monument and vicinity, Utah and Colorado. U. S. Geological Survey Miscellaneous Investigations Map I-1407, scale 1:50,000.

Hayden, F. V., 1872. Preliminary Report of the U. S. Geological Survey of Wyoming and Portions of the Contiguous Territories. Washington, p. 41-70.

Herr, R. G., Picard, M. D., and Evans, S. H., Jr., 1982. Age and depth of burial, Cambrian Lodore Formation, northeastern Utah and northwestern Colorado. University of Wyoming Contributions in Geology 21:115-121.

Hoggan, R. D., 1970. Paleontology and paleoecology of the Curtis Formation in the Uinta Mountains area, Daggett County, Utah. Brigham

Young University Geology Studies 17(2):31-65.

Holland, W. J., 1915. A new species of *Apatosaurus*. Annals of the Carnegie Museum 10:143-145.

Hunt, C. B., 1969. Geologic history of the Colorado River. U. S. Geological Survey Professional Paper 669-C:59-130.

Imlay, R. W., 1980. Jurassic paleobiogeography of the conterminous United States in its continental setting. U. S. Geological Survey Professional Paper 1062, 134 p.

Izett, G. A., 1981. Volcanic ash beds. Recorders of Upper Cenozoic silicic pyroclastic volcanism in the western United States. Journal of Geophysical Research 86(B11):10200-10222.

Kay, J. L., 1934. The Tertiary Formations of the Uinta Basin, Utah. Annals of Carnegie Museum, 23:357-371.

——, 1957. The Eocene vertebrates of the Uinta Basin, Utah. *In:* Seal, O.G. (editor), Guidebook to the Geology of the Uinta Basin, Intermountain Association of Petroleum Geologists, 8th Annual Field Conference, p. 110-114.

Kayser, R. B., 1964. Petrology of the Nugget-Navajo Sandstone at outcrops near Hanna, Utah and Dinosaur National Monument. Intermountain Geological Association Guidebook on Uinta Basin, 13th Annual Field Conference, p. 105-108.

Kinney, D. M., 1956. Geology of the Uinta River-Brush Creek area, Duchesne and Uintah Counties, Utah. U. S. Geological Survey Bulletin 1007, 185 p.

Kocurek, G. and Dott, R. H., Jr., 1983. Jurassic paleogeography and paleoclimate of the central and southern Rocky Mountains Region. In: Reynolds, M. W., and Dolly, E. D., (editors), Mesozoic Paleogeography of West-central United States. Rocky Mountain Section, Society of Economic Paleontologists and Mineralogists, Denver, Colorado, p. 101-116.

Koesoemadinata, R. P., 1970. Stratigraphy and petroleum occurrence, Green River Formation, Red Wash Field, Utah. Colorado School of Mines Quarterly 65(1), 77 p.

Lawton, R., 1977. Taphonomy of the dinosaur quarry, Dinosaur National Monument. University of Wyoming Contributions in Geology 15:119-126.

Lewis, G. E., Irwin, J. H., and Wilson, R. F., 1961. Age of the Glen Canyon Group (Triassic and Jurassic) on the Colorado Plateau. Geological Society of America Bulletin 72:1437-1440.

Lindsay, J. B., (editor), 1969. Geologic Guidebook to the Uinta Mountains — Utah's maverick range. Intermountain Association of Geologists, 16th Annual Field Conference, 237 p.

Lockley, M., 1991. Tracking the rise of dinosaurs in eastern Utah. Canyon Legacy 6:2-8.

McCormick, C. D. and Picard, C. D., 1969. Stratigraphy of the Gartra Formation (Triassic), Uinta Mountain area, Utah and Colorado. Intermountain Association of Geologists, 16th Annual Field Conference Guidebook — Uinta Mountains, p. 169-180.

McIntosh, J. S., and Berman, D. S., 1975. Description of the palate and lower jaw of *Diplodocus* (Reptilia. Saurischia) with remarks on the nature of the skull of *Apatosaurus*. Journal of Paleontology 49(1):197-199.

MacGinitie, H. D., 1969. The Eocene Green River flora of northwestern Colorado and northeastern Utah. University of California Publications in Geological Science 83, 140 p. + 31 plates.

Madsen, J. H., Jr. and Miller, W. E., 1979. The fossil vertebrates of Utah, an annotated bibliography. Brigham Young University Geology Studies 26(4), 147 p.

Maione, S. J., 1971. Stratigraphy of the Frontier Sandstone Member of the Mancos Shale (Upper Cretaceous) on the south flank of the eastern Uinta Mountains, Utah and Colorado. Earth Science Bulletin 4:27-58.

Marsh, O. C., 1871. On the geology of the eastern Uinta Mountains. American Journal of Science and Arts 1(3rd Series):191-198.

Mauger, R. L., 1977. K-Ar ages of biotites from tuffs in Eocene rocks of the Green River, Washakie, and Uinta Basins, Utah, Wyoming, and Colorado. University of Wyoming Contributions in Geology 15:17-41.

McDowell, F. W., Wilson, J. A., and Clark, J., 1973. K-Ar dates for biotite from two paleontologically significant localities-Duchesne River Formation, Utah and Chadron Formation, South Dakota. Isochron/West 7:11-12.

McKenna, M. C. and others, 1973. K/Ar recalibration of Eocene North American land-mammal "ages" and European ages. Geological Society of America. Abstracts with Programs, 5(7):733.

Mullens, T. E., 1971. Reconnaissance study of the Wasatch, Evanston, and Echo Canyon Formations in part of northern Utah. U. S. Geological Survey Bulletin 1311-D, 31 p.

Murany, E. E., 1964. Wasatch Formation of the Uinta Basin. Intermountain Geological Association Guidebook on Uinta Basin, 13th Annual Field Conference, p. 145-156.

Osmond, J. C., 1964. Tectonic history of the Uinta Basin. Intermountain Geological Association Guidebook on Uinta Basin, 13th Annual Field Conference, p. 47-58.

Otto, E. P., and Picard, M. D., 1976. Petrology of Entrada Sandstone (Jurassic), northeastern Utah. Rocky Mountain Association of Geologists 1976 Symposium — Cordilleran Hingeline, p. 231-246.

Peterson, F., 1988. Stratigraphy and nomenclature of Middle and Upper Jurassic rocks, Western Colorado Plateau, Utah and Arizona. U. S. Geological Survey Bulletin 1633-B. p. 17-56.

Peterson, F.,and Turner-Peterson, C. E., 1987. The Morrison Formation of the Colorado Plateau. Recent advances in sedimentology, stratigraphy, and paleotectonics. Hunteria 2(1), 18 p.

Peterson, J. A., 1955. Marine Jurassic rocks, northern and eastern Uinta Mountains and adjacent areas. Wyoming Geological Association 10th Annual Field Conference Guidebook — Green River Basin, p. 75-79.

Peterson, O. A. and Kay, J. L., 1931. The upper Uinta Formation of northeastern Utah. Carnegie Museum Annals 20(3-4):293-306.

Picard, M. D., 1975. Facies, petrography and petroleum potential of Nugget Sandstone (Jurassic), southwestern Wyoming and northeastern Utah. *In:* Bolyard, D.W. (editor), Symposium on Deep Drilling Frontiers of the Central Rocky Mountains, Steamboat Springs, Colorado Rocky Mountain Association of Geologists, p. 109-127.

Picard, M. D. (editor), 1985. Geology and Energy Resources, Uinta Basin of Utah. Utah Geological Association 12, 338 p.

Pipiringos, G. N., and Imlay, R. W., 1979. Lithology and subdivisions of the Jurassic Stump Formation in southeastern Idaho and adjoining areas. U. S. Geological Survey Professional Paper 1035-C.

Pipiringos, G. N., and O'Sullivan, R. B., 1978. Principal unconformities in Triassic and Jurassic rocks, Western Interior United States — A preliminary survey. U. S. Geological Survey Professional Paper 1035-A, 29 p.

Poole, F. G., and Stewart, J. H., 1964. Chinle Formation and Glen Canyon Sandstone in northeastern Utah and northwestern Colorado. Intermountain Geological Association Guidebook on Uinta Basin, 13th Annual Field Conference, p. 93-104.

Powell, J. W., 1876. Report on the Geology of the Eastern Portion of the Uinta Mountains and a Region of Country Adjacent Thereto. U. S. Geological and Geographical Survey of the Territories (Rocky Mountain Region), Washington, D. C., 218 p.

Rigby, J. K., 1964. Some observations of the stratigraphy and paleoecology of the Carmel and Twin Creek Formations in the Uinta Mountains. Intermountain Geological Association Guidebook on Uinta Basin, 13th Annual Field Conference, p. 109-114.

Ritzma, H. R., 1974. Dating of igneous dike, eastern Uinta Mountains. Utah Geology 1:95.

——, 1983. Igneous dikes of the eastern Uinta Mountains, Utah and Colorado. Utah Geological and Mineral Survey, Special Studies 56:1-23.

Rowley, P. D., and Hansen, W. R., 1979. Geologic map of the Plug Hat quadrangle, Moffat County, Colorado. U. S. Geological Survey Geological Quadrangle Map GQ-1514.

Rowley, P. D., Hansen, W., Tweto, O. and Carrara, P., 1985. Geologic

Map of the Vernal 1° x 2° Quadrangle, Colorado, Utah, and Wyoming. U.S. Geological Survey Map I-1526.

Rowley, P. D., Kinney, D. M., and Hansen, W. R., 1979. Geologic map of the Dinosaur Quarry Quadrangle, Uintah County, Utah. U. S. Geological Survey Map GQ-1513.

Ryder, R. T., Fouch, U. D., and Elison, J. H., 1976. Early Tertiary sedimentation in the western Uinta Basin, Utah. Geological Society of America Bulletin 87:496-512.

Sabatka, E. F. (editor), 1964. Guidebook to the geology and mineral resources of the Uinta Basin — Utah's hydrocarbon storehouse. Intermountain Association of Petroleum Geologists 13th Annual Field Conference, 277 p.

Sadlick, W., 1955. Carboniferous formations in northeastern Uinta Mountains. *In:* Wyoming Geological Association Guidebook 10th Annual Field Conference — Green River Basin, p. 49-59.

———, 1956. Some Upper Devonian — Mississippian problems in eastern Utah. Intermountain Association of Petroleum Geologists, Geology and Economic Deposits of East Central Utah, 7th Annual Field Conference, p. 65-77.

Sales, J. K., 1969. Regional tectonic setting and mechanics of origin of the Uinta Uplift. Intermountain Association of Geologists 16th Annual Field Conference Guidebook — Uinta Mountains, p. 65-78.

Sanborn, A., and Goodwin, J., 1965. Green River Formation at Raven Ridge, Uintah County, Utah. Mountain Geologist 2(3):109-114.

Schell, E. M., 1969. Summary of the geology of the Sheep Creek Canyon Geological Area and vicinity, Daggett County, Utah. Intermountain Association of Geologists 16th Annual Conference Guidebook — Uinta Mountains, p. 143-152.

Seal, O. G. (editor), 1957. Guidebook to the Geology of the Uinta Basin. Intermountain Association of Petroleum Geologists 8th Annual Field Conference, 224 p.

Sears, J. W., Graff, P. J., and Holden, G. S., 1982. Tectonic evolution of lower Proterozoic rocks, Uinta Mountains, Utah and Colorado. Geological Society of America Bulletin 93:990-997.

Stewart, J. H., Poole, F. G., and Wilson, R. F., 1972. Stratigraphy and origin of the Chinle Formation and related Upper Triassic strata in the Colorado Plateau region. U. S. Geological Survey Professional Paper 690, 336 p.

Stokes, W. L., 1944. Morrison Formation and related deposits in and adjacent to the Colorado Plateau. Geological Society of America Bulletin 55(8):951-992.

Stokes, W. L., 1952. Lower Cretaceous in Colorado Plateau. American Association of Petroleum Geologists Bulletin 36(9):1766-1776.

Stokes, W. L., 1986. Geology of Utah. Utah Geological and Mineral Survey and Utah Museum of Natural History Occasional Paper No. 6, 280 p.

Thomas, H. D. and Krueger, M. L. 1946. Late Paleozoic and early Mesozoic stratigraphy of Uinta Mountains, Utah. American Association of Petroleum Geologists Bulletin 30(8):1255-1293.

Tidwell, W. D., 1990. Preliminary report on the megafossil flora of the Upper Jurassic Morrison Formation. Hunteria 2(8), 12 p.

Untermann, G. E., and Untermann, B. R., 1955. Geology of the eastern end of the Uinta Mountains, Utah-Colorado. *In:* Geology of Eastern Colorado, Intermountain Association of Petroleum Geologists 6th Annual Field Conference Guidebook, p. 18-20.

———, 1964 (revised 1968). Geology of Uintah County. Utah Geological and Mineral Survey Bulletin 72, 112 p.

———, 1969. Geology of the Uinta Mountain area, Utah-Colorado. Intermountain Association of Geologists 16th Annual Conference Guidebook — Uinta Mountains, p. 79-86.

Utah Geological Association, 1983. Road logs for energy resources and geologic overview of the Uinta Basin, 1983. Utah Geological Association Publication 12A, 35 pp.

Vaughn, R. L., and Picard, M. D., 1976. Stratigraphy, sedimentology, and petroleum potential of Dakota Formation, northeastern Utah. Rocky Mountain Association of Geologists 1976 Symposium — Cordilleran Hingeline, p. 257-280.

Wallace, C. A., and Crittenden, M. D., Jr., 1969. The stratigraphy, depositional environment, and correlation of the Precambrian Uinta Mountain Group, western Uinta Mountains, Utah. *In:* Lindsay, J.B. (editor), Geologic Guidebook of the Uinta Mountains. Intermountain Association of Geologists, 16th Annual Field Conference, p. 127-141.

White, T. E., 1964. The Dinosaur Quarry. Intermountain Association of Petroleum Geologists Guidebook, 13th Annual Field Conference, p. 21-48.

Williams, J. S., 1969. The Permian System in the Uinta Mountains area. Intermountain Association of Geologists 16th Annual Field Conference Guidebook — Uinta Mountains, p. 153-168.

Wiltschko, D. V., and Doer, J. A., Jr., 1983. Timing of deformation in overthrust belt and foreland of Idaho, Wyoming, and Utah. American Association of Petroleum Geologists Bulletin 67:1304-1322.

Yochelson, E. L., and van Sickle, D. H., 1968. Biostratigraphy of the Phosphoria, Park City, and Shedhorn Formations. U. S. Geological Survey Professional Paper 313-D:571-660.

Young, R. G., 1960. Dakota Group of the Colorado Plateau. American Association of Petroleum Geologists Bulletin 44(2):156-194.

STRATIGRAPHIC SECTION FOR THE EASTERN UINTA MOUNTAINS, UINTA BASIN, UTAH AND BRIDGER BASIN, WYOMING

By Sue Ann Bilbey
Utah Field House of Natural History
235 East Main
Vernal, UT 84078

PERIOD	EPOCH	FORMATION	DESCRIPTION
Quaternary	Holocene	Alluvium and colluvium	Silt, sand and gravel.
	Pleistocene	Alluvial fan, glacial and river terrace deposits	Silt, sand and gravel associated with identifiable geomorphologic deposits.
Tertiary	Miocene	Brown's Park	Tuffaceous sandstone, conglomerate, and limestone. K-Ar dates 25 to 10 Ma.
Tertiary	Oligocene	Bishop Conglomerate	Fluvial tuffaceous conglomerate, sandstone, and ash-fall tuff. Clasts mainly from the Uinta Mountain Group. K-Ar dates 41 to 26 Ma.
Tertiary	Oligocene? and Eocene	Duchesne River - four members	Fluvial and locally lacustrine rocks. Light red to red sandstone and conglomerate with light gray, tan, yellow sandstone, mudstone, and shale. K-Ar date is 40 Ma. Type locality for the Duchesnean Land Mammal Age.
Tertiary	Eocene	Unita (south side of the Uinta Mountains) - two or three members.	Variegated fluvial and lacustrine shale, marlstone, siltstone, and sandstone. K-Ar date is 43 Ma. Type locality for the Uintan Land Mammal Age.
Tertiary	Eocene	Bridger (north side of the Uinta Mountains)	Gray to variegated fluvial and lacustrine shale, mudstone, marlstone, and sandstone. Famous for Eocene mammals (Bridgerian Land Mammal Age).
Tertiary	Eocene	Green Fiver - numerous members.	Lacustrine and locally fluvial rocks - light gray to buff marlstone, oil shale, limestone, siltstone, sandstone, and conglomerate. Well known plant and insect localities in this area.
Tertiary	Eocene and Paleocene	Wasatch - several members	Fluvial with some lacustrine rocks - sandstone, claystone, shale, and conglomerate. Type locality for the Wasatchian Land Mammal Age.
Tertiary	Paleocene	Fort Union	Fluvial and lacustrine rocks - light gray to brown sandstone, shale, and claystone.
Cretaceous	Upper	Mesaverde Group - Williams Fork and Iles, Sego Sandstone, and Trout Creek Sandstone	Continental with minor marine beds - crossbedded sandstone, dark gray shale, and minor coal.
Cretaceous	Upper	Mancos (south) Hilliard or Baxter (north)	Medium to dark gary, yellow weathering marine shale and minor sandstone.

PERIOD	EPOCH	FORMATION	DESCRIPTION
Cretaceous	Upper	Frontier	Yellow and tan, fossiliferous, marine sandstone and minor continental carbonaceous shale and coal.
Cretaceous	Lower	Mowry	Silver-gray and bluish-bray siliceous marine shale and bentonite. Abundant fish scales. K-Ar date 97 Ma.
Cretaceous	Lower	Dakota	Yellow and light-gray crossbedded, littoral sandstone and conglomerate and minor shale and coal.
Cretaceous	Lower	Cedar Mountain	Two members of fluvial origin: lower discontinuous Buckhorn Conglomerate, upper lightly variegated shale, mudstone, limestone, and minor sandstone.
Jurassic	Upper Jurassic and Lower Cretaceous?	Morrison	Two members of fluvial origin: lower sandstones of the Salt Wash Member, upper claystone, limestone, and conglomerate of the Brushy Basin Member. Dinosaur fossils found in both members. K-Ar date of 135.2 ± 5.5 Ma for bentonite 11 m above the Dinosaur National Monument Quarry.
Jurassic	Upper	Stump/Curtis	Three members of marine origin: lower Curtis Member, fossiliferous, crossbedded sandstone; middle Redwater Shale, olive-green fissile glauconitic shale, oolitic limestone, fossiliferous; Windy Hill Member, intermittent, gray sandstone. Marine reptiles.
Jurassic	Middle	Entrada	Eolian, light gray to pink crossbedded sandstone. Near Manila contains reddish-brown siltstone (= Preuss formation?).
Jurassic	Middle	Carmel	Interbedded marine and continental beds of medium to dark red and green sandy shale, sandstone, mudstone, and light gray limestone and gypsum. Marine fossils and dinosaur footprints.
Jurassic/ Triassic	Lower	Glen Canyon Sandstone Navajo/Nugget Sandstone	Light gray to pink, eolian crossbedded sandstone with minor lacustrine, parallel bedded calcareous sandstones. Dinosaur footprints along lake shore.
Triassic	Upper	Chinle/Popo Agie	Continental deposits of darkly variegated siltstone, sandstone, shale, and conglomerate. Numerous reptilian footprints in the upper beds.
Triassic	Upper	Gartra Grit/Shinarump Member of Chinle	Light yellow to pink crossbedded fluvial sandstone and conglomerate, with fragments of petrified wood - *Araucaria.*

PERIOD	EPOCH	FORMATION	DESCRIPTION
Triassic	Lower	Moenkopi	Medium to dark red, green and gray, ripple-marked siltstone and shale, littoral origin with reptilian footprints.
Triassic	Lower	Dinwoody	Light to greenish gray, thin bedded shale, siltstone, sandstone, and minor limestone, marine in origin.
Permian	Lower	Park City	Light to greenish gray, locally fossiliferous siltstone, sandstone, dolomite, limestone, claystone, and phosphatic shale.
Permian and Pennsylvanian		Weber	Light gray to buff, crossbedded sandstone. Eolian and marine in origin. Major oil producer in the Vernal area.
Pennsylvanian	Middle	Morgan	Light red to gray, locally crossbedded sandstone and interbedded limestone, marine fossils.
Pennsylvanian	Lower	Round Valley	Light to medium gray to blue-gray limestone with interbedded light gray and red shale. Marine in origin with fossils and chert concretions.
Mississippian	Upper	Doughnut/Manning Canyon	Dark gray, green, and red clay shale and light gray to yellow sandstone and limestone, marine and continental in origin. Some plant imprints.
Mississippian	Upper	Humbug	Light gray to tan, pink to red, locally crossbedded sandstone, limestone, and red and black shale. Marine in origin.
Mississippian	Lower	Deseret	Medium gray limestone, breccia, cherty limestone, and dolomite. Marine in origin.
Mississippian	Lower	Madison	Tan to light to dark gray, locally fossiliferous, cherty marine limestone, some dolomite.
Cambrian	Middle to Upper	Lodore	Light brown to greenish-gray sandstone and pebble conglomerate: overlain by pink to tan to greenish-gray, fossiliferous glauconitic shale and crossbedded sandstone. Marine in origin.
Precambrian	Middle Proterozoic	Uinta Mountain Group	Light to dark red, crossbedded, locally pebbly sandstone and locally gray, green, and red silty shale. Marine and fluvial in origin. Rb-Sr shale date of about 1 billion years.
Precambrian	Early Proterozoic? and Late Archean	Red Creek Quartzite	White, gray, tan, and light-green metaquartzite, with quartz-muscovite schist, orthoamphibolite, and minor marble. Rb-Sr muscovite date of >2,300 Ma.
Precambrian	Archean	Owiyukuts Complex	Granitic and quartzofeldspathic gneiss. Rb-Sr isochron of 2,700 Ma.

—ROADLOG— VERNAL, UTAH TO DINOSAUR NATIONAL MONUMENT

Sue Ann Bilbey
Utah Field House of Natural History
235 East Main, Vernal, Utah 84078

INTRODUCTION

This road log originates in Vernal, Utah, and covers approximately 41 miles to the east and north to Dinosaur National Monument on the Utah-Colorado border. The course traverses Mesozoic and Cenozoic continental deposits with a rich paleontologic record and complex structural history. For additional road log information to the west and north from Vernal, see "Roadlog — Vernal, Utah, to Manila, Utah" (Bilbey and Hamblin, this volume). A brief history and comprehensive bibliography covering these two road logs and the general vicinity are presented in "Uinta Mountains and Basin — A Brief Historical Review and Selected Bibliography" (Bilbey, this volume). For a general stratigraphic section of this area, see "Stratigraphic Section for the Eastern Uinta Mountains, Uinta Basin, Utah and Bridger Basin, Wyoming" (Bilbey, this volume).

A map for this road log is presented in the "Introduction" (Gillette, this volume).

ROAD LOG

MILEAGE	CUMULATIVE	Description
0.0	0.0	Utah Field House of Natural History State Park in Vernal, Utah.
2.0	2.0	Asphalt Ridge at 3:00 — oil impregnates sandstones in the Mesaverde and Duchesne River formations. Red and maroon beds of the Upper Eocene Duchesne River Formation unconformably overlie the gray and tan beds of the Upper Cretaceous Mesaverde Formation.
1.7	3.7	Highway 40 turns east out of Naples, Utah.
2.0	5.7	Split Mountain at 10:00, Blue Mountain at 11:00. Driving in Ashley Valley (named for William L. Ashley, 1825 explorer) on Cretaceous Mancos Shale.
0.4	6.1	Relatively flat area in the middle distance to the northeast is the Quaternary Jensen pediment surface cut on the Mancos Shale. Pebbles in the gravel contain Paleozoic and Mesozoic fossils.
2.2	8.3	Ashley Valley oil field to the south at 2:00. Oil is produced from the Frontier, Morrison, Park City, and Weber formations. Oil field was discovered in shallow wells in 1925 (first commercial oil field in Utah), deeper wells in 1948. This is a structural play in the Weber Sandstone, an anticline that has no surface expression.
1.0	9.3	Bridge over Ashley Creek.
3.4	12.7	Junction with Utah Highway 149 in Jensen, Utah. Road north leads to Dinosaur National Monument (DNM).
0.6	13.3	Bridge over the Green River.
0.2	13.5	Turn left (north), bluff to the east is in the Frontier Sandstone. Local fossil collectors report abundant shark teeth in the ant hills on the Frontier.
1.4	14.9	Turn right onto dirt road, climb hill out of the Mancos onto the Frontier. Most of the hilltop is covered with Quaternary pediment deposits for the next 1.5 miles.
1.7	16.6	Stop 1. Walk along jeep trail to the top of

		the hill. In the distance to the north is Split Mountain Gorge, a westward-plunging anticline bisected by the Green River. Dinosaur National Monument lies north of the river. Morrison Formation is seen in the foreground south of the river (Brushy Basin Member to the west, Salt Wash Member to the east). Abundant dinosaur bone has been found in this area: Jensen/Jensen Quarry and the McStego Quarry.
3.9	20.5	Return to Jensen, turn north to Dinosaur National Monument.
2.5	23.0	Junction of Dinosaur National Monument road with the Brush Creek Road. This is the access road to the north side of Split Mountain.
1.7	24.7	Dinosaur National Monument entrance sign. This is the site of the Dominguez/Escalante crossing of the Green River in 1776. View to the east beginning north: Split Mountain anticline (south limb), Jensen syncline, Blue Mountain (Stuntz Ridge) monocline. See the enclosed cross section. Mancos shale is exposed in the "buckskin" hills along the road.
2.5	27.2	Turn left. Entrance to the Dinosaur National Monument Quarry. As you proceed up the hill to the quarry, you will be crossing this sequence of strata: Frontier Sandstone, Mowry Shale, Dakota Sandstone, Cedar Mountain Formation, and Morrison Formation.
0.7	28.1	Stop 2 — Dinosaur National Monument Quarry. It was discovered in 1909 by Earl Douglass of the Carnegie Museum, made a National Monument in 1915. Preserved in the Morrison Formation at this site are 12 species of dinosaur, a crocodile, and 2 turtles. Elsewhere in the Monument a variety of microvertebrates have been found. The view to the east from the parking lot looking north to south: Jurassic Navajo/Nugget, Carmel, Entrada, Stump/Curtis, Morrison, Cretaceous Cedar Mountain, Dakota, Mowry, Frontier, and Mancos formations.
0.7	28.8	Return to main road, turn left proceeding east toward campgrounds.
0.2	30.0	Swelter Shelter — Fremont Culture shelter (a very small cave) with petroglyphs in the Frontier Formation.
1.7	31.7	Intersection to Split Mountain Campground, turn left. Road cuts through Jurassic and Triassic rock as you proceed toward Split Mountain.
0.8	32.5	Scenic overlook at Split Mountain Gorge. Pennsylvanian Weber through Jurassic Navajo/Nugget formations.
0.2	32.7	STOP 3. Split Mountain Campground at the boat ramp. Take a closer look at the Weber Formation — primarily a cross-bedded sandstone, part of which has been identified as eolian. This is the primary oil producer at Ashley Valley and Rangely oil fields.
1.0	33.7	Back to the main road, proceed east.
1.2	34.9	Green River Overlook. Several Quaternary river terraces above the Green River; near the axis of the Jensen syncline; Morrison Formation to the south, excellent exposures of both members above the river.
1.2	36.1	Morrison Formation cross section cut by the Green River.
1.0	37.1	Bridge across the Green River. Placer mining has occurred several times at this bend in the river. Only gold flour has been recovered. Entrada Sandstone exposed in the cliffs above the river.
0.3	37.4	Stump/Curtis Formation at 3:00.
0.5	37.9	Morrison Formation is exposed along the road and in the mounds to the west.
0.4	38.3	Road turns east following very closely the axis of the Jensen syncline.
0.7	39.0	Entrada and Carmel formations exposed at 9:00.
0.5	39.5	Dinosaur National Monument boundary. At 6:00 view the race track of the Moenkopi Formation around the edge of Split Mountain.
0.1	39.6	Intersection. Turn left and cross Cub Creek.
0.2	39.8	Navajo/Nugget Sandstone in hills to the left and right. Elephant Toes Butte to the south shows excellent examples of cross-bedding and parallel truncation surfaces.
0.4	40.2	STOP 4. Petroglyphs at Cub Creek. Fremont petroglyphs are etched on the patina (desert varnish) of the Navajo/Nugget Sandstone. These petroglyphs are thought to date about 1000 AD. This is assumed because Fremont pit houses dating to that period have been excavated in this area.
0.2	40.4	Around the bend more petroglyphs are seen high on the cliff face of the Navajo/Nugget. Below them is the formational contact between the Navajo/Nugget and the Chinle/Popo Agie formations. Monument personnel report vertebrate bone fragments in the uppermost Chinle/Popo Agie. Elsewhere in DNM this interval has produced numerous vertebrate trackways as identified by Martin Lockley, Kelly

Conrad, and crew from University of Colorado, Denver.

0.2 40.6 Exposure of Gartra Grit/Shinarump along the left side of the road. Also three petroglyphs are seen above the arroyo.

0.1 40.7 To the north are box canyons formed in the Weber Sandstone. The phosphate-rich Park City Formation forms well-vegetated flat irons along the edge of the anticline. To the east are the Weber, Park City, Dinwoody?, Moenkopi, Gartra Grit/Shinarump from north to south.

0.5 41.21 STOP 5. Josie Morris cabin. Josie was a local character whose friends included Butch Cassidy and the Wild Bunch. She lived here late in her life until her death in 1964 at the age of 90. In 1953 she was named Rodeo Queen in Vernal. As is often found at the base of these box canyons, a spring provided Josie and her animals with fresh water.

Return to Vernal. If time permits, the personnel of Dinosaur National Monument will show the group an ongoing paleontological excavation.

—ROADLOG— VERNAL, UTAH TO MANILA, UTAH

Sue Ann Bilbey and Alden H. Hamblin
Utah Field House of Natural History
235 East Main, Vernal, Utah 84078

INTRODUCTION

This road log commences in Vernal, Utah, and follows a main highway route northward for 80 miles to Manila, Utah. The continuation of this road log is Evanoff (this volume) into southwestern Wyoming which readily connects to Interstate 80 and points west. This road log traverses Paleozoic and Mesozoic marine and continental sedimentary rocks with a rich and varied paleontological record. For additional road log information to the east from Vernal, see "Roadlog — Vernal, Utah, to Dinosaur National Monument" (Bilbey, this volume). A brief history and comprehensive bibliography covering these two road logs and the general vicinity are presented in "Uinta Mountains and Basin — A Brief Historical Review and Selected Bibliography" (Bilbey, this volume). For a general stratigraphic seciton of this area, see "Stratigraphic Section for the Eastern Uinta Mountains, Uinta Basin, Utah and Bridger Basin, Wyoming" (Bilbey, this volume).

A map for this road log is presented in "Introduction" (Gilette, this volume).

ROADLOG

MILES	CUMULATIVE	Description
0.0	0.0	Utah Field House of Natural History State Park, Vernal, Utah.
0.2	0.2	Intersection of US Highway 40 with US Highway 191, turn north (right).
3.6	3.8	Drive Through The Ages road sign. Through a cooperative effort between the U. S. Bureau of Land Management, U. S. Forest Service, and the Utah Field House of Natural History, signs have been installed along U. S. Highway 191 indicating the various geological formations encountered along the route.
0.1	3.9	Mancos Shale: thickness 5000 ft (1525 m), composed of soft, dark gray shale that weathers to light gray or tan. It forms the badlands between here and Jensen. The sediments represent deep-water clays and muds of a seaway that extended westward from near the Mississippi River to central Utah during middle and late Cretaceous time.
0.1	4.0	Frontier Formation: thickness 250 ft (76 m), forms the prominent ridge (hogback) running northeast-southwest from here. It consists of a basal sandstone unit overlain by shale, the top of which has some coal seams, and an upper fossiliferous sandstone unit. This unit contains cannonball concretions as large as 10 ft (3 m) in diameter. These sediments were deposited as beach sands, nearshore marine sands, and coastal swamp debris. Dinosaur tracks are occasionally found associated with interbedded coal and shale beds. Marine fossils, like ammonites and shark's teeth, can often be found by looking through ant beds along outcrops of the Frontier.
0.2	4.2	Stop 1. Mowry Shale: thickness 95-125 ft (29-38 m), K-Ar dates of 97-94 Ma. Dark gray siliceous shales which weather to

silvery-gray. The most distinguishing characteristic of the Mowry Shale is the abundance of scales and small bones of teleost fish. This shale was deposited on the sea bottom. The high content of silica is due to volcanic ash falls. These also may have been responsible for the dead fish. Identified types of fish are *Beryciforme* and *Aleposaurid,* both rare as complete specimens.

0.25 4.45 Dakota Sandstone: thickness 50 ft (15 m). Yellow and white pebbly sandstone with minor coal seams can be found, as well as varying amounts of silicified wood, ripple marks, and mud cracks. This formation is widespread, ranging from Montana to New Mexico and from central Utah to the Great Plains. The Dakota represents marine-nonmarine sediments deposited as the Mancos sea transgressed the area about 110 Ma.

0.25 4.7 Cedar Mountain Formation: thickness 100 ft (30 m). Conglomeratic sandstone and lightly variegated mudstone formed by stream and floodplain deposits. Fossil bones from two dinosaurs, a carnivore *(Deinonycus)* and an ankylosaur have been found in the Vernal area. This formation, originally named in central Utah, is sometimes difficult to distinguish from the underlying Morrison Formation.

0.3 5.0 Morrison Formation: thickness 800 ft (244 m). The Morrison Formation, graveyard of the dinosaurs, is a varicolored formation of mudstone, claystone, and shale, with interbedded sandstone, conglomerate, and limestone. Colors vary from white, gray and green to lavender and red. Its is a widespread formation, extremely heterogeneous in nature. It was deposited on a broad, low-lying plain by intermittent shifting streams, floodplains, and local lakes in a semi-arid to temperate climate. The dinosaur quarry at Dinosaur National Monument is attributed to accumulation through time of dead dinosaurs in a sand bar along a Morrison river.

0.8 5.8 Road to the left goes to Steinaker State Park.

4.2 10.0 Stop 2. Stump/Curtis Formation: thickness 15-260 ft (5-79 m). The Stump/ Curtis Formation is composed of interbedded marine sandstone, shale, and limestone. It is generally gray-green due to the occurrence of glauconite. It contains a number of invertebrate fossils, the most notable is the belemnite, *Pachyteuthis densis,* a cigar-shaped cuttlebone or guard of a squid-like animal. Bones of ichthyosaurs and pliosaurs, large marine reptiles, are occasionally found. Ripple marks and oyster beds are common, indicators of a warm shallow sea.

0.3 10.3 Entrada Sandstone: thickness 165-240 ft (50-73 m). This is a ridge-forming sandstone, white to pink or buff, which often weathers to round knobs. The Entrada here is barren of fossils and is composed primarily of wind-deposited sand dunes with a few interbedded red mudstone beds. Near Moab, Utah, it contains vast numbers of dinosaur footprints in the uppermost beds.

0.15 10.45 Carmel Formation: thickness 125-380 ft (38-116 m). The Carmel generally is found in depressions between ridges of the Entrada and Navajo Sandstones where bedding is tilted. This weak, non-resistant formation is composed of sandy shale, fine-grained sandstone, mudstone with minor gypsum and limestone. These beds vary from reddish-brown to light gray and green. The occurrence of dinosaur footprints and marine shellfish reveal an eastern marine shoreline of a northern seaway.

0.05 10.5 Intersection with road to Red Fleet Reservoir. Turn right.

2.0 12.5 Stop 3. Red Fleet Reservoir. This reservoir was established as part of the Central Utah Project. A paleontological survey noted that sensitive formations would be impacted by the seasonal water level variation. This has become increasingly important with the discovery of dinosaur tracks in the Navajo/Nugget Sandstone, in the Carmel Formation, and in the Frontier Formation near or along the lake shore. In addition each autumn new dinosaur bone and plant material are exposed in the Morrison Formation as the water level drops.

2.0 14.5 Return to US Highway 191, turn right.

0.2 14.7 Navajo/Nugget Sandstone (also Glen Canyon): thickness 700-1000 ft (213-305 m). Former sand dunes with related oases are preserved in this cross-bedded unit. North and northwesterly winds in a desert environment deposited quartz sand in dunes over most of the intermountain west. Rare oases or lakes were watering holes, as proved by abundant dinosaur tracks at the site on Red Fleet Reservoir. This formation is well represented state wide in many of our National Parks, Monuments, and State Parks as impressive domes, arches, and canyons.

0.5 15.2 Chinle/Popo Agie Formation: thickness 235-276 ft (72-84 m). Continental deposits (streams, lakes, and soils) influenced by volcanic activity are represented in this formation. Variegated shale, sandstone, and conglomerate preserve petrified wood, phytosaur remains, and reptilian footprints of several types. Similar deposits are represented at Petrified Forest in Arizona.

0.1 15.3 Shinarump Conglomerate/Gartra Grit: thickness 28-75 ft (8-23 m). This set of buff to yellow cross-bedded conglomerate and coarse sandstone beds was formed by braided stream deposition. Erosion of the underlying Moenkopi, as identified by a slight angular unconformity, is seen at the base of the conglomerate.

0.4 15.7 Moenkopi Formation: thickness 800-900 ft (244-275 m). This strata was deposited on periodically exposed mudflats associated with a western seaway. Dark to brick red shale, siltstone, and sandstone beds are predominant with minor occurrences of thin interbeds of gypsum and grayish green siltstone. Fossil footprints (probably from a phytosaur) are occasionally found.

1.5 17.2 Park City Formation: thickness 144 ft (44 m). The Park City Formation is composed of gray to white cherty limestone, some red to white sandy shale, and a 17-20 ft (5-6 m) layer of phosphate rock at the base. It is of marine origin, with the shoreline somewhat east of here. The phosphate beds were formed along the margin of a continental shelf by upwelling currents of organic-rich water.

1.8 19.0 Chevron Resources Co. Vernal phosphate operation. The basal unit of the Park City Formation is being mined for fertilizer. The phosphate is pumped in a slurry over the Uinta Mountains to Rock Springs, Wyoming. The company has provided an overlook point to see this operation.

2.1 21.1 Stop 4. Windy Point Geological turnout. Excellent viewpoint for the Mesozoic of eastern Utah. Large red exposures of the Shinarump protrude above the landscape suggesting battleships — the "Red Fleet."

0.4 21.5 Ashley National Forest Sign

1.4 22.9 Weber Formation: thickness 1000 ft (305 m). The Weber Formation is a thick, buff to light gray cross-bedded sandstone. Because it is poorly cemented and highly jointed, erosion tends to cut deep, steep-walled canyons in it, creating some of the major scenic attractions in the area. The sandstone was deposited primarily as beach and windblown dune deposits. The Ashley oil field, about 8 mi (13 km) southeast of Vernal, and the Rangely oil field in eastern Colorado produce from the Weber.

1.2 24.1 Red Cloud Loop Turnoff to the left. Notice the mountain tops in this area, most are flattened and imply an extensive erosional surface, the Gilbert Peak erosional surface.

2.0 26.1 Morgan Formation: thickness 1400 ft (427 m). As seen along this drive, this unit includes both the Morgan and Round Valley formations. In is composed of alternating red to gray fine-grained sandstone, limestone, and red to lavender shale. Some beds are quite fossiliferous. Mud cracks and ripple marks are fairly common. It shows variation from nearshore shallow to deep water marine deposition.

2.5 28.6 Madison Limestone: thickness 100 ft (30 m). Several formations have been combined as members of what is shown as the Madison Limestone along this roadway. These are the Doughnut/Manning Canyon, Humbug, Deseret, and Lodgepole formations, in descending order. These consist of limestone, dolomite, sandstone, and dark colored shales. Numerous caves have formed in some of the limestone layers. Fossils include gastropods, crinoids, brachiopods, and corals which indicate deposition in a shallow nearshore marine environment.

There is a major hiatus at the base of the Mississippian rocks in the Uinta Mountains, with the Ordovician, Silurian, and Devonian periods missing. This hiatus suggests either a period of nondeposition or that rocks were deposited but subsequently eroded away prior to Mississippian time.

0.6 29.2 Lodore Formation: thickness 155-450 ft (49-137 m). Although not well exposed along the highway, the Lodore Formation is seen as white to red, green, and gray siltstone and sandstone interlayered with green and red shale. Portions of this formation were deposited in a marine environment as evidenced by the occurrence of brachiopods and rare trilobites.

6.1 35.1 Uinta Mountain Group: thickness 12,000 to 24,000 ft (3660-7220 m). These rocks make up the core of the Uinta Mountains and are the oldest rocks seen along the highway. The Uinta Mountain Group is composed of red, lavender, and buff sandstone and conglomerate with interbedded red to green shale. These rocks have been

		partially metamorphosed, with the sandstone becoming quartzite in some areas. The Uinta Mountain Group was deposited in streams and rivers along an east-west-trending rift valley (an aulacogen). Marine incursions may be recorded in some of the shale beds. Fossils are very rare, although some very ancient life forms have been found. During the Laramide orogeny east-west compression reactivated the Precambrian fault system, thrusting the entire sequence eastward and upward to form the Uinta Mountains.
5.0	40.1	Junction with US Highway 191 and Utah Highway 44. Continue west toward Manila, Utah on Highway 44.
3.5	43.6	Junction to Red Canyon Overlook, turn right.
2.6	46.2	Stop 5. Red Canyon Visitor's Center. Exposed in the Red Canyon below the visitor's center are 1400 ft (427 m) of the Uinta Mountain Group. The lake at the bottom of the canyon is Flaming Gorge Reservoir. It extends nearly 80 miles (128 km) along the course of the Green River from Wyoming into Utah.
1.0	47.2	Turn left to Canyon Rim.
0.3	47.5	Stop 6. Red Canyon Overlook Picnic area, Lunch. Similar vistas to those seen at the visitor's center.
2.0	49.5	Return to Utah Highway 44. Turn right (west).
1.5	51.0	Dowd Mountain turnoff to the right.
0.8	51.8	Turnoff to Sheep Creek Geologic Area. Turn left. This area was designated as National Geological Area on May 13, 1962. Along the route through Sheep Creek as much as 2 billion years of geologic history can be viewed.
5.6-6.7	57.4-58.5	Views of the uppermost 3,000 to 4,000 ft (915-1220 m) of Precambrian Uinta Mountain Group metasediments in the canyon to the west and Uinta fault. The mottled red and white sandstone probably lost most of its color due to leaching by water. Precambrian rocks are thrust up next to Mississippian rocks. The Uinta fault zone includes Mississippian and lower Pennsylvanian rocks. Drag on the north-easterly side tilted most of the Mississippian and Pennsylvanian rock to a nearly vertical configuration. Away from the fault zone the strata gradually flatten.
0.8	59.3	Stop 7. Palisade Park. The canyon floor is covered with considerable debris due to spring flooding. Seven people who were camping here were killed by one of these floods on June 10, 1965. One of the bodies was never found.
0.3	60.3	Uinta Fault Zone: Precambrian-Mississippian contact to left.
0.2	60.5	At 9:00 Pennsylvanian Round Valley in fault contact with Mississippian rocks near the western terminus of Uinta fault zone.
0.1	60.6	In road cut to the right, black shales of the Doughnut/Manning Canyon Formation. Generally this formation is covered by vegetation.
0.1	60.7	Morgan-Round Valley gradational contact. Round Valley Formation: thickness 400 ft (122 m), light- to medium light-gray, thick to massive bedded nodular limestone. Both of these formations contain numerous marine fossils like brachiopods, coral, and crinoids.
0.2	60.9	Bridge over Sheep Creek. During September this is an excellent spot to watch the Kokanee salmon run to their spawning grounds along upper Sheep Creek. As with other salmon their appearance during this time of their lives changes dramatically — they become bright red and form deeply hooked jaws.
0.4	61.3	Weber-Morgan contact beneath the upper massive tan sandstone and at top of the grassy slope. Morgan Formation: thickness 120 ft (37 m), composed of red and purple shale and thin limestone.
0.4	61.7	Tower Rock (Weber Formation) at 12:00.
0.7	62.8	Ashley National Forest boundary. Park City Formation at 9:00.
0.1	62.9	Ranch house on the left. Weber Formation: thickness 1560 ft (476 m).
0.3	63.2	Park City, Moenkopi, and Shinarump formations at 7:00. Park City Formation: thickness 400 ft (122 m). The Meade Peak Phosphatic Shale: thickness 48 ft (15 m), but contains only low grade ore. The brilliant red color of the Moenkopi Formation as seen by John Wesley Powell prompted him to name this section of the Green River, Flaming Gorge.
0.8	64.0	At 3:00 Shinarump underlying Chinle/Popo Agie, at 9:00 massive Navajo/Nugget Sandstone.
0.1	64.1	Driving on Chinle/Popo Agie. At 4:00, anomalously greenish-gray mudstones of the Triassic Moenkopi Formation (thickness 725 ft, or 221 m) are underlain by Permian Park City Formation (thickness 330 ft, or 101 m).
0.4	64.5	Sheep Creek Bridge.

0.5	65.0	Carmel Picnic area.
0.5	65.5	Carmel-Navajo/Nugget contact.
0.5	66.0	Jurassic section exposed at 12:00. Stump/Curtis is at the top of the ridge, top of the Entrada is at the top of the uppermost red shale. Top of the Carmel below the massive yellow sandstone. Somewhere in these Jurassic rocks of Sheep Creek Canyon O. C. Marsh collected the first Jurassic reptilian bone (a crocodile — ***Diplosaurus nanus*** femur) found in this area in 1870.
0.1	66.1	Intersection with Highway 44, turn left.
0.2	66.3	Carmel Formation: thickness 320 ft (98 m) at 9:00.
0.2	66.5	Entrada Sandstone: thickness 220 ft (67.1 m) at 9:00 underlain by the Jurassic Carmel Formation.
0.4	66.9	Stump/Curtis Formation: thickness 180 ft (55 m) at 9:00.
1.0	67.9	Morrison Formation along the road way, although generally covered with vegetation.
0.3	78.2	Dakota-Morrison contact in road cut. Morrison Formation: thickness 920 ft (281 m). Carbonaceous layers are part of the Dakota Formation in the road cut.
0.3	78.5	Dakota-Mowry contact. Dakota Formation: ranges in thickness from 130 ft to 250 ft (40-76 m). Nearby petroleum exploration has found abundant gas in the Dakota.
0.1	78.6	Frontier-Mowry contact. Mowry Formation: thickness 200 ft (61 m).
0.1	78.7	Frontier-Mancos/Hilliard/Baxter contact. Numerous similarities can be found between the Mancos, Baxter, and Hilliard formations. All are deposits from the same epicontinental seaway in the Cretaceous. Correlation is sometimes difficult due to the Uinta uplift.
0.1	78.8	Frontier dip slope at 4:00. The Upper Cretaceous Frontier Formation: thickness ranges from 190 ft to 260 ft (58-79 m).
0.8	79.6	A good view of the Mesaverde "racetrack" at 3:00. This phenomenon is due to differential erosion of sedimentary rocks along the south side of the Uinta Mountain arch.
0.9	80.5	Manila, Utah. END OF ROAD LOG.

—ROADLOG—
MANILA, UTAH, TO FORT BRIDGER, WYOMING, ALONG UTAH 43 AND WYOMING 414. THE BRIDGER FORMATION OF THE BRIDGER BASIN

Emmett Evanoff and Logan D. Ivy
Geology Section, University of Colorado Museum
Boulder, CO 80309-0315

INTRODUCTION

The road from Manila, Utah, to Fort Bridger, Wyoming, runs along the north edge of the Uinta Mountains and into the Bridger Basin (southern Green River Basin; Figure 1). Along almost its entire length, the road crosses one of the most fossiliferous middle Eocene continental deposits in North America, the Bridger Formation. The Bridger is famous for its vertebrate fossils (especially turtles and mammals), but it also contains nonmarine mollusks, plants, and stromatolites. Fossils have been collected in the region for more than 130 years, and Bridger Basin specimens are housed in almost every major museum in the United States. The accompanying roadlog emphasizes the stratigraphic and historic features of this region. This roadlog is a continuation of the roadlog contained in "Roadlog — Vernal, Utah, to Manila, Utah" (Bilbey and Hamblin, this volume), which commenced in Vernal, Utah.

HISTORY OF WORK IN THE REGION

A list of collectors in the Bridger Basin prior to 1900 reads like a *"Who's Who"* of early American vertebrate paleontologists. Fossil bones were found in the area prior to the Civil War, but the first specimens to be described were collected by Dr. J. Van A. Carter and described by Joseph Leidy (1869). O. C. Marsh of Yale University was the first vertebrate paleontologist to visit the area, bringing his field school to the Bridger Basin in 1870, 1871, and 1873. Many of the specimens Marsh described in his Dinocerata monograph (1886) came from these explorations. The 1870 Hayden Survey also visited the region and F. V. Hayden named the Bridger Formation in his report on this expedition, published in 1871. E.D. Cope and Joseph Leidy visited the area in 1872, and Cope returned in 1873. Princeton University expeditions lead by H. F. Osborn and W. B. Scott collected in the Bridger Basin in 1877 and 1878, and Scott returned in 1886. Jacob Wortman collected in the region in 1893.

The first studies to relate vertebrate fossils to the detailed stratigraphy of the Bridger Formation were done by the American Museum of Natural History (AMNH) expeditions of 1903 to 1906 that were led by Walter Granger, W. J. Sinclair, and W. D. Matthew. Matthew's 1909 memoir set the stage for all subsequent stratigraphic studies of the Bridger, and his informal units A-E are still used today (Figure 2). Largely relying on this work, H. E. Wood (1934) divided the Bridger Formation into the Blacks Fork and Twin Buttes members based on a major faunal break in the middle of the formation.

From the 1930s to the late 1960s, researchers from the U.S. National Museum (USNM) led episodic collecting expeditions in the Bridger Basin. The most intensive effort was by C. L. Gazin from 1941 to 1969, which produced one of the more extensive collections of Bridgerian age mammals. In the 1970s, R.M. West, L. Kristalka, and crews from the Milwaukee Public Museum collected Bridger Basin microfaunanas by screen washing. Previously this portion of the fauna had not been well sampled.

Many researchers have collected fossils from the Bridger Basin over the years, often while enroute to other areas of interest. As a result, many museums and universities have vertebrate collections from the Bridger Basin. Institutions

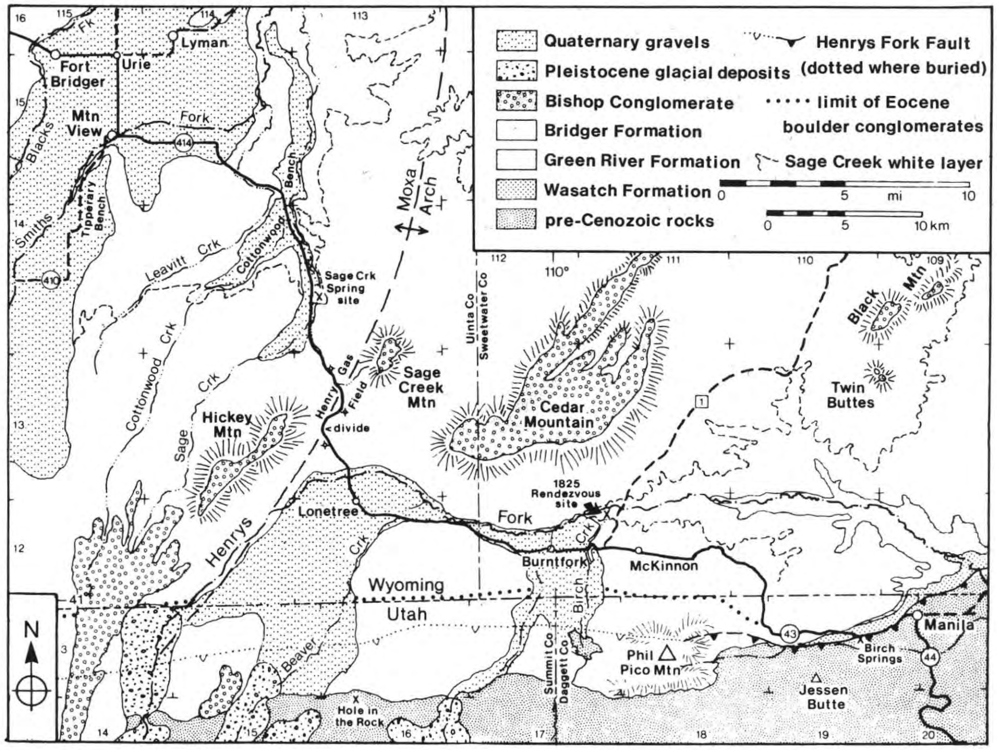

Figure 1. Map of the Bridger Basin showing the geologic and geographic features discussed in the roadlog. Adapted from Bradley (1961), Love and Christiansen (1985), and Rowley et al. (1985).

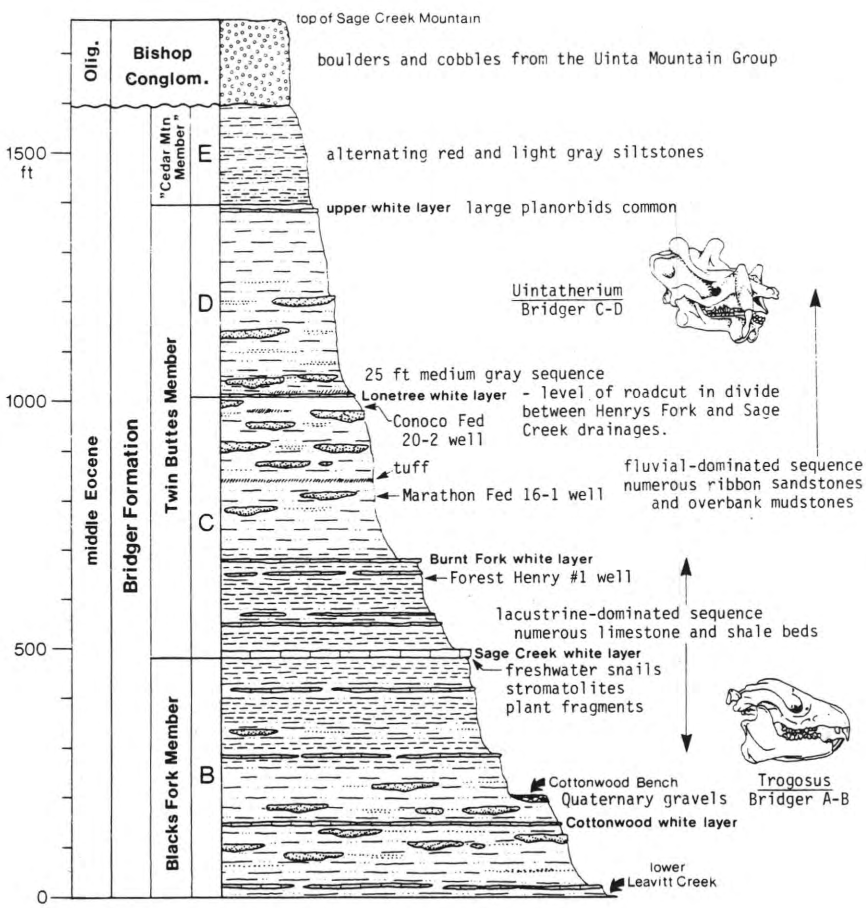

Figure 2. Diagrammatic columnar section of the Bridger Formation exposed from Sage Creek Mountain to the base of Leavitt Creek.

that have Bridger Basin collections that are known to the authors include the AMNH, Burke Museum (University of Washington), University of California (Berkeley and Riverside), University of Colorado (Boulder), Cranbrook Institute (Michigan), University of Kansas, University of Michigan, Harvard Museum of Comparative Zoology, USNM, University of Wyoming, and Yale Peabody Museum.

SUMMARY OF BRIDGER FORMATION GEOLOGY

The Bridger Formation is a thick sequence of fluvial and lacustrine volcaniclastic mudstones, sandstones, and limestones. Green and brown smectitic mudstones and shales are the most common lithology. The smectite in the mudrocks is from the weathering of volcanic glass, and the mudrocks typically form rounded badland slopes mantled with "popcorn" surfaces. Some of the shales are carbonaceous and contain plant fossils, and all mudrocks contain vertebrate fossils. The sandstones represent channel deposits and contain well-preserved lateral-accretion deposits indicating high-sinuosity streams. The mineralogy of the sandstones also suggests a volcanic source (Sinclair, 1906; Bradley, 1964). Bones are common in many of these sandstones, especially in point-bar deposits. Limestones are volumetrically small but are areally widespread. Some limestone beds support benches, and are the marker beds or "white layers" of Matthew's (1909) informal stratigraphic units. Most of these limestones contain abundant freshwater snails, and several contain microvertebrates. Thin, widespread fall-out tuffs also occur, but have not been used as marker-beds by previous workers. Fluvial-dominated intervals, characterized by abundant ribbon sandstones and mudstones, alternate with lacustrine-dominated intervals, characterized by limestones and shales. Areally, lacustrine rocks are more common in the eastern part of the route while fluvial rocks are more common in the northwest part. The general stratigraphic sequence of lithologies in the Sage Creek Mountain/ Leavitt Creek areas is shown in Figure 2.

The total thickness of the Bridger Formation ranges from 1,560 ft (475 m) in the Twin Buttes area to over 2,285 ft (696 m) in the Sage Creek Mountain area (Bradley, 1964). The Bridger Formation was deposited over a 2 m.y. interval (between 49.5 and 47.5 Ma, McKenna et al., 1974; West and Hutchison, 1981). Thus, the rock accumulation rate in the Sage Creek Mountain area (1.14 ft/k.y.; 0.35 m/k.y. is one of the highest in the Eocene record of the Rocky Mountains. The volcanic sediment in the Bridger was derived from the contemporaneous Absaroka volcanic field in northwest Wyoming (Bradley, 1964; West, 1976). The volcanic debris choked the streams in the Green River Basin, and prevented the Green River lakes from forming despite a time of rapid subsidence in the basin.

ACKNOWLEDGMENTS

We thank Mary L. Gillam and Kenneth Carpenter for reviewing the manuscript, and Holly Cunningham of the Wyoming State Geological Survey for providing information on the natural gas wells in the Henry Field.

ROADLOG

This roadlog originates in Manila, Utah, and ends 54 miles (87 km) further, in Fort Bridger, Wyoming. It is a continuation of the Vernal to Manila road log (Bilbey and Hamblin, this volume) which traverses 80 miles (129 km) of Mesozoic and Paleozoic exposures in northeastern Utah.

Mileage	Cumulative	Description
0.0	0.0	Junction of Utah 44 and 43, Manila. Turn left (west).
0.6	0.6	Manila town line. Road turns left onto the Henrys Fork fault. Cliffs to the north (right) are steeply dipping conglomerates and sandstones of the lower Eocene Wasatch Formation. Lucerne Valley to the south (left) is underlain by the Upper Cretaceous Hilliard (Baxter/Mancos) Shale. The Henrys Fork fault thrust the Hilliard Shale northward onto the Wasatch Formation, with a local displacement of about 4,000 feet (1,220 m) (Hansen, 1965). The Henrys Fork fault was active during the early Eocene, as indicated by angular unconformities in the Wasatch Formation along the mountain front. Straight ahead and across Lucerne Valley is Jessen Butte, with the Nugget (Glen Canyon) Sandstone exposed at the top.
2.1	2.7	Right curve at Birch Spring Ranch. Road leaves the Henrys Fork fault and climbs up the Wasatch ridge. The conglomerates in the Wasatch show a classic unroofing sequence with pieces of petrified wood derived from the Morrison and Dakota formations at the base, and limestone cobbles and boulders derived from the Curtis, Morgan, Round Valley, and Madison formations at the top. The upper Wasatch here interfingers with the Laney Member of the Green River Formation, and contains thin laterally persistant limestones. These limestones contain freshwater mussels *(Plesielliptio* spp.), freshwater snails *(Goniobasis* sp.), and freshwater ostracodes *(Candona* sp. and *Cypridea* sp.). The rather indistinct contact between the Wasatch and the middle Eocene Bridger Formations is at the top of the ridge.
2.3	5.0	Milepost 3, on the divide between Antelope Hollow (to the north) and Birch Spring Draw (to the south). Straight ahead is Phil Pico Mountain (el. 9,575 ft, 2,918 m), com-

posed of about 1,450 ft (442 m) of unnamed lower and middle Eocene conglomerates. The conglomerates interfinger with the Wasatch, Green River, and Bridger formations. These conglomerates include boulders as much as 10 feet (3 m) in diameter, derived primarily from Paleozoic and Mesozoic units in the northern Uintas. Clasts from the Uinta Mountain Group do not occur except near the top. The conglomerates occur along the mountain front but do not extend for more than about 6 miles (9.7 km) northward from the mountain front.

2.9 7.9 Utah-Wyoming state line; Utah 43 becomes Wyoming 414. The buttes in the distance to the north (at 1:00) include Black Mountain (covered with trees) on the left, and Twin Buttes on the right. The buttes are capped by the upper Oligocene Bishop Conglomerate, and have extensive badland exposures of the Bridger Formation on their flanks. These buttes are the type area for the Twin Buttes Member (Bridger C and D) of the Bridger Formation.

1.4 9.3 Milepost 139. Straight ahead (to the northwest) is Cedar Mountain (el. 8,580 ft, 2,615 m), a broad mesa capped by the Bishop Conglomerate. The Bishop is a widespread conglomeratic unit containing abundant clasts derived from the Uinta Mountain Group. The conglomerate has not produced fossils, but biotite and hornblende from interbedded tuffs on the south side of the Uintas have yielded fission track ages of about 29 Ma (Hansen, 1986). The Bridger Formation underlies the Bishop Conglomerate, and is well exposed in the badlands below the cap. In Matthew (1909), Cedar Mountain was called Henrys Fork Table.

5.1 14.4 The community of McKinnon. The benches in this area are covered by Quaternary gravels derived from the Uinta Mountains and Tertiary conglomerates.

1.4 15.8 Junction of Wyoming 414 with road to Green River (Converse County Road 1). Continue ahead on 414.

0.5 16.3 Road cut on left (milepost 132) exposing mudstones and sandstones of the Bridger Formation. The bluff is capped by Quaternary gravels. The stream at its base is Birch Creek, a southern tributary of the Henrys Fork. The first Rocky Mountain trappers' rendezvous (June and July, 1825) was held near the junction of Birch Creek and Henrys Fork, about 1.5 miles to the northeast.

1.3 17.6 State historical marker about the 1825 Rocky Mountain Rendezvous.

0.4 18.0 The community of Burntfork.

2.7 20.7 Sweetwater County/Uinta County line. The white unit in the bench near the base of Cedar Mountain (to the north) is the Lonetree white layer. This layer is a thin sequence of tuffs and lacustrine limestones which Matthew (1909) used to separate the Bridger C (below) from the Bridger D (above). Straight ahead at the skyline is Hickey Mountain (el. 8,817 ft, 2,687 m), another mesa capped with Bishop Conglomerate.

2.7 23.4 Milepost 125. To the north (4:00) near the skyline and on the west end of Cedar Mountain is a thick sequence of alternating red and gray layers of the uppermost Bridger Formation, the Bridger E of Matthew (1909) or the "Cedar Mountain Member" of West and Hutchison (1981). This member is composed of alternating red and orange-banded siltstones interbedded with gypsum layers. Fossils are rare in these rocks, but include turtles and mammals of the Bridgerian Land Mammal Age (West and Hutchison, 1981). These outcrops on the west end of Cedar Mountain are the type section for the member. The Twin Buttes Member (Bridger C and D) occurs below the Bridger E, and includes the gray rocks exposed in the badlands between the lowest red bed and the Henrys Fork.

1.5 24.9 Junction with Hole in the Rock Road (Uinta County 295) on the south (left) side. Hole in the Rock is a small arch in the Madison Limestone about 7 miles (11 km) to the south. The highest conical peak to the southwest (10:00) is Gilbert Peak (el. 13,442 ft, 4,097 m). Gilbert Peak is supported by Proterozoic arkoses of the Uinta Mountain Group. The road is on outwash gravels derived from Pinedale glaciers which extended to the base of the mountain front. The terminal moraines of one of these glaciers can be seen directly below Gilbert Peak, as the tree-covered ridge at the mouth of the valley 8 miles (13 km) to the southwest.

1.6 26.5 Lonetree, Wyoming. The combined post office-store was founded in 1897 but closed in 1982. Hickey Mountain is straight ahead, Sage Creek Mountain (el. 8,454 ft, 2,557 m), a high butte capped by Bishop Conglomerate, is to the north (at 1:30). Sage Creek Mountain was also called "Big Bone Butte" by O. C. Marsh because of the abundance of *Uintatherium* bones in the badlands on its flanks.

1.3 27.8 Bridge across Henrys Fork Creek (milepost 120.61). The Lonetree white layer caps the near ridges straight ahead and to the left (west).

1.7 29.5 Milepost 119. OPTIONAL STOP. To the left (west) is the Conoco Fed 20-2 natural gas well. The well is one of the southernmost in the Henry Field, which produces gas from the Dakota Sandstone on the southwest end of the Moxa Arch. The arch is buried under early Tertiary rocks which are essentially horizontal at the surface. This well was drilled to the Morrison Formation at a depth of 13,950 ft (4,252 m), and produces from the Dakota at a depth of 13,760 ft (4,194 m).

The road is just below the Lonetree white layer, at the base of the Bridger D. The square-topped butte beyond the gas well near Hickey Mountain is almost at the top of the Bridger D. The white bench at the base of the square-topped butte is the upper white layer of Matthew (1909), and contains abundant shells of the large planorbid snail *Biomphalaria pseudoammonius* (Schlotheim).

The road will enter a roadcut through the divide between the Henrys Fork drainage and the Sage Creek drainage. This is the highest stratigraphic position the road reaches in the Bridger Formation — at the level of the Lonetree white layer. The road drops into badlands of the upper Bridger C, which is composed of brown tuffaceous mudstones interbedded with scattered green ribbon sandstones. The mudstones are fluvial overbank deposits and the sandstones are channels deposits. The mudstones support rounded hills covered by a "popcorn" surface formed by the weathering of smectitic clays. The channel sandstones show paleoflow to the southeast. The badlands in this area include the classic Lonetree localities of Matthew (AMNH expeditions of 1903-1906) and Gazin (USNM expeditions between 1941 and 1969).

1.6 31.1 Approaching the road to Marathon Fed 16-1 natural gas well on the right (east) side of the road. OPTIONAL STOP. Sage Creek Mountain is straight ahead (to the northeast). About 800 ft (244 m) of Bridger rocks are exposed in these badlands. The upper part of the Bridger C extends from the road to the Lonetree white layer, the prominent white band in the lower middle ground at the base of the lowest juniper trees. The Bridger D extends from the Lonetree white layer to the base of the first red bed high on Sage Creek Mountain. The Bridger E extends from the red-beds to the base of the Bishop Conglomerate which caps Sage Creek Mountain.

1.9 33.0 Forest Oil Henry Unit #1 natural gas well to the right (northeast) next to the road. The thin prominent ledge behind the well and just above the holding tanks is a thin but widespread cherty limestone in the middle of the Bridger C. This is probably the Burnt Fork white layer of Matthew (1909), and marks the top of the lacustrine part of the Bridger C. This lacustrine sequence is characterized by brown shaly claystones and widespread thin limestones (white layers), with few interbedded channel sandstones and overbank mudstones. Around the corner to the north is a second, laterally discontinuous limestone layer about 20 ft (6 m) below the Burnt Fork white layer.

3.0 36.0 Junction with graded dirt road to Forest Oil Henry Unit to the east (right). Thick white limestone outcrop below the highway and across Sage Creek (at 2:00) is the Sage Creek white layer, the boundary between the underlying Blacks Fork Member (Bridger A and B) and the overlying Twin Buttes Member. This outcrop was next to Sage Creek Spring along the old Lonetree stage road, and was photographed and described by Sinclair (1906). The Sage Creek white layer here is a 13 ft (4 m) sequence of alternating lacustrine limestones and carbonaceous shales. The limestones contain freshwater snails (planorbids, lymnaeids, and physids), plant fragments, stromatolites, and scattered vertebrates (mostly turtles). Bradley (1961) mapped this limestone throughout the southern Bridger Basin, where it covers approximately 600 square miles (1,550 square km). The rim (below the highest butte) to the northeast is supported by the Burnt Fork white layer. Three other limestone layers occur between the Burnt Fork and Sage Creek white layers in the lacustrine-dominated lower part of the Bridger C.

3.3 39.3 Bridge over Cottonwood Creek (milepost 109.15). The bluffs to the east (right) expose the upper part of the Bridger B, with the Sage Creek white layer supporting the bench at the skyline. Channel sandstones are rare and two discontinuous limestone layers occur in these outcrops, indicating a lacustrine-dominated sequence. The road rises slightly onto the Cottonwood Bench, which is supported by Quaternary gravels derived from the Uinta Mountains and the Bishop Conglomerate.

1.1 40.4 Milepost 108. The road turns left and drops off the Cottonwood Bench into the badlands of Leavitt Creek. The badlands are developed in the lower and middle parts of the Bridger B. Channel sandstones and overbank mudstones are common, indicating a fluvial-dominated sequence.

2.0 42.4 Milepost 106. The badland buttes to the west (10:00) include the middle and lower parts of the Bridger B. The Bridger B is well exposed along the north-trending panel of badlands to the northeast (right) that includes the type area for the Blacks Fork Member on its north end.

1.9 44.3 Junction with Uinta County Road 253 to right (north) just after the road turns to the left. Road crosses onto the Quaternary gravels of the Smiths Fork. Butte at the skyline at 11:30 is Tipperary Bench, capped by Pleistocene gravels on mudstones and sandstones of the Bridger B. H.E. Wood (1934, p. 241) identified this bench as the "Grizzly Buttes" of early collectors. The American Museum of Natural History expeditions of 1903-1906 collected thousands of vertebrate specimens from the lower Bridger B at Grizzly Buttes, including many nearly complete skulls and skeletons.

3.9 48.2 Junction of Wyoming 414 and 410 in Mountain View just across the Smiths Fork bridge. Continue north on 414 across Quaternary deposits of the Smiths Fork.

3.2 51.4 Junction of Wyoming 414 and I-80 business loop in Urie. Turn left (west) on I-80 business loop. Road is on bench supported by Quaternary gravels of the Smiths Fork, and drops off to the valley of the Blacks Fork. The large mesa on the skyline at 11:00 (after the turn) is Bridger Butte, capped by Quaternary gravels with the Bridger B exposed on its flanks.

2.5 53.9 Town line of Fort Bridger. Fort Bridger was founded in 1843 by Jim Bridger and Louis Vasquez along the emigrant trail to Oregon, California, and Utah. The fort was an important stop for the geographical and geological expeditions of Stansbury (1849), Simpson (1859), King (1869), and Hayden (1870). O. C. Marsh of Yale brought his field classes to Fort Bridger in 1870, 1871, and 1873 to collect in the Bridger Formation along our route. E. D. Cope and Joseph Leidy collected in the area in 1872. Marsh's influence with the fort's personnel resulted in Cope being lodged in the government hay yard. The fort was closed by the War Department in 1890. The original fort, on the west side of town, is a state historical site and has been partially reconstructed.

REFERENCES

Bradley, W. H. 1961. Geologic map of a part of southwestern Wyoming and adjacent states. U. S. Geological Survey, Miscellaneous Geologic Investigations Map I-332, scale 1:250,000.

——. 1964. Geology of Green River Formation and associated Eocene rocks in southwestern Wyoming and adjacent parts of Colorado and Utah. U. S. Geological Survey Professional Paper 496-A, 86 p.

Hansen, W. R. 1965. Geology of the Flaming Gorge area, Utah-Colorado-Wyoming. U. S. Geological Survey Professional Paper 490, 196 p.

——. 1986. Neogene tectonics and geomorphology of the eastern Uinta Mountains in Utah, Colorado, and Wyoming. U. S. Geological Survey Professional Paper 1356, 78 p.

Hayden, F. V. 1871. Report of F. V. Hayden, *in* F. V. Hayden survey, preliminary report of the United States Geological Survey of Wyoming and portions of contiguous territories, 2nd annual report. U. S. Government Printing Office, Department of the Interior, p. 9-188.

Leidy, J. 1869. Notice of some extinct vertebrates from Wyoming and Dakota. Proceedings of the Academy of Natural Sciences of Philadelphia, 21:63-67.

Love, J. D., and Christiansen, A. C. 1985. Geologic map of Wyoming. U. S. Geological Survey Map, 3 sheets, scale 1:500,000.

Marsh, O. C. 1886. Dinocerata, a monograph of an extinct order of gigantic mammals. U. S. Geological Survey Monograph 10, 243 p.

Matthew, W. D. 1909. The Carnivora and Insectivora of the Bridger Basin, Middle Eocene. American Museum of Natural History Memoir, 9(6):291-567.

McKenna, M. C., Russell, D. E., West, R. M., Black, C. C., Turnbull, T. D., Dawson, M. R., and Lillegraven, J. A. 1973. K-Ar recalibration of Eocene North American land-mammal "ages" and European ages. Geological Society of America Abstracts with Programs, 5:733.

Rowley, P. D., Hansen, W. R., Tweto, Ogden, and Carrara, P. E. 1985. Geologic map of the Vernal 1 degree by 2 degree Quadrangle, Colorado, Utah, and Wyoming. U. S. Geological Survey, Miscellaneous Geologic Investigations Map I-1526, scale 1:250,000.

Sinclair, W. J. 1906. Volcanic ash in the Bridger beds of Wyoming. American Museum of Natural History Bulletin, 22(15):273-280.

West, R. M. 1976. Paleontology and geology of the Bridger Formation, southern Green River Basin, southwestern Wyoming. Part 1. History of field work and geological setting. Milwaukee Public Museum, Contributions in Biology and Geology, no. 7, 12 p.

West, R. M., and Hutchison, J. H. 1981. Geology and paleontology of the Bridger Formation, southern Green River Basin, southwestern Wyoming. Part 6. The fauna and correlation of Bridger E. Milwaukee Public Museum, Contributions in Biology and Geology, no. 46, 8 p.

Wood, H. E. 1934. Revision of the Hyrachyidae. American Museum of Natural History Bulletin, 67(5):181-295.

TAPHONOMY OF AN *ALLOSAURUS* QUARRY IN THE DEPOSITS OF A LATE JURASSIC BRAIDED RIVER WITH A GRAVEL-SAND BEDLOAD, SALT WASH MEMBER OF THE MORRISON FORMATION, DINOSAUR NATIONAL MONUMENT, UTAH

John F. Hubert
Department of Geology and Geography
University of Massachusetts, Amherst MA 01003
Daniel J. Chure
Dinosaur National Monument
Jensen, UT 84035

ABSTRACT

During Late Jurassic time, a shallow braided river with a gravel-sand bedload deposited the fluvial strata of the Salt Wash Member of the Morrison Formation in Dinosaur National Monument. An articulated *Allosaurus* skeleton is being excavated at the Monument from the upper portion of a 60-cm layer of conglomerate at the bottom of a paleochannel 1.4 m deep. A high-energy flood cut the channel into a coset of planar crossbed sets built by coalescing transverse bars, probably of linguoid shape. The flood waters transported and deposited the gravel and the *Allosaurus* carcass. As the flood stage fell, the carcass was rapidly buried, mostly by down channel migration of trains of three-dimensional dunes of the lower flow regime that deposited a coset of trough crossbedded sands. Simultaneously, the carcass was partly covered by plane-bedded sand deposited in the upper flow regime, the lateral transition from dunes being caused by slightly higher velocities in that part of the channel. The skeleton was preserved due to its location in a topographic low and rapid burial, which protected it from scavengers and exhumation by subsequent floods.

INTRODUCTION

The staff of Dinosaur National Monument are currently excavating an articulated *Allosaurus* skeleton from the Salt Wash Member of the Morrison Formation at a site located about 1 km east of the quarry building (Figure 1). The site is in fluvial sandstones and conglomerates of Late Jurassic age in the upper half of the Salt Wash Member (Figure 1). Our paper uses sedimentological data from these well-exposed strata to reconstruct the hydrodynamic processes and bedforms of the river that transported, deposited, and preserved the skeleton.

The rivers that deposited the Salt Wash Member in northeastern Utah flowed from highlands in western Utah and eastern Nevada, based on regional maps of fluvial paleocurrent azimuths, sandstone mineral composition, and isopach thicknesses (Craig et al., 1955; Cadigan, 1967; Dawson, 1970; Peterson, 1984). The highlands were roughly parallel to a magmatic arc associated with subduction during the Nevadan orogeny (Peterson, 1984).

Regional semiaridity during deposition of the Salt Wash Member is suggested by eolian sandstones in the Tidwell, Bluff-Junction Creek, Salt Wash, and Recapture members of the Morrison Formation in the Colorado Plateau (Peterson and Turner-Peterson, 1987) and by eolian sandstones recently discovered in the Dinosaur National Monument by Peterson and Turner (unpublished data, 1991). These dune fields were of limited areal extent in a landscape dominated by braided rivers and their floodplains. A pronounced rainy season may be indicated by the presence of minor detrital kaolinite in the mudstones of the Salt Wash Member at the Monument (Dodson et al., 1980; Bilbey et al., 1974; Bilbey, 1991).

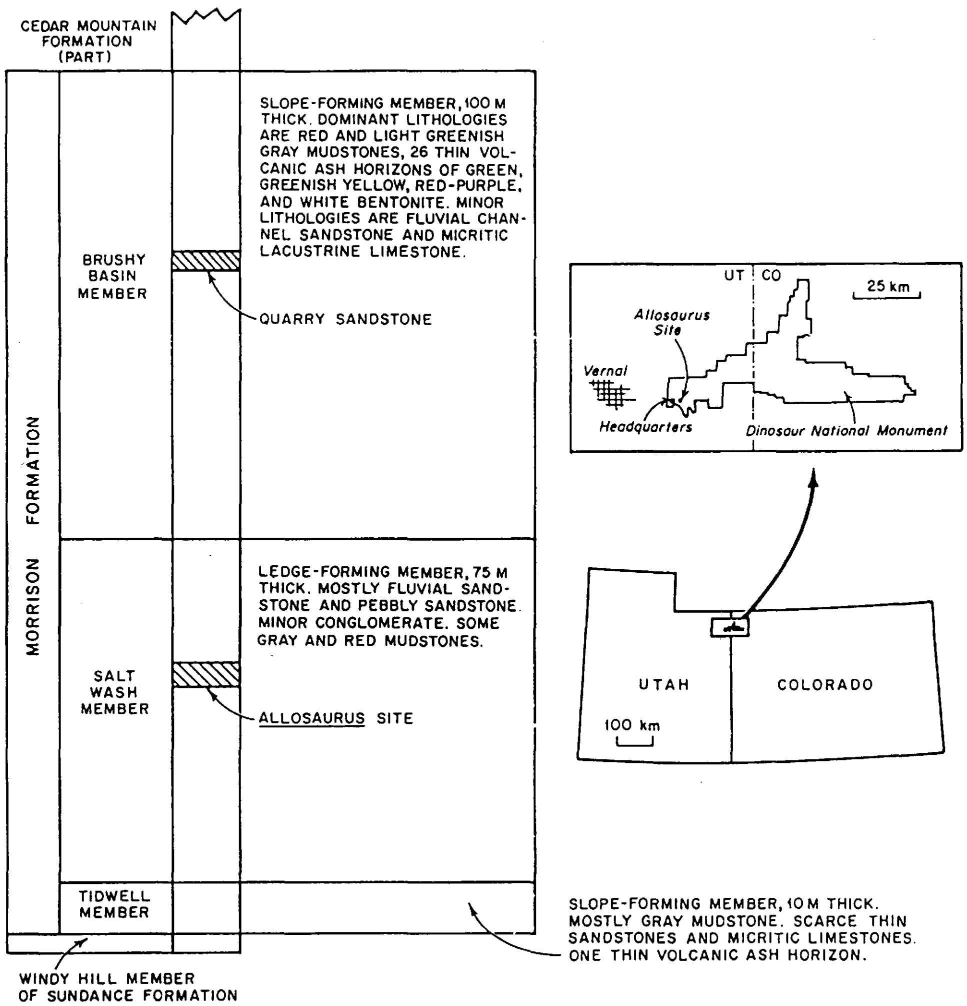

Figure 1. Index map and stratigraphic section showing the locations of the *Allosaurus* site in the Dinosaur National Monument and in the Salt Wash Member of the Morrison Formation. The measured section is simplified from Peterson and Turner (unpublished data, 1991) and Bilbey et al. (1974).

DESCRIPTION OF THE SPECIMEN

Although the Morrison Formation is renowned for the abundance of its dinosaurs, much remains to be learned about the dinosaur fauna. All of the large dinosaur quarries in the Morrison are in the Brushy Basin Member or its equivalents, although the relationship of the Morrison in the Front Range to other subdivided Morrison exposures is currently unclear.

On the other hand, the dinosaurs of the Salt Wash Member are poorly understood, with articulated, identifiable remains being almost non-existent. The Fruita Paleontological Area of Colorado contains a rich and diverse small vertebrate fauna from near the top of the Salt Wash, but dinosaur remains are fragmentary (Callison, 1987), with the exception of a large, uncollected, partial theropod skeleton (J. Kirkland, pers. comm., 1988). Young (1991) reported a dinosaur nest with eggs from the Salt Wash in western Colorado, but the only dinosaur remains found at the site are isolated teeth. Finally, Bartleson and Jensen (1988) have described a partial skeleton of *Apatosaurus* sp. from basal Morrison beds near Gunnison, Colorado. Thus, the specimen reported on here is a significant addition to our limited knowledge of Salt Wash dinosaurs.

Although excavation of the specimen is still underway, a number of useful observations can be made. The material uncovered to date is a single, articulated individual lying on its left side. It is composed of at least the following material: a nearly complete series of caudal vertebrae (including chevrons), two articulated caudal vertebrae lying atop the left pes, the right ilium, complete left and right hindlimbs, and nearly complete right and left pes. All missing foot bones were almost certainly originally preserved, but have been lost through erosion of the outcrop. The large pes (metatarsal III is 22.5 cm in length) is of a size found in *Allosaurus* specimens with a total length of 10.7 m (J. Madsen, pers. comm., 1991), indicating that this specimen is adult. Excavation of the site is on-going and we expect that more of the specimen will be found.

To date only the right pes has been collected and completely prepared. The specimen (catalog number DINO 11541) includes the articulated right metatarsals (MT) II, III, and IV, with tarsal III adpressed to the proximal end of MT III; the distal part of MT I; and phalanges II-1 (incomplete), II-2, III-1, III-2, IV-1, and articulated IV-2 through IV-5 (Figure 2).

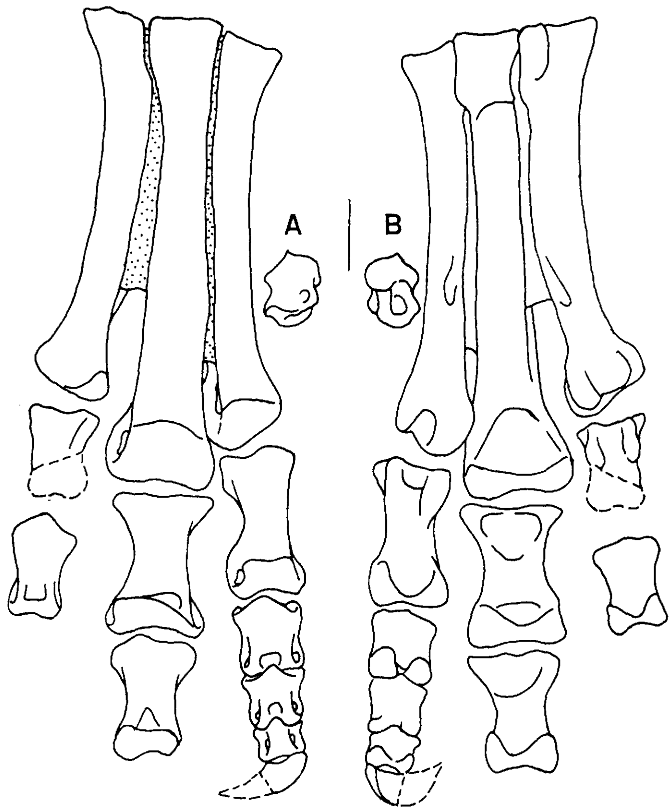

Figure 2. DINO 11541, *Allosaurus* sp., right pes, matrix stippled. A) superior, B) inferior views. Scale = 5 cm.

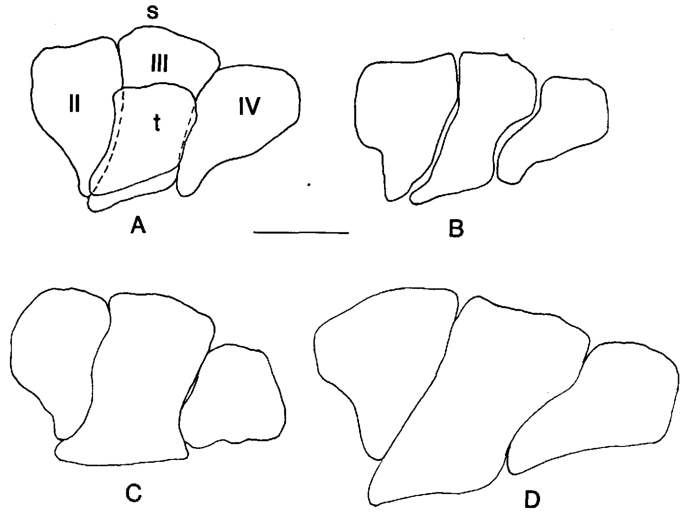

Figure 3. Morrison theropod right metatarsals in proximal view. A) *Allosaurus* sp. DINO 11541. B) *Allosaurus fragilis* (after Madsen, 1976, fig. 25, reversed). C) *Ceratosaurus nasicornis* (after Gilmore,1920, plate 24, reversed). C) *Torvosaurus tanneri* (after Britt, 1991, compiled from fig. 24, reversed). S = Superior Face. t = tarsal III. Scale = 5 cm.

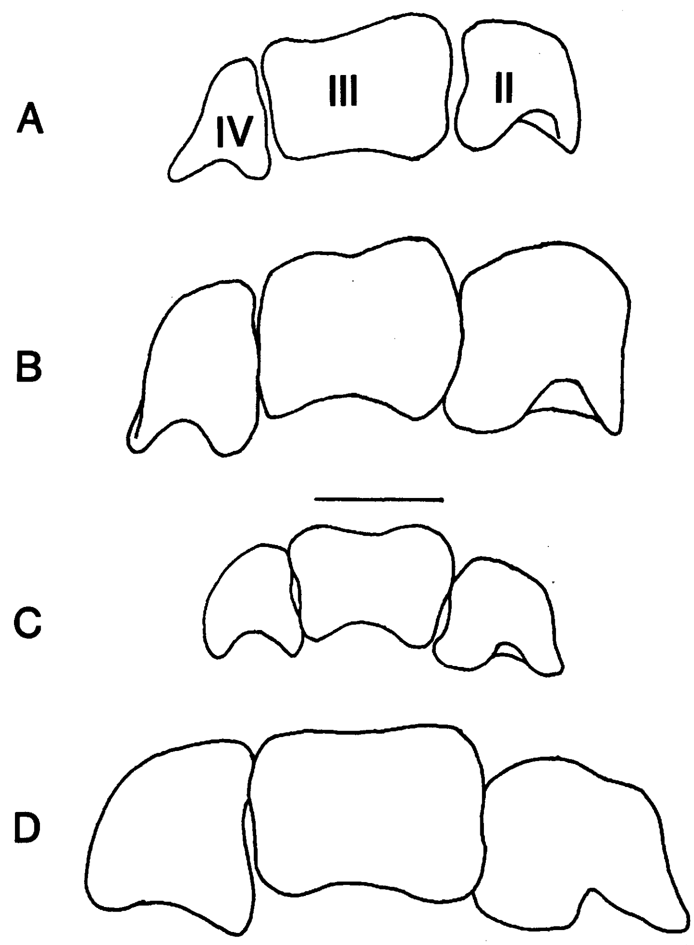

Figure 4. Morrison theropod right metatarsals in distal view. A) *Allosaurus* sp. DINO 11541. B) *Allosaurus fragilis* (after Madsen, 1976, compiled from plate 54, reversed). C) *Ceratosaurus nasicornis* (after Gilmore, 1920, plate 25, reversed). D) *Torvosaurus tanneri* (after Britt, 1991, compiled from fig. 24, reversed). Scale = 5 cm.

Detailed description of these elements awaits future publication when all of the specimen is collected and prepared. However, identification of the material collected to date is possible because metatarsals are diagnostic at the generic level for Morrison theropods. The configuration of the proximal ends of the metatarsals is characteristic of *Allosaurus* and unlike that seen in the other large Morrison theropods *(Torvosaurus, Ceratosaurus)* for which feet are known (Figures 3, 4). In contrast to the condition in *Ceratosaurus,* the proximal end of MT III in DINO 11541 does not overlap the inferior faces of MT II and IV, and MT IV is not rectangular in outline. In contrast to the condition in *Torvosaurus,* the proximal end MT III is hourglass shape in outline and the inferior end of MT IV is narrow and curved. The distal ends of the metatarsals also agree with those seen in *Allosaurus.* In contrast to the condition in *Torvosaurus* and *Ceratosaurus,* the distal ends of MT II has a flat medial edge and MT IV is narrow. These features are characteristic of *Allosaurus.*

A number of taphonomic factors such as scavenging, pre-burial decay, and transport often result in the disarticulation of vertebrate skeletons. Among the features indicating that the present specimen was either not transported far before burial or that it had not been scavenged are 1) the articulated nature of the metatarsals, 2) the presence of tarsal III in natural contact with the metatarsals, 3) the articulated phalanges of digit IV, 4) the presence of the distal half of metatarsal I which is only loosely articulated with the rest of the foot, 5) the left pes (still in situ) shows that the left metatarsals II,III, and IV are articulated (although the distal half of each has been lost through erosion), 6) the right femur, tibia, and fibula are articulated and the right pes was found articulated with the right limb, and 7) the articulated caudal series also includes chevrons for all vertebrae so far exposed. The high degree of articulation of all bones found to date indicates rapid burial, especially in light of the occurrence of the specimen in conglomeratic deposits in a braided river. This is in sharp contrast to the more common occurrence of broken and isolated dinosaur bones in other Salt Wash fluvial sandstones in Dinosaur National Monument.

A wafer about 48 mm in diameter was cut transverse to the length of phalanx III-1 of the right pes and prepared as a petrographic thin section. The central 36.5 mm of the phalanx is cancellous bone. It is surrounded by 3.1 mm of Haversian compact bone with densely packed cross sections of cylindrical secondary osteons around vascular canals. Overlying this layer is a 3.1-mm layer of fibro-lamellar bone with primary osteons, a bone type which forms by rapid growth (Reid, 1987). The outermost 5.3 mm is a layer of zonal bone ("growth rings" of Reid, 1990) made of alternating zones of fibro-lamellar bone and lamellated bone. Evidently, the *Allosaurus* grew rapidly to adult size, followed by alternating rapid and slow growth.

Many cancellous openings and Haversian canals are partially lined by authigenic iron sulfide that forms spheres, hemispheres, or a thin layer of crystals. These openings and canals are largely filled by authigenic calcite that lies upon the iron sulfide. Typically, a single calcite crystal fills as many as 20 adjacent cancellous openings with optical continuity of the crystal in all the openings. The bone is partly replaced by iron sulfide, but not calcite. Authigenic iron oxide partly replaces bone adjacent to cracks, especially near the outside of the bone. Younger authigenic gypsum fills veins that cross through the bone and though the calcite-filled openings. Gypsum locally forms mm-scale crusts around the bones.

Angular fragments of bone occur locally within the calcite in the cancellous canals. This brecciation of a bone otherwise undamaged by chewing or trampling was apparently caused by the displacive pressure of the growing calcite crystals as suggested by Thomas (1984) who observed similar "crush zones" in Upper Cretaceous dinosaur bones in southern Alberta.

OBSERVATIONS OF THE SANDSTONES AND CONGLOMERATES

The conglomerate layer that contains the *Allosaurus* skeleton and the contiguous strata were sketched in the field on squared graph paper with equal horizontal and vertical scales (Figures 5, 6). The 5 by 8-m area covered by the sketch includes the accessible strata. The strata strike N80°W and dip 62°SW. The orientation of the rock face sketched is N59°E-S59°W so that when viewing Figure 6, you are looking to the southeast in the direction S31°E, equivalent to an azimuth of 149°. The sketch shows 1) the position of each of the *Allosaurus* bones as exposed in June, 1991, 2) the dimensions and grain sizes of the planar and trough crossbed sets and plane-bedded sandstone, 3) the stratigraphic architecture of the sedimentary structures, 4) the paleocurrent azimuths for 19 crossbed sets, and 5) the locations of carbonized wood fragments.

The paleoflow directions of the river recorded in Figure 5 vary from into the diagram, to towards the right side of the diagram. The average direction of flow of the river at the *Allosaurus* site was southwest towards an azimuth of 204° as recorded by the paleocurrent readings for 19 crossbed sets (Figure 7). The spread in azimuth directions for the combined group of azimuths is 153°, from southeast at 117° to directly west. The average direction of flow of the Salt Wash rivers in Dinosaur National Monument and surrounding area was to the southeast as measured at several locations by Peterson and Turner (unpublished data, 1991).

The planar crossbed sets average about 40 cm in thickness, reaching a maximum of 85 cm (Figure 5). On the classification scheme of the Society of Sedimentary Geology (Ashley, 1990), these sets vary in scale from small to large, averaging medium. The crossbeds are made of couplets of coarser and finer-grained laminae. Pebbles up to a cm in size are concentrated along the lower surfaces of the sets and along the lower parts of the crossbeds. The crossbeds tangentially meet the lower bounding surfaces of the sets. Cosets of superimposed planar crossbed sets reach 1.6 m in thickness.

The trough crossbed sets increase in average thickness from about 10 cm for the sandstones to about 40 cm for pebbly sandstones and conglomerates (Figure 5). The overall size of the sets also increases with grain size. These trough sets range from small to medium size. The cosets of trough crossbed sets exceed 1.6 m, being covered at the bottom of the sketch.

Round spherical quartz grains of medium-sand size are common in the sandstones, and visible with a hand lens. Fragments of mudstone and tan-weathering micritic limestone up to 30 cm in size occur in the conglomerates.

Carbonized wood fragments, up to 32 cm in size, are present in 7 of the crossbed sets and in the plane-bedded sandstone (Figure 5).

The gravel matrix around the *Allosaurus* and the overlying sandstones are weakly cemented by authigenic calcite and gypsum. Three petrographic thin sections of the sandstones show that they contain both intergranular calcite cement and scattered patches of calcite crystals a mm or so in size that engulf a few sand and silt grains. A younger gypsum cement in the sandstones fills veins, forms crusts around grains, and occurs as mm-size crystals that engulf neighboring grains.

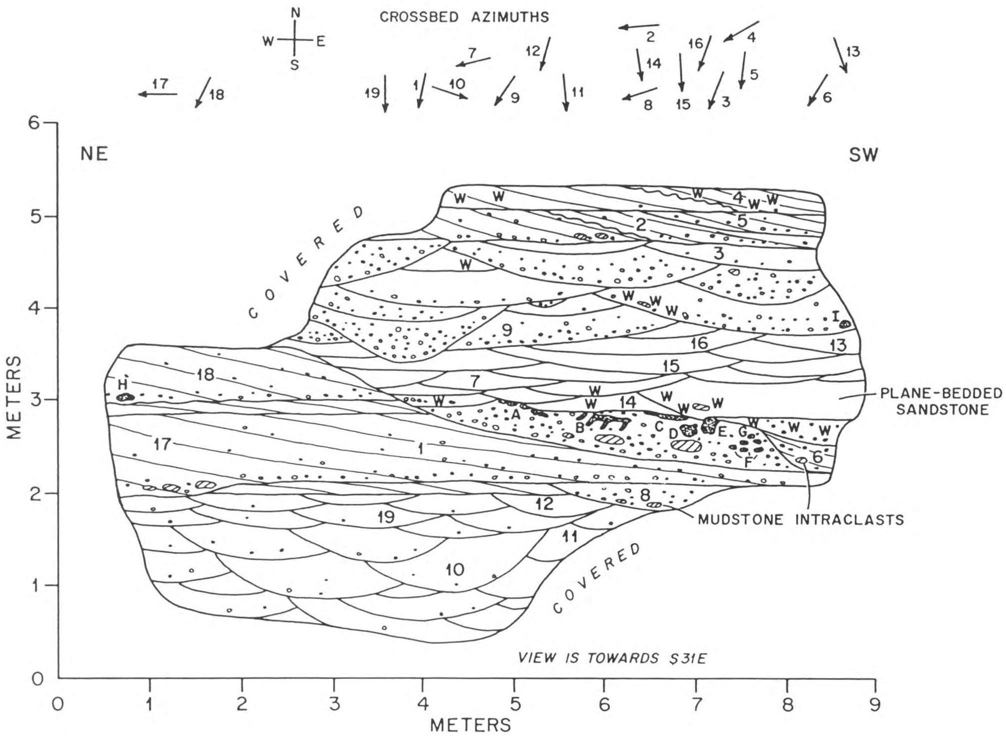

Figure 5. Sketch of the sequence of sandstone, pebbly sandstone and conglomerate that contains the ***Allosaurus.*** The exposed bones of the skeleton are A) five caudal vertebrae, **B) four chevrons, C) fibula, D) tibia, E) femur, F) three caudal vertebrae, and G) three phalanx bones of the left pes. Two partly exposed** dinosaur bones of unknown type are H and I. The skeleton is embedded in conglomerate with a maximum size of the pebbles of about 3 cm, except for mudstone intraclasts which are shown with a diagonal pattern. Planar crossbed sets are drawn with light lines to show crossbeds. Trough crossbed sets are differentiated from planar crossbed sets by the omission of crossbeds and the presence of curved bounding surfaces. The area with horizontally laminated sandstone is left blank and is labelled on the sketch. Paleocurrent readings in crossbeds sets are labelled 1 through 19. Occurrences of abundant carbonized wood are labelled W.

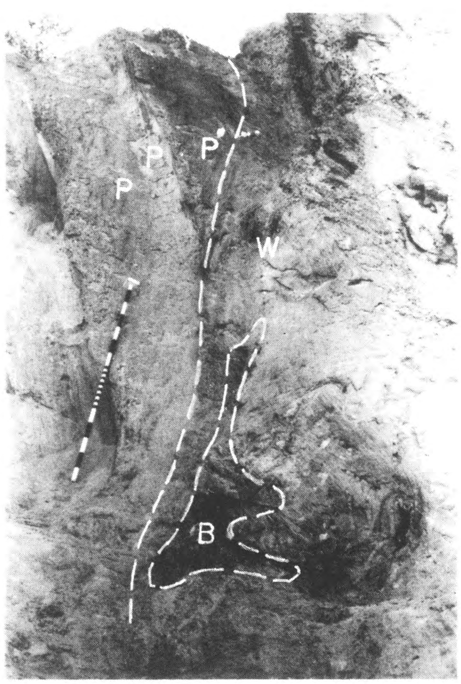

Figure 6. Field photograph of part of the *Allosaurus* site. The strata dip steeply to the right. Labelled on the diagram are the bones (B), paleochannel that contains the *Allosaurus* (dashed line), planar crossbed sets (P), and fragment of charcoal (W). These features are shown in the sketch of Figure 5. The sandstones immediately over the bones have been removed parallel to the bedding, causing the area with the bones to project to the right in the photograph. The 1.5-m stick is divided into 10-cm intervals.

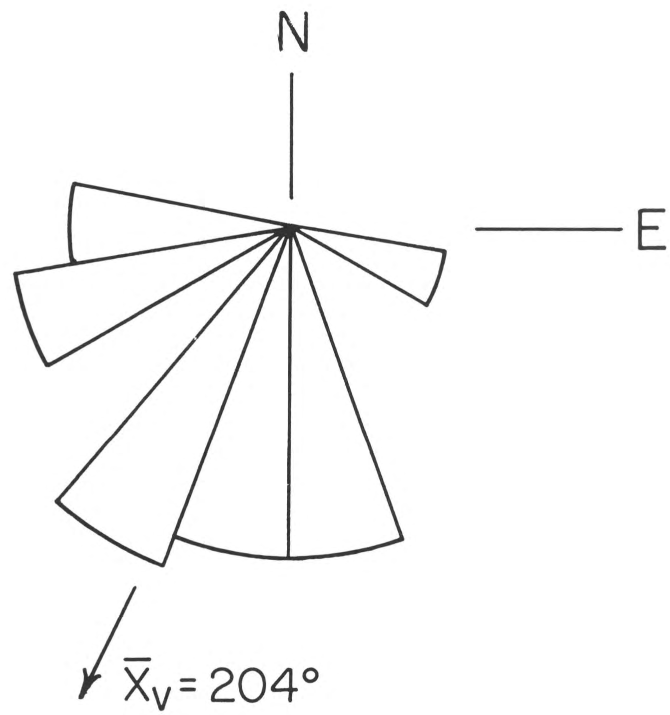

Figure 7. Equal-area plot of the 19 paleocurrent azimuths at the *Allosaurus* site. The vector mean of 204° is statistically significant at less than the 0.001 level when the consistency ratio of L = 79.3% is tested by the Rayleigh statistic.

INTERPRETATIONS

The river that deposited the Salt Wash Member at and near the *Allosaurus* site was braided as evidenced by numerous channels filled with pebbly sandstone and conglomerate, the absence of lateral accretion surfaces and crevasse splay sandstones typical of meandering rivers, and the high ratio of sandstone and conglomerate to mudstone. The river was wide and shallow with multiple channels, some of which during flood stages abruptly shifted their positions within the bed of the river.

The skeleton occurs within a layer of conglomerate 60 cm in thickness at the bottom of a channel 1.4 m deep (Figures 5, 6). A high-energy flood cut the channel, and transported and deposited the gravel and *Allosaurus* carcass. The carcass lay close to the top of the layer of gravel, partly covered by a thin veneer of gravel, but with at least the fibula, femur, and part of the tail exposed at the sediment-water interface (Figure 5). The carcass evidently was partly decomposed as indicated by two caudal vertebrae that broke off the tail, coming to rest with phalanx bones of the left pes.

The planar crossbed sets formed by avalanching of sand and pebbles down the slipfaces of transverse bars with non-cuspate crestlines as the bar crests migrated down river. The bars probably were tongue-shaped linquoid bars of the lower flow regime based on the similarities of the thickness, bounding surfaces, and crossbeds with the crossbed sets deposited by modern linquoid bars, and the common occurrence of linquoid bars in braided rivers with a pebbly sand bedload. The transverse bars at the *Allosaurus* site migrated to the southwest, with an average direction for sets 1, 17 and 18 of 220° and an average direction of 232° for sets 2, 4, and 5. To the left of paleocurrent readings 2 and 4 on Figure 2, there are reactivation surfaces that record a fall in river stage, followed by a rise in river stage and renewal of bar progradation.

Thus we infer that the planar crossbed sets were deposited by downriver migration of trains of transverse bars, some of which exceeded 85 cm in height. The superposition of four planar crossbed sets, including sets 1, 17 and 18, to form a coset 1.6 m in thickness suggests that they may have formed part of a sandflat. The pattern of superposition of planar crossbed sets is repeated by the three planar sets at the top of the sketch.

During the flood event which transported the *Allosaurus* carcass, the channel was cut into the coset of planar crossbeds and the gravel and carcass came to rest at the bottom of the channel. The upper part of the channel was then filled by a coset of trough crossbedded sands, built by trains of three-dimensional (cuspate crestline) dunes of the lower flow regime that migrated to the southwest towards 191° (sets 7, 13, 14, 15, and 16). The carcass was probably covered in a few hours based on the rate of advance of three-dimensional dunes in modern rivers.

The sedimentary features of the strata at the *Allosaurus* site share numerous similarities to those seen in the pebbly sands of the Platte River in Nebraska, where trains of linquoid bars become active during bankfull and flood stages to coalesce laterally and vertically, forming sandflats. During the subsequent fall in river level, the flow becomes confined to anastomosing channels that erode the sandflats and individual linquoid bars, giving the river its braided character. At the lowest river stages, the sandflats and linquoid bars are exposed and flow is in the channels, with the sand and pebbles moved down river in three-dimensional dunes and as plane beds.

In the upper half of the section shown in Figure 2, from the base of the conglomerate with the *Allosaurus* to the base of the planar crossbed sets at the top of the sketch, there are three cycles that fine upward from conglomerate or pebbly sandstone to sandstone. This pattern suggests three repetitions of high discharge followed by a fall in river stage. Mud drapes due to fallout from suspension were not observed on the crossbed sets, but this could reflect a combination of low suspended load in the river and removal of the mud by erosion during the next flood.

Keys to preservation of the articulated skeleton were its location in a topographic low and rapid burial, which protected the carcass from scavengers and exhumation by subsequent floods. The gravel layer was rapidly buried, mostly by trough crossbedded sand, and to lesser extent by plane-bedded sand. The absence of scour at the surface of the gravel layer suggests that the river level did not fall low enough to expose the gravel with its *Allosaurus.* The gravel layer and at least the first few, and perhaps all, of the overlying trough crossbed sets of sand were deposited more or less continuously as the flood stage of the river fell, producing the relatively lower flow velocities necessary for establishment of dunes of the lower flow regime. Simultaneously, the plane beds of sand that covered the femur and metatarsals were deposited under upper flow regime conditions, due to slightly higher velocities than the laterally equivalent dunes. Such lateral transitions from dune to plane beds are common in shallow flows of some tens of centimeters depth. The low position of the *Allosaurus* relative to the top of the adjoining sandflat, and presumably also the upper surfaces of other nearby sandflats, meant that it was less apt to be exhumed by the rushing waters of subsequent floods.

The conglomerates contain numerous sand to boulder-size fragments of mudstone and micritic limestone, indicating that compacted and partially lithified pieces of floodplain mud and lacustrine calcareous mud were eroded and transported down river. As the river level rises during a flood, the banks of a braided river tend to be undercut and collapse, dropping chunks of sediment onto the river bed. In contrast, the maximum size of the terrigenous pebbles, largely chert, is about 3 cm. When in flood, the river was capable of carrying much larger terrigenous clasts, but they were not available to be transported.

The numerous fragments of carbonized plant fragments in the sandstones and conglomerates came from plants along the river banks. During flood stage, abundant plant debris was carried down river to settle on the foresets of the prograding transverse bars and three-dimensional dunes. The absence of root traces in the crossbedded sandstones and conglomerates shows that the transverse bars and dunes were not parts of vegetated islands.

The round, spherical quartz grains of medium sand size in the sandstones at the *Allosaurus* site are of eolian origin. Most of these distinctive grains were recycled from older eolian sandstones as indicated by occasional abraded silica overgrowths. The discovery by Peterson and Turner (unpublished data, 1991) of eolian sandstones in the Salt Wash Member of the Morrison Formation in Dinosaur National Monument raises the possibility that some of these grains either blew from nearby eolian dunes into the river, or the river cut through eolian dunes. The paleoclimate of the area through which the braided river flowed was arid for most of the year, but subject to a rapid increase to flood-stage discharge, either during a major storm or at the beginning of a rainy season.

CONCLUSIONS

An *Allosaurus* skeleton now being excavated from the Salt Wash Member of the Morrison Formation in Dinosaur National Monument occurs within a conglomerate layer in a sequence of sandstones, pebbly sandstones, and conglomerates deposited by a broad, shallow braided river. During a high-energy flood, the gravel and *Allosaurus* were deposited at the bottom of a channel cut into a coset of planar crossbed sets built by superimposed transverse bars, probably of linquoid shape. As the river stage fell, the carcass was rapidly buried, mostly by down channel migration of trains of three-dimensional dunes of the lower flow regime that laid down a coset of trough crossbedded sands. In part, the carcass was covered simultaneously by plane-beds of sand deposited in the upper flow regime, due to a lateral transition to slightly higher velocities. The topographically low position and rapid burial of the carcass protected it from scavengers and exhumation by subsequent floods.

ACKNOWLEDGMENTS

The line drawings in Figures 1, 5, 6, and 7 were prepared by Marie Litterer. The research of J. F. Hubert was done while a Visiting Scientist at the Utah Geological Survey, Salt Lake City, Utah. Hubert thanks the Utah Geological Survey for financial support of field work and purchase of petrographic thin sections. The site was discovered by G. F. Englemann and T. Fowler during a National Park Service contracted paleontological inventory of the Morrison Formation in Dinosaur National Monument. Ann Elder, Scott Madsen and volunteers collected the material described in this paper and continue excavations at the site. Ann Elder prepared the right pes.

REFERENCES CITED

Ashley, G. M. 1990. Classification of large-scale subaqueous bedforms: a new look at an old problem. Journal of Sedimentary Petrology 60:160-172.

Bartleson, B.L. and Jensen, J. A. 1988. The oldest (?) Morrison Formation dinosaur, Gunnison, Colorado. The Mountain Geologist 25: 129-139.

Bilbey, S. A. 1991. Stratigraphy and sedimentary petrology of the Upper Jurassic-Lower Cretaceous rocks at the Cleveland-Lloyd dinosaur quarry with a comparison to the Dinosaur National Monument quarry. Unpublished manuscript for the Ph. D. Dissertation, University of Utah, Salt Lake City, Utah, 243 pp.

Bilbey, S. A., Kerns, R. L., Jr., and Bowman, J. T. 1974. Petrology of the Morrison Formation, Dinosaur Quarry Quadrangle, Utah. Utah Geological and Mineral Survey, Special Studies No. 48, 15 pp.

Britt, B. B. 1991. Theropods of Dry Mesa Quarry (Morrison Formation, Late Jurassic), Colorado, with emphasis on the Osteology of *Torvosaurus tanneri.* Brigham Young University Geology Studies 37:1-72.

Cadigan, R. A. 1967. Petrology of the Morrison Formation in the Colorado Plateau region: U. S. Geological Survey Professional Paper 556, 113 pp.

Callison, G., 1987. Fruita: a place for wee fossils. *In:* Averett, W.R. (editor), Paleontology and Geology of the Dinosaur Triangle. Museum of Western Colorado, Grand Junction, Colorado: p. 91-96.

Craig, L. C. and others. 1955. Stratigraphy of the Morrison Formation and related formations, Colorado Plateau region, a preliminary report. U. S. Geological Survey Bulletin 1009E:125-168.

Crowley, K. D. 1983. Large-scale bed configuration (macroforms), Platte River Basin, Colorado and Nebraska: primary structures and formative processes. Geological Society of America Bulletin 94:117-133.

Dawson, J. C. 1970. Sedimentology and stratigraphy of the Morrison Formation (Upper Jurassic) in northwestern Colorado and northeastern Utah. Ph. D. Dissertation, University of Wisconsin, Madison, Wisconsin, 142 pp.

Dodson, P., Behrensmeyer, A. K., Bakker, R. T., and McIntosh, J. S. 1980. Taphonomy and paleoecology of the dinosaur beds of the Jurassic Morrison Formation. Paleobiology 6:208-232.

Gilmore, C. W. 1920. Osteology of the carnivorous Dinosauria in the United States National Museum, with special reference to the genera *Antrodemus (Allosaurus)* and *Ceratosaurs.* Smithsonian Institution, U. S. National Museum Bulletin 110: 159 pp.

Madsen, J.H. 1976, *Allosaurus fragilis:* a revised osteology. Utah Geological and Mineral Survey Bulletin 109, 163 pp.

Peterson, F. 1984. Fluvial sedimentation on a quivering craton: influence of slight crustal movements on fluvial processes, Upper Jurassic Morrison Formation, western Colorado Plateau. Sedimentary Geology 38:21-49.

Peterson, F., and Turner-Petersen, C. E. 1987. The Morrison Formation of the Colorado Plateau: recent advances in sedimentology, stratigraphy, and paleotectonics. Hunteria 2:1-18.

Reid, R. E. H. 1987. Bone and dinosaurian "endothermy". Modern Geology 11:133-154.

Reid, R. E. H. 1990. Zonal "growth rings" in dinosaurs. Modern Geology 15:19-48.

Thomas, R. G. 1984. Cementation histories of Upper Cretaceous dinosaur bones, southern Alberta, and their relevance to taphonomic studies. Abstracts Volume, Fourth North American Paleontological Convention, p. A46.

Young, R. G. 1991. A dinosaur nest in the Jurassic Morrison Formation, western Colorado. *In:* Averett, W.R. (editor), Guidebook for Dinosaur Quarries and Tracksites Tour, western Colorado and eastern Utah. Grand Junction Geological Society, Grand Junction, Colorado, p. 1-15.

LATE TRIASSIC VERTEBRATE TRACKS IN THE DINOSAUR NATIONAL MONUMENT AREA

Martin G. Lockley, Kelly Conrad, Marc Paquette
Geology Department, University of Colorado at Denver
1200 Larimer St. Denver CO 80204.
and
Alden Hamblin, Utah Field House of Natural History
235 E. Main, Vernal, UT 84078

ABSTRACT

Recent studies indicate that the older Mesozoic sedimentary rocks of the Dinosaur National Monument (DNM) area are rich in vertebrate tracksites. A total of 21 tracksites have been discovered in the Late Triassic Popo Agie/Chinle Formation in the last few years. Three tracksites have also been discovered in the lower part of the Glen Canyon Group. The Popo Agie/Chinle sites are particularly significant because they yield the trackways of most of the major groups of reptiles known from this epoch (dinosaurs, reptile-like mammals, phytosaurs, aetosaurs, lepidosaurs, ?trilophosaurs and tanystropheids). In fact the diversity of tracks rivals the diversity of Late Triassic tetrapod body fossils known from many sites in the well-known Chinle Formation, for example at the Petrified Forest National Park, and in the fossiliferous Dockum Group.

The discovery of aetosaur tracks *(Brachychirotherium)* in the lower part of Glen Canyon Group provides strong evidence for a Late Triassic age for the track-bearing bed. This is a significant contribution to unresolved questions about the age of the Glen Canyon Group in this area.

INTRODUCTION

Studies of the Popo Agie/Chinle Formation, and the lower part of the Glen Canyon Group (Wingate equivalent) in the area around Dinosaur National Monument (DNM) have revealed remarkably diverse Late Triassic vertebrate track assemblages. Although a single dinosaur tracksite was reported from the Popo Agie of Wyoming by Branson and Mehl (1932) and a second site recorded at Vermillion Creek in Moffat County, Colorado (Pipiringos and O'Sullivan, 1978), it was not until the 1980s and 1990s that the vertebrate track assemblages received serious attention.

Two of us (M.G.L. and K.C.) began investigating the Vermillion Creek site in 1985 and accumulated a substantial collection of track-bearing slabs from a single stratigraphic level approximately 20 m below the top of the formation (Lockley, 1986; 1987; 1990; 1991; Lockley and Conrad, 1989; Conrad, in preparation).

In the late 1980s and early 1990s one of us (A.H.) began to discover tracksites in the area of Red Mountain and Redfleet Reservoir north of Vernal, Utah. Most of these sites are new discoveries, though one may have been known to Untermann and Untermann (1954), who reported footprints without publishing any detailed information. To date we know of at least five Popo Agie/Chinle sites and one in the lower part of the Glen Canyon Group, in the Red Mountain/Redfleet Resevoir area.

The present study received a significant boost with the initiation of a National Park Service grant to look for tracks in Dinosaur National Monument. To date we have discovered 16 tracksites within the DNM boundaries — 14 in the Popo Agie/Chinle and two in the Glen Canyon Group, (see Lockley, et al., 1990; 1991).

STRATIGRAPHY

There is some confusion about stratigraphic nomenclature in the study area (Uintah County, Utah and Moffat County, Colorado). Fortunately however a new consensus is emerging and can be summarized briefly. The Late Triassic red bed sequence, referred to as the Chinle Formation in many parts of Utah and the Colorado plateau (e.g., Rowley, et al., 1979), is referred to as the Popo Agie Formation in Wyoming (High and Picard, 1969). Spencer Lucas (written communication 1991) suggests that in the study area the lower part of the formation, the conglomeratic Gartra Member and the overlying yellow and variagated zeolitic and bentonitic Ochre Member both belong to the Popo Agie and are different from the upper Red Siltstone member (sensu Pipiringos and O'Sullivan, 1978) which consists of whitish and pink ripple marked sandstones alternating with brick red and purple siltstones and shales (siltstones and shales change from red to purple in the upper 10 meters). Lucas suggests that this upper member (about 20 to 25 meters) is equivalent to the Rock Point member of the Chinle Formation and is separated from the lower Popo Agie members by an unconfomity. We agree that the upper member is quite distinctive. All the tracks and invertebrate traces occur in this member. Currently we use the compound term Popo Agie/Chinle Formation to refer to this red bed sequence (Lockley et al., 1990; 1991).

In reference to the overlying predominantly white, cross-bedded sandstone sequence, some authors use the term "Glen Canyon Group" whereas others use the compound term "Navajo/Nugget." We prefer the former nomenclature because it can be demonstrated that the lower part of the Glen Canyon group in this area contains a pre-Navajo, Late Triassic unit or Wingate Formation equivalent (Poole and Stewart, 1964a, p. D 38; 1964b, p. 102; Peterson, personal communication). Tracks are particularly useful in clarifying the age of the lower part of the Glen Canyon Group in this area.

LOCATION AND CATALOGUING OF TRACKSITES AND TRACKS

Tracksites in the study area are catalogued according to their geographical location and stratigraphic position. Tracksites in the Vernal area, west of DNM are treated as a separate cluster and have been assigned Utah locality numbers as well as locality names (e.g., Redfleet West = 42Un564T, see Appendix). A single site at Cliff Creek, east of Jensen, Utah (Figure 1) has also been catalogued this way.

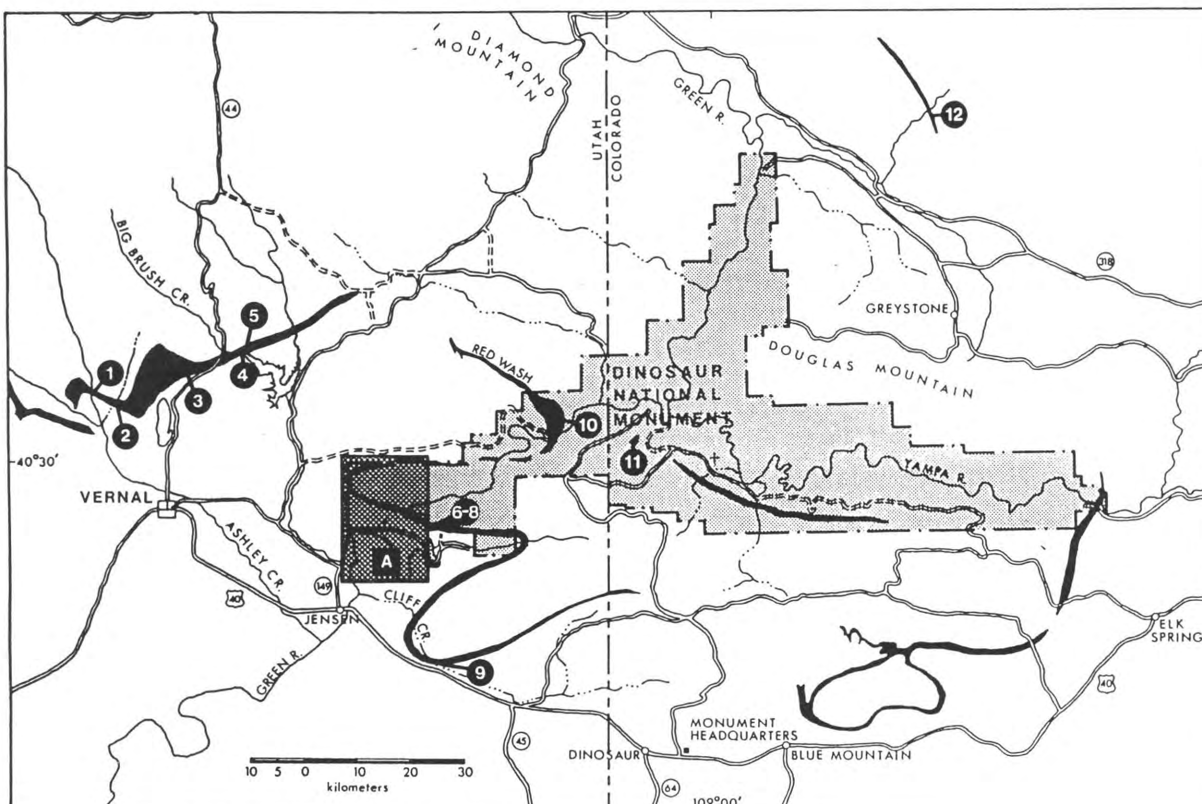

A. Split Mountain West sites (see figure 2): Lockley, Conrad, & Fleming.
1. Old Power Plant (Ashley Creek) site: A. Hamblin
2. Red Mountain West (Spring Creek) site: A. Hamblin
3. Red Mountain East site: A. Hamblin
4. Big Brush Creek (Red Fleet West) site: A. Hamblin
5. Red Fleet North site: A. Hamblin
6-8. Split Mountain East sites: Lockley, et al.
9. Cliff Creek site: A. Hamblin
10. Red Wash site: M. Pacquette
11. Chew Ranch site: M. Pacquette
12. Vermillion Creek site: Conrad & Lockley

Figure 1. Map of Dinosaur National Monument area showing the location of Late Triassic tracksites in the Popo Agie Formation (solid pattern). Localites 1-5 refer to sites discovered by A. Hamblin north of Vernal (Red Mountain and Redfleet areas). The basal Glen Canyon Group, McConkie Ranch Site is also in this area. Detail of tracksite locations in the Split Mountain West area is shown in Figure 2. Details of other sites are explained in the text.

Sites in Dinosaur National Monument have been referred to in chronological order of discovery by the University of Colorado at Denver Dinosaur Trackers Research Group as UCD 90-1 to UCD 90-4 and UCD 91-5 to UCD 91-16; see Figure 2. These sites have also been keyed to their correct stratigraphic position (Figure 3). DNM Sites 8 and 11 are in the Glen Canyon Group, but all others are in the Popo Agie/Chinle Formation. At three of these sites (UCD91-5,6 and 15) we have recorded two stratigraphic levels with tracks and used "a" (lower) and "b" (upper) suffixes to distinguish sites. (Lockley et al., 1990; 1991). In the future these sites will also be given DNM locality numbers.

The Vermillion Creek site in Colorado is treated as a single locality for the purposes of this report. Unpublished U.S. Geological Survey documentation suggests that these tracks come from two different levels. Our field observations indicate that this is not the case. However, tracks do occur in outcrops that extend for about three kilometers along strike.

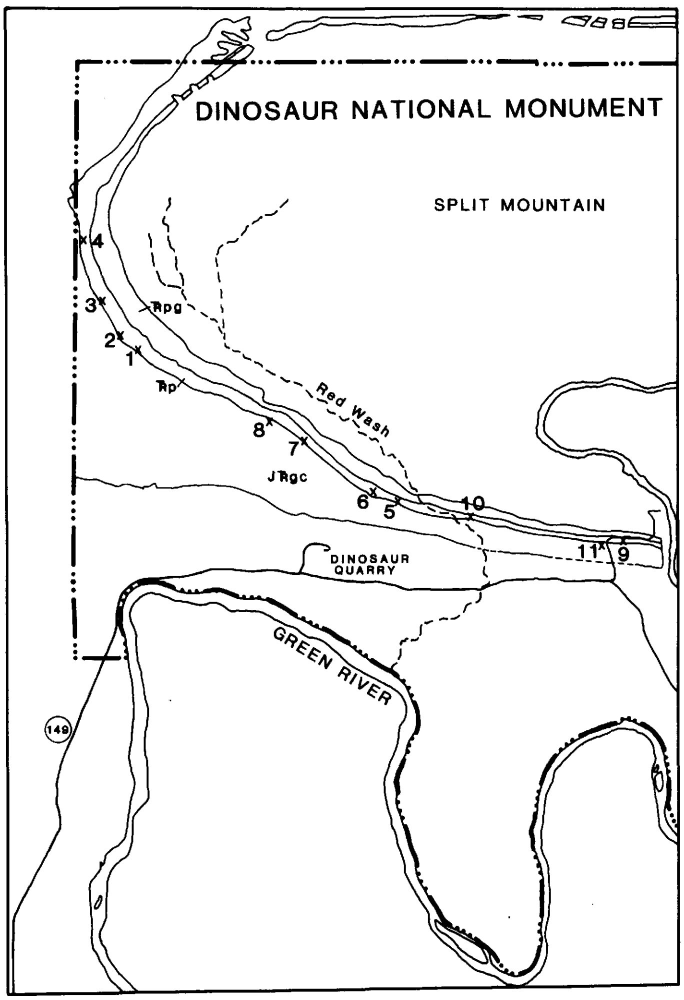

Figure 2. Location of Late Triassic tracksites in the western part of Dinosaur National Monument (Split Mountain West sites of Figure 1). UCD90-1 through 90-4, and UCD91-5 through 91-10 were discovered and investigated by Lockley, Conrad, Paquette and Fleming in 1990-1991. All except locality 91-8, which is in the Glen Canyon Sandstone, are in the Popo Agie Formation. Locality 11, in the Glen Canyon Group, was reported to us by Dr. David Loope. See text for details. Ꞧpg = Popo Agie Formation, Gartra Member; Ꞧp = Popo Agie Formation; JꞦgc = Glen Canyon Group.

Original footprints (natural impressions and casts) and invertebrate traces have been collected from many, but not all sites. In addition we have made replicas of several tracks and trackways using latex for molding, and plaster and/or fiberglass for casting. Specimens from the Vernal area and from Cliff Creek have numbers corresponding to the Utah Locality Numbers. DNM specimens are numbered with the "DINO" prefix (e.g., DINO 15000 from UCD 91-8). Specimens from Vermillion Creek are catalogued in the U.S.G.S. collections and in the joint University of Colorado at Denver — Museum of Western Colorado (CU-MWC) collections. All cataloguing was done by the authors in conjunction with curators at these institutions.

TRACK TYPES (ICHNOLOGY)

Rather than list the track types known from each of the 26 sites (and levels) in the study area, we have summarized the ichnofauna for the whole area and referred to specific sites only in cases where the ichnology warrants special attention. A list of curated specimens and track identifications from Dinosaur National Monument and the Redfleet/Red Mountain area is also included in the appendix.

Popo Agie/Chinle Formation: Vernal area and Cliff Creek. — To date five sites are known in this area referred to as Redfleet West, Redfleet North, Red Mountain East, Red Mountain West and Old Power Plant. These have yielded the ichnogenera *Agialopus* (a small three toed dinosaur track similar to *Grallator*) and *Brachychirotherium* (the tracks of a large quadruped, probably an aetosaur: see Figure 4). The exact stratigraphic position of most localities is known but sections have not been measured in detail. All sites are in the upper Red Siltstone member (same interval as in Figure 3 at DNM) and several are close to the member's upper contact with the overlying Glen Canyon Group.

The Cliff Creek site has yielded only a single *Agialopus* track, but also a delicate invertebrate (?insect) trail.

Popo Agie/Chinle Formation: Dinosaur National Monument. — To date 14 sites (17 levels) are known from DNM. There is a large concentration of sites at the west end of the monument on the southern flank of the anticline that comprises the "race track" area between the park's western boundary and the Green River at Split Mountain Campground. Three additional sites were recorded just east of the Green River (Figure 1) and two more are now known to the northeast (Red Wash) and east (Chew Ranch). The DNM track assemblage is more diverse than that currently known from the Vernal area. In addition to *Agialopus* (sites 1, 4, 5a, 7, 12, 13, 14 and 16) and *Brachychirotherium* (sites 2 and 3), at least five other distinctive ichnotaxa are known. These include the lacertilian *Rhynchosauroides* (made by a lizard or sphenodontid) from sites 7, 15 and 16 and *Gwyneddichnium* (probably made by the tanystropheiid reptile *Tanytrachelos*) from sites 5b, 9, 15 and 16. In addition, a track which

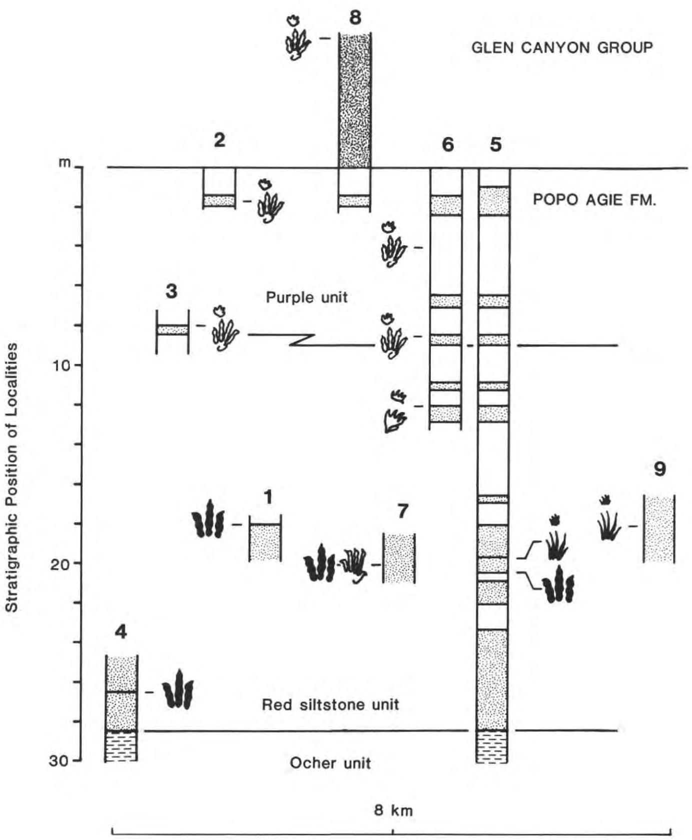

Figure 3. Stratigraphic sections showing the levels at which Late Triassic tracksites have been recorded in the western part of DNM (compare with Figure 2). Appropriate symbols are used to show different track types; see text for explanations. (Stratigraphic positions of localities 1 and 4 are only approximate.)

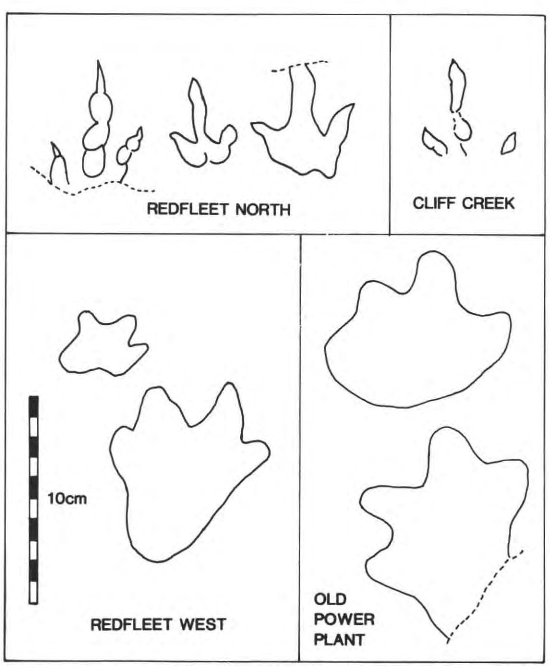

Figure 4. *Agialopus* (top) and *Brachychirotherium* (bottom) from Cliff Creek and three sites in the Vernal area. Note that manus and pes tracks from Redfleet West are a set but tracks from Old Power Plant site are not from the same trackway.

we assign to *?Apatopus* (possibly of trilophosaurian affinity) was recovered from site 6b, a synapsid or reptile-like mammal track was replicated from site 2 and two phytosaur trackways were mapped and measured at site 6a. This suggests a minimum diversity of seven vertebrate track types each representing a different reptile (or mammaloid) taxon. In addition *Scoyenia gracilis* s.s. and other invertebrate burrows are abundant at many localities and a well preserved limulid trail (*Kouphichnium*: DINO 15003) was collected from locality 9, we have also recovered well-preserved *Isopodichnus* traces from locality 16.

The Vermillion Creek site has yielded abundant tracks attributable to *Agialopus, Gwyneddichnium* and *Rhynchosauroides* as well as numerous invertebrate traces including *Scoyenia gracilis, Bifurcalapes, Cochlichnus, Aeripes,* cf. *Pterichnus, Treptichnus* and others.

Trackways and tracks of special interest and significance. — Two of the aforementioned vertebrate track types are interesting because of their rarity. *?Apatopus* is currently only known from one other Late Triassic locality in the western United States (i.e., from the Dockum Group of New Mexico, Conrad et al., 1987). The same is true for the phytosaur trackways (Figure 5), which are also only known from this particular New Mexico locality . Synapsid tracks remain elusive in the Late Triassic of the West. We have elsewhere reported *Pentasauropus*-like tracks from the Chinle and Dockum (Lockley, 1986; Conrad, et al. 1987; Lockley and Conrad, 1989) but have yet to find well-preserved trackway sequences.

The most interesting discoveries in the study area to date are the trackways of *Gwyneddichnium* engaged in both walking and swimming activity. When originally named by Bock (1952), *Gwyneddichnium* was an obscure ichnogenus of uncertain affinity, based only on isolated tracks. The discovery of complete trackway segments at the Moffat County site (Baird, unpublished written communication to

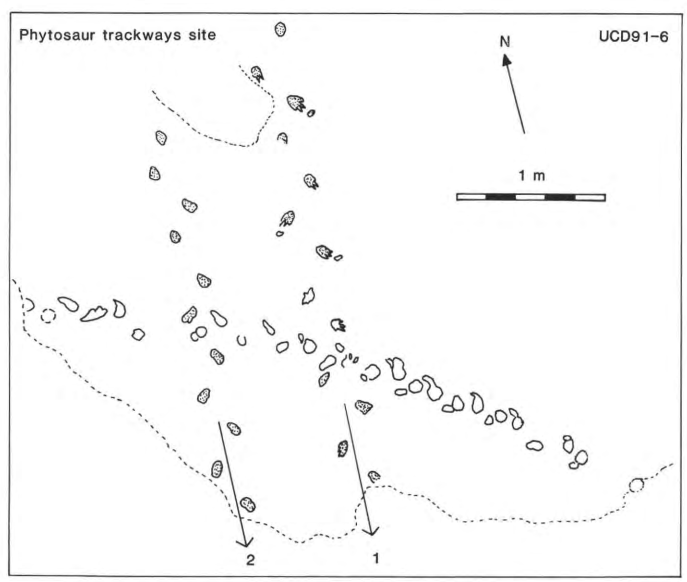

Figure 5. Phytosaur trackways from DNM site UCD91-6, Popo Agie Formation.

USGS 1964; Lockley 1986, 1990) helped shed light on the size and gait of the trackmaker. However it was not until after Olsen (1979) described the aquatic reptile *Tanytrachelos* in the Late Triassic of Virginia that Baird (1986) and Lockley (1986) suggested this genus as the *Gwyneddichnium* trackmaker.

As is often the case in ichnology, precise efforts at trackmaker identification are somewhat conjectural and compromised by limited knowledge of extinct faunas. In this case however, new evidence strongly supports the *Gwyneddichnium—Tanytrachelos* correlation.

Two well-preserved trackway segments from site UCD 91-5b show evidence of the *Gwyneddichnium* trackmaker engaged in swimming activity. Instead of progressing on all fours with alternating steps of hind and front feet, the "swimming" trackways show only hind foot impressions situated in paired or side-by-side arrangement reminiscent of a hopping gait (except for the wider spacing between left and right footprints: see Figure 6, and discussion by Thulborn 1989). The tracks also show a very wide splay between the digit imprints and clear impressions of interdigital webbing between toes one and three. These features indicate a partially bouyant aquatic animal using the substrate to gain purchase in propelling itself forward with synchronous strokes of its hind feet. As shown by trackway specimen DINO 15006 the animal was evidently accelerating or at least increasing the length of strokes as it progressed. All other known *Gwyneddichnium* occurrences at DNM reveal widely splayed digit impressions and isolated tracks evidently indicative of swimming or bouyant activity. By contrast all the Vermillion Creek *Gwyneddichnium* trackways reveal evidence of animals that were walking on all fours with digits held close together and directed forward in the direction of progression.

To the best of our knowledge this is the first example of an ichnogenus for which such well-preserved walking and swimming trackways are documented. Certainly it is the only example for a trackmaker identified with confidence down to the genus level. Moreover it is the only example we know of in which tracks can be used to demonstrate the exact configuration of interdigital webbing. Slab DINO 15006 also reveals elongate impressions that might possibly be interpreted as *Tanytrachelos* resting traces. Further detailed description of these traces is outside the scope of this paper and will be presented elsewhere in due course. However, we stress that DNM *Gwyneddichnium* traces are remarkable in the quality of their preservation and the significant insights they offer into tanystropheid anatomy and behavior.

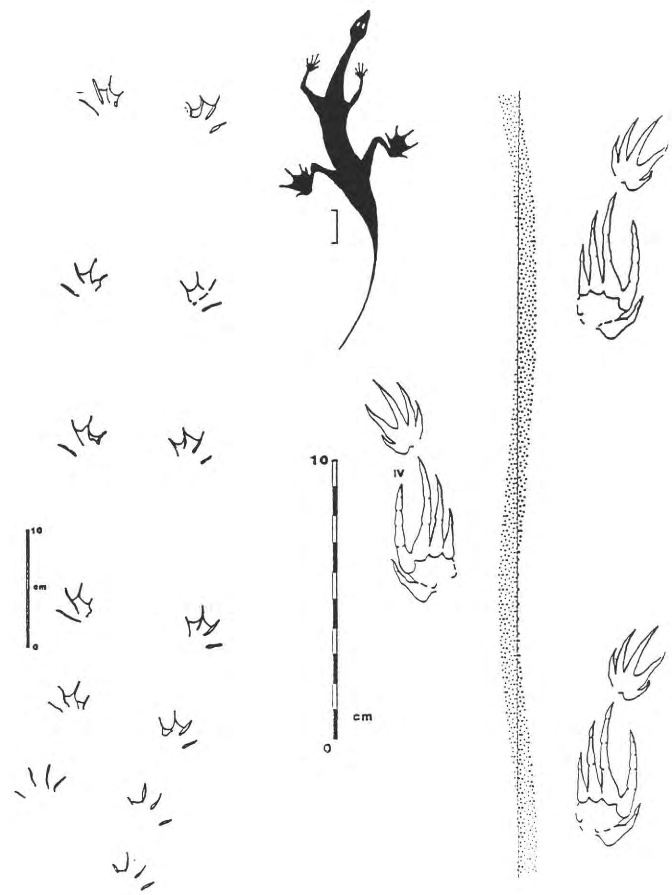

Figure 6. Comparison of *Gwyneddichnium* trackway indicative of swimming behavior (left = DINO 15006) and walking (right = USGS specimen from Popo Agie Fm. Vermillion Creek, Moffat Co. Colorado). Trackmaker was probably *Tanytrachelos* (see silhouette of 20-25 cm long animal for general morphology, and text for details).

Glen Canyon Group tracksites. — To date we have discovered three tracksites in the Glen Canyon Group all at about the same stratigraphic level, in red playa sediments approximately seven meters above the base of the White Sandstone sequence. The most important locality, UCD91-8, reveals a *Brachychirotherium* manus-pes set and a large semi-spherical to ovoid track of unknown affinity. UCD 91-11 mainly reveals trampling and tracks in cross section, but one poorly preserved three-toed track has been recorded. The third locality, McConkie Ranch, in the Vernal area reveals several small tridactyl tracks as well as the enigmatic large semi-spherical to ovoid tracks. It is conceivable that these large footprints are attributable to reptile-like mammals (synapsids), but we have yet to find well-preserved trackway segments.

DISCUSSION OF POPO AGIE TRACKS

The study to date has also shown that there is a pattern to the stratigraphic distribution of Popo Agie tracks. The well exposed sandstones and siltstones of the lower part of the Red Siltstone Member have so far yielded a *Gwyneddichnium, Rhynchosauroides,* and small theropod tracks (*Agialopus* and cf. *Grallator*) assemblage at a level about 20 meters below the top of the formation. This is exactly the same assemblage as has been reported from this stratigraphic level in Moffat County Colorado some 35-40 miles (about 60 km) to the northeast (Lockley 1986). Moreover, these levels are associated with abundant invertebrate traces (*Scoyenia* and others) both at DNM and in Moffat County Colorado.

By contrast the upper 8-9 meters of the formation, both in the DNM and Vernal areas, appear to yield a preponderance of *Brachychirotherium* tracks, from siltstones and sandstones that are notably more purple and grey than the underlying brick-red stata. Apart from the occurrence of tridactyl tracks in the Vernal area, the only other ichnotaxa recorded from this upper unit are isolated occurrences of phytosaur, synapsid and ?trilophosaurid (=?*Apatopus*) footprints. We therefore tentatively conclude that the upper beds contain a different, facies-controlled, or biostratigraphically distinct ichnofauna. We also noted that the uppermost sandstone beds at DNM, a purple and grey unit 1-2 meters below the base of the Glen Canyon Group, contains abundant small bone fragments throughout the area, and as far west as Redfleet Resevoir and Red Mountain. The bone remains have a distinctive purple tinge and/or halo and resemble coprolite fragments.

When looked at as a whole the Popo Agie vertebrate ichnofauna in the DNM area can be summarized as follows (cf. Figures 7 and 8).

Dinosaur tracks	*Agialopus* and ?*Grallator*
Sphenodontid/lizard tracks	*Rhynchosauroides*
Tanysropheiid tracks	*Gwyneddichnium*
Phytosaur tracks	?*Chirotherium* sp.
Aetosaur tracks	*Brachychirotherium*
Synapsid tracks	-no name-
?trilophosaur tracks	*Apatopus*

The invertebrate traces can be summarized as follows:

Limulid tracks	*Kouphichnium*
?small arthropod traces	*Scoyenia*
?beetle traces	*Bifurcalapes* spp.
?oligochaete trails	*Cochlichnus*
?conchostrachan traces	*Isopodichnus*
?conchostrachan traces	*Acripes*
?arthropod surface trails	*Pterichnus*
?invertebrate trace	*Treptichnus*

This list indicates that, within the study area, most of the major groups of Late Triassic vertebrate trackmakers known from western North America are represented. Moreover, it indicates an abundance of invertebrate life in various fluvio-lacustrine habitats where the trackmakers were active. This allows for the reconstruction of the animal communities of this well known epoch along the lines of the stratigraphic partitioning suggested above, but no doubt with some overlap. As discussed elsewhere (Lockley, 1986; 1987; 1991; Lockley and Conrad, 1989) the *Agialopus, Rhynchosauroides, Gwyneddichnium* assemblage probably represented a community of small reptiles that frequented shoreline habitats in fluvio-lacustrine environments, per-

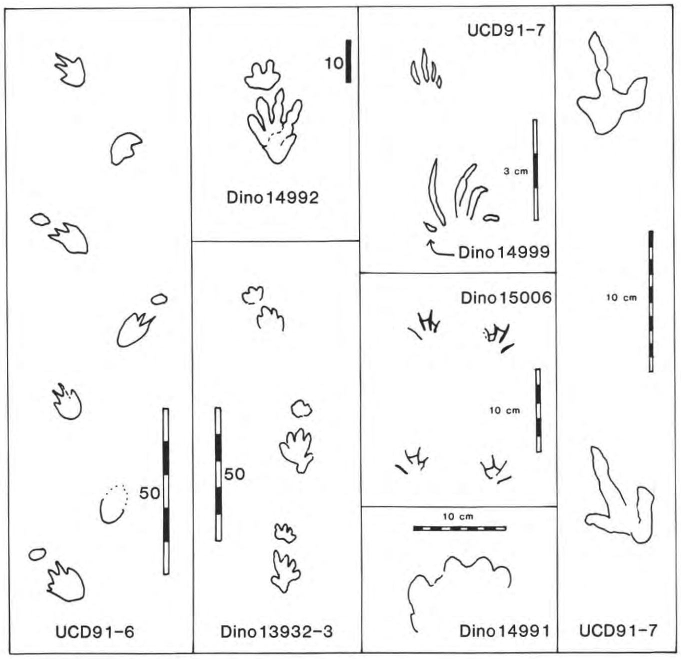

Figure 7. Summary of all known Late Triassic vertebrate track types from the Popo Agie Formation at Dinosaur National Monument (except for *Apatopus*). UCD91-6 = Phytosaur trackway, Dino 13932-3 and 14992 = *Brachychirotherium*, Dino 14999 and UCD91-7 = *Rhynchosauroides*, Dino 15006 = *Gwyneddichnium*, Dino 14991 = ?synapsid track, and UCD91-7 = *Agialopus* (trackway of a small bipedal dinosaur).

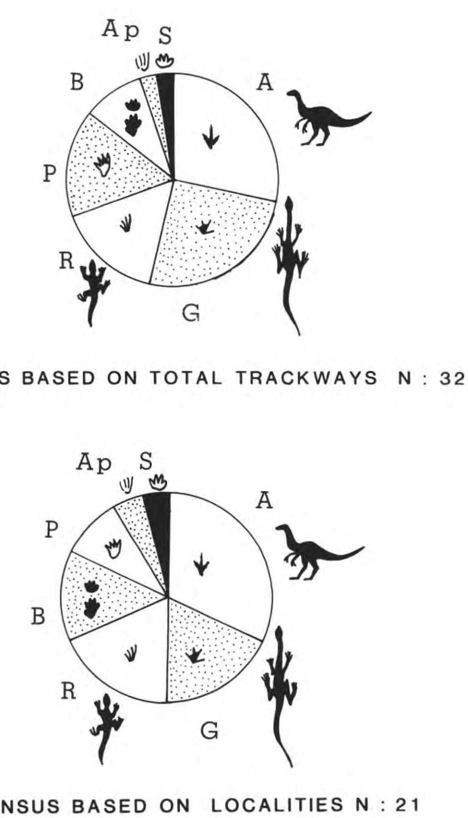

Figure 8. Relative abundance of various trackway types in the Popo Agie/Chinle Formation of the Dinosaur National Monument area based on number of trackways (above), and number of localities with various trackway types (below). Trackway census does not include the large Vermillion Creek site. Locality census includes all known sites and levels.

haps feeding on the invertebrate tracemakers that were so abundant. The *Brachychirotherium* assemblage may represent a more terrestrial community associated with different substrates (paleosols); however, the presence of presumed phytosaur tracks evidently indicates aquatic habitats nearby. As discussed by Lockley and Conrad (1989) preservational factors also come into play, allowing for the preservation of small, delicate traces in certain facies but not in others.

Given that there are virtually no identifiable body fossils known from this stratigraphic unit (the Red Siltstone Member), the tracks provide a useful census of the vertebrate fauna. As shown in Figure 8, the relative abundance of trackmakers can be assessed either by counting the total number of individual trackways, or by counting the number of localities at which particular trackway types occur. Both census methods yield similar results, and show that *Agialopus, Gwyneddichnium,* and *Rhynchosauroides* were the dominant trackmakers in the unit as a whole. As suggested above, the remaining, less common trackways may belong to a different assemblage associated with the upper part of the unit. However in other areas, for example in the Dockum beds of New Mexico (Conrad, et al., 1987) representative trackways from both assemblages are found together. For this reason we have pooled the data for the whole unit. Whether treated separately or together, the track assemblages indicate a mixture of aquatic and terrestrial animals inhabiting environments close to water (shorelines). This evidence appears consistent with the regional evidence of "abundant precipitaion and shallow watertables", even "monsoonal" conditions (Dubiel, et al., 1991). Indeed the high water tables alone may account for the abundance of tracks in this unit.

DISCUSSION OF THE GLEN CANYON SANDSTONE TRACKS

DNM locality UCD91-8 is situated about 7m above the base of the Glen Canyon Group, sometimes referred to as the Navajo/Nugget sandstone, but in all probability a Wingate Formation equivalent (Poole and Stewart 1964a,b). *Brachychirotherium* tracks (DINO 15000) occur in a thin unit of red sandstones, siltsones and shales sandwiched between underlying and overlying cross bedded white sandstones. The red bed sequence exhibits mud cracks, ripple marks, and several other tracks in cross section. *Brachychirotherium* is traditionally regarded as a Late Triassic index ichnite, and is known from the upper part of the Popo Agie Formation in this area, as well as from the upper parts of the Chinle Formation and Dockum Group in Utah and New Mexico, respectively.

The UCD91-8 find is important because it strongly suggests that the lower part (at least 7 meters) of the Glen Canyon Sandstone (so-called Navajo/Nugget) is Late Triassic. Further south, in the Moab region of eastern Utah, the transition from Late Triassic red beds (Chinle Formation) to the overlying eolian units of the Glen Canyon Group (i.e.,the Wingate Formation) is marked by a change from diverse Late Triassic reptile footprint faunas to assemblages dominated by dinosaur tracks (*Grallator* and *Eubrontes* assemblages of probable Liassic age, Lockley 1990). By contrast, in northeastern Utah, this *Grallator-Eubrontes* assemblage appears in the middle part of the sequence at Redfleet Reservoir (Hamblin, 1988) quite high in the Glen Canyon succession. In the Moab area the base of the Navajo Formation is high in the Glen Canyon Group and is undoubtedly of Liassic if not late Liassic age. In the DNM area the term Navajo/Nugget has been used as a synonym for the Glen Canyon sequence. The track evidence however suggests that the base of the Glen Canyon at DNM is significantly older than the base of the Navajo Formation elsewhere in the Colorado Plateau region. This implies a pre-Navajo (Wingate) facies in the lower part of the Glen Canyon sequence in this area (Poole and Stewart, 1964a,b; Fred Peterson and Dan Chure, personal communications, 1991). Furthermore the presence of *Brachychirotherium* implies a temporal correlation with the upper part of the Chinle Formation and the upper part of the Dockum Group (Conrad et al., 1987).

Dr. David Loope (Univ. of Nebraska) reported a site where vertebrate tracks / trampling could be seen in cross section. Measurement of the section at this site revealed tracks at about 8-9 meters above the base of the Glen Canyon Group in thin tabular red bed units intercalated in a sequence of cross-bedded sandstones. Thus the tracks are at approximately the same stratigraphic level as the *Brachychirotherium* tracksite UCD91-8. We were able to recognise this red bed 'playa' sequence throughout much of the western part of DNM as well as in the Vernal area. The fact that the predominantly eolian sandstones of the Glen Canyon Group are broken by a red bed sequence appears to support the suggestion (above) that the Group can be subdivided on lithological grounds.

CONCLUSIONS

1. The Late Triassic ichnofaunas of the Dinosaur National Monument area indicate the former existence of diverse reptile (=archosaur) -dominated faunas in humid, fluvio-lacustrine habitats.

2. The ichnofaunas are typical of this epoch and compare favorably, in diversity and quality of preservation, with coeval track assemblages from the Chinle Formation and Dockum Group elsewhere in the western USA.

3. The high density of tracksites in a small area and at several stratigraphic levels suggests a good potential for further discovery and paleoecological and biostratigraphical synthesis in the future.

4. Well-preserved *Gwyneddichnium* tracks and trackways provide new insights into the anatomy of soft parts (foot web configuration) and behavior (swimming style) of the trackmaker, now thought to be the tanystropheid *Tanytrachelos.*

5. The occurrence of Late Triassic tracks in the basal part of the Glen Canyon Group provides important age constraints for a unit that was not previously dated with any certainty.

ACKNOWLEDGMENTS

This work was funded primarily by the National Park Service (1990-1991) with additional support from the National Science Foundation prior to 1990. Dr. Farley Fleming (U.S. Geological Survey) participated in the project in 1990 and discovered DNM site UCD 90-3. Dan Chure, Sue Ann Bilbey and Fred Peterson assisted with valuable discussions.

BIBLIOGRAPHY

Baird, D. 1986. Some Upper Triassic reptiles, footprints, and an amphibian from New Jersey. The Mosasaur. Journal of the Delaware Paleontological Society 3:125-153.

Bock, W. 1952. Triassic reptilian tracks and trends of locomotor evolution. Journal of Paleontology 26:395-433.

Branson, E.B., and Mehl, M.G., 1932. Footprint records from the Paleozoic and Mesozoic of Missouri, Kansas and Wyoming. Geological Society of America Bulletin 43:383-398.

Conrad, K. (in prep). Vertebrate Ichnology of the Popo Agie Formation, Colorado, Utah and Wyoming. Master's Thesis, Department of Geology, University of Colorado, Boulder (provisional title).

Conrad, K., Lockley, M. G. and Prince N. K. 1987. Triassic and Jurasssic vertebrate dominated trace fossil assemblages of the Cimmaron Valley region : implications for paleoecology and biostratigraphy. New Mexico Geological Society Guidebook. 38th Field Conference, p. 127-138.

Dubiel, R. F., Parrish, J. T., Parrish, M. and Good, S. 1991. The Pangean Megamonsoon — evidence from the Upper Triassic Chinle Formation, Colorado Plateau. Palaios 6:347-370.

Hamblin, A. 1988. Tracksite in the Navajo/Nugget Sandstone Redfleet Reservoir, Uintah County, Utah. Abstracts with Program, International Symposium on Vertebrtae Behavior Derived from the Fossil Record. Museum of the Rockies (Sept 8-10, 1988) 20 p.

High, L. R. Jr. and Picard, M. D. 1969. Stratigraphic relations within the upper Chugwater Group (Triassic, Wyoming). American Association of Petroleum Geologists Bulletin 53:1091-1104.

Lockley, MG., 1986. Dinosaur Tracksites: a fieldguide published in conjunction with the First International Symposium on Dinosaur Tracks and Traces. University of Colorado Geology Deptartment Magazine Special Issue #1. 56 p.

Lockley, M.G. 1987. Dinosaur Trackways. In: Olsen, E., and Czerkas, S. (editors), Dinosaurs Past and Present. Los Angeles County Museum, p. 81-95.

Lockley, M. G. 1990. Tracking the rise of dinosaurs in eastern Utah. Canyon Legacy. (Dan O'Laurie Museum, Moab, Utah) 2:2-8.

Lockley, M. G. 1991. Tracking Dinosaurs: A New Look at an Ancient World. Cambridge University Press. 238 p. (in press)

Lockley, M. G. and Conrad, K. 1989. The paleoenvironmental context, preservation and paleoecological significance of dinosaur tracksites in the Western USA. p. 121-134 In: Gillette, D. D. and Lockley, M. G. (editors) Dinosaur Tracks and Traces. Cambridge University Press, 454 p.

Lockley, M. G., Fleming, R. F. and Conrad, K. 1990 Distribution and significance of Mesozoic vertebrate trace fossils in Dinosaur National Monument. In: Boyce, M. S., and Plumb, G. E. (editors), 14th Annual Report, University of Wyoming National Park Service Research Center, p. 39-41.

Olsen, P. E. 1979. A new aquatic Eosuchian from the Newark Supergroup (Late Triassic—Early Jurassic) of North Carolina and Virginia. Postilla 176:1-14.

Olsen, P. E., and Flynn, J. J. 1989. Field guide to the vertebrate paleontology of Late Triassic age rocks in the southwestern Newark Basin (Newark Supergroup, New Jersey and Pennsylvania). The Mosasaur, Journal of the Delaware Valley Paleontological Society 4:1-43.

Pipiringos, G. N., and O'Sullivan, R. B. 1978. Principal unconformities in Triassic and Jurassic rocks, Western Interior United States — A preliminary Survey. U.S. Geological Survey Professional Paper 1035-A, 29 p.

Poole, F. G., and Stewart, J. H. 1964a. Chinle Formation and Glen Canyon Sandstone in northeastern Utah and northwestern Colorado. U. S. Geological Survey Professional Paper 501-D, p. D 30-39.

Poole, F. G., and Stewart, J. H. 1964b. Chinle Formation and Glen Canyon Sandstone in northeast Utah and northwest Colorado. In: Sabatka, E. F. (editor), Guidebook to the Geology and Mineral Resources of the Uinta Basin, Utah's Hydrocarbon Storehouse. Intermountain Association of Petroleum Geologists, 13th Annual Field Conference, September 16-19, 1964.

Rowley, P. D., Kinney, D. M., and Hansen, W. R. 1979. Geologic map of the Dinosaur Quarry Quadrangle, Uintah County, Utah. U. S. Geological Survey Map GQ-1513.

Thulborn, R.A. 1989. The gaits of dinosaurs, p. 39-50 In: Gillette, D. D. and Lockley, M. G. (editors), Dinosaur Tracks and Traces. Cambridge University Press, 454 p.

Untermann, G. E., and Untermann, B. R. 1954. Geology of Dinosaur National Monument and vicinity. Utah Geological and Mineralogical Survey Bulletin 42:46.

APPENDIX:

VERTEBRATE AND INVERTEBRATE TRACE FOSSIL SPECIMENS DINOSAUR NATIONAL MONUMENT

Locality number	Track name/type	DINO specimen #
UCD90-1	tridactyl (theropod)	
UCD90-2	*Brachychirotherium*	14992
"	mammal-like reptile	14991
UCD90-3	*Brachychirotherium*	13932
"	"	13933
UCD90-4	tridactyl (theropod)	
UCD91-5a	tridactyl (?*Agialopus*)	14997
"	"	14998
UCD91-5b	*Gwyneddichnium*	15006
"	"	15007
UCD91-6b	?*Apatopus*	15110
	"	15111a
	"	15111b
UCD91-7	*Rhynchosauroides*	14999
UCD91-8	*Brachychirotherium*	15000
UCD91-9	*Gwyneddichnium*	15001
"	?*Brachychirotherium*	15002
UCD91-10	*Kouphichnium*	15003
"	*Scoyenia*	15008
UCD91-14	Tridactyl track	15112
UCD91-15a	*Rhynchosauroides*	15113
UCD91-15b	*Gwyneddichnium*	15114
	Rhynchosauroides	15115
UCD91-16	*Rhynchosauroides*	15119
	"	15120
	Gwyneddichnium	15121
	Isopodichnus	15122

VERNAL AND JENSEN AREAS: Redfleet, Red Mountain and Cliff Creek sites
(specimen numbers not assigned).

42Un563T	(Redfleet North)	Tridactyl dinosaur tracks
42Un564T	(Redfleet West)	*Brachychirotherium* manus pes set
42Un625T	(Old Power Plant)	*Brachychirotherium*
42Un626T	(McConkie Ranch)	Tridactyl dinosaur tracks (not collected)
42Un627T	(Cliff Creek)	*Agialopus*, unnamed insect trail
42Un628T	(Red Mountain West)	Tridactyl dinosaur tracks
	Red Mountain East	? tridactyl dinosaur tracks

GENERAL GEOLOGY OF THE OGDEN AREA, UTAH
A Field Guide and Road Log for Teachers and Students of Geology

by
James R. Wilson
Dept. of Geology
Weber State University
Ogden, UT 84408-2507

This road log begins at the intersection of U.S. 89 and Harrison Boulevard in South Ogden, Utah. Cumulative mileage is shown in the first column. The number in bold after the description is the mileage to the next mentioned feature in the road log.

0.0 Intersection of U.S. 89 and Harrison Boulevard. Proceed east on U.S. 89 to the first road on the right. **0.3**

0.3 Turn right on paved road and immediately turn left into the parking lot of the Baptist Church. **0.1**

0.4 **STOP 1: OVERVIEW OF THE MOUTH OF WEBER CANYON AND LAKE BONNEVILLE SHORELINES.** Park in the southeastern corner of the church parking lot and walk to the crest of the small knoll about 50 m to the east. From this point there is a spectacular view of the mouth of Weber Canyon, cut by the Weber River into the Wasatch Range. This immediately raises the question of which was here first. Did the Weber River begin flowing across a gently sloping landscape that gradually rose beneath it, forcing the river to erode a deep canyon to maintain its course across the rising mountain range? If so, the river would be referred to as antecedent. Or, was an old mountain range buried by immense amounts of sediment across which the ancestral Weber River began flowing. As time passed, the sediment was eroded, the mountains exhumed, and the river eroded through the mountains as it was lowered onto them. This latter scenario would mean that the river was superimposed. The terms superimposed and antecedent were first suggested by John Wesley Powell as a result of his explorations on the Green and Colorado Rivers of Utah during the 1860 s and 1870 s. To adequately answer the question as to whether a particular stream represents antecedence or superimposition, it is necessary to know something of the geologic history of the area. It is now known that many western mountain ranges were deeply buried by Tertiary sediments and are even now still being exhumed. In the Wasatch, remnants of Tertiary gravels are common on some of the mountain summits and form extensive deposits in the area of Echo Junction along the route of I-84 that you see here. However, the mountains from which these sediments were derived lay to the west of us, implying that drainage should have been to the east. Could the Weber River have reversed its course? All this would suggest superimposition. But now let us examine the mountains. The mountain front here is marked by spectacular examples of triangular facets. Triangular facets result when fault movement along a mountain front cuts off the toe of ridges. Upward movement of the mountain block and erosion result in triangular terminations of the ridges and these are known as facets. Most of you are probably aware of the Wasatch Fault and features such as these facets are prime evidence of its presence. The uplift of the mountains along the

Wasatch Fault presumably continues today and the effect of this rising mountain mass beneath the channel of the Weber River would suggest that antecedence is an important component of the river's history. Many rivers in the west illustrate evidence for both antecedence and superimposition. While it may be impossible to discern the specific importance of each, ample opportunity for generating discussions of cause and effect with students can be found when contemplating a river canyon through a mountain range.

At this point, the mountains are formed in the metamorphic rock of the Farmington Canyon Complex. Named for Farmington Canyon, outside of Farmington, Utah, where it is well exposed along the road up the canyon, the rocks were formed deep within the Earth by extreme heat and pressure approximately 1.8 billion years ago (Hedge and others, 1983) during the Precambrian Era. The degree of heat and pressure can be appreciated by observing the incipient melting of the rocks that occurred during metamorphism. In the Farmington area white streaks visible on the cliffs and seen more closely in road cuts going up Farmington Canyon represent pegmatites (coarse-grained quartz-feldspar rocks) which formed as silica-rich minerals began to melt during metamorphism. The darker minerals have a higher melting point and rather than melting became oriented during metamorphism to form rocks such as gneiss and schist. Many rocks in this part of the Wasatch represent combinations of pegmatite veins in the darker gneiss and schist. Mixed rocks of this type, resulting from the near-melting during metamorphism are referred to as migmatites. They commonly exhibit folding that occurred while the rocks were in a plastic state, similar to what you see upon squeezing a large amount of toothpaste out of a tube.

From this viewpoint we have two prominent shorelines of Lake Bonneville spread out before us. The highest shoreline, seen as the distinct bench on the triangular facets of the mountain front, is the Bonneville shoreline and is approximately 5200 feet in elevation. The surface on which we stand, and its counterpart seen across the valley, represents the Provo level of Lake Bonneville. This is the largest, widest bench created by Lake Bonneville and is found at approximately 4800 feet in elevation along the Wasatch Front. At its highest, Lake Bonneville extended up Weber Canyon and into the valleys beyond. Sediments from the mountains were washed down into the valleys and filled them. When Lake Bonneville broke through its threshold in Idaho resulting in a catastrophic flood and a rapid drop in lake elevation in this area, sediment was washed out of the higher valleys and canyons. During the Provo level, sediment accumulated here at the mouth of the canyon to form a broad delta. Driving south on U.S. 89, you come down off the delta as you travel from Kaysville to Farmington and it extends northward to North Ogden. As the lake shrank from the Provo level to its present elevation, the Weber River has adjusted to the changing base level by eroding into the lake sediments to create the broad valley we see before us. The lake sediments are mixtures of clay, sand, and gravel, although here in the river-deposited sediments of the delta there is a preponderance of sand and gravel. This makes the sediments a valuable resource as evidenced by the large gravel pits. The lake sediments are not particularly strong and not cemented, thus slumps and landslides are common along the steep slopes of the valley.

From this site it is also possible to see the effects of different climate on north-facing and south-facing ridges. The north-facing slopes are generally steeper and rockier than the south-facing slopes. The south-facing slopes have smoother slopes and more vegetation indicating greater soil accumulation through the effects of chemical weathering and favorable conditions for plant growth. North-facing slopes may experience more physical weathering through frost wedging, creating steeper slopes that are less favorable for soil accumulation, and thus, plant growth. Botanists would probably find distinctive plant communities on the two contrasting slopes.

Return to the intersection of U.S. 89 and Harrison. **0.4**

0.8 Intersection of U.S. 89 and Harrison Boulevard. Drive north on Harrison Boulevard. **0.5**

1.3 Intersection. Wilshire Theater on the left. Exposures of Lake Bonneville sediments behind the gas station and shopping center northeast of the intersection. **0.4**

1.7 Crossing Burch Creek. Note the intensive development which is now occurring in this valley west of Harrison Boulevard. **1.5**

3.2 Intersection with 42nd South St. Turn right onto Country Hills Drive. **0.7**

3.9 **STOP 2: BEUSS POND PARK.** Beuss Pond is a small sag pond created either by a graben along the Wasatch Fault or by tilting of slump blocks along the fault. Ponds and marshy areas are common along the trace of faults and many examples of this can be found along the Wasatch Fault. These features result in the accumulation of organic material that can be dated by radiometric carbon 14 which can allow us to time recurrent faulting events. Large boulders of pink Tintic Quartzite border the parking area. **0.4**

4.3 To the right on the mountain slope above the houses is a rounded depression in the mountain that marks the scar of a prehistoric rockslide. Rock falls and rock slides have occurred sporadically, but continuously, throughout the geologic past along the

Wasatch Front and will continue to do so. In the event of a major earthquake, catastrophic rock falls, slides, and avalanches are a possibility. Continue along Country Hills Drive as it curves around to become 36th South St. and intersects Harrison Boulevard. **1.0**

5.3 Intersection of 36th South St. with Harrison Boulevard. Turn right (north) on Harrison. **1.8**

7.1 **STOP 3: DEE MEMORIAL PARK.** Stop on the north edge of the park and proceed to one of the small hills in the park for a view of the rocks and structure of the Wasatch Front. The pink and tan rocks of the Tintic Quartzite dominate the scene. These were formed in Cambrian-Precambrian time and unconformably rest upon the metamorphic rocks of the Farmington Canyon Complex. An unconformity results when there is a period of erosion or non-deposition in which rocks may be removed to create an erosional surface. This period of erosion may last tens or hundreds of millions of years, but is represented in the geologic record only as a surface between rock layers. When the period of erosion eventually comes to an end, sediment deposited in the area covers the irregularities of the old erosion surface. An unconformity of the type that we see here, where sedimentary rocks overlie metamorphic rocks,is known as a nonconformity.

Folding of the rocks is visible as you look at the face of the mountains and see how the rocks drape across the front. In addition to the young, still active, Wasatch Fault at the foot of the mountain front, there are other older, inactive faults that make up the mountains. Many of these are thrust faults wherein rocks from the west were literally shoved eastward to pile up repetitive layers as they overlapped each other. Repetition of rock layers by thrust faults can be seen during a drive up Ogden Canyon to Ogden Valley, where gray limestone layers can be seen being repeated.

As you look at the scene in front of you it can be seen how the Tintic Quartzite comes down and is cut off south of the canyon and then reappears high up on the mountain front to the north of the canyon. Discontinuity of rock layers such as seen here is one of the primary ways by which we recognize that faulting has occurred.

Proceed around the block on which the park is located and re-enter Harrison heading north (turn right). **1.0**

8.1 Intersection with 20th South St. Turn right and immediately turn left onto Valley Drive. **0.7**

8.8 The vegetation on the right conceals a slump that came down across the road and flowed out onto the golf course to the left. **0.5**

9.3 Turn right into the parking lot of Rainbow Lanes and proceed straight ahead to the rear of the lot.

STOP 4. SLUMPS IN LAKE BONNEVILLE SEDIMENTS.

This area is noteworthy for the development of a large circular amphitheater from numerous slumps that have occurred here. A slump is a form of mass movement (movement by gravity rather by erosion) in which the block or blocks of material is rotated along a curved surface as it moves down. Slumps are common forms of slope failure and frequently occur in unconsolidated material that has become saturated with water. For this reason slumps are most common in spring in our area when snow melt has saturated the ground and rains may occur as well. It should be noted that one of the worst scenarios for earthquakes in our area is to have a major earthquake in the spring when the ground is saturated. Shaking during the earthquake would greatly increase the likelihood of slumps and other slope failures occurring.

The slump directly south of the parking lot occurred in 1985 and was witnessed by many people. The slump destroyed a steel power line support similar to the ones you see up the hill resulting in a power outage to a large area.

The Wasatch Fault is located just beyond the building and parking lot, toward the mountain front. A prominent fault scarp is visible in the Lake Bonneville sediments on the Provo terrace above the head of the slumps. The fault in this vicinity is also marked by the occurrence of hot springs. The Ogden Hot Springs are located near river level in the mouth of Ogden Canyon. A tufa deposit from a hot spring is located along the trail leading east out of the rear of the parking lot. The hot springs at the mouth of the canyon have a temperature of 56°C (122°F) and have almost 5000 mg/l of chloride (Cole, 1982). Hot springs are common in areas with recent volcanic activity, such as Yellowstone, because very hot rocks can be found close to the land surface. In areas such as the Wasatch Front, where there is no evidence of recent volcanism, water must travel very deep to reach rocks that are sufficiently hot to heat it to high temperature. For this reason, hot springs are uncommon in areas without young volcanic rocks. When hot springs are found in nonvolcanic areas, such as the Wasatch Front, it usually suggests that there are deep fractures or faults in the rock that allow the water to reach great depth and return to the surface. In this area, the Wasatch Fault and associated breaks provide the conduits through which the water can move. As a result there are several hot springs that occur along the length of the Wasatch Fault.

Continue down Valley Drive to its intersection with 12th South St. **0.2**

9.5 Intersection with 12th South St. Turn left (west). **1.0**

10.5 Intersection with Harrison Boulevard. Turn right (north) and proceed up the hill. **0.5**

11.0 Traffic light. Intersection with 9th South Street. Turn right (east) onto 9th South. **0.3**

11.3 Fault Line Gas Station on left. **0.4**

11.7 9th South Street terminates and turns into a restricted gravel road. Park at the end of the pavement and walk about 100 m up the hill to a level area at the top of the steep gravel road.

STOP 5. ROCKS OF THE FARMINGTON CANYON COMPLEX.

At this location we have an excellent view to the south back toward the mouth of Ogden Canyon, our last stop. The amphitheater created by slumping is clearly visible. On the Provo terrace, to the left (east) of the amphitheater, a distinct scarp or break in the ground is visible. This is the trace of the Wasatch Fault. The fault continues on into the general area where we are standing at this stop.

It is possible to make a small rock collection at this stop which will have many different types of metamorphic and some igneous rocks from the Farmington Canyon Complex. In general, you should be able to find several varieties of gneiss, possibly schist, and perhaps a dark-colored rock known as amphibolite. You may find masses of quartz-feldspar-mica rock which represents pegmatite material. Additionally, numerous boulders of pink to brown Tintic Quartzite litter the ground. Many of these boulders show metaconglomerate (gravel) layers as well. Rocks from higher up in the mountain may sometimes be found where they have tumbled down from their original locations. Gray limestone is the most obvious of these.

If we return to the bus by walking northwest along a gravel road and trail to the rusty rocks forming cliffs and talus about 75 m north of the bus, we will find slickensides on the rock surfaces. Slickensides are polish and striations created by fault movement, further evidence of the nearby Wasatch Fault.

Reboard the bus and return down 9th South St. to Harrison. **0.7**

12.4 Intersection with Harrison. Turn right (north). **1.3**

13.7 For the next mile, you should note the steep cliffs and talus formed in the Tintic quartzite. An area like this would be particularly subject to rockfall, especially so during an earthquake. **1.6**

15.3 Fork in the road. Bear right on Mountain Road. From the left side of the bus there are views of the alluvial fan at the foot of the canyon coming down from Mt. Ben Lomond. **1.5**

16.8 Turn left on 2600 North. **1.6**

18.4 Turn right at Washington Boulevard and proceed straight north on 400 East Street. Follow this road up the hill as it changes to 450 East Street (about 1.5 miles), heading toward the Lakeview Heights Water Tank high on the hill. The bus will park somewhere in the vicinity of the water tank depending upon construction activity in the area. From the parking area we will walk up the hill to the prominent escarpment.

STOP 6. BONNEVILLE BEACH.

During the time of the highstand of Lake Bonneville, between 19,000 and 13,000 years ago (Currey, 1980), prominent beaches were created along the Wasatch Front. The beach you see here was incised into alluvial fan deposits at the foot of Mt. Ben Lomond. More recent alluvial fan deposits east of this location have erased the beach from that area. The large number of boulders in this area may be a result of the waves winnowing fine material from the beach leaving the boulders behind.

Numerous stacks, small rocky islands in Lake Bonneville, are present in this area as isolated rocky outcrops. Lake Bonneville features, such as beaches and stacks, along with spits and bars seen in other areas around the lake allow the teaching of coastal geomorphology and oceanography with some local examples, in spite of there not being an ocean in the immediate vicinity.

Return to bus and proceed back down the hill to near the head of Washington Boulevard. **1.3**

19.7 Turn right on 2650 North St., just before the head of Washington Boulevard. **0.1**

19.8 Turn right on Pleasant View Drive. **3.8**

23.6 Intersection with U.S. 89. Turn right (north). **0.1**

23.7 Turn left (west) on dead end road. **0.2**

23.9 Park off the road near the railroad tracks. Don't block any of the roads.

STOP 7: UTAH HOT SPRINGS

Several hot springs occur along the railroad tracks in this area. The temperature and chemistry of these springs is very similar to the Ogden Hot Springs described earlier (Cole, 1982). In the past water from the springs was used for recreation in a swimming complex nearby. Ogden residents would ride the trolley out to this area for a day in the country. Presently the water from the hot springs is used to heat greenhouses that you see to the west.

Across the old road there is a road cut in pink Tintic Quartzite. Close examination of the outcrop reveals numerous slickensides indicating fault movement. The Wasatch Fault or one of its subsidiaries passes through here. Once again, the occurrence of hot springs is an indication of water traveling to great depths along the fractures created by faulting, being heated, and rising back to the surface along other fractures.

Return to the bus and go back to U.S. 89. **0.2**

24.1 Intersection with U.S. 89.

From this point you may continue on U.S. 89 back into Ogden, continue north along the highway to view features in the Willard-Brigham City area, or travel south and west to Little Mountain and the shores of the Great Salt Lake.

REFERENCES

Cole, D.R., 1982, Tracing fluid sources in the East Shore area, Utah: Ground Water, v. 20, no. 5, p. 586-593.

Currey, D.R., 1980, Coastal geomorphology of Great Salt Lake and vicinity: Utah Geological and Mineral Survey Bulletin 116, p. 69-82.

Hedge, C.E., Stacey, J.S., and Bryant, Bruce, 1983, Geochronology of the Farmington Canyon Complex, *in* Miller, D.M., Todd, V.R., and Howard, K.A. eds., Tectonic and stratigraphic studies in the Eastern Great Basin: Geological Society of America Memoir 157, p. 37-44.

MIOCENE MONZONITIC INTRUSIONS AND ASSOCIATED MEGABRECCIAS OF THE IRON AXIS REGION, SOUTHWESTERN UTAH

by
H. Richard Blank, Peter D. Rowley*, and David B. Hacker=*
**U.S. Geological Survey, P.O. Box 25046, Denver, C0 80225*
=Dept. of Geology, Kent State Univ., Kent, OH 44242

GEOLOGIC SETTING

This two-day field trip begins and ends each day in Cedar City, located 250 miles south of Salt Lake City in southwestern Utah. The route is entirely within the Cedar City 1° x 2° quadrangle (Fig. 1). The geologic history of this quadrangle is summarized by Winkler and Shubat (1990); reviews of the Cenozoic stratigraphy and structure are given by Anderson and Rowley (1975), Rowley and others (1979), and Siders and Shubat (1986). Just east of Cedar City, the dramatic Hurricane Cliffs (Anderson and Mehnert, 1979) mark the physiographic boundary separating the highly extended Basin and Range Province from the mildly extended High Plateaus section of the Colorado Plateau. This boundary follows a structural hinge line associated with an eastward change from miogeoclinal to cratonic sedimentary facies in Paleozoic and Mesozoic rocks. It also corresponds roughly to the eastern limit of the foreland fold-and-thrust belt of the late Mesozoic Sevier orogeny (Armstrong, 1968). Structures produced by Tertiary magmatism and regional extension are commonly superimposed on the compressional features, and occur both in the Basin-and-Range and on the adjacent Colorado Plateau; the structural transition between these two provinces, in contrast to the physiographic transition, is diffuse, encompassing much of the Cedar City quadrangle. Multidisciplinary studies currently being carried out under the aegis of the U.S. Geological Survey's BARCO (Basin and Range-Colorado Plateau transition zone) project are aimed at a better understanding of the tectonic and magmatic evolution of this complex zone (see Blank and Kucks, 1989, for preliminary compilations of the geophysics and geology of the BARCO area).

A generalized, composite stratigraphic column for the field trip area is given on figure 2. The oldest exposed rocks are marine limestone, shale, and siltstone of the Jurassic Carmel Formation and overlying synorogenic clastic sedimentary rocks of the Iron Springs Formation of apparent Late Cretaceous age. These rocks were tectonically raised during eastand southeast-directed Sevier thrusting. The resulting topographic forms were reduced by erosion during

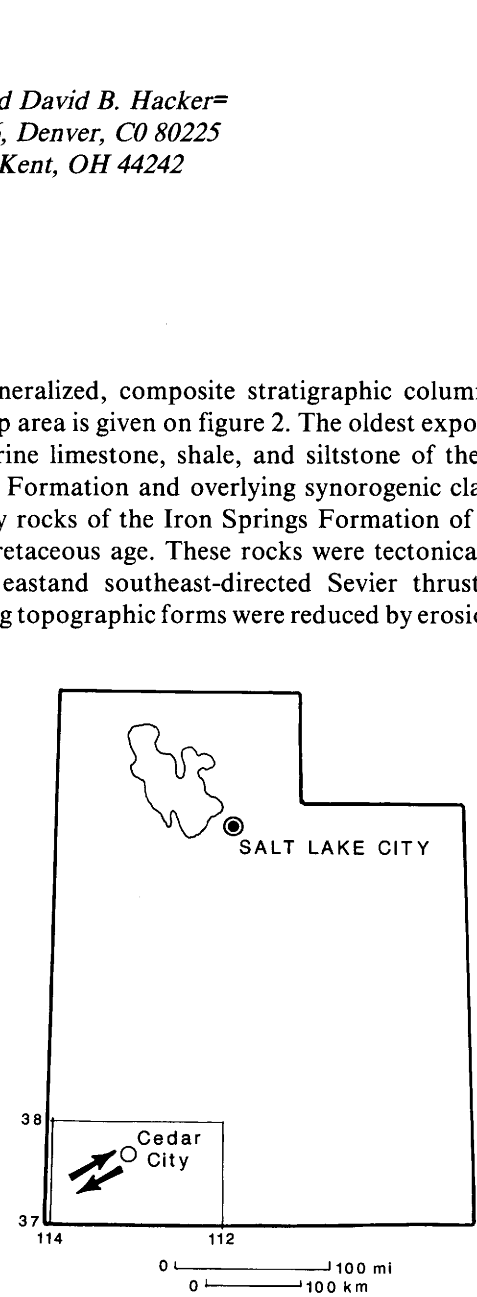

Figure 1. Index map of Utah, showing Cedar City 1° x 2° quadrangle and area of field trip (arrows).

AGE	(Ma)	FORMATION (excluding intrusive rocks, thin sedimentary intervals, and unconsolidated deposits)	MEMBER	MAXIMUM THICKNESS (m)
QUATERNARY AND PLIOCENE	<2?	YOUNG BASALT		180
	<5?	BASIN FILL		2-3000?
PLIOCENE(?)	5?	RHYOLITE AND DACITE OF SHINBONE CREEK AND EIGHTMILE SPRING		120
MIOCENE	8-9	RHYOLITE AND DACITE OF ANTELOPE RANGE		80
	10-11?	BASALT OF FLATTOP MOUNTAIN		120
	>12	VOLCANICLASTIC ROCKS OF NEWCASTLE RESERVOIR		370
	5-12?	VOLCANICLASTIC ROCKS OF ENTERPRISE RESERVOIR		370
	11-15	RHYOLITE AND DACITE OF FLATTOP MOUNTAIN COMPLEX		380
		TUFF OF HONEYCOMB ROCKS		180
	12-13?	OX VALLEY TUFF		170
		TUFF OF CEDAR SPRING		90
		BASALT OF PILOT CREEK		120
	19-20	RACER CANYON TUFF	UPPER MEMBER	460
			LOWER MEMBER	
		ANDESITE PORPHYRY OF MAPLE RIDGE		90
		ANDESITE OF SHOAL CREEK AND NORTH HILLS		250
		PINE VALLEY LATITE		610
	21	RENCHER FORMATION	LAHAR MEMBER	300
			UPPER TUFF MEMBER	
			LOWER TUFF MEMBER	
		DACITE OF PIÑON PARK WASH		150
	22	HARMONY HILLS TUFF		170
		ANDESITE OF LITTLE CREEK		370
	23	CONDOR CANYON FORMATION	BAUERS TUFF MEMBER	180
			ANDESITE	80
			SWETT TUFF MEMBER	30
OLIGOCENE	24	LEACH CANYON FORMATION	TABLE BUTTE TUFF MEMBER	290
			NARROWS TUFF MEMBER	
	27	ISOM FORMATION	HOLE-IN-THE-WALL TUFF MEMBER	50
			BALDHILLS TUFF MEMBER	300
		ANDESITE		40
	28-30	WAH WAH SPRINGS FORMATION		50
OLIGOCENE AND EOCENE		CLARON FORMATION	UPPER(WHITE)LIMESTONE MEMBER	500
			MIDDLE RED LIMESTONE MEMBER	
			BASAL CONGLOMERATE MEMBER	
LATE CRETACEOUS		IRON SPRINGS FORMATION (EQUIVALENT TO KAIPAROWITS FORMATION, STRAIGHT CLIFFS AND WAHWEAP SANDSTONE, TROPIC FORMATION, AND DAKOTA SANDSTONE OF COLORADO PLATEAU)		1200
JURASSIC		CARMEL FORMATION	WINSOR MEMBER	250
			BANDED MEMBER	
			HOMESTAKE LIMESTONE MEMBER	
			BASAL SILTSTONE MEMBER	

Figure 2. Generalized, composite stratigraphic column for *iron axis* region, Utah (Basin and Range sector). See appendix for descriptions and references.

early to middle Tertiary time and largely buried beneath conglomerate, siltstone, and lacustrine limestone of the Claron Formation, which is generally considered to be Eocene and Oligocene, although the base may locally include Paleocene strata (see Goldstrand, 1990). With the onset of calc-alkalic volcanism during the Oligocene, at about 33 Ma, and continuing into the early Miocene, deposits of ash-flow tuff of the Needles Range Group, Isom Formation, and Quichapa Group were spread over the region from sources to the west and northwest (mostly in the Caliente and Indian Peak nested-caldera complexes; see Ekren and others, 1977; Rowley and Siders, 1988; and Best, Christiansen, and Blank, 1989). In the field trip area, these tuffs are intercalated with lava, laharic breccia, and near-vent explosion-breccia erupted from local andesitic volcanoes, but for the most part they were deposited on surfaces of low relief.

Structural and topographic relief were again produced during the early Miocene, this time as a result of regional monzonitic magmatism. Hypabyssal intrusions were emplaced as bulbous laccoliths, sills, and other, at least partly concordant, bodies of various forms. More than a dozen discrete intrusive bodies have been mapped within this magmatic province and others are known from drilling or inferred from their cover-rock structures and aeromagnetic signatures. Many bodies are interconnected and much more extensive at depth, as indicated by the regional aeromagnetic anomaly pattern (Fig. 3). The intrusions occur in a broad northeast-trending belt that follows the trend of the Sevier orogenic front. Sevier trends are oriented about 45° off the average northerly strike of the Hurricane fault and other major extensional structures of the Basin-and-Range to Colorado Plateau transition zone in this region, but are nearly parallel to northeast-trending offsets of the Plateau margin. Thus the older structures (thrusts, folds, intrusions) likely had a significant influence on the evolution of late Cenozoic extensional structures.

Alignment of laccolithic intrusions and associated iron deposits in the Bull Valley and Iron Springs mining districts along a Sevier thrust fault (Mackin, 1954; Van Kooten, 1988) inspired the term *iron axis* (Mackin, 1960), which has subsequently been used in reference to the entire magmatic province (e.g., Tobey, 1976). The exposed bodies yield K-Ar ages of 20-22 Ma. Most are quartz monzonite to granodiorite porphyries, although the Mineral Mountain intrusive, at the southwest end of the belt, is a granite porphyry (Morris, 1980; Adair, 1986), and the Iron Peak (Iron Point) intrusive, at the northeast end, is composed of gabbro-diorite (Spurney, 1984). Rock of all nine iron-axis intrusions that can be seen on this field trip is characterized by phenocrysts of plagioclase (andesine-labradorite), biotite, hornblende and/or pyroxene (diopsidic augite), and magnetite; the groundmass, comprising 1/3 to ½ the total volume, is mainly fine-grained quartz and potassium feldspar. Hereafter such rock is referred to simply as *monzonite,* and its extrusive equivalent, as latite, regardless of its mineralogical or chemical classification according to any particular standard. Typical monzonite or latite rock has been altered to some extent by deuteric or vapor-phase processes.

Allochthonous sheets, slabs, wedges, and irregular blocky masses of lateral dimensions in the range 0.1-10 km and thicknesses up to several hundred meters, and consisting of highly brecciated volcanic and sedimentary rock, 21 Ma and older, are widely distributed throughout the monzonite province, both in the Basin and Range sector and on the western Markagunt Plateau. They commonly sole on shallow, subhorizontal *detachment* structures that truncate little disturbed pre-monzonite formations. In some places rocks of different ages are chaotically mixed; in others, stratigraphic continuity tends to be preserved but formations are internally broken and rotated or pervasively brecciated on macro-to microscopic scales. These megabreccias, locally mapped as chaos in early work (Blank, 1959), have been interpreted as slide masses related variously to intrusion (Blank, 1959, 1991; Mackin, 1960; Rowley and others, 1989), to plateau uplift (Sable and Anderson, 1985), and to fault scarps (Anderson, 1985, 1988; unpub. data); or formed by regional shallow low-angle detachment faulting (Maldonado and others, 1990; in press). Mapping of megabreccias in the region is not yet complete and at present there is no compelling reason to attribute a common origin to all occurrences.

The main purpose of this field trip (Fig. 4) is to examine megabreccia deposits southwest of Cedar City in the Iron Springs district, northern Pine Valley Mountains, and eastern Bull Valley Mountains, and to evaluate field evidence bearing on their structural relations to the Iron Mountain, Stoddard Mountain, Pine Valley, and Bull Valley-Big Mountain intrusives. As a working hypothesis, we attribute the distribution of these megabreccias and their association in many places with regional low-angle normal faults to regional distension resulting from pervasive upper-crustal monzonitic magmatism; and the characteristics of specific megabreccia deposits are explained as local accommodation to structural and topographic distortions resulting from rapid emplacement of magma in local near-surface environments. At Iron Mountain, the breccias consist of isolated narrow ribs of steeply dipping Claron strata distributed in an arcuate pattern around the intrusion and overlain by flat slabs of pulverized volcanic rocks of the Isom Formation and Quichapa Group, strongly suggesting emplacement as gravity slides from the oversteepened intrusive dome. Farther southwest, in the Bull Valley district, megabreccias are composed of rock apparently sloughed from the roof of the Bull Valley-Big Mountain intrusive arch as the monzonitic magma rose rapidly, broke through to the surface, and was spread over the region as latite ash flows. The age of the oldest ash-flow tuff deposits (upper Rencher Formation) blanketing the megabreccias and the age of the youngest rocks within the megabreccia (lower Rencher Formation) constrain the time of emplacement to be penecontemporaneous with Rencher and the Bull Valley-Big Mountain intrusive, that is, about 21-22 Ma. Stacked megabreccias between the Bull Valley-Big Mountain area and the Pine Valley Mountains are interpreted as material initially emplaced as slides from the west and north and subsequently

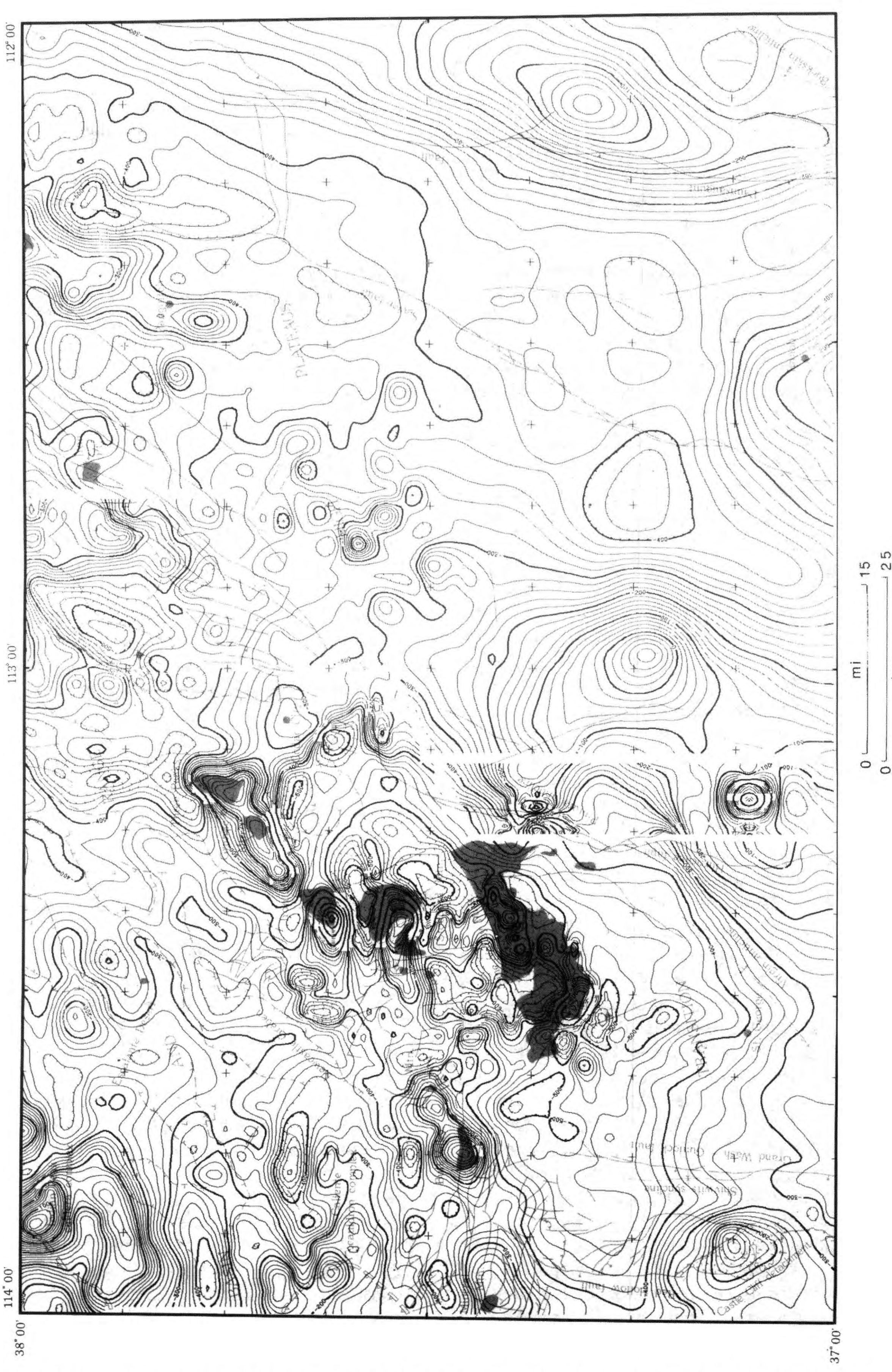

Figure 3. Residual total-intensity aeromagnetic anomaly map of Cedar City 1° x 2° quadrangle, southwestern Utah, after Blank and Crowley (1990). Isopleth interval 20 nanoteslas. Tertiary monzonitic intrusions shaded.

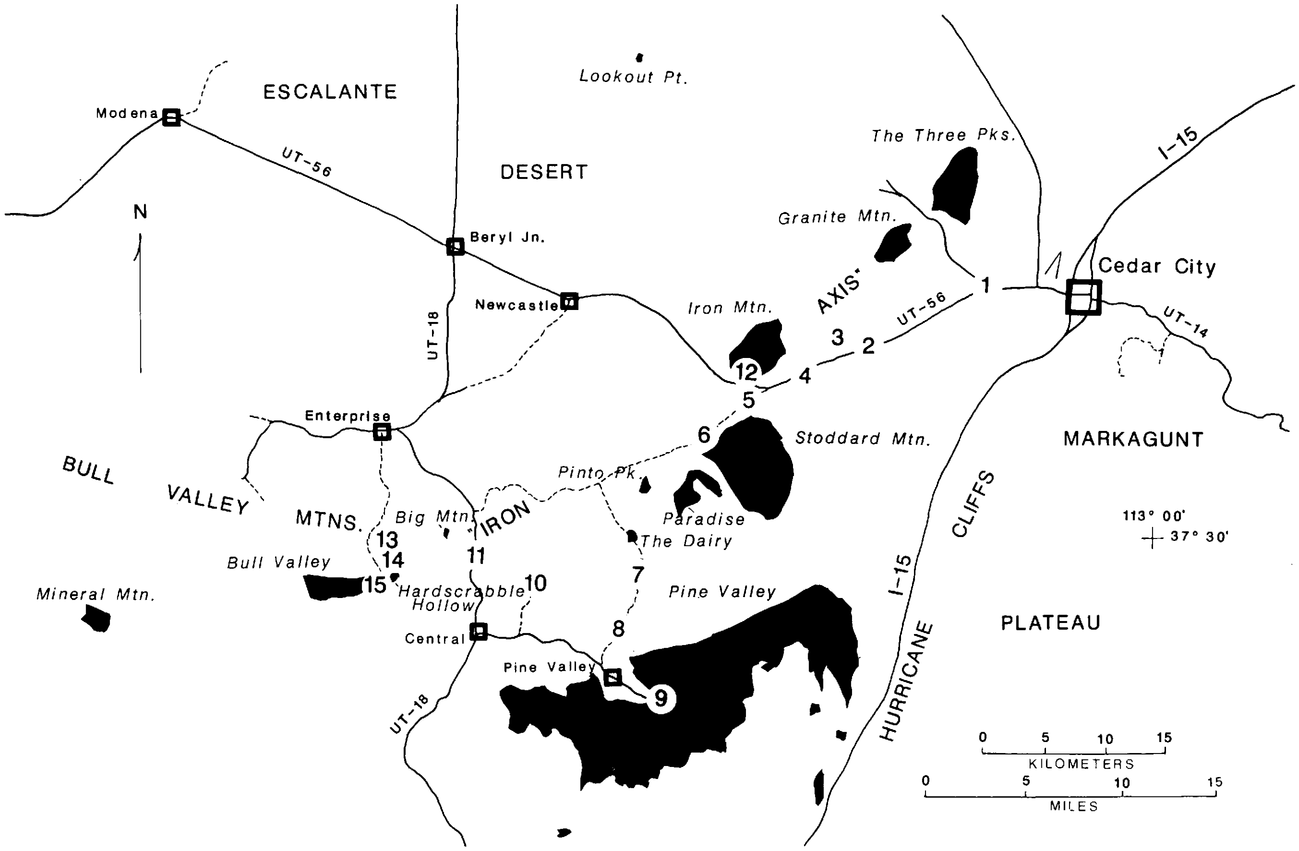

Figure 4. *Iron axis* region, showing early Miocene monzonitic intrusions (solid black) and route of field trip (stops 1-12, DAY ONE; stops 13-15, DAY TWO).

deformed and overidden by new slides and thrust sheets emplaced during growth of the Pine Valley laccolith. These rocks form a vast allochthonous complex of pre-intrusive formations and Rencher ash-flow, mudflow, and alluvial deposits, locally capped by lava genetically related to the laccolith (Pine Valley Latite).

Following the monzonite episode, the region received additional ash-flow deposits from the west (Racer Canyon Tuff); the distribution of these younger sheets was strongly influenced by local topography. Andesitic volcanism continued intermittently. Bimodal (rhyolite-basalt) volcanism began at 14-15 Ma and has persisted sporadically through the late Cenozoic. The peak of the bimodal phase of magmatic activity may have been reached during the interval 11-15 Ma, which saw the development of major silicic eruptive centers in the Bull Valley Mountains and emplacement of the youngest regional ash-flow sheet (Ox Valley Tuff). This interval approximately coincides with a period of rapid regional extension in adjacent parts of the Basin and Range province (Wernicke and others, 1988). Middle to late Miocene extension in the Bull Valley Mountains was accompanied by west-northwest dextral faulting, as emphasized by Anderson (1987) and Anderson and Barnhard (in press). Northeast-striking, high-angle normal faults characteristic of basin-range structure were active only after about 8.5 Ma ago (Shubat and Siders, 1988; Blackett and others, 1990).

ROAD LOG

DAY ONE Cedar City to Iron Mountain slide area, Pinto, Pine Valley, Atchinson Mountain, and Mountain Meadow, then return via Newcastle, with brief stop at Blowout pit on Iron Mountain. Day's agenda includes optional excursion up Coal Creek Canyon for panoramic views of Hurricane fault scarp and Iron Springs monzonite intrusions, and group dinner at Sugar Loaf Restaurant, Cedar City.

ASSEMBLE ON EAST SIDE OF CITY PARK, 200 N AND 100 E STREETS, FOR 8:00 AM DEPARTURE.

Mileage

Interval	Cumulative	
0	0	200 N and Main St. (traffic light). Proceed W on UT-56.
1.0	1.0	I-15 overpass.
4.5	5.5	**STOP 1.** The Y intersection between UT-56 and road to Iron Springs and Desert Mound. Overview of some aspects of the Iron Springs mining district first discussed in a classic report by Mackin (1947). Maps

of the area include those by Mackin (1954), Blank and Mackin (1967), Mackin and Rowley (1976), and Mackin and others (1976). Five monzonitic intrusions (Pine Valley, Stoddard Mountain, Iron Mountain, Granite Mountain, and The Three Peaks) are visible from this vantage point. Pete Rowley will describe the geologic setting. Iron Mountain, Granite Mountain, and the Three Peaks are the three intrusions of the Iron Springs district. These bodies, as well as intrusions of the Bull Valley district, SW of here, were emplaced concordantly at the base of the Homestake Limestone member of the Jurassic Carmel Formation. From here continue SW on UT-56.

2.9 8.4 Quichapa Lake (playa) on L.

3.0 11.4 Crest of low hill of old alluvium.

1.4 12.8 **STOP 2.** Leach Canyon (see Fig. 5): relatively unbroken Quichapa ash-flow sheets dipping E off the Iron Mountain intrusive. Note characteristic lithologies of Harmony Hills Tuff, Bauers Tuff Member of Condor Canyon Formation, and Leach Canyon Formation, all of Quichapa Group (22-24 Ma).

0.5 13.3 **STOP 3.** Still in Leach Canyon: pulverized tuffs of Quichapa Group and Isom Formation (27 Ma) above a low-angle detachment.

0.6 13.9 Roadcut of pulverized Eocene and Oligocene Claron Formation on R. Almost directly W of this cut is a view of Mt. Claron (type locality of the Claron Formation) at about 1:30.

0.5 14.4 Duncan Creek turnoff and old Woolsey Ranch on L. The Woolsey Ranch fault, a WNW-striking left-lateral tear fault at the base of a line of high cliffs one mile to the N of us, bounds a zone of gravity slides from the Iron Mountain intrusive dome.

0.8 15.2 Pulverized Claron conglomerate in roadcut on R.

1.1 16.3 Turnoff to Diamond Z Ranch. Turn L and follow this road, turning L again at the ranch house and again on a track leading steeply up a small knob to a buried water tank near the summit.

1.2 17.5 **STOP 4.** Park vehicles at the water tank and walk a short distance NE to the summit of the knob. This vantage point affords good views of the Iron Mountain pluton and associated slide structures. Resistant ribs of steeply dipping and overturned Claron beds, keeled in soft rocks of the Iron Springs Formation, form an arcuate outcrop pattern around the Iron Mountain dome; slide masses of less steeply dipping Quichapa rocks can be seen to the ESE (Flat Top Mountain) and SW (Duncan Mountain). The geology of the area has been outlined by Rowley and Barker (1978). After discussion led by Rowley we will retrace our route back to UT-56.

1.3 18.8 Turn L (WSW) on UT-56 and continue.

1.1 19.9 Road to the Comstock Mine, which is on the NE flank of Iron Mountain.

0.3 20.2 Junction, UT-56 and Pinto road (Dixie N.F. 009). Leave the pavement, turning onto the gravel-surfaced Pinto road and continuing WSW.

1.3 21.5 **STOP 5.** Park vehicles just NE of a low divide and hike NW to the rocky crest of a hillock of brecciated Quichapa and Claron. To the N is the Iron Mountain pluton, to the S is the Stoddard Mountain pluton; we are in a crush zone between these two intrusive domes. It is uncertain whether the brecciation is result of sliding or compression or both. From here, continue SW on the Pinto road and descend to Ritchie Flat.

3.2 24.7 **STOP 6.** Road cut in Stoddard Mountain pluton on L. Sample the monzonite if you wish, then walk a few meters SW to read the historical marker at Page Ranch, and resume.

0.2 24.9 Junction with a road leading SE to New Harmony. Continue WSW toward Pinto.

3.0 27.9 Junction with a road leading S to Pinto Spring. Continue WSW.

0.3 28.2 Drainage divide; roadcuts of white Claron.

3.3 31.5 Junction with the Pinto road leading N to UT-56 at Newcastle. Continue WSW.

0.2 31.7 Junction with the Pinto Creek road (Dixie N.F. 011) leading to Grass Valley and Pine Valley. Turn L (S).

3.4 35.1 The Dairy pluton of Cook (1957). White Claron (chiefly lacustrine carbonate beds) dips N and S off a small boss of monzonite, which may be connected to the Paradise and Stoddard Mountain intrusives in the subsurface. All three bodies and the Pine Valley laccolith were mapped by Cook for his Ph.D. dissertation. More recent mapping includes work by Grant (1991) and current work of Rowley and Hacker.

0.3 35.4 Leach Canyon Formation, then Harmony Hills Tuff in road cuts on R.

0.2 35.6 Tuff of Rencher Formation (about 21 Ma) on L. Cook (1957) defined the Rencher Formation as “a complex assemblage of ignimbrite, breccia, air-fall tuff, bedded

Figure 5. Geologic map of Iron Mountain area, Iron Springs district. From Blank and Mackin (1967), with additions by P.D. Rowley. Selected geologic features are labeled; contours are of aeromagnetic total-intensity residual anomaly (isopleth interval 20 nanoteslas). Dotted lines are inferred subsurface extensions of intrusions. Closed barbs indicate gravity slide; open barbs, thrust. Iron deposits in solid black. Numbers 2-5 and 12 indicate field trip stops on DAY ONE. Letter symbols: Jec, Carmel Fm; Kis, Iron Springs Fm; Tc, Claron Fm; Tin, Isom Fm. and Needles Range Group; Tq, Quichapa Group; Tp, monzonite porphyry; Tbq, Tbc, tectonic breccia; Tpr, Racer Canyon Tuff and Rencher Fm; Qs, surficial deposits.

tuff-breccia, volcanic sandstone, and lenticular limestone and conglomerate [that] overlies the Quichapa group unconformably." Modal and chemical compositions of Rencher tuff are similar to those of Harmony Hills, the chief modal distinction being that Harmony Hills has sparse phenocrysts of quartz and sanidine.

0.2 35.8 Bridge over S fork of Pinto Creek.

0.3 36.1 Large glassy latite blocks in a Rencher tuffaceous matrix (*blue boulder breccia member* of Cook's Rencher Formation). Similar material locally occurs at the very base and very top of the Rencher Formation in the Bull Valley district.

0.4 36.5 Cliffs of Pine Valley Latite of Cook (1957) on skyline at 10:00; probable Rencher Formation at road level. The Pine Valley latite lava extruded shortly after emplacement of Rencher tuffs and mudflows. The precise location of the lava source(s) is not known; the NW margin of the Pine Valley laccolith is a likely candidate, as is the vicinity of Rencher Peak, 7 km ENE of here. Chemical and mineralogical data indicate that the latite and monzonite of Pine Valley are comagmatic.

0.6 37.1 Roadcut through andesitic breccia of slide mass. This is believed to be Little Creek Breccia of the Bull Valley district (Blank, 1959). Allochthonous masses of similar breccia are widespread between here and Big Mountain, 15 km to WNW. We are uncertain whether this particular slide has moved from the Bull Valley-Big Mountain intrusive arch or from a closer, as yet unidentified source area. Thick deposits of andesitic lavas, near-vent explosion breccia, and laharic breccia typically occur in the stratigraphic interval between the Bauers Tuff Member of the Condor Canyon Formation and Harmony Hills Tuff in the vicinity of the arch, but elsewhere in the region Harmony Hills Tuff rests directly on Bauers Member or on relatively thin andesitic laharic breccia above Bauers.

0.2 37.3 *White tuff breccia* phase of Rencher in roadcut on L. This rock is correlative with lower Rencher of the Bull Valley district (Blank, 1959).

0.4 37.7 **STOP 7.** Megabreccia composed of tuff of probable lower part of Rencher Formation, Leach Canyon Formation, and pyroxene-plagioclase andesite porphyry lava of the interval between Isom and Claron Formations. Polymict volcanic megabreccia similar to this mass is widespread in a broad belt extending at least from Panguitch Lake on the Markagunt Plateau, SSW to the vicinity of Mineral Mountain at the Nevada border. The megabreccia always involves rocks at least as old as Rencher. Geologic and geophysical mapping to date suggest that the distribution of these breccias is similar to that of exposed and concealed hypabyssal monzonite.

0.5 38.2 Brecciated Claron in roadcut on L.

0.2 38.4 Pass at Pinto Creek-Grass Valley Creek drainage divide.

0.3 38.7 Road to Broken Arrow Ranch (formerly Rencher Ranch, type locality of the Rencher Formation).

2.1 40.8 **STOP 8.** Crest of hill; on flank of cinder cone of quartz-bearing basalt. Overview of Grass Valley and ramparts of Pine Valley Latite above a gravity slide and a thrust sheet that includes an earlier slide mass. Due E of us a few km is the ENE-striking monzonite-latite contact. Dave Hacker will point out important features and discuss the structural relationships.

2.2 43.0 Road turns to SE; first good view of Pine Valley. The valley is enclosed by high, rugged topography of the Pine Valley Mountains, composed almost entirely of monzonite of the Pine Valley laccolith (which has also been described as a thick sill). Alluviation of the valley floor began when basalt flows of late Pliocene to early Pleistocene age blocked the drainage of the Santa Clara River, a tributary of the Virgin River, which in turn joins the Colorado River at Lake Mead.

0.1 43.1 Junction with Central-Pine Valley paved road. Turn L (SE). 1.1 44.2 Junction with main street of town of Pine Valley. Turn L (SE).

0.2 44.4 USFS Pine Valley Work Center.

2.0 46.4 Red Claron under the floor of the laccolith makes red soil on L. Note blocks of monzonite from talus or a landslide.

0.2 46.6 Pine Valley Reservoir on R, caretaker residence on L.

0.5 47.1 **STOP 9.** LUNCH STOP AT PONDEROSA PICNIC AREA. Examine monzonite in talus blocks (but collect any samples far from the developed area, please!). At this site we are well within mapped margins of the laccolith and about level with its base. Contacts (intrusive faults?) with Quichapa Group, Rencher Formation, and Pine Valley Latite are 2-3 km to the NNW and N. The floor of the laccolith occupies a broad, shallow, N-plunging syncline (Sevier downwarp?) developed on the underlying rocks and is typically at or near the top of the Claron Formation. The total preserved thickness of the laccolith exceeds that of the pre-intrusive section above its base and below Pine Valley Latite, which seems to imply that monzonite of Pine Valley erupted onto the surface or intruded its own extrusion. The monzonite-latite contact was mapped by Cook as an intrusive fault, but at least in some places the contact appears to be completely gradational. After lunch, retrace the route back to the junction with the Grass Valley road and continue on toward Central.

2.9 50.0 Town of Pine Valley: junction with road to Central. Turn R(N) at the church. Note Atchinson Mountain at 10:00. It is capped by Rencher, above which is basalt. Basalt also caps Rencher at 11:00 on the skyline. The southern part of the Atchinson Mountain area is included in Cook's dissertation work but only a reconnaissance map is presently available for the remainder (Cook, 1960). Currently the area is being remapped by Blank and Hacker.

1.1 51.1 Junction with Grass Valley-Pinto road. Go straight on the main (paved) road, toward Central. The road is now on a surface of basalt; when we pass a low crest, look back for a pleasing view of Pine Valley, with the Pine Valley Mountains as backdrop.

1.1 52.2 View of Square Top Mountain at 10:30 in far distance. Flat-lying Pennsylvanian and Permian rocks forming the upper surface were thrust over rocks as young as the Late Cretaceous Iron Springs Formation during the Sevier orogeny (Hintze, 1986). Jackson Peak, the conical peak directly to R(NE) of Square Top, is part of the same thrust sheet. Atchinson Mountain is now at 2:00; the white slope midway up the mountain is lower Rencher, overlain by upper Rencher. Lower Rencher (white tuff breccia) rests on megabreccia. Bull Valley Mountains at 12:00.

2.3 54.5 Good view of red and white Claron north of road. Claron here is overlain by autochthonous Quichapa (lacking intercalated Little Creek Breccia); above that are slide breccias composed of rock of all Quichapa formations but predominantly of Little Creek Breccia of Blank (1959) and Cook (1960).

0.9 55.4 Junction with jeep track (Dixie N.F. 824) leading to Eightmile Spring on the west flank of Atchinson Mountain. The hill in the foreground, at 2:00, is Eight Mile Dacite of Cook (1957). Cook considered this flow to be Pleistocene because it seems to fill a paleovalley not much different from modern valleys; however, it may prove to be a product of NNE-aligned fissure eruptions and to be Pliocene. Make a sharp right turn at the obscure entrance to a jeep track descending to a gulley. The track leaves basalt and leads N up the drainage between Eight Mile Dacite on the W and nearly flat-lying Claron and Quichapa strata on the E. In places, the autochthonous Quichapa section, consisting of Leach Canyon Formation, Bauers Tuff Member of Condor Canyon Formation, and Harmony Hills Tuff, is severely attenuated by bedding-plane faults.

1.5 56.9 Cross drainage twice and head E. Another track leads SW from here, toward Central. The mass of Eight Mile Dacite directly on our L apparently rests on thin pyroxene-plagioclase andesitic lava that overlies white Claron (no contacts have been found). This and other andesites commonly occur in the stratigraphic interval between Claron and Isom Formations.

0.7 57.6 Eightmile Spring. Plenty of room for vehicles, and depending on the condition of the jeep track, we may leave them here and walk the last half mile to the base of the megabreccia section.

0.5 58.1 **STOP 10.** Atchinson Mountain. End of passable jeep track, at spring (tight for vehicle turn-arounds). From here, ascend to the ridge crest (not to the summit of Atchinson Mountain) through megabreccia, starting in andesite of Little Creek Breccia of Blank (1959) and climbing up through five lenses of Harmony Hills Tuff encased in the andesite. Most low-lying knobs to the N and S of us are thoroughly brecciated Bauers Tuff Member, which served as the basal zone of detachment for the overlying stack of low-angle fault slices. Little Creek Breccia of the allochthonous mass was tentatively considered by Cook (1957) to be a post-Quichapa, post-Rencher deposit, and he named it the *Atchinson Mountain Formation.* In places, white Claron, pre-Isom andesite, Leach Canyon Formation, and Bauers Tuff Member are present in their usual stratigraphic order below Little Creek Breccia, but above the base of the allochthon. Cook (1957) named this package of rocks the *Grass Valley*

Formation. Later, recognizing that the apparently fortuitous repetition of lithologies was due to tectonic emplacement of the section above a low-angle fault, these two formation names were abandoned (Cook, 1960). We will see the proposed source area for the allochthon on Day 2 of this field trip. On the ascent through the megabreccia, note rotation of blocks of Harmony Hills Tuff as indicated by orientation of eutaxitic structures. Rotation on a much finer scale occurred in rock of Bauers Member. Also, note complex interpenetration of Harmony Hills Tuff and Little Creek Breccia on steep faces. Capping these rocks in some places are small isolated slices of pre-Isom andesite and Claron sedimentary rocks (both red and white Claron are present). In general, however, Harmony Hills Tuff and Little Creek Breccia comprise the upper part of the megabreccia section, and lower formations of the Quichapa Group comprise the lower part. Mapping at 1:24,000-scale is still in progress, and we do not know how many individual fault planes will eventually be discriminated nor whether all fault slices have a common provenance.

On Atchinson Mountain, as in the Bull Valley district, megabreccia is locally intercalated with lower Rencher ash-flow deposits but mantled by upper Rencher, indicating that these slides occurred before the culminating Rencher eruptions. However, small-scale folds involving both upper and lower Rencher tuff as well as the underlying megabreccia have been mapped in this vicinity, and just E of the area traversed this morning (Pinto Creek-Grass Valley), slide masses have been overridden by one or more thrust sheets. Post-Rencher compressional deformation associated with growth of the Pine Valley laccolith may partly account for the extraordinary thickness of megabreccia in the Atchinson Mountain area.

After checking Rencher on the ridge crest, descend to the spring again via a more northerly route and meet at the vehicles for return to the pavement.

2.7 60.8 Intersection of jeep trail with Central-Pine Valley road. Turn R (SW).

0.2 61.0 Apparent dike of basalt in old alluvium on R.

0.9 61.9 Dixie N.F. boundary. Cinder cones at 9:00-11:00. Hill at 2:00 is mainly composed of autochthonous Claron and Quichapa, with some outliers of allochthonous Quichapa (mostly Bauers Member) on the crest. Enter Central.

1.5 63.4 Intersection with UT-18 (stop sign). Turn R (N).

0.3 63.7 Knobs of brecciated Bauers Member at 1:00-2:00 on hillcrest. On the L, basalt caps hills of Rencher Formation on the downthrown side of a probable strand of the NNE-striking Gunlock high-angle normal fault.

2.5 66.2 Slide masses at 11:00-3:00, with numerous prominent scabby outcrops of Bauers Member and less resistant outcrops of brecciated Harmony Hills Tuff.

1.2 67.4 Hill at 2:00 containing construction scar (cut during installation of the Wyoming-Bakersfield gas pipeline in 1991) is composed of lower and upper tuff of Rencher Formation. The lower unit (white tuff breccia) directly overlies slide megabreccia of Quichapa. The pipeline cut exposed a contact between the lower and upper Rencher here and again about 1.5 km NW of Central. This contact is characterized by an upward darkening and by an increase in the phenocryst content. In places the location of the contact is uncertain, as the lower unit contains several partial cooling breaks that result in similar contrasts. South and W. of the Bull Valley vent, thin (<1 m-thick) deposits of bedded Rencher ash (base-surge deposits?), largely converted to jaspilite (by iron-rich exudations from the underlying tuff?), occur between lower and upper Rencher, but elsewhere no ash intervenes and the contact is gradational across several cm, with no evidence of weathering or erosion. Samples of both units yielded essentially identical K-Ar ages for biotite (determined by E.H. McKee; reported by Rowley and others, 1989). Thus the hiatus between upper and lower Rencher is inferred to be brief, although possibly a complete cooling break. As we shall see on Day 2, immediately adjacent to the E to SE side of the Bull Valley vent the two units are locally separated by huge masses of pre-intrusive (roof) rocks, chiefly Claron and Iron Springs Formations.

0.6 68.0 Roadcuts of Quichapa megabreccia on L and Rencher Formation, which overlies it, on R.

0.8 68.8 **STOP 11.** Roadcuts of megabreccia. Examine the megabreccia and view the Big Mountain monzonite-cored dome at 10:00 across Mountain Meadow. Monzonite is exposed on the SW flank of the dome, which marks the NE end of the Bull Valley-Big Mountain intrusive arch. Subsurface continuity of intrusive rock between exposed extremities of the arch is inferred from aeromagnetic data. The crest of the Big Mountain dome consists mainly of Iron Springs sandstone, and locally, of Homestake Limestone Member. Claron and Quichapa strata dip generally away from the dome at lower elevations around its base and in some places are so severely brecciated and intermixed that they are mapped as megabreccia.

0.3 69.1 Road to Mountain Meadow monument on L. Mountain Meadow is traversed by the Old Spanish Trail, and is the site of the infamous 1857 massacre in which about 120 emigrants perished. An account of this tragic event and its historical setting is given in *The Mountain Meadows Massacre* (Brooks, 1991).

0.3 69.4 Junction with road leading E to Pinto and Iron Mountain. Continue N on UT-18.

1.5 70.9 Low pass where road crosses N flank of Big Mountain. Roadcuts are in N-dipping Iron Springs sandstone overlain to N and E of the road by red Claron conglomerate and siltstone.

1.2 72.1 Cross N-striking hinge fault, the Big Mountain fault of Blank (1959), which forms the W boundary of the Big Mountain dome. Normal, up-to-the-E, throw on this fault increases southward from perhaps 0.1 km here to nearly 1.0 km SW of the apex of the dome, where Claron is juxtaposed with Carmel. For the next half-mile or so along the road, roadcuts are in N-dipping Claron. The road then crosses into a slide block of extensively brecciated Quichapa.

1.2 73.3 Roadcut through brick-red, 3-m-thick ledge of Hole-in-the-Wall Tuff Member of Isom Formation. Look closely to the R as we pass through this cut to see a 0.3-m-thick basal vitrophyre separated from the overlying stony red ledge by about 1.0 m of soft white powdery material. The vitrophyre is the probable base of the ash-flow unit and the intervening material is probably completely decomposed ash-flow tuff. Stratigraphically beneath the vitrophyre are several tens of meters of lacustrine clays and coarser clastic material, which in turn rest on an Isom-Claron pyroxene-plagioclase lava flow similar to that seen near Atchinson Mountain.

From here, UT-18 turns sharply R (NNW) down Cottonwood Wash. The road initially is cut in Quichapa, Isom, and Claron strata, but after about half a kilometer it is flanked on both sides by old (Pliocene-Pleistocene) valley-fill deposits.

1.7 75.0 Enter Escalante Valley (Escalante Desert), named after the Spanish padre whose expedition passed through this area in 1776 in search of a route from Santa Fe to California (he is also the namesake of a valley, river, and town in south-central Utah). Buried, NE-trending, basin-and-range topography beneath valley alluvium has been delineated by gravity surveys (Pe and Cook, 1980). The low mountains directly ahead, N to NW of Enterprise, are the so-called North Hills, comprised mostly of hornblende-andesite flows and laharic breccias erupted in post-Rencher, pre-Racer Canyon time, that is, at about 19-21 Ma. Farther N and W the andesites are overlain by rhyolite flows and tuffs of 11-13 Ma age (Siders, 1985a, b, 1991).

0.9 75.9 Junction with paved road that leads W to Enterprise. Turn R and head E and then NE on the continuation of UT-18.

2.8 78.7 Junction with paved road that leads ENE toward Newcastle (UT-18 curves to N here and heads toward Beryl Junction). Turn R onto the Newcastle road. For most of its distance, this road is gravel-surfaced and follows the SE margin of Escalante Valley, parallel to the Antelope Range fault zone (range-front fault) of Siders and others (1990). Excellent exposures of the fault zone were created by the 1991 pipeline project, then buried again. The range SE of the road has no formal name but is considered by some to be an eastern extension of the Bull Valley Mountains. It is composed of Iron Springs Formation and younger rocks and is bounded on the SE by a buried ridge of monzonite that extends ENE from near the E margin of Mountain Meadow.

7.7 86.4 Enter Newcastle (Main St.). A prominent (25 mgal) NE-trending Bouguer gravity low centered 2-3 km NW of here is produced by a 3-km-deep graben bounded by the range-front fault (Pe and Cook, 1980). Geophysical surveys and drilling, most recently by the Utah Geological Survey, have delineated a *blind* geothermal resource (Newcastle KGRA) in the graben (Mabey and Budding, 1987; Blackett and others, 1990). The resource heats various buildings in the town, including commercial greenhouses.

0.7 87.1 Junction of Main St., Newcastle, with UT-56 (stop sign). Turn R(E).

0.4 87.5 View of mouth of Newcastle Reservoir at 3:00. The north wall of the reservoir is composed of resistant upper Miocene polymict volcanic conglomerate, sandstone, and mudflow breccia (Siders and others, 1990).

0.5 88.0 Cross Wyoming-Bakersfield pipeline again. The road heads toward Silver Peak, the high point of the Antelope Range. The range is a broad, asymmetrically domed, complexly faulted, hydrothermally altered, and mineralized (mainly with silver) area of Jurassic (Homestake Limestone Member of Carmel Formation) and younger rocks, including rhyolite flows and domes of post-monzonite age (post-20 Ma) (Shubat and McIntosh, 1988; Shubat and Siders, 1988). Rhyolite of Silver Peak, for example, has been dated at 8.4 Ma, the apparent age of alteration and mineralization. A Bouguer gravity anomaly high associated with the range is contiguous with a broad high associated with intrusions of the Iron Springs district (Cook and Hardman, 1967); monzonite crops out in several small areas near Table Butte, a few km N of the range, but there is no aeromagnetic indication of near-surface monzonite beneath the Antelope Range dome.

4.0 92.0 Desert Mound turnoff.

4.5 96.5 Old Irontown turnoff. Irontown is the site of an early iron ore smelting industry by Dixie pioneers (MacDonald, 1991).

1.4 92.5 Turnoff to Blowout pit on Iron Mountain. If we are on schedule we will visit the pit, with permission of its owners (Gilbert Development Co., Cedar City).

0.7 98.6 **STOP 12.** Blowout pit, about 120 m deep. Overturned Homestake Limestone Member of the Carmel Formation in the upper plate of the Iron Springs Gap thrust is mineralized by iron-rich fluids derived from the Iron Mountain pluton (Mackin, 1947, 1968; Mackin and Ingerson, 1960). A comprehensive study of the mineralogy, petrology, and geochemistry of the monzonites of the Iron Springs district and associated ore deposits has recently been completed by D.S. Barker (Univ. of Texas-Austin, written communication, 1991). Intense intrusive deformation is indicated by overturning of the Claron around the SE border zone of the intrusion. We shall see evidence of similar asymmetric (SE-vergent) deformation produced by the Bull Valley-Big Mountain intrusive. Our purpose here is to view the monzonite, note the SE structural vergence, and relate these features to the gravity slides that we saw from the Diamond Z Ranch. Return to UT-56.

0.6 99.2 Junction with UT-56. Turn L (E), and continue to Cedar City.

17.7 116.9 200 N and Main St., Cedar City.

DAY TWO Cedar City to Enterprise, Ox Valley, Gardner Spring and return; includes 4-5 mi loop hike from Gardner Spring.

ASSEMBLE ON EAST SIDE OF CITY PARK, 200 N AND 100 E STREETS, FOR 7:00 AM DEPARTURE.

Mileage

Interval	Cumulative	
0	0	200 N and Main St. (traffic light). Proceed W on UT-56.
29.9	29.9	Newcastle, Main St. Continue WNW toward Beryl Junction.
1.5	31.4	Views of the Big Mountain dome to L(S), and Table Butte, which consists of ash-flow tuff of the Leach Canyon and Condor Canyon Formations, to R(N). Monzonite 2-3 km SW of Table Butte is the Lookout Point intrusive of Grant and Proctor (1988).
4.9	36.3	Beryl Junction. Turn L(S) on UT-18.
1.2	37.5	Road on R leads 4 mi W to Escalante silver mine (Hecla Mining Co.), Utah's largest primary silver producer until it was shut down recently. Mineralization occurred along a NNE-striking vein in 11-13 Ma *mine series* volcaniclastics of Siders (1985b), equivalent to volcaniclastics in the north wall of Newcastle Reservoir; vein adularia at the mine has yielded a K-Ar age of 11.6 Ma (Siders, 1985b).
1.0	38.5	Potato sheds on R. Potatoes, cubed alfalfa, and rebuilt tires are the main exports of the southern Escalante Valley.
5.1	43.6	Washington County line.
0.7	44.3	Newcastle turnoff. Continue on UT-18.
2.8	47.1	Junction, UT-18 and road to Enterprise. Bear due W (do not turn S on the continuation of UT-18); the road we follow becomes Main St. in Enterprise.
0.6	47.7	Enterprise, 200 E and Main. Turn L(S). The Enterprise area has recently been mapped at 1:24,000-scale by Blank (unpublished data). As we pass Enterprise High School, note Flattop Mountain and Enterprise cinder cone at 1:00-2:00. The surface of Flattop Mountain is olivine basalt (Enterprise Basalt of Blank, 1959). This basalt

appears to be about the same age as morphologically similar basalt S of Modena dated at 10.8 Ma (Best and others, 1980). The basalt caps a rhyolite eruptive center; the sharp point just to the L of Flattop is Pilot Peak, a satellite rhyolite plug or tholoid. Continuing S, the road gradually ascends a ridge of old alluvium.

2.4 50.1 Calf Springs junction. Continue straight S on Dixie N.F. 007 toward Ox Valley. The road leads S up Calf Creek, which follows the E margin of andesite of Black Hills (formerly Black Hills basalt of Blank, 1959). This rock has not yet been dated but drainage on flow surfaces is not integrated. The flows issued from a vent at the base of Ox Valley peak on the W side of Ox Valley, and blocked the drainage, resulting in aggradation of the valley and formation of an ephemeral lake.

1.5 51.6 Confluence of Spring Creek and Shinbone Creek. Exposures of Claron Formation here.

2.1 53.7 Enter gorge of Shinbone Creek. The enclosing cliffs are composed of rhyolite of Shinbone Creek (formerly Shinbone Rhyolite of Blank, 1959), a locally vented flow with a whole-rock K-Ar date of 4.7 Ma (E.H. McKee, unpublished data)—as far as we are aware, the youngest rhyolite in SW Utah. The flow was emplaced on soft, salmon-colored tuffaceous sandstone (Reservoir Formation of Blank, 1959; see Cook, 1960, p. 45) that occupies a broad arcuate depression SW, S, and SE of Flattop Mountain. This depression may be bounded by partial ring structures related to the Flattop Mountain rhyolite center.

0.4 54.1 Tom Spring. Confluence of Shinbone Creek and Bullrush Creek. The road leads SW up Bullrush.

0.3 55.4 Enter Ox Valley. Ox Valley Peak is straight ahead on the far side of the valley, and Ox Valley Lake (usually dry) occupies its northern extremity.

0.2 55.6 First full view of Ox Valley. The road swings sharply S. A jeep track running due W along a fence line (section line) provides access to the Pilot iron claims area at the W end of the Bull Valley vent zone, about 2 mi SW of Ox Valley. Ox Valley is confined on the S and E by hills of dense, rust-colored ash-flow tuff of the upper Rencher Formation. This rock is a near-vent facies and may have moved as a flow breccia during the final stage of its emplacement. Rencher is locally capped by Ox Valley Tuff (12-13 Ma), a major high-silica rhyolite ash-flow sheet apparently derived from the eastern part of the Caliente caldera complex of Nevada-Utah (Blank, 1959; Noble and McKee, 1972; Ekren and others, 1977; Rowley and others, 1979; Anderson and Hintze, 1991). Ash-flow tuff of earlier eruptions in the eastern Caliente caldera complex (Racer Canyon Tuff, 19 Ma; see Siders and others, 1990) does not occur on or SE of the Bull Valley-Big Mountain intrusive arch, which was probably a topographic barrier.

1.9 57.5 Junction with Dixie N.F. 356 leading to southernmost extremity of Ox Valley, our objective. Track 007 continues up Valley Canyon and at one time provided access to the NE (upper) end of Hardscrabble Hollow. Turn R(W).

0.5 58.0 Junction. The track that leads straight ahead ascends to a low pass 0.15 km S of here, on the drainage divide between interior Great Basin and the Colorado River. From this pass, a pack trail leads straight down Gardner Draw. The track leading L(E) follows topographic contours along the W side of a ridge and then drops steeply to Gardner Spring in the draw. Depending on conditions after the winter wet season, we will either park here and walk the ridge route to the spring, returning via the Gardner Draw pack trail; or drive both ways on the jeep trail, leaving the vehicles at the spring for the day's loop traverse on foot. The jeep-trail distance to the spring is about two miles and the route is almost entirely through well exposed vent-facies Rencher. Studies of the area include work by Wells (1938), Blank (1959), Tobey (1976), and current mapping by Blank and R.E. Anderson.

0.6 58.6 **STOP 13.** Mineralized Rencher along a probable E-W fault zone (Farnsworth claims; see Bullock, 1970), interpreted as covering the E extremity of the Rencher vent (Fig. 6). Note cognate inclusions in fresh rock faces of the Rencher. The rock generally appears structureless except on fresh surfaces, where inclusions can always be seen; their shape ranges from lenticular to subangular. The crest to the S of this locality is composed of brecciated Rencher mapped by Tobey (1977) as *intrusive Rencher breccia.* Similar breccia occurs at the level of Gardner Draw W and SW of here.

0.4 59.0 **STOP 14.** Leave the track here and scramble a short distance up the ravine to see

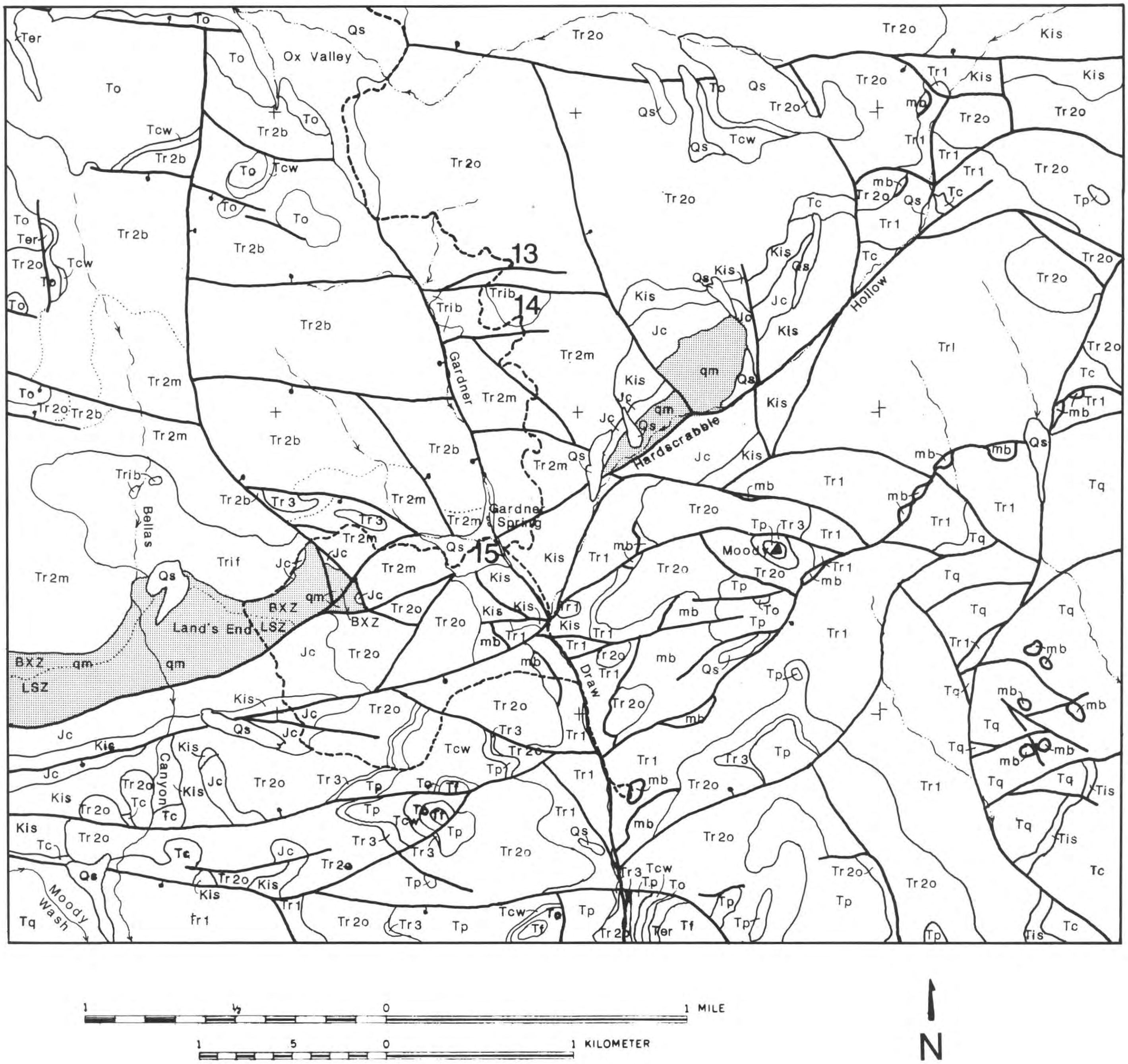

Figure 6. Geologic map of Gardner Spring-Hardscrabble Hollow area, Bull Valley district. After Tobey (1976), with modifications and additions by H.R. Blank. Gradational contacts dotted; heavy dashed line is route of field trip (DAY TWO); numbers indicate stops.

MAP UNITS

Quaternary			Qs	Surficial deposits
Miocene			Tf	Basalt of Flattop Mountain
			Ter	Volcaniclastic rocks of Enterprise Reservoir
			To	Ox Valley Tuff
			Tcw	Tuff of Cedar Spring
			Tp	Basalt of Pilot Creek
	Rencher Formation	Intrusive member	Trib	Breccia facies
			Trif	Flow-layered facies
		Lahar member	Tr3	
		Upper ash-flow member	Tr2b	Flow-breccia near-vent facies
			Tr2m	Massive near-vent facies
			Tr2o	Outflow facies
		Lower ash-flow member	Tr1	
			mb	Megabreccia
			qm	Monzonite (LSZ, lower shell zone; BXZ, brecciated zone)
Miocene and Oligocene			Tq	Quichapa Group
Oligocene			Tis	Isom Formation
Oligocene and Eocene			Tc	Claron Formation
Late Cretaceous			Kis	Iron Springs Formation
Jurassic			Jc	Carmel Formation

MAP UNITS

Quaternary Qs surficial deposits

Tf basalt of Flattop Mtn. Ter volcaniclastic rocks of Enterprise Reservoir To Ox Valley Tuff Tcw tuff of Cedar Spring Tp basalt of Pilot Creek Trib breccia facies intrusive member Miocene Trif flow-layered facies Trl laharic breccia member

Tr2b flow-breccia near-vent facies Rencher Fm. upper ash-flow member Tr2m massive near-vent facies Tr2o outflow facies mb megabreccia Tr1 lower ash-flow member qm quartz monzonite (LSZ, lower shell zone; BXZ, brecciated zone) Tq Quichapa Group Oligocene and Eocene Tc Claron Fm. Late Kis Iron Springs Fm. Cretaceous Geology after Tobey (1976), with modifications and additions by H.R. Blank (unpub. data)

Jurassic Jc Carmel Fm. AGE FORMATION (excluding thin sedimentary intervals and unconsolidated deposits) good exposures of the intrusive breccia.

0.8 59.8 Approximate contact of Rencher and Iron Springs Formations. We have never seen this contact perfectly exposed, probably because sandstone at the contact is too highly shattered.

0.2 60.0 **STOP 15.** Gardner Creek (Gardner Spring is just upstream). Cross the creek and park the vehicles anywhere in the Cottonwood grove. Bring lunch and adequate water: the loop hike from here is 4-5 miles long with plenty of scrambling, including a 600-ft ascent up a steep gully. Start by following the jeep track W from Gardner Spring. Fresh rock surfaces in road cuts reveal that we are in vent-facies Rencher; we have crossed back out of a window of Iron Springs sandstone exposed at creek level. After half a kilometer of gentle ascent, the track reaches the ridge crest, still in vent facies. On our R are outcrops of faintly layered Rencher breccia, the layering indicating gentle northerly dips. The breccia includes large blobs of glassy material and was interpreted by Tobey as a laharic deposit. Continue to follow the main track W and SW along topographic contours and pass into dark red Rencher that shows distinct flow layering rather than lenticulitic or breccia structures. The layering is roughly parallel to the contact with underlying brecciated monzonite. Rencher of this facies is limited to a zone about 0.15 km wide and extending to the W about 1.5 km. One interpretation is that the rock represents viscous material extruded as a vent spine at the conclusion of ash-flow eruption phases. Continue to the iron prospect at the end of the track. Mineralization is mainly in screens of Homestake Limestone Member in the contact zone between Rencher and monzonite. Directly downslope are the outcrops of brecciated monzonite. From here, continue at the same elevation SW toward the knob of monzonite known as *Land's End.* In the saddle just N of Land's End, basal Rencher consists of gray, fine-grained to glassy latite exhibiting fluidal layers and drag folds, and (rarely) containing angular fragments of monzonite.

1.1 61.1 *LUNCH STOP AT LAND'S END.* This is a good vantage point for viewing structure. The Rencher-monzonite contact strikes E-W and dips about 30° N. Rencher rests directly on monzonite, or on thin mineralized screens of Carmel or Claron, for a distance of almost 4 km along strike; this is considered to be the minimum strike length of the vent zone. If the breccia seen on our descent to Garden Spring this morning is indeed intrusive, then the vent zone may actually be 5.5-6 km in strike length. Monzonite here is in Tobey's *lower shell zone* of the intrusion; to the W, in the western sector of the vent, Rencher overlies an *upper shell zone,* which is separated from this lower shell zone by an interior, fine grained, highly altered, brecciated zone believed to represent residual magma from the Rencher eruptions. The intrusive-extrusive relationship was first recognized by Wells (1938), who mapped the district in reconnaissance and studied the iron ores. An uninterrupted section of pre-intrusive strata dips S off the western sector of the intrusive arch and is capped by ash-flow tuff of both upper and lower units of Rencher. Dips steepen toward the contact with monzonite, but no detachment faults have been found within the S-dipping section. Strata of Homestake Member at the contact with monzonite W of our present position are near-vertical to overturned as much as 45°. Such steep dips are at least partly a result of the rise of late-stage monzonitic magma and extrusion of Rencher, although Sevier deformation may also be a factor. To the E and ENE, on the crest of the intrusive arch, upper Rencher rests directly on sedimentary rock of the Carmel, Iron Springs, and Claron Formations but nowhere on monzonite; the upper two sedimentary formations are greatly attenuated and pre-intrusive volcanic rocks and lower Rencher are missing. Immediately SE of the crest, however, lower Rencher occurs as a thick (to 200 m) tuff breccia overlying and locally including Quichapa slide megabreccia. Isolated slabs and irregular masses of Iron Springs and Claron Formations, some as large as 1 km in strike length, occur between lower and upper Rencher units. The megabreccia and Iron Springs and Claron rocks are interpreted as gravity slide masses sloughed from the intrusive arch just before and during emplacement of lower Rencher. No such masses occur in upper Rencher.

Next descend SSE from Land's End, passing across a concealed contact between monzonite and underlying, overturned Carmel. Traverse three low divides beyond the first SW-directed gully before reaching a major W-directed gully which will be followed upstream.

0.5 61.6 Contact between upper Rencher ash-flow tuff and Carmel Formation. Basal Rencher here is glassy and pulverulent and contains rare angular fragments of monzonite. The Carmel is contorted but not shattered. Climb up through upper Rencher, via the gully. Near the top of the ash-flow tuff, Rencher exhibits rude layering and contains abundant blobs of gray glassy cognate material weathering as cavities. Overlying this Rencher phase are well-bedded, laharic Rencher deposits. These are in turn overlain by dark purple lava (Pilot Creek Basalt of Blank, 1959; Hausel and Nash, 1977) and then by 50-100 m of mudflow and other volcaniclastic deposits (Cedar Spring Member of Cove Mountain Formation of Blank, 1959; Hausel and Nash, 1977).

0.6 62.2 At ridge crest, still in Cedar Spring Member. To the S, Cedar Spring deposits are overlain by Ox Valley Tuff, and the entire section is capped by basalt, possibly equivalent to that on Flattop Mountain. The ridge crest provides good views of the Gardner Draw and Hardscrabble Hollow sections to the E and ENE. The Hardscrabble Hollow intrusive crops out about mid-way up the hollow; though much faulted, it clearly has a conformable roof of Homestake Limestone Member. Between one and two km of pre-upper Rencher section are missing from above the Homestake. These rocks presumably are distributed as megabreccia in terrain between the arch and Atchinson Mountain.

Follow the ridge crest about 0.3 km to the NE and then descend due E into Gardner Draw. About 50-75 m above the creek level, pass through a poorly exposed slab of shattered Iron Springs sandstone and possibly red Claron, which directly overlie lower Rencher. This is an intra-Rencher slide block. Beneath the slab are excellent exposures of white tuff breccia, the principal component of the lower Rencher cooling unit. At this locality, lower Rencher tuff contains large blocks (as much as 4 m in diameter) of earlier formed Rencher material, some with flow structure.

0.5 62.7 Gardner Creek. Proceed S down the draw following the left-bank trail for about one km, to exposures of a megaclast of Little Creek Breccia. A zone of brecciated gray glassy Rencher tuff is traversed enroute. This glassy rock is the basal vitrophyre of lower Rencher, and is interpreted to be the sole of a south-directed gravity slide; it can be traced discontinuously to the ridge crest E of Gardner Draw.

0.5 63.2 Slide mass of Little Creek Breccia. From here, we retrace our path one km and continue upstream to the vehicles.

1.0 64.2 Gardner Spring. Retrace the route to Enterprise and Cedar City.

60.0 124.2 Cedar City, 200 N and Main St., by 6:00 PM.

REFERENCES

Adair, D.H., 1986, Structural setting of the Goldstrike district, Washington County, Utah: p. 129-135 *in* Griffin, D.T., and Phillips, W.R., eds., Thrusting and extensional structures and mineralization in the Beaver Dam Mountains, southwestern Utah: Utah Geol. Assoc. Pub. 15, 217 p.

Anderson, J.J., 1985, Mid-Tertiary block faulting along west and northwest trends, southern High Plateaus, Utah: Geol. Soc. of America, Abstracts with Programs, v. 17, no. 7, 1985 (abstr.).

Anderson, J.J., 1988, Pre-basin-range block faulting along west and northwest trends, southeastern Great Basin and southern High Plateaus: Geol. Soc. of America, Abstracts with Programs, v. 20, no. 3, p. 139 (abstr.).

Anderson, J.J., and Rowley, P.D., 1975, Cenozoic stratigraphy of southwestern high plateaus of Utah: p. 1-51 *in* Anderson, J.J., Rowley, P.D., Fleck, R.J., and Nairn, A.E.M., Cenozoic Geology of Southwestern High Plateaus of Utah: Geol. Soc. of America Special Paper 160, 88 p.

Anderson, R.E., 1987, Neogene geologic history of the Nevada-Utah border area at and near lat. 37°30'N: Geol. Soc. of America, Abstracts with Programs, v. 19, no. 7, p. 572 (abstr.).

Anderson, R.E., and Barnhard, T.P., in press, Heterogeneous Neogene strain and its bearing on horizontal extension and horizontal and vertical constriction at the margin of the extensional orogen, Mesquite Basin area, Nevada and Utah: U.S. Geol. Survey Bulletin.

Anderson, R.E., and Christensen, G.E., 1989, Quaternary faults, folds, and selected volcanic features in the Cedar City 1° x 2° quadrangle, Utah: Utah Geol. Mineral Survey Misc. Pub. 89-6, 29 p., map scale 1:250,000.

Anderson, R.E., and Hintze, L.F., 1991, Geologic map of the Dodge Spring quadrangle, Lincoln County, Nevada, and Washington County, Utah: U.S. Geological Survey Open-File Report 91-360, scale 1:24,000.

Anderson, R.E., and Mehnert, H.H., 1979, Reinterpretation of the history of the Hurricane fault in Utah: p. 145-166 *in* Newman, G.W., and Cooke, H.D., eds., 1979 Basin and Range Symposium and Great Basin Field Conference: Denver and Salt Lake City, Rocky Mountain Association of Geologists and Utah Geological Association, 662 p.

Armstrong, R.L., 1968, Sevier orogenic belt in Nevada and Utah: Geol. Soc. of America Bull., v. 70, p. 429-458.

Armstrong, R.L., 1970, Geochronology of Tertiary igneous rocks, eastern Basin and Range Province, western Utah, eastern Nevada, and vicinity, U.S.A.: Geochimica et Cosmochimica Acta, v. 34, no. 2, p. 203-232.

Best, M.G., Christiansen, E.H., and Blank, H.R., Jr., 1989, Oligocene caldera complex and calc-alkaline tuffs and lavas of the Indian Peak volcanic field, Nevada and Utah: Geol. Soc. of America Bull., v. 101, p. 1076-1090.

Best, M.G., Christiansen, E.H., Deino, A.L., Gromm, C.S., McKee, E.H., and Noble, D.C., 1989, Excursion 3A: Eocene through Miocene volcanism in the Great Basin of the western United States: p. 91-133 *in* Chapin, C.E., and Zadek, Jiri, eds., New Mexico Bur. of Mines and Mineral Resources Memoir 47, 265 p.

Best, M.G., and Grant, S.K., 1989, Stratigraphy of the volcanic Oligocene Needles Range Group in southwestern Utah: p. 3-28 in U.S. Geological Survey Prof. Paper 1433-A.

Best, M.G., McKee, E.H., and Damon, P.E., 1980, Space-time composition patterns of late Cenozoic volcanism, southwestern Utah and adjoining areas: Am. Jour. of Science, v. 280, p. 1035-1050.

Blackett, R.E., Shubat, M.A., Chapman, D.S., Forster, C.B., Schlinger, C.M., and Bishop, C.E., 1990, The Newcastle geothermal system, Iron County, Utah: Utah. Geol. and Mineral Survey Open-File Rept. 189, 178 p.

Blank, H.R., Jr., 1959, Geology of the Bull Valley district, Washington County, Utah: Seattle, Univ. of Washington, unpub. Ph.D. dissertation, 177 p.

Blank, H.R., Jr., 1991, Megabreccia sheets derived from deroofing of a monzonitic intrusion in southwestern Utah: Geol. Soc. of America, Abstracts with Programs, v. 23, no. 5, p. A450 (abstr.).

Blank, H.R., Jr., and Crowley, J.K., 1990, Geophysical studies: p. 24-42 *in* Eppinger, R.G., Winkler, G.R., Cookro, T.M., Shubat, M.A., Blank, H.R., Jr., Crowley, J.K., Kucks, R.P., and Jones, J.L., Preliminary assessment of the mineral resources of the Cedar City 1° by 2° quadrangle, Utah: U.S. Geol. Survey Open-File Report 90-34, 146 p.

Blank, H.R., Jr., and Kucks, R.P., 1989, Preliminary aeromagnetic, gravity, and generalized geologic maps of the USGS Basin and Range-Colorado Plateau transition zone study area in southwestern Utah, southeastern Nevada, and northwestern Arizona (the BARCO project): U.S. Geological Survey Open-File Report 89-432, 16 p., 3 maps, scale 1:250,000.

Blank, H.R., Jr., and Mackin, J.H., 1967, Geologic interpretation of an aeromagnetic survey of the Iron Springs district, Utah: U.S. Geol. Survey Prof. Paper 516-B, 14 p.

Brooks, Juanita, 1991, The Mountain Meadows Massacre: Norman, Okla., Univ. of Oklahoma Press, 318 p. (paperback edition).

Bullock, K.C., 1970, Iron deposits of Utah: Utah Geol. and Mineralogical Survey Bulletin 88, 101 p.

Cashion, W.B., 1967, Carmel Formation of the Zion Park region, southwestern Utah—A review: U.S. Geol. Survey Bull. 1244-J, p. J1-J9.

Cook, E.F., 1957, Geology of the Pine Valley Mountains, Utah: Utah Geol. and Mineralogical Survey Bulletin 88, 111 p. Cook, E.F., 1960, Geologic atlas of Utah, Washington County: Utah Geol. and Mineralogical Survey Bulletin 70, 119 p.

Cook, E.F., 1965, Stratigraphy of Tertiary volcanic rocks in eastern Nevada: Nevada Bur. of Mines Report 11, 61 p.

Cook, K.L., and Hardman, Elwood, 1967, Regional gravity survey of the Hurricane fault area and Iron Springs district, Utah: Geol. Soc. of America Bull., v. 78, no. 9, p. 1063-1076.

Ekren, E.B., Orkild, P.P., Sargent, K.A., and Dixon, G.L., 1977, Geologic map of the Tertiary rocks, Lincoln County, Nevada: U.S. Geological Survey Miscellaneous Investigations Map I-1041, scale 1:250,000.

Fillmore, R.P., 1989, Sedimentology and provenance of the Upper Cretaceous Iron Springs Formation, southwestern Utah: Flagstaff, Northern Arizona University, M.S. thesis, 263 p.

Fleck, R.J., Anderson, J.J., and Rowley, P.D., 1975, Chronology of mid-Tertiary volcanism in High Plateaus region of Utah: p. 53-62 *in* Anderson, J.J., Rowley, P.D., Fleck, R.J., and Nairn, A.E.M., eds., Cenozoic geology of southwestern High Plateaus of Utah: Geol Soc. of America Spec. Paper 160, 88 p.

Goldstrand, P.M., 1990, Stratigraphy and ages of the basal Claron, Pine Hollow, Canaan Peak, and Grapevine Wash Formations, southwest Utah: Utah Geol. and Mineral Survey Open-File Report 193, 186 p.

Grant, S.K., 1991, Geologic map of the New Harmony quadrangle, Washington County, Utah: Utah Geological and Mineral Survey Open-File Report 206, 33 p., scale 1:24,000.

Grant, S.K., and Proctor, P.D., 1988, Geologic map of the Antelope Peak quadrangle, Iron County, Utah: Utah Geological and Mineral Survey Open-File Report 130, 20 p., scale 1:24,000.

Hausel, W.D., and Nash, W.P., 1977, Petrology of Tertiary and Quaternary volcanic rocks, Washington County, southwestern Utah: Geol. Soc. of America Bulletin, v. 88, p. 1831-1842.

Hintze, L.F., 1986, Stratigraphy and structure of the Beaver Dam Mountains, southwestern Utah: p. 1-36 *in* Griffin, D.T., and Phillips, W.R., eds., Thrusting and extensional structures and mineralization in the Beaver Dam Mountains, southwestern Utah: Utah Geol. Assoc. Pub. 15, 217 p.

Jaffe, H.W., Gottfrield, David, Waring, C.L., and Worthing, H.W., 1959, Lead-alpha age determinations of accessory minerals of igneous rocks (1953-1957): U.S. Geol. Survey Bulletin 1097-B, p. 65-148.

Mabey, D.R., and Budding, K.E., 1987, High-temperature geothermal resources of Utah: Utah Geological and Mineral Survey Bulletin 123, 64 p.

MacDonald, G.D., III, 1991, The Magnet—Iron ore in Iron County, Utah: Cedar City, Utah, G.D. MacDonald III, 63 p.

Mackin, J.H., 1947, Some structural features of the intrusions in the Iron Springs district: Utah Geol. Soc., Guidebook to the Geology of Utah, no. 2, 62 p.

Mackin, J.H., 1954, Geology and ore deposits of the Granite Mountain area, Iron County, Utah: U.S. Geological Survey Mineral Investigations Field Studies Map MF-14, scale 1:12,000.

Mackin, J.H., 1960, Structural significance of Tertiary volcanic rocks in southwestern Utah: Amer. Journ. of Science, v. 358, p. 81-131.

Mackin, J.H., 1968, Iron ore deposits of the Iron Springs district, southwestern Utah: p. 992-1019 *in* Ridge, J.D., ed., Ore Deposits of the United States, 1933-1967 (Graton-Sales volume), v. 2, New York: Amer. Inst. of Mining, Metallurgical, and Petroleum Engineering, p. 992-1880.

Mackin, J.H., and Ingerson, Earl, 1960, An hypothesis for the origin of ore-forming fluid, p. B1-B2 in Short papers in the geological sciences: U.S. Geological Survey Prof. Paper 400-B.

Mackin, J.H., Nelson, W.H., and Rowley, P.D., 1976, Geologic map of the Cedar City NW quadrangle, Iron County, Utah: U.S. Geol. Survey Geologic Quadrangle Map GQ-1295, scale 1:24,000.

Mackin, J.H., and Rowley, P.D., 1976, Geologic map of the Three Peaks quadrangle, Iron County, Utah: U.S. Geol. Survey Geologic Quadrangle Map GQ-1297, scale 1:24,000.

Maldonado, Florian, Sable, E.G., and Anderson, J.J., 1990, Shallow detachment of mid-Tertiary rocks, Red Hills (Basin and Range), with implications for a regional detachment zone in the adjacent Markagunt Plateau (Colorado Plateau), southwest Utah: Geol. Soc. of America, Abstracts with Programs, v. 22, no. 3, p. 63 (abstr.).

Maldonado, Florian, and Williams, V.S., in press, Geologic map of the Parowan Gap quadrangle, Iron County, Utah: U.S. Geological Survey Geologic Map GQ-1712, scale 1:24,000.

Maldonado, Florian, Sable, E.G., and Anderson, J.J., in press, Evidence for a Tertiary low-angle shear zone, Red Hills, Utah, with implications for a regional shear zone in the adjacent Colorado Plateau: Utah Geological Association, 1992 Field Trip and Guidebook: Engineering and Environmental Geology of Southwestern Utah.

Mattison, G.D., 1972, The chemistry, mineralogy and petrography of the Pine Valley Mountains, southwestern Utah: College, PA, The Pennsylvania State Univ., Ph.D. dissertation, 141 p.

Morris, S.K., 1980, Geology and ore deposits of Mineral Mountain, Washington County, Utah: Brigham Young Univ. Studies in Geology, v. 27, pt. 2, p. 85-102.

Noble, D.C,. and McKee, F.H., 1972, Description and K-Ar ages of volcanic units of the Caliente volcanic field, Lincoln County, Nevada, and Washington County, Utah: Isochron/West, no. 5, p. 17-24.

Pe, Win, and Cook, K.L., 1980, Gravity survey of the Escalante Desert and vicinity, Iron and Washington Counties, Utah: Earth Science Laboratory/University of Utah Research Institute Report No. DOE/ID/12079-14, 169 p.

Peterson, Fred, and Pipiringos, G.N., 1979, Stratigraphic relations of the Navajo Sandstone to Middle Jurassic Formations, southern Utah and northern Arizona: U.S. Geol. Survey Prof. Paper 1035-B, 43 p.

Rowley, P.D., and Barker, D.S., 1978, Geology of the Iron Springs mining district, Utah: p. 49-58 *in* Shawe, D.R., and Rowley, P.D., eds., Field Excursion C-2, Guidebook to mineral deposits of southwestern Utah: Utah Geol. Assoc. Pub. 7, 75 p.

Rowley, P.D., McKee, E.H., and Blank, H.R., Jr., 1989, Miocene gravity slides resulting from emplacement of the Iron Mountain pluton, southern Iron Springs mining district, Iron County, Utah: EOS, v. 79, no. 43, p. 1309 (abstr.).

Rowley, P.D., and Siders, M.A., 1988, Miocene calderas of the Caliente caldera complex, Nevada-Utah: EOS, v. 69, no. 44, p. 1508 (abstr.).

Rowley, P.D., Steven, T.A., Anderson, J.J., and Cunningham, C.G., 1979, Cenozoic stratigraphic and structural framework of southwestern Utah: U.S. Geol. Survey Prof. Paper 1149, 22 p.

Sable, E.G., and Anderson, J.J., 1985, Tertiary tectonic slide megabreccias, Markagunt Plateau, southwestern Utah: Geol. Soc. of America, Abstracts with Programs, v. 17, no. 4, p. 263.

Shubat, M.A., and McIntosh, W.S., 1988, Geology and mineral potential of the Antelope Range mining district, Iron County, Utah: Utah Geol. and Mineral Survey Bulletin 125, 26 p.

Shubat, M.A., and Siders, M.A., 1988, Geologic map of the Silver Peak quadrangle, Iron County, Utah: Utah Geol. and Mineral Survey Map 108, scale 1:24,000.

Siders, M.A., 1985a, Geologic map of the Pinon Point quadrangle, Iron County, Utah: Utah Geol. and Mineral Survey Map 84, scale 1:24,000.

Siders, M.A., 1985b, Geologic map of the Beryl Junction quadrangle, Iron County, Utah: Utah Geol. and Mineral Survey Map 85, scale 1:24,000.

Siders, M.A., 1991, Geologic map of the Mount Escalante quadrangle, Iron County, Utah: Utah Geol. and Mineral Survey Map 131, scale 1:24,000.

Siders, M.A., Rowley, P.D., Shubat, M.A., Christenson, G.E., and Galyardt, G.L., 1990, Geologic map of the Newcastle quadrangle, Iron County, Utah: U.S. Geol. Survey Geologic Quadrangle Map GQ-1690, scale 1:24,000.

Siders, M.A., and Shubat, M.A., 1986, Stratigraphy and structure of the northern Bull Valley Mountains and Antelope Range, Iron County, Utah: p. 87-102 *in* Griffin, D.T,. and Phillips, W.R., eds., Thrusting and extensional structures and mineralization in the Beaver Dam Mountains, southwestern Utah: Utah Geol. Assoc. Pub. 15, 217 p.

Spurney, J.C., 1984, Geology of the Iron Peak intrusion, Iron County, Utah: Kent, Ohio, Kent State Univ., unpub. M.S. dissertation, 84 p.

Tobey, E.F., 1976, Geology of the Bull Valley intrusive-extrusive complex and genesis of the associated iron deposits: Eugene, Univ. of Oregon, unpub. Ph.D. dissertation, 244 p.

Van Kooten, G.K., 1988, Structure and hydrocarbon potential beneath the Iron Springs laccolith, southwestern Utah: Geol. Soc. of America Bulletin, v. 100, no. 10, p. 1533-1540.

Wells, F.G., 1938, The origin of the Iron ore deposits in the Bull Valley and Iron Springs district, Utah: Econ. Geology, v. 23, p. 477-507.

Wernicke, Brian, Axen, G.J., and Snow, J.K., 1988, Basin and Range extensional tectonics at the latitude of Las Vegas, Nevada: Geol. Soc. of America Bull., v. 100, no. 11, p. 1738-1757.

Winkler, G.R., and Shubat, M.A., 1990, Geologic setting: p. 4-23 *in* Eppinger, R.G., Winkler, G.R., Cookro, T.M., Shubat, M.A., Blank, H.R., Jr., Crowley, J.K., Kucks, R.P., and Jones, J.L., Preliminary assessment of the mineral resources of the Cedar City 1° x 2° quadrangle, Utah: U.S. Geological Survey Open-File Report 90-34, 146 p.

APPENDIX
DESCRIPTION OF ROCK UNITS, IRON AXIS REGION

(AR, Antelope Range and Newcastle area; BV, Bull Valley district, including northern and eastern Bull Valley Mtns.; IS, Iron Springs district, Red Hills, and Cedar City area; PV, northern Pine Valley Mtns., including Stoddard Mtn.)

YOUNG BASALT	Black, sparsely porphyritic, augite-hypersthene andesitic lava and tephra of Black Hills, BV (Blank, 1959; Hausel and Nash, 1977); dark gray to black olivine-augite basaltic lava and tephra of Enterprise (Blank, 1959, unpub. data); quartz-bearing basaltic lava and tephra of Pine Valley-Central area (Cook, 1957, 1960; Hausel and Nash, 1977); and basaltic, lava and tephra of Red Hills, Cedar City-Parowan area, and western Markagunt Plateau (Fleck and others, 1975; Anderson and Christensen, 1989; Maldonado and Williams, in press).
BASIN FILL	Loosely consolidated, fine to coarse clastic rocks and mudstone of valley-fill deposits; includes Pliocene and Pleistocene graben fill of southern Escalante and Cedar City-Parowan areas. Exposed strata near range fronts capped by dissected alluvial fan deposits.
RHYOLITE AND DACITE OF SHINBONE CREEK AND EIGHTMILE SPRING	Light tan to gray, pink, or purplish, biotite-bearing, phenocryst-poor, rhyolitic to dacitic lava of Shinbone Creek, BV (Blank, 1959; E.H. McKee, unpub. data). Occurs as low, domoform mass with flow-layered interior and vesiculated margins; modal composition similar to Racer Canyon Tuff. Also, brown to bluish- or greenish gray, massive to platy hornblende dacitic lava of Eightmile Spring area NE of Central, which may be Pleistocene (Cook, 1957, 1960; Hausel and Nash, 1977).
RHYOLITE AND DACITE OF ANTELOPE RANGE	Purplish gray, biotite-bearing, glassy, vesicular rhyolite to trachyte andesite porphyry lava of Silver Peak domes; purplish, biotite-bearing, diktytaxitic, phenocryst-rich dacite porphyry of Bullion Canyon dome (Shubat and Siders, 1988).
BASALT OF FLATTOP MOUNTAIN	Dark gray to bluish black olivine-augite basaltic lava and tephra forming caprock of Flattop Mountain (BV), and approximately coeval caprock near Modena, near North Hills of Enterprise area (Siders, 1985a), and on W side of Pine Valley Mountains (Cook, 1957, 1960). Overlies soft, salmon-colored volcaniclastic rocks and rock of silicic domes and flows at Flattop Mountain (Blank, 1959).
VOLCANICLASTIC ROCKS OF NEWCASTLE RESERVOIR	Dark, red-brown, coarse volcanic conglomerate, mainly of alluvial fan origin; and subordinate laharic breccia and sandstone. Correlative with mine series of Siders (1985b), host for silver ore at Escalante mine (Siders and others, 1990).
VOLCANICLASTIC ROCKS OF ENTERPRISE RESERVOIR	Soft, pink to salmon-colored, largely volcaniclastic sandstone, siltstone, and mudstone; semi-consolidated volcanic pebble-cobble conglomerate of alluvial fan and fluvial origin, with subordinate white and gray airfall ash. Also includes minor tan, coarse, polymict mudflow breccia and tan, fragment-rich, crystal-poor rock of probable sillar. Overlain by basalt of Flattop Mountain. As mapped, may include young valley fill or tuff and volcaniclastic deposits of Cedar Spring (Blank, 1959). Assigned by Cook (1960) to Muddy Creek Formation of southern Nevada (also see Hintze, 1986).
RHYOLITE AND DACITE OF FLATTOP MOUNTAIN COMPLEX	Blue-gray to dark purple, sparsely porphyritic to aphanitic rhyolitic lava and hypabyssal intrusive rock of Cow Creek, Little Pine Creek, and Pilot Peak (BV); includes gray glassy rhyolitic breccia phases of vent and flow margins (Blank, 1959; Cook, 1960; E.H. McKee, unpub. data). Also included are similar rhyolitic rock of Pinon Point and Beryl Junction (Siders, 1985 a,b); and reddish to tan, moderately crystal-rich biotite dacite of Hogs Back, BV (Blank, 1959; unpub. data).
TUFF OF HONEYCOMB ROCKS	White to gray, non-welded to lightly welded, crystal-poor, rhyolitic ash-flow tuff with abundant purple and red rhyolitic aphanite and subordinate andesite fragments. Overlies Ox Valley Tuff S of Enterprise Reservoir in BV; not present E of Flattop Mountain (Blank, unpub. data).
OX VALLEY TUFF	Pale blue or lavender to pink, moderately welded, moderately crystal-rich rhyolitic ash-flow tuff, characterized by insets of blue iridescent sanidine; contains sparse, generally altered, pumice lapilli and sparse purple aphanite fragments. Where silicified, resembles massive rhyolitic lava of Cow Creek flow-dome, BV; correlation with similar ash-flow tuff of Caliente area uncertain (Blank, 1959; Noble and McKee, 1972; Ekren and others, 1977).

TUFF OF CEDAR SPRING	Soft, white, gray, and salmon-colored, massive, crystal-poor, rhyolitic (?) sillar tuff and fine to coarse, poorly consolidated volcaniclastic rocks; includes thin, gray-green, highly welded rhyolitic (?) ash-flow tuff of Lower Moody Wash, BV (Blank, 1959).
BASALT OF PILOT CREEK	Purple, brown, and black olivine-augite basaltic lava, commonly with platy structure and displaying abundant fine- to medium-grained reddish iddingsitic olivine insets. Includes varicolored intrusive and near-vent facies in Pilot Wash area, BV (Blank, 1959); may be correlative with basaltic andesite from lower Moody Wash area analyzed by Hausel and Nash (1977).
RACER CANYON TUFF	White to pale gray or tannish, moderately welded, moderately crystal-rich rhyolitic to dacitic ash-flow tuff, with sparse biotite and abundant red and purple lithic fragments; modally similar to Leach Canyon Formation. Volcaniclastic interbeds separate upper and lower compound cooling units near top of formation. Upper zone of lower cooling unit exhibits rude layering and coarsely spherulitic devitrification. In part correlative with tuff of Kane Point (Mackin, 1960) and upper part of Page Ranch Formation of Cook (1960). Described by Blank (1959), Siders (1985a), Siders and others (1990), and others; radiometric ages reported by Jaffe and others (1959), Noble and McKee (1972), Siders (1991), and L.W. Snee (unpub. data).
ANDESITE PORPHYRY OF MAPLE RIDGE	Dark purple (less commonly red or brown) andesite (?) porphyry lava characterized by coarse-zoned plagioclase and sparse, smaller biotite insets; overlies laharic breccia of Shoal Creek in BV district (Blank, 1959; unpub. data).
ANDESITE OF SHOAL CREEK AND NORTH HILLS	Varicolored hornblende andesitic and 2-pyroxene andesitic lava, near-vent breccia, and laharic breccia of eruptive complex NW of Enterprise. Typically is dark brown with coarse long-prismatic hornblende phenocrysts. Overlies crystal-rich ashflow tuff (Harmony Hills Tuff and/or Rencher Formation) in BV (Blank, 1959), but may be in part pre-Quichapa, as specimen from North Hills gave K-Ar age of 24.2 Ma (Siders, 1985 a,b).
PINE VALLEY LATITE	Gray to red-purple, crystal-rich, augite-biotite latitic lava of PV (Cook, 1957, 1960). Characterized by coarse plagioclase insets, platy flow structure, and thick black glassy basal zone (Cook, 1957; Grant, 1991; D.B. Hacker, unpub. data). Comagmatic with monzonite of Pine Valley. Shown by Mattison (1972) to be mineralogically andesitic and chemically dacitic.
RENCHER FORMATION	White to tan, brown, reddish or purple, lightly welded to moderately welded, crystal-rich, biotite-hornblende-augite andesitic to dacitic ash-flow tuff and tuff breccia (Cook, 1957; Blank, 1959). Contains abundant angular to ovoidal cognate inclusions (in part vapor-phase-altered pumice). Thickest in BV; erupted from intrusion of Bull Valley. Formation includes intrusive, near-vent, and laharic phases; lower, compound cooling unit in BV is locally overlain by thin, jaspilitized basal ash (base-surge deposit?) of overlying simple cooling unit, which is darker, has higher crystal and cognate inclusion content, and (near vent) flow-breccia top (Blank, 1959; Tobey, 1976). Laharic breccia of Rencher Formation overlain by Pine Valley Latite in N PV (D.B. Hacker, unpub. data). Radiometric age reported in Rowley and others (1989).
DACITE OF PINON PARK WASH	Reddish to gray or lavender, porphyritic, dacitic lava exposed NW of Enterprise. Characterized by coarse, blocky insets of zoned plagioclase; modal composition close to that of Harmony Hills Tuff. Stratigraphic position not known from field relations but dated at 21.7 Ma (Siders, 1985a); similar rock overlies hornblende andesite of Shoal Creek W of Enterprise (Blank, unpub. data).
HARMONY HILLS TUFF	Upper Formation of Quichapa Group, which is widespread in SW Utah and SE Nevada. Reddish to pink, moderately welded, crystal-rich, biotite-hornblende-augite trachyandesitic (latitic-andesitic ash-flow tuff. Distinguished from overlying Rencher tuff in BV and PV chiefly by presence of sparse phenocrysts of quartz and sanidine. Contains abundant ovoidal cognate inclusions (pumice and crystallized pumice). Pre-dates monzonitic intrusions of iron axis (except intrusion of Lookout Point; see Grant and Proctor, 1988); (Mackin, 1960; Cook, 1965; Williams, 1967; Armstrong, 1970; Noble and McKee, 1972; Rowley and others, 1979; age relations summarized in Siders and others, 1990).
ANDESITE OF LITTLE CREEK	Varicolored, porphyritic aphanitic to glassy, pyroxene andesitic lava, autobrecciated lava, flow breccia, near-vent breccia, and laharic breccia. Thickest at Copper Mountain, W of intrusion of Bull Valley; similar rock occurs at this stratigraphic horizon as mudflow breccia in IS and northern PV (Blank, 1959; Grant, 1991; P.D. Rowley, unpub. data).

ANDESITE OF CONDOR CANYON INTERVAL	Dark andesitic mudflow breccia occurring between tuff members of Condor Canyon Formation in IS and northern PV (Mackin and others, 1976; Shubat and Siders, 1988; Grant, 1991).
CONDOR CANYON FORMATION	Red to light blue-gray, densely welded, crystal-poor, biotite-bearing rhyolitic ash-flow tuff with characteristically extreme eutaxitic foliation of flattened pumice lenticules and pronounced sheeting developed in red zone above thick black basal vitrophyre. Bauers Member (Mackin, 1960) has both plagioclase and sanidine in phenocryst mode and Swett Member lacks sanidine; both lack quartz, and are distinguishable from one another only with difficulty in the field. Swett Member (Mackin, 1960) absent in BV (Cook, 1965; Williams, 1967; Armstrong, 1970; Best, Christiansen, Deino, and others, 1989).
LEACH CANYON FORMATION	Basal formation of Quichapa Group. Pale cream to pink and gray, moderately welded, moderately crystal-rich, biotite and hornblende-bearing, rhyolitic ashflow tuff with abundant red lithic fragments. Members generally not discriminated; separated by 1-2 m of lacustrine limestone S of Central (H.R. Blank, unpub. data) (Mackin, 1960; Williams, 1967; Best, Christiansen, Deino, and others, 1989).
ISOM FORMATION	Purplish gray to brick-red and brown, densely welded, crystal-poor trachydacitic ash-flow tuff, commonly with well-developed black basal vitrophyre. Sparse phenocrysts of plagioclase and subordinate clinopyroxene are more abundant in Baldhills Member. Also contains sparse gray altered pumice fiamme, with elongate vesicles and flow-sheeting. Thickest in AR and IS; thin or absent in BV (Mackin, 1960; Shubat and Siders, 1988; Best, Christiansen, and Blank, 1989).
ANDESITE OF ISOM-CLARON INTERVAL	Brown aphyric lava characterized by abundant elongate amygdaloidal vesicles; red-brown lava with abundant coarse glomeroporphyritic clinopyroxene; purple, coarsely trachytic plagioclase porphyry (Blank, 1959; unpub. data). Andesite of this interval in places mapped as lower part of Isom Formation (Anderson and Rowley, 1975; Siders and others, 1990).
WAH WAH SPRINGS FORMATION	Pink to brown or green, moderately welded, crystal-rich, hornblende-biotite dacitic ash-flow tuff of Needles Range Group (Mackin, 1960; Best and Grant, 1989). Is thickest in IS area and Red Hills, where underlain by Cottonwood Wash Formation of Group and by a succession of volcaniclastic rocks, limestone, and ash-flowtuff (Maldonado and others, 1989; Maldonado and Williams, in press). Tongues into upper Claron Formation in BV (Blank, 1959; Mackin, 1960; Best and Grant, 1989).
CLARON FORMATION	Fluvial and lacustrine limestone, sandstone, siltstone, and conglomerate, but dominantly massive to thin-bedded gray limestone in upper part and gray to pink, red, or orange cobble conglomerate at base; as mapped, may be locally in part Paleocene (see Goldstrand, 1990). Coarsens westward; upper part equivalent to what was called pink cliffs Wasatch in early reports on the Cedar Breaks area. Five members mapped in IS (Mackin and Rowley, 1976; Mackin and others, 1976).
IRON SPRINGS FORMATION	Varicolored, thin-bedded to massive, but commonly mustard-colored, thick-bedded fluvial and lacustrine clastic rocks with subordinate limestone and coal. Three to five members mapped in IS; equivalent formations of Colorado Plateau distinguished only on E side of PV (Mackin and Rowley, 1976; Mackin and others, 1976; Fillmore, 1989).
CARMEL FORMATION	Cream to blue-gray massive to thin-bedded and platy marine limestone, red and maroon siltstone, and gray to maroon shale, in part fossiliferous. Not subdivided in W part of region. Underlain by Middle Jurassic Temple Cap(?) Sandstone and Early Jurassic Navajo Sandstone in Red Hills (Maldonado and others, in press) and E and S part of PV area (Cook, 1957, 1960; also see Peterson and Pipiringos, 1979). Base of formation is horizon of Miocene monzonite intrusion in IS (Mackin and others, 1976) and BV (Blank, 1959, Tobey, 1976).

PROCESSES AND PRINCIPLES ALONG THE WASATCH FRONT

by Susan Morgan
Department of Geology & Geophysics
University of Alaska
Fairbanks, Alaska 99775-0760

This field trip guide is modified from Tour 4 and Tour 5 of a booklet by Susan Morgan published by the Utah Geological Survey. We revised the order of stops and added additional information about geologic processes in a few places.

Susanne U. Janecke
Peter T. Kolesar
Department of Geology
Utah State University
Logan, UT 84322-4505

OGDEN TO BRIGHAM CITY

Ogden North Along Highway 89 to Brigham City

0.0 Starting Point. Junction Highway 203 and Highway 39. Start trip, driving west on Highway 39 (Fig. 1).

1.4 Junction Highway 89 — Turn right (North) on Highway 89.

2.4 Junction Highway 235 — Stay on Highway 89.

3.3 Junction Highway 204 (Wall Street) —Stay on Highway 89.

4.1 **Stop 1 — View of the Wasatch Mountain Front to the Right (East).** The Wasatch is an imposing mountain range formed by complex thrust and normal faulting during the geologic past. The dark, lower rocks, the Farmington Complex metamorphic rocks, are overlain by the lighter, pink, Cambrian Tintic Quartzite. All of these rocks have been moved from west to east by thrust faulting. Here one captures a glimpse of Earth's complexity, since several thrust sheets are stacked one on top of another. Two thrusts that occur below the Willard thrust, the Ogden and Taylor thrust faults, are exposed in the Wasatch Range east of Ogden and repeat the rock sequence. Geologists have shown that the rocks above the thrust moved eastward about 140-110 million years ago.

Most thrust faults are flat or tilted gently back in the direction from which the rocks above the thrust came. The thrust faults in the Wasatch Mountains near Ogden are unusual because they are tilted toward the east, toward the direction of transport. Why might this be?

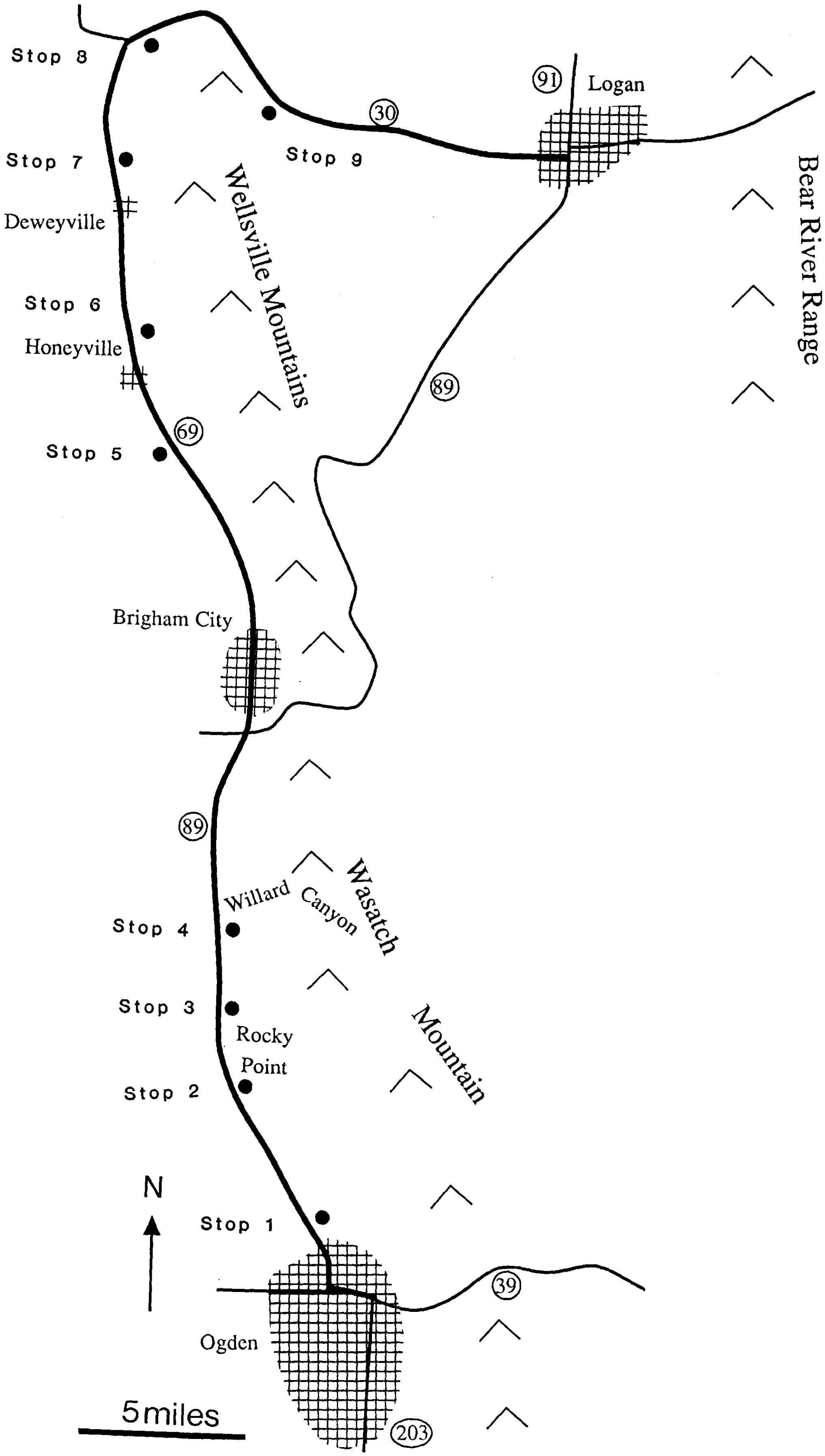

Figure 1. Location of road log stops.

8.3 Peter Skene Ogden Historical Marker on the right (East).

8.6 Road cut through the Tintic Quartzite; enter Box Elder County. The Wasatch Range is bounded on the west side by the Wasatch fault, an active normal fault that continues to uplift the Wasatch Range. Fault scarps of the Wasatch fault, steep slopes created by movement along the active fault, are not easy to distinguish from Bonneville shoreline features.

Studies indicate that the Wasatch fault is divided into a series of segments that behave somewhat independently. The segments are separated from one another by zones called segment boundaries. Several segment boundaries of the Wasatch fault coincide with salients, a geologic term for a major bedrock spur that extends out into a basin or valley.

9.0 **Stop 2 — Rocky Point.** The road curves around Rocky Point, part of the Pleasant View salient. Complex faulting extends this bedrock point, or salient, some distance from the mountain front. Even though the point is composed of Cambrian Tintic Quartzite, only a few outcrops of quartzite can be seen above the Lake Bonneville sediments that blanket the underlying rocks.

Rocky Point is a segment boundary that separates the Brigham City segment of the Wasatch fault to the north from the Weber segment to the south. The Brigham City segment generated a large earthquake about 3,600 years ago, whereas the most recent event along the Weber segment occurred about 500 years ago.

9.1 Junction Highway 89 and Interstate 80. Lake Bonneville-Wasatch Fault. This section of Highway 89 sometimes is referred to as "fruit way" because of all the orchards and fruit stands lining the highway. The pervasive Lake Bonneville shorelines form prominent benches along the base of the Wasatch Range to your right (east). From here, north past Brigham City, the mountains are bounded by the Brigham City segment of the Wasatch fault.

11.4 **Stop 3 — Toe of an Alluvial Fan.** The road traverses the toe of an alluvial fan. You can get a close look at the boulders dotting the alluvial fan. These boulders were most likely moved by mass wasting.

12.1 Enter Willard.

12.3 Alluvial Fans. A small canyon, to the south of Willard Canyon, with a very nice alluvial fan developed at its mouth, is coming into view. Alluvial fans form when a confined mountain stream spreads out across a plain in the adjacent valley. Deposition is caused by changes in channel geometry (stream widens, water becomes more shallow, velocity drops), infiltration of water and evaporation of water. This depositional process gradually builds a fan-shaped feature called an alluvial fan. All of the small canyons along the mountain front have alluvial fans at their mouths. If you look closely you will notice that large boulders comprise part of the fan material. Streams probably didn't move such big rocks; more likely these were old debris-flow deposits. Because no shoreline features are developed on them, the alluvial-fan deposits postdate Lake Bonneville, and are therefore younger than about 14,000 years old.

13.8 **Stop 4 — Debris Flow Basin.** On your right, you will soon be passing a rock wall that is really a spill-over for a debris flow basin constructed in the early 1920s. A debris flow is an example of a mass-wasting event. Mass wasting is defined as the downslope movement of rock, debris, or soil under the influence of gravity. In 1910 the uppermost slopes of the Willard Canyon drainage basin were heavily overgrazed. The removal of soil-stabilizing vegetation by overgrazing resulted in two debris flows that moved through the canyon and deposited material. These debris flows damaged structures in the town of Willard. A debris flow is a water-saturated mixture of mud, sand, gravel, and boulders that becomes unstable and moves down slope. After the 1910 disaster two things were done to mitigate the situation. First, grazing was limited on the upper slopes and those slopes were terraced and planted with trees. Second, a debris basin was constructed to channel and contain any future debris flows. A debris basin is just what it sounds like, a large basin, constructed directly below the hazard area, that will hopefully contain any debris flow coming off the mountain slopes. The rock spillway you see from the highway allows water, collected in the basin behind it, to run off. Since its construction, the debris basin has been nearly filled by debris flows. Debris basins are still being constructed in many areas of the United States where mass-wasting hazards are present.

From here you can see Willard Canyon, a large canyon carved into the western slopes of the mountains (Fig. 2). The last outcrops of pink, steeply-dipping, Lower-Middle Cambrian Tintic Quartzite are to the right (north) side of Willard Canyon. The light-colored Tintic has been visible along the mountain front as we drove north from Ogden. This quartzite is a "sedimentary quartzite," a quartz-cemented sandstone. It consists of sand-sized quartz particles and scattered rounded pebbles and exhibits small-scale cross-bedding, a sedimentary structure that tells a story about how the original sand grains were deposited. Small-scale cross beds are slices through ripple marks, which occur in streams and along beaches today, and are formed by moving water. By looking at modern features and making comparisons to the ancient rock record, geologists unravel the mysteries hidden within the rocks. Since the Tintic Quartzite is composed of ripple-marked, deposits of well-rounded

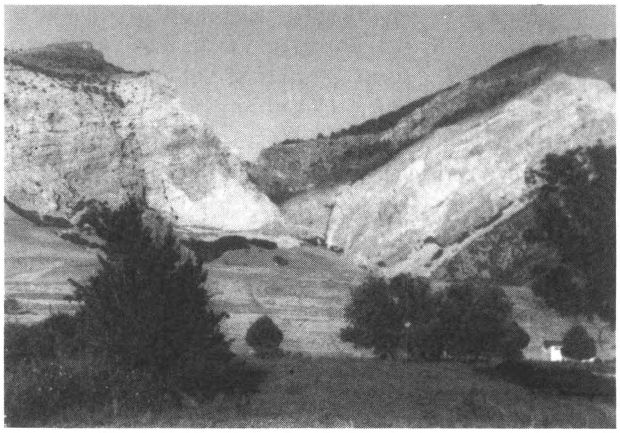

Figure 2. Mile 13.8. The light colored, east-dipping, Lower-Middle Cambrian Tintic Quartzite overlies the dark, 1.8 billion-year-old Farmington Complex at Willard Canyon. The boundary between the two rock units is a nonconformity and represents over 1 billion years of missing time.

sand grains and pebbles, geologists postulate it was probably deposited in a near-shore or beach environment. In Cambrian time, the sands most likely were eroded from exposed continental rock to the east, were transported by rivers to the ocean, and finally formed beaches rippled by shoreline currents.

From Ogden north to Willard Canyon we have been driving past spectacular rugged outcrops of some of the oldest rock in Utah. The dark, lower rocks are part of the Precambrian Lower Proterozoic Farmington Complex, metamorphic schist and gneiss that have been radiometric age-dated to be at least 1.8 billion years old and possibly as old as 2.5 billion years. The Farmington Complex is directly overlain by the much younger Cambrian Tintic Quartzite, 550 million years old. Color differences make the boundary between these two rock types apparent. You may recognize that there is a big chunk of time missing, or not represented by the rock record, between these two rock units. This surface is called an unconformity and results when erosion removes pre-existing rock or sediment. An unconformity may also result if no material is deposited during an interval of time. When sedimentary rock unconformably overlies metamorphic or intrusive igneous rock the contact between the two rock units is called a nonconformity.

Metamorphism refers to changes that occur to the rocks, a result of changes such as increased heat and/or pressure in the rocks' environment. Geologists studying the Farmington Complex have determined that most of the gneiss was originally a granitic intrusion, whereas some of the lenses of gneiss and schist were originally sedimentary rock. Most of these rocks are tightly folded, a common result of regional metamorphism and directed pressure.

The Willard thrust is located just above the pink cliffs of the Tintic Quartzite and places older Precambrian sedimentary rock on top of younger Cambrian rock.

15.7 Enter Perry.

16.6 Great Salt Lake to the left (West). Willard Bay, the northern end of the Great Salt Lake, is on your left. The Salt Lake has no outlet and is a remnant of the once-larger, ancient Lake Bonneville. A change to a warmer and drier climate at the end of the last Ice Age, approximately 12,000 years ago, led to the shrinkage of the lake waters as evaporation exceeded precipitation. The level of the Great Salt Lake still responds to climate variations. In the 1983-1985 wet climate cycle, the lake level rose several feet and flooded adjacent land, including most of the Bear River Wildlife Refuge. The Refuge encompasses most of the wetlands formed where the Bear River enters the Great Salt Lake, just west of Brigham City. The Bear River delivers most of the fresh water that enters the Great Salt Lake.

Precambrian rocks are exposed on the hillsides to the right (east) and are part of the rock sequence of the upper plate of the Willard thrust. Near Willard Canyon the road crosses the trace of the thrust, and the rocks forming the magnificent cliffs from Willard south are part of the Precambrian to Cambrian rock sequence of the lower plate (underneath) of the Willard thrust.

19.2 Stoplight at the intersection of Highway 89 and Main Street just south of Brigham City.

BRIGHAM CITY TO LOGAN VIA CACHE BUTTE

Brigham City North on Highway 69 Then East
Via Highway 30 to Logan

0.0 Starting Point. Junction of Highway 69 and Highway 89. From here you have a good view of the Wellsville Mountains. These mountains trend north-south and are bounded by normal faults on both the east-facing and west-facing sides (the side you are looking at). This range is often referred to as the steepest mountain range in the world, that is, they are very high in relation to the width of their base. It is such a narrow range, that if you stood on the ridge top, you would look almost directly down into the Cache Valley.

1.6 Downtown Brigham City. Continue through town from the junction with Highway 89. The outcrops making up the mountain front are Cambrian Brigham Group Quartzite.

6.0 Alluvial Fan, Mines, and Fossils. You are now traveling over the toe of an alluvial fan that includes mudflow and debris-flow material from Cascade Canyon to the right (east). The numerous large boulders indicate such mass-wasting events.

The Cambrian Spence Shale, a member of the

Langston Formation, crops out in the lower part of Cascade Canyon. The Spence Shale is a fossiliferous unit, with trilobites and brachiopods among its more common fossils. Brigham City resident Lloyd Gunther has collected extensively in the Spence Shale over many years. He has uncovered a variety of world-class fossils, some of which are new species. If you care to hunt fossils in the Spence Shale, note that the property adjacent to the mountains is private land and that you must have the land owner's permission before crossing private property.

At this point, an old road scar begins to cross the mountain front and leads to an old antimony mine in Antimony Canyon, the next large canyon to the south. The road starts from private land and is now nearly impassable due to rockfalls. During World War II, antimony was highly valued as an alloy in metals for airplanes. Antimony is relatively rare in the United States, so large amounts of money were spent developing the mine even though prospectors found only small amounts of this element. Mine buildings, including a mill and living quarters for mine workers, were constructed in Antimony Canyon and in several of the smaller canyons to the north. However, very little ore was actually shipped out for the war effort.

Due to normal faulting, the Spence Shale crops out high up on the steep slopes of Antimony Canyon. This is the location of one site where Mr. Gunther and others have collected numerous fossil specimens.

7.1 Shorelines. From here is a good view directly south along the range front to Brigham City and the well-developed Bonneville and Provo-level shorelines.

8.8 Enter Honeyville. In 1939, a mammoth tooth was found near the small community of Bear River City, southwest of Honeyville, a reminder of the different creatures that roamed this area in the past. Mammoths and many other large mammals (such as camels, giant ground sloths, giant beavers, and saber-toothed tigers) became extinct about 12,000 years ago at the end of the last ice age. Some geologists think that the dramatic change in climate at that time caused the extinctions.

8.9 **Stop 5 — Call's Fort Canyon on the Right (East) Call's Fort Historical Marker on the Left (West).** The historical marker tells the history of Call's Fort, which was built in 1855. The local history is fascinating, but so are the rocks that make up the historical marker. The distinctly color-banded boulders are gneiss from the Farmington Complex that crops out south of Brigham City. The more common rounded, pink quartzite boulders are from the lower Cambrian Brigham Group that crops out just south of Call's Fort Canyon. This unit is equivalent to the Tintic quartzite discussed previously. Why are so many of the quartzite boulders rounded? Stream action would round the boulders; however, these stones were taken from an early flour mill where the grinding action would also produce rounded boulders. What better stone could be used to grind flour than a hard, quartz-rich rock such as this?

Besides all of the wonderful rocks making up the historical marker, there is a beautiful view of the spectacular cliffs of Paleozoic limestone and dolostone in Call's Fort Canyon to your right (east) (Fig. 3). There is also a characteristic alluvial fan formed at the mouth of the canyon. Just south of this canyon are the last outcrops of the Cambrian Brigham Group Quartzite. These are the dark brown to rusty colored rocks at the base of the mountains.

9.2 Gravel Pit. A large gravel pit, to your right (east), is against the base of the mountains just north of Call's Fort Canyon. By now you probably realize that the gravel and sand, a valuable resource, are a result of Lake Bonneville shoreline deposits.

10.4 Alluvial Fan. The road crosses an alluvial fan emanating from the mouth of Cottonwood Canyon.

11.1 Junction Rt. 240 to I-15 on the Left (West) — Stay on 69 North. As you drive north along the base of the Wellsvilles, you move up-section, that is, the rocks are becoming younger (since the rocks dip northeast). Several small normal faults have also helped to rearrange the rocks so they are younger as you drive north.

12.9 **Stop 6 — Wellsville Homocline and Crystal Hot Springs.** From here there is a good view of the thick pile of Paleozoic limestone and dolostone, including a thick sequence of quartzite, that comprises the Wellsville Mountains. The layers, or strata, all dip steeply to the northeast, and are cut by numerous small-scale normal faults. You may notice that faults offset some of the more obvious rock layers.

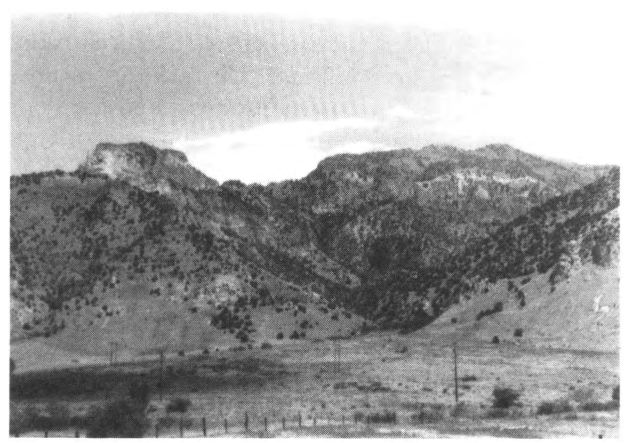

Figure 3. Mile 8.9. Paleozoic limestone and dolostone form the spectacular cliffs in Call's Fort Canyon. An alluvial fan has formed at the mouth of the canyon.

When the strata all dip in one direction, as they do in this portion of the Wellsville Mountains, they form a structural feature called a homocline.

Crystal Hot Springs. The hot spring to your left (west) is located in proximity to the fault-bounded Wellsville Mountain Front. Fault zones are areas where rock is fractured and broken by the grinding movement of rock. Fluids can flow easily through these fractured zones. The water that reaches the surface at Crystal Springs is most likely heated deep below the Earth's surface. It then moves to the surface via the path of least resistance — a fractured and consequently permeable fault zone.

14.6 Alluvial Fans. As you travel toward Deweyville there is a good view of what appears to be a ramp jutting out into the valley (Fig. 4). This is an alluvial fan made of stream deposits and mudflow and debris-flow material.

16.4 Enter Deweyville.

17.3 Junction with Highway 102 and Highway 69. Continue north on Highway 69.

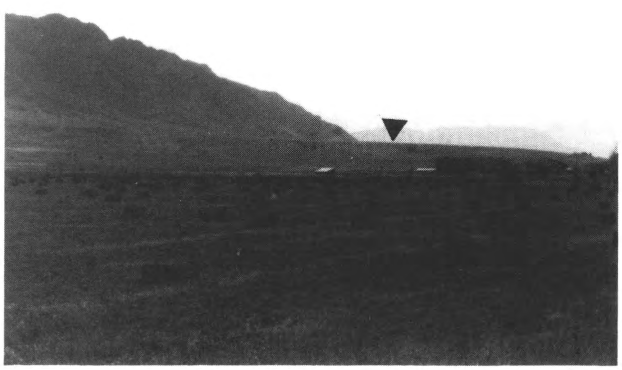

Figure 4. Mile 14.6. An alluvial fan (arrow) south of Deweyville.

17.5 Rock Outcrops. South of the gravel pit at the next stop, outcrops of Paleozoic rock form cliffs that jut out of the steep hillsides. The rocks are inclined, or gently dipping, to the northeast and are Pennsylvanian to Permian age limestone of the Oquirrh Formation. Abundant angular talus forms slopes under the cliffs (Fig. 5). Talus forms mainly as a result of frost action, the repeated freeze and thaw of water, which eventually breaks rock apart.

18.3 **Stop 7 — Gravel Pit.** This is a great place to look at different ways sediment can be deposited. Two gravel pits south of Collinston offer nice cross-section views of layered Lake Bonneville shoreline deposits. Some of the gravel and sand layers are horizontal, some are on an angle, and some are contorted into swirls. The swirled sediment may have liquefied during a large prehistoric earthquake. The varying grain sizes can be related to different energy levels of water that transported and deposited the sediment. In areas along the gravel pit walls, you may see cross-bedded gravel overlying horizontally-bedded silt. High energy is needed to move coarse material, and silt, which is generally carried in suspension, requires quiet water to settle out. What kind of story does this change in sediment type tell?

21.2 Enter Collinston. The rock outcrops to the right (east) are the Collinston Conglomerate, a member of the Tertiary Salt Lake Group. This conglomerate consists of rounded to somewhat angular gravel fragments eroded from the rocks on the surrounding hillsides. In places, it contains numerous gastropod (snail) shells.

The two prominent shorelines in this area are the upper Bonneville level and the lower Provo level. To your left (west) is a good view of what was once the flat-floored lake bottom. The Bear River has eroded into the lake bottom sediment after the lake dried up about 10,000 years ago.

22.3 Junction with Highway 30. Turn east on Highway 30.

22.7 **Stop 8 — Gullies.** The road crosses a small gully eroded by Cottonwood Creek, an intermittent creek, into the soft Lake Bonneville sediment. Several narrow but deep draws, or gullies, formed in these easily erodible sediments are skirted by the road.

Bear River. From here you have a good view of the Bear River and its flood plain, both of which are incised into old lake-bottom sediment. This portion of the Bear River is considered to be a mature stream; that is, it is close to its temporary base level, the lowest level to which a stream can erode. In this case the Great Salt Lake forms a temporary base level. Most of the erosional work of the river is extended laterally, instead of downward, to form elegantly curved meanders.

The notch, or lowest point, in the ridge to the left (north) that separates Cache Valley and Malad

Figure 5. Mile 17.5. Talus forms slopes beneath cliffs of the Pennsylvanian to Permian age Oquirrh Formation.

River-Bear River Valley is the Bear River Narrows. The Bear River eroded the notch through Silurian and Ordovician limestone and dolostone. Cutler Dam was built in the gap.

Many intermediate Bonneville shorelines are developed on the mountains on the west side of the Salt Lake Valley.

24.9 Cutler Dam Road to the Left (North).

26.1 Provo-level Shoreline. At this point, the road crosses the somewhat obscure Provo-level shoreline.

26.4 Crest of Hill — Cache Butte Divide. As you crest the hill, you will see behind you a good view of the Malad River-Bear River Valley.

The Malad Range to the left (north) and the Wellsville Mountains to the right (south) are separated by Cache Butte Divide.

26.9 Enter Petersboro.

27.3 **Stop 9 — Road Cut.** A volcanic tuff, an ash-fall deposit of the Tertiary Salt Lake Group, is exposed to your left (north). Since the highest level of Lake Bonneville covered this area, it is likely that the tuff was reworked by wave action and currents.

29.4 Junction with Highway 23. Stay on Highway 30 heading East. You are in the Cache Valley, a classic Basin and Range half graben. The major fault, the east Cache fault, is along its eastern edge. Locally, the western margin of the graben is faulted.

29.7 Cross Railroad Tracks.

To this point the road has been on a gentle decline, and passes over old lake shorelines of Lake Bonneville. When the lake was at its highest level, this pass was covered with water. The lowest point along the ridge, where the water of Lake Bonneville initially entered Cache Valley, is just north of the road, at Bear River Narrows, the site of Cutler Dam. Bear River Narrows was also the connection between the western portion of the lake and Red Rock Pass, in northern Cache Valley, when the lake began to empty about 15,000 to 14,000 years ago.

30.7 Logan Marsh Bridges. There are four bridges, in a short distance, that span the waters of the Logan Marsh. The Little Bear River enters the marsh from the right (south) and eventually flows into the Bear River to the north. The marsh provides habitat for many different creatures, including a variety of waterfowl such as pelicans, sandhill cranes, ducks, and geese.

The two most prominent Lake Bonneville levels, the highest Bonneville level and the lower Provo level, are easy to observe along the mountains on the east side of Cache Valley. In addition to these two levels, you can see many minor shorelines on the west side of Cache Valley.

33.0 Road to Benson to the Left (North).

36.2 Cross Railroad Tracks.

37.0 Cache County Courthouse, Main and 200 North. End of trip.

MESOZOIC TECTONICS OF THE NORTHERN WASATCH RANGE, UTAH

W. A. Yonkee, Department of Geology, Weber State University, Ogden, UT 84408
J. P. Evans, Department of Geology, Utah State University, Logan, UT 84322
P. G. DeCelles, Department of Geological Sciences, University of Rochester, Rochester, NY 14627

INTRODUCTION

The geometry and chronologic development of regional structures in the Idaho-northern Utah-Wyoming fold and thrust belt are well constrained (Armstrong and Oriel, 1965; Royse and others, 1975; Dixon, 1982; Lamerson, 1982; Wiltschko and Dorr, 1983; Oriel, 1986), making this an excellent area to study kinematics of thrust systems. Major thrusts cut up section to the east and transported Paleozoic and Mesozoic shelf and miogeoclinal strata relatively eastward above a regional decollement. Large-scale fault-bend and fault-propagation folds with concentric and kink geometries are associated with the thrusts. Synorogenic conglomerates record the successive emplacement of thrust sheets from west to east during the Mesozoic to early Tertiary Sevier orogeny. The fold and thrust belt forms a salient convex to the east, and is separated from thrust systems in central Utah by the Cottonwood and Uinta arches. The four major thrust systems exposed in northern Utah are from west to east the Willard, Ogden, Crawford, and Absaroka systems (Figs. 1 and 2). The frontal Hogsback thrust is exposed to the east in Wyoming. Basement rocks are absent in the frontal thrust sheets but are incorporated into thrust sheets in the Wasatch Range (Bell, 1951; Bruhn and Beck, 1981; Yonkee, 1990) and farther west (Snoke and Miller, 1988). The frontal thrust sheets are unmetamorphosed, but metamorphic grade locally reaches greenschist facies in the Wasatch Range (Yonkee, 1990), and increases in overall grade to the west (Snoke and Miller, 1988).

The Willard thrust system (Crittenden, 1972), the structurally highest and oldest system, carries a distinct stratigraphic package that includes about 4 km of upper Proterozoic strata and 8 km of Paleozoic strata (Figs. 2A and 3). The Willard thrust has a minimum displacement of 35 km, based on cutoff relations of Cambrian strata (Yonkee and others, 1989). The thrust juxtaposes upper Proterozoic low-grade metasedimentary rocks over Paleozoic rocks within much of the Wasatch Range, but thin slices of the lower Proterozoic Facer Formation, a sequence of intermediate grade metamorphic rocks, are locally incorporated into the base of the sheet (Crittenden and Sorensen, 1979). The thrust has a footwall flat in Cambrian shale and limestone and an oblique ramp that climbs southeast to Mississippian strata. The thrust has a footwall flat to the east in Jurassic strata, and juxtaposes Proterozoic and imbricated Paleozoic rocks over Jurassic strata along its eastern leading trace. Rocks in the upper and eastern parts of the thrust sheet are relatively undeformed, but the western lower part of the sheet displays tight inclined folds, minor thrusts, and well-developed foliation. Major movement on this thrust was probably synchronous with deposition of the Aptian (120 to 110 m.y.) Ephraim Conglomerate (Heller and others, 1986), and equivalent Kelvin Formation. Ages of sericite from syntectonic veins in part of the Willard sheet are between 140 and 110 m.y., recording internal deformation that partly preceded and was synchronous with large-scale thrusting (Yonkee, 1990).

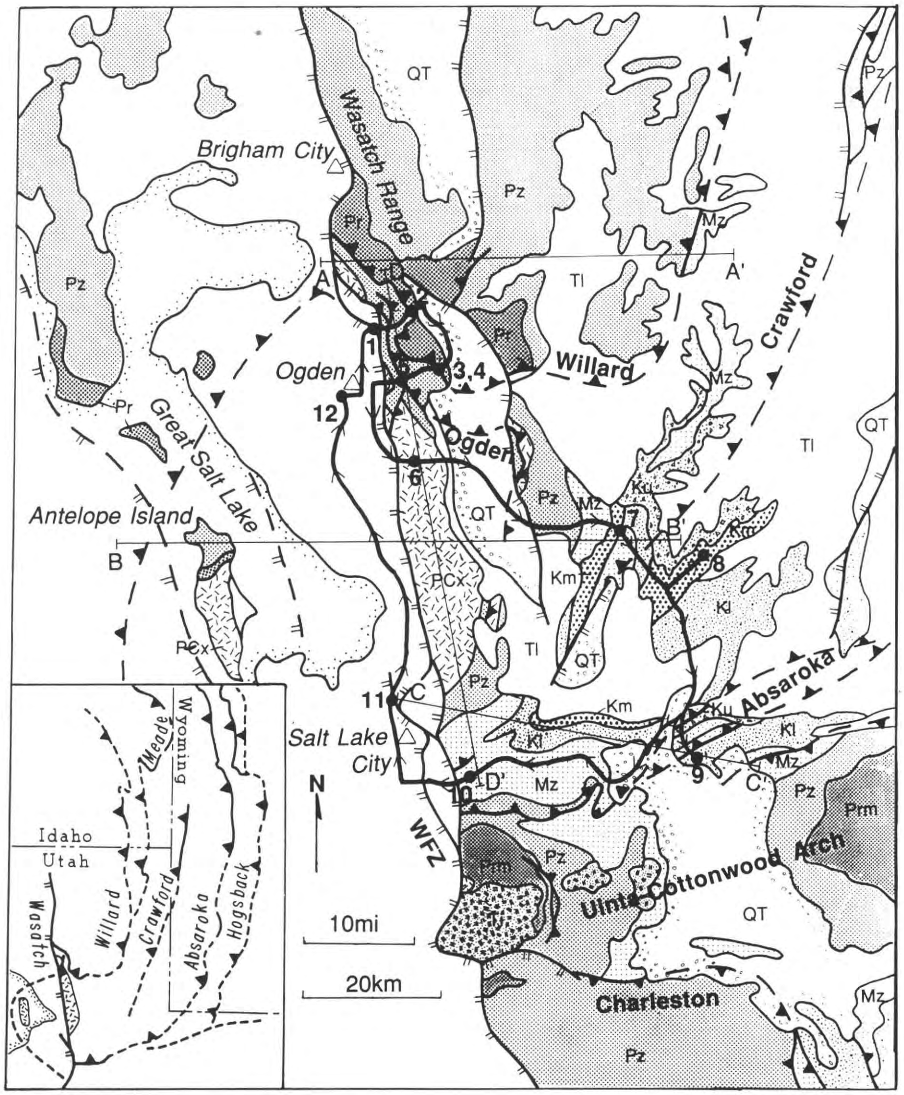

Figure 1. Index map of northern Utah showing locations of major thrusts. Locations of sections A-A', B-B', C-C', and D-D' in Figure 2 are shown. Route of field trip indicated by solid heavy line and stops are numbered. PЄx-crystalline basement, Prm-middle Proterozoic sedimentary rocks of Big Cottonwood and Uinta Mountain Group, Pr-upper Proterozoic sedimentary and low-grade metamorphic rocks of Huntsville Group, Pz-Paleozoic strata, Mz-Triassic and Jurassic strata, Kl-Cretaceous lower synorogenic deposits including Kelvin, Frontier, and Henefer Formations, Km-Cretaceous middle synorogenic deposits including Echo Canyon Conglomerate, Ku-Cretaceous upper synorogenic deposits including Hams Fork Conglomerate, Tl-early Tertiary synorogenic deposits of Wasatch Formation, Ti-Tertiary intrusive igneous rocks, QT-Cenozoic post-thrusting deposits. Modified from Hintze (1980), Lamerson (1982), Davis (1985), and Bryant (1990). Inset shows location of major thrusts within the Idaho-Utah-Wyoming thrust belt.

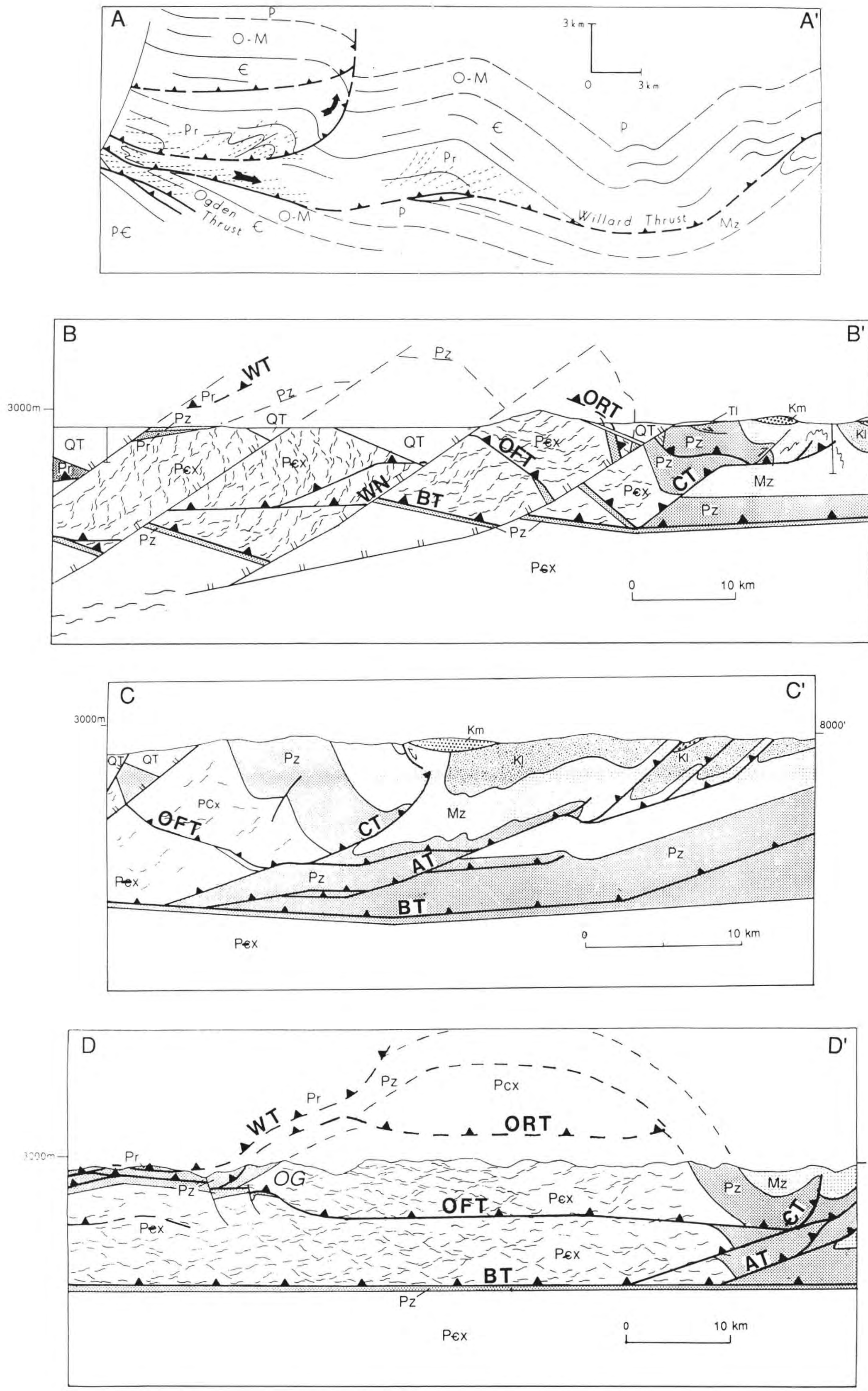

Figure 2. Generalized cross sections A-A', B-B', and C-C' subparallel to transport direction and longitudinal section D-D'. Units are same as in Figure 1 except Paleozoic strata divided into: €-Cambrian; OM-Ordovician to Mississippian; and P-Pennsylvanian to Permian strata. Faults are labeled: AT-Absaroka thrust; BT-basal thrust; €T-Crawford thrust; OFT-floor thrust of Ogden system; ORT-roof thrust of Ogden system; WT-Willard thrust, and WN-Wasatch normal fault zone. Section A-A' from Yonkee and others (1989), sections B-B' and D-D' modified from Yonkee (in press).

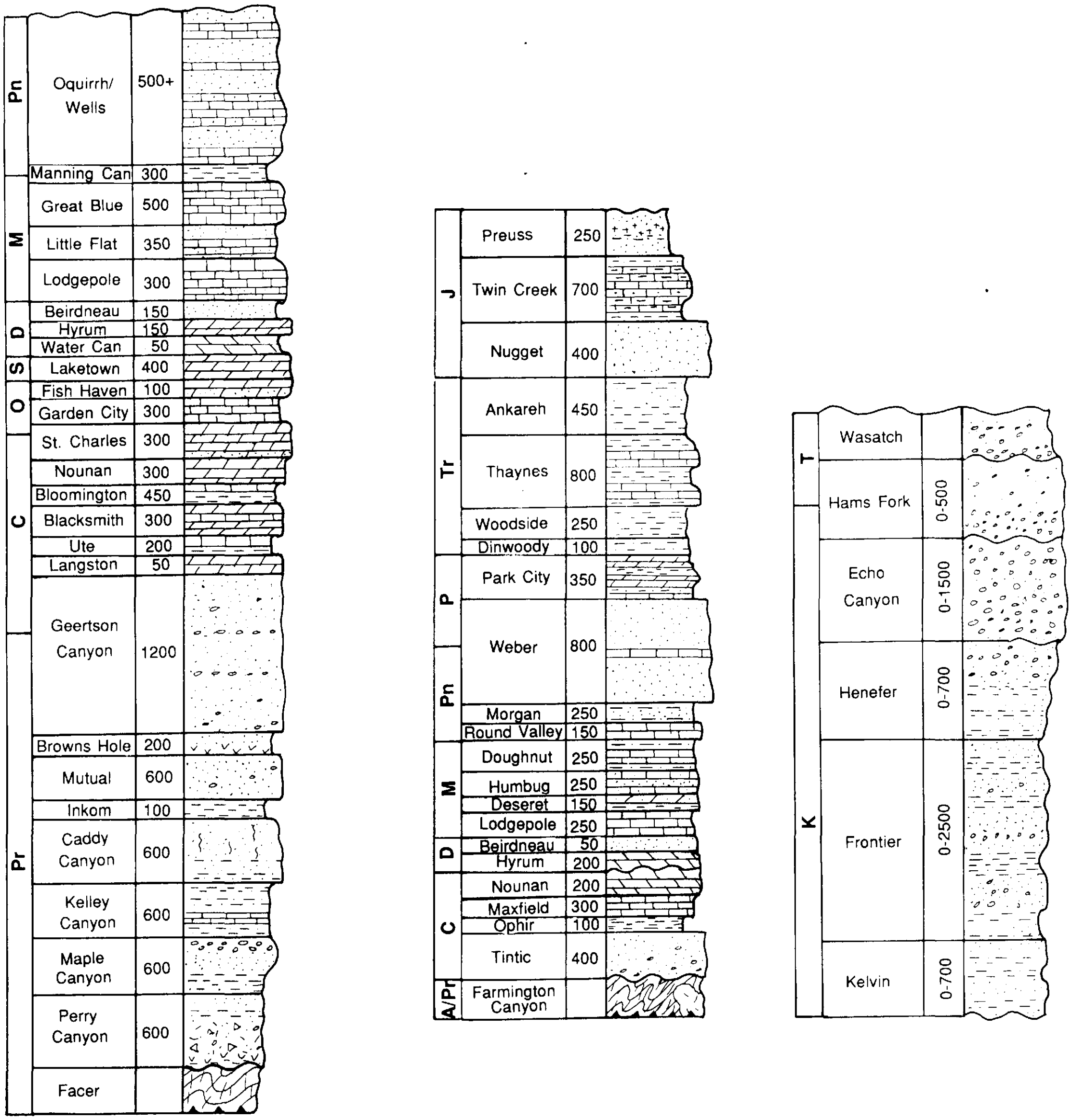

Figure 3. Generalized stratigraphic sections modified from Hintze (1988). Approximate formation thicknesses are given in meters. A. Stratigraphic section for part of Willard thrust sheet in northern Utah. The upper part of the Permo-Pennsylvanian Oquirrh Group and Triassic strata have been removed by erosion in this area. The Oquirrh Group is up to 7 km thick to the west in the Promontory Mountains, but probably decreases in thickness to the east. B. Stratigraphic section for parts of Crawford and Absaroka thrust sheets in north-central Utah. Cretaceous to Tertiary synorogenic deposits in the right hand column are highly variable in thickness.

Precambrian crystalline basement forms the core of a regional anticline structurally below the Willard thrust (Figs. 1 and 2B; Bell, 1951; Bryant, 1984; Yonkee, 1990). Basement rocks have a structural thickness of about 9 km and are directly overlain by a thin sedimentary cover consisting of about 3 km of Paleozoic and 3 to 5 km of Mesozoic strata (Fig. 3). The anticline has a culmination in the Wasatch Range, and may continue in the subsurface into southern Idaho, based on aeromagnetic data reported by Mabey and others (1978). This regional fold is a ramp anticline that is locally imbricated by the Ogden thrust system and lies above the Absaroka thrust system. The anticline is asymmetric with a steep east-dipping limb and a gently dipping western limb. Large-scale folding and thrusting in the anticline produced 50% shortening, and slip on thrusts within the anticline was largely transferred eastward into 50 to 60 km of slip on the frontal Crawford, Absaroka, and Hogsback thrusts (Yonkee, in press). Basement in the anticline is also internally deformed by an anastomosing network of shear zones that accommodated 5 to 20% internal shortening. The anticline had a protracted uplift and deformation history between about 90 and 50 m.y. Ages of syndeformational sericite from the shear zones are mostly between 140 and 110 m.y., recording internal deformation that mostly preceded large-scale folding (Yonkee, 1990).

The Ogden thrust system imbricates Precambrian crystalline basement and the sedimentary cover within the anticline (Schirmer, 1988; Yonkee, in press). North of Ogden, Utah, the thrust system includes a main thrust that juxtaposes lower Cambrian quartzite over upper Cambrian dolomite. Toward the south, the main thrust branches into a floor thrust and roof thrust. The floor thrust ramps laterally down to the south from lower Cambrian quartzite into Precambrian basement in the hanging wall, and from upper Cambrian dolomite to basement in the footwall. Stratigraphic separation increases to the south to 4 km, and estimated slip reaches 10 to 15 km. The roof thrust ramps laterally down section to the south in the hanging wall, and the interpreted southeastern continuation of the fault juxtaposes basement over Cambrian limestone at Durst Mountain, Utah (Hopkins, 1983). The amount of slip on the roof thrust is poorly constrained. The age of major movement on the Ogden thrust system is uncertain, and the system may be linked with the Crawford and Willard systems.

The Crawford thrust is poorly exposed in northern Utah, but drill hole data partly constrain its geometry (Link and others, 1985). The thrust has a major ramp from Cambrian strata to a footwall flat in Cretaceous strata. Cambrian rocks are locally juxtaposed over Cretaceous strata recording up to 15 km of slip on the thrust (Dixon, 1982). A hanging-wall anticline cored by Paleozoic strata is found along the frontal trace of the thrust in the Crawford Mountains (Fig. 1). Slip probably decreases to the south, and the thrust is interpreted to core an anticline which contains complexly deformed, salt-bearing Preuss Formation near Henefer, Utah (stop 7 in Fig. 1). Faulted rocks of the Preuss Formation can be traced 15 km south, and the anticline may continue southwest toward Salt Lake City where it is cored by faulted Triassic strata (Fig. 1; Bryant, 1990). Movement on the Crawford thrust was probably synchronous with initial large-scale folding and uplift of the basement-cored anticline and with deposition of the Echo Canyon Conglomerate at about 85 to 90 m.y. (Royse and others, 1975; Jacobson and Nichols, 1982; DeCelles, 1988). The Echo Canyon Conglomerate locally displays intraformational unconformities and has been divided into three informal members which will be examined on this field trip. Fission track ages for apatite from the highest elevations of basement exposed in the Wasatch Range (Naeser and others, 1983) also record initial uplift of the anticline about 90 m.y.

The Absaroka thrust system includes the Mount Raymond thrust exposed in the Wasatch Range and the Crandall Canyon and Cherry Canyon thrusts exposed near Rockport Reservoir (Figs. 1 and 2C; Crittenden, 1974; Bryant, 1990). These thrusts are probably linked with the Absaroka thrust to the northeast and have an aggregate slip greater than 15 km, based on map patterns and stratigraphic relations (Bradley, 1988). The Mount Raymond thrust dips north, reflecting tilting on the north flank of Cottonwood arch, and places Cambrian strata over Mississippian strata at its westernmost exposure. The thrust has a hanging wall and footwall flat in Mississippian strata, and ramps up to a footwall flat in Jurassic strata to the east. Farther east, this thrust may connect with the Crandall Canyon and Cherry Canyon thrusts which place Jurassic strata over Cretaceous strata. The Mount Raymond, Crandall Canyon, Cherry Canyon, and Absaroka thrusts vary systematically in strike and define a salient convex to the east. Early movement on the Absaroka thrust is recorded by the Santonian (80 m.y.) Little Muddy Creek Conglomerate, and major movement occurred synchronous with deposition of the Campanian-Maestrichtian (75 to 65 m.y.) Hams Fork Conglomerate (Royse and others, 1975; Jacobson and Nichols, 1982). The Hams Fork Conglomerate displays intraformational unconformities and contains clasts of basement rock, recording renewed uplift of the basement-cored anticline during thrusting.

The Hogsback thrust, locally exposed to the east in Wyoming, has an estimated slip of 15 to 20 km (Dixon, 1982). Movement on the Hogsback thrust was partly synchronous with deposition of the Paleocene to Eocene Wasatch Formation (Wiltschko and Dorr, 1983). The Wasatch Formation is areally extensive and contains clasts of basement rock, recording renewed translation and minor uplift of the basement-cored anticline. The Hogsback thrust may ramp laterally down to the south and merge into the North Flank thrust which bounds the Uinta arch (Bradley, 1988).

The Uinta arch is a regional east-trending anticlinorium bounded on the north by the North Flank thrust, and on the south by the Uinta Basin Boundary thrust (Hansen, 1965; Bruhn and others, 1986; Bradley, 1988). The Cottonwood arch exposed in the Wasatch Range probably represents the western continuation of the Uinta arch (Crittenden, 1976). Both arches are cored by crystalline basement, overlain by a distinctive 5- to 8-km-thick sequence of middle Proterozoic sedimentary rock. The arches divide thrust systems in northern Utah and Wyoming from thrust systems in central Utah. Development of these two thrust systems overlapped temporally, but ages of deformation, amounts of displacement, and stratigraphy vary between the systems. Uplift of the Uinta arch began during the late Cretaceous and culminated during the Paleocene and Eocene, synchronous with subsidence of the Green River and Uinta Basins (Bruhn and others, 1986). Earlier formed thrusts were rotated to north dips along the north flank of the arches. The younger Hogsback thrust may have linked with the North Flank thrust, recording overlapping thrusting and development of foreland basement uplifts (Bradley and Bruhn, 1988).

Basin and Range extension probably initiated in the Miocene with development of normal faults that cross cut earlier thrust-related structures (Hintze, 1988), and was accompanied by a switch to bimodal volcanism (Best and others, 1980). The Wasatch normal fault zone (WFZ) marks the eastern margin of the Basin and Range Province and lies within the Intermountain seismic belt (Fig. 4; Arabasz and others, in press). The WFZ extends for 370 km from southern Idaho to central Utah and is divided into eight segments which rupture independently and have individual trace lengths of 35 to 70 km (Schwartz and Coppersmith, 1984; Machette and others, 1987; Machette and others, 1991). The WFZ has up to 11 km of displacement that accumulated over the last 17 m.y. (Parry and Bruhn, 1986), and average uplift rates over the last 10 m.y. ranged from about 0.4 to 0.8 mm/yr (Naeser and others, 1983; Evans and others, 1985). The WFZ has also had repeated surface-rupturing events during the Holocene and is capable of generating magnitude 7.0 to 7.5 earthquakes (Schwartz and Coppersmith, 1984), although no large surface-faulting earthquakes have occurred in historic time. Time intervals between large earthquakes on individual segments during the Holocene range from 1,100 to 5,000 years, with about 1 to 5 m of slip per large earthquake, giving Holocene displacement rates of about 0.5 to 2 mm/yr (Machette and others, 1987; Nelson, 1988; Machette and others, 1991). Nishenko and Schwartz (1990) estimated a 12 to 24% chance (depending on model) of a magnitude 7.0 or greater earthquake occurring on the WFZ in the next 50 years. Earlier thrust-related structures may partly control segmentation; e.g., the Weber segment extends along the culmination of the basement-cored anticline from the Pleasant View salient south to the Salt Lake salient (Figs. 1 and 4).

On this field trip we will examine critical outcrops and discuss evidence for the interpreted tectonic evolution of the northern Wasatch Range. The following questions will be addressed. (1) What are the kinematics and timing relations of major thrust systems? (2) What are the mechanisms of deformation? (3) What are the relations between deformation of basement and cover rocks? (4) What was the paleogeography of the area, as recorded in synorogenic conglomerates? (5) What are the geometric relations of younger extensional structures to older thrust-related structures?

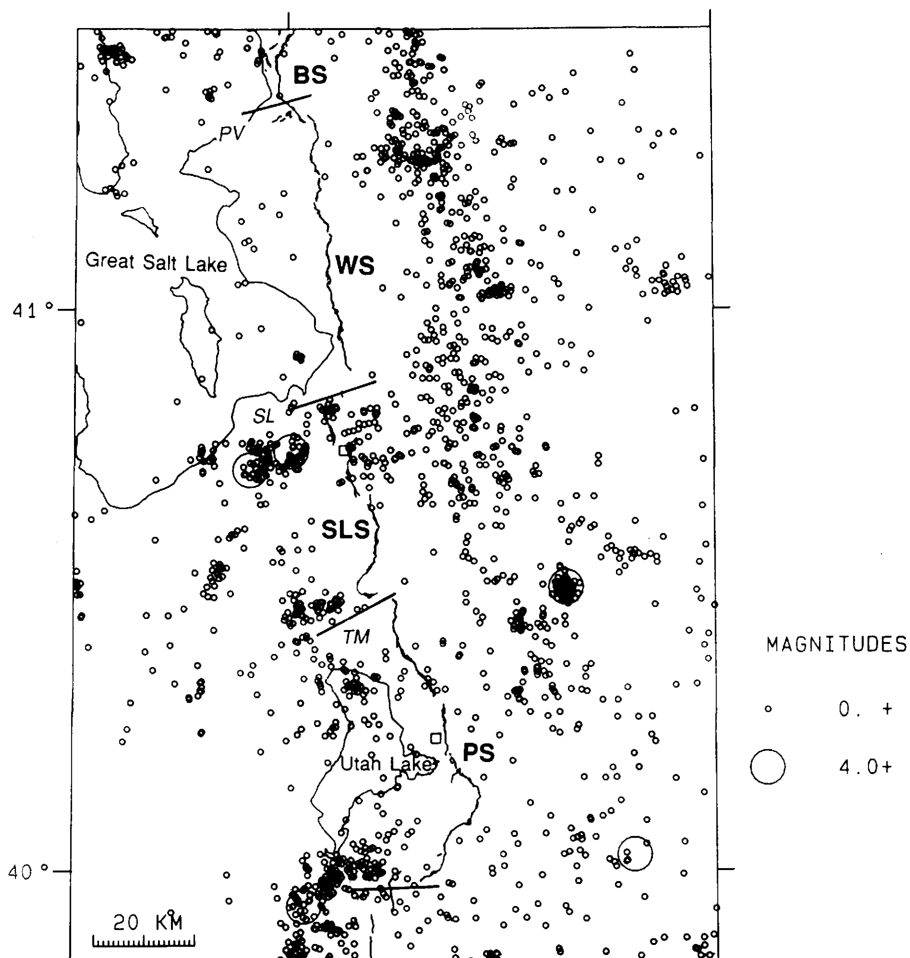

Figure 4. Generalized map showing trace of Wasatch fault zone and epicenters of earthquakes for period from 1960 to 1990 provided by University of Utah Seismograph Station. Segments are labeled: BS-Brigham segment; WS-Weber segment: SLS-Salt Lake segment; and PS-Provo segment. Segment boundaries indicated by heavy solid lines include the Pleasant View salient (PV), the Salt Lake salient (SL), and the Traverse Mountains (TM). Epicenters of small earthquakes are concentrated along segment boundaries and along a belt east of the Wasatch fault zone.

ROAD LOG

Mileage interval	cumulative	description
0.0	0.0	Depart from Radisson Suite Hotel in downtown Ogden, Utah. Proceed north on U.S. Highway 89 (Washington Blvd.).
1.8	1.8	Junction with Utah Highway 39 (1200 North). Continue north on U.S. 89.
1.0	2.8	Junction with Utah Highway 235. Continue straight north on Utah 235. Willard and Ben Lomond Peaks are visible to the north along the skyline. The Willard thrust juxtaposes Proterozoic Facer Formation over highly deformed Cambrian limestone and shale at Willard Peak. Folded and faulted Cambrian rocks beneath Ben Lomond Peak are underlain by Precambrian basement rocks.
3.2	6.0	Junction with Utah Highway 231. Continue north on Utah 235.
0.1	6.1	Turn right and head east on 2600 North Street.
1.1	7.2	Turn left and head north on 1050 East Street.
0.8	8.0	Turn right and head east on North Ogden Drive (3100 North).
0.7	8.7	**Stop 1.** Regional tectonic overview.

Turn off south side of road into open area that affords excellent view of the Wasatch Front and of ranges to the west. The trace of the Willard thrust lies near the crest of the Wasatch Range from Willard Peak south to Ogden Canyon (Crittenden and Sorensen, 1985a, 1985b; Davis, 1985). The lower part of the Willard sheet consists mostly of upper Proterozoic low-grade metasedimentary rocks with slices of lower Proterozoic Facer Formation. Rocks within the Willard sheet have been translated east a minimum of 35 km, and are placed over a footwall flat in variably deformed Cambrian shale and limestone within part of the Wasatch Range. Cambrian limestone and shale are underlain by the Cambrian Tintic Quartzite, and by Precambrian basement (named the Farmington Canyon Complex by Eardley and Hatch, 1940) which cores a regional anticline that continues south to Bountiful, Utah (Yonkee, 1990). The Tintic Quartzite is placed over upper Cambrian dolomite, limestone, and shale along the Ogden thrust to the southeast (Schirmer, 1988). South of Ogden, the Ogden thrust branches and laterally ramps into a floor thrust and a roof thrust that imbricate cover and basement rocks along the steeply dipping eastern limb of the basement-cored anticline. A branch of the Ogden thrust repeats the Tintic Quartzite to the east, and underlying windows of Cambrian limestone and shale may mark another branch that ramps laterally down to the north beneath basement rock (Schirmer, 1988). Complexly folded and imbricated Cambrian Tintic, Ophir, and Maxfield Formations beneath Ben Lomond Peak form part of an antiformal duplex that may connect with the Willard thrust to the north and with the Ogden thrust system to the south (Beck, 1982).

Thick sequences of Proterozoic and Paleozoic rocks exposed on Fremont Island, Little Mountain, and the Promontory Range to the west lie within the Willard thrust sheet. Antelope Island visible to the southwest consists of Precambrian basement and gently dipping sedimentary cover rocks that lie on the western limb of the basement-cored anticline (Yonkee, in press). The Pilot and Raft River Ranges farther west contain Precambrian basement, Proterozoic, and Paleozoic cover rocks locally metamorphosed to amphibolite facies synchronous with Jurassic igneous activity (Snoke and Miller, 1988). Metamorphic grade in the lower part of the Willard sheet and in basement rocks in the Wasatch Range reached greenschist facies, and most deformation probably occurred during the Cretaceous. Relations between deformation and metamorphism in the western ranges and development of the Utah-Idaho-Wyoming thrust belt remain enigmatic (Oriel, 1986; Snoke and Miller, 1988).

The trace of the Wasatch normal fault zone (WFZ) lies just to the east of the stop. The bench visible to the northwest near Pleasant View consists of complexly faulted bedrock that is bounded on the southwest and northeast by major splays of the WFZ (Gilbert, 1928; Crittenden and Sorensen, 1985a). Discontinuous Holocene fault scarps are developed in parts of the bench (Personius, 1988). The bench is part of a structural and seismogenic boundary between the Weber segment to the south, and the Brigham segment to the north (Schwarz and Coppersmith, 1984). The Weber segment last ruptured about 0.5 ka, whereas the last surface rupture event on the Brigham segment occurred about 3.6 ka (Machette and others, 1987, 1991). Net displacement across the WFZ in the Ogden area probably exceeds 5 km, and a deep basin filled with Miocene and younger deposits underlies the area to the west (Fig. 2B). The WFZ marks the approximate eastern boundary of the Basin and Range Province, and most ranges to the west are bounded by normal faults.

Remains of a recent debris flow are visible here and to the southwest. The flow formed when 8 inches (20 cm) of rain fell during September 7-8, 1991. The rain saturated debris in Slide Canyon to the northeast, and the debris formed a flow that moved rapidly down the canyon and onto an old alluvial fan. The flow produced about 5.9 million dollars of damage.

0.5 9.2 Fractured Tintic Quartzite dips gently north and west in a series of road cuts. Limestone of the Maxfield Formation forms ledges south of an east-striking normal fault near base of North Ogden Canyon. Displacement across the normal fault decreases to the east.

0.9 10.1 Quaternary colluvium covers bedrock in this area.

0.3 10.4 A klippe of the Willard thrust sheet overlies Cambrian strata along the skyline to the northeast. The Cambrian strata are rotated into a syncline that continues 10 km to the south and is locally truncated by the Willard thrust.

0.8 11.2 North Ogden Pass. View of Ogden Valley down and to the east. The mountains east of Ogden Valley lie within the Willard thrust sheet and consist mostly of the thick Proterozoic Huntsville Group, locally overlain unconformably by the Tertiary Wasatch Formation.

0.4 11.6 Tintic Quartzite forms small ledges north of road.

0.2 11.8 Limestone of the Maxfield Formation in road cut displays weak to strong foliation. Foliation is defined by recrystallized and flattened calcite ooids and grains, but dolomite ooids are equant with only limited twinning and fracturing. The contact with the underlying Tintic Quartzite is a semi-brittle shear zone.

0.4 12.2 Dolomite layers in the Maxfield Formation are highly fractured and locally brecciated.

0.4 12.6 **Stop 2.** Willard thrust near North Ogden Canyon. The Willard thrust zone, exposed in a road cut northwest of a 90° bend in the road, has been studied by Evans and Neves (in press). The thrust juxtaposes upper Proterozoic low-grade metasedimentary rocks of the Perry Canyon Formation in the hanging wall over limestone, siltstone, and dolomite of the Cambrian Maxfield Formation in the footwall (Fig. 5). The thrust dips 10° to 40° northeast, partly reflecting rotation on the east limb an underlying basement-cored anticline. Graywacke and argillite of the Perry Canyon Formation exhibit intense slatey cleavage, and brecciated argillite forms a 1- to 3-m-thick zone in the hanging wall. The thrust

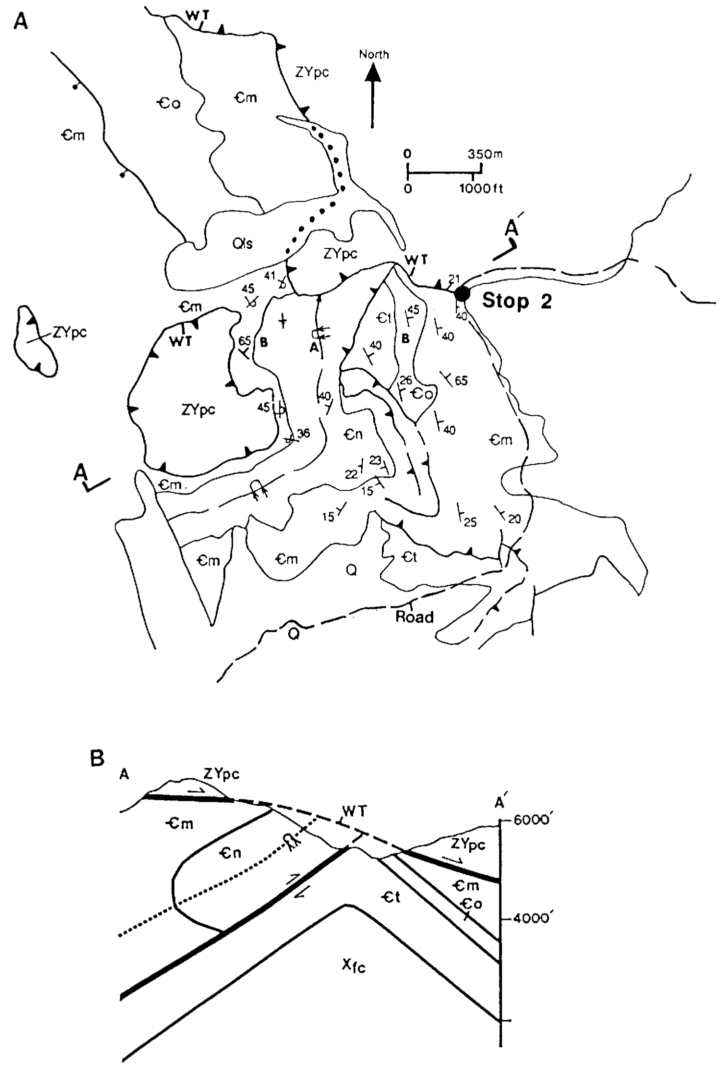

Figure 5. (A). Geologic map of the North Ogden Canyon area near stop 2. An eastward-opening, nearly recumbent syncline in the Maxfield, Ophir, and Nounan Formations is cut by the Willard thrust. ZYpc-Perry Canyon Formation, Ꞓt-Tintic Quartzite, Ꞓo-Ophir Formation, Ꞓm-Maxfield Formation, Ꞓn-Nounan Formation, Q-Quaternary alluvium and colluvium, Qls-Quaternary landslide deposits, WT-Willard thrust. Mapping adapted from Crittenden and Sorensen (1985a) with reinterpretation from Evans and Neves (in press). (B). Cross section of the North Ogden Canyon area. The axial surface of the footwall syncline is truncated by the Willard thrust, and both the footwall syncline and Willard thrust are refolded above a broad anticline. Symbols for strata the same as above. Xfc-Farmington Canyon Complex.

zone in the footwall is a 3- to 5-m-thick, well-foliated limestone mylonite, which formed by dynamic recrystallization (Fig. 6A). Outcrop-scale structures near the thrust include kink folds, small shear zones, and a late-stage, pervasive fracture system that cuts folds and shear zones. Rocks 20 to 100 m structurally below the thrust display primary bedding structures, numerous fractures and calcite-filled veins (Fig. 6B), and strong to weak cleavage that refracts across bedding. Thin shear zones cut some limestone layers, reflecting heterogeneous top-to-the-east shear, and some dolomite layers are intensely brecciated.

Map-scale structures of this area include an overturned footwall syncline within Cambrian strata and a small thrust which may be cut by the Willard thrust (Fig. 5). The fold axis of the overturned syncline is nearly parallel to the strike of the thrust and at high angles to the inferred eastward transport direction. Rocks in the overturned limb of the syncline dip 40° to 60° west and cutoff angles between bedding and the Willard thrust range from 30° to 90°. A small thrust cuts the lower limb of the syncline. Rocks east of the small thrust dip 30° to 45° east-northeast and are at low angles to the Willard thrust. Footwall folding occurred prior to or during slip along the Willard thrust at this location, and the thrust ramps to the northeast from overturned to upright Cambrian strata in the footwall. Minor folds and shear zones are widespread in the footwall syncline and are cut by small veins and fractures.

Twenty kilometers to the north near Willard Peak and Willard Canyon, limestone mylonite and strongly foliated slate of the Ophir and Maxfield Formations form a zone up to 200 m thick beneath the Willard thrust. The Willard thrust sheet in this area also contains a basal sequence of imbricated, tightly folded, and intensely foliated rocks of the lower Proterozoic Facer Formation. Plastic deformation is more intense and pervasive at Willard Peak and at Willard Canyon compared to the North Ogden Canyon area.

A

B

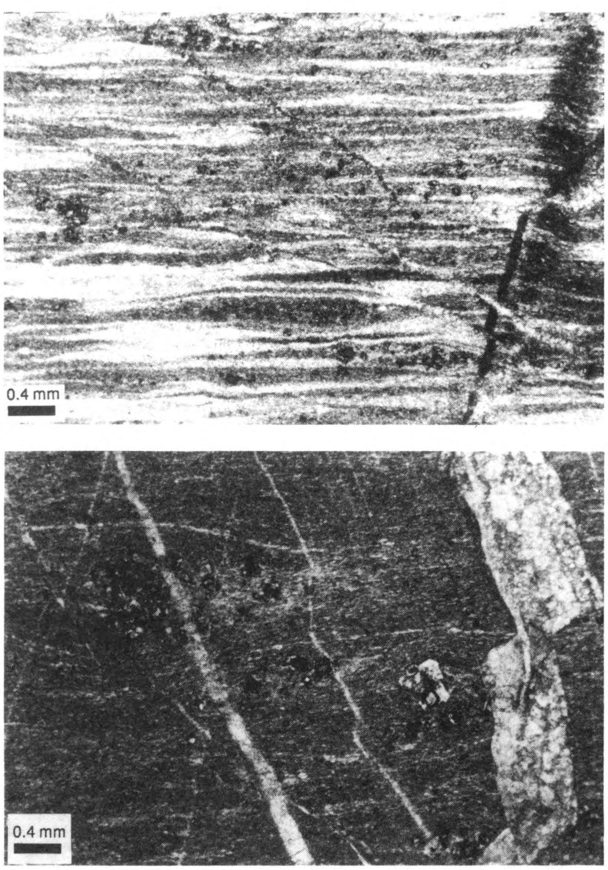

Figure 6. Photomicrographs of rocks in North Ogden Canyon area. (A). Limestone mylonite from Willard fault zone at Stop 2. Recrystallized and elongate calcite grains define mylonitic foliation. Foliation is rotated by a small kink band. (B). Dolomite 50 m structurally below the Willard thrust is cut by vein arrays. Dolomitic ooids display little or no ductile strain.

0.7	13.3	Continue east and reach floor of Ogden Valley. The valley floor is mostly covered by Quaternary deposits, but Tertiary strata that were deposited after thrusting are locally exposed along the west flank of the valley (Sorensen and Crittenden, 1979). These strata dip about 30° east, possibly due to rotation above a listric normal fault that bounds the east side of the valley. An east-dipping antithetic normal fault bounds part of the western side of the valley.
0.7	14.0	Junction with Utah Highway 162. Continue straight east on Utah 162.
0.2	14.2	Enter Liberty. Veer right and continue south on Utah 162.
2.1	16.3	Bridge over North Fork of Ogden River.
1.0	17.3	Junction with Utah Highway 158. Turn right and head west on Utah 158.
0.6	17.9	Junction with spur on left. Continue southwest on Utah 158.
0.2	18.1	Bridge over North Fork of Ogden River.
1.0	19.1	Views to southwest of Mount Ogden and to southeast of Durst Mountain. Mount Ogden consists of Precambrian basement and steeply east-dipping Tintic Quartzite, overlain by imbricated and folded Cambrian shale and limestone above the east-dipping, folded Ogden roof thrust. At Durst Mountain a slice of basement is placed over Cambrian rocks along an east-

dipping thrust interpreted to be part of the roof thrust. Basement rocks at Durst Mountain are overlain by a steeply east-dipping panel of Paleozoic and Mesozoic rocks which form the eastern limb of the regional basement-cored anticline.

1.4 20.5 East-dipping low-grade metasedimentary rocks of the Proterozoic Perry Canyon Formation are poorly exposed in road cuts and display gently dipping foliation that increases in intensity southwest toward the Willard thrust. Pineview Reservoir on southeast side of road.

0.6 21.1 **Stop 3.** Willard thrust at Pineview Reservoir. The Willard thrust is exposed in a large road cut along the north side of the highway. The thrust dips 20 to 30° east and places east-dipping diamictite, quartzite, and argillite of the Proterozoic Perry Canyon Formation over east-dipping limestone beds of the Mississippian Humbug Formation (Fig. 7; Sorensen and Crittenden, 1979). Strongly developed foliation in the Perry Canyon Formation dips gently east and is defined by recrystallized quartz grains, flattened clasts, and preferred orientation of mica. Syntectonic quartz veins cross cut and are deformed by foliation. Sericite in the veins has $^{40}Ar/^{39}Ar$ ages between 140 and 110 m.y., recording early plastic deformation that was synchronous or partly preceded large-scale thrusting (Yonkee, 1990). Breccia zones at low angles to the thrust cross cut foliation and veins, recording later cataclasis. A tightly folded quartzite layer and intensely foliated argillite crop out 1 to 5 m above the thrust. Asymmetric quartz-fiber overgrowths on pyrite grains record top-to-the-east shear in the argillite. Regionally, folds and foliation increase in intensity and rotate into parallelism with the thrust recording localized penetrative deformation near the base of the Willard sheet (Crittenden,1972; Beck, 1982; Yonkee and others, 1989).

Mississippian limestone in the footwall, however, is relatively undeformed and unmetamorphosed. Small pits dug across the fault trace revealed fractured limestone 3 to 4 m below the fault. Rocks along the fault included highly weathered ultracataclasite and rare limestone protomylonite. This style contrasts with the thrust zone exposed at stop 2, and with the thick zone of penetrative deformation along the Willard thrust at Willard Peak (Evans and Neves, in press). The Willard thrust ramps up section toward the southeast in its footwall (Schirmer, 1988), and the higher level of the Willard thrust in the Pineview area may have precluded plastic deformation of footwall rocks. Other possibilities for the transition in footwall deformation style include changes in differential stress, differences in fluids, and lithologic variations in footwall rocks (Evans and Neves, in press).

Fluid inclusion and mineralogic data, combined with thermal models, indicate that emplacement of the Willard thrust sheet increased temperatures and pressures within the footwall (Yonkee and others, 1989). Estimated maximum temperatures of 400 to 500°C and depths of 10 to 13 km occurred within the base of the Willard sheet just prior to large-scale thrusting. Estimated maximum temperatures of 300 to 400°C and depths of 12 to 15 km occurred within basement rocks in the footwall after emplacement of and burial beneath the Willard sheet.

0.3 21.4 Road cut in gently east-dipping Mississippian Humbug Formation. Contraction faults cut bedding at low angles.

0.3 21.7 Junction with Utah Highway 39. Turn right and head west on Utah 39.

0.1 21.8 **Stop 4.** "Z-fold" in Ogden Canyon.

Highway 39 commonly has a great deal of traffic, and care must be taken in parking for this stop. The parking area is on the south side of the road approximately 75-100 m west of the junction of Highways 39 and 162.

The "Z-fold" has been central in interpretations of folding and thrusting in the northern Wasatch Range. Crittenden (1972) indicated that the fold developed as a result of east-west shortening below the east-directed Willard thrust. The "Z-fold", viewed north across the canyon, is developed in thin- to medium-bedded limestone and sandstone of the Mississippian Gardison, Deseret, and Humbug Formations (Fig. 7; Sorensen and Crittenden, 1979; Pavlis and Bruhn, 1988). The fold has planar limbs and very narrow hinge zones. Bedding dips gently east in the upper and lower limbs, and is overturned and west-dipping in the central limb. Fold axes are nearly horizontal and trend approximately N 10° W, and axial surfaces dip gently west. The fold extends over a north-south distance of about 5 km, but the shape of the fold changes. About 2 km south of the canyon the "Z-fold" gives way to a gently east-dipping homocline, probably due to south-

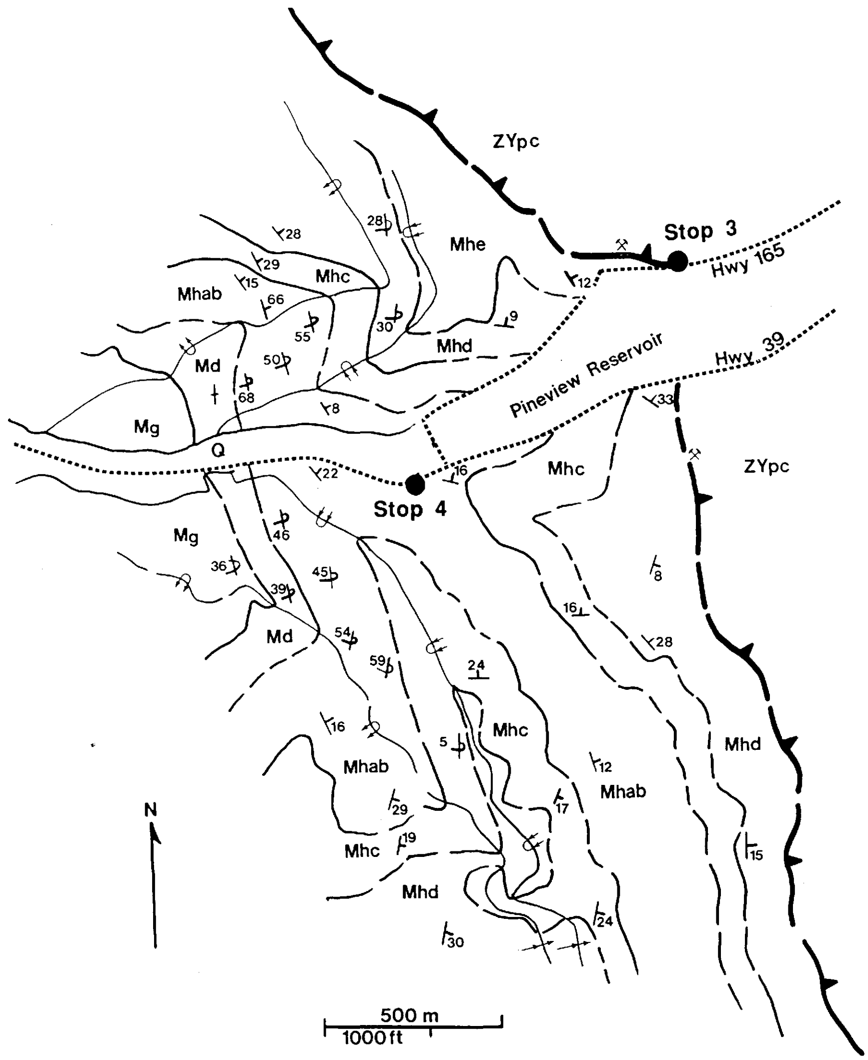

Figure 7. Geologic map of the upper Ogden Canyon area near stops 3 and 4. The Willard thrust (WT) places Proterozoic Perry Canyon Formation (ZYpc) on the Mississippian Humbug Formation (members include Mhab, Mhc, Mhd, and Mhe). Other units are Md-Deseret Formation and Mg-Gardison Formation. An overturned anticline-syncline pair define a Z fold on the north side of Ogden Canyon. This fold pair merges into a monocline 2 km south of the canyon. Map adapted from Sorensen and Crittenden (1979) and Pavlis and Bruhn (1988).

ward merging of anticlinal and synclinal hinges during propagation of the fold tip (Pavlis and Bruhn, 1988). The "Z-fold" probably developed by a combination of flexural slip and flexural flow mechanisms during slip on the overlying Willard thrust. Flexural slip in the Humbug Formation is evident by numerous bed-parallel faults, and by contraction faults which cut bedding at low angles in the shallow-dipping limbs. Flexural flow is suggested by complex folds and fault networks in the Gardison Formation within the lower hinge zone of the "Z-fold" exposed near the power plant.

North of Ogden Canyon, Mississippian to Ordovician strata are rotated into a recumbent, east-vergent syncline that is cut by the Willard thrust (Sorensen and Crittenden, 1979). Hansen (1980) and Neves (1989) also documented minor breccia zones and minor isoclinal folds immediately beneath the Willard thrust.

0.4 22.2 Power plant. Mississippian Gardison Formation is exposed in cliffs northwest of highway. Successively deeper levels of the Paleozoic section are encountered heading west.

0.3 22.5 Devonian Bierdneau Formation is exposed in quarry north of highway.

0.2 22.7 Small slide area north of Oaks Restaurant.

0.2 22.9 Small road cut in Ordovician Fish Have Dolomite. Cambrian St. Charles and Nounan Formations are exposed in slopes to northwest.

1.0 23.9 Bridge across Ogden River. Tight recumbent fold is developed in Maxfield Formation south of bridge.

0.1 24.0 Ophir Formation forms small outcrops in road cuts.

1.0 25.0 Tintic Quartzite in road cut. An upper branch of the Ogden thrust, exposed along Johnson Draw to the north, dips 40° east and juxtaposes the Tintic Quartzite over Cambrian shale and limestone. The upper branch probably merges with a lower branch of the Ogden thrust to the north near the head of Johnson Draw and to the south near the base of Ogden Canyon.

0.3 25.3 Cross approximate trace of Ogden thrust. Fractured dolomite of the St. Charles Formation is in road cut.

0.2 25.5 **Stop 5.** Ogden thrust system in the Ogden area. Stop at pullout on south side of highway and hike southwest to small quarry. The lower branch of the Ogden thrust, visible on the north side of Ogden Canyon, dips about 40° east and places Tintic Quartzite over St. Charles Formation (Fig. 8; Crittenden and Sorensen, 1985b; Yonkee, 1990). The thrust has a stratigraphic throw of about 1000 m. Secondary folds and cleavage are locally developed in the Maxfield and Ophir Formations in the footwall of the Ogden thrust. Limestone beds of the Maxfield Formation exposed in the quarry are cut by vein arrays and by contraction faults at low angles to bedding.

To the south, the Ogden thrust system bifurcates into a lower floor thrust and an upper roof thrust (Fig. 8; Yonkee, in press). The floor thrust ramps down laterally southward from upper Cambrian strata to Precambrian crystalline basement in the footwall, and from Tintic Quartzite to basement in the hanging wall. The maximum structural separation reaches 4 km to south, and estimated slip reaches 10 to 15 km. The roof thrust ramps laterally up section in its footwall from the Ophir to St. Charles Formation, but may ramp laterally down section in its hanging wall from Cambrian strata to basement rocks southeast toward Durst Mountain. Basement in the Ogden area is cut by widely spaced minor shear zones that accommodated top-to-the-east shear in the lower parts of the Ogden thrust sheet. The cover is deformed by gently north- to northwest-plunging folds, by northeast-plunging minor folds at low angles to lateral ramps, and by cleavage. Cleavage in the cover and basement is gently dipping in most areas, but cleavage is intensely developed and steeply dipping near lateral ramps within a detachment zone in Cambrian strata. Finite strain estimates for deformed ooids in Cambrian limestone record 15 to 65% shortening and 20 to 200% principal extension during combined thrust-parallel shear, wrench shear parallel to lateral ramps, and layer parallel shortening (Yonkee, in press).

The Ogden floor thrust includes an outer 50- to 200-m-wide zone of altered and fractured gneiss, and an inner 5- to 50-m wide zone of intensely deformed phyllonite and cataclasite within basement rocks (Yonkee and Mitra, in press). Slip on fracture networks in the gneiss accommodated a small increment of top-to-the-east simple shear above the thrust (Bruhn and Beck, 1981). Phyllonite contains fine-grained mica and recrystallized quartz, and cataclasite consists of angular basement fragments sitting in a very fine-grained micaceous matrix, recording mixed plastic and cataclastic deformation, grain size reduction, and concentrated greenschist-facies retrograde alteration within the fault zone. These textures are broadly similar to textures within basement shear zones observed to the south, but plastic deformation is less pervasive in the Ogden area which lies at a shallower structural level.

0.3 25.8 Shale of Ophir Formation displays cleavage and minor folds in road cut.

0.1 25.9 East-dipping beds of Tintic Quartzite form bold cliffs.

0.3 26.2 Unconformity between Tintic Quartzite and underlying Precambrian granite gneiss. The gneiss has an estimated age of 1,795 m.y. (Hedge and others, 1983), and is part of the Farmington Canyon Complex (Bryant, 1988). Precambrian high-grade metamorphic and igneous rocks of the Farmington Canyon Complex crop out over a north-south distance of 60 km in the Wasatch Range, and include a large northern region of granite gneiss, a central region of migmatitic gneiss, and a southern region composed mostly of paragneiss, schist, and quartzite (Bryant, 1988). Cemented fluvial gravels that locally cover

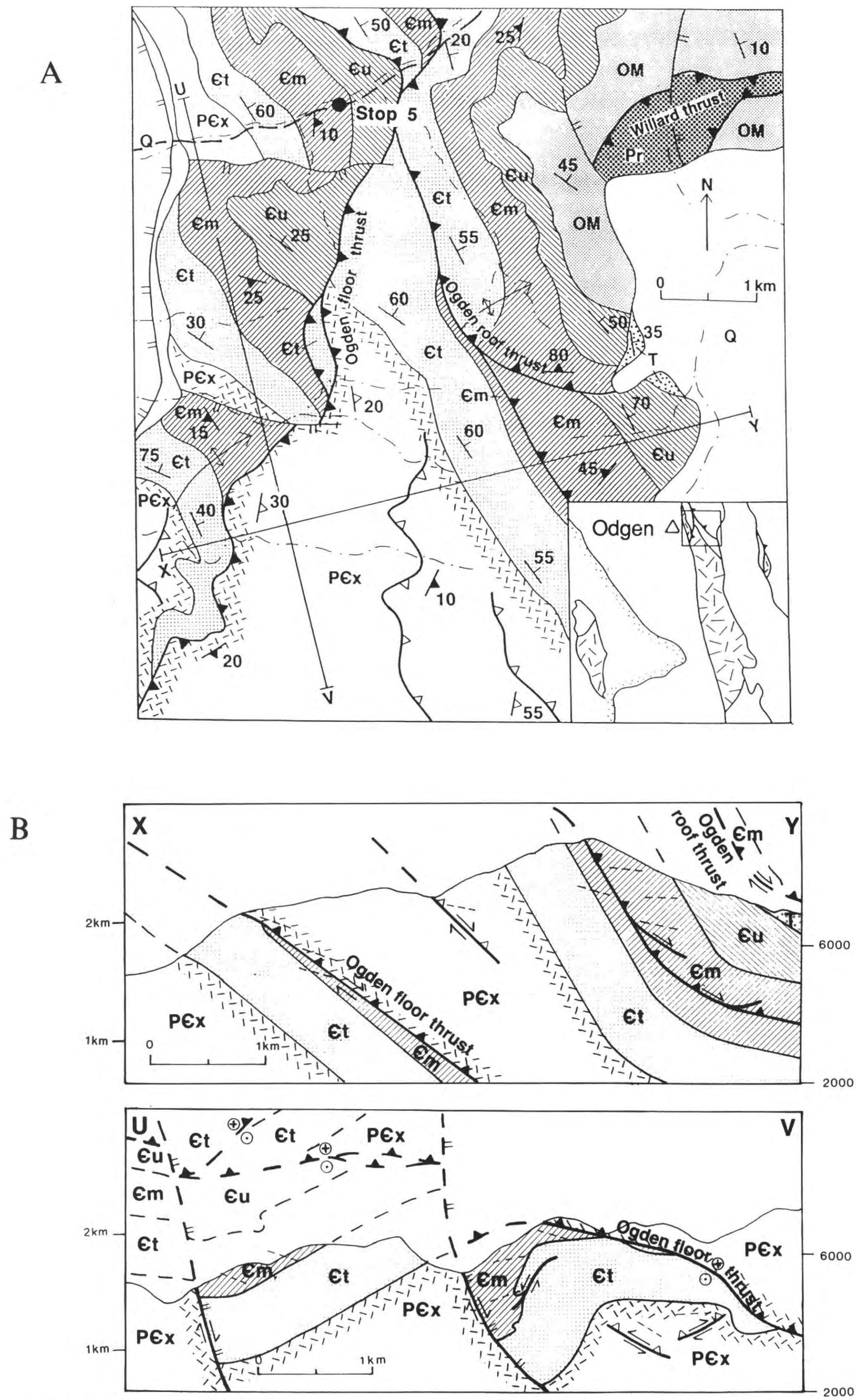

Figure 8. A-Generalized geologic map of the Ogden area near stop 5. The basement and cover are imbricated by the Ogden thrust system and a small klippe of the overriding Willard sheet is preserved in the northeastern part of the area. Cleavage in the basement and cover is gently dipping except near lateral ramps. PЄx-Precambrian crystalline basement, Pr-Proterozoic rocks of Willard sheet, Єt -Tintic Quartzite, Єm-middle Cambrian shale and limestone, Єu -upper Cambrian dolomite, OM-Ordovician to Mississippian strata, T-Tertiary Wasatch Formation, Q-Quaternary deposits. Map modified from Yonkee (in press). B -Sections X-Y and U-V drawn using down-plunge projection of data. Section X-Y shows folded, east-dipping Ogden thrust system. Cleavage traces (dashed lines) are shallowly raking and make acute angles with the Ogden thrust system. Section U-V shows Ogden floor thrust ramping laterally down section to the south. Anticlines cored by shear zones partly rotate the overlying Ogden floor thrust, and cleavage traces partly fan about these folds.

bedrock along the highway were probably deposited during a high stand Lake Bonneville.

0.7 26.9 Cross approximate trace of Weber segment of the Wasatch normal fault zone (WFZ) at mouth of Ogden Canyon. The WFZ displays multiple Holocene scarps in the Ogden area (Gilbert, 1928; Nelson, 1988). Trenching studies north of the mouth of Ogden Canyon indicate a total of 5 to 8 m of slip in the last 6,000 years with surface rupturing events at about 0.5, 1.0, 2.8, and 3.8 ka (Nelson, 1988; Machette and others, 1991). Terraces visible on slopes to the south and north correspond to shorelines of the Bonneville and Provo levels of ancient Lake Bonneville. A landslide complex is developed in the lake deposits along a north-facing slope southwest of the highway.

1.0 27.9 Junction with Utah Highway 203. Turn left and head south on Utah Highway 203 (Harrison Blvd).

1.6 29.5 View to east up Taylor Canyon toward Mount Ogden. A steep, east-striking fault along Taylor Canyon places Precambrian rocks on the north against Cambrian rocks to the south. Prominent tan beds of the Tintic Quartzite curve around an anticline that is cored by basement rock south of the canyon. Above the anticline, the Ogden floor thrust places Precambrian basement rocks over Tintic, Ophir, and Maxfield Formations. The thrust is partly rotated by the anticline, but also partly cuts the anticline, recording overlapping folding and thrusting (Fig. 8).

1.8 31.3 Weber State University to east. The Ogden floor thrust is the prominent structure in the mountain front. The thrust ramps laterally down section to the south and places basement over basement at its south end where displaced down by the WFZ.

2.4 33.7 View to south. Precambrian rocks of the Farmington Canyon Complex form the core of a regional anticline which extends south toward Bountiful, Utah. Farther south, high peaks of the Wasatch Range above Salt Lake City are visible.

0.5 34.2 Junction with U.S. Highway 89. Turn left and proceed southeast on U.S. 89.

0.5 34.7 Start down hill to Weber River. Road cuts consist of delta deposits which formed where the Weber River drained into ancient Lake Bonneville. Shorelines for the Bonneville and Provo levels are visible as discontinuous benches along the mountain front.

1.4 36.1 Junction with Interstate 84. Go under overpass and veer right onto interstate entrance. Proceed east on Interstate 84 toward Morgan, Utah.

0.9 37.0 Cross approximate trace of the WFZ at mouth of Weber Canyon. A minor graben bounded by Quaternary fault scarps is visible to the south along U.S. 89.

0.2 37.2 Migmatitic gneiss of the Farmington Canyon Complex forms cliffs along Weber Canyon. Gneissic layering dips overall to the southwest, but is locally folded. The migmatitic gneiss contains garnet-, biotite-, and sillimanite-bearing layers of paragneiss, amphibolite, and lenses of granite gneiss (Bryant, 1988). Rb-Sr data for migmatite gneiss samples do not define an isochron, but the data may record a complex Archean to early Proterozoic history of metamorphic and igneous activity (Hedge and others, 1983).

0.7 37.9 Power plant at bridge over Weber River.

0.6 38.5 **Stop 6.** Weber Canyon shear zone.

Pull over onto dirt road on south side of Interstate 84. Take short hike south and up to reach cut along a buried pipeline. Be careful of loose rocks and snakes.

A 5- to 10-m-wide, subhorizontal shear zone consisting of green phyllonite and mylonite cross cuts gray migmatitic gneiss in the pipeline cut (Hollett, 1979; Yonkee, 1990). Phyllonite displays pervasive greenschist alteration, well-developed cleavage, and shear bands (Fig. 9A). Cleavage is defined by preferred orientation of mica and flattened quartz aggregates, and shear bands correspond to thin zones of extremely fine grain size and intense deformation. Cleavage generally dips 10 to 40° west, but is rotated into parallelism with gently dipping shear bands, recording heterogeneous top-to-the-east simple shear. Shear bands vary from being subparallel to and being at acute angles to the boundary of the shear zone. The shear zone is bounded by a 2- to 10-m-thick transition zone of fractured and variably altered gneiss and protomylonite. Mesoscopic gractures, veins, and thin (<1-m wide) shear zones form a connected network within the transition zone along which greenschist facies alteration is concentrated. Surrounding migmatitic gneiss is relatively undeformed and unaltered. Foliation in the gneiss dips 10 to 40° southwest, but is locally folded and cut by widely spaced fractures.

A traverse across the shear zone reveals important changes in strain, chemistry, mineralogy, microtextures, and interpreted deformation mechanisms (Fig. 10; Yonkee and Mitra, in press). Migmatitic gneiss consists of about 35% quartz, 50% total feldspar, and lesser amounts of biotite, hornblende, and equant garnet grains. Quartz and feldspar show evidence of only limited plastic deformation and microcracking (Fig. 9B).

Fractured gneiss and protomylonite in the transition zone formed by variable cataclasis, plastic deformation, and alteration during influx of hydrothermal fluids concentrated along fracture and microcrack networks (Fig. 9C). Samples in the transition zone contain an average of about 35% quartz, 40% total feldspar, and 25% sericite, chlorite, and epidote produced by alteration (Fig. 10). Matrix, consisting of recrystallized mica and quartz grains with sizes less than 50μm, comprises 15 to 35% of samples from the transition zone. Quartz displays widespread undulatory extinction and limited recrystallization recording plastic deformation. Feldspar grains are cut by numerous microcracks and mineral-filled veins, and are partly altered to very fine-grained mica and recrystallized albite. Axial ratios of strain, estimated from boudinaged and partly altered garnet grains, are between 2:1 and 5:1.

Phyllonite in the shear zone formed by pervasive plastic deformation and alteration (Fig. 9D). Phyllonite samples contain an average of about 50% quartz, 5% total feldspar, and 45% sericite, chlorite, and epidote. Fine-grained, recrystallized matrix comprises greater than 80% of most phyllonite samples. Quartz displays widespread recrystallization, subgrains, and deformation bands recording plastic deformation. Feldspar grains are largely replaced by foliated, very fine-grained aggregates of mica. Axial ratios of strain, estimated from lengths and shapes of quartz fibers in pressure shadows, range from 10:1 to 40:1 (Yonkee, 1990).

Thicknesses and displacements of shear zones in the Wasatch Range are positively correlated, probably indicating that zones grow in thickness with increasing time and displacement (Yonkee, 1990). Thus textures observed across a shear zone can be interpreted in terms of temporal evolution. The concentration of deformation into narrow shear zones probably requires

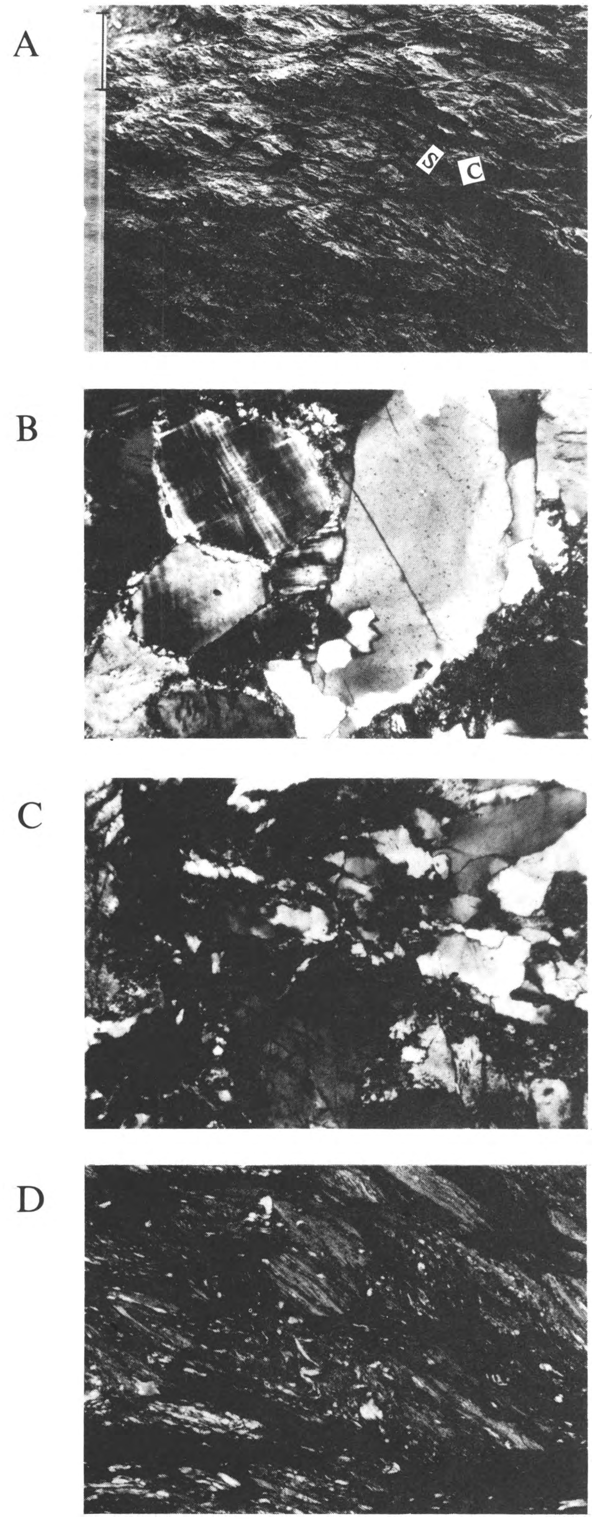

Figure 9. Structures and textures for Weber Canyon shear zone. A. S-C phyllonite in the shear zone. Scale bar is 5 cm long. B. Basement gneiss away from shear zone has granoblastic texture. Minor recrystallization of feldspar is concentrated along grain boundaries, and crack cuts quartz grain. C. Protomylonite in transition zone shows increased microcrack and alteration intensity. Local recrystallization results in grain size reduction. D. Phyllonite from shear zone consists of strongly foliated, fine-grained mica aggregates and highly recrystallized and ribboned quartz. Gently raking, extremely fine-grained shear bands rotate foliation.
Widths of B, C, D equal 0.5 mm of sample.

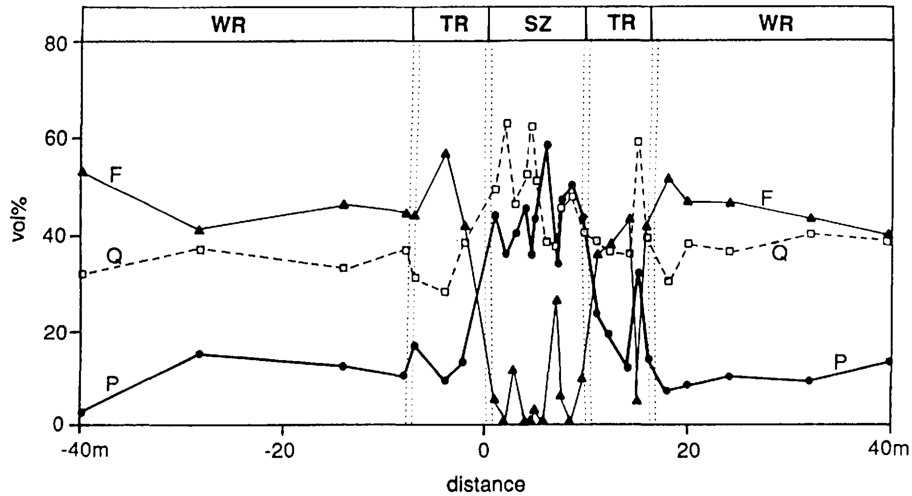

Figure 10. Variations in vol% minerals for samples on a traverse across the Weber Canyon shear zone, modified from Yonkee and Mitra (in press). Symbols are: Q-quartz; F-total feldspar; and P-total phyllosilicates. The amount of feldspar decreases and the amount of phyllosilicates increases going from wall rock (WR), into the transition zone (TR), and across the shear zone (SZ).

strain softening of the zones relative to the country rock (Mitra, 1978). Influx of fluids along fracture and microcrack networks is interpreted to have altered the gneiss, resulting in production of a fine-grained quartz- and mica-rich matrix that deformed plastically in the shear zone. Strain softening mechanisms include reaction softening during alteration of strong feldspar to relatively weak mica, hydrolytic weakening of quartz, and grain size reduction with an increase in the rate of diffusive mass transfer deformation.

The Weber Canyon shear zone is part of a complex network of shear zones that accommodated internal deformation of the basement-cored anticline (Yonkee, in press). Shear zones in this area along the steeply dipping east limb of the anticline include: moderately southwest- and northwest-dipping sets with top-to-the-west shear, and very gently southeast- and northeast-dipping sets with top-to-the-east shear (Fig. 11). These sets define a flattened octahedral pattern, and gently west-dipping cleavage is parallel to the acute bisector of the sets. Shear zones on Antelope Island on the gently dipping west limb of the anticline include: steeply east-dipping sets with east side up, and west-dipping sets with west side up. Cleavage on Antelope Island dips moderately west parallel to the acute bisector of the shear zone set. Cleavage and shear zones define a partial fan about the anticline (Fig. 2B), and if the steeply dipping east limb of the anticline is rotated back to horizontal, then the west-dipping shear zones exposed in the Wasatch Range become steeply east-dipping with east side up and the very gently east-dipping zones become steeply west-dipping with west side up. This geometry is consistent with generation of shear zones during early subhorizontal shortening, followed by rotation during large-scale folding. $^{40}Ar/^{39}Ar$ ages of sericite from the Weber Canyon and nearby shear zones mostly range from 140 to 110 m.y., consistent with initial development of shear zones before large-scale thrusting and folding of the anticline (Yonkee, 1990).

0.7	39.2	Cross Weber River. Fractures partly covered with epidote cross cut migmatitic gneiss on south side of highway. The fractures appear to have provided pathways for limited alteration and fluid circulation. Devils Gate, a steep-sided channel cut into basement rock on the north side of the highway, formed where the Weber River was diverted around landslide. Minor shear zones cut basement rock north and above Devils Gate.
0.7	39.9	Rest area. Lunch.
1.0	40.9	Enter Morgan Valley. A landslide complex in Quaternary slope deposits and Tertiary strata is visible to the north.
0.5	41.4	View to northwest of east flank of Mount Ogden. Steeply east-dipping Cambrian quartzite and complexly deformed Cambrian

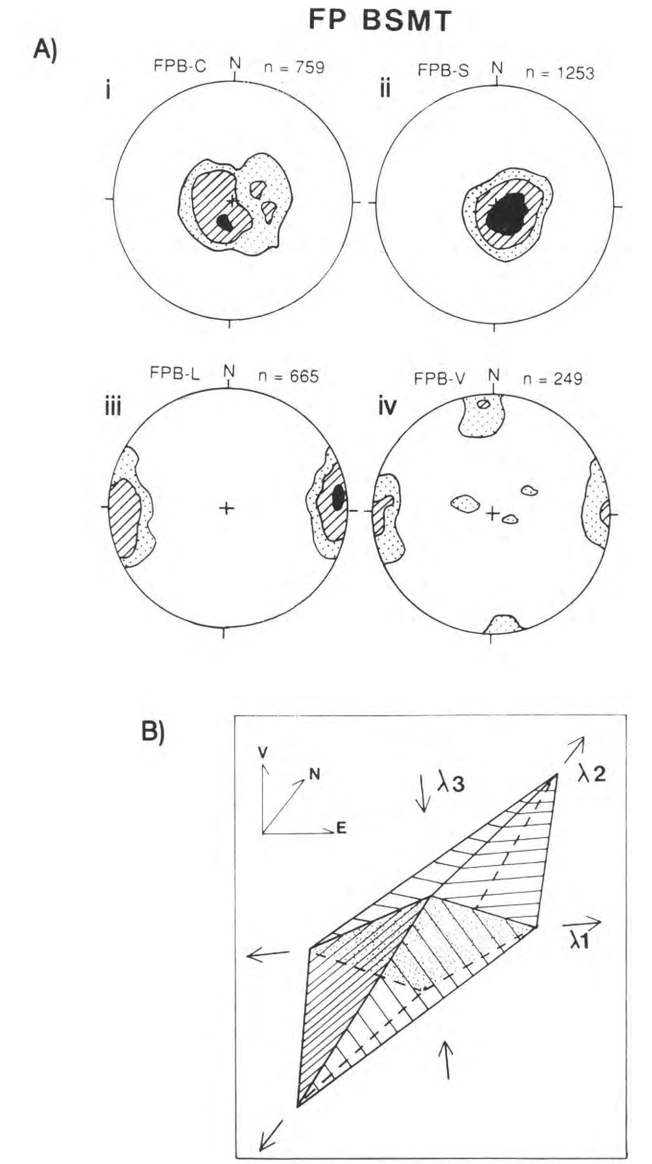

Figure 11. A. Contoured equal area stereograms illustrating geometric relationships of basement structures in Francis Peak area along and south of Weber Canyon taken from Yonkee (1990). Shown are: (i) poles to C surfaces and shear-zone boundaries; (ii) poles to cleavage; (iii) stretching and mineral lineations; and (iv) poles to veins. Contour intervals are 2, 4, and 10% per 1% area. B. Schematic diagram of octahedral three-dimensional geometry of shear zones and principal directions of bulk strain.

limestone and shale exposed along the mountain flank are unconformably overlain by the Tertiary Wasatch Formation. Strata of the Wasatch Formation are poorly exposed along the mountain base to the north and south and dip about 30° east into Morgan Valley.

1.3 42.7 Poorly exposed volcanic sandstone, mudstone, tuff, flow breccia, and lahar deposits of Norwood Tuff underlie much of Morgan Valley (Mullens and Laraway, 1973), and are visible in railroad cuts to the south. Beds dip 20 to 40° east. K-Ar and fission track ages of the volcanics, summarized by Bryant (1990), range from 29 to 37 m.y. The volcanics are intermediate to silicic in composition.

4.4 47.1 A possible continuation of the Ogden roof thrust juxtaposes Precambrian basement over Cambrian quartzite, shale, and limestone at Durst Mountain to the east (Hopkins, 1983; Mullens and Laraway, 1973). The fault currently dips east, probably due to rotation of the steep east limb of the basement-cored anticline. The fault probably initiated as a gently west-dipping thrust fault.

1.2 48.3 Gravels of ancient Lake Bonneville are exposed in a road cut. Lake Bonneville formed an estuary into Morgan Valley during its high stand. Terrace at Bonneville level is above highway to northeast.

4.0 52.3 Pass exit to Morgan, Utah. Cross approximate trace of Como fault zone. This west-dipping normal fault continues north and bounds the east side of Morgan Valley where it places Devonian to Cambrian strata against the Norwood Tuff (Mullens and Laraway, 1973). South of Morgan, the fault juxtaposes the Wasatch Formation on the east against the Norwood Tuff, and displacement probably decreases farther to the south. The Norwood Tuff is locally rotated into an open syncline just west of the fault trace. The fault marks a boundary between dip domains of post-thrusting Tertiary strata. Tertiary strata in Morgan Valley, along the Wasatch Range, and farther west generally dip about 30° east, possibly reflecting rotation above listric normal faults or isostatic adjustments during regional extension. Tertiary strata to the east of the Como fault are gently dipping to horizontal.

0.8 53.1 Enter Upper Weber Canyon. Limestone and dolomite beds of the Mississippian Gardison (or Lodgepole) Formation dip 20 to 50° east to southeast and are cut by minor faults in road cut. Successively younger levels of the Paleozoic and Mesozoic section are encountered proceeding east across east-dipping limb of regional basement-cored anticline (Mullens and Laraway, 1964, 1973; Schirmer, 1985).

0.6 53.7 Silty carbonate and sandstone beds of the Mississippian Humbug and Doughnut Formations dip 50 to 80° east and are cut by minor faults in road cuts.

0.4 54.1 Gray limestone beds of the Pennsylvanian Round Valley Formation in road cut dip

50° east.

0.3 54.4 Approximate contact between Round Valley Formation and reddish siltstone and silty limestone of the Pennsylvanian Morgan Formation lies along the valley to the north. Hills south of the Weber River consist mostly of the Tertiary Wasatch Formation.

0.6 55.0 Approximate contact between the Morgan and Pennsylvanian Weber Formations. The Weber Formation crops out to the east and consists mostly of light gray to tan, well-indurated sandstone, with some interbedded cherty limestone.

0.5 55.5 Faulted hinge region of a minor syncline is visible to north. Bedding east of the hinge zone is gently dipping to horizontal.

2.0 57.5 The hinge of a secondary anticline on the east limb of the regional basement-cored anticline is visible to the north. This secondary fold has long, relatively planar limbs and a narrow, but rounded, hinge zone. The western limb of the secondary fold is gently dipping and the eastern limb dips steeply east. The fold may reflect translation of strata over a ramp-flat geometry in the underlying Ogden or Crawford thrust system (Schirmer, 1985).

0.5 58.0 Contact between Weber and Permian Park City Formations. Disharmonic minor folds are developed in thin-bedded limestone, siltstone, and shale of the Park City Formation.

0.3 58.3 Gray siltstone and limestone of the Triassic Dinwoody Formation and red shales of the overlying Triassic Woodside Formation are rotated into disharmonic minor folds to the north and east.

0.2 58.5 The hills to the north consist of gray to tan limestone and siltstone of the Triassic Thaynes Formation. Beds are rotated into open folds.

0.7 59.2 Red siltstone and sandstone beds of the Triassic Ankareh Formation dip about 60° east in road cuts to the north.

0.3 59.5 Contact between Ankareh Formation and resistant, orange to tan sandstone of the Jurassic Nugget Formation.

0.3 59.8 Contact between the Nugget Formation and red shales and evaporites of the Gypsum Spring Member of the Jurassic Twin Creek Formation.

0.1 59.9 Resistant limestone layers in the Twin Creek Formation form Devils Slide to the south. The layers dip 80 to 90° east and are cut by widely spaced stylolites that define a weak spaced cleavage at high angles to bedding. The cleavage may have initiated during early layer parallel shortening and was rotated along with bedding during large-scale folding.

0.6 60.5 Contorted, subvertical micrite and siltstone beds of the Twin Creek Formation are visible in road cut to the south. Gently east-dipping conglomerate beds unconformably overly the Twin Creek Formation and are well exposed along large road cut to the east.

1.2 61.7 **Stop 7.** Weber Canyon conglomerate.

Veer right off I-84 onto exit 112 (Henefer exit). Pull over to south of stop sign for discussion, then proceed east back onto entrance to I-84.

Cobble- to boulder-conglomerate is exposed for a distance of 1.5 km in the road cut along Interstate 84. The conglomerate consists of coarse stream-flow and debris-flow facies that were deposited on the upper parts of laterally intertonguing ancient alluvial fans, visible along the mountain flank to the southwest (named Rocky Ridge). The conglomerate is very poorly sorted and packaged in 5- to 25-m-thick units separated by thin siltstone units. The average modal clast composition of the conglomerate is 53% sandstone and quartzite, 32% limestone, 9% siltstone, and 6% chert. Identifiable clasts include fragments from the Nugget, Park City, Weber, and Tintic Formations. All of these clasts could have been derived from sources along the east limb of the regional basement-cored anticline exposed along Upper Weber Canyon. Basement clasts and distinctive Proterozoic clasts from the Willard sheet are not apparent. The level of the basement does not appear to have been breached by this time, and an ancient drainage divide may have separated this area from the Willard sheet. This facies is informally referred to as the Weber Canyon conglomerate, and may be slightly younger or partly correlative with the main body of the Echo Canyon Conglomerate.

Near the western edge of the road cut, beds in the lower part of the Weber Canyon conglomerate lie with angular unconformity over subvertical Jurassic strata and dip 20° east, but beds in the upper part of the conglomerate are subhorizontal (Fig. 12). At the eastern edge of the outcrop, bedding in the lower part of the conglomerate is steeply dipping to overturned,

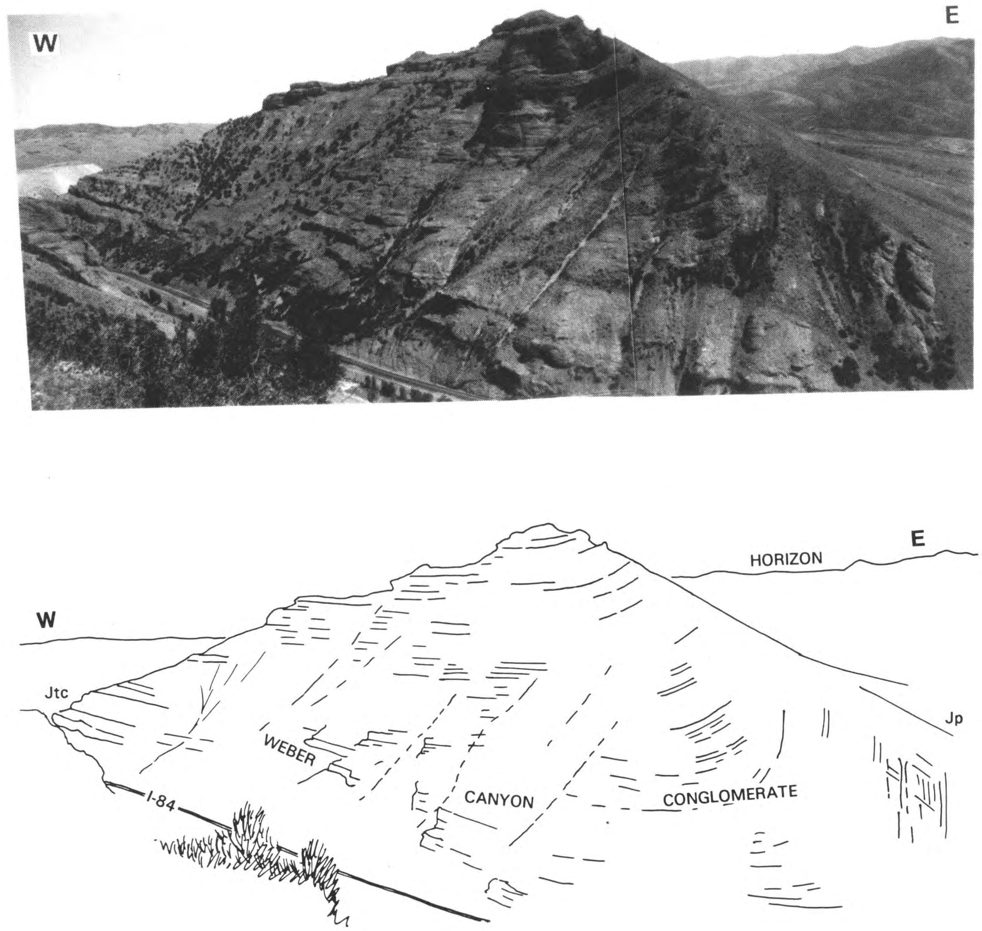

Figure 12. Photomosaic and sketch of Weber Canyon conglomerate exposed along Interstate 84 (I-84) near Henefer, Utah. The conglomerate displays intraformational unconformities, with dips of bedding decreasing toward the top of the conglomerate. The lower, eastern part of the conglomerate is deformed by east-dipping reverse faults near a contact with the Preuss Formation (Jp), and the western part of the conglomerate unconformably overlies the Twin Creek Formation (Jtc).

and probably overlies poorly exposed beds of the Preuss and Kelvin Formations (Mullens and Laraway, 1964). Progressive unconformities are present in the conglomerate within each limb of the syncline. The progressive unconformity in the eastern limb of the syncline is most prominent with dips of bedding decreasing upward from overturned, to 50° west, to 30° west, to subhorizontal near the top of the section (Fig. 12). Unconformities and changing dips within the conglomerate across the outcrop record growth of an asymmetric syncline. This syncline can be traced 15 km south to East Canyon Reservoir, and possibly as far southwest as the Emigration syncline near Salt Lake City. East of the syncline, poorly exposed Jurassic and Cretaceous strata may form part of a tip anticline above the Crawford thrust, called the Henefer anticline by Schirmer (1985). The Amoco-Gulf Franklin Canyon #1 well near Henefer, Utah, encountered 2,200 m of complexly deformed salt, sandstone, and siltstone Preuss Formation, and an underlying imbricated sequence within the Twin Creek Formation. The normal thickness of the Preuss Formation is less than 250 m, and the unusual thickness may reflect repetition of strata or flowage of salt in the core of the anticline. The anticline may continue to the southwest and link with the Spring Canyon anticline near Salt Lake City (Crittenden, 1965b). The East Canyon fault zone extends along the west flank of the anticline and had a protracted history. The fault zone includes west-directed, east-dipping reverse faults (or back thrusts) that locally place the Preuss Formation over faulted Weber Canyon conglomerate, recording overlapping deposition and development of the anticline (Fig. 12). The fault zone also includes west-dipping thrusts that connect with the Ogden or Crawford thrust (Schirmer, 1985), and a younger east-dipping Tertiary normal fault that places Norwood Tuff on the east against the Preuss Formation (Bryant, 1990).

No palynological dates have yet been obtained from the Weber Canyon conglomerate. This conglomerate facies, however, can by physically traced south to East Canyon Reservoir where it lies east of and beneath west-dipping beds of the Hams Fork Conglomerate. The Hams Fork Conglomerate has been dated here as Campanian-Maestrichtian by Nichols and Warner (1978), and contains distinctive clasts of basement rock and Proterozoic rock derived from the Willard sheet. The main source for the Weber Canyon conglomerate appears to have been to the west in the east limb of the basement-cored anticline, and the non-resistant beds in the adjacent tip anticline appear to have been incapable of generating coarse detritus.

2.6 64.3 The valley to the southwest near Henefer is probably underlain by the Kelvin and Preuss Formations, locally covered by the Wasatch Formation (Mullens and Laraway, 1964). Proceeding east-southeast, we pass through the Cretaceous Frontier and Henefer Formations exposed along the northwest limb of the Stevenson Canyon syncline.

0.7 65.0 Sandstone layers in the Frontier Formation dip 60 to 70° east.

0.7 65.7 Beds of the Henefer Formation dip about 30° east in road cut. The Henefer Formation here consists of four to five upward-coarsening progradational sequences that were deposited in marine and fluvial environments on the distal parts of a fan-delta. Clasts in coarser conglomeratic layers were probably derived from upper Paleozoic and Mesozoic strata, and have an average modal composition of 30% sandstone and quartzite, 27% limestone, 27% siltstone, and 16% chert. The Henefer Formation grades upward into fluvial conglomerates of the Echo Canyon Conglomerate.

0.7 66.4 Approximate contact with the main body of the Echo Canyon Conglomerate. The dip of bedding decreases east within the trough of the Stevenson Canyon syncline.

0.5 66.9 Knobs of Echo Canyon Conglomerate visible to northeast display subhorizontal bedding.

1.3 68.2 Conglomerate layers in the cliffs to the east dip gently and are on the southeast limb of the Stevenson Canyon syncline (northwest limb of the Coalville anticline).

0.6 68.8 Junction with Interstate 80. Veer left and head east on I-80 toward Evanston, Wyoming.

0.5 69.3 Veer right off I-80 onto exit 169 (Echo Canyon exit). Take left at stop sign and head north under interstate and railroad overpasses.

0.2 69.5 Turn right and head east on old highway. Cliffs to the north and east provide excellent exposures of the upper facies of the Echo Canyon Conglomerate. The average modal composition of clasts in the upper facies is 82% sandstone and quartzite, 7% limestone, 5% siltstone, and 6% chert. The dominant clast type is tan to light gray quartzite derived from the Weber Formation. Paleocurrents are directed mostly to the east and southeast.

2.7 72.2 Approximate contact between upper facies and lower facies of the Echo Canyon Conglomerate to the northeast.

2.0 74.2 **Stop 8.** Echo Canyon Conglomerate. After stop retrace route southwest back to I-80.

The lower facies of the Echo Canyon Conglomerate is exposed along the lower part of the hillslope to the northwest, and consists of stream-flow conglomerate and minor sandstone. Conglomerates here are not as coarse as units to the west and were probably deposited on the outer reaches of alluvial fans. Paleocurrents indicate flow to the east and southeast. Clasts in the lower facies have an average modal composition of 50% sandstone and quartzite, 20% limestone, 12% siltstone, 6% chert, and 12% distinctive red to green quartzite and graywacke derived from Proterozoic rocks of the Willard sheet. Beds in the conglomerate dip 10 to 20° northwest. The main body of the Echo Canyon Conglomerate is Coniacian-Santonian (about 85 to 90 m.y.; Jacobson and Nichols, 1982), and records early uplift of the basement-cored anticline and possible movement on the Crawford thrust.

A prominent angular unconformity is visible at the base of the overlying, gently dipping Campanian-Maestrichtian (75 to 65 m.y.) Hams Fork Conglomerate. The Hams Fork Conglomerate contains distinctive clasts of Proterozoic quartzite derived from the Willard thrust sheet and rare clasts of basement rock, recording renewed uplift and erosion of the basement-cored anticline. Deposition of the conglomerate was probably synchronous with main movement of the Absaroka thrust (Royse and others, 1975). Preservation of locally folded Hams Fork Conglomerate within the southern part of the Absaroka thrust sheet reflects deposition east of a growing basement-cored anticline during movement on the Absaroka thrust (Yonkee, in press).

The assemblage of clast types in the different conglomerate facies records the progressive development and denudation of the basement-cored anticline, with six idealized temporal stages recognized. (1) Conglomerate layers in the Kelvin, Frontier, and Henefer Formations were probably derived from Mesozoic and upper Paleozoic rocks during emplacement and erosion of the Willard thrust sheet, and possibly during initial, minor uplift of the basement-cored anticline. (2) The lower facies of the Echo Canyon Conglomerate records early rapid uplift and erosion of Mesozoic to middle Paleozoic rocks on the east limb of the basement-cored anticline, and continued erosion of lower parts of the Willard sheet as it was passively uplifted to the northwest. (3) The upper facies of the Echo Canyon Conglomerate probably accumulated during continued uplift and erosion of middle Paleozoic rocks on the east limb of the growing basement-cored anticline. The apparent lack of clasts from the Willard sheet may reflect development of an ancient drainage divide to the northwest. (4) The Weber Canyon conglomerate facies probably records continued uplift and erosion of middle to lower Paleozoic rocks on the east limb of the basement-cored anticline, synchronous with development of the tip anticline. (5) The Hams Fork Conglomerate, which lies with angular unconformity over the Echo Canyon Conglomerate, records later uplift and erosion of middle Paleozoic to basement rocks on the east limb of the basement-cored anticline during movement on the Absaroka thrust. The lower part of the Willard thrust sheet was also passively uplifted and eroded. (6) Conglomerate beds of the Paleocene to Eocene Wasatch Formation, which lie with angular unconformably over the Hams Fork Conglomerate, record erosion and minor uplift of the basement-cored anticline during movement on the underlying Hogsback thrust.

2.1	76.3	Approximate contact between upper facies (to southwest) and lower facies of Echo Canyon Conglomerate.
2.7	79.0	Turn left and head under railroad overpass. Take right and head southwest onto entrance of Interstate 80.
0.3	79.4	Junction with Interstate 84. Veer left and continue south on Interstate 80.
0.4	79.8	Small slide area is developed in surficial deposits and Echo Canyon Conglomerate.
0.4	80.2	Echo Reservoir to east. The contact between the Echo Canyon and Henefer Formations in hillslopes east of the reservoir is marked by an upward transition to more massive conglomerates.
0.8	81.0	Conglomerate, sandstone, and black shale interbeds of Henefer Formation are exposed in a road cut.
1.2	82.2	Rest area. Sandstone beds of Frontier Formation are exposed in hillslopes to west.
0.9	83.1	Thick sandstone unit of Frontier Formation dips about 20° northwest.
0.7	83.3	Bridge over Weber River. Ridge north of Coalville, Utah, includes northwest-dipping sandstone and conglomerate beds of the Turonian Oyster Ridge Member of the Frontier Formation. This area lies on the northwest limb of the Coalville anticline.
1.7	85.5	Hills to east expose gently dipping beds of the Tertiary Wasatch Formation.
3.5	89.0	Road overpass. Hills to southwest are underlain by poorly exposed lahar, flow, tuff, and volcaniclastic deposits of the Keetley Volcanics. K-Ar dates of the volcanics, summarized by Bryant (1990), range from 33 to 38 m.y. Volcanic rocks are intermediate in composition and contain plagioclase, hornblende, clinopyroxene, and rare biotite.
2.4	91.4	Veer right onto exit 156 toward Wanship, Utah.
0.3	91.7	Junction with U.S. Highway 89. Turn left and proceed south on U.S. 89 through Wanship.
0.4	92.1	Pass under Interstate 80.
0.3	92.4	Northwest-dipping beds of the Kelvin and Preuss Formations are poorly exposed in hillslope to west.
0.4	92.8	Cross approximate trace of Cherry Canyon thrust which places the Preuss Formation on northwest against Hams Fork Conglomerate on southeast (Bradley, 1988). Conglomerate beds dip northwest and are well exposed across the Weber River.

0.9 93.7 Rockport Reservoir to east. Northwest-dipping beds of Frontier and Kelvin Formations are visible on east side of reservoir.

0.7 94.4 Cross approximate trace of southwest-trending Dry Canyon fault which repeats part of the Kelvin Formation and is onlapped by the Hams Fork Conglomerate (Bradley, 1988). The fault may be an imbricate of the Crandall Canyon thrust, but the amount of slip and dip on the fault are uncertain. Sandstone, conglomerate, and claystone beds of Kelvin Formation dip 50 to 60° northwest and are exposed in road cuts heading south along the highway.

1.1 95.5 Red siltstone beds of Preuss Formation dip 60° northwest in road cut.

0.3 95.8 Cross approximate trace of Crandall Canyon thrust. Southeast of the thrust, beds of Frontier Formation dip 45 to 55° northwest.

0.2 96.0 **Stop 9.** Southern part of the Absaroka thrust system. Pull into turnout on east side of road for overview and discussion. Then return north along U.S. 89.

Northwest-dipping faults imbricate Mesozoic strata within the Absaroka thrust sheet around Rockport Reservoir (Fig. 13; Crittenden, 1974; Bradley, 1988; Bryant, 1990). The Crandall Canyon thrust dips about 60° northwest and juxtaposes red beds of the Preuss Formation over sandstone and black shale of the Frontier Formation. To the east, the dip of the thrust steepens and the thrust is locally overturned and southeast-dipping, reflecting rotation along the north flank of the Uinta arch. Slickenlines indicate east- to southeast-directed slip, and the amount of slip may exceed 15 km based on stratigraphic relations across the thrust (Bradley, 1988). The thrust is locally onlapped by the Campanian-Maastrichtian Hams Fork Conglomerate, and movement on the thrust may correlate with early movement of the Absaroka thrust in Santonian time.

The trace of the Cherry Canyon thrust lies approximately 5 km to the north. This thrust dips about 55° northwest and juxtaposes the Jurassic Preuss Formation over the Hams Fork Conglomerate. The thrust has a hanging wall ramp up to the Cretaceous Kelvin Formation to the northeast, and an imbricate of this fault appears to bound the southeast limb of the Coalville anticline farther to the northeast. The fault is onlapped by Oligocene Keetley Volcanics to the southwest. The amount and direction of slip on the Cherry Canyon thrust are uncertain. The thrust probably formed concurrent with main movement on the Absaroka thrust and with deposition the Campanian-Maestrichtian Hams Fork Conglomerate which displays intraformational unconformities in this area (Bradley, 1988).

Additional imbricate faults, including the Dry Canyon and Rockport faults, repeat Jurassic and Cretaceous strata in the hang-

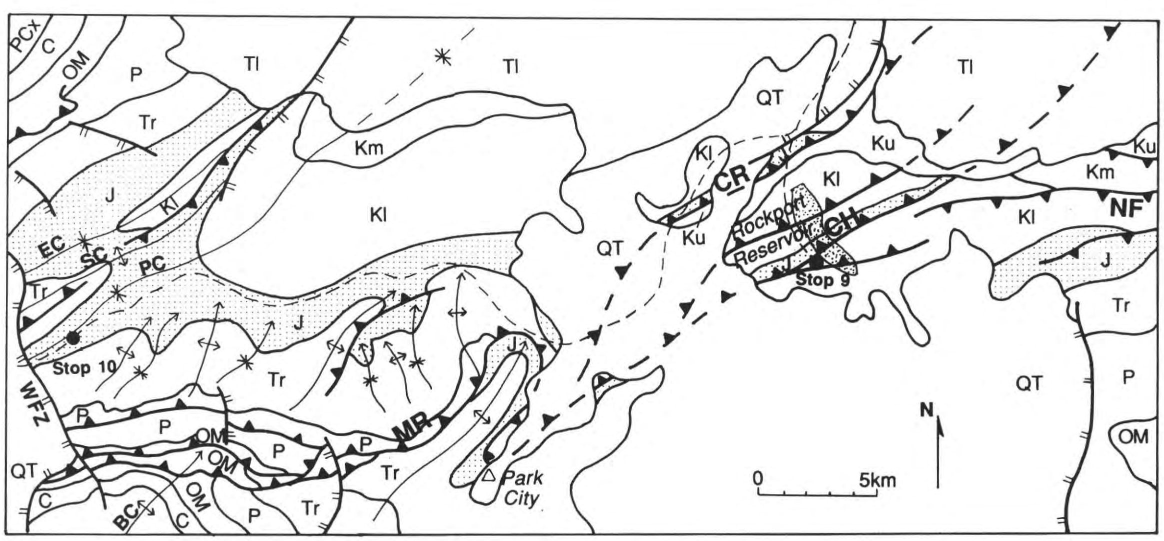

Figure 13. Generalized geologic map of area round Rockport Reservoir. Positions of Mount Raymond thrust (MR), Crandall Canyon thrust (CR), Cherry Canyon thrust (CH), and North Flank (NF) fault system indicated. Axial traces of major folds are labeled BC-Big Cottonwood anticline, EC-Emigration Canyon syncline, PC-Parleys Canyon syncline, and SC-Spring Creek anticline. Pr-middle Proterozoic sedimentary rocks, C-Cambrian strata, OM-Ordovician to Mississippian strata, P-Pennsylvanian and Permian strata, Tr-Triassic strata and Nugget Formation, J-Jurassic strata (stippled), Kl-Cretaceous Kelvin, Frontier, and Henefer Formations, KM-Cretaceous middle synorogenic deposits including Hams Fork Conglomerate, Tl-early Tertiary deposits of Wasatch Formation, QT-Cenozoic post-thrusting deposits. Modified from Bradley (1988) and Bryant (1990).

ing wall and footwall of the Crandall Canyon thrust (Bradley, 1988). The Crandall Canyon, Cherry Canyon, and imbricate thrusts are interpreted to link with the Mount Raymond thrust to the southwest in the Wasatch Range, and with the Absaroka thrust to the northeast. The Absaroka thrust system varies systematically in strike and defines a salient convex to the east. The salient may have formed by variation in bulk transport direction (fanning of slip directions), decreasing slip to south with dextral wrench shear, and rotation of thrusts along the north flank of the Uinta arch.

The north flank of the Uinta arch, visible to the southeast, regionally consists of gently north-dipping Proterozoic, Paleozoic, and Mesozoic sedimentary rocks (Hansen, 1965; Bradley, 1988). The arch is a major east-trending anticlinorium, bounded on the north by the North Flank thrust and Green River Basin. This fault dips 40 to 70° south and has up to 10 km of stratigraphic separation. The arch had a protracted uplift history beginning in latest Cretaceous and culminating in Eocene time (Bruhn and others, 1986). The Uinta arch may continue west into the Cottonwood arch within the Wasatch Range, and these arches divide the northern Idaho-Utah-Wyoming thrust belt from the thrust belt of central and southern Utah. The major frontal thrust south of the Uinta arch is the Charleston thrust which had Late Cretaceous movement, possibly overlapping with movement on the Absaroka thrust. The major frontal thrust north of the Uinta arch is the Hogsback thrust which had Paleocene to Eocene movement. The Hogsback thrust may ramp laterally down to the south and connect with the North Flank thrust, requiring 15 to 20 km of dextral wrench shear to be accommodated across the Uinta arch (Bradley and Bruhn, 1988).

0.2 96.2 Cross approximate trace of Crandall Canyon thrust.

1.4 97.6 Cross approximate trace of Dry Canyon fault.

1.6 99.2 Cross approximate trace of Cherry Canyon thrust.

0.7 99.9 Pass under Interstate 80. Take left onto interstate entrance and head west on I-80 toward Salt Lake City, Utah.

0.8 100.7 Road cut in poorly exposed Keetley Volcanics.

1.1 101.8 Beds of Kelvin Formation dip 30 to 50° northwest within road cuts here and to southwest. These beds are probably continuous beneath the cover of Keetley Volcanics with rocks exposed north of Rockport Reservoir in the hanging wall of the Cherry Canyon thrust.

2.0 103.8 Red siltstone beds of Preuss Formation dip 55° northwest in road cut.

0.4 104.2 Cross approximate trace of fault that places Preuss Formation on northwest over Hams Fork Conglomerate (?) on southeast. The fault may be the southwestern continuation of the Cherry Canyon thrust.

0.4 104.6 Lahar deposits of Keetley Volcanics are exposed in road cuts here and to south along canyon.

1.8 106.4 Leave mouth of canyon. View of Wasatch Range to west.

1.7 108.1 Junction with U.S. Highway 40. Continue west on I-80.

3.1 111.2 Junction with Utah Highway 224 from Park City. Continue northwest on I-80. Approximate trace of the Mount Raymond thrust lies just southwest of interstate (Crittenden and others, 1966). Sandstone beds of the Jurassic Nugget Formation exposed in the hill to the north are within a hanging-wall ramp anticline above the thrust and dip 50 to 70° east. The ramp anticline is cored by Permian strata farther west. Limestone beds of the Twin Creek Formation exposed to the southwest are in the footwall of the thrust, and dip northwest to southeast around the hinge of a northeast-trending anticline that also folds the thrust. The folded thrust places Nugget Formation over a footwall flat in the Twin Creek Formation to the south and east. Two cleavages, each defined by spaced stylolites, are developed in limestones of the Twin Creek Formation, and are interpreted to record early west-northwest layer parallel shortening, development of north- to northeast-plunging folds, later north-northwest shortening, and development of east-northeast-plunging folds (Bradley and Bruhn, 1988).

0.7 111.9 East-dipping beds of the Triassic Ankareh Formation within the hanging wall of the Mount Raymond thrust are poorly exposed in the hillslope to the northeast.

1.0 112.9 Pass exit to Jeremy Ranch. Sandstone beds of Nugget Formation exposed in the quarry to the west lie within the northwest limb of the hanging-wall ramp anticline. Successively younger rocks will be encountered heading west as the highway cuts obliquely across the north-northwest dipping limb of the Parleys Canyon syncline (Crittenden, 1965a, 1965b). This syncline lies within the hanging wall of the Mount Raymond thrust and has a gently east-northeast plunging fold axis. North- to northeast-plunging secondary folds also locally rotate beds along Parleys Canyon.

2.3 115.2 Road cut in micrite beds of Twin Creek Formation. Summit Park is to southwest.

0.9 116.1 Red siltstone and sandstone beds of Preuss Formation dip about 60° north-northwest in road cut.

2.4 118.5 Lambs Canyon exit. Sandstone beds of Kelvin Formation are visible to north. North-dipping beds of the Frontier Formation crop out farther north toward the trough of the Parleys Canyon syncline.

1.3 119.8 View to west of east-northeast plunging Spring Canyon anticline (Crittenden, 1965b). The anticline is cored by faulted Triassic rocks, and may continue northeast into the Henefer anticline. Conglomerate beds exposed to the north along East Canyon lie with angular unconformity over the Frontier Formation, and are rotated into an open syncline along the trend of the underlying tighter Parleys Canyon syncline. Angular unconformities may be present in the conglomerate, ages of beds are uncertain, and parts of the conglomerate may correlate with the Echo Canyon, Hams Fork, and Wasatch Formations (Mullens, 1971).

1.2 121.8 Siltstone and silty micrite beds of Twin Creek Formation display ripple marks in road cut.

1.4 123.2 Ranch exit. Micrite and siltstone beds are cut by complex fault zones in road cut northwest of exit.

1.6 124.8 Overpass. Complex folds are developed in limestone of the Watton Canyon Member of the Twin Creek Formation. Spaced cleavage is strongly fanned about the folds.

0.7 125.5 **Stop 10.** Internal deformation of the Twin Creek Formation along Parleys Canyon.

Pull over along entrance ramp on north side of highway for view of large roadcut in the Twin Creek Formation. Then continue southwest on I-80.

Micrite, limestone, and silty limestone of the Twin Creek Formation exposed along Parleys Canyon are deformed by cleavage, minor folds, veins arrays, and minor faults (Fig. 14). Cleavage is defined by spaced seams that are enriched in clay and strongly depleted in calcite. These seams both cross cut and are cut by calcite-filled veins recording overlapping development of cleavage and multiple vein sets. Two spaced cleavages are locally present: (1) a strongly developed cleavage (termed S1) that is generally steeply dipping and strikes north to north-northeast; and (2) a weakly developed cleavage (termed S2) that is generally gently dipping and strikes east to northeast. S2 cleavage seams dissolve some veins that cross cut S1 seams, indicating that S1 formed first. Some veins are grouped in en echelon arrays along shear zones where cleavage is more intensely developed.

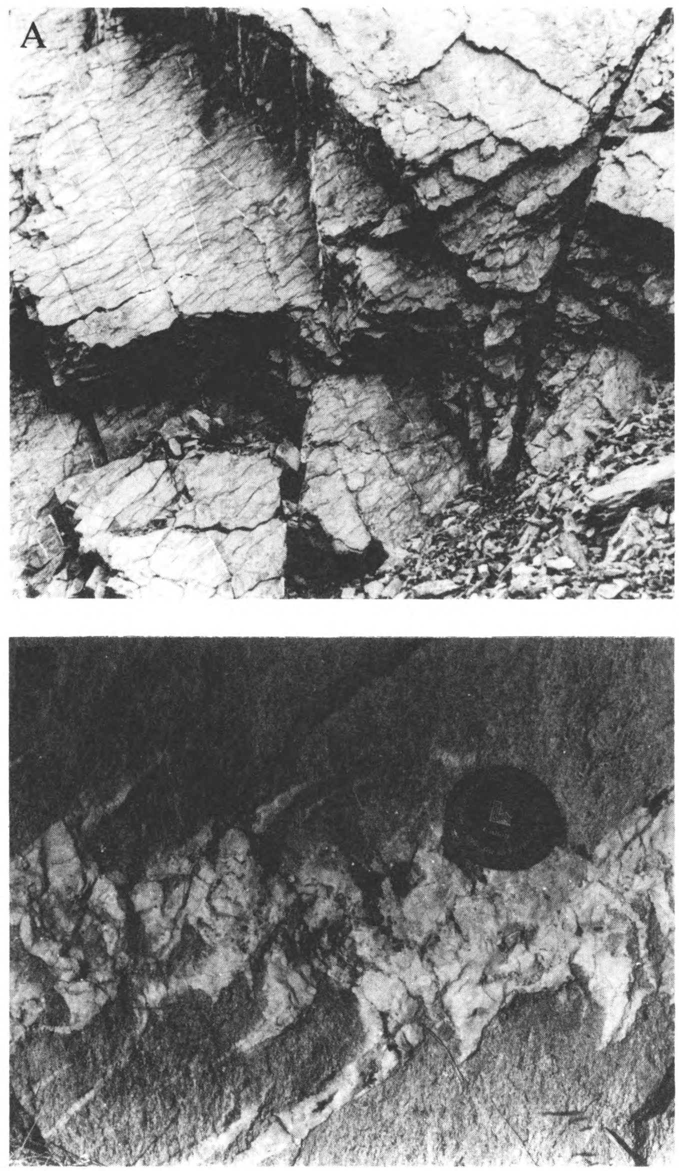

Figure 14. (A). Well-developed spaced cleavage in micritic limestone of the Twin Creek Formation along Parleys Canyon is defined by spaced seams of residue that are enriched in clays. (B) Veins locally form en echelon arrays reflecting heterogeneous shear.

S1 is parallel to hinge lines of north- to northeast-plunging minor folds (termed F1 folds), but remains at high angles to bedding around folds, forming partial fans (Fig. 15). These secondary F1 folds are well developed on the south flank of the Parleys Canyon syncline, but are locally conical and decrease in amplitude to the north. The F1 folds are disharmonic and formed above detachments in Pennsylvanian and Triassic strata, and some folds are cored by reverse faults. Some S1 seams contain thin calcite-filled veins that may have formed when the incremental extension direction rotated during folding. These relations are consistent with early development of S1 during west-northwest layer parallel shortening, followed by F1 minor folding.

S2 is parallel to the hinge lines of larger-scale gently east-northeast plunging F2 folds, including the Parleys Canyon syncline, Spring Canyon anticline, and Emigration Canyon syncline. This cleavage is strongly fanned about the F2 folds, remaining subperpendicular to bedding in the hinge and limb regions. These relations record later north-northwest subhorizontal shortening followed by development of larger-scale F2 folds.

The timing and kinematic relations of F1 and F2 folds are uncertain. F1 folds may record early west-northwest shortening, prior to large-scale movement along the Crawford and Mt. Raymond thrusts. The east-northeast-trending F2 folds (Parleys Canyon syncline, Spring Canyon anticline, and Emigration syncline) may continue in the subsurface and connect with the northeast-trending Stevenson Canyon syncline, Henefer anticline, and the syncline in the Weber Canyon conglomerate (Bryant, 1990). Thus F2 folds may be related to propagation and movement along the Crawford and Absaroka thrust systems. Changes in orientations of F2 fold axes and thrusts define a salient and may reflect variation in transport direction, dextral wrench shear, or rotation on the north flank of the Cottonwood arch. Alternatively, F2 folds may have formed synchronously with the Cottonwood arch during Laramide deformation (Bradley, 1988). Future kinematic analysis of en echelon vein arrays, slickenside surfaces, shear-vein fibers, and asymmetric fibers in pressure shadows may better constrain models for development of the folds and salient.

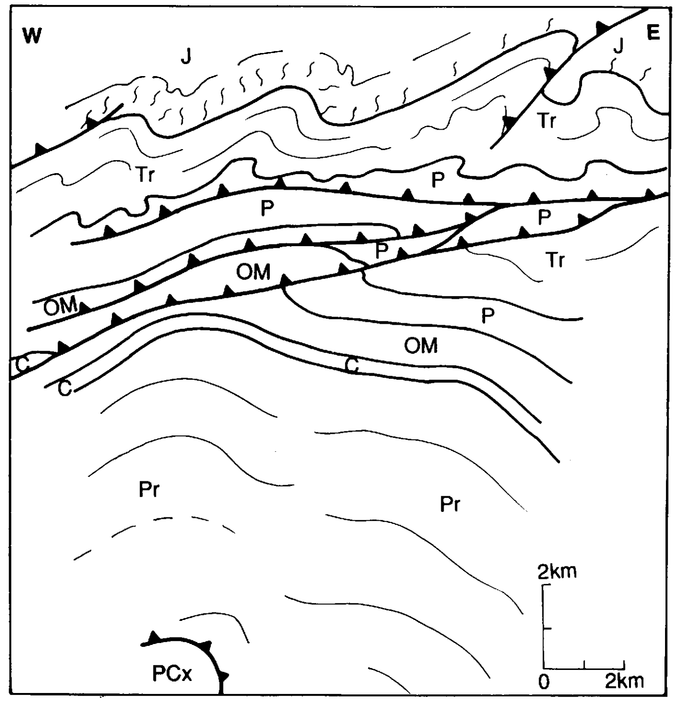

Figure 15. Generalized cross section along part of Parleys Canyon drawn using down-plunge projection of data. A series of disharmonic minor folds is developed in Triassic and Jurassic strata above a detachment zone in Permo-Pennsylvanian strata. Jurassic strata of the Twin Creek Formation are cut by cleavage (wavy lines) that fans about minor folds. The Mount Raymond thrust (MR) continues out of the back limb of the Big Cottonwood anticline which is cored by crystalline basement of the Little Willow series (PCx). Units same as in Figure 13. Modified from Bradley and Bruhn (1988), including data from Crittenden (1965a, 1965b).

0.6	126.1	Locally faulted contact between Nugget Formation and Sliderock and Gypsum Spring Members of the Twin Creek Formation is in gully to north and west. Faulted and brecciated sandstone beds of Nugget Formation are exposed in road cut to southwest.
0.4	126.5	Junction with Interstate 215. Continue west on I-80. Contact between Nugget and Triassic Ankareh Formations in hill slope to north.
1.0	127.5	Cross approximate trace of eastern splay of WFZ along base of mountains. Twin Creek Formation is exposed in road cut to northeast.
2.9	130.4	Cross approximate trace of western splay of WFZ which has Holocene fault scarps. View to southeast of central part of the Wasatch Range. The steep slope of Mount Olympus consists of Tintic Quartzite in the footwall of the Mount Raymond thrust. Precambrian Big Cottonwood Formation and basement rock of the Little Willow Series core the Cottonwood arch to the south. Oligocene granite and quartz monzonite intrusions locally cut the crest of the arch.

2.2 132.6 Junction with Interstate 15. Veer right and head north on I-15.

2.9 135.5 Junction with Interstate 80. Continue heading north on I-15.

1.8 137.3 Veer right onto 6th North exit and head east.

0.7 138.0 Junction with U.S. Highway 89. Turn left and head north on U.S. 89.

1.9 139.9 **Stop 11.** Tectonics of the Warm Springs fault zone and Salt Lake segment of the WFZ.

Stop at pull out near MONROC headquarters and discuss tectonics of the Wasatch normal fault zone (WFZ). Then proceed north on U.S. 89.

The Salt Lake segment of the WFZ is about 35 km long and consists of several approximately planar sections, each 3 to 12 km in length, that meet along fault bends and branches (Fig. 16; Bruhn and others, 1987). Estimated dips of fault sections range from 30 to 60°, and strikes vary from northwest to northeast. Paleostress analyses along the Salt Lake segment have indicated a subhorizontal minimum compressive stress trending between 230 and 250°, consistent with west to southwest-trending normal to oblique slip along the fault sections (Bruhn and others, 1987; Yonkee and Bruhn, unpublished data).

The Salt Lake salient, a complexly faulted and partly buried west-southwest-trending ridge of Tertiary and Paleozoic bedrock (Van Horn, 1982; Van Horn and Crittenden, 1987; Scott, 1988), forms the northern boundary of the Salt Lake segment (Fig. 16). Gravity and drill hole data indicate that the bedrock ridge continues westward into the Salt Lake Valley (Zoback, 1983), and a diffuse belt of epicenters of small earthquakes lies above this ridge (Fig. 4). The Salt Lake salient is a nonconservative barrier that separates the Weber and Salt Lake segments which have had different Holocene rupture histories (Schwartz and Coppersmith, 1984; Machette and others, 1991). The salient is largely covered by gently east-dipping clastic and volcaniclastic deposits of the late Tertiary Salt Lake Formation, and these deposits are separated from Precambrian bedrock and steeply dipping Paleozoic rocks by the Rudys Flat fault along the eastern boundary of the salient. This west-dipping normal fault is "scoop-shaped" and varies in strike from northwest to northeast. The fault has an estimated slip of about 6 km and has probably been active in the Quaternary, although Holocene fault scarps are absent. The interior of the salient contains several north- to northwest-striking synthetic and antithetic normal faults, and several northeast-striking faults. The salient is partly bounded on the south by the west-northwest-striking Virginia Street fault. The north-striking Warm Springs fault separates Paleozoic and Tertiary bedrock from Quaternary deposits along the western margin of the salient. This fault appears to bend around the salient and a northeast-striking branch bounds the northwestern margin of the salient. A possible fault branch also continues north of the salient (Van Horn, 1982). The southern extent of the Warm Springs fault is uncer-

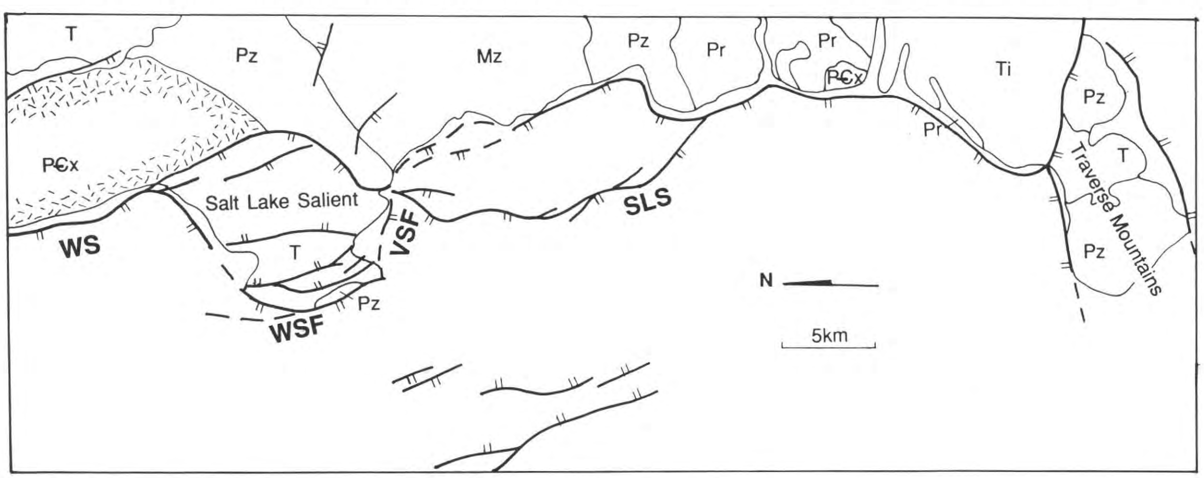

Figure 16. Generalized map of Salt Lake segment (SLS) and part of the Weber segment (WS) of the Wasatch normal fault zone. The Salt Lake salient, a west-southwest-trending bedrock ridge that is internally deformed by fault networks, marks the boundary between the two segments. The Traverse Mountains mark the southern boundary of the SLS. WSF-Warm Springs fault and VSF-Virginia Street fault. Units are P€x-Precambrian crystalline rocks, Pr-middle Proterozoic sedimentary rocks, Pz-Paleozoic strata, Mz-Mesozoic strata, T-Tertiary strata, and Ti-Tertiary intrusive igneous rocks. Modified from Bruhn and others (1987) and Bryant (1990).

tain, and this fault may be en echelon or merge with the main part of the Salt Lake segment.

The Warm Springs fault dips 40 to 80° west within the MONROC quarries, and places southeast-dipping beds of Mississippian limestone in the footwall against Quaternary deposits in the hanging wall. Deposits of Lake Bonneville are offset by 10 to 15 m across the fault, probably recording multiple slip events (Gilbert, 1928). Fault surfaces display two dominant sets of slickenlines, a west-southwest-trending set and an older west-northwest-trending set (Pavlis and Smith, 1980). Fault surfaces also display undulations with wavelengths and amplitudes of millimeters to meters. Most undulations are aligned subparallel to slickenlines approximately down the dip of the fault.

The Salt Lake salient lies along the southern end of the basement-cored anticline, and the Weber segment to the north appears to have formed near the axial surface of the anticline (Fig. 2B). The Salt Lake segment to the south cuts east- to northeast-striking Mesozoic to Precambrian bedrock and Tertiary igneous rocks in its footwall. These rocks lie at the southern boundary of the Idaho-Utah-Wyoming thrust belt and along the Cottonwood arch. Farther south, the Provo segment cross cuts the Charleston thrust sheet. Segments of the WFZ crudely correlate with lateral changes in thrust-related structures, and the geometry of thrust-related structures may have partly controlled the location and segmentation of the WFZ.

1.0 140.9 Veer left onto entrance to Interstate 15 and continue north on I-15.

4.8 145.7 View to east of basement rocks of Farmington Canyon Complex which lie on the steeply dipping eastern limb of the basement-cored anticline. "B" on hill slope to the east is at the Bonneville level.

5.1 150.8 Quaternary landslide complex is visible to east.

2.0 152.8 Junction with U.S. Highway 89. Continue heading north on I-15.

1.0 153.8 Bumpy terrain in golf course to east is part of a lateral spread deposit that may have formed by ground failure during past earthquakes.

4.0 157.8 View of Antelope Island to west. Antelope Island lies on the gently dipping western limb of the basement-cored anticline.

4.5 162.3 The highway passes along the western (distal) edge of the Weber delta which was built out into ancient Lake Bonneville.

7.3 169.6 Descend onto alluvial deposits of Weber River.

3.9 173.5 Junction with Utah Highway 79. Veer right onto exit 344B and proceed west on Utah Highway 79 (Hinckley Drive) toward Ogden airport.

0.8 174.3 Take left into entrance to Ogden airport.

0.3 174.6 **Stop 12** (optional). Summary of regional tectonics. Pull into first parking lot on east side of road for regional overview and discussion. After discussion, turn back to Utah 79.

The Willard and Ogden thrust systems display complex lateral ramps and branching of thrusts in the Wasatch Range to the east (Fig. 17). The thrust systems are downdropped along Weber segment of the WFZ, and lie below the valley floor. A basal thrust is interpreted to lie beneath the Ogden thrust system. The steeply dipping eastern limb of the basement-cored anticline is visible along the Wasatch Range to the east and southeast, and the gently dipping western limb of the basement-cored anticline is preserved on Antelope Island to the southwest.

The progressive development of regional thrust systems is illustrated in Figure 18,

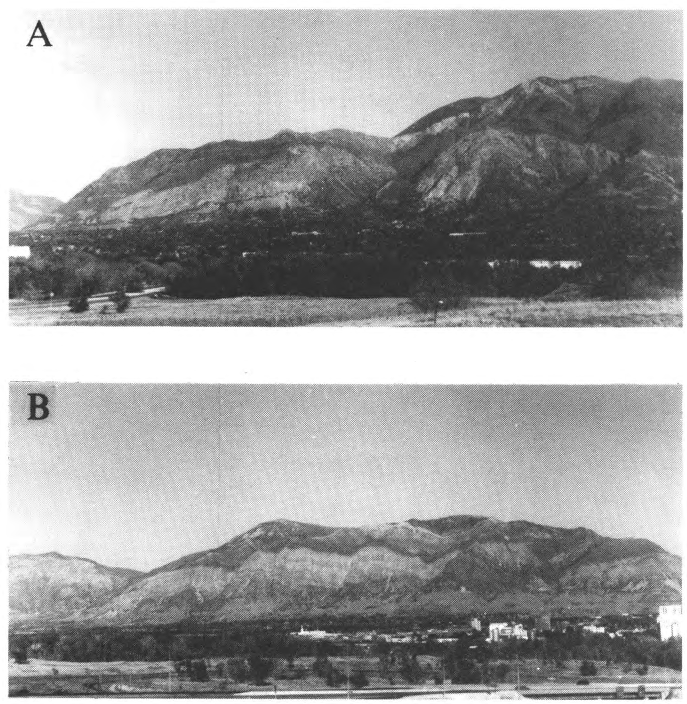

Figure 17. View from stop 12 near Ogden airport looking east at Wasatch Range. Photograph A covers area south of Ogden Canyon and photograph B covers area north of Ogden Canyon.

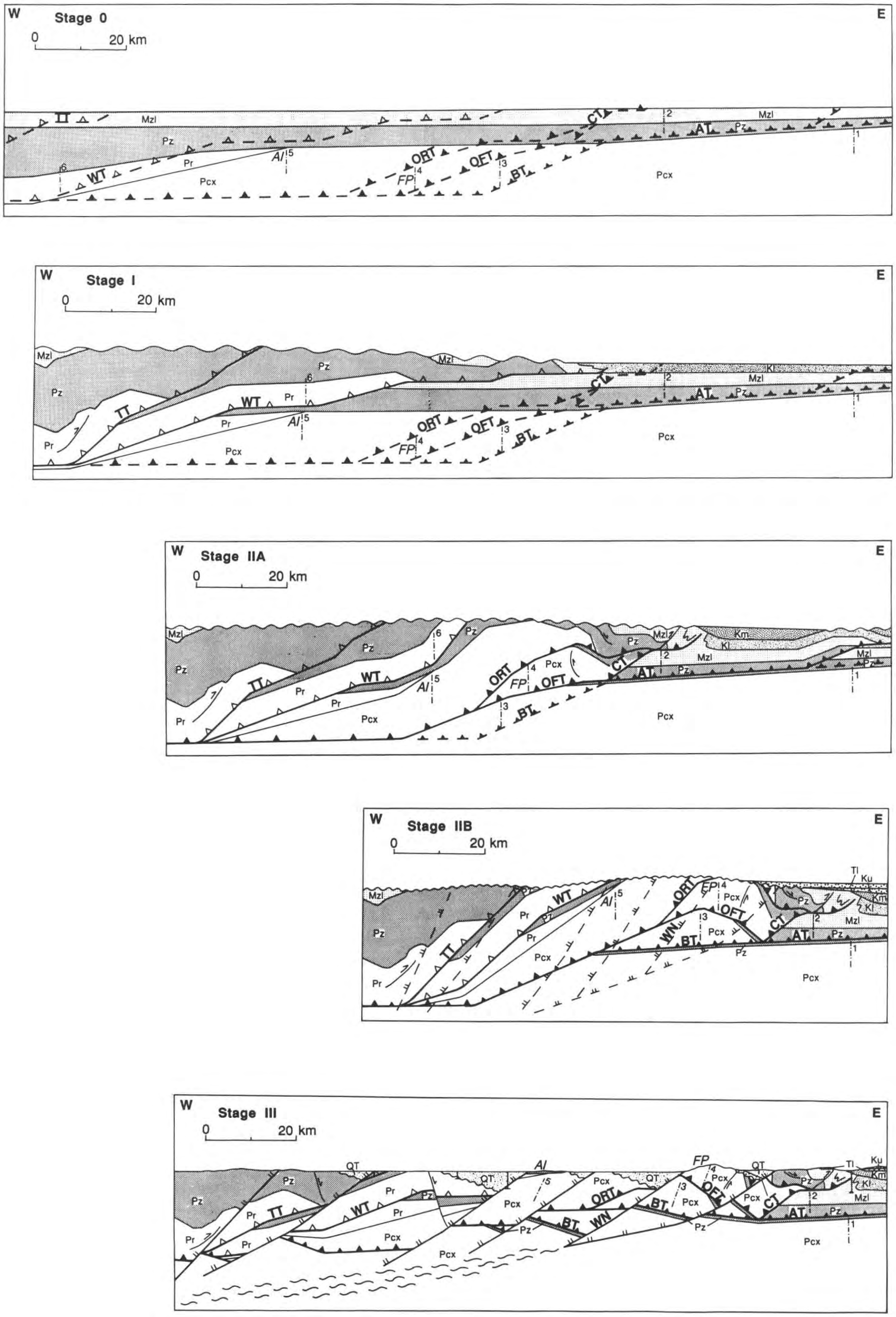

Figure 18. Generalized cross sections obtained by undeforming section B-B' in Figure 2. Sections illustrate successive development of thrust systems in northern Utah. Idealized stages are: 0-pre-deformational sedimentary wedge; I-movement on the Willard thrust system; IIA-movement on Ogden thrust system; IIB-final movement on basal thrust; III-Tertiary extension. Estimated approximate positions of erosion surfaces, based on compositions of clasts in synorogenic deposits, are shown by wavy lines. Solid lines with different teeth types represent geometrically related thrust traces, and dashed lines represent positions of restored faults. Units same as in Figure 1. Faults are labeled: AT-Absaroka thrust; BT-basal thrust; CT-Crawford thrust; OFT-floor thrust of Ogden system; ORT-roof thrust of Ogden system; TT-Tintic Valley thrust; WT-Willard thrust; and WN-Wasatch normal fault zone. Taken from Yonkee (in press).

based on the discussion of Yonkee (in press). The sections are drawn using a fault-bend-fold model which conserves the length of the horizontal datum. Length balancing provides an initial approximation, although the geometry may be locally modified by heterogeneous internal shortening.

Stage 0. The undeformed cover formed a westward-thickening wedge prior to initiation of Cretaceous thrusting. A major sedimentary basin, with about 8 km of relief on the top of the basement, marked the westernmost part of the area.

Stage I. The Willard thrust sheet was emplaced between 140 and 110 m.y., overlapping with early internal shortening of the basement, recorded by $^{40}Ar/^{39}Ar$ ages of syndeformational sericite from basement shear zones and from veins in the Willard sheet. Emplacement of the Willard sheet buried the footwall to greater depths and probably resulted in increased temperatures and fluid influx within the basement (Yonkee and others, 1989). The Willard thrust had a lower flat at the base of a western sedimentary basin and ramped up to a second flat within Cambrian strata. Synorogenic strata of the Ephraim and Kelvin Formations were deposited.

Stage IIA. Movement on the Ogden thrust system between about 110 and 80 m.y. produced a major ramp anticline. The synorogenic Echo Canyon Conglomerate was deposited between 85 to 90 m.y., recording initial large-scale uplift and unroofing of the basement-cored anticline (DeCelles, 1988). The Ogden thrust system continued from a lower flat within the sedimentary basin eastward into the basement. The Ogden floor and roof thrusts ramped up to a higher flat in Cambrian strata that continued farther east as the regional decollement of the frontal Crawford, Absaroka, and Hogsback thrusts, marking a fundamental change from basement-involved deformation. The ramps had about 9 km of structural relief, corresponding to the estimated thickness of basement in the anticline and to the relief on the top of the basement within the western sedimentary basin (modified from minor internal shortening). The estimated slip of about 30 km within the Ogden system was largely transferred eastward into slip on the Crawford thrust, early movement on the Absaroka thrust, and internal shortening of the cover to the east above a detachment in Jurassic strata (Mitra and Yonkee, 1985). Approximately 5 km of slip was taken up in flexural slip folding and internal deformation within the anticline. The Ogden thrust system also has major lateral ramps, resulting in a complex three-dimensional geometry.

Stage IIB. Slip on a basal thrust system between 80 and 50 m.y. resulted in renewed uplift, and an increase in width and amplitude of the basement-cored anticline. The synorogenic Hams Fork Conglomerate, related to late movement on the Absaroka thrust, and part of the Wasatch Formation, related to movement on the Hogsback thrust, were deposited east of the anticline. These deposits contain basement clasts, recording continued erosion of the anticline. The Ogden thrust system was rotated to the observed east dip, and shear zones and cleavage which initiated during early shortening were rotated and modified into a partial fan about the anticline. An estimated 40 km of slip on the basal thrust was largely transferred eastward into later movement on the Absaroka thrust and into movement on the Hogsback thrust. The remaining slip was taken up by flexural slip folding and internal shortening within the anticline. Large-scale imbricate thrusts and folds within the anticline produced about 60% total shortening. Smaller shear zones and cleavage accommodated an additional 5 to 20% internal shortening.

Stage III. Tertiary extension modified thrust-related structures into their current geometry. Tertiary strata were rotated to east dips as fault bounded blocks rotated and extended.

0.3	174.9	Turn right and head east on Utah Highway 79.
1.3	176.2	Junction with Utah 204 (Wall Avenue). Continue east on Utah 79 (3100 South).
0.5	176.7	Junction with U.S. Highway 89 (Washington Blvd.). Turn left and head north on U.S. 89.
0.9	177.6	Return to Radisson Suite Hotel. End field trip.

REFERENCES

Arabasz, W. J., Pechmann, J. C., and Brown, E. D., in press, Observational seismology and the evaluation of earthquake hazards and risk in the Wasatch Front area, Utah: U.S. Geological Survey Professional Paper.

Armstrong, F. C., and Oriel, S. S., 1965, Tectonic evolution of the Idaho-Wyoming thrust belt: American Association of Petroleum Geologists Bulletin, v. 11, p. 1847-1866.

Beck, S. L., 1982, Deformation in the Willard thrust plate in northern Utah and its regional implications [M.S. thesis]: Salt Lake City, Utah, The University of Utah, 79 p.

Bell, G. L., 1951, Farmington Canyon Complex of the north-central Wasatch [Ph.D. dissertation]: Salt Lake City, Utah, The University of Utah, 101 p.

Best, M. G., McKee, E. H., and Damon, P. E., 1980, Space-time-composition patterns of late Cenozoic mafic volcanism, south-western Utah and adjoining areas: American Journal of Science, v. 280, p. 1035-1050.

Bradley, M. D., 1988, Structural evolution of the Uinta Mountains, Utah, and their interaction with the Utah-Wyoming salient of the Sevier overthrust belt [Ph.D. dissertation]: Salt Lake City, Utah, The University of Utah, 178 p.

Bradley, M. D., and Bruhn, R. L., 1988, Structural interactions between the Uinta arch and the overthrust belt, north-central Utah: Implications of strain trajectories and displacement modeling, *in* Schmidt, C. J., and Perry, W. J., Jr., eds., Interaction of the Rocky Mountain foreland and the Cordilleran thrust belt: Geological Society of America Memoir 171, p. 431-445.

Bruhn, R. L., and Beck, S. L., 1981, Mechanics of thrust faulting in crystalline basement, Sevier orogenic belt, Utah: Geology, v. 9, p. 200-204.

Bruhn, R. L., Gibler, P. R., and Parry, W. T., 1987, Rupture characteristics of normal faults: an example from the Wasatch fault zone, Utah: *in* Coward, M. P. Dewey, J. F., and Hancock, P. L., eds., Continental Extensional Tectonics: Geological Society of London Special Publication 28, p. 337-353.

Bruhn, R. L., Picard, M. D., and Isby, J. S., 1986, Tectonics and sedimentology of the Uinta arch, western Uinta Mountains and Uinta Basin, *in* Peterson, J. A., ed., Paleotectonics and sedimentation in the Rocky Mountain region, United States: American Association of Petroleum Geologists Memoir 32, p. 333-352.

Bryant, B., 1984, Reconnaissance geologic map of the Precambrian Farmington Canyon Complex and the surrounding rocks in the Wasatch Mountains between Ogden and Bountiful, Utah: U.S. Geological Survey Miscellaneous Geologic Investigations Map I-1447.

——, 1988, Geology of the Farmington Canyon Complex, Wasatch Mountains, Utah: U.S. Geological Survey Professional Paper 1476, 54 p.

——, 1990, Geologic map of the Salt Lake City 30′ x 60′ quadrangle, north-central Utah, and Uinta County, Wyoming: U.S. Geological Survey Map I-1944.

Crittenden, M. D., Jr., 1965a, Geologic map of the Mount Aire quadrangle, Salt Lake County, Utah: U.S. Geological Survey Map GQ-379.

——, 1965b, Geologic map of the Sugar House quadrangle, Salt Lake County, Utah: U.S. Geological Survey Map GQ-380.

——, 1972, Willard thrust and Cache allochthon, Utah: Geological Society of America Bulletin, v. 83, p. 2871-2880.

——, 1974, Regional extent and age of thrusts near Rockport Reservoir and relation to possible exploration targets in northern Utah: American Association of Petroleum Geologists Bulletin, v. 58, p. 2428-2435.

——, 1976, Stratigraphic and structural setting of the Cottonwood area, Utah: *in* Hill, J. G., ed., Symposium of the Cordillera Hingeline: Rocky Mountain Association of Geologists, p. 363-379.

Crittenden, M. D., Jr., Calkins, F. C., and Sharp, B. J., 1966, Geologic map of the Park City West quadrangle, Utah: U.S. Geological Survey Map GQ-535.

Crittenden, M. D., Jr., and Sorensen, M. L., 1979, The Facer Formation, a new early Proterozoic unit in northern Utah: U.S. Geological Survey Bulletin 1482-F, 28 p.

——, 1985a, Geologic map of the Mantua quadrangle and part of the Willard quadrangle, Box Elder, Weber, and Cache Counties, Utah: U.S. Geological Survey Map I-1605.

——, 1985b, Geologic map of the North Ogden quadrangle and part of the Ogden and Plain City quadrangles, Box Elder and Weber Counties, Utah: U.S. Geological Survey Map I-1606.

Davis, F. D., 1985, Geologic map of the northern Wasatch front, Utah: Utah Geological and Mineral Survey Map 53A.

DeCelles, P. G., 1988, Lithologic provenance modeling applied to the Late Cretaceous synorogenic Echo Canyon Conglomerate, Utah: A case of multiple source areas: Geology, v. 16, p. 1039-1043.

Dixon, J. S., 1982, Regional structural synthesis, Wyoming salient of western overthrust belt: American Association of Petroleum Geologists Bulletin, v. 66, p. 1560-1580.

Eardley, A. J., and Hatch, R. A., 1940, Precambrian crystalline rocks of north-central Utah: Journal of Geology, v. 48, p. 58-72.

Evans, J. P., and Neves, D. S., in press, Footwall deformation along the Willard thrust, Sevier Orogenic Belt: Implications for mechanisms, timing, and kinematics: Geological Society of America Bulletin.

Evans, S.H., Parry, W.T., and Bruhn, R.L., 1985, Thermal, mechanical, and chemical history of Wasatch fault cataclasite and phyllonite, Traverse Mountains area, Salt Lake City, Utah: From K/Ar and fission track measurements: U.S. Geological Survey Open-File Report 86-31, p. 410-415.

Gilbert, G. K., 1928, Studies of Basin-Range structure: U.S. Geological Survey Professional Paper 153, 89 p.

Hansen, R. L., 1980, Structural analysis of the Willard thrust fault near Ogden Canyon, Utah [M.S. thesis]: Salt Lake City, Utah, The University of Utah, 82 p.

Hansen, W. R. 1965, Geology of the Flaming Gorge area, Utah-Colorado-Wyoming: U.S. Geological Survey Professional Paper 490, 196 p.

Hedge, C. E., Stacey, J. S., and Bryant, B., 1983, Geochronology of the Farmington Canyon Complex, Wasatch Mountains, Utah, *in* Miller, D. M., Todd, V. R., and Howard, K. A., eds., Tectonic and stratigraphic studies in the eastern Great Basin: Geological Society of America Memoir 157, p. 37-44.

Heller, P. L., Bowdler, S. S., Chambers, H. P., Coogan, J. C., Hagen, E. S., Schuster, M. W., and Winslow, N. S., 1986, Time of initial thrusting in the Sevier orogenic belt, Idaho-Wyoming and Utah: Geology, v. 14, p. 388-391.

Hintze, L. F., 1980, Geologic map of Utah: Utah Geological and Mineral Survey Map A-2, scale 1:500,000.

Hintze, L. F., 1988, Geologic History of Utah: Brigham Young University Geology Studies Special Publication 7, 202 p.

Hollett, D. W., 1979, Petrological and physiochemical aspects of thrust faulting in the Precambrian Farmington Canyon complex, Utah [MS. thesis]: Salt Lake City, Utah, The University of Utah, 99 p.

Hopkins, D., 1983, Geology of the Durst Mountain area [MS. thesis]: Salt Lake City, Utah, The University of Utah, 80 p.

Jacobson, S. R., and Nichols, D. J., 1982, Palynological dating of syntectonic units in the Utah-Wyoming thrust belt: The Evanston Formation, Echo Canyon Conglomerate and Little Muddy Creek Conglomerate, *in* Powers, R. G., ed., Geologic studies of the Cordilleran thrust belt: Denver, Colorado, Rocky Mountain Association of Geologists, p. 735-750.

Lamerson, P. R., 1982, The Fossil Basin and its relationship to the Absaroka thrust system, Wyoming and Utah, *in* Powers, R. B., ed., Geologic studies of the Cordilleran thrust belt: Rocky Mountain Association of Geologists Guidebook, v. 1, p. 279-340.

Link, P. K., Crook, S. R., and Chidsey, T. C., Jr., 1985, Overthrusts and stratigraphy in the Wasatch, Bear River and Crawford Ranges and Bear Lake Plateau, north-central Utah, *in* Kerns, G. J., and Kerns, R. L., eds., Orogenic patterns and stratigraphy of north-central Utah and southeastern Idaho: Utah Geological Association Publication 14, p. 269-328.

Mabey, D. R., Zeitz, I., Eaton, G. P., and Kleinkopf, M. D., 1978, Regional magnetic patterns in part of the Cordillera in the western U.S.: Geological Society of America Memoir 152, p. 93-106.

Machette, M. N., Personius, S. F., and Nelson, A. R., 1987, Quaternary geology along the Wasatch fault zone-segmentation, recent investigations, and preliminary conclusions: U.S. Geological Survey Open File Report 87-585, p. A1-72.

Machette, M. N., Personius, S. F., Nelson, A. R., Schwartz, D. P., and Lund, W.R., 1991, The Wasatch fault zone, Utah: Segmentation and history of Holocene earthquakes: Journal of Structural Geology, v. 13, p. 137-149.

Mitra, G., 1978, Ductile deformation zones and mylonites: The mechanical processes involved in the deformation of crystalline basement rocks: American Journal of Science, v. 278, p. 1057-1084.

Mitra, G., and Yonkee, W. A., 1985, Spaced cleavage and its relationship to major structures in the Idaho-Utah-Wyoming thrust belt of the Rocky Mountain Cordilleras: Journal of Structural Geology, v. 7, p. 361-373.

Mullens, T. E., 1971, Reconnaissance study of the Wasatch, Evanston, and Echo Canyon Formations in part of northern Utah, U.S. Geological Survey Bulletin 1311-D, p. 1-31.

Mullens, T. E., and Laraway, W. H., 1964, Geology of the Devils Slide quadrangle, Morgan and Summit Counties, Utah: U.S. Geological Survey Map MF-290.

——, 1973, Geologic map of the Morgan 7½ minute quadrangle, Morgan County, Utah: U.S. Geological Survey Map MF-318.

Naeser, C. W., Bryant, B., Crittenden, M. D., Jr., and Sorensen, M. L., 1983, Fission-track ages of apatite in the Wasatch Mountains, Utah: an uplift study, *in* Miller, D. M., Todd, V. R., and Howard, K. A., eds., Tectonic and stratigraphic studies in the eastern Great Basin: Geological Society of America Memoir 157, p. 29-36.

Nelson, A. R., 1988, The northern part of the Weber segment of the Wasatch fault zone near Ogden, Utah, *in* Machette, M. N., ed., In the Footsteps of G. K. Gilbert—Lake Bonneville and Neotectonics of the Eastern Basin and Range Province: Utah Geological and Mineral Survey Miscellaneous Publication 88-1, p. 33-37.

Nishenko, S.P., and Schwartz, D. P., 1990, Preliminary estimates of large earthquake probabilities along the Wasatch fault zone, Utah: EOS, v. 71, p. 1448.

Neves, D. S., 1989, Footwall deformation and structural analysis of the footwall of the Willard thrust fault, northern Wasatch Range, Utah [M.S. Thesis]: Logan, Utah, Utah State University, 158 p.

Nichols, D. A., and Warner, M. A., 1978, Palynology, age, and correlation of the Wanship Formation and their implications for the tectonic history of northeastern Utah: Geology, v. 6, p. 430-433.

Oriel, S.S., 1986, The Idaho-Wyoming salient of the North American Cordillera foreland thrust belt: Bulletin of the Geological Society of France, v. 8, p. 755-765.

Parry, W. T., and Bruhn, R. L., 1986, Pore-fluid chemistry and chemical reactions on the Wasatch normal fault, Utah: Geochimica et Cosmochimica Acta, v. 52, p. 2053-2063.

Pavlis, T. L., and Bruhn, R. L., 1988, Stress history during propagation of a lateral fold-tip and implications for the mechanics of fold thrust belts: Tectonophysics, v. 145, p. 113-127.

Pavlis, T. L., and Smith, R. B., 1980, Slip vectors from faults near Salt Lake City from Quaternary displacement and seismicity, *in* Arabasz, W.J., Smith, R. B., and Richins, W. D., eds., Earthquake Studies in Utah: Salt Lake City, Utah, University of Utah, p. 378-382.

Personius, S. F., 1988, Preliminary surficial geologic map of the Brigham City segment and adjacent parts of the Weber and Colliston segments, Wasatch fault zone, Box Elder and Weber Counties, Utah: U.S. Geological Survey Map MF-2042.

Rigo, R. J., 1968, Middle and Upper Cambrian stratigraphy in the autochthon and allochthon of northern Utah: Brigham Young University Geology Studies v. 15, p. 31-66.

Royse, F. C., Warner, M. A., and Reese, D. L., 1975, Thrust belt of Wyoming, Idaho, and northern Utah: Structural geometry and related stratigraphic problems, *in* Boylard, D. W., ed., Deep drilling frontiers of the central Rocky Mountains: Rocky Mountain Association of Geologists Guidebook, p. 41-54.

Schirmer, T. W., 1985, Basement thrusting in north-central Utah: A model for the development of the northern Utah highland, *in* Kerns, G. J., and Kerns, R. L., eds., Orogenic patterns and stratigraphy of north-central Utah and southeastern Idaho: Utah Geological Association Publication 14, p.129-144.

Schirmer, T. W., 1988, Structural analysis using thrust fault hanging-wall sequence diagrams: Ogden duplex, Wasatch Range, Utah: American Association of Petroleum Geologists Bulletin, v. 72, p. 573-585.

Schwartz, D. P., and Coppersmith, K. J., 1984, Fault behavior and characteristic earthquake: Examples from the Wasatch and San Andreas fault zone: Journal of Geophysical Research, v. 89, p. 5681-5698.

Scott, W. E., 1988, G. K. Gilbert's observations of post-Bonneville movement along the Warm Springs fault, Salt Lake County, Utah, *in* Machette, M. N., ed., In the Footsteps of G. K. Gilbert—Lake Bonneville and Neotectonics of the Eastern Basin and Range Province: Utah Geological and Mineral Survey Miscellaneous Publication 88-1, p. 44-46.

Snoke, A. W., and Miller, D. M., 1988, Metamorphic and tectonic history of the northeastern Great Basin, *in* Ernst, W. G., ed., Metamorphism and crustal evolution of the western United States: p. 607-648.

Sorensen, M. L., and Crittenden, M. D., Jr., 1979, Geologic map of the Huntsville quadrangle, Weber and Cache Counties, Utah: U.S. Geological Survey Map GQ-1503.

Van Horn, R., 1982, Surficial geologic map of the Salt Lake City North quadrangle, Davis and Salt Lake Counties, Utah: U.S. Geological Survey Map I-1404.

Van Horn, R., and Crittenden, M. D., Jr., 1987, Map showing surficial units and bedrock geology of the Fort Douglas quadrangle and parts of the Mountain Dell and Salt Lake City North quadrangles, Davis, Salt Lake, and Morgan Counties, Utah: U.S. Geological Survey Map I-1762.

Wiltschko, D. V., and Dorr, J. A., Jr., 1983, Timing of deformation in overthrust belt and foreland of Idaho, Wyoming, and Utah: American Association of Petroleum Geologists Bulletin, v. 67, p. 1304-1322.

Yonkee, W. A., 1990, Geometry and mechanics of basement and cover deformation, Farmington Canyon Complex, Sevier orogenic belt, Utah [Ph.D. dissertation]: Salt Lake City, Utah, The University of Utah, 255 p.

——, in press, Basement-cover relations, Sevier orogenic belt, northern Utah: Geological Society of America Bulletin.

Yonkee, W. A., and Mitra, G., in press, Comparison of basement deformation styles in parts of the Rocky Mountain Foreland, Wyoming, and the Sevier orogenic belt, northern Utah: Geological Society of America Special Paper.

Yonkee, W. A., Parry, W. T., Bruhn, R. L., and Cashman, P. C., 1989, Thermal models of thrust faulting: Constraints from fluid inclusion observations, Willard thrust sheet, Idaho-Utah-Wyoming thrust belt: Geological Society of America Bulletin, v. 101, p. 304-313.

Zoback, M. L., 1983, Structure and Cenozoic tectonism along the Wasatch fault zone, *in* Miller, D. M., Todd, V. R., and Howard, K. A., eds., Tectonic and stratigraphic studies in the eastern Great Basin: Geological Society of America Memoir 157, p. 3-27.

LATE PROTEROZOIC AND EARLY CAMBRIAN STRATIGRAPHY, PALEOBIOLOGY, AND TECTONICS: NORTHERN UTAH AND SOUTHEASTERN IDAHO

Paul Karl Link
Department of Geology
Idaho State University
Pocatello Idaho, 83209
Loren H. Smith
Department of Organismic and Evolutionary Biology
Harvard University
Cambridge Massachusetts, 02138

ABSTRACT

Strata exposed in the lower part of the Willard thrust sheet on the west face of the Wasatch, Malad, Pocatello, and Bannock Ranges (Fig. 1) provide a record of latest Precambrian and Early Cambrian time (approximately 800 Ma to 530 Ma). These rocks generally consist of the Pocatello Formation at the base and the Brigham Group above, and they contain evidence of several key pieces of geologic and paleontologic history. In particular, they were deposited when multicellular life was first developing and diversifying, that is, in Late Riphean, Ediacaran-Vendian, and Cambrian time (Fig. 2), and the upper units contain Early Cambrian fossils. Furthermore, they record one or more periods of glaciation and basaltic volcanic activity, events that preceded rifting of the western margin of North America. This rifting was completed by latest Proterozoic time. The Brigham Group contains shallow-marine and adjacent fluvial braid-plain deposits which were deposited in the Cordilleran miogeocline along the eastern margin of the proto-Pacific ocean and which record, as abrupt but subtle unconformities, incised canyons, and gravity-flow deposits, the rise and fall of the Proterozoic sea. The upper part of the Brigham Group contains abundant ichnofossils, evidence of burrowing and feeding activities of Early Cambrian organisms.

INTRODUCTION

This field trip is designed to provide a one-day introduction to the Late Proterozoic and Lower Cambrian strata present along the front of the Wasatch and Bannock Ranges from Ogden, Utah, north to Pocatello, Idaho. Our purpose is to provide descriptions of fieldtrip stops accessible via passenger vehicles, and from which further study may commence. Several of these field-trip-stop descriptions have been published before (Link and Lefebre, 1983; Link and others, 1985b; Link, 1987; Christie-Blick and Levy, 1989a). Persons interested in these field-trip stops should obtain topographic maps at 1:250,000 scale (Pocatello, Preston, Ogden, and Brigham City) or 1:100,000 scale (Pocatello, Malad City, Tremonton, Logan, Promontory Point, and Ogden).

Late Proterozoic and lower Paleozoic strata crop out along the length of the North American Cordillera (Crittenden and others, 1983; Eisbacher, 1985; Miller, 1985). These rocks record protracted rifting of the western margin of North America and the establishment of a passive continental margin by Early Cambrian time (Stewart, 1972, 1976; Stewart and Poole, 1974; Burchfiel and Davis, 1975; Young, 1982; Armin and Mayer, 1983; Bond and others, 1983, 1985; Devlin and Bond, 1988; Christie-Blick and Levy, 1989a; Ross, 1991).

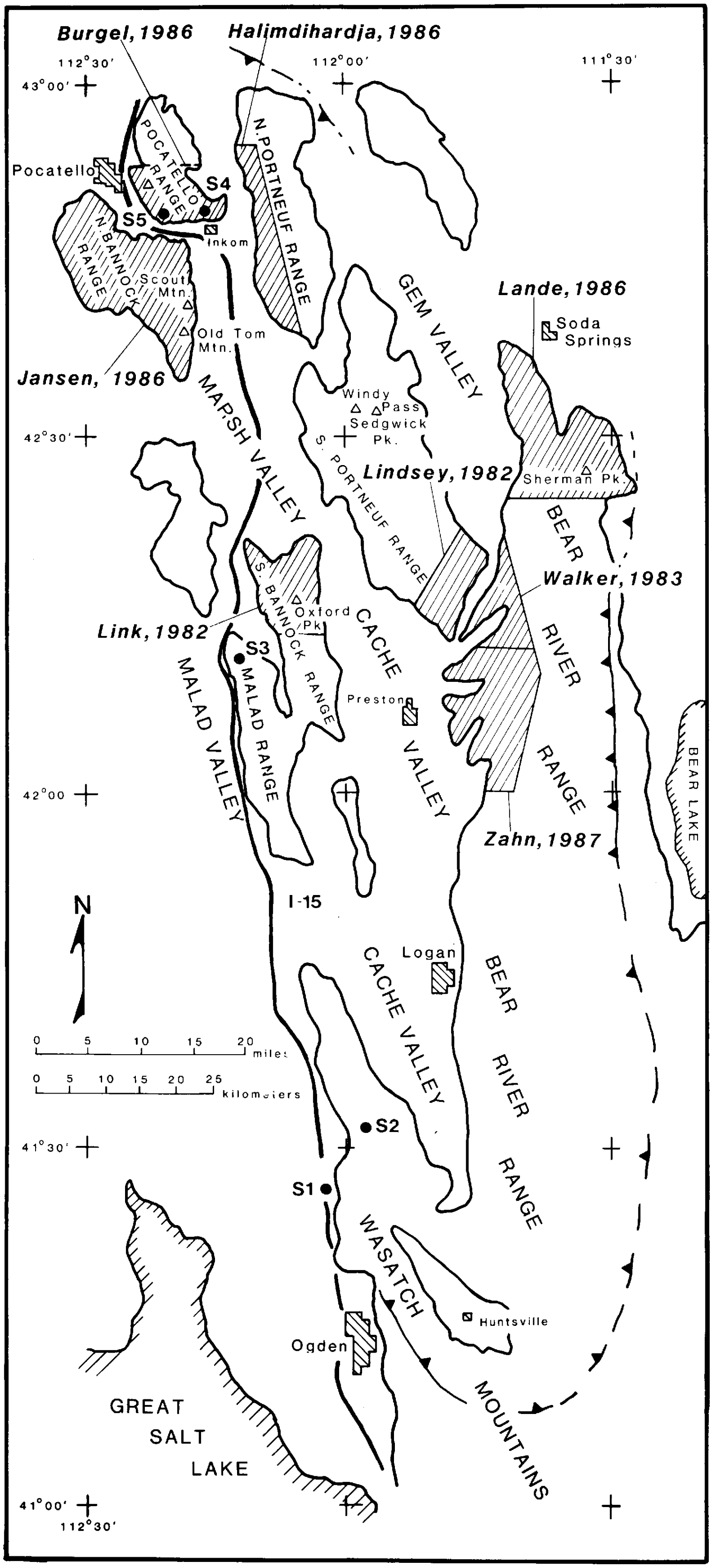

Figure 1. Location map with names of ranges and field trip stop locations (S1 to S5), from Link and others, 1987. Stop one will provide an overview of the Wasatch front and the tectonic history of the region. Stop two, in Box Elder Canyon east of Brigham City, is the type area of the Brigham Quartzite of Walcott (1908), cut by the Box Elder thrust. Stop 3, Two Mile Canyon, features the upper Brigham Group and overlying Cambrian strata, with abundant trilobite fossils. Stop 4, north of Inkom, examines the detailed sequence stratigraphy of the Caddy Canyon Quartzite and the overlying Inkom Formation. Stop 5 at Portneuf Narrows concludes with the Pocatello Formation, including diamictites and the overlying carbonate strata.

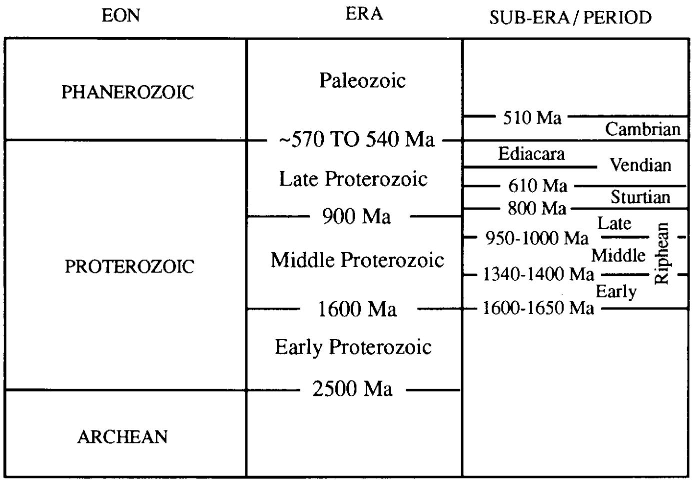

Figure 2. Proterozoic to Cambrian time scale, following U.S.G.S terminology for eras, modified from Christie-Blick and Levy (1989a). The age of the base of the Vendian at 610 Ma is from Harland and others (1990), though they call the preceding sub-era "Sturtian," whose base (and the top of the underlying Riphean) is placed at 800 Ma. Note that recent assessment of the age of the base of the Cambrian period suggests that it may be 540 Ma (Hoffman, 1991; Knoll and Walter, in press).

The Late Proterozoic miogeoclinal rocks of northern Utah and southeast Idaho were divided into a lower diamictite and volcanic succession (the Pocatello Formation and equivalent strata) and an upper terrigenous detrital succession (the Brigham Group) by Stewart (1972). Broadly equivalent strata are present beneath Paleozoic carbonate rocks along the length of the United States cordillera, from northeastern Washington to Death Valley in southeastern California and in Canada to the north (Young and others, 1979). These rocks are dominantly unfossiliferous, except for microfossils from the glaciogenic Mineral Fork Formation (Knoll and others, 1981), and abundant Early Cambrian trace and body fossils, examples of which we will examine at Two Mile Canyon in the Malad Range (stop 3). Recent syntheses of studies of these rocks include Crittenden and others (1983), Link and others (1985a; 1987), Christie-Blick and others (1988), Christie-Blick and Levy (1989a), and Levy and Christie-Blick (1991a, 1991b).

GEOLOGIC OVERVIEW

Diamictite and Volcanic Succession

The diamictite-and-volcanic succession (deposited after about 770 Ma) crops out extensively in allochthonous thrust plates of Utah and Idaho. In these locations, sedimentary-facies associations suggest marine settings in basins at least tens of kilometers across, influenced by contemporaneous volcanism and faulting (Link, 1983a; 1986; Christie-Blick, 1985).

The Pocatello Formation of southeastern Idaho and the correlative formation of Perry Canyon in Utah (Anderson, 1928; Ludlum, 1942; Trimble, 1976; Link, 1981; 1983a; 1986; 1987; Crittenden and others, 1983; Link and LeFebre, 1983; ChristieBlick, 1985) contain as much as 1,000 m of extrusive basaltic volcaniclastic rocks and poorly sorted detrital strata that include graywacke and diamictite. The base of these rocks is not exposed.

Stratigraphic and geochemical data suggest that the glacial strata accumulated in an extensional tectonic setting, probably related to the early stages of continental rifting. Abrupt vertical and lateral changes in facies, thickness, and provenance of the Pocatello Formation suggest syndepositional basement-involved faulting, although unequivocal associated Late Proterozoic faults have not been identified (Link, 1983a; 1986).

The exposed lower part of the Pocatello Formation contains mafic volcanic flows and intrusive and volcaniclastic rocks which have undergone low-grade metamorphism (Stewart, 1972; Crittenden and others, 1983; Christie-Blick, 1985; Harper and Link, 1986). Chemical analyses of the volcanic rocks indicate that they are tholeiitic and alkalic basalts. These compositions suggest within-plate tectonic settings, and are consistent with volcanism during continental rifting (Stewart, 1972; Harper and Link, 1986). The basalts of the Bannock Volcanic Member will be seen at the bottom of the hill at Portneuf Narrows (stop 5).

The glacial origin of the Late Proterozoic diamictites of northern Utah was advocated first by Blackwelder (1932). Recent studies have established four lines of evidence for glacial-marine sedimentation: (1) regional persistence, (2) inclusion of a wide variety of extrabasinal clasts, (3) a few striated clasts and dropstones, and (4) regional facies arguments which suggest both glacial and tectonically influenced sedimentation (Christie-Blick, 1983; 1985; Crittenden and others, 1983; Link and Lefebre, 1983; Link, 1983a; 1986; 1987; Christie-Blick and Levy, 1989a). Massive or crudely stratified diamictite may have been deposited from floating ice or by mass-flow processes that redistributed glacially derived debris. Many of the glacial-marine rocks are better sorted and bedded than the distinctive diamictite. Basinal facies assemblages include conglomerate, laminite with dropstones, sandstone, thin diamictite beds, and siltstone. These are interpreted to represent sediment reworked from ice-contact deposits or subaqueous glacial outwash and redeposited by turbidity currents, debris flows, and suspension fallout. The post-glacial transgression was a world-wide event that provides a stratigraphically valuable record of sea-level rise (upper member, Pocatello Formation, seen at Portneuf Narrows, stop 5, and Kelley Canyon Formation, seen at Box Elder Canyon, stop 2).

Terrigenous Detrital Succession

The terrigenous detrital succession of northern Utah and southeastern Idaho is represented by the Brigham Group, 2,000 to 4,000 m thick, composed mainly of quartzose sandstone, with subordinate conglomerate, mudstone, limestone, and volcanic rock (Fig. 3). These rocks traditionally are called "quartzite", even though metamorphic grade is usually low (lower greenschist facies or below). The stratigraphic terminology of the Brigham Group and its constituent formations is applicable through nearly 500 km, north to south, in the miogeocline (Crittenden and others, 1971; Oriel and Armstrong, 1971; Christie-Blick, 1982; Lindsey, 1982; Link and others, 1985a; 1987; Christie-Blick and others, 1988; Christie-Blick and Levy, 1989a). The Brigham Group was defined in Utah by Crittenden and others (1971), reexamined in Utah by Sorensen and Crittenden (1976b), and formally defined in Idaho by Link and others (1985a).

The Brigham Group contains mainly mineralogically and texturally mature sediment, (observed at Box Elder Canyon, stop 2, and Inkom, stop 4), deposited primarily in braided fluvial and shallow-marine environments. Offshore (substorm wavebase) facies are subordinate. Formations are regionally extensive, and exhibit gradual lateral changes in thickness and facies (Crittenden and others, 1971). Paleocurrents tend to be consistent through broad regions (Link and others, 1987).

Dominant lithologies in the Brigham Group are fine- to coarse-grained, white- to tan-colored quartz arenites and medium- to coarse-grained, red to purple, arkosic arenites that are locally conglomeratic. Siltstones are present in several parts of the group, notably in the Inkom Formation. Shale and limestone are sparse. There are discontinuous limestone and dolomite beds in the Caddy Canyon Quartzite and in the Gibson Jack Formation in the northern Bannock Range (Trimble, 1976).

The Caddy Canyon Quartzite varies in both thickness and lithology. In Idaho, the unit is generally of shallow-marine facies (Link and others, 1987) whereas in Utah, braided fluvial and braid-delta facies are dominant (Levy, 1991; Levy and Christie-Blick, 1991a). The upper part of the Caddy Canyon Quartzite and the overlying Inkom formation contain several horizons of incised channels filled with chaotic conglomerates.

Above the fine-grained Inkom Formation, the Mutual Formation and the base of the overlying Camelback Mountain Quartzite are persistently conglomeratic and feldspathic, especially in Idaho. The contact between these units is

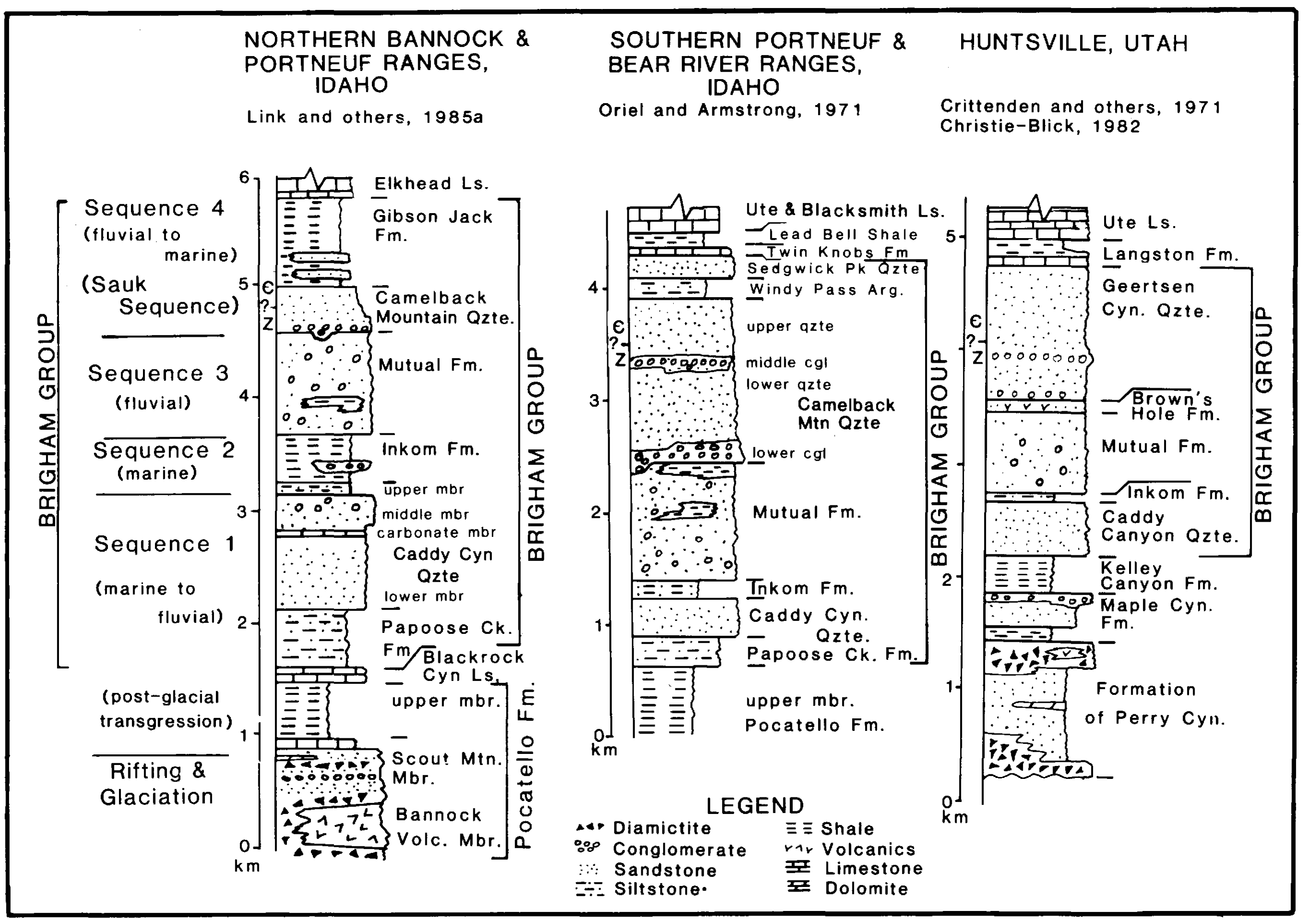

Figure 3. Correlation chart of late Proterozic rocks in southeast Idaho and northern Utah from Link and others (1987). The glacial and volcanic rocks of the Pocatello Formation will be seen at stop 4, Inkom, Idaho, and at stop 2, Box Elder Canyon. The upper Brigham Group and overlying Middle Cambrian strata will be examined at stop 3, Two Mile Canyon.

locally an incised channel, inferred to be a sequence boundary (Link and others, 1987; Christie-Blick and Levy, 1989a). Intercalated basalt lava flows and felsic tuff beds are present in the Browns Hole Formation, correlative with the upper Mutual Formation in isolated locations (Huntsville, Utah, not visited on this field trip, but see Christie-Blick and Levy, 1989a). Feldspathic sandstones are present at several stratigraphic levels (Geertsen Canyon Quartzite, visited at Box Elder Canyon, stop 2 and Mutual Formation, visited at Inkom, stop 4), which suggests influxes of detritus from newly uplifted basement source areas (Link and others, 1987; Christie-Blick and Levy, 1989a).

The terrigenous detrital succession, represented by the Brigham Group, was deposited on a broad, episodically subsiding shelf, in both marine and fluvial environments. Some workers have suggested that the entire terrigenous detrital succession accumulated as a passive-margin deposit (Stewart, 1972; Stewart and Suczek, 1977; Link and others, 1987). Later workers (Devlin and Bond, 1988; Christie-Blick and Levy, 1989) suggest that the lower part of the succession may have accumulated in an intracratonic basin, and that the passive continental margin was not established until deposition of the upper part. In either event, the final continental separation and associated tectonic subsidence occurred in latest Proterozoic time during deposition of the Brigham Group (Stewart and Suczek, 1977; Bond and others, 1983; Devlin and Bond, 1988; Lindsey and Link, 1988; Christie-Blick and Levy, 1989a).

Recently the Brigham Group has been subdivided using techniques of sequence stratigraphy that include the identification of subtle regional unconformities (depositional sequence boundaries, Fig. 4) (Vail and others, 1977; Christie-Blick and Levy, 1985; Link and others, 1987; Christie-Blick and others, 1988; Christie-Blick and Levy, 1989a; Levy and Christie-Blick, 1991a). Correlation of sequence boundaries is difficult in deformed rocks and limited exposures, but the boundaries tend to be associated with abrupt vertical changes in sedimentary facies that represent a basinward shift in depositional environment (for example, offshore, muddy marine, to braided stream, as observed in the upper part of the Caddy Canyon Quartzite at Inkom, stop 4). Where such facies discontinuities can be traced through large areas, unconformities of regional extent are indicated (Christie-Blick and others, 1988, Christie-Blick and Levy, 1989a; Levy and Christie-Blick, 1989). In Idaho and Utah at least five sequences have been inferred to date (Fig. 3). The oldest contains the glacial deposits and the youngest represents the lower part of the Cambrian-Ordovician Sauk I sequence of the craton (Sloss, 1988).

AGE AND CORRELATION

Ages

A problem central to the interpretation of both the diamictite and volcanic succession and the terrigenous detrital succession is the lack of geochronologic data for most of the rocks. The age of only the upper part of the Brigham Group is known directly. An alkali trachyte in the Brown's Hole Formation in Utah yielded an $^{40}Ar/^{39}Ar$ age of 580 Ma (recalculated by N. Christie-Blick from Crittenden and Wallace, 1973). The age of the diamictite and volcanic succession is estimated at about 750 Ma, based on a Sm/Nd date of 762 +/-44 Ma from apparently correlative mafic volcanic and diamictite-bearing strata in northeast Washington by Devlin and others (1988).

Paleontology

Although a biostratigraphic framework has been developed for terminal Proterozoic strata, the paucity of fossils in the Pocatello Formation and the Brigham group has hindered dating using these methods. The diamictite and volcanic succession is dominantly unfossiliferous, though acritarchs of apparent Vendian affinity have been found in the Mineral Fork Formation (Knoll and others, 1981). The base of the Brigham Group is also unfossiliferous, while the upper sandstones and mudstones contain Early Cambrian fauna and trace fossils (Crittenden and others, 1971; Oriel and Armstrong, 1971; Campbell, 1974; Christie-Blick, 1982; Link and others, 1987). The Brigham Group grades up into Middle Cambrian shales and limestones (exposed at the top of the traverse at Two Mile Canyon, stop 2).

Isotope Chemostratigraphy

It may be possible to correlate the Pocatello Formation and Brigham Group with other late Precambrian sequences through the use of carbon and strontium isotopes (Derry and others, 1989; Knoll and others, 1986; Magaritz and others, 1991). Although carbonates are uncommon within the Brigham Group, and are slightly metamorphosed, several horizons have been sampled, and are being isotopically analyzed (A.J. Kaufman and L.H. Smith, in prep).

Correlations Using Late Proterozoic Glaciations

Late Proterozoic glacial rocks are present worldwide (Hambrey and Harland, 1981; Harland, 1983). Although precise chronostratigraphic correlation of individual ice ages is not yet possible, their available ages cluster at approximately 940, 770, and 615 Ma (Crowell, 1983). The age of the third cluster, representing the Varanger glaciation, has been recently estimated at 610-590 Ma (Harland and others, 1990). The similarity of facies, of homotaxial relationships, and of tectonic settings of the various Late Proterozoic glaciogenic successions of the western United States suggests that they are broadly synchronous within the second (770 Ma) glacial age cluster, and implies glaciation having significant regional extent (Christie-Blick and others, 1980; Crittenden and others, 1983; Eisbacher, 1985). Evidence for several rapid sea-level changes associated with the third (Varanger) glaciation may be present in the upper Caddy Canyon Quartzite and the Inkom Formation as seen at

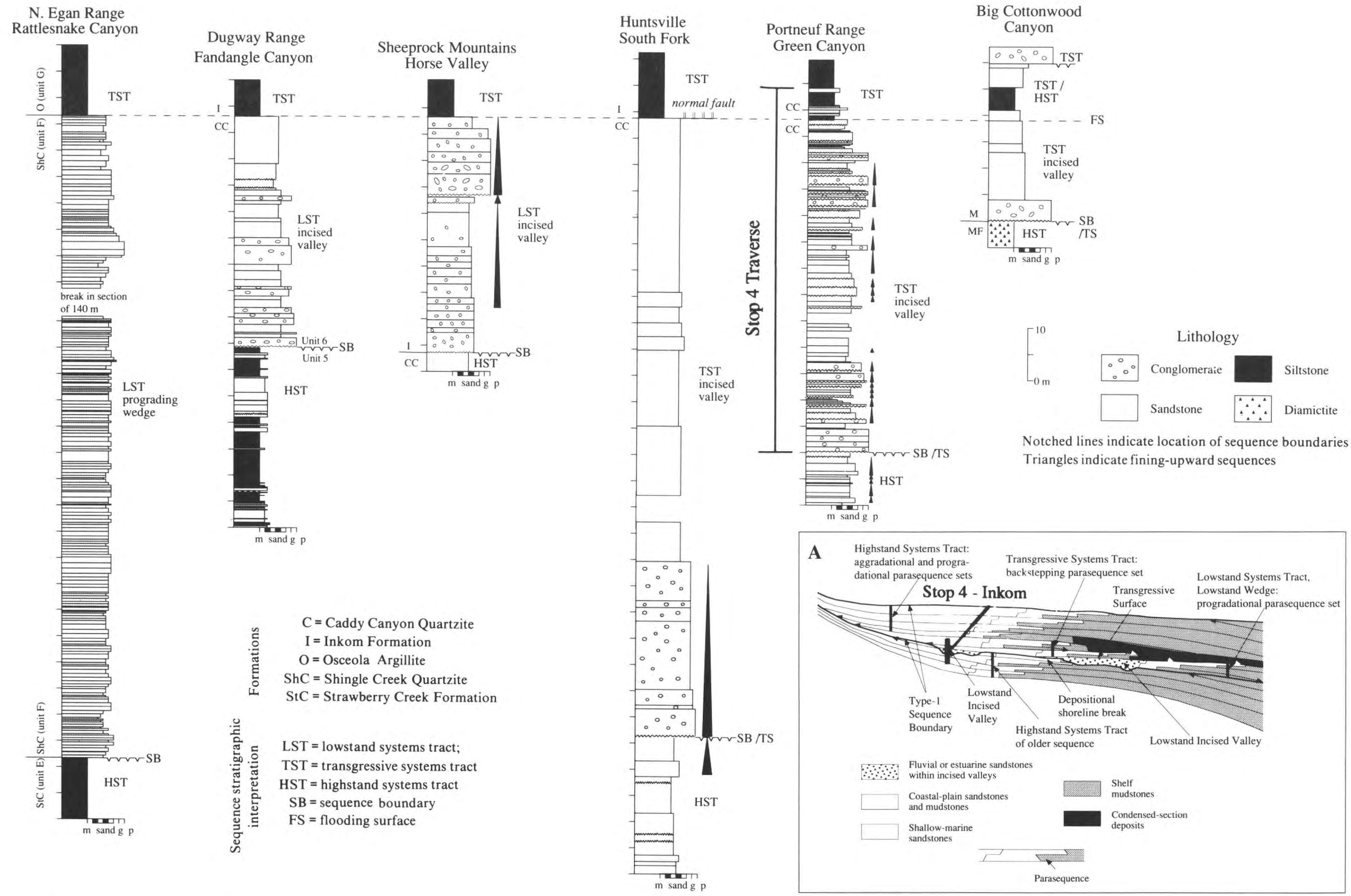

Figure 4. Stratigraphic cross-section for the sequence boundary near the top of the Caddy Canyon Quartzite from Big Cottonwood Canyon in the central Wasatch Range to the northern Egan Range in eastern Nevada. Datum is a prominent flooding surface, generally at the base of the Inkom Formation, although not necessarily the same flooding surface in each section. Stop 4 (Inkom) is just west of the Portneuf Range section, and the base of the first conglomerate at the field trip stop is the transgressive surface. The base of the green matrix-rich sandstone with contorted sandstone beds is interpreted to be a flooding surface. There are two stratigraphically higher flooding surfaces upward in the section below the Inkom formation. These parasequences may be caused by eustatic sea-level changes caused by the Varanger glaciations (Levy and others, 1991). The diagram indicates that a flooding surface may or may not be the same as the transgressive surface. Note that in different localities, different criteria have been used for defining the lithostratigraphic boundary between the Caddy Canyon Quartzite and the Inkom Formation. Sequence boundaries and flooding surfaces are interpreted on the basis of stratigraphic sedimentology, not gross lithic character, and do not necessarily coincide with formal stratigraphic units. The Egan Range section is continuous and unfaulted, and the break is shown solely for the ease of presentation. Diagram is modified from Levy (1990) and Levy and Christie-Blick (1991). Inset A: Conceptual cross sections of a basin margin with a ramp setting showing stratal geometry and system tracts within unconformity-bounded depositional sequences (modified by M. Levy from van Wagoner and others, 1990; figure is after Levy and Christie-Blick, 1991a and Levy, 1990).

Inkom, field trip stop 4 (Levy and others, 1991). The irregular pattern of incised valleys filled with sediment-gravity flow deposits in these formations suggests several periods of ravinement and drowning of incised valleys.

Analysis of Tectonic Subsidence

Atlantic-type rifted margins have characteristic subsidence curves which can be analyzed to provide the time of initiation of the subsidence, itself induced by cooling of the rifted continental crust, following the heating associated with rifting and its associated mafic magmatism. For the Cordilleran miogeocline, the age of initiation of tectonic subsidence has been calculated to be latest Proterozoic to Early Cambrian, 575 +/-25 Ma (Bond and others, 1983, 1985; Bond and Kominz, 1984; Devlin and Bond, 1988; Christie-Blick and Levy, 1989; Levy and Christie-Blick, 1991b). In Idaho and Utah, there is little evidence of synsedimentary faulting associated with the final rifting event, and the stratigraphic position of the event must be inferred from the subsidence curve analysis rather than from geologic evidence (Link and others, 1987; Christie-Blick and others, 1988; Christie-Blick and Levy, 1989c). The final rifting event that led to the Cordilleran miogeocline or passive margin is thus probably near the stratigraphic level of the Mutual Formation or Camelback Mountain Quartzite (Fig. 3).

Indeed, rocks which contain evidence for rifting (the Pocatello Formation and correlative units) apparently are 200 Ma older than the tectonic subsidence associated with the miogeocline. This apparent paradox was noted by Stewart and Suczek (1977), Stewart (1982), and Ross (1991), who proposed that the rift history was protracted. There may have been one or more early rift events, starting at about 770 Ma, that did not lead to continental separation (Devlin and Bond, 1988; Lindsey and Link, 1988; Christie-Blick and Levy, 1989a; Levy and Christie-Blick, 1991b). The Pocatello Formation and the lower portion of the Brigham Group (at least including strata below the Mutual Formation) are thus not part of the subsidence cycle that produced the early Paleozoic Cordilleran miogeocline, but were deposited in continental rift basin or intracratonic basin settings (Christie-Blick and Levy, 1989a; Levy and Christie-Blick, 1991a).

LATE PRECAMBRIAN PALEOBIOLOGY

Recent Work

Strata of Late Proterozoic age (900-570 Ma) have become the focus of recent paleobiological research due to the discovery of important fossil taxa and a reappraisal of the nature of the Cambrian explosion of Metazoans (multicellular, potentially motile, heterotrophic organisms that develop from embryos: Barnes, 1987). The Late Precambrian is no longer viewed as a monotonous, static landscape dominated by microbial mats, but rather as a time of key evolutionary innovations. It is also clear that geological, atmospheric and evolutionary events were intimately associated (Knoll 1991a, 1991b).

Ediacaran Fauna

Perhaps the most spectacular component of the Late Precambrian fossil record is the soft-bodied Ediacaran fauna. First discovered in the Adelaide Geosyncline of South Australia more than forty years ago (Sprigg, 1947), this unusual fossil assemblage has subsequently been identified from over 20 localities worldwide (Glaessner, 1984).

The Ediacaran assemblage contains numerous medusoid fossils, which may be early relatives of modern coëlenterates, however, it is better known for the more enigmatic components, such as Dickinsonia, Charnia, and Tribrachidium. There is no evidence for differentiated respiratory or digestive systems in any of these taxa, and they appear to be constructed in a manner analogous to air mattresses or quilted pneu (Seilacher, 1990). With their unique morphology, mode of construction and symmetry, these organisms seem to represent a highly successful yet short-lived (perhaps less than 20 m.y. [590-570 Ma, Harland and others, 1990]) experiment with multicellularity. Although it has been suggested that the Ediacaran fauna is not closely related to any modern taxa (Fedonkin, 1986; Seilacher, 1990), there is still great uncertainty concerning their biology, ecology and phylogeny.

Although elliptical impressions have been documented from the Late Proterozoic Inkom and Cambrian Gibson Jack formations of southeast Idaho (Jansen, 1987), it is doubtful that they are biogenic. The impressions are circular to oval in outline, range from 5 to 40 mm in diameter, and are often divided by radial lines or concentric rings. Many specimens contain central pyrite cubes, and the orientation of the discoidal impressions is frequently along cleavage planes subparallel to bedding, which suggests secondary concretionary formation. Cloud (1973) reported pseudofossils with similar morphology from the Lower Silurian Shawangunk Formation of eastern Pennsylvania. Similar specimens at large angles (20 to 30 degrees) to bedding in the Belt Supergroup also support the hypothesis that these specimens are concretionary in nature (R.J. Horodyski, personal communication, 1991).

Microbial Organisms

In contrast to our understanding of the megascopic organisms of the Late Precambrian, the knowledge of the biology and paleoecology of microbial organisms is now known at a level comparable with that of Phanerozoic communities. For example, the Draken Conglomerate Formation of Spitsbergen contains five distinct communities of microfossils which exhibit onshore-offshore trends in diversity and composition (Knoll and others, 1991). Microfossils are also being used to develop a biostratigraphic framework for the Late Precambrian (Knoll and Butterfield, 1989).

Acritarchs (organic-walled microfossils with uncertain taxonomic affiliations, but possibly related to dinoflagellates) underwent a marked increase in size, morphological complexity (spines, processes and other ornamentations; Knoll and Butterfield, 1989), and diversity during the Late Riphean and Early Vendian (Knoll, 1989). This was followed by a sharp decline in the middle to Late Vendian. It has been proposed that a mass extinction was responsible for this decline in diversity (Knoll, 1989), although conclusive evidence is lacking. The simple microfossil *Bavlinella faveolata* and simple unadorned unicells have been described from the Mineral Fork Formation of the central Wasatch Mountains southeast of Salt Lake City.

Small Shelly Fossils

Although the Precambrian-Cambrian boundary traditionally has been defined at the first appearance of skeletonized fossils (specifically trilobites), it has been realized recently that there are several "small shelly fossils" which precede this biostratigraphic datum (Signor and others, 1987; Grant, 1990; Conway Morris and others, 1990). The most widespread of these is *Cloudina,* which is now known to have global distribution (Grant, 1990, Conway-Morris and others, 1990). *Cloudina* is often found in great abundance, and may have formed small thickets. Small shelly fossils, some of which may belong to the same genus as *Cloudina* (Grant, 1990) are well known from the Deep Spring Formation of the White-Inyo mountains of eastern California and western Nevada (Signor and others, 1987; Signor and Mount, 1989).

Although the *Cloudina*-bearing strata are correlative with the Late Precambrian and Early Cambrian strata of northeastern Utah and southeastern Idaho, similar fossil taxa have not been found in this are. *Cloudina* and related taxa may become important index fossils for Ediacaran rocks, as fossils continue to be documented from additional localities and placed within the existing biostratigraphic framework of the Late Precambrian.

Biomineralization prior to the traditionally defined Precambrian-Cambrian boundary was not limited to metazoans. Carbonate crusts from the Nama Group of Namibia have been described as probable calcified metaphytes by Grant and others (1991). This discovery implies that biomineralization may have originated in diverse biological systems nearly simultaneously at the end of the Precambrian.

Ichnofossils

Ichnofossils also demonstrate an increase in the diversity of both the feeding modes which were utilized and the soft-bodied taxa which originated during the Late Precambrian. Unequivocal trace fossils are preserved in rocks containing the Ediacaran soft-bodied fossils, indicating that coelomic organisms (organisms with a body cavity and capable of making traces) were present although they were not able to secrete skeletal elements. Early trace fossils such as *Bilinichnus* and *Nenoxites* (restricted to Vendian rocks), *Nereites, Monomorphichnus,* and *Planolites* (not exclusively limited to the Vendian) are limited to the upper few millimeters below the sediment-water interface, and are relatively simple in morphology (cylindrical or rope-like tubes generally less than 3-5 mm in diameter). During the Late Vendian, trace fossils increased in size (*Didymaulichnus* can have a diameter as great as 10-12 mm), complexity of feeding strategy, and depth of bioturbation. The distinctive trace fossils *Skolithos* and *Planolites* (originating in the Vendian but abundant through the Phanerozoic) are extremely common at stop 3.

The diversity of Late Precambrian-Early Cambrian trace fossils is such that they can be used as index fossils for rocks of this age (Crimes, 1987). The degree and depth of bioturbation continue to increase through the Cambrian, as determined by simple indices of bioturbation based primarily upon the degree to which bedding is disturbed (Droser and Bottjer, 1988). The difference between Precambrian and Cambrian rocks should be clearly visible during this field trip, and it may be possible to detect trends in the depth and intensity of bioturbation upsection at Two Mile Canyon (stop 3).

Stromatolites

Contrary to the pattern of increased diversification seen in microfossils, in metazoans and in metaphyte-grade organisms (multicellular algae), stromatolites underwent a significant decline in both diversity and abundance during the latest Precambrian (Grotzinger, 1990, and references therein). Many hypotheses have been suggested to explain this decline. Until recently, the general consensus held that the evolution of complex metazoan taxa resulted in an increase in grazing on stromatolites within previously protected habitats. Grotzinger (1990) suggested that since their decline apparently preceded the evolution of grazing metazoans, it may be due to a decrease in the carbonate saturation of Proterozoic seawater, which resulted in a decrease in the ability of stromatolite-building microorganisms to secrete carbonate cements.

The only possible stromatolites known from the Pocatello Formation are in the carbonate and marble unit of the upper Scout Mountain Member (Link and LeFebre, 1983). These structures are visible at stop 5, north of the Portneuf Narrows.

The Role of Oxygen in Late Precambrian Biotic Events

Changes in the composition of the early atmosphere have long been invoked to govern the rate of Precambrian biological evolution (Nursall, 1959; Cloud, 1968; Runnegar, 1982). Early theories suggested that increases in the partial pressure of oxygen (pO_2) reduced the amount of ultraviolet radiation penetrating to the Earth. Recent work (Kasting, 1987) has shown that the bulk of ultraviolet radiation is filtered out by the atmosphere at pO_2 levels attained by the Middle Proterozoic (approximately 1600 Ma). However, new biogeo-chemical models suggest that oxygen may still have played a pivotal role in the evolution of Precambrian life.

Although it is difficult to place absolute values on oxygen levels during the Late Proterozoic, there are several lines of evidence that suggest significant increases during the Late Riphean. Increases in the rate of burial of organic carbon, as implied by the carbon-isotope record, suggest significant increases in pO_2 (Knoll 1991a; Knoll and others, 1986; Kaufman and others, 1991). The sharp rise in the strontium $^{87}Sr/^{86}Sr$ ratio from sea water in Vendian time, which implies that increased rates of erosion of continental rocks allowed the permanent burial of organic carbon (Knoll, 1991a, 1991b; Derry and others, in press), also suggests that oxygen levels increased during this time. This rise is inferred to have occurred immediately after the Varanger glaciation, just prior to the appearance of abundant, large Ediacaran taxa.

Increases in ambient oxygen concentrations would have allowed Ediacaran organisms to overcome limits to rates of oxygen supply to cells that were imposed by the slow rate of diffusion, without the organisms having to construct complex respiratory systems. For example, Runnegar (1982) has calculated that *Dickinsonia* could have satisfied its oxygen requirements through diffusion alone at oxygen levels 6% to 10% of present atmospheric levels. Increases in oxygen concentration also have enabled single-celled organisms (such as the morphologically complex Late Vendian acritarchs) to attain a large size in spite of the constraints on rates of transport by diffusion. It seems reasonable to hypothesize that increases in body size facilitated the evolution of complex internal structures. In this framework, increases in the oxygen content of the Late Precambrian atmosphere are seen as the key to the explosion of animal taxa characteristic of the Phanerozoic world.

CONCLUSIONS

The Late Precambrian world can no longer be viewed as static and monotonous, but must be understood as dynamic and complex. Our understanding of the tectonic events and their implications for ocean circulation patterns, geochemical cycling and climate change has increased greatly. In turn, it must be realized that these facets of the Late Precambrian world impinged directly upon biotic events. Knowledge of the basin scale processes, such as those occurring in the Pocatello Formation and the Brigham Group, can be used to corroborate global trends and events.

ACKNOWLEDGMENTS

This research was supported by the Kackley Family Endowment to Idaho State University, the Idaho Initiative project of the Idaho Geological Survey, and a Paleontological Society/ Margaret C. Wray Trust grant to LHS. We especially thank Marjorie Levy for permission to use Figure 4. Nicholas Christie-Blick has been a source of insight for both of us. Jay Kaufman and Nan Arens read the manuscript and made many useful suggestions. Minos and Blue (complex, [semi]-motile quadrupedal metazoans) were faithful companions through the development of this manuscript.

DESCRIPTION OF FIELD TRIP STOPS

Mile

0.0 Field trip starts at intersection of 12th Street and Interstate highway I-15 in Ogden, Utah. Head north on I-15.

The view to the east and north is of the front of the Wasatch Range, exposed by the Neogene Wasatch fault system (Machette and others, 1991). The west face of the range north of Pleasant View contains at the base, Early Proterozoic basement of the Farmington Canyon Complex (Bryant, 1984). The striking pink-colored cliff above the Farmington Canyon Complex is the Cambrian Tintic Quartzite, the lithostratigraphic equivalent of the upper Brigham Group (Crittenden, 1972; Crittenden and others, 1973). Cambrian limestones and shales lie above the Tintic.

Structurally above these cratonal-facies strata is the Willard thrust, which carries allochthonous miogeoclinal facies strata of the Late Proterozoic formation of Perry Canyon and Brigham Group. A series of thrust-bounded duplexes are present below the Willard thrust below Ben Lomond Peak, and in the west-facing slopes of the Wasatch Range south to Weber State University in South Ogden (Bruhn and Beck, 1981; Schirmer, 1985, 1988).

The area near Huntsville, reached by going east up the Ogden River, contains the best exposures of the Brigham Group in northern Utah (Crittenden and others, 1971; Sorensen and Crittenden, 1979). The field trip guidebook edited by Christie-Blick and Levy (1989a) contains descriptions of stops near Huntsville, as well as an excellent summary of the Late Proterozoic strata of the western Cordillera.

4.6. Prominent shorelines of Lake Bonneville are visible on the Pleasant View salient.

12.5. Willard Exit (exit 360) Utah Highway 315. Take northbound exit.

13. **FIELD TRIP STOP 1.** Pull off for view to the east of the Willard thrust.

This field trip stop sets the structural background for the rest of the field trip. The following description is condensed from Link and others (1985b). We are looking east at Willard Canyon. The Willard thrust is located just above the thick trees on the south wall of the canyon (Sorensen and Crittenden 1972; Sorensen and Crittenden, 1976a). It places Early Proterozoic Facer Formation and the overlying Huntsville sequence (formation of Perry Canyon and Brigham Group) over Early Proterozoic-Archean Farmington Canyon Complex, the nonconformably overlying pink cliff of Cambrian Tintic Quartzite and Cambrian Maxfield Limestone, poorly exposed in the trees (Yonkee and others, 1989). As interpreted by Schirmer (1985, 1988) the Willard thrust system here is dipping northward off a lateral ramp in the Farmington Canyon Complex below.

The front of the Wasatch Range here contains a complex of landslides and rotational slump features, formed along the trace of the Brigham City segment of the Wasatch fault (Machette and others, 1991). Mass movements on this mountain front, generally triggered by spring runoff, periodically disrupt activities in the fruit orchards and suburban homes of Willard and Perry.

We will be spending the day in the lower part of the Willard thrust sheet, which extends north from here along the Wasatch front to the Snake River Plain, a distance of 130 miles (210 km).

Continue north on I-15. Excellent shorelines of Lake Bonneville are exposed on the Wasatch front from Willard north to Brigham City (Fig. 10).

Mile 16.2. Perry Canyon is directly east (Fig. 10). It is a good place to examine the formation of Perry Canyon (Sorensen and Crittenden, 1976b; Crittenden and others, 1983). A field trip stop here is described in Link and Lefebre (1983).

Mile 17.4. Take exit 364, US Highway 89 and 91 north to Brigham City and Logan. Box Elder Canyon (Fig. 10) is directly east of Brigham City, and will be the site of stop 2. It is generally the type area of the Brigham Quartzite of Walcott (1908), though it contains a gently east-dipping fault which cuts the section (Sorensen and Crittenden, 1976a; 1976b).

Mile 19.3. Stop light. Go straight at intersection with Main Street, Brigham City.

We are entering Box Elder Canyon. Several stops are possible here, depending on time and interest. The stops are designated 2a, 2b, 2c, and 2d.

Mile 22.0. **FIELD TRIP STOP 2a:** BOX ELDER CANYON-KELLEY CANYON FORMATION. Figure 5 contains a geologic map of this area.

Pull out on right. Black argillite on the north side of the highway is the Late Proterozoic Kelley Canyon Formation. The rock is laminated, black, pyritic, orange-brown weathering shale and argillite. The tightly folded rock is cut by a feldspar-porphyritic lamprophyre dike of unknown age (Sorensen and Crittenden, 1976a).

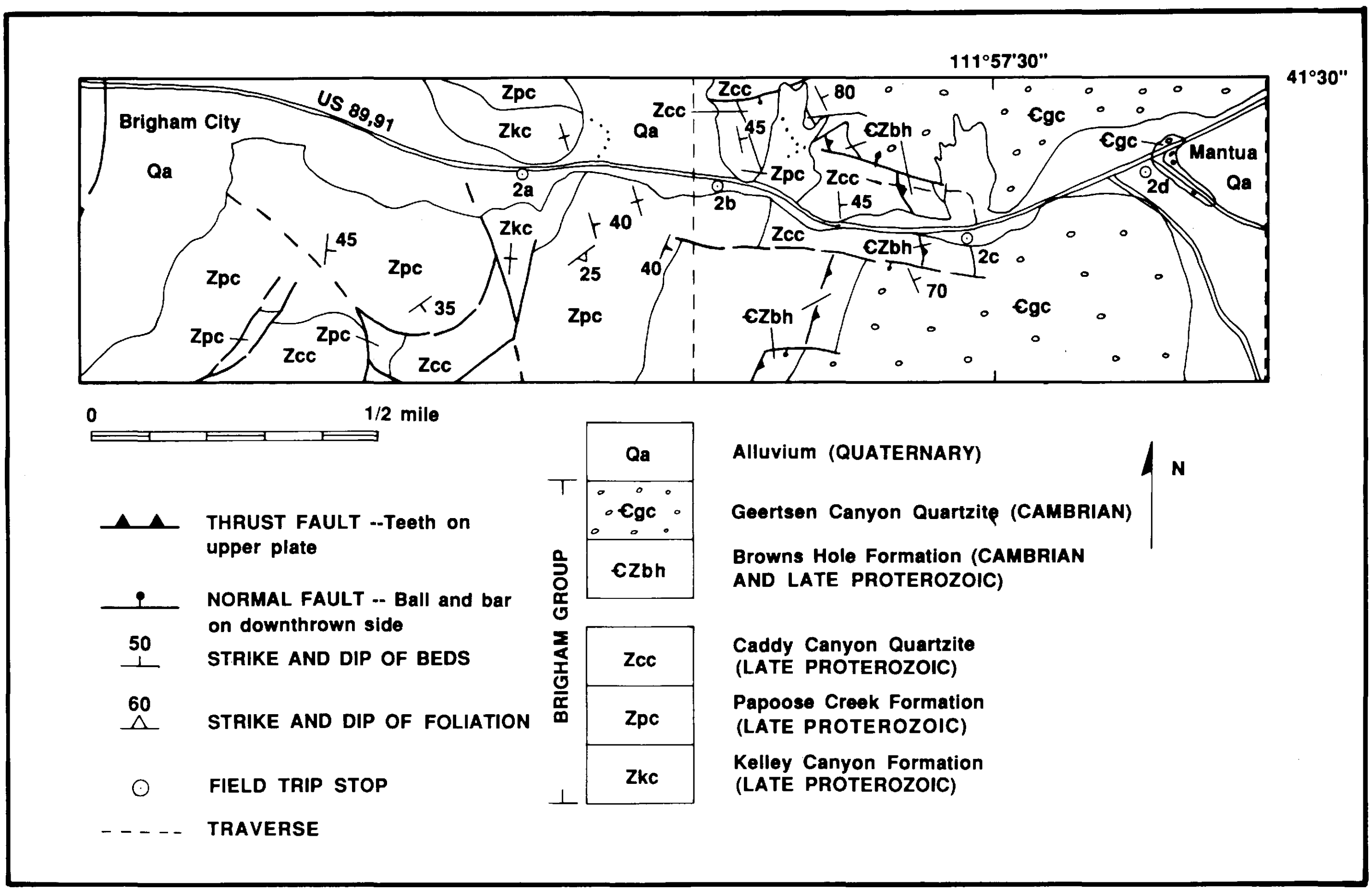

Figure 5. Geologic map of Box Elder Canyon and field trip stop 2. The traverse described in the text starts at stop 2C. Map is redrawn from Sorensen and Crittenden, 1976a.

22.4 National Forest Boundary, welcome to the Cache National Forest.

22.7. **FIELD TRIP STOP 2b:** PAPOOSE CREEK FORMATION. Stop on right at outcrop of Papoose Creek Formation. A cliff containing a shear zone cutting the Papoose Creek Formation is exposed south of the creek. At this locality, a boulder on the north side of the road displays fine-grained sandstone dikelets intruding intercalated siltite which characterize the Papoose Creek Formation from here to the Pocatello area.

23.0. **FIELD TRIP STOP 2c:** GEERTSEN CANYON QUARTZITE, BROWNS HOLE FORMATION, BOX ELDER THRUST, AND CADDY CANYON QUARTZITE. Park on south side of highway and climb ridge north of the road to the gravel road (aqueduct service road) about 200 feet above the highway. Here, away from roaring trucks and lumbering Winnebagos are excellent exposures of the Geertsen Canyon Quartzite, the Browns Hole Formation, the Box Elder thrust, and the Caddy Canyon Quartzite. Walking down section, to the west, the medium bedded Geertsen Canyon Quartzite contains planar beds typical of marine depositional facies (Fig. 6).

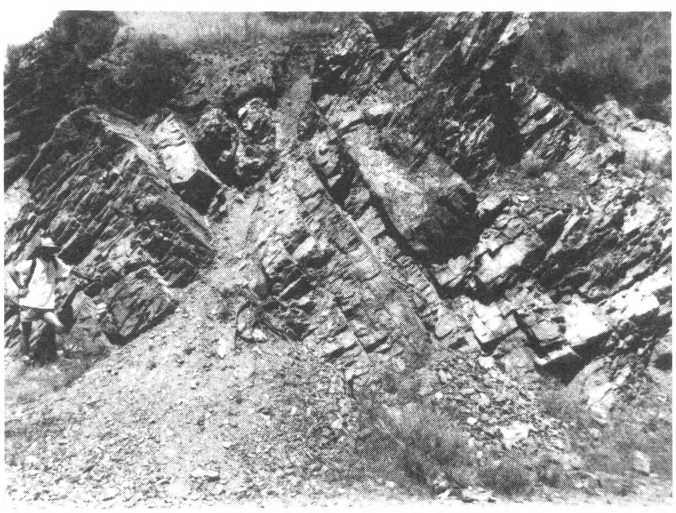

Figure 6. The Geertsen Canyon Quartzite exposed by the aqueduct service road at stop 2c, showing planar medium to thick beds typical of marine depositional facies.

The underlying Browns Hole Formation (Fig. 7) is distinctly trough cross bedded, pebbly, coarse-grained sandstone or quartzite. Near Huntsville the Browns Hole Formation contains tuff and tuffaceous conglomerate (Crittenden and others, 1976a; Christie-Blick and Levy, 1989a). The Browns Hole Formation lies unconformably on the Mutual Formation, and represents the base of

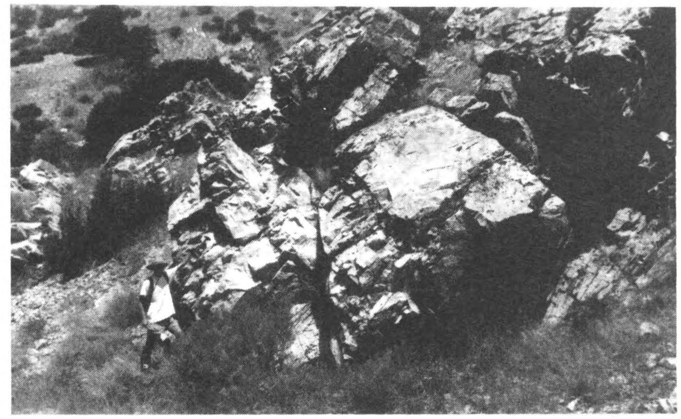

Figure 7. Trough cross bedded, pebbly, coarse-grained sandstone or quartzite of the Browns Hole Formaiton, interpreted as fluvial facies. The photograph is taken along the aqueduct service road, stop 2c.

the fourth stratigraphic sequence of the Brigham Group (Fig. 3). In Idaho, the basal Camelback Mountain Quartzite, which locally occupies incised channels in the underlying Mutual Formation, is equivalent to the Browns Hole Formation.

The Box Elder thrust of Sorensen and Crittenden (1976a) is well-exposed where a sharp bedding discordance separates chloritic, medium- to-coarse grained sandstone of the Caddy Canyon Quartzite below, from trough cross-bedded Browns Hole Formation above (Fig. 8). The Caddy Canyon Quartzite contains distinctive green silty partings and thin beds (Fig. 9). The Inkom Formation and overlying Mutual Formation are eliminated along this fault, which has normal separation. The general pattern in the Wasatch and Bannock Ranges is for faults which dip at shallow angles to eliminate stratigraphic section. These faults have been interpreted as both

Figure 8. The Box Elder thrust at stop 2c along the aqueduct service road in Box Elder Canyon, with the Browns Hole Formation faulted above the Caddy Canyon Quartzite.

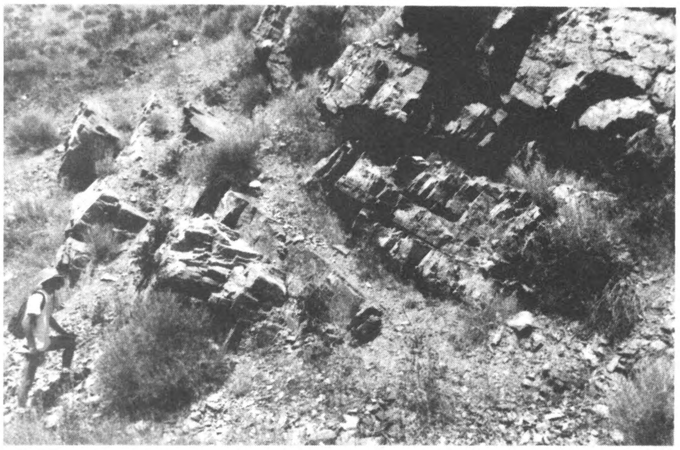

Figure 9. The Caddy Canyon Quartzite along aqueduct service road at Box Elder Canyon (stop 2c), with silty partings and thin beds.

younger-on-older Mesozoic decollement (thrust) faults, or as normal faults of probable Neogene age (Allmendinger and Jordan, 1981; Link, 1982; Link and others, 1985a; Burgel and others, 1987).

23.4. **FIELD TRIP STOP 2D:** GEERTSEN CANYON QUARTZITE. Beyond Cache National Forest sign, cross Box Elder Creek. Pebbly sandstone or quartzite of the Geertsen Canyon Quartzite (Fig. 6) is exposed on the south side of the road. Quartz pebbles reach 1 cm in diameter. This is typical of the base of the Geertsen Canyon, and of the correlative Camelback Mountain Quartzite in Idaho.

Return to Brigham City and I-15, northbound.

29.4 enter freeway, northbound.

As we drive north on I-15, the Wellsville Mountains are east of the highway (Fig. 10) and the Blue Spring Hills and West Hills are west of the road (Fig. 10). Shorelines of Lake Bonneville are prominent on both sides of the valley. The Wellsville Mountains contain a complete Late Proterozoic and Paleozoic stratigraphic section. The quartzites of the Brigham Group are present at the base of the range. They are overlain by Cambrian and Ordovician limestone with minor shale and quartzite. The Silurian and Devonian strata are mainly dolomites. Mississippian limestones are present near the top of the range, with sandy Pennsylvanian and Permian Oquirrh Formation at the summit (Doelling, 1980; Link and others, 1985; Oviatt, 1986a).

The West Hills, to the west of the highway, are a southern extension of Samaria Mountain in Idaho, and contain mainly upper Paleozoic strata (Beus, 1968; Platt, 1977).

52.1. Riverdale-Logan exit, Utah Highway 30. Cutler Dam is visible to the east. This was the location where water from the main body of Lake Bonneville spilled eastward into Cache Valley during the Lake Bonneville overflow (Oviatt, 1986b). The outlet for the Lake Bonneville flood was at Red Rock Pass on the north end of Cache Valley.

59.3. Exit 394, Plymouth, Utah 13 South. The Malad Range is east of the road. It contains east-dipping strata, mainly of Cambrian age, and overlying lower Paleozoic limestone. The high point is Gunsight Peak, underlain by Silurian Laketown Dolomite (Doelling, 1980).

67.9. Welcome to Idaho. Samaria Mountain is west of the Malad Valley, west of the highway.

80.2 Take exit 13, Malad City, Highway 38; turn left under freeway and continue west into Malad on 50 South St.

80.7 Turn left on South Main street, heading south.

82.3 Turn left on Two Mile Road, heading east toward the Malad Range. Cross under freeway.

83.9 **FIELD TRIP STOP 3:** TWO MILE CANYON. Stop at small quarry on north side of road. This is the Two Mile Canyon section of the top of the Brigham Group and base of the overlying fossiliferous Lower Middle Cambrian limestones studied by Resser (1939a; 1939b) Oriel and Armstrong (1971), and Campbell (1974).

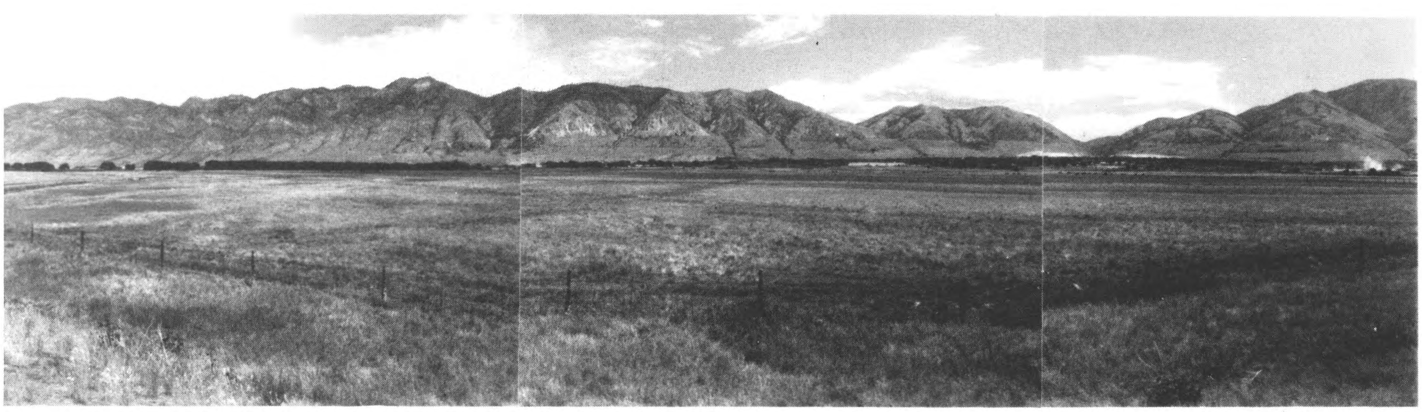

Figure 10. Composite photograph of the front of the Wasatch Range, looking east from Interstate I-15 west of Brigham City. From right (south) to left, the prominent topographic features are Perry Canyon, Box Elder Canyon, with prominent terraces of Lake Bonneville deposits below and to the north of it, and the long ridge of Wellsville Mountain, which contains a gently northeast-dipping succession of Late Proterozoic to Permian rocks.

Through examination of the trilobites found at this locality and at Antimony Canyon, near Brigham City Utah, Campbell (1974) developed a detailed biostratigraphic zonation for the strata exposed at this locality. Faunules (informal biologic units within each zone) are strongly facies dependant, somewhat complicating the precision of biostratigraphic correlations.

In a climb of about 1,000 feet up the ridge, starting about 100 m north of the quarry, the upper part of the Brigham Group (including rocks correlated with the Camelback Mountain Quartzite, Windy Pass Argillite, and Sedgwick Peak Quartzite) is very well exposed. These units were discussed as members of the Brigham Quartzite (of formation rank) by Oriel and Armstrong (1971). Link and others (1985a) formally changed the Brigham Quartzite to Brigham Group in Idaho, thus elevating these three members to formation rank (Fig. 3).

The strata at the base of the hill belong to the Camelback Mountain Quartzite (equivalent to the Kasiska Quartzite Member of the Brigham Quartzite of Oriel and Armstrong, 1971). The lowest exposed beds are tan and maroon, poorly sorted, pebbly coarse sandstone with planar cross beds and wedge bed geometry. They are interbedded with fissile, green, micaceous siltite containing abundant *Skolithos* and *Planolites* trace fossils.

The upper part of the quartzite section (Windy Pass Argillite) contains more siltstone and is thinner- and more even-bedded (Fig. 11). The rock is a green (glauconitic?) and maroon sandstone, with thin shale beds. The uppermost quartzite bed is included in the Sedgwick Peak Quartzite. The upper part of the Brigham Group contains both the *Olenellus* and *Plagiura-Kochaspis* biostratigraphic zones, which would indicate that the Lower Cambrian-Middle Cambrian boundary lies between 210 and 430 feet above the base of the section, within the uppermost Brigham Group strata (Campbell, 1974).

Figure 11. The Windy Pass Argillite at Two Mile Canyon showing interbedded siltstone and medium-grained sandstone. The siltstone beds contain abundant ichnofossils.

The top of the Brigham Group is placed at the first mappable limestone above the dominantly quartzite section. At this location there are about 30 m of dark gray bioclastic micrite of the Twin Knobs Formation of Oriel and Armstrong (1971), (formerly included in the Langston Formation by Resser, 1939b).

The Twin Knobs Formation contains a high diversity of trilobites, with low abundances of most taxa (Campbell, 1974). Although the majority of fossils found are sponge spicules and disarticulated trilobite exuviae, complete specimens are not uncommon. Inarticulate brachiopods are also abundant, but have not been studied in detail. Over 50 species of trilobites have been found at this locality, limited primarily to the sandstone and limestone units lower in the section, and the uppermost limestone unit. The most common genus is *Albertella*, defining a zone which contains several distinct faunules.

Gray platy limy shale or siltstone with sponge spicules and trilobite spines overlies the Twin Knobs Formation. It was included in the Spence Shale Member of the Ute Limestone by Resser (1939b), and in the Lead Bell Shale by Oriel and Armstrong (1971). The upper part of the Lead Bell Shale contains red-weathering dolomite containing cross bedding. Red- and gray-weathering, silty mottled limestone of the Bancroft Limestone of Oriel and Armstrong (1971) overlies the shale and continues to the top of the hill. This is typical of bioturbated limestone of the Blacksmith Limestone to the east and north (Oriel and Platt, 1980).

Drive back to Malad City and to Freeway.

85.5. Turn right on South Main.

87.1. Turn right on 50 S Street.

87.6. Enter I-15 Northbound.

91.2. Preston exit, Idaho 36, exit 17. Oxford Mountain is east of the highway. The summit ridge is composed of Camelback Mountain Quartzite. The area, which contains younger-on-older faults with shallow dip, was mapped by Link (1983a; 1983b).

92.7. Level of Bonneville shoreline.

96.1. Devil Creek Reservoir Exit, exit 22. The white rock on the east side of the highway is rhyolitic tuff of the Miocene and Pliocene Salt Lake Formation (Starlight Formation). It was erupted from vents to the north and west, and is a product of the passage of the Snake River Plain-Yellowstone hot spot.

99.2. Malad Summit. The rocks at the summit are much-faulted Ordovician and Cambrian limestone and quartzite. Here the highway crosses over the Bannock Range. Elkhorn Peak is to the west, and Oxford Peak to the east. Marsh Valley is to the north, with the Portneuf Range behind. The

Portneuf Range contains east-dipping Late Proterozoic and lower Paleozoic strata, and is bounded on the west side by a normal fault, similar to the other ranges is the area.

101.6. Freeway passes over Marsh Valley road. The flat-topped peak in the Portneuf Range to the north is Haystack Mountain. Mt. Bonneville is the peak just north of it. To the northwest is the Bannock Range; the prominent summit is Old Tom Mountain, underlain by east-dipping strata of the Brigham Group. The Pocatello Range, which forms the country north of the Portneuf River, lies to the north-northwest.

104.2 Woodland Road, crossing path of Lake Bonneville flood.

105.3. Exit 31, Idaho Highway 40 to Downey and Preston. To the west is Wakley Peak of the Bannock Range. Hawkins Basin, one of the Miocene-Pliocene eruptive centers, lies to the west (Carlson, 1968).

110.3. Exit 36, to Virginia. Garden Creek Gap, a superposed stream canyon cut across the Bannock Range (Ore, 1982) can be seen to the west. Garden Creek Gap contains east-dipping pebbly quartzites of the Scout Mountain Member of the Pocatello Formation (Platt, 1985; Thompson, 1982). A field trip stop in Garden Creek Gap is described in Link and Lefebre (1983).

112.4. Gravel bars north of here were deposited by the Lake Bonneville flood.

113.1. The right of way for the Utah and Northern Railroad (narrow-gauge) railroad crosses the highway here. The railroad was built in 1878 along Marsh Creek to the west, in an area prone to flooding (Albi and others, 1981). The route was abandoned in 1881 after broad-gauge track was built on higher ground on the present right-of-way of the Union Pacific Railroad (Oregon Short Line), which follows the Portneuf River on the east side of Marsh Valley. The narrow-gauge railroad had been started northward from Brigham City, Utah, in 1871 by interests associated with the Mormon Church (and named the "Utah Northern Railway Company"). Construction only reached Franklin, sixty-one miles away, on the Idaho-Utah border, before funding became short. The initial owners suffered bankruptcy, and the railroad was purchased and its name modified to "Utah and Northern Railroad Company" in 1877 by Jay Gould and interests associated with the Oregon Short Line. Construction was immediately started northward toward Pocatello (Albi and others, 1981).

114.9. Exit 40 to Arimo. The Utah and Northern Railroad station of Oneida was located on the longitudinal bar left by the Lake Bonneville flood, east of Marsh Creek, to the west of the highway. Garden Creek Gap may be reached by driving west from Arimo.

117.7. The basalt of Portneuf Valley is present on both sides of the road. This basalt was erupted from source vents in Gem Valley east of the Portneuf Range and flowed down the course of the ancestral Bear River (now the Portneuf River) about 600,000 years ago (K-Ar date of 0.583 +/-0.104 Ma; Scott and others, 1982).

121.5. US Highway 30 exit to Lava Hot Springs and Soda Springs. Link and others (1985b) describe the geology along this highway. North of here the freeway travels along the basalt of Portneuf Valley, which forms high ground in the middle of Marsh Valley. This is an example of inverted topography, with the Portneuf River forced to the east side of the valley and Marsh Creek occupying the west side of the valley. The lava flow, which flowed along low ground of the original river channel, occupies the center of the valley.

129.2. The highway slopes downward off the lava flow just south of Inkom. Cambrian Elkhead Limestone forms the hill directly east of the road, and is quarried west of the road at Idaho's only cement plant, in Inkom.

130.2 Boulders deposited during the Lake Bonneville flood form a longitudinal bar east of the road. The highway and river here bend to the west, and cross the Bannock Range via Inkom, Blackrock and Portneuf Narrows. This canyon affords easy access to the entire Late Proterozoic section of the Willard thrust sheet.

131.0. Exit 57, Inkom, exit to the right and go under the freeway.

132.0. Turn right, north, on Main street.

132.3. Cross under freeway and stop for **FIELD TRIP STOP 4.** Our traverse involves climbing the steep hill to the north, below the concrete "I" (Fig. 12 and 13).

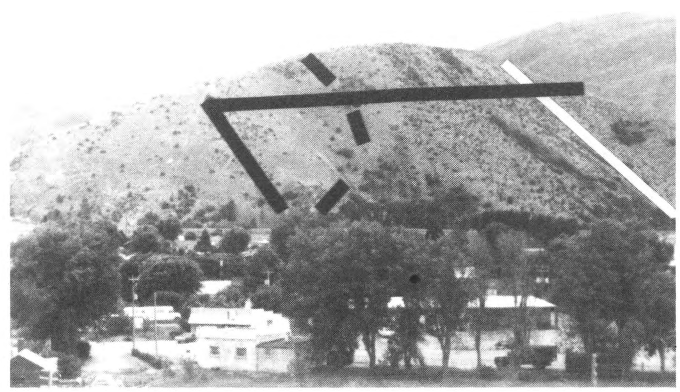

Figure 12. View of field trip stop 4 at Inkom, looking north from south of the Portneuf River. Solid black line — traverse; dashed black line — fold; solid white line — contact between the Caddy Canyon Quartzite (to the left) and the Inkom Formation (to the right).

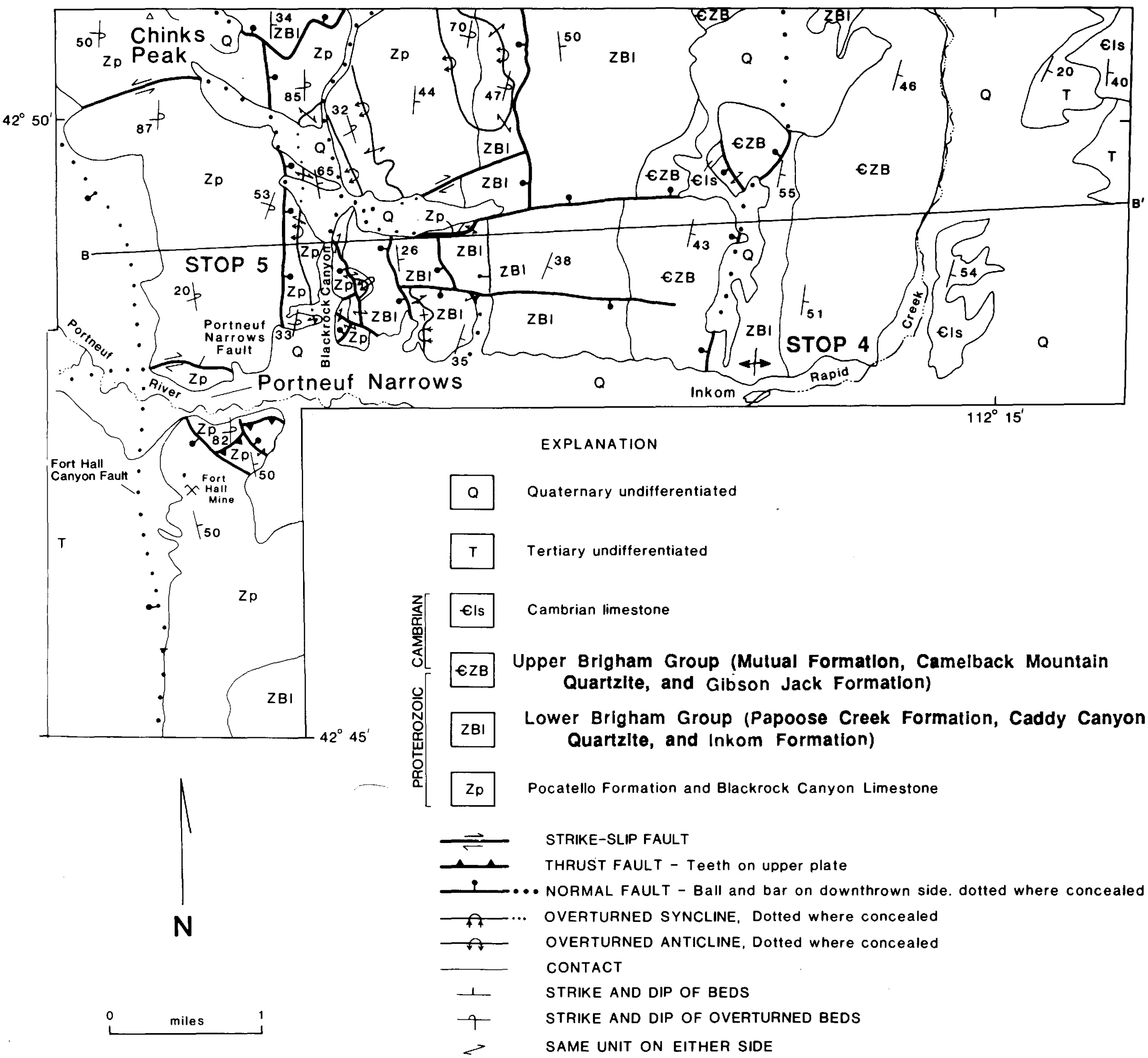

Figure 13. Geologic map of Inkom-Portneuf Narrows area east of Pocatello, Idaho, showing locations of field trip stops 4 and 5. Line of cross section (Fig. 14) is shown. Map is modified from Burgel and others, 1987.

The Brigham Group here is folded into reclined folds with shallowly west-dipping axial planes (Fig. 14). At the base of the hill strata dip west, overturned, but at the level of the "I", beds dip steeply east, right-side up. Climb up to the ridge west of the "I" and traverse eastward, up section, through the upper part of the Caddy Canyon Quartzite and Inkom Formation (Fig. 3, Fig. 12).

This traverse demonstrates the sedimentary facies of the Brigham Group across a stratigraphic sequence boundary in the upper Caddy Canyon Quartzite (shown regionally on figure 4) On that figure, our traverse is near the column shown for Green Canyon. On the west end of the traverse are granule-bearing coarse sandstones containing planar and trough cross beds, interpreted as braided fluvial and shallow marine facies. They are overlain abruptly by a disorganized, channelized conglomerate or diamictite containing both pebble-sized clasts of vein quartz and soft-sediment clasts of fine grained sandstone and siltstone to 1 m in length, in a matrix of maroon-colored siltstone and fine-grained sandstone. The base of this conglomerate is interpreted as the transgressive surface (Fig. 4). This conglomerate becomes finer grained upward over 3 m to a medium- to coarse-grained sandstone. A second

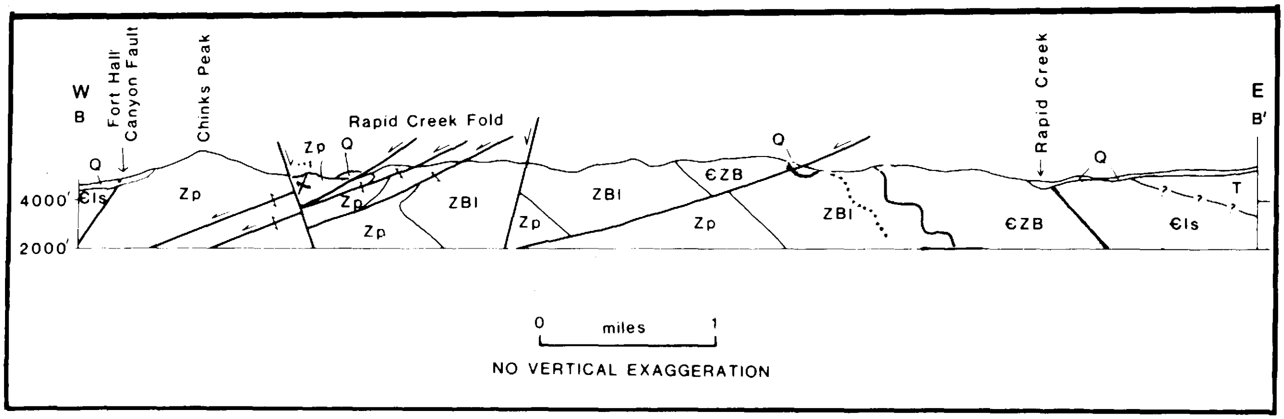

Figure 14. Cross section B-B′ from geologic map of Figure 13, after Burgel and others, 1987. Symbols are the same as in Figure 13. Geologic position of field trip stop 4 is west of the folded beds west of Rapid Creek. Geologic position of field trip stop 5 is on the east slope of Chinks Peak near the west end of the section.

conglomerate is present above, which also becomes finer-grained upward to an abrupt contact with greenish-brown, matrix-rich, medium-grained sandstone with contorted rip-up clasts. This sandstone is interpreted as an outer shelf or slope facies, as opposed to the pink, coarse-grained sandstones below, because of the darker color, prevalence of high matrix content, and presence of contorted sandstone and mudstone clasts. The contact between this sandstone and the underlying conglomerate is interpreted to be a flooding surface.

Stratigraphically higher is another cycle of conglomerate overlain by laminated green siltite and argillite of the Inkom Formation, interpreted as an outer shelf or basin deposit. These eustatic cycles may be related to sea-level changes associated with the Varanger glaciation (ca 590-610 Ma, Krogh and others, 1988; Kaye and Zartman, 1985; Harland and others, 1990) evidence for which is present in broadly correlative strata from northwestern Canada (Aitken, 1991; see discussion above).

Return to vehicles and proceed back to U.S. highway 30 in Inkom.

132.7. Turn right on Highway 30.

133.2. Turn left on Grant Avenue, a frontage road on the south side of the freeway. We are proceeding down section in the Brigham Group.

134.5. Rest area and weigh station is to the north. Brown cliff at the east end of the rest area is dolomite of the Caddy Canyon Quartzite, a marker bed in the middle of the formation.

135.4. Lower contact of the Caddy Canyon Quartzite and upper contact of the Papoose Creek Formation crop out to the north, as the road descends the hill.

136.1. Top of Blackrock Canyon Limestone crops out on the right.

137.2. Ski View Drive. Folded upper member of the Pocatello Formation crops out on the right.

137.4 Blackrock Canyon road. Turn right. Pass under I-15.

137.7. Take immediate left after crossing under freeway. continue to end of dirt road.

138.0. Pull out on left for **FIELD TRIP STOP 5, POCATELLO FORMATION.** This description is modified from Link (1987) and Christie-Blick and Levy (1989a).

The purpose of this stop is to examine the transition from glacial-marine to post-glacial sedimentation in a structurally overturned block of Pocatello Formation in the Pocatello Range (Crittenden and others, 1971; Trimble, 1976; Link, 1983a, 1987; Link and LeFebre, 1983).

This stop consists of a traverse, down stratigraphic section, from phyllite and siltstone of the upper member of the Pocatello Formation to diamictite of the underlying Scout Mountain Member. At the start of the traverse, we shall briefly examine an outcrop of the Bannock Volcanic Member of the Pocatello Formation. This unit, which interfingers with and underlies diamictite in the Pocatello area, is of tholeiitic to alkalic affinity, and represents important evidence for Late Proterozoic continental rifting at about 770 Ma (Harper and Link, 1986).

Portneuf Narrows is a deep valley occupied by the Portneuf River between the Bannock Range to the south and Pocatello Range to the north, and is located approximately 5 km (3 miles) southeast of Pocatello. The geological structure is dominated by a large-scale east-vergent fold, the Rapid Creek fold of Burgel and others (1987), located in the upper plate of the Putnam thrust. The fold is disrupted by a Mesozoic tear fault (the Portneuf Narrows fault, Fig. 13) that separates overturned beds north of the Narrows from upright beds to the south (Link and Lefebre, 1983; Burgel and others, 1987).

Portneuf Narrows is thought to have been cut during the last few million years by the ancestral Bear River before that river was diverted southward into the Lake Bonneville basin (Ore, 1982). The valley is floored by the late Pleistocene basalt of Portneuf Valley (Trimble, 1976; Scott and others, 1982). About 14,500 years ago, a catastrophic failure of an alluvial dam at Red Rock Pass, about 65 km (40 miles) to the south, resulted in the lowering of Lake Bonneville by at least 100 m (300 ft) and a discharge through the Narrows that was capable of moving boulders as large as 3.5 m (12 ft) in diameter (Currey and others, 1984; Bright and Ore, 1987).

Siltstones of the upper member of the Pocatello Formation are exposed near the parking area and in the bottom of the canyon. They are tightly folded and display a phyllitic cleavage, which is itself deformed into kink bands (Link and LeFebre, 1983).

From the parking area, continue more or less due westward uphill and down section (Fig. 15). The elevation gain to the ridge top is about 400 m (1300 ft). Note that most of the prominent gullies contain small faults (Fig. 13).

The contact between the upper member and the Scout Mountain Member of the Pocatello Formation is marked by a prominent white carbonate and marble marker unit, which appears to grade stratigraphically upward into siltstones of the upper member.

These carbonate rocks rest with sharp contact on an upward-fining assemblage of fine- to very fine-grained sandstone and shale which contains abundant structurally overturned sedimentary structures. These include scours, load structures, normal grading, current ripples (some resembling flaser bedding), parallel laminae, convolute laminae, and water-escape structures. The sandstone and shale grade downward into poorly stratified feldspathic coarse- to fine-grained sandstone that forms the prominent brown cliff near the top of the hill. Sedimentary features of this unit are minor erosion surfaces, load structures and possible flute marks, diffuse parallel laminae and parting lineation, possible dish structures, and in places, large-scale cross-stratification. The sandstone gradationally overlies pink dolomite-chip breccia with a sandy matrix. Intact dolomite is not observed in this section, but is present at the same stratigraphic level in the area south of Portneuf Narrows. However, dolomite breccia can be found along the contact.

The top of the hill is underlain by poorly stratified black sandy diamictite containing pebbles and

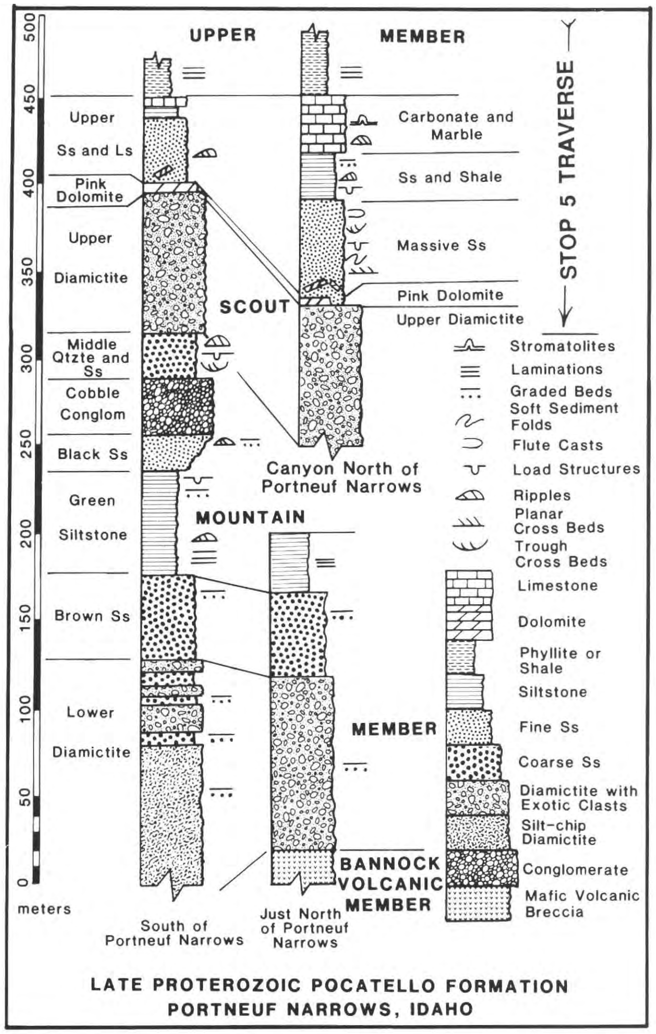

Figure 15. Stratigraphic column of the Late Proterozoic Pocatello Formation near Portneuf Narrows, Bannock County, Idaho. Field trip traverse is shown, in upside down beds. After Link, 1987 and Christie-Blick and Levy, 1989a.

cobbles of quartzite, granitic rocks, vein quartz and volcanic rocks. The contact between the diamictite and overlying breccia is sharp and concordant with stratification. This diamictite has yielded a few examples of glacially striated and faceted clasts (Link, 1983a). The rock appears massive. However, a careful search reveals evidence for stratification in the form of wisps in the matrix and diffuse layers of pebbles. The diamictite appears to consist largely of ice-rafted debris derived from an ice sheet, and in places reworked by bottom currents and by sediment gravity flow in a glacial-marine environment (Crittenden and others, 1983; Link, 1983a). There is no firm evidence for deposition from grounded ice.

The most impressive feature of the predominantly clastic sedimentary rocks in the upper part of the Scout Mountain Member is the abundant evidence for deposition from turbulent, high-concentration sediment gravity flows (sole marks, normal grading, parallel laminae with parting lineation, convolute laminae, various water-escape structures). The strata above the diamictite may have accumulated below wave base, and the carbonate rocks may be among the deepest-water sediments present in the section.

Christie-Blick and Levy (1989b) suggest the following interpretation of the section north of Portneuf Narrows. Deposition of carbonate sediment (now dolomite) on glacial-marine diamictite was due to a marked decrease in the terrigenous sediment supply (e.g., Bjorlykke and others, 1978), and is not necessarily an indicator of either shallow water conditions or of shoreline transgression. The dolomite may instead represent an interval of sediment starvation within a depositional sequence. The diamictite beneath the dolomite is interpreted as representing all or part of the transgressive systems tract. Facies arrangements in glaciated basins are controlled strongly by both ice sheet dynamics and changes in depositional base level, and glacial-marine diamictite would be expected to accumulate preferentially during times of glacial retreat and rising sea level. Retreat of the ice margin to an entirely terrestrial position would lead to a significant decrease in the flux of rafted sediment. Hence the dolomite may represent the feather edge of the highstand systems tract within the basin and perhaps part of the underlying transgressive systems tract. The sandstones and shales overlying the dolomite are interpreted as lowstand and transgressive deposits above a sequence boundary. This is suggested by the predominance of sediment-gravity-flow deposits and by the locally erosional lower contact of the sandstones. The carbonate and marble unit, whose thickness and proportion of carbonate varies markedly from one section to another, is thought to represent another interval of sediment starvation.

The upper member of the Pocatello Formation, which overlies these carbonate rocks, is interpreted as the lower part of the next highstand systems tract.

Walk southward along the crest of the hill, and the proceed westward down the southernmost spur. The contact between diamictite (overturned Scout Mountain Member) and greenstones (upright Bannock Volcanic Member) is the Portneuf Narrows fault, interpreted by Burgel and others (1987) as a generally southward-dipping strand of a Mesozoic tear fault.

Several components of the Bannock Volcanic Member can be observed on the southwest flank of the ridge (Link and Lefebre, 1983; Link, 1987). These include greenstone breccia, volcaniclastic sandstone, and locally, pillow breccia. The Bannock Volcanic Member grades upward into diamictite of the Scout Mountain Member that contains abundant argillite fragments and sparse clasts of quartzite. Geochemical data obtained by Harper and Link (1986) from volcanic rocks at Chinks Peak about 3 km north of this locality reveal high Ti and high Zr/Y ratios indicative of within-plate volcanism, and Nb/Y ratios and patterns of light REE enrichment consistent with an alkalic composition.

To the south, correlative rocks are of transitional tholeiitic-alkalic composition (Harper and Link, 1986). These data are taken to indicate that volcanic rocks of the Bannock Volcanic member accumulated at a time of continental rifting.

138.3. Turn right on Blackrock Canyon Road.
138.6. Turn right on Portneuf Road.
139.4. I-15 southbound entrance.
140.0 I-15 northbound entrance.
End of field trip.

BIBLIOGRAPHY

Aitken, J.D., 1991, Two Late Proterozoic glaciations, Mackenzie Mountains, northwestern Canada: Geology v. 19, p. 445-448.

Albi, C., Chappell, G.S., Meyers, R.C., and Richardson, R.W., eds., Idaho-Montana Issue: Colorado Rail Annual No. 15: Golden, Colorado Railroad Museum, 215 p.

Allmendinger, R.W. and Jordan, T.E., 1981, Mesozoic evolution, hinterland of the Sevier orogenic belt: Geology, v. 9, p. 308-313.

Anderson, A.L., 1928, Portland cement materials near Pocatello, Idaho: Idaho Bureau of Mines and Geology Pamphlet 28, 15 p.

Armin, R.A. and Mayer, L., 1983, Subsidence analysis of the Cordilleran miogeocline: Implications for timing of late Proterozoic rifting and amount of extension: Geology, v. 11, p. 702-705.

Barnes, R.D., 1987, Invertebrate zoology: Philadelphia, Saunders College Publishing, 893 p.

Beus, S.S., 1968, Paleozoic stratigraphy of Samaria Mountain, Idaho-Utah: American Association of Petroleum Geologists Bulletin, v. 52, p. 782-808.

Bjorlykke, K., Bue, B., and Elverhoi, A., 1978, Quaternary sediments in the northwestern part of the Barents Sea and their relation to the underlying Mesozoic bed rock: Sedimentology, v. 25, pp. 227-246.

Blackwelder, E., 1932, An ancient glacial formation in Utah: Journal of Geology, v. 40, p. 289-304.

Bond G.C., Christie-Blick, N., Cominz, M.A., and Devlin, W.J., 1985, An early Cambrian rift to post-rift transition in the Cordillera of western North America: Nature, v. 316, p. 742745.

Bond, G.C., Kominz, M.A., and Devlin, W.J., 1983, Thermal subsidence and eustasy in the Lower Paleozoic miogeocline of western North America: Nature, v. 306, p. 775-779.

Bright, R.C., and Ore, H.T., 1987, Evidence for the spillover of Lake Bonneville, southeastern Idaho: *in* Beus, S.S., ed., Centennial field guide volume 2, Geological Society of America, Rocky Mountain section, p. 143-146.

Bruhn, R.L. and Beck, S.L., 1981, Mechanics of thrust faulting in crystalline basement, Sevier orogenic belt, Utah: Geology, v. 9, p. 200-204.

Bryant, Bruce, 1984, Reconnaissance geologic map of the Precambrian Farmington Canyon Complex and surrounding rocks in the Wasatch Mountains between Ogden and Bountiful, Utah: U.S. Geological Survey Map I-1447, scale 1:50,000.

Burchfiel, B.C. and Davis, G.A., 1975, Nature and controls of Cordilleran orogenesis, western United States: extensions of an earlier synthesis: American Journal of Science, v. 275-A, p. 97-118.

Burgel, W.D., 1986, Structural geology of the Rapid Creek area, Pocatello Range, north of Inkom, southeast Idaho, [M.S. Thesis]: Pocatello, Idaho State University, 67 p.

Burgel, D., Rodgers, W., and Link, P.K., 1987, Mesozoic and Cenozoic structures of the Pocatello region, southeastern Idaho: *in* Miller, W.R. ed., The thrust belt revisited, Wyoming Geological Association, 38th annual field conference guidebook, p. 91-100.

Campbell, D.P., 1974, Biostratigraphy of the Albertella and Glossopleura Zones (Lower Middle Cambrian) of northern Utah and southern Idaho [M.S. thesis]: Salt Lake City, University of Utah, 295 p.

Carlson, R.A., 1968, Geology and petrography of the volcanic rocks south of Hawkins Basin, southeastern Idaho: M.S. Thesis, Pocatello, Idaho State University.

Christie-Blick, N., 1982, Upper Proterozoic and Lower Cambrian rocks of the Sheeprock Mountains, Utah: Regional correlation and significance: Geological Society of America Bulletin, v. 93, p. 735-750.

Christie-Blick, N., 1983, Glacial-marine and subglacial sedimentation, Upper Proterozoic Mineral Fork Formation, Utah: *in* Molnia, B.F., ed., Glacial Marine Sedimentation, New York, Plenum Press, p. 703-776.

Christie-Blick, N., 1985, Upper Proterozoic glacial-marine and subglacial deposits at Little Mountain, Utah: Brigham Young University Geology Studies, v. 32, part 1, p. 9-18.

Christie-Blick, N., and Levy, M., 1985, A new approach to time correlation in Proterozoic rocks: sequence boundaries in the Brigham Group, Utah: Geological Society of America Abstracts with Programs, v. 20, p. 298.

Christie-Blick, N., and Levy, M., eds., 1989a, Late Proterozoic and Cambrian tectonics, sedimentation, and record of Metazoan radiation in the western United States: Field Trip Guidebook T331, 28th International Geological Congress, Washington D.C., American Geophysical Union, 113 p.

Christie-Blick, N., and Levy, M., 1989b, Concepts of sequence stratigraphy, with examples from strata of Late Proterozoic and Cambrian age in the western United States: *in* Christie-Blick, N., and Levy, M., eds., 1989, Late Proterozoic and Cambrian tectonics, sedimentation, and record of Metazoan radiation in the western United States: Field Trip Guidebook T331, 28th International Geological Congress, Washington D.C., American Geophysical Union, p. 23-38.

Christie-Blick, N., Grotzinger, J.P., and von der Borch, C.C., 1988, Sequence stratigraphy in Proterozoic successions: Geology, v. 16, p. 100-104.

Christie-Blick, N., Link, P.K., Miller, J.M.G., Young, G.M., and Crowell, J.C., 1980, Regional geologic events inferred from Upper Proterozoic rocks of the North American cordillera: Geological Society of America Abstracts with Programs, v. 12, p. 402.

Cloud, P., 1968, Atmospheric and hydrospheric evolution and the primitive earth: Science v. 160, p. 729-736.

Cloud, P., 1973, Pseudofossils: a plea for caution: Geology, v. 1, p. 123-127.

Conway Morris, S., Mattes, B.W. and Menge, C., 1990, The early skeletal organism Cloudina: new occurrences from Oman and possibly China: American Journal of Science v. 290-1, p. 245-260.

Crimes, T.P., 1987, Trace fossils and correlation of late Precambrian and early Cambrian strata: Geological Magazine v. 124, p. 97-189.

Crittenden, M.D., Jr., 1972, Geologic map of the Browns Hole Quadrangle, Utah: U.S. Geological Survey Geologic Quadrangle Map GQ-968, scale 1:24,000.

Crittenden, M.D., Jr, and Wallace, C.A., 1973, Possible equivalents of the Belt Supergroup in Utah: in Belt Symposium, v. 1: Moscow, University of Idaho, Idaho Bureau of Mines and Geology, p. 116-138.

Crittenden, M.D., Jr. Schaeffer, F.E., Trimble, D.E., and Woodward, L.A., 1971, Nomenclature and correlation of some upper Precambrian and basal Cambrian sequences in western Utah and southeastern Idaho: Geological Society of America Bulletin, v. 82, p. 581-602.

Crittenden, M.D., Jr., Christie-Blick, N., and Link, P.K., 1983, Evidence for two pulses of glaciation during the Late Proterozoic in northern Utah and southeastern Idaho: Geological Society of America Bulletin, v. 994, p. 437-450.

Crowell, J.C., 1983, The recognition of ancient glaciations: *in* Medaris, L.G., Jr., Nickelson, D.M., Byers, C.W., and Shanks, W.C., eds., Proterozoic Geology: Selected papers from an International Proterozoic symposium: Geological Society of America Memoir 161, p. 289-297.

Currey, D.R. Atwood, G. and Mabey, D.R., 1984, Major levels of Great Salt Lake and Lake Bonneville: Utah Geological and Mineral Survey Map 73.

Derry, L.A., Kaufman, A.J., and Jacobsen, S.B., Sedimentary cycling and environmental change in the Late Proterozoic: Evidence from stable and radiogenic isotopes: Geochimica et Cosmochimica Acta (in press).

Derry, L.A., Keto, L.S., Jacobsen, S.B., Knoll, A.H. and Swett, K., 1989, Sr isotopic variations in Upper Proterozoic carbonates from Svalbard and East Greenland: Geochimica et Cosmochimica Acta, v. 53, p. 2331-2339.

Devlin, W.J. and Bond, G.C., 1988, The initiation of the early Paleozoic Cordilleran miogeocline: evidence from the uppermost Proterozoic-Lower Cambrian Hamill Group of southeastern British Columbia: Canadian Journal of Earth Sciences, v. 25, p. 1-19.

Devlin, W.J., Brueckner, H.K., and Bond, G.C., 1988, New isotopic data and a preliminary age for volcanics near the base of the Windermere Supergroup, northeastern Washington, U.S.A.: Canadian Journal of Earth Sciences, v. 25, p. 1906-1911.

Doelling, H.H., 1980, Geology and Mineral Resources of Box Elder County, Utah: Utah Geological and Mineral Survey Bulletin 115, 251 p., map scale 1:125,000.

Droser, M.L. and Bottjer, D.J., 1988, Trends in depth and extent of bioturbation in Cambrian carbonate marine environments, western United States: Geology v. 16, p. 233-236.

Eisbacher, G.H., 1985, Late Proterozoic rifting, glacial sedimentation, and sedimentary cycles in the light of Windermere deposition, western Canada: Palaeogeography, Palaeoclimatology, Palaeoecology, v. 51, p. 231-254.

Fedonkin, M.A., 1986, Precambrian problematic animals: their body plan and phylogeny: *in* Hoffman, A. and Nitecki, M.H., eds., Problematic Fossil Taxa: Oxford, Oxford University Press, p. 59-67.

Glaessner, M.F., 1984, The dawn of animal life: Cambridge, Cambridge University Press, 244 p.

Grant, S.W.F., 1990, Shell structure and distribution of Cloudina, a potential index fossil for the terminal Proterozoic: American Journal of Science, v. 290a, p. 261-294.

Grant, S.W.F., Knoll, A.H., and Germs, G.J.B., 1991, Probable calcified metaphytes in the latest Proterozic Nama Group, Namibia: origin, diagenesis, and implications: Journal of Paleontology v. 65, p. 1-19.

Grotzinger, J.P., 1990, Geochemical model for Proterozoic stromatolite decline: American Journal of Science, v. 290a, p. 80-103.

Halimdihardja, P., 1986, Stratigraphy and depositional environment of the Brigham Group in a portion of the northern Portneuf Range: M.S. Thesis, Idaho State University, 164 p.

Hambrey, M.J. and Harland, W.B., eds., 1981, Earth's pre-Pleistocene glacial record: Cambridge, England, Cambridge University Press, 1004 p.

Harland, W.B., 1983, The Proterozoic glacial record: *in* Medaris, L.G., Jr., Nickelson, D.M., Byers, C.W., and Shanks, W.C., eds., Proterozoic Geology: Selected papers from an International Proterozoic symposium: Geological Society of America Memoir 161, p. 279-288.

Harland, W.B., Armstrong, R.L., Cox, A.V., Craig, L.E., and Smith, A.G., 1990, A geological timescale 1989: Cambridge, England, Cambridge University Press, 263 p.

Harper. G.D. and Link, P.K., 1986, Geochemistry of Upper Proterozoic rift-related volcanics, northern Utah and southeastern Idaho: Geology, v. 14, p. 864-867.

Hoffman, P.F., 1991, Did the breakout of Laurentia turn Gondwanaland inside-out: Science v. 252, p. 1409-1411.

Jensen, M.F., 1989, Geology of Bear River City quadrangle, Box Elder County, Utah, Utah Geological and Mineral Survey Open-File Report 145, scale 1:24,000.

Kasting, J.F., 1987, Theoretical constraints on oxygen and carbon dioxide concentrations in the Precambrian atmosphere: Precambrian Research, v. 90, p. 10497-10510.

Kaufman, A.J., Hayes, J.F., Knoll, A.H., and Germs, G.J.B, 1991, Isotopic compositions of carbonates and organic carbon from upper Proterozoic successions in Namibia: stratigraphic variation and the effects of diagenesis and metamorphism: Precambrian Research, v. 49, p. 301-327.

Kaye, C.A. and Zartman, R.F., 1985, A late Proterozoic Z to Cambrian age for the stratified rocks of the Boston Basin, Massachusetts, U.S.A.: *in* Wones, D.R., ed., Proceedings 'The Caledonides in the USA', Department of Geological Sciences, Virginia Polytechnical Institute, State University Memoir 2, p. 257-261.

Knoll, A.H., 1989, Evolution and extinction in the marine realm: some constraints imposed by phytoplankton: Philosophical Transactions of the Royal Society of London B, v. 325, p. 279-290.

Knoll, A.H., 1991a, End of the Proterozoic Eon: Scientific American, v. 265, p. 64-73.

Knoll, A.H., 1991b, Biological and biogeochemical preludes to the Ediacaran Radiation: *in* Lipps, J.H. and Signor, P.W., eds., Origins and early evolutionary history of the Metazoa: New York, Plenum (in press).

Knoll, A.H. and Butterfield, N.J., 1989, New window on Proterozoic life: Nature v. 337, p. 602-603.

Knoll, A.H., Blick, N., and Awramik, S.M., 1981, Stratigraphic and ecologic implications of late Precambrian microfossils from Utah: American Journal of Science, v. 281, p. 247-263.

Knoll, A.H., Hayes, J.M., Kaufman, A.J., Swett, K., and Lambert, I.B., 1986, Secular variation in carbon isotope ratios from Upper Proterozoic successions of Svalbard and East Greenland: Nature, v. 321, p. 832-838.

Knoll, A.H., Swett, K. and Mark, J., 1991, Paleobiology of a Neoproterozoic tidal flat/lagoonal complex: the Draken Conglomerate Formation, Spitsbergen: Journal of Paleontology, v. 65, p. 531-569.

Krogh, T.E., Strong, D.F., O'Brein, S.J. and Papezik, V., 1988, Precise U-Pb zircon dates from the Avalon Terrain in Newfoundland: Canadian Journal of Earth Sciences v. 25, p. 442-453.

Lande, A.C., 1986, Stratigraphy and depositional environment of the Brigham Group, Oneida Narrows, southeastern Idaho [M.S. Thesis]: Pocatello, Idaho State University, 106 p.

Levy, M., 1991, Late Proterozoic and Early Cambrian Sedimentation, sequence stratigraphy, and tectonic evolution of the eastern Great Basin [Ph.D. dissertation]: New York City, Columbia University, 380 p.

Levy, M., and Christie-Blick N., 1989, Pre-Mesozoic palinspastic reconstruction of the eastern Great Basin (western United States): Science, v. 245, p. 1454-1462.

Levy, M., and Christie-Blick, N., 1991a, Late Proterozoic paleogeography of the eastern Great Basin: *in* Cooper, J.D., and Stevens, C.H., Paleozoic paleogeography of the western United States: Pacific Section, Society of Economic Paleontologists and Mineralogists, Publication 67, v. 1, p. 371-386.

Levy, M. and Christie-Blick, N., 1991b, Tectonic subsidence of the early Paleozoic passive continental margin in eastern California and southern Nevada: Geological Society of America Bulletin, v. 103, p. 1590-1606.

Levy, M.E., Christie-Blick, N. and Link, P.K., 1991, Late Proterozoic incised valleys of the eastern Great Basin: fluvial response to relative falls in sea level: Geological Society of America Abstracts with Programs, v. 23, no. 5, p. 242.

Lindsey, K.A., 1982, The Upper Proterozoic and Cambrian "Brigham Group," Oneida Narrows, southeastern Idaho: Northwest Geology, v. 11, p. 13-21.

Lindsey, K.A., and Link, P.K., 1988, Stratigraphic evidence for two episodes of continental rifting in the basal Cordilleran miogeocline from the northern Great Basin to northeastern Washington: Geological Society of America Abstracts with Programs, v. 20, no. 3, p. 176.

Link, P.K., 1981, Upper Proterozoic diamictites in southeastern Idaho, U.S.A.: *in* Hambrey, M.J. and Harland, W.B., eds., Earth's pre-Pleistocene glacial record: Cambridge, Cambridge University Press, p. 736-739.

Link, P.K., 1982, Structural geology of the Oxford and Malad Summit Quadrangles, Bannock Range, southeastern Idaho, *in* Powers, R.B., ed., Geologic studies of the Cordilleran thrust Belt, Volume 2: Denver, Rocky Mountain Association of Geologists, p. 851-858.

Link, P.K., 1983a, Glacial and tectonically influenced sedimentation in the Upper Proterozoic Pocatello Formation, southeastern Idaho, *in* Miller, D.M., Todd, V.R., and Howard, K.A., eds., Stratigraphic and tectonic studies in the eastern Great Basin: Geological Society of America Memoir 157, p. 165-181.

Link, P.K., 1983b, Geology of the upper Proterozoic Pocatello Formation, Bannock Range, southeastern Idaho [Ph.D. dissertation]: Santa Barbara, University of California, 131 p.

Link, P.K., 1986, Tectonic model for deposition of the Late Proterozoic Pocatello Formation, southeastern Idaho: Northwest Geology, p. 15, p. 1-7.

Link, P.K., 1987, The Late Proterozoic Pocatello Formation; A record of continental rifting and glacial marine sedimentation, Portneuf Narrows, southeastern Idaho: *in* Beus, S.S., ed., Rocky Mountain Section of the Geological Society of America, Centennial Field Guide Volume 2, p. 139-142.

Link, P.K. and LeFebre, G.B., 1983, Upper Proterozoic diamictites and volcanic rocks of the Pocatello Formation and correlative units, southeastern Idaho and northern Utah, *in* Gurgel, K.D., ed., Geologic excursions in stratigraphy and tectonics: from southeastern Idaho to the southern Inyo Mountains, California, via Canyonlands and Arches National Parks, Utah, guidebook, part II, Geological Society of America Rocky Mountain and Cordilleran sections meeting: Utah Geological and Mineral Survey Special Studies 60, p. 1-32.

Link, P.K., LeFebre, G.B., Pogue, K.R., and Burgel, W.D., 1985a, Structural Geology between the Putnam thrust and the Snake River Plain, southeastern Idaho: *in* Kerns, G.L., and Kerns, R.L., Jr. eds., Orogenic Patterns and stratigraphy of north-central Utah and southeastern Idaho, Utah Geological Association Publication 14, p. 97-117.

Link, P.K., Crook, S.R., and Chidsey, T.C., Jr., 1985, Hinterland structure, paleozoic stratigraphy and duplexes of the Willard thrust system; Bannock, Wellsville and Wasatch ranges, southeastern Idaho and northern Utah: *in* Kerns, G.L., and Kerns, R.L., Jr. eds., Orogenic Patterns and stratigraphy of north-central Utah and southeastern Idaho, Utah Geological Association Publication 14, p. 314-328.

Link, P.K., Jansen, S.T., Halimdihardja, P., Lande, A., and Zahn, P., 1987, Stratigraphy of the Brigham Group (Late ProterozoicCambrian), Bannock, Portneuf, and Bear River Ranges, southeastern Idaho, *in* Miller, W.R., ed., The thrust belt revisited: Wyoming Geological Association, 38th annual field conference guidebook, p. 133-148.

Ludlum, J.C., 1942, Pre-Cambrian formations of Pocatello, Idaho: Journal of Geology, v. 50, p. 85-95.

Machette, M.M., Personius, S.F., and Nelson, A.R., 1991, The Wasatch fault zone, Utah—segmentation and history of Holocene earthquakes: Journal of Structural Geology, v. 13, p. 137-149.

Magaritz, M., Kirschvink, J.L., Latham, A.J., Zhuravlev, A.Yu., Rozanov, A.Yu., 1991, Precambrian/Cambrian boundary problem: Carbon isotope correlations for Vendian and Tommotian time between Siberia and

Morocco: Geology, v. 19, p. 847-850.

Miller, J.M.G., 1985, Glacial and syntectonic sedimentation: The upper Proterozoic Kingston Peak Formation, southern Panamint Range, eastern California: Geological Society of America Bulletin, v. 96, p. 1537-1553.

Nursall, J.R., 1959, Oxygen as a prerequisite to the origin of the metazoa: Nature v. 183, p. 1170-1172.

Ore, H.T., 1982, Tertiary and Quaternary evolution of the landscape in the Pocatello, Idaho, area: Northwest Geology, v. 11, p. 31-36.

Oriel, S.S. and Armstrong, F.C., 1971, Uppermost Precambrian and lowest Cambrian rocks in southeastern Idaho: U.S. Geological Survey Professional Paper 394, 52 p.

Oriel, S.S. and Platt, L.B.. 1980, Geological map of Preston 2 degree Quadrangle, southeast Idaho and western Wyoming: U.S. Geological Survey Miscellaneous Investigations Map I-1127, Scale a:250,000.

Oviatt, C.G., 1986a, Geologic map of the Honeyville quadrangle, Box Elder and Cache Counties, Utah: Utah Geological and Mineral Survey Map 88, scale 1:24,000.

Oviatt, C.G., 1986b, Geologic map of the Cutler Dam quadrangle, Box Elder and Cache Counties, Utah: Utah Geological and Mineral Survey Map 91, scale 1:24,000.

Platt, L.B., 1977, Geologic map of the Ireland Springs-Samaria area, southeastern Idaho and northern Utah: U.S. Geological Survey Miscellaneous Field Studies Map MF-890, scale 1:48,000.

Platt, L.B., 1985, Geologic map of the Hawkins Quadrangle, Bannock County, Idaho: U.S. Geological Survey Miscellaneous Field Studies Map MF-1812, scale 1:24,000.

Resser, C.E., 1939, The Spence shale and its fauna [Utah and Idaho]: Smithsonian Miscellaneous Collection, v. 97, no 12, Publication 3490, 29 p.

Resser, C.E., 1939b, The Ptarmigania strata of the northern Wasatch Mountains: Smithsonian Miscellaneous Collection, v. 98, no. 24, Publication 3550, 72 p.

Ross, G.M., 1991, Tectonic setting of the Windermere Supergroup revisited: Geology, v. 19, p. 1057-1152.

Runnegar, B., 1982, Oxygen requirements, biology and phylogenetic significance of the late Precambrian worm Dickinsonia, and the evolution of the burrowing habit: Alcheringa, v. 6, p. 223-239.

Schirmer, T.W., 1985, Basement thrusting in north-central Utah: a model for the development of the northern Utah highland: *in* Kerns, G.J. and Kerns, R.L., Jr., eds., Orogenic patterns and stratigraphy of north-central Utah and southeastern Idaho: Utah Geological Association Publication 14, p. 129-143.

Schirmer, T.W., 1988, Structural analysis using thrust-fault hanging-wall sequence diagrams: Ogden Duplex, Wasatch Range, Utah: American Association of Petroleum Geologists Bulletin, v. 72, p. 573-585.

Scott, W.E., Pierce, K.L, Bradbury, J.P., and Forester, 1982, Revised Quaternary stratigraphy and chronology in the American Falls area, southeastern Idaho: *in* Bonnichsen, Bill, and Breckenridge, R.M., editors, Cenozoic geology of Idaho, Idaho Bureau of Mines and Geology Bulletin 26, p. 581-596.

Seilacher, A., 1990, Vendozoa: organismic construction in the Proterozoic biosphere: Lethaia, v. 22, p. 229-239.

Signor, P.W. and Mount, J.F., 1989, Paleontology of the Lower Cambrian Waucoban Series in eastern California and western Nevada: *in* Christie-Blick, N. and Levy, M., eds., Late Proterozoic and Cambrian tectonics, sedimentation, and record of metazoan radiation in the western United States: Field Trip Guidebook T331, 28th International Geological Congress, Washington D.C., American Geophysical Union, p. 23-38.

Signor, P.W., Mount, J.F., and Onken, B.R., 1987, A pre-trilobite shelly fauna from the White-Inyo region of eastern California and western Nevada: Journal of Paleontology, v. 61, p. 425-438.

Sloss, L.L., 1988, Tectonic evolution of the craton in Phanerozoic time, *in* Sloss, L.L., ed., Sedimentary Cover—North American Craton; U.S.: Boulder, Colorado, Geological Society of America, The Geology of North America, v. D-2, p. 25-51.

Sorensen, M.L. and Crittenden, M.D., Jr., 1972, Preliminary geologic map of part of the Wasatch Range near North Ogden, Utah: U.S. Geological Survey Miscellaneous Field Studies Map MF-428, scale 1:24,000.

Sorensen, M.L., and Crittenden, M.D., Jr., 1976a, Preliminary geological map of the Mantua quadrangle and part of the Willard quadrangle, Box Elder, Weber, and Cache Counties, Utah: U.S. Geological Survey Miscellaneous Field Studies Map MF-720, scale 1:24,000.

Sorensen, M.L., and Crittenden, M.D., Jr., 1976b, Type locality of Walcott's Brigham Formation, Box Elder County, Utah: Utah Geology, v. 3, p. 117-121.

Sorensen, M.L., and Crittenden, M.D., Jr., 1979, Geologic map of the Huntsville quadrangle, Weber and Cache Counties, Utah: U.S. Geological Survey Geologic Quadrangle Map GQ-1503, scale 1:24,000.

Sprigg, R.C., 1947, Early Cambrian (?) 'Jellyfishes' of Ediacara, South Australia, and Mount John, Kimberley District, Western Australia: Transactions of the Royal Society of South Australia, v. 73, p. 72-99.

Stewart, J.H., 1972, Initial deposits in the Cordilleran geosyncline: evidence of a Late Precambrian (< 850 m.y.) continental separation: Geological Society of America Bulletin, V. 83, p. 1345-1360.

Stewart, J.H., 1976, Late Precambrian evolution of North America: plate tectonics implication: Geology, v. 4, p. 11-15.

Stewart, J.H., 1982, Regional relations of Proterozoic Z and Lower Cambrian rocks in the western United States: *in* Cooper, J.D., Troxel, B.W., and Wright, L.A., eds., Geology of Selected Areas in the San Bernadino Mountains, Western Mojave Desert, and Southern Great Basin: Guidebook for Fieldtrip No. 9, Cordilleran Section Geological Society of America, Shoshone Ca., Death Valley Publishing Company, p. 171-186.

Stewart, J.H. and Poole, F.G., 1974, Lower Paleozoic and uppermost Precambrian Cordilleran miogeocline, Great Basin, western United States: *in* Dickinson, W.R., ed., Tectonics and sedimentation: Society of Economic Paleontologists and Mineralogists Special Publication No. 22, p. 28-57.

Stewart, J.H. and Suczek, C.A., 1977, Cambrian and latest Precambrian paleogeography and tectonics in the western United States, *in* Stewart, J.H., Stevens, C.H., and Fritsche, A.E., eds., Paleozoic paleogeography of the western United States: Society of Economic Paleontologists and Mineralogists, Pacific section, Pacific Coast Paleogeography Symposium 1, p. 1-17.

Thompson, B.J., 1982, Geology of Garden Creek Cap, Bannock Range, southeastern Idaho [M.S. thesis]: Pocatello, Idaho State University, 41 p.

Trimble. D.E., 1976, Geology of the Michaud and Pocatello quadrangles, Bannock and Power Counties, Idaho: U.S. Geological Survey Bulletin 1400, 88 p.

Vail, P.K., Mitchum, R.M., Jr., and Thompson, S.,III, 1977, Seismic stratigraphy and global changes in sea level: *in* Payton, C.E., ed., Seismic stratigraphy — applications to hydrocarbon exploration: American Association of Petroleum Geologists Memoir 26, p. 49-212.

Walcott, C.D., 1908, Cambrian geology and paleontology; No. 1, Nomenclature of some Cambrian Cordilleran formations: Smithsonian Miscellaneous Collections, v. 53, p. 1-12.

Walker, C.S., 1983, The stratigraphy and depositional environment of the upper Proterozoic and Cambrian Brigham Group, near Mink Creek, Idaho [M.S. Thesis]: Pocatello, Idaho State University, 55 p.

Yonkee, W.A., Parry, W.T., Bruhn, R.L., and Cashman, P.H., 1989, Thermal models of thrust faulting: Constraints from fluid-inclusion observations, Willard thrust sheet, Idaho-Utah-Wyoming thrust belt: Geological Society of America Bulletin, v. 101, p. 304-313.

Young, G.M., 1982, The Late Proterozoic Tindir Group, east-central Alaska: Evolution of a continental margin: Geological Society of America Bulletin, v. 93, p. 759-783.

Young, G.M., Jefferson, C.W., Delaney, G.D., and Yeo, G.M., 1979, Middle and Late Proterozoic evolution of the northern Canadian Cordillera and Shield: Geology, v. 7, p. 125-128.

Zahn, P., 1987, Stratigraphy and depositional environment of the Brigham Group, Cub River area, Idaho [M.S. Thesis]: Pocatello, Idaho State University, 96 p.